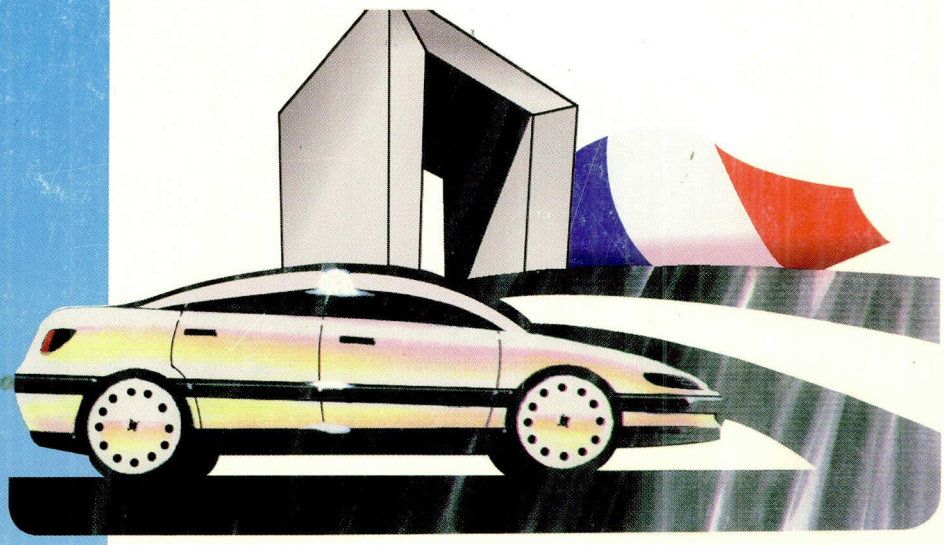

13th International Technical Conference on Experimental Safety Vehicles

13th Conférence Technique Internationale sur les Véhicules Expérimentaux de Sécurité

Proceedings Volume 2

PARIS LA VILLETTE
CITÉ DES SCIENCE
ET DE L'INDUSTRIE
PARIS, FRANCE
NOVEMBER 4 - 7, 1991

13th International Conference
on Experimental Safety Vehicles

Volume 2

The Thirteenth International Technical Conference on Experimental Safety Vehicles

Sponsored by:
U.S. Department of Transportation
National Highway Traffic Safety Administration

Hosted by:
French Government

Held at:
Paris, France
November 4-7, 1991

Foreword

This report of the proceedings of the Thirteenth International Technical Conference on Experimental Safety Vehicles was prepared by the National Highway Traffic Safety Administration, U.S. Department of Transportation.

We wish to thank the authors and all those responsible for the excellence of the material submitted, which aided materially in the preparation of this report.

For clarity and because of some translation difficulties, a certain amount of editing was necessary. Apologies are, therefore, offered where the transcription is not exact.

Introduction

The International Experimental Safety Vehicles (ESV) Program originated under NATO's committee on the Challenges of Modern Society (CCMS) and was implemented through bilateral agreements between the United States Government and the governments of France, the Federal Republic of Germany, Italy, the United Kingdom, Japan, and Sweden. The participating nations agreed to develop experimental safety vehicles to advance the state-of-the-art in safety engineering and to meet periodically to exchange technical information on their progress.

To date, twelve international conferences have been held, each hosted by one of the participating Governments. These conferences have drawn participants from government, the worldwide automotive industry, and the motor vehicle safety research community. International cooperation in motor vehicle safety research continues at the highest level. As work on experimental safety vehicles was completed, the research program expanded to cover the entire range of motor vehicle safety. The ESV Conferences now serve as the international forum through which progress in motor vehicle safety technology is reported.

The proceedings of each Conference have been published by the United States Government and distributed worldwide. These reports, which detail the safety research efforts underway worldwide, have been recognized as the definitive work on motor vehicle safety research. We are sure that this outstanding example of international cooperation seeking reductions in motor vehicle deaths and injuries will continue its past success.

Attendees

AUSTRALIA

Brian Fildes
Monash University
Accident Research Centre

Michael Griffiths
Roads & Traffic Authority

Peter Makeham
Dept. of Transport

Jack McLean
University of Adelaide

BELGIUM

Tadaomi Akiba
Nissan European Tech. Center

Kazuhito Asakawa
J.A.S.I.C.

Kazuhiko Hayashi
Toyota Motor Europe

Yoshihiro Heishi
Nissan European Tech. Center

Herbert Hennsler
C.E.E.

Susumu Ino
Daihatsu Motor Co., Ltd.

Henk Mannekens
Nissan European Tech. Center

Masami Misaki
Nissan European Tech. Center

Hideo Obara
Nissan European Tech. Center

Keiichi Okabayshi
Toyota Motor Europe

Ushio Ueno
Toyota Motor Europe

Yves Van der Straaten
General Motors Europe

Hans Van Driessche
Honda Motor Europe

Daniel Verdiani
Commission of European Communities

Udo Westfal
ACEA

BULGARIA

Krouin Valkov
Ministry of Transport

CANADA

Duncan McPherson
University of British Colombia

James Newman
Biokenetics Assoc. Ltd.

Stephen Read
University of Waterloo

Christopher Wilson
Road Safety & Motor Vehicle Regulations

CZECHOSLOVAKIA

Vojtech Rieger
U.S.M.D.

DENMARK

Per Frederiksen
Justice Ministry - Road Safety Div.

Ib Rasmussen
Ministry of Justice/Road Safety

FRANCE

Alain Achard
Renault

Francois Alonzo
I.N.R.E.T.S.

Yves Aubin
Comite des Const. Franc. d'Auto.

Claude Aubry
Autoliv Klippan

Eugene Auffray
F.F.C.

Daniel Augello
Renault

Jean-Jacques Azuar
Chausson Engineering

Jean Barge
E.C.I.A.

Marc Behaghel
Comite des Const. Franc. d'Auto.

Agnes Bellini
L.A.B./PSA - Renault

Farid Bendjallal
L.A.B./PSA - Renault

J. M. Berard
D.S.C.R.

Roger Biard
I.N.R.E.T.S. - L.C.B.

Pierre Bigot
P.S.A. Peugeot Citroen

Georges Blanc
Automobile Normalisation Bureau

Charles Blanot
Renault - Direction des Etudes

Jean Bloch
I.N.R.E.T.S.

Jean-Claude Bluet
I.N.R.E.T.S.

Felix Bocaly
Peugeot S.A. Research

Marc Bocque
Peugeot S.A.

Serge Bohers
Peugeot S.A.

Jean Bonnoit
I.N.R.E.T.S. - LBA

Veronique Bordes
I.N.R.E.T.S. - LBA

Antoine Bossard
Automobiles Peugeot

Patrick Botto
Renault - IRACBA

Laurent Bouchard
Renault - IRBA

Robert Bouquet
I.N.R.E.T.S. - L.C.B.

Denis Bourcart
Autoliv Klippan

Jean-Luc Brard
Peugeot S.A. Research

Pierre Brun
P.S.A.

Francoise Brun-Cassan
L.A.B./PSA - Renault

Gilles Brutel
Peugeot S.A. Research

Jean-Loup Burgaud
Ecole Centrale de Paris

Marie-Christine Cailleret
Renault - IRACBA

Herve Calmelly
Matra Automobiles

Serge Care-Colin
C.E.T.E. de l'Est

Roland Caroff
Peugeot S.A.

Nelson Casadei
Renault, Research Directorate

Francoise Cassan
Renault

Claude Cavellero
I.N.R.E.T.S. - LBA

Dominique Cesari
I.N.R.E.T.S. - L.C.B.

Francois Chamouard
Renault - Biomech./Accident Lab

Paul Charlety
Autoliv Klippan

Remi Chavanne
Automobiles Peugeot - Sochaux

Martine Chereau
Peugeot S.A. Research

Claude Chevalier
Fondation M.I.A.F.

Jean Chevrier
R.A.T.P.

Jean-Pierre Cheynet
U.T.A.C.

Alain Clerc
Automobiles Peugeot

Pierre Colinot
P.S.A. Direction des Etudes

Paul Philippe Cord
LIVBAG

Franck Dauvilliers
Renault - AARMT

Christophe de Baynast
Peugeot S.A. Research

Pascal Deloof
INRETS - CRESTA

Igor Demay
Automobiles Citroen

Andre Deperrois
P.S.A.

Jean Derampe
Peugeot S.A.

Veronique Desgardins
Automobile Citroen

Lambert Detoux
F.F.C.

Louis DeVaulx
P.S.A.

Serge Diet
Renault

Georges Dobias
I.N.R.E.T.S.

Claude Dolivet
I.N.R.E.T.S. - L.C.B.

Marie-France Dondel
Renault - Direction des Etudes

Regis Dornez
Renault

Yves Drouadaine
Framasoft CSI
Tour Fiat

Alain Dubos
Renault

Alain Duchesne
Davey Bickford

B. Durand
D.S.C.R.

Marc Ellenberg
C.E.T.E. de l'Est

Philippe Eurin
Ministere, Recherche/Technologie

Denis Even
TELMA

Leonce Evin
Auto Klippan

Jean-Pierre Faidy
P.S.A. DRAS

Gerard Faverjon
L.A.B./Peugeot Renault

Andre Fayon
Renault

Michel Ferlay
I.N.R.E.T.S.

Francis Ferrandez
I.N.R.E.T.S.

Serge Ficheux
U.T.A.C.

Claude Fline
Ministere Recherche/Technologie

Helene Fontaine
I.N.R.E.T.S.

Jean-Yves Foret-Bruno
Renault

Arnaud Froumajou
Peugeot S.A. Research

Jean Fructus
U.T.A.C.

Philippe Gaches
Peugeot S.A. Research

Gilles Garret
Autoliv Klippan

Bernard Gauvin
D.S.C.R.

Louis Germain
Renault Vehicules Industriels

Olivier Gignoux
Renault

Jean-Claude Goaer
Renault

Camille Gontier
Ecole Centrale de Paris

Christian Goualou
P.S.A./E.C.P.

Silvie Goujon
Peugeot S.A. Research

Raymond Guasco
F.I.E.V.

Louis-Robert Guy
PYROSPACE

Mouloud Haddak
I.N.R.E.T.S./L.C.B.

Jean Hamon
P.S.A. DRAS

Jean-Marie Heinrich
L.A.B./PSA - Renault

Claude Henry
L.A.B./PSA - Renault

Francois Hordonneau
Renault

Jean-Francois Huere
Peugeot S.A. Research

Christophe Jacob
Renault - AARMT

Jacques Jolivet
Autoliv Klippan

Marco Klingler
INRETS - CRESTA

Serge Koltchakian
Renault - Biomech./Accident Lab

Michel Kozyreff
Autoliv Klippan

Jean Jacques Laine
C.E.T.E., Nord Picardie

Marc Laliere
Renault Automobiles Centre Technique

Patrice Larguier
P.S.A. - DRAS

Francois Laurent
Peugeot S.A. Research

Aime LeCalve
Renault

Jean-Yves LeCoz
L.A.B./PSA-Renault

Evelyne Lepoivre
Renault

Francois Leygue
Ministry of Transport

Richard Loinard
PYROSPACE

Roland Lucquiad
U.T.A.C.

Philippe Mack
Renault

Jean-Paul Magnier
Davey Bickford

Vincent Maillard
E.C.I.A.

Bruno Marguet
GEC ALSTHOM - CIMT

Gerard Martigny
Peugeot S.A. Research

Veronique Martin
Automobiles Citroen

Yves Martin
Automobiles Citroen

Therese Martinet
Peugeot S.A.

Gerard Mauron
Peugeot S.A. Research

Jean-Pierre Medevielle
I.N.R.E.T.S.

Menard
INNOVATION 128

Serge Morlan
PYROSPACE

Francois Mounier-Poulat
Renault Vehicules Industriels

Richard Najchaus
Renault

Henri Novel
Huliez France

Sean O'Riordain
I.N.R.E.T.S. - L.C.B.

Laurent Oudenard
Renault - IRBA

Jean-Frederic Outters
Automobiles Citroen

Jean Pages
F.I.E.V.

Christian Perotto
LIVBAG

Claire Petit
Renault - IRBA

John L. Phelps
O.I.C.A.

Yvette Pincemaille
L.A.B./PSA - Renault

Sophie Planque
Renault - AARMT

Yves Portier
A.P.S.A.D., Direction Automobile

Daniel Pouget
Renault

Alain Priez
Renault - IRACBA

Eric Ramaioli
Renault

Michelle Ramet
I.N.R.E.T.S. - L.C.B.

Philippe Ranc
Automobiles Citroen

Raymond Ravenel
Comite des Const. France D'Auto

Jean-Pascal Reille
Renault, Direction des Etudes

Francois Renaudin
SERAM, lab. de Biomecanique

Joel Rio
Renault

Nicholas Rogers
IMMA

Jean-Paul Rouet
SAGEM

Patrice Roulois
Heuliez Automobiles

Nakoto Sakai
NIPPONDENSO

Rene Sallen
Automobiles Citroen

Patrick Siarry
Ecole Centrale de Paris

Donggang Song
Renault - IRACBA

Olivier Soulie
Automobiles Peugeot-Sochaux

Jean-Pierre Spagnol
Autoliv Klippan

Georges Stcherbatcheff
Renault

Christian Steyer
Renault

Xiang-Tong Tao
INRETS LCB

Philippe Tardivon
P.S.A. Direction des Etudes

Claude Tarriere
Renault

Christian Thevenet
C.C.F.A.

Christian Thomas
L.A.B./PSA- Renault

Pierre Toursel
Peugeot S.A. Research

Xavier Trosseille
Renault

Jerome Uriot
Renault - IRBA

Harold Vallee
L.A.B./PSA - Renault

Gilles Vallet
I.N.R.E.T.S.

Jacques Van Bunderen
Autoliv Klippan

Kyriakos Vavalidis
Autoliv Klippan

Philippe Ventre
Renault

Michele Vergne
Fondation M.I.A.F.

Roel Verhoog
CESA

Louis-Claude Vrignaud
Siemens Automotive S.A.

Gilbert Walfisch
Renault

Remy Willinger
I.N.R.E.T.S.

GERMANY

Horst Albrecht
Volkswagen AG

Winfried Asmuth
TUV Rheinland

Toshio Ban
Honda R & D Europe

Hartmut Burger
Volkswagen AG

Bo Cavell
Autoliv GmbH

Horst Dalibor
Volkswagen AG

Karl Frederick Ditsch
Ministry of Transport

Jens Eberius
Porsche AG

Harald Eggelmann
Mercedes-Benz AG

Willi Elsenheimer
Adam Opel AG

Eberhard Faerber
Federal Highway Research Institute

Joerg Fellerer
Bayerische Motoren Werke AG

Detlef Frank
Bayerische Motoren Werke AG

Joachim Franz
Siemens AG

Bernd Friedel
Federal Highway Research Institute

Wolf-Richard Frielingsdorf
Mercedes-Benz AG

Klaus-Peter Glaeser
Federal Highway Research Institute

Jurgen Grandel
DEKRA

Johann Guggenberger
Siemens AG

Josef Haberl
Bayerische Motoren Werke AG

Hans Hagen
Karl Kassbohrer Fahrzeugwerke GmbH

Lothar Heider
Mercedes-Benz AG

Wolfram Hell
University Munich

Thomas Hummel
HUK - Verband

Dimitrios Kallieris
University of Heidelberg

Karl-Heinz Kartenberg
Porsche AG

Jorg Kerwath
Honda R & D Europe

Kikuzo Kitaori
Mitsubishi Motors Europe, B.V.

Juergen H. Kloeckner
BASt, Federal Highway Research Institute

Hubert Koch
Industrie Verband Motorrad

Bernhard Koonen
TUV Rheinland e.V.

Gerald Krabbel
Technische Universitat Berlin

Bernd Kraemer
TUV Rheinland e.V.

Hans-Joachim Kraft
Bayerische Motoren Werke AG

Heinz Kunert
SEKURIT-Glas Union GmbH

Klaus Langwieder
HUK - Verband

Bog-Soo Lee
Institute of Automobilengineering

Heinz Leffler
Bayerische Motoren Werke AG

Herbert Loffelholz
Federal Industry of Transport

Horst-Georg Marks
Volkswagen AG

Gunther Menzel
Volkswagen AG

Yoshimoto Nagamoto
Mazda Motor Corp.

Hiroyaki Nishioka
Toyoda Gosei Co., Ltd.

Michael Popp
Universitat der Bundeswehr

Berud Richter
Volkswagen AG

Ernst-Rudiger Rohr
Mercedes-Benz AG

Klaus Rompe
TUV Rheinland e.V.

Willibald Roth
Kolbenschmidt AG

Dieter Schaper
Electrolux Autoliv

Thomas Scharnhorst
Volkswagen Research Forschung Fahrzeugtechnik

Dieter Scheunert
Mercedes-Benz AG

Andreas Schindler
TUV Rheinland e.V.

Friedrich-Karl Schlotterbeck
European Components Deutschland

Achim Schmitz
TUV Rheinland e.V.

Gerhard Schontag
Mercedes-Benz AG

Ruprecht Sinnhuber
Volkswagen AG

Alexander Sporner
HUK Verband

Armin Starck
DEKRA

Hans-Eggert Tonnesen
Anton Ellinghaus GmbH & Co. KG

Hidenori Uki
Mitsubishi Motors Europe B.V.

Hans-Josef Vasen
Kolbenschmidt AG

Jesko Veenhuis
Volkswagen AG

Elmar Vollmer
Audi AG

Klaus Von Versen
Engineering Systems International

Lothar Wech
T.U.V. Bayern eV.

Hanns-Peter Weisbarth
Bayerische Motoren Werke AG

Ulrich Wezel
Porsche AG

Frank Wolf
Mercedes Benz AG

Robert Zobel
Volkswagen AG

HUNGARY

Csaba Siklos
Ministry of Transportation

IRELAND

Denis Wood
Wood and Associates

ISRAEL

Ran Cohen
A.D.A.

ITALY

Elisabetta Amici
Centro Sviluppo Mayterial

Pierluigi Ardoino
Fiat Auto SpA - Centro Sicuarezza

Andrea Benedetto
Fiat Auto SpA - Centro Sicurezza

Dante Bigi
Fiat Auto SpA - Centro Sicurezza

Buscaglione
Fiat Auto SpA - Centro Sicurezza

Stefano Buscaglione
Fiat Auto

Fissore
Fiat Auto

F. Fissore
Fiat Auto SpA - Centro Sicurezza

F. Fossati
Fiat Auto SpA - Centro Sicurezza

C. Lomonaco
Ministero dei Trasporti

Fabrizio Luccetti
Fiat Auto SpA - Centro Sicurrezza

Lamberto Milani
Italdesign

Silvia Monticelli
Fiat AutoSpA - Centro Sicurezza

A. Pastorino
Fiat Auto SpA - Centro Sicurezza

Claudio Schinaia
Ministero dei Trasporti

F. Zacchilli
Ministero dei Trasporti

JAPAN

Akihiko Akiyama
Honda R & D

Kenji Araki
Sumitomo Metal Industries, Ltd.

Yoshinori Boda
M.I.T.I.

Mr. Clepkenn
Nissan Motor Company, Ltd.

Hidehiko Enomoto
Hino Motors, Boxy Research & Development

Naoto Fukushima
Nissan Motor Company, Ltd.

Satoshi Fukushima
Toyota Motor Corporation

Kenichi Goto
Japan Automobile Research Institute

Takeshi Harigae
Japan Automobile Research Institute

Kazuo Higuchi
Honda R & D, 12th Research Section

Kaneo Hiramatsu
Japan Automobile Research Institute

Masaki Hitotsuya
Fujitsu Ten Ltd.

Kiyoshi Honda
Honda R&D, 12th Research Section

Noritoshi Horigome
Ministry of Transport

Masaru Igarashi
Suzuki Motor Corporation

Haruyuki Ikesue
NSK, Ltd.

Namio Irie
Nissan Motor Company, Ltd.

Hirotoshi Ishikawa
Japan Automobile Research Institute

Shin-ichi Ishiyama
Toyota Central R & D Labs, Inc.

Keiji Isoda
Mitsubishi Motors Corporation

Kazuyoshi Katou
Toyota Motor Corporation

Junichi Kishimoto
Nippon Koki Co., Ltd.

Toru Kiuchi
Toyota Motor Corporation

Ikuya Kobayashi
Fujitsu Ten Ltd.

Akira Koike
Hino Motors, Vehicle Research & Exper.

Norio Komoda
Toyota Motor Corp. R&D Planning

Yutaka Kondoh
Toyota Motor Corporation

Ichiro Kurawaki
Yamaha Motor Co., Ltd.

Keiji Kusaka
Kawasaki Heavy Industries, Ltd.

Tohru Kuwahara
Isuzu Motors Limited

Hiroyuki Matsumoto
Mazda Motor Corporation

Inukai Mitsuo
Tokai Rika Co., Ltd.

Toshihito Miyagawa
Toyota Motor Corporation

Kyoichi Miyazaki
Japan Automobile Research Institute

Yoshiyuki Mizuno
Nissan Motor Co., Ltd.

Itsuro Muramoto
Nissan Motor Company, Ltd.

Kosuke Nagao
Ashimori Industry Co., Ltd.

Kenji Nakagawa
Toyobo Co., Ltd.

Akihisa Nakamura
I.A.T.S.S.

Muneo Nishizawa
Takata Corp.

Hideo Obata
CRC Research Institute Inc.

Akihiro Ohtomo
Nissan Motor Company, Ltd.

Katsumi Oka
Honda R&D, Tochigi Center

Shinichi Sakamoto
Suzuki Motor Corporation

Toshiaki Sakurai
Mitsubishi Motors Corporation

Shouichi Sano
Honda R&D Co., Ltd.

Michihisa Sasonoi
Suzuki Motor Corporation

Kazuhiro Seki
Honda R & D

Katsuhiro Sekine
Pyro Safety Device Co.

Iichi Shingu
Toyota Motor Corporation

Teruhisa Sugita
Takata Corp.

Katsunobu Sumida
Toyota Motor Corporation

Norio Sumitomo
Toyobo Co., Ltd.

Keizo Suzuki
Tokai Rika Co., Ltd.

Moriyuki Taguchi
Yamaha Motor Co., Ltd.

Nobuhiko Takahashi
Nissan Motor Company, Ltd.

Hideo Takeda
Takata Corporation

Masatoshi Tanaka
Daihatsu Motor Co.

Toshi Tanaka
Sensor Technology Co.

Katsunori Taneda
Japan Automobile Research Institute

Izumi Tokunaga
Ministry of Transport

Junji Tonomura
Suzuki Motor Corporation

Yutaka Tsukiji
Mazda Motor Corporation

Takahiro Tsuruga
Toghigi R&D Center

Hiroshi Ueno
Nissan Motor Company, Ltd.

Shuji Yamaguchi
Toyota Motor Corporation

Kuniaki Yamakuse
Honda Motor Co., Ltd.

Takenori Yamamoto
Honda R&D., Ltd.

Yugi Yokoya
Toyota Motor Corporation

Hiroshi Yoshida
Mitsubishi Motors Corporation

Keigo Yoshida
Honda R & D Co., Ltd.

KOREA

Youngtai Choi
Korea Auto. Test & Res. Instit.

NETHERLANDS

Anna Agter
Ministry of Transport and Public Works

Hans Ammerlaan
Ministry of Transport

Peter De Coo
TNO Road Vehicles Research Institute

Hans Driever
TNO Road Vehicles Research Institute

Hans Huijbers
Ministry of Transport

Paul Jacobs
Volvo Car BV

Edgar Janssen
TNO Road Vehicles Research Institute

Dirk Landheer
Eindhoven University of Technology

Henk Lupker
TNO Road Vehicles Research Institute

Jaap Maartense
Volvo Car BV

Gerard Meekel
Ministry of Transportation and Public Works
Department of Road Transportation

Yashishi Mizutani
Tokai Rika Co., Ltd.

John Nieboer
TNO Road Vehicles Research Institute

Joop Pauwelussen
TNO Road Vehicles Research Institute

Jan Paul Peters
Yamaha Motor Europe N.V.

Bernard Reys
TNO Road Vehicles Research Institute

Albert Roelfsema
Volvo Car BV

L.T.B. Van Kampen
Institute for Road Safety Research

Carla Van Moorsel
Ministry of Transport

Jan Van Santen
J.P.M. Van Santen Public Relations

Fred Wegman
Institute for Road Safety Research

Jac Wismans
TNO Road Vehicles Research Institute

Willem Witteman
Eindhoven University of Technology

RUSSIA

Serguei Efjmenko
State Science and Technology Committee

Anatolie Ejov
City of Moscow

Vladimir Federov
Ministry of the Interior

Vladimir Fedorov
Inspection D'Automobiles de la Russie

Evgenii Semenov
Foundation for Road Safety

Igor Vengerov
S.T.C.E.C.

Igor Venguerov
Technical Center

SPAIN

Javier Alvarez-Montalvo
Ministry of Industry and Commerce

Mercedes Menendez
I.N.T.A.

SWEDEN

Rune Almquist
Volvo Car Corporation

Roger Alven
Alvatec AB

Sture Andersson
Electrolux Autoliv

Nils Bohlin
Bohlin Consulting/Olstorp

Per Branneby
Saab Automobile AB

Gustaf Celsing
Autoliv Svenge AB

Anders Eugennson
Volvo Car Corporation

Erik Falk
Volvo Car Corporation

Lennart Fremling
Swedish Road Safety Office

L. Yngue Haland
Electrolux Autoliv AB

Soren Hedberg
Swedish Road Safety Office

Jan Holmgren
F.T.S.S.

Jan Ivarsson
Volvo Car Corporation

Goran Kahler
Saab Automobile AB

Janusz Kajzer
Chalmers University of Technology

Birgitta Kamren
Folksam Research

Magnus Koch
Volvo Car Corporation

Maria Koch
Folksam Research

Anders Kullgren
Folksam Research

Tony Landh
Saab Automobile AB

Kas Larsson
Saab Automobile

Stefan Larsson
Volvo Truck Corporation

Thomas Lekander
Swedish Road Safety Office

Anders Lie
Folksam Research

Mats Lindquist
Saab Automobile AB

Per Lovsund
Chalmers University of Technology

Bjorn Lundell
Volvo Car Corporation

Fritz Hugo Martin Mellander
Volvo Car Corporation

Gert Nilson
Chalmers University of Technology

Curt Nordgren
Assoc. of Swedish Auto. Manuf. (BIL)

Hans Norin
Volvo Car Corporation

Anders Ohlund
Volvo Car Corporation

Jan Olsson
Autoliv Svenge AB

Michael Persson
Volvo Car Corporation

Jan Petzall
Chalmers University of Technology

Bengt Pipkorn
Chalmers University of Technology

Kare Rumar
Swedish Road & Traffic Res. Institute
V.T.I.

Lennart Strandberg
Swedish Road & Traffic Res. Institute
V.T.I.

Mats Svensson
Chalmers University of Technology

Sven-Erik Svensson
Volvo Car Corporation

Claes Tingvall
Folksam Research

Thomas Turbell
Swedish Road & Traffic Research
V.T.I.

SWITZERLAND

Robert Kaeser
ETH Zurich

Urs Maag
University of Montreal

Masahiko Naito
Auto. Stand. International Center

Gottfried Treviranus
Universtat Zurich

Felix Walz
Institute of Forensic Medicine

UNITED KINGDOM

Gordon Bacon
M.I.R.A.

John F. S. Bidgood
RAC Motoring Services

Philip Bly
Transport & Road Research Laboratory

Alan Bowker
UK Transport Dept.-Vehicle Inspectorate

Jeanne Breen
PACTS

David W. Burleigh
Britax Excelsior Ltd.

Bryan Chinn
Transport & Road Research Laboratory

Keith Clemo
M.I.R.A.

Laurence Clift
ICE Ergomanics

Anthony Denniss
T.R.R.L.

William H. Dixon
Society of Motors Manufacturers & Traders

Mark Dorn
RSEL, Middlesex Polytechnic

Eric Dunn
Department of Transport

Alan Dyche
First Technology Systems

Nigel Earle
Ford Motor Company, Ltd.

Malcolm Eden
Ford Motor Company, Ltd.

Paul Fleming
Breed Automotive

Geoffrey Fletcher
Ford Motor Company, Ltd.

Alan Randell Giles
Rover Group, Ltd.

K. Goense
Airbags International

John Harris
Transport & Road Research Laboratory

Julian Hill
University of Birmingham

C. Adrian Hobbs
Transport & Road Research Laboratory

Frederick John Hope
Hope Technical Developments, Ltd.

John Anthony Jeyes
U.K. Department of Transport

Christopher Kavanagh
Airbags International

Douglas Kendall
M.I.R.A.

Michael Lewis
Rolls Royce Motors Ltd.

Richard Lewis
Ford Motor Company, Ltd.

Richard Lowne
Transport & Road Research Laboratory

Murdoch Macaulay
TRRL

Murray Mackay
University of Birmingham

John Miles
Ove Arup and Partners

Andrew Morris
University of Birmingham

Pat Murphy
U.K. Department of Transportation

Ian Douglas Neilson
P.A.C.T.S.

Robert Newton
ICE Ergonomics

Rock Nigel
ICE Ergonomics

Muir Parker
First Technology Safety Systems

Steve Parkin
University of Birmingham

Geoffrey Platten
Ogle Design Ltd.

Mostafa Rashidy
Ford Motor Company, Ltd.

Adrian Keith Roberts
Transport & Road Research Laboratory

Brian Robinson
Transport & Road Research Laboratory

Peter Roy
RSEL, Middle Polytechnic

Majid Sadeghi
Cranfield Impact Center

Geoffrey Savage
RSEL, Middlesex Polytechnic

Peter Victor Skuse
Rover Group, Ltd.

Peter Slater
Ford Motor Company, Ltd.

Viv Stephens
M.I.R.A.

Richard Sturt
Ove Arup and Partners

Peter Thomas
ICE Ergonomics

S. Valkenburg
Airbags International

Roger Vingoe
HW Structures Ltd.

John Wall
Transport & Road Research Laboratory

Edmund Ward
ICE Ergonomics

Paul Wellicome
M.I.R.A.

Nigel Wemyss
Ogle Design Ltd.

Christopher Williams
Ford Motor Company, Ltd.

Christopher Witherington
RSEL, Middlesex Polytechnic

UNITED STATES

Steven Anderson
ASL

Kenichi Ando
Jetro New York

Robert Arnold
Motor Vehicle Manufacturers' Assoc.

Robert A. Assunacao
Morgan Melhuish et al.

Thomas Baloga
Mercedes-Benz NA

Douglas Bennett
U.S. House of Representatives

Barry Berson
Hughes Aircraft

Donald Bischoff
NHTSA

Russell Brantman
Breed Automotive

Alex Butt
American Suzuki Motor Corp.

Terence Chorba
Centers for Disease Control - F36

Carl Clark
Safety Systems Company

Robert M. Clarke
NHTSA

Scott Cooper
U.S. House of Representatives

Jerry Ralph Curry
NHTSA

Gregory Dana
Association of International Auto. Manufacturers

Robert Davenport
University of Zurich

George Davis
NHTSA

Bruce Decker
Toyota Motor Sales, U.S.A.

Robert Denton
Robert A. Denton, Inc.

Kennerly H. Digges
University of Virginia

James Donovan
Wilson, Elser, Moskowitz, Edelman, Dicker

Deborah Ederer
First Technology Safety Systems

William Randall Edwards
Chrysler Corporation

Karl-Heinz Faber
Mercedes-Benz of North America

Eugene Farber
Ford Motor Co., Ltd.

Michael Finkelstein
Michael Finkelstein & Associates

David Finnegan
U.S. House of Representatives

John Fleck
J & J Technologies Inc.

Donald Friedman
Liability Research

Thomas Fugger
Kinematics Research

Junichi Fukuda
Honda R&D North America, Inc.

Peter Fuller
University of Louisville

Yoshihiro Goi
Mitsubishi Motors of America

James Hackney
NHTSA

Dietmar Haenchen
Volkswagen of America

Chester L. Hale
American Honda Motor Corp., Inc.

Toni Harrington
Honda North America, Inc.

Philip Hight
Accident Research & Analysis

Ralph Hitchcock
NHTSA

Jan Holgren
First Technology Safety Systems

William Hollowell
NHTSA

Toshio Horiuchi
Nissan Research & Development

Saburo Inui
Toyota Motor Corp, Services of N.A.

Joseph Kanianthra
NHTSA

Joseph Kennebeck
Volkswagen of America, Inc.

Tawfik Khalil
Motor Vehicle Manufacturers Association
GM Corporation

Albert King
Wayne State University

William King
Ford Motor Company, Ltd.

Tadao Kobayashi
American Honda Motor Corp., Inc.

William Leasure
NHTSA

Robert LeFevre
General Motors Corporation

John Leinonen
Ford Motor Company, Ltd.

David Lemmon
University of Cincinnati

Paul Lisovicz
Morgan Melhuish et al.

John Lisowski
Morgan Melhuish et al.

Francois Louis
Renault USA

Richard H. Lucki
PSA - USTR

James Mahern
Honda R&D North America, Inc.

Seiji Matsumura
Kawasaki Motors Corp., USA

Ed Michel
Harley Davidson, Inc.

Manabu Morisaka
Toyota Motor Corp. Services of N.A.

Robert Munson
Ford Motor Company, Ltd.

John R. Musgrave
Coburn, Croft & Putzell

Alberto Negro
Fiat Auto USA, Inc.

George Nield
Assoc. of International Auto. Manufacturers

Satoshi Nishibori
Nissan Research & Development

Linda O'Connor
NHTSA

Brian O'Neill
Insurance Institute for Highway Safety

John Orlando
U.S. House of Representatives

George L. Parker
NHTSA

Helen Petrauskas
Ford Motor Company, Ltd.

Elaine Petrucelli
A.A.A.M.

George Pittara, Jr.
First Technology Safety Systems

Wes Pittman
Vehicle Consultants Inc.

Gordon Plank
R.S.P.A.

Priyaranjan Prasad
Ford Motor Co., Ltd.

Nagarajan Rangarajan
G.E.S.A.C.

Ronald Robbins
Consultant

David Romeo
Romeo Engineering

Anthony Sances
Medical College of Wisconsin

Albert Schlecter
Chrysler Corporation

Greg Schmeling
Harley Davidson, Inc.

Henry Seiff
M.V.M.A.

Tariq Shams
G.E.S.A.C.

William Shapiro
Volvo Cars of North America

Philip Sheets
Kawasaki Motors Corp., USA

Philip Siracuse
American Suzuki Motor Corp.

Howard M. Smolkin
NHTSA

John Snider
The University of Tennessee

Douglas W. Toms
American Honda Motor Corp., Inc.

Frank Turpin
NHTSA

James Ughetta
Wilson, Elser, Moskowitz,
Edelman, Dicker

Chris Von Will
First Technology Safety Systems

William H. Walsh
NHTSA

Ronald Wasko
Motor Vehicle Manufacturers'
Association

Emroy Watson
Yamaha Motor Corp.

Bill Weber
Hughes

David Weir
Dynamic Research, Inc.

Marc Weiss
Naval Biodynamics Lab

Kenneth Yadvish
Lester, Schwab, Katz & Dwyer

Albert Yamada
Masaoka & Assoc.

Narayan Yoganandan
Medical College of Wisconsin

John Zellner
Dynamic Research, Inc.

Karl-Heinz Ziwica
B.M.W.

Volume 1. Opening Ceremonies Thru Session 5 Contents

SECTION 1. OPENING CEREMONIES

SECTION 2. GOVERNMENT STATUS REPORTS

Chairman: Howard M. Smolkin, United States

SECTION 3. TECHNICAL SESSIONS

Technical Session 1: Crash Investigation and Data Analysis

Chairperson: Fred Wegman, The Netherlands

Technical Session 2: Safety Improvements from Advanced Vehicle/Highway Technology

Chairperson: Claudio Schinaia, Italy

Technical Session 3: Specialized Road Users

Chairperson: Kenichi Goto, Japan
Co-Chairperson: Kaneo Hiramatsu, Japan

Technical Session 4: Safety Improvements from Advanced Vehicle/Highway Technology

Chairperson: Bernard Durand, France

Technical Session 5: Side Impact Occupant Protection

Chairperson: Richard Lowne, United Kingdom
Co-Chairperson: Ian Neilson, United Kingdom

Volume 2. Session 6 Thru Session 10 Contents

SECTION 3. TECHNICAL SESSIONS (CONTINUED)

Technical Session 6: Light Vehicle Rollover

Chairperson: William Leasure, United States

Technical Session 7: Crash Avoidance Research
Chairperson: Kare Rumar, Sweden

Technical Session 8: Biomechanics and Dummy Development

Chairperson: Dominique Cesari, France

Technical Session 9: Frontal Crash Protection

Chairperson: S. Christopher Wilson, Canada

Technical Session 10: Heavy Truck Safety

Chairperson: Bernd Friedel, Federal Republic of Germany

Technical Session 6
Light Vehicle Rollover

Chairperson: William Leasure, United States

S6-O-01

Pivotal Characterization of Car Rollovers

A.C. Malliaris, J. H. DeBlois
DeBlois Associates, Inc.

Abstract

This paper addresses and traces the influence of several rollover pre-initiation, independent, variables on intermediate and final outcomes, regarding the crashing car/occupant complex system and the resulting casualties. The primary vehicles under investigation are cars. The data for the development of the desired results are extracted from the US field experience of rollover involved cars and car occupants. Six independent variables are addressed in the rollover pre-initiation stage: car travel speed, roadway speed limit, car maneuver, accident precursor, first harmful event, and the location of this event. Five intermediate outcomes are distinguished: the number of quarter turns; loss of passenger compartment integrity through doors that come open in the crash; loss of integrity through disintegrated glazing; occupant ejections, complete or partial; and intrusion of roof, roof borders, and pillars. The final outcomes addressed in the investigation are occupant fatalities, injured survivors, and overall harm. A most informative aspect of this investigation is the comparative evaluation of rollover versus nonrollover crashes. Car travel speed is found to be the source of profound differences. Car travel speed is suggested as a most informative descriptor of "rollover severity," especially when considered in conjunction with accident precursor and car maneuver conditions that promote lateral speed development.

Introduction

Because of the complexity in the relationship between circumstances and outcomes in rollover associated crashes, a rollover severity descriptor and pivotal determinants of outcomes have been elusive goals to date. This paper develops the foundation for achieving these goals.

In addition to their demonstrable influence on rollover outcomes, the independent variables in this investigation are emphasized on the basis of two criteria: (a) availability in the records of accident experience; and (b) applicability in dynamic simulations and tests of rollovers. The purpose of this investigation is to establish the grounds for useable parameters, and a range of pertinent values for these parameters, that influence profoundly car rollover outcomes, as observed in the accident experience, at all stages between pre-rollover maneuvers and final outcomes.

Note that the scope of the paper is limited to the investigation of rollover attributes as they influence the severity of this event and its outcomes, irrespective of conditions that promote or reduce rollover propensity.

Background

Rollover is a serious highway threat. In the US, nearly 10,000 people are killed each year in crashes of rollover involved motor vehicles; about 6,000 of these fatalities are occupants of cars.

In spite of such concerns, little progress has been made to date in serious and quantitative research of rollover. This is so not only because of the complexities of rollover associated crashes, but also because of the fact that until recently neither the data nor the analytical tools were available to conduct such research.

In addition to a missing descriptor of rollover severity, and missing pivotal determinants of rollover outcomes, also missing is a rollover test protocol that represents adequately the unfolding of rollover events, post-initiation.

All of these are important prerequisites for the formulation of rollover performance requirements, and for the development and evaluation of proposed interventions aimed at casualty reduction.

Rollover crashes have been usually characterized by a large number of parameters, that may influence rollover outcomes at a varying and often unknown degree. Examples of such parameters are the terrain topography and the time of the rollover crash; the first harmful event and its location with respect to the roadway; roadway grade, curvature and surface conditions.

Although such parameters provide good background for rollover research, they are marginally useful in establishing the relatively few, simple, and pivotal conditions needed in dynamic simulation or testing of cars for crashworthiness performance in rollovers.

Two useful parameters suggested by this investigation are: a car's translational velocity (available through an estimate of the car's travel speed or through the roadway speed limit) and the likelihood of an angular impulse, developing as a result of pre-rollover car states that promote lateral slide, irrespective of circumstances that led to such states.

Data Sources and Applications

Because of the required many categories of variables and needed resolution, the primary source of data used all across the board in this investigation is the US National Highway Traffic Administration's (NHTSA's) National Accident Sampling System (NASS).

Within this system, we rely primarily on the nationally representative sample of the NASS/Crashworthiness Data System, [NASS/CDS 1988-1990], concerning cars of recent vintage and other light vehicles that were towed away due to crash damage in the US, in 1988-1990.

The sample counts, i.e. the counts before inflation to national estimate levels, available within this system for the investigation of rollover injuries are: about 1,400 rollover involved cars and 2,000 rollover exposed occupants. Most of the attributes of interest in this investigation are available for these sample counts.

Because of the relatively small sample of fatalities in the NASS we address NHTSA's Fatal Accident Reporting System [FARS 1988-90], census of all fatal accidents, every year on US roads, to obtain baseline fatality counts. This source of data provides us with a rollover involved populations of about 16,400 cars and 17,500 occupant fatalities.

In conjunction with the above, for general estimate purposes, we address a companion file: the NASS/General Estimates System which is a national sample of all police reported accidents in the US [NASS/GES 1988-1990]. The sample of rollover involved cars in this file is about 4,200.

Furthermore in integrating all casualties, whether fatalities or injured survivors, we apply the "Harm" descriptor as a bottom line measure of all casualty outcomes. Several data sources of injury outcomes and injury costs have been reviewed for this purpose. Particularly applicable are the cost and injury outcome schedules appearing in the work of Miller et al conducted in the Urban Institute, [Miller 1991a], [Miller 1991b], and [Miller 1991c].

Perspective

Rollover Involved Cars and Car Occupants

About 11,600,000 motor vehicles of all body types become crash involved every year on US roads. This is an annualized average for 1988-1990, according to NASS/GES. Of these, about 87% or 10,200,000 are light vehicles used for personal transportation including: 8,200,000 cars, 1,300,000 pickups, 410,000 vans, and 260,000 multipurpose vehicles (MPVs) per year.

Only a small proportion of these crash involvement rates are rollover related. This proportion for cars is 1.74% and represents about 142,000 cars per year. However the corresponding proportion for casualties and harm is much higher.

For example, the fatalities associated with rollover exposed occupants represent more than 25% of all car occupant fatalities. This is so because of the high severity of the rollover crashes in general, and in particular because of the high incidence of occupant ejections in rollovers.

A total of 14,700,000 occupants per year are crash involved in the US. Of these 11,900,000 are car occupants. About 208,000 car occupants per year are rollover exposed, with these outcomes:

5,820: Dead
7,650: Survivors with Serious or Higher Injuries
121,800: Survivors with Moderate or Minor Injuries
72,800: Uninjured

Total Harm

Fatalities and injured survivors may be combined into Harm. We do this by essentially summing all injured car occupants, including fatalities, each weighted in proportion to the monetary consequences, according to a recently suggested schedule [Miller 1991b], as summarized in Table 1 below.

Table 1. Monetary Cost of Occupant Casualties by Severity of Outcome

Occupant Casualties	Monetary Cost Thousands '88 $
Fatalities	644
Survivors @ MAIS=5	511
@ MAIS=4	133
@ MAIS=3	69.9
@ MAIS=2	21.1
@ MAIS=1	2.8

Note that, for simplicity, at this stage we make no provisions for costs relating to the lost quality of life of car occupant casualties and their families, or for property damage. Neither do we make provisions for resolving monetary cost differences according to injured body region or system/organ. Based on the cited specifics we estimate the monetary cost of car occupants injured in rollovers to be about $6.1 billion ('88 dollars).

Harm Distributions

Harm in Rollover versus Non Rollover Crashes. As recalled from an earlier part of the investigation about 208,000 car occupants are rollover exposed every year in the US, out of a total of 11,900,000 car occupants exposed to all highway crashes. This proportion is about 1.75 rollover exposed per 100 crash exposed car occupants.

Because of the high severity of rollover accidents and the high incidence of ejections, rollover exposed car occupants incur about 21% of the harm to all crash exposed car occupants. This is about a 12 to 1 disparity in harm per exposed occupant, and underscores the urgent need for rollover casualty control.

Harm by Safety Belt Use and Ejections. We further estimate how the cited total harm is distributed among the two restraint conditions (unrestrained and restrained),

and the three degrees of ejection (none, complete and partial) for car occupants exposed to rollover crashes.

Unrestrained, Nonejected	37.6%
Unrestrained, Completely Ejected	37.7%
Unrestrained, Partially Ejected	8.6%
Restrained, Nonejected	14.3%
Restrained, Completely Ejected	0.4%
Restrained, Partially Ejected	1.4%
Total	100.0%

Based on the data sources used in this investigation, safety belt use by car occupants on US roads in 1988-1990 is estimated to be about 50%, varying very significantly as a function of crash mode, crash severity, and occupant demographic attributes. In addition safety belt use rates are often mischaracterized due to occupant reporting inaccuracies.

Accordingly, the relatively small harm proportions cited above for restrained occupants, should not be entirely assigned to safety belt effectiveness. Other factors that may account for the said small harm proportions are: (a) a much lower belt use rate in rollovers, e.g. under 20%; and (b) when exposed to rollovers, belt using car occupants are most likely involved in less severe rollovers than unbelted occupants, as a result of more safety awareness.

Further Harm Distributions. In order to conclude the general perspective addressed in this section we show further distributions of rollover exposed car occupants and of the harm they incur. This is done in Table 2 below.

Table 2. Rollover Exposed Car Occupants and Harm Distribution

	Occupants Percent	Harm Percent	Relative Harm per Occupant
All	100.0	100.0	1.00
Distributed by:			
Travel Speed, mph			
40 or Under	26.0	11.0	0.42
41 to 60	53.1	40.9	0.77
Over 60	20.9	48.1	2.30
By Crash Type			
Single Vehicle	87.3	77.3	0.89
Multi-Vehicle	12.7	22.7	1.79
By Rollover Axis			
Roll	96.4	94.6	0.98
Pitch	3.6	5.4	1.50
By Quarter Turns			
One	17.2	10.1	0.59
Two or Three	49.1	35.5	0.72
Four or More	33.7	54.4	1.61
By Ejection Occurrence			
No	91.0	44.3	0.49
Yes	9.0	55.7	6.19

Note that Percent Occupants and Percent Harm in this Table add to 100% in each part of the table. Also note that the Relative Harm per Occupant is the Percent Harm divided by the Percent Occupants. As such it is always equal to 1.00 for the total in each part of Table 2.

Three of the attributes shown in Table 2, Car Travel Speed, Number of Quarter Turns, and Ejection Occurrence, are discussed extensively in later sections. However at this point consider two significant rollover attributes: the Number of Vehicles involved in rollover events and the Primary Rotation Axis.

Specifically, note that the large majority of car rollovers are single driver accidents, and that the rollover axis is almost exclusively the car's roll axis. The proportion of end-over-end car rotation (pitch) is very small. In view of these circumstances, this investigation will focus primarily on roll axis rollovers, without reference to the number of vehicles involved in the crash.

Criteria in the Selection of Key Variables

The investigation has provided substantial perspective for car rollovers in relation to a number of characteristics, but most of the attributes discussed so far are not particularly helpful in the formulation of either rollover test or dynamic simulation protocols. Moreover no major suggestions have been advanced yet for the selection of one or a few variables to represent "rollover severity."

Key variables for the investigation will be selected in each of the three main areas of interest: pre-crash, intermediate outcomes, and final outcomes. For clarity, pre-crash variables are best thought of as independent variables, while the intermediate and final outcomes are the dependent variables.

A preliminary list of key variables is limited first by the availability of such variables with appropriate resolution in the accident records. In addition, priority considerations for key variables in the pre-crash stage are established on the basis of a variable's strength of influence on intermediate and especially final outcomes.

For the investigation reported here, pre-crash variables are pre-rollover variables addressed from the viewpoint of what happens once rollover has been initiated, without any relevance to the question of whether or how rollover is initiated.

The most important criterion in the selection of such key variables is their applicability to be used simply and readily as pivotal parameters in dynamic simulations or testing of cars in the post-initiation stages of rollover, leading to results concerning intermediate and final outcomes.

For example, a car's travel speed, preceding the rollover, is both influential and practicable. By contrast, variables such as the urban or rural location of the crash, or the location of the first harmful event (whether on the roadway or off it), may be influential but are neither simple nor practicable pivotal parameters in rollover simulations or testing.

Key Pre-Rollover Variables

In order to apply the criteria discussed above, we address the following pre-crash variables: Car Travel Speed, Roadway Speed Limit, Car Maneuver, Crash Precursor, First Harmful Event, and Location of First Harmful Event. These are examined separately in crashes with and without rollover occurrence, for comparison.

Car travel speed, is a prime candidate for a pivotal parameter, because, as will be shown shortly, it has a very strong influence on both intermediate and final outcomes of rollover crashes, as well as it is practicable for applications in rollover tests and dynamic simulations.

Car travel speed is available both in the NASS and in the FARS accident records, although in about 50% of the records. For this reason, the distribution of each key variable in the investigation, whether dependent or independent, was checked for relative agreement and consistency, in a comparison of the two accident record populations: one with known and the other with unknown car travel speeds.

The results of this comparison show no significant differences between the two populations and thus suggest that it is a fair approximation to use the records of known car travel speeds for the characterization of all records in the NASS and FARS used in this investigation.

Furthermore, in order to strengthen the analyses based on estimated travel speed, we also address the readily available roadway speed limit, a fair surrogate of travel speed, as an additional independent variable. The working assumption here is that car travel speed is at least as high as the roadway speed limit, especially at night when rollovers show a high incidence; and in roadways through non heavily populated areas, where most of the rollovers take place.

Car Maneuver (pre-crash) as a variable is offered in both the NASS and the FARS data sources. This variable assumes several possible values concerning car travel well before critical conditions developed, leading ultimately to a crash. Examples of such maneuvers are: Going Straight, Negotiating a Curve, Passing, Lane Changing, Slowing in Traffic, Starting in Traffic, etc.

Crash Precursor is an independent variable offered only in the NASS, where it is known as the "Type of Accident." The values assumed by this variable are vehicle specific and help identify what transpired in the relatively short time, say seconds, before a crash occurrence became inevitable.

Examples of values assumed by the Crash Precursor are: many distinct configurations in two vehicle crashes such as vehicle path crossings, head on paths, head to rear paths, and sideswipes; and many single driver crash configurations. Of particular interest in a rollover investigation are values such as: roadway departure, collision avoidance, loss of control, or loss of traction.

Two more variables are addressed as independent variables: the First Harmful Event (FHE), and the Location of FHE relative to the roadway. Both variables are available in both the NASS and FARS.

Beyond the six independent variables mentioned above, an examination of all other available variables revealed only weak candidates for pivotal independent variables.

The Importance of Travel Speed

The proportion of cars traveling at a given speed is shown in Figure 1, as a function of this speed, for all police reported car crashes, rollover involved and all other.

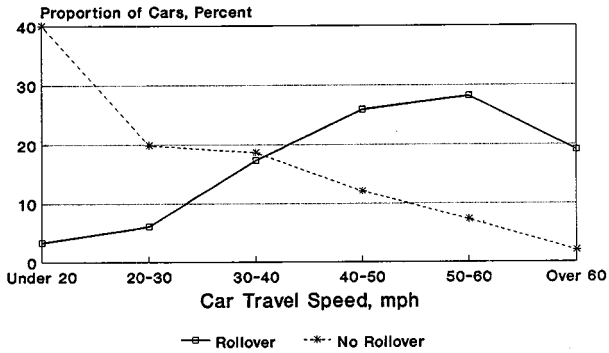

Source: The NASS/GES 1988-1990

Figure 1. Car Travel Speed in Crashes of All Severities

A major difference between the shown distributions is evident, since the distribution for rollovers is clearly shifted by more than 20 mph toward higher travel speeds. The mean speeds for these distributions are: 50.1 mph for the rollover involved cars, and 27.7 mph for cars in all other crashes.

Another illustration of travel speed distributions is shown in Figure 2, for cars involved in fatal accidents. The same major difference between rollover and non rollover distributions is evident. In this case the mean speeds are: 63.4 mph for the rollover involved cars, and 45.3 mph for cars in all other crashes.

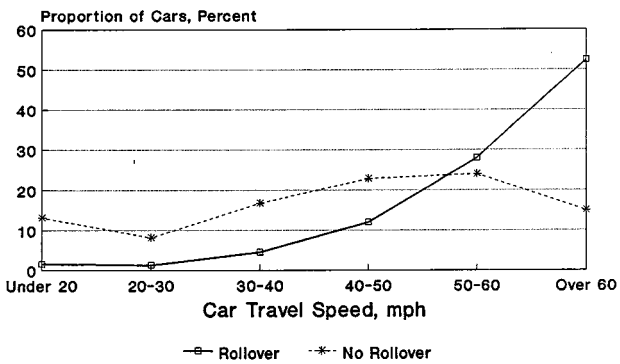

Source: The FARS 1988-1990

Figure 2. Car Travel Speed in Fatal Crashes

The large proportion of travel speeds above say 50 mph, for rollover involved cars, and the large disparity between rollover and non rollover travel speed distributions, is not limited only to the data shown in Figures 1 and 2. As shown in Table 3, high travel speeds of rollover involved cars, and the rollover/nonrollover disparities are evident in every available source of data, concerning cars, occupants, occupant fatalities, and harm in general.

Table 3. Distribution of Car Rollover Records over Car Travel Speeds, 1988-1990

(1) Cars in All Police Reported Rollovers [NASS/GES]
(2) Towaway Rollover Involved Cars [NASS/CDS]
(3) Rollover Involved Cars in Fatal Accidents [FARS]
(4) Rollover Exposed Occupants in Towaway Cars [NASS/CDS]
(5) Fatalities in Car Rollovers [FARS]
(6) Total Harm (Fatalities & Survivors) in Car Rollovers

Travel Speed, mph	Rollover Accident Records % (1)	% (2)	% (3)	% (4)	% (5)	% (6)
20 & Under	3.2	3.2	1.6	3.4	1.6	1.1
21-30	6.1	2.3	1.3	5.8	1.2	1.9
31-40	17.3	21.1	4.5	16.7	4.1	8.0
41-50	25.9	24.7	12.0	25.8	11.5	14.7
51-60	28.2	28.3	28.0	27.2	27.3	26.2
Over 60	19.1	20.1	52.4	20.8	54.0	48.0
Total	100.0	100.0	100.0	100.0	100.0	100.0
Mean (mph) for R/O	50.0	51.2	63.4	50.3	64.5	60.5
Mean (mph) for All Other	27.7	31.9	45.3	28.1	46.5	38.5

Furthermore, the cited findings are confirmed by a detailed analysis of the readily available roadway speed limit, a fair surrogate of travel speed.

An illustration of results concerning the distribution of cars, either rollover involved or involved in other crashes, over the roadway speed limits is given in Figure 3. A summary of similar results from several other sources is presented in Table 4.

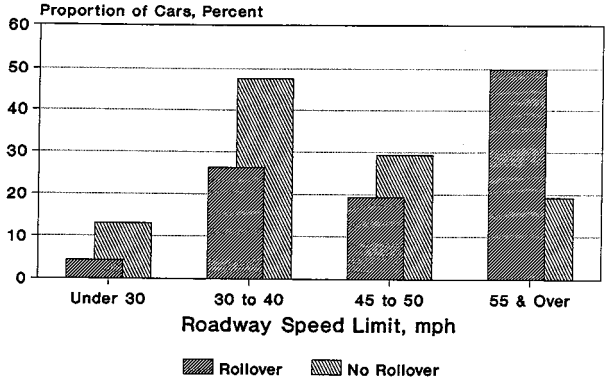

Source: The NASS/CDS 1988-1990

Figure 3. Proportions of Rollover Involved and Other Crash Involved Cars as Function of Roadway Speed Limit

It is evident that these results are essentially consistent with the conclusions reached earlier concerning the large proportions of rollover involved cars that travel at high speeds, say above 50 mph.

Table 4. Distribution of Car Rollover Records over Roadway Speed Limits

(Each Column Adds Up to 100%)
(1) Cars in All Police Reported Rollovers [NASS/GES]
(2) Towaway Rollover Involved Cars [NASS/CDS]
(3) Rollover Involved Cars in Fatal Accidents [FARS]
(4) Rollover Exposed Occupants in Towaway Cars [NASS/CDS]
(5) Fatalities in Car Rollovers [FARS]
(6) Total Harm (Fatalities & Survivors) in Car Rollovers

Roadway Speed Limit, mph	Rollover Accident Records % (1)	% (2)	% (3)	% (4)	% (5)	% (6)
Under 30	5.4	4.3	2.9	7.2	2.9	3.9
30 to 40	19.7	26.4	14.4	20.7	14.4	13.8
45 to 50	19.4	19.3	12.9	20.3	13.1	21.9
55 & Over	55.5	49.9	68.0	51.9	69.6	60.4

As recalled, the working assumption in relating roadway speed limit to car travel speed is that car travel speed is at least as high as the roadway speed limit, especially at night when rollovers show a high incidence; and in roadways through non-heavily populated areas, where most of the rollovers take place.

Potential for Lateral Slide

Lateral car slide is a condition likely to promote rollover. However, the available car accident records offer no measures of lateral velocity. For this reason we take advantage of the resolution offered in the records of Car Maneuver and/or Crash Precursor, discussed earlier, in order to produce a composite variable that we shall call: "Lateral Slide Potential" that is potential for lateral velocity development.

Our interest in addressing the variables: Car Maneuver and Crash Precursor in this investigation is evident from the point of view of conditions, in either one or in both variables, that lead to lateral velocity development.

An illustration of the distribution of car maneuvers encountered in fatal car accidents is given in Figure 4, concerning rollover involved cars as well as cars involved in other crashes. It is evident in this figure that rollover has a higher incidence for maneuvers such as "Negotiating Curve," "Avoidance," and "Lane Change" maneuvers such as passing, merging, etc.

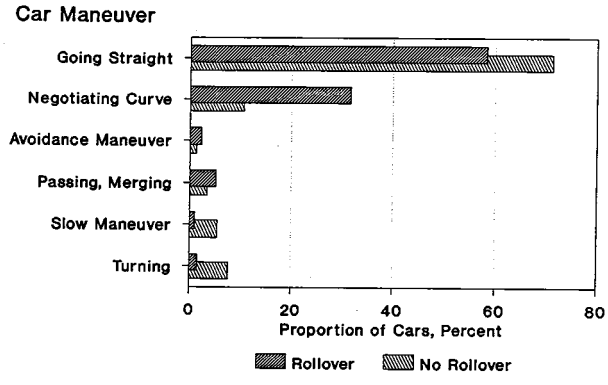

Source: The FARS 1988-1990

Figure 4. Car Maneuver Proportions in Rollover and Non-Rollover Crashes

The Crash Precursor, is an event that may be concurrent with or follow a maneuver. A relevant grouping and distribution of Crash Precursor values for rollover or nonrollover crashes is shown in Figure 5. The predominant proportions of certain maneuvers for rollover involved cars is evident, including "Loss of Control," "Roadway Departure" and "Avoidance."

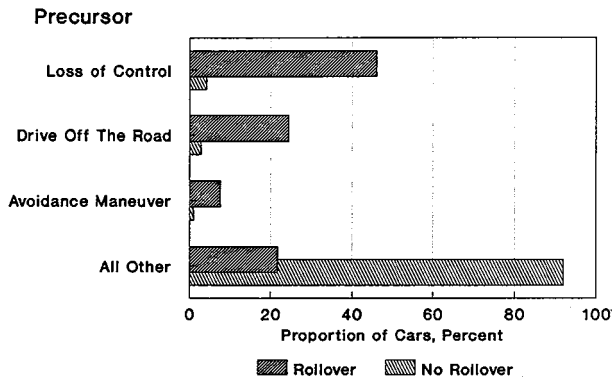

Source: The NASS/GES 1988-1990

Figure 5. Crash Precursor Proportions in Rollover and Non-Rollover Crashes

With full awareness that variables: Car Maneuver and Crash Precursor, have limitations, we formulate a composite variable assumes paired values as shown below:

- No, No: (No Negotiating Curve, No Lane Change; No Collision Avoidance); -- (No Roadway Departure; No Loss of Control; No Loss of Traction)
- Yes, No: (Negotiating Curve, or Lane Change, or Collision Avoidance); -- (No Roadway Departure; No Loss of Control; No Loss of Traction)
- No, Yes: (No Negotiating Curve, No Lane Change; No Collision Avoidance); -- (Roadway Departure or Loss of Control or Loss of Traction)
- Yes, Yes: (Negotiating Curve, or Lane Change or Collision Avoidance); -- (Roadway Departure or Loss of Control or Loss of Traction)

where the first parenthesis in each case designates values assumed by the Car Maneuver variable, while the second parenthesis refers to values assumed by the Crash Precursor variable.

In a further simplification we define the lateral slide potential to be low under the "No, No" conditions , and high under conditions: "Yes, No," or "No, Yes" or "Yes, Yes."

Intuitively speaking, we would expect a small likelihood of rollover when the lateral slide potential is low, while a high potential for lateral slide would lead us to expect a high likelihood for rollover.

The accident experience validates this notion. Specifically, we find that the lateral slide potential is high in 83.2% of the rollovers (versus in 27.3% of other crashes), while the lateral slide potential is low in 16.8% of the rollovers (versus 72.7% of other crashes).

Intermediate Outcomes

Intermediate outcomes is a collective characterization of dependent variables that follow the independent variables in the chain of events that unfold in a crash. Five intermediate outcomes are distinguished in this investigation, based on availability in the accident records and on desired resolution.

The five intermediate outcomes are: (1) the number of quarter turns in the rollover; (2) loss of passenger compartment integrity through doors that come open in the crash; (3) loss of integrity through disintegrated glazing; (4) occupant ejections, complete or partial; and (5) intrusion of roof, roof borders, and pillars.

We now address each of these intermediate outcomes as a function of the most important pre-crash variable, namely car travel speed.

Number of Rollover Quarter Turns

The number of quarter turns (QT) is an important intermediate variable. It is also a strong link between pre- and post-rollover initiation conditions. Moreover, it may be a good candidate for "rollover severity," in addition to or instead of the pre-rollover car speed, as will be seen later in this investigation.

Based on available resolution, QT in car rollovers assumes the values: one, two or three, and four or more. Rollover involved cars, irrespective of travel speed, are distributed as follows:

17.7% with QT = 1,
39.1% with QT = 2 or 3, and
43.2% with QT = 4 or more
100.0% Total

However, this mix is very sensitive to a car's travel speed as seen in Table 5 below.

Table 5. Car Rollover Quarter Turns as a Function of Car Travel Speed

Car Travel Speed, mph	Row Proportion, % by Car Rollover Quarter Turns: One	2 or 3	4 or More	Total Percent
40 or Less	37.3	39.9	22.6	100.0
41 to 50	19.0	48.9	32.0	100.0
51 to 60	7.0	42.4	50.5	100.0
Over 60	7.2	19.6	73.2	100.0

Essentially, the proportion of cars with 4 or more quarter turns increases steadily as the travel speed increases, while the proportion of cars with a lower QT is steadily reduced.

This is an indication that rollover severity increases as car travel speed increases, given that an increasing number of QT introduces higher risks of (a) loss of passenger compartment integrity; (b) occupant ejections; (c) roof and roof support intrusion; and (d) harmful occupant contacts.

Loss of Passenger Compartment Integrity (Through Doors)

The proportion of rollover involved cars with a door that comes open during the rollover is about 8%, averaged over all car travel speeds or QTs. This proportion shows the following sensitivities:

- Car Travel Speed, mph:

40 or Less	1.0%
41 to 50	2.9%
51 to 60	4.5%
Over 60	28.1%

- Number of Quarter Turns:

1	3.7
2 to 3	5.2
4 or More	13.8

Loss of Passenger Compartment Integrity (Through Glazing)

The proportion of rollover involved cars with at least one window (including windshield and roof window) entirely disintegrated is about 65% when averaged over all car travel speeds or all QT's.

In spite of such a large proportion for the average rollover involved car, there are still sensitivities as shown below:

- Car Travel Speed, mph

40 or Less	40.7
41 to 50	85.1
51 to 60	67.2
Over 60	84.0

- Number of Quarter Turns

1	35.0
2 to 3	62.1
4 or More	87.7

Car Occupant Ejections

Table 6 summarizes the car occupant proportions that are ejected in rollovers and, separately for comparison, in all other crashes. The same table also shows the harm to ejectees as a proportion of the harm to all rollover exposed occupants.

Table 6. Ejected Car Occupants and Related Harm

Degree of Ejection	Rollover Crashes	All Other Crashes
	% Ejectees	% Ejectees
Complete	5.99	0.29
Partial	2.95	0.32
Total Ejections	8.94	0.61
	% Harm	% Harm
Complete	35.9	5.72
Partial	19.8	6.64
Total Ejections	55.7	12.36

The proportions shown in Table 6 are averaged over all car travel speeds or over all QT values. There is however a large variation in the proportion of ejectees and of the ejection harm across the values assumed by car travel speeds or QTs in this investigation.

For example, the value 55.7% appearing at the bottom of the Rollover column in Table 6, varies between 10% and 78% as the car speed is varied from under 40 mph to over 60 mph. Similarly wide excursions are observed in ejection proportions as a function of QT.

Final Outcomes

Fatalities, injured survivors, and the integration of these into harm have been addressed in several sections of this investigation, especially in the part dealing with rollover exposed car occupants in perspective. We shall summarize here the principal findings.

Based on data presented in earlier sections, the rollover involvement of car occupants is about 1.75 per 100 crash exposed; but the harm to rollover exposed occupants is about 21% of the harm to all crash exposed. This is a disparity of 12 to 1 and underscores the need for casualty control in rollovers.

Furthermore, harm distribution in rollovers, is very sensitive to car travel speed and, by association to the number of rollover quarter turns, and to ejection occurrence. This was discussed in connection with Table 2. As may be seen in this table wide variations take place in the harm per occupant, as the car travel speed varies from under 40 mph to over 60 mph.

Similarly, a significant sensitivity is seen in harm per occupant, as a function of the number of quarter turns in the rollover, and especially as a function of ejection occurrence.These sensitivities hold for injured survivors as well as for fatalities.

Conclusions

In search of a pivotal characterization of car rollovers, this investigation addressed parameters and values of parameters that must be taken into account in developing rollover simulation, and test and evaluation protocols, that are relatively simple, practicable, and representative of conditions in the field experience.

In addressing pre-rollover conditions, two parameters proved to be influential: the car travel speed, and the potential for lateral slide development. Travel speed in conjunction with the lateral slide potential appear to influence profoundly not only the incidence, but also the severity of rollovers. These parameters deserve further attention in the development of a "rollover severity" descriptor.

Travel speed is also the most important parameter that distinguishes rollovers from all other categories of crashes. Rollover involved cars travel at a mean speed of 50 mph (63.4 mph for fatal crashes); by contrast cars in all other crashes travel at 27.7 mph (45.3 mph in fatal crashes).

Irrespective of this comparative evaluation, rollover test and dynamic simulation protocols will have to

address these rather high speeds. This could be accomplished by either considering a pertinently high test or simulation speed in the travel direction or, if not, by introducing part of the energy that is implied by a higher travel speed in a subsequent stage, e.g. as roll energy through an angular impulse.

Acknowledgement

This work is sponsored by the Division of Injury Control, Centers for Disease Control, US Department of Health and Human Services, under a grant: "The Mechanics and Biomechanics of Rollover Casualties." This paper is a companion paper to: Digges, K., "A Framework for the Study of Rollover Crashworthiness," 13th Safety Vehicle Conference, Paris, France, November 1991 (Paper No. 91-S6-O-05).

References

Digges, K., "Recent Improvements in Occupant Crash Simulation Capabilities of the CVS/ATB Model," SAE 880655, 1988.

Digges, K., Malliaris, A.C., and Ommaya, A., "The Mechanics and Biomechanics of Rollover Casualties," Wayne State Biomechanics Symposium, March 1991.

Digges, K., "Application of Human Models to Evaluate Improvements in Motor Vehicle Crash Safety," 8th Conference of Mathematical Modeling, College Park, Maryland, May 1991.

Digges, K., Malliaris, A.C., Ommaya, A., and McLean, "Characterization of Rollover Casualties," 1991 IRCOBI, Berlin, Germany, September 1991.

Digges, K., "A Framework for the Study of Rollover Crashworthiness," 13th Safety Vehicle Conference, Paris, France, November 1991.

"Fatal Accident Reporting System," Automated Files, National Highway Traffic Safety Administration, Annual Issues 1988-1990.

Malliaris, A. C. and K. H. Digges, "Crash Protection Offered by Safety Belts," Proceedings of the 11th International Conference on Safety Vehicles, Washington, DC, May 1987.

Miller, T., et al, "The Costs of Highway Crashes," The Urban Institute, Washington, DC, 1991.

Miller, T., "The Comprehensive Cost of Motor Vehicle Injuries by Body Region and AIS Severity," 35th Annual Proceedings of the AAAM, 1991.

Miller, T., and Associates "New Estimates of Highway Crash Costs," The Urban Institute Press, Washington DC, 1991.

"The National Accident Sampling System /CDS," (NASS) Automated Files 1988-1990, National Highway Traffic Safety Administration.

S6-O-05

Analysis of the Factors Which Influence Rollover Crash Severity

K. Digges, S. Klisch
University of Virginia

Introduction

The research reported in this paper is a continuation of that reported by Cohen, Digges, and Nichols [1] and by Malliaris and DeBlois [2]. These related papers report analyses of rollover crash data, and are published in the 12th and 13th ESV Conference Proceedings. This earlier research proposed crash variables which were shown to by data analysis to be indicators of occupant injury severity. These "crash severity" variables are needed to assist in defining test conditions for rollover evaluations and for setting goals for injury mitigation measures. The objective of the research reported here is to apply computer modeling, supplemented by studies of "hard copy" documentation of rollover accidents and crash tests, to assess the influence of the crash severity indicators suggested in the literature.

Past Research

A summary of the data analysis research which describes the characteristics of rollover crashes in the United States is given in the earlier paper by Cohen, Digges, and Nichols, and will not be repeated here. These earlier studies included the following observations:

- Ejections are extremely harmful events, and are the predominate cause of harm in rollover crashes.
- In fatal crashes, fatality odds for ejectees are 6 to 8 times higher than for occupants not ejected.
- Injury and ejection are related to number of quarter turns and distance traveled.
- Extent of vehicle damage is related to injury severity.
- In most rollover crashes, the vehicle has a significant lateral velocity component prior to the occurrence of rollover.

Papers dealing two different types of full scale car rollover tests have been reported by Habberstad, et.al. [3] and Orlowski, et. al. [4]. The Orlowski paper documented pure roll tests of Chevrolets with and without roof reinforcement. The authors concluded that a roll cage did not reduce injury measures on a test dummy for the vehicle and roll condition tested. The Habberstad paper reported full vehicle testing which involved severe tripping prior to the roll. The tests showed that severe dummy impacts with the vehicle interior could be induced early in the rollover event.

Robertson [5,6] found that fatal rollover of utility vehicles per 100,000 registered vehicles relative to cars during 1982-87 was strongly correlated to the static stability of the vehicles. Brewer and Harwin [7] examined vehicle, driver and environmental factors which could be deduced from Cardfile and found that vehicle stability factor had a strong influence on rollover involvement risk.

Malliaris [8] examined FARS and Cardfile to determine the significance of motor vehicle characteristics on rollover propensity, after controlling for nonvehicular influences. He found that wheelbase and stability factor were both influential. Four wheel drive vehicles also exhibited higher rollover risks, after controlling for exposure differences.

Mengert, et. al. [9] examined the single vehicle rollover risks for 40 vehicle make/models in the states of Maryland, Texas, and Washington. Vehicle stability factor and urban/rural location were found to be important predictors of rollover risk. Harwin and Emory [10] examined the CARS data for precrash conditions. They found that 80 to 90% of the rollovers were tripped, generally by soil. They reported that injury severity correlated strongly with speed. Stability factor, and number of quarter turns were also influential.

Malliars and DeBlois [2] investigated 1988-90 NASS and found that vehicle pre-crash speed is a pivotal crash severity parameter. The pre-crash speed for rollovers is much higher than for other crashes. Approximately 50% of rollovers occur at speeds above 50 mph, compared with 10% for other crashes.

Framework for the Study of Rollover Outcomes

In studying the rollover phenomena, we are examining separately each of the individual events which influence the motion of the vehicle and its occupants. Our approach is to apply computer models which have been developed and validated by NHTSA. These models include the STI vehicle model for tripped rollover, the ATB Vehicle Model for vehicle post trip motion, and the ATB Occupant Model for occupant motion.

The first event considered is the tripping mechanism. The consequences to be determined in this case are the pre-roll dynamics and kinematics of the vehicle, and those of each occupant. The STI Vehicle Model, and the ATB Occupant Model provide the instruments for this study. We apply these instruments to determine the consequence of tripping for a matrix of initial conditions which represent the rollover spectrum in the field experience. The result is a spectrum of output conditions which are used as input to study the next event.

The second event considered is the free roll and translation of the vehicle and its occupants after tripping and prior to the vehicle impacting the ground. The ATB Vehicle Model is used to predict vehicle motion and the ATB Occupant Model is used for occupants. This phase of simulation includes the motion from the time the tires have lost contact with the ground until the first vehicle body-to-ground impact occurs.

The third event considered is the first vehicle body-to-ground impact. This phase includes the motion from the time the vehicle roof or side impacts the ground, until the next impact. The consequences to be determined are the dynamics of the vehicle and its individual occupants. Again, the ATB models developed and validated by NHTSA are the instruments for this study.

In a similar way, studies of fourth and fifth events can be constructed for those rollovers which involve multiple ground contacts. Consequently, a complete roll of several revolutions can be simulated.

For the purpose of our initial study, we are conducting parametric studies to evaluate how crash variables influence the first three events.

Tripping Simulations

The STI Tripped Rollover Model is used to simulate the tripping event. This model is described in References 11 and 12.

The STI model was developed for NHTSA by Systems Technology, Inc. This model is a seven degree of freedom vehicle model which was developed to permit the analysis of conditions which produce tripped rollover. The model simulates a skidding vehicle impact with a curb. The curb to wheel force is characterized by four functions: (1) a spring force between 0 and 2 inches of 2000 lb/in, (3) a constant wheel deflection force of 4000 lb/in between 2 and 8 inches, (3) a spring force of 8000 lb/in above 8 inches, and (4) a curb damping force of .25 lb-sec/ft.

The model permits the variation of vehicle geometry, inertia, suspension, and external force parameters; and the magnitude and direction of the initial displacement, speed and acceleration.

The model predicts the incidence of a dynamic instability which irreversibly leads to rollover. The roll angle, roll rate and roll acceleration are all calculated at each time increment as the simulation progresses, and are available as output variables. The simulation terminates when rollover is predicted.

An initial application of the STI model was the evaluation of parameters which are sensitive to changes in the tripping velocity. For this study, the geometric and inertia properties were averages taken from the 38 passenger cars published in reference 13. Suspension properties were scaled from the baseline data provided with the STI model. The tripping mechanism was a 6 inch curb which developed force properties as described earlier.

The STI model predicts a large sensitivity of roll rate to lateral velocity. The sensitivity is relatively independent of car size, as shown in Figure 1.

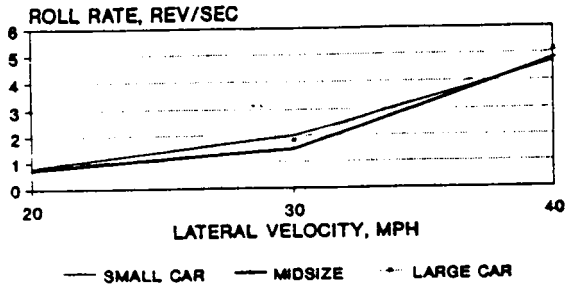

Figure 1. STI Model—Tripping Velocity Influence on Roll Rate (Three Car Sizes)

A further analysis of the factors which influence roll rate is presented in Figure 2. This figure shows the sensitivity of roll rate to other variables which are independently increased by 20%. The baseline case for this analysis was a 20 mph tripped rollover. As anticipated, the lateral velocity has a large amplification factor on roll rate.

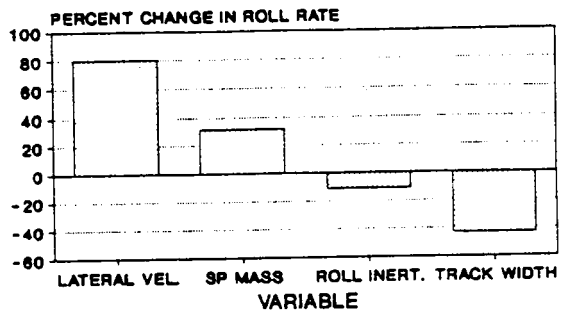

Figure 2. STI Model - Roll Rate Change for 20% Increase in Other Variables (20-mph, .75 rev/sec Baseline)

Vehicle dimensional and inertia parameters have varying influence on roll rate. As the car size increases, the mass, roll inertia, and track width all increase. The offsetting influence on roll rate among these parameters reduces the sensitivity of roll rate to car size.

Occupant motion during the tripping event is being simulated by the ATB Occupant model. This research will be addressed later, in the Discussion section.

Roll Simulations

The dynamic conditions resulting from tripping, as predicted by the STI model can now be used as input data to the ATB vehicle and occupant models which have been validated for predicting the post tripping motion of the vehicle and occupants. The ATB model has been used extensively by NHTSA and the Air Force to simulate vehicle and occupant motion during a crash.

The ATB Vehicle Model was developed and validated by the Air Force Armstrong Aerospace Medical Laboratory (AAMRL). In this model, the vehicle is simulated by one inertia ellipsoid, and eight contact hyperellipsoids. The hyperellipsoid has the capability of producing shapes which resemble boxes with rounded corners—not unlike modern cars and light trucks. Separate ellipsoids and hyperellipsoids are used to represent the four wheels, the hood, trunk, roof, and body. The specific configuration of the ellipsoids is discussed in reference 14. The output of the ATB simulation includes the time history of all forces acting on the vehicle, and the resulting accelerations, velocities, and displacements—both linear and angular.

The ATB Vehicle Model been validated for predicting the complex motion of a 1983 Dodge Aires which rolled four times during a test of highway barriers [14]. The model has also been validated for predicting the motion of vehicles roll tested by the NHTSA roll cart. These tests involve ejecting a vehicle from a test cart traveling at about 30 mph. The longitudinal axis of the vehicle is approximately 90 degrees to the direction of the cart's motion. At the time of ejection, the vehicle is flipped off by a hydraulic system, which imparts a roll velocity of approximately one revolution per second.

The model used for occupant simulation is the ATB Occupant Model. This model is configured to represent the occupant. The ATB Occupant Model has been extensively validated for predicting occupant motion in a crash. In the case of rollover, the AAMRL has simulated numerous rollover tests from the NHTSA rollover cart, thereby providing a body of validated data. A published example of validated occupant motion in rollover is found in reference 15.

Pure Roll Modeling of Occupants

The influence of roll rate on the occupant was examined using the ATB Occupant Model. The data set used was for a mid-size car similar to the one for which valid data is available in Reference [15]. The roll rate was achieved by introducing a pure roll acceleration, similar to that produced by the NHTSA roll test cart. The acceleration was terminated when the desired constant roll rate was achieved. The resulting occupant motion, and occupant to vehicle forces were then observed.

Selected results of simulations of a driver undergoing a counter clockwise roll are presented in Figure 3. For this case, the presence of restraints has little influence on the occupant motion. The resulting forces on the door and window for roll rates up to 3 revolutions per second are shown.

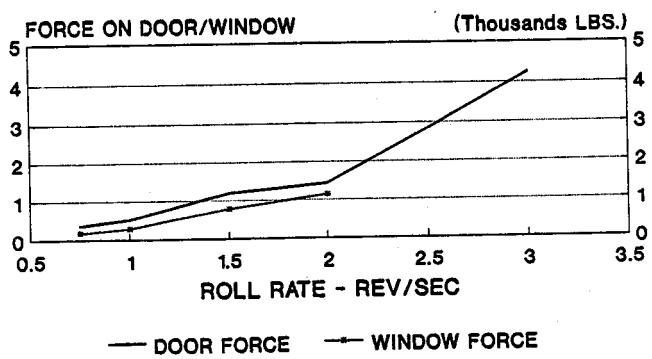

Figure 3. ATB Occupant Model—Roll Rate vs Force Exerted by Occupant (Constant Roll Rate)

Modeling of the Vehicle First Impact

Many researchers have suggested that in rollover events, vehicle damage is an indicator of crash severity. An objective of the vehicle first impact modeling is to gain insight into relationships between vehicle damage and other crash parameters. The establishment of relationships between velocity loss and vehicle damage would be useful in predicting the initial crash velocity.

The model applied was the ATB Vehicle Model. The data set used was that validated for the Dodge Aries in a one rev/sec guardrail induced rollover at 60 mph [14]. Four revolutions of roll ensued. The vehicle stiffnesses were not changed from those in the base data set. The values were inferred from comparing the model and test results.

For the purpose of this sensitivity analysis, the vehicle initial position is an initial roll angle of 100 degrees, and the roof is approximately 1 inch from touching the ground. From this initial condition, the following variables are independently varied: (1) lateral velocity, (2) surface coefficient of friction, (3) roll rate. The results are shown in Figures 4 through 6.

The evaluation of vertical velocity is reported in Figure 7. In this Figure, vertical velocity is expressed in terms of the drop distance required to produce the vertical velocity. For this analysis, the vertical velocity was varied and the other initial conditions were constant. The initial position was approximately 100 degrees, one inch above the surface. The initial lateral speed was 30 mph, and the roll rate was one rev/sec. The vertical velocity was varied through a change in initial velocity, not by changing the initial position.

Analysis of Accident Cases

In order to gain information from accident cases, a detailed analysis was conducted of 140 rollover cases from the 1988-89 NASS files. These cases were selected to represent those with significant vehicle damage. Attempts were made to verify the initial speed, to determine the nature and extent of the tripping mechanism, and to estimate the initial roll rate.

The results of the study are incomplete. However, estimates of the roll rates suggest that the maximum roll rate observed is in the order of 2.5 to 3 rev/sec. The estimates are based on vehicle and scene evidence including initial velocity, distance between trip and initial impact, and vehicle angular rotation between trip and first impact.

Discussion of Results

The results presented are based principally on computer simulation. In these simulations, the crash events in tripping, pure roll, and first vehicle impact are separated and analyzes independently. The objective is to explore how pivotal parameters which influence crash severity interact in each phase of the crash.

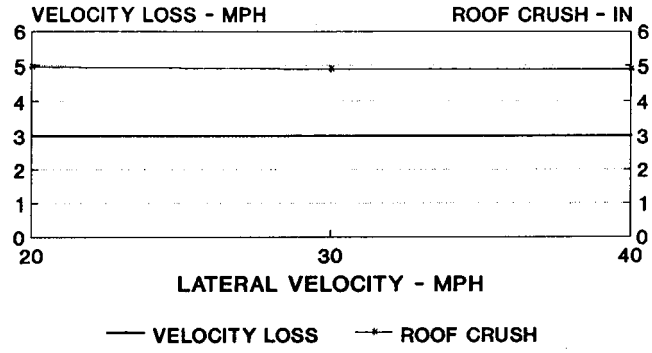

Figure 4. ATB Model—Lateral Velocity vs. Velocity Loss and Roof Crush (1 rev/sec Roll Rate)

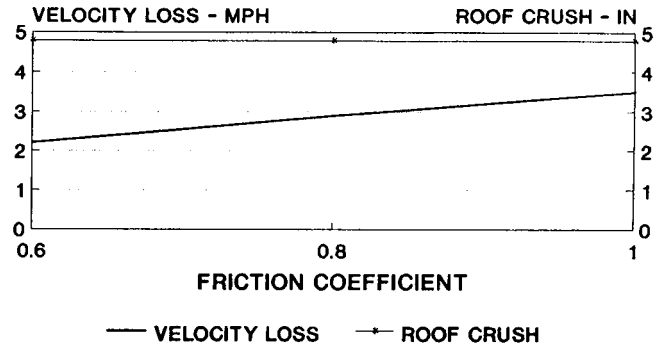

Figure 5. ATB Model—Surface Friction vs. Velocity Loss and Roof Crush (1 rev/sec Roll Rate)

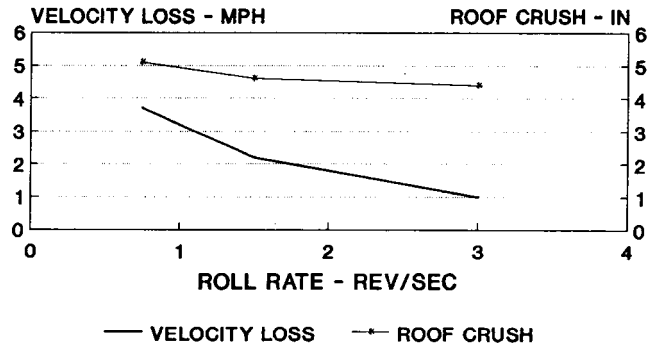

Figure 6. ATB Model—Roll Rate vs. Velocity Loss and Roof Crush (30 mph Lateral Velocity)

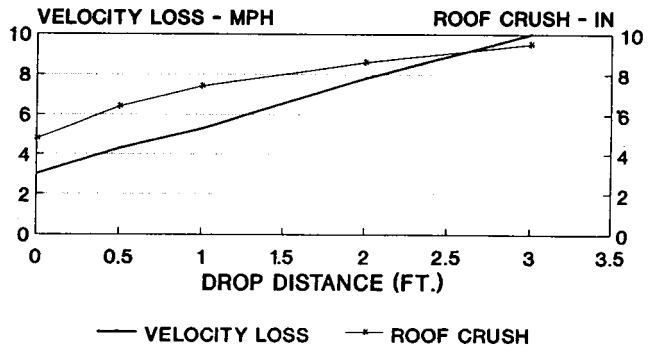

Figure 7. ATB Model—Vertical Velocity vs. Velocity Loss and Roof Crush (1 rev/sec; 30 mph Lateral Velocity)

Data analysis by Malliaris has identified initial velocity as a pivotal parameter in rollover crashes. The STI model suggests that roll rate is strongly related to initial velocity for tripped rollover (Figures 1 & 2). The tripping mechanism simulated by the STI model may be more severe than seen in high speed rollover crashes. The roll rates predicted by the STI model were in excess of 5 rev/sec for the range of crash speeds which account for 50% of the rollovers. However, analysis of NASS rollover data suggests that roll rates above 2.5 rev/sec are rare.

The high tripping forces permitted by the STI model may account for this disparity. Nevertheless, the the strong relationship between linear velocity and roll velocity, is worthy of further investigation and verification.

The pure roll simulations show that high roll rates, independent of other impacts, can produce conditions to induce ejection (Figure 3). These results indicate that in pure rolls, the occupant forces on the door and window can exceed 1000 pounds at roll rates of 2 rev/sec. This load is generally sufficient to cause glass breakage. At 2.5 rev/sec the force on the can door exceed 2500 lbs. By way of comparison, the Federal Motor Vehicle Safety Standard on door latch strength requires a 2500 lb. test. These simulation results suggest that high values of roll rate may have a profound influence on the potential for ejection.

The correlation between ejection and number of quarter turns of roll which is reported in the literature has been postulated to be related to increased time of exposure to the risk of ejection. However, the modeling suggests that the increased severity of the roll rate may also be a dominant factor.

The acceleration produced by the initial tripping acceleration can have a profound influence on the position of the occupant prior to the time the rollover begins. For example, in tests reported by Habberstad [3], the tripping impact produced sufficient acceleration to eject the occupant prior to rollover. For many roll configurations, the tripping acceleration acts to mitigate the initial roll acceleration. This interaction an important part of the accident data analysis, and occupant modeling studies which are currently underway.

The simulations of first vehicle impact provide insight into those variables which influence roof crush and velocity loss (delta-V). The condition simulated was a mid-size vehicle impacting on its roof at a roll rate of one revolution per second. In the validating test for this simulation, the test vehicle roof was not greatly damaged. As a result, the parameters do not recognize the failure characteristics of the structure. Results may be considered as indicators of trends, but should not be considered as absolute.

The simulation shows that roof crush and roll velocity loss are largely independent of lateral velocity (Figure 4). The implication of this result is that high speed testing may not be needed to evaluate high speed protection in rollover crashes.

Coefficient of surface friction has negligible influence on roof crush, but a significant influence on velocity loss (Figure 5). This result is intuitively appealing.

Roll rate sensitivity is shown in Figure 6. At high roll rates, some rotational energy is transferred to translational energy during impact. Consequently, the translational velocity loss decreases with increasing roll rate. Roof crush is relatively insensitive to roll rate.

Vertical velocity, expressed in terms of drop height is shown in Figure 7. The results show that the vertical velocity has a strong influence on both the roof crush and velocity loss.

One of the objectives of this research is to provide guidance to crash investigators. Ultimately it is desired to assess crash severity from the damage to the vehicle. For the conditions examined, vehicle damage was influenced most by vertical velocity, not roll rate or lateral velocity. The only basis found for estimating roll rate and horizontal velocity was from measurements of impact locations at the crash scene.

Additional data collection elements will be required to evaluate the significance of the tripping mechanism, the roll rate and the vertical velocity on rollover crash severity.

References

1. Cohen, D., Digges, K., and Nichols, H., "Rollover Crashworthiness Classification and Severity Indices," 12 ESV Conference, Paper Nr. 89-2B-0-012, May 1989.
2. Malliaris, A, and DeBlois, H., "Pivotal Characterization of Rollover," Proceedings of the 13th ESV Conference, 1991.
3. Habberstad, J., Wagner, R., and Thomas, T., "Rollover and Interior Kinematics Test Procedures Revisited," Proceedings of 30th Stapp Conference, SAE 861875, 1986.
4. Orlowski, K., Bundorf, and Moffatt, E., "Rollover Crash Tests—The Influence of Roof Strength on Injury Mechanics," SAE 851734.
5. Robertson, L., and Kelly, B., "Static Stability as a Predictor of Rollover Crashes Fatal to Occupants of Cars and Utility Vehicles," Journal of Trauma.
6. Robertson, L., "Risk of Fatal Rollover in Utility Vehicles Relative to Static Stability," Presentation to 1988 SAE Government/Industry Meeting, May 3, 1988.
7. Harwin, A., and Brewer, H., "Analysis of the Relationship Between Vehicle Rollover Stability and Rollover Risk Using NHTSA Cardfile Accident Data Base," NHTSA Interim Report, 1987.
8. Malliaris., A., "Rollover in Motor Vehicle Accidents," NHTSA-TSC-HS978-1, July, 1989.

9. Mengert, P., Salvatore, S., DiSario,R., and Walter, R., "Statistical Estimation of Rollover Risk," DOT-HAS-807-446, August 1989.
10. Harwin, A., and Emory, L., "The Crash Avoidance Rollover Study: A Database for the Investigation of Single Vehicle Rollover Crashes," NHTSA Internal Report, May 1989.
11. Rosenthal, T. J., et.al., "Users Guide and Program Description for a Tripped Rollover Vehicle Simulation," STI Document 1216-2, Contract DTNH-84-D-17080, June, 1985.
12. Nalecz, A.G., et. al., "Sensitivity Analysis of Vehicle Tripped Rollover Model," NHTSA Report DOT HAS 807 300 July, 1988.
13. Garrott, W. R., and Monk, M. W., "Vehicle Inertial Parameters, Measured Values and Approximations," SAE Paper 881767, November, 1988.
14. Kaleps, I., and Rizer, A., "Simulation of Vehicle Crash and Rollover Dynamics," NHTSA Report DOT HAS 807 049, June, 1986.
15. Obergefell, L. A., et. al., "Prediction of an Occupant's Motion During Rollover Crashes," SAE Paper 861876, 1986.

S6-O-06

Manufacturer's Overview of Rollover Resistance Test Technology

Robert L. LeFevre, Richard E. Rasmussen
General Motors Corporation

Abstract

Rollover accidents are among the most difficult of the major accident categories to analyze through the application of full-scale test procedures. Because of this difficulty, industry and governments worldwide have not reached a consensus on a full-scale test technology to assess a vehicle's ability to resist rollover motion. Additionally, progress in developing test procedures to define rollover resistance has been retarded by the factors of accident complexity and a reluctance to separate maneuver handling issues from those specifically related to the rollover event. The relevance of field accident data to test procedure selection will be described with examples from U.S. experience. Candidate procedures from around the world will be discussed and a set of criteria for judging and comparing the merits of these proposals will be suggested. All procedures represent compromises between the desire to include every contributing factor and a need to distinguish differences in rollover performance. Also, problems associated with validating candidate procedures with field accident data are described.

Introduction

Since the earliest days of the automotive industry, the role of vehicle design in rollover accidents has been intensively investigated as pictured in Figures 1 and 2. Many improvements in body structure, chassis component integrity, tire bead retention, mass distribution, and passenger restraint systems have been introduced as passenger car and light truck designs have evolved. This evolution will continue as light trucks move toward independent front suspensions for all wheel drive configurations. Independent front suspensions will permit lower powertrain components, hence, the lowering of center of gravity heights.

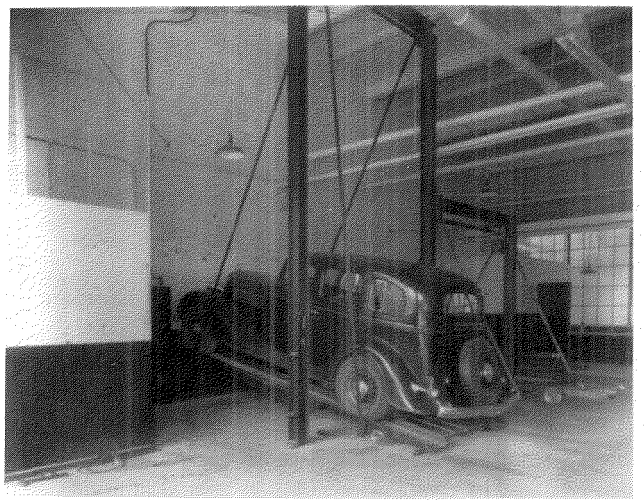

Figure 1. Early Center of Gravity Height Test Facility at the GM Proving Ground

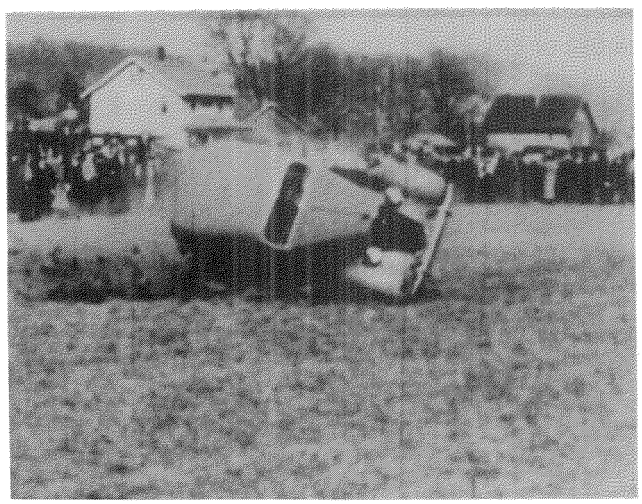

Figure 2. Early Lateral Rollover Test on Level Ground at the GM Proving Ground

However, vehicle design is not the only consideration in rollover accident prevention. Of equal or greater

importance in rollover prevention are design improvements for roadside geometries and barrier systems [1]. Further, statistical analysis of accident data provides a wealth of information on the dominant role of driver impairment and demographics in this special class of accident.

Despite considerable public and private sector attention, significant gaps remain in the technology of full-scale vehicle rollover performance evaluation. There are no objective test procedures that have received worldwide industry and government acceptance for evaluating the ability of a design to resist rollover during a precrash maneuver. In fact, there are nearly as many test proposals as investigations into the subject. Among the factors retarding progress in identifying an agreed upon test procedure are the complexity of the real world event, the difficulty in isolating a vehicle's resistance to rollover from driver and road-environment issues, and the problems associated with drawing appropriate conclusions from trends suggested by the accident data.

This paper provides an evaluation and comparison of candidate rollover resistance test procedures and examines the basic compromises that may be inherent with the available choices.

System Overview

The three-element, closed-loop system illustrated in Figure 3 is essential to every analysis of rollover events. Each element needs to be factored into 1) evaluation of field accident data, 2) assignment of causation responsibility, or 3) comparison of objective test procedures. Totally focusing on one element, excluding the other two, has led to conclusions and recommendations that are misleading. For development of objective test procedures that are intended to define the vehicle's role in the rollover event, it is absolutely necessary to consider the driver and road contributions in order to control or eliminate them.

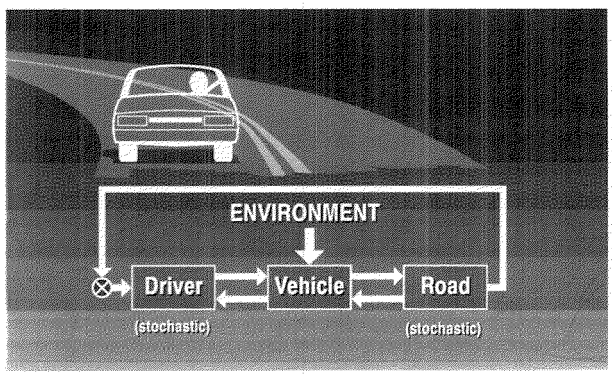

Figure 3. Control System for Rollover Analysis

This three-element, closed-loop system is conceptually simple and has been modeled with a degree of success for many years. However, the properties of the driver and road components as elements of a control system must be viewed as nonlinear, stochastic, and lacking in the important properties of stationarity and ergodicity that are basic assumptions for conventional systems analysis. Few statistical parameters describing the performance of these stochastic control elements are tabulated in the literature and the limited available data show wide ranges: driver control strength has been observed to vary over a range of four-to-one, surprise reaction time can vary by six-to-one, and road friction can vary by ten-to-one with even broader ranges of spectral content in road profiles.

Recent studies of large accident data files are beginning to demonstrate a large degree of interdependence in these three basic system elements. For example, a particular vehicle design is not exposed to a random selection of drivers, nor is it operated in a randomly selected portion of the available road environment. Rollover accident rates evident from field data for particular vehicle designs are not necessarily the result of the design, but are strongly influenced by these driver and road-environment elements. These influences must be used in correlating rollover resistance test results with field accident data.

Test Selection Criteria

Two factors influence industry views on the most appropriate approach to measure rollover resistance of a vehicle design.

- Historically, automotive testing has been comparative in nature. Engineers and decision makers want to know how Vehicle A compares to Vehicle B with confidence and precision, particularly where regulatory compliance margins are involved.
- Accident data show that all vehicles experience rollover regardless of their size and mission.

Therefore, industry is most interested in test procedures which are capable of assigning numbers to product performance with distinguishable resolution and having the broadest possible applicability. At a minimum, a test procedure would be expected to encompass the full range of light duty vehicles. It is recognized that heavy trucks and articulated vehicles often require test procedures which are tailored to their special characteristics and use. Other considerations that influence industry views on test procedures are:

- Field Relevance—The test should comprehend phenomena that contribute to field performance to the greatest extent possible.
- Performance Criteria—The test should produce performance on a continuous rating spectrum, rather than just provide a pass/fail measure.
- Reproducibility—The test should be capable of being run so that different laboratories obtain the same results, particularly in the context of regulations.

- Responsiveness—The test should be relatively short in duration and low in cost to help with the rapid pace of automotive developments.
- Computer Modeling—While virtually all physical systems can be modeled, the resources required to model some situations can exceed those associated with full scale testing of prototypes. These situations need to be avoided where possible.
- Low Risk and Nondestructive—The test should pose minimal risk to the safety of personnel and result in minimal damage to expensive prototype vehicles.

Accident Data Issues

Several levels of government in the United States have compiled a number of extensive accident data files over the past decade. These files vary from special purpose files containing about 1000 reports, to one very large general purpose file with over 6 million reports. The quantity and quality of the information in each of these files varies with the size and intended purpose of the file. As the following paragraphs will explain, it is essential that information in these files be applied to the problem of selecting appropriate rollover resistance test procedures.

Figures 4 and 5 depict rollover accident statistics for passenger cars and light trucks from the National Accident Sampling System (NASS) file which consists of samples of severe accidents that occur on U.S. roadways. Several relevant findings are immediately evident from this most simple array of accident statistics:

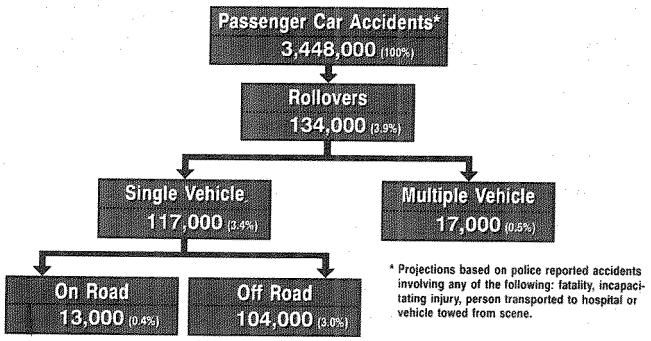

Figure 4. Passenger Car Rollover Projections Based on 1986 NASS Data

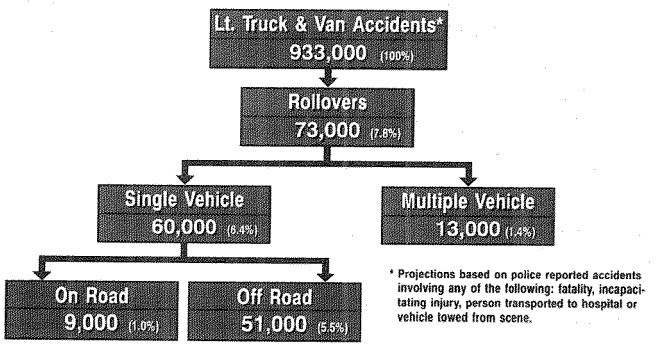

Figure 5. Light Truck/Van Rollover National Projections Based on 1986 NASS Data

- Rollover accidents represent a small portion of the total spectrum of vehicle accidents, even at the relatively high level of severity represented by the NASS file.
- Rollovers on the roadway represent a very small portion of total rollover accidents.
- The most prevalent rollover accident scenarios are off-road and multiple vehicle collisions which are often the most complicated.
- Rollover accidents are a higher portion of all light truck accidents than is the case with passenger cars. It should be noted that this finding may reflect a lower prevalence for other classes of light truck accidents.

In the U.S., there has been considerable publicity and literature about the rollover rates for sport utility vehicles. Figure 6, reproduced from a 1990 NHTSA publication on light truck safety, implies a rapid and unexplained reduction in rollover fatality rates for this class of vehicle for a four year period from 1985 to 1988 [2]. Rollover fatality rates for sport utility vehicles during 1988 were slightly lower than those for small pickup trucks according to this report. It is very unlikely that a 35% reduction in rollover fatality rates over a four year period is related to vehicle design improvements. This trend remains a subject worthy of further investigation.

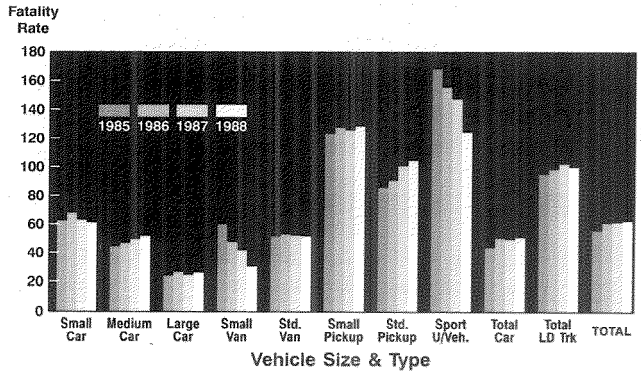

Figure 6. Rollover Fatality Rates, Fatalities per Million Registered Vehicles

The sport utility vehicle situation provides an illustration of the difficulty associated with interpreting rollover accident rate data. Figure 7 is a tabulation of fatal rollover accident rates over an extended period [3]. The 18 vehicle designs studied are a mixture of sporty cars and light duty trucks, with heavy emphasis on vehicles classified as sport utility vehicles. The following observations further exemplify the particular attention that needs to be given when analyzing such data:

- The rollover rates for this group of vehicles vary by a factor of 10.
- Both the lowest and highest rollover rate vehicles are "4 X 4" sport utility vehicles.

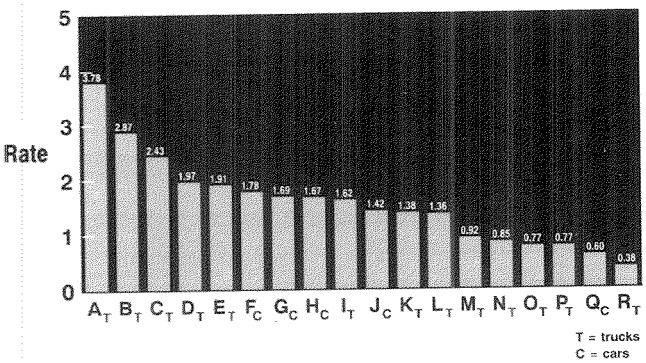

Figure 7. Fatal Rollover Events Per 10,000 Registered Vehicle Years: Single Vehicle Accidents (1984-87 FARS Data)

- One third of the top half of this sample's rollover rates belong to sporty cars, these being the lowest and widest vehicle designs operated on public roads.

The driver factors recorded for the vehicles and accidents of the sample are summarized in Figures 8(a), 8(b), and 8(c) [3]. Driver age demographics varies by a factor of six; alcohol involvement varies by a factor of three; and poor driving records also vary by a factor of three. The low, wide sporty cars consistently make up one third or more of the vehicles in the upper half for each driver category.

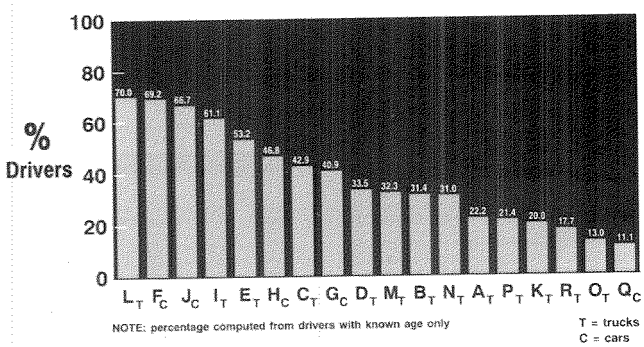

Figure 8(a). Percentage of Drivers Less than 25 Years of Age (1984-87 FARS Data)

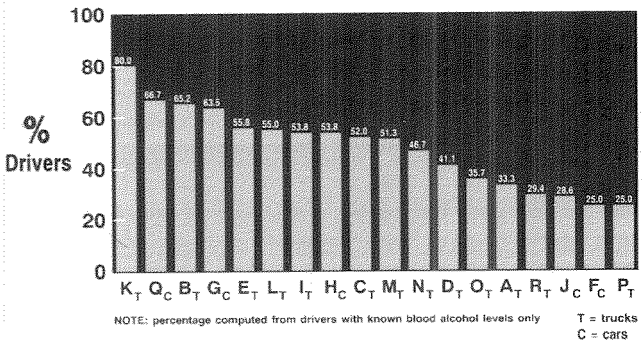

Figure 8(b). Percentage of Drivers With Blood Alcohol Above 0.1% (1984-87 FARS Data)

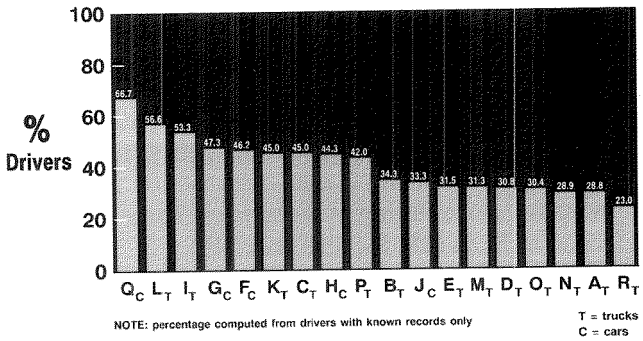

Figure 8(c). Percentage of Drivers With Prior Speeding Conviction (1984-87 FARS Data)

Similar characteristics are evident in available data on environmental factors and rollover. Figure 9 illustrates the range in rollover rates for eastern urban centers as compared to western mountain states in the U.S. [4]. Neglecting the District of Columbia, there is a factor of five in this comparison of rollover rates between states.

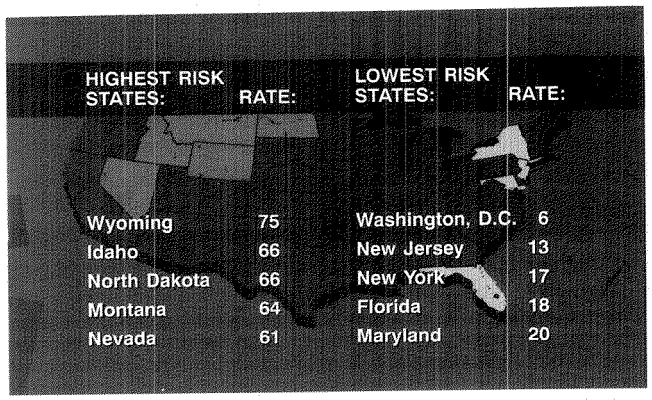

Figure 9. Rollover Rates by Geographic Location

The above few excerpts from the very extensive rollover accident data literature are quoted here as a caution for those who attempt to validate rollover resistance test proposals from raw rollover rates derived from field data. While it may be possible to empirically model the rollover situation from the large body of accident information that has been collected, these few findings demonstrate that causation models must contain a balance of driver, vehicle, and environment factors in order to represent the situation for confident identification and extraction of vehicle factors.

Test Procedure Proposal Categories

Since there are many proposals for test procedures to measure a vehicle's ability to resist rollover, it is appropriate to create categories of these proposals so they can be discussed and compared in an organized manner. The category system used in this paper is as follows:

- Physical Properties Tests—These are laboratory tests intended to measure basic physical properties with a conceptual relationship to rollover resistance.
- Rollover Simulations—These are also laboratory tests intended to estimate, comparatively, the level of maneuver severity that a vehicle can achieve at its threshold of rollover.
- Dynamic Road Tests—This category includes all procedures that involve operation of a vehicle on a roadway. Since many of the procedures that have been publicized are ad hoc evaluations conducted by magazines, these procedures are usually not as specified nor as documented as those conducted by automotive testing organizations. For purposes of this paper, the general problem of dynamic road testing for rollover performance will be discussed without detailed reference to specific procedures.

Physical Properties Tests

Analysts and modelers generally agree that three vehicle properties are fundamental factors in rollover equations of motion: 1) track width, 2) center of gravity height, and 3) roll moment of inertia. There are additional important factors that have not received the attention from investigators inside and outside the transportation industry which are outside the scope of this paper.

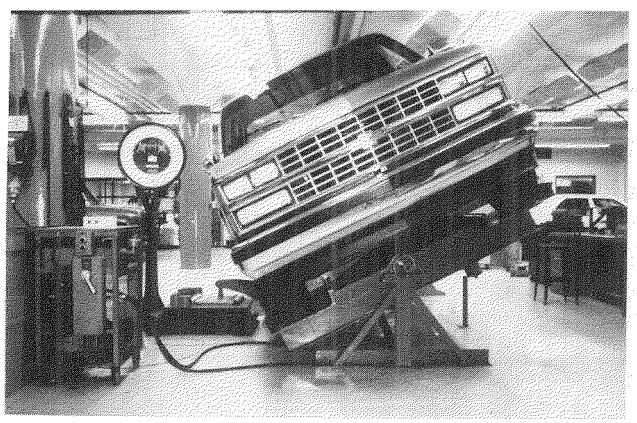

Figure 10. Test Facility Used to Measure Center of Gravity at the GM Proving Ground

Vehicle	Lab A		Lab B		Lab C		Lab D	
	High	Low	High	low	High	Low	High	Low
Vehicle 1	27.94	27.46	27.25	27.19	26.34	26.16	27.05	25.30
Vehicle 2	28.13	27.59	26.52	26.21	25.60	25.48	24.64	23.96
Vehicle 3	26.19	25.63	25.35	25.20	24.94	24.63	26.24	22.51
Buck	25.16	24.91	24.01	23.76	24.26	23.96	25.17	20.69
Average	26.71	26.54	25.72	25.65	25.21	25.13	24.89	24.00

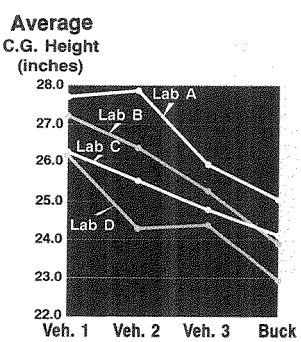

Figure 11. Center of Gravity Measurement by Laboratory

While roll moment of inertia is a physical factor that should relate to a vehicle's ability to resist large transient lateral forces associated with curb impact and soil mechanics, it has received less media attention than c.g. location. Many automotive laboratories have facilities for measurement of whole vehicle moments of inertia because they are fundamental to a variety of dynamic performance modeling activities. A roll moment of inertia test facility is shown in Figure 12. Such facilities are configured so that vehicle inertia magnitude contributes directly to the period of a simple and predictable oscillating system. The period of oscillation, measured with great precision is proportional to the moment of inertia where the c.g. location is known and appropriate mathematical axes compensation has been accomplished. The facility in Figure 12 holds the vehicle on a platform supported by knife edges and springs. Other facilities use air bearing supports or multifilar pendulum systems. Roll moment of inertia, for passenger cars, has been found to be a simple function of vehicle total mass and dimensions [6]. It can often be predicted empirically from these properties with an acceptable degree of precision. Similar formulas for light trucks are not available. The authors are unaware of any investigation to establish repeatability or correlation between industry facilities for inertia measurement. Use of large, simple structures with mass and geometry approaching that of vehicles and inertia properties that are readily calculated can be helpful in validation of inertia test facilities.

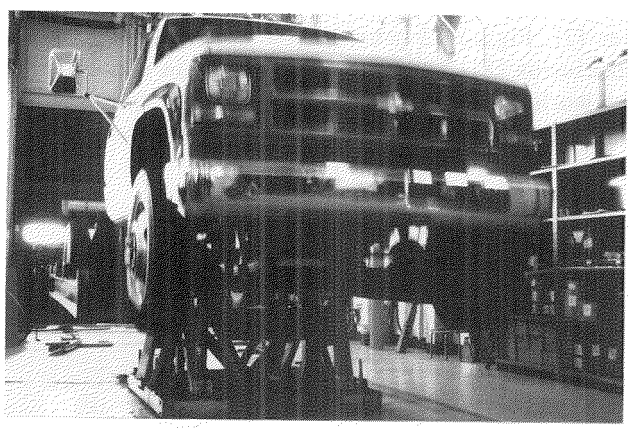

Figure 12. Roll Moment of Inertia Test Facility at the GM Proving Ground

Rollover Simulations

The rollover simulation laboratory tests most often discussed for measurement of rollover resistance use the tilt table and sidepull procedures. Of these, the tilt table test is the most widely used around the world because it accommodates a broad range of vehicles. The tilt table procedure is viewed as simple and modest in cost. Two factors seem to support usage of this test:

- Field data shows that operation on a sideslope to be the most prevalent rollover accident circumstance such as may be the case with earthmovers and heavy trucks.
- A need to evaluate or regulate rollover resistance for the least stable portion of the vehicle population, such as double decker buses, articulated tanker trucks, three-wheeled passenger cars and three-wheeled light commercial vehicles.

Many four-wheeled passenger cars and light trucks initiate rollover only in response to high levels of lateral force. For these vehicles, the tilt table approach may have limitations or lack credibility. Where the lateral force required to initiate rollover begins to approach the weight of the vehicle, very large tilt angles are necessary for wheel lift. For these cases, the vehicle suspension will move to full rebound, the tires will become lightly loaded and difficult to restrain as the angle for wheel lift is approached. Some proponents of the tilt table conduct the test at maximum cargo load to lower the tilt angle required for wheel lift. While this strategy may make the test easier to obtain credible results for passenger-carrying light trucks with large cargo capacities, the influence of cargo may not be sufficient for testing sporty cars and other vehicles with small capacity.

In addition to the above difficulties, the tilt table test procedure also does not comprehend that lateral rollovers are often a result of tripping. Accident investigators in the U.S. have concluded that tripping for a broadsliding vehicle is the most prevalent rollover circumstance encountered in light vehicle accident reconstruction activities [7]. Figure 13 provides statistics that support this conclusion [8]. The road environment in other parts of the world may increase the prevalence of sideslope as a dominant factor in rollover accidents. However, in the U.S. this is not the case.

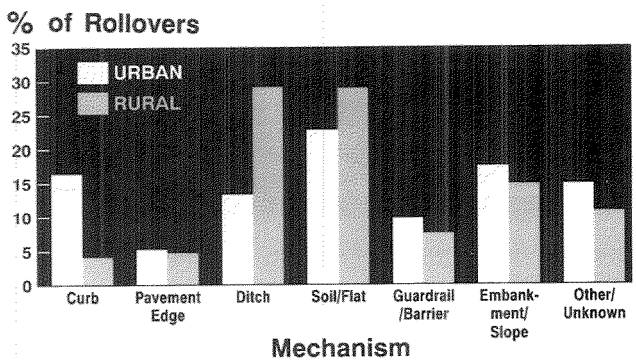

Figure 13. Initiating Mechanism in U.S. Rollover Accidents

Recognizing the limitations of the tilt table test and the long, frustrating and nonproductive experience with dynamic road tests, investigators in the U.S. began to look for a hybrid lab/road test that would combine the advantages of lab testing with the realism of road testing. A cable was used to pull on the side of a moving vehicle to determine the lateral force required for two wheel lift. The cable was mounted from a heavy truck to provide a sufficient and stable reaction for this test. Some test facilities used rail mounted vehicles or tracked vehicles. While the variability in tire-road friction made this approach to rollover resistance testing impractical, investigators noted that lateral force for two wheel lift for a rolling vehicle was virtually identical to levels for a nonrolling vehicle. Subsequent tire testing revealed that tire vertical and lateral spring rates, for these severe conditions, rolling and nonrolling, are very similar while many other tire properties are significantly different. Since tire vertical spring rate and lateral spring rate (more properly termed overturning moment) are among the major tire factors contributing to rollover resistance, this finding suggested that a nonrolling laboratory side-pull test might provide a precise measure of rollover resistance where broadslide related tripping is known to be a most prevalent rollover accident circumstance.

A facility for this purpose is shown in Figure 14. The vehicle is pulled laterally with a measured force that is controlled to be horizontal, oriented at ninety degrees to the plane of symmetry, and arranged to pass through the gravity center location as it moves vertically as a result of the lateral force. This is accomplished with simple closed loop controls that sense center of gravity height, cable angle, and vehicle yaw motion. Rate of increase in the pull force is slow to result in a test that is essentially steady state. Vehicle restraint is assured with a low curb restraint of the tire. Innertubes are used to prevent tire bead unseating and air loss for these extreme conditions. A sling is used for most cars and trucks to spread the pull force and minimize body damage. The test is replicated six times to provide resolution in the range of 0.02 for the sidepull ratio which is the ratio of lateral force at two wheel lift versus vehicle test weight. This would correspond to test resolution of 0.02 G's if this situation could be reproduced with a road maneuver test.

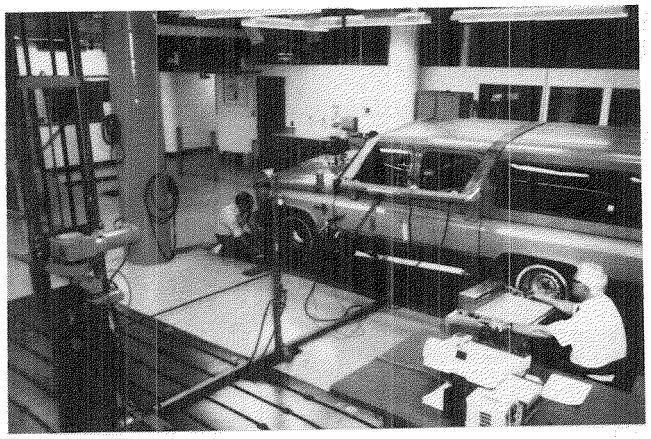

Figure 14. Side Pull Test Facility at the GM Proving Ground

This test has been used for some years on a variety of passenger cars, light trucks, and sport utility trucks.

While vehicles without roof structures require special fixturing and minor body damage is frequent, indications are that the approach has so far been applicable to every light duty vehicle submitted for testing. Only three labs in the U.S. are known to have used this procedure and limited test correlation work has been accomplished at this time. The major problem with lab-to-lab correlation may be associated with c.g. location.

The obvious limitation of the laboratory rollover resistance simulation tests described here is neglect of dynamics. For example, neither the sidepull nor the tilt table test results are influenced by vehicle roll axis moment of inertia. It may be possible to construct a more sophisticated sidepull test device that would provide a controlled pull force at a higher time rate of change, so that inertia would be able to influence the result. One related procedure was reported in early 1990 [9]. In this case, vehicles were pulled laterally over a slippery surface at speeds in the range of 30 mph. The broadsliding vehicles then encountered either a curb or a prepared soil condition intended to produce rollover. The soil situation produced lateral force sufficient for deceleration in the range of 1.5 to 2.0 g, while the curb provided a pulse of force sufficient for deceleration in the range of 10 g. These high forces often produced component collapse. The vehicle lateral acceleration versus time graphs included in the referenced paper show data too noisy to adequately discern differences in rollover resistance of various vehicle designs.

In the U. S., some researchers have been investigating rollover resistance using the ratio of T/2H, where T is the track width and H is the c.g. height. It is possible to compare T/2H with the sidepull ratio and the tangent of the tilt table angle at two wheel lift.

The NHTSA facility at the Vehicle Research and Test Center has run all three test procedures on the same population of 13 cars and trucks [10]. Because of the diversity of the vehicles used, which ranged from a subcompact car to a full-sized passenger van, c.g. height and track width tend to dominate the results. If T/2H, tangent of the tilt table angle, and sidepull ratio are each used as an estimator of the steady state lateral acceleration level that will initiate rollover motion, T/2H provides the highest estimate of lateral acceleration, sidepull the lowest estimate, with the tangent of tilt angle falling between the two. The tests were performed under light load conditions and the order of the estimates could change at higher loads. More experience with the simulation tests is needed to obtain a complete understanding of their relationship to vehicle design factors other than basic height and width.

Dynamic Road Test Issues

Industry efforts to develop a road test for rollover performance began in the early 1 920's and continued into the mid-1 960's. SAE Recommended Practice J857a, Roll-over Tests Without Collision, is an interesting written record of the frustrations experienced in pursuing a controlled and repeatable approach to the testing. Most of this work was probably intended for evaluation of occupant protection, but similar difficulties were encountered by those attempting to develop road tests for rollover resistance. The NHTSA continued to work on rollover resistance road tests in the 1970's after most industry efforts were abandoned for lack of success.

So far, at least two problems have remained unresolved despite these efforts:

- Ability to precisely define the severity of a road maneuver that results in rollover, or out-rigger contact, so that vehicles can be compared in terms of their resistance to maneuver severity. The "Drastic Steer and Brake Test" investigated by NHTSA used a very transient steering input that often resulted in high levels of vehicle vibration and noisy measures of motion severity.
- Ability to control the contribution of the tire-road interface to the rollover event.

The tire-road interface situation is demonstrated by Figure 15 derived from industry studies of tire braking traction [11]. In this case, the peak tire braking traction was measured with a traction reference tire on a number of dry road surfaces used for testing at different industry proving ground facilities. These road surfaces did not include anything that would be judged artificial or polished to produce peculiar performance. Plotted for comparison is the range of sidepull test data for a population of vans and sport utility vehicles. The point of this comparison is that the variability in the lateral acceleration which can be developed on various roads is almost as large as the range of rollover resistance performance that would be observed in a population of light trucks. Assuming that sidepull ratio is a true measure of rollover resistance and the peak traction data a true measure of the ability of the road friction to create lateral rollover force, nearly all of the population of vehicles could, theoretically, be shown to rollover on the highest friction surface, while 11 of the 13 would not rollover on the lowest friction surface. If the band of uncertainty associated with resolution of maneuver severity (the order of 0.2 G) is added to the uncertainty associated with road friction, the result is a test process uncertainty as broad as the range of performance for the population of vehicles to be compared. Although the problem of obtaining repeatable driver control inputs was solved in one experiment with a sophisticated steering, braking, and accelerating robot controller, investigators found that the control inputs required for the most severe lateral motion was a function of the vehicle design to a major degree.

Recent proponents of driver-controlled, path-constrained, task-performance road tests for rollover resistance have asserted that such tests can be relied upon. The proponents have suggested that outrigger

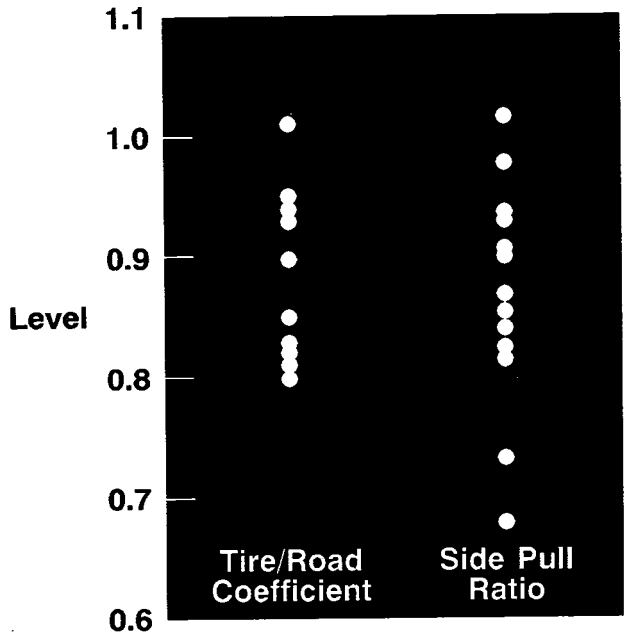

Figure 15. Comparison of the Range of Tire/Road Friction and Rollover Potential as Evidenced by Side Pull Ratio for 10 Roads and 13 Vehicles

contact for any severe maneuver on an arbitrary flat road should be viewed as indicative of a vehicle deficiency, and lack of contact is judged as proof of adequacy. This strategy is seriously flawed because certain classes of vehicles cannot pass such a test. In addition to the problems with control of road friction and driver inputs, this simplistic approach ignores the large population of cargo carriers and bus type vehicles that are unlikely to meet this standard when loaded to design intent even though their "real world" performance is judged acceptable. When judged using the metrics of T/2H, tilt table, or probably sidepull, many of these vehicles will show less than half the resistance to rollover of sport utility vehicles.

Summary

The motor vehicle industry has had a long term interest in evaluating rollover resistance of its products. While progress on rollover procedures has been limited, success has been realized in developing consensus test procedures for the more prevalent front and rear collisions and for assessing the maneuver properties associated with braking, steering and acceleration. The various candidate procedures for rollover resistance testing represent compromises among the desires for face validity and effectiveness versus the practical considerations of complexity, repeatability, reproducibility and resolution capability. In many ways, compromise issues have been successfully resolved for other collisioh scenarios to the benefit of both users and manufacturers. The compromise process for rollover needs further effort to meet both domestic and international needs. Meaningful progress in reducing rollover events will require a better understanding of the technical facts and tradeoffs, plus a commitment to an objective treatment of the influences of the driver and environment as well as the vehicle. Hopefully, the discussion of these issues within this paper has contributed to this process.

References

(1) Stonex, K. A. *Roadside Design for Safety,* Highway Research Board Proceedings, Volume 39, 1960.

(2) *Safety Programs for Light Trucks and Sport Utility Vehicles,* 1990, U.S. Department of Transportation, National Highway Traffic Safety Administration.

(3) Suzuki Submission to NHTSA, 1990.

(4) Data Link, Inc., *Rollover in Motor Vehicle Accidents,* Final Draft Report, August 1988. An Investigation Conducted for the Office of Crash Avoidance Research, NHTSA.

(5) Winkler, C. and Campbell, K. *Center of Gravity Height: A Round-Robin Measurement Program,* Technical Report to The Motor Vehicle Manufacturers Association, January, 1991.

(6) Riede, P.M, Cobb, W. A., and Leffert, R. L., *Typical Vehicle Parameters for Dynamics Studies—Revised for the 1980's,* SAE Preprint 840561, February, 1984.

(7) Orlowski, K.R., Moffatt, E.A., Bundorf, R.T., and Holcomb, M.P., *Reconstruction of Rollover Collisions,* SAE Preprint 890857, 1989.

(8) Harwin, E. A. and Emery, L., *The Crash Avoidance Rollover Study: A Database for the Investigation of Single Vehicle Rollover Crashes,* National Highway Traffic Safety Administration, May, 1989.

(9) Cooperrider, N. K., Thomas, T. M., and Selim, A. H., *Testing and Analysis of Vehicle Rollover Behavior,* SAE Preprint 900366, February, 1990.

(10) Chrstos, J. P., *An Evaluation of Static Rollover Propensity Measures,* National Highway Traffic Safety Administration, May, 1991.

(11) Ebert, N. E., *SAE Tire Braking Traction Survey: A Comparison of Public Highways and Test Surfaces.* SAE Preprint 890638, February, 1989.

S6-O-08

The Urban Rollover: Characteristics, Injuries, Seat-Belts and Ejection

G.M. Mackay, S. Parkin, A.P. Morris, R.N. Brown
Accident Research Unit,
University of Birmingham

Abstract

This paper presents an analysis of rollover crash characteristics and the injury consequences for occupants. 158 rollover cases are analyzed involving 282 occupants. Comparisons are made, where appropriate, between this study and previous studies conducted in the 1970's. The study found that generally, the urban rollover is not a dramatic crash. Injury severity was found to be low to both restrained and unrestrained occupants, but ejectees were more likely to be fatally injured than non-ejectees. That however does not imply a causal relationship between ejection and the specific mechanism of injury. Roof crush was not found to be responsible for injury causation and therefore no recommendations for changes in current roof strength are made. This sample may under represent high velocity crashes as the study was conducted in an urban environment, a view supported by the fact that only 20% of vehicles rolled more than one revolution.

Introduction

A rollover accident, defined here as at least 90 degrees of vehicular rotation about any horizontal axis (after Huelke et al, 1972 (1)) can on occasion, be one of the more life threatening types of crashes. This is due to the unbelted occupant being exposed to high energy, specific interior contacts or ejection from the vehicle which, Huelke et al, 1977 (2) claim, is consistently more life threatening than containment. Secondly, during such crashes, the non-ejected occupant is exposed to a greater risk of serious injuries to the head, neck and spine when the vehicle is upside down due to the rapidly changing nature of several force vectors applied over a very short period of time (Huelke et al, 1972.

Previous studies have suggested some consistency in the incidence of rollover accidents (in which injuries occur) in relation to the general accident pattern. Mackay and Tampen, 1970 (3) found that rollovers account for 8% of such collisions in the UK, while Mackay, 1981 (4) reviewing sample studies in Europe showed that rollover accidents constituted 8-12% of all accidents. In addition, the Fatal Accident Reporting System, 1985 (5) shows that 9% of American car crashes are rollovers.

Methodology

This study examined 158 vehicles containing 282 occupants involved in rollover accidents in and around the West Midlands conurbation. All vehicles were examined retrospectively and medical data were obtained from local hospitals. Additionally, the occupants themselves were interviewed by questionnaire. Mackay et al, 1985 (5) give a more comprehensive outline of the methodology of this ongoing Occupant Injury Study.

Accident Types

Table 1 shows the numbers of vehicles involved in rollover events. Of the accidents in which the number of vehicles involved was positively identified, 73.5% involved only one vehicle.

Table 1. Number of Vehicles per Accident

Vehicles in accident	Number	Percentage of Total (%)	Percentage of knowns (%)
Single vehicle	111	70.3	73.5
Two+ vehicles	40	25.3	26.5
Not known	7	4.4	-
Total	158	100.0	100.0

Huelke et al, 1972 (1) found that in a sample of 253 rollover accidents, 79% were single vehicle, and Mackay and Tampen, 1970 (3) found in their sample of 89 rollover accidents, 70% were single vehicle.

Occupant Age and Sex

The age and sex distribution of the occupants is shown in Table 2.

Table 2. Age and Sex Distribution of the Occupants

Sex / Age	MALE n	MALE %	FEMALE n	FEMALE %	TOTAL n	TOTAL %
0-10	3	1.7	2	2.9	5	2.0
11-15	5	2.9	5	7.1	10	4.1
16-20	54	30.9	13	18.6	67	27.3
21-25	41	23.4	18	25.7	59	24.1
26-30	20	11.4	11	15.7	31	12.7
31-40	23	13.1	9	12.9	32	13.1
41-50	11	6.3	3	4.3	14	5.7
51+	18	10.3	9	12.9	27	11.0
Total *	175	100.0	70	100	245	100.0
Not known	29	87.9	4	12.1	33	100.0
Total	204	73.4	74	26.6	278	100.0

* This total includes known values only
(4 occupants, sex not known)

73.4% of the occupants were male, compared with 65.5% male occupancy for all accident types (the latter figure taken from the entire Birmingham database, from which the rollovers were selected for this study). Of the sample where the age and sex is known 38.8% are males in the age range 16-25 (compared with 18.7% for all accident types). Clearly, males in this age range are heavily over-represented in rollover accidents, there being twice as many involved in rollovers than the figure for all accident types. If the age range 16-25, for both male and female, is omitted out of the totals, males still constitute 71.7% of the total remaining, showing that

males in general are more often involved in rollover accidents. 34.8% of the vehicles in the sample contained at least one male in the age range 16-25. On average there were 1.8 occupants per vehicle in the sample. The occupancy for a vehicle that had at least one male in age range 16-25 rose to 2.5, leaving the occupancy in the remaining vehicles at 1.4. Females constituted 26.6% of the whole sample, but only 12.6% of the sample of occupants that were in vehicles that had at least one male in the age range 16-25, leaving the female occupancy of the remaining vehicles at 39.8%.

Restraint Use

Table 3 shows restraint use for the occupants in the sample. Restraint use for front seat occupants was 89.9%, which is comparable to observed national restraint use in general (variously observed at 85-95% in 1990).

Table 3. Restraint Use by Seating Position

Seat position / Restraint use	FRONT n	FRONT %	REAR n	REAR %	TOTAL n	TOTAL %
Restrained	142	89.9	1	2.1	143	69.4
Unrestrained	16	10.1	47	98.9	63	30.6
Total *	158	100.0	48	100.0	206	100.0
Not known	71	93.4	5	6.6	76	100.0
Total	229	81.2	53	18.8	282	100.0

* This total includes known values only

Number of Rolls

The number of rolls experienced by the vehicles in the sample is shown in Figure 1, in quarter turns. There were additionally 47 cases in which the number of rolls could not be established, an inherent feature of a retrospective study. It was also not possible to establish how many of the known sample had vaulted, but Mackay and Tampen, 1970 (3) and Hight et al, 1972 (7) both showed that this occurs in only about 5% of rollovers and it was therefore considered that the results would not be unduly affected. Figure 1 shows that after the first quarter turn, vehicles do not tend to stay on their sides, but topple over onto either the roof or wheels, this being the more stable condition. The majority, (63%), of the vehicles that rolled over experienced a maximum of half a revolution. There is a very rapid, almost exponential, decrease in the number of rolls. In 20% of the known sample the vehicle rolled more than 1 revolution. 6% rolled more than 2 revolutions, and only 3% rolled 3 revolutions or more.

In contrast Mackay and Tampen, 1970 (3) found that only 7% of their sample rolled more than 1 revolution. This may partly be due to the change of design of vehicles used in the UK in the past 20 years. Hight et al, 1972 (7) found that 30% of their sample rolled more than 1 revolution, possibly illustrating the difference between American vehicles involved in mainly rural rollovers, versus UK vehicles involved in urban rollovers. The high level of restraint use in the current

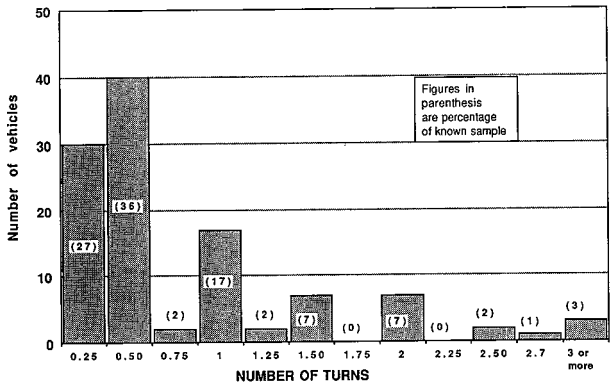

Figure 1. Number of Rolls

study, however, undoubtedly requires a more severe event to occur in order for a case to get into the sample.

Final Resting Position

Figure 2 shows the final resting positions of the vehicles in this study (Birmingham 1991), and these results are compared to Mackay and Tampen's, 1970 (3) earlier Birmingham work, Hight et al, 1972 (7) rural US work, and Huelke et al, 1972 (1) larger US sample.

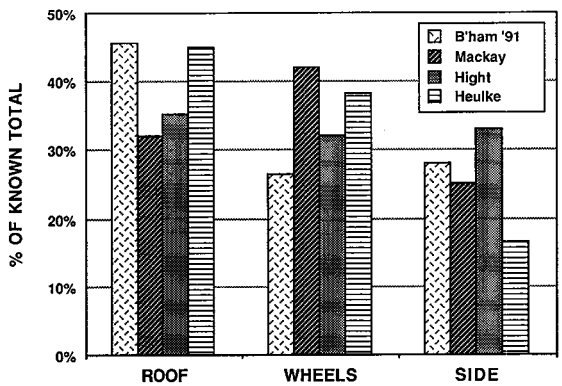

Figure 2. Final Resting Positions

(Mackay and Tampen's results include the rollovers that experienced no more than 1 revolution, being 93% of their sample. Hight et al's results include the rollovers that experienced no more than 2 revolutions, being 94% of their sample).

Of the vehicles that had a final resting position on their sides there were no differences between the results found in this study, and Mackay and Tampen's earlier work, both being at about a quarter of the known sample. Both studies also found that of the vehicles that had a final resting position on their sides, about 3/4 experienced only 1/4 of a revolution. In contrast, Hight et al's mainly rural US study found that 1/3 of the vehicles had a final resting position on their side, of which only 36.5% rolled only 1/4 of a revolution (half the frequency found in the Birmingham studies). Huelke et al found in

their larger US sample that in only 16.5% of the known sample did the vehicle have a final resting position on the side, with no mention made of the number of turns.

Impact Types

Table 4 shows the types of accident in which the rollovers occurred. In 27% of the known cases the vehicles suffered no, or no major impact before or after the rollover. This is very different to the results observed by Mackay and Tampen, 1970 (3) in which the figure was 55%.

Table 4. Impacts Before and/or After Rollover

Impact type		Number of vehicles	Percentage of knowns(%)
None, or no major impact before or after rollover	Pure	14	9.2
	Tripped	13	8.5
	Off-road	14	9.2
Rollover after impact		85	55.6
Rollover before impact		12	7.8
Impact before and after rollover		15	9.8
Total		153	100
Not known		5	-

In 65.4% of the known cases the vehicles did suffer a major impact previous to the rollover (compared with 35%, Mackay and Tampen). These results are clearly a feature of the urban environment.

First Object Struck

Table 5 shows the first objects struck that initiated a rollover. 33.5% of the vehicles suffered no major impact before the rollover. This is significantly less than Mackay and Tampen found (55.1%). This study found that of the objects struck that initiated a rollover, 34.7% were other cars or light vans, and 6.1% were heavy commercial vehicles. These are considerably lower frequencies than were found by Mackay and Tampen, the figures being 55% and 12.5% respectively. Mackay and Tampen found that trees and posts represented 22.5% of the primary impacts in their study, whereas the same objects comprise 40.9% of the primary impacts in this study.

Table 5. First Objects Struck

Object struck	Number of vehicles	Percentage of known struck objects(%)
Other car or light van	34	34.7
Heavy commercial vehicle	6	6.1
Post	27	27.6
Tree	13	13.3
Other road furniture	3	3.1
Wall or fence	15	15.3
Not known	7	-
None, or no major impact	53	-
Total	158	100.1

Of the 53 cases in which there was none, or no major impact before the rollover, about a third were pure rolls, a third were due to running off-road, and a third were due to some tripping mechanism. The curb represented over two thirds of the objects that tripped the vehicles.

Door Performance

Table 6 gives details of door performance. In only 37.3% of cases did all the doors function correctly, post-crash. At least one door jammed in 46.8% of the vehicles, and at least one door opened in 15.8% of the vehicles. In no instances did a door open and another become jammed. Door jamming may be a concern when a vehicle also incurs a fire. This problem did not occur in this study, with less than 1% of the rollover vehicles subsequently igniting (one case).

Table 6. Door Performance

Door state	Number of vehicles	Percentage of total (%)
Doors function correctly	59	37.3
Door(s) jamming	74	46.8
Door(s) opening	25	15.8
Doors opening and jamming	0	0
Total	158	99.9

Door opening, in contrast, is of interest as the chances of occupant ejection are exacerbated as a result. The injury consequences of ejection are discussed later in the paper.

Windscreen Performance

There are two general methods for fixing windscreen into cars. The traditional method is that of a rubber gasket between the windscreen aperture and the glass. The other technique is for the windscreen to be bonded, or glued, directly to the aperture. Of the 158 vehicles in this study, 129 (81.6%) had a windscreen fixed with a gasket. The remainder, 29 (18.4%) were bonded. Table 7 and Figure 3 show the performance of the two types of fixing.

Table 7. Windscreen Fixing Performance

State / Fixing type	Fully intact	Part separated	Fully separated	Total	%
Gasket	26	23	80	129	81.6
Bonded	11	12	6	29	18.4
Total	37	35	86	158	100.0
%	23.4	22.2	54.4	-	100.0

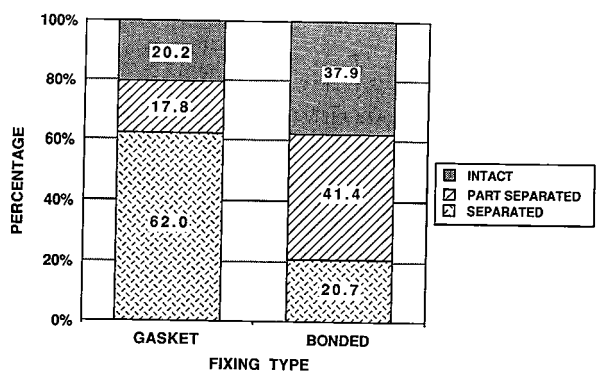

Figure 3. Windscreen Fixings Performance

In over half of the rollovers the windscreen became fully separated from its fixing. In addition to this, 20% of the windscreen were made from toughened glass, which when broken also leaves a large aperture. Therefore, in over 60% of the vehicles involved in this study there was a large aperture in front of the front seat occupants, available for possible ejection.

Seat Belts and Ejection

The effectiveness of seat belts in all types of accidents has been well documented. Huelke et al, 1977 (2) noted that belt use reduced fatal and serious injuries by 20-50%.

Huelke et al, 1973 (8) found that 30% of non-restrained occupants were ejected during rollover collisions compared to 0% of restrained occupants. Of ejected front seat occupants, 52% received critical to fatal (AIS 5-6) (AIS as defined by Marsh, 1972 (9)) injuries compared to 8% of non-ejected occupants. By comparison, Hight et al, 1972 (7) found that 20% of unrestrained occupants were ejected compared to 0.4% of restrained occupants. Their study found that 52.2% of occupants received critical to fatal (MAIS 5-6+) (AIS as defined by States, 1969 (10)) as a result of either total or partial ejection compared to 2% of non-ejected occupants. However, it does not follow that the specific causes of the injuries were contacts occurring outside the vehicle. It may well be that the process of ejection is an indicator of a severe collision and the actual specific mechanism of the injury may be a contact within the vehicle prior to ejection taking place. Both ejection and severe injury may be the outcome of a high energy rollover, they are not necessarily related causally.

Tables 8, 9 and 10 show the results of the current study. A significantly greater proportion of unrestrained occupants were ejected either partly or totally from vehicles in rollover accidents ($X^2 = 27.61$, $P < 0.01$). A significant number were more likely to be fatally injured than occupants who were contained within the vehicle ($X^2 = 55.59$, $P < 0.01$). This finding is supported by data in table 10. Table 10 shows that 47% of occupants are likely to receive MAIS 5-6 injuries when they are ejected (wholly or partially) compared to 2.3% of contained occupants and again this is a statistically significant relationship ($X^2 = 65.54$, $P < 0.01$). This study compares similarly with both the study by Hight et al, 1972 (7) and Huelke et al, 1973 (8). However, none of these studies, including the present one, have a good independent variable for assessing the severity of a rollover. Until such a parameter is available, and numbers of rolls, roll distance and roof deformation have all been proposed, but have not proved to be satisfactory, it is not possible to isolate the specific part played by the ejection process. It is of interest that there were three cases of restrained occupants being ejected.

Table 8. Restraints Versus Ejection

Ejection	Restrained	Unrestrained	Total
YES	3 (13.2)	16 (5.8)	19
NO	140 (129.8)	47 (57.2)	187
Total	143	63	206 *

$\chi 2 = 27.61$ With Yates' correction factor
$P < 0.01$
* Restraint use not known has been ignored
Numbers in parentheses represent expected values

Table 9. Fatalities Versus Ejection

Ejection	Fatal	Non-fatal	Total
YES	10 (1.4)	9 (17.6)	19
NO	11 (19.6)	252 (243.4)	263
Total	21	261	282

$\chi 2 = 55.59$ With Yates' correction factor
$P < 0.01$
Numbers in parentheses represent expected values

Table 10. MAIS Score Versus Ejection

Ejection	MAIS 0-4*	MAIS 5-6*	Total
YES	10 (17.7)	9 (1.0)	19
NO	253 (241.5)	6 (13.8)	259
Total	263	15	282

$\chi 2 = 65.54$ With Yates' Correction Factor
$P < 0.01$
* As defined by the Abbreviated Injury Scale, 1985 revision
Numbers in parentheses represent expected values

Head and Neck Injuries, Restraints and Ejection

Table 11 represents combined head and neck injury rates for restrained and unrestrained ejectees and non-ejectees. There is a significantly greater chance of experiencing higher level head and neck injuries (AIS 3-6) by unrestrained ejected occupants compared to non-ejected restrained occupants ($X^2 = 26.04$, $P < 0.02$). It is of interest that the incidence of AIS 3-6 injuries to the head and neck for unrestrained unejected occupants at 13% is only slightly greater than for the restrained unejected group at 10%.

Table 11. Head and Neck AIS Versus Ejection and Restraint Use

Ejection (restraint use)	AIS 1-2	AIS 3-6	Total
Ejected (unrestrained)	5 (11.7)	9 (2.3)	14
Non-ejected (unrestrained)	27 (25.9)	4 (5.1)	31
Non-ejected (restrained)	79 (73.4)	9 (14.6)	88
Total	111	22	133

$\chi 2 = 26.04$
$P < 0.02$
Numbers in parentheses represent expected values

Roof Crush

There appears to be little to support the view that roof crush is *directly* related to occupant injury severity in rollover accidents. Automobiles, especially after rolling

more than one revolution, often sustain a certain amount of roof displacement. Huelke et al, 1972 (1), using data from the Highway Safety Research Institute (HSRI) noted a weak but consistent association between roof crush and injury severity as measured by the Abbreviated Injury Scale (AIS as defined by Marsh, 1972 (9)). They suggested a strong association with injury when there was an extreme case of roof crush, i.e, in order of 25 inches or more. However, the authors suggested that otherwise the relationship was more tenuous ("It is only when the roof is crushed downwards more than two feet, thereby obliterating the compartment space—found only in severe crashes—that the average injury level reaches the 'serious' category"). The authors concluded that other than suggesting an association between roof crush and injury severity, roof crush is merely an indication of accident severity and that injury severity increases with accident severity. Huelke's initial view was supported by a later study (Huelke and Compton, 1983 (11)) which looked at rollover injuries in the National Crash Severity Study. They found that only 15% of serious to maximum (AIS 3-6) injuries in rollovers were attributable to direct contact with the roof or other structures at the top of the car.

Plastiras et al, 1985 (12) analyzed the relationship between roof crush and injury risk. They examined twelve sub-compact cars of model years 1974-1978 and computed injury rates per 100 rollovers. They found no significant linear correlation between crush and injury rate and thus concluded that "there is no apparent relationship between roof crush as measured by the roof crush test specified in FMVSS 216 and occupant protection as measured by injury rates reported in the Washington State Accident Database."

In our study, a comparison was made between roof crush and MAIS. Occupants who had MAIS-0 scores or where the MAIS score was not known were excluded from this study as were occupants in vehicles which did not suffer roof crush or where the roof crush was not known. Table 12 gives the results of the study. This table was used to perform a Chi-square analysis (Table 13). From the available data, it would appear that roof intrusion and injury severity are not causally related.

Table 12. MAIS Versus Roof Intrusion

MAIS / Intrusion(cm)	1	2	3	4	5	6
1-5	9	9	0	1	1	0
6-10	12	3	2	0	0	0
11-15	11	4	2	0	0	0
16-20	5	1	3	0	0	0
21-25	4	1	0	0	0	0
26-30	3	1	0	0	0	0
31-35	5	0	1	0	0	0
36-50	1	3	1	0	0	1
50+	1	0	3	0	0	0

Table 13. MAIS Versus Roof Intrusion

Roof intrusion	MAIS 1-2	MAIS 3-6	Total
1-15cm	45 (42.0)	6 (9.0)	51
>15 cm	25 (28.0)	9 (6.0)	34
Total	70	15	85

χ^2 =2.36 With Yates' correction factor
P is not significant
Numbers in parentheses represent expected values

Occupant Injuries

Table 14 gives details of 82 restrained drivers and their injuries. Only these occupants were considered in this section in order that a direct comparison can be made with the findings made by Mackay and Tampen, 1970 (3) which examined predominantly unrestrained occupants who were seated in the front.

Table 14. Injuries Received by 82 Restrained Drivers

MAIS / Region	1	2	3	4	5	6	Total n	Total %
Head	42	13	8	0	0	1	64	30
Neck	18	4	1	0	1	1	25	12
Chest	21	2	6	2	2	0	33	16
Abdomen	9	0	0	0	1	0	10	5
Upper limbs	35	6	4	0	0	0	45	21
Lower limbs	28	2	5	0	0	0	35	16
Total	153(72%)	27(12%)	24(11%)	2(1%)	4(2%)	2(1%)	212	100

Notable comparisons can be made in Figure 4. 96% of unrestrained drivers in the Mackay and Tampen study suffered head and face injuries compared to 78% of restrained drivers in the current study which suggests that restraints serve a purpose for preventing head contacts with the steering wheel, roof, 'B' pillar and side glass.

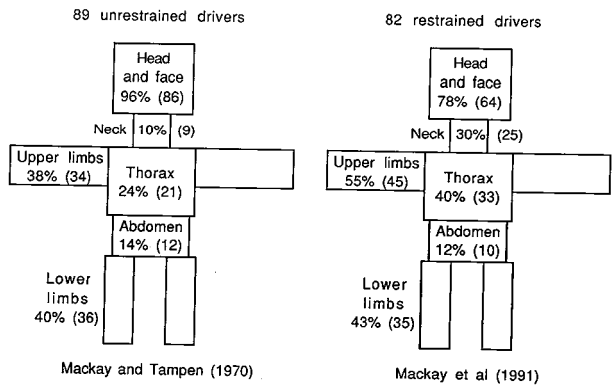

Figure 4. Distribution of Injuries

Neck injuries in the current study were found to have increased from 10% to 30%. This could be explained by an increase on soft tissue neck injuries.commonly sustained by correctly restrained occupants and this view is supported by the fact that 72% of neck injuries are in the AIS-1 category. Both upper limb and thoracic injuries show moderate increases. 72% of thoracic and

upper limb injuries are AIS-1. It is therefore suggested that the moderate, relative increase in thoracic and upper limb injuries are explained by the effects of wearing seat belts.

Table 15 gives details of all occupant injury scores regardless of both seating position and restraint use. These scores are represented in Figure 5. What is immediately clear from the table is that slight injuries (AIS 1-2) are far more likely to occur than serious to life threatening (AIS 3-6) injuries (85%-15%). Such data may suggest that rollover accidents are not as potentially life threatening as has been previously thought. However, it is reiterated that accidents in this study are urban in nature and therefore perhaps do not contain a more representative proportion of violent crashes of this type. A follow up study could take this into consideration.

Table 15. Occupant Injury to All Occupants

MAIS / Region	1	2	3	4	5	6	Total
Head	95	37	12	1	4	4	153
Neck	51	8	3	0	1	3	66
Chest	41	10	10	6	6	2	75
Abdomen	14	2	1	3	7	0	27
Upper limbs	95	28	6	0	0	0	129
Lower limbs	78	11	11	0	0	0	100
Total	374	96	43	10	18	9	550

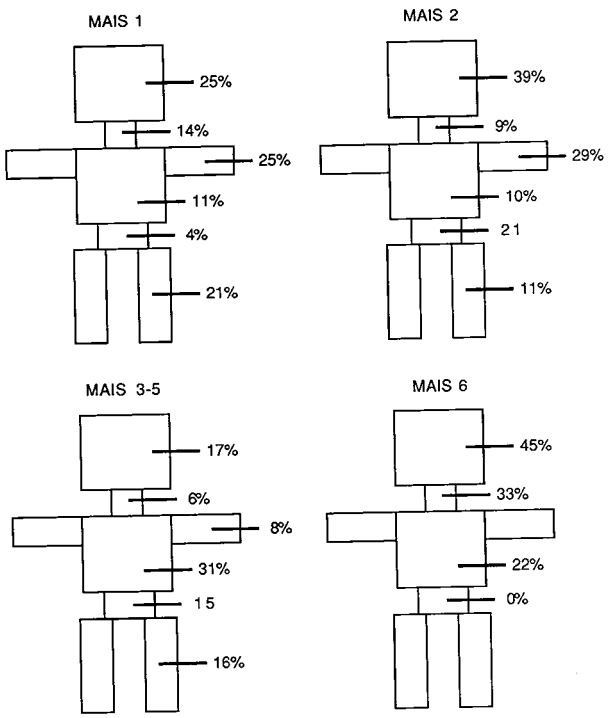

Figure 5. Distribution of MAIS Scores

Summary and Recommendations

This paper presents analyses of rollover crash characteristics and injury consequences for occupants. From the study, the following conclusions can be drawn:

- Males in the age-range 16-25 are over represented in the sample used for this study.
- Modern vehicles tend to roll one revolution or less in an urban environment. The majority experience a maximum of half a revolution.
- In known cases, 27% of vehicles suffered no major impact before or after the roll; in 65.4% of known cases, vehicles did suffer a major impact prior to rolling.
- At least one door jammed in 46.8% of vehicles and at least one door opened in 15.8% of vehicles.
- In over 60% of cases, windscreen separation or breakage provided a possible forward ejection route.
- A significantly greater proportion of unrestrained occupants were ejected (wholly or partially) than correctly restrained occupants. Ejectees are more likely to be fatally injured than non-ejectees.
- Unrestrained ejectees are more likely to receive high level head and neck injuries than restrained non-ejectees. Such injuries however may well occur prior to the ejection process. Non-ejected restrained occupants are more likely to suffer lower level (AIS 1-2) injuries than higher level (AIS 3-6) injuries.
- Roof crush in this study did not relate to injury severity.
- Restraint use may serve a purpose for preventing head contacts with steering wheel, roof, B-Pillar and side glass, but may result in relatively more minor injuries to upper limb and thoracic areas.
- 85% of injuries in this study are AIS 1-2 compared to 15% AIS 3-6.

In summary, the urban roll-over is not a dramatic crash and overall injury severity is low to both restrained and unrestrained occupants. The use of seat belts is advised, but seat belts themselves are not necessarily effective in the reduction of minor injuries and indeed injuries may be sustained through their use.

Roof crush is not a factor in determining injury severity. Rather, injury severity is an outcome of accident severity and restraint use. This suggests that roof strength regulations are adequate; indeed increased roof strength may raise the centre of gravity of the vehicle, reduce visibility and effect a reduction in the absorption of crash energy.

It should be remembered that the accidents in this study are urban in nature and therefore violent rollover accidents may be under-represented in the sample. Future research should consider rural data so that a comprehensive overview can be attained.

Acknowledgements

We are grateful to all members of the Co-operative Crash Injury Study and also acknowledge the help of the sponsors; the Transport and Road Research Laboratory of the Department of Transport, Ford Motor Company, Rover Group and Nissan (UK) Limited.

References

1. Huelke, D. F. et al; "Analysis of rollover factors and injury causation;" pp. 62-79, Proceedings of sixteenth conference of the American Association for Automotive Medicine, 1972.
2. Huelke, D. F. et al; "Injuries, restraints and vehicle factors in rollover car crashes;" pp. 93-107, Accident Analysis and Prevention, Vol 9, 1977.
3. Mackay, G. M. and I. D. Tampen; "Field studies of rollover performance;" pp. 969-977, 1970 International automobile safety conference compendium. SAE paper 700417.
4. Mackay, G. N. "Seat belts in Europe—their use and performance in collisions;" International symposium on occupant restraint, 1981.
5. National Highway Traffic Safety Administration; "Belt laws in 8 states in 1985 saved 200 to 300 lives;" Fatal Accident Reporting System, 1985.
6. Mackay, G. M. et al; "The methodology of in-depth studies of car crashes in Britain;" pp. 365-390, Field accidents, data collection, analysis, methodologies, and car crash injury reconstructions. SAE Technical Paper Series 850556, 1985.
7. Hight, P. V. et al; "Injury mechanisms in rollover collisions;" pp. 204-227, Sixteenth Stapp Car Crash Conference, 1972. SAE paper 720966.
8. Huelke, H. F. et al; "Injury causation in rollover accidents;" pp. 87-115. Proceedings of seventeenth conference of the American Association for Automotive Medicine, 1973.
9. Marsh, J. C. "Existing traffic accident injury causation data recording methods and the proposal of an accident injury classification scheme;" pp. 44-61, Proceedings of sixteenth conference of the American Association for Automotive Medicine, 1972.
10. States, J. D. "The Abbreviated and the Comprehensive Research Injury Scales;" SAE Transactions Vol.78 (1969) paper 690810.
11. Huelke, D. F. and Compton C. P. "Injury frequency and severity in rollover car crashes as related to occupant ejection contacts and roof damage—an analysis of National Crash Severity Study Data;" pp. 395-401, Accident Analysis and Prevention, Volume 15, 1983.
12. Plastiras, K. P. et al; "An examination of the correlation between vehicle performance in FMVSS 216 versus injury rates in rollover accidents;" SAE paper 850335, 1985.

S6-O-10

Study on Passenger Car Rollover Simulation

Toshiaki Sakurai, Yoshiharu Takigawa, Hitoshi Ikeno
Mitsubishi Motors Co., Ltd.

Abstract

This paper describes belted dummy injury and roof deformation in rollovers, based on analyzation of field accident investigations results. In the rate of rollover events to the amount of passenger car traffic accidents, occupants' physical injury, and roof crash are studied from analyzing the database originally investigated by the Ministry of Transport in Japan. The ramp roll-over tests based on SAE J857, are carried out in the laboratory. Comparison of dummy neck loadings and injury criterion (HIC) to the roof crash are presented for production vehicles. By utilizing a three-dimensional Finite Element code (PAM-CRASH), rollover simulations are conducted to observe the behavior of the roof crash in detail. Portions of this paper have been revised to incorporate new findings, results of reviews and examinations after the presentation in Paris, France.

Introduction

There are few studies of ramp roll-over crash tests using restrained dummies. The following study considers the effects of roof structure on the belted occupants injury in rollovers. The objective of this report illustrates the results of four programs:

- Field accident investigations for rollovers in Japan are studied.
- Twelve ramp roll-over tests using 3-point seat belted dummies are conducted utilizing a variety of production vehicles.
- Inverted dummy drop tests are carried out.
- Rollover simulation using the Finite Element Method predicts a roof crash behavior in detail.

Field Accident Investigations

The Results of Field Accident Investigations in Japan

Field accident investigations are mainly conducted by the Police Department and the Ministry of Transport (MOT) in Japan. About one hundred field accident investigations with which MOT entrusts the Japan Automobile Research Institute (JARI), are carried out every year at the Ibaragi prefecture and its adjacent prefectures in Japan. Using the MOT data from 235 restrained/unrestrained front seat occupants in rollovers studies are carried out.

Figure 1 shows the relative distribution of collision types for occupant victims at the Ibaragi prefecture and

its adjacent prefectures in Japan, using 1985 to 1989 accident data of passenger cars. One of the findings is that the percentage of rollovers had relatively fewer occurrences than that of frontal collisions.

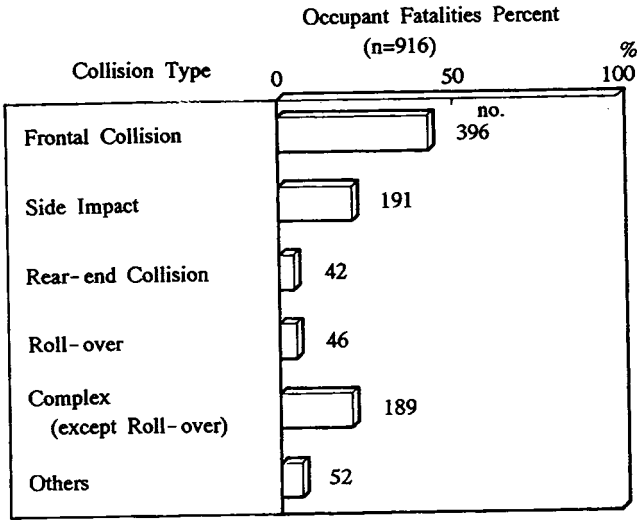

Figure 1. Relative Distribution of Collision Type for Occupant Victims at the Ibaragi Prefecture in Japan, 1985 to 1989 Accident Data

Figure 2 also describes the relative distribution of collision types for occupant fatalities in the United Kingdom incidents, using 1983 to 1986 accident data. This data shows that rollovers are few in comparison with the total number of accidents, and the distribution is similar to that of Japan.

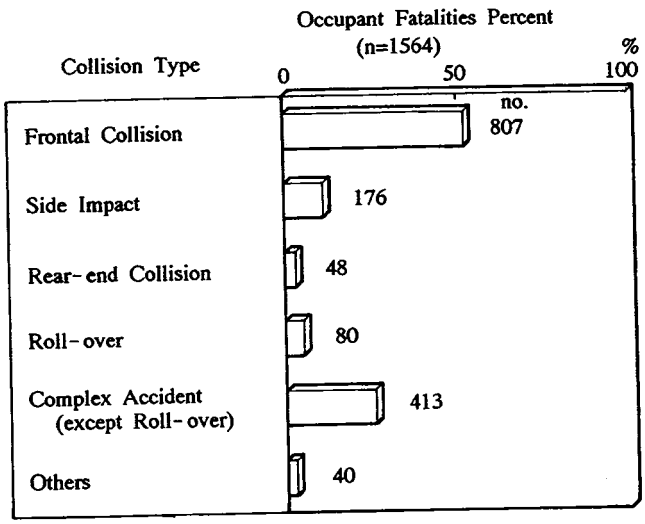

Figure 2. Relative Distribution of Collision Type for Occupant Victims in the United Kingdom, 1983 to 1986 Accident Data

The Unrestrained Occupants to Ejectees

The relative distribution of collision types for occupant non-ejection or ejection with unrestraints is illustrated in Figure 3. As shown in this Figure, it is found that the rate of ejection for rollover is relatively greater than that of other traffic collision types.

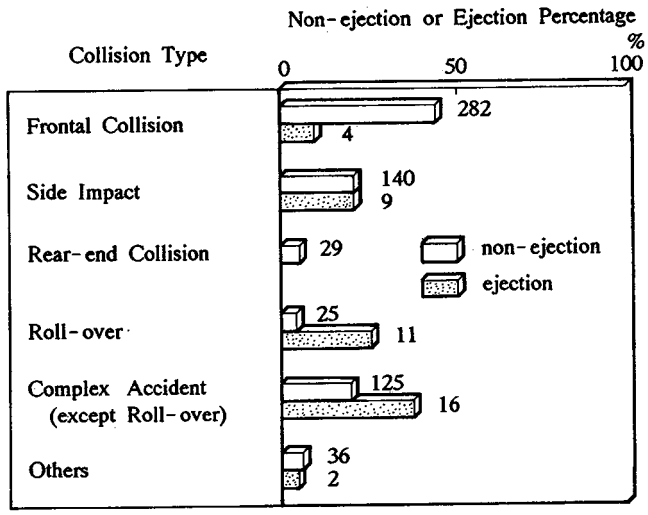

Figure 3. Relative Distribution of Collision Type for Occupant Non-ejection or Ejection with Unrestraint, 1985 to 1989 Accident Data

The relative contribution of injury severity (Abbreviated Injury Scale; AIS) for non-ejection or ejection is shown in Figure 4. This Figure illustrates that non-ejected occupants with an AIS over 4 are apt to be less, and ejected occupants with an AIS over 3 are relatively larger. It is unclear whether a restraint system is available for reduction of injury in rollovers, but it is clear that the use of restraints is the primary prevention of ejection in rollovers. Huelke (1) concluded that for those occupants not ejected from the car, belts effectively reduce fatalities and the more serious injuries in rollovers.

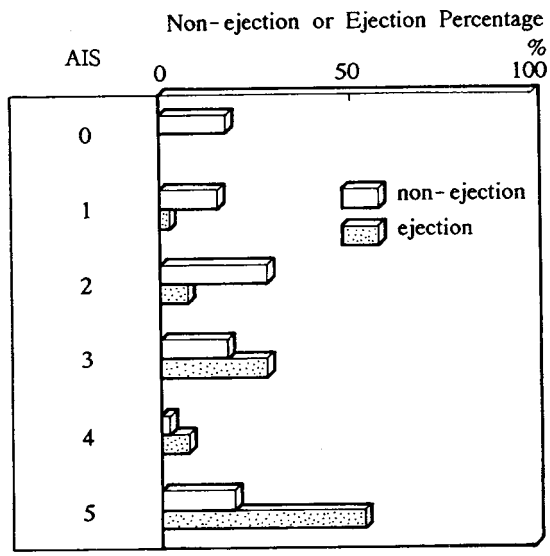

Figure 4. Relative Distribution of Injury Severity (AIS) for Non-ejection or Ejection with Unrestraint, 1985 to 1989 Accident Data

The Occupants Injury to Non-Ejection

Figure 5 presents the relative distribution of injury severity (AIS) for the roof deformation in cases of non-ejection with unrestraint. It is seen that occupants injuries are few at AIS over 4 with non-ejection. Also, it is found that no significant statistical relationship exists between AIS and roof deformation for non-restrained occupants in rollovers.

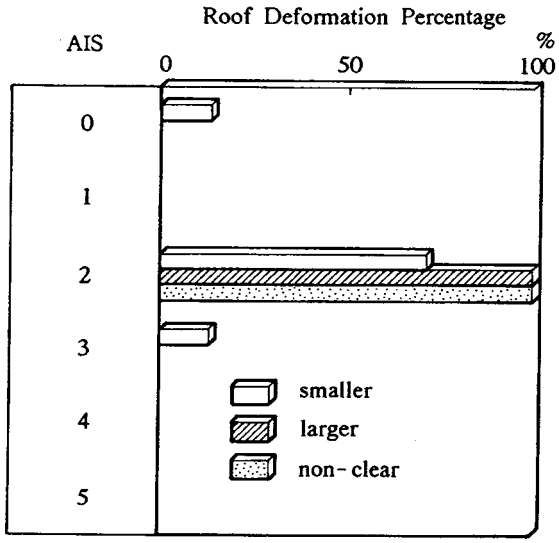

Figure 5. Relative Distribution of Injury Severity (AIS) for the Roof Deformation in Cases of Non-Ejection with No Restraint

Huelke (2) indicated that for contained occupants, those belted had fewer severe injuries and fewer fatalities. Strother (3) found NCSS rollover/restrained data sparse, but noted that the existing data showed no restrained rollovers with an AIS 4. His studies results happened to be similar to ours. Huelke (4) observed that, even in those accidents where there was 13 to 24 inches of roof crash, the average injury to lap belted occupants was moderate.

Table 1 presents the comparison of injury severity to various parts of the human body from aggressive parts of vehicle body, without ejection from the vehicles. The rate of injury severity to the head is the highest of total number of injuries. Also, the most aggressive part of vehicle is the roof when compared to other vehicle body parts, as illustrated in Table 1.

Ramp Rollover Tests

Test Methodology

Various test procedures for passenger car roll-over tests have provided techniques and instrumentation for study and evaluation of vehicle structural effects. Also, occupant behavior resulting from rollovers produced by the ramp test are specified (5). The ramp procedure, which is reproducible between different types of passenger cars, provides realistic simulations of rollover accidents without collision.

Table 1. Relative Distribution of Injury Severity to Various Parts of the Human Body from Aggressive Parts of Vehicle Body

Parts of Vehicle body	Parts of human body				
	Head	Neck	Chest	Abdomen	Legs
Roof	75				
Front Pillar 1 Side-rail	25				
window shield				100	
Steering			100		
Door trim					100
Others		100			
	(100)	(100)	(100)	(100)	(100)

The schematic ramp test is shown in Figure 6. As a severe turn usually will not produce enough of a rolling moment to cause the vehicle to rollover, two techniques are proposed. One is with the ramp located so as to lift the front wheel which provides the needed rolling moment (5). The other is with an adaptation of control system of steering wheel. In the first method, the rail curvature and ramp height are designed to produce a rollover at a speed of 50km/h (see Figure 6). With the adaptation, the rolling moment can be precisely generated by quick moment of steering wheel (see Figure 6).

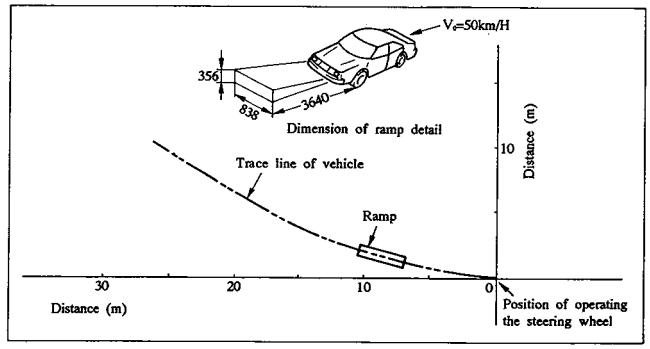

Figure 6. The Schematic Ramp Test

Twelve ramp roll-over tests were conducted using different types of Mitsubishi Motors passenger cars at a nominal speed of 50km/h. They were a front engine, front wheel driver car weighing approximately 1300kg, including an additional weight with a 2500mm wheelbase taken as a rough average. For these tests, the production cars of four-door sedans, two-door coupes, and sports-car types were selected. In order to take a photograph, head restraints on the front and rear seats were removed. The doors were locked and windows closed prior to the test. The steering wheel was automatically controlled by using an accumulator unit on board. The emergency brake was also on board. All tests are carried out on flat concrete in dry conditions.

Overall vehicle accelerations are measured triaxially by accelerometers located on the center pillars at their intersection with side sill.

The Hybrid III 50th percentile male dummies were set in the left and right front in the seated position. Accelerometers were placed in their head and neck. Dummies were restrained with three point seat belts with an inertial locking belt system. Also, a tension reliever and load cell were located in line with the seat belt to measure the dynamic loads.

Two on-board high speed cameras were equipped at the rear position to document dummy movement. Off-board high speed cameras photographed the behavior of the vehicles. One high speed camera, to document the overall vehicle movement, was located at points on the right side of the test site.

Ramp Roll-Over Test Results

Vehicle Kinematics. The data from twelve ramp roll-over tests results are shown in Figure 7, with regard to a number of revolutions of vehicles. When the vehicles just reach the position of operating the steering wheel, the steering wheel is automatically controlled quickly to right direction. The vehicles are driving leaning and rolled obliquely off the ramp with the passenger side leading at around 50km/h. First, the driver side of the roof immediately contacted the ground, followed by the passenger side. Typically, one revolution occurs in these tests. The difference of vehicle type does not clearly correspond to the number of revolutions.

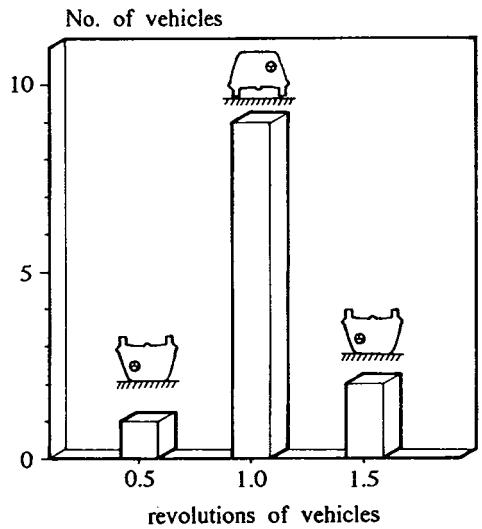

Figure 7. Number of Revolutions of Vehicles

Dummy Kinematics. The dummies movement is documented by using two on-board cameras. As the dummies are nearly obligated on centrifugal force during the rollovers, dummies are almost always moved upward and outward to the extent permitted by the belts. After contact is made with the roof, the dummies heads remain adjacent to the roof or the roof rail. Once the driver dummy head is set, this orientation is kept until the test is over. The passenger dummy tends to lean to the driver dummy to the extent which the belt can extend.

Dummy Measurements vs Vehicle Deformation. The head acceleration and neck compression loads of the Hybrid III dummy are measured. The time-history of the roof deformation is observed by using a high speed camera attached to the body structure at the rear seat. From these measurements and observations, the time-history results for the neck compression load and the roof deformation are schematically shown in Figure 8. According to the observations obtained by using the high speed camera, the dummy sitting on the side of the vehicle that approaches the ground first will contact the side glass due to the rotational inertia force. At this time, the neck compression load contributes slightly to the component of lateral load. As the vehicle rotation increases, the dummy becomes inverted and contacts the adjacent side roof rail and remains there. When the dummy's head stops, its torso keeps moving towards its head stopping at maximum compression. The maximum neck load is assumed to occur at this time. This is the reason for the high compression load in the neck. By observation from the high speed camera and confirmed by instrumented measurements, most of the roof deformation occurs after the peak neck load. According to Bahling, et al. (6) in the dolly rollover test, the maximum neck load occurs before the structural deformation causes maximum load.

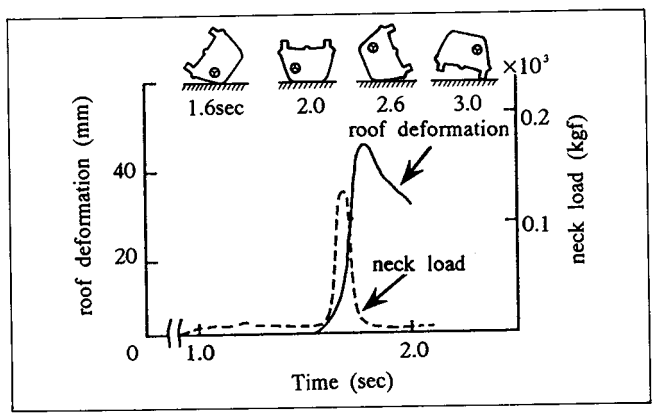

Figure 8. The Relationship Between the Neck Load, Roof Deformation and Time History

Dummy Injuries and Roof Geometry. Here a factor affecting of the structural deformation on dummy injury is introduced, considering field accident investigations and ramp roll-over tests described above.

Figure 9 show the geometric roof height H defined as a factor. The roof height H' is assumed to be a perpendicular distance between two parallel lines. The distance is a clearance between the line L connected the vertex point A of engine hood with the point B intersected the center-pillar, and the side roof rail in a side view, and the line L' parallel to the line L through the point C intersected the front pillar and the side roof rail. By introducing factor H, comparison of roof deformation on factor H, we are able to understand clearly, the rollover phenomenon.

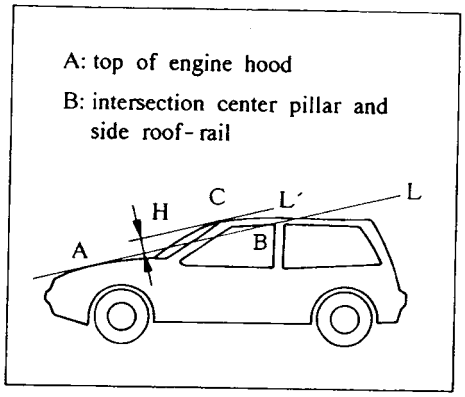

Figure 9. The Geometric Roof Height H

Figure 10 shows the relation between roof deformation and roof height H. It is found that relations between the roof deformation and roof height H seem to be linear.

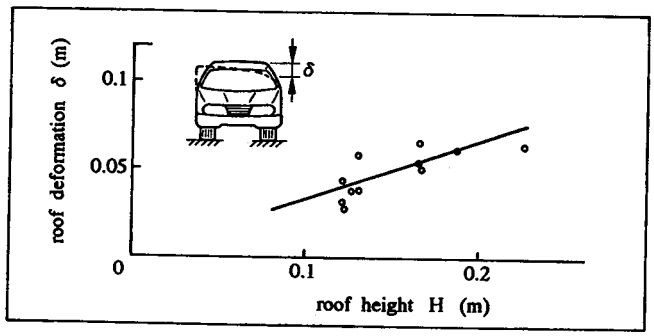

Figure 10. The Relation Between Roof Deformation and Roof Height

If a linear relationship exists between the roof deformation and the roof height H, the roof height H may relate to dummies injuries.

Figure 11 illustrates the neck load versus the height H. Figure 12 presents HIC versus roof height H. As seen in the Figures, that as H increases, the neck load and HIC tend to increase.

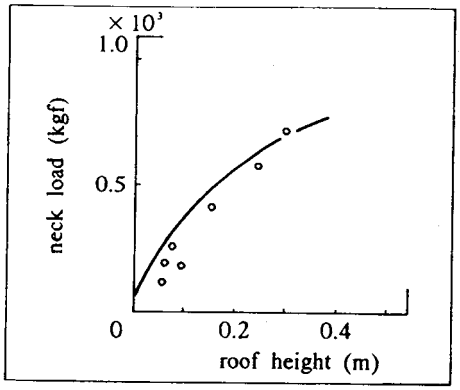

Figure 11. The Neck Load Versus the Roof Height

As the result of the introduced factor H, a possible relationship is identified between the initial geometric configuration of a vehicle and roof deformation or dummy injury.

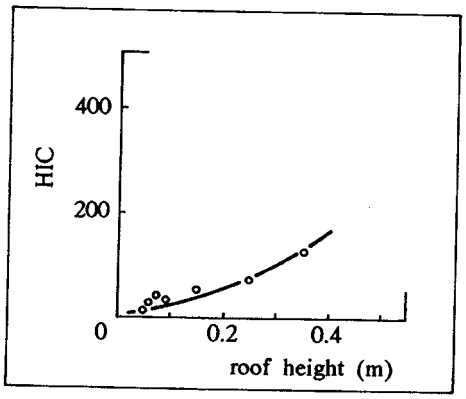

Figure 12. HIC Versus Roof Height

Even in case of higher roof height H, the value of dummies HIC and neck load is lower level relatively compared with a criterion of injuries.

Roof Height H and Roof Strength. Comparison of the static roof strength (FMVSS 216) for the roof deformation is investigated. As shown in Figure 13, there is no stronger correlation than between the roof strength and the roof deformation. Therefore, the static roof strength is a weaker relation to the dummy injury in the sense that it is stronger relation to the roof deformation. Here the static roof strength is given place to displacement X, defined as the load, and satisfied with loads required in FMVSS 216 (see Figure 14).

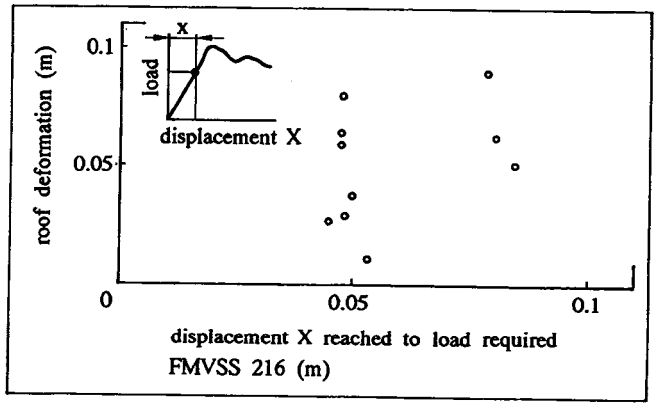

Figure 13. The Roof Deformation Versus the Displacement X

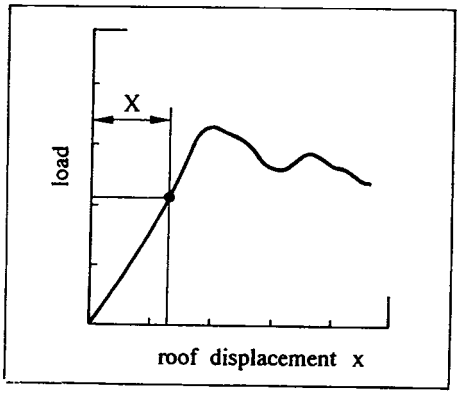

Figure 14. Static Roof Strength (FMVSS 216)

Inverted Dummy Drop Test

There are, however, a few problems related to these methods with respect to the repeatability due to the various type vehicles selected. Among each test, initial conditions always have to decide, for the steering wheel to be operated quickly and timely. So only the inverted dummy drop test is conducted in order to gain precisely repeatable data.

Drop Test Procedure

The dummy is allowed to free fall from the inverted position, which is designed for each vehicle. In the area of dummy-to-ground, the part of roof cut off from the production vehicle is placed directly on the ground. Figure 15 describes the schematic dummy drop test.

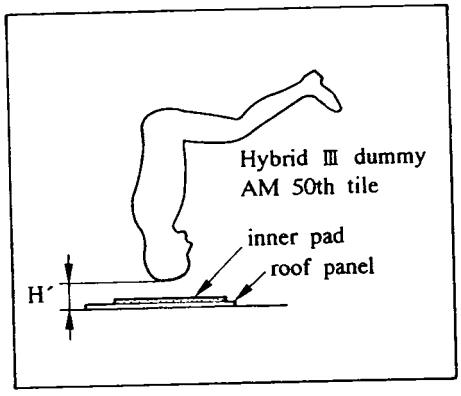

Figure 15. The Schematic Dummy Drop Test

Drop Test Results

Drop test results with combinations of the drop height and dummy injury as shown in the insets of Figures 11 and 12, are presented in Figures 16 and 17. As the height of drop position increases, the dummy injury also increases accordingly. It is found that the tendency of the dummy injury in the drop test corresponds to results of the ramp roll-over test.

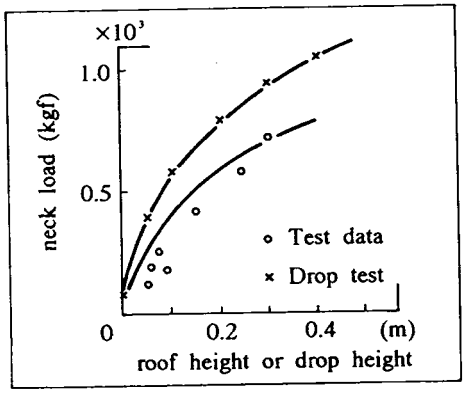

Figure 16. Combinations of the Drop Height and the Load of Dummy in the Insets of Figure 11

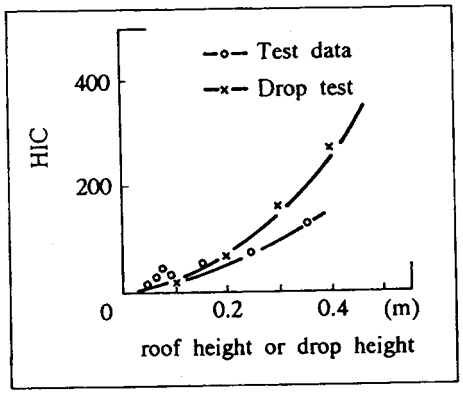

Figure 17. Combination of the Drop Height and HIC of Dummy in the Insets of Figure 12

Rollover Simulation

Finite Element Method (FEM)

For calculation of the rollover phenomenon using FEM, it is necessary to solve the motion equation with time integration. Explicit integration is preferable for solving crash simulation problems such as a frontal fixed barrier compared with implicit integration, but implicit integration may be better than explicit in relatively longer behavior such as rollover. However, it is not yet established for calculation. One program vectorized for the supercomputer, is used to conduct the rollover simulation.

FEM Model

FEM model is explained as follows (7). Body panels such as the frame, outer panel, floor and roof are modified with thin shell elements to calculate the impact buckling modes. Suspension unit and other chassis components are modeled as bar elements with the equivalent stiffness. Flanges of panels connected with spot welding are modeled with each plate thickness. The weight of components is attributed to lumped mass respectively. Rigid walls may be defined providing external impact surfaces, while slide lines prevent penetration of internal structure surfaces during collision. Slide lines are available for frames. Mesh element sizing is 20mm x 20mm on an average considering sound velocity. The number of mesh elements is approximately 15000.

Figure 18 shows the FEM model for rollover simulation. Figure 19 illustrates the calculation result.

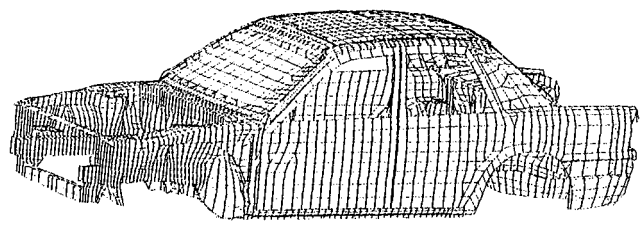

Figure 18. FEM Model

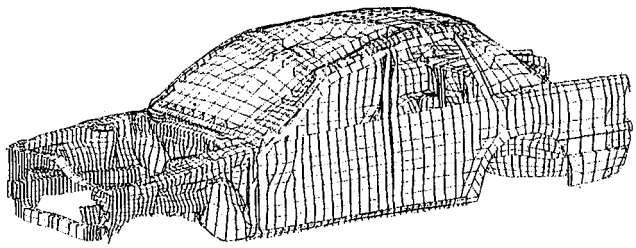

Figure 19. Deformation Mode

Conclusions

- In field accident investigations in Japan, rollovers are relatively little, compared to other accidents. A highest severe injury rate to occupants not ejected is to the head.
- The comparison of the roof deformation or the roof height H on dummy injury in the improved ramp rollover tests is as follows:
  - Maximum neck load of dummy occurs before most structural deformation of the vehicle in ramp rollover test.
  - The relative distribution of roof deformation for neck loads is not stronger respectively.
  - The roof deformation and dummy injury are possibly related to the roof height H, derived from the initial geometric configuration of the vehicle.
- The results of the inverted dummy drop test is able to be corresponded to the ramp roll-over test.
- By using the FEM, the rollover phenomenon is clarified in detail.

References

1. Huelke, D. F., Lawson, T. E., Marsh, J. C., Injuries, Restraints and Vehicle Factors in Rollover Car Crashes, Accid. Anal. and Prev., Vol. 9, 1977.
2. Huelke, D. F., Lawson, T. E., Scott, R., and Marsh, J. C., The Effectiveness of Belt Systems in Frontal and Rollover Crashes, SAE 770148, 1977.
3. Strother, C. S., Smith, G. C., James, M. B., and Warner, C. Y., Injury and Intrusion in Side Impacts and Rollovers, SAE 840403, 1984.
4. Huelke, D. F., Marsh, J. C., and Sherman, H. W., Analysis of rollover Accident Factors and Injury Causation, 16th Conference of the American Association for Automotive Medicine, 1972.
5. SAE Handbook, J857, 1982.
6. Bahling, G. S., Bundorf, R. T., and Kaspzyk, G. S., Rollover and Drop Test—The Influence of Roof Strength on Injury Mechanics Using Belted Dummies, 34th Stapp Car Crash Conference Proceedings, SAE 902314, 1990.
7. Sakurai, T., Aoki, T., On the Safety Body Structure of Finite Element Method Analysis, 12th International Technical Conference on ESV, 89-2A-O-015, 1989.

S6-O-11

Roof Collapse and the Risk of Severe Head and Neck Injury

Donald Friedman, Keith D. Friedman
Liability Research Group

Abstract

A survey of accident statistics and harm to the head and neck from side impact and rollovers, suggest that vehicle upper structure should be the next high priority goal in reducing severe casualties. Contrary to contentions that roof strength has little influence on these injuries, these results from a multiplicity of studies, indicate that roof collapse should be eliminated, passive interior padding improved, laminated and retained glazing be installed and restraints improved by pretensioning retractors. A statistical analysis of the 1982 and 1983 NASS files of rollover accidents, indicates a greatly increased risk of severe injury to occupants under a collapsing roof section. The increased risk was also demonstrated by detailed investigation and analysis of 15 rollover accidents using the protocol of SAE #890382 (Live Subject Safety Research). The instrumented data from sixteen nearly identical, rollover tests conducted by General Motors with conventional and rollcaged roofs and unrestrained and belted Hybrid III dummies were analyzed and confirmed the increased risk. Limiting the deformation extent of vehicle roofs by lightweight structural changes and simple and inexpensive force limiting, energy absorbing interior surface modifications, were demonstrated to reduce the risk of severe injuries by a factor of at least four. Further reductions can result from maintaining the vehicle's directional stability by Anti-Lock Braking Systems, limiting an occupant's contact velocity by emergency tensioning retractors on restraints and by minimizing partial ejection potential by laminated and retained glazing.

Introduction

Automotive rollover impacts critically injure and kill thousands of people each year[1-6] through head and neck injuries[7-10] as shown in Figure 1. The tragic human consequences of a quadriplegia injury under an obviously collapsed roof naturally leads to the presumption that the roof isn't strong enough.

These studies indicate that while the roof isn't strong enough, explaining what happened usually isn't that

simple and research agreement on the vehicle design features which cause rollover injuries has until now been masked by misrepresentation.

* 27% of all HARM involves the Head and Neck
* 41% of Head and Neck HARM comes from contact with the Roof, Roof-edge, and A-Pillar.
* 8% of HARM in Side impacts is from head contacts with the Roof Area.
* 12,000 Head Injuries per year of which 2000 are totally disabled and 5400 have severe partial disability.
* 3100 Life threatening, but surviving Spinal Cord Injuries.
* 5900 Fatal Cervical Spine Injuries
* 500 Quadriplegics per year

Figure 1. Head and Neck Accident Injury Statistics

Perhaps because rollovers aren't publicly well understood and of lower priority, virtually no regulatory attention has been given to manufacturer's countermeasures for reducing or eliminating the number of people annually killed and critically injured in rollover accidents.

Moreover NHTSA seems to have given up on the dynamic rollover test of paragraph S8.3 of FMVSS 208 because in regulatory terms it isn't repeatable enough, although GM's 16 Malibu series tests illustrate useful repeatability. Instead there is now an NHTSA initiative on FMVSS 214 head injury testing, on FMVSS 216 applicability to light trucks and vans and for an adjusted static roof crush test as means of improving head impact protection.[11]

To address the issue of critical injury risk to occupants of vehicles in rollover impacts, analyses of several data sources have been conducted. The analyses utilize data from:

- Rollover Potential and Rate Studies,[12-14]
- National Accident Sampling System,[3]
- Rollover Accident Case Studies,
- Head and Neck Injury Data,[15-19]
- Rollover test data,[20-31]
- Head contacts[7,8] and padding studies[32-33] and
- Computer simulations[34-37].

The results of these analyses provide insight into:

- the vehicle characteristics that initiate and exacerbate the injury potential of Rollover accidents;
- the restrained and unrestrained occupant kinematics during the rollover event;
- the injury mechanism of head and neck contact and,
- the countermeasures which would mitigate the injuries.

Background

A rollover accident is usually the result of an instability associated with the vehicle inadvertently traveling with a velocity vector whose principal component is no longer in the direction of the vehicles longitudinal axis. Rollover propensity and the effect of Anti-Lock Braking Systems (ABS) to deal with directional stability during braking may be part of the solution.[12-13]

Several studies have been conducted on behalf of vehicle manufacturers suggesting that stronger roof structures are of little value in terms of occupant protection.[25-30]

However, there is reason to question such conclusions. For example, some studies restrict themselves to consideration of impacts in which the ground contact and head impact point are identical in space and/or time. They conclude that stronger roof structures are of no value in protecting occupants, and they imply that nothing can be done to reduce the consequence of these impacts.

They do not consider the implications of stronger roof structures on vehicle dynamics, windshield/glazing retention on roof strength and occupant ejection, or of stronger roofs to limit deformation and collapse in the proximity of the occupant location. Furthermore, they do not consider the implications of padded, energy absorbing, or shaped roof structures, nor do they address the issue of roof structure performance on the risk of critical injury to occupants with head strikes not at the exact location of ground contact.

Most current production cars use less then .04" of steel and 1/2" of acoustic deadening material to contain and/or separate an occupant's head from the ground; the increased window area of tempered side glazing facilitates ejections. Additionally, the roof support structures allow the roof to collapse in a one foot drop test (much less a dynamic rollover event), and the occupant's head is exposed to numerous unpadded interior hard points.

In short, many previous studies do not consider the implications of current roof structure design on the risk of critical injury, nor what can be done with available countermeasures. Therefore, the two primary purposes of this paper are to: define the factors on which Head and Neck Injury Risk depends; and to identify safety features which could reduce the frequency and severity of such injuries particularly in rollover accidents.

Propensity to Rollover and Rollover Rates Per 100 Fatalities

Collision Avoidance. An NHTSA and a confidential study[13] has derived estimates of field rollover rates for cars and other light vehicles; determined the extent to which these rollover rates are influenced by half the track width divided by the center of gravity elevation (T/2H), after control for other vehicular factors and normalization to common exposure conditions; and has characterized the rollover rates by injury severity; among other comparative evaluations.

Light trucks, vans and utility vehicles experience much higher (1.5 to 2 times) overturning rates than automobiles.[5] Our experience and investigations indicate that these vehicles are frequently used as passenger cars

with lightly loaded rear wheels. When so loaded, an emergency steering maneuver accompanied by braking tends to lock up the rear wheels resulting in a loss of directional control, lateral skidding and rollover.

Shorter wheelbases also result in higher yaw rates and indicate vehicles with a lower yaw moment of inertia which combine to produce lateral skidding and potential for roll. The use of Anti-Lock Braking Systems (ABS) on such vehicles may be a most important everyday safety feature on lightly loaded pickups, vans and utility vehicles with as much or more safety benefits than other crashworthiness improvements. Running-off-the-road is usually the first event in a rollover of any vehicle and ABS could significantly reduce the frequency of such occurrences.

Crashworthiness. As in most studies of those types, an inherent assumption is that equal protection is provided for the occupants and no attempt is made to correlate the fatality or severe injury rates with intrusion or restraint features nor to assess the likelihood of reducing the rates with practical modifications.

The resulting claim is that vehicles which overturn more frequently are less safe than ones which do not and should be taken off the market. Manufacturers who have a duty to provide comparable state-of-the-art protection can do so either with collision avoidance features or with occupant protection features such as stronger roofs, roll bars, emergency tensioning retractors, passive interiors, laminated glazing, etc. or preferably all.

As addressed in a previous study[38] dealing with frontal impacts, there is no doubt that as designed and inherently (by the laws of physics) "small cars are less safe than large cars," but by attention to occupant protection and restraint design, the disparity can be substantially ameliorated. As air bags are installed in all vehicles (probably by 1994) and as increased CAFE forces large cars to lighten, their compatibility and the disparity will improve[39] although some intrusion in small cars may remain. When that happens, the frequency of occurrence of severe to fatal injury in frontal accidents will reach a lower limit as a result of vehicle factors and the residual will be more occupant related and more independent of size.

The same situation applies to side impact and rollover accidents, using the same specific amelioration techniques of reduced intrusion, improved passive interiors, and automatic tensioning of belts.

National Accident Data Analysis

A study of rollover impacts[40] was conducted in 1986/1987 using data from the 1982 and 1983 National Accident Sampling System. Rollover cases involving hardtop automobiles with known data for variables of interest were considered.

A review of the actual hardcopy data aided in identifying rollover types and the nature of damage associated with the occurrence of injury. The results suggested that roof damage descriptions relative to occupant locations would correlate with critical injury occurrence.

It was also noted that ejection and ejection paths may also be related to roof crush and distortion or may be a secondary effect relative to the roof crush. The hardcopy data study suggested the following:

- Cases with significant roof crush at the occupant location or expected contact area appear to generally result in substantial injury;
- Cases with substantial other damage may distort data analysis results (e.g. frontal or side impacts in which there was also a rollover); and,
- Ejection and ejection paths may also be related to roof crush and distortion or may be a secondary effect relative to the roof crush.

As a result of the hardcopy data study, the computerized data were utilized to characterize the proximity of roof crush to occupant location, and cases were excluded from data study in which non-top damage extent was greater than 3 as were those occupants totally ejected through the door area. The details of the recoding and methodology are contained in Appendix A.

The Statistical Analysis System was then used to study the computerized data. The results show a dramatic difference in the risk of critical injury or death when the damage in the proximity of the occupant exceeds a damage extent of 3. Specifically, the increased risk in rollover impacts for occupants in the proximity of significant roof crush is approximately 4 to 1.

Table 1. Analysis Results Showing Comparison of Risk for Occupants not in the Proximity of Significant Roof Crush in Rollover Impacts

	Raw Data		Weighted Results		Risk of
Category	AIS 0-3	AIS 4-6	AIS 0-3	AIS 4-6	AIS 4,5,6
Proximal Damage 0-3	307	5	58541	229	.0039
Proximal Damage >3	138	5	15170	243	.0158

The tabular results are shown in Table 1 and show a factor of 4 increase in the risk of critical injury or death in rollover impacts when the occupant location is in the proximity of significant roof crush compared with occupants who are not.

Rollover Case Studies

Fifteen cases of critical injury or fatality have been investigated, most but not all on an in-depth basis. These real world rollover cases described in Table 2, were analyzed by computer simulation to characterize the accident, the occupant kinematics and the injury mechanism.

In each case alternative means to reduce the level of injury were considered and then demonstrated to be feasible within practicality and economic constraints.

The mitigation means considered were a stronger roof, a shaped roof (like cars of the 50's and the Minicars

Table 2. Rollover Accident Case File Summaries

Case Vehicle	Roof Deform Extent	Injured by roof # / AIS	Other Injured # / AIS	Effective Countermeasure
1. 1975 Pinto	= 5	1CS/ 5	1 / < 2	Strt.
2. 1983 Blazer	> 3	1BD/ 6	2 / < 2	Strt. & Pad.
3. 1986 Escort	= 5	2CS/ 5	1 / < 2	Strt. & Pad.
4. 1981 LeSabre	> 3	1CS/ 5	3 / < 2	Strt. or Pad.
5. 1984 Toy P/U	> 4	1CS/ 4	1 / < 2	Strt. or Pad.
6. 1980 280 Z	> 2	1BD/ 4	0	Strt. or Pad.
7. 1976 Dodge	= 5	2CS/ 5	1 / < 2	Strt. & Pad.
8. 1983 Camaro	= 5	1CS/ 5	0	Strt.
9. 1981 F150 P/U	> 2	1BD/ 5	4 / < 3	Padding
10.1988 2500 P/U	= 5	1CS/ 5	0	Strt.
11.1985 Bronco	= 4	1CS/ 5	1 / < 3	Strt.
12.1988 BMW	= 1	2BD/ 6	5 / > 1	Padding
13.1981 Subaru	= 1	1CS /5	1 / 1	Padding
14.1988 Samurai	= 0	1CS /5	0	Padding
15.1976 260 Z	= 3	1CS /5	0	Padding
Subtotal	8 Veh w/RC >3	10 Inj >4 u/RC,		8 Inj <3 nu/RC
Subtotal	7 Veh w/RC <3	8 Inj >4 and		12 Inj <3

CS=Cervical Spine, BD=Brain Damage, Strt.=Structure, Pad.=Padding, < =less than, > =greater than.

RSV), padding, headroom and restraint emergency tensioning. The proof was the comparative level of injury resulting from the alternative, relative to the original contact.

These cases indicate that:

- passenger side rolls are most frequently occurring and far-side (driver side) roof crush is most significant.
- occupants under a significantly crushing roof suffered a critical neck or brain injury while those not in the proximity of the crushing roof suffered no critical injuries.
- occupants on the far side of the roll suffer the most significant Injuries.
- all of the critical injuries would have been eliminated by the inclusion of a stronger roof structure and 2 inches of interior force limiting metal padding on the roof, roof pillars and rails.

In the real world, the initiation of roll is usually preceded by a violent yaw maneuver which also moves the human occupant's upper torso and head forward as well as to the right. Human drivers usually have their hands on the wheel allowing them to resist such forward and lateral motion to perhaps 0.5 g.

The initial position of the occupant, how they hold or brace themselves and where they are (their body part attitude and orientation) at the instant of first touch down, are major factors in establishing their injury level. This is because severe neck injury generally occurs when the head impact contact velocity is 2 to 3 m/s and the cervical spine is aligned and generally perpendicular to the contact surface. Brain damaging head contact requires higher velocities and forces not frequently occurring in rollovers (unless the roof is also moving), long interior paths to surface contact, or partial ejection and head contact with the ground.

While the lateral delta V (which generates the roll) tends to move the occupants sideways (at 4 to 8 m/s), during a rollover, the occupants are thrust into contact with the interior surfaces of the vehicle closest to them by centrifugal forces as soon as the roll rate is high. While the driver has his hands on the wheel, passengers have a tendency to use their arms to protect their head, perhaps by extending them over the back or top of their head, thereby reducing contact velocity. Also tilting the head so that the chin is close to the chest (tucking it in) is natural. This increases head to roof clearance and misaligns the cervical spine.

Injury Measures. The computer simulation analyses use the Hybrid III dummy as a tool in comparing alternate designs, although the neck is thought to be too stiff and lacks compliance, particularly in compression to represent absolute human neck injury.[18-19] The GM suggested Hybrid III Biomechanical tolerance[15] (injury criteria) for axial compression is shown in Figure 2. Also shown are the Hodgson and Thomas[17] data and the resulting NHTSA[16] upper and lower limits for predicting a critical (AIS = 5) injury. Other neck injury criteria such as moments in flexion and extension exceeding 190nm and 57nm respectively have been published from the same sources.[15-16]

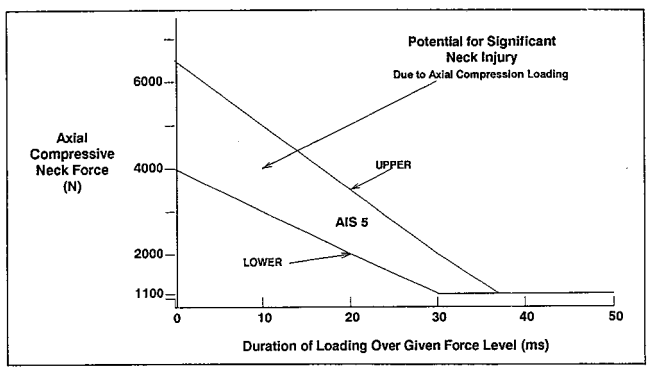

Figure 2. Hybrid III Dummy Neck Axial Compression Tolerance

Injury Criteria are dummy forces representing "predictive" probability functions for when 25 to 50% of the people will be so injured. Design engineers use these criteria to adjust the force/deflection properties of the vehicle interior where the dummy might contact it. The authors and others[15,18,19,37,42,46] have shown that the Injury Criteria must be increased by about 25% to represent the "descriptive" probability function of a person who has actually been so injured.

The case studies included several ways to receive an incapacitating (AIS level 4 or 5) injury with the interior of the car in a rollover. The most common are as follows:

- Building up a high relative velocity and then violently striking the head on the roof or its support structure. There were five brain damaged victims and two quads resulting from a head to surface closing velocity in an unpadded or inadequately padded area (#2,6,9,12,13,14) under areas without roof collapse (extent less than 3) but some deformation. There were 12 other people with moderate or less injuries

in the same vehicles seated where there was no significant roof deformation.

- Receiving an aligned neck compression load of more than 4000 n (interpreted from Biomechanical Research Criteria and applied to the Hybrid III simulations) often in conjunction with a moment torque or shear force. This is projected to result in some form of compression fracture and subluxation. Fourteen of the victims became quadriplegic from crushing of the cervical vertebrae (1,3,4,5,7,8,10, 11,15) with roof collapse (extent greater than 3) over their seating position while all thirteen other occupants of the same vehicles not under collapsed roof sections received minor to moderate injuries.
- The above injuries were sometimes in combination with shear forces and moment (torque) loads on the head and neck resulting in posterior or anterior cervical fracture and displacement.

A Sample Case study involving Roof Crush

This 65 mph loss of control, running-off-the-road accident resulted in a 20 mph 360 degree roll on dirt in a vehicle with a secondary supplier's undeveloped Targa (substantially weakened) roof which collapsed (at about 3300 pounds and 2300 ft-lbs) to the window sill on a restrained woman with more than five inches of normally seated head clearance. The injury was a severe extension compression of the cervical spine with posterior fractures of C-2 as well as symmetrical posterior burst fractures at C-6.

The vehicle trajectory was simulated in 3-D from take-off and touchdown marks in the soft earth, the roof crash pulse and deformation were modeled from FMVSS 216 and computer derived stiffness estimates. The occupant kinematics and injury mechanism computer simulations resulted in the injury measures of Table 3.

Table 3. Resulting Injury Measures from Actual and Alternative Simulations of Example Rollover

Parameter	Actual	Stiffer Roof	Stiffer Roof & pretensioning
Crush over victim	30cm	15cm	15cm
Belt Slack (each)	1.75"	1.75"	0"
Torso Belt load (n)	0	0	1095 n
Lap Belt load (n)	405 n	1303 n	2607 n
HIC	343	67	26
Neck Shear Forces	-95 n	178 n	245 n
Neck Moment	2 nm	1.5 nm	-37 nm
Peak Neck Compressive Force	4727	2309	1061

The analysis indicated that the roof was collapsing at about 15 feet/second at about 200 degrees of roll in alignment with her cervical orientation at contact with her head somewhat in extension due to a concurrent violent vehicle yaw motion. She was off the seat, moving towards the roof with about an eight foot/second velocity, which was in the process of being arrested by the belts with 1.75" of slack on each side. The contact produced dummy neck compression (from head contact with the earth) injury measures at the AIS = 5 quadriplegic level.

When we substituted a 6000 pound stiff 2300 ft-pound roof, deformation was limited to about 15 cm, the neck compression was about 2300 newtons (a much lower probability of permanent debility). When we added belt emergency tensioning retractors,[45-48] of the belt wind-up type patented in the 1970's, to this alternative roof configuration the neck compressive load dropped to 1061 n. A parametric analysis was also conducted for a range of stiffer earth surfaces with a similar range of results.

Analysis of GM Rollover Test Data

Rollover crash test data available from General Motors were reviewed.[25-26] GM made no attempt to make these tests representative of the real world. Therefore, careful analysis and judgement must be applied when comparing these injury measure results with the human injury results of accident statistics and case investigations.

Care must be taken to properly interpret tests with dummies, who can neither hold on, brace themselves, protect their head and neck with the arms, nor keep their chin on their chest. In fact, dummies are designed to be "in position" with its head erect and neck aligned for an axial compression load through the top of the head. And while a person might drop their head after a first impact, the dummy resets itself for many impacts in the course of a roll.

The GM rollover tests are right roll dolly launch tests. In the first series of 8 tests the driver and right front passenger dummies were unrestrained, while in the second set of 8, the dummies were restrained but with a belt which was significantly slackened to represent how human occupants wear them and allow 4" of vertical motion at 1 g.

The tests were conducted with a vehicle initial roll position 23 degrees to the horizontal and launched from about 9 to 12 inches above the ground with a speed of approximately 51 Kilometers Per Hour (KPH). That means the launch produces a clockwise roll (looking from the rear) and that the driver dummy experiences a significant force to move, actually moving upward and to its right at launch.

These tests with 1983 Chevrolet Malibu four door vehicles are most likely to produce a first roof to ground contact on the drivers side roof (the far side in this case), and are most likely to collapse there first (with standard roofs) and produce a driver injury.

Half the vehicles in each series were also modified to include an unpadded 160# roll cage. None of the roll-caged vehicles deformed, and two of the eight standard vehicles did not collapse. This suggests that a much more modest weight increase for roof support structure would be sufficient to achieve the benefits of the rollcaged vehicles in reduced injuries.

In the eight unrestrained GM tests there were inside the car, 43 Potentially Injurious Impacts (PII) = or >2000

newtons—the GM presumed threshold of any axial compression injury for an average of 3.5 such impacts per test for the far side driver, while @ 4000 newtons (the GM serious injury probability measure) or more there are less than 2 per test. For the nearside passenger, there are only about 1.5 PII per test and only two total interior contacts above 4000 n.

In the eight restrained tests inside the car, there were a similar 39 PII's but there were 5 passenger contacts above 4000 n; estimated dummy contact velocities were .83 to 3.3 m/s.

As explained in Figure 2, Biomechanical researchers suggest using 4000 newtons of short duration axial compression (Metric 1) for relating neck injury measures to the onset of severe neck injury probability. They also relate neck moments exceeding 190 nm in flexion and 57 nm in extension (Metric 2) to critical injury.

Table 4. Results of GM Test Data Showing the Fraction of Cases Exceeding Neck and Moment Criterion (Metric 1)

Roof Type	Position Relative to Roll	Restraint Condition: Unrestrained	Restraint Condition: Restrained	Total
Standard	Far side	4/4	4/4	8/8
Roll cage	Far side	4/4	2/4	6/8
Standard	Nearside	2/4	1/4	3/8
Roll cage	Nearside	2/4	3/4	5/8

For the Hybrid III dummy injury measure results to correspond to the certainty of a real world critical neck injury occurring, we assumed that axial compression greater than 5000 newtons accompanied by 1000 newtons of shear (Metric 3) would be appropriate.

Table 5. Results of GM Test Data Showing the Fraction of Cases Exceeding Neck Moment Criterion (Metric 2)

Roof Type	Position Relative to Roll	Restraint Condition: Unrestrained	Restraint Condition: Restrained	Total
Standard	Far side	2/4	2/4	4/8
Roll cage	Far side	2/4	0/4	2/8
Standard	Nearside	0/4	0/4	0/8
Roll cage	Nearside	1/4	0/4	1/8

Thus, three metrics have been identified for interpreting the data from the Hybrid III dummy, two of which (Metrics 1 and 2) are interpreted (Tables 4 and 5) as corresponding to predicting the onset of severe neck injury probability while the third (Metric 3) represents a median probability of critical neck injury (such as might be appropriate for modeling a known, having-actually-occurred critical injury) shown in Table 6.

These metrics were evaluated using the data available; the results from each test are presented in Appendix B, while the results are summarized below.

Of these results perhaps the most notable is the dramatic difference in the results for the far side metric 3 between standard and roll caged vehicles. As can be seen in Table 6, there were *no* cases in which a far side occupant in the *roll caged* Malibu ever exceeded the Metric 3 criterion, while *all* of the far side restrained occupants in the *standard* Malibu exceeded the limit. And the roofs of the standard vehicles whose occupants did not exceed the metric, did not collapse.

Table 6. Results of GM Crash Test Data Showing the Fraction of Cases Exceeding the 5000 n Axial Neck Compression and 1000 n Shear Force Criterion (Metric 3)

Roof Type	Position Relative to Roll	Restraint Condition: Unrestrained	Restraint Condition: Restrained	Total
Standard	Far side	2/4	4/4	6/8
Roll cage	Far side	0/4	0/4	0/8
Standard	Nearside	1/4	0/4	1/8
Roll cage	Nearside	0/4	2/4	2/8

There are a number of other interior injury measure results which are of interest. For example there were only 2 cases of HIC greater than 1250, 1 in standard roof and 1 in roll cage vehicles. There were two cases of partial and one total ejection.

Unfortunately, GM did not publish photographic derived data such as when, where and how much the roof crushed as a function of time. There were only three plots of neck compression force vs time for PII 2L3, 3L4 and 7L4 on which roof contact was displayed at the beginning of the neck compression and indicated that roof crush occurred later. The electronic data from 4 vertical accelerometers indicated that contact occurred some 25 to one hundred milliseconds earlier as shown in Figure 3.

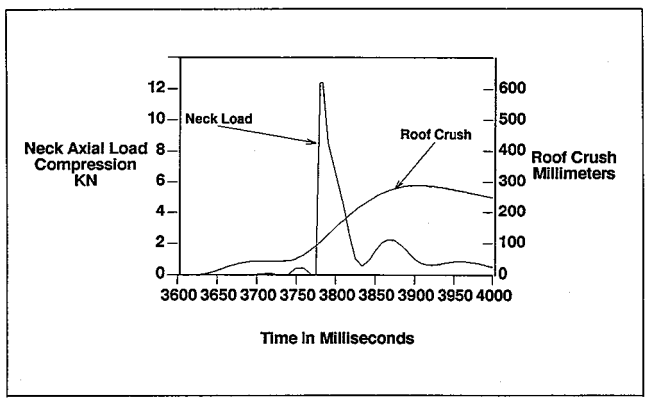

Figure 3. Estimated Relationship Between PII 7L4 Roof Crush and Head Strike Timing

One clear conclusion from the GM tests is that a stronger roof, which does not collapse, changes the dynamics of the rollover so that far side roof rail contact is less severe and therefore less injurious. In both sets of production vehicle tests when the roof collapsed the magnitude of the far side neck compression load was as high as 13,200 newtons, often exceeded 7000 newtons, but in both sets of rollcaged tests, the neck compression never exceeded 6600 newtons.

There were more PIIs (and a few > 4k newtons) on the near side of the rollcaged than production vehicles, the magnitude of the hits are mostly mitigatable.

Countermeasures. GM published no comment on how mitigation measures would effect the injury results of the 3200 pound 1983 Chevrolet Malibu rollover tests. They were considered in this study on a group and individual basis and the applicability of alternate designs were determined. An assessment of the ability to significantly mitigate each of the injury impacts was made using Metric 3 as the evaluation criterion. Since most roof contact velocities in the GM tests were between .8 and 3.3 m/s, we concluded that if the roof could be strengthened just enough to resist collapse as occurred in the Number 8 unrestrained and the Number 8 belted conventional roof tests, the padding would mitigate the remaining interior neck compression forces.

Of course, in addition to the larger gauge-and-section roof support strengthening design and added metal padding, the countermeasure system should include retained and improved side glazing to limit ejection.[43] These results are shown in Table 7. The total production weight increase of this countermeasure system is estimated to be less than 50 pounds.

Table 7. Results of GM Tests Considered with Appropriate Countermeasures Showing Expected Number of Potentially Critical Injuries

	Original Potential Critical Injury Impacts	Expected Number of Potential Critical Injury Impacts with Countermeasures
Standard Far side	8/8	0/8
Roll cage Far side	6/8	0/8
Standard Nearside	3/8	0/8
Roll cage Nearside	5/8	0/8

Rollover Tests Relative to Real World Accident Studies. This analysis of GM rollover tests has provided injury measure insights, one test relative to another, but a comparison to actual case work studies has shown that the test conditions used are not representative of real world accidents since:

- Many rollovers have a violent yaw maneuver prior to the initiation of roll causing the far side occupant to move forward and toward what will become the near-side occupant;
- The dummy is launched with about a 10 ft/sec vertical velocity vector from the dolly which causes unrestrained dummies and several of the dummies in the restrained tests to move to the roof as the wheels touch down, and to incur significant injury measures suggesting risk of critical injury in the process;
- The dummies cannot hold on and/or brace themselves as would be the reflex action of people in impacts;
- The erect dummy neck is probably not representative of a persons neck in rollover impacts, nor representative of human reflex actions;
- The far side occupant is much better off with a non-collapsing and strengthened roof (although a 160# rollcage is not necessary);
- A stronger roof structure alone is not sufficient to eliminate the potential for critical injuries for all occupants;
- Roof collapse increases the potential for critical injury by increasing the effective head contact velocity; and,
- While torso augmentation is a significant factor in some contacts with an unpadded roof, the contacts frequently occur when the roof is not yet displaced, nor in contact with the ground, making padding countermeasures effective.

Head Strike, Padding and Computer Simulations Studies

A number of independent real world injury accident studies were conducted or reviewed in conjunction with head and neck injuries in other accident modes to validate Injury Measure results and confirm the effects of padding. These included:

- three helmeted football players receiving quadriplegic injuries through the inefficient 1" of padding at the top of the helmet and strike velocities in the 8 to 12 ft/sec range. These cases had the advantage of filmed occurrence on a marked grid, physical dummy tests and 2 and 3 D corresponding computer simulations.
- five side impact car cases involving head studies on inadequately padded roof rails and sail panels;
- a parametric computer study of a far side, side impact occupant contacting a conventional and/or a padded roof at vertical velocities of 2 to 3.5 m/s, horizontal velocities of 0, +7/-2, +/-4 meter/sec and 0°, 10° and 20° head flexion[37];
- one case of a frontal head strike on a passenger side GM "X" car instrument panel whose force/deflection properties yielded effectively 4" of stroke;
- NHTSA study on head strikes and A pillar padding effectiveness;[32-33, 41]
- GM study on A pillar and roof rail padding;[44]
- GM drop tests of restrained and unrestrained Hybrid III dummies in conventional and roll caged roof vehicles;[26] and,
- rollover test data of a physical and a 3-D simulated dummy in a 1982 Dodge Aries FHWA/NHTSA/ Aeromedical Lab. test.[34]
- rollover data from the design configuration of the Minicars' Research Safety Vehicle (RSV)

The last point is illustrated in Figure 4. Considering current automotive styling trends, an alternate counter-

measure approach is the monocoque rounded roof structure of the Minicars Research Safety Vehicle which rolled three times without excessive far side roof rail acceleration or deformation. It provided 4 inches of roof deformation without intruding on the occupant's survival space. The angled interior roof contact surface was designed to flex the head and neck to preclude axial loading.

Figure 4. Research Safety Vehicle

A case example involves a heavy 220# man, unrestrained in a partial (20-30 degree) roll as the result of a far side, side impact. The vehicle and near side occupant motion resulted in an effective vertical contact velocity of about 2.5 meters/second with the roof, producing C5-C6 quadriplegia.

The first thing done[37] was to conduct a parametric analysis of the possibilities for dummy neck injury when striking a roof at various vertical and horizontal velocities and with various head orientations. We also considered the very same circumstances but with a mathematically padded, non-pocketing roof. The results indicated that at 2 to 3 m/s contact velocities neck compression injury measures could be limited to the 2500 newton range.

Next an exemplar car was located and the static force/deflection properties of the roof were measured with a head form. A 22 gauge plate with 1" high tabs on 6" centers were then inserted between the headform and the roof and the measurements repeated. The measurements are shown in Figure 5.

This data shows that the lined roof limits the force to about 500 pounds (2200 newtons), over 800 inch-pounds of energy absorption, while the conventional roof exceeds 500 pounds at 400 inch-pounds. Translated to case related neck compression injury measures, as shown in Figure 6, it means that a padded roof can limit neck forces to below 2500 newtons at up to 140% of the conventional roof's acceptable (2 to 3 m/s) contact velocity or, when at the same speed, the conventional roof produces 15,000 newtons, the padded roof will limit to less than 2500 n.

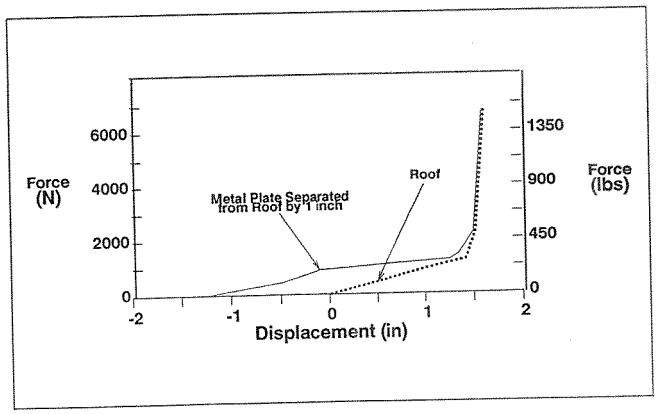

Figure 5. Force/Deflection Properties of a Typical Passenger Vehicle Roof and With 1-Inch Tabs on Six-Inch Centers on a 22 Gauge Metal Inner Roof Liner

3-D Test Number	105	106	102
Roof Characteristic	Baseline	Baseline	Padded
Victim Roof Contact Velocity	2 m/s	2.5 m/s	2.5 m/s
Initial "X" velocity	2.0	2.0	2.0
Initial "Y" velocity	4.0	4.0	4.0
Initial Head Angle	90	90	90
Initial Neck Angle	90	90	90
Head to Roof (Lbs)	485	5000	406
Neck Compression (Lbs)	370	4142	303

Figure 6. The Comparative Characteristics and Dummy Injury Measures for this Case, Derived in 3-D from Figure 5 Measurements

Summary

A loss of directional control resulting from the vehicle response to a combination of emergency steering and braking inputs initiates lateral skidding and rollover accidents.

Data analysis shows significantly greater risk of critical injury when an occupant is in the proximity of roof crush with deformation extent index greater than 3.

Case study analyses show that occupants under a crushed roof section suffer more severe injuries than those not under a significantly crushed roof section.

GM test data shows a significantly greater chance of critical injury when an occupant is under a crushed roof. Previous published information obscured facts by using a low threshold of "potential injury" rather than a measure consistent with critical injury.

The risk of head/neck injury from roof contact in rollovers is related to the relative contact velocities of the head/neck, and the orientation of the head, neck and torso upon contact with the roof.

Risk of critical head/neck injury is dependent on:

- roof interior head/neck clearance
- roof shape
- extent >3 of roof deformation
- interior force/deflection characteristics
- restraint system performance
- glazing performance

The results suggest that such alternative rollover safety design improvements, adding approximately 50 pounds to the vehicle weight and $250 in cost, could save as many as 5000 lives per year and 5000 critical neck injuries in all accident modes.

BENEFITS	
FATALITIES ELIMINATED	5000
CRITICAL INJURIES REDUCED	2500
SEVERE INJURIES REDUCED	2500
COSTS	
WEIGHT	50 lbs
COST	$250

Figure 7. Estimated Head/Neck Injury Countermeasure and Benefit/Cost in All Accident Modes

Further and more detailed observations, comments and conclusions are in APPENDIX C.

Recommendations

The roof support structure should be strengthened to avoid buckling collapse.

The interior of all roof and roof support surfaces should be padded with force limiting material to allow two inches of deformation at 2500 to 3500 newtons without pocketing.

Restraint systems should be equipped with emergency tensioning retractors.

Side window glazing should be laminated and retained to reduce roof deformation, shattering and limit ejection. Anti-lock Braking Systems should be installed to improve emergency directional control thereby reducing the frequency of rollover accidents.

References

1. Fatal Accident Reporting System (FARS), NHTSA.
2. National Crash Severity System (NCSS), NHTSA.
3. National Accident Sampling System, (NASS), NHTSA.
4. The Severity of Rollover Crashes in the National Crash Severity Study; Robert McGuigan, December 1980.
5. Light Truck and Passenger Car Rollover and Ejection in Single-Vehicle Crashes, Kenneth W. Terhune, PH.D. Arvin/Calspan.
6. Statistical Estimation of Rollover Risk; Peter Mengert, Santo Salvatore, Robert DiSario, Robert Walter, August 1989.
7. A Search for Priorities in Crash Protection; SAE 820242, Malliaris et al, page 6 & 7.
8. Crash Injury Impairment and Disability: Long Term Effects, SAE SP-661 860505 S. Luchter, page 94 & 96.
9. Cervical Injuries Suffered in Automobile Crashes, J. Neurosurg. March 81, Mendelsohn et al p. 316.
10. Head Injuries in Highway Accidents—Current Incidence and Potential Abatement; Malliaris and Digges, Univ. of Virginia, 1991.
11. Advanced Notice of Proposed Rulemaking for FMVSS 214 February 1991 and Amendment to FMVSS 216 Docket No. 89-22, April 1991.
12. The Crash Avoidance Rollover Study: A Database for the Investigation of Single Vehicle Rollover Crashes; E. A. Harwin, Lloyd Emery, May 1989.
13. Comparative Evaluation of Rollover Rates, Prepared by Data Link, Inc. CONFIDENTIAL, not publicly available.
14. Rollover Potential of Vehicles on Embankments, Sideslopes, and Other Roadside Features August 1986 Final Reports; Federal Highway Administration-Office of Research and Development, Note: Vol. I and II, File dated November 1986. Also SAE 870234.
15. Injury Assessment Values used to Evaluate Hybrid III Response Measurements; Harold J. Mertz, Safety and Crashworthiness Systems, Current Product Engineering, General Motors Corporation, Feb. 1984.
16. Injury Criteria and Mathematical Analogs for Selected Body Areas; Rolf H. Eppinger, NHTSA, July 6, 1982.
17. The Biomechanics of Neck Injury from Direct Impact to the Head; V. R. Hodgson, L. M. Thomas, Head and Neck Injury Criteria—Consensus Workshop.
18. Kinematic and Anatomical Analysis of the Human Cervical Spinal Column Under Axial Loading; Pintar, Yoganandan, Sances, Reinartz, Harris and Larson SAE 892436.
19. Epidemiology and Injury Biomechanics of Motor Vehicle Related Trauma to the Human Spine; Haffner, Maiman, Pintar, Yoganandan, Sances, Nichols, Jentzen, Weinshel and Larson SAE 892438.
20. NHTSA Rollover Tests: Vehicle and Dummy Kinematics in a Controlled Rollover Crash—1) 1988 Chevrolet Standard Regular Bed Pickup, 2) 1989 Nissan Standard Regular Bed Pickup, 3) 1988 Nissan Standard Regular Bed Pickup, 4) 1989 Nissan Pickup Truck, 5) 1989 Nissan Pickup Truck; Transportation Research Center of Ohio.
21. Vehicle Inertial Parameters-Measured Values and Approximations-SAE Technical Paper Series, W. Riley Garrott, Mickael W. Monk, Jeffrey Chrstos Date, October 31-November 3, 1988 SAE #: 881767.
22. Status Report on NHTSA Sponsored Research on Computer Modeling of Rollover Vehicle Dynamics, Presentation to Rollover Subcommittee, Motor Vehicle Safety Research Advisory Committee, NHTSA, March 16, 1989; Andrzej G. Nalecz.
23. NHTSA Research Safety Vehicle (RSV), Phase I, 1974, DOT-HS4-00844, Phase II, 1975, DOT-HS-5-01215, Phase III, 1977, DOT-HS-7-01552, Phase IV, 1978, DOT-HS-8-02096, Minicars, Inc.
24. Occupant Motion During a Rollover Crash; Arnold K. Johnson, David A. Knapton NHTSA, November 1984.

25. Rollover Crash Tests-The Influence of Roof Strength on Injury Mechanics; Kenneth F. Orlowski, R. Thomas Bundorf, General Motors Corporation; Edward A. Moffat, Biomech, Inc. SAE 851734.
26. Rollover and Drop Tests—The Influence of Roof Strength on Injury Mechanics using Belted Dummies; G. S. Bahling, GM/CPE, R. T. Bundorf, GM/CPE, G. S. Kaspzyk, GM/CPE, E. A. Moffatt, Consultant, K. F. Orlowski, Consultant, J. E. Stocke, GM/CPE; SAE 902314.
27. Real World Rollovers—A Crash Test Procedure and Vehicle Kinematics Evaluation; T.M. Thomas, N.K. Cooperrider, S.A. Hammoud, P.F. Woley, Failure Analysis Associates, Inc., March 10, 1989.
28. Reconstruction of Rollover Collisions; K.R. Orlowski, E.A. Moffatt, R.T. Bundorf and M.P. Holcomb SAE #: 890857.
29. Rollover and Interior Kinematics Test Procedures Revisited; John L. Habberstad, Roger C. Wagner, Terry Thomas SAE #: 861857.
30. Testing and Analysis of Vehicle Rollover Behavior; Neil K. Cooperrider, Terry Thomas, Selim A. Hammoud, Test and Engineering Center SAE #: 900366.
31. Development of a Tumble Number for Use in Accident Reconstruction; Thomas A. Bratton SAE #: 890859.
32. Side Interior Stiffness Measurements; Donald T. Willke and Michael W. Monk, NHTSA SAE 861880.
33. Injury and Intrusion in Side Impacts and Rollovers; Charles E. Strother, Greg C. Smith, Michael James, Charles Y. Warner Collision Safety Engineering, SAE #: 840403.
34. Prediction of an Occupant's Motion During Rollover Crashes; Louise A. Obergefell, Ints Kaleps, Arnold Johnson, NHTSA SAE #: 861876.
35. MVMA 2-D Modeling of Occupant Kinematics in Rollovers; D. Hurley Robbins, David C. Viano SAE #: 840860.
36. Live Subject Safety Research-Side Impact; Donald Friedman, S. Forrest, F. Gott, and G.D. Dyne-Liability Research, Inc. SAE #: 890382.
37. Improved Product Design by Impact Testing of Human Subjects, D. Friedman, 18th International Workshop on Human Subjects Biomechanical Research, November 1990.
38. The Safe Road to Fuel Economy; D. Friedman, K.D. Friedman, Clarence Ditlow and D. Nelson, April 1991.
39. Large Car-Small Car Offset Crash Test at 70 mph Closing Speed with Air Bags; Insurance Institute for Highway Safety, Brian O'Neill, February 1991.
40. Statistical Analysis of Injured Occupants by Seating Position & Location of Roof Deformation; Keith Friedman, Donald Friedman, unpublished.
41. Sub-System and Full System Testing to Assess Side Impact Safety; D. Willke, D. Guenther, M. Monk, 18983, SAE #830465.
42. Comparison of New Car Assessment Program Crash Test Results with Real World Crash Test Data; NHTSA Rulemaking Office of Market Incentives, March 1988.
43. Car Crash Tests of Glass-Plastic Side Glazing, Carl Clark, Peter Sursi, 1984.
44. General Motors Vehicle Safety Improvement Program (VSIP) Confidential, Unpublished.
45. U.S. Patent Numbers 4285479, 4023746, 4684077, 4540137.
46. Biomechanical Evaluation of the Axial Compressive Responses of the Human Cadaveric and Manikin Necks; N. Yoganandan, A. Sances, F. Pintar, August 1989.

Appendix A. Statistical Methodology

The availability of the National Accident Sampling System[3] represents a substantial resource for the calculation of nationally representative data associated with crash conditions and consequences. While the data is available from 1979 through the present, two years of the data (from 1982 and 1983) were selected for use in this study due to their similarity of file formats which simplified the formulation of working data sets. The effort required to process the additional years available has been left for further study.

In order to put the data into a form consistent with the analysis requirements the files were:

1. Converted to an occupant level file
2. Filtered for occupant vehicle rollover involvement Variable 112 in 1983 Vehicle Record Format
3. Filtered for Unknown Data
   a) Known Maximum Injury Level Variable 98 in 1983 Occupant Record Format
   b) Known Rollover Details (Exclude 3 on Variable 112 on 1983 Vehicle Record Format)
   c) Passenger Compartment Integrity not equal 0 (O = no passenger compartment) (Exclude 0 on Variable 106 of 1983 Vehicle Record Format)
   d) Exclude non-passenger cars and convertibles (Exclude all but 2-9 Vehicle Body Type on Variable 23-24 in 1983 Vehicle Record Format)
   e) Known Magnitude of Intrusion Variable 108 in 1983 Vehicle Record Format
   f) Known First Collision Deformation Classification for General deformation location (see Figure below)
      Longitudinal/lateral location
      Vertical/lateral location
      Type of damage Distribution
      Deformation Extent

g) Occupant seat positions 1, 3, 4, 6, 7, 9 (no occupants in mid seat locations and no unknown seat positions)

Cases with non-top damage greater than 4 were not considered. Occupants who were totally ejected through the door were not considered.

Occupant	General Damage	Specific Top Longitudinal Damage	Specific Top Lateral Damage
Left Side	Top	Center Center & Front Center & Rear Distributed	Distributed Left Left & Center
Right Side	Top	Center Center & Front Center & Rear Distributed	Distributed Right Right & Center

Variables of interest in the files were recoded where necessary to provide for consistency between years; after this was done, the files were merged into one file.

Following the creation of the analysis data file exploratory analysis of the data was conducted. Various factors were examined to assess the significance of the factors on injury consequences. The Statistical Analysis System package was used for all analysis work. Based on initial work new variables were created combining various variables into physically sensible combinations reflecting the considerations inherent in the hypothesis under investigation.

After initial reviews of the data, cases were selected for review of the underlying hardcopy records to gain additional insight into the implications of the coding procedures in use.

The hardcopy review aided in identifying rollover types and the nature of damage associated with the occurrence of injury. The results suggest that roof damage descriptions relative to occupant locations would correlate with severe injury occurrence. It was also noted that ejection and ejection paths may also be related to roof crush and distortion or may be a secondary effect relative to the roof crush. The study suggested among other things that:

- Cases with significant roof crush at the occupant location or expected contact area appear to generally result in substantial injury.
- Cases with substantial other damage may distort data analysis results (e.g. frontal or side impacts in which there was also a rollover).

The final analyses took into account the above considerations. It was also recognized that detail at the level of the hardcopy cases for the classification of roof crush would yield substantially better precision with regard to the location and amount of the roof crush relative to the occupant.

While confidence intervals can be calculated for the data, substantial effort is required. As a result, it was decided for this analysis to observe the consistency of the results across analyses and across alternative injury level thresholds. Depending on the results of the analyses further work on formal confidence interval estimation may be desirable to establish statistical significance. However, in the event of large differences in probability or in the case where the relations are consistently upheld the likelihood is that the large effort required to compute the confidence intervals would not be justified particularly when more data can be added to simply enlarge sample sizes.

Based on the exploratory and hardcopy analysis results a variable was created to reflect the general proximity of damage to the occupant location. The general form of the variable was dependent on the occupant location as illustrated below.

The proximity coding was assumed as shown below such that cases meeting these requirements were considered to be in the proximity of roof damage (and otherwise they were not).

It is clear that this coding scheme can, of course, be refined. Further, the addition of better precision in the data through the use of the hardcopy results to implement a more detailed coding scheme may provide for better resolution in the analysis of the data. Presumably, the additional precision would make the difference in the results discussed in the paper even more pronounced.

Appendix B. Detailed Driver and Passenger Head/Neck Contact Loads in GM Rollover Tests

APPENDIX B - Unejected, DRIVER head/neck contact loads from 16 GM Right Rollover tests (8 Restrained and 8 Unrestrained)

TEST #	CONDITION Standard Roof	AXIAL NECK LOADS PII >2kn	Std >4kn	Max kn	>5kn+1kn shear	NECK MOMENTS flex>190nm lat,ext>57nm	HIC
3	rest/dr	5	3	12.	1	3 lat	90
4	rest/dr	4	4	7.9	1	1 flex 3 lat	200
7	rest/dr	4	2	13.2	2	2 lat	740
8	rest/dr	2	2	5.3	1	2 lat	640
	Subtotal	15	11		5	10	0
1a	unrs/dr	3	1	5.2	1	3	2820
4a	unrs/dr	4	3	7.8	1	1	n/a
5a	unrs/dr	2	1	4.50	0	0	n/a
8a	unrs/dr	4	3	5.10	0	0	190
	Subtotal	13	8		2	4	1
Total Number >		28	19		7	14	1

TEST #	CONDITION RollCage Roof	AXIAL NECK LOADS PII >2kn	Std >4kn	Max kn	>5kn+1kn shear	NECK MOMENTS flex>190nm lat,ext>57nm	HIC
1	rest/dr	0	0		0	0	530
2	rest/dr	1	1	5.6	0	0	420
5	rest/dr	0	0		0	0	80
6	rest/dr	3	1	4.1	0	1 lat	130
	Subtotal	4	2		0	1	0
2a	unrs/dr	5	2	4.9	0	0	330
3a	unrs/dr	2	1	5.	0	1	20k
6a	unrs/dr	2	1	4.8	0	0	n/a
7a	unrs/dr	2	1	5.7	0	1	100
	Subtotal	11	5		0	2	1
TOTAL NUMBER >		15	7		0	3	1

APPENDIX B - PASSENGER head/neck contact loads from 16 GM Right Rollover tests (8 Restrained and 8 Unrestrained)

TEST #	CONDITION Standard Roof	PII >2kn	AXIAL NECK LOADS Std >4kn	Max kn	>5kn+1kn shear	NECK MOMENTS flex>190nm lat,ext>57nm		HIC
3	rest/rfp	0	0		0	0		90
4	rest/rfp	4	2	4.8	0	0		100
7	rest/rfp	3	1	4.75	0	0		70
8	rest/rfp	0	0		0	0		160
	Subtotal	7						
1a	unrs/rfp	5	1	4.6	0	0	(3 ground)	640
4a	unrs/rfp	3	2	7.8	1	0	(2 ground)	n/a
5a	unrs/rfp	3	0	3.8	0	0	(2/grd/ej)	n/a
8a	unrs/rfp	2	0	2.2	0	0		140
	Subtotal	13	3		1	0		
Total Number >		20	3		1	0		0

TEST #	CONDITION RollCage Roof	PII >2kn	AXIAL NECK LOADS Std >4kn	Max kn	>5kn+1kn shear	NECK MOMENTS flex>190nm lat,ext>57nm		HIC
1	rest/rfp	4	1	6	0	0		200
2	rest/rfp	3	1	4.5	0	0		180
5	rest/rfp	6	2	6.6	1	2		130
6	rest/rfp	1	0	2.3	0	0		190
		14	4		1	2		
2a	unrs/rfp	2	0		0	0	(1 ground)	280
3a	unrs/rfp	4	0		0	0	(3 ground)	240
6a	unrs/rfp	3	1	4.5	0	1	(1 ground)	n/a
7a	unrs/rfp	5	1	4.8	0	0	(1 ground)	110
		14	2		0	1		
Total Number >		28	6		1	3		0

Appendix C. Other Observations, Comments and Conclusions

More effort should be made to utilize the real world data available, to identify safety problems and to improve vehicle product safety design.

Crash pulses with longer rolls and lower angular accelerations appear to result in reduced risk of occupant injury. Such pulses are characteristic of roofs shaped like the Minicars RSV, cars of the 1950's and some current sporty cars.

In rollover impacts, the roof edge (corner) frequently experiences rolling contact with the ground, when the translational velocity at touchdown is 5 or more mph higher than the roll rate times the roll radius, resulting in a low (3 to 4g) long duration, or a high (10 to 20g) short duration shearing force at the roof rail. The consequence is to plow a 1 to 2 foot ground patch, collapsing the leading side "A and B" pillars towards the center of the vehicle, shifting the roof and destroying the integrity of the trailing pillars leading to their compression buckling.

The shape of the roof of current cars is thought to be inviolate, but they could easily have more rounded roof rails and greater tumblehome, allowing the cars to roll more easily with less peaked lateral deceleration. A monocoque roof design should improve rollover crashworthiness at lower cost and weight than present designs.

A squared, rollcaged roof edge radically alters the dynamic roll rate, vertical and lateral velocity and occupant contact velocity.

In rollover impacts, occupants seated under a portion of the roof which crushes are at significantly greater risk of critical injury than those seated under a roof without significant roof crush.

In rollover impacts limiting roof crush to a few inches (deformation index of 3 or less), significantly reduces the risk of critical injury.

Stronger roof structures:

- change the kinematics and dynamics of rollovers
- allow more vehicle energy to be absorbed in translation rather than in the crushing of the roof and hence not adding to the occupant's head and neck vertical contact velocity
- reduce the occurrence of injury measures associated with critical injury for far side occupants

Roof crush is resisted not only by the structure but by the strength of the windshield and closed side windows.

Any structural roof crush in the area of conventional side glazing produces breakage allowing the potential for subsequent head ejection and contact with the ground.

Stronger roof structures provide for the ability to retain windshield and improved side glazing, and they in turn increase roof strength.

A rounded, mildly deforming roof, rolls more smoothly, resulting in lower instantaneous decelerations, lower occupant contact velocities and potentially less injurious impacts with the interior.

Most current roofs only need minor structural change to limit deformation extent and avoid collapse and injury.

General Motors utilized a low injury measure threshhold to conclude that there is no difference in occupant injury whether the roof crushes or not. Their use of a "potentially injurious" criterion rather than the potential for critical injury, would appear to mislead regulators into believing that a stronger roof with force limiting interior is unnecessary.

A "potentially injurious" criterion may be consistent with corporate objectives for minimizing costs but highlights the differences between manufacturer corporate objectives, insurance company objectives of minimizing injury costs, and government objectives for maximizing overall societal benefit.

The seated, back inclined, body position significantly reduces potential neck loading from the torso.

The contact velocity and energy of the torso in rollover collisions is low relative to the interior, and head and neck orientation is usually not aligned, so "torso augmentation" of axial compression injuries are improbable.

Increased usage of seat belt shoulder harnesses may substantially increase the risk of axial compression neck injuries in current collapsible roof vehicles, by guiding the alignment of the head/neck with the intruding roof surface.

Upper vehicle interior contact surfaces with 2" of force limiting "padding" would significantly reduce the potential for critical head/neck injuries.

Strengthening the roof structure in all cars so that they won't buckle or collapse after bending and absorbing energy for a few inches will eliminate more than 50% of

the paraplegic/quadriplegic level injuries in the rollover accident population.

History has shown that a regulating authority or the consumer has to require improved safety. NHTSA and GM expressed enthusiasm for the Airbag in 1970. When regulatory implementation was delayed, it took until 1984 to require by 1987, the 1974 GM ACRS driver system performance in all cars by 1994. And during that interval, there was much discussion between NHTSA, industry spokesmen and the press about the practicality, effectiveness and cost of Airbags. Since about 1975 we have been following the same course to improve side impact and rollover protection for the head and neck. Is this necessary or appropriate to meet safety objectives?

S6-W-12

Effect of Car Size on the Frequency and Severity of Rollover Crashes

Charles J. Kahane
National Highway Traffic Safety Administration

Abstract

Narrower, lighter, shorter cars have higher rollover rates than wide, heavy, long ones under the same crash conditions. During model years 1970-82, as the market shifted from large domestic cars to downsized, subcompact or imported cars, the fleet became more rollover prone. The net effect of all car size changes since 1970 is an increase of approximately 1340 rollover fatalities per year in the United States. The methods of this report do not identify which individual vehicle size parameter (track width, curb weight, wheelbase, etc.) is the principal "cause" of rollover proneness.

Introduction

Rollover crashes are a major safety problem, resulting in about 4,500 fatalities a year to occupants of passenger cars. This report analyzes the influence of car size on rollover propensity, crashworthiness and fatality risk. The issues are studied in the context of the overall trend in fatality risk of unrestrained occupants of passenger cars of model years 1970-82 in rollover crashes, for those are the years in which passenger cars became substantially smaller in the United States.

In 1989, the National Highway Traffic Safety Administration (NHTSA) published *An Evaluation of Door Locks and Roof Crush Resistance of Passenger Cars* [5], which includes a detailed literature review and analyses of the effect of car size on rollover crash involvements. The material in this report is excerpted from the evaluation.

What Happened to Cars in 1970-82?

It is obvious that cars became "smaller" during 1970-82, but there are several ways to measure car "size." Three measures of size that are often used in analyses are curb weight, wheelbase and track width. The parameters are highly intercorrelated, in that "large" cars tend to be heavy, long and wide while "small" cars, with few exceptions, are light, short and narrow. For 1970-82 cars, the correlation coefficients of curb weight with wheelbase, curb weight with track width and wheelbase with track width are .93, .92, and .91, respectively.

Between model years 1970 and 1982, the median curb weight of cars in fatal crashes decreased by about 1000 pounds (from 3700 to 2700); the median wheelbase decreased by 10 inches (from about 115 to 105); and the median track width, by 2 or 3 inches (from 60 to about 57). Since model year 1982, the parameters have remained rather stable. At this time (1990), the size and weight of the average car on the road in the United States is close to the average model year 1982 car, as more and more pre-downsized cars are retired.

The size reductions of the 1970-82 period were achieved by two mechanisms. The more important is a market shift from full-sized cars to subcompact and imported cars. The shift was already underway in 1970 and gained strength throughout the period. Secondarily, there was downsizing within many domestic car lines, primarily after 1975 (until 1974, they were still growing). Imports grew during the late 1970's and early 1980's.

Factors Affecting Rollover Proneness

The following example of a sequence of events leading up to a rollover crash illustrates a variety of factors affecting rollover. The first event is that the driver, through inattention or speeds in excess of driving abilities, fails to keep the car aimed in the direction of the roadway. Upon noticing that the car is about to run off the road, the driver may try drastic corrective maneuvers, such as slamming on the brakes or swerving. The attempt is unsuccessful and puts the car into a skid. Now it is heading off the roadway with a partly sideways orientation. After the car leaves the roadway it encounters tripping mechanisms such as loose soil or a ditch, resulting in a rollover.

The preceding example suggests that rollover propensity has two components, so to speak: *directional* stability and *rollover* stability. A car is directionally unstable if it tends to skid or spin out of control or is hard to steer on course. A directionally unstable car will have many off-road excursions into terrain where rollover is likely to occur. "Rollover stability" is the

tendency of a car to remain upright *given* that it has come in contact with a typical off-road tripping mechanism. Short light cars usually have less directional stability than long, heavy ones. Narrow cars have less rollover stability than wide cars. Since "small" cars are shorter, lighter and narrower than full-sized cars, they tend to have lower directional and rollover stability.

Literature Review

In 1968, Garrett studied the relationship of car size to rollover propensity [1], defining the rollover rate of a car to be the ratio of principal rollovers to other single vehicle crashes. His idea is that rollovers and other single vehicle crashes typically involve about the same type of driver behavior—i.e., losing control of the car and running off the road. The other single vehicle crashes act as a sort of control group and cancel out biases due to differences in driving exposure or aggressiveness. He performed a regression of the rollover rates of 1950-67 cars by track width, curb weight and height. "The data indicate that there is a strong correlation between rollover frequency and vehicle dimensions: rollover increases as car size shifts from heavy, wide track, low vehicles to light, narrow track, high cars. Car weight and track width appear to have the greatest influence on vehicle overturn."

Jones [4], Griffin [2] and Harwin and Brewer [3] performed similar regressions and obtained excellent correlations of the rollover rate with the "stability factor" (half the track width divided by the height of the center of gravity) and wheelbase.

Malliaris et al [6] emphasized the roles of directional stability and rollover stability as components of rollover risk. They found that lighter cars have lower directional *and* rollover stability than heavy cars. NHTSA's 1988 Technical Evaluation [8] of Congressman [now Senator] Timothy Wirth's petition further explores this concept, stating that a number of vehicle size parameters, especially wheelbase, are related to directional stability. NHTSA stressed that the high intercorrelation of vehicle size parameters makes it hard to draw firm conclusions on which individual parameter is the most important factor in rollover risk.

During 1988-89 Partyka and Boehly of NHTSA studied the correlation of car weight and fatality risk in various crash modes [7]. Their regression equation for the rollover fatality rate per 100,000 vehicle years is

$$\text{fatality rate} = 8.01 - .00123 \text{ car weight}$$

The paper does not address whether this is a "cause and effect" relationship or a result of the strong correlation of car weight with other vehicle size parameters. Although the authors do not themselves use the formula this way, it will yield a fatality rate prediction if the average weight, by model year, is substituted for "car weight." The 1970-82 reduction of curb weight from 3700 to 2700 pounds would be associated with an increase in the fatality rate from 3.46 to 4.69, a 36 percent increase, nearly identical to the findings of this report.

Analysis Method and Data Sources

The measure of rollover propensity throughout this report is the ratio of rollovers to *frontal* impacts with fixed objects. The intuitive reason for the choice is that frontal impacts with fixed objects come closest to being a "control" group. They control for driver and exposure differences but not for vehicle factors affecting rollover risk. The number of frontal impacts with fixed objects, intuitively, is proportional to the frequency at which aggressive or inattentive driving results in a failure to keep the car aimed in the direction of the roadway—i.e., a potential rollover scenario. The greater the directional and/or rollover stability of a car, the fewer of these potential rollover scenarios become actual rollovers—and the lower the ratio of rollovers to frontal impacts with fixed objects.

The data sources for the analysis are the Fatal Accident Reporting System (FARS) for calendar years 1975-86 and Texas accident files for 1972-74 and 1977-83. FARS data are used to calculate the ratios of fatal rollovers to fatal frontal impacts with fixed objects. Texas data are used to calculate ratios for [primarily] nonfatal crashes. The study relies on Texas data because that is the only State for which NHTSA has files dating back to the early 1970's. Both files needed adjustments for calendar year differences and vehicle age effects [5], pp. 93-101 and 130-140.

Rollover Propensity Trends, 1970-82

The main products of the analysis are year to year trend lines or risk indices for model years 1970-82. Figures 1-4 are based on Texas data (primarily nonfatal crashes) and indicate the trends in rollover propensity.

Figure 1 shows the rollover propensity index by model year. The data points "U" ("unadjusted" for car size) show the actual ratios of rollovers to frontal fixed object

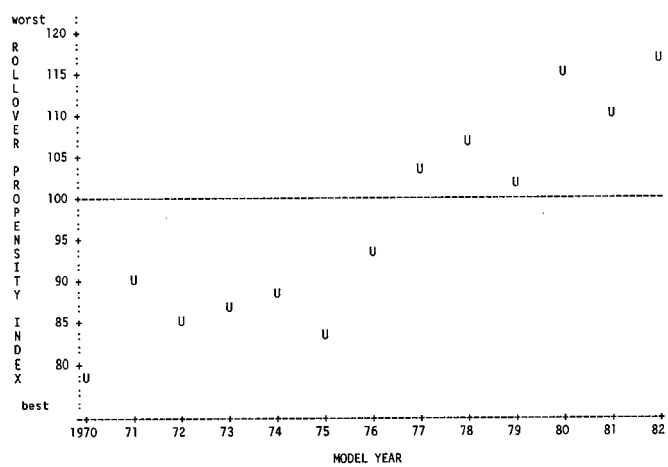

Figure 1. Rollover Propensity Index by Model Year (1975-80 Average = 100)

impacts in Texas data, indexed so that the average ratio for 1975-80 comes out to 100. The rollover propensity index starts at 80-85 in the early 1970's and rises steadily year after year, especially after 1975, to an all time high close to 120 in model year 1982. In other words, rollover propensity increased by almost 50 percent during model years 1970-82. In 1970-74, rollover propensity remained fairly stable: the market shift to smaller car classes was partly offset by the growth of cars within market classes. The real increases began after 1975, the period of downsizing within car lines as well as a market shift to smaller car lines.

In Figure 2, rollover propensity is graphed separately for 5 market classes of cars: I = Import, S = Subcompact (domestic), C = Compact, M = Midsized, F = Full-sized. The dependent variable is LOGR2, the logarithm of the ratio of rollovers to frontal fixed object impacts [5], pp. 100-109. The logarithm is used because it is more suitable for statistical analyses and for comparing one graph to another. The most obvious phenomenon in Figure 2 is that smaller cars consistently have higher rollover rates. Full-sized cars are always the best and imports are almost always the worst.

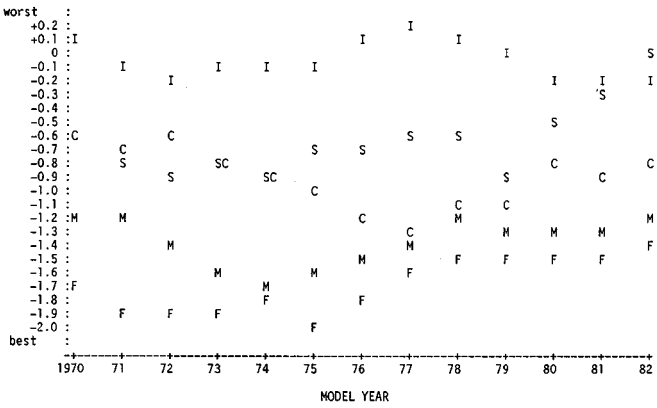

Figure 2. Rollover Propensity by Model Year and Car Market Class (LOGR2; I = Import, S = Subcompact, C = Compact, M = Midsized, F = Full Sized)

It is possible to see the effects of size changes within market classes. Full-sized cars were downsized in 1977-79; mid-sized cars in 1975-78; and compact cars in 1980—there are corresponding increases in rollover propensity during those years. Domestic subcompacts became narrower and lighter during 1970-82 while imports became wider, longer and heavier. Figure 2 shows that domestic subcompacts had lower rollover risk than imports in the 1970's but lost their advantage in the 1980's.

While Figure 1 shows a large, steady increase in aggregate rollover propensity, Figure 2 shows only moderate increases, if any, within market classes. As noted earlier, the size reductions of the 1970-82 period were achieved by two mechanisms. The more important was the market shift from full-sized cars to subcompact and imported cars, reflected in Figure 1 but not Figure 2. The effect of downsizing within market classes, reflected by both figures, is only of secondary importance and partially offset by size increases in imported cars.

A principal task of the analysis is to determine the extent to which the trends in Figures 1 and 2 are due to car size as opposed to other factors. The task is accomplished by a log-linear regression of rollover propensity (LOGR2) by curb weight, track width, wheelbase and vehicle age. The dependent variable in the regression is the aggregate value of LOGR2 for all cars belonging to a particular class interval of weight, width, wheelbase and age [5], pp. 109-118. Driver age was also tried as an independent variable and found to have negligible influence on the regression coefficients of the other variables. The regression coefficients for the model that best fit the data are:

INTERCEPT	5.561
TRACK WIDTH	-.0962
CURB WEIGHT	-.000259
VEHICLE AGE	-.0317

R squared is .97, a very high correlation. Although wheelbase did not have a significant effect in this model, that does not necessarily mean it is unimportant. As noted earlier, wheelbase, curb weight and track width are highly intercorrelated and the regression analysis could easily confuse their relative effects.

Based on the regression, a new variable

PROPEN2 = LOGR2 + .0962 TRACK WIDTH
+ .00259 CURB WEIGHT + .0317 VEH AGE

is defined and graphed by model year and market class in Figure 3. PROPEN2 measures rollover propensity adjusted for car size. Figures 2 and 3 are graphed to the same logarithmic scale—i.e., vertical distances have the same meaning in both graphs. It is evident that most of the variation across market classes and model years is explained by the car size parameters. The large variations across market classes in Figure 2 shrink to a narrow band in Figure 3, where no single market class is consistently at the top or bottom of the graph.

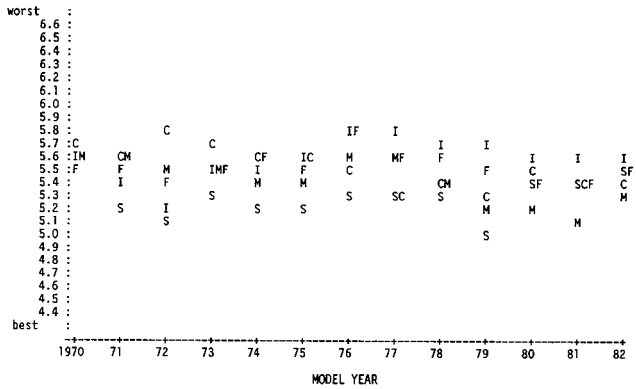

Figure 3. Rollover Propensity by Model Year and Market Class, *Ajusted for Car Size* (PROPEN2; I = Import, S = Subcompact, C = Compact, M = Midsized, F = Full Sized)

Figure 4 shows the rollover propensity index by model year—*adjusted for car size*. The data points "A" ("adjusted" for car size) are the antilogarithms of the average values of PROPEN2 across the various market classes, indexed so that the average ratio for 1975-80 comes out to 100. The adjusted rollover propensity index is close to 100 and remains essentially unchanged throughout 1970-82. There may be a few models with exceptional rollover rates, but none of them has sufficiently high sales or extreme rollover rates to pull the index (average for all cars) away from 100. Rollover propensity, on the average, is very well correlated with car size.

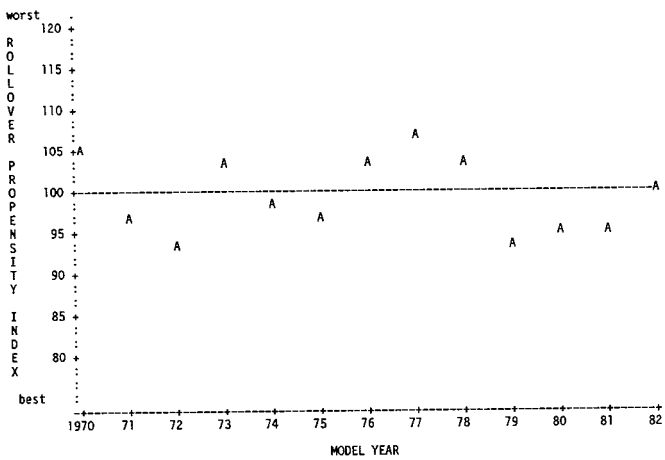

Figure 4. Rollover Propensity Index by Model Year, *Adjusted for Car Size*

Rollover Fatality Risk Trends, 1970-82

Figures 5-8 are based on FARS data and indicate the trends in rollover fatality risk. Figure 5 shows the rollover fatality risk index by model year, comprising the net effects of changes in rollover propensity *and* crashworthiness. The data points "U" ("unadjusted" for car size) show the actual ratios of fatal rollovers to fatal frontal impacts with fixed objects, based on FARS data, indexed so that the average ratio for 1975-80 comes out to 100. The rollover fatality risk index starts at about 90 in the early 1970's and rises steadily after 1975 to about 123 in model year 1982 (based on continuing the 1977-81 trend line through 1982; the actual data point for 1982 is even higher). In other words, rollover fatality risk increased by about 37 percent (123 vs. 90) during model years 1970-82. The trend in rollover fatality risk is quite similar, although not as steep as the trend of nonfatal rollover propensity (Figure 1); in both cases the real increases began after 1975, the period of downsizing within car lines as well as a market shift to smaller car lines.

In Figure 6, rollover fatality risk is graphed separately for the 5 market classes of cars. The dependent variable is LOGROLL, the logarithm of the ratio of fatal rollovers to fatal frontal impacts with fixed object [5], pp. 140-142. It is obvious from Figure 6 that smaller cars

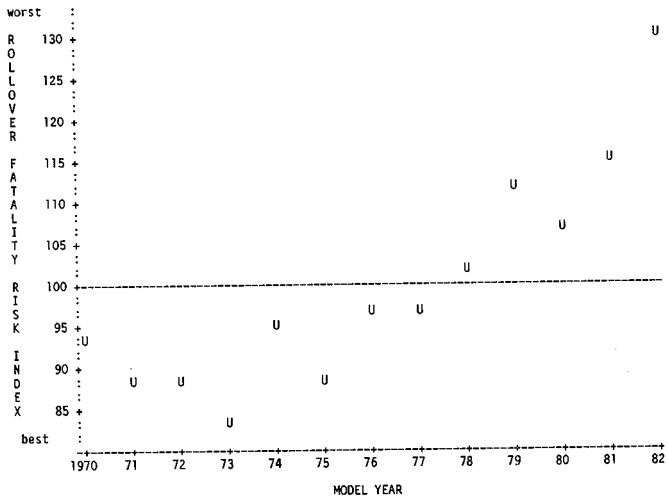

Figure 5. Rollover Fatality Risk Index by Model Year (1975-80 Average = 100)

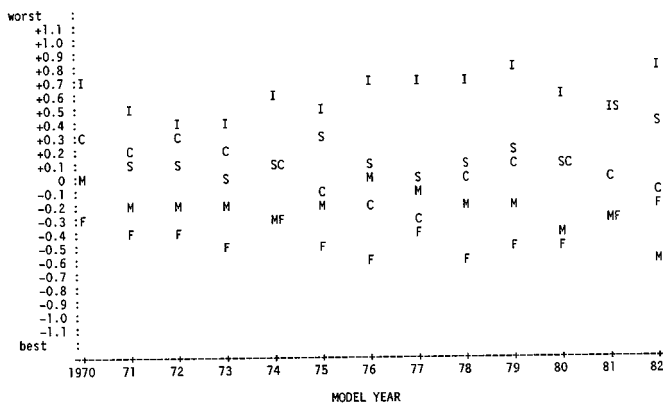

Figure 6. Rollover Fatality Risk by Model Year and Car Market Class (LOGROLL; I = Import, S = Subcompact, C = Compact, M = Midsized, F = Full Sized)

have higher fatality risk. Consistently, full-sized cars are at the bottom of the chart and imports at the top.

Figures 2 (nonfatal rollover propensity) and 6 (fatal rollover propensity) are graphed on the same logarithmic scale. Although the figures look quite similar, it is readily seen that the range of values in Figure 2 is larger than in Figure 6. In other words, the increased rollover propensity of small cars relative to large cars translates to a somewhat smaller increase in fatality risk. That is because many of the additional rollovers of small cars (in situations where a large car would have stayed on the road or at least remained upright) are in crashes of low severity unlikely to result in fatalities.

A key task of the analysis is to separate the effects of rollover propensity and crashworthiness in the fatality index. NHTSA's evaluation uses two independent methods for separating the effects. One is a log-linear regression of rollover fatality risk (LOGROLL) by curb weight, track width, wheelbase and vehicle age [5], pp. 149-167 (actually, separate regressions are performed for ejection and nonejection fatalities). The regression equations are similar to those obtained from the Texas

data (see above) and indicate little or no change in crashworthiness after the early 1970's.

The other approach is to adjust the rollover fatality risk index (LOGROLL, based on FARS data) for changes in rollover propensity (LOGR2, based on Texas data, as shown in Figure 2). NHTSA's evaluation [5], pp. 169-183, suggests that

NEWROLL2 = LOGROLL - LOGR2/1.9

is the mathematical combination of LOGROLL and LOGR2 which most closely indicates the trend in overall fatality risk in rollovers, after controlling for changes in rollover propensity—i.e., it is a measure of rollover crashworthiness. Since car size is the prime determinant of rollover propensity, NEWROLL2 also measures rollover fatality risk adjusted for car size. NEWROLL2 is graphed by model year and market class in Figure 7. Figures 6 and 7 are graphed to the same logarithmic scale—i.e., vertical distances have the same meaning in both graphs. Virtually all of the variation across market classes and model years in Figure 6 is eliminated in Figure 7. The various market classes have nearly identical crashworthiness values (except toward the right end of the graph where sparse data result in some variation).

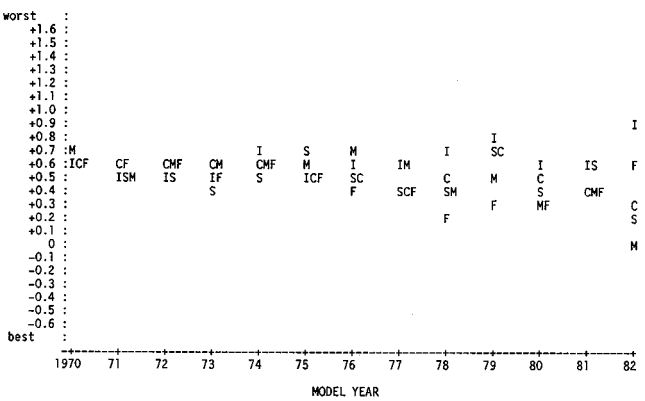

Figure 7. Rollover Fatality Risk by Model Year and Market Class, *Adjusted for Car Size* (NEWROLL2; I = Import, S = Subcompact, C = Compact, M = Midsized, F = Full Sized)

Figure 8 shows the rollover fatality risk index by model year—*adjusted for rollover propensity/car size*. The data points "A" ("adjusted" for car size) are the anti-logarithms of the average values of NEWROLL2 across the various market classes, indexed so that the average ratio for 1975-80 comes out to 100. This crashworthiness index is close to 100 and remains essentially unchanged throughout 1970-82. The large increase in rollover fatality risk during 1970-82 (Figure 5) is not due to a change in crashworthiness but rollover propensity—i.e., car size.

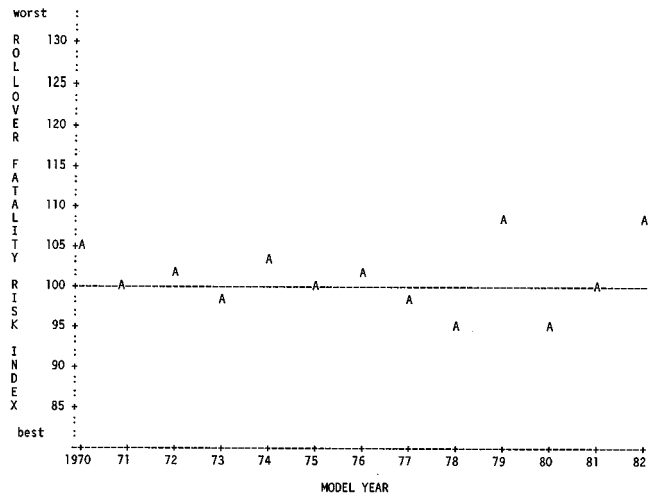

Figure 8. Rollover Fatality Risk Index by Model Year, *Adjusted for Car Size*

Estimation of the Fatality Increase

During calendar years 1987-88, there were an average of 4500 fatalities per year in primary rollover crashes of passenger cars. By 1988, the mix of passenger cars on the road had size and weight characteristics similar to the model year 1982 fleet. In other words, the "baseline" estimate of rollover fatalities, given model year 1982 car sizes and the calendar year 1987-88 driving environment is 4500 per year.

How much lower would the number of fatalities had been, given model year 1970-75 car sizes in the calendar year 1987-88.driving environment? Figure 5 displays the rollover fatality risk index by model year. A smooth curve through the data points yields the following values [5], p. 209:

1970	91	1975	90	1979	103
1971	90	1976	93	1980	107
1972	89	1977	96	1981	115
1973	88	1978	100	1982	123
1974	89				

The baseline fleet of model year 1982 vehicles, with a fatality risk index of 123, experiences 4500 rollover fatalities per year. A fleet of model year 1970-75 vehicles, with an average risk index of 90, would experience 4500 (90/123) = 3300 rollover fatalities, which is 1200 fewer than the baseline model year 1982 cars. The increase of 1200 fatalities between model years 1975 and 1982 occurred despite a major shift from 2 door cars to 4 door cars during the same period. According to NHTSA's evaluation, the shift from 2 door to 4 door cars prevents 140 ejection fatalities per year [5], pp. 218-219. Thus, the net fatality increase due to car size reductions is 1200 + 140 = 1340 fatalities per year.

NHTSA's evaluation attempts to subdivide the net loss of 1340 lives per year according to the various mechanisms of car size changes [5], pp. 216-227:

	Lives per Year Saved	Lost
Market shift from full-sized to imported/subcompact cars		1220
Downsizing within domestic car lines		350
Wider tracks for some imported cars	230	
SUBTOTALS	230	1570
NET LIVES LOST PER YEAR		1340

These individual estimates are derived from the evaluation's regression equations of rollover fatality risk by curb weight, track width and wheelbase [5], pp. 149-167. These regression models assigned a large influence to track width and less influence to wheelbase and curb weight. Since the vehicle size parameters are highly intercorrelated, it is possible that the models partly confused their effects. If so, the benefits of "wider tracks for imported cars" would be overstated and the losses for market shift and downsizing likewise overstated. The net loss of 1340 lives per year, on the other hand, is a more accurate estimate which does not depend on the regression coefficients.

While the methods of this report are appropriate for estimating the effect of historical changes in car size on rollover fatality risk, it would be inadvisable to use them to predict what might happen in the future if a single parameter (say, curb weight) is changed while others are held constant.

References

[1] Garrett, John W. "A Study of Rollover in Rural U.S. Automobile Accidents." SAE Paper No. 680772 in *Proceedings of Twelfth Stapp Car Crash Conference*. New York: Society of Automotive Engineers, 1968.

[2] Griffin, Lindsay I. III. *Probability of Overturn in Single Vehicle Accidents as a Function of Road Type and Passenger Car Curb Weight*. College Station, TX: Texas Transportation Institute, [1981].

[3] Harwin, E. Anna, and Brewer, Howell K. *Analysis of the Relationship between Vehicle Rollover Stability and Rollover Risk Using the NHTSA CARDfile Accident Database*. Washington: National Highway Traffic Safety Administration, to appear in 1989.

[4] Jones, Ian S. "Overturning in Single Vehicle Accidents." *Accident Analysis*. London: Planning and Transport Research and Computation Co., 1973.

[5] Kahane, Charles J. *An Evaluation of Door Locks and Roof Crush Resistance of Passenger Cars—Federal Motor Vehicle Safety Standards 206 and 216*. Report No. DOT HS 807 489. Washington: National Highway Traffic Safety Administration, [1989].

[6] Malliaris, A. C.; Nicholson, Robert M.: Hedlund, James H.; and Scheiner, Stanley R. *Problems in Crash Avoidance and in Crash Avoidance Research*. SAE Paper No. 830560. Warrendale, PA: Society of Automotive Engineers, [1983].

[7] Partyka, Susan C., and Boehly, William A. "Passenger Car Weight and Injury Severity in Single Vehicle Nonrollover Crashes." *Twelfth International Technical Conference on Experimental Safety Vehicles*. Washington: National Highway Traffic Safety Administration, 1989.

[8] Technical Evaluation of Rulemaking Petition. Attachment to memorandum by Scott Shadle to NHTSA Docket No. PRM-MP-004-13. Washington: National Highway Traffic Safety Administration, August 12, 1988.

Technical Session 7
Crash Avoidance Research

Chairperson: Kare Rumar, Sweden

S7-O-01

Wheels Anti-Lock Systems for Big Series Passenger Cars

P. Brun
PSA Peugeot - Citroen

Introduction

From the outset, braking system development has made a considerable contribution to automobile safety progress. Thus, successively, with the arrival of hydraulic control (Peugeot 202 in 1946), front disc brakes as standard and high-pressure regulated braking (Citroen DS in 1954), ventilated discs (504, in 1968), then anti-lock brakes (CX in 1981 and 505 in 1985), Peugeot and Citroen have never stopped developing active automotive safety.

Today, in this field, the PSA Group breaks new ground by offering an anti-lock system on 309, 205, 106 and AX. In fact, until now, only higher-segment vehicles, for reasons of cost, could be fitted with this equipment. Henceforth, technological development has enabled the fitting on small vehicles of a new twin-captor specific anti-locking device for a modest price. Thus PSA offers the greatest number of possibilities of acquiring this major safety system.

Anti-Lock Braking System (ABR)

When a vehicle brakes, the maximum deceleration to which it can be subject is limited by the laws of physics. It depends on the adhesion between the tyre and the road. This adhesion is characterised by a factor which can vary from 0 (no adhesion) to more than 1, and generally equates to 0.9 on a dry tarmac road, 0.6 in rain, and can drop to 0.1 on icy surfaces.

As soon as braking starts, a slight sliding of the wheels on the ground appears. Longitudinal adhesion is a function of the wheels sliding on the road and thus determines the vehicle deceleration capability. According to the graph below, potential deceleration is at its maximum for a slide between 10 and 30%. However, if the force applied by the driver on the brake pedal is too great in relation to the available adhesion, sliding rapidly increases to reach the 100% value, i.e. the wheels lock, (Figure 1).

This has three consequences:

- total loss of vehicle directional control resulting in the inability to avoid an obstacle or to stay on the road (the tyre slides on the road surface instead of turning).

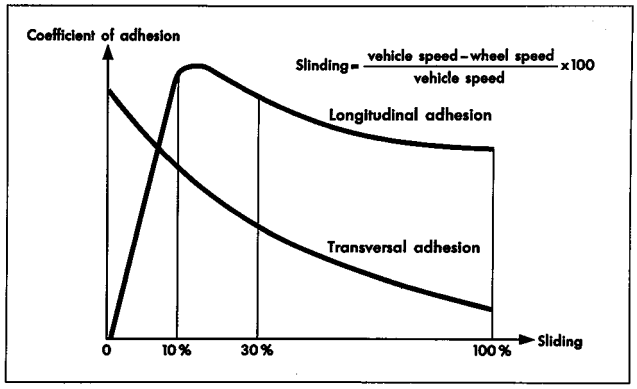

Figure 1. Adhesion as a Function of the Wheel Speed

- major vehicle instability, which may cause spinning (due to a fall in the transversal adhesion of the rear axle).
- stopping distance increase (due to a decrease in longitudinal adhesion).

Furthermore, wheel locking on high adhesion causes major tyre wear with the tread being scraped and a "flat spot" being produced. For reasons of safety and comfort, early tyre replacement is then necessary.

Therefore the ABR system aims at optimising vehicle braking in all circumstances, under all conditions of adhesion. It maintains wheel sliding within the ideal sliding band and naturally removes any risk of locking, (Figure 2).

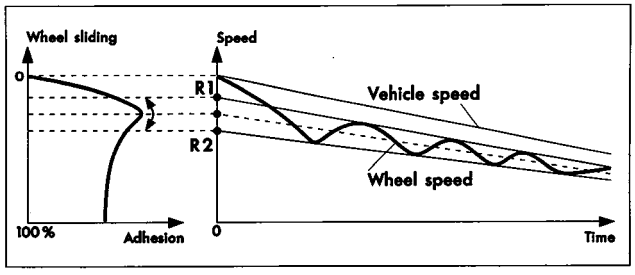

Figure 2. ABR Wheel Speed Control in Relation to Optimum Sliding

For this, an electro-hydraulic system is used which, during braking and if required, reduces hydraulic pressure to the brakes and quickly regulates it in relation to available adhesion. The complete system is controlled by an electronic calculator which receives wheel rotation speed signals. After comparing and analysing these

signals, the calculator can determine the actual speed of the vehicle and the wheels which are close to locking.

The ABR Evolution for Big Series Passenger Cars

Anti-lock brake systems are today widespread in France, Europe and worldwide. However, their application is generally limited to the higher market segments. The main reason for this is the relatively high cost of these systems (FF.9,600 for a 605, FF9,300 for a 405, FF9,500 for a BX or an XM). This renders such systems almost incompatible with vehicles of the bottom and lower middle segments.

Thus, in order to increase the availability of this safety system, henceforth PSA offers on certain vehicles (309 GTI, XS and Srdt, 205 GTI and TurboD, AX GTI, 106 XT and XSi, ...) a new type of anti-lock system: ABR with twin wheel-speed sensors and twin independent regulation channels (one per brake circuit). In fact, whilst usually the speed of each of the four vehicle wheels is monitored, here only the two front wheel speeds are measured and transmitted to the calculator.

This new system, developed here by the BENDIX Company, is perfectly suited to the vehicles already mentioned, due to its lower cost (notably fewer components), its lower weight and smaller volume (installation problems on small vehicles). As an example, in November 1991, the twin sensor ABR offered as an option on the 205 costs FF6,000, whilst the basic price of a 205 GTI 1 .9L is FF101,300 and the TurboD FF85,900. In the same vein, ABR for the 309 costs FF6,200, whilst the 309 GTI costs FF108,900, and the 309 XS 1 .9L costs FF85,100. Finally, the AX GTI, sold at FF83,100, requires an extra FF6,000 for ABR.

ABR Twin Sensor System Description

The twin sensor ABR system is part of the add-on anti-lock braking system family: it is added to a conventional braking system. The system comprises:

- brake pedal
- vacuum brake servo
- dual master cylinder with special anti-lock valves (in order to withstand back-pressure)
- dual "X" braking circuits
- additional pressure regulator hydraulic block with four solenoid valves
- calculator: separate electronic box with 35-way connector and corresponding electrical wiring. It can be fitted in the boot (205), in the central dashboard inside the vehicle (309) or even in the engine compartment (106, AX) which requires very high mechanical and thermal resistance.
- system check warning light on the dashboard
- special transmission with a hemispherically-cut 48-tooth acoustic crown wheel
- two wheel-speed inductive sensors, mounted on each front wheel pivot (specific). They detect variations in magnetic flux caused by the teeth passing across the pole. These variations induce an alternating current (sinusoidal signal) in the coil and their frequency and amplitude are proportional to the wheel rotational speed, (Figure 3, Figure 4).
- two axle-load dependent compensators to distribute braking effort to the rear wheels
- front disc brakes
- rear disc or drum brakes, (Figure 5).

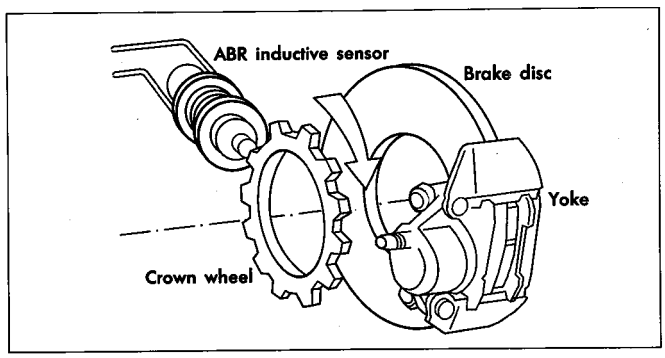

Figure 3. Wheel Speed Sensor

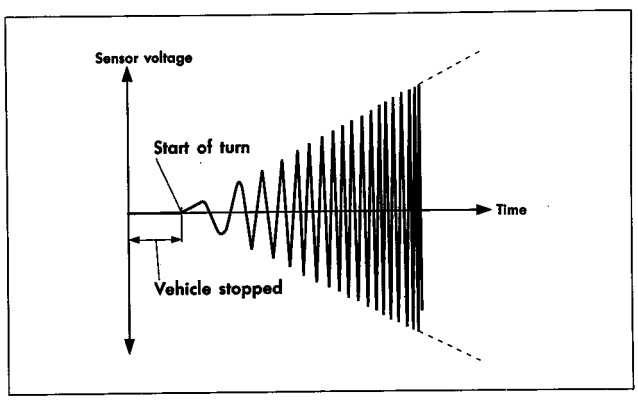

Figure 4. Signal Produced by Wheel Speed Sensor

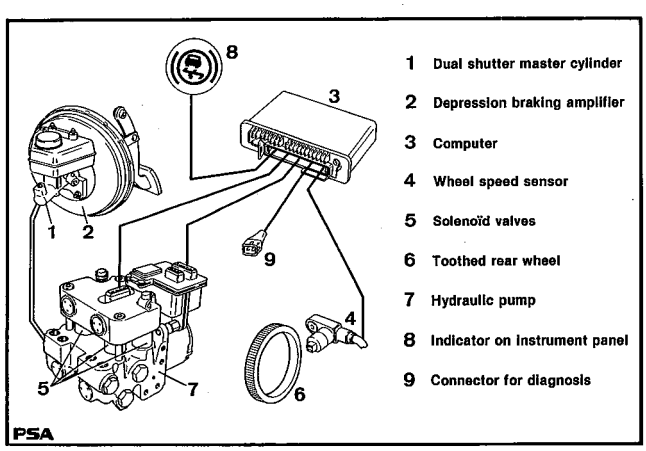

Figure 5. Additional 2 Sensor-ABR System (Anti-Lock System)

Specific Features of the Twin Sensor Anti-Lock System

- **"X" braking circuit requirement.** In order to be able to optimise the front and rear brake pressure regulation, the twin sensor ABR system must be installed on a dual "X" braking system (left-front linked to right-rear, with interlinkage for symmetry). A front-rear brake system such as on the 205 GTI 1600, would not enable good results to be obtained (no regulation at the rear), and for this reason it is changed to an "X" system, with the ABR option, (Figure 6).

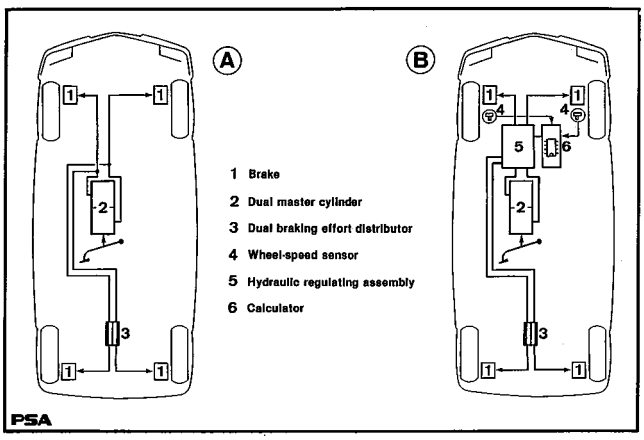

Figure 6. A: Dual "X" Braking Circuit. B: Dual "X" Braking Circuit with Additional Dual Sensor ABR

- **Special hydraulic assembly.** The hydraulic assembly used for the anti-lock system has two sensors and two regulation channels, comprising four solenoid valves. The latter modulate braking pressure in situations outside the optimal wheel sliding band. These solenoid valves operate in an "all or nothing" mode, with a reaction time of around 3 to 7 ms. Two valves are fitted on each channel, the first being an inlet-exhaust solenoid valve and the second acting as a restrictive valve for slow pressure variation. Therefore, four basic pressure variation categories are available: inlet and release, quick or slow. From this, by modifying the control time of each solenoid valve, intermediate pressure rise and fall curves can be obtained, thus ensuring fine pressure regulation, (Figure 7). The group also comprises:
  - an electric motor driving two pumps (one per channel) to return brake fluid towards the master cylinder after the pressure reduction phases.
  - two low-pressure reservoirs (one per channel) which fill rapidly when pressure drops.
  - two high-pressure reservoirs (one per channel) limiting pulsation due to pump pressure rise waves.
  - two anti-pulsation valves (one per channel) used as a restriction between the pump and the master cylinder in order to reduce brake pedal movement under regulation.

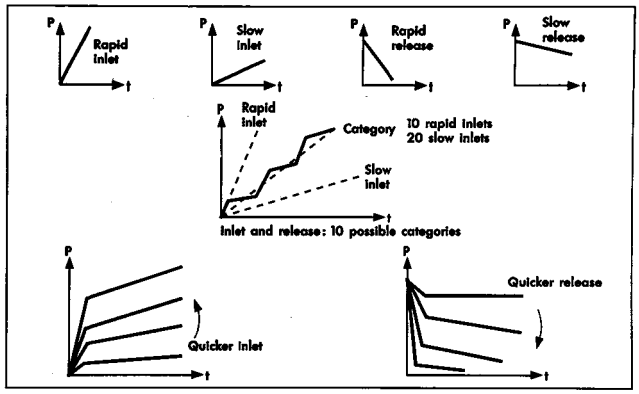

Figure 7. Pressure Categories

- **More precise regulation logic.** Only the speed of the two front vehicle wheels is known. This renders the all-important determining of absolute vehicle speed in relation to the ground much more delicate. The problem is further increased by the fact that these wheels are motorised, notably the difficulty of interpreting wheel-spin and regaining adhesion. Due to this, additional algorithms are required in the ABR regulation logic and this has led to a far more complex development of the system.
- **Optimising braking effort distribution.** In the absence of speed sensors on the rear wheels, their locking can only be avoided by judicious front-rear distribution of braking effort. In fact, it is required that under all circumstances and notably under all loads, each rear brake has:
  - a pressure lower than that required to lock the wheel,
  - a pressure as high as possible in order to obtain best benefit of available adhesion and to have the shortest stopping distances.

  In order to achieve these high-level performances, relating as far as possible to those of a four-sensor system, a high-performance braking distribution system has been adopted: two axle-load dependent compensators (one upstream of each rear brake on the dual "X" circuit). This enables the system to operate as close as possible underneath the ideal pressure distribution curve, (Figure 8).

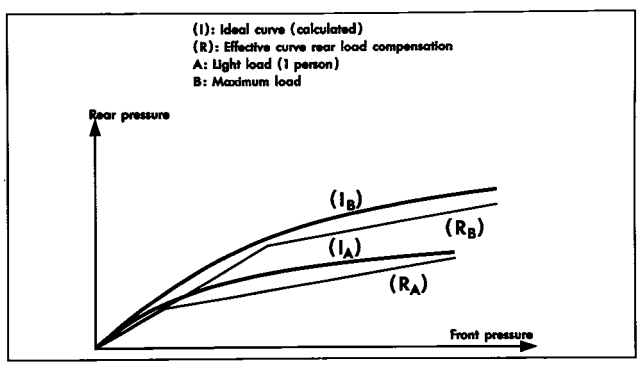

Figure 8. Braking Distribution

Load compensation control is in fact highly recommended for light vehicles which are particularly sensitive to mass variations over the rear axle, and for short wheel-base vehicles which are sensitive to mass transfers towards the front under braking.

The Twin Sensor ABR System Calculator and Safety

For operational safety reasons, the numerical calculator designed by BENDIX for this ABR has two distinct micro- processors:

- a main 16-bit Intel 8096 main processor which:
  - executes the solenoid valve software programme
  - carries out fault detection: sensors, solenoid valves, pump motor, relays, loom
  - controls self-diagnosis and stores fault codes in non-volatile memory.
- a monitoring 8-bit Motorola 6805 processor which:
  - calculates the coherence of the speed sensors
  - checks the coherence of the solenoid valve controls performed by the 8096
  - dialogues with the 8096, (Figure 9).

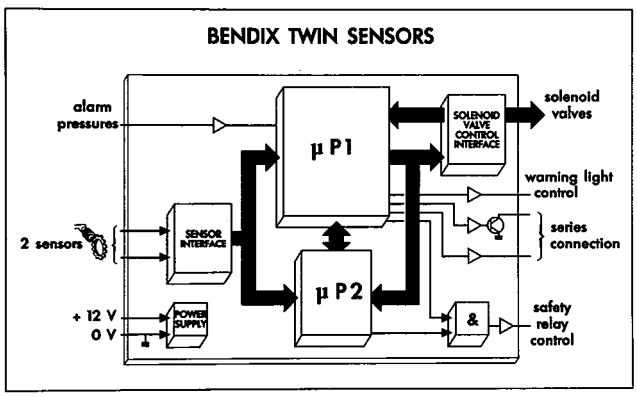

Figure 9. Electronic Calculator

In the event of disagreement between the two microprocessors, the safety relay is activated and cancels the ABR function without modifying the conventional braking system and the ABR warning light is illuminated on the dashboard. In certain cases, with very localised faults in the ABR system, the calculator can adapt itself and continue to operate in "degraded" mode.

ABR Self-Diagnostics

To help maintenance and trouble-shooting, the calculator is fitted with a self-diagnostic device, enabling the detection by a series of luminous flashes of the type of defect present in memory. It operates as follows:

- each element is linked to a number (e.g. for the front-left inlet-exhaust solenoid valve: code 44);
- when the fault appears, the code is memorised in the calculator's non-volatile memory (code saved in the event of the box being removed from the vehicle);
- this code remains in memory even if the fault disappears;
- this code can be sent on request either by a serial connection (at the factory), or by luminous flashes by connecting a bulb to the diagnostic socket, or by using a special device, the TAD 99 (Self-diagnostic Tester), which automatically carries out the diagnostic request and clearly registers the fault code;
- after repair, it is necessary to wipe this code from the calculator memory by earthing the diagnostic lead for 10 seconds or by pressing the "erase" button on the TAD 99, (Figure 10).

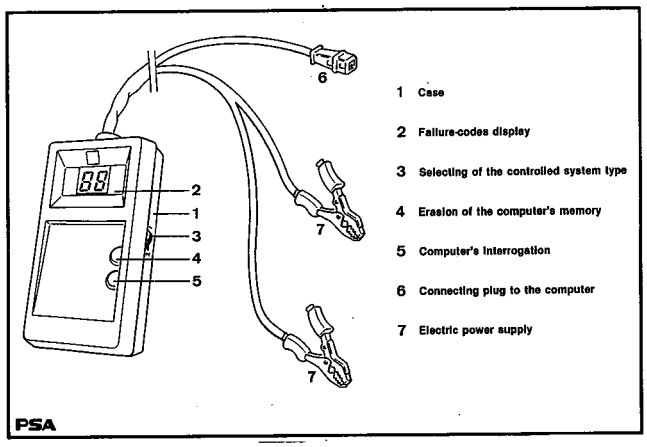

Figure 10. Auto-Diagnosis Tester TAD 99

The Twin Sensor ABR Development

The development and manufacture of anti-lock systems such as the twin sensor ABR fitted to PSA vehicles are entrusted to outside suppliers such as BENDIX, in the present example. In fact, the relative complexity of the product and the high investment costs—notably in terms of testing—make this activity difficult to integrate within the structure of a large general manufacturer such as PSA.

Thus, for each new model study, the supplier has for several months a sufficient supply of mechanically representative vehicles to be able to adapt his anti-lock system. After fitting out these vehicles, they are taken for the entire winter for testing on the large frozen lakes in Sweden. In a small town near the Arctic Circle, one can find the majority of anti-lock manufacturers. There, they have many low- adhesion test tracks on which it is possible to travel at 150 kph and to brake hard in almost complete safety. Under these conditions, which cannot be reproduced in France, the delicate development of the anti-lock system software programme for each vehicle is perfected.

Validating the Twin Sensor ABR System at PSA

On receipt of the new ABR system, PSA validates it by a test programme which takes place:

- in Sweden, on the frozen lakes used by the suppliers,
- in France, on special tracks which are particularly valid for high and average adhesion.

The PSA validation tests are as follows (in each situation there is maximum braking with ABR intervention):

- Directional control. Vehicle directional control in the following cases:
  - braking whilst avoiding an obstacle
  - braking whilst changing one or two lanes
  - braking on skid pans
  - braking in a straight line and on entering bends
  - braking on leaving bends
- Vehicle stability. Correct rear axle tracking (same conditions as directional control).
- Stopping distances. Measurements in relation to initial speed and adhesion.
- Left-right asymmetric adhesion (or mu-split). This occurs when two wheels on the same side have high adhesion (tarmac) and the two others have low adhesion (snow, wet grass on the verge, for example). In these conditions, braking inevitably creates an often brutal yawing movement, which takes the vehicles towards the most adhesive side. Strong and sharp correction of the steering wheel is then necessary. In the most critical cases (high adhesion asymmetry), the vehicles spins round. ABR prevents any locking of the front wheel, notably on the side with less adhesion (with this twin sensor system, locking of the rear wheel on low adhesion is permissible). This enables the tyres to maintain optimal transversal adhesion and thus the vehicle resists as far as possible the turning torque. Furthermore, ABR can delay the pressure rise in the more adhesive side (momentary partial under-braking). This diminishes the yawing effect and the steering wheel correction can be made by any driver.
- Adhesion transition. This is the study, during straight-line braking, of the passing from high to low adhesion and vice versa. Pedal height variations and system reaction speed are the particular fields of analysis.
- Pedal comfort-filtering. Pedal movement in the regulation phase is unavoidable and must be attenuated, but not necessarily suppressed; in fact these are the warning signals alerting the driver that he is at the limit of adhesion. The three analysis criteria are: oscillation, vibration, travel.
- Comfort-operating noise. The noise is basically caused by the pump and solenoid valve operation and this highlights the importance of selecting the correct location for the hydraulic block and acoustically insulating it.
- ABR extreme operating conditions:
  - rapid braking release and re-application
  - linked over-acceleration and braking
  - rebound braking/jumping (instantaneous locking)
  - braking over mixed adhesion surfaces.

All these tests are carried out at different speeds, with the clutch engaged and disengaged, and with varying levels of adhesion.

Dual Sensor and Four Sensor ABR System Comparison

In order to highlight the effectiveness of the BENDIX twin sensor ABR system in the vehicles into which it is fitted, below is a comparison with a four sensor system, in accordance with two of the previously listed criteria: stopping distance and directional stability.

Two vehicles, A and B, are used. A is fitted with the BENDIX twin sensor ABR, whilst B has a competitor's highly reputed four sensor ABR system.

Furthermore, these two vehicles are absolulely identical and tested under the same conditions:

- identical vehicle mass
- identical tyres, same wear condition, same inflation pressure
- identical braking distribution systems
- identical brake pads, with the same degree of wear.

The vehicle comparison is simultaneous to remove any variations in adhesion.

- Stopping distance comparison. The distance required to come to a complete halt is measured, with the vehicle's ABR system in permanent use (therefore with maximum pedal pressure). Comparison is made for varying levels of adhesion and at different speeds. Each result is taken from the average of 10 tests, 5 of which were completed with the clutch engaged, (Figure 11).

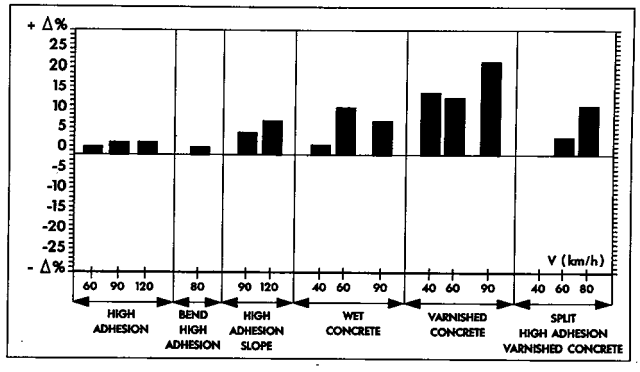

Figure 11. Stopping Distance Variations: Twin Sensors ABR BENDIX Compared with the Four Sensors Benchmark (Vehicle in Charge)

It was noted, in accordance with our expectations, that on average the twin sensor ABR system offers a slightly lower performance than a four sensor system. However, the measured average increase in stopping distance—about 10%—remains well below the 30 to 40% measured between braking with

locked wheels and braking with four sensor ABR. In the specific example of high adhesion, the performance of both systems is comparable, as the stopping distance increase is only 3%, whilst with locked wheels + 20% was measured.

- Low adhesion directional stability comparison. The vehicle is in a circle of radius 250m, with a solid ice surface. Vmax is the maximum speed around this curve without steering wheel correction. The initial test speed is taken as 0.9 x Vmax and braking to come to a halt is carried out in the curve, clutch engaged, without steering wheel correction. The stopping distances and deviation at the end of braking are measured, (Figure 12, Figure 13).

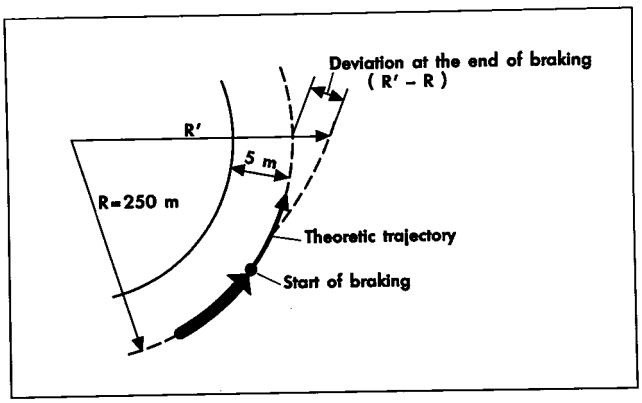

Figure 12. Operating Method

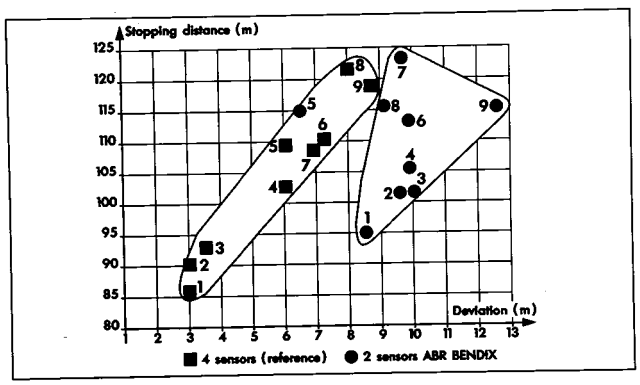

Figure 13. Directional Stability on Natural Low Adhesion Surface: Stopping Distances and Comparative Curve Deviation

The results show that the variation in stopping distances correlate with previous tests. The deviation becomes greater with the twin sensor ABR system, but remains within acceptable limits, as it is low, bearing in mind the low levels of adhesion. Furthermore, it is incontestably superior to that (hypothetical) that would be measured with locked wheels because, in this case, the vehicle would spin around at the start of braking. The notions of deviation and stopping distance would therefore be academic.

Furthermore, to enable comparisons to be made, the test described here was carried out without steering wheel correction. However, any driver could of course reduce deviation by taking appropriate corrective action.

ABR: Pratical Driving Recommendations

The anti-lock wheel system thus enables optimum automatic use of available adhesion. But it is not able to correct for a style of driving which is not appropriate to traffic and road conditions. It is not a licence for imprudent driving. In particular, stopping distances must still be considered as well the speed at which bends are negotiated, because these are governed by unchangeable physical laws. Furthermore, the serviceable condition of the vehicle remains of primary importance: shock absorbers, brakes, tyres.

In the event of heavy braking:

- On a slippery surface, as soon as one wheel has a tendency to lock, the ABR is activated. Then maximum brake pressure should be applied without pumping. For the driver, this is felt by brake pedal oscillations and heavy clicking noises (solenoid valve actuation) and some shudders in vehicle deceleration, corresponding to the successive brake pressure rises and falls during the ABR regulation phase.
- On a dry surface, it is also possible to hear tyre squeal, which corresponds to optimum wheel sliding (governed by the ABR system) representing the best possible use of the available adhesion.

Conclusion

The advantage of the ABR twin sensor system, proven and fitted on small vehicles at PEUGEOT and CITROEN, clearly shows through the various tests. Without equalling that of a system with four sensor reference points, it does achieve a very high level of performance, under any tyre/road adhesion conditions. Its modest price and its excellent price/performance ratio have thus become major advantages which today enable the PSA Group to offer to the widest clientele a true anti-lock system, a fundamental element in automobile safety.

Acknowledgment

We express our thanks to: BENDIX France for all their assistance in producing this article.

S7-O-02

Improvements in Active Safety by Innovation for Automatic Stability Control Systems

Dr.-Ing. Heinz Leffler
BMW AG

Abstract

Additionally to the already available ASC and ASC+T of the BMW top models newly designed stability control systems will become introduced in the 3-series and 5-series BMW cars. All these systems are applicable on mechanic and automatic gearbox-equipped cars. Whereas ASC, available at BMW since '87, is a pure engine-control system, where reduction of engine torque is used to avoid stability-critical situations on low-μ road surfaces, the latest Automatic Stability Control Systems of BMW (ASC+T) additionally apply active braking to the driven wheels. The engine control of BMW's ASC-systems is based on a selected interface structure of engine management and transmission control units. Throttle control as well as active braking is realized differently depending on the respective model range. Whereas the BMW 750i and 850i use bifluid hydraulic units in add-on technique for ASC, ABS-integrated hydraulics in open or semi-open versions will be applied to the other types of the BMW model range. The newly designed ABS-integrated ASC-systems form the basis for further increased penetration of the car market with stability control systems. The different systems described in this paper show remarkable improvements in vehicle stability as well as in traction capability during critical driving situations. Performance data and statistical analysis of test results obtained with ASC-equipped cars prove, that the Automatic Stability Control Systems contribute significantly to improve active safety.

Introduction

Safety control systems suffer from the matter of fact, that their presence in nearly all cases is not recognizable inside or outside the car. To convince a customer of the advantages cf a safety system, thus requires a well-established argumentation or customer's experience having mastered a critical situation only because of the safety control system in his car.

Among other safety control systems Anti-Lock Braking Systems (ABS) and—as a quasi inversion of the ABS—Automatic Stability Control Systems ASC, contribute greatly to improve active safety of passenger cars as well as of commercial vehicles and buses. BMW as a manufacturer of passenger cars have rewarded the safety consciousness of their customers and are equipping all their models with ABS as a standard.

Automatic Stability Control Systems ASC have been introduced in 1987 for some top-of-the-range cars and meet just nowadays the phase of integration and application from top to bottom range of the production line.

As a result of the engineering work linked with this introduction-phase, BMW have designed—together with their suppliers Bosch and Teves—two ABS-integrated stability- and traction-control systems which will be introduced in the 325i and 525i at the beginning of 1992. The integration of the ASC-controller and the ASC-hydraulics in the existing ABS-system forms a very space- and weight-optimized design, which will become the basis for further future engineering work around brake and stability-control systems.

ASC-Systems at BMW

Two categories of ASC-systems are available at BMW nowadays. Pure stability-control systems which influence engine only, were introduced in 1987. To improve traction especially on friction-splitted surfaces, the introduction of a differential brake effect with the ASC+T in 1989 led to a remarkable progress [1]. Further integration of hydraulics and electronics resulted in innovative ASC-systems, with a common hardware which simultaneously is applied for ABS- and ASC-control.

Figure 1 gives a general view of the control circuits applied to the different systems as well as a relation to the adjacent BMW models. The rate of integration of the hydraulics and the electronics can also be picked-up.

	ASC	ASC+T		
BMW Model Range	535i/iA, 730i/iA, 735i/iA, 750i/iA, 850iA	750iA, 850i/iA	525i/iA	325i/iA
Throttle	X (EML)	X (EML)	X (ADS2)	X (ADS2)
Ignition/ Injection Cutout	X	-	X	X
Ignition Timing	X	X	X	X
Differential Brake	-	X	X	X
Add-On ASC-Hydraulics	-	X	-	-
ABS-Integrated ASC-Hydraulics	-	-	X	X
ABS-Integrated ASC-Electronics	X	X	X	X

EML: Electronically Controlled Throttle
ADS2: Electro-Mechanical Throttle Actuator

Figure 1. ASC/ASC+T, Comparison of Control Circuits

The ASC communicates with the engine and transmission management to reduce excessive wheel slip at the driven wheels, starting or driving on stability-critical road surfaces. The control circuits to be used for this purpose are the throttle control, the injection- and ignition-cutout and the ignition-timing adjustment. Throttle control takes place by interfacing with the control unit of an electronical accelerator. This

communication link provides the reduction of wheel slip also during situations in which the driver shifts down in low gear or releases the accelerator pedal on low-friction roads, whereby engine drag may be sufficient for causing brake slip at the driven wheels.

Via an interface to the electronics of the automatic gearbox ASC influences the gear-shifting logic in such a manner, that unnecessary gear changing during ASC-control is stopped or modifications of the gear-changing program are initiated to allow earlier shifting in higher gear.

The first ASC+T—T is the abbreviation for traction—used a bi-fluid add-on ASC-hydraulic unit with integrated piston-type nitrogen accumulator to produce a differential brake effect at the driven wheels, which stops excessive wheel slip at one or both wheels of the drive axle, starting or driving on adhesion-critical road surfaces. Besides brake control, throttle control as well as ignition timing are available as control circuits on the ASC+T actually used on BMW's 750i and 850i. Ignition and injection cutout in this system are replaced by the fast brake-control circuit.

In contrast to the add-on ASC+T of the BMW 750i, 850i the ASC+T of the BMW 325i as well as of the 525i are fully ABS-integrated systems, where not only the electronics but also the hydraulics are commonly used for ABS- and ASC-purposes. Both systems are provided with control circuits for brake, throttle, ignition/injection-cutout and ignition timing. The throttle position during ASC-control is modified via an electric motor with integrated gear ratio (ADS2), to reduce the throttle against driver's demand. For this purpose the throttle is equipped with a decoupling unit.

The ASC+T of the BMW 325i is based on the TEVES ABS MKIV with an open hydraulic system, whereas the system foreseen for the BMW 525i uses the ASC-extended Bosch ABS2E with semi-open hydraulics during ASC-mode and closed hydraulic system during ABS-mode. All ASC-systems in use at BMW are applicable on manual gearbox-equipped cars as well as on automatic gearbox one's.

ABS-Integrated ASC+T

System Diagram

The ASC+T of the BMW 325i is based on TEVES' ABS MKIV which was extended hydraulically to allow individual wheel braking at the rear axle and to provide active braking to reduce excessive drive slip. In case of the 325i each modulator consists of a pair of 2/2-stage valves, to allow different pressure steps during ABS- or ASC-control. In Figure 2 the basic layout of the ASC+T of the 325i is presented.

To generate a very fast brake application especially during the first ASC-control cycle a spring-loaded piston accumulator is integrated in the system. System pressure is controlled between 70 bar and 110 bar via an electric pressure switch. To isolate the piston accumulator from

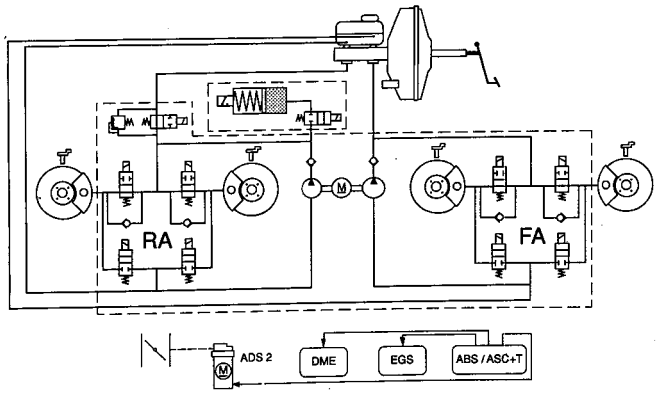

Figure 2. ASC+T of BMW 325i (TEVES System)

the basic brake system a normally closed 2/2-stage valve is incorporated in the accumulator. Separation of master cylinder and rear axle brake circuit during ASC-control is achieved by another—normally opened—2/2-stage valve. Parallel to the latter valve a pressure-relieve valve is required, allowing maximum pressure of 140 bar.

Because of the open hydraulics being used by the TEVES system, certain precautions were required to achieve at least the same safety standard and pedal comfort as with commonly used closed hydraulic-ABS systems. By a sophisticated brake pedal travel logic—a travel sensor is incorporated in the vacuum booster—this ambitious goal was achieved. Additionally the function of the electric-driven pump is monitored by a speed sensor fixed at the electric motor. Wheel-speed sensing takes place via conventional inductive speed pickups detecting speed information of toothed wheels.

The ASC-control of engine and transmission is achieved via an interface structure to the digital motor electronics DME and the control unit of the automatic gearbox EGS. Throttle control is carried out by a separate electric-driven throttle actuator ADS2, which with a bowden wire connected to the throttle can reduce the throttle position with its decoupling mechanism against driver's demand.

Figure 3 shows the basic layout of the Bosch system used on the BMW 525i. Similar to the system of the 325i the ASC+T is based on the ABS. In case of the Bosch system the hydraulic unit is of a slightly different design compared to the non-ASC model. The modulators of the ASC+T of the 525i are of the 3/3-stage type. Like the 325i the number of modulators of the 525i hydraulic unit had to be extended by one, to allow individual wheel braking at the rear axle.

A 3/2-stage solenoid was introduced in the line between master cylinder's rear-axle connection and rear-axle input of the hydraulic unit. In the case of ASC-function this solenoid is energized and interrupts the rear-axle line to the master cylinder. In the energized position the 3/2-stage solenoid connects the pressure circuit via a pressure-relief valve with the reservoir. Relief pressure is nominally 80 bars.

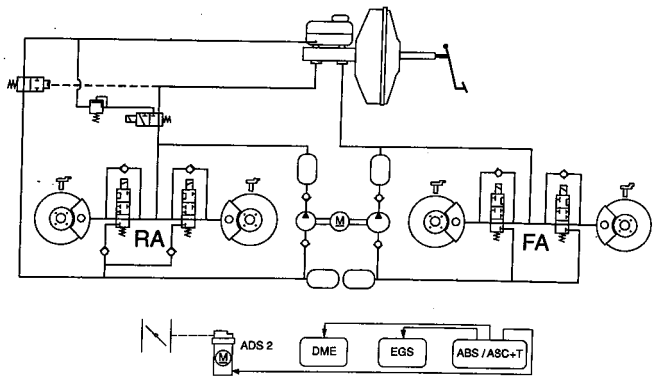

Figure 3. ASC+T of BMW 525i (Bosch System)

In the suction line between pump and reservoir a hydraulically actuated 2/2-stage valve is introduced. Its purpose is to interrupt the connection between open reservoir and closed hydraulic circuit during normal braking or ABS-application.

The engine control during ASC-mode operates basically like with the 325i's system: interfaces exist to the control units of engine and transmission, the throttle is controlled with the same electric actuator ADS2.

Electronic's Block Diagram

The block diagrams of both system's electronics (Fig. 4, 5) indicate that the throttle actuator (ADS2) is controlled by the ABS/ASC-control unit. Whereas the TEVES-system uses 3 identical 87 C 54 controllers to implement the control and safety logic of ABS and ASC as well as for the ADS2 throttle actuator, the Bosch system prefers two C 196 KR micro controllers for ABS/ASC-function and a 68 HC 11 for the ADS2.

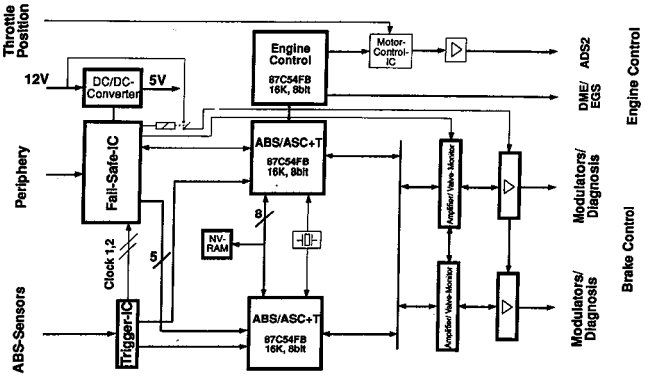

Figure 4. Block Diagram of ABS/ASC+T-Control Unit for BMW 325i

The word length in the TEVES-system is 8 bit, Bosch uses 16 bit for ABS/ASC-logic and 8 bit for the ADS2-control. Practical differences from the word-length limited resolution of the micro-controllers cannot occur, because internal arithmetic operation in the TEVES controller allow the same resolution as the Bosch control unit.

Both electronics serve ISO diagnosis, so that permanent or sporadic system failures can be detected easily. System failures of the ABS or the ASC+T are indicated

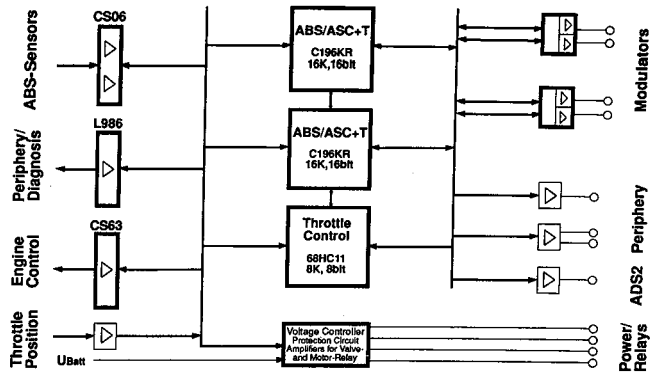

Figure 5. Block Diagram of ABS/ASC+T-Control Unit for BMW 525i

to the driver by two different warning lamps. System failure is indicated by a permanently lighted lamp of the adjacent system, ASC-control is indicated with a 3 Hz flashing of the ASC-lamp.

To generate a position control circuit for the throttle, a throttle potentiometer serves the actual throttle angle to the electronic control unit. Engine speed is considered as well.

ASC+T Controller BMW 325i/525i

ASC-Controllers so far available at BMW either were developed for pure engine control (ASC) or for combined engine and brake control system ASC+T, the latter based on bifluid plunger hydraulics. The ASC+T systems presented here are fully ABS-integrated systems, concerning electronics as well as hydraulics. Therefore new logic structures had to be designed to optimize the respective car and control system on each other.

Outstanding high-lights of the new ASC+T-logic for the BMW 525i are new algorithms for cornering, variable slip thresholds considering different gradients and an increased control frequency. The degree of stability during cornering could be determined more precisely and hill-climbing ability was improved also by selective treatment of individual wheel behaviour driving on a gradient or in hair-pin bends.

By consideration of the engine map, depending on the respective situation, digressive or progressive routines for throttle-control will be applied. As a result of this saw-tooth shaped engine speed behaviour during ASC-control is prevented and the utilization of adhesion is increased.

Figure 6 shows a control cycle of the ASC+T of the BMW 525i on a split-μ test track. Split-μ was between ice and asphalt. Throttle demand was nearly 100%, when the ASC+T by suitably adapted activation of the different control circuits for engine and brake assisted the driver in starting on this critical road surface. Average brake pressure was approximately 30 bars at the brake of the low-μ wheel.

The logic for ASC+T of the BMW 325i has features similar to those of the BMW 525i, but is realized differently of course. Apart from logic-combinations for the

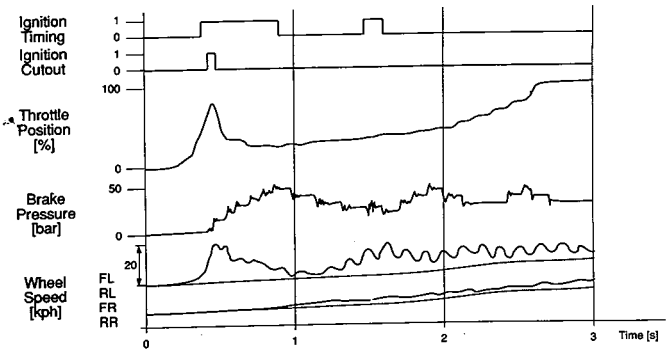

Figure 6. Control Cycle on μ-Split, BMW 525i

detection of cornering and hill-climbing special precautions for the excessive power of the BMW 325i had to be taken into account in order to guarantee control comfort and high utilization of adhesion. Continuous transitions between Select-High and Select-Low control are possible by selective treatment of the control deviation of the tractive wheels. The speed of throttle control is adapted automatically to the momentary slip of the driven wheels.

As an example of a control cycle Figure 7 shows the relevant control circuits of the ASC+T, when starting the BMW 325i on a split-μ road very similar to the one used in Figure 6. The throttle actuation was faster than for the BMW 525i, resulting in slightly longer injection/ignition-cutout. Brake control-pressure with approximately 35 bars also is slightly higher with very small variations about the mean value.

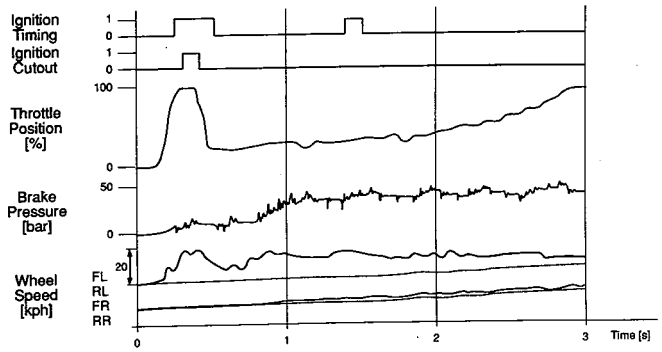

Figure 7. Control Cycle on μ-Split, BMW 325i

Both examples of ASC+T control cycles on μ-splitted roads indicate, that independently of the different basic ASC+T-systems and vehicle concepts a similar system performance is achieved. The vehicle dynamics on different test tracks being presented in the following part will underline this statement.

Stochastic Driving Tests

Comparing cars with and without ASC, very soon leads to the conclusion, that traction and stability are remarkably improved, especially when driving on low-adhesion surfaces. But not only these very obvious singularities prove the benefits of modern brake and drive-slip control systems: also instationary driving tests show, that ASC+T can reduce driver's physiological stress very significantly and improve the active safety of the car/driver system.

Tests on four different test tracks were carried out, to find out, how the benefits of ASC can be quantified. These tracks were

- a handling course with bends of different radii,
- a typical part of this course stimulating ASC-control with bends of changing direction,
- a sinusoidal course,
- another handling course with bends of greater radii allowing maximum speeds up to 180 kph.

From earlier investigation work [2] it was known that the spectral analysis and statistical evaluation of instationary driving manoeuvres was an appropriate technique to compare the influence of ASC on road holding and on driver's effort controlling a car. In this case the description of the interesting vehicle motions in terms of effective values was considered. As a result of this Figure 8 to 10 show by an assessment of yaw rate and steering angle, measured at the steering wheel, to what extent ASC+T influences vehicle dynamics.

Comparing the BMW 325i on wet and dry asphalt handling course, it can be seen, that when switching off the ASC the driver has to generate up to 13.3% higher steering effort to control a car that shows an increase in yaw of 25.8%. The respective figures on dry asphalt are lower: the yaw rate increases by 2.5% only, whereas steering requires 8.0% higher steering angles (Fig. 8).

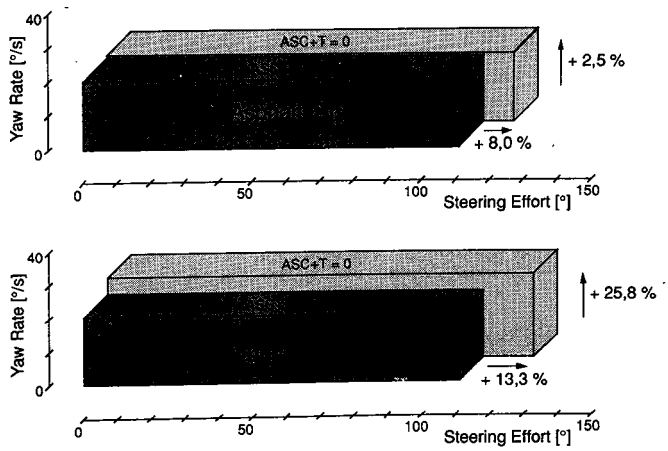

Figure 8. Steering Effort and Yaw Rate, BMW 325i, Handling Course

On a special section of a test track used with the BMW 525i with and without ASC, steering effort increase-c between 7.6% (dry road) and 19.5% (wet road) driving without ASC (Fig. 9). The adjacent yaw rate increase amounts between 5.3% (dry) and 8.0% (wet). The section considered for this investigation consists of a bend with progressively decreasing radius, two bends anti-clockwise and a gradient with a hair-pin bend. Both results prove that with ASC+T a remarkable reduction of driver's stress as well as a lower yaw rate of the car is achievable.

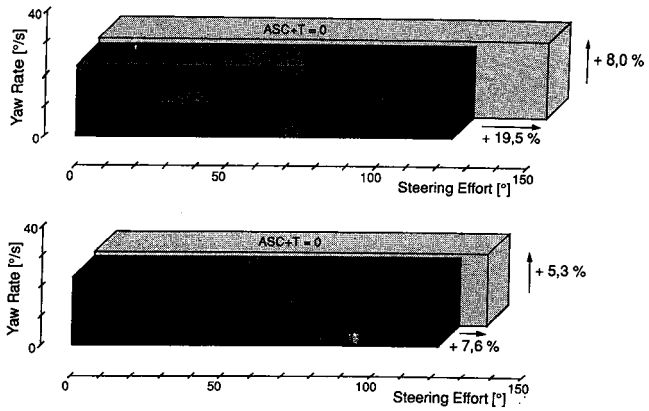

Figure 9. Steering Effort and Yaw Rate, BMW 525i, ASC Section

Comparing the BMW 325i and the BMW 525i on a wet asphalt track with sinusoidal arrangement of bends show, that the improvement in vehicle stability and the reduction in steering effort amount nearly to the same value, independently of the higher adhesion required by the BMW 325i (Fig. 10). Approximately 20% reduced steering effort and 8% lower yaw rate were achieved thanks to ASC+T.

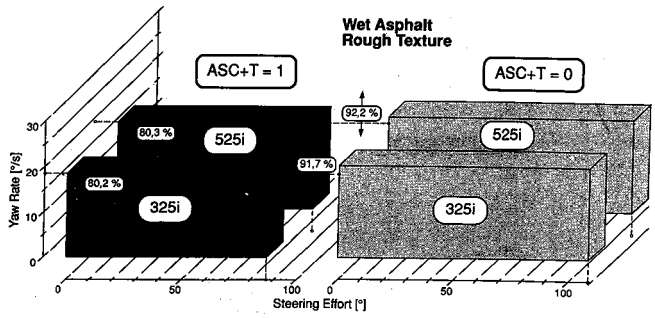

Figure 10. Steering Effort and Yaw Rate, BMW 325i/525i, Sinusoidal-Course

Sometimes people argue, that the increased stability of an ASC-equipped car results from a remarkably lower average speed. Fig. 11 shows a result obtained with the BMW 325i on a high-speed handling course. Driving with ASC indeed reduces average speed by 0.5%—for the sake of a 5.3% reduced yaw rate and a 7.4% decreased steering effort. This result shows, that the improved vehicle stability influences vehicle speed in a neglectable way.

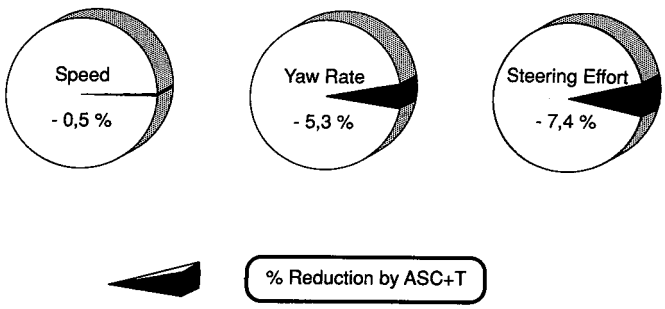

Figure 11. High-Speed Handling-Course, BMW 325i

Traction Performance

By introduction of a differential-brake effect traction performance improves remarkably especially on split-μ surfaces. Fig. 12 shows an example of traction improvement on split-μ gradients of 12% and 16%. Split-μ was 0.15/0.8, whereby the low-μ was represented by an epoxy surface artificially watered so that a water film of constant thickness was generated.

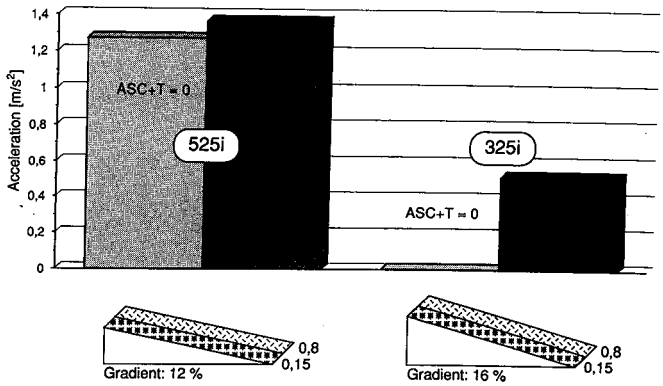

Figure 12. Traction on μ-Split Gradients, BMW 325i/525i

In case of the 12% gradient the BMW 525i was compared with and without ASC+T. Driver's best achieves a mean acceleration of 1.27 m/s², whereby careful application of accelerator pedal is required. Starting with ASC+T, the mean acceleration amounts to 1.36 m/s². This improvement by 7% is achievable without any special precaution from driver's side. All these results were achieved with manual gearbox-equipped cars.

Starting with a 325i on the split-μ 0.15/0.8 gradient of 16% without ASC+T was not possible. Trying the same with control system engaged results in a mean acceleration of 0.52 m/s². This is a convincing result to which degree the superiority also under such extreme conditions is enhanced by ASC+T.

Similarly as with ABS also for ASC+T still some road surfaces are existing, where the controller is asked too much. These surfaces generally consist of loose material like gravel, grit or sandy material. Normally such surfaces produce wheel-slip characteristics where control systems cannot achieve optimal utilization of adhesion.

With the BMW 325i as well as with the 525i a test was carried out on loose gravel. The goal was to accelerate the car from O to 500 m as fast as possible and to do sa with and without ASC+T. Fig. 13 shows the results: driver's best in this case beats the ASC-controller by 7% but of course for the price of increased effort for the driver to keep the car in lane. The BMW 525i with its higher rear axle load achieves in this special test a slightly better acceleration than the 325i (4%).

Cornering

Open-loop and closed-loop tests on a circle of 66.5 m radius were carried out with a BMW 325i. The car was equipped with ASC+T, whereby the system could be

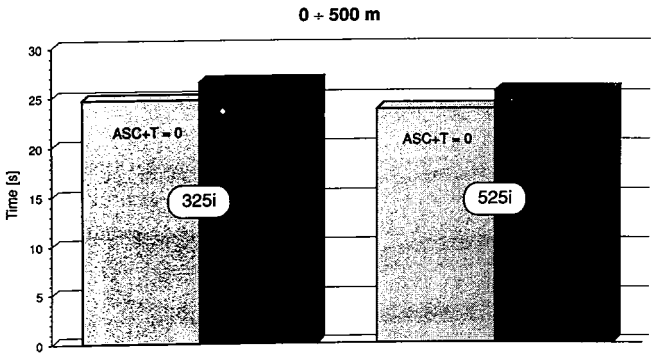

Figure 13. Traction on Loose Gravel, BMW 325i/525i

switched off. The surface of the circle consisted of blue basalt which was permanently watered to reduce its grip. The friction coefficient was approximately 0.3 with some variations depending on the individual shape of the basalt stones.

The car was accelerated on the blue basalt, until it reached its stationary-limit speed. At a predetermined point of the circle the driver had to apply a step input to the accelerator. Depending on the individual test the driver either had to control the vehicle to keep it in lane or to fix the steering wheel in a constant position.

The open-loop test proves, that the ASC+T-equipped car holds its course without bigger variations in its yaw rate. The car with the disengaged ASC+T shows an increased yaw rate which nearly doubles within 1 s (Fig. 14).

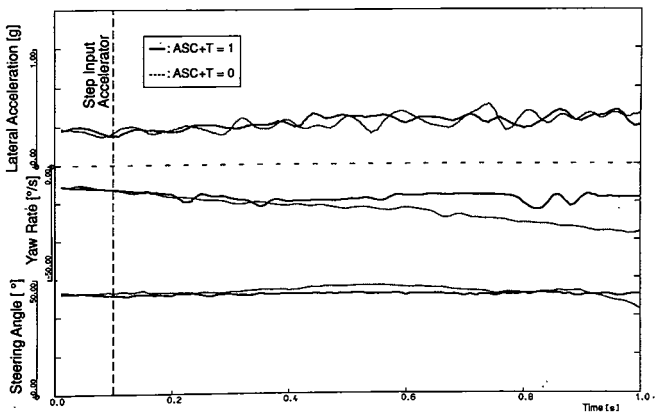

Figure 14. Cornering, Open-Loop, BMW 325i

In the closed-loop test with ASC+T the driver doesn't need to correct the steering angle, when he applies a step input on the accelerator pedal, because the engine torque is limited to a non-critical value. In contrast to the ASC+T not in function the driver starts after 0.5 s countersteering to control the car but again the car ends up with a doubled yaw rate 1 s after step input to the accelerator (Fig. 15).

Results achieved with the BMW 525i show the same tendency, the ASC+T assists the driver very strongly under adhesion-critical conditions driving in bends.

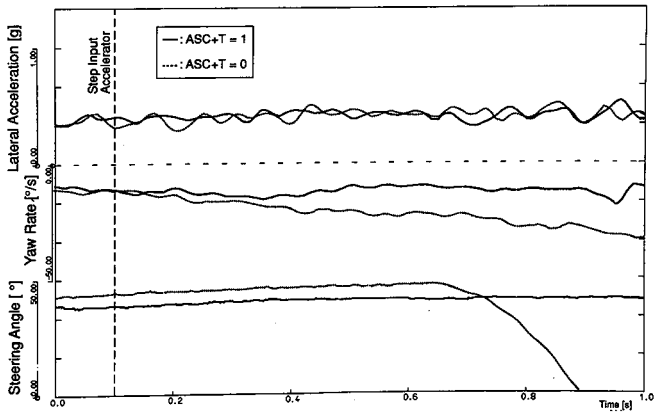

Figure 15. Cornering, Closed-Loop, Step Input to Accelerator, BMW 325i

Car/Trailer Combination

Very often cars are used as tour caravans or boat-trailers. Such combinations normally ar,e speed-limited in most countries because of their more complicated road-holding properties. Generally the increased rear-axle load of a car towing a trailer does not create traction problems, but stability-critical situations very easily can be produced by drivers not aware of the actual adhesion properties between tyre and road.

If the driver doesn't apply the accelerator-pedal carefully while driving around a bend with a car/trailer combination, and encountering drastic changes in the adhesion coefficients from high-μ to low-μ, the stability is heavily impaired. Side force at the rear axle of the car under such conditions can be reduced dramatically, which results in oscillations around the vertical axis of the whole combination. Carrying out the same driving manoeuvre with an ASC+T-equipped car assists the driver in controlling the combination. Fig. 16 shows the comparison with a BMW 325i and a caravan with and without ASC.

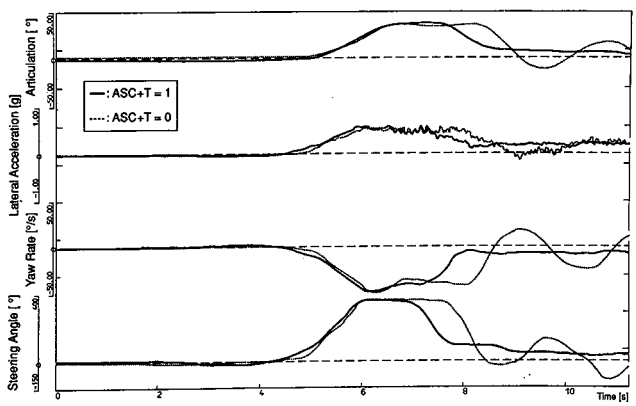

Figure 16. Turning-Off Manoeuvre with Car/Trailer Combination, BMW 325i

Starting from standstill, accelerating the combination to 30 kph, results in a geometrically determined angle

between car and trailer. Within the first 2 seconds, having started turning-off, yaw rate and steering effort show the same values for the car with and without ASC+T. After this time the combination starts to oscillate, because of impaired side stability at the rear axle of the car without ASC+T. In contrast to this the car/trailer combination with ASC+T reduces engine torque during turning off on the changing adhesion condition to such an amount, that an absolutely uncritical behaviour of the combination results.

The stability of the combination of a BMW 525i and a trailer principally shows the same tendency, ASC+T reduces driver's effort to control the combination and improves stability.

Avoidance of Accidents by ASC+T

ASC+T can remarkably improve active safety within the physical limits of tyre/road interaction concerning the maximum transmittable longitudinal and lateral forces. Depending on their driving experience, the safety margin of car drivers in different driving situations can differ significantly. To illustrate this context, Figure 17 was created. In situations, when no special reactions are required, average drivers as well as professional drivers control their car within the stable range with sufficient safety reserve.

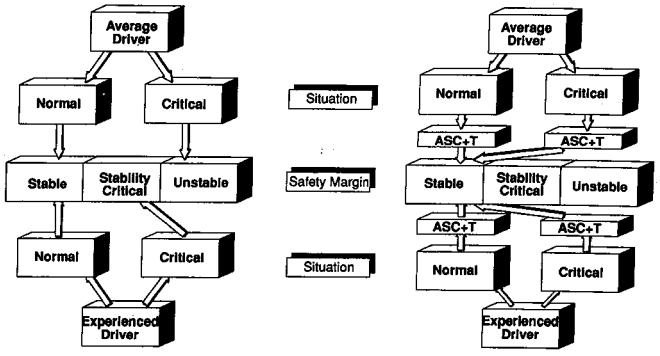

Figure 17. ASC+T, Influence on Driver's Performance

This situation changes totally, when drivers become aware of unexpected changes in the normal run of events. During stability-critical driving manoeuvres experienced drivers in most of the cases will control their car by reducing the safety reserve. The average driver in contrast generally over-reacts and looses control of his car.

Unexpected occurring critical driving situations with excessive drive-slip are the main field of application where ASC+T assists the driver to control his car. Average drivers will be hindered to induce instability in the car, whereas the experienced driver automatically will be kept in a more stable range.

ASC+T improves road holding of a car by adhesion-adapted drive-slip and thus improved driving safety. The driver can withstand stability-critical driving manoeuvres with reduced physiological stress. Road conditions with adverse traction potential can be mastered more easily in superior style. Additionally drivers can identify adhesion-critical road conditions, the perception safety is also improved (Fig. 18).

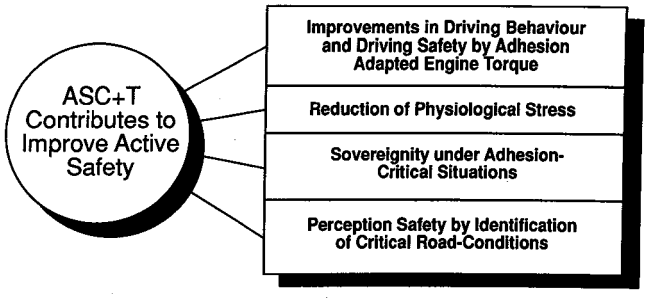

Figure 18. ASC+T, a Contribution to Improve Active Safety

The better knowledge of road conditions, the physiological relief under critical traffic conditions and the automatically adapted engine torque when driving on unexpected changing road conditions help the driver to prevent accidents.

The accident avoidance potential of ASC+T has not yet been established exactly, but can be expected to be at least as high as with ABS. To promote engineering work in this field of electronics application is an important contribution towards an even safer traffic than already achieved. The introduction of ABS-integrated drive slip control systems ASC+T for the BMW 325i and 525i beside the ASC+T already available for the upper class models of the 7- and 8-series range has to be treated as one important step towards the penetration of the whole model range with ASC+T.

References

[1] H.J., Kraft, H., Leffler, The Integrated Brake and Stability Control System of the New BMW 850i, SAE Paper 900 209.

[2] H. Leffler, ABS-Integrated Drive Slip Control Systems, Evaluation and Performance Comparison by the Car Manufacturer, FISITA Paper 905092.

S7-O-03

Traction Control Technology for Improved Driving Safety

Hiroshi Yoshida, Tadao Tanaka,
Keiji Isoda, Koichi Kamiya
Mitsubishi Motors Corporation

Abstract

A traction control system improves vehicle acceleration and stability; however the traction control systems already developed have only a slip restrictive feature that prevents wheel spin when a vehicle starts or accelerates on a slippery road surface. This paper presents the advanced traction control system with unique and innovative technologies, which enables a driver to trace corners safely and smoothly even on a paved road by prevention of an excessive lateral acceleration. In addition to vehicle dynamics, human factors were introduced to determine the control algorithm. As a result, the system provided us with an appropriate mental condition and a further improvement in vehicle maneuverability.

Introduction

Even through the remarkable development of chassis control technology, driving safety should have priority over any other demand in the recent traffic society. From this standpoint, various types of chassis control system have been developed to improve vehicle mobility through the effective utilization of tire forces, which has also been contributing to the preventive safety [1] [2]. Namely what these technologies have been aiming at is the improvement in the relationship between a vehicle and a road environment. A traction control system is also one of those effective methods to improve a vehicle maneuverability mainly on a slippery road surface. The current traction control system recently spreading over Europe and Japan provides a function that prevents the driving wheels from developing an excessive slip through the reduction in traction force (hereinafter called slip control) [3]. In this way, the slip control supports driver's operation, and remarkable improvements in a safe driving on a slippery road surface has been achieved without driver's proficient skill.

On the other hand, even on an ordinary road surface such as an asphalt paved road, a vehicle does not always maneuver according to driver's intention under a marginal turning condition, because tire cornering force is almost used up against an excessive lateral acceleration. In this condition, since the tire slip of driving wheels is considerably small, it is not significant to improve a vehicle controllability by applying the slip control through the detection of tire slip. In order to ensure a safe driving even in such a condition, we have challenged to apply another concept to a traction control system, which prevents a vehicle from approaching a marginal turning condition by regulating traction force. This concept results in the development of an innovative traction control system[4]. This system has a preventive safety feature that improves course traceability in a turn by the automatic regulation of traction force so as not to generate an excessive lateral acceleration (hereinafter called trace control). As a result, the trace control provides a better traceability according to the driver's desired courses in various road surface conditions. This also enables a vehicle to avoid accidents due to an excessive vehicle speed in a turn. Namely this system supports to compensate a driver for his operational errors for a vehicle to maneuver in a safer condition before it approaches a marginal turning condition.

Through the development of the control algorithm, it was found that human factors were more important on such a driver supporting system deeply related to driver's information processing, and that it is all the more important to regard the relationship between a driver and a vehicle as the closed loop included a road environment as well.

The system combined the trace control function with the slip control function is called TCL. TCL has been applied to Diamante, Mitsubishi s new car model introduced into Japanese market in May of 1990. This paper mainly describes the concept and the effects of the trace control concerning active safety that have not been previously offered by any current traction control system.

Concept of Trace Control

Steering Characteristics of Front Wheel Drive Vehicle in a Turn

When a vehicle is turning, a lateral acceleration ay can be formulated by vehicle speed V, steering wheel angle δH, etc. as follows:

$$ay = \delta H \cdot V^2 / \{is \cdot L \cdot (1 + K \cdot V^2)\}$$

where is = Steering gear ratio, L = Wheelbase, and K = Stability factor.

As the passenger car is normally designed to exhibits under-steering tendency (K>O : US characteristics), a steering wheel angle increases according to the increase in vehicle speed under the condition of the circle turning with a fixed radius as shown in Fig. 1.

Once a vehicle approaches a marginal turning condition, the steering wheel has to rapidly increased to trace a turning circle, which means that the vehicle hardly maneuvers according to the driver's intention. When a vehicle is accelerated in a marginal condition, that tendency is slightly strengthened because of the reduction in the cornering power of the front tires caused by a load transfer from the front to the rear. Furthermore, when tire slip occurs in such a condition as snow covered roads, the lateral acceleration at a marginal condition hardly develops in spite of the extreme

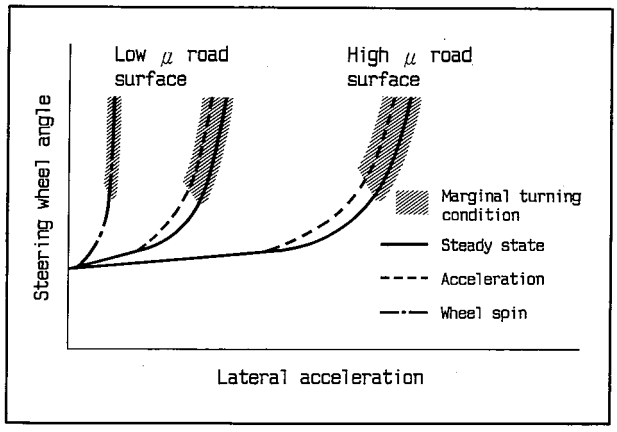

Figure 1. Steering Characteristics of Front Wheel Vehicle

increase in a steering wheel angle because of the deterioration of tire s lateral road holding capability. In this way, since vehicle controllability almost deteriorates near a marginal turning condition, it would be one of the most available approaches to prevent a vehicle from approaching a marginal condition for a further safety.

Basic Concept of Trace Control

Restriction of Excessive Lateral Acceleration. It would be effective that a vehicle speed is restricted by the detection of a marginal condition before a vehicle approaches that condition. For example, the automatic regulation of traction force according to a detected lateral acceleration could prevent a vehicle from developing an excessive lateral acceleration, and that would mean to prevent a vehicle from approaching a marginal turning condition accidentally caused by the imprudent operation of the accelerator pedal. That results in giving a driver enough time to control a vehicle safely and smoothly and therefore could be called a preventive safety.

Control Reference of Lateral Acceleration Level. In order to obtain the appropriate value of a lateral acceleration for a safe driving, the experiments were carried out under various driving conditions. The concept of human factors was introduced to set up the appropriate value, that is, the lateral acceleration criterion was derived from the experiments, where a driver considered that he would drive a vehicle without an excessive mental tension. (Details concerning a mental tension are described below.)

Fig. 2 shows an example of measurement results which represents the relationship between a lateral acceleration and a vehicle speed. It can be seen in the figure that the higher is a vehicle speed, the lower is a lateral acceleration level where a driver negotiates a corner without an excessive mental tension. In urban areas, a driver seems to have a weak sensation on a lateral acceleration, which causes a higher allowance of a lateral acceleration not to give a driver an excessive mental tension. It could be why a driver receives so many information to be processed besides a lateral acceleration.

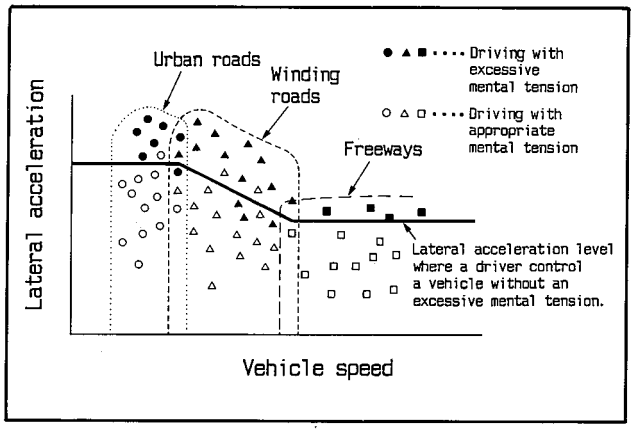

Figure 2. Lateral Acceleration Level for Trace Control Reference

On a winding road, a driver seems to feel a lateral acceleration more sensitively according to the increase in a vehicle speed. On a free way, a driver has the strongest sensation on a lateral acceleration, but the allowance level does not seem to vary corresponding to a vehicle speed. In this way, the reference level of a lateral acceleration for the trace control was established, where a driver negotiates a corner without an excessive mental tension.

Control Target of Longitudinal Acceleration. From the viewpoint of a driver's operation, the following typical patterns should be considered, where a lateral acceleration exceeds the reference level as shown in Fig. 3, where Case A = Increase in steering wheel angle with vehicle speed constant, and Case B = Increase in vehicle speed with steering wheel angle fixed.

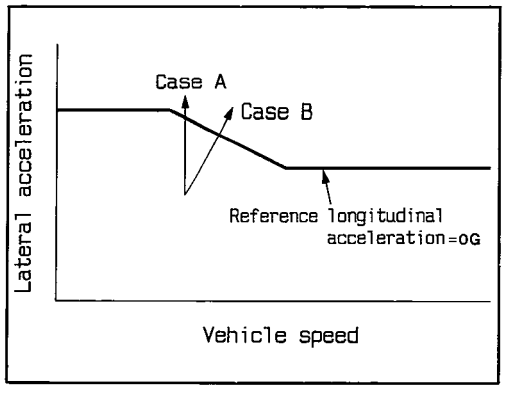

Figure 3. Typical Patterns Which Exceed Reference Acceleration Level

What the trace control aims at is to compensate a driver for a response delay in his operation. So it would be effective that a vehicle is decelerated using engine braking in case A, and that a longitudinal acceleration is restricted according to the allowable longitudinal acceleration determined by the estimation of the secure

time while a driver can afford to control a vehicle so as not to exceed the reference level of a lateral acceleration in case B.

Thus each reference lateral acceleration level was set up by each allowable longitudinal acceleration as the control map shown in Fig. 4. The target engine torque is finally determined so as to adapt the reference lateral acceleration level to the degree of longitudinal acceleration.

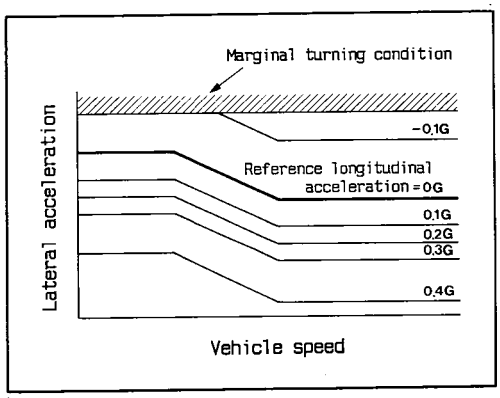

Figure 4. Control Map for the Trace Control

Detection of Lateral Acceleration. The following methods have generally been used to detect a lateral acceleration. One is to use a lateral acceleration sensor, and the other is to calculate it from the speed difference between the left and right rotating wheel. Even the method with a lateral acceleration sensor, however, has a time delay compared with the acceleration expected by a driver's steering motion, which could result in the delay of the control if the methods mentioned above are applied to the detection of a lateral acceleration as shown in Fig. 5.

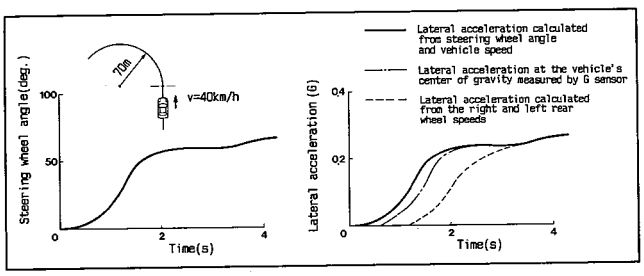

Figure 5. Lateral Acceleration Response for Various Detecting Methods

For this reason, the method was adopted where a lateral acceleration is obtained from the calculation with a vehicle speed and a steering wheel angle in accordance with Eq. (1). This control with a predictive lateral acceleration is a feedforward detective one, which would assure a good control response for the trace control.

Furthermore, this feedforward detection method for a marginal turning condition would be still available even on a slippery road surface, such as snow covered road where an actual lateral acceleration is not well developed with the increase in steering wheel angle. That is, a marginal turning condition is predictively detected by a steering wheel angle and a vehicle speed in any road condition. Fig. 6 illustrates how the marginal turning condition is detected on a slippery road surface by using this method.

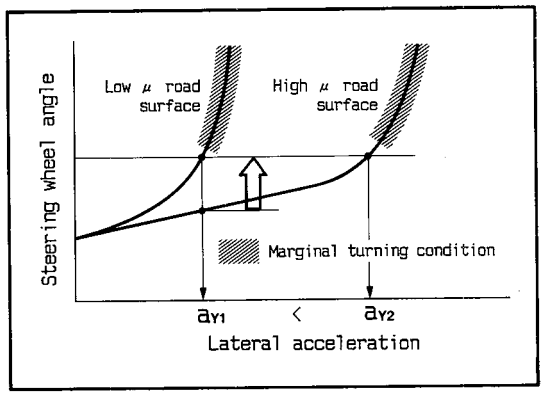

Figure 6. Detection of Marginal Turning Condition on Low μ Surface

TCL System Description

System Configuration of TCL

The schematic diagram of TCL applied to a front wheel drive vehicle is shown in Fig. 7. This system is equipped with various sensors: the rear wheel speed sensors for calculating a vehicle speed, the transmission output shaft speed sensor and the transmission position signal for a rotating speed of driving wheels, the steering wheel angle sensor for calculation of a lateral acceleration, and the accelerator position sensor for estimating a driver's accelerating intention. Based on those information, the target engine torque is calculated by the traction electronic control unit (ECU), and informed to the engine ECU, which finally controls a engine torque. In addition the slip ratio of driving wheels is obtained by comparing a driving wheel speed with a vehicle speed, which is used as the information of the slip control.

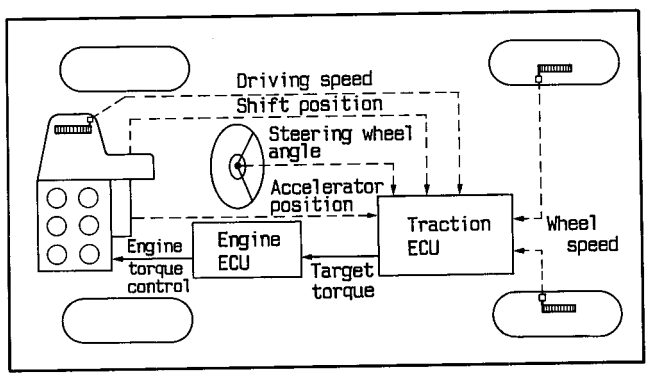

Figure 7. Schematic Diagram of TCL

Control Algorithm of Trace Control

Fig. 8 shows the trace control diagram based on the feedforward control of a lateral acceleration described

above. The control is performed in accordance with the following flow.

- The lateral acceleration of a vehicle ay is calculated with a steering wheel angle δH and a vehicle speed V according to Eq. (1).
- The reference longitudinal acceleration axr is determined by V and ay according to the control map as shown in Fig. 4.
- The reference engine torque Tr that realizes axr is calculated using vehicle mass M,a tire rolling radius R and a total reduction ratio ρ, considering various running resistances, such as a tire rolling resistance and a cornering drag.
- The engine torque TM that corresponds to the driver's intention for acceleration is obtained by an accelerator position ΘA and an engine speed NE.
- The target engine torque TT is finally fixed by Tr, TM and corrective factors α1 and α2, which were experimentally determined in consideration of a driver's intention for acceleration. The trace control functions to regulate the engine torque as far as TM exceeds Tr.

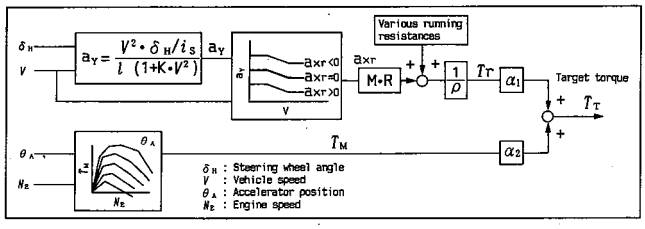

Figure 8. Trace Control Diagram

Superiority of Trace Control to Driver's Operation

It is needless to say that a response delay in a driver's operation has great influence on a crush avoidance. It is showed that if a driver's reaction time is shortened by only half a second, the collision probability could be reduced by a half [5]. So it might be preferable that a driver gets rid of a response delay in his operation, especially in a trace control marginal turning condition.

The trace control compensates a driver for his operational error for a vehicle to maneuver in a safer condition before a vehicle approaches a marginal turning condition.

Fig. 9 shows the breakdown of a necessary time for a engine torque regulation. As shown in Fig. 9, the necessary time is reduced considerably by the trace control with the feedforward detection of a lateral acceleration.

Reliability of the System

Electronic components and sensors of TCL themselves have a sufficient reliability which has already been developed for the current chassis control systems, such as ABS, 4WD and electronically controlled suspension. TCL also has the following feature to keep a high reliability as a total system constitution.

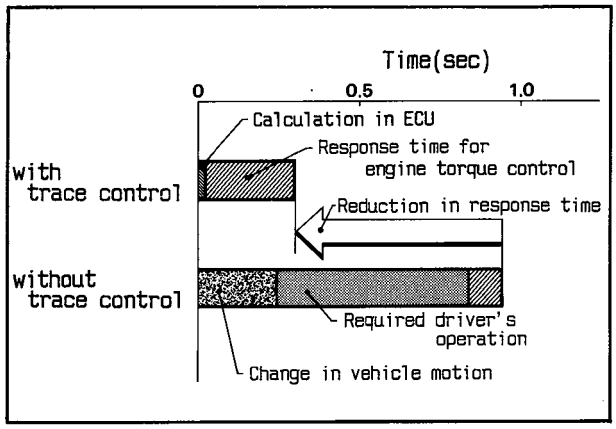

Figure 9. Necessary Time for Engine Torque Regulation

- The calculation in a engine-ECU and TCL-ECU is carried out separately, which also enables each ECU to detect some trouble through a mutual observation.
- Troubles detection is also made by various check program through the microcomputer, sensors and actuators.
- Fail-safe is secured to prevent a vehicle behavior from occurring a sudden change even if the system fails by some trouble.
- When some trouble occurs a driver can easily recognize the condition with the warning indicator, and a vehicle is put back to the condition without TCL.

Effect of Trace Control on Vehicle Maneuverability

Course Traceability under Acceleration in a Turn

When a vehicle is accelerated in a circular turn, the yaw velocity of a vehicle ψ increases in proportion to a vehicle speed V according to the following equation.

$$\psi = V / R$$

where R denotes turning radius.

Here the course traceability in circular turn would be evaluated by the degree of the increase in a yaw velocity to a vehicle speed. Fig. 10 shows the test results that the vehicle was rapidly accelerated from the steady state circular turn of a 30m radius with a steering wheel angle fixed. The oblique line in Fig. 10 indicates the yaw velocity when the vehicle traced the reference circle. Each pair of plotted data corresponds to the condition at the start of the acceleration and at two seconds after the start. It says that the smaller the deviation from the reference oblique line is, the more a driver can afford to control a vehicle. As a result of the tests, the vehicle with trace control had a smaller deviation from the reference line, which means a better course traceability than that of the vehicle without the trace control.

Operation of Steering Wheel and Accelerator Pedal

Effect on a Operation Manner. Fig. 11 and Fig. 12 present the effect of the trace control on the manner of operating a steering wheel and an accelerator pedal in

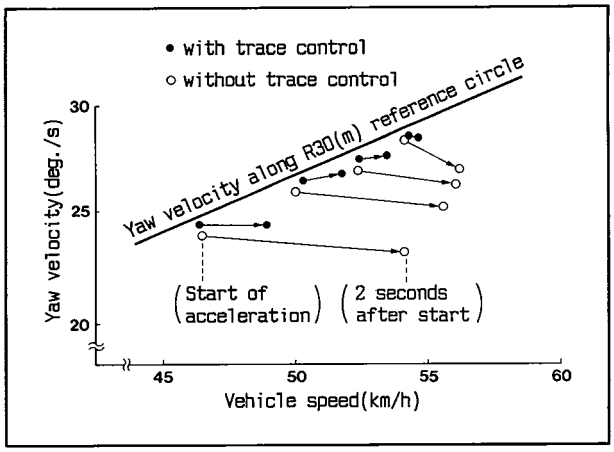

Figure 10. Course Traceability During Acceleration in a Turn

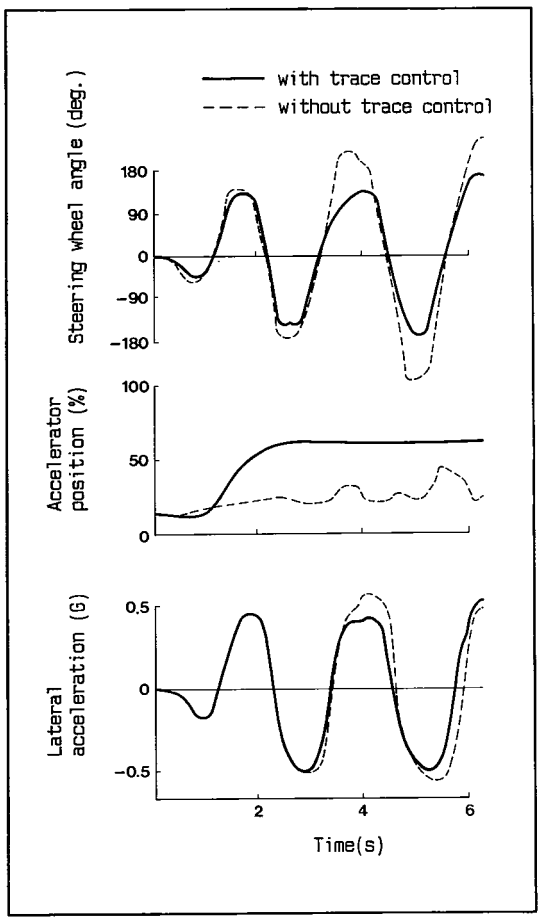

Figure 11. Driving on Slalom Course

the slalom course driving. Fig. 11 shows the angle of steering wheel, the position of an accelerator pedal and the lateral acceleration of the vehicle when it was driven at a target speed of 55km/h with pylons located at a pitch of 18m. The vehicle provided with trace control showed a stable steering wheel operation as compared to the vehicle without trace control. As to an accelerator pedal operation, the operation with the trace control was more stable than the vehicle without the trace control.

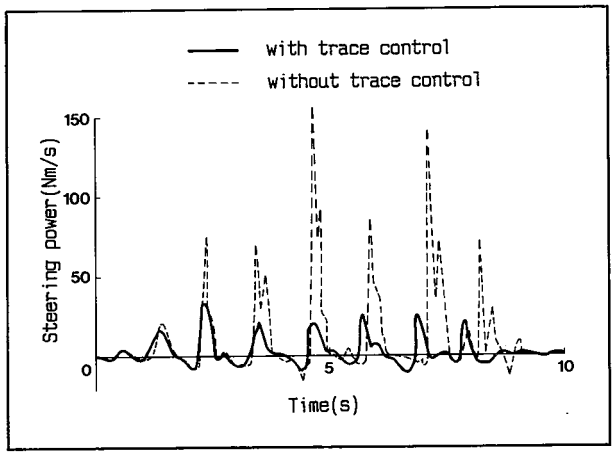

Figure 12. Physical Load in Steering Operation

Those mean that a driver easily control the vehicle with the trace control because he need not care much about a steering wheel and an accelerator pedal operation.

Effect on a Physical Load. In addition this result is also represented as the effect on the physical load of a driver, that is, the steering power as shown in Fig. 12. A steering power is defined as the product of a steering wheel angular velocity and a steering torque, and the smaller a steering power, the less a driver's physical load. As shown in Fig. 12, a driver's steering physical load was considerably reduced by the trace control.

Effect on the Time to Drive through a Slalom Course

The reduction in a driver's physical load also enables a driver to perform a more efficient driving, decreasing the wasteful vehicle behavior by the excessive operations of a steering wheel and an accelerator pedal. Fig 13 shows the test results of the necessary time passing through a slalom course in comparison between average skilled drivers and expert drivers. As shown in Fig. 13, the trace control contributes to the reduction in the necessary time through the slalom course not only in case of an average skilled driver but also in case of an expert driver.

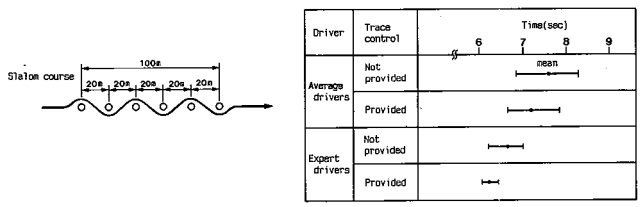

Figure 13. Reduction in Time by the Trace Control Effect

Effect on the Mental Load

A driver has to process various information for tracing a course, confirming a road holding condition and avoiding a crash, which causes to raise a driver's mental tension and especially an excessive mental tension might lead to a wrong information processing.

An attempt was made quantitatively to measure a driver's mental tension. It is generally known that when

a human being receives an emotional stimulus, he reacts physiologically such as heart rate, a galvanic skin response and a brain wave. From the viewpoint of quantitative and continuous measurement, a galvanic skin response was applied, which is utilized the physiological phenomenon that a cell depolarization by receiving an emotional stimulus causes the variation of a skin electric resistance, so-called a skin impedance level. Fig. 15 shows a measurement example of skin impedance level on the winding road driving shown in Fig. 14. In Fig. 15, the vertical axis represents the degree of mental tension in a dimensionless form, and the higher a vertical level, the lower a skin impedance level and the higher a driver's mental tension. The experiment were carried out under three control references, that is A , B , C as shown in Fig. 15. It is found that a driver's mental tension is greatly affected by those control references, and it is considerably decrease so long as suitable control condition would be applied. As shown in Fig. 15, "B" would give a driver an appropriate mental tension. It would be why a driver has no need to process the information for road holding condition. Namely a driver can afford to pay more attention to a course tracing and a crash avoidance.

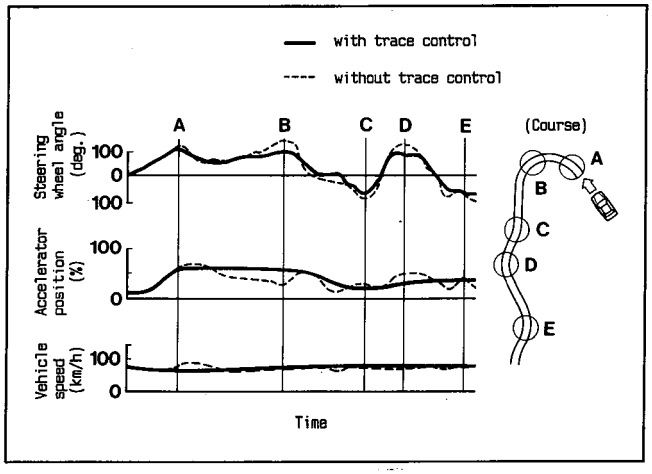

Figure 14. Driving on Winding Road

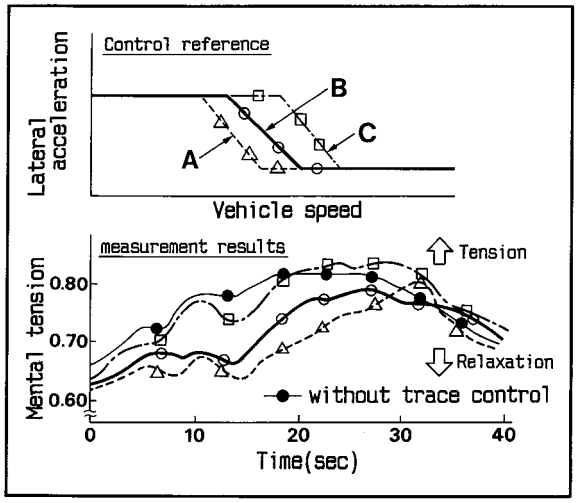

Figure 15. Effect of Trace Control on Mental Tension

In addition another measurement regarding a driver's physiological response was tried, that is, an electro-encephalogram (EEG); brain wave. Fig. 16 shows the analyzed results of EEG measured on the winding road shown in Fig. 14. As shown in Fig. 16, the trace control worked to reduce the power of EEG in the range of β wave (14~50Hz), which means that the active level of the brain was approximately kept in the same condition as the driving on a straight road, or not excessively.

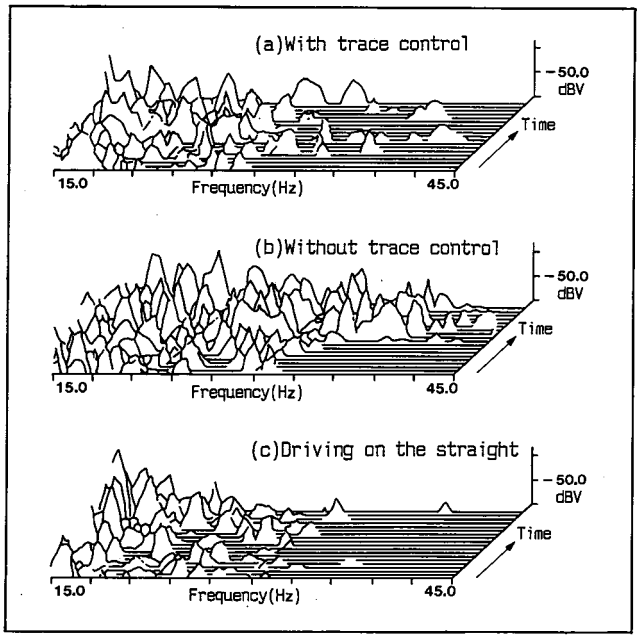

Figure 16. Effect of Trace Control on Mental Tension (Brain Wave)

Conclusions

Although a high performance vehicle shows an excellent mobility, it also has a high possibility to approach a marginal driving condition, especially in a turn. Once a vehicle enters a marginal condition, a driver has hardly enough time to control a vehicle. From this standpoint it is the most effective that a vehicle never approaches a marginal condition and a driver never has an excessive mental tension. This concept has been applied to the traction control technology under the name of trace control. Namely in the construction of the traction control algorithm, human factors such as a driver's mental stress were also introduced in addition to the improvement of vehicle dynamics. That also means that the system has been built up by regarding the relationship between a driver and a vehicle as the closed loop included a road environment as well.

The test result proved that the trace control contributes to the reduction not only in a driver's physical load but also in a mental tension with good traceability kept. Furthermore, those effects would mean that the trace control secures the enough time for a driver to recover a vehicle maneuver even if any errors are made in a steering and an accelerating operation. It would be just

a preventive safety or an active safety. In that sense the trace control could be one of the most innovative systems for further improvement in driving safety.

Lastly, we authors are sure that the realization of this preventive or active safety concept indicates the starting point of a new generation: Human-oriented vehicle.

References

1. R. Mitamura, M. Tani, T. Tanaka, & H. Yuasa: System integration for New Mobility, SAE Paper 881773 (1988).
2. H. Yoshida and M. Tani: Future Trends of Vehicle Control Technology, Journal of JSAE, Vol. 43, No. 1, 1989 (in Japanese).
3. H. Demel and H. Hemming: ABS and ASR for passenger cars-goals and limits, SAE 890834, 1989.
4. K. Isoda, M. Osaki, M. Hashiguchi, & K. Otake: Mitsubishi Traction Control System (TCL) and Chassis Integrated Control Technology, Mitsubishi Motors Technical Review, No. 3, 1991.
5. Hans-Georg Metzler: Computer Vision Applied to Vehicle Operation, SAE 881167, 1988.

S7-O-04

Controlled Suspension for Better Safety

Jean-Pascal Reille, Charles Blanot
Renault Direction des Etudes

Abstract

The field of controlled suspension is developing rapidly. By improving the trade off between ride comfort and handling, such systems have bettered the global car performance. Up until now, controlled suspension made it possible to improve comfort and performance in most cases, with the result being at least equal to that of the reference passive suspension vehicle. The new system described here affords superior passenger comfort and safety irrespective of the road profile and driving situation. The experimental vehicle built by Renault, which was developed in conjunction with Lipmesa associated with Sagem, is equipped with four quick-acting variable-damping shock absorbers. The damping force is controlled in real time on the basis of information qualifying the pilot's driving, e.g. steering-wheel information, and information obtained from the road profile, such as the absolute car-body and wheel velocity. The set value of force is calculated taking into account the velocity of shock absorber displacement and the map of its force-velocity pattern. The results of the simulation calculations and the dynamic tests performed on the vehicle show the effectiveness of this new concept, which provides a substantial improvement in safety combined with increased comfort.

Introduction

The number of controlled suspension systems on offer is increasing. Such systems give an improvement in overall vehicle performance, especially for strongly characterized road or driver stresses.

Very often, however, when the shock absorber allows only discrete settings, the system fixes a mean calibration position which then gives a result similar to that obtained with a standard vehicle.

To allow simultaneous improvement of comfort and road holding, a system must be developed to allow real-time control of damping forces. We therefore selected quick-acting variable-damping shock absorbers which, in association with an original control strategy, are undoubtedly the *ne plus ultra* in controlled damping suspension systems.

The vehicle used for the study is a Renault 19, and an application of this concept is implemented on the Renault Cover safety vehicle. This application is implemented taking into account the industrial constraints for a vehicle of the Renault range.

System Architecture

The system installed on the vehicle is shown in Figure 1.

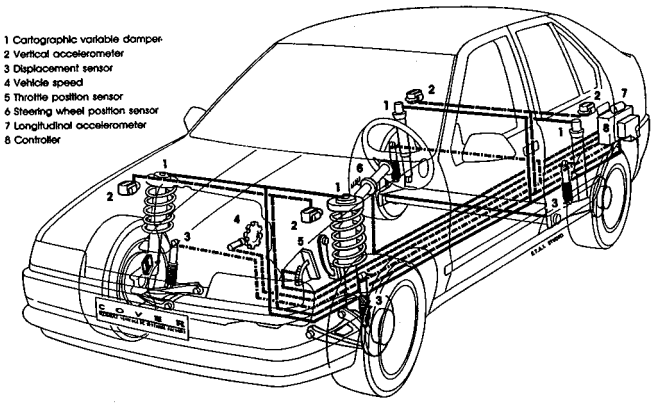

Figure 1. System Architecture

Sensors

The following information is used in the strategy:

- 4 wheel/body displacements
- 4 body vertical accelerations
- Steering-wheel position
- Throttle-valve position
- Longitudinal accelerometer
- Vehicle speed.

Shock Absorbers

For optimum performance the shock absorber must have the largest possible setting dynamics and the

shortest possible response time. The damping force must be as close as possible to the calculated force, and it is advisable to have numerous possible shock absorber settings. A continuous variable-damping shock absorber was therefore selected.

An oil flow between the rebound chamber and the shock absorber reserve chamber is controlled by solenoid valve. This allows damping forces to be varied both in expansion and compression. To avoid changing the existing shock absorber structure, oil passes through a counter-rod. The control valve is incorporated at the top the rod. A cross section view of the shock absorber is shown in Figure 2.

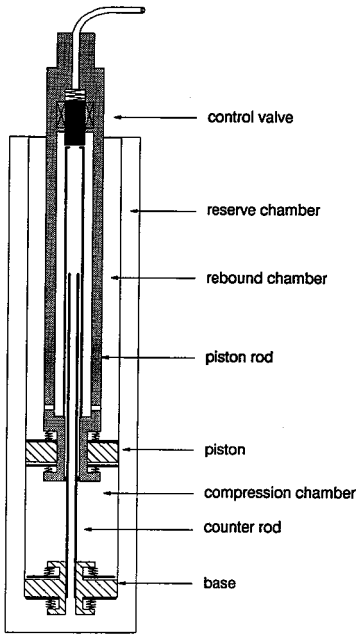

Figure 2. Damper Cross Section

The shock absorber's response time is 10 ms. It is important to obtain a minimal phase shift between the damping force required and the force obtained.

Control Strategy

Vertical Strategy

The control strategy ensures independent, real-time control of the damping force on each wheel. The optimum damping force one wishes to obtain at each moment depends on the absolute wheel velocity, V_{wheel} and body velocity V_{body} of the vehicle quarter in question.

$$F = C_1 * V_{wheel} - C_2 * V_{body}$$

The difference of this strategy by comparison with the usual "skyhook" type patterns is the addition of the term $C_1 * V_{wheel}$, which allows a compromise to be reached between wheel grip (safety/performance) and body movements (the comfort achieved being weighted by the term $C_2 * V_{body}$). This compromise can be shifted from one pole to another by adjusting the coefficients C_1 and C_2 an increase in coefficient C_1 displaces this compromise towards the "safety" pole, while an increase in C_2 displaces it towards the "comfort" pole.

Safety Strategy

Driving situations are detected by the following parameters:

- *Steering-wheel position.* Can detect that the vehicle is in a cornering situation. In this case, it must be possible to increase the transverse capability for transmitting tyre force.
- *Steering-wheel speed.* Can detect emergency collision avoidance manoeuvres when it is necessary both to increase tyre capacities and limit the vehicle's roll velocity.
- *Throttle position.* This variable makes it possible to know the engine torque demanded by the driver and to increase the tyre's longitudinal capability.
- *Throttle speed.* Allows detection of engine torque variations which could generate a vehicle pitch motion.
- *Longitudinal acceleration.* Allows detection of braking situations where it is necessary to increase the vehicle's longitudinal capability. This sensor could be replaced by a braking pressure measurement.

The choice of the pair of coefficients (C_1, C_2) is determined from the preceding parameters and the vehicle speed. For straight-line driving, the compromise centres on the comfort coefficient, and C_1 is therefore very small. When one of the parameters exceeds a predefined threshold, the pair (C_1, C_2) is altered in order to improve vehicle safety. For multiple stresses, the pair of coefficients offering the greatest safety is adopted. The coefficient pair (C_1, C_2) is specific to each suspension train.

We can take as an example the operation of the system on cornering, where driving safety is to be increased. In the [steering-wheel angle, vehicle speed] plane, four threshold levels are defined, thus defining five coefficient pairs (see Figure 3). When the [steering-wheel angle, vehicle speed] operating point enters a region, the coefficient pair for the region in question is applied to the force calculation. This allows a gradual change of the comfort/performance compromise. When

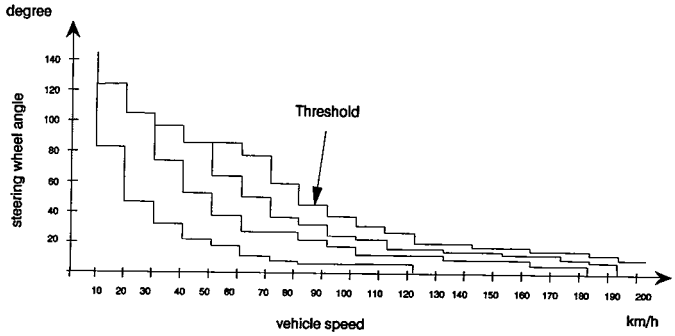

Figure 3. Safety Strategy Example

the thresholds are crossed downwards, a time lag is applied.

Shock Absorber Control

Once the damping force has been calculated, the actuator control current is determined. A shock absorber control map, determined by machine tests, is stored in memory. With this map, knowing the shock absorber's displacement speed and the force required, it is possible to calculate the control current. Specific maps exist for the front and rear suspensions.

It may be that the calculated force is not attainable:

- either because it does not come within the shock absorber's setting range;
- or because it is in the "active" part of the force-velocity plane (this is the region in which energy would have to be applied to achieve the required force).

Figure 4 illustrates this phenomenon. In the force/velocity plane are shown the operating points required by the calculation, for a "bad road" type of excitation. This is an eloquent demonstration of the difference between an active suspension and a semi-active suspension.

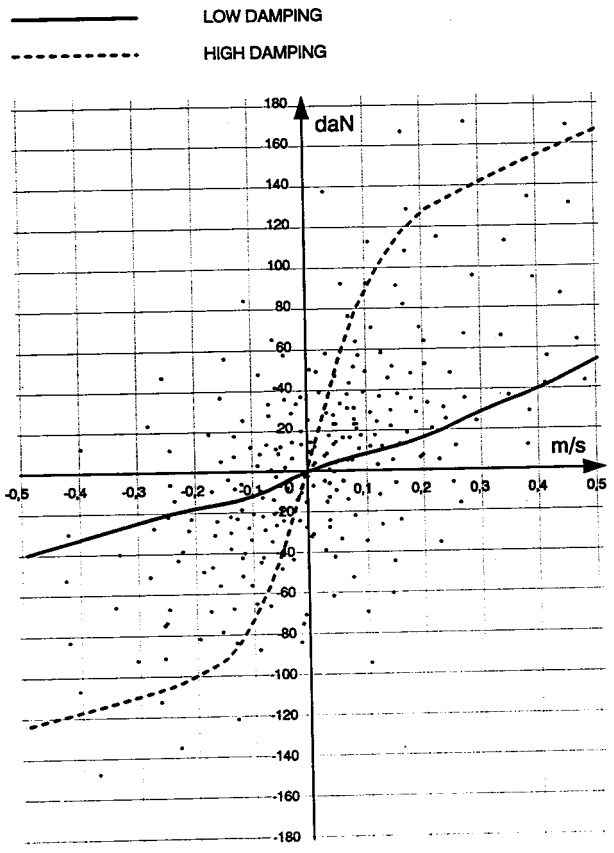

Figure 4. Damping Force Restriction

In both these cases, the strategy selects the control current so as to minimize the difference between the force exerted and the desired optimum force.

The entire loop, from the choice of coefficients through to suspension control, is implemented in less than 10 ms. The flow chart of the control strategy for a vehicle quarter is shown in Figure 5.

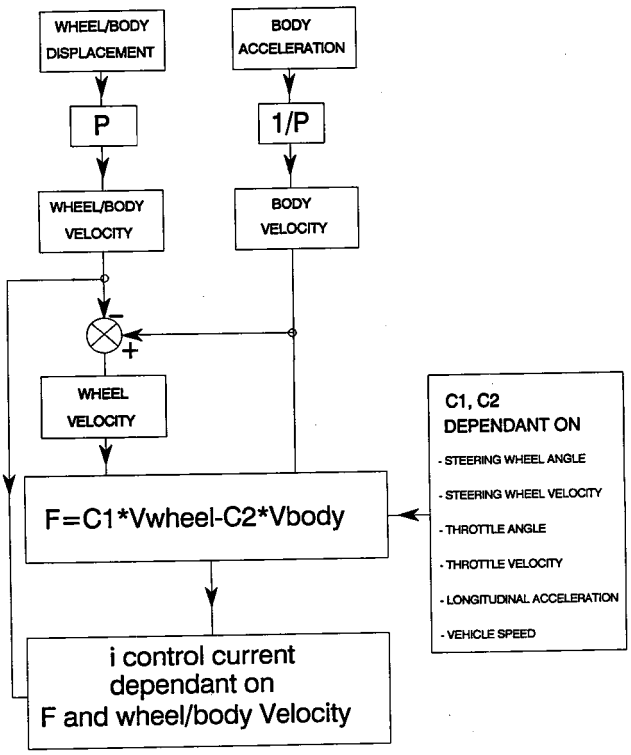

Figure 5. Control Algorithm

Simulation

In the initial phase, the calculation made it possible to validate the control strategy defined above. Subsequently, the calculation was used to define the system profile: response time, sensor precision, and numerical calculus methods. Ultimately, calculation is a tool allowing pre-definition of the strategy coefficients so as to reduce the time required for development tests.

Figure 6 shows an example in which the obstacle adopted is a road hump of wavelength 40 m. One observes that the constant increase in coefficient C_2, C_1

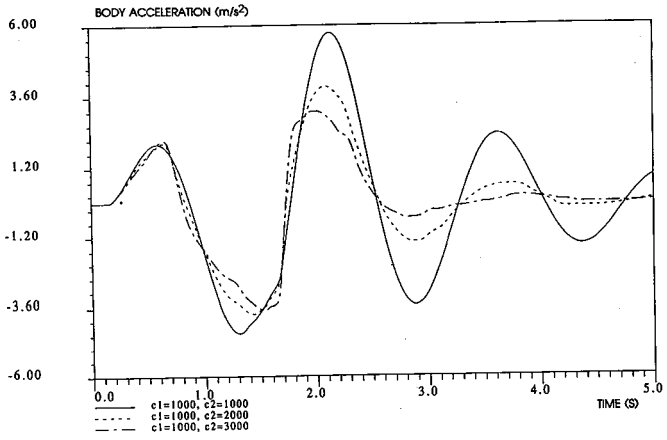

Figure 6. Road Bump Response

constant, produces a major reduction in vertical acceleration of the vehicle when passing over the obstacle.

Test Results

All the tests performed showed the advantages of this type of suspension system, from both the safety and comfort viewpoints.

The gains achieved include the following:

- *straight-line travel:* reduction in low-frequency body movements, and reduction in car vibration levels;
- *braking:* reduction in dive effect, improved road grip by the wheel, especially on poor roads;
- *acceleration:* reduced nose-up, improved traction;
- *cornering:* reduction in spurious body movements, improved control of wheel grip especially on bad roads. Improved body behaviour when negotiating a corner.

It can therefore be seen that major gains are achieved in all customary driving conditions.

Comfort Tests

Gains in comfort are illustrated particularly well by Figure 7. This test was performed on a four-cylinder hydropulse bench. The figure shows a comparison between the vertical acceleration spectra at the body level for a "road" type signal on a car body equipped with a standard passive suspension system or the cartographic suspension system.

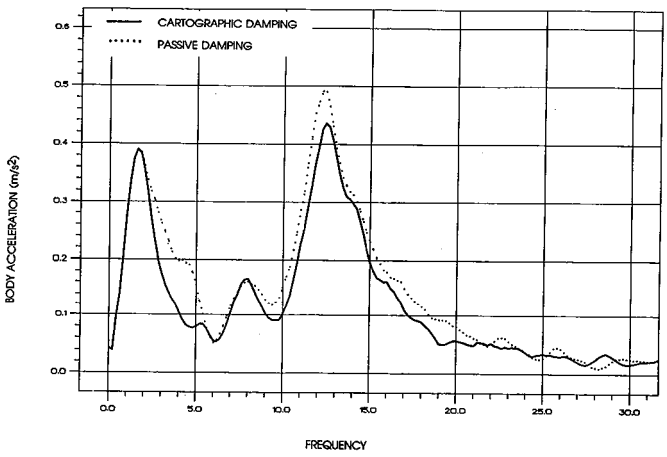

Figure 7. Comfort Bench Test

Cartographic suspension gives a lower accelerometric level at medium and high frequencies than the standard suspension system, without detracting from low-frequency movements. This results in better overall comfort and hence less driver fatigue.

Performance Tests

An example of a gain in vehicle performance is shown in Figure 8. The test involves a lane change at 80 km/h. The resultant roll velocities for a standard suspension and the cartographic suspension are compared (these roll velocities were measured by an inertial unit). A major reduction in roll velocity is observed with the cartographic suspension system. This will mean a far better subjective impression for the driver and, once again, improved driving comfort.

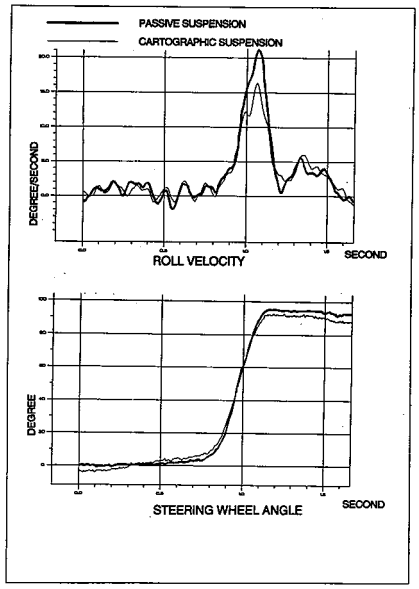

Figure 8. Lane Change Test

Real-time control of the vertical force applied to the tyre allows the stopping distance on a poor road to be reduced by comparison with a standard vehicle. This means a 20% reduction in deterioration of stopping distance due to a degraded road surface. Of course, this result depends on the severity of the road profile.

Conclusion

This cartographic suspension system is the most sophisticated industrial controlled damping system available today. The strategy described here could be still further improved, while retaining the same number of sensors, to allow finer monitoring of roll and pitch modes.

The quick-acting cartographic suspension system, with extensive setting dynamics, provides the optimum match between the damping force exerted and the damping force required. This feature makes it possible to obtain exceptional performance in terms of safety, on the one hand by improved vehicle control and on the other hand by reducing the vibration level, which is a source of fatigue.

The system in its present configuration is homogeneous, since there is a match between the number and quality of sensors, and the actuator performance. This solution can be regarded as an envelope solution which will have to be broken down into various systems, adapted to each vehicle range, according to a compromise centering around three main criteria: complexity, cost and performance.

S7-O-05

Improvement in High-Speed Safety Through Active Suspension Control

Naoto Fukushima, Namio Irie
Nissan Motor Co., Ltd.

Abstract

This paper describes the hydraulic active suspension which is mounted in the Nissan Infiniti Q45 and is effective in improving high-speed safety. This active suspension has been designed specifically to provide improved vehicle stability at high speed through the use of skyhook damper control, a frequency-dependent damping mechanism and active roll and pitch control. The system design concept is presented along with an analytical explanation of the three major functional features. The results of theoretical and experimental analyses are presented which clarify quantitatively the effects of the control procedures and parameters on the vertical vibration characteristics of the vehicle body during high-speed driving, as well as on the road contact of the tires when traveling on an undulating road, cross-wind stability and steering response characteristics. These results confirm that this active suspension provides outstanding performance unobtainable with conventional suspensions, especially under high-speed driving conditions.

Introduction

Active suspensions have become a central focus of passenger car chassis development today because they hold out the potential for achieving dramatic improvements in performance over conventional passive control systems. The latter have mainly controlled vehicle motions by switching the spring and damper rates according to the condition of the vehicle.

Research on active suspensions dates back approximately twenty years and was originally aimed at application to railway vehicles [1]. The first serious attempt to apply an active suspension to the automobile was a mechanical system developed by Automotive Products Co. which was based on a hydropneumatic suspension [2]. Subsequently, Lotus developed an active suspension incorporating an electro-hydraulic servo system. The Lotus suspension has been tested in sports cars and also installed in racing cars [3].

More recently, Nissan and Toyota successively announced hydraulic active suspensions for certain passenger car models [4] [5] and thus ushered in an era of active suspension use in production vehicles.

This paper first discusses the types and features of typical active suspensions developed to date and then describes the Nissan hydraulic active suspension installed in the Infiniti Q45 sedan. The construction of the system is presented along with an analysis of its performance characteristics, the design method used, and the system's contribution to improvements in vehicle dynamics.

Types and Features of Hydraulic Active Suspensions

Three typical types of hydraulic active suspensions that have been developed to date are classified in Figure 1.

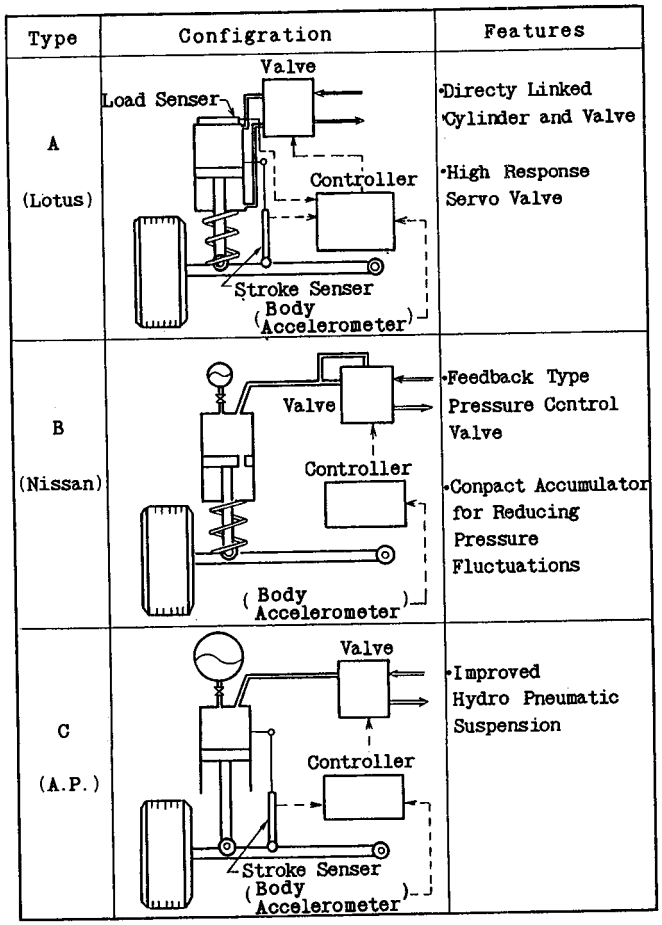

Figure 1. Configuration of Typical System

Type A, a system under development at Lotus, is characterized by its direct linkage of a double-acting cylinder and a high-response control valve. While the control capability of the system is quite high, the control valve must provide fast response in order to absorb vibrational inputs from the road surface. As a result, the system necessarily consumes a large amount of energy especially on rough road surfaces where unsprung resonance is conspicuous.

Type C was a hydropneumatic suspension developed by Automotive Products and was constructed as a hydropneumatic suspension. It employed a flow control valve to accomplish active control by filling the accumulator and sending the hydraulic fluid to the cylinder. Because

of this method of operation, it consumed a great deal of energy in controlling bounce, roll and other sprung motions that occur during travel on an undulating road surface or in slalom-like driving.

Type B has been developed by Nissan with the specific aim of suppressing the increase in energy consumption seen with the other two types. One of its major features is the combination of a pressure control valve with a small accumulator and a hydraulic cylinder. Vibrational inputs from a rough road surface are absorbed by the accumulator, which reduces the flow rate required of the system as a whole. Control of sprung vibrations is accomplished by active damping control and the passive damping action of the hydraulic system to reduce the required hydraulic fluid flow rate when traveling on undulating road surfaces. Thus, the large energy consumption that becomes a problem in the type A and C systems under certain driving conditions is avoided. In terms of overall energy consumption, type B can be characterized as an energy-saving active suspension system.

The following discussion will describe the type B system featured in the Infiniti Q45 as a representative example of active suspension systems.

Construction of Hydraulic Control System

Required Control System Function

One major feature of active suspension control is that the active element added to the system necessarily becomes an element that transmits road surface inputs, as seen in Figure 2. Consequently, the actuator used in an active suspension must be capable of both generating the necessary force to control sprung motions and counterbalancing vibrational inputs from the road surface. In developing the control system for the active suspension, this was both the most critical and the most difficult issue that had to be addressed.

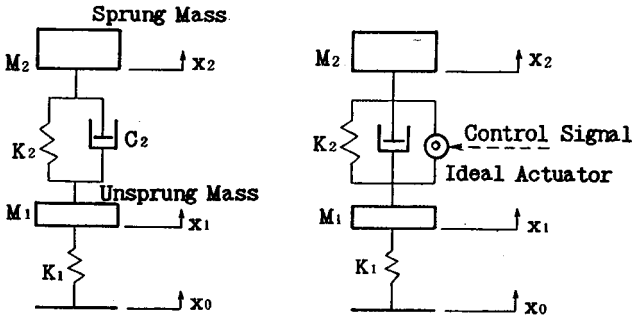

(a) Passive Suspension (b) Active Suspension

Figure 2. Suspension Model

A great deal of theoretical research has been conducted on active suspensions and there are many reports in the literature of analyses involving the use of an ideal actuator [6] [7]. What is meant by an ideal actuator is one that generates force according to control inputs but does not produce any reactive force against vibrational inputs from the road surface. The function required of the control system of an active suspension therefore differs from that required of an ordinary servo system.

Hydraulic Control System Configuration

In actuality, the hydraulic control system is configured such that it includes dampers, in addition to an ideal actuator. A detailed system configuration is shown in Figure 3.

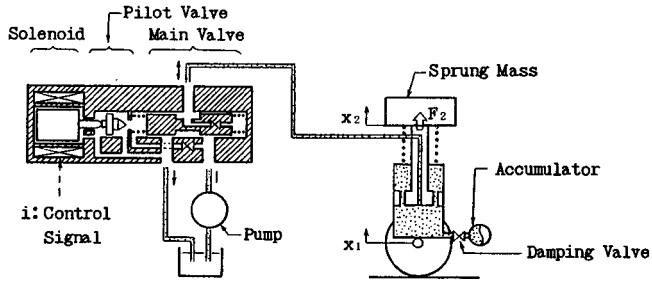

Figure 3. Electrohydraulic Pressure Control System

As indicated in the figure, high-pressure hydraulic fluid is sent from the pump and introduced through the main valve, from where it is sent to the wheel actuator. When the spool is in a neutral position, the valve is completely closed. Movement of the spool to the right opens the port on high-pressure side. Conversely, when the spool moves to the left, the return-side port is opened.

The cylinder pressure is fed back and applied to the right end of the spool, while control pressure produced by the solenoid and pilot valves is applied to the left end. When the two pressure levels are unbalanced, the spool moves accordingly, changing the cylinder pressure. As a result, the spool returns to its neutral position and the cylinder pressure is thus regulated so that it is equal to the control pressure.

The accumulator and hydraulic cylinder are connected by means of a damping valve. As will be explained in detail in the following section, the passive damping action of the hydraulic active suspension is produced by a system which combines this damping valve with the accumulator and the pressure control valve. This results in an ideal frequency-dependent damping characteristic.

Basic Characteristics of Hydraulic Control System

This section explains two typical characteristics of the active suspension control system. One is the response characteristic of the force F2 generated by the cylinder in relation to the control current, i. The other is the characteristic of the force F2 generated by the cylinder in relation to the velocity, x1 - x2, which corresponds to road surface inputs. Experimental data on these two characteristics are shown in Figure 4. The parameter denoted as Po in the figure indicates the biased hydraulic pressure.

The i-F2 characteristic shows sufficient responsiveness to control the pitch, roll and bounce motions of the

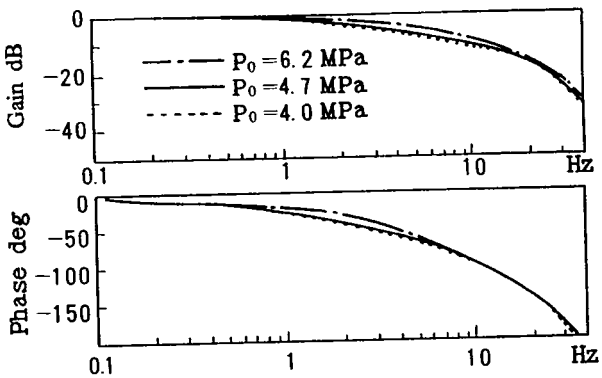

(a) Force F_2/Control Signal i

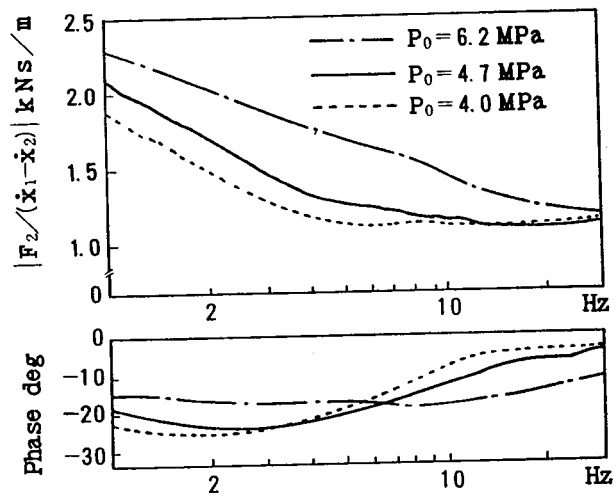

(b) Force F_2/Velocity$(\dot{x}_1-\dot{x}_2)$

Figure 4. Frequency Response of Electrohydraulic System

vehicle body. The characteristic of F2 in relation to x1 - x2 shows a damping tendency, the value of which becomes smaller at higher frequencies. This result indicates that the transmission of road surface inputs to the body is reduced in the high frequency region.

In-Vehicle Configuration

The layout of the system when installed in a vehicle is shown in Figure 5. All of the major components were newly developed for the hydraulic active suspension.

Analysis and Design of Hydraulic Active Suspension

This section explains the procedure followed in designing the hydraulic active suspension. First, an analytical explanation is given of the three major functional features of the system—skyhook damper control, frequency-dependent damping mechanism and roll/pitch control. The concept applied in determining their control constants is also explained. After that, an explanation is given of the performance characteristics of the mechanical suspension used in conjunction with the

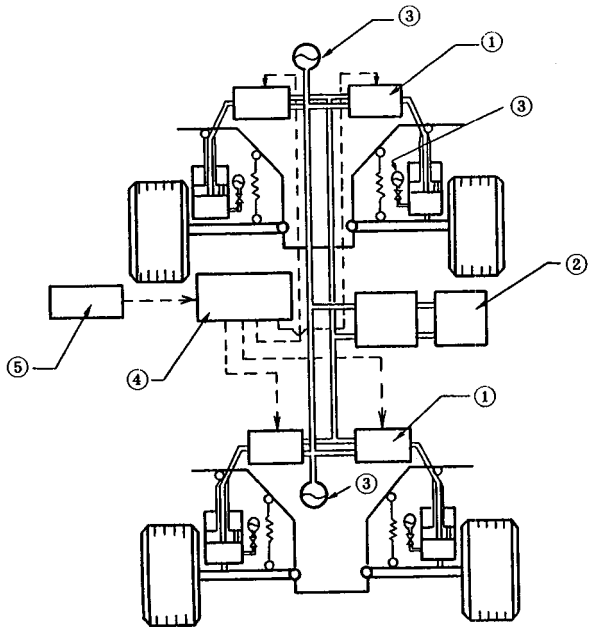

① Feedback Type Pressure Control Valve
② Radial Plunger Pump : 7 cylinders, 10 MPa
③ Accumulator : Free Piston Type
④ Controller : Built in High Speed 16 bit CPU
⑤ Accelerometer : Ball Detection Type

Figure 5. Schematic Diagram of Active Suspension System

hydraulic active suspension and of the sharing of the performance load between the two systems.

Skyhook Damper Control and Frequency-Dependent Damping Mechanism

The combination of skyhook damper control and the frequency-dependent damping mechanism is notably effective in damping both the sprung and unsprung resonances of the vehicle and in reducing the transmission of road surface inputs to the body. The following explanation indicates how this is accomplished.

Skyhook damper control. It has been noted that a skyhook damper, which produces damping force in proportion to the absolute vertical velocity of the vehicle body, is a rational approach to reducing body vibration [6]. This concept has been incorporated in the hydraulic control system of the Nissan active suspension. The equivalent models shown in Figure 6-(c) and (d) were used in analyzing the characteristics of a passive damper and the skyhook damper. When a passive damper is employed, the vertical vibration characteristic of the body in relation to road surface inputs is given by

$$\frac{x_2}{x_1} = \frac{2j\omega_2\zeta_2\omega + \omega_2^2}{-\omega^2 + 2j\omega_2\zeta_2\omega + \omega_2^2} \quad (1)$$

The vibration transmission ratio at the resonant point is

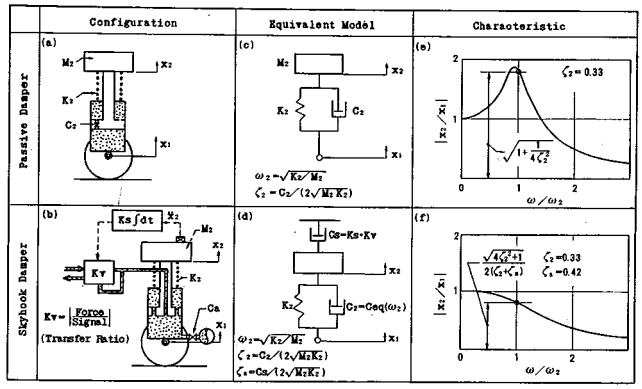

Figure 6. Configuration and Characteristics of Skyhook Damper

$$\left|\frac{x_2}{x_1}\right|_{\omega=\omega_2} = \sqrt{1+\frac{1}{4\zeta_2^2}} \tag{2}$$

and it always has a value greater than 1.

With the skyhook damper, on the other hand, the vibration characteristic is given by

$$\frac{x_2}{x_1} = \frac{2j\omega_2\zeta_2\omega+\omega_2^2}{-\omega^2+2j\omega_2(\zeta_2+\zeta_s)\omega+\omega_2^2} \tag{3}$$

The vibration transmission ratio at the resonant point is

$$\left|\frac{x_2}{x_1}\right|_{\omega=\omega_2} = \frac{\sqrt{4\zeta_2^2+1}}{2(\zeta_2+\zeta_s)} \tag{4}$$

Therefore,

$$\zeta_s \geq \sqrt{\zeta_2^2+1/4}\ -\zeta_2 \tag{5}$$

This makes it possible, then, to reduce the vibration transmission ratio to a value less than 1.

The skyhook damper system thus allows considerable design freedom for setting the damping ratio of active control, ζ_s, and that of the passive damper, ζ_2. In the Nissan hydraulic active suspension, these two damping ratios are set at $\zeta_2 = 0.33$ and $\zeta_s = 0.42$. These values have been set so that they satisfy Eq. (5)

Frequency-dependent damping mechanism. In the control system shown in Figure 3, the pressure control valve functions as a damping element against road surface inputs. As a result, the mechanism by which the suspension generates damping force is formed as shown in Figure 7(a). Using the equivalent model shown in (b) in the figure, the transmissibility characteristic can be found as

$$\frac{F_2}{\dot{x}_1-\dot{x}_2} = Cv\cdot\frac{jCa\omega+Ka}{j(Cv+Ca)\omega+Ka} \tag{6}$$

It is seen in Figure 7-(c) that the calculated result thus obtained agrees well with the experimental data, which indicates that the system has been modeled accurately.

The equivalent damping constant of this system, Ceq(ω), can be calculated with the following expression by letting H(ω) represent the right side of Eq. (6).

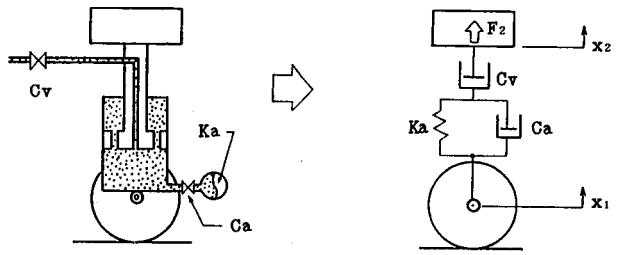

(a) Damping System (b) Equivalent Model

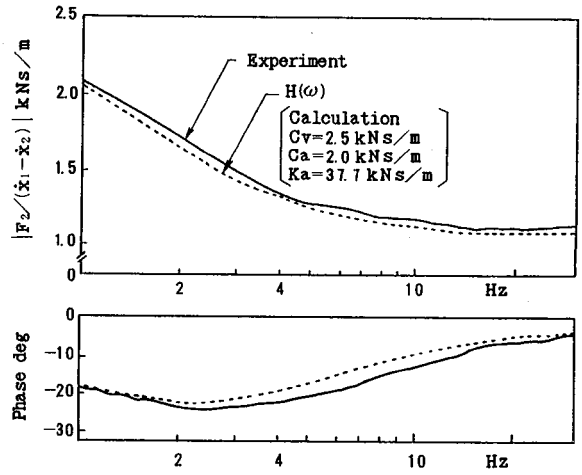

(c) Comparison between Experiment and Calculation

Figure 7. Frequency-Dependent Damping Characteristics

$$Ceq(\omega) = |H(\omega)|\cos(\angle H(\omega)) \tag{7}$$

Equation (7) is dependent on the design parameters of the hydraulic system. This means that the sprung and unsprung damping ratios, ζ_2, ζ_1, can be adjusted according to the hydraulic system design parameters. Further, their values can be set independently to match vehicle performance requirements. In the Nissan hydraulic active suspension, the 0.33 value of ζ_2, together with the effect of the skyhook damper, provides sufficient damping to attenuate sprung resonance. In addition, ζ_1 has been set at 0.17 so as to minimize the transmission of vibration from the road surface within the range where the tires can maintain good road surface contact.

Effect of skyhook damper and frequency-dependent damping mechanism. A calculation model was made by adding the skyhook damper in Figure 6-(b) and the frequency-sensitive damping mechanism in Figure 7-(c) to the suspension model in Figure 2-(a) having two degrees of freedom. The resulting model was used to calculate the vibration characteristics of a vehicle in relation to road surface inputs. The results obtained are compared in Figure 8.

We will define two typical indexes of ride comfort: α indicates the extent to which sprung resonance is damped and β indicates the extent to which the transmission of road surface inputs to the body is isolated. In both cases,

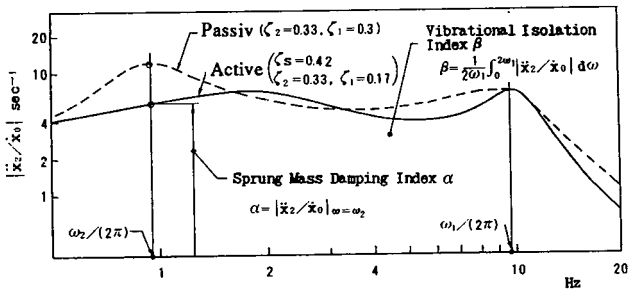

Figure 8. Comparison of Transmissibility (Calculation)

a smaller value means better ride quality. The two indexes are given by the following equations.

$$\alpha = |\ddot{x}_2/\dot{x}_0| \quad \omega = \omega_2 \tag{8}$$

$$\beta = \frac{1}{2\omega_1} \int_0^{2\omega_1} |\ddot{x}_2/\dot{x}_0| \, d\omega \tag{9}$$

Figure 9 compares the performance of an active suspension and a passive suspension with respect to the indexes α and β. With the passive suspension, a trade-off is required between α and β. In contrast, the skyhook damper of the active suspension works to reduce α and simultaneously the frequency-dependent damping mechanism is effective in reducing β. As a result, the performance characteristic of the active suspension shifts to the lower left region of Figure 9, surpassing the limits of the passive suspension.

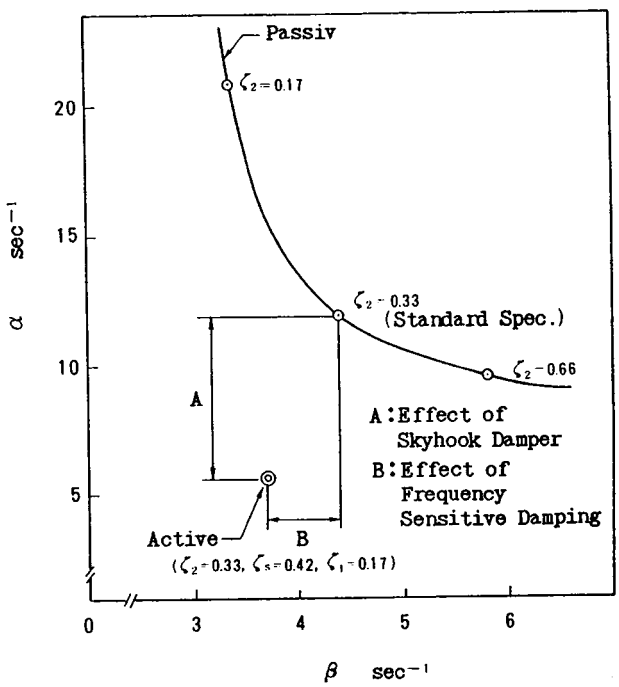

Figure 9. Improvement of Ride Comfort (Calculation)

Roll and Pitch Control

Body roll resulting from the effect of lateral acceleration, such as what occurs during cornering, is suppressed by generating a counter roll moment, referred to here as roll control. This is accomplished by increasing the hydraulic pressure at the outside wheels of a turn and reducing it at the inside wheels so as to produce a counter force that is proportional to the output of lateral accelerometers.

Pitch control is also effected in the same way. A counter pitching moment is generated that is proportional to the output of a longitudinal accelerometer. This works to suppress dive and squat motions during braking and rapid acceleration.

Since roll and pitch control is used in combination with skyhook damper control, the model shown in Figure 10 was prepared so that the entire control system could be analyzed. While this model focuses on roll, bounce and lateral motions, a similar model can also be created for pitching.

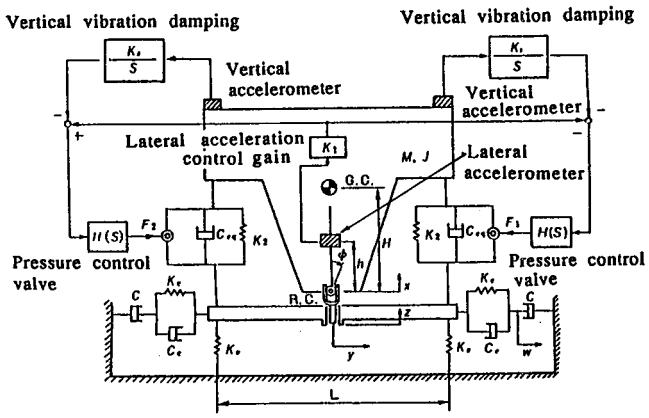

M: vehicle mass
L: tread
J: roll moment of inertia
C: tire cornering power/vehicle speed
K_ω: vertical spring rate of tires
K_ε: lateral stiffness of tires

Figure 10. Analytical Model

Roll control response in relation to crosswind inputs. Using the model in Figure 10, a crosswind input was applied to the vehicle body in the form of a sine wave and the roll rate response was calculated. The calculated results are shown in Figure 11. Since this analysis did not include yaw motion, the conditions were slightly different from those of real-world driving. Nonetheless, the results clearly indicate the effects of roll control and skyhook damper control. It is seen that roll control is effective in suppressing body roll during cornering by counterbalancing the force of inertia (centrifugal force), although it produces the opposite effect in relation to a crosswind. On the other hand, skyhook damper control works to suppress body roll even in a crosswind. It suppresses roll motion sufficiently to more than offset the increased body roll that is induced when roll control is applied in a crosswind.

Control of transient steer characteristics. Yaw stability generally declines at higher driving speeds because of the reduced gripping power of the tires and the increased inertial force of the vehicle owing to the occurrence of

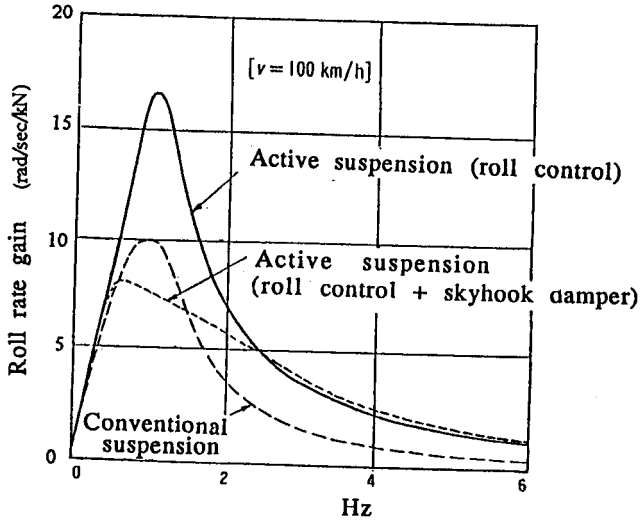

Figure 11. Body Roll Response in Relation to Crosswind Input

yaw motion. To overcome this problem, the Nissan hydraulic active suspension provides transient control over lateral load shifts that occur during roll control, which works to improve high-speed stability.

The specific method used is a very simple one in which the lateral accelerometer for the front wheels is installed aft of the lateral accelerometer for the rear wheels. Typical experimental results obtained with this control procedure are shown in Figure 12. These data are for a sudden lane change that was executed at a speed of 100 km/h. The notation ε in the figure indicates the amount of change in transient steer characteristics and is given by

$$\varepsilon = |\Delta W| \cdot \left(\frac{\Delta W_f}{\Delta W} - 0.6\right) \qquad (10)$$

where ΔW_f is the lateral load shift at the front wheels and ΔW is the total lateral load shift for both the front and rear wheels.

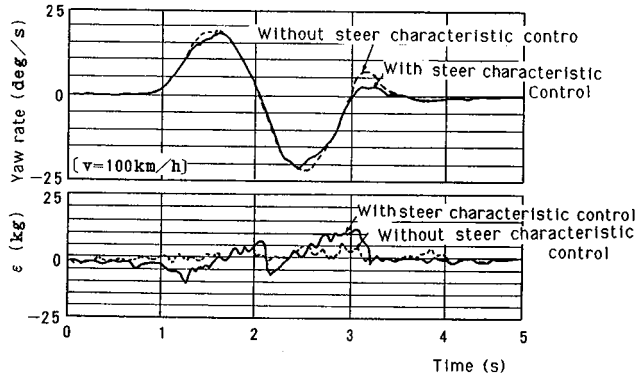

Figure 12. Effects of Steer Characteristic Control

A comparison with the results obtained when the same lateral accelerometer was used for both the front and rear wheels indicates that the above-mentioned control procedure was effective in reducing yaw rate overshoot. This is attributed to the fact that it caused ε to shift to the positive, i.e., understeer, side at the time of convergence.

Characteristics of Mechanical Suspension and Sharing of Performance Load Between the Two Suspensions

When a production vehicle is equipped with the hydraulic active suspension, it is necessary to return the mechanical suspension system to achieve a good match between the two systems. The procedure for matching active control and a mechanical suspension is outlined in the flowchart in Figure 13.

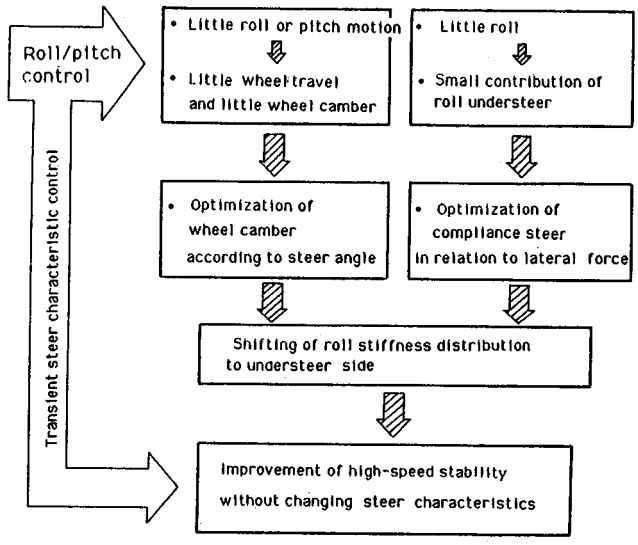

Figure 13. Procedure for Matching Active Control and Mechanical Suspension Characteristics

The aim of this matching procedure is to improve yaw stability at high-speed without substantially altering the steer characteristics.

The procedure is explained here following the order in the flowchart. The effects of roll and pitch control are clarified in the first step. At the front end, the travel of the outside wheels of a turn is reduced by the application of roll/pitch control. As a result, a larger effect is achieved by applying negative camber according to the steer angle than by applying it on the bound side as has been done traditionally. At the rear, the reduction of roll motion makes it impossible to attain improved stability through the use of roll steer. Consequently, it is necessary to provide for a sufficiently large compliance steer characteristic.

The second step concerns the optimization of the performance required of the mechanical suspension. The third step indicates the direction taken in tuning the mechanical suspension. The fourth step indicates the final performance objective, including the addition of transient steer characteristic control.

In this example the mechanical suspension is adapted to active control in order to obtain the final performance objective. Depending on the nature of that objective, it may be necessary to tune both the active control method and the characteristics of the mechanical suspension.

Improvement in High-Speed Safety

Contribution of Each Control Function to Performance Improvements

The respective areas of vehicle performance that are improved by skyhook damper control, frequency-dependent damping mechanism and roll/pitch control, the three major control features of the hydraulic active suspension, are outlined in Figure 14.

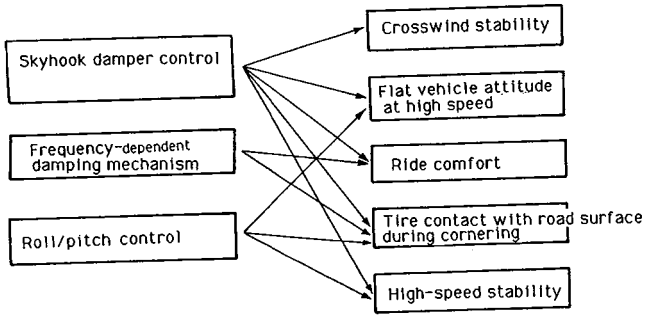

Figure 14. Contribution of Each Control Function to Improved Vehicle Dynamics

Improvement in high-speed stability works to stabilize vehicle behavior following the execution of an emergency driving maneuver to avoid a forward obstacle when traveling at high speed. This improved stability helps to some extent to prevent accidents caused by unstable vehicle behavior resulting from the execution of such sudden driving operations by the driver.

Improved tire contact with the road surface during cornering can reduce the possibility of an accident due to swerving by the vehicle toward the road shoulder. Such vehicle behavior can occur as a result of a reduction in the cornering force of the tires while cornering on a rough road surface.

Better crosswind stability and maintenance of a flat vehicle attitude at high speed both increase the capacity to stabilize vehicle behavior against external disturbances. Improvements in these performance parameters help to reduce the driver's workload during high-speed driving.

Improved ride comfort resulting from a reduction in body vibration is effective in mitigating occupant fatigue especially during long trips.

As those examples illustrate, the improvements in vehicle performance obtained with the hydraulic active suspension all help to stabilize vehicle behavior during high-speed driving and thus they serve to reduce the workload of the driver. In this way, they are effective in improving active safety at high speed.

Steering Performance

Steer characteristics. Figure 15 compares the change in steer characteristics for an active suspension vehicle and one equipped with a mechanical suspension. The vehicles were gradually accelerated from a very low speed while turning in a circle, 15 m in radius, at a fixed steering wheel angle. As was expected, the active suspension vehicle displayed performance on a par with its mechanical suspension counterpart.

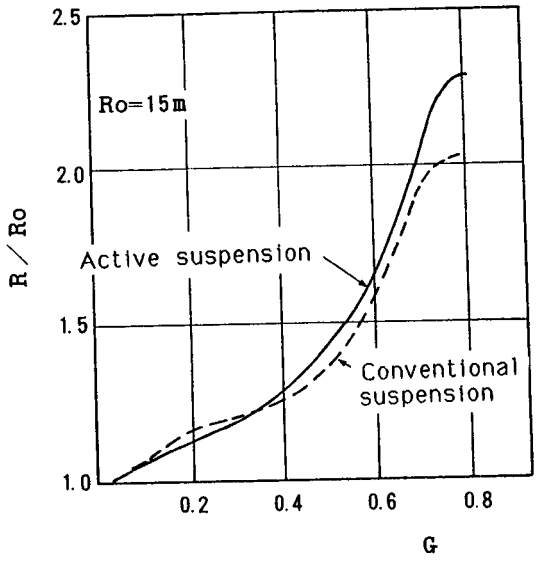

Figure 15. Steer Characteristics

Frequency response characteristic. Figure 16 compares the yaw rate response of the two vehicles in relation to a steering input of ±30 degrees when traveling at a speed of 100 km/h. The active suspension vehicle shows a smaller increase in the peak gain of the yaw resonance frequency, indicating better yaw stability.

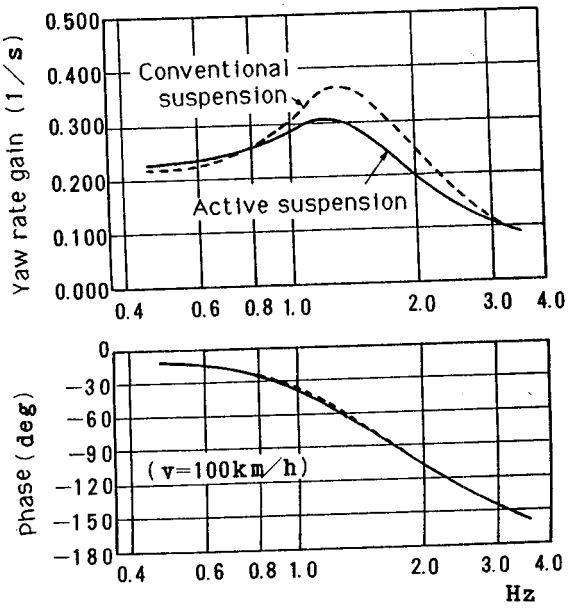

Figure 16. Frequency Response of Yaw Rate

Figure 17 shows a similar comparison for the roll rate response. The results for the active suspension vehicle show effective suppression of body roll at a roll resonance frequency of 1 Hz and phase improvement is also seen. While the reduction in the steady-state gain is attributed to the effect of roll control, the reduced gain

seen at the resonance point is also due in part to the roll damping effect of the skyhook damper.

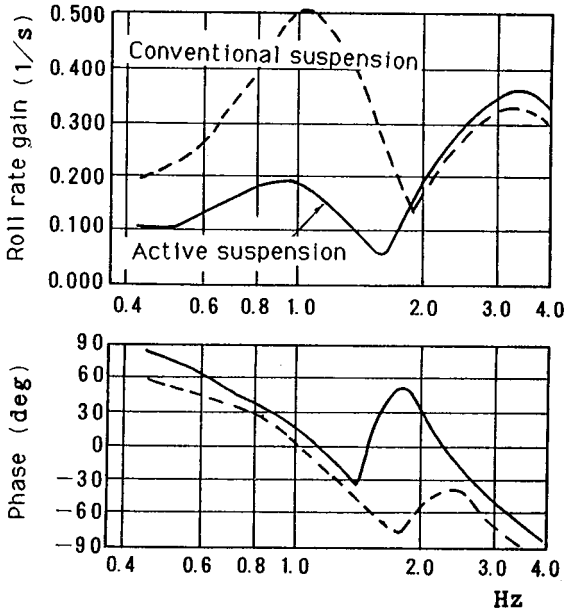

Figure 17. Frequency Response of Roll Rate

Ride Comfort and Tire Contact with Road Surface

Figure 18 compares the vertical vibration of the floor that was measured when the two vehicles were driven on a level road surface at a speed of 100 km/h. The active suspension car shows a lower vibration level in nearly every frequency range and the measured data validate the calculated results presented in Figure 8. The reduced vibration level at sprung resonance frequencies of 1~2 Hz is attributed to the effect of skyhook damper control. At higher frequencies, the reduction is attributed to the effect of the frequency-dependent damping mechanism. These results indicate that the Nissan hydraulic active suspension provides a soft, pliant ride together with a flat, stable vehicle attitude.

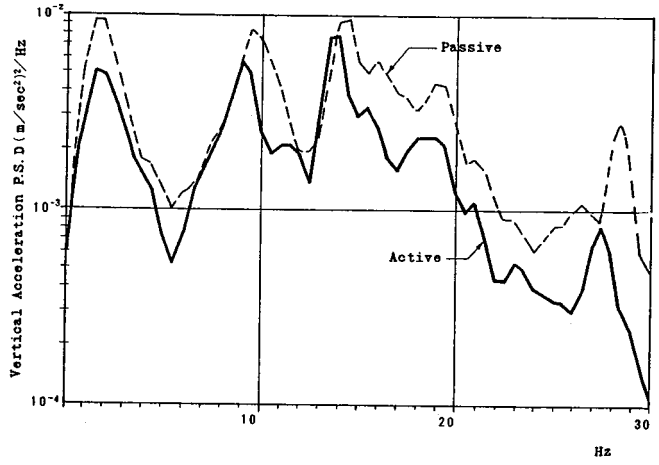

Figure 18. Body Vibration on a Level Road Surface

Figure 19 compares the body vibration that was measured in the two vehicles when they were driven at high speed over an undulating road surface which tends to cause sprung resonance. Although this figure shows only the results for vertical vibration, similar tendencies were also observed for pitching. The low level of vibration seen at low frequencies where sprung resonance typically occurs indicates that there was little change in tire contact with the road surface. This result clearly shows the effectiveness of the active suspension in improving the road surface contact of the tires. In real-world driving, tire contact with the road surface becomes an issue of concern during cornering. By effectively suppressing body roll, the Nissan hydraulic active suspension assures sufficient suspension travel in the bound direction at the outside wheels of a turn and this also contributes to improved tire contact with the road surface.

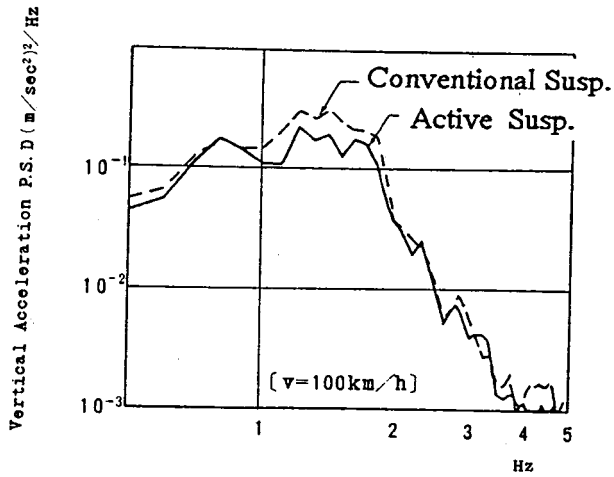

Figure 19. Body Vibration on an Undulate Road Surface

Crosswind Stability

The results of a crosswind stability test indicated that there was a large difference in roll rates between the two vehicles, while virtually no difference was seen in their yaw rates. Measured data on the roll rates of the vehicles are given in Figure 20. The results for the active suspen-

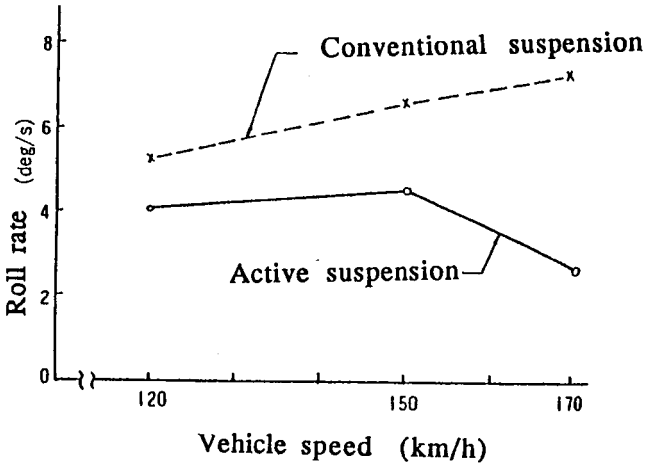

Figure 20. Crosswind Stability

sion vehicle show that skyhook damper control was noticeably effective in mitigating body roll even in a crosswind, as mentioned earlier in 4.2.1. This damping effect contributed to the improved crosswind stability seen for the active suspension vehicle.

Conclusion

The results of theoretical analyses, simulations and experimentation show that the Nissan hydraulic active suspension mounted in the Infiniti Q45 achieves vehicle dynamic performance that was previously unobtainable with conventional suspensions. This performance results from skyhook damper control, a frequency-dependent damping mechanism and roll/pitch control, the three major functional features of the suspension system, and from the good matching achieved between active control and the characteristics of the mechanical suspension.

The improved performance achieved with this suspension system works to stabilize vehicle behavior by minimizing attitude changes that can be induced by sudden driving maneuvers, crosswinds, road surface inputs or other changes in the driving environment. Improved stability, in turn, reduces the driver's workload under all sorts of driving conditions and thereby enhances active safety.

References

1. Hedlick, J.K., "Railway Vehicle Active Suspension," Vehicle System Dynamics, 10, (1981), p. 267.
2. Packer, M.B., "Active Ride Control—A Logical Step from Static Vehicle Attitude Control," SAE paper 780050.
3. Wright, P.G. and Williams, D.A., "The Application of Active Suspension to High Performance Road Vehicles," I Mech E Paper, C 239, (1984), p. 123.
4. Kawarazaki, Y., et al., "Development of the Nissan Hydraulic Active Suspension," pre-print of SAE-Japan (in Japanese), 892 (1989-10).
5. Yonekawa, T., "Vehicle Dynamics of Active Suspension Control," pre-print of SAE-Japan (in Japanese), 901 (1990-5).
6. Kamopp, D., "Active Damping in Road Vehicle Suspension System," Vehicle System Dynamics, 12, (1983), p. 291.
7. Thompson, A.G, "Optimal and Suboptimal Linear Active Suspension for Road Vehicles," Vehicle System Dynamics, 13, (1984), p. 61.

S7-O-06

Development of Tyre Checking Equipment

Roland Lucquiaud
U.T.A.C.

Abstract

In order to reduce the number of accidents due to tyre blow-outs on motorways, it has now become important to find technical solutions to improve road safety. Experience has shown that driving at high speed on long distances with underinflated tyres may result in a fatal blow-out. This may even happen at an earlier stage because tyres store many former aggressions. So we are currently developing methods and technical means to check the tyre pressures and the good condition of tyre structures:

- T*yre pressures using a stationary equipment located outside the vehicle.* This device consists of a propelled mass and a force transducer hitting the tyre tread. Parameters calculated from form and duration of the delivered signal are related to inflation pressure. The next step now consists in implementing the equipment where vehicles are likely to stop for a short period of time (e.g. toll gates).
- *The good condition of tyre structures (mainly the internal condition of the casing).* A microphone set close to a running tyre on a drum delivers time and frequency signatures based on specific signal processing methods. A statistical analysis is then necessary to correlate signature parameters and danger criteria for good and damaged tyres.

Introduction

A great amount of car accidents on motorways are due to factors which differ from those on roads, namely fatigue, drowsiness, not taking account of bad weather conditions, blow-out of tyres. Though driving on motorways is four or five times safer than driving or roads and tyre blow-outs are responsible for merely 10% of motorway car accidents, the automotive industry has to carry out studies to reduce as far as possible the amount of accidents due to this.

The blow out of a tyre could be linked to a mechanical failure of one tyre. However, analysis often reveals that the involved tyre was underinflated and rolling for a long time at high speed. Analysis may also reveal that the involved tyre may have stored former aggressions (when hitting the curb, or running over potholes).

Consequences of Driving with Tyres in Bad Conditions

Driving with under-inflated tyres has the following consequences: it increases the car consumption, modifies

the road holding qualities (when braking or taking bends) at high speed without the driver's knowing. In this case, casing and tread plies are submitted to an overheating, that may bring about the detachment of the tread pattern.

On-Board Devices for Inflation Pressure Control

These devices are under development in order to control continuously the inflation pressure of the four wheels and to warn the driver if a tyre is going flat (made by Michelin, Bosch, Dunlop, Labinal, . . .). These devices will only be supplied on "haut de gamme" vehicles on option within a few years.

Checking the Inflation Pressure: Our External Device

The Principle

We developed a measurement system that allows to check the inflation pressure of tyres, at toll gates where vehicles still have to stop for a short time. It relies on the following measurement principle: a mass fitted with a force transducer is propelled and hits the tread pattern under the tyre. Form and duration of the delivered signal have to be analyzed in order to estimate the inflation pressure: on figure 1, we can see that the longer the impact, the less inflated is the tyre. But the impact duration depends on the tyre structure (figure 2).

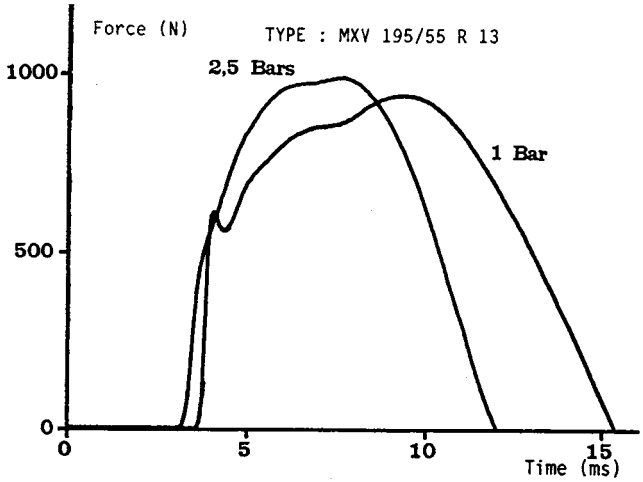

Figure 1. Influence of Inflation Pressure on the Shock Signal (for Two Extreme Pressure Values)

Data Processing

Several parameters (shock energy, asymmetric coefficient and kurtosis based on the 2nd, 3rd, 4th statistical moments) can be calculated. For each tyre, a linear relation between parameters and air pressure can be found (see figure 3 for relation between kurtosis and inflation pressure for two tyres). A prediction model for inflation pressure has to be improved with a covariance analysis of a large amount of tyres. Our preliminar study shows that the model can't apply to all the tyres together. The

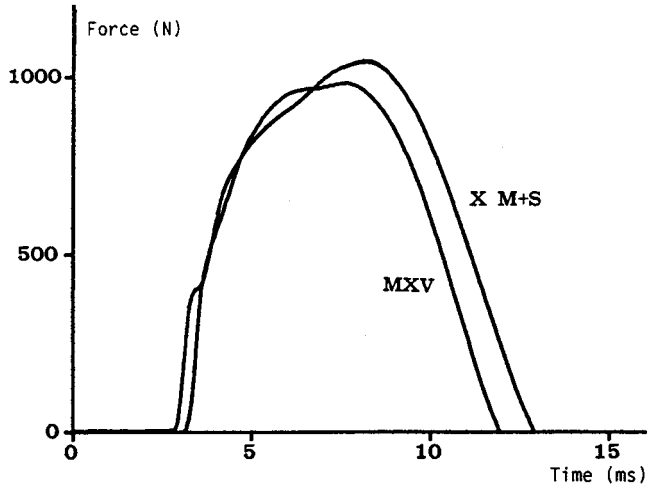

Figure 2. Influence of Tyre Structure on the Shock Signal (Inflation Pressure = 2 bars, with Two Different Tyres: Michelin MXV 195/55R13 and Michelin X M+S 145R13)

multiple correlation coefficient increases when we classify the tyres in three classes: tyres for small range, medium range and high range of passenger cars. The prediction model gives more reliable results for the first class which looks the most homogeneous: tyres with an overall width lower or equal to 165 mm and with an aspect ratio between 80 and 65).

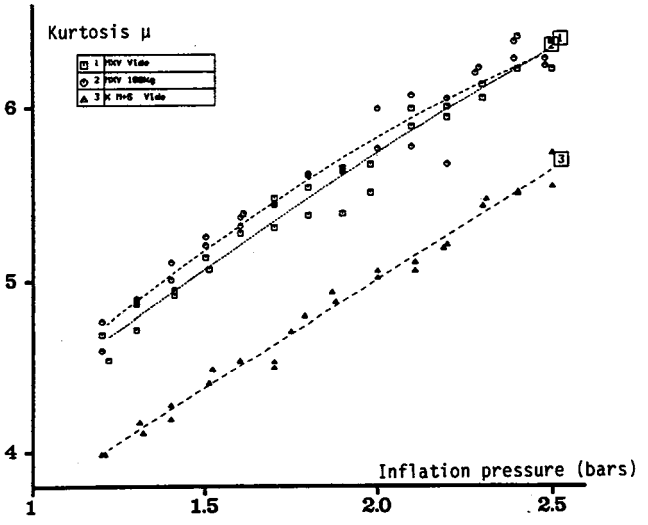

Curve 1: Michelin MXV with normal load.
Curve 2: Same tyre with an additional load.
Curve 3: Michelin X M+S. $\mu = (\int F^4(t)dt)/\int F^2(t)dt)^2$.

Figure 3. Kurtosis Coefficient Calculated for Different Inflation Pressures, for Two Different Tyres

The Device

The next step is to design the device that could test at once one axle of passenger cars, taking into account different aspects, such as car passengers safety and the vehicle's wheels position. For this, all the mobile parts have to be implemented under the ground; the guns containing the equipped mass have to move quickly left or

right according to vehicle position and gauge (figure 4). This device will allow us to improve our prediction model in order to obtain a better accurary of inflation pressure estimation. Furthermore, we have to study the influence of other parameters, such as tyre temperature, ambient temperature, tread wear . . . .

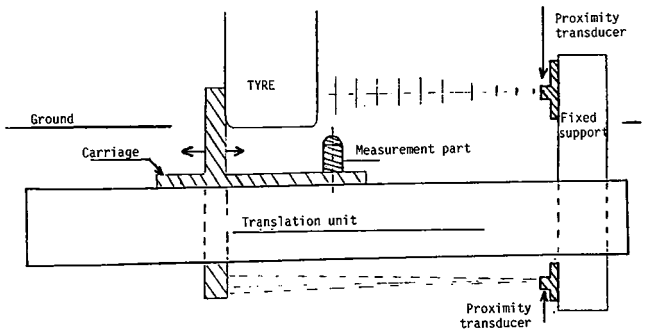

Figure 4. Sketch of the Checking Equipment for Inflation Pressure

Checking the Tyre Structure

About Technical Checking

A complete investigation of tyre conditions must be performed with the control of the tread wear and an internal control of the casing. The irregular wear of the tread is due to shock absorbers, wheel train, steering or braking parts that need to be repaired. But, it appears to be more difficult to assess whether shocks on the casing plies or breakers are serious or not without removing the tyre. It is also possible to detect inside the casing (by mottlings on the sidewall) when a vehicle has been driven with under inflated type for a long time.

Our Method

In order to detect the faults of tyres that can't be detected by a visual inspection, we investigated on a method using acoustics means. The principle is similar to the one applied for fault detections in rotating machines (gears and bearing of gearboxes, blades of fans or turbines). We have to analyze the sound pressure of a microphone closed to the tyre running on a drum. On figure 5, a fault can be revealed on a time signature. These time signatures are obtained by a "conditioned" averaging: each signature lasts one tyre revolution and is averaged synchronous with each revolution in order to extract the tyre-periodic signal. The spectral signatures of the sound pressure signal show many peaks at harmonics of the revolution frequency. With these spectral data, we need to apply specific signal processing methods (cepstrum analysis, Hilbert transform) that allow us to come back to the time domain. These methods may help diagnose the periodic faults on a tyre.

Development Work

In order to improve the analysis, we have to fill in a bank of signatures of tyres, some with well-known faults and some without any faults. The study of the signatures

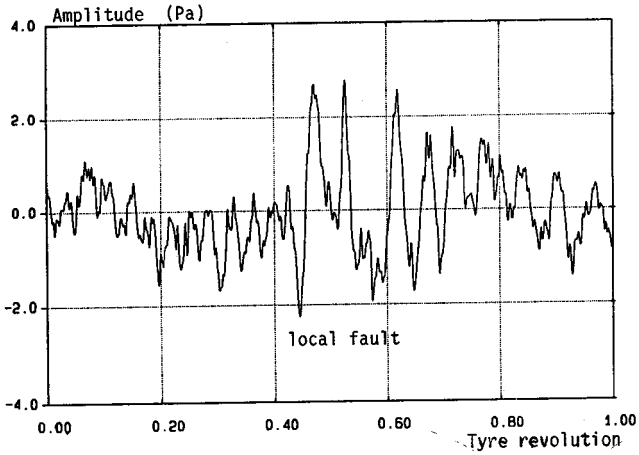

Figure 5. Time Signature for a Tyre Without Any Fault (60 km/h, Inflation Pressure 4 Bars)

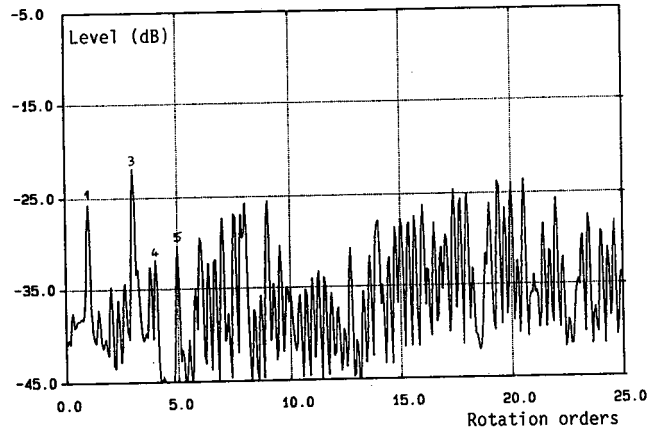

Figure 6. Spectral Signature for a Tyre Without Any Fault (60 km/h, Inflation Pressure 4 Bars)

content requires knowledge about how tyres are manufactured in most cases and about the noise generation mechanisms. We also have to study the influence of rolling conditions and find the best (for inflation pressure, revolution speed).

Acknowledgments

The author gratefully acknowledges the help of ASSECAR (Association Securite Autoroute) for the development of the inflation pressure checking equipment, and the support of SERT (Service des Etudes de la Recherche et de la Technologie du Ministere de l'Equipement, du Logement, des Transports et de l'Espace) for the investigations on both methods.

References

1. R. Lucquiaud: Sous gonflage des pneumatiques. Rapport UTAC 90/1385. Novembre 1990.
2. R. Lucquiaud: Controle de l'état interne des pneumatiques. Rapport UTAC 90/1986. Novembre 1990.
3. ASSECAR: Sous gonflage des pneumatiques—enseignements à tirer de l'opération. Plein d'Air été 1985 Fevrier 1 986.

4. M. Scholz: "Fahrzeugreifen: Ungleichförmigkeiten an Luftreifen." Teil 1 + Tell 2 - F + K 11/1984 pp 30-32 F + K 12/1984 pp 34-36.
5. "Les causes d'usure et de détérioration prématurées des pneus." Le relais - Total. Mai 1985 et Juin 1985.
6. J.F. Gaillochet: "Méthodes de surveillance de l'état mécanique des machines au moyen de l'analyse des vibrations." Note interne Cetim. Juillet 1979.
7. P. Coudray: "Surveillance des machines par analyse de vibrations. Application aux réducteurs à engrenages." Ingenieur de l'Automobile. Janvier-Fevrier 1983, n° 1, pp 60-65.
8. G. Sapy: "Une application du traitement numérique des signaux au diagnostic vibratoire de panne: la détection des ruptures d'aubes de turbines." Automatisme tome xx, n° 10, Octobre 1975, pp 392-395.
9. R.B. Randall: "Cepstrum analysis and gearbox fault diagnostic." Bruel & Kjaer application. Note 233-80.

S7-O-07

How About the Average Driver in a Critical Situation? Can He Really Be Helped by Primary Safety Improvements?

Alain Priez
Institut de Recherche Anatamo-Chirurgical et de Biomécanique Appliquée
Claire Petit
Institut de Recherche Biomécanique et Accidentologique
Bruno Guézard, Lionel Boulommier
Association d'Aide à la Recherche intéressant la Médecine du Travail
André Dittmar, Alain Delhomme
Laoratoire de Thermorégulation CNRS URA
Evelyne Vernet-Maury
Université C. Bernard
Edwidge Pailhous
Psychologist, 82 bd. Buzenval, Paris
Jean-Yves Foret-Bruno, Claude Tarriere
Renault France

Abstract

Since primary safety is the unique possibility to protect automobilists in 1/2 of the crashes, it needs to quantify the efficiency of these systems. The authors consider that a primary safety system is efficient only if it avoids dead or injured people; Both the driver and the system have to be trailed at the same time. The ABS has recently been studied in this aim through a 100-drivers experiment. Preliminary results are shown. Although the ABS is famous, it appears that most drivers don't know how it works and misused it.

Introduction

In 1990, road accidents in France resulted in 10,289 deaths (6,295 automobilist deaths). Despite all the improvements which it is possible to make to different restraint systems (assuming that everyone uses these devices), and taking into account all the improvements in vehicle structural reinforcement still possible, in at least 51% of the cases, impact severity is so great that it seems to be outside the realm of current secondary safety technical capabilities and economic possibilities (Thomas, 89). This being the case, then in more than 1/2 of accidents, the only solution is primary safety and accident avoidance.

Accident avoidance systems are already available in vehicles (anti-lock braking systems (ABS), controlled suspension systems, . . .) or are being studied by different car or fittings manufacturers, they're even being studied within the framework of extensive international research programs (PROMETHEUS, DRIVE). These devices are going to allow a better management of some situation reaching the limits of the vehicle potential, maybe even traffic rules. Yet such changes in the way of driving are useful only if the system's efficiency is real.

Need to Evaluate Primary Safety System Efficiency

Primary safety system efficiency can be evaluated in terms of performance improvement. It is possible to measure in a precise way the improvements to road stability or vehicle braking obtained from the use of such a device. However, improvements in vehicle potential do not necessarily correspond to actual improvements in occupant safety.

Another method of approach is to evaluate the efficiency of a primary safety system in terms of accidents causing injury which have been avoided or lives saved due to the use of the system. The information thus obtained is directly useable to show the benefits possible from the generalized use of the given system.

However, this approach is much more difficult to carry out. In fact, in order to have reliable statistical data, it is necessary to test the primary safety system on a large scale, which means having a large number of vehicles equipped with the system and carrying out measurements over a sufficiency long period of time and across a sufficiently vast geographical area. Thus, the first drawback to such an approach is that information is

not available immediately but rather after a long delay which hinders the development of the system and improvement of its performance.

The other drawback is the very complexity of carrying out such an approach. The study cannot be carried out if the data collected at the scene of an accident is not precise or sufficient enough. Collecting such precise and adequate data means having people trained in gathering such data at the scene of an accident. As well, the given device's effect can only be determined by determining the cause of the accident, which is long and tricky work as it is susceptible to the injured or witness account reliability and to the interpretation of those doing the study. Lastly, accident study cannot be complete. In 1990, the French National Gendarmerie recorded 59,799 road accidents involving injuries. To this already high figure, it is necessary to add the accidents recorded by the National Police; in other words, the amount of data involved is considerable. Accidents resulting in only damage to property are not recorded although the safety device may have been responsible for making it possible to avoid injury in such accidents. In this case, only the damage to property is regretted, while perhaps the accident itself could have been avoided! Even insurance companies can only count the fatal, injury provoking or property damaging accidents, they cannot take into account "almost accidents" which every driver experiences at sometime, and which were avoided thanks to the safety device which needs to be evaluated. If the non-analyzed data in one year is difficult to interpret, it is possible to study the evolution of this data from year to year and compare the results from year to year.

If this approach involves complex implementation, it is the only one which can potentially quantify the gain in terms of lives saved through the use of a given device.

A last approach consists of evaluating the efficiency of a device during a test where the performance of the driver-vehicle pair is studied. This approach does not allow the direct quantification of the gain in terms of lives saved, but it does considerably simplify the study. The fact that it consists of a test situation, means that the same accident can be duplicated as many times as necessary, thus obtaining data from perfectly comparable circumstances. The number of experiments being known, it is very easy to measure the number of accidents avoided or involving low level impact. Last of all, the driver and the vehicle can be equipped with captors thereby simplifying considerably the collection of data concerning the pre-collision phase, in comparison to the collection of post-accident data. If the collection of statistically reliable data is easier using this method, the population studied will always remain limited as will the accident provoking configurations looked at. Only estimates will be possible from the situations tested.

Evaluation of Anti-lock Braking System Efficiency

The anti-lock braking system is the most promising primary safety system which has been put into general use in vehicles over the last 10 years. When it came out, certain insurance companies offered lower insurance premiums for vehicles equipped with the ABS system. After a number of years, these same insurance companies are now cancelling this advantage since equipped vehicles do not seem to be less involved in accidents than unequipped vehicles. The advantage in having an ABS braking system is however obvious. It allows vehicle control while braking through optimal use of adherence conditions and reduces braking distance to a minimum in all situations. So, while the efficiency of the ABS system is clear, its road efficiency remains to be seen, at least in terms of reducing the number of accidents and accident victims.

A number of studies have been carried out to measure the efficiency of the ABS system. Its usefulness was demonstrated on a test course while braking in a curve (Lechner et al., 1989). Non-professional drivers were to brake violently upon passing a marker placed at the beginning of a curve while driving at the instructed speed of 75 km/h. The increase in steering control is evident: most braking with the ABS system maintained to the vehicle's trajectory and the vehicle was stopped without leaving the road. This tendency was reversed when braking was carried out under the same test conditions without an ABS system. However, even if the drivers were not professionals, the fact that drivers were requested to brake upon passing a marker took away the element of surprise and renders this test closer to a mere vehicle performance test. Driver participation is in fact conditioned by the experimental circumstances, which limit the effect of the driver-vehicle interaction. In a study of drivers' emergency manoeuvres during a critical intersection situation, using a Daimler-Benz simulator, (Malaterre and Lechner, 1989; Lechner and Malaterre, 1990) the efficiency of the ABS system was not directly measured (the simulator was not equipped with the ABS system). However, the possible gain from such a system was extrapolated as a function of the measures carried out. 20 % of the accidents were avoided without the ABS system. With an ABS system, an additional 14 % of the accidents would have been avoided and the consequences of the accidents would have been lessened in 40% of the remaining cases. The difficulty in duplicating, with a simulator, the behavior of a vehicle equipped with the ABS system limited this study to making projections about the efficiency of the ABS system. Recent progress in simulation models should improve simulator credibility.

Experimental Procedures

The above two examples reveal the need to carry out an ABS system study under real driving conditions. Of the 37,972 accidents leading to injury involving at least one car which occurred on French roads in 1990, 13,749 were two-car accidents. Of these, 3,243 took place outside of city limits and at an intersection. This accident configuration, which corresponds to a quarter of the accidents involving two vehicles, seems typical of a configuration where the ABS system would have considerable positive effect on safety. The study described in this article is based on this accident type.

100 volunteer subjects were recruited from among Renault personnel. They were selected with the help of psychometric tests in order to evaluate their level of emotionality (Eysenck personality test and the Stroop stress test). All those chosen had a driver's license but the length of time they had it varied. None of them were professional drivers. Four groups of 25 subjects were formed:

- Group 1 used a car without an ABS system
- Group 2 used a car equipped with an ABS system but were not aware of this
- Group 3 used a car equipped with an ABS system and were aware of this
- Group 4 used a car equipped with an ABS system and had attended a half-day training in its use. This training consisted of a theoretical part explaining the objective and functioning of the ABS system, as well as a practical part involving demonstrations and avoidance exercises. This training took place two months before testing.

Dividing up of the subjects was carried out based on the psychometric test results so as to obtain homogeneous groups in terms of age, length of time in possession of a driver's license and emotionality. The fact that the test population was recruited from a sample of the working population lead to the under-representation of older people. However 70% of the drivers involved in this kind of situation were represented.

The subjects were informed that they were taking part in a study on primary safety and that their behavior, as well as that of the car, would be recorded during a driving run on a circuit which could present "critical situations." The car used was a Renault 25 TXI. In the cars used by Group 1 subjects, the ABS system was disconnected and braking was therefore of the normal sort.

The course was a closed circuit made up of connecting roads, parts of the circuit track and a two-lane road (7 m wide) delimited by cones placed in an open area. The course crossed a number of intersections, of which two were in the part of the course delimited by cones. At these two intersections, Renault 19 cars were stopped at stop signs with a driver at the wheel. Subject visibility was restricted by safe, artificial (polystyrene) walls which made it impossible to see the stopped Renault 19s, up until the last minute, at these two intersections. The other intersections can be relatively open or masked by vegetation.

The subject generally completed three runs of the course to become familiar with the car and the course. The number of runs can be varied so that those subjects waiting cannot figure out the length of the experiment. The course was new to each subject at the beginning of the test and the subjects waiting had no contact with those who had already completed the test. One run lasted 4 minutes and the total length of time to complete the test was about 12 minutes. The instructed speed was 100 km/h on straightaways and 80 km/h on curves. An experimenter, always the same, was next to the subject in the car in order to give speed and driving instructions and to verify if these instructions were carried out. The experimenter also ensured the safety of the subject by correcting any manoeuvres that could be dangerous.

During the last run, the Renault 19 positioned to the right of the second intersection was replaced by an inflated dummy car having the same features as a Renault 19. The subject's car passed in front of an optical beam which triggered a synchronization signal which released the obstacle. The walls concealing the intersection did not allow the subjects to see the obstacle until it pulled out into their lane. At this moment, given the speed of 100 km/h and a mean reaction time estimated at 0.8 seconds, the braking distance was 15 meters too short to avoid the obstacle. The average speed of the subject's car when it arrived at the obstacle was 40-50 km/h. The obstacle car crossed half of the intersection and then stopped. The left lane was free, allowing the subject's car to pass. This situation being very difficult, the first avoidance reaction was the only chance to avoid the obstacle.

The aim of the study was to evaluate the ABS system's efficiency considering the driver's use of it. To do this, a number of parameters were recorded from the car and from the subject. These were the following:

- From the car (16 parameters)
  - speed of each wheel
  - the ABS system's solenoid valve setting
  - steering wheel angle
  - longitudinal and transversal acceleration
  - brake pedal displacement
  - actions carried out on the accelerator, clutch and brake
  - actions carried out on the emergency brake
  - engine speed (to determine shifting)
  - obstacle car start up synchronization (photoelectric cells)
  - sync signals
- From the subject (12 parameters)
  - capillary flow
  - skin potential
  - skin resistance
  - skin temperature

- breathing rate
- heart rate
- biceps brachialii and finger flexor electromyograms (EMG)
- horizontal and vertical electro-occulogram (EOG)
- a micro-camera attached to the subject's right forehead to record his/her field of vision
- a video camera attached to the right-hand comer of the dashboard to film the subject's upper body during the experiment

The measurements were recorded throughout the entire experiment.

The first six measurements collected from the subject were designed to measure his/her concentration and stress level. All changes in concentration, even a simple mental computation, lead to neurophysiological changes. The first four measurements were collected from the palm of the left hand. The captors were placed in such a way so as not to hamper driving. The breathing rate was constantly measured by using a temperature sending unit placed under the nose. These measurement systems were developed by the URA CNRS 1341 Laboratory of Thermoregulation (Dittmar et al., 1985).

The EMG measured on the arm was designed to measure the subject's force and clutch on the wheel. The EOG and the micro-camera were used to evaluate where the subject was looking.

Furthermore, in order to examine the overall emotionality level of the subjects confronted with such a situation, all subjects filled out a self-evaluation questionnaire (ASTA test) before and after undergoing testing.

The aim of all these measurements was to objectify the subject's capacity to use the potential of the vehicle driven. The different tests made it possible to obtain homogeneous groups in terms of emotionality and to determine the emotional state of each subject before and after the experiment. The first two runs established the reference level for the parameters collected from the subject and determined the way the subject dealt with an intersection and his reactions in an emergency situation.

Results

Testing was carried out during the summer of 1991. Therefore, only preliminary results from 87 subjects will be presented here.

Influence of Group

The population studied was divided into four groups as a function of the information given to the subjects about the ABS braking system. The ages and sensitivity to stress of group members were homogeneous across groups:

- Group 1: the ABS braking system was disconnected ("normal" braking)
- Group 2: the car was equipped with an ABS system but the driver wasn't aware of it
- Group 3: the car was equipped with an ABS system and the driver was aware of this
- Group 4: the car was equipped with an ABS system and the driver had training

Results by group are given in Table 1.

Table 1

	group 1	group 2	group 3	group 4
Successfully avoided	0 %	21.8 %	17.7 %	29.2 %
Tried to avoid	39.1 %	30.4 %	23.5 %	50 %
Braking only	56.9 %	38.8 %	46.8 %	20.8 %
No attempt	4 %	9 %	12 %	0 %

The term "tried to avoid" refers to subjects who carried out a complex avoidance manoeuvre, that is to say braking and steering wheel movement. Even if they did not succeed, such a manoeuvre was necessary to avoid the obstacle. In the case of those that tried to avoid the obstacle, impact might have been less violent but data analysis to date has not gone so far as to let us break this down further.

If we want to look more closely at driver behavior and his/her ability to use all the ABS system's potential in the given situation, it is necessary to look at the first two lines of Table 1. The efficiency of the ABS system is demonstrated in the results obtained with group 1 for none of these subjects, who were driving cars not equipped with the ABS system, succeeded in avoiding the obstacle.

40 to 50 % of subjects attempted (successfully or not) to avoid the obstacle by turning the wheel. This percentage reaches 80 % for those in group 4 who attended a half-day training in avoidance manoeuvres.

The test was judged realistic by all of the subjects. Only a few subjects judged the obstacle insufficiently realistic. It should be noted that none of the subjects who judged the obstacle insufficiently realistic succeeded in avoiding it and all of them had a very belated reaction. It is difficult, given the limited data analyses having been carried out to date, to determine if the statement that the obstacle was insufficiently realistic is due to the real opinion of the subject, or is an attempt on the subject's part to excuse his bad reaction.

Influence of Age

If we study the population as a whole, age does not seem to effect results. The average age of subjects who avoided the obstacle is 32.5 (+ 7.3 years), the average age of those who carried out a complex avoidance manoeuvre is 30.1 (+ 6.5 years), and that of those who tried nothing is 31.7 (+ 7.3 years). It is however interesting to study this point in more detail by breaking down the population as a function of age (see Table 2).

Subjects between the ages of 26 and 36 have the highest success rate. Approximately 60 % of subjects over 26 completed a proper manoeuvre, while only 45 % of those under 26 and over 37 completed a proper manoeuvre.

Table 2

	< 26 years old	26 to 36 years old	37 to 47 years old
Successfully avoided	9.1 %	21.8 %	15.8 %
Tried to avoid	36.4 %	39.1 %	31.6 %
Braking only	50 %	39.1 %	47.4 %
No attempt	4.5 %	0 %	5.2 %

None of the subjects in the study were over 47 years old. This definitely results in a skewed study as 29 % of French drivers on the roads are over this age. As well they make up 37 % of those involved in this type of accident and 50.5 % of those presumed responsible for such accidents. This over 47 age group are mainly the drivers of the car which cuts across the road, represented in this study by the obstacle. However, considering only the drivers who are not responsible, the Renault 25 drivers, the test population covers more than 70 % of the age groups concerned.

Length of Driving Experience

The amount of driving experience can be measured by the number of years the person has had his/her driver's license. Subjects who avoided the obstacle had their license, on the average, for 13.7 years (+ 6.4 years). Those who carried out an avoidance manoeuvre had it, on the average, for 11.9 years (+ 6.8 years). Those who did not attempt an avoidance manoeuvre had it for 12.8 years on the average (+ 7.3 years). These differences are not significant. A detailed breakdown is given in Table 3.

Table 3

	< 10 years	10 à 20 years	20 à 30 years
Successfully avoided	15.5 %	20 %	17.7 %
Tried to avoid	35.6 %	40 %	29.4 %
Braking only	46.7 %	20.8 %	52.9 %
No attempt	2.2 %	16.7 %	0 %

As in Table 2, the middle column of Table 3 shows the highest success rate and the highest rate of choosing the proper manoeuvre.

It is interesting to breakdown first column results. Of those subjects having had their driver's license for fewer than 5 years, none succeeded in avoiding the obstacle. Of those who had obtained their license < 6 years ago, only one in 17 succeeded in avoiding the obstacle. From there on, the figures become progressively those found in Table 3.

Influence of Driver Personality

During the pre-selection period, all subjects took a series of tests designed to evaluate their personality (Eysenck test) and their reaction speed (Stroop test). These tests, carried out by Mrs. Pailhous, were used to divide the subjects into four groups as a function of their ability to react to a stressful situation. These groups were Group A - insensitive; Group B - not very sensitive; Group C - rather sensitive; Group D - very sensitive. The influence of this measure is summarized in Table 4.

Table 4

	Group A	Group B	Group C	Group D
Successfully avoided	13.4 %	25 %	13.8 %	13.3 %
Tried to avoid	53.3 %	42.8 %	34.5 %	13.3 %
Braking only	33.3 %	21.5 %	48.2 %	66.7 %
No attempt	0 %	10.7 %	3.5 %	6.7 %

A subject's ability to carry out an avoidance manoeuvre seems to be strongly linked to his/her emotional reactions. The first two columns give results for subjects who are not highly sensitive to stressful situations. Only one third of them did not react correctly to the situation. Of the more sensitive subjects, half, indeed even three quarters, experienced stress loads too high to allow them to carry out the proper manoeuvre.

Discussion

The experimental conditions used correspond to a critical situation, braking alone in such a situation being insufficient to avoid the accident. In this sort of critical situation, the efficiency of the ABS braking system is evident. The simple fact of having the system allows accident avoidance in 20 % of the cases. Training subjects in the use of the ABS system contributes to avoiding almost a third of accidents.

In the first three groups, 50 to 60 % of the subjects did not try to turn the steering wheel even though the distance between the obstacle and their car was too short for braking alone to be enough to avoid the accident. In the group which received training, 80 % of the drivers undertook the appropriate manoeuvre. This considerable improvement in performance reveals the usefulness of such training.

This half-day training took place 2 months before testing. In the first part of the training period, how the ABS braking system works was described, as were the advantages of this system in comparison to a conventional braking system. The theory behind the limitations of the system were explained (stopping distance equal to that of the conventional braking system given a dry surface and that the driver was trained and not surprised). During the second part of the training, the subjects attended (as passengers and as observers from the outside) demonstrations on the efficiency of the ABS braking system on wet surfaces (little adherence) or mixed surfaces (two wheels on a wet surface and two on a dry one). Lastly, each subject carried out "emergency" braking while on a straightaway, on a dry surface, and an avoidance manoeuvre. This avoidance manoeuvre was done within a course marked by cones, activating the ABS braking system and requiring that the steering wheel be turned. This manoeuvre was different from the manoeuvre required in the test situation. It is interesting to note that none of the subjects succeeded in activating

the ABS braking system during their first try at straight line "emergency" braking. All subjects had to try again at least once in order to succeed (for each of the two exercises, the subject continued trying until s/he succeeded).

The fact that setting up such a short training is relatively simple, increases the interest in doing so. Moreover, 4 of the subjects owned cars equipped with an ABS system. They were placed in the first group (2 subjects), the third group (1 subject) and the fourth group (1 subject). Even thought this number is too small to be statistically significant, the first three subjects did not try to turn the wheel during the test, only the subject in the fourth group carried out the proper manoeuvre (and avoided the obstacle). Despite the fact that their use of the ABS system was not good, these subjects felt more confident because their car was equipped with the system.

It may be initially surprising to note the results of the third group, which was informed that their vehicle was equipped with an ABS system, were not as good as the results from group 2, which was not informed their vehicle was equipped with an ABS system. This below standard performance however can be explained by a generally poor understanding of the system and a feeling of increased safety due to this system, which is generally badly used. This hypothesis is upheld by the interviews done during the tests. In these interviews, the subjects described the ABS system as a device enabling more effective and higher quality braking (i.e. optimal, stronger braking with braking distance greatly shortened under all circumstances).

The difficulties experienced by the subjects in spontaneously activating the ABS system may be due to a high level of conditioning to normal breaking and the fear of locking the wheels. These would suggest that the presence of an audible signal or a signal light indicating whether the ABS system has been activated or not would be helpful.

It is of interest to note that a large number of subjects who could not avoid the obstacle considered the manoeuvre too difficult, even impossible, to carry out. These subjects expressed surprise when they learned that others had succeeded in avoiding the obstacle. Professional test drivers who participated in the preparation of this experiment rated the manoeuvre doable but difficult. This demonstrates the interest in carrying out further testing on safety systems with non-professional drivers.

The influence of age currently cannot be considered as it can only be seen as a reflection of the importance of the length of a person's driving experience (determined by the length of time a person has had his/her driver's license). It is important to note at this point, the poor performance of subjects who have had less than 6 years driving experience.

References

Dittmar, A., Saumet, J.-L. and Vernet-Maury, E.; "Apports des paramètres thermovasculaires dans l'analyse de la réponse électrodermale;" J. Physiol., Paris, pages 80, 3, 22, 1985.

Lechner, D., Van Elslande, P. and Jourdan, J.-L.; "Utilisation d'un système ABS par des conducteurs non professionels lors d'un freinage en courbe;" INRETS report #4; 1989.

Lechner, D., and Malaterre, G.; "Expérimentations de manoeuvres d'urgence sur simulateur de conduite;" Second part : "L'analyse détaillé des manoeuvres;" INRETS report #103; 1990.

Malaterre, G. and Lechner, D.; "Expérimentations de manoeuvres d'urgence sur simulateur de conduite;" First part: "comportement des conducteurs;" INRETS report #104; 1989.

Thomas, C., Koltchakian, S., TarriËère, C., Tarrière, B., Got, C., and Patel, A.; "Les priorités en sécurité primaire que désignent les limites de faisabilité technique en sécurité secondaire automobile;" XXIII F.I.S.I.T.A. conference; May 7-11, 1990.

S7-O-08

Crash Avoidance Capability of 50 Drivers in Different Cars on Ice

Lennart Strandberg
Swedish Road and Traffic Research Institute, VTI

Abstract

Experiments were carried out with more than 50 non-professional drivers making acceleration, deceleration and lane change manoeuvres on ice at speeds where skidding was expected. The subjects drove their own car and four reference cars (Volvo 440 or 740) with front or rear wheel drive, and with differently studded tyres. The ABS-function was switched on or off. The reference cars were tested by the drivers in different order according to a Latin-Square design. In a combined braking and smooth lane change manoeuvre, ABS increased the average deceleration significantly. Steerability and stability were also superior with ABS: lane marks hit in one (1) of 208 tests compared to 30 of 208 tests without ABS. Deceleration was 20% greater with fully studded tyres than with basic studding on all wheels. In a non-braking but more severe double lane change manoeuvre, Loss-of-Control (LoC) occurred in 40% of the tests with oversteering properties, induced by front biasing stud

protrusion and number. If front and rear tyres were switched to understeering, less than 20% of the tests resulted in LoC. With all tyres fully studded, front driven cars had 30% LoC, which was 2-3 times greater than for the larger rear driven cars. Still, the larger cars were superior in manoeuvre severity quantities, such as lateral acceleration derived from speed and path geometry. The correlation of these quantities to LoC relative frequency was not confirmed by the present study. Several observations give cause for more emphasis on vehicle dynamics in driver education.

Introduction

Background

The safety potential of modern vehicle technology may be lost, if drivers do not utilize the crash avoidance properties in emergencies. But also in normal driving on slippery roads, appropriate driver behaviour varies considerably between cars. The need of driver education in safety-relevant car differences has been confirmed in personal communication with driving teachers and from vehicle dynamics oriented analyses of individual accidents. Also accident statistics indicate that considerable safety improvements may be achieved with more emphasis on natural science knowledge in driver education and in vehicle maintenance, see Strandberg (1989).

It is true that the physical efficiency of crash avoidance equipment such as anti-lock brake systems (ABS) have been demonstrated by several investigators: e.g. Johnsson & Knutsson (1973); Rompe et al (1987); Robinson & Riley (1989). But in recent years the effect on the real accident risk from ABS and other safety justified measures has been questioned by researchers, see OECD (1990). Even if one does not accept the Risk Homeostasis "theory" (Wilde, 1988) as a fruitful explanation of negative results, Biehl et al (1987) and Aschenbrenner et al (1991) showed scientifically that a group of taxi drivers drove more risky when their car had ABS (compared to identical cars without ABS).

Unfortunately, many non-scientists interpret such results as a proof of ABS uselessness for safety. However, with minor educational efforts, ABS may contribute substantially to crash avoidance. Priez et al (1991) found encouraging improvements in the avoidance manoeuvre performance of non-professional drivers with ABS cars after a half day's education. Their experiments were carried out two months after the ABS-course, hence pointing at lasting effects. Many ABS car drivers without ABS-education did not grasp the opportunity to steer while braking, because they thought that ABS makes the stopping distance much shorter. Thereby, they were less successful than their matches (also without education and in an ABS car) who were not aware of that the car had ABS.

Though we did not intend to investigate the ABS training effects, the results and experiences from the present study indicate that proper ABS behaviour may be achieved with only a few minutes demonstration and driving practice. Unexpected result differences in this investigation between tyres and between front and rear wheel driven cars are other examples of the safety potential in better knowledge on driver-vehicle interaction.

Objectives

The main and general purpose of the experiments reported here was to increase our knowledge on how the average driver copes with the differences on ice between cars and tyres, that are common on the roads and that may have contributed to serious skidding accidents. Data allow comparisons between ABS and conventional brakes, between four different mountings of two types of studded tyres, between lateral, forward, and rearward acceleration (deceleration) capability, between different drivers (and between Front and Rear Wheel Drive, provided that other differences between the actual FWD and RWD cars can be neutralized or neglected). Such comparisons will be presented in this paper.

Since this knowledge will be (and has been) used in a development programme for driver education and skid training (VTI, 1990), we had to put realism (validity) and overview before statistical power (reliability) on a few predetermined issues. However, the recordings from the experiments constitute a data base intended for pilot investigations of a number of other questions—relevant also in the development of vehicle technology and automotive systems that help the driver to avoid accidents. One of the four test cars was equipped with an onboard computer and motion sensors for recordings and later (not in this paper) evaluations within the European research programme PROMETHEUS.

Method

Time History and Overview

The experiments were carried out on a frozen lake (Hemsjon) in the county of Dalarna during the three winter vacation weeks of 1990 (Swedish schools are closed one week in February-March every year for winter sport activities). Most of the driver subjects were tourists contacted by invitation to addresses supplied by the tourist office in the town of Orsa.

A few days before commencement, the mild weather forced us to move the test station 60 km away from Orsa. The late move to a comparatively isolated spot made it virtually impossible to keep the test track in the same intended condition. Some planned measurements and other activities had to be abandoned or simplified on days when the weather and failing equipment took all available resources. In addition, high temperature and melting ice caused various practical problems disturbing the experimental procedure. Therefore, a sound scientific skepticism towards the results is recommended. Due to the practical problems our team sometimes had to work 15-20 hours a day. Though some fatigue mistakes have

been discovered and compensated for, other problems may impose unknown bias. For instance, the participating subjects drove 120 km extra distance in their own cars on slippery winter roads during their vacation. They are probably representative for a more skilled driver population than the average on Swedish roads.

A test session took about 3 hours and involved 2 subjects driving their own car in the first and last test runs. The tests with (and data on) the drivers' own cars are not considered in detail in this paper. In the major part of a session, 2 front and 2 rear wheel driven Volvo "reference cars" were used with anti-lock brakes (ABS) in function or disconnected by the instructor occupant. Winter (Mud+Snow) tyres with two dissimilar stud configurations were mounted in pairs at the front and rear axles to give the reference cars neutral, under- or oversteering properties.

Normally, two sessions were carried out per week-day. Due to unusually high temperature on February 20 and similar problems during the week-end between weeks no.8&9, four sessions had to be called off. (We almost gave up after ten sessions when the ice was covered with some hundred millimeters of water and broke up at the ordinary entrance path.) Hence, data from 26 sessions have been collected. The weather problems forced us to use up almost all granted resources in the field experiments, leaving too little for a reasonably quick and exhaustive evaluation. In the project team we are therefore interested to continue evaluation and analysis in cooperation with people outside the Swedish Road and Traffic Research Institute (VTI).

Reference Cars

The reference cars provided by Volvo were designated A&B (front wheel driven Volvo 440GL), and C&D (rear wheel driven Volvo 744 GL). All of them were 1990 year model with manual 5-speed transmission and their maker's number of chassis were A: KX183ELC063932, B: KX183ELC064326, C: 744882L1400122, D: 744883-L1400227. Some of their technical specifications are given in Table 1. Drivers' own cars were designated E and F, but in computer recorded data and in result tables both cars of the drivers in a session have been labelled E. The same Mazda 6264 Wheel-Steering with unstudded M+S tyres (provided for our 4WS practice by the Swedish Mazda importer) was lent to four car-less drivers as their "own" car in sessions no.2, 18, 19, 22. Otherwise, all own cars are different. In this paper data will not be presented on drivers' own cars and they will be disregarded in most of the test result presentations.

In all reference cars a video camera was mounted behind the front seats. In car D computerized measurement equipment occupied the front passenger seat. The computer and its operator-instructor were in the rear seat of car D, hence being more rear biased in weight distribution than car C, which had no measuring equipment. The instructor was seated in the front passenger seat in all other cars (A, B, C, E, F). An optional switch made it possible to connect or disconnect the ABS from the front seat.

Table 1. Manufacturer's (Volvo, 1989 & Hansson, 1991) Technical Specifications for Reference Cars Used in Experiments

Reference Car designation	A&B	C&D
Volvo model	440GL	744GL
Driven wheels	Front	Rear
Length (m)	4.31	4.85
Width (m)	1.67	1.75
Wheel-base (m)	2.50	2.77
Track width-front (m)	1.42	1.47
Track width-rear (m)	1.43	1.46
Nominal kerb weight with 70kg driver (kg)	1100	1370
Nominal weight distribution Front:Rear (%)	61:39	55:45 [D: rear bias]
Maximum engine power (kW at Rev. per second)	75 at 93	85 at 90
Nominal ratio weight/power (kg/bhp)	10.8	11.8
Rear to front ratio of brake lining hydraulic pressure	Reduced at high press.	Rear same as front
ABS make (both have 3 channels, mutual rear control)	Teves	Bosch

Measurements were also recorded with a driver from the investigation team in a Volvo 745 "calibration" car equipped with unstudded M+S tyres of the same type (Gislaved Frost) as on the cars A-D. See section below on Experimental Design.

Tyres

Two studding configurations were used with the same type of tyre, see Figure 1&2. The Nivis Gislaved company provided 22 wheels with studded tyres, that had been run-in at low speed on bare roads to secure the studs in the rubber for constant stud protrusion during the experiments. However, measurements on 12 studs per tyre after the experiments revealed substantial deviations from the requested protrusion, see Table 2. (On Swedish roads, cars must not have more than 150 studs per tyre and the maximum permissible protrusion is 1.5 mm.)

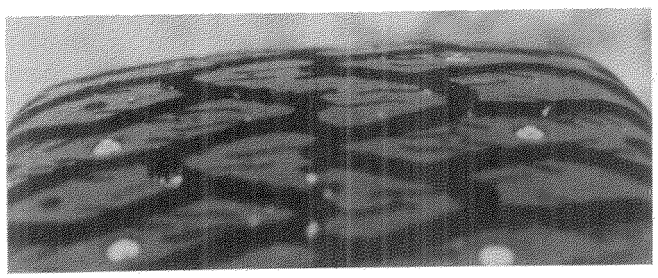

Figure 1. Detail of a Basic Studded Tyre After the Experiments

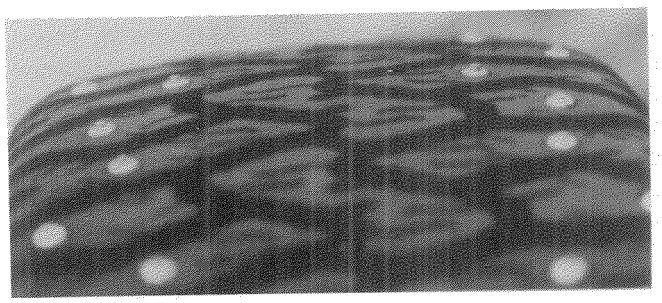

Figure 2. Detail of a Fully Studded Tyre After the Experiments

Table 2. Tyre Studding: Protrusion as Intended Before the Experiments, and Measured on 12 Studs/Tyre Afterwards

Tyre Studding FWD: carA&B RWD: carC&D	Basic: (70 studs/tyre) Front Wheel Drive	Basic: (70 studs/tyre) RearWheel Drive	Full: (140 studs/tyre) Front Wheel Drive	Full: (140 studs/tyre) RearWheel Drive
Protrusion before (requested)	About 0.5 mm	About 0.5 mm	About 1.5 mm	About 1.5 mm
Protrusion after (measured sample)	69% (of 48 studs) 1.0 mm or more	21% (of 48 studs) 1.0 mm or more	52% (of 84 studs) 2.0 mm or more	25% (of 84 studs) 2.0 mm or more

M + S Gislaved Frost Tyres made by Nivis about four months before the experiments. Dimension 175/65R14 (Front Wheel Driven cars A&B) and 185/65R15 (Rear Wheel Driven cars C&D). Tyre tread pattern about 9 mm.

Unfortunately, we were too short of resources to follow the Nivis people recommendations to move the wheels between sessions from one position to another in the cars. Therefore, the protrusion varied also within the four groups in Table 2. Nevertheless, the deviations are consistent with the observation that the increase in protrusion (occurring particularly when driving with great adhesion utilization on ice) is more pronounced for FWD cars, Strandberg (1989). This will be discussed under a separate subhead in the Double Lane Change chapter below.

The tyres were mounted differently on the cars to give them pure handling properties, see Table 3.

Table 3. Denomination of the Four Studding Configurations Used on the Reference Cars A-D

Tyre Studding Configuration of a car	Understeer	Basic	Maxi	Oversteer
Tyres at front axle (notation in Table 2)	Basic	Basic	Full	Full
Tyres at rear axle (notation in Table 2)	Full	Basic	Full	Basic

Measuring Equipment and Recordings, Personnel

Three stationary speed sensors and the stopping position reported by an observer beside the test track made it possible to calculate average acceleration and deceleration values on basis of the path geometry (the lateral acceleration equation takes the car width into account, as well).

One Speed Sensor (SS) consists of two infrared light emitters and two detectors. These components were put at a reasonably safe distance from the path and the lane-marks, the emitters to the left and the detectors to the right. The distance between the two emitter-detector pairs was S m for SS no. 1 and 8 m for SS2 and SS3. The time between light beam disruptions was determined with a computer also calculating the speed (average between the emitter-detector pairs) and presenting the value at a display in the testing base. The computer has been developed at VTI for use with cables and other types of vehicle detectors in a system called PTA (Portable Traffic Analyzer) for determination of speed, lateral position, vehicle type, etc.

The tests were governed from the testing base (a warmed-up Van-type car) by the test manager. The base was put behind snow banks about 10m to the right of the first lane-marks in the test track. A video camera outside the base was recording the tests but frequent drop outs occurred due to wind, snow and electro-magnetic noise from the PTA computers close to the video recorder.

In all reference cars a video camera was mounted behind the front seats, normally recording a whole session including sound from the radio communication. The pictures may be used for qualitative information on car and steering wheel motions. During pauses between the test runs, the instructors filled in a questionnaire on the drivers personal data, annual mileage and experience from different car types, from winter-time driving and from accidents. The same form and the same instructor followed the driver when changing between cars. This "driver form" was also used for test outcomes and data such as notes on skidding, clutch depressing, subjective judgements on steering corrections (used to distinguish between 0 and 1 in the Loss-of-Control Score, see section on Loss-of-Control statistics below), demanded speed and speedometer reading (for determining a suitable speed change for the next Double Lane Change manoeuvre in radio discussions between the instructor and the test manager).

The measuring computer in car D recorded the time histories of throttle position, steering wheel angle, longitudinal and lateral acceleration, longitudinal velocity, yaw velocity, in addition to events such as depressing the brake or clutch pedal. The 8 channels were sampled with 20 Herz during 40 seconds per test. Such records from several hundred tests are available on PC-media for further analysis. Successful attempts have been made to compute non-recorded variables such as yaw and sideslip angles. These data may improve our knowledge on how different drivers perceive and negotiate skidding motions, though they are not elaborated on in this paper. Hitherto, data have been processed with Excel in MS-Windows and are stored on IBM compatible PC-media.

Since important parts of the experiments were unrehearsed and required a great deal of practical experience from both driving and teaching other drivers as well as of extemporary engineering, the presentation would not be complete without a few words on the personal background of the test team relevant to their roles on site. (Of course, other people have contributed substantially to the investigation during preparation and evaluation. But this description concentrates on the test site activities.) Names in alphabetical order.

Stefan Berglund (instructor and computer operator in car D) has practical experience from mechanical and electronical engineering at VTI and privately with various cars. Now also racing a go cart of his own.

Sven-Åke Lindén (test manager and responsible for selection, preparation and operation of the test site as well as for lodging and social arrangements) has decades of similar experience from VTI. He is also considered (one of) the institute's most reliable test drivers. Now teacher at the Volvo Dynamic Safety Driving School.

Lennart Strandberg (project manager, responsible for experimental design and for safety-relevant manoeuvres) has experience from driving rallies and Swedish ice racing championships, from accident analyses and driving school cooperation on skid-pad training, and from scientific testing of technical properties with human subjects.

Harry Sörensen (instructor and operator in car D also responsible for its computer programming and its measuring equipment) has a long time experience from VTI on design and management of measuring equipment for testing of car handling properties.

Jerry Wallh (car testing manager and "calibration" driver, responsible for transports and communications at the test site) has several years professional experience as an ambulance driver in the fire brigade. Now responsible for the test vehicle fleet and vehicle techniques laboratory at VTI.

The Swedish Federation of Women's Motor Transport Corps (SKBR) contributed most of the time four workers in different roles.

Kicki Hellström chairperson for the Dalarna county branch of SKBR found extremely capable ladies working one week at a time as instructors, track managers and observers, lane-mark positioners, duty vehicle drivers, video operators, photographers, ice drillers, snow removers, receptionists, etc. They fulfilled their tasks under primitive conditions after a few hours training on Sunday afternoon before their week on duty. In spite of our poor knowledge at that time on the frequent ABS-confuses among non-professional drivers, the results from the (Combi) braking tests show that the instructors in a few minutes succeeded to teach the drivers how to improve their deceleration capacity with ABS. Their names are Berith Andersson, Eva Bäcksholm, Inga-Lill Camitz, Rita Eriksson, Sylvia Krenn, Christina Lekman, Ing-Marie Persson, Kerstin Sunnerby.

Driver Subjects

Thanks to cottage rental agencies we could mail invitations to about 300 tourists, intending to spend their winter sport vacation close to the town of Orsa. The number of people who accepted to participate was more than sufficient as long as we stuck to our plans to test on the Orsa Lake. However, the high temperature in Orsa the weeks before the experiments forced us to move the test site about 60 km as mentioned above. Of course, a number of subjects then withdrew from participation, but the mild weather made also skiing difficult.

Therefore, we could find driver subjects to all sessions, particularly after asking the local inhabitants around lake Hemsjon, where the tests finally were carried out. Six of the SKBR women and Stefan Berglund from VTI have also participated as subjects in sessions when the drivers on schedule did not appear. However, no person has participated twice and all 52 subjects are different individuals. Many of the participating tourists accepted to drive 120 km extra distance in their own cars on slippery winter roads during their vacation. Hence, our driver sample is biased and probably representative for a more skilled driver population than the average on Swedish roads. Drivers' sex and year of birth are given in Table 4, but other compilations from the questionnaire in the "driver form" will not be presented in this paper.

Combi Manoeuvre: Accelerating, Braking, Steering, Stopping

The combination (Combi) manoeuvre was designed to challenge the driver-vehicle ability to keep control in acceleration, deceleration, and steering while braking. The driver was asked to accelerate as much as possible from standstill about 200 m before the first lane-marks at X=0 in Figure 3. After having continued the acceleration for 80 meters in the left lane, the driver should make a quick change to maximum deceleration bringing the car to a full stop without hitting the lane-marks.

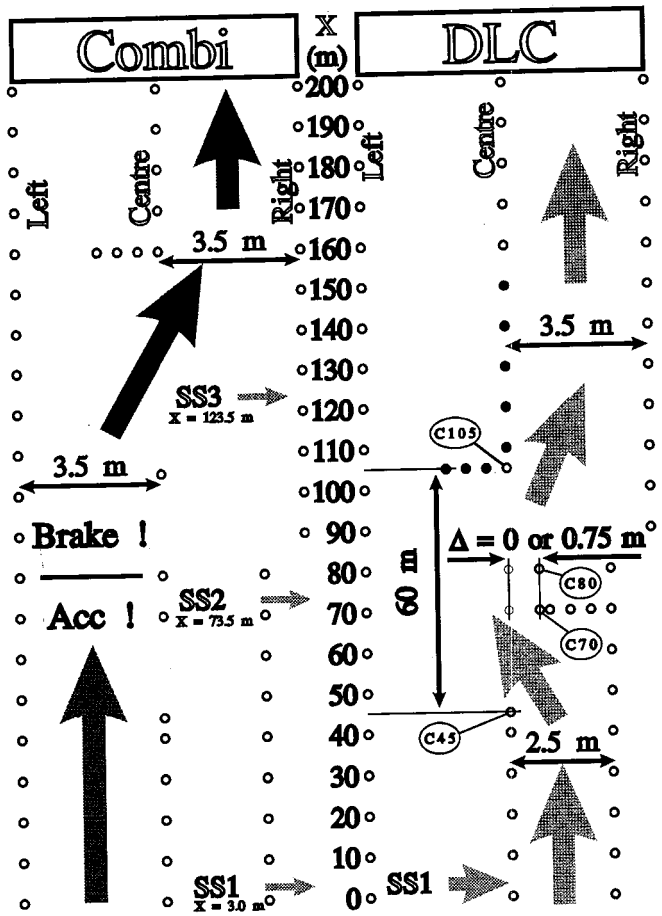

Marks at filled circles were removed when changing between manoeuvre types. SS1, SS2, SS3 indicate the X-coordinates of the infrared light Speed Sensors (put some meters beside the test path to avoid damage upon loss-of-control).

Figure 3. Path Layout and Lane-Mark Positions in Combi and in Double Lane Change Tests

In most of the tests the car did not stop before X=160 m. Therefore, it was necessary to turn right during the deceleration. However, the lane change could easily be made without need of skid provoking steering, provided the brakes were properly used. When the car had stopped, an observer reported its front end position by radio to the test manager, who wrote it down in his "session form" together with the readings from the three Speed Sensors (SS1, SS2, SS3 in Figure 3). The car position was determined with an accuracy of about ± 1 m by looking at the nearby lane-marks put in holes in the ice 10 meters from each other. However, in 60 (of 520) Combi tests the car stopped after X=205 m. Then it was more difficult to assess the position, since only two lane-marks were present after the ones at X=200 m. If some lane-marks were hit, it was reported to the session form by the observer.

In sessions when we judged the ice particularly slippery, the starting point was moved from 150m to 200m before the first lane-marks in the test track (distance to SS1 designated S_{01}). A too short acceleration distance would give too low speeds in the path and make it too easy to stop before X=160m without need of steering into the right lane. In Table 4 the comparatively small decelerations at sessions with S_{01}=200m indicate that the subjective judgements of slipperiness were not too bad.

Most of the lane-marks and the exit in the right lane were the same for both Manoeuvre types. However, the exchanges between Combi and Double Lane Change arrangements were comparatively time-consuming and their number were therefore minimized in the session agenda.

Double Lane Change Manoeuvre

The Double Lane Change (DLC) test track geometry had been adjusted to impose problems with stability and (rear wheel) skid control when the tyres were similar at both front and rear wheels (Basic or Maxi Studding). In the pretests with Oversteering tyres, we found the same geometry to be even more skid provoking. Understeering tyres, on the other hand, made the tests comparatively insensitive to the skills of the driver. When the demanded speed was too great, loss-of-steering and "plow out" occurred often before completion of the first lane change to the left, which resulted in hitting of the lane-marks C70 & C80, see Figure 3. Therefore, few tests were scheduled with Understeering tyres in the main program.

In the ordinary DLC test, drivers were asked to keep constant a certain speed and to avoid hitting lane marking tubes. Since the obstacle marks blocking the right lane (C70&C80 in Figure 3), determined the lateral motion and the severity of the manoeuvre, we had to exclude (disapprove) a test from analysis, if both these lane-marks were overrun, see Eq. 7. (In sessions no. 21-22 inflatable car dummies helped the drivers to avoid such disapproval).

The speed was demanded on radio by the test manager to provoke skidding—and loss-of-control in certain tests with unskilled drivers. The instructor and test manager judged the driver proficiency during the initial training runs and in about four recorded DLC tests with the drivers' own car. In these first DLC tests, the driver increased the speed in small steps. However, the succeeding ordinary tests with the reference cars were only two per driver car combination and in some cases were both runs on the same side of the limit for loss-of-control. To minimize the number of driver-cars with such unspecific results, the speed was demanded as follows. If the driver had no problem in the first DLC with a reference car, the test manager requested a specified increase (5 or 10km/h) of the speed in the second test and vice versa. Only if the first run exhibited pronounced skidding with recovery and if lane-marks were hit in the first run, the same speed was demanded in the second DLC test.

Experimental Design

To neutralize driver learning and fatigue effects on the differences between reference cars and between tyre configurations, they were tested by the drivers in different order. In sessions 1-8 & 9-16 respectively, every reference car was presented to four drivers in each sequential position (1st, 2nd, 3rd, 4th), and in session 17-18 to one driver in each position. Tyre configurations remained unchanged within these groups of sessions, see Table 4.

Sessions no. 14, 17 and no. 19-26 included so called pedal tests (Double Lane Change with clutch, throttle or ABS-brake activation). They were carried out only with the computerized Rear Wheel Driven car D and with one of the Front Wheel Driven cars (A or B). To avoid learning or confusing effects on the ordinary DLC manoeuvres, all pedal tests were scheduled to be the driver's last DLCs with the two cars in question. Due to excessive time consumption for the additional pedal tests in sessions 14 & 17, the ordinary program had to be reduced to allow for pedal tests in the last eight sessions (no. 19-26). It was decided to abandon the DLC tests with car C, because the weight distribution and handling properties were considered more different between car C&D than between car A&B. Since we intend to present the results of pedal tests elsewhere, they are normally disregarded in this paper.

When excluding car C from the DLC-tests in sessions 19-26 we also decided to mount Understeering tyres on it. The Combi tests would then be complete with all car-studding combinations. And in the DLC-manoeuvre we expected that many tests had to be withheld from analysis, since both marks blocking the right lane (C70 & C80 in Figure 3) often were hit in the pretests with understeering.

Since car C was not used at all in the DLC manoeuvre, only two (anti-symmetrical) car permutations were scheduled in sessions 19-26. Comparisons of DLC results from these sessions should therefore be made with caution—and preferably between car A and B (Front Wheel Driven). However, comparisons between cars C and D seem justified in Combi tests.

Table 4. Experimental Conditions in Ordinary Sessions

Session no.	Week no. Day time of day	Date	Distance S01 (m)	Tyre Studding Car A	Tyre Studding Car B	Tyre Studding Car C	Tyre Studding Car D	Driver no.1 & no.2: Sequential order of reference cars A, B, C,D	Driver 1: Seq. order of brake config. in Combi-test	Driver 1: Sex, Year of birth	mean (A-D) Decel. d_{mac} (m/s²)	Driver 2: Sex, Year of birth	mean (A-D) Decel. d_{mac} (m/s²)	Remark Foot note
1	7, Mon a.m.	Feb.12	150	Max	Ovr	Max	Ovr	1:ABCD 2:CADB	ABS, STD	M, 1939	1.74	M, 1946	1.65	
2	7, Mon p.m.	Feb.12	150	Max	Ovr	Max	Ovr	1:BDAC 2:DCBA	ABS, STD	M, 1963	1.57	F, 1943	1.67	
3	7, Tue a.m.	Feb.13	150	Max	Ovr	Max	Ovr	1:BDAC 2:CADB	STD, ABS	F, 1942	1.90	M, 1939	2.01	
4	7, Tue p.m.	Feb.13	150	Max	Ovr	Max	Ovr	1:ABCD 2:DCBA	STD, ABS	F, 1943	1.96	M, 1942	2.35	
5	7, Wed a.m.	Feb.14	150	Max	Ovr	Max	Ovr	1:BDAC 2:DCBA	ABS, STD	F, 1945	2.06	F, 1947	2.43	
6	7, Wed p.m.	Feb.14	150	Max	Ovr	Max	Ovr	1:CADB 2:ABCD	STD, ABS	M, 1971	2.55	M, 1966	2.51	
7	7, Thu a.m.	Feb.15	150	Max	Ovr	Max	Ovr	1:ABCD 2:DCBA	STD, ABS	M, 1940	2.39	M, 1945	2.51	
8	7, Thu p.m.	Feb.15	150	Max	Ovr	Max	Ovr	1:CADB 2:BDAC	ABS, STD	F, 1970	2.19	F, 1948	2.51	
9	7, Fri a.m.	Feb.16	150	Max	Bas	Bas	Max	1:ABCD 2:DCBA	STD, ABS	M, 1949	2.47	M, 1947	2.26	
10	7, Fri p.m.	Feb.16	150	Max	Bas	Bas	Max	1:CADB 2:BDAC	ABS, STD	M, 1968	2.18	M, 1971	2.15	
11	8, Mon a.m.	Feb.19	150	Max	Bas	Bas	Max	1:BDAC 2:DCBA	ABS, STD	M, 1931	2.48	F, 1965	2.54	
12	8, Mon p.m.	Feb.19	150	Max	Bas	Bas	Max	1:CADB 2:ABCD	STD, ABS	M, 1944	2.52	M, 1938	2.37	
13	8, Wed p.m.	Feb.21	200	Max	Bas	Bas	Max	1:BDAC 2:CADB	STD, ABS	M, 1943	1.53	F, 1947	1.43	
14	8, Thu a.m.	Feb.22	200	Max	Bas	Bas	Max	1:ABCD 2:DCBA	STD, ABS	M, 1949	1.41	M, 1941	1.22	14)
15	8, Thu p.m.	Feb.22	200	Max	Bas	Bas	Max	1:BDAC 2:CADB	ABS, STD	M, 1940	1.77	M, 1952	1.75	
16	8, Fri a.m.	Feb.23	200	Max	Bas	Bas	Max	1:ABCD 2:DCBA	ABS, STD	M, 1932	1.29	M, 1971	1.61	
17	8, Fri p.m.	Feb.23	150	Max	Bas	Max	Bas	1:ABCD 2:DCBA	ABS, STD	F, 1961	1.87	M, 1946	1.90	17)
18	9, Mon p.m.	Feb.26	150	Max	Bas	Max	Bas	1:CADB 2:BDAC	ABS, STD	F, 1946	1.99	F, 1932	1.95	
19	9, Tue a.m.	Feb.27	150	Und	Ovr	Und	Ovr	1:ABCD 2:DCBA	ABS, STD	M, 1943	1.96	M, 1942	2.08	19)
20	9, Tue p.m.	Feb.27	150	Und	Ovr	Und	Ovr	1:ABCD 2:DCBA	STD, ABS	M, 1965	1.92	F, 1967	1.93	20)
21	9, Wed a.m.	Feb.28	150	Und	Ovr	Und	Ovr	1:ABCD 2:DCBA	ABS, STD	M, 1947	2.29	M, 1941	1.82	21)
22	9, Wed p.m.	Feb.28	150	Und	Ovr	Und	Ovr	1:ABCD 2:DCBA	STD, ABS	M, 1962	1.98	M, 1950	2.05	22)
23	9, Thu a.m.	Mar.1	150	Und	Ovr	Und	Ovr	1:ABCD 2:DCBA	ABS, STD	M, 1945	2.07	M, 1943	2.11	23)
24	9, Thu p.m.	Mar.1	150	Und	Ovr	Und	Ovr	1:ABCD 2:DCBA	STD, ABS	F, 1947	1.84	M, 1920	1.85	24)
25	9, Fri a.m.	Mar.2	150	Und	Ovr	Und	Ovr	1:ABCD 2:DCBA	ABS, STD	M, 1938	1.89	M, 1963	1.74	25)
26	9, Fri p.m.	Mar.2	200	Und	Ovr	Und	Ovr	1:ABCD 2:DCBA	STD, ABS	M, 1941	1.62	M, 1940	1.63	26)

Comment 14, 17) Complete test program + additional pedal tests with cars A&D.
Comment 19-26) With Car C only Combi-tests were carried out (no DLC-manoeuvres). Additional pedal tests with cars B&D.
Comment 21-22) Inflatable car dummies (reinforcing the visual impression of ordinary plastic tube lane-marks) put where lane change should be completed.

S01=acceleration distance from start to "entrance gate" (first lane-marks). The Driver 1&2 d_{mac} (Eq.4) deceleration results (mean values over car A-D) indicate the variation between sessions in ice friction.

Two Combi tests were carried out with each pair of car and driver. Therefore, learning and fatigue effects on comparisons between ABS and Standard (STD) brakes were neutralized by reversing the testing order for the two drivers in each session. When Driver no. 1 began with ABS, Driver no.2 had Standard brakes in the first Combi test with all cars A-D. To minimize the variance from the successive within-session changes in ice roughness (due to the studded tyres and because of weather), ABS and STD tests were made directly after each other. Only one test run by the other driver came in between.

Even if the changes in ice roughness and friction may be neutralized within the sessions, considerable variations have been observed between sessions. See the last columns in Table 4 and Figure 4. Separate tests were carried out with a driver from the investigation team in the "calibration" car with unstudded tyres of the same type as on the cars A-D. However, time constraints and practical problems limited the possibilities to run calibration tests frequently enough. Snowfall and weather changes in many sessions introduced substantial friction variations with time and with driver path selection. In addition, the corresponding variation in the relationship between studded and unstudded tyres is so poorly known that we have not yet found any satisfactory method to utilize these calibration data.

Consequently, the evaluation should be based on variables as insensitive as possible to friction fluctuations. Some attempts will be presented below, but skepticism is recommended and the author will gratefully receive constructive criticism and ideas for future research.

Since the pretests were impeded by the move between the lakes of Orsa and Hemsjön (68 + 97 + 147 + 130 = 442) additional tests were made after session no. 26 during four days (March 3-6). Only three drivers (S-Å Lindén, L Strandberg, J Wallh) from VTI were involved—to reduce the variance in the handling property assessments for the reference cars and tyre studding configurations in Table 1&3. The calibration car was also used in these tests to facilitate analyses which may increase our knowledge on the questions mentioned above. A considerable number of computer recorded car D motions are included in these data, which are being evaluated in proportion to available resources.

Results and Discussion: Combined Manoeuvre

Assessment of Deceleration and Forward Acceleration

Two deceleration values (d_2 and d_3) has been assessed for each Combined Manoeuvre (Combi) Test. Data on the stopping distance (S_2 & S_3) from the Speed Sensors no. 2 & 3 (SS_2 & SS_3 in Figure 3) and on the corresponding speeds (v;) were used together with the simple expression in Eq.1, where subscript i denotes the actual speed sensor (no. 2 or no. 3).

$$d_i = \frac{v_i^2}{2S_i} \qquad (1)$$

Since the drivers were instructed to accelerate up to SS2, the brakes were not always fully applied during the initial part of the S2-distance. Therefore, $d_3 > d_2$ in the average Combi test, and d_3 may be considered a more precise measure of the stopping capability than d_2. On the other hand, missing data is more frequent from SS3, since we had to give priority to SS2 (necessary for evaluation of the Double Lane Change Manoeuvre) when snow and other factors caused drop-outs of the sensors.

The accelerations a_1 (from start to Speed Sensor SS1) and a_{12} (from SS1 to SS2) were determined similarly from the SS1 and SS2 speed records, v, and from the sensor positions.

$$a_1 = \frac{v_1^2}{2S_{01}} \qquad (2)$$

$$a_{12} = \frac{v_2^2 - v_1^2}{2S_{12}} \qquad (3)$$

The distance S_{12} between SS1 and SS2 was 70.5 m in all sessions, while S_{01} was either 153 m or 203 m since the starting point sometimes (when the ice was particularly slippery) was moved from 150m to 200m before the first lane marks in the test track, see Table 4 and Figure 3.

Table 5 displays statistics on these quantities expressed as the "macro" (subscript mac) values of acceleration and deceleration. A few of the recorded sensor speeds gave unreasonably great deceleration values, probably because flying lane marks triggered the speed sensors. Therefore, the next greatest value for each driver-car pair was selected by the computer program as a maximum of the medians of all (up to four) deceleration or acceleration triples according to the formulas:

$$d_{mac} = \mathrm{MAX}(Median(d_{2(ABS)}, d_{3(ABS)}, d_{2(STD)}), Median(d_{3(ABS)}, d_{2(STD)}, d_{3(STD)}), Median...) \quad (4)$$

$$a_{mac} = \mathrm{MAX}(Median(a_{1(ABS)}, a_{12(ABS)}, a_{1(STD)}), Median(a_{12(ABS)}, a_{1(STD)}, a_{12(STD)}), Median...) \quad (5)$$

where the decelerations d_2 and d_3 are given by Eq. 1 and accelerations a_1, a_{12} by Eq. 2 & 3. The result sensitivity to variations in ice friction and in driver deceleration performance are illustrated in Figure 4. Substantial differences are exhibited between sessions, but also between drivers in certain sessions. Within a session it was not expected to find driver differences of such a magnitude, since each value is an average of the "best" tests with the same four reference cars.

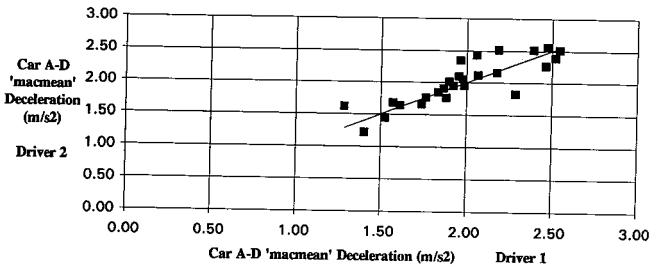

(in m/s² as the "macmean" deceleration (driver's average over car A-D of the "macro" deceleration value: d_{mac} in Table 4 & Eq.4). Line y=x overlayed. Linear regression forced through origin (y=mx) yields slope m= 1.01 and r^2=0.72)

Figure 4. Relationship Between the Two Drivers in Each Session Regarding Their Deceleration Capability

Deceleration and Controllability With and Without ABS

When evaluating the influence from ABS on the deceleration capability, the (d_i) deceleration values were paired for the same driver and car. Since the Combi tests with and without ABS were made consecutively for every car driver combination, such pairing makes the results less sensitive to the time variation of friction, and to differences between drivers, tyres, cars, etc. Therefore, an ABS deceleration enhancement Ratio (R_{diABS}) was calculated (one for each d_2- or d_3-deceleration value) according to Eq.6:

$$R_{diABS} = \frac{d_{i(ABS)}}{d_{i(STD)}} \quad (6)$$

where subscript; means the speed sensor number (2 or 3), subscript (ABS) denotes a test run with ABS, while subscript (STD) is used for the corresponding test run (same car and driver) with standard or conventional brakes, i.e., when the Anti-Lock function was disconnected. Table 5 exhibits statistics on these Ratios for the four tyre studding configurations defined in Table 3.

Table 5. Number of Driver-Stud Combinations with Complete Data (n), Corresponding Average (Mean) and Standard Error

Table 5a) Reference cars A&B (Front Wheel Driven Volvo 440).

Tyre Studding	n	R_{d2ABS} Mean	R_{d2ABS} Std.err.	n	R_{d3ABS} Mean	R_{d3ABS} Std.err.	n	a_{mac} Mean	a_{mac} Std.err.	n	d_{mac} Mean	d_{mac} Std.err.
Basic	20	1.059	0.036	18	1.125	0.058	20	0.843	0.061	20	1.768	0.116
Oversteer	32	1.166	0.037	23	1.269	0.108	29	1.021	0.034	32	2.125	0.056
Understr.	15	1.102	0.034	11	1.146	0.043	13	0.999	0.053	16	1.790	0.067
Maxi	33	1.078	0.025	30	1.098	0.059	36	0.985	0.036	36	2.181	0.069
All types	100	1.106	0.017	82	1.158	0.040	98	0.968	0.022	104	2.024	0.042

Table 5b) Reference cars C&D (Rear Wheel Driven Volvo 740).

Tyre Studding	n	R_{d2ABS} Mean	R_{d2ABS} Std.err.	n	R_{d3ABS} Mean	R_{d3ABS} Std.err.	n	a_{mac} Mean	a_{mac} Std.err.	n	d_{mac} Mean	d_{mac} Std.err.
Basic	19	1.078	0.055	16	1.051	0.041	20	0.749	0.074	20	1.703	0.118
Oversteer	30	1.148	0.048	20	1.158	0.055	29	0.806	0.038	32	1.915	0.054
Understr.	16	1.168	0.063	11	1.207	0.080	13	0.951	0.053	16	1.987	0.062
Maxi	34	1.130	0.024	28	1.110	0.049	36	0.886	0.034	36	2.117	0.061
All types	99	1.132	0.022	75	1.125	0.028	98	0.843	0.024	104	1.955	0.039

Table 5c) All reference cars A-D (both Front and Rear Wheel Driven).

Tyre Studding	n	R_{d2ABS} Mean	R_{d2ABS} Std.err.	n	R_{d3ABS} Mean	R_{d3ABS} Std.err.	n	a_{mac} Mean	a_{mac} Std.err.	n	d_{mac} Mean	d_{mac} Std.err.
Basic	39	1.068	0.032	34	1.090	0.036	40	0.796	0.048	40	1.735	0.082
Oversteer	62	1.157	0.030	43	1.217	0.063	58	0.913	0.029	64	2.020	0.041
Understr.	31	1.136	0.036	22	1.177	0.045	26	0.975	0.037	32	1.888	0.048
Maxi	67	1.104	0.017	58	1.104	0.038	72	0.936	0.025	72	2.149	0.046
All types	199	1.119	0.014	157	1.142	0.025	196	0.906	0.017	208	1.990	0.029
Tests out of lane	30	1.126	0.047									

(Std.err. = Std.dev./√n) of ABS deceleration enhancement (R_{diABS}, Eq. 6) as well as the "macro" values of acceleration (a_{mac} Eq. 5) and deceleration (d_{mac}, Eq. 4) given in m/s².

If the means are assumed to be t-distributed, the standard error may be considered greater than a 1/4 confidence interval (level 95% if n>60, 90% if n>6) for the mean. See e.g. Fisher (1958) or Draper & Smith (1981). Hence, the deceleration enhancement with ABS may be considered statistically significant.

Under these conditions, the average driver succeeded to increase the deceleration with about 10% (lower limit of the 95%-confidence interval: 1.09<Rd_{2ABS}-mean< 1.15 and 1.09<R_{d3ABS}-mean< 1.19) when ABS was in function. The deceleration enhancement with ABS tended to be more pronounced when tyre studding was different at the front and rear axles (Oversteer and Understeer rows in Table 5).

However, raw data on the stopping position reveal that the driver succeeded to stop before the "end" of the left lane (at X=160m in Figure 3) in 56 tests with ABS but in only 37 tests without. Therefore, one must not conclude that ABS improves deceleration to the same extent when steering is unnecessary.

A separate evaluation of the tests where lane marking tubes were hit, revealed only one test (of 208) with ABS, while mark-hitting occurred in 30 tests when ABS had been disconnected (the car left the lane completely in 16 of these 30 non-ABS tests). The last row of Table Sc indicates that the drivers in question did not significantly

improve their deceleration capability by locking the wheels and ignoring the lane-keeping task (which has been suggested in car- and tyre test reports in some newspapers). This evaluation of driver control points at an ABS advantage, which may be even more important to safety than the deceleration enhancement.

Deceleration With Different Tyre Configurations, Examples of Bias

The advantage of having well-studded tyres on the driven wheels is reflected by the greater acceleration (a_{mac}) mean values in Table 5a (Oversteer row) and in Table 5b (Understeer and Max studding rows).

Considering the Front Driven cars in Table 5a, the comparatively great acceleration capability of the Understeered configuration may reflect a bias due to greater friction on the acceleration path during the last eight sessions (no. 19-26), which were the only ones with Understeer studding on the reference cars. See Table 4.

Paired comparisons of the acceleration assessments a_1 and a_{12} between Under- and Oversteered studding in these sessions contradicted the paradoxical relationship between the average values. The qualitative results after matching were as expected from common-sense: Better studding at the driven wheels (Oversteered in Front Driven cars) gave greater acceleration values in more than 70% (35 of 48) of the available data pairs (8 sessions x 2 drivers x 2 acceleration values x 2 brake configurations = 64 minus 16 sensor drop-outs make 48 pairs).

Such sources of bias should be investigated before overinterpreting differences between average values over several sessions. Therefore, it is desirable to continue the analysis and to check some of the primary evaluations in this paper with methods and variables, that are insensitive to bias due to ice friction variation between sessions.

One must also bear in mind that the discrimination here between Front and Rear wheel drive may be misleading, since the cars in question (Volvo 440 and Volvo 740 respectively) are different in many other ways, as well, see Table 1. Particularly when comparing the deceleration levels (d_{mac} in Table 5), it may be informative to know that the 440-model has a valve in the hydraulic brake system allowing for greater friction utilization at the rear wheels (before front wheel locking) on medium slippery surfaces. No such function has been included in the 740 model, due to the emphasis on stability in its design philosophy.

Compared to the Front or Rear wheel drive issue, these details in the brake systems may be more decisive of the contradiction between Table 5a and Table 5b regarding the qualitative difference between Oversteer and Understeer in ABS deceleration enhancement (R_{diABS}). Though the differences may lack statistical significance, the R_{diABS} is greater for the Oversteered configuration in the 440-model, while the 740 benefits more from ABS with Understeering tyres. This is consistent with the 440-740 difference in brake force distribution. Without ABS the 740 will lock up its front wheels at a deceleration which is more inferior to the lock-up limit of the rear wheels than in the 440-model.

Nevertheless, the average deceleration values differ substantially between Basic- and Maxi-studded tyres, as should be expected. The difference seems significant both statistically and practically, since the average driver improved the deceleration with more than 20 % when changing from Basic- to Maxi-studded tyres on all wheels.

Driver Brake Release Upon ABS Vibrations, Accident Risks and Driver Education

During preparation and training of the subjects, many drivers became surprised and released the brake pedal when they perceived the noise and vibration from the activated ABS. According to driving teachers at Swedish skidpads, this reaction and lack of sensory experience is common even among ABS car owners. Suitable information and training might therefore be offered to drivers who rent, borrow or buy a car with anti-lock brakes.

The ABS surprise reaction and spontaneous brake releases in emergency situations may have contributed to accidents. Perhaps that has contributed to the negative or lack of positive effect on safety from ABS, which has been reported by a few investigators. However, Biehl, Aschenbrenner & Wurm (1987) interpret their negative results as a support for Wilde's risk homeostasis "theory" (since it cannot be generally falsified, it is doubtful if it should be considered a scientific theory). Risk homeostasis means that drivers keep the accident risk at a constant level by increasing speed and by changing "towards a riskier or less cautious manner of driving" (OECD, 1990), when they become aware of active safety improvements, e.g. ABS.

Though Biehl et al (1987) only were unsuccessful in their attempts to find significant effects from ABS on the accident risk (no effect found = "negative results"), the risk homeostasis idea seems to convince some people that ABS is worthless—as well as many other driver supporting measures intended to reduce the accident risk. Such a destructive attitude may be encouraged by belief in risk homeostasis, but is questioned from a scientific point of view by Stottrup-Hansen et al (1990).

According to Aschenbrenner (1991), data from their study (Biehl et al, 1987, further evaluated by Aschenbrenner et al, 1991) "indicate that ABS drivers had less accidents when they used the brakes and more accidents in which they did not brake at all, e.g. losing one's way in an icy curve." This statement put doubts into the above mentioned assumption that spontaneous brake releases in emergency situations may have contributed to accidents. Nevertheless, it also points at a considerable safety potential of ABS, which may become better

reflected in accident statistics, if drivers are effectively informed of the limitations of ABS—and trained in utilizing ABS (even in icy curves).

The potential safety gains of ABS education and training is clearly demonstrated in driving experiments by Priez et al (1991). Trained drivers were about twice as prone as their untrained matches to behave adequately in a surprising simulated emergency (car dummy automatically pulled out at a crossing with restricted visibility). The "training consisted of a theoretical part explaining the objective and functioning of the ABS system, as well as a practical part involving demonstrations and avoidance exercises. This training took place two months before testing" and occupied the participants a half-day.

In a double-blind classification of the driving behaviour of their subjects (taxi drivers in Munich), Biehl et al (1987) found that their observers (acting as if they were ordinary passengers to the taxi driver) had judged the average driver behaviour as less cautious with ABS in all 18 variables taken into account. Though it was possible to identify an ABS car by the control light in the instrument panel, the observers were not informed whether the car had ABS or not. Neither were they told that the study dealt with the influence from ABS (as far as has been interpreted from Aschenbrenner et al, 1991).

The conscientious investigation by Aschenbrenner-Biehl-Wurm offers strong evidence that drivers behave more risky due to unrealistic expectations on the safety improvements with ABS. However, though the subjects were professional taxi drivers, they had not received any specific education on ABS. The question is if adequate training might improve safety in real traffic also—as on the test track for Priez et al (1991) mentioned above.

Data from the present study are encouraging in this respect. Though our driver subjects received only very short and improvised "training," they performed better with ABS (see above)—and through their speed selection in the Combi manoeuvre (see below) they did not exhibit any greater self-confidence with ABS than without.

Since they may be due to the sessions' training effect, a couple of differences will be pointed out here between the first and the last Combi test made with the driver's own car. In the introductory tests of the session, 23 drivers succeeded in stopping their own car before the left lane "end" (X= 160m in Figure 3), but in the corresponding test at the end of the session only three (3) drivers succeeded. Data were available for 40 drivers in this comparison. The details behind have not yet been investigated, but probably the drivers were more able to accelerate and reach a higher speed with their car at the end of the session. This may have undesirable effects on traffic behaviour and safety. On the other hand, the deceleration performance increased for a majority of the drivers. A simple count revealed that 21 of 36 drivers (where data were complete in this respect) achieved a greater deceleration value with their own car after the reference car tests than before.

One apprehension concerning ABS was reinforced during the author's own test driving a front wheel driven car with both ABS and Automatic Spin Reduction (ASR). A rear wheel skid developed to unrecoverable when the ASR prevented spinning of the front wheels. Then it became desirable to lock up all wheels and keep the car motion straight to shy on the path. However, ABS made that impossible and the car continued turning. Finally, it went backwards into a stack of hard snow. Similar property damage has been reported from skid-pad driving with ABS buses. In a critical situation on the road it may also be more injurious to crash in a side impact after an ABS supported yaw motion than to lock up all wheels into a frontal impact. Perhaps an emergency lock-up function should be available in ABS cars or automatically triggered when the skid (sideslip angle and yaw motion) exceeds the recoverable level.

Speed Selection With and Without ABS

According to risk homeostasis, drivers should drive faster with ABS than without in the Combi Manoeuvre, since they were explicitly told by the instructor if the ABS was switched on or off before the test. In order to test this hypothesis, the records from Speed Sensor SS2 were evaluated. Each driver made 4 Combi tests with ABS and 4 tests without (one test pair per reference car). The speed level at SS2 was mostly about 70 km/h with driver averages ranging from 62 km/h (for the Basic-studded Rear wheel driven cars) to 75 km/h (for the Oversteered Front wheel driven car).

The average speed ratio (speed with ABS divided by speed without ABS) over 199 test pairs (4 cars x 52 drivers minus missing data) was 1.01, which is not significantly different from unity. For each subject the number of test pairs with greater speed in the ABS run, was counted according to Table 6. Comparisons with tables on the binomial distribution confirm that the null hypothesis cannot be rejected. Hence, data do not support the idea that (instructed) drivers choose another speed with ABS than without.

Table 6. Number of Subjects Driving Faster with ABS in a Majority of Cars, in Fifty-Fifty, and in a Minority of the Four Reference Cars

Speed greatest in:	More tests withABS	Equal number of tests	More tests without ABS
Number of subjects:	21	17	14

Data from Speed Sensor SS2 in 197 Combi test pairs (ABS & STD).

Perhaps did the drivers learn sufficiently of ABS during the short pre-test exercise to avoid unjustified speeding. The frequent losses-of-control in the introductory Double Lane Change tests with their own cars may also have imposed a more careful driving attitude. The poor effects on safety in the studies mentioned above may therefore be explained by lack of knowledge and experience rather than by the somewhat fatalistic risk homeostasis idea. Thereby are these results

pointing at the potential of more precise knowledge and of continued efforts from experienced safety promoting professionals.

Results and Discussion: Double Lane Change Manoeuvre

Loss-of-Control Statistics

Since lane-marks were hit in only 31 of 416 Combi tests, the lane keeping task seems to have been comparatively simple for this driver group, as was intended when the Combi test track was outlined. The Double Lane Change (I)LC) Manoeuvre, on the other hand, was designed to challenge the lateral stability and skid recovery performance to a greater extent.

To distinguish tests with different degrees of driver control, a Loss-of-Control Score (LCS, with four levels from 0 to 3) was determined by the onboard instructor or by the trackside observers and the test manager.

0 No steering wheel corrections and no hitting of lane marks gave LCS 0.
1 Steering wheel corrections only gave LCS 1 (determined subjectively by the onboard instructor).
2 LCS 2 was recorded if (trackside observers discovered that) lane-marks were hit without a complete loss of control.
3 LCS 3 means that the driver lost control and the car left the lane completely.

In 348 normally recorded DLC tests with the reference cars, 94 tests (27%) resulted in Loss-of-Control (LCS= 3). For individual drivers the Loss-of-Control ratio varied from 0 of 9 tests to 5 of 7 tests (71%).

However, the LCS statistics should not be used alone for ranking the drivers and for assessments of their individual skills. Eight drivers had no LCS 3 at all, but four of them drove slower than demanded—resulting in smaller adhesion utilization laterally than what they had longitudinally in the Combi tests. When skidding to the left in the left lane, other drivers tried harder than normally to avoid the "oncoming car" lane-marks (C105, 110, etc in Figure 3). Their prolonged steering to the right made the clockwise yaw more pronounced and increased the risk of an LCS 3 outcome (leaving the lane). Drivers who countersteered earlier to the left had an easier task to avoid LCS 3, if they accepted LCS 2 and deliberately run over the centre lane-marks in the vicinity of no.C105.

When ranking cars and tyre studding configurations, it is also important to consider differences in speed and manoeuvre severity. With a "better" car, the test manager could request a greater speed in the first DLC run of each driver. Therefore, a greater percentage of tests with complete Loss-of-Control (LCS 3) may be justified for tyres with greater adhesion. However, no such distinct statistical relationship between speed and Loss-of-Control percentage has been found, see the discussion on Figure 10 below.

Anyhow, the test procedure aimed at speeds which were on both sides of the border of losing control for each car-driver combination. At these speeds it must have been possible to move the car laterally from the right to the left lane, if the test should be considered in this evaluation. A similar motion may be initiated by the driver in traffic, as well. Irrespective of the speed level, it seems safety-relevant to determine the likeliness of such a possible manoeuvre leading to Loss-of-Control. Therefore, LCS statistics has been computed to illustrate the tyre influence on the control properties of the reference cars (A-D). See Table 7.

Table 7. Number of Double Lane Change Tests Grouped into Two Loss-of-Control Score (LCS) Levels

Compari son No.	Tyre Studding Configuration Cnf.1	Cnf.2	... Wheel Drive Cars	Number of tests recorded Approved *+disapproved* Cnf.1	Cnf.2	Number with Maintained Control (LCS<3) Cnf.1	Cnf.2	Number with Loss-of-Control (LCS=3) Cnf.1	Cnf.2	Percent with LCS=3 *(including disapprovals)* Cnf.1	Cnf.2	Comments on Data Selection (Some data sets exclude tests, where some of the three Speed Sensors were malfunctioning)
1	Bas	Max	Rear	38	39	27	37	11	2	29%	5%	Sessions 9-18 only. Standard DLC-
			C D	+2	+1					*33%*	*8%*	tests.
2	Bas	Max	Front	41	39	31	30	10	9	24%	23%	As above but only Front Wheel
			B A	0	+1					*24%*	*25%*	Drive.
3	Bas	Max	Sum	79	78	58	67	21	11	27%	14%	Sum of both above. (Data available
			above	+2	+2					*28%*	*16%*	from all three Speed Sensors).
4	Bas	Max	Rear	38	70	27	62	11	8	(29)	11%	Sessions 1-18. Approved Standard
			C&D	*(+2)*	*+3*						*15%*	DLC-tests.
5	Bas	Max	Front	41	69	31	48	10	21	(24)	30%	As above but only Front Wheel
			B A	*(0)*	+2						*32%*	Drive.
6	Bas	Max	Sum	79	139	58	110	21	29	(27)	21%	Sum of both above. (Data available
			above	*(+2)*	*+5*						*24%*	from all three Speed Sensors).
7	Over	Max	Rear	32	31	18	25	14	6	44%	19%	Sessions 1-8 only. Standard DLC-
			D C	*+1*	+2					*45%*	*24%*	tests.
8	Over	Max	Front	25	31	14	19	11	12	44%	39%	As above but Only Front Wheel
			B A	*+5*	*+1*					*53%*	*41%*	Drive.
9	Over	Max	Sum	57	62	32	44	25	18	44%	29%	Sum of both above. (Data available
			above	*+6*	*+3*					*49%*	*32%*	at least from Speed Sensor no.2).
10	Over	Max	Rear	55	70	33	62	22	8	40%	(11)	Data mixed from all Sessions.
			C&D	*+1*	*+3*					*41%*	*15%*	Approved Standard DLC-tests.
11	Over	Max	Front	37	69	20	48	17	21	46%	(30)	As above but only Front Wheel
			B A	*+5*	+2					*52%*	*32%*	Drive.
12	Over	Max	Sum	92	139	53	110	39	29	42%	(21)	Sum of both above. (Data available
			above	*+6*	*+5*					*46%*	*24%*	from all three Speed Sensors).
13	Over	Und	Front	14	30	8	26	6	4	43%	13%	Sessions 19-26 only. Standard
			B A	*0*	+2					*43%*	*19%*	DLC-tests. (Data available at least
												from Speed Sensor no.2).
14	Over	Und	Front	101	30	61	26	40	4	40%	(13)	As above completed with Sessions
			+Rear	*+6*	+2					*43%*	*19%*	1-8 and Oversteering Rear Wheel
			ABCD									Drive (carD) in Ss 19-26.
15	Over	Und	Front	205	30	121	26	84	4	41%	(13)	As above completed with all
			+Rear	*6+3*						*43%*	*19%*	approved Pedal DLC-tests. Note:
			ABCD	*=+9*	+2							Pedal tests only with Oversteering.

Bold text indicate the most suitable rows for comparisons between different combinations of Reference car (Front Wheel Drive: Volvo 440 & Rear Wheel Drive: Volvo 740) and Tyre Studding Configuration. Underlined percentages are repeated later (within parentheses). When both obstacle marks (C70 & C80 in Figure 3) were hit, the test had to be *disapproved* for Lateral Acceleration Assessment. If such tests are included, their numbers appear in *italics*.

When the Loss-of-Control Score is dichotomized to either LCS 3 or smaller (LCS 0-2), distinct differences appear between the Over- and Understeered configurations. While complete loss-of-control occurred in only four (13 %) of the 30 approved DLC-tests with Understeering tyres (all four were rear wheel skids ending in spin-out), the Oversteering tyres exhibit LCS 3 in 84 (41 %) of 205 DLC-tests, see row 15 in Table 7. However, row 13 shows that only 14 Oversteering DLC-tests are fully comparable to the 30 Understeering ones (i.e. with Front Wheel Drive, recording in sessions 19-26, and without intervening Pedal tests which unintentionally excluded about 15 such normal DLC tests from evaluation).

If one counts Loss-of-Control (LCS=3) tests together with *disapproved* tests (because of Early Plow-Out and hitting both obstacle marks C70&C80, *italics* in Table

7), the "failure" percentages increase, but the rank order remains the same in most of the comparisons in Table 7.

Figure 5 presents some of the percentages from Table 7: row 1 & 2 (Basic Studding), row 10 & 11 (Oversteering and Maxi), row 13 (Understeering). The confidence intervals in Figure 5 are estimated from Binomial Parameter tables (Dowdy & Wearden, 1991).

While Oversteering tyres result in inferior handling in most of the Table 7 comparisons, Maxi studded tyres on all four wheels result in substantially greater Loss-of-Control ratios for the smaller FWD cars (A&B) than for the larger RWD cars (C&D). See row pairs 1 & 2 or 7 & 8 merged on rows 4 & 5 (versus Basic Studding) and on rows 10&11 (versus Oversteering Studding). In addition, it appears from Figure 8 that the average manoeuvre was less severe with the smaller car type A&B, which emphasizes the inferiority of its control properties.

The inferiority in stability of the A&B cars in the Loss-of-Control statistics (Table 7, Figure 5) is remarkable, since their smaller width puts less demand on lateral motion and lateral acceleration in the DLC manoeuvre than for car C&D. In Figure 8&9 it will be demonstrated that the lateral acceleration assessments at transition to Loss-of-Control were smaller for the FWD cars A&B in comparison to car C&D in the same sessions Nevertheless, the FWD car inferiority in the tests may be valid and safety-relevant on public roads, as well. See the section below on Hazards with Front Bias.

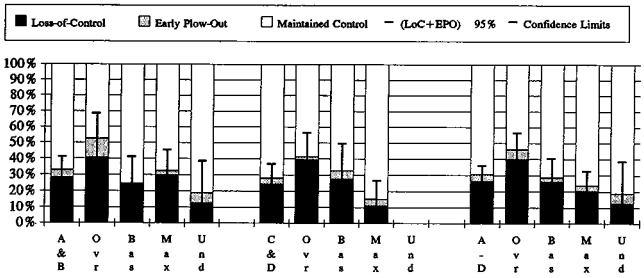

Approximate 95% confidence intervals for "failures." Column groups for Car types: A&B; C&D; all types A-D. Separate columns for Tyre Studding config: Σ; Ovr; Bas; Max; Und.

Figure 5. Proportions of "Failures" (Loss-of-Control or Early Plow-Out) and "Successes" (Maintained Control) in the Double Lane Change Tests

Assessment of Lateral Acceleration from Speed and Distances

In this kind of driving experiments, crash avoidance capability is often determined as a threshold speed (or similar physical quantity), which only "better" driver-vehicle combinations can exceed without losing control. To make the results more general and possible to judge for other investigators, we aimed at quantities comparatively independent of the test path geometry. In both the Combi and the Double Lane Change tests it was also important to make the results and their variance insensitive to fluctuations in ice friction, which should be expected in a three week outdoor test program.

Therefore, we designed the experiments for assessments of lateral (and longitudinal) accelerations and ratios thereof, such as in Table 4 & 5. A typical value of the lateral acceleration in the Double Lane Change manoeuvre may be assessed from the path geometry and from the Speed Sensor recordings. A Driver model (Approximation) for Vehicle Investigation by computer Simulation, DAVIS, developed by Strandberg (1972), determines the lateral acceleration from the speed (v, assumed to be constant during the manoeuvre) and the following parameters:

L (ideal) Manoeuvre Length is defined as twice the longitudinal distance from the beginning of left motion in right lane to the centre of the "right lane obstacle" (where the lateral motion will change from leftwards to rightwards in a symmetrical DLC about the 10 m long blocking of the right lane). From wheel traces on the ice, the value L=80m has been used in the evaluations here. (Even if the longitudinal "gate" was 60m, see Figure 3, the lateral displacements are very small at the ends of this trajectory.)

Y lateral motion amplitude needed to avoid hitting the plastic tube marks between the lanes and at the left corners of the simulated obstacle (C70 & C80 in Figure 3).

Δ position of the obstacle lane-marks (distance Δ to the right of the centre line between the marks C45 to C105). It varied between certain sessions (Δ = 0.75m except in sessions 5-12 when Δ =0.0m).

c car width (c=1.67m for car A & B, c = 1.75m for car C & D. Drivers' own cars E & F schematized here to c = 1.70m).

Hence, the reference car tests have been evaluated with four alternative Y-values (1.75, 1.67, 1.00, 0.92 m), since Y = c - Δ. According to Strandberg (1978), the DAVIS' peak lateral (Sideways) Acceleration, SA is given by Eq.7.

$$SA = \frac{6(4+5\pi)^2}{(6\pi^2+9\pi+8)} \frac{v^2}{L^2} Y \qquad (7)$$

It should be noted that the constants Y and L have not yet been fitted to data. All SA-values in this paper should therefore be considered relative and not absolute. However, it may be possible to make better assessments of the constants L, c, and Δ by using regression analysis with the computer recorded acceleration data from car D, speed sensor data, and Eq. 7.

Even if the constant L and the parameter Y are inaccurate descriptions of an individual test trajectory, they quantify (through Eq. 7) the effect from speed on the lateral acceleration needed in an an ideal manoeuvre. And if the space given by a smaller car width (c) or by a smaller obstacle (greater Δ) is better utilized in one

test than in another, Eq. 7 offers an optimal-manoeuvre reference expressed as a well-known physical quantity (peak acceleration) which may be given in a standardized unit (here m/s^2).

The smaller SA-values achieved at a certain speed with cars A&B due to their smaller c- and Y-measures compared to cars C & D may then be considered unfair, since smaller car dimensions contribute to reduce the DLC-manoeuvre severity even in real traffic situations. Nevertheless, a greater SA-value reflects a more demanding manoeuvre when different tyres or drivers are compared from tests with the same type of car.

Lateral Acceleration at the Transition to Loss-of-Control

In the last mentioned respect, the crash avoidance capability for each driver has been quantified through the maximum SA-value achieved without complete Loss-of-Control (SA_{OK}) and through the minimum value where the driver lost control (SA_{LC}). Referring to the Loss-of-Control Score levels in Table 7, these two SA-values (if both exist) have been determined as follows for each combination of driver, Studding configuration and car type

$$SA_{OK} = \text{driver-MAX(SA with LCS} < 3) \text{ for one car or a group of cars} \quad (8)$$

$$SA_{LC} = \text{driver-MIN(SA with LCS=3) for one car or a group of cars} \quad (9)$$

Figure 6 illustrates that most drivers lost control in a less severe manoeuvre than in their "best" one with maintained control. This indicates that the test manager's speed demand was reasonable and that it may be worthwhile to elaborate on the influence from parameters in cars and tyres. The possibilities to demonstrate the importance of such parameters are noticeable and might be used in driver education.

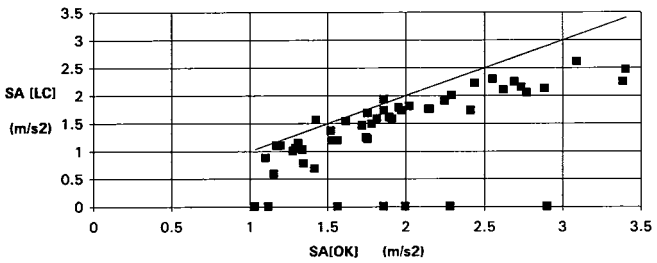

Includes all cars A-E, where the width c= 1.7m for Eq. 7 was made to pattern for driver's own car E). Smallest value (SA_{LC}) from tests resulting in Loss-of-Control versus greatest value (SA_{OK}) from tests with maintained control. Line y = x for reference. Plot on x-axis for drivers with no LoC test.

Figure 6. Each Driver's Pair of Lateral Acceleration Extreme Values from All Standard Double Lane Change Tests in the Session

Taken over all drivers and sessions, the mean values of the manoeuvre severity quantities (defined in Eq. 7-13) do not differ much more between studding configurations than what may be expected from random variation. One clear-cut exception has been found, though: The average driver lost control in RWD cars at less severe manoeuvres with Basic Studding (SALC= $1.3m/s^2$) than with Oversteer Studding (SALC= $1.9m/s^2$) or with Maxi Studding (SA_{LC}= $1.8m/s^2$). The Basic Studding was inferior also with the FWD cars. See Table 8. The rear biased weight distribution in car D compared to car C may have contributed to the great values with Oversteer studding (only car D) in comparison to the Basic Studding, where car C dominated the RWD tests.

Table 8. Greatest Lateral Acceleration with Maintained Control (SA_{OK}) and Smallest with Loss-of-Control (SA_{LC}) for Different Combinations of Reference Cars and Tyre Studding Configurations

Cars (cf. Table 1&4)	Tyre Studding (cf. Table 3)	SA_{OK} (m/s^2) Mean value	SA_{OK} Std.err. (m/s^2)	SA_{LC} (m/s^2) Mean value	SA_{LC} Std.err. (m/s^2)
A&B (FWD)	Oversteer	1.51	0.09	1.75	0.09
A&B	Maxi	1.48	0.08	1.95	0.12
A&B	Basic	1.40	0.11	1.51	0.22
A&B	Understeer	1.49	0.06	1.68	0.14
D not C (RWD)	Oversteer	1.80	0.06	1.94	0.10
C&D	Maxi	1.84	0.08	1.80	0.17
80%C & 20%D	Basic	1.58	0.16	1.30	0.22

Mean values over all drivers in normal Double Lane Change tests. Std.err. (standard error = sample standard deviation divided by $\sqrt{n}$) designates usual estimate of standard deviation of the mean.

Paired comparisons in Table 8 (as well as in the figures with 95% confidence intervals) may reveal several "significant" differences on the 5% level. However, the number of possible comparisons is too great for this level and the likelihood of mass-significance must be considered to avoid misinterpretation of the results.

When trying to rank order the cars, their effect is obscured by the great "noise" from driver and session variances in SA_{OK}. This is illustrated in Figure 7, where SA_{OK} values for each combination of driver and reference car A,B,D is plotted versus SAOK for car C with the same driver (but only from session 1-8, where the studding configurations were unchanged, see Table 4). The values for Car C (with Maxi studding) were selected as the independent (x) variable, since they were the greatest with most drivers.

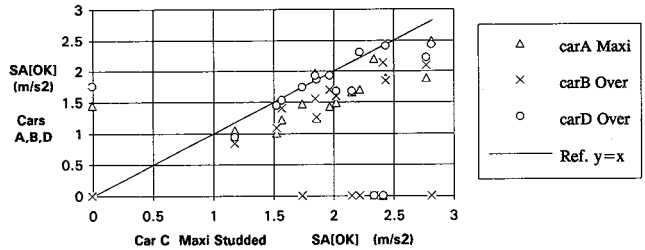

SAOK-values from session 1-8 for reference car A,B,D plotted versus SA_{OK} for car C with same driver. Plot on x-axis corresponds to loss-of-control in drivers' all DLC tests with that car.

Figure 7. Sixteen Drivers' Greatest Lateral Acceleration in Double Lane Change Tests with Maintained Control (SAOK in Eq. 7 & 8)

The differences in SA_{OK}-level between tyre studding configuration cannot easily be distinguished only by comparing their mean values over the 16 drivers. Their confidence intervals overlap considerably, as can be seen in Figure 8. However, the resolution increases, if differences in SA_{OK} values are calculated for each driver and averaged. Then the Maxi-studded cars may be considered "significantly" superior to the Oversteering ones, since the lower confidence limit of their average within-driver difference is greater than zero. See Figure 8, also exhibiting more pronounced differences between the cars A&B and the larger RWD cars C&D. Even if the car A values are extended with up to 9% by assessing its width equal to that of car C in Eq.7, the differences appear to remain.

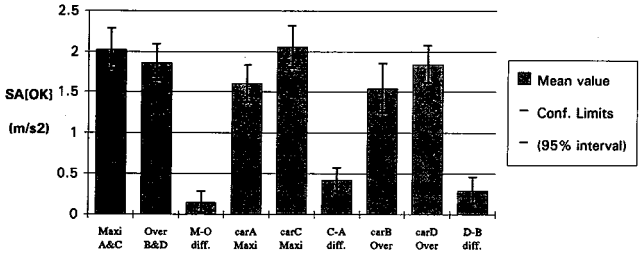

Grouping between Maxi or Oversteering Stud configurations; between Car A,B (FWD) or Car C,D (RWD); and within-driver Differences. Mean values over drivers in sessions 1-8 with 95 % confidence intervals.

Figure 8. Driver's greatest lateral acceleration in DLC tests with maintained control, SA_{OK}

Ratios Between Lateral and Longitudinal Acceleration

When considering the ratio between the DLC lateral and the Combi longitudinal accelerations, the differences also seem distinct between the two reference car types, see Figure 9. The within-car variation of SA_{OK} between drivers and sessions is evidently almost neutralized when one divides the lateral acceleration with the longitudinal one. Compare Figures 7 & 9. The remaining and clear-cut difference between the two car types may be partly due to stud protrusion deviations and to the nonlinear functional relationship between wheel load and friction of studded tyres on ice, which will be commented in the last section.

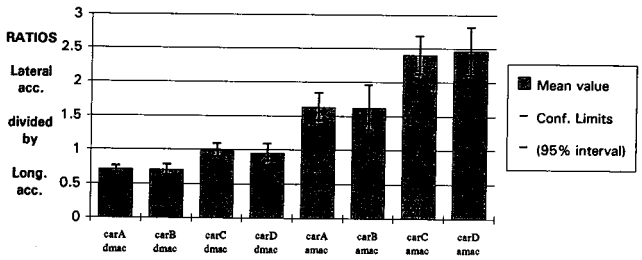

See ratios R_{SdOK} and R_{saOK} in Eq. 10 & 11. Car mean values over drivers in sessions 1-8 with 95% confidence intervals.

Figure 9. Lateral Acceleration Divided by Deceleration (d_{mac}) or by Forward Acceleration (a_{mac})

The mentioned ratios may be expressed as follows according to the definitions in Eq. 4-5 & 8-9. The controlled lateral-backwards acceleration ratio is a measure of the maximum severity of an evasive manoeuvre in relation to the current deceleration capability:

$$R_{SdOK} = \frac{SA_{OK}}{d_{mac}} \tag{10}$$

The controlled lateral-forward acceleration ratio is a measure of the maximum severity of an evasive manoeuvre in relation to the current acceleration capability:

$$R_{SaOK} = \frac{SA_{OK}}{a_{mac}} \tag{11}$$

The uncontrolled lateral-backwards acceleration ratio is a measure of the minimum manoeuvre severity which led to Loss-of-Control in relation to the current deceleration capability:

$$R_{SdLC} = \frac{SA_{LC}}{d_{mac}} \tag{12}$$

The uncontrolled lateral-forward acceleration ratio is a measure of the minimum manoeuvre severity which led to Loss-of-Control in relation to the current acceleration capability:

$$R_{SaLC} = \frac{SA_{LC}}{a_{mac}} \tag{13}$$

Statistical Relationship Between Speed and Loss-of-Control Likeliness

Since better tyres allowed for higher speeds, a great Loss-of-Control percentage does not necessarily mean poor handling qualities. Therefore, several plots have been made in pursuit for a positive correlation between the test failure percentage and speed (quantified through various normalized variables based on Eq.7-13). However, with our testing procedures and criteria for speed demand, tyre Studding and Car type (such as in Figure 5), appear more decisive of the LoC likeliness than their differences in speed and manoeuvre severity, see Figure 10.

Nevertheless, Table 8 demonstrate that the greatest possible speed in an evasive manoeuvre was lower with Basic Studding than with Oversteer Studding, while Figure 5 illustrated the distinct inferiority of Oversteer Studding when it comes to driver control. A question which remains to be answered is: what happens on the road to the average driver at the same speed? Will Oversteering properties result in unnecessarily severe manoeuvres provoking spin-outs to a greater extent than with Basic Studding properties? Or will the steerability offered by the superior front wheels in an Oversteering

car just be utilized in emergencies, that are impossible to cope with in a Basic Studded car?

It may be difficult to design experiments for valid investigations of driver behaviour from this viewpoint, but it would be clarifying to apply the case-control method from epidemiology to assess the relative risks associated with tyre differences within cars. See Schlesselman (1982), Jones & Stein (1987), Strandberg (1991). Even if only minor effects may result from a conscious and safety-promoting positioning of tyres, the costs seem negligible to the individual. According to the present study, traffic safety would benefit from improved knowledge and more extensive driver education on the substantial differences between cars and tyres in handling properties.

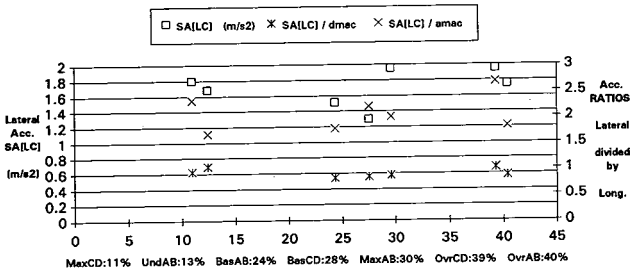

Y-values are means over all drivers for mentioned Studding-Car combinations.

Figure 10. Three Manoeuvre Severity Quantities (SA_{LC} in Eq. 9 and Ratios Thereof as in Eq. 12 & 13) Plotted Versus Loss-of-Control Percentages in Double Lane Change Tests with Same Vehicle

Comments on Hazards with Front Bias in Wheel Load and in Stud Protrusion

Considering sessions 1-8 only (rows 7 & 8 in Table 7), the car A percentage with Loss-of-Control (LCS=3) was about twice that of car C. The handling inferiority of the smaller FWD cars A & B compared to the larger RWD cars C&D, may be more due to other factors than to the Front Wheel Drive per se. For instance, a shorter wheelbase deteriorates stability (Strandberg et al, 1982).

Another explanatory factor with greater potency was suggested by Nordstrom (1991). Like the average FWD car, the A&B cars may have had front/rear wheel loads close to the opposite extremes of the Side Force Coefficient curve (SFC as a nonlinear function of wheel load for studded tyres on ice). According to Elgeskog & Brodd (1976) an increment in wheel load of about 1000N (100kg) or more may raise the SFC by about 25%. With a driver and at nominal curb weight the A&B cars exhibit about 120kg greater load at a front wheel than at a rear one, see Table 1. The front-rear wheel loads for the C&D cars differ less (about 70kg) and are on a higher weight level, which may be more distant from the steep ascent in the √-shaped SFC-curve.

Even if the numbers are small, rows 1&7 in Table 7 illustrate the influence on stability from rear wheel load. The Loss-of-Control percentage with Maxi Studded RWD cars was 19 % when car C was used (row 7), while car D exhibits the smallest ratio in the whole table (5% on row 1). It may be statistically dubious (because known data cannot be used for hypothesis testing) to point out that these percentages are almost outside each other's 95% confidence interval. Nevertheless, this difference in Loss-of-Control ratios offers support to the above mentioned explanation, since the wheel load of car D was rear biased in comparison to car C and to the numbers in Table 1, mainly due to the rear-seated instructor / computer operator.

In addition to this hazard in rear-light cars, measurements have indicated that the average car on Swedish winter roads has a greater stud protrusion at the driven wheels. In a study of 200 randomly selected cars, reported by Strandberg (1989), the difference was statistically significant for FWD cars. It should be noted that this stud diverging phenomenon improves stability with RWD and deteriorates it with FWD.

The protrusion increases faster when driving on ice with great adhesion utilization (Nilsson, 1990). In spite of the tyre contributor's careful running-in procedure, the stud protrusion was found to be substantially greater after the experiments than before, particularly for the FWD tyres, see Table 2. Since we did not move the wheels between front and rear regularly, it cannot be ruled out that the tyres on car A&B increased their adhesion more at the front through successively greater protrusion.

However, this develops in most FWD cars even in traffic on winter roads, where rear wheel skidding accidents with FWD cars are frequent, contrary to common belief. Official statistics indicate that such instability accidents take more lives than loss-of-steering accidents (Strandberg, 1989). Though spin-outs may be less common than plow outs, side impacts are more injurious than frontal impacts in conventional automobiles.

In rear wheel driven cars, also excessive throttle or engine braking may surprise the driver with unexpected power oversteering. One of our driver subjects was very close to a severe crash into the testing base. When car D began to yaw during acceleration for a Combi manoeuvre, the driver did not release the throttle. After a couple of recovered skids he spun out with almost constant speed and hit the speed sensors before the car came to rest. According to our questionnaire, he had a driver's license even for heavy vehicle combinations but almost no experience from rear wheel drive on winter roads.

Since rear wheel skids may be controllable (for a skilled driver with plenty of lateral space) and less common than loss-of-steering—at least in FWD cars, many drivers reject understeering more than oversteering properties. Therefore, drivers should be informed about these potential instability hazards in the average FWD car—and one simple remedy (mounting wheels with

greater stud protrusion at the rear). Of course such mounting may deteriorate the deceleration performance (see dmac in Table Sa) and increase the risk of understeering or plow out accidents. Hence, further accident analysis is needed before it should be generally recommended to mount the best tyres at the rear. A suitable epidemiological method has been adapted to the routines of the Swedish police, see Strandberg (1991).

In follow-up tests with car D after the ordinary 26 sessions, we found that steerability with poor tyres (Basic Studding) at the front wheels could be improved, if rear wheel skidding was initiated by a couple of small steering reversals before the actual DLC-manoeuvre. Such intentional skidding may belong more to the racing or rally course than to public roads. But it must be remembered that similar skids may be initiated unintentionally by any driver when it is slippery—in spite of the car exhibiting clear-cut understeering properties in most common manoeuvres.

Acknowledgements

This study has been jointly sponsored as a part of the Swedish research and development programme for skid training. Funding organizations are (in alphabetical order of the Swedish abbreviations) The Service Company of the Swedish Insurance Industry (FSAB), the National Society for Road Safety (NTF), the Swedish Association of Driving Schools (STR), the Swedish Transport Research Board (TFB), the National Road Safety Office (TSV), the Swedish Road and Traffic Research Institute (VTI). Grants for the experiments were also offered from Volvo Car Corporation within the European PROMETHEUS programme. Substantial contributions with equipment and knowledge were supplied by Volvo and by Nivis Tyre Inc. Audi, Mazda, Saab, and Subaru have also provided high-tech cars, giving the members of the project group hands-on driving experience from disconnectable ABS, 4-Wheel-Steering, Automatic Spin Reduction, and 4 Wheel-Drive. Valuable and appreciated assistance was given by members of the Swedish Federation of Women's Motor Transport Corps (SKBR). The Tourist Office in the town of Orsa kindly acted as intermediary to the drivers. People living in the village Sandsjo at lake Hemsjon stood behind the practical arrangements in spite of the short notice. Their concern of our personnel, equipment, and activities was a relief to the whole testing team.

References

Aschenbrenner, K.M., (1991). Personal correspondence. Hoechst, A.G., Frankfurt am Main, Germany.

Aschenbrenner, K.M., Biehl, B., Wurm, G.W., (1991). Mehr Vehrkehrssicherheit durch bessere Technik? Feldtuntersuchungen zur Risikokompensation am Beispiel des Antiblockiersystem (ABS). Final report to Bundesanstalt für Strassenwesen. In press.

Biehl, B., Aschenbrenner, M., Wurm, G., (1987). Einfluss der Risikokompensation auf die Wirkung von Vehrkehrssicherheitsmassnahmen am Beispiel ABS. Unfall und Sicherheitsforschung Strassenverkehr, Heft 63. Bundesanstalt für Strassenwesen.

Dowdy, Shirley & Wearden, S., (1991). Statistics for Research. John Wiley & Sons, New York.

Draper, N., & Smith, H., (1981). Applied Regression Analysis. John Wiley & Sons, New York.

Elgeskog, E., & Brodd, S., (1976). The Influence of Wheel Slip Control Dynamics on Vehicle Stability during Braking and Steering. In Braking of Road Vehicles, I Mech E Conf. Publ. 1976-5, pp. 59-68 (ref. to Fig. 4).

Fisher, R.A., (1958). Satistical Methods for Research Workers. In J.H. Bennet (ed.): A Re-issue of Statistical Methods for Research Workers, The Design of Experiments, and Satistical Methods and Scientific Inference, Oxford University Press, 1990.

Hansson, R., (1991). Personal communication on braking systems. Volvo Car Corporation, Göteborg, Sweden.

Johnsson, L., & Knutsson, K., (1973). Field Testing Statistical Tests. In Swedish Experimental Safety Vehicle program "Steerability During Emergency Braking," Report 4-01.

Jones I.S., & Stein, H.S., (1987). Defective Equipment and Tractor-Trailer Crash Involvement. Insurance Institute for Highway Safety, 1005 N.Glebe Road, Arlington, Virginia 22201, USA.

Nilsson, H., (1990). Personal communication on studded tyres. Nivis Tyre Inc. Gislaved, Sweden.

Nordström, (1991). Personal communication on tyre characteristics, ABS, and vehicle dynamics. VTI, Linkoeping, Sweden.

OECD (1990). Behavioural adaptations to changes in the road transport system. Organisation for Economic Cooperation and Development, Road Transport Research, Paris. IRRD No 824028.

Priez, A., Petit, C., Guezard, B., Boulommier, L., Dittmar, A., Delhomme, A., Vernet-Maury, E., Pailhous, E., Foret-Bruno, J.Y., Tarriere, C., (1991). How About the Average Driver in a Critical Situation? Can He Really Be Helped by Primary Safety Improvements? To be published in proceedings of the 13th ESV Conference, Paris, November, 1991. Paper no.91-S7-O-07.

Robinson, B.J., & Riley, B.S., (1989). Braking and Stability Performance of Cars Fitted with Various Types of Anti-Lock Braking Systems. Proceedings (pp.836-846) on the 12th ESV Conference, Göteborg, Sweden, May 29 - June 1, 1989.

Rompe, K., Schindler, A., Wallrich, M., (1987). Advantages of an Anti-Wheel Lock System (ABS) for the Average Driver in Driving Situations. Proceedings (pp.442-448) on the 11th ESV Conference, Washington, D.C., May 12-15, 1987.

Schlesselman, J.J., (1982). Case-Control Studies. Oxford University Press.

Strandberg, L., (1972). Mathematical Description of Vehicle Motion in a Double Lane Change Manoeuvre. Chapter B.7 in VTI Repon 9. (In Swedish).

Strandberg, L., (1978). Lateral Stability of Road Tankers. VTI Report 138A (ref. to Volume II, pp. D18-D21).

Strandberg, L., Tengstrand, G., Lanshamrnar, H., (1982). Accident Hazards of Rear Wheel Steered Vehicles. In G. Johannsen & J.E. Rijnsdorp (eds.), IFAC Analysis, Design and Evaluation of Man-Machine Systems. Pergamon Press, Oxford and New York, 1983.

Strandberg, L., (1989). Skidding Accidents and their Avoidance with Different Cars. Proceedings (pp. 825-828) on the 12th ESV Conference, Göteborg, Sweden, May 29 - June 1, 1989. Also in VTI Reprint 158.

Strandberg, (1991). Case-Control Studies for Assessment of Accident Risks in Drivers and Vehicles (in Swedish: Bestärnning av olycksrisker hos trafikant och fordon). VTI Note TF 50-20 (to appear as VTI Repon 367).

Stöttrup-Hansen, E., Ahlbom, A., Axelson, O., Hogstedt, C., Juul Jensen, U., Olsen, J., (1990). Negative Results—no effect or information? Arbete och Hälsa 1990:17, National Institute of Occupational Health, Solna, Sweden.

Wilde, G.J.S., (1988). Risk Homeostasis Theory and Traffic Accidents: Propositions, deduction and Discussion of Dissension in Recent Reactions. ERGONOMICS, vol.31(4), pp.441-468.

Volvo (1989). Volvo Pocket Guide 1990 (In Swedish: Volvo Fickdata 1990). Volvo Car Corporation, Göteborg, Sweden.

VTI, Swedish Road and Traffic Research Institute (1990). Annual Report 1989/90. Linköping, 1990 (ref. to pp. 19-21).2

S7-O-10

Simulation as a Design Aid

E. Girardot, P. Tardivon
PSA Peugeot-Citroen

Introduction

The improvement of automotive vehicle road performance and the manufacturers' concern to optimize handling characteristics by adapting them to the driver's capabilities as well as today's road environment, has led PSA to develop effective research and study methods used as a preliminary modelling tool in the design office. This tool must be capable of being adjusted nonempirically to take account of the numerous parameters which govern the dynamic response of an automotive vehicle.

The method chosen by PSA brings together the use of open-loop numerical simulation and track testing, associated with results analysis enabling both objective (variations curves) and subjective (representation of vehicle behaviour using synthesized images) judgements.

Numerical Simulation

Numerical simulation consists of using a mathematic model to represent the dynamic behaviour of a vehicle. PSA has several types of model at its disposal. The mathematic model used as an example in this paper has been produced by defining:

- The kinetics of a system formed from 5 rigid solids
  - chassis
  - 4 wheels
  - engine (reduced to its flywheel) and a material point: the steering rack location.
- The kinetics define the steering and suspension systems (wheel plane orientation, induced effects, etc)
- The forces
  - suspension efforts
  - ground/tyre efforts (from tyre condition parameters such as longitudinal slip, tyre slip angle, etc.)
  - aerodynamic efforts
  - engine and braking efforts.

The vehicle is characterized by about 600 parameters, the model is driven by a steering wheel angle, an engine torque and a brake pressure. Its response forms the vehicle road behaviour (within a certain field of validity). The use of these numerical tools is justified for many reasons. They enable:

- the study of a vehicle which does not yet physically exist
- parametric studies:
  - quick
  - with perfectly repeatable outside conditions
- a better understanding of the physical phenomena (notably due to the availability of any required variable)
- the replacement of actual tests when these are difficult to undertake (particularly when they are dangerous) or difficult to interpret.

However, these numerical tools require validation for them to be considered as true vehicle behaviour in a reliable fashion. A test and measurement programme on real vehicles must be carried out to precisely define the model's field of validity of which limitation is known (particularly due to the stationary functional description of the tyre).

Track Testing (Reconstructing Trajectories)

The measurement of certain fundamental dynamic vehicle parameters is difficult (vehicle trajectory, chassis, tyre slip angle). PSA has developed a software programme to reconstruct trajectories from simple measurements taken on the vehicle:

- Linear accelerations at a point according to the three body axes (reference)
- Chassis and angle rates (gyroscopic unit)
- Vehicle speed (Correvit system)

This software programme enables access to:

- Chassis condition variables as well as their derivatives
- Normal and tangential acceleration as well as the trajectory curve radius.

Results Presentation Tool

Apart from the presence of different variables resulting from the numerical simulation and track tests in the form of groups of curves, the analysis of which gives rise to a considerable workload, and so PSA has equipped itself with an animated vehicle movement sequence representation system.

This is achieved using a synthesized image generator (G1 10 k SOGITEC) animating 5 bodies (the chassis plus the four wheels) from their co-ordinates relative to a fixed reference frame. The image calculation is carried out in real time at a frequency of 25Hz.

This type of presentation is a great help in the work of result analysis by enabling a subjective visual appreciation of the overall vehicle evolution and thus being a complement to the objective judgements made using curves.

The different possibilities linked to synthesized image generation such as:

- the ability of the observer to be positioned anywhere in relation to the vehicle
  - fixed observer
  - observer linked to vehicle movement
  - observer at the driving controls
  - zoom
  - the replacement of a solid by a linked trihedron to demonstrate angular movement.
- multiplication of the elements to be observed by using a constant (body angles, wheel angles..).
- slow motion, forward/rewind projection.
- replays

leaving the researcher complete freedom to focus in on a particular point.

Reconstructing an Accident (Leaving the Road on a Left-Hand Bend)

In association with other manufacturers and the relevant authorities, P.S.A. is working towards improving vehicle safety. Notably in the area of primary safety, the numerical simulation and analysis tools described can lead to a better understanding of the sequence of events and the mechanism of an accident.

The type of accident selected (leaving the road on a bend) represents 13% of serious road accidents. The one studied is described as "low dynamics" as the vehicle speed on entering the bend was well below the maximum possible speed for this type of bend.

Accident Description and Reconstruction

The police report enables the various phases of the accident to be reconstructed:

- A top range car on a 3-lane main road mounted the verge on the right-hand side of the road in a left-hand bend.
- The vehicle travelled a distance of 76 metres with the right-hand wheels at a maximum of 1.6 metres onto the verge.
- The vehicle then regained the road, travelling about 20 metres before leaving skid marks over a distance of 21 metres and crashing into a vehicle coming in the other direction.

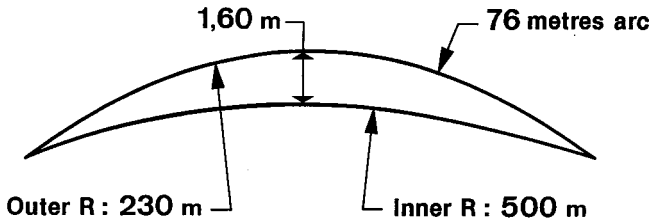

Figure 1. Accident Reconstruction

This report also informs us of:

- The vehicle type.
- The approximate vehicle trajectory (trajectory whilst on the grass and whilst in the final known braking phase).
- The road condition during the accident: dry road.
- The vehicle's final speed of about 60 kph determined from the state of the damage.
- The bend curve radius for the two vehicles involved.

Certain data remain unknown:

- The driver's behaviour: steering wheel angle, braking pressure.
- The vehicle's initial speed.
- The vehicle load (according to the photos, a relatively heavy load installed towards the rear).
- The actual road adhesion conditions (type of surface and above all the grass adhesion conditions).

From relatively realistic hypotheses, it is however possible to re-calculate certain accident data. The calculations show that the vehicle was travelling at between 95 and 117 kph when it went onto the grass. The marks left in the grass by the vehicle show that the driver was not braking during this phase.

The drawing produced by the police enables us to evaluate the trajectory curve radius in the grass.

The 500 metre bend curve radius enables us, knowing the distance covered in the grass and the maximal distance from the road to the marks left in the grass, to determine the vehicle's curve radius on leaving the road: 230 metres.

The various speeds and rates of deceleration appear on the Reconstructed Accident diagram, Figure 2.

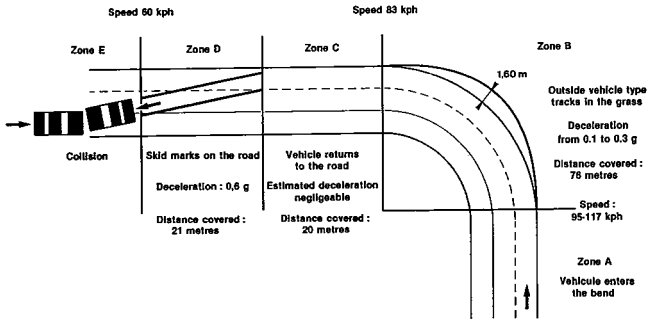

Figure 2. Reconstructed Accident Diagram

Simulation Produced

By using the numerical simulation model, from the available accident data and hypotheses on the driver's behaviour, we have reconstructed the vehicle evolution up to its return to the road (subject vehicle: XM).

Throughout the simulation, brake pressure is nil and resistive engine torque 40 mN corresponding to the accelerator in its highest position.

The simulation is carried out in two stages: Figure 3.

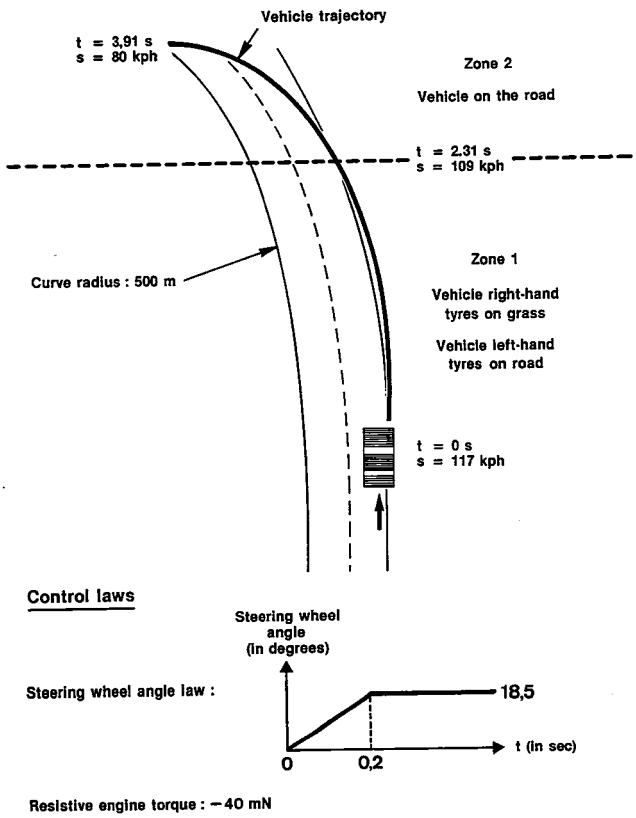

Figure 3. Simulated Accident

- The vehicle has two wheels on the road and two wheels on the grass from t=0s to t=2.31s (at the end of which time the 76 metres in the grass would have been covered). The first stage starts when the two right-hand vehicle wheels enter the grass. The vehicle speed at this point is 117 kph and it is in a rectilinear trajectory. The driver turns the steering wheel at this point from an initial 0 value to a value of 18.5 degrees in a linear manner, taking 0.2s (predetermined angle to enable the vehicle to describe in a steady manner a curve radius of 230 metres; the steering wheel angle rate corresponds to an average value). At the end of this first phase, the vehicle is travelling at 109 kph and has covered 76 metres (average deceleration 0.1g).
  N.B. The low adhesion of the grass has been represented by tyres, the characteristics of which were noted on a surface with an adhesion factor of 0.3.
- The vehicle has four wheels on the road (as from t = 2.31s). The second stage starts when the vehicle has returned to the road. Steering wheel angle, engine torque and brake pressure have been maintained constant. It is noted that this stage ends with the vehicle spinning nose to tail.

Interpretation

This reconstruction does not faithfully reproduce the accident, but above all, highlights the influence of the lack of adhesion continuity when the right-hand wheels pass from the road to the grass. This lack of continuity in reality causes the driver to lose control of the vehicle which goes into a nose to tail spin.

The curves drawn on the figures 4 to 7 illustrate the following phenoma:

- The discontinuity of transversal effort on the two vehicle right-hand wheels at the moment of the change of adhesion (Figure 4 and 5), as well as the low evolution of transversal effort on the left-hand wheels at the same time (Figure 6 and 7).
- The effect of imbalance on the trajectory which shows:
  - a sharp increase in yawing speed (Figure 8),
  - evolution in time of the attitude angle which characterizes the start of a nose to tail spin (Figure 9).

Compared with the actual accident, the major differences are probably:

- the laws of control applied by the driver (impossible to determine after the event)
- the road profile (probable height variation between road and verge)

However, having taken the simplest possible hypotheses for the simulation, we have obtained a movement which perfectly reproduces the general features of the accident but not necessarily the exact values of actual movements.

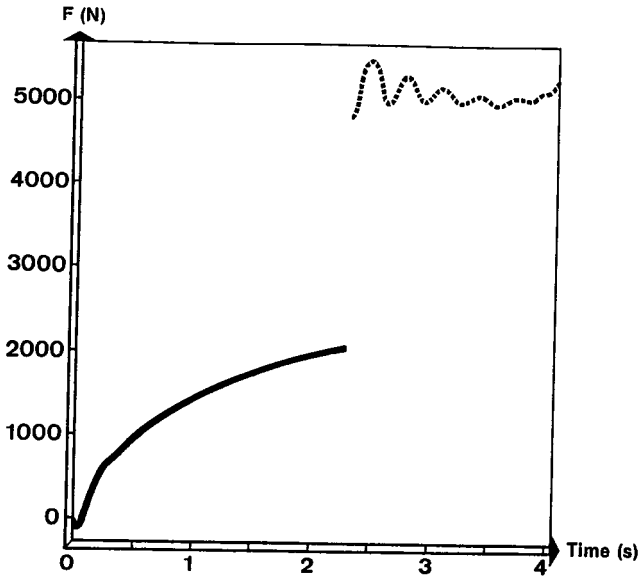

Figure 4. Ground/Tyre Transversal Effort (Front Right Wheel)

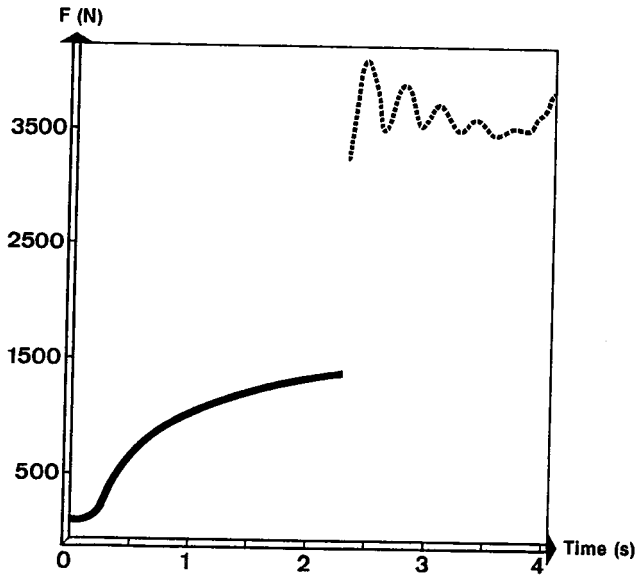

Figure 5. Ground/Tyre Transversal Effort (Rear Right Wheel)

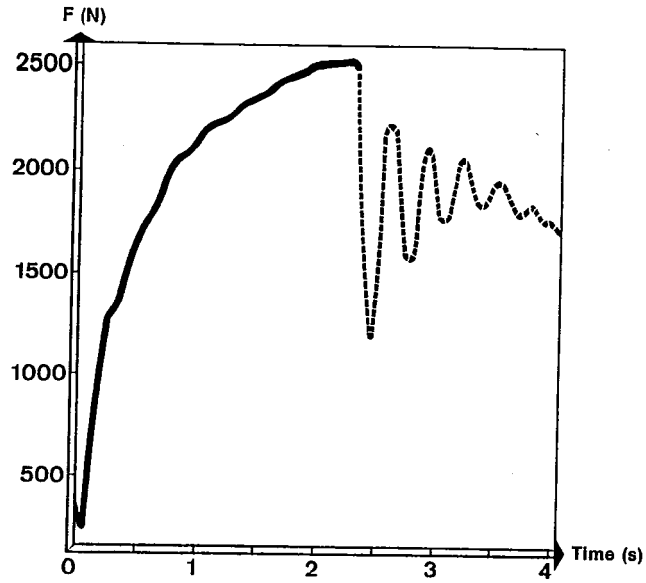

Figure 6. Ground/Tyre Transversal Effort (Front Left Wheel)

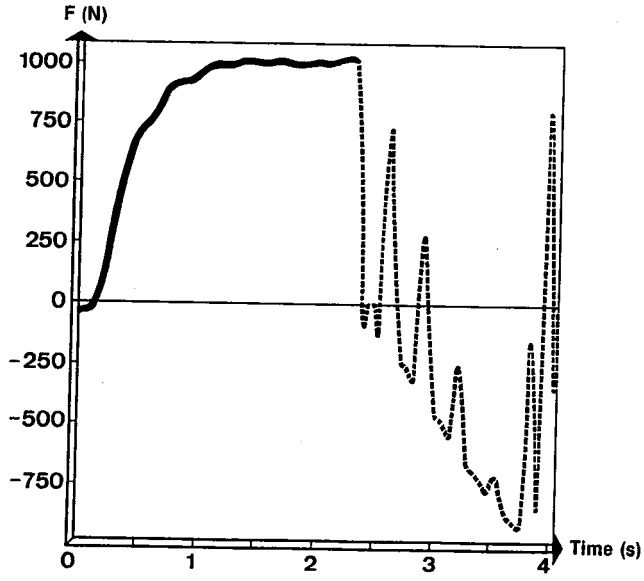

Figure 7. Ground/Tyre Transversal Effort (Rear Left Wheel)

It can therefore be shown that the lack of continuity of adhesion between the road surface and the verge can be the cause of a loss of control in a bend and this simulation can be used as the point of departure for the study of suitable counter-measures.

Conclusion

This presentation has shown, using an application based on a true case, the results that can be obtained by linking numerical simulation and animation with the aim of representing overall vehicle behaviour in a synthesized manner. Direct observation, in real time, of the vehicle's movement on its trajectory, as well as the accompanying timing diagram, provides very useful data explaining the physical phenomena.

Beyond the present application of linking vehicle engine, braking and steering with animation, the introduction of the driver in the control loop is a way of further advancing automobile vehicle behaviour analysis method.

Reference

1. From accidentology analysis to the intelligent vehicle. 13th ESV Document, Reference 91-S4-W-15, M. Colinot (PSA) Lechner (INRETS) France.

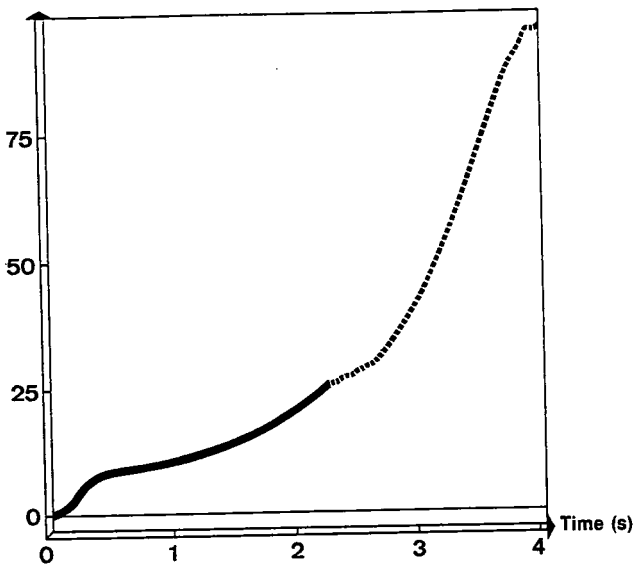

Figure 8. Yaw Rate (in Degrees)

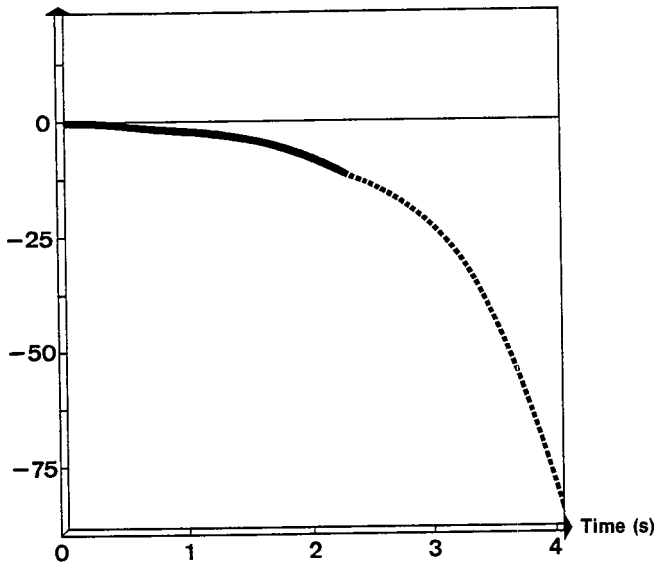

Figure 9. Vehicle Body Slip Angle (in Degrees)

S7-O-11

Analysis of Accidents in Right Turns Using a Fuzzy Logic Simulation Model

Hiroshi Ueno, Kiyoshi Ochiai
Nissan Motor Co., Ltd.

Abstract

The objective of this research was to develop and confirm the validity of a simulation model incorporating fuzzy logic that could be used in analyzing the mechanism involved in the occurrence of accidents in right turns. This model is applicable to accidents occurring at intersections in which a vehicle making a right turn collides with an oncoming vehicle traveling straight ahead. Such accidents can be traced to driver error stemming from ambiguous recognition and judgment. The model is capable of analyzing separately and quantitatively each factor involved in the mechanism causing such accidents. It can be also used to evaluate the risk involved in the execution of right turns. It was noted that older drivers tend to underestimate the speed of oncoming cars. Right turn simulations were conducted with the model reflected this recognition characteristic. The results of the simulations revealed that for older drivers the time allowance for executing a right turn was shorter by a maximum of 1.0 second in comparison with younger drivers. In addition, evaluations were also made for oncoming cars and motorcycles and for differences in the perception of oncoming vehicle speeds and the perception of distance under daytime and nighttime driving conditions.

Introduction

The operation of a motor vehicle entails a repetitive process of recognition and judgment on the part of the driver with respect to the condition of the vehicle and that of the surrounding traffic environment. These acts of recognition and judgment contain various ambiguities that can become the cause of an accident in all too many instances.

In developing preventive safety systems, which are classified under the category of active safety, it is essential to understand the mechanism behind the occurrence of accidents due to human error in recognizing or judging a situation. Such understanding provides the basis for devising safety system concepts which will be most effective in helping drivers to avoid errors that lead to accidents. Another crucial aspect of this development work is to establish methods that make it possible to predict the improvement in safety that can be achieved through the implementation of a newly developed safety device or technology.

The aim of the present work was to develop and confirm the validity of a simulation model that could be used in making quantitative analyses of the factors at work in the occurrence of accidents in right turns (left turns in the U.S. and most European countries). Such accidents seem to be caused by ambiguities in recognition and judgment on the part of the driver of the turning vehicle, even though the person is aware of the presence of an oncoming vehicle that is traveling straight ahead.

To accomplish this aim, a comprehensive simulation model incorporating fuzzy logic has been developed that takes into account the entire right turn process, including recognition, judgment and execution of driving operations.

Analysis of Right Turns

In order to develop the fuzzy logic simulation model, it was necessary to analyze the driver behavior that the model is intended to simulate. This was accomplished by analyzing video tape recordings of approximately 400 right turns executed at actual intersections. In addition, approximately 100 right turns were executed at intersections without traffic signals by a vehicle equipped with various measurement instruments. The vehicle behavior data thus collected were also used in analyzing right turns.

Video Tape Analysis

Whether a turning vehicle stopped or not showed a stronger correlation with the time headway, including the information on the speed of the oncoming vehicle, than with the distance from the center of the intersection to the oncoming vehicle. This suggests that right turn judgments are based on the perceived distance to and speed of an oncoming vehicle.

Figure 1 shows the percentage of the number of vehicles that turned right without stopping and the number that stopped and waited before turning as a function of the time headway between the oncoming vehicles. When the time headway between oncoming vehicles was shorter than three seconds, all vehicles stopped and waited before turning. Conversely, when the time headway was longer than six seconds, virtually all vehicles turned without stopping. With a time headway of 4.2 seconds, the number of vehicles was divided almost evenly between those that did and did not stop before turning.

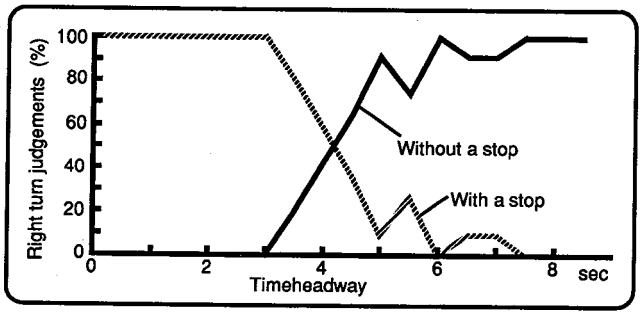

Figure 1. Right Turn Judgments as a Function of Time Headway of Oncoming Vehicles

Analysis of Right Turn Data Obtained With an Actual Vehicle

As seen in Figure 2, up to the point where the drivers made a right turn judgment, the deceleration pattern in approaching the intersection was the same regardless of whether the vehicles stopped or not before turning.

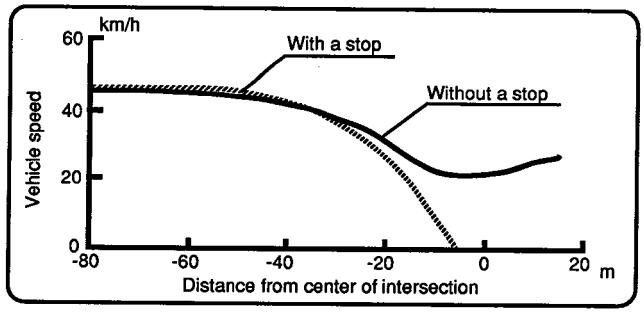

Figure 2. Typical Intersection Approach-Deceleration Pattern and Stop-Deceleration Pattern

An analysis of all the data showed that drivers switched to a deceleration pattern with a stop at a distance of 60 to 20 m before the intersection. From this result, it is concluded that during this interval the drivers made a judgment as to whether a right turn was possible or not.

Overall Configuration of Simulation Model

Task Analysis

The various tasks involved in executing a right turn were analyzed in order to determine the overall configuration of the fuzzy simulation model. A macroanalysis of right turn tasks indicated that right turns could be broadly divided into those involving a stop and those without. Each type of right turn was then divided into six and four phases, respectively.

Figure 3 shows the flow of tasks executed by the driver in making a right turn involving a stop.

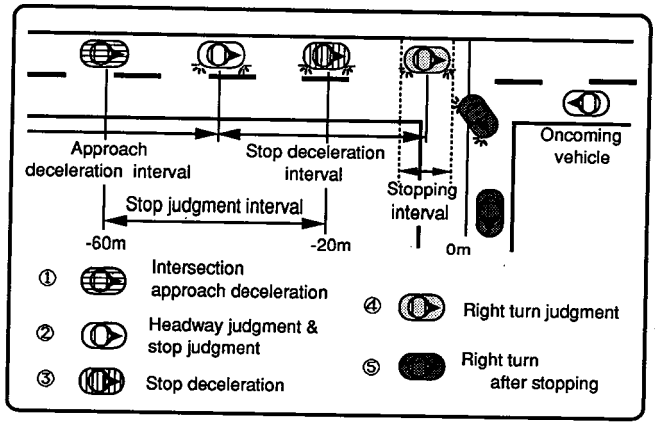

Figure 3. Right Turn Tasks with a Stop

In right turns involving a stop, the driver makes a decision to stop in the stop judgment interval and then proceeds to the task of decelerating the vehicle so as to bring it to a stop within the stopping interval. Subsequently, the driver makes a right turn judgment while the vehicle is stopped; when a right turn is judged possible, the driver proceed to execute the turn. In right turns where the driver decides during the judgment interval not to stop, he continues with the task of approaching the intersection and then proceeds to the task of executing a right turn at a point about 20 m before the intersection.

Construction of Model

As indicated by the task analysis results in the preceding section, the judgment and operational tasks of right turns with and without a stop were divided into six and four phases, respectively. The first three phases of both types of right turns are identical. Thus, the tasks performed by the driver in executing a right turn consist of seven phases in total.

A submodel has been prepared that corresponds to each individual phase. This was necessary because the information inputs needed to make judgments and perform driving operations in each phase differ, as do the outputs (i.e., driver judgment and behavior) of each phase and the rules used in deriving those outputs. The fuzzy logic simulation model for analyzing right turns consists of seven submodels, as shown in Figure 4, including three judgment models, which recognize the status of oncoming vehicles and determine the next action by the driver of the turning vehicle, and four types of right turn behavior models.

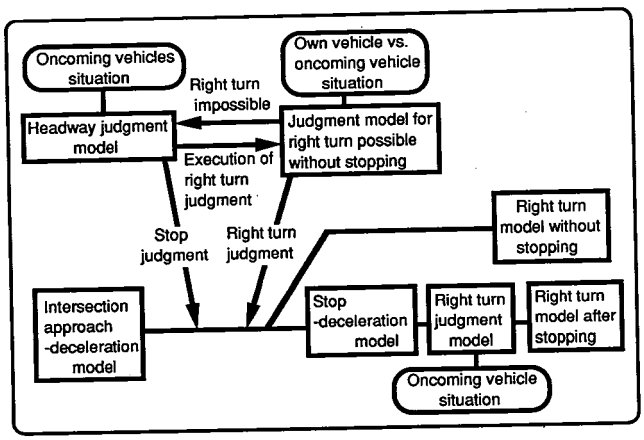

Figure 4. Configuration of Right Turn Simulation Model

Right Turn Judgment Model

One of the major features of a fuzzy model is that it is capable of simulating the ambiguous nature of human recognition, judgment and operational behavior. Moreover, it can also be used to perform quantitative evaluations of the characteristics of these human actions.

As an example of the application of the model, we will consider a situation in which a right turn judgment is made while a vehicle is stopped at an intersection waiting to turn right. This example will illustrate the major feature of a fuzzy model.

Concept of Right Turn Judgment Model

While the vehicle is stopped at an intersection waiting to turn right, it is assumed that the driver makes a preliminary right turn judgment based on the perceived speed of and distance between two oncoming vehicles. At the moment when the preceding oncoming vehicle passes through the center of the intersection, a final right turn judgment is made on the basis of the perceived speed of and distance from the center of the intersection to the second oncoming vehicle, i.e., the object of the driver's judgment.

The object of the driver's judgment shifts to the next oncoming car at the point where the driver judges that it is completely impossible to execute a right turn in front of the first oncoming car.

Construction of Right Turn Judgment Model

Inputs. Inputs include the speed of the oncoming vehicle that is the object of the driver's judgment and its distance from the center of the intersection.

Outputs. It is assumed that driving operation judgments are made under a situation of competition between subjective feelings of safety and risk. Accordingly, judgments that a right turn is possible or impossible are output as a "judgment level," representing a ratio of the driver's conflicting feelings about the possibility of executing a right turn.

When either of the judgment levels showed a value other than 100%, it indicated an ambiguous situation in which a definite right turn judgment could not be made.

In real-world driving, it is assumed that there is a certain threshold at work in the determination of driver judgments in such situations. This threshold value for making such judgments is assumed to vary depending on a variety of factors, such as the personality and psychological state of the driver and the environmental circumstances at the time.

Membership functions. The degree of ambiguity and resolution of human perception of distance and speed correspond respectively to the width of the membership functions and their number of divisions. Accordingly, experiments were conducted to obtain basic information on the accuracy of human judgment with respect to distance and speed.

Rules. Drivers posses knowledge based on learned experience that enables them to judge and execute the degree of response that is suitable for a certain level of input. In the fuzzy logic simulation model, this knowledge has been expressed in production rules having an IF-THEN format.

Tuning of membership functions and rules. The analyses of the video tape recordings of right turns indicated that all vehicles turning right stopped at the intersection before turning when the time headway to an oncoming vehicle was shorter than three seconds. When the time headway was longer than six seconds, all vehicles turned right without stopping. The input and output membership functions and rules were tuned and optimized to simulate such patterns.

Simulation Results

The simulation faithfully reproduced the results of the analyses of the video tape recordings of right turns. Figure 5 shows the simulation results for the relationship between right turn judgments and the position and speed

of oncoming vehicles. The step-like lines in the figure indicate the critical lines for right turn judgments with respect to the threshold values of the right turn judgment levels. Above this line a right turn is judged to be possible while below the line it is judged to be impossible. The upper and lower straight lines indicate time headways of six and three seconds, respectively, for the oncoming vehicles.

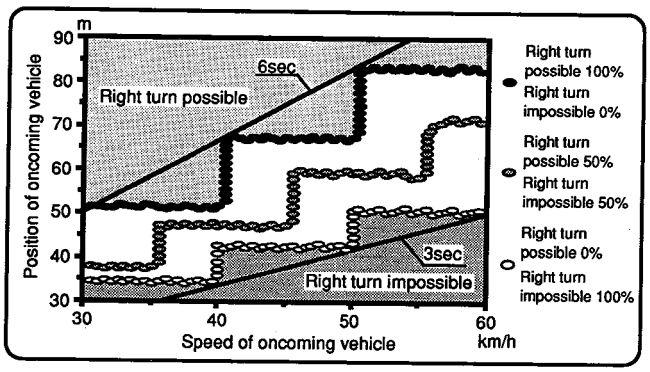

Figure 5. Relationship Between Judgments Level Threshold and Critical Line in Right Turn Judgment

When the threshold value for judging that a right turn is possible is low, the right turn involves a high degree of risk because there is only a short interval between the completion of the turn and the arrival of the oncoming vehicle at the center of the intersection. Conversely, when the threshold value is high, the right turn involves little risk because there is a long interval from the completion of the right turn until the oncoming vehicle reaches the center of the intersection.

Evaluation of Risk in Right Turns

Present Situation for Right Turn Accidents

Traffic accident data in the U.S. show that the percentage of left turn accidents (right turn in this paper) among all accidents involving drivers over 60 years of age is approximately double the corresponding figure for younger drivers. Accident analysis results in Japan indicate that right turn accidents involving an oncoming motorcycle represent 75% of all right turn accidents. Approximately 20% of all right turn accidents occurred even through the driver of the turning vehicle had checked for oncoming traffic and judged that a right turn was possible.

Concept Underlying Evaluation of Risk

Right turn accidents occur in a "conflict zone," representing the space traversed by an oncoming vehicle as it passes through an intersection. Accordingly, the index used in evaluating the degree of risk in right turns in this investigation was the time allowance from the moment the rear end of the turning vehicle cleared the conflict zone until the oncoming vehicle reached the zone.

A misjudgment that an oncoming vehicle is farther away than its actual position corresponds to an overall shift in fuzzy set of the position toward the near side. Since the oncoming vehicle reaches the intersection in less time than expected, the time allowance is reduced, resulting in greater risk. Similarly, a misjudgment that an oncoming vehicle is traveling more slowly than its actual speed corresponds to an overall shift in fuzzy set of the speed toward the high speed side. The time allowance is thus reduced, resulting in a higher degree of risk.

Consequently, the model can provide quantitative estimates of the degree of risk in right turns and of the contribution of each factor involved.

Evaluation Index for Risk in Right Turns

Collision zone. A simulation conducted with the right turn model with a stop, one of the seven submodels, showed that it took the turning vehicle a maximum of 3.2 seconds to pass through the conflict zone. Consequently, if the time headway of the oncoming vehicle that was the object of the driver's judgment was less than 3.2 seconds at the point the right turn judgment was made, a right turn accident would occur unless the oncoming vehicle decelerated. This was defined as the collision zone.

Danger zone and safety zone. It is reported that a time allowance of at least two seconds is generally necessary for vehicle maneuvers under ordinary traffic conditions. When following another vehicle on the freeway, drivers generally allow a time headway of around 1.5 seconds on average. It is assumed that a time allowance of at least 1.5 seconds is also necessary for executing right turns.

In view of these figures, a danger zone was defined here as an interval of less than 4.7 seconds in terms of the time from the moment the driver decides to turn right and begins to execute the turn until the oncoming vehicle reaches the center of the intersection. This interval includes the maximum right turn execution time of 3.2 seconds plus 1.5 seconds as the minimum value of the time allowance.

When the interval from the completion of the right turn judgment until the oncoming vehicle reaches the center of the intersection is longer than 4.7 seconds, there is more than ample time to execute a right turn safely. This region was defined as the safety zone in this work.

Simulation Results for Evaluation of Risk

Effect of Different Oncoming Vehicle Speeds on the Evaluation of Risk in Right Turns

Oncoming vehicle speed recognition characteristics. Experiments were conducted to examine the accuracy of human judgment with respect to the speed of oncoming vehicles traveling straight ahead. It was noted that in a speed range of 30 to 60 km/h, the speed of oncoming vehicles was recognized accurately irrespective of the

vehicle speed. The results of an experiment involving high oncoming vehicle speeds of more than 70 km/h showed that the degree of ambiguity in the subjects' perception of oncoming vehicle speeds increased with increasing vehicle speed.

A simulation was carried out to determine what effect the tendency for greater ambiguity to occur in speed judgments in the high speed range would have on the degree of risk in right turns.

Simulation results. Figure 6 shows the critical line for right turn judgments as a function of the position and speed of oncoming vehicles in a speed range of 30 to 100 km/h. The threshold values of the judgment levels in this case were 50% for and 50% against the possibility of executing a right turn.

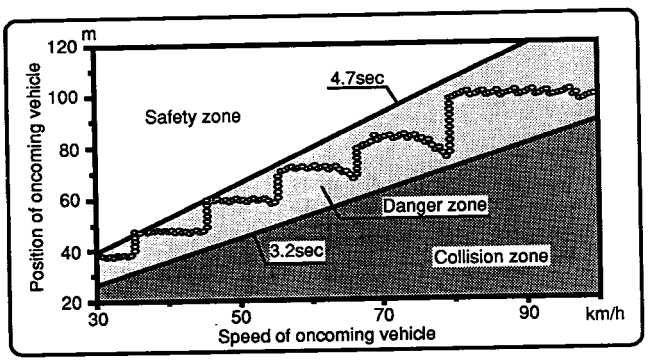

Figure 6. Critical Line for Right Turn Judgments When Oncoming Vehicle Speed is Extended to High-Speed Region

In an oncoming vehicle speed range of 30 to 50 km/h, the average time allowance was 1.1 seconds and the shortest time allowance was 0.6 second. In an oncoming vehicle speed range of 75 to 100 km/h, the average time allowance was 0.76 second and the shortest time allowance was 0.23 second. Compared with the low to medium speed range, the average time allowance was 0.34 second shorter and the shortest time allowance was reduced by more than 60%.

These results suggest that the time allowance with respect to the collision zone is somewhere in the range of oncoming vehicle speeds ordinarily observed at intersections. However, the time allowance is reduced as the oncoming vehicle speed increases. When oncoming vehicles approach intersections at exceptionally high speeds, there is a much greater possibility of an accident occurring.

Effect of Differences Between Daytime/Nighttime Perception of Oncoming Vehicle Distances on the Evaluation of Risk in Right Turns

Characteristics of daytime/nighttime perception of distance. The results of an experiment concerning the perception of distance to objects indicated that distance judgments at night were around 20 to 50 % less accurate than during the daytime. A simulation was carried out to examine what effect this increase in ambiguity with respect to the perception of distance to oncoming vehicles would have on the degree of risk in right turns.

Simulation results. Figure 7 shows the critical lines for right turn judgments during the daytime and nighttime as a function of the speed and position of oncoming vehicles. The threshold values of the right turn judgment levels were 50% for and 50% against the possibility of executing a right turn.

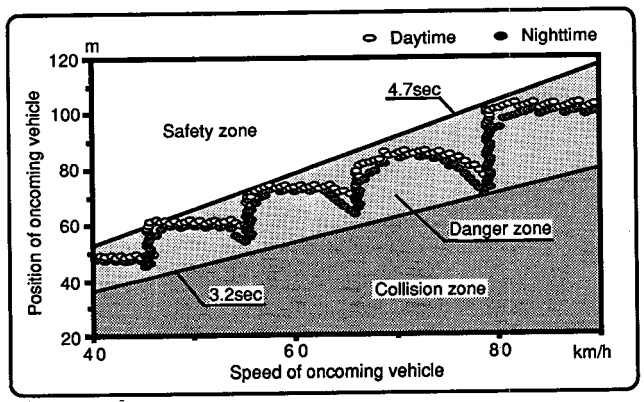

Figure 7. Comparison of Critical Lines of Right Turn Judgments During Daytime and Nighttime According to Differences in Perception of Oncoming Vehicle Speed

The results indicate that daytime and nighttime right turn judgments differed in approximately 40% of all the regions included in the simulation. In the areas where the judgments differed, the time allowance at night was shorter by an average of 0.89 second and a maximum of 1.55 seconds. Compared with the shortest time allowance of 0.34 second during the daytime, the shortest time allowance at night was an extremely small 0.01 second, which meant there was virtually no leeway at all. This results suggest there is a strong possibility that right turns in nighttime driving may involve a higher degree of risk than during the daytime.

Evaluation of Risk in Right Turn Behavior of Older Drivers

Judgment of speed by older drivers. According to a study done by B. Hills et al., older drivers tend to underestimate the speed of oncoming vehicles by as much as 8 km/h in comparison with the perception of vehicle speed by younger drivers in general. This poses a greater degree of risk in right turns because oncoming vehicles approach the intersection faster than older drivers expect. A simulation was carried out to evaluate how much this tendency on the part of older drivers to underestimate vehicle speeds would increase the degree of risk in right turns.

Simulation results. Figure 8 shows the critical lines for right turn judgments by older and younger drivers as a function of the position and speed of oncoming vehicles. The threshold values of the right turn judgment levels were 50% for and 50% against the possibility of executing a right turn.

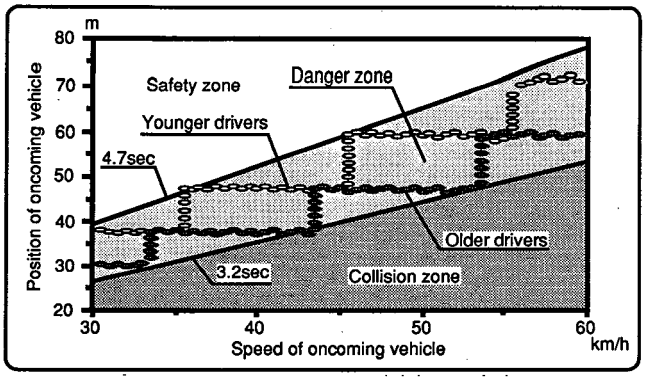

Figure 8. Comparison of Critical Lines of Right Turn Judgments Between Younger and Older Drivers According to Difference in Perception of Oncoming Vehicle Speed

Judgments made by younger drivers that a right turn was possible showed somewhat of a margin with respect to the collision zone. However, in some cases, the older drivers judged that a right turn was possible when the time headway to the oncoming car was close to the collision zone limit of 3.2 seconds. This suggested that older drivers would face a greater possibility of being involved in a right turn accident than younger drivers.

This possibility was also seen in quantitative terms. The critical line for right turn judgments by the older drivers showed an average time allowance of 0.39 second, which was much shorter and only around 36% of the 1.08 second time allowance seen for the younger drivers.

In approximately 80% of the cases simulated, the judgments of the older drivers differed from those of the younger drivers. In the cases where different judgments were made, the time allowance for the older drivers was shorter by an average of 0.85 second and a maximum of 1.0 second. These figures confirmed quantitatively that older drivers faced a higher degree of risk in right turns than their younger counterparts.

Evaluation of Risk in Right Turns Involving Oncoming Motorcycles

Acceptable time headway for motorcycles. A study done by Nagayama et al. examined the acceptable time headway of oncoming cars and motorcycles.

They found that the average critical time of the acceptable headway for cars and motorcycles was 2.9 and 2.5 seconds, respectively. They also reported that no significant difference was observed between cars and motorcycles with respect to the perception of speed and distance.

Based on these results, it was assumed that psychological factors rather than perceptional elements had a larger effect on differences in right turn judgments between oncoming motorcycles and cars. This difference corresponded to the change in judgment rules in the fuzzy logic simulation model.

Simulation results. Figure 9 shows the critical lines for right turn judgment in the case of oncoming cars and motorcycles as a function of the position and speed of the oncoming vehicles. The threshold values of the right turn judgment levels were 50% for and 50% against the possibility of executing a right turn.

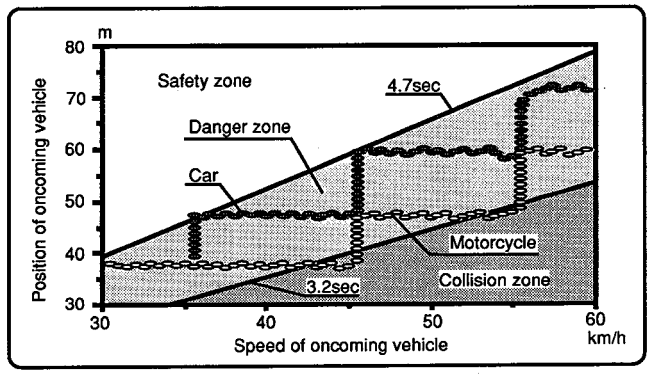

Figure 9. Comparison of Critical Lines of Right Turn Judgments for Oncoming Car and Motorcycle

The results for cars show that there was some time allowance with respect to the collision zone. However, the results for motorcycles indicate that even in the collision zone judgments were still made that a right turn was possible. This result suggests that the possibility of an accident occurring would be higher when the oncoming vehicle was a motorcycle rather than a car.

This possibility was also borne out in quantitative terms. The critical line for right turn judgments when the oncoming vehicles were motorcycles showed an average time allowance of 0.38 second as opposed to 1.08 second when the oncoming vehicles were cars.

In approximately 82% of the cases, different right turn judgments were made between oncoming motorcycles and oncoming cars. In cases where different judgments were made, the time allowance for motorcycles was shorter by an average of 0.85 second and a maximum of 1.0 second.

Conclusion and Future Outlook

This simulation model can reproduce with exceptional fidelity the real-world behavior displayed by drivers and vehicles in right turns. Simulation results confirmed the effectiveness of this fuzzy logic model in conducting qualitative evaluations of the ambiguous nature of human recognition, judgment and driving operations.

The model incorporates the results of extensive studies of various human recognition characteristics. That body of knowledge supports quantitative analyses of the factors causing right turn accidents due to errors of recognition, judgment or vehicle operation on the part of the driver of the turning vehicle. Such analyses are carried out using the contribution of each factor.

The same procedure as that followed in developing the simulation model presented here can be used to create

similar models for analyzing other accident patterns. The knowledge and know-how gained through the development of this model should make it possible to explain different accident mechanisms according to each factor involved.

By analyzing various accident mechanisms according to each of the different factors involved and storing the results in a database, it should be possible to construct a system for assessing the improvement in safety that might be obtained through the introduction of a new device or technology. Such an assessment system would be a valuable tool in designing the most effective preventive safety systems, in studying and determining the optimum system specifications and in evaluating and predicting the improvement in safety that could be achieved by implementing the system.

References

1. B. Hills, "Vision, visibility, and perception in driving," Perception, 1980, volume 9.
2. Y. Nagayama, et al., "Speed Judgment of Oncoming Motorcycles," Proceedings of the International Motorcycle Safety Conference, 955-971, Washington, DC, 1980.

Technical Session 8
Biomechanics and Dummy Development

Chairperson: Dominique Cesari, France

S8-O-01

Evaluation of Impact Responses of the EUROSID-1 and BIOSID

Takeshi Harigae, Koji Ohsaki, Haruo Ohmae
Japan Automobile Research Institute, Inc.
Tatsumasa Okamoto, Masayoshi Hayashida
Japan Automobile Manufacturers Association, Inc.

Abstract

A series of side impact tests have been conducted to evaluate the biofidelity of the EUROSID-1 and BIOSID side impact dummies. These tests were conducted to assess the biofidelity of the side impact dummies as specified by the impact response requirements by Draft Proposals at ISO/TC22/SC12(ISO/DP9790-1 to 6). The test results show that both dummies do not completely satisfy the ISO biofidelity requirements. Some portions of the dummies show best compliance with the ISO requirements, while other portions fail to comply with the requirements. In Addition, dummy performance in terms of the proposed thorax injury criteria, i.e., TTI, Rib Deflection, and V*C is analyzed with these test results. Of these results, the better correlation between the EUROSID-1 and BIOSID was obtained for V*C, and the better equivalence for TTI.

Introduction

The protection of automobile occupants from side impact is a subject of world-wide importance, and various research programs have been conducted by automobile engineers and constructors in the several countries. In addition, the several governments of interest have endeavored to draw up test procedures for evaluating the vehicle performance for occupant protection in side impact.

Under these circumstances, the Japan Automobile Research Institute,Inc. (JARI) and the Japan Automobile Manufacturers Association,Inc.(JAMA) have been studying since 1983 on side impact occupant protection. JARI/JAMA study is centered on following three items:

- Investigation of road traffic accidents in Japan
- Study of side impact test procedure
- Evaluation of side impact dummies

Of these items, an earlier evaluation tests for side impact dummies were implemented from 1987 to 1988 for the SID and EUROSID. Both dummies were tested in terms of the ISO biofidelity requirements, and the results have already been reported at ISO/TC22/SC12/WG5 meetings (7). Similar dummy tests were also conducted by experts from the United States (8), France (9), and the Netherlands (10). Based on the results of these evaluation studies, the ISO concluded that "neither SID nor EUROSID satisfied the biomechanical impact response requirements of ISO/DP9790-1 to 6" (11).

After this, the EUROSID-1 was developed by EEVC WG9, which is an improved model of production prototype of EUROSID (12). Also, in the United States, the SAE Side Impact Dummy Task Force was set up, resulting in development of the BIOSID (13).

From 1990 to 1991, JARI/JAMA carried out evaluation tests on both the EUROSID-1 and BIOSID to assess their biofidelity in terms of the latest version of documents ISO/DP9790-1 to 6 (1,2,3,4,5,6).

Comparison of the Dummy Specifications

The EUROSID-1 is the model with improvements in or redesign of, the neck, shoulder, thorax, abdomen, and pelvis of the production prototype EUROSID. In addition to the EUROSID-1 delivered in a complete set, a retrofit kit is also provided, which is for updating the production prototype EUROSID to EUROSID-1. JARI/JAMA purchased a retrofit kit and, incorporated the kit parts into the production prototype EUROSID which had been purchased in 1987. The Serial Number is 006 for the production prototype EUROSID, and 20004 for the retrofit kit.

The BIOSID was developed by the SAE Side Impact Dummy Task Force. The model which JARI/JAMA purchased was delivered in December, 1989. However, subsequent design change and improvements were made by Humanetics,Inc. and the dummy was redelivered in August, 1990. The Serial Number of the dummy is 003.

While both the EUROSID-1 and BIOSID are designed corresponding to the 50th percentile adult male, the dimensions and the mass distribution for each part are not identical according to the differences in structure of the two dummies.

Figure 1 compares the height, depth, width, and angles for each part between the EUROSID-1 and BIOSID which were seated on a flat, rigid, horizontal surface with a seat back perpendicular to that surface and become the back surface of the spine is parallel to the seat back.

The following points are observed in comparing the dimensions of the two dummies.

- The shoulder pivot height of the EUROSID-1 is higher than that of the BIOSID.
- The distance from the head C.G., shoulder pivot, H-point and knee pivot to the seat back for the

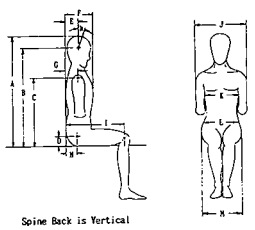

Measured Position	EUROSID-1	BIOSID
A : Sitting Height	890	880
B : Head C.G Height	770	770
C : Shoulder Pivot Height	550	505
D : H.Point Height	90	90
E : Head C.G to Seat Back	245	205
F : Chest Depth	255	270
G : Shoulder Point to Seat Back	175	145
H : H.Point to Seat Back	175	140
I : Knee Pivot to Seat Back	570	545
J : Shoulder Width	465	415
K : Chest Width(at Middle Rib)	325	340
L : Abdominal Width	280	340
M : Hip Width(at H.Point)	355	355
N : Head Angle Relative to Spine	27°	10.5°

Figure 1. Comparison of External Dimensions for the EUROSID-1 and BIOSID

EUROSID-1 are all greater than that for the BIOSID.

- The shoulder width of the EUROSID-1 is greater than that of the BIOSID. (This is because only one arm on the impact side is provided for the BIOSID).
- The abdominal width of the EUROSID-1 is less than that of the BIOSID.
- The head angle relative to the spine of the EUROSID-1 is greater than that of the BIOSID.

Table 1 gives a comparison of the masses for each part of the EUROSID-1 with the BIOSID, together with the mass distribution for the 50th percentile adult male, estimated by UMTRI (14). The following points are noted on comparing the mass distributions.

- Although the Hybrid-III head is used with either of these dummies, the EUROSID-1 head is lighter than that of the BIOSID. This is because the EUROSID-1, as opposed to the BIOSID, cannot be equipped with a 6-axis neck transducer.
- The abdomen of the EUROSID-1 is about 1kg less than that of the BIOSID.
- The pelvis of the EUROSID-1 is about 4kg less than that of the BIOSID.
- The total mass of the EUROSID-1 is about 4kg less than that of the BIOSID.

Table 1. Comparison of Mass Distribution for the EUROSID-1 and BIOSID

Unit: kg

Body Region	EUROSID-1	BIOSID	50th Percentile Adult Male*1
Head	4.05	4.50	4.13
Neck	1.06	1.06	0.96
Thorax	22.50*2	23.12*3	23.76
Arms	1.26×2	1.30	3.79×2
Abdomen	5.07*4	6.08*5	2.36
Pelvis	11.91*6	16.16	11.41
Legs	12.60×2	11.65×2	13.18×2
Total	72.30	76.59	76.56

*1 ; Values were estimated by UMTRI (Ref. 14)
*2 ; with $^2/_3$Jacket
*3 ; with Jacket
*4 ; Flesh, Abdominal-Instruments and Lumbar
*5 ; 2ribs, Lumbar and Lumbar-Spine Interface
*6 ; with $^1/_3$Jacket

Biofidelity Evaluation Tests

The documents ISO/DP9790-1 to 6 describes the impact test set-up and response requirements of six body regions—the head, neck, thorax, shoulder, abdomen, and pelvis—of side impact dummy to assess their biofidelity. Response requirement corridors are set up for each body regions, based on the results of test with cadavers and human volunteers conducted by the several research laboratories in Europe and the United States. In addition, the normalization procedures which are to compensate for changes in effective mass caused by slight differences in dummy positioning, are also required for the thorax, shoulder, abdomen, and pelvis.

The evaluation tests of the EUROSID-1 and BIOSID were carried out according to the latest version of documents ISO/DP9790-1 to 6. Table 2 summarizes the biofidelity evaluation test matrix of the JARI/JAMA studies.

Table 2. ISO Biofidelity Evaluation Test Matrix Performed by JARI/JAMA

Body Region	Test Condition	No. of Tests Performed/ 1 Dummy	Normalized or Not	ISO Reference No.
Head	0.2m Rigid Drop	3	Not Specified by ISO	ISO/DP9790-1 (Nov. '87)
	1.2m Padded Drop	Not Performed		
Neck	7.0G Sled	2	Not Specified by ISO	ISO/DP9790-2 (Nov. '87)
	6.7G Sled	Not Performed		
	12.0G Sled	Not Performed		
Thorax	1.0m Rigid Drop	3	Yes	ISO/DP9790-3 ISO/TC22/SC12/WG5-N249 "Proposed Revisions of DP9790-3" (Sep. '89)
	2.0m Padded Drop	3		
	6.8m/s Rigid Sled	3		
	8.9m/s Padded Sled	3		
	8.9m/s Rigid Sled	3		
	4.3m/s Lateral Impact	3		
	6.7m/s Lateral Impact	3		
Shoulder	4.5m/s Lateral Impact	3	Yes	ISO/DP9790-4 (Jul. '88)
Abdomen	1.0m Drop	3	Yes	ISO/DP9790-5 (Jul. '88)
	2.0m Drop	1		
Pelvis	6.0m/s Lateral Impact	3	Yes	ISO/DP9790-6 (Aug. '88)
	6.7m/s Lateral Impact	3		
	7.5m/s Lateral Impact	3		
	9.0m/s Lateral Impact	3		
	0.5m Rigid Drop	3		
	1.0m Rigid Drop	3		
	2.0m Padded Drop	3		
	3.0m Padded Drop	Not Performed		
	6.8m/s Rigid Sled	3		
	8.9m/s Padded Sled	3		
	8.9m/s Rigid Sled	3		

The padded 1200mm-drop head test was not performed because the test conditions were considered too severe than necessary. The neck bending test with 6.7G sled was not conducted because a satisfactory decelerator sled were not available in our facilities. The neck bending test with 12G sled was omitted because the response requirements were based on the results only of cadaver tests and deemed as having lower priority. The pelvis 3.0m drop test with padded surface was not performed because the setting-up was difficult to maintain an appropriate dummy position.

The response data for the thorax, shoulder, abdomen, and pelvis were normalized with the procedure given by the ISO documents. Effective masses and the normalizing factors of both dummies are summarized in Appendix-1 and Appendix-2 respectively.

Head Test

In ISO/DP9790-1 (November '87), two types of drop tests are required for dummy's head. These are a drop tests onto a rigid surface from a height of 200mm and a

drop test onto a padded surface from a height of 1200mm. In the JARI/JAMA studies, only 200mm drop test was performed.

Figure 2 shows the test set-up of the head 200mm drop test. The dummy's head was suspended at a 200mm height above a flat, rigid, horizontal impact surface. The midsagittal plane of the head made an angle of 35° to the surface and its anterior-posterior axis was horizontal. A "quick release" device was used to drop the head onto the impact surface.

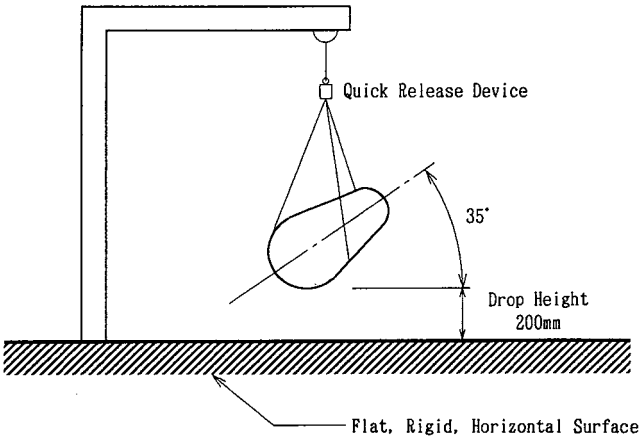

Figure 2. Test Set-up for Head 200mm Drop Test

In this test, the dummy's head was instrumented with a triaxial accelerometer attached on the non-impacted side of the head cavity. Accelerations were filtered using SAE channel class 1000.

Table 3 shows the resultant peak head accelerations for both the EUROSID-1 and BIOSID for the head 200mm drop test. The responses of the both dummies were completely within the requirement. The repeatability of these responses were excellent for both dummies.

Table 3. Resultant Peak Head Accelerations for the EUROSID-1 and BIOSID Obtained from Head Drop Test

Test Condition and ISO Requirement	EUROSID-1 (SAE1000)			BIOSID (SAE1000)		
200mm Drop 100 - 150 G	134.8	131.6	137.5	141.1	144.9	136.8

Neck Test

In ISO/DP9790-2 (November '87), three types of tests are required for the neck. These are the 7G HYGE test, the 6.7G decelerator sled test, and the 12G HYGE test. In the JARI/JAMA studies, only the 7G HYGE test was performed.

In this test, an upright rigid seat with a vertical side board that was rigidly attached to the seat was securely fastened to a HYGE sled in a sideward facing, and the dummy was seated in an upright position. The dummy was restrained to the seat using a seat-belt with its shoulder and pelvis placed against the vertical side board.

The accelerations of the head and T1 (thorax upper spine) of the dummy were measured in this test. Both accelerations were filtered according to SAE-J211. In addition, the motions of the head and T1 were analyzed from a 16mm high-speed film.

The test results are summarized in Table 4. The lateral accelerations of the head were completely within the response requirement for both the EUROSID-1 and BIOSID, and the vertical head accelerations were at the lower boundary of the requirement for both dummies. The lateral acceleration of T1 of the EUROSID-1 was completely within the requirement and that of the BIOSID was at the lower boundary. The lateral and vertical displacements of the head C.G. relative to T1 were below the requirement for both dummies, in particular the BIOSID responses were outside more than one corridor width below the requirements. The time of maximum head displacement of both dummies were within the requirement. The EUROSID-1 satisfied the requirements for the displacement of the T1 relative to the sled and for the head flexion at upper boundary, but those of the BIOSID were below the lower bounds of the requirements.

Table 4. Neck Peak Response Measurements for the EUROSID-1 and BIOSID Obtained from 7G HYGE Test

Measurement	ISO Requirement	EUROSID-1		BIOSID	
Lat. Head Acc. (SAE1000)	8 - 11 G	10.0	10.1	9.9	10.3
Vert. Head Acc. (SAE1000)	8 - 10 G	8.0	8.0	8.2	8.3
Lat. T1 Acc. (SAE180)	12 - 18 G	15.2	14.5	12.0	12.4
Lat. Head Disp.	130 - 162 mm	107.0	106.0	82.9	88.5
Vert. Head Disp.	64 - 96 mm	39.2	41.0	20.9	21.8
Time of Max. Head Disp.	159 - 175 ms	168.0	174.0	163.0	164.0
Lat. T1 Disp.	46 - 63 mm	62.7	54.5	28.2	31.2
Angle of Flexion	44 - 59 deg.	56.9	57.3	35.1	35.8

Thorax Test

Three types of tests are required for evaluation of the thorax in ISO/DP9790-3. These are the drop test, sled test, and pendulum impact test. The JARI/JAMA has been performed these three types of tests for both the EUROSID-1 and BIOSID. The test conditions, normalization procedures, and response requirement corridors conform to the document ISO/TC22/SC12/WG5-N249 (September,1989) that is a proposed revision of ISO/DP9790-3.

Drop Test. Two types of tests are required for thorax drop test. The first test is a whole dummy drop onto a rigid surface from a height of 1 meter, and the second one is a drop onto a padded surface from 2 meters.

Figure 3 shows the test set-up for the thorax drop test. The whole dummy was suspended with midsagittal plane horizontal, and a "quick release" device was used to provide a free fall onto the impact surface. The impact surface consists of two separate force-measuring sur-

faces, one for the thorax and the other for the pelvis. Each impact surface instrumented with three load-cells. In the rigid impact test, the impact surface for the thorax includes the shoulder-impact target, and one edge of that surface was corresponded to the lower edge of the 3rd rib of the dummy, and the center-line of the pelvis impact surface was aligned to the H-point of the dummy. In the padded impact test, the center of the thorax padding was in line with the 2nd rib of the dummy while avoiding shoulder impact to the padding, and the center-line of the pelvis padding was aligned to the H-point of the dummy. For both test conditions, the upper arms of the dummy were rotated 20° forward of the spine. The paddings used in this test were made by polyethylene developed in Japan with the same dimensions and characteristics as the APR padding. The dimensions, and force-displacement curve are given in Appendix 3.

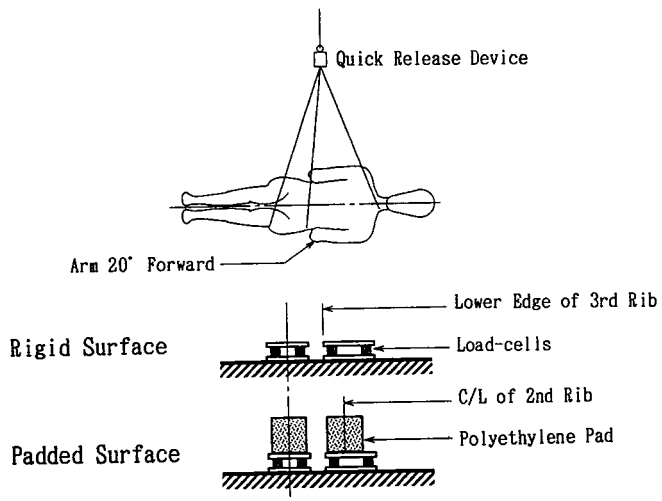

Figure 3. Test Set-up for Whole Dummy Drop Test

In these tests, the forces at each impact surface and the deflection of the impacted ribs relative to the spine were measured. The forces and deflections were filtered using SAE channel class 180, and then normalized by the procedure given in document N249.

Figure 4 shows the force-time curves at the thorax-impact surface for both the EUROSID-1 and BIOSID to the 1 meter rigid drop test compared with ISO response requirement corridor as described in document N249. The peak force for the EUROSID-1 was at the lower boundary of the requirement corridor but the time duration was longer than the corridor. The force-time curve at the thorax-impact surface for the BIOSID, on the other hand, was completely within the corridor.

Figure 5 shows the force-time curves at the thorax-impact surface for both dummies to the 2 meter padded drop test compared with N249 requirement corridor. The peak force for the EUROSID-1 was within the response requirement corridor but the time duration was slightly longer than the corridor. The force-time curve at the thorax-impact surface for the BIOSID, was completely within the corridor, the same as 1 meter rigid drop test.

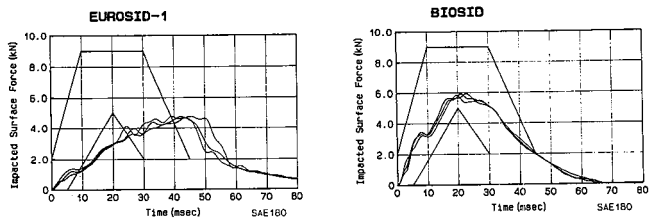

Figure 4. Normalized Thorax Impact Surface Force-Time Obtained from 1 meter Rigid Drop Test: EUROSID-1 and BIOSID Responses Compared with ISO Requirement Corridor

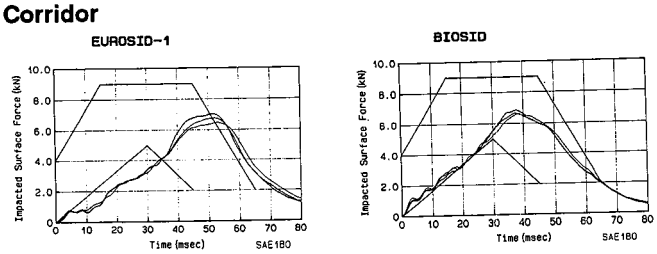

Figure 5. Normalized Thorax Impact Surface Force-Time Obtained from 2 meter Padded Drop Test: EUROSID-1 and BIOSID Responses Compared with ISO Requirement Corridor

Table 5 gives the normalized peak rib deflections of the EUROSID-1 and the BIOSID for both the 1 meter and 2 meter drop tests. In the 1 meter test, the lower rib of the EUROSID-1 satisfied the requirement for only one drop; all other responses exceeded the upper bound of the requirement. For the BIOSID, the upper rib deflections in two tests were slightly below the requirement, while the other responses were all within the requirement. In the 2 meter test, the upper rib of the EUROSID-1 satisfied the requirement in two tests, and the lower rib in one test, but other than these, all responses exceeded the upper bound of the requirement by large amounts. For the BIOSID, on the other hand, the upper rib deflections of two tests were slightly below the requirement, but all other responses satisfied the requirement.

Table 5. Normalized Peak Rib Deflection for the EUROSID-1 and BIOSID Obtained from Thorax Drop Test

Test Condition and ISO Requirement	EUROSID-1 (SAE180)			BIOSID (SAE180)		
1.0m Rigid Drop						
26 - 38 mm	Upper Rib	39.7	39.8 41.6	Upper Rib	25.2	25.9 26.1
	Middle Rib	38.2	39.3 40.6	Middle Rib	26.1	27.3 27.4
	Lower Rib	37.0	38.6 38.4	Lower Rib	27.3	29.1 28.7
2.0m Padded Drop						
26 - 40 mm	Upper Rib	36.3	33.5 44.4	Upper Rib	26.5	25.7 25.8
	Middle Rib	45.4	45.6 46.8	Middle Rib	33.3	31.7 33.2
	Lower Rib	43.0	44.4 38.9	Lower Rib	37.6	35.8 38.4

Sled Test. Three types of tests are required for thorax sled test. These are a rigid wall impact test at a velocity of 6.8m/s, a padded wall impact test at 8.9m/s, and a rigid wall impact test at 8.9m/s. For these tests, a HYGE sled was used instead of the decelerator sled in the JARI/JAMA studies.

A seat with instrumented side wall was securely attached to the HYGE sled, transverse to the direction of

travel. The side wall had two impact surfaces, one for the thorax and the other for the pelvis. Three load-cells were attached to each impact surface. Figure 6 shows the dimensions of the seat and impact surfaces used in this test. The surface of the seat was covered with a teflon sheet to prevent the rotation of the dummy. The dummy was placed at sufficient distance from the impact surface to assure the dummy impact after a prescribed sled velocity is built up. The positioning of the arms is not clearly specified in the test set-up procedure of document N249, so in JARI/JAMA tests the upper arms were placed parallel to the spine for both the EUROSID-1 and BIOSID. For the padded wall impact test, polyethylene paddings were used as is the same in the thorax drop test.

In these tests, the forces at the impacted wall, and the accelerations of the upper spine, lower spine, and upper rib were measured. Forces and the accelerations were filtered using SAE channel class 1000 and again filtered using a 100Hz FIR filter. These responses were normalized by the procedure as specified in document N249.

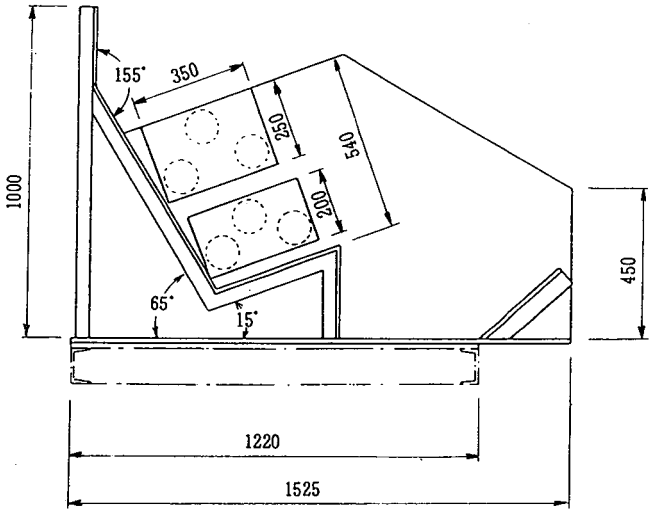

Figure 6. Dimensions of the Test Seat and Impact Surface for Sled Test

Figure 7 shows the force-time curves at the thorax-impact surface for the EUROSID-1 and the BIOSID for the 6.8m/s rigid wall impact test, compared with response requirement corridor of document N249. The force-time curve at the thorax-impact surface for the EUROSID-1 was completely within the requirement corridor. The peak force for the BIOSID, on the other hand, was slightly exceeded the upper bound of the requirement, while the time duration was rather shorter than the corridor.

Figure 8 shows the force-time curves at the thorax-impact surface for both dummies for the 8.9m/s padded wall impact test, compared with requirement corridor of document N249. For both the EUROSID-1 and BIOSID, the peak forces slightly exceeded the upper bound of the requirement, while the time durations satisfied the corridor.

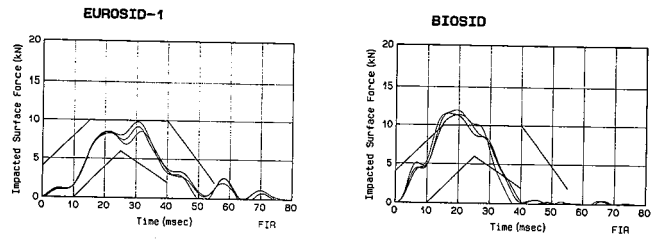

Figure 7. Normalized Thorax Impact Surface Force-Time Obtained from 6.8m/s Rigid Wall Impact Test: EUROSID-1 and BIOSID Responses Compared with ISO Requirement Corridor

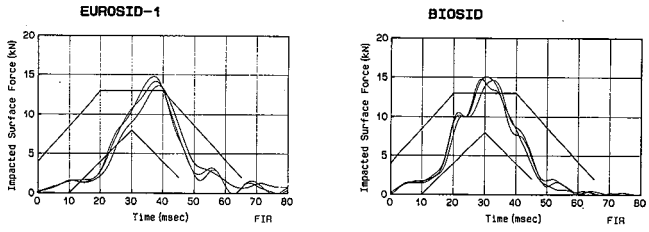

Figure 8. Normalized Thorax Impact Surface Force-Time Obtained from 8.9m/s Padded Wall Impact Test: EUROSID-1 and BIOSID Responses Compared with ISO Requirement Corridor

Figure 9 shows the force-time curves at the thorax-impact surface for both dummies for the 8.9m/s rigid wall impact test, compared with requirement corridor of document N249. For the EUROSID-1, the peak force slightly exceeded the upper bound of the requirement, while the time duration was almost within the corridor. The peak force for the BIOSID, on the other hand, exceeded the upper bound of the requirement, while the time duration was slightly shorter than the corridor.

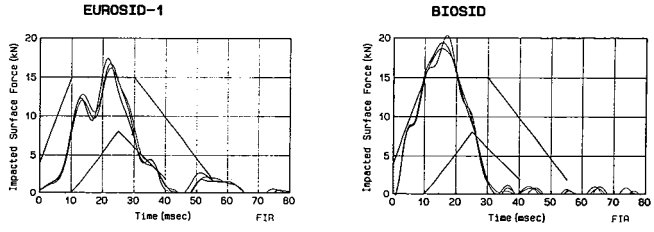

Figure 9. Normalized Thorax Impact Surface Force-Time Obtained from 8.9m/s Rigid Wall Impact Test: EUROSID-1 and BIOSID Responses Compared with ISO Requirement Corridor

Table 6 gives the normalized peak accelerations of the upper spine, lower spine, and upper rib of both the EUROSID-1 and BIOSID in the sled tests. In the rigid wall impact at 6.8m/s, the accelerations of the upper spine and lower spine of the EUROSID-1 were below the lower bound of the requirement, while the upper rib acceleration was within the response requirement. For the BIOSID, the upper spine and lower spine accelerations were smaller than the lower bound, while the upper rib acceleration exceeded the requirement. For the padded wall impact at 8.9m/s, the EUROSID-1, as is the same in the 6.8m/s tests, the upper and lower spine

accelerations were smaller than the response requirement while the upper rib acceleration was within the requirement. For the BIOSID, again in the same manner as for 6.8m/s tests, the upper and lower spine accelerations were smaller than the response requirement, while the upper rib acceleration was slightly larger. For the EUROSID-1 impacted against a rigid wall at 8.9m/s, in the same manner as for the other test conditions, the upper and lower spine accelerations were smaller than the lower bound, while the upper rib acceleration was within the requirement. On the other hand, the upper spine and upper rib accelerations of the BIOSID satisfied the response requirement, but the lower spine acceleration was below the requirement by small amount.

Table 6. Normalized Peak Accelerations for the EUROSID-1 and BIOSID Obtained from Thorax Sled Test

Test Condition and ISO Requirement	EUROSID-1 (FIR100)			BIOSID (FIR100)		
6.8m/s Rigid Wall Impact						
Upper Spine 82 - 122 G	29.0	24.9	25.8	49.7	52.3	50.3
Lower Spine 71 - 107 G	36.2	37.7	36.2	51.6	54.2	62.1
Upper Rib 66 - 100 G	79.2	79.5	75.4	115.0	113.6	109.4
8.9m/s Padded Wall Impact						
Upper Spine 66 - 98 G	41.9	38.9	41.0	56.8	55.3	50.2
Lower Spine 82 - 129 G	52.2	56.4	51.0	73.9	71.2	67.3
Upper Rib 72 - 108 G	91.3	76.7	80.5	108.6	112.5	117.5
8.9m/s Rigid Wall Impact						
Upper Spine 69 - 103 G	41.8	40.7	41.9	83.8	80.4	76.3
Lower Spine 129 - 193 G	67.1	64.8	65.1	118.5	115.1	127.0
Upper Rib 133 - 199 G	139.6	141.5	139.8	193.5	189.6	180.3

Impactor Test. Two types of thorax pendulum impact tests are required in document N249, for both 4.3m/s impact and 6.7m/s impact. A linearly guided impactor was used instead of the pendulum impactor in the JARI/JAMA tests.

The tests were carried out by applying a pure lateral impact to the side of the rib structure, using a 23.3kg impactor with a 150mm-diameter face. The dummy was seated in an upright position on a flat, rigid, horizontal surface, without back support. The seating surface was covered by a teflon sheet. The upper arms of both dummies were removed during these tests (but only of impacted side for EUROSID-1). Because the impact position is not clearly specified in document N249, the impactor was aimed at positions shown in Figure 10, specifically, the center-line of the impactor was aligned to the mid-point of the middle rib cylinder for the EUROSID-1, or the impactor was aligned to the mid-point of the 2nd rib for the BIOSID.

In these tests, the accelerations of the impactor and the upper spine of the dummy were measured, and filtered using SAE channel class 1000 and SAE channel class 180 respectively, and, these responses were again filtered with the 100Hz FIR filter. The acceleration of the impactor was used to calculate the impactor force. The impactor force and upper spine acceleration were normalized by the procedure given in document N249.

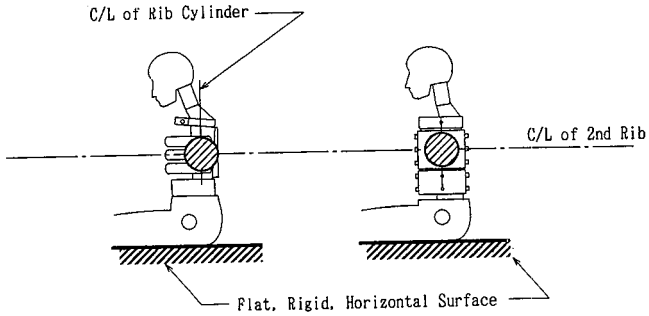

Figure 10. Positioning of the Impactor Face for Thorax Impact Test

The impactor force-time responses and the upper spine acceleration-time responses for both the EUROSID-1 and BIOSID at 4.3m/s impact test were shown, compared with the response requirement corridor given in document N249, in Figure 11 and Figure 12, respectively (in which corridors are from HSRI pure lateral impact tests together with WSU/GMR oblique lateral impact tests). The peak force of the impactor for the EUROSID-1 was within the requirement corridor, but the time duration was slightly shorter than the corridor. In addition, the peak acceleration of the upper spine exceeded the upper bound of the requirement, but the time duration satisfied the corridor. The test results for the BIOSID, as is for the EUROSID-1, shows the impactor peak force was within the requirement corridor while the time duration was slightly shorter, and upper spine peak acceleration exceeded the upper bound while the time duration satisfied the corridor.

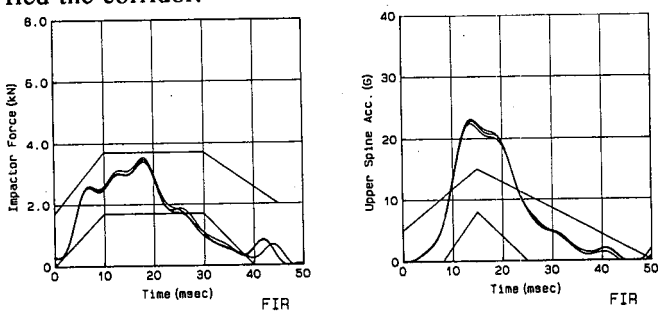

Figure 11. Normalized Impactor Force-Time and Upper Spine Acceleration-Time Obtained from 4.3m/s Thorax Impact Test: EUROSID-1 Responses Compared with ISO Requirement Corridor

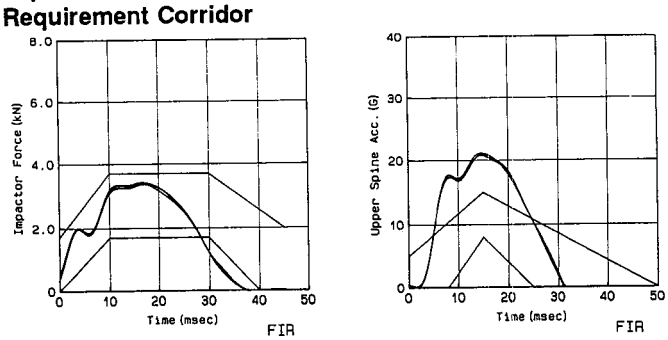

Figure 12. Normalized Impactor Force-Time and Upper Spine Acceleration-Time Obtained from 4.3m/s Thorax Impact Test: BIOSID Responses Compared with ISO Requirement Corridor

The impactor force-time responses and the upper spine acceleration-time responses for both dummies at 6.7m/s impact test were shown in Figure 13 and Figure 14. For the impactor force-time response, the corridor from the cadaver oblique lateral impact tests by WSU/GMR was shown. The upper spine acceleration-time response is not required in this test, but the responses were normalized by the procedure as is for 4.3m/s impact test in the JARI/JAMA studies. The peak force for the impactor force-time response for the EUROSID-1 was almost within the response requirement corridor, but the time duration was slightly shorter. The peak force of the impactor for the BIOSID was also within the corridor, as is for the EUROSID-1, but the time duration fell slightly shorter than the corridor.

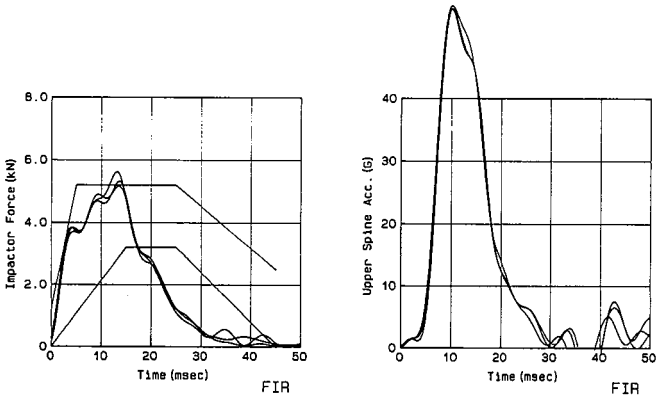

Figure 13. Normalized Impactor Force-Time and Upper Spine Acceleration-Time Obtained from 6.7m/s Thorax Impact Test: EUROSID-1 Responses Compared with ISO Requirement Corridor

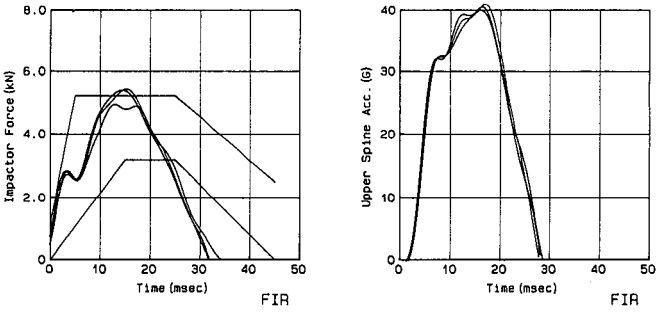

Figure 14. Normalized Impactor Force-Time and Upper Spine Acceleration-Time Obtained from 6.7m/s Thorax Impact Test: BIOSID Responses Compared with ISO Requirement Corridor

Shoulder Test

To evaluate the shoulder of the dummy, a pendulum impact test is required in ISO/DP9790-4 (July '87). In the JARI/JAMA tests, a linearly guided impactor identical with that used in the thorax impact test was used instead of the pendulum impactor.

Figure 15 shows the test set-up for the shoulder impact test. The tests were carried out by applying a pure lateral impact to the shoulder at 4.5m/s, using a 23.3kg impactor with a 150mm-diameter face. The center-line of the impactor was aligned to the shoulder pivot for both dummies. The seating position of the dummy was identical with that of the thorax impact test, except that the upper arms were placed parallel to the spine along the thorax.

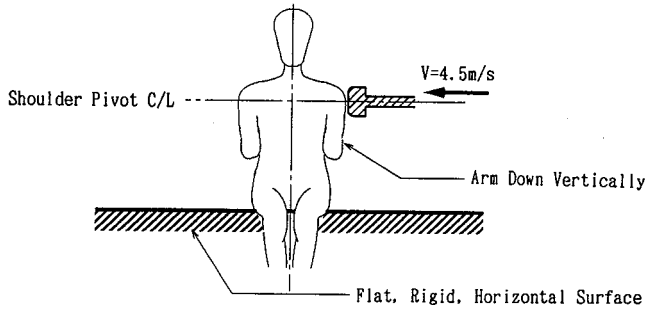

Figure 15. Test Set-up for Shoulder Impact Test

The acceleration of the impactor was measured, and filtered using SAE channel class 1000. The impactor acceleration was used to calculate the impactor force and the response was normalized by the procedure given in ISO/DP9790-4. The shoulder displacement relative to the spine is required for this test, but was not measured in the JARI/JAMA test.

Figure 16 shows the impactor force-time curves for the shoulder impact test for both the EUROSID-1 and BIOSID, compared with the response requirement corridor. Although the peak impactor force for the EUROSID-1 was slightly higher than the upper bound of the requirement corridor, the overall shape and time duration of the impactor force-time curve fit on the corridor. The peak force of the impactor for the BIOSID was twice as high as the upper bound of the requirement, and the time duration fell in short.

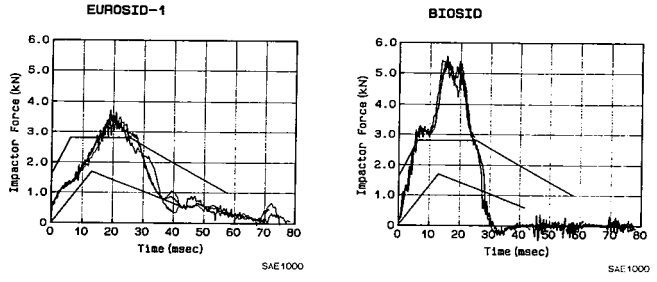

Figure 16. Normalized Impactor Force-Time Obtained from Shoulder Impact Test: EUROSID-1 and BIOSID Responses Compared with ISO Requirement Corridor

Abdomen Test

According to ISO/DP9790-5(July '88), drop tests from height of 1 meter and 2 meters onto a simulated armrest are required to evaluate the abdomen of the dummy.

Figure 17 shows the test set-up for the abdomen drop test. The dummy was suspended with the midsagittal plane horizontal, and a "quick release" device was used to provide a free fall onto the impact surface. The simulated armrest protruding 41mm above the surrounding surface and mounted on three load-cells which were

secured to the horizontal surface. In the document ISO/DP9790-5, positioning of the dummy's abdomen relative to the armrest is specified as "abdomen region including the area of the 9th rib in line with the top surface of the simulated armrest." However, in the JARI/JAMA tests, as shown in Figure 18, the center-line of the armrest was aligned to the abdominal force transducers for the EUROSID-1, and on the center-line of the gap between two abdominal ribs for the BIOSID. These positioning of both dummies were decided with the knowledge from their calibration tests so that the best abdominal performance is thought to be expected. The upper arm of the dummy was removed for both the EUROSID-1 (impacted side only) and BIOSID during the tests.

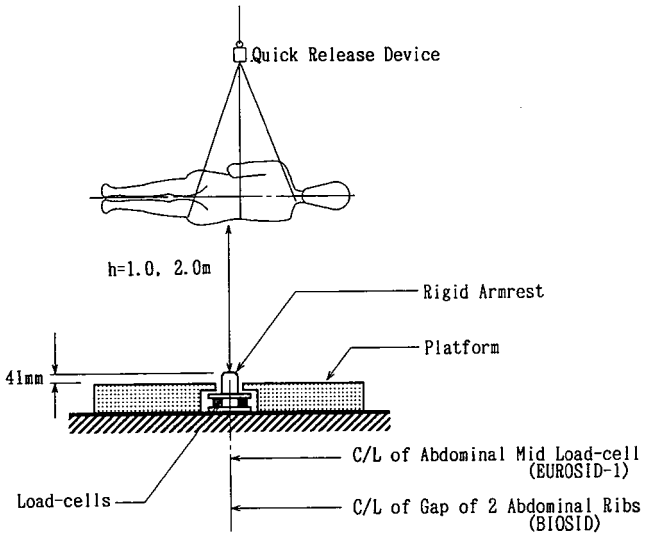

Figure 17. Test Set-up for Abdomen Drop Test

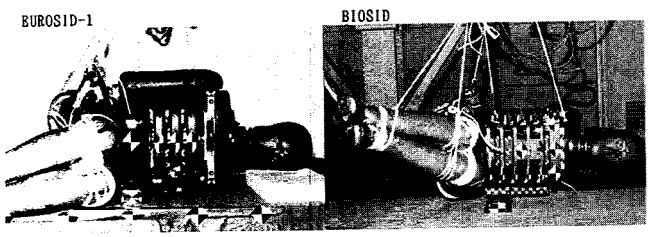

Figure 18. Positioning of the Abdomen to Rigid Armrest for Abdomen Drop Test

The force applied to the armrest and acceleration of the lower spine were measured. The acceleration of the abdominal upper rib was also measured for the BIOSID. All responses were filtered using SAE channel class 180, and were then normalized by the procedure specified by ISO/DP9790-5.

Figure 19 shows the force-time responses at the armrest for the 1 meter drop test for the EUROSID-1 and the BIOSID, compared to the response requirement corridor. With the EUROSID-1, the peak force of the armrest exceeded the upper bound of the requirement corridor, but the time duration almost fell within the corridor. For the BIOSID, on the other hand, the peak force of the armrest fell within the requirement corridor but the time duration was slightly longer. And the overall shape and time duration of the armrest force-time curve for the BIOSID nearly fits on the corridor.

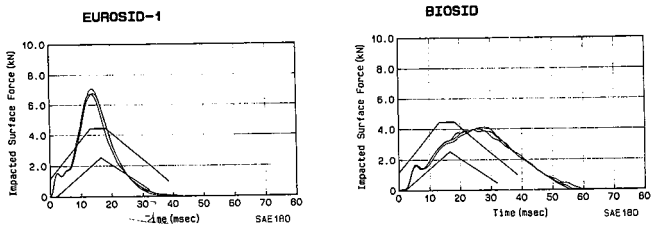

Figure 19. Normalized Armrest Force-Time Obtained From 1 meter Drop Test: EUROSID-1 and BIOSID Responses Compared with ISO Requirement Corridor

Figure 20 shows the force-time responses at the armrest for the 2 meter drop test for both dummies, compared with the requirement corridor. The 2 meter drop test was performed only once for both dummies. As in the 1 meter drop test, the armrest peak force exceeded the upper bound of the requirement for the EUROSID-1, but the time duration almost fell within the corridor. For the BIOSID the armrest peak force exceeded the upper bound of the requirement, and the time duration was slightly longer than the corridor.

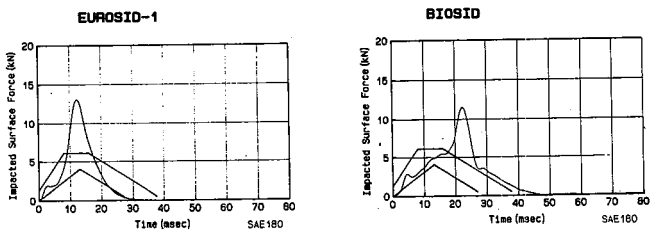

Figure 20. Normalized Armrest Force-Time Obtained From 2 meter Drop Test: EUROSID-1 and BIOSID Responses Compared with ISO Requirement Corridor

Table 7 gives the normalized peak accelerations of the lower spine of the EUROSID-1 and the BIOSID for both 1 meter and 2 meter tests. The normalized peak acceleration of the abdominal upper rib of the BIOSID are also given in this table. For the EUROSID-1, the peak accelerations of the lower spine exceeded the upper bound of the requirement in both 1 meter and 2 meter tests. For the BIOSID, on the other hand, the peak accelerations of the lower spine were within the requirement, and the

Table 7. Normalized Peak Accelerations for the EUROSID-1 and BIOSID Obtained from Abdomen Drop Test

Test Condition and ISO Requirement	EUROSID-1 (SAE180)			BIOSID (SAE180)		
1.0m Drop						
Lower Spine 29 - 35 G	45.4	45.6	45.7	29.3	33.2	32.4
Impacted Rib 100 - 125 G	N.M	N.M	N.M	117.6	118.0	129.5
2.0m Drop						
Lower Spine 75 - 91 G	92.5			75.8		
Impacted Rib 160 - 200 G	N.M			191.5		

N.M ; Not Measured

peak accelerations of the abdominal upper rib were almost within the response requirement in both the 1 meter and 2 meter tests.

Pelvis Test

In ISO/DP9790-6 (August, '88), three different types of tests are required to evaluate the pelvis of the dummy, namely, the impactor test, drop test, and sled test. The JARI/JAMA has been performed these three types of tests for both the EUROSID-1 and BIOSID.

Impactor Test. The Impactor test was carried out by applying a lateral impact to the pelvis of the dummy, using a 17.3kg linearly guided impactor. This test requires impact velocity between 6m/s and 10m/s. In the JARI/JAMA tests, four different velocities were chosen, namely, 6.0, 6.7, 7.5, and 9.0m/s. The impactor had a spherical face of 175mm-radius, and diameter of 120mm as shown in Figure 21. This was smaller than that specified by ISO/DP9790-6. However, as mentioned in the report of EEVC WG9 (15), this dimensions are corrected values to errata in the original INRETS report. The seating position and the upper arm position of the dummy were identical to those for the shoulder impact test. The center-line of the impactor was aligned to the H-point of the dummy.

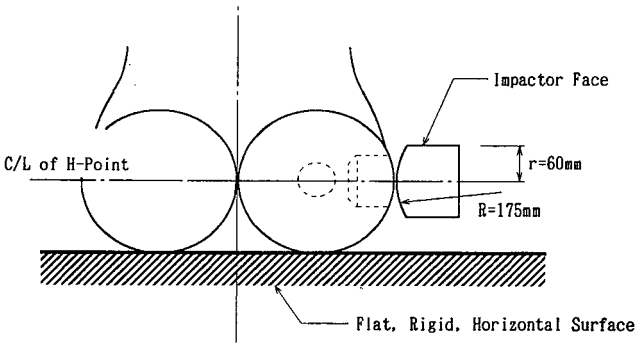

Figure 21. Positioning of the Impactor Face for Pelvis Impact Test

The acceleration of the impactor was measured and used to calculate the impactor force, which was filtered using SAE channel class 1000, and then normalized by the procedure given in ISO/DP9790-6.

Figure 22 shows the relationships between the normalized peak force of the impactor and impact velocity for both the EUROSID-1 and BIOSID, as well as the response requirement corridor. The normalized peak impactor force vs impact velocity response of the EUROSID-1 shows linear relationship, but that of the BIOSID does not. In the 6.0 to 9.0m/s test range for the EUROSID-1, the impactor peak forces showed a higher values than the upper bound of the requirement. For the BIOSID, in the 6.0m/s and 6.7m/s tests, the impactor peak forces fell within the requirement corridor, but for the 7.5m/s test, the impactor peak force was almost at the upper bound, and for the 9.0m/s test, the value was greater than the corridor.

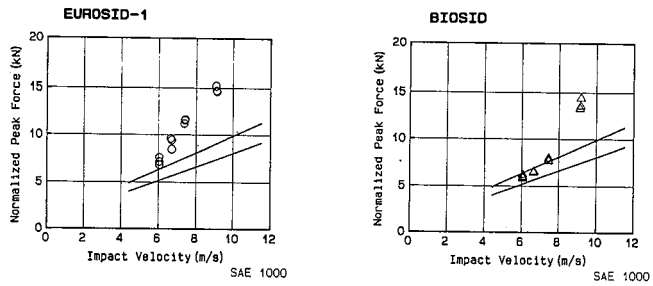

Figure 22. Normalized Peak Impactor Force vs. Impact Velocity Obtained from Pelvis Impact Test: EUROSID-1 and BIOSID Responses Compared with ISO Requirement Corridor

Drop Test. Four different conditions were required for drop test for the pelvis, namely, drop tests from heights of 0.5 and 1 meters onto a rigid surface; drop tests from heights of 2 and 3 meters onto a padded surface. In the JARI/JAMA tests, three types of drop tests were carried out, omitting the 3 meter drops.

The set-up procedure of the dummy for these tests is identical with that of the drop tests for the thorax. The same type of polyethylene pad was also used in the padded tests for the pelvis as used in the thorax drop tests. The pelvis acceleration was measured, and was filtered using SAE channel class 180, and then normalized by the procedure specified in ISO/DP9790-6.

Table 8 shows the normalized peak pelvis accelerations of both the EUROSID-1 and BIOSID, for three types of pelvis drop tests. The pelvis peak acceleration of the EUROSID-1 in the drop test from 1 meter onto a rigid surface fell within the requirement. However, in the other two types of tests, the values obtained were less than the lower bounds. The pelvis peak accelerations of the BIOSID in all three types of tests were less than the lower bounds of the requirements except the one test in 2 meter padded drop test.

Table 8. Normalized Peak Pelvis Accelerations for the EUROSID-1 and BIOSID Obtained from Pelvis Drop Test

Test Condition and ISO Requirement	EUROSID-1 (SAE180)			BIOSID (SAE180)		
0.5m Rigid Drop 39 - 45 G	34.5	34.8	37.0	32.0	29.2	37.7
1.0m Rigid Drop 63 - 77 G	65.3	65.4	67.1	36.6	40.5	37.1
2.0m Padded Drop 39 - 47 G	30.0	30.7	33.7	41.3	30.8	32.3

Sled Test. Three types of sled tests are required for the pelvis as is the case for the thorax, namely, a rigid wall impact at 6.8m/s and 8.9m/s and a padded wall impact at 8.9 m/s.

The sled and the dummy settings in these tests were identical with that used in the thorax sled tests. In

addition, a polyethylene pad was also used in the padded impact tests.

In these tests, the force at the impacted wall and the acceleration of the pelvis were measured. These responses were filtered using SAE channel class 1000, followed by the 100Hz FIR filtering, and then normalized by the procedure specified by ISO/DP9790-6.

Table 9 shows the normalized peak forces of the pelvis-impact surface and the pelvis peak accelerations for both the EUROSID-1 and BIOSID, for three types of sled tests. The peak forces at the pelvis-impact surface for the EUROSID-1 under the three test conditions exceeded the upper bounds of the requirements. The pelvis acceleration of the EUROSID-1 was less than the lower bound for the 8.9m/s padded wall impact test, but in the other two tests the values exceeded the upper bound of the requirements. The peak forces at the pelvis impacted-surface for the BIOSID, as with the EUROSID-1, exceeded the upper bounds for all three test conditions. The pelvis peak acceleration of the BIOSID for the 6.8m/s rigid wall impact test was almost at the upper bound; for the 8.9m/s padded wall impact test, almost at the lower bound; and for the 8.9m/s rigid wall impact test, the value exceeded the upper bound of the requirement.

Table 9. Normalized Peak Impact Surface Forces and Pelvis Accelerations for the EUROSID-1 and BIOSID Obtained from Pelvis Sled Test

Test Condition and ISO Requirement	EUROSID-1 (FIR100)			BIOSID (FIR100)		
6.8m/s Rigid Wall Impact						
Force 6.4 - 7.8 kN	28.4	28.8	29.8	22.7	24.3	27.5
Acceleration 66 - 77 G	96.3	98.2	98.7	73.9	78.0	95.0
8.9m/s Padded Wall Impact						
Force 11.6 - 13.6 kN	18.2	17.8	17.4	22.6	22.4	22.0
Acceleration 61 - 75 G	49.5	51.5	48.1	63.2	57.6	62.2
8.9m/s Rigid Wall Impact						
Force 22.4 - 26.4 kN	39.9	39.8	39.7	42.3	43.4	41.7
Acceleration 96 - 116 G	177.3	177.5	182.8	167.8	174.6	171.6

Overall Dummy Biofidelity

The results obtained from the tests for each part of both the EUROSID-1 and BIOSID were evaluated with the following three-level ranking.

A: Peak within response corridor

B: Peak within one corridor width above or below requirements

C: All other responses

In Table 10, evaluation of all parts of both dummies are summarized. By comparing both dummies in each part of the body in terms of the above ranking, we see that:

- The head of the both dummies show excellent performance in 200mm rigid drop test.
- The neck of the both dummies on 7G sled test, show rank A responses for acceleration of head and T1, however displacement responses of the EUROSID-1 are in better agreement to the requirements than that of the BIOSID.
- The thorax of the both dummies show high biofidelity rank on different three test conditions. In particular, the BIOSID shows excellent performance in the drop test. On the other hand, the EUROSID-1 shows more biofidelic responses than BIOSID in the sled test.
- The shoulder of the EUROSID-1 shows more biofidelic response rather than BIOSID in 4.5m/s impactor test.
- The abdomen of the BIOSID shows best compliance with the response requirements except the armrest force in the 2 meter drop test.
- Although the pelvis of the EUROSID-1 shows considerable responses in the drop test, but all responses in the other tests did not. The pelvis of the BIOSID shows more biofidelic responses rather than EUROSID-1, in the impactor test and sled test.

Table 10. EUROSID-1 and BIOSID Biofidelity Rankings

Body Region	Test Condition	Measurement	Biofidelity Ranking EUROSID-1	Biofidelity Ranking BIOSID
Head	0.2m Rigid Drop	Res.Head Acc.	A	A
Neck	7.0G Sled	Lat.Head Acc.	A	A
		Vert.Head Acc.	A	A
		Lat.T1 Acc.	A	A
		Lat.Head Disp.	B	C
		Vert.Head Disp.	B	C
		Time of Max.Head Disp.	A	A
		Lat.T1 Disp.	A	C
		Angle of Flexion	A	B
		Angle of Twist	N.M	N.M
Thorax	1.0m Rigid Drop	Impacted Surface Force	A	A
		Rib Deflection	B	A
	2.0m Padded Drop	Impacted Surface Force	A	A
		Rib Deflection	B	A
	6.8m/s Rigid Sled	Impacted Surface Force	A	B
		Upper Spine Acc.	C	B
		Lower Spine Acc.	B	B
		Upper Rib Acc.	A	B
	8.9m/s Padded Sled	Impacted Surface Force	B	B
		Upper Spine Acc.	B	B
		Lower Spine Acc.	B	B
		Upper Rib Acc.	A	B
	8.9m/s Rigid Sled	Impacted Surface Force	B	C
		Upper Spine Acc.	B	A
		Lower Spine Acc.	B	B
		Upper Rib Acc.	A	A
	4.3m/s Lateral Impact	Impactor Force	A	A
		Upper Spine Acc.	B	B
	6.7m/s Lateral Impact	Impactor Force	A	A
Shoulder	4.5m/s Lateral Impact	Impactor Force	B	C
		Shoulder Deflection	N.M	N.M
Abdomen	1.0m Drop	Armrest Force	C	A
		Lower Spine Acc.	C	A
		Impacted Rib Acc.	N.M	A
	2.0m Drop	Armrest Force	C	C
		Lower Spine Acc.	B	A
		Impacted Rib Acc.	N.M	A
Pelvis	6.0m/s Lateral Impact	Impactor Force	C	A
	6.7m/s Lateral Impact	Impactor Force	C	A
	7.5m/s Lateral Impact	Impactor Force	C	B
	9.0m/s Lateral Impact	Impactor Force	C	C
	0.5m Rigid Drop	Pelvis Acc.	B	B
	1.0m Rigid Drop	Pelvis Acc.	A	C
	2.0m Padded Drop	Pelvis Acc.	C	B
	6.8m/s Rigid Sled	Impacted Surface Force	C	C
		Pelvis Acc.	C	B
	8.9m/s Padded Sled	Impacted Surface Force	C	C
		Pelvis Acc.	B	A
	8.9m/s Rigid Sled	Impacted Surface Force	C	C
		Pelvis Acc.	C	C

A	16 / 46	21 / 48
B	16 / 46	15 / 48
C	14 / 46	12 / 48

A : Peak within Response Corridor
B : Peak within 1Corridor Width Above or Below Requirements
C : All Other Responses
N.M : Not Measured

The number of items with A and B ranks, with which we think a dummy is applicable in practice, are 32 items among a whole 46 items for the EUROSID-1, and are 36 items among a whole 48 items for the BIOSID.

Discussion

Full-Scale Side Impact Test Procedure enacted in the United States (16) requires the TTI (Thoracic Trauma Index) as an index for scaling thoracic injuries. On the other hand, both the Rib Deflection and V*C (Viscous Criterion) are discussed to apply in the proposed Full-Scale Side Impact Test Procedure in Europe (17,18).

Both the EUROSID-1 and BIOSID can measure these three types of injury criteria, but possibly different responses would be expected, even under identical test conditions.

Utilizing the data obtained from the biofidelity evaluation tests covered in this report, a comparison was made of the responses of both the EUROSID-1 and BIOSID to the thorax injury criteria proposed for the Full-Scale Side Impact Test Procedure. Accordingly, the responses of the two dummies with respect to TTI, Rib Deflection, and V*C were compared, using the data obtained from the drop tests and sled tests performed in this research.

Table 11 summarizes the responses of three injury criteria for both dummies obtained from drop tests and sled tests. The figures in Table 11 are average values for three sets of test performed under identical conditions. The figures in parentheses are the coefficient of variation. These data were not subjected to ISO normalization. The repeatability of these injury criteria were good for both dummies, except the V*C of the BIOSID in the 0.5m rigid drop Test. It is seen that in the padded and rigid sled tests at 8.9m/s the TTI and V*C were reduced by a polyethylene pad, but the Rib Deflection was not lessened for both the EUROSID-1 and BIOSID.

Table 11. Thorax Injury Criteria for the EUROSID-1 and BIOSID Obtained from Drop Test and Sled Test

Test Condition	EUROSID-1			BIOSID		
	TTI (G)	Rib Defl. (mm)	V*C (m/s)	TTI (G)	Rib Defl. (mm)	V*C (m/s)
0.5m Rigid Drop	24.2(2.4)	19.7(4.1)	0.10(0.0)	23.7(2.4)	15.1(6.3)	0.06(16.1)
1.0m Rigid Drop	53.2(5.1)	33.9(1.8)	0.29(3.1)	44.7(4.9)	27.7(1.4)	0.21(6.3)
2.0m Padded Drop	40.1(8.1)	42.6(2.4)	0.37(3.2)	35.4(4.2)	34.5(3.3)	0.28(4.9)
6.8m/s Rigid Sled	65.9(2.7)	40.2(1.6)	0.60(2.2)	82.6(2.0)	51.1(0.7)	0.68(5.0)
8.9m/s Padded Sled	69.5(4.9)	54.7(1.6)	0.98(1.4)	80.6(1.4)	65.4(0.3)	1.32(2.1)
8.9m/s Rigid Sled	130.1(0.4)	52.1(1.4)	1.24(5.4)	127.9(1.5)	65.8(0.0)	1.50(1.4)

( ): Coefficient of Variation %

Figure 23 shows the correlations between the EUROSID-1 responses and the BIOSID responses under the same conditions. The correlations of the two dummies can be expressed by the following equations.

TTI (BIOSID) = 1.026 x TTI (EUROSID-1) + 0.318 (r = 0.968)

Rib Defl.(BIOSID) = 1.524 x Rib Defl.(EUROSID-1) - 1.851 (r = 0.934)

V*C (BIOSID) = 1.378 x V*C (EUROSID-1) - 0.149 (r = 0.991)

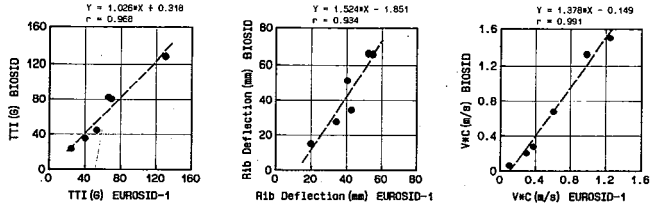

Figure 23. Correlation of Thorax Injury Criteria between the EUROSID-1 and BIOSID: Responses Obtained from Drop Test and Sled Test

From these relationships, as far as the drop tests and the sled tests are concerned, the TTI gives the better equivalence between the two dummies (the linear coefficient for the TTI closest to unity), and the V*C gives the better correlation. However, these correlations, which stand at least for the tests covered by this test report, do not automatically stand for the full-scale test.

Conclusions

As part of the research carried out by JARI/JAMA, a series of side impact tests have been conducted on both the EUROSID-1 and the BIOSID, to evaluate their biofidelity compared to the latest version of the response requirements of ISO/DP9790-1 to 6. The results can be summarized as follows.

(1) Both the EUROSID-1 and BIOSID are designed to the 50th percentile adult male size, but the dimensions and mass distributions are not identical.

(2) Both the EUROSID-1 and BIOSID do not completely satisfy the response requirements of ISO/DP9790-1 to 6. In other words, both dummies have parts of better biofidelity as well as poor biofidelity. Therefore, we might be able to say that both dummies are still premature for practical use. And, by comparing both dummies in each part of the body in terms of the biofidelity rankings, we see that: both are in the same level for head and thorax responses; EUROSID-1 is advantageous in neck and shoulder responses; and BIOSID is advantageous in abdomen and pelvis responses.

(3) An analysis was made to the proposed thorax injury criteria utilizing the data obtained from the biofidelity evaluation tests covered in this report. As far as the drop tests and sled tests performed in this research, the TTI gives better equivalence, and the V*C gives better correlation between the two dummies.

Tasks in Future

Although we obtained better correlation and better equivalence in terms of thoracic responses in comparison of the EUROSID-1 and the BIOSID by the biofidelity evaluation tests, this can be said as more or less a natural outcome, since both dummies have been developed so as to comply with ISO biofidelity requirement corridors. On the other hand, in full-scale vehicle side

impact tests by new FMVSS 214 in a preliminary JARI/JAMA study not yet reported, we observed responses of the two dummies do not always go in parallel, although tests are not many yet. Therefore we are much conscious of the need for a comprehensive evaluation based on all including the study in full-scale or full-scale-equivalent tests.

References

1. ISO/DP9790-1, "Road Vehicles—Anthropomorphic Side Impact dummy—Lateral Head Impact Response Requirements to Assess the Biofidelity of the Dummy," ISO/TC22/SC12, November 1987.
2. ISO/DP9790-2, "Road Vehicles—Anthropomorphic Side Impact dummy—Lateral Neck Impact Response Requirements to Assess the Biofidelity of the Dummy," ISO/TC22/SC12, November 1987.
3. ISO/TC22/SC12/WG5-N249, "Proposed Revision of ISO-9790-3, Road Vehicles—Anthropomorphic Side Impact dummy—Lateral Thoracic Impact Response Requirements to Assess the Biofidelity of the Dummy," September 1989.
4. ISO/DP9790-4, "Road Vehicles—Anthropomorphic Side Impact Dummy—Lateral Shoulder Impact Response Requirements to Assess the Biofidelity of the Dummy," ISO/TC22/SC12, July 1988.
5. ISO/DP9790-5, "Road Vehicles—Anthropomorphic Side Impact Dummy—Lateral Abdomen Impact Response Requirements to Assess the Biofidelity of the Dummy," ISO/TC22/SC12, July 1988.
6. ISO/DP9790-6, "Road Vehicles—Anthropomorphic Side Impact Dummy—Lateral Pelvis Impact Response Requirements to Assess the Biofidelity of the Dummy," ISO/TC22/SC12, August 1988.
7. ISO/TC22/SC12/WG5-N213, "The Biofidelity Test Results on SID and EUROSID," JARI/JAMA, October 1988.
8. Irwin, A.L. et al, "Comparison of the EUROSID and SID Impact Responses to the Response Corridor of the International Standards Organization," SAE-890604, February 1989.
9. Bendjellal, F. et al, "Comparative Evaluation of the Biofidelity of EUROSID and SID Side Impact Dummies," SAE881717, October 1988.
10. Janssen, E.G. et al, "Comparison of EUROSID and Cadaver Responses in Side Impacts", Proceedings of 12th Conference on Experimental Safety Vehicles, Göteborg, May 1989.
11. ISO/TC22/SC12/WG5-N218, "Summary of WG5 Evaluation of SID and EUROSID," October 1988.
12. European Experimental Vehicle Committee, "Specifications of the EEVC Side Impact Dummy EUROSID-1," April 1990.
13. Beebe, M.S, "What is Biosid," SAE900377, February 1990.
14. The University of Michigan Transportation Research Institute, "Anthropometry of Motor Vehicle Occupants, Volume 2—Mid Size Male," DTNH22-80-C-07502,December 1983.
15. Roberts,A.K. et al, "Review of Cadaver Responses to Lateral Impact and Derived Biofidelity Targets for Dummy," Proceedings of IRCOBI Conference, September 1990.
16. NHTSA, Federal Motor Vehicle Safety Standards, "Side Impact Protection," 49 CFR Part 571 (Docket No. 88-06; Notice 8), October 1990.
17. Economic Commission for Europe, "Proposal for Draft Regulation: Uniform Provisions Concerning the Approval of Vehicles with Regard to the Protection of the Occupants in the Event of A Lateral Collision," TRANS/SC1/WP29/GRSP/R.48/Rev. 1, January 1991.
18. Commission of the European Communities, Ad hoc Working Group "ERGA-Passive Safety," "Proposal for a Directive on the Protection of Car Occupants During Side Impact Collision," ERGA S/65 final, June 1989.

Appendix 1. Effective Masses and Normalizing Factors for EUROSID-1 Tests

Body Region	Test Condition	Effective Mass Me(kg)		Mass Ratio	Normalizing Factors			
		Dummy	Standard	Rm	Rf	Ra	Rx	Rt
Thorax	1.0m Rigid Drop	26.32	38.0	1.444	1.202		1.202	1.202
		28.23	38.0	1.346	1.160		1.160	1.160
	2.0m Padded Drop	25.79	38.0	1.473	1.473		1.473	1.473
		33.46	38.0	1.136	1.066		1.066	1.066
		31.22	38.0	1.217	1.103		1.103	1.103
		33.31	38.0	1.141	1.068		1.068	1.068
	6.8m/s Rigid Sled	30.86	38.0	1.231	1.110	0.901		1.110
		30.13	38.0	1.261	1.123	0.890		1.123
	8.9m/s Padded Sled	29.85	38.0	1.273	1.128	0.886		1.128
		35.62	38.0	1.066	1.033	0.968		1.033
		35.90	38.0	1.059	1.029	0.972		1.029
	8.9m/s Rigid Sled	37.61	38.0	1.010	1.005	0.995		1.005
		34.07	38.0	1.115	1.056	0.947		1.056
		33.73	38.0	1.127	1.061	0.942		1.061
		33.71	38.0	1.127	1.061	0.942		1.061
	4.3m/s Lateral Impact	31.54	20.8	0.659	0.905	1.374		0.905
		31.93	20.8	0.651	0.903	1.387		0.903
	6.7m/s Lateral Impact	31.88	20.8	0.653	0.904	1.385		0.904
		35.18	15.2	0.432	0.810	1.875		0.810
		35.52	15.2	0.428	0.808	1.895		0.808
		33.25	15.2	0.457	0.819	1.793		0.819
Shoulder	4.5m/s Lateral Impact	21.70	20.5	0.945	0.972		0.972	0.972
		22.23	20.5	0.922	0.960		0.960	0.960
		21.29	20.5	0.963	0.981		0.981	0.981
Abdomen	1.0m Drop	17.00	16.4	0.965	0.982	1.018		0.982
		16.83	16.4	0.975	0.987	1.013		0.987
	2.0m Drop	16.89	16.4	0.971	0.985	1.015		0.985
		17.65	16.4	0.929	0.963	1.037		0.963
Pelvis	6.0m/s Lateral Impact	14.70	14.5	0.986	0.993			
		14.54	14.5	0.997	0.998			
	6.7m/s Lateral Impact	15.07	14.5	0.962	0.981			
		14.51	14.5	0.999	0.999			
		14.36	14.5	1.010	1.005			
	7.5m/s Lateral Impact	14.55	14.5	0.997	0.998			
		14.39	14.5	1.008	1.004			
		14.43	14.5	1.005	1.002			
		14.53	14.5	0.998	0.999			
	9.0m/s Lateral Impact	14.68	14.5	0.988	0.994			
		14.46	14.5	1.003	1.001			
		14.28	14.5	1.015	1.007			
	0.5m Rigid Drop	72.30*1	76.0*2	1.051		0.975		
	1.0m Rigid Drop	72.30*1	76.0*2	1.051		0.975		
	2.0m Padded Drop	72.30*1	76.0*2	1.051		0.975		
	6.8m/s Rigid Sled	72.30*1	76.0*2	1.051	1.025	0.975		
	8.9m/s Padded Sled	72.30*1	76.0*2	1.051	1.025	0.975		
	8.9m/s Rigid Sled	72.30*1	76.0*2	1.051	1.025	0.975		

*1 ; Whole body mass of the dummy.
*2 ; Whole body mass of the standard cadaver.

Appendix 2. Effective Masses and Normalizing Factors for BIOSID Tests

Body Region	Test Condition	Effective Mass Me(kg)		Mass Ratio	Normalizing Factors			
		Dummy	Standard	Rm	Rf	Ra	Rx	Rt
Thorax	1.0m Rigid Drop	38.48	38.0	0.988	0.994		0.994	0.994
		35.67	38.0	1.065	1.032		1.032	1.032
	2.0m Padded Drop	34.41	38.0	1.104	1.051		1.051	1.051
		31.71	38.0	1.198	1.095		1.095	1.095
		32.41	38.0	1.173	1.083		1.083	1.083
		33.13	38.0	1.147	1.071		1.071	1.071
	6.8m/s Rigid Sled	49.03	38.0	0.775	0.880	1.136		0.880
		51.12	38.0	0.743	0.862	1.160		0.862
	8.9m/s Padded Sled	50.89	38.0	0.747	0.864	1.157		0.864
		49.81	38.0	0.763	0.873	1.145		0.873
		50.22	38.0	0.757	0.870	1.150		0.870
	8.9m/s Rigid Sled	48.17	38.0	0.789	0.888	1.126		0.888
		61.27	38.0	0.620	0.788	1.270		0.788
		61.55	38.0	0.617	0.786	1.273		0.786
		60.96	38.0	0.623	0.790	1.267		0.790
	4.3m/s Lateral Impact	39.90	20.8	0.521	0.864	1.658		0.864
		38.79	20.8	0.536	0.869	1.620		0.869
	6.7m/s Lateral Impact	40.12	20.8	0.518	0.863	1.666		0.863
		39.84	15.2	0.382	0.791	2.073		0.791
		39.99	15.2	0.380	0.790	2.079		0.790
		40.24	15.2	0.378	0.790	2.090		0.790
Shoulder	4.5m/s Lateral Impact	24.05	20.5	0.852	0.923		0.923	0.923
		23.89	20.5	0.858	0.926		0.926	0.926
		23.64	20.5	0.867	0.931		0.931	0.931
Abdomen	1.0m Drop	14.68	16.4	1.117	1.057	0.946		1.057
		15.01	16.4	1.092	1.045	0.957		1.045
	2.0m Drop	15.59	16.4	1.052	1.026	0.975		1.026
		13.97	16.4	1.174	1.084	0.923		1.084
Pelvis	6.0m/s Lateral Impact	14.35	14.5	1.010	1.005			
		14.10	14.5	1.028	1.014			
	6.7m/s Lateral Impact	14.32	14.5	1.013	1.006			
		14.75	14.5	0.983	0.991			
		14.32	14.5	1.013	1.006			
	7.5m/s Lateral Impact	14.23	14.5	1.019	1.009			
		14.74	14.5	0.984	0.992			
		14.67	14.5	0.988	0.994			
	9.0m/s Lateral Impact	14.57	14.5	0.995	0.997			
		15.05	14.5	0.963	0.981			
		15.09	14.5	0.961	0.980			
		15.01	14.5	0.966	0.983			
	0.5m Rigid Drop	76.59*1	76.0*2	0.992		1.004		
	1.0m Rigid Drop	76.59*1	76.0*2	0.992		1.004		
	2.0m Padded Drop	76.59*1	76.0*2	0.992		1.004		
	6.8m/s Rigid Sled	76.59*1	76.0*2	0.992	0.996	1.004		
	8.9m/s Padded Sled	76.59*1	76.0*2	0.992	0.996	1.004		
	8.9m/s Rigid Sled	76.59*1	76.0*2	0.992	0.996	1.004		

*1 ; Whole body mass of the dummy.
*2 ; Whole body mass of the standard cadaver.

Appendix 3. Dimensions and Characteristics of the Polyethylene Pad

Material ; Polyethylene Foam
Foam Density ; 68kg/m³

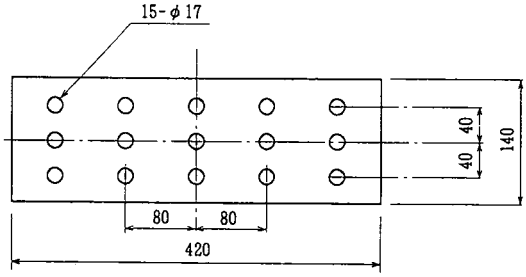

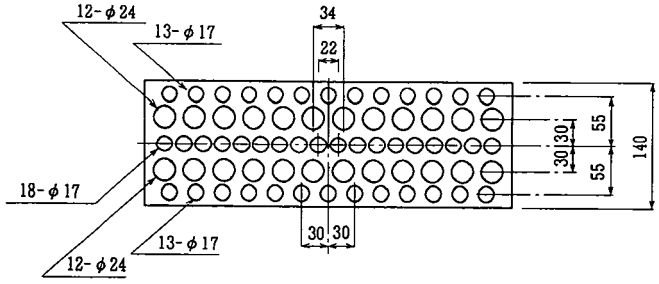

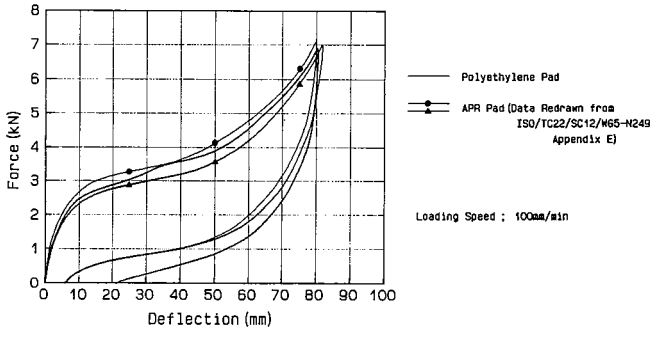

S8-O-02

The Biofidelity of the Production Version of the European Side Impact Dummy "EUROSID-1"

A.K. Roberts, M. Beusenberg, D. Cesari, K-P. Glaeser
European Experimental Vehicles Committee—Working Group 9

Abstract

Development of the European Side Impact Dummy EUROSID-1 was completed early 1990. EEVC Working Group 9 comprehensively reviewed the lateral impact cadaver data base and have published detailed biofidelity test procedures and design targets for dummies, based on the original cadaver data. This report describes and presents the results of a large biofidelity test programme performed within the EEVC test laboratories on four samples of the EUROSID-1 dummy. The results of this test programme are compared with the biofidelity targets produced by the EEVC Working Group 9.

Introduction

Development and Status of EUROSID

The specification for EUROSID-1 was finished in May 1989 (1) and the production version of the specification became available in 1990. No further development of the dummy is being undertaken. Many of the Production Prototype EUROSID dummies have been upgraded to the EUROSID-1 specification (the production specification) and several new dummies have been produced. The principal improvements made to the dummy were incorporated to improve its biofidelity, since this was the main area of criticism. During the general evaluation period of EUROSID, EEVC Working Group 9 published two status papers (2,3). These papers examined the problem areas that were being reported by users. The steps taken to resolve the problems were discussed and the improvements that were being incorporated to resolve these difficulties were described. Since the first batch of EUROSID (Production Prototype) dummies were produced the following improvements have been made and are incorporated in the EUROSID-1 dummy.

- Head—No Change.
- Neck—A minor detailed design change to the central section has been made to improve durability. Circular buffers of varying stiffness are now available to permit certification tuning.
- Arm/Sho.—Stub arms are now used and detent stops at the shoulder joint are incorporated to improve in-vehicle setting up. The arm skeletal design has changed slightly to improve durability.
- Thorax—The original optical displacement transducers have now been replaced by high specification linear displacement potentiometers. A revised rib flesh system in now used and the ribs have a lower dynamic mass, to improve biofidelity. Improved rib guides have been developed.
- Lumbar—No Change.
- Abdomen—The original tape switches have now been replaced by strain gauged beams.
- Pelvis—Detailed design changes made been made to improve durability and impact repeatability. The pubic symphysis force cell has been replaced and the ilium force gauges have been removed. A molded plastic ilium, replacing the aluminum one, is now incorporated with a revised hip insert block. The sacrum block has been re-profiled to permit increased ilium deformation.
- Legs—No change.

In addition to the above design changes the mass distribution of the dummy has been corrected. As a consequence of these improvements the User's Manual has been updated and the certification procedures reviewed. New pendulum based certification procedures for the lumbar and neck have been developed, using a new symmetrical headform.

Requirements of a Crash Test Dummy

A crash test dummy has to satisfy several different requirements. One of the important requirements is that it exhibit a good degree of biofidelity. Apart from biofidelity there are other requirements of equal importance and priority—repeatability, reproducibility, durability, robustness to name a few. Unfortunately the quality of a dummy is all too frequently assessed solely in terms of its biofidelity. The test programme described in this report concentrates on the biofidelity aspects, since that was the main purpose of the test programme. More than one dummy, test establishment and impact test procedure was used in this test programme therefore to a limited extent some of these other requirements can also be evaluated from these results. The principle evaluation of a dummy must be based on its performance in a vehicle in a crash test. One further assessment of biofidelity can be made in a vehicle impact test. This particular aspect was not evaluated in this part of EUROSID-1s evaluation but vehicle based cadaver comparative tests are being planned with EUROSID-1, based on the FAT Opel Kadet cadaver tests (4,5).

Biofidelity Targets

EEVC Working Group 9 carried out a comprehensive review of the cadaver data base in 1990 and derived a set of biofidelity design targets for a lateral impact test dummy (6). This paper not only reviewed the cadaver data base but also prioritized the test procedures based on the quality of the cadaver test procedure, the rele-

vance of the test and its reproducibility as well as the injury severity/risk in accidents. The paper developed a set of biofidelity targets appropriate for any side impact dummy, to be used in a vehicle impact test procedure. All of the biofidelity test procedures, adopted by WG9, were based on simple, easily reproduced test procedures in which test variability could be minimized. The cadaver data used to derive the targets was normalized according to the procedures developed by Mertz and Lowne (7) with against standard masses derived by WG9 (8).

The response targets for EUROSID-1 were obtained by reprocessing the cadaver data. The targets were mathematically derived from the mean cadaveric responses for the particular test. The normalized cadaveric responses were first time shifted to a "best fit" position based on the peak response and overall pulse shape. A mean response curve was then determined. The width of the tolerance curve was based on an examination of the cadaver results for tests in which there were sufficient data for statistical analysis. Based on this analysis a band of width ± 25% of the peak mean value was applied to the whole time history of mean normalized cadaver curve, this approximating to a tolerance band of about ± one standard deviation. A ± 25% tolerance band was constructed around the mean response curve. To enable the corridor to be easily specified a straight line corridor was then constructed through the ± 25 % responses. The actual corridor coordinates are described in the EEVC WG9 test procedure paper (8).

Test Programme

The EEVC WG9 biofidelity test programme has consisted of three test procedures, free fall drop, linear guided impactor and impact sled tests. The basic test procedures adopted for this programme were first described in a 1990 EEVC WG9 paper reviewing the lateral impact cadaveric data base (6) and have since been slightly refined, based on test experience and increased knowledge of the cadaver tests. The actual test procedures and targets were re-published at the 1991 ESV conference (8). The main difference in the two versions of the two WG9 papers being with respect to the wall dimensions for the sled based tests. Impact tests have been carried out by four research institutes—the BASt, Germany; INRETS, France; TNO, Netherlands; and the TRRL in the United Kingdom. Table 1 details the complete test programme carried out at each establishment. It should be noted that each of the test institutes used a different sample of the EUROSID-1 dummy and that for most of the test procedures the particular test was repeated by more than one institute. The priority rating of the test and body part was determined by WG9 based on the quality of the cadaver data, the test procedure and injury severity/risk from accidents.

It should be noted that the 1m drop test procedure used to assess the abdomen was not considered by WG9 to be a good quality test procedure. Due to this the target was considered to be a low quality target but since injury to the abdomen is important the abdomen was classified as a high priority body part.

Table 1. Scope of Biofidelity Test Programme Presented in this Report

Research Institute -		BASt	INRETS	TNO	TRRL
High Priority Targets					
Head -	1m Drop	20	-	10	6
Thorax -	4.3m/s Imp	-	-	5	5
	7.6m/s RW	-	3	-	5
	10.3m/s RW	-	3	-	5
	10.3m/s PW	-	2	-	5
Abdomen -	1m Drop	-	-	6*	-
Pelvis -	Imp	-	8	6	-
	7.6m/s RW	-	3	-	5
	10.3m/s RW	-	3	-	5
	10.3m/s PW	-	2	-	5
Low Priority Targets					
Neck -	Dummy sled	-	-	1	-
Shoulder -	Quasi static	-	-	-	**
	4.5m/s Imp	-	-	5	5

[Imp = Guided Impactor : RW = Rigid Wall : PW = Padded Wall]

* See Section 3.1.3.
** See Section 3.2.2.

EUROSID-1 Responses

It should be noted that most of these results cannot be compared to other performance requirements published by other groups since both normalization procedures and test procedures could be different. Only the head drop test procedure is equivalent (9).

High Priority Targets

Head biofidelity. The original cadaver tests were carried out on a complete cadaver, the cadavers being strapped to a pivoting pallet. The biofidelic test—a 200 mm free fall drop test onto a rigid surface—has been adopted, due to its ease and repeatability.

The biofidelity test is a simple free fall drop test onto a rigid surface from a height of 200mm. Table 2 shows the response of three EUROSID-1 heads subjected to this test procedure. BASt also tested two other heads. In an un-tuned condition they gave mean responses of 145.7 g

Table 2. Head Drop Tests

	Peak Resultant deceleration (g)	
Target	83 - 141	
Test condition	Un-tuned head	Tuned head
BASt	156.3	139.4
	159.8	138.6
	158.6	133.7
	151.3	138.0
	153.5	138.9
	154.4	134.5
	156.1	146.6
	156.1	140.4
	153.0	136.2
	154.8	136.0
TNO	146.8	114.9
	145.9	122.5
	151.1	116.0
	150.4	117.9
	149.7	118.9
TRRL	151.9	137.1
	161.4	138.2
	163.7	136.6

and 140.2 g. It is thought that both of these heads could easily have been tuned into the biofidelity targets.

Thorax biofidelity. Thorax biofidelity is assessed by two test procedures, a simple linearly guided impactor test and three sled based tests.

Thorax impactor test. The thorax biofidelity impactor test is performed at a velocity of 4.3 m/s using a 6" diameter impactor with a mass of 23.4 kg. Two normalized parameters are assessed, impactor deceleration and lateral acceleration of the upper spine measured at the T1 position. Figure 1 and Figure 2 show the impactor decelerations responses for the TNO and TRRL dummies, compared to the target corridor. Figure 3 and Figure 4 show the T1 lateral accelerations responses.

Thorax sled tests. Thorax biofidelity in the sled tests are based on three test procedures. Two tests are into two rigidly mounted force plates and one further test into the same plates onto which is attached two defined pads. The impact velocities, 7.6 and 10.3 m/s are defined as the impact velocity of the dummy into the wall. This velocity allowing for any possible rebound velocity. *Previous test specifications for this type have test have defined impact velocity purely on impact sled velocity (9). Re-examination of the base cadaver data showed significant wall rebound at the time of cadaver to wall impact. The EEVC specified velocities reflect the actual cadaver to wall impact.* The assessment of biofidelity in this test procedure is based on the inertia compensated wall forces measured at the upper load plate. Figure 5 and Figure 6 show the upper rigid wall force response at 7.6 m/s. Figure 7 and Figure 8 show the rigid wall force response at 10.3 m/s. Figure 9 and Figure 10 show the padded wall force response at 10.3 m/s.

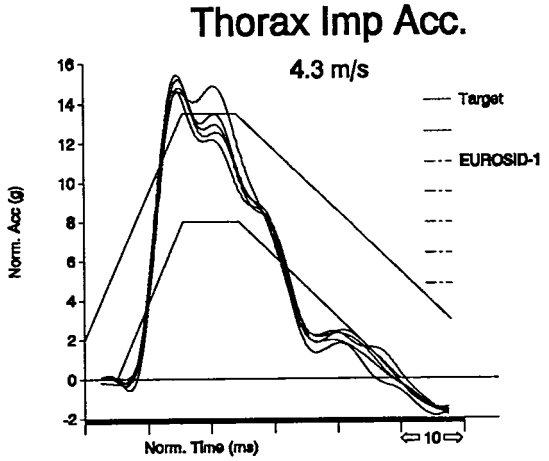

Figure 1. Thorax Impactor Deceleration—TNO

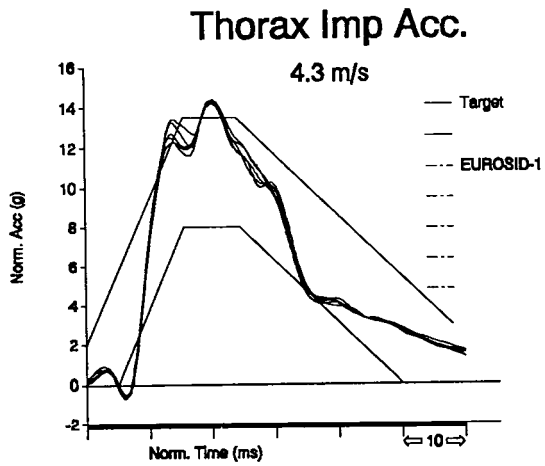

Figure 2. Thorax Impactor Deceleration—TRRL

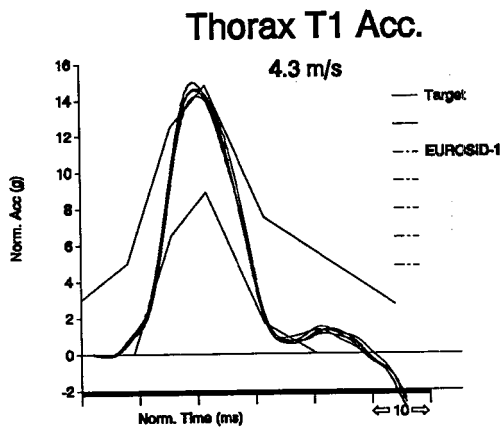

Figure 3. Thorax T1 Lateral Acceleration—TNO

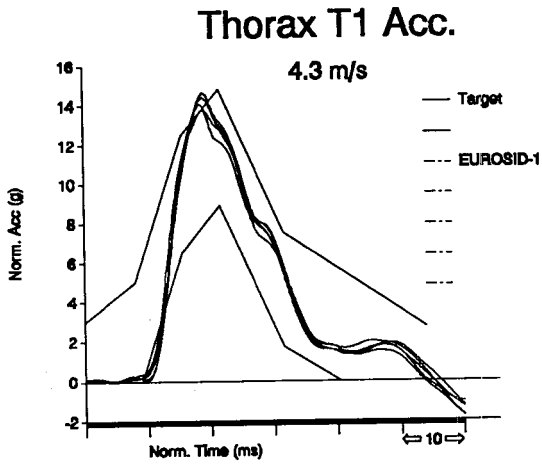

Figure 4. Thorax T1 Lateral Acceleration—TRRL

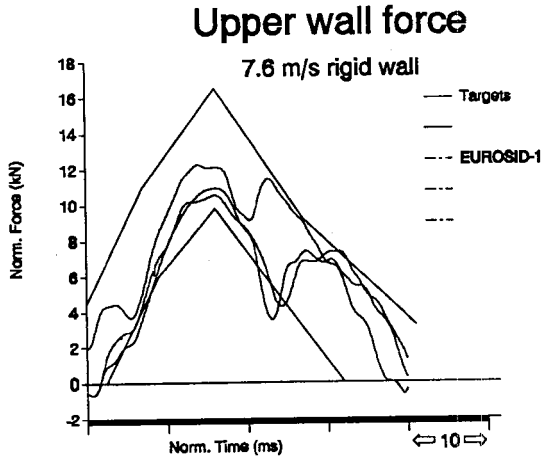

Figure 5. Thorax Rigid Wall Force (7.6 m/s)—INRETS

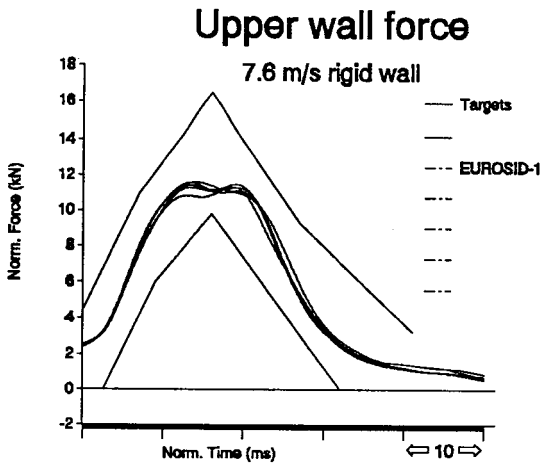

Figure 6. Thorax Ridge Wall Force (7.6 m/s)—TRRL

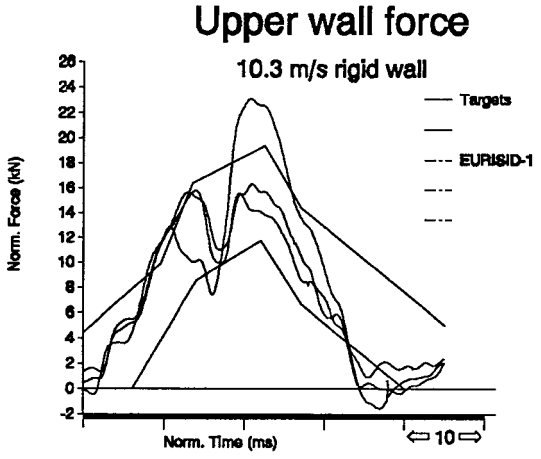

Figure 7. Thorax Ridge Wall Force (10.3 m/s)—INRETS

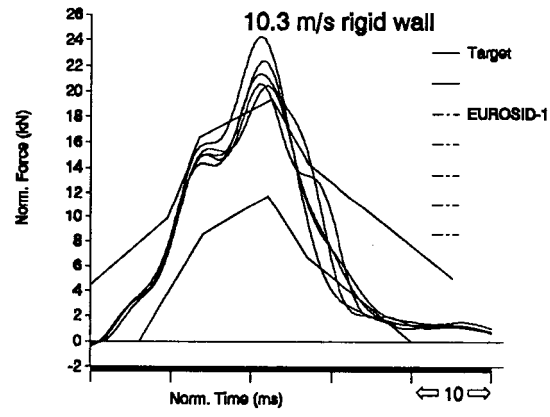

Figure 8. Thorax Ridge Wall Force (10.3 m/s)—TRRL

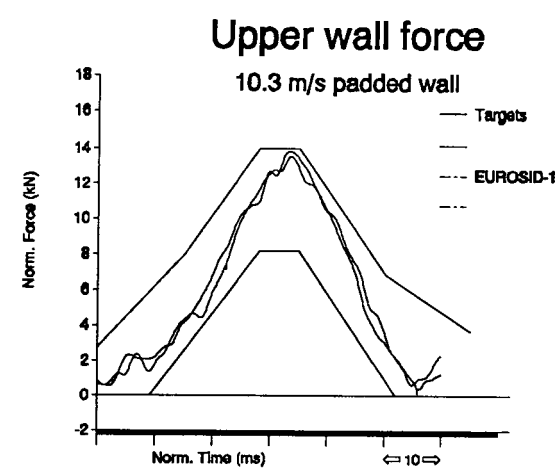

Figure 9. Thorax Padded Wall Force (10.3 m/s)—INRETS

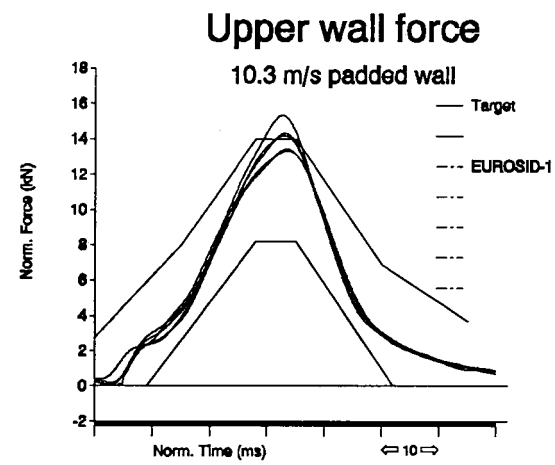

Figure 10. Thorax Padded Wall Force (10.3 m/s)—TRRL

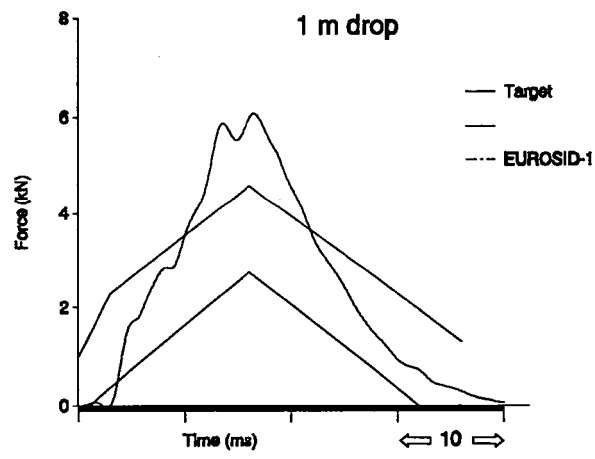

Figure 11. Abdomen Drop Test—TNO

Abdomen Biofidelity

Abdomen biofidelity is assessed in a free fall drop test, that is very difficult to perform accurately. Of the 6 tests performed only was considered of adequate quality and capable of full normalization in terms of biofidelity. The abdomen is assessed by the normalized force measured at the simulated arm rest. In addition abdominal penetration should be ≥41mm. Figure 11 shows the inertial compensated armrest force response of EUROSID-1, from a drop height of 1m in the one processed test.

Pelvis Biofidelity

As for the thorax pelvis biofidelity is assessed in two dynamic test procedures, impactor and sled based.

Pelvis impactor test. The impactor test is based on a special light weight impactor with a spherical impact

surface. The mass of the impactor is 17.3 kg with a spherical face of 175 mm radius and an outer diameter of 120 mm. The dummy is sat on a special defined seat. A range of impact velocities are permitted for the test between 6.0 and 10.0 m/s. A force/velocity response target corridor is defined for this test. Figure 12 shows this response corridor and the peak responses from a number of impact tests performed on two EUROSID-1 dummies.

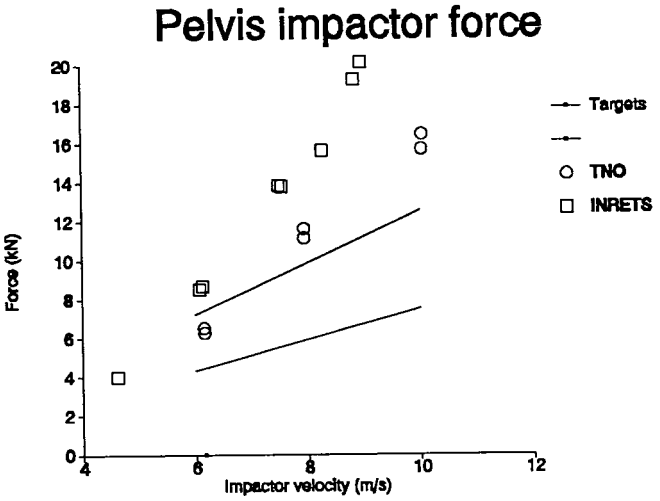

Figure 12. Pelvis Impactor Force/Velocity

Pelvis sled tests. The test procedure for the pelvis is exactly the same as for the thorax, both test being carried out at the same time. Pelvis biofidelity in this test is assessed by two requirements at each test condition, peak pelvis deceleration and lower inertia compensated wall force. Table 3 shows the peak decelerations for the three sled test conditions. Figure 13 and Figure 14 show the lower rigid wall force response at 7.6 m/s. Figure 15 and Figure 16 show the lower rigid wall force response at 10.3 m/s. Figure 17 and Figure 18 show the lower padded wall force response at 10.3 m/s.

Table 3. Pelvis Decelerations in Sled Tests

	Peak Pelvis Deceleration (g)		
Test Condition	7.6 m/s RW	10.3 m/s RW	10.3 m/s PW
Target	52.7 - 87.9	79.5 - 132.5	65.8 - 109.7
INRETS	134.8 124.8 110.0	211.5 188.9 213.5	95.0 98.0
TRRL	Inst. Fail 129.1 120.4 116.2 128.8	174.4 189.8 185.5 195.9 230.9	71.9 72.9 74.6 72.6 75.4

Low Priority Targets

Neck biofidelity. Neck biofidelity is assessed in a sled based test procedure, reproducing human volunteer test. The test specifies both the sled deceleration as well as the dummies T1 lateral deceleration. Both test procedures being based on the same cadaver data set. The same peak response targets are specified for both test procedures. Table 4 tabulates the peak responses of the EUROSID-1 neck to the targets.

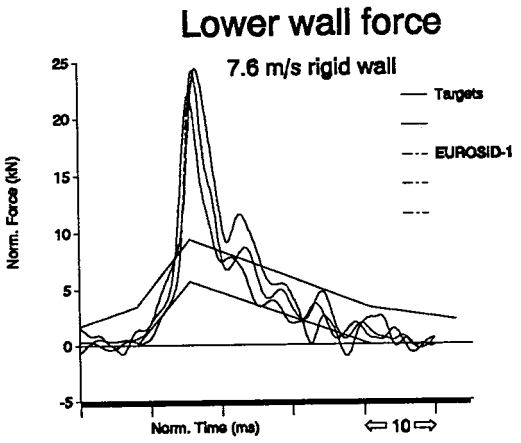

Figure 13. Pelvis Ridge Wall Force (7.6 m/s)—INRETS

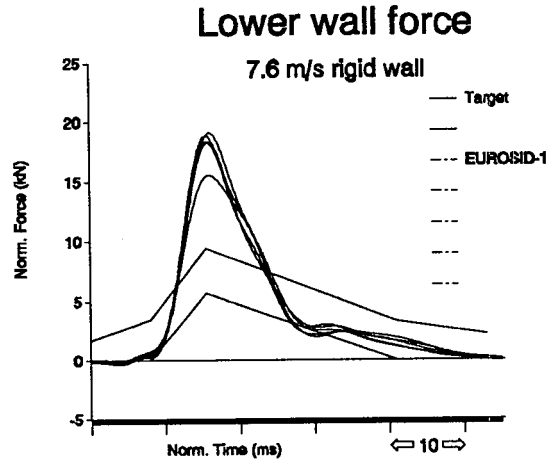

Figure 14. Pelvis Ridge Wall Force (7.6 m/s)—TRRL

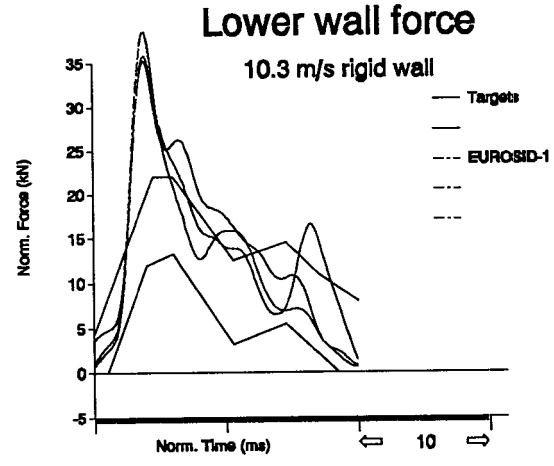

Figure 15. Pelvis Ridge Wall Force (10.3 m/s)—INRETS

Shoulder biofidelity. Shoulder biofidelity is assessed in two tests, a very simple lateral quasi-static test and a linearly guided impactor test at 4.5 m/s using the 6" diameter 23.4 kg impactor. Figure 19 and Figure 20 show the responses of two EUROSID-1 dummies this the dynamic test. Table 5 shows the maximum deflection observed in the TRRL tests.

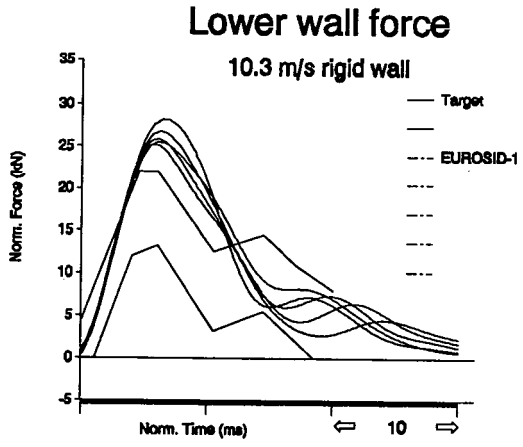

Figure 16. Pelvis Ridge Wall Force (10.3 m/s)—TRRL

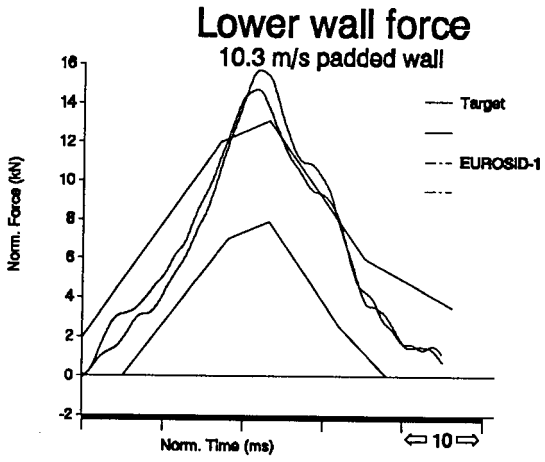

Figure 17. Pelvis Padded Wall Force (10.3 m/s)—INRETS

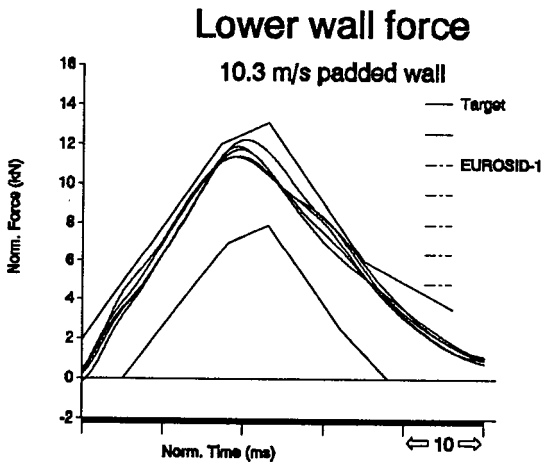

Figure 18. Pelvis Padded Wall Force (10.3 m/s)—TRRL

Table 4. Neck Pendulum

	Maximum Angular Flexion (Deg)	Maximum Horizontal Disp. of CoG (mm)	Maximum Downward Vertical Disp. of CoG (mm)
Target	44 - 59	130 - 162	64 - 94
TNO Test Result	53	122	51

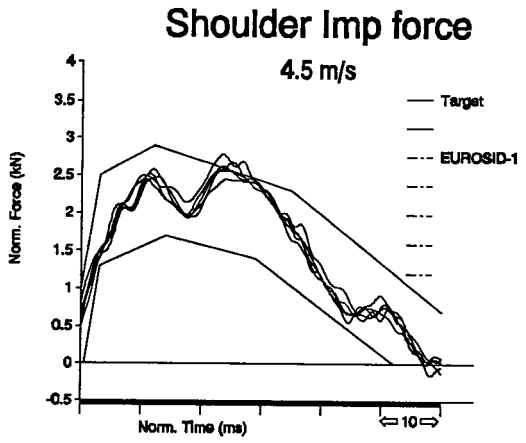

Figure 19. Shoulder Impactor Force/Time—TNO

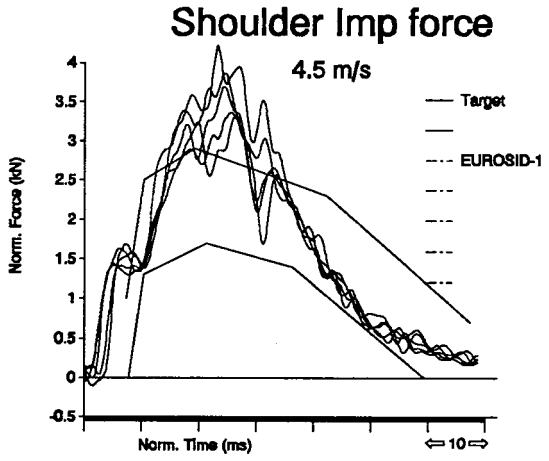

Figure 20. Shoulder Impactor Force/Time—TRRL

Table 5. Shoulder Impactor Tests Displacements—TRRL

Shoulder Impactor Test	Maximum Lateral Displacement mm
Test 1	71
Test 2	68
Test 3	61
Test 4	74
Test 5	63

A large number of quasi static tests were performed by TRRL. The test as specified is a simple one but great difficulty was found in performing it due to alignment difficulties. The results, although not listed, have a high level of variance dependant upon the adjustment and orientation of the external dummy suit. Without the suit in place around the dummy the force displacement targets are easily met. With the suit in position the force to achieve the displacement target can range between the specified level and about 50-100% greater.

Discussion of Results

As was previously described the biofidelity design targets were based on a mathematically derived mean response from a group of cadaver tests. The quality of the biofidelity target is based not only on the number of repeat cadaver tests but also upon the reproducibility of the test procedure itself. Much of the discussion must be

based as much on the sparsity of the usable cadaver data and the severity of the test procedure as to the ability of the dummy to conform to the targets. It should be noted that only for the pelvis impactor test is there a reasonable number of cadaver tests on which to develop biofidelic targets with confidence. Only the EEVC head drop test is identical to the equivalent test procedure specified by ISO (9).

It is most important for the dummy to be humanlike in its response under impact conditions where the stiffness of the body part is similar to the stiffness of the impacted part of the vehicle interior. This is most likely to be the case with the thorax and abdomen. This is less critical for the pelvis whose stiffness is likely to be greater than the stiffness of the padding provided for its protection.

It should be noted that when the targets were derived it was decided not to attempt to compensate for the human muscle tone in living subjects. It is thought that muscle tone would increase the lateral stiffness, principally of the thorax.

High Priority Body Areas

Head drop test. The head of EUROSID-1 has not changed from the original production prototype dummy, and is based on the Hybrid III dummy head, but certified for lateral impact. It should be noted that the head of EUROSID-1 is similar to that used on BIOSID.

The results from the three institutes that performed biofidelic tests on the EUROSID-1 head clearly show that the head can be tuned to meet the biofidelity requirements for a side impact dummy.

Thorax impactor test. The two sets of thorax impactor results from TNO and TRRL show good agreement. Mean peak acceleration values for impactor acceleration are only 7% and 3% above the upper target boundary and the T1 accelerations are in the peak limit range. For both sets of results the rate of rise in acceleration is consistent but slightly greater than that measured with cadavers. The dummy response might be more representative of live human response when muscle tone is present. Overall the response of the thorax in the impactor test is very close to the targets.

Thorax sled test. The thoracic wall forces in the 7.6 m/s rigid wall and 10.3 m/s padded wall impacts are in very good agreement with the design targets, lying almost entirely within the corridors. The peak amplitudes of the results from INRETS and TRRL are almost identical.

Even for the 10.3 m/s rigid wall impact tests the responses, for the most part, are within the corridors, although some peaks exceed the upper limit. This sled test must be interpreted not only against the design targets and the size of the cadaver data base but also against the severity of the in-vehicle impact situation. The 10.3 m/s rigid wall test is an extremely severe impact both to a cadaver and to a dummy. The injury parameters well exceed the accepted performance limits. This test condition can therefore be regarded as being less relevant to the in-car situation than the other two sled impact conditions.

For the more important test conditions (7.6 m/s rigid wall and 10.3 m/s padded wall) the response of the thorax is in very good agreement with the targets and is close to the target for the extreme rigid wall test at 10.3 m/s.

Abdomen drop test. The cadaver target for the abdomen is based on a set of tests on arm rests of differing heights involving a wide range of injury severity. Because of poor test repeatability only one test result on the abdomen can be discussed at length. The one result does indicate that the peak force generated on the armrest is above the target. The average internal abdominal force measured in the drop test with a 41 mm armrest was 3.5 kN which is 40% greater than the performance limit of 2.5 kN at a penetration of 39 mm. The abdomen was not designed to be biofidelic up to this high level (cadaver injury equivalent to AIS 4). In the drop test the abdomen will bottom out against the strain gauged beams which would generate the high peak force observed.

It should be noted abdomen design changes from the Production Prototype dummy to EUROSID-1 relate to instrumentation techniques rather than biofidelity. This was the principal cause of concern expressed by users of the earlier version of the dummy.

The period of the abdomen force pulse is similar to the target corridor but the peak value exceeds the upper limit by about 30% in the one valid test. The abdomen is considered to be a high priority body part, but the cadaver data is only of limited value. Based on this limited data the biofidelity of the abdomen is considered to be adequate.

Pelvis impactor test. The impactor test results from both INRETS and TNO indicate that the forces exceed the target corridor at speeds greater than about 5.5 m/s for the INRETS tests and about 6.5 m/s for the TNO tests.

The performance is close to the target at low speeds but agreement at higher speed is poor. It should be noted that during development of EUROSID the performance of the pelvis in the impactor test was influenced by lumbar stiffness. A stiffer lumbar than would be required for optimum performance in the impactor tests was chosen to improve dummy seating stability. This test only loads the pelvis which would not be the situation for in-car testing.

While the forces exceed the target values at the higher velocities they are closer for EUROSID-1, which uses a polymeric ilium, than those found with the Production Prototype EUROSID which had an aluminum ilium.

Pelvis sled test. The peak responses for the padded wall test are in good agreement with the target but in the rigid wall tests at both impact speeds they are somewhat in excess. While the forces and accelerations for the

rigid wall tests exceed the target values they are again closer for EUROSID-1 than those found with the Production Prototype EUROSID.

Low Priority Body Areas

Neck sled test. The neck test procedure is a difficult one to perform since there are two input requirements, sled and T1 lateral acceleration. It is not possible to achieve a perfect match for both input requirements on a non HY-GE sled. The test procedure defined by EEVC WG9 places greater importance on reproducing T1 acceleration rather than the sled pulse. Three dimensional film analysis is necessary to measure displacements and flexion angles. A close match to the T1 requirement was achieved in the one test performed by TNO.

Although neck injuries are not currently considered in side impact testing, the translational and rotational measurements relate to the possibility of the head impacting the vehicle interior in a lateral impact. Any head contact with the vehicle interior is likely to occur well before the maximum head displacement measured in this test are achieved. From the one test, satisfactory responses were measured for angular flexion but small deviations from the targets were observed for the displacements. Thus compliance is considered to be sufficient for good neck biofidelity.

Shoulder impactor test. Fairly good overall repeatability was seen in the shoulder impact tests within each test laboratory, the TNO tests being closer together than the TRRL results. The TNO dummy results are very close to the target corridor but the TRRL dummy gave slightly higher force levels outside of the target and in addition the "noise" level was much greater. The minimum shoulder deflection target of 32 mm was easily exceeded.

The shoulder of EUROSID-1 has two degrees of freedom. When struck laterally the arm moves both forward as well as laterally. A possible explanation for the differences between the two test results lies in the test equipment and test procedure. It is believed that the cadaver tests were performed with a linearly guided impactor with the response of the shoulder being determined purely by force and shoulder lateral displacement criteria. Since the shoulder of EUROSID-1 slides across the surface of the impactor it generates bending moments in the impactor guide which could influence frictional forces. The impactor used by TRRL uses linear ball races and the TNO impactor uses plain linear bearings. An impactor based on plain bearings is more likely to suffer from frictional damping problems than one using linear roller races, but the roller races can cause oscillations as rollers engage and disengage. These oscillations may be seen superimposed on the TRRL pulses. This could explain the differences between the TNO and TRRL responses. It should be noted that the certification of EUROSID-1 is based on a suspended impactor to overcome this problem. These differences are not observed in this type of impactor. Overall the shoulder responses of EUROSID-1 are in close agreement with the targets.

Shoulder quasi-static test. This is a low priority body part and a low priority test procedure if it is compared to the in-vehicle impact severity situation. This test is intended to ensure sufficient lateral compliance of the shoulder. Tests performed according to this prescribed procedure have shown that under very low loads the jacket of EUROSID-1 greatly influences the motion of the shoulder. Tests indicate that maximum translational motion of the shoulder well in excess of 55 mm is possible. It should be noted that the shoulder does not have any associated injury threshold criterion attached to it.

Repeatability and Reproducibility

An assessment of dummy repeatability can be gained by examining peak dummy responses from repeated tests with the same dummy. In addition dummy reproducibility can be assessed by comparing different dummies' peak responses in the same test at different research laboratories. Where a test has been repeated more than once the Coefficient of Variation (%) can give an indication of the quality of a dummy. It is acknowledged that the greater the number of repeat tests the better is the quality of the estimate of the Coefficient. The Coefficient of Variation is derived from the mean response value and the standard deviation (Equation 1).

$$Coef.\,Var.\,(\%) = \frac{Standard\,Deviation}{Mean\,Value} * 100 \quad (1)$$

It is generally considered that a Coefficient of Variation of about 10% is acceptable under these types of test conditions. Table 6 shows the peak mean responses and

Table 6. Comparisons Between Dummies and Tests Institututes

Body Part	Test	Parameter	Dummy	Sample Size	Mean Value	% Coef of Var.
Head	Drop	Head g	BASt	10	138.2	2.6
			TNO	5	118.0	2.5
			TRRL	3	137.3	0.5
Thorax	Impactor	Imp g	TNO	5	15.0	2.1
			TRRL	5	14.4	0.6
		T1 lat g	TNO	5	14.6	1.9
			TRRL	5	14.3	2.6
	7.6 Rig W	Wall kN	INRETS	3	11.2	7.9
			TRRL	5	11.5	1.2
	10.3 Rig W	Wall kN	INRETS	3	18.4	4.1
			TRRL	5	21.8	7.2
	10.3 Pad W	Wall kN	INRETS	2	13.7	1.4
			TRRL	5	14.2	5.6
Abdomen	Drop	Arm Rest kN	TNO	1	6.1	na
Pelvis	7.6 Rig W	Wall kN	INRETS	3	23.6	5.5
			TRRL	5	18.0	7.9
		Pelv Lat g	INRETS	3	123.2	8.3
			TRRL	5	123.6	4.5
	10.3 Rig W	Wall kN	INRETS	3	36.6	4.6
			TRRL	5	26.3	4.6
		Pelv Lat g	INRETS	3	204.6	5.4
			TRRL	5	195.3	9.8
	10.3 Pad W	Wall kN	INRETS	2	15.2	4.5
			TRRL	5	11.7	3.0
		Pelv Lat g	INRETS	2	96.5	1.6
			TRRL	5	73.8	1.8
Shoulder	Impactor	Imp g	TNO	5	2.5	4.4
			TRRL	5	3.7	10.1
Neck	Sled	Ang Flex °	TNO	1	53	na
		Horz Disp mm	TNO	1	122	na
		Vert Disp mm	TNO	1	51	na

Coefficient of Variation for the different dummies tested at different research institutes and in the differing test procedures. The Coefficient of Variation is as high as 10% for only two of the 26 test series reported and is well below this figure for the remainder.

Conclusions

- For the high priority body areas the biofidelity of EUROSID-1 is considered to be good or adequate.
  - Head—It has been shown that the head can be adjusted to meet the biofidelity target set for a lateral impact test dummy.
  - Thorax—It is important that this body area behaves in a humanlike manner. The biofidelity results indicate that the performance of the dummy thorax either achieves or is very close to achieving the targets set for a dummy. The biofidelity of the thorax is considered to be good.
  - Abdomen—The abdomen performance approaches that of the set target, although the peak force observed exceeded the target level by about 30% in the biofidelity test which is considered to be excessively severe in terms of injury level. The biofidelity of the abdomen is considered to be adequate.
  - Pelvis—The pelvis response in the padded wall test is good, being almost entirely within the set targets. The forces and accelerations in the rigid wall sled and the higher speed impactor tests exceed the target values set, although they are much closer than the results found with the Production Prototype EUROSID. The biofidelity of the pelvis is considered to be adequate for the in-vehicle situation.
- For the low priority body areas the EUROSID-1 is considered to be sufficiently biofidelic.
  - Neck—The neck flexion angular flexion response is within the target range and the maximum displacements are close to the targets. As any head to vehicle interior contacts are likely to occur before maximum displacement the biofidelity is considered to be sufficient.
  - Shoulder—The shoulder impactor force is within or close to the target and the maximum displacement targets are easily met. The biofidelity of the shoulder is considered to be reasonably good.
- The repeatability of EUROSID-1 in the biofidelity tests has been shown to be good, having a Coefficient of Variation of well under 10% in most tests.
- Overall the biofidelity and repeatability of EUROSID-1 has been shown to be good and EUROSID-1 is considered to be satisfactory for use in legislative side impact tests and for vehicle research and development.

Acknowledgements

Participating members of EEVC Working Group 9 are D. Cesari, E.G. Janssen, K-P. Glaeser, G.D. Suthurst (retired), R.W.Lowne (Chairman), A. Pastorino, A.K. Roberts (Secretary), and M. Beusenberg.

References

1. Specification of the EEVC Side Impact Dummy, EUROSID-1. Report of the EEVC Working Group 9. 1989.
2. Roberts A.K. et al. Status Report of the Production Prototype EUROSID's 1988. Report of the EEVC Working Group 9. IRCOBI/EEVC Workshop on the Evaluation of Side Impact Dummies. 13th Sept. 1988. BASt Germany.
3. Roberts A.K. Report on EUROSID 1989. EEVC Working Group 9 report. 12th ESV Conference Göteborg, Sweden 1989.
4. Forschungsvereinigung Automobiltechnik e.V. (1989). FAT Schriftenreihe, to be published.
5. Forschungsvereinigung Automobiltechniek e.V. (1984). Belastbarkeitsgrenze und Verletzungsmechanik des angegurteten Fahrzeuginsassen beim Seitenaufprall. Phase I: Kinematik und Belastungen beim Setienaufprall im Vergleich Dummy/Leiche. FAT Schriftenreihe nr. 36. Frankfurt am Main.
6. Roberts A.K. Review of Cadaver Responses to Lateral Impact and Derived Biofidelity Targets for Dummies. 1990 IRCOBI Conference. Lyon France. Sept. 1990.
7. Mertz H.J. A Procedure for Normalizing Impact Response Data. SAE Paper 840884, Warrendale, PA. USA. 1984.
8. Roberts A.K. et. al. Test Procedures for Defining Biofidelity Targets for Lateral Impact Test Dummies. Written report of the European Experimental Safety Committee Working Group 9. Twelfth ESV Conference. Paris. France.
9. (a) ISO/TC22 Road Vehicles—Anthropomorphic Side Impact Dummy—Lateral Head Response Requirements to Assess the Biofidelity of the Dummy. ISO/DTR 9790-1 Ref No ISO/TC22/SC22/WG5 N1554 E. (b) ISO/TC22 Road Vehicles—Anthropomorphic Side Impact Dummy—Lateral Neck Response Requirements to Assess the Biofidelity of the Dummy. ISO/DTR 9790-2 Ref No ISO/TC22/SC22/WG5 N1554 E. (c) ISO/TC22 Road Vehicles—Anthropomorphic Side Impact Dummy—Lateral Shoulder Response Requirements to Assess the Biofidelity of the Dummy. ISO/DTR 9790-3 Ref No ISO/TC22/SC22/WG5 N1554 E. (d) ISO/TC22 Road Vehicles—Anthropomorphic Side Impact Dummy—Lateral Thoracic Response Requirements to Assess the Biofidelity of the Dummy. ISO/DTR 9790-4 Ref No ISO/TC22/SC22/WG5 N1554 E. (e) ISO/TC22 Road Vehicles—Anthropomorphic Side Impact Dummy—Lateral Abdominal Response

Requirements to Assess the Biofidelity of the Dummy. ISO/DTR 9790-5 Ref No ISO/TC22/SC22/WG5 N1554 E. (f) ISO/Road Vehicles—Anthropomorphic Side Impact Dummy—Lateral Pelvic Response Requirements to Assess the Biofidelity of the Dummy. ISO/DTR 9790-6 Ref No ISO/TC22/SC22/ WG5 N1554 E.

Annex: Normalization Factors

The factors used to normalize the EUROSID-1 test data are shown in the following Tables. Although the numbers in themselves are of little importance they do give some indication of dummy and test procedure repeatability. They also show by how much the dummy responses have been modified, using the same normalization techniques applied to the original cadaver data by WG9.

Shoulder. The normalization factors for the shoulder impactor tests used by TNO and TRRL are shown in Table 7 and Table 8.

Thorax Impactor Tests. The normalization factors for the thorax impactor tests used by TNO and TRRL are shown in Table 9 and Table 10.

Thorax and Pelvis Sled Tests. The normalization factors for the sled tests used by INRETS and TRRL are shown in Table 11 and Table 12.

Abdomen Drop. The normalization factor for the abdomen drop test used by TNO is shown in Table 13.

Pelvis Impactor. The normalization factors for the pelvis impactor tests used by INRETS and TNO are shown in Table 14 and Table 15.

Table 7. TNO

TEST	IMPACTOR & TIME.
Test 1	1.17
Test 2	1.18
Test 3	1.18
Test 4	1.16
Test 5	1.20

Table 8. TRRL

TEST	IMPACTOR & TIME.
Test 1	1.22
Test 2	1.25
Test 3	1.23
Test 4	1.26
Test 5	1.25

Table 9. TNO

TEST	IMPACTOR ACC.	T1 ACC.	TIME
Test 1	0.99	1.06	0.99
Test 2	0.98	1.09	0.98
Test 3	0.97	1.11	0.97
Test 4	0.98	1.09	0.98
Test 5	0.98	1.08	0.98

Table 10. TRRL

TEST	IMPACTOR ACC.	T1 ACC.	TIME
Test 1	0.98	1.02	0.98
Test 2	0.97	1.03	0.97
Test 3	0.98	1.02	0.98
Test 4	0.98	1.02	0.98
Test 5	0.98	1.02	0.98

Table 11. INRETS

TEST	THORAX (Time & Force)	PELVIS (Time & Force)	PELVIS Acceleration
7.6 m/s Rigid Wall			
Test 1	0.90	0.82	1.11
Test 2	1.01	0.86	1.08
Test 3	0.95	0.90	1.06
10.3 m/s Rigid Wall			
Test 1	0.99	0.82	1.11
Test 2	1.00	0.86	1.08
Test 3	1.02	0.81	1.11
10.3 m/s Padded Wall			
Test 1	0.93	0.77	1.14
Test 2	0.95	0.79	1/13

Table 12. TRRL

TEST	THORAX (Time & Force)	PELVIS (Time & Force)	PELVIS Acceleration
7.6 m/s Rigid Wall			
Test 1	0.99	0.82	1.10
Test 2	0.98	0.79	1.12
Test 3	1.00	0.80	1.12
Test 4	0.99	0.79	1.12
Test 5	1.00	0.82	1.10
10.3 m/s Rigid Wall			
Test 1	1.00	0.78	1.13
Test 2	1.01	0.78	1.13
Test 3	1.01	0.78	1.17
Test 4	1.02	0.80	1.12
Test 5	0.97	0.75	1.15
10.3 m/s Padded Wall			
Test 1	0.96	0.73	1.17
Test 2	0.95	0.74	1.16
Test 3	0.93	0.74	1.16
Test 4	0.95	0.74	1.16
Test 5	0.96	0.77	1.14

Table 13. TNO

TEST VELOCITY	ARMREST FORCE & TIME.
Test 1 - 1m drop	1.00

Table 14. INRETS

TEST VELOCITY	IMPACTOR & TIME.
Test 1 - 4.62 m/s	0.99
Test 2 - 8.27 m/s	1.03
Test 3 - 6.13 m/s	1.01
Test 4 - 6.08 m/s	1.01
Test 5 - 7.55 m/s	0.99
Test 6 - 8.84 m/s	1.02
Test 7 - 8.97 m/s	1.03
Test 8 - 7.50 m/s	1.01

Table 15. TNO

TEST VELOCITY	IMPACTOR & TIME.
Test 1 - 6.16 m/s	0.98
Test 2 - 6.15 m/s	0.98
Test 3 - 7.94 m/s	0.98
Test 4 - 7.94 m/s	0.98
Test 5 - 10.05 m/s	0.99
Test 6 - 10.04 m/s	0.98

S8-O-03

A Comparison of Hybrid III and Cadaver Thorax Response Under Diagonal Belt Loading

Seán ó Ríordáin, Michelle Ramet, Dominique Cesari, Robert Bouquet
INRETS

Abstract

This paper presents the results of a series of thorax loading tests, in which the aim was to analyze the response of human surrogates in an inline frontal impact when restrained by a diagonal seatbelt. The general results of 33 tests on 20 cadavers and 42 tests on 2 different Hybrid III dummies are reported. The tests show that the energy required to fracture 6 ribs is lower than previously reported at 417 joules. They also show that the Hybrid III is twice as stiff as the cadavers tested in this mode of thorax compression.

Introduction

The purpose of the paper is to present and compare the results of a series of test which were carried out on the thoraxes of the Hybrid III dummy and on cadavers. The tests were designed to test the response of the thorax to a belt loading simulating a frontal inline impact. The tests were carried out by INRETS-LCB in cooperation with NHTSA and Transport Canada. Previous test have been carried out (1) to determine the response of the thorax of volunteers and the Hybrid III to this belt loading. This project was conceived with the aim of extending the severity of the impact using cadavers. In total 33 tests were carried out on cadavers and 42 tests on two different types of Hybrid III dummy. The tests took place over a period of more than two years. These tests clearly demonstrate the comparative reproducibility of the Hybrid III dummy when compared with the very scattered response of cadavers.

Test Methodology

The cadaver and Hybrid III tests were carried out under essentially the same conditions. The human surrogate was placed flat on its back with its lower legs placed on a box to approximate a sitting posture, refer figure 1. A webbing belt supplied by Transport Canada, similar to that used in a car, was placed diagonally across the thorax in a manner similar to that of the diagonal seat belt of a car driver (left hand drive) and such that it passed directly over the sternum. The belt angle was 36 degrees to the centre line of the surrogate. The extremities of the webbing were passed over two low friction bearings and were attached to the ends of a horizontal bar at a pair of force cells. This bar was then

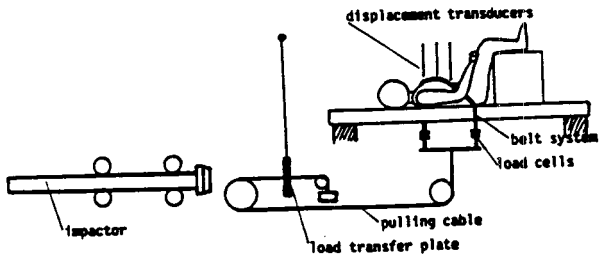

Figure 1. Test Setup

pulled vertically downwards and around a system of pulleys to a suspended catcher plate.

In this series of tests the plate was struck by an impactor which was propelled by a system of powerful elastic bands. The impactor was in "free-flight" for a short period prior to its impact with the catcher plate. The speed of the impactor was measured during this "free-flight" period. Two alternative impactor masses were used in the tests, 22.4 kgs and 76.1 kgs. There was an accelerometer behind the head of the impactor. In addition to the internal thoracic deflections measured on the Hybrid III thorax, 8 (and in some cases 9) external linear displacement transducers were placed vertically above the thorax to measure dynamic compression, a further transducer was placed horizontally on each side (in some cases only on the right hand side) of the thorax to measure lateral enlargement as a result of the compression. Three of the transducer rods were attached directly to the belt, the others were attached to the rib cage directly through the flesh (for both cadavers and Hybrid III). Figure 2 shows the location of the displacement transducers. A high speed camera (1000 f/s) showed the side profile of the cadavers during the tests.

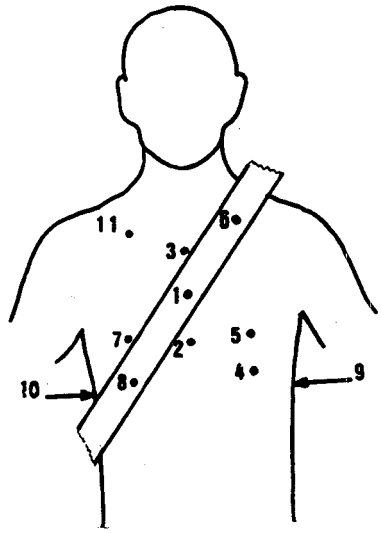

Figure 2. Transducer Locations

Hybrid III Test Results

Forty-two dynamic tests were performed on two different Hybrid III dummies, using both the light (22.4 kgs) and the heavy (76.1 kgs) impactor.

Points 1 (mid-sternum on the belt) and 8 (the lowest floating rib on the right hand side) consistently had the highest deformations. The externally measured deflection was always higher than the internally measured deflection using the original Hybrid III thoracic potentiometer. The internal transducer is attached to the front face of the metal spine of the dummy and measures the deflection of the inside of the metal ribs of the dummy. However the external transducer measures the compression of the dummy with reference to the table on which the dummy is lying, so there are two layers of vinyl skin which are compressed, in addition to the way in which the skin will conform with the shape of the 6 ribs. Regressions are given in appendix 2.

Cadaver Test Results

There were 20 cadavers, 5 female and 15 male of average mass 58 kgs (range 41 to 92.5 kgs), and average age 62 years (range 17 to 86 years). L'Abbé et al. (1) used 7 male volunteers, average mass 77 kgs, and average age 21 years. The average stature of the cadavers was quite high at 1.71 metres. The Livi index for the cadavers varied from 20.3 to 26.6 with an average of 22.3, i.e., comparatively thin. Before any cadaver test the cause of death was determined; cadavers having had a long hospitalization were rejected.

Table 1

	Cadavers	Hybrid III	L'Abbé Volunteers
Age	61.0		21
Height (m)	1.71		
Mass (kgs)	59.8	75.0	77
Li	22.7		

Before each cadaver was tested, they were weighted and measured to determine their detailed anthrometry. A tracheotomy tube was installed in each cadaver, and immediately before a test, the lungs were inflated to restore "normal" thoracic shape; typically, this increased chest depth by the order of 2.5 cm. The tracheotomy tube was left open during the tests.

Two different impactor masses were used, 7 cadavers were tested with an impactor mass of 22.4 kgs, and the other 13 were tested with an impactor mass of 76.1 kgs, 5 of which had previously been tested with a static test in which the deflection did not exceed 1.71 cm. Note that in the previous tests on volunteers (1), deflections of 1.6 to 2.5 cm at the centre of the sternum were considered admissible.

As in the Hybrid III tests, deflection transducers 1 (centre of the sternum) and 8 (at the lowest of the floating ribs on the right hand side, where the thorax is widest) gave the largest deflections. Note that this is almost directly above the liver and gall bladder and that any significant detection at this level (with or without fractures) will impinge on these organs. Note also that the spleen is in a similar position on the left hand side. Transducer number 9 measured lateral extension of the rib cage at the left hand side, however it was found that the measurement values were always less than 0.5 cm, so it was decided to use this transducer in position 11 during the later tests. At autopsy, it was found that more than half of the cadavers had at one or more rib fractures.

Table 2

		NRF	Def.8 (cm)
THC14	Liver damage; Gall bladder torn away	16	7.66
THC20	Liver damage	18	6.22
THC73	Liver tears	9	6.81
THC79	Liver and Spleen damage	3	6.16

There were in general no differences in injury at the same energy level between the two different masses. However the impact duration was significantly different for the heavy and light masses, being of the order of 80 ms for the lighter mass and between 110 and 120 ms for the heavy mass. In addition, there was significant rebound after an impact with the heavy mass, but negligible rebound with the lighter mass. Note also that for an impact of the same energy, the belt tension was significantly higher for the heavy impact mass than with the light mass.

The majority of rib fractures were on the right hand side, the others on the left at the anterior face, under the arc of the belt. In three cases, when using the heavy weight, there were fractures mid-sternum, in the case of THC 71 it was associated with the fractures of the middle rib arches. In the cases of THC 73 and THC 65, there were no rib fractures. In only one cadaver were there fractures on the posterior rib arches, THC 14, which is rarely seen in accidentology.

Based on the regressions on Number of Ribs Fractured (NRF) we have the following (refer to appendix 1 for regression equations):

Table 3

NRF	average deflection cm	95% CI deflection cm	% deflection	95% CI % deflection
1	3.7	3.2 / 4.3	0.19	0.16 / 0.22
6	5.3	4.3 / 6.4	0.27	0.22 / 0.33
10	6.2	4.8 / 8.0	0.32	0.24 / 0.41

NRF	average energy J	95% CI energy J	average total belt force N	95% CI TBF N
1	250	202 / 309	3634	2870 / 4601
6	417	321 / 540	5614	4201 / 7503
10	532	384 / 736	6898	4803 / 9897

Conclusion

This study looked at thorax compression of cadavers and Hybrid III and provided data on human tolerance to belt loading; 6 rib fractures correspond to a belt load of

5600 N and an impact energy of 420 joules. However, it is clear from the confidence intervals above that the variability of the cadavers is indeed large. Furthermore 75% of the cadavers were more than 50 years old, compared with an average of 21 years for the volunteers in L'Abbé's study. However, will we not also protect the younger population when we protect our elders?

Acknowledgements

The results presented in this paper are obtained from a joint programme between NHTSA, Transport Canada and INRETS. The authors would like to thank Mr. Stan Backaitis and Mr. Dainius Dalmotas who organized the technical support for this research programme. The authors would also like to thank the technical staff at INRETS-LCB for their assistance. In particular the authors appreciate the collaboration of Professor Morin and Dr. Bouallegue of the Lyon Faculty of Medicine. The first author would like to extend his thanks and appreciation to Mr. Cesari for the opportunity to be involved in this programme.

References

1. L'Abbé R.J., Dainty D.A., Newman J.A. "An experimental analysis of thoracic deflection response to belt loading" 7th IRCOBI Conference Cologne, 1982
2. Cesari D., Bouquet R. "Behaviour of Human Surrogates Thorax under Belt Loading" SAE 902310; 34th Stapp Car Crash Conf. Proc. 1990

Appendix 1

Regressions on cadaver tests, are given below in a compact format, based on the regression of the dependent variable y on the independent variable x to give the regression equation $y = a + bx$; the coefficients a and b being given in the table below. In addition the Student-t test values are given for each of the coefficients for the null hypothesis H_0: the coefficient {a|b} is zero.

Table 4

		Coefficient		Student's T-test			
Y variable	X variable	a	b	a	b	r^2	n
ln(nrf+1)	ln(%defl)	4.05	1.22	7.05	4.89	0.443	32
ln(%defl)	ln(nrf+1)	-2.03	0.36	-18.67	4.87	0.443	32
ln(nrf+1)	ln(defl)	0.94	0.37	8.90	5.19	0.474	32
ln(defl)	ln(nrf+1)	0.00	0.86	n/a	8.82	(0.715)	32
ln(nrf+1)	ln(energy)	-4.27	0.97	-4.15	5.36	0.525	28
ln(energy)	ln(nrf+1)	4.98	0.54	31.69	5.36	0.525	28
ln(nrf+1)	ln(tbf)	-5.88	0.85	-3.38	4.09	0.391	28
ln(tbf)	ln(nrf+1)	7.74	0.46	44.24	4.09	0.391	28
ln(tbf)	ln(defl)	6.32	1.36	31.71	10.38	0.806	28

Notes

1. "ln(x)" means the natural log of x, i.e., $\log_e(x)$.
2. "nrf+1" means the total Number of Ribs Fractured plus 1, a statistically valid transformation to avoid ln(zero).
3. "defl" means the deflection measured at mid-sternum, i.e., point number 1 attached to the belt.
4. "%defl" means the deflection defl (refer note 2) divided by the pre-test and un-inflated chest depth.
5. "energy" means the impact energy; calculated from the impactor speed immediately prior to impacting the catcher plate and the impactor mass.
6. "tbf" means the Total Belt Force, being the sum of the forces measured at the two ends of the bar underneath the table, as described previously.

Appendix 2

Hybrid III Regressions

Table 5

		Coefficient		Student's T-test			
Y variable	X variable	a	b	a	b	r^2	n
ln(tbf)	ln(defl)	7.05	1.30	66.66	17.96	0.895	40
defl	ln(tbf)	-17.90	2.50	-12.74	15.86	0.869	40
ln(defl)	ln(defh3)	0.77	0.68	21.67	20.61	0.922	38
ln(defh3)	ln(defl)	-0.96	1.36	-9.96	20.61	0.922	38

Notes

1. "tbf" and "defl" as defined in notes in Appendix 1.
2. "defh3" means the deflection measured internally in the Hybrid III thorax.

S8-O-04

The Use of a Multi-Accelerometric Method in Automotive Safety Tests

L. Oudenard, F. Bendjellal, A. Bellini, J. Uriot
Peugeot S.A./Renault

Abstract

Following the specific work of evaluation of methods for computing angular acceleration from the measurement of linear accelerations, the results of which are set out in a previous publication, two concrete applications were implemented with complementary objectives:

- Evaluate the sensitivity of angular acceleration measurement for an impact with airbag as compared to a direct impact on the steering wheel.
- Estimate the precision of the measurements taken by studying the 3D kinematics of a steering column (with dummy) by comparison with a vehicle without a conventional film study.

In both cases, the results obtained have shed light on aspects which could not have been detected any other way (influence of the airbag on head data other than the HIC, dummy/steering column interaction). This study also provided an opportunity of evaluating the Nxl computation method developed in the laboratory. This method allows full use to be made of the measurement potential provided by accelerometer mounts APR 89/II and APR 89/III, composed of 5 or 6 accelerometric triaxes.

Introduction

The determination of angular acceleration and head dynamics in biomechanics experiments is one of the main centres of research at the APR. Up until now, the studies performed at the APR in this field were chiefly concerned with the tolerance of the head in frontal impact and the development of a methodology allowing angular acceleration to be determined by means of a multi-accelerometric approach (1).

The present paper, which is a continuation of this work, proposes describing concrete cases of application of the multi-accelerometric methodology, especially in relation to the interests of car makers.

Reminder Concerning Angular Acceleration Computation Methods

There are four possible methods of computing angular acceleration based on linear acceleration measurements (the figures in brackets refer to the bibliographic references). Three have already been described (1):

- the 3x3x3 method, developed by N.M. Alen et al. (UMTRI) (2)
- the 3x2x2x2 method, developed by Padgaonkar et al. (WSU) (3)
- the in-line method, developed by Viano et al. (GM) (4)

The fourth, which will now be described, is called:

- Nx1. This method was developed by D. Lestrelin (5). It is a generalization of the 3x3x3 method extended to a number of channels in the range between 6 and 18. This method has the advantage of considering each of the channels separate from one another and thus allowing computation when the channels required for computation by the aforementioned methods are missing.

Comment: The mathematical development of this method is presented in the Appendix.

Experimental Conditions and Methodology

Multi-Accelerometric Mount for Head of Hybrid III 50th Percentile

The APR 89III mount, shown in Figure 1, consists of a monobloc part in light alloy which can be fitted onto the Hybrid III head.

This mount, measuring 112 x 92 x 69.5 mm and weighing 290 g, is attached directly to 3- or 6-axis upper neck transducers. It is designed to receive up to 6 ENTRAN EGA SY three-axis accelerometers, thus allowing measurement of up to 18 linear accelerations. The centre of gravity of the mount was designed to coincide on the one hand with the centre of gravity of the dummy's head, and on the other hand with the centre of seismic masses of sensor No. 4. Figure 2 illustrates the position of the mount in the dummy's head. The characteristics of the APR 89III mount are as follows:

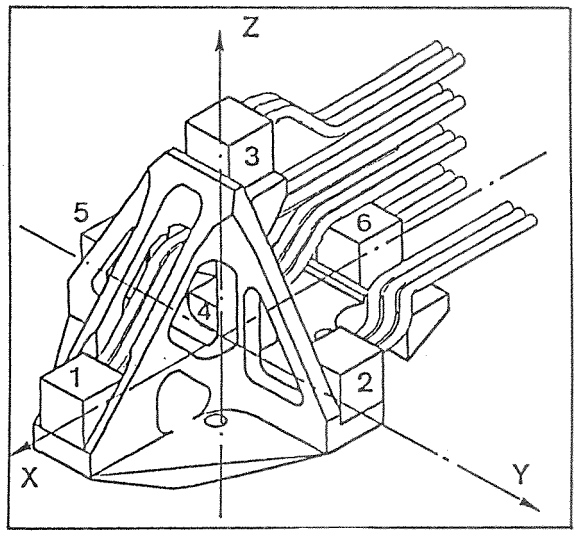

Figure 1. APR 89III Mount - A 18: Rigid Accelerometer Mount Specially Designed for the Hybrid III Test Dummy

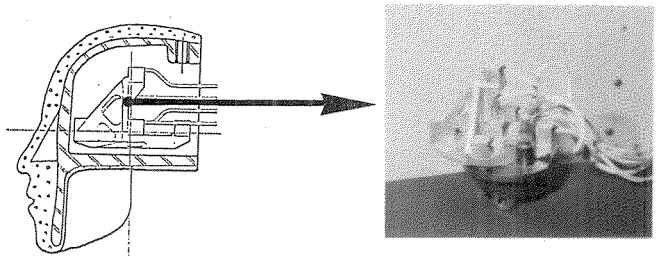

Figure 2. APR 89III Accelerometric Mount as Fitted to the Hybrid III Head

- Lightweight device of sufficient stiffness to give a satisfactory frequency response at up to 3000 Hz. Its vibration behaviour is described later.
- Use of CAD techniques to facilitate manufacture.
- Mount dimensions compatible on the one hand with the computing criteria in particular the distances between linear acceleration measurement points—and also with the space available inside the Hybrid III head.
- Easy assembly on the neck transducers (3- or 6-axis) and easy installation of measurement wires.
- Number of three-axis sensors and layout of sensor measurement axes allowing angular acceleration of the head to be computed by various methods.

Comment: This mount can also be used to analyze the kinematics of other items, such as the steering column. This configuration, moreover, is dealt with elsewhere in this paper.

Vibratory Assessment of the Accelerometer Mount

To be sure that the mount is not likely to affect the measurements, a vibration study was performed. This study showed that the mount's first resonant frequency (mode 1) is situated at approximately 3500 Hz on the XOZ plane, at more or less 45° from the X and Z axes

(cf Figure 3). The second mode, at more than 4 kHz, is oriented along the Y axis.

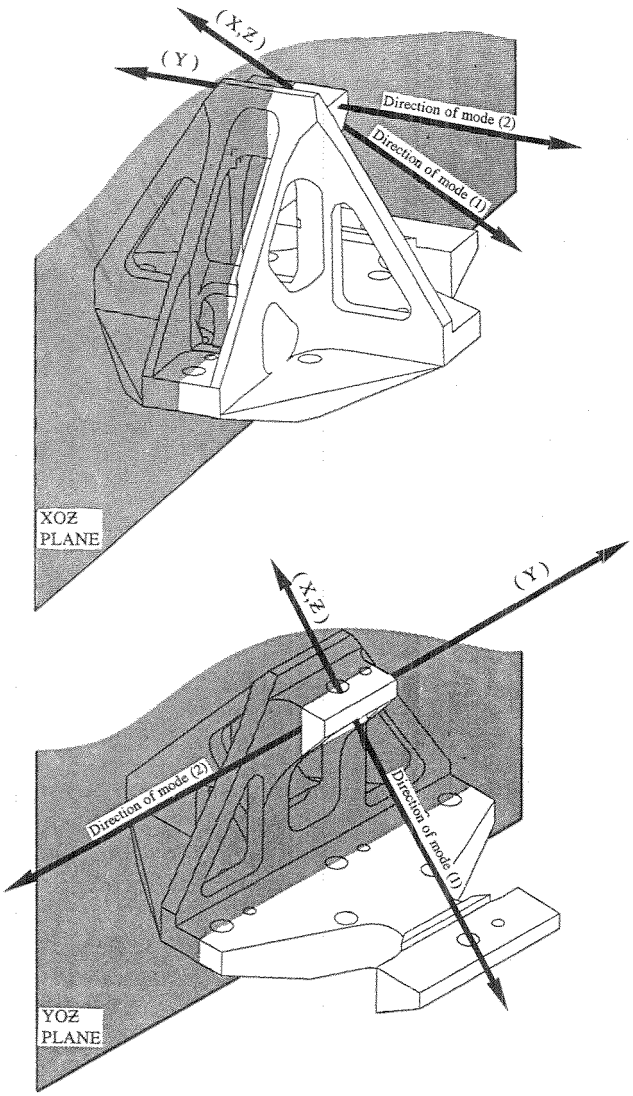

Figure 3. Orientation of Vibration Modes of the Mount as Obtained from Evaluation Tests

Overall, the frequency of the first mode and the corresponding resonance amplitudes are consistent with the filtering quality required by the head signals (filtering at 1650 Hz at -24 dB per octave).

Moreover, from the very structure of the mount one can observe that the sensor located at the top is the most exposed to vibrations. The vibration study performed on the mount confirms this hypothesis. However, the level of the first vibration modes is satisfactory (cf. Table 1).

Comment: The measurements were performed with BRUEL and KJAER 4374 sensors assembled in the same way (on a triaxial cube) as the ENTRAN EGA SY 500G sensors. A typical curve obtained during this study is shown in Figure 4.

Table 1. Vibration Behaviour of the APR 89III Mount: First Modes and their Amplitude Measured at the Location of the "SUMMIT" Sensor

EXCITATION AXIS	SENSOR LOCATION	SUMMIT		
	MEASUREMENT AXIS	X	Y	Z
X	Mode 1 (Hz)	3465	3465	3465
	Level (dB)	31.33	17.09	24.99
Y	Mode 1 (Hz)	3500	/	/
	Level (dB)	2.30	/	/
Z	Mode 1 (Hz)	3485	3485	3485
	Level (dB)	18.26	4.34	11.89

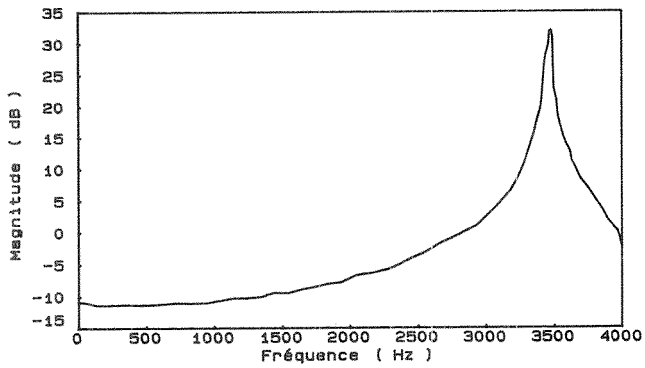

Figure 4. Frequency Response of the Accelerometric Mount Obtained from Vibration Tests

Application to Crash Tests

The two tests used for the study, while based on the same methodology, have different objectives.

The first test, which is a comparison of head/steering wheel impacts with and without airbag, is designed to provide additional criteria for evaluating the safety gained by using the airbag.

The second test is designed to evaluate the precision of the angular acceleration computing methods and the technologies employed to determine the kinematics of a steering column in impact, on the basis of linear acceleration measurements.

Comparison of Impact between Head and Standard Steering Wheel and Head and Steering Wheel Provided with an Airbag

This study was performed on a sled at 52 km/h in 0° frontal impact. The deceleration law is that of a vehicle of the PSA range. The airbag used is of the EUROBAG type (inflated volume = 25l).

For the purpose of the test, a Hybrid III dummy is equipped with the 18-channel mount used in its complete configuration (6 triaxial sensors) and mounted on the upper 6-axis neck transducer.

Measurement of Steering Column Displacement in the Presence of a Dummy

This crash test was performed on a vehicle of the PSA range at 56 km/h in 0° frontal impact.

The 18-channel mount (reduced to 15 channels, or five 3-axis transducers in a specific variant to allow for these new test conditions) was mounted directly on the steering column (cf. Figure 5).

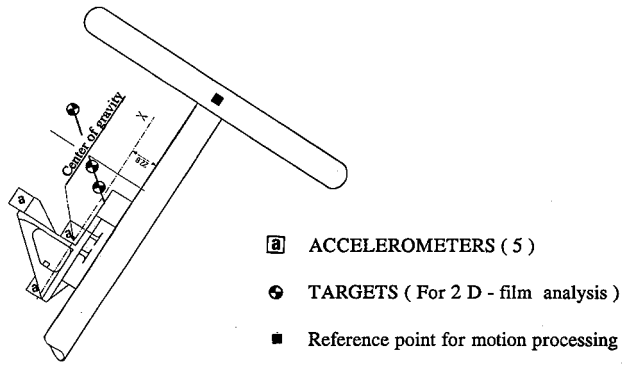

Figure 5. Position of the 12-Accelerometer Array with Respect to Steering Column Assembly

It can show the 3D kinematics of the steering column relative to the laboratory reference. The 3D kinematics of the column relative to the vehicle was obtained by determining the vehicle's kinematics with respect to the laboratory by means of a 3D film analysis.

It was decided to limit the application of the accelerometric method to steering column movement, knowing that this part of the vehicle is not easily accessible to film analysis during an impact, especially in the presence of a dummy. For the vehicle kinematics, movements were analyzed by monitoring the movements of photographic targets attached at the rear as shown in Figure 6.

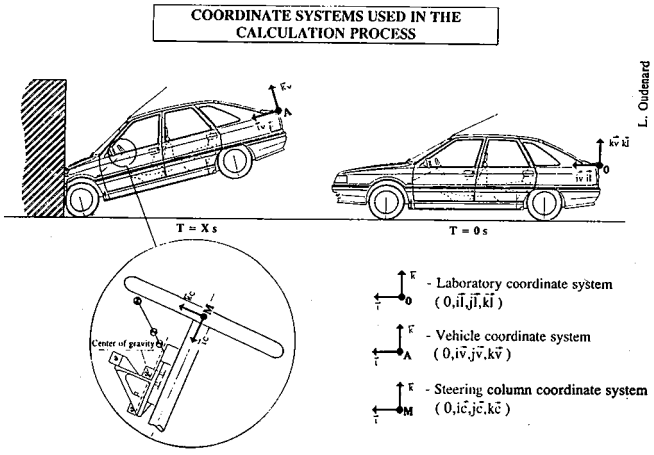

Figure 6. Definition of the Necessary Coordinate Systems Used in the Computation of Steering Wheel Motion (in a 0°, 56 Km/h Crash Test)

The orientation and positioning of the 15-channel mount were determined from dimensions measured at several points by a 3D test bench.

The origin of the measurement reference was confounded with one of the 3 spherical targets (in this case, the rear left) used for film analysis of the 3D kinematics. This reference is confounded with the laboratory reference at t = 0 ms (cf. Figure 6).

Results

Comparison of Impact Between Head and Standard Steering Wheel and Head and Steering Wheel Provided with an Airbag

General. Both tests were performed in repetitive conditions, since the speeds at impact and the deceleration laws are similar.

Before considering the head/neck segment of the Hybrid III dummy, it is very interesting to compare the main results for the other body segments for both tests, so as to evaluate the influence of the Airbag on those segments (cf. Table 2).

Table 2. Main Results Obtained With and Without Airbag, Respectively, for the Thorax and Pelvis Segments (Hybrid III Dummy in Driver Position)

			STEERING WHEEL	AIRBAG
LINEAR ACCELERATION (MAX) (G)	THORAX	X	56	60
		Z	16	18
	PELVIS	X	57	52
		Z	19	16
FORCE (MAX) (daN)	LUMBAR	Fx	360	415
		Fz	-145	-238
	External Lap-Belt		884	810
	External Shoulder-Belt		983	919
LUMBAR (MAX)	MOMENT (Nm)	My	302	288
THORACIC (MAX)	DEFLECTION (mm)		49	47

This table shows the similarity between the two series of tests. The gain at the level of seat-belt forces is slight, and at the thorax level it is zero. Deviations are observed on the level of lumbar forces, which are hard to explain. Accordingly, the influence of the airbag is insignificant for the body segments mentioned, which is normal given that its volume is small (25 litres) and it covers only the head, the neck and the upper part of the thorax.

Head/neck segment: determination of angular acceleration. After checking the accelerometric signals measured on the APR mount, it was decided to discard the signals measured by the 3-axis transducers located at the level of the nose (1) and the right temple (5) (cf. Figure 1), and to use only the remaining 3-axis transducers with

the WSU 3-2-2-2 computing method. In this way, the best computation agreement was obtained.

Table 3 allows the effectiveness of the airbag to be assessed from the data measured and computed at the head and neck levels.

Table 3. Comparison of Head and Facial Data Obtained from Head/Steering Wheel and Head/Airbag Impacts

			STEERING WHEEL IMPACT	AIRBAG
HIC			1043	555
HIC 36 ms			785	459
ANGULAR ACCELERATION OF HEAD (rad/s²)	X	min.	- 1675	- 1999
		max.	2342	721
	Y	min.	- 4241	- 2651
		max.	4039	2936
	Z	min.	- 3261	- 1047
		max.	4497	1337
LINEAR ACCELERATION OF HEAD CG (MAX) (G)	X		- 104	- 43
	Y		12	10
	Z		- 47	- 43
INITIAL CONDITIONS	HEAD ANGULAR VELOCITY (rad/s)		0	0
	HEAD ANGLE OF INCLINE (degrees)		19	14
	INITIAL VELOCITY (m/s)		14.26	14.20
Max. FACIAL CONTACT FORCE	(k N)		4.65	2.25
DURATION OF HEAD CONTACT	(m s)		29	54

Angular acceleration is considerably reduced by the airbag (by about 30%). Linear accelerations, the HIC and the force applied to the face are reduced by approximately 50%. However, one observes that contact time is doubled by the airbag (spreading effect), which is logical given the equivalent energy to be dissipated.

Angular acceleration of the head. The analysis proposed below allows interpretation of the angular acceleration values obtained (cf. Figure 7).

The high level of angular acceleration around the OY axis shows that the movement is virtually planar except at the end of contact, when torsion is distinguished around the OZ axis visible on the film.

The oscillations observed over time can be explained by the different stiffnesses of the impacted regions on the steering wheel (rim less stiff than the hub).

The same procedure is applicable to the airbag test. However, we merely give the curves of angular acceleration (cf. Figure 8). ωy is preponderant with respect to ωx and ωz, throughout the impact. Thus, the movement remains planar (absence of torsion at end of impact, and ωz remains insignificant). The contact (longer) shows numerous oscillations generated by the instability of the

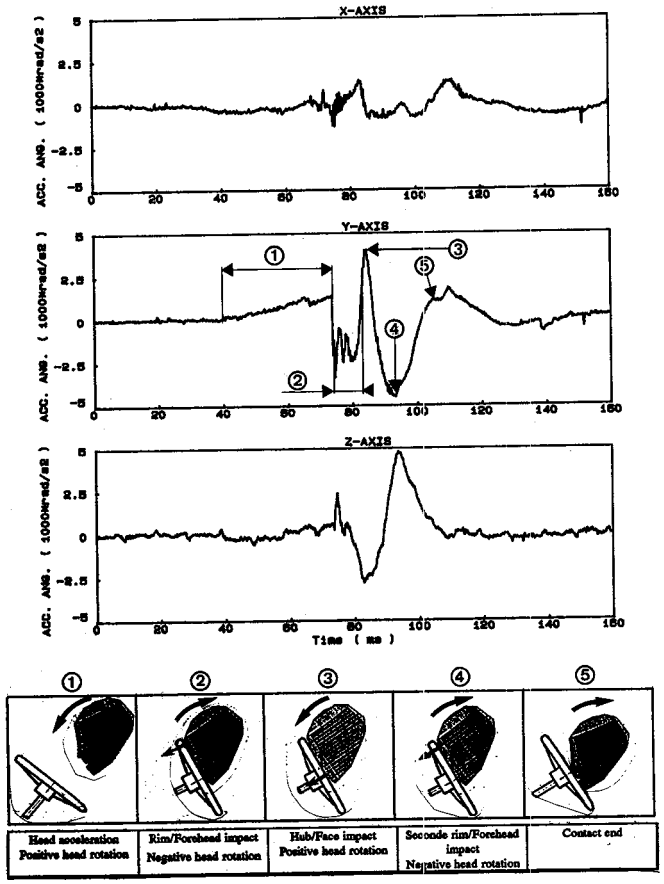

Figure 7. Angular Acceleration of the Head and Head/Steering Wheel Contact Sequences (Frontal Sled, 3 pts Belted Dummy, 52 Km/h)

head/airbag system. Phase 1 of the head's forward movement is shorter than during the head/steering wheel test due to inflation of the airbag, and accordingly much less angular acceleration is generated.

Determination of the point of impact of head contact. The determination of the point of impact over time provides us with two important items of information.

- The duration of contact is doubled with the airbag (54 ms instead of 29 ms).
- The point of impact moves with time. This movement can easily be monitored for head/steering wheel impact.

Moreover, it can be determined that two areas are affected:

- the forehead by the rim;
- the lower part of the face by the hub (cf. Figure 9). This area is less affected for the airbag impact, since the head is thrust into the airbag and the point of impact given by the computation corresponds to the position of the resultant force vector applied to the face (cf. Figure 10).

Force applied to the face. Computation of the force applied to the face shows that:

- The airbag reduces the force by a factor of 2. Moreover, a phenomenon of filtering of maxima peaks is observed (cf. Figure 11);

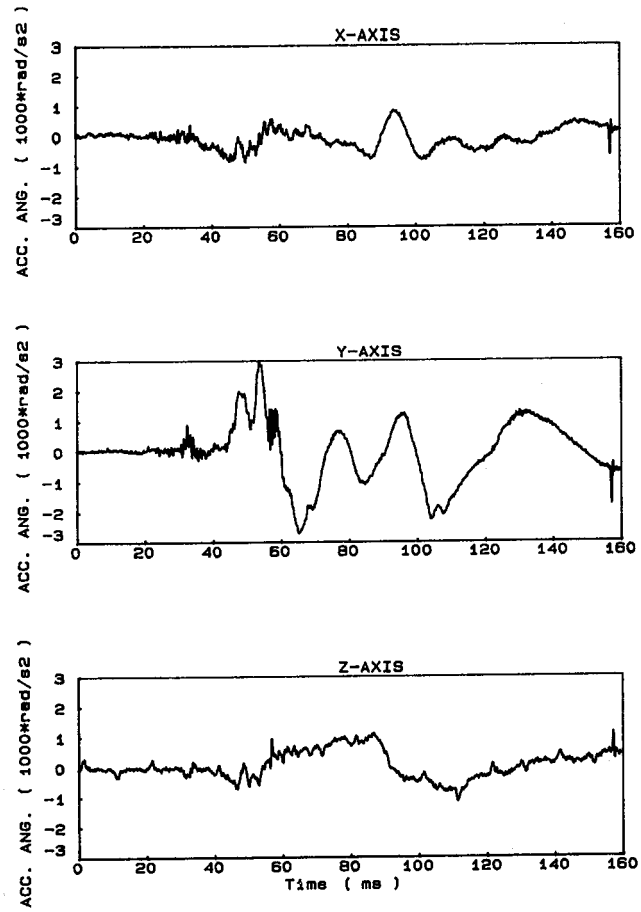

Figure 8. Head Angular Acceleration in a 52 Km/h Frontal Sled Test: 3 pts Belted Dummy + Airbag

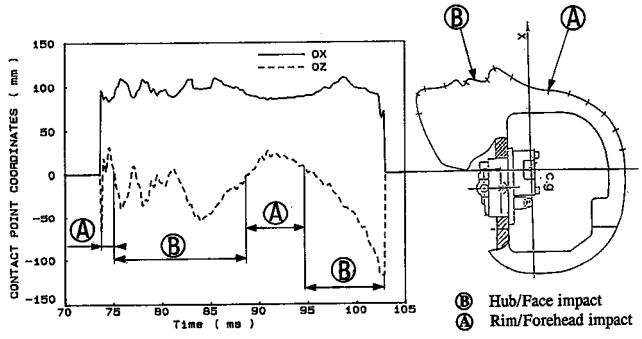

Figure 9. Coordinates of Head Contact Point as a Function of Time in Frontal Sled Test (With Head/Steering Wheel Contact)

- On the contrary, the head/steering wheel impact generates rather strong peaks which, when correlated in time to the point of impact, show (cf Figure 12) that there are two force peaks at approximately 4600 N and 3100 N applied to the maxillary.

Measurement of Steering Column Displacement in the Presence of a Dummy

General. A fairly comprehensive comparative study of the available computation methods was able to be performed, given the good quality of the 15 measurement channels.

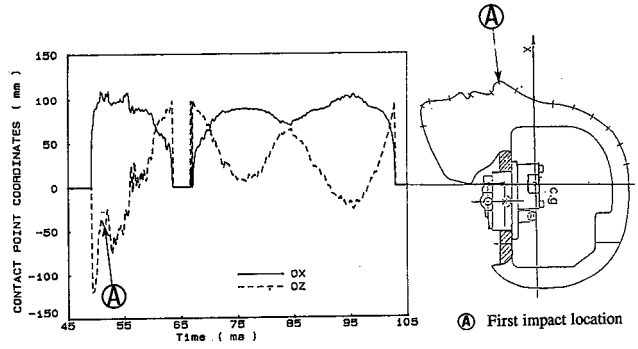

Figure 10. Coordinates of Head Contact as a Function of Time in Frontal Sled Test with Driver Airbag

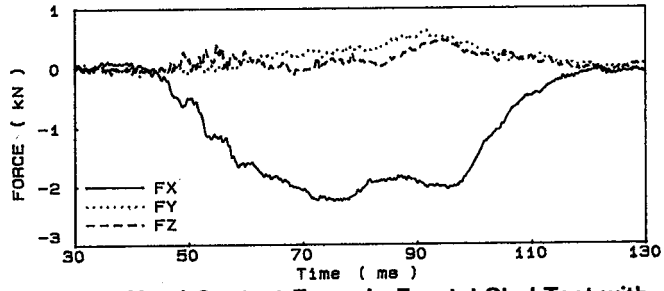

Figure 11. Head Contact Force in Frontal Sled Test with Driver Airbag

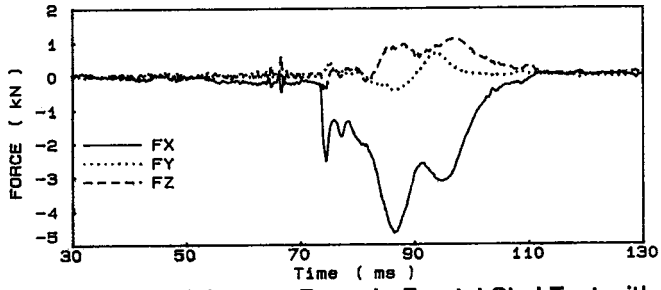

Figure 12. Head Contact Force in Frontal Sled Test with Head/Steering Wheel Impact

With the 3-2-2-2 and 3x3x3 methods we obtain satisfactory results, which are very similar. However, it appears that the Nx1 method, due to the use of redundant channels (and the optimization of data in the sense of the least squares), provides greater precision in term of kinematics. Accordingly, the following results were obtained by that method.

The measurement of angular acceleration at the steering column level showed that (cf Figure 13):

- The angular acceleration peaks are correlated to interactions of the column with its immediate environment. The curve in Figure 13 can be broken down into three phases:
  - Series of positive peaks: thrust of the front part of the vehicle against the column ==> rearward displacement and rising of the column;
  - Series of negative peaks corresponding to the thrust of the dummy against the column ==> the first two peaks correspond to the action of the femurs, the following two to the action of the thorax and head;

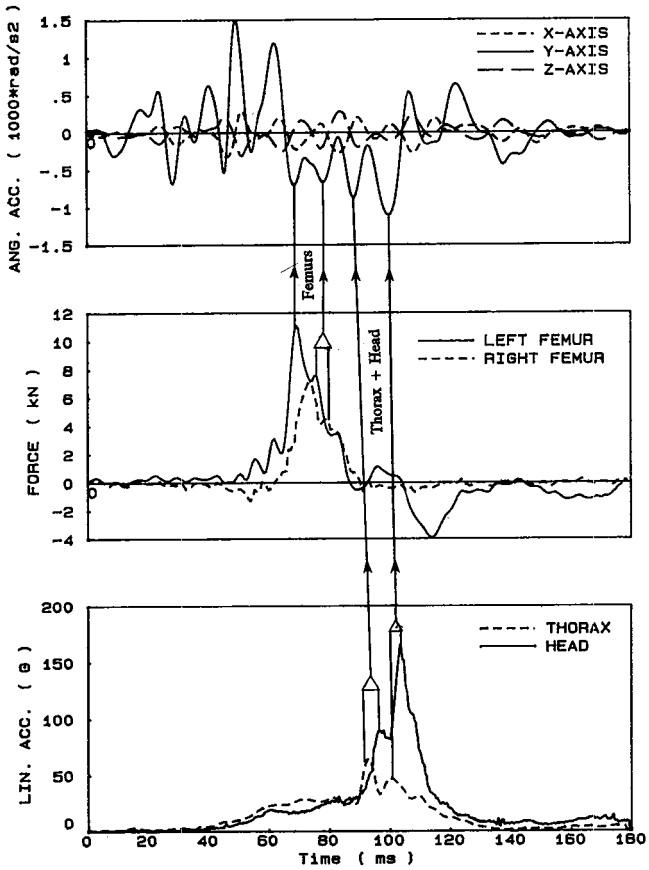

Figure 13. Correlation Between Steering Column Angular Accelerations and Dummy Parameters Obtained in a 56 Km/h, 0° Frontal Crash Test

- New series of positive peaks: further interaction of the vehicle on the column at end of impact.

Comment 1: The curves are filtered to CFC 60 to comply with the filtering class used for the vehicle.
Comment 2: Note that the linear speed curves for the column show that the column is virtually motionless during head/thorax impacts (cf. Figure 14).

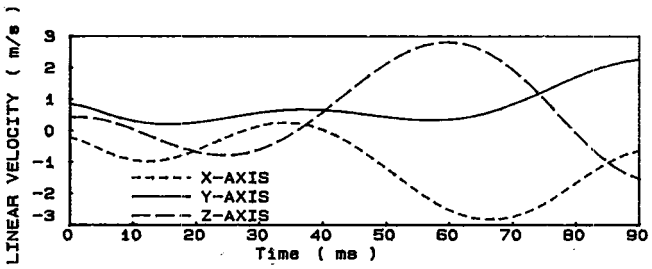

Figure 14. Linear Velocity of the Steering Wheel Hub with Respect to Vehicle Coordinate System: Data Obtained Using a Multi-Accelerometric Method

3D Kinematics of the Steering Wheel Column with Respect to Vehicle Coordinate System

Quality of results. The imprecisions related to computation of the double integration of linear accelerations and the orientation matrix at every moment generate a divergence which appears mainly after the maximum of column movement along the X axis (which expresses the retraction). Thus, the results presented should be taken into account only up to approximately 90 ms.

Steering column movements. One observes (cf Figure 15) that the column movement is three-dimensional:

- column retraction (negative X)
- column offset (positive Y)
- column rising (positive Z)

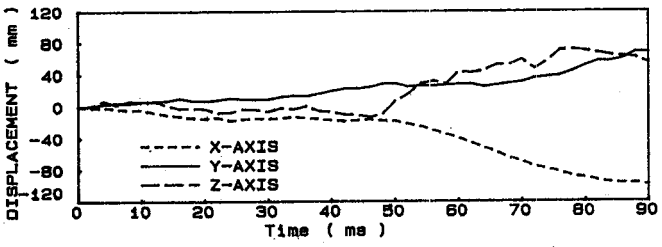

Figure 15. Linear Rearward Displacement of the Steering Wheel Hub with Respect to Vehicle Coordinate System (in a 56 Km/h Crash Test)

Trajectories. The trajectories in the 3 main planes show that (cf. Figure 16):

- on the one hand, the movements along X and Z are correctly correlated, i.e., $f(X) = Z$.
- on the other hand, the movements along X and Y and along Y and Z are weakly correlated. Accordingly, in this case, the column movement is composed of a rotation combined with a translation in the XOZ plane and a pure translation along the OY axis.

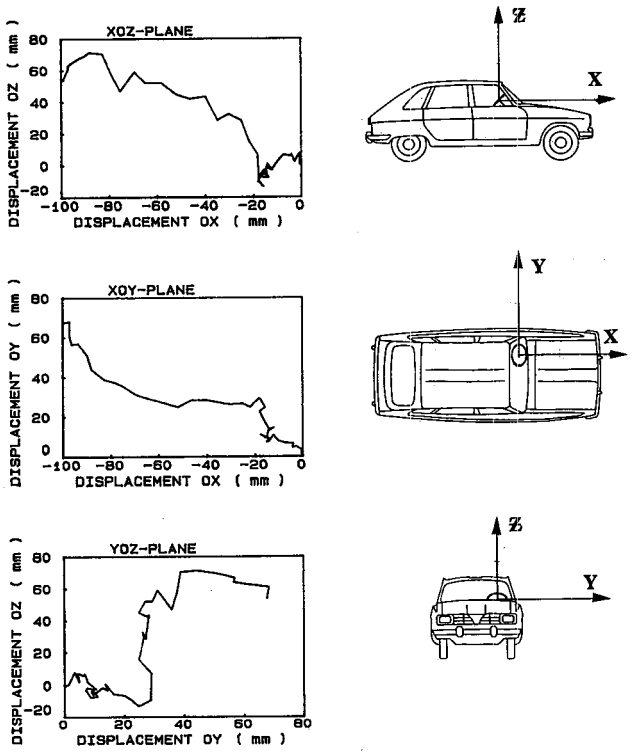

Figure 16. Trajectories of the Steering Wheel Hub with Respect to Vehicle Coordinate System in Resp. 3 Principal Planes

Orientation. Figure 17 expresses the column orientation over time (the non-null initial angles express the column orientation relative to the vehicle reference at t = O ms).

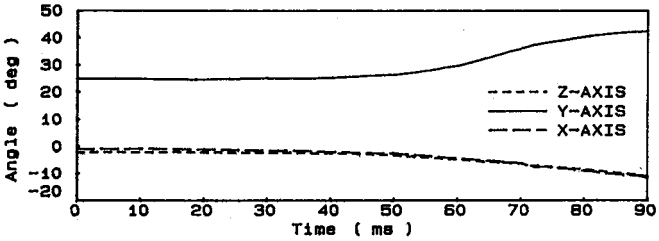

Figure 17. Steering Column Rotations (Euler Angles) Expressed in the Vehicle Coordinate System

Euler's angles show that column rotation takes place exclusively around the OY axis. The regular increase in value of rotation around the X and Z axes reflects the trend to divergence of the computation.

Verification of results. To validate the results obtained, two types of checks were performed:

- the first on the basis of a 2D film analysis allowing the film movements to be compared with those of the computation in the XOZ plane (cf Figure 18);
- the second by comparing the maximum movements obtained with the measurements obtained on 3D test bench before and after the impact (static measurement).

On the whole, the results are satisfactory.

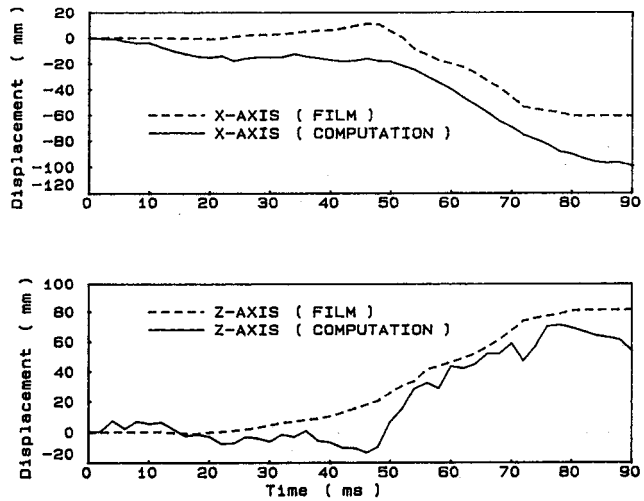

Figure 18. Comparison of Computed Steering Column Displacements with those Obtained from Film Analysis

Quite expectedly, the computed column retraction X (dynamic) is twice as great as the static retraction measured:

Xdyn = -99.3 mm
Xstat = -43.07 mm

The computed column offset Y is close to the measured value:

Ydyn = 67.5 mm
Ystat = 51.5 mm

The same applies to column retraction:

Zdyn = 58.2 mm
Zstat = 61.34 mm

The computed steering column rotations (Euler's angles) along the three axes are consistent with those recorded during 3D film analysis. However, one observes an attenuation of the main rotation [around OY (σ)] and an increase in the secondary angles [(ψ and ρ)] related to a slight divergence in computation over time.

- Measurements (static)
  ψ = -0.63°
  σ = 21.97°
  ρ = -5.59°
- Computation
  ψ = -10.74°
  σ = 17.34°
  ρ = -9.14°

Summary and Conclusions

The objective of this study is to evaluate application of a multi-accelerometric method, already developed for dummies, to car safety tests.

Two concrete applications are presented. In the first case the contribution of the angular acceleration to the analysis of two types of head impacts is evaluated. The second application consists of the calculation of steering column rearward displacement in frontal crash test.

In the first case, by determining:

- the angular acceleration (factor regarded as very important in the process of cerebral lesions);
- the force vector applied to the face in the form of a modulus and a point of application;
- the duration of impact;

it is possible to refine the analysis of head impact.

The second case shows that it is possible to approximate the kinematics of a solid object such as the steering wheel without having to analyze a film. The displacements obtained from the accelerometric approach are compared with those provided by conventional film analysis. This comparison shows acceptable convergence during the whole dynamic motion of the steering wheel column. This can be especially useful when the object to be analyzed is hard to track by camera.

However, the operation is still complicated to perform, and analysis is fairly long due to the combination of accelerometry and 3D film analysis.

As a consequence, and to optimize the analysis of steering column rearward displacement, it is conceivable to adopt one of the following options:

- The accelerometric approach with reduced measurement channel number but applied to the solid bodies formed by the column and vehicle.
- The approach combining accelerometry (3 channels) and direct measurements of angular velocity, likewise applied to the two solids.

Generally speaking, this article is one step in a process which aims at optimizing the application of accelerometry to concrete cases of automotive safety.

Acknowledgements

We should like to thank Philippe Mack and Laurent Bouchard for their help in obtaining the published results and Nathalie Merle for typing of the manuscript. We express our gratitude to the PSA crash test laboratory at La Garenne Colombe for carrying out the tests, and in particular to Messrs Mauron, Brutel, Huere and Fournier.

References

(1) F. Bendjellal et al., "Dynamics in various impact situations," Proceedings of the 34th Stapp Car Crash Conference, SAE Technical Paper 902320, November 1990.

(2) M. Nabih Alem and Holstein, L. Garry, "Measurement of 3D Motion," HSRI, Ann Arbor, Michigan, October 1977.

(3) A.J. Padgaonkar, K.W. Krieger and A.I. Wing, "Measurement of Angular Acceleration of a Rigid Body Using Linear Accelerometers," ASME, Journal of Applied Mechanics, September 1975, 552-556.

(4) D.C. Viano, J.W. Melvin, J.D. McCleary, R.G. Madeira, T.R. Shee, J.D. Horsch, "Measurement of Head Dynamics and Facial Contact Forces in the Hybrid III Dummy," Proceedings of the 30th Stapp Car Crash Conference, SAE Technical Paper 861891, October 1986.

(5) D. Lestrelin, "Calcul de l'Accélération Angulaire de la Tête: Programmes Disponibles au Laboratoire APR," Personal paper, 1983.

Appendix: N x 1 Accelerometric Method

In the following, a brief presentation of this method is presented. As mentioned previously the N x 1 method is a generalization of the 3-3-3 method developed by Alem (2). The N x 1 method was developed to solve the cases of rigid body motion where some data channels are missed. It consists of an extension of the 3-3-3 case by processing each data channel separately.

Notation

In the following, we shall note:

- { P } as a vector of dimension n
- [P] as a matrix of dimension n x n in such a way that the matrix product [P] { v } represents the vector product { P } x { v }
- (A) as a matrix 1 x n.

The 3-3-3 Method

This method is applied to 3 sets of 3 accelerometers, located respectively at points P_1, P_2 and P_3. The absolute acceleration A_{pi}, of a point P_i, in a rigid body is given by the vector equation:

$$(1) \quad \vec{A}_{P_i} = \vec{A}_R - \vec{PiR} \times \vec{\dot{\omega}} + \vec{\omega} \times (\vec{\omega} \times \vec{PiR}) \; i = 1 \ldots 3$$

Where

$\vec{A}_R$ is the linear acceleration of a reference point

$\vec{PiR}$ is the position vector of point Pi relative to R

$\vec{\dot{\omega}}$ is the angular acceleration vector of the rigid body

$\vec{\omega}$ is the angular velocity vector of the rigid body

$\times$ is the vector product

Using notations presented previously the equation (1) can be written as follows:

$$(2) \quad \{A_{P_i}\}_{i=1\_3} = \{A_R\} - [PiR]\{\dot{\omega}\} + [\omega]\{[\omega]\{PiR\}\}$$

If we considered point R as the center of gravity of points P_1, P_2 and P_3, then it can be shown that:

$$(3) \quad \{A_R\} = \{\{A_{P_1}\} + \{A_{P_2}\} + \{A_{P_2}\}\} / 3$$

This yields a resulting expression with a system of 3 simultaneous differential equations in which unknowns are the angular velocity components and their derivatives:

$$(4) \quad [PiR]_{i=1\_3}\{\dot{\omega}\} = \{A_R\} - \{A_{P_i}\} + [\omega]\{[\omega]\{PiR\}\}$$

Which can be written as follows:

$$(5) \quad \{\dot{\omega}\} = ([P]^t [P])^{-1} [P]^t \{V\}$$

Where

$$[P] = \begin{bmatrix} [P_1R] \\ [P_2R] \\ [P_3R] \end{bmatrix} \text{ with dimension of } P : 9 \times 3$$

$$\{V\} = \begin{Bmatrix} \{A_R\} - \{A_{P_1}\} + [\omega]\{[\omega]\{P_1R\}\} \\ \{A_R\} - \{A_{P_2}\} + [\omega]\{[\omega]\{P_2R\}\} \\ \{A_R\} - \{A_{P_3}\} + [\omega]\{[\omega]\{P_3R\}\} \end{Bmatrix}$$

System (5) can be therefore solved using conventional numerical technics. The resulting angular accelerations and velocities are the best estimates of the true solution, in the least-squares sense.

The N x 1 Method

If one or more channel measurements are missed, the use of the center of gravity of points Pi becomes impossible. Let N_v is the number of available acceleration measurements with $N_v \geq 6$. If each acceleration component is expressed with respect to the head anatomical coordinate system, then the set of equations (2) becomes:

$$(6)\quad A_{Pi} = (C_i\{A_R\} - (C_i)\{[PiR]\{\dot{\omega}\}\} + (C_i)\{[\omega]\{[\omega]\{PiR\}\}\} \qquad i = 1..N_V$$

Where

subscript i refers to channel i

(C_i) are the components of a unit vector oriented along the measurement direction of channel i

[PiR] is the position vector of channel i located at point Pi with respect to the reference point

$\{A_R\}$ is the linear acceleration of the reference point (unknown)

System (6) is a set of N_V simultaneous differential equations in which the unknowns are the angular velocity components (ω), their derivatives ($\dot{\omega}$) and the linear acceleration components (A_R).

Equation (6) can be written as follows:

$$(7)\quad R\{X\} = \{V\}$$

Where

$$R = \begin{bmatrix} (C_1)\{P_1R\} & -(C_1) \\ (C_2)\{P_2R\} & -(C_2) \\ \cdot & \\ \cdot & \\ (C_{N_V}\{P_{N_V}R\} & -(C_{N_V}) \end{bmatrix} \quad \text{Dimension of } R : N_v \times 6$$

$$\{V\} = \begin{matrix} (C_1)\{[\omega]\{[\omega]\{P_1R\}\}\} - \{A_{P1}\} \\ (C_2)\{[\omega]\{[\omega]\{P_2R\}\}\} - \{A_{P2}\} \\ \cdot \\ \cdot \\ (C_{N_V})\{[\omega]\{[\omega]\{P_{N_V}R\}\}\} - \{A_{N_V}\} \end{matrix}$$

and

$$\{X\} = \begin{Bmatrix} \dot{\omega} \\ A_R \end{Bmatrix}$$

The task now is to solve, using the conventional numerical techniques (Runge Kutta or Predictor Corrector) the following system:

$$(8)\quad \{X\} = (R'R)^{-1}R'\{V\}$$

where R^t is the transpose matrix of R.

S8-O-05

EUROSID I and BIOSID Impact Response Characteristics vs. ISO Biofidelity Requirements

F. Bendjellal, G. Fuld, E. Hautmann, M. Koch, H. Marks, A. Pastorino
ACEA Working Group on Dummies

Abstract

This paper deals with responses of BIOSID and EUROSID I side impact dummies as regards biofidelity requirements set up by ISO/TC22/SC12/WG5. Each dummy was subjected to a series of sled, impactor, and drop tests in order to assess the behavior of dummy segments such as the neck, shoulder, thorax, abdomen and pelvis. Besides the biofidelity evaluation, other dummy characteristics are discussed, i.e., repeatability and reproducibility. The main results of the present study confirm that both dummies, although showing better performance than their predecessors, still need to be further developed so that they could be used as a development and certification tool.

Introduction

Soon after the introduction, a few years ago, of the "prototype" EUROSID side impact dummy, CCMC (now ACEA) launched an extensive laboratory and full-scale impact test programme [1] to compare it to the other then available side impact dummy, the SID, developed by NHTSA. The main conclusion drawn at that time was that neither dummy seemed to meet the need for a biomechanically representative human surrogate, which furthermore also could withstand the severe impact forces in full-scale testing and give reproducible and repeatable results.

Since then the EUROSID has been further developed resulting in the present "production type" EUROSID I. Other efforts to produce a testing device which better corresponds to established requirements have led to the creation of the SAE-BIOSID. Consistent with its original goal of assessing the characteristics of different side impact dummies, CCMC decided to also evaluate the performance of these devices. This programme, initiated by ACEA, represents the contribution from the European automobile industry to similar activities being performed by MVMA and JAMA.

It is important for the automobile industry, and for its customers—the car occupants, to introduce safety related design changes and improvements based on decisions from the use of test tools as reliable as possible. These

tools should be developed and supported by a broad data base. CCMC/ACEA therefore decided to include also the BIOSID in an evaluation programme.

Given the difficulties experienced with the purchase of either dummy due to long backlogs in orders at their producers and the high purchase prices involved, CCMC/ACEA's evaluation programme had to be limited to laboratory tests. It is recognized that a final decision on which version of the EUROSID will have to be used for a European side impact test should be based on a broader footing, including full-scale test results. However, as the implementation of mandatory compliance testing cannot be the responsibility of the regulated industry, it is suggested that governments and other public authorities participate in the creation of the full-scale test data base.

The following laboratories have been entrusted with performing the actual testing of the different body segments of the dummies:

- Institute of forensic Medicine of the University of Heidelberg (in the following referred to as "HEIDELBERG": Rigid and padded wall sled tests to evaluate the behavior of the thorax and pelvis);
- TNO: Drop tests involving the abdomen, and lateral neck bending tests;
- UTAC: impactor tests of the thorax and pelvis.

These tests were performed according to the procedures defined in documents TR 9790 except for the thorax for which the latest reference TC22/SC12/WGS N 249 was used. The data reported in the following were provided by the laboratories mentioned above and analyzed by ACEA/WG.D members.

For each dummy segment, the test results were investigated according to two response criteria, biofidelity and repeatability. Durability findings are reported where possible. In assessing the dummies' biofidelity, the method and weighing factors proposed by ISO in references [4] and [7] were taken into account, well aware of the limitations of findings based solely on laboratory testing.

The paper itself has been jointly drafted by ACEA's Working Group on Dummies (WG.D), with contributions on individual dummy segments from the following WG.D members:

- Head,neck and shoulder: F. Bendjellal, APR
- Thorax: M. Koch, Volvo Car Corp.
- Abdomen: A. Pastorino, FIAT
- Pelvis: E. Hautmann, BMW; G. Fuld, Mercedes-Benz
- Introduction/Conclusion: H. G. Marks, Volkswagen AG

Impact Responses of EUROSID I and BIOSID

Dummy Head Performances

The data discussed in this section came from an earlier ACEA program, where EUROSID P.P. (Production Prototype) was compared to the SID [1]. Since EUROSID and BIOSID have the same head as the EUROSID P.P., the results obtained with this latter are applicable to the first dummies.

The biofidelity of the head segment was evaluated on the basis of two types of response specifications recommended by ISO. The first specification was formulated from rigid surface tests performed by Hodgson [2] on cadavers. The second refers to free falls onto a padded surface, performed by APR [3], and also on cadavers. Both specifications recommend a simple free fall test in which only the head of the dummy is involved.

Test set-up and measurement conditions. The dummy's head was suspended above the impacting surface, at a height of 200 mm, and 1200 mm respectively for specifications N° 1 and N° 2. This height was defined by the distance between the surface to be impacted and the lowest point of the head. The head was oriented to an angle of 35° with respect to the horizontal, and 10° in the second. During the first specification tests, a 50 mm thick dry clean steel plate formed the rigid impact surface, while, for the second specification test, this plate was covered with a thin sheet of 5 mm thick padding (Figure 1). A quick-release mechanism was used to ensure the head drops. The instrumentation used comprised equipment for measurement of acceleration at the head c of g, in both evaluation cases. For the tests reproducing the HODGSON condition, the head was, in addition, equipped with a sensor for measurement of acceleration of a point of the head located opposite the impact point. All the measurement channels were class CFC 1000 filtered.

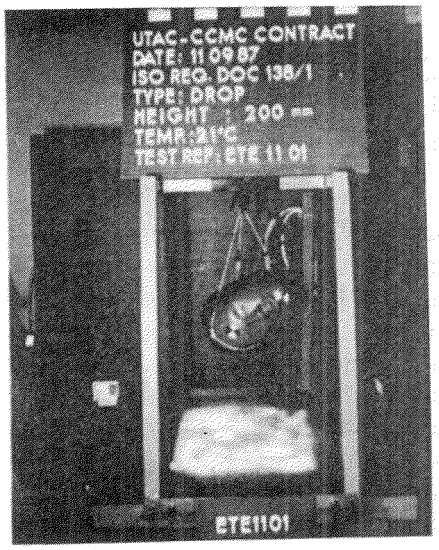

Figure 1. Test Set-Up Used in Rigid Drop Tests Involving the Dummy's Head

EUROSID I and BIOSID Head Responses in Rigid Impact

The resultant acceleration of the head, measured at the non-impacted side is presented in Figure 2, where

EUROSID I and BIOSID responses are compared to ISO requirements. Both dummies show higher peak values with respect to the upper limit of the cadaver corridor. Dummy responses are here 28% higher than this corridor limit.

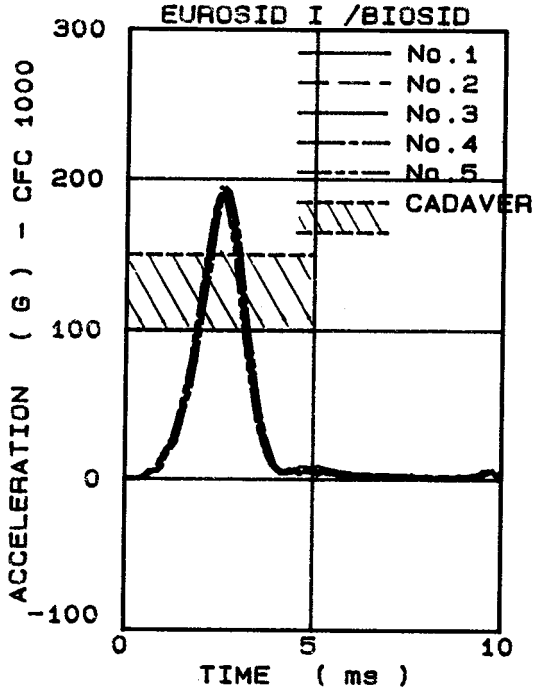

Figure 2. Head Resultant Acceleration vs Time Obtained from Rigid Drop Tests EUROSID and BIOSID Responses Compared with ISO Requirements

EUROSID I AND BIOSID Head Responses in Padded Impact

In Figure 3, the resultant acceleration of the head c.g., obtained from padded drop tests, is presented as a function of time in order to allow a more in-depth analysis. When compared to ISO corridor and to the cadaver curve, the dummy response is beyond the required limit (1.4 times the limit) and shows a short duration pulse.

EUROSID I AND BIOSID Biofidelity Scores for the Head Segment

According to ISO [4] the general formula for establishing the head score is:

$$B_1 = (\sum_{j=1,2} V_{i,j} \cdot B_{1,j}) / (\sum_{j=1,2} V_{1,j})$$

where

B_1 is the biofidelity score for the head

$V_{1,j}$ is the weighing factor for test condition j

$B_{1,j}$ is the biofidelity score of the head in test condition j

Since the head is involved in two test conditions the biofidelity partial scores $B_{1,1}$ and $B_{1,2}$ are established according to the equation developed in appendix.

Table 1 summarizes this calculation process.

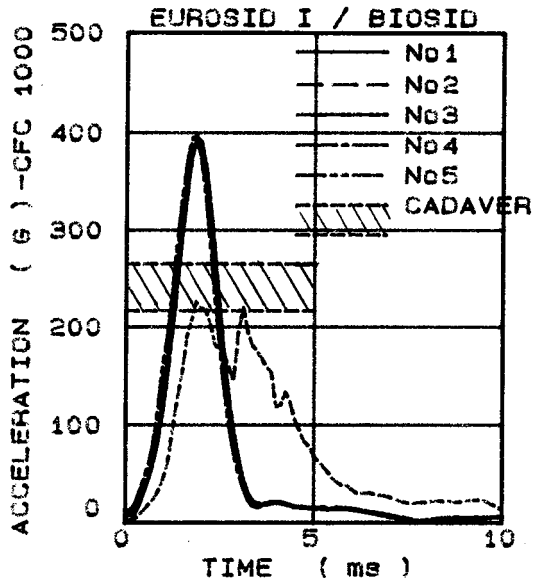

Figure 3. Resultant Acceleration of the Head c.g. vs Time Obtained from Padded Drop Tests: EUROSID and BIOSID Responses Compared with ISO Requirements

Table 1. Weighing Factors and Scores for EUROSID I and BIOSID in Head Tests

TEST	i	PARAMETER	$V_{1,i}$	$W_{1,i}$*	$R_{1,i}$** BIOSID / EUROSID
200 mm - Rigid drop	1	Head Acc. (res)	8	9	5
1200 mm - Padded drop	2	Head Acc. (res)	4	9	0

* Weighting factor of the parameter
** Response value of the dummy

$$B_{1,1} = (W_{1,1} \cdot R_{1,1})/W_{1,1} = 5$$
$$B_{1,2} = (W_{1,2} \cdot R_{1,2}) = /W_{1,2} = 0$$

Hence

$$B_1 = (V_1 \cdot B_{1,1} + V_1 \cdot B_{1,2})/(V1 + V2) = 3.3$$

Therefore for both dummies, the biofidelity score is: $B_1 = 3.3$.

EUROSID I and BIOSID Repeatability in Head Impact Tests

The results, expressed in terms of peak values and obtained from the previously discussed tests, are reported in Table 2. For each impact conditions mean response, standard deviation and coefficient of variation were calculated. With a C.V. of respectively 0.8% and 1.8 the repeatability of the dummy's head in these test conditions appears to be excellent.

Table 2. EUROSID I and BIOSID Head: Response Results Obtained from Rigid and Padded Drop Tests

	RIGID DROP TESTS					PADDED DROP TESTS				
TEST REFERENCE	1	2	3	4	5	1	2	3	4	5
Max.resultant head acceleration:										
- non impacted side,rigid impact	193	195	192	194	191					
- c.g. for padded impact						393	396	400	412	403
Mean (g) / SD / CV (%)	193 / 1,6 / 0,8					400 / 7,3 / 1,8				

Dummy Neck Performances

Three neck response characteristics in lateral flexion are defined by ISO in document [5]. One response characteristic was selected for this program in order to evaluate the biofidelity of EUROSID I and BIOSID necks. The corresponding requirements originate from volunteer tests conducted by EWING et al. [6].

Test set-up and instrumentation. The dummy, seated on a chair attached to the sled in the upright position, was restrained by belts around the chest and the pelvis (see Figure 4). The harness system originally used in the reference tests was not used since time consideration made it difficult to reproduce for the present test programme. The shoulder and hip of the dummy were wedged against a vertical side wall. The anteroposterior axis of the head of the dummy was horizontal.

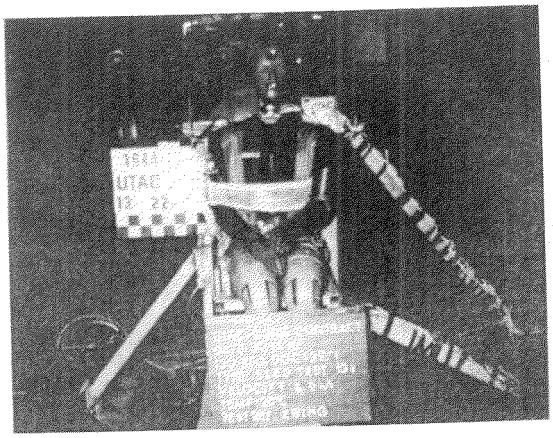

Figure 4. Test Set-Up Used in Neck Evaluation Tests According to ISO Requirements (Nb 1)

Starting from this initial position, the dummy was submitted to a deceleration pulse. The object of the response characteristics is to evaluate the kinematic of the head and that of the base of the neck (T1 level), with respect to the sled.

As far as measurements are concerned, the dummy was equipped with accelerometers at the head c.g., at T1 and T4. Two other sensors were provided for measurement of seat and sled decelerations.

In addition, photographic targets, fixed on the head and T1, were used to evaluate head 3D kinematics with respect to T1. For this purpose, a specific method based on photogrammetry principles and combining several high speed cameras was applied.

The filtering classes for the various measurements were as follows:

- CFC 1000 for head acceleration,
- CFC 180 for thoracic and sled accelerations.

In conformance with the above-mentioned conditions, 2 tests were performed with each dummy at a nominal level of sled deceleration of 7 G and a velocity of 6 m/s.

EUROSID I AND BIOSID Neck Responses in 7 G Sled Tests

There are 9 biofidelity response requirements specified by ISO for neck sled tests as shown in Table 3. These requirements concern mainly the head (3D kinematics) and T1 (lateral displacement and acceleration). According to reference [7], the 9 responses do not have the same importance. From the weighing factors reported in Table 3, the highest factors are assigned respectively to the head lateral displacement and head flexion angle while the lowest factor is assigned to head twist angle.

Table 3. Dummy Responses in Neck Sled Tests

TESTS PARAMETERS	k	TESTS RESULTS EUROSID 1 91236	EUROSID 1 91237	BIOSID 91238	BIOSID 91239	REQUIREMENTS		WEIGHTING FACTORS FOR PARAMETERS $w_{2,1,k}$
^{a}T1, max (G)	1	16.1	16.6	16.3	15.9	12 to 18	G	5
$^{a}Hcg\ y$-direction (lateral) (G)	2	11.0	10.9	12.5	12.8	8 to 11	G	5
$^{a}Hcg\ z$-direction (vertical) (G)	3	12.1	12.7	7.8	8.8	8 to 10	G	5
Max. hor. displ. T1 w.r.t. sled (mm)	4	106	110	35	50	46 to 63	mm	5
Max. head flexion (degrees)	5	71	73	39	42	44 to 59	degrees	7
Max. head twist (degrees)	6	17	20	16	20	-32 to -45	degrees	4
Max. hor. displ. H_{cg} w.r.t. T1 (mm)	7	108	115	99	107	130 to 162	mm	8
Max. vert. displ. H_{cg} w.r.t. T1 (mm)	8	50	44	32	32	-64 to -94	mm	6
Time of max. head excursion (s)*	9	0.142	0.142	0.120	0.124	0.159 to 0.175	s	5

* The time of maximum head excursion is defined here as the time of maximum horizontal (x-) displacement of H_{cg}

The results obtained are reported in Table 3, where peak values of the 9 response requirements are presented. It appears for some parameters, i.e head twist angle and T1 acceleration that both EUROSID I and BIOSID show almost identical responses. Main differences can be observed in terms of head displacement (trajectory), head flexion angle and T1 lateral displacement where EUROSID I gives larger magnitudes.

The comparison of EUROSID I and BIOSID neck performances with ISO requirements suggests the following comments if the "best" test for each dummy is considered:

- Except for 2 responses (T1 displacement and time of max head excursion), the EUROSID 1 dummy meets completely (2 cases) or partially other requirements;
- The BIOSID fails in 3 cases, including head displacements, and meets completely (3 cases) or partially other requirements;
- EUROSID I neck performances are better than those of BIOSID. The relative and slight superiority of EUROSID I neck is mainly due to the larger magnitude of the head trajectory (see Figure 5).

EUROSID I and BIOSID Biofidelity Scores for Neck Segment

According to data reported in Table 3, on the basis of formula provided in reference (4), biofidelity scores for both dummies were established (test n° 91237 and 91239). It follows that:

- B2 (EUROSID I) = 5
- B2 (BIOSID) = 4.6.

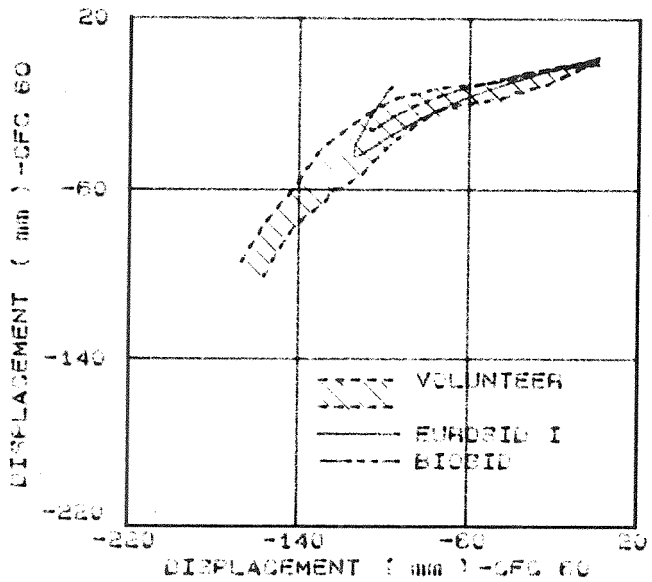

Figure 5. Trajectory of the Head c.g. Relative to T1 Obtained from 7G Sled Tests EUROSID 1 and BIOSID Responses Compared with Volunteer Corridor as Suggested by ISO Requirements

Dummy Shoulder Performances

Evaluation of the biofidelity of the shoulder segment consists in a side impact centered on the shoulder joint, with an impactor of 23.4 kg and a velocity of between 4.4 and 4.6 m/s. The response characteristics of the shoulder, as defined by ISO in document DTR 9790-4, were obtained from impactor tests conducted with cadavers by APR. Shoulder requirements comprise a corridor as a function of time of the impactor normalized load and two limits of the normalized shoulder deflection relative to the spine.

The ISO specifications also recommend that the dummy's shoulder biofidelity has to be evaluated on the basis of displacement and acceleration of the base of the neck obtained in sled tests conducted with volunteers.

Test set-up and instrumentation. The dummy was seated in an upright position on flat, rigid surface. The seating surface, with no back support, was clean. A linearly guided impactor, with a mass of 23.4 kg, was used to strike the dummy shoulder. The impactor axis was perpendicular to the dummy's midsagittal plane. In EUROSID I and BIOSID tests the impactor axis was aligned with the axis of the left upper arm joint. Figure 6 illustrates the test set-up used for EUROSID I and BIOSID. Measurements comprised for both dummies the acceleration respectively of the impactor and of the upper spine T1. These data were filtered according to class CFC 180. The required CFC 1000 filter, which was also used, showed high-frequency vibration responses. For both dummies the relative shoulder deflection was measured from high speed film. According to the test set-up mentioned above five tests were performed with each dummy.

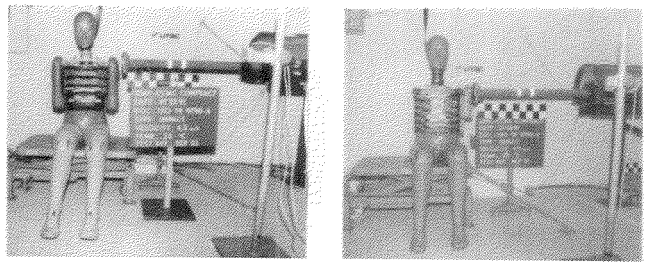

Figure 6. Test Set-up Used in Shoulder Tests According to ISO Requirements (8)

EUROSID I and BIOSID Shoulder Responses in Impactor Tests

The principal results obtained with EUROSID I and BIOSID dummies in 4.5 m/s impactor tests are presented in Tables 4 and 5, where are reported respectively raw data and normalized data. For biofidelity evaluation two parameters are here analyzed. These are the normalized impact force time history (see Figure 7) and the normalized peak shoulder deflection (see Figure 8).

Table 4. Raw Data as Obtained from Impactor Tests Involving the Shoulder

	EUROSID I					BIOSID				
TEST REFERENCE	1	2	3	4	5	1	2	3	4	5
Impact velocity (m/s)	4,55	4,45	4,55	4,55	4,52	4,40	4,40	4,40	4,50	4,40
T1 max. acceleration (g)	26	23	25	23	25	22	22	22	23	23
Mean (g)/ SD(g)/ CV (%)	24 / 1,3 / 5,4					23 / 0,4 / 1,9				
Max.impactor acceleration (g)	12	11	12	11	12	22	22	22	22	21
Max.impactor load (kN)	2,8	2,6	2,9	2,7	2,8	5,1	5,1	5,3	5,3	5,0
Mean (g)/ SD(g)/ CV (%)	2,8 / 0,11 / 4,0					5,2 / 0,13 / 2,6				
Max.rel.impactor displacemt (mm)	61	56	54	61	58	37	42	40	41	37

Table 5. EUROSID I and BIOSID Shoulder Responses in Impactor Tests (Normalized Data)

	EUROSID I					BIOSID				
TEST REFERENCE	1	2	3	4	5	1	2	3	4	5
Eff.Mass m_e (kg)	16,85	17,17	16,84	17,05	17,31	22,68	22,67	22,63	22,45	22,37
Mass Ratio R_m	1,22	1,19	1,22	1,20	1,18	0,90	0,90	0,91	0,91	0,92
Nmlized Factors $R_z=R_t=R_x=R_m^{1/2}$	1,10	1,09	1,10	1,10	1,09	0,95	0,95	0,95	0,96	0,96
Max nmlzd imp. displemt (mm)	67	61	59	67	63	35	40	38	39	36
ISO requiremt. shoulder (mm)	Minimum : 34					Maximum : 41				
Max nmlzd. imp. load (kN)	3,0	2,8	3,1	2,9	2,9	4,7	4,8	4,8	5,0	4,7

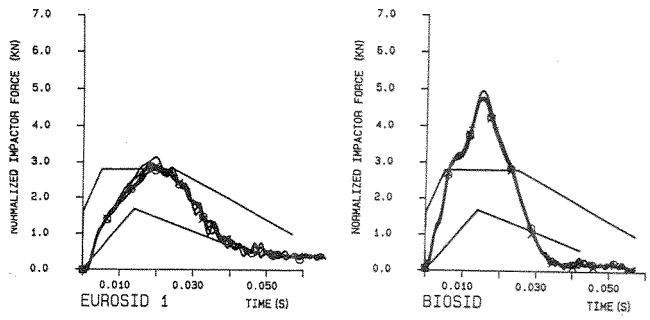

Figure 7. Normalized Impactor Force vs Time: EUROSID 1 and BIOSID Responses Compared to ISO Requirements

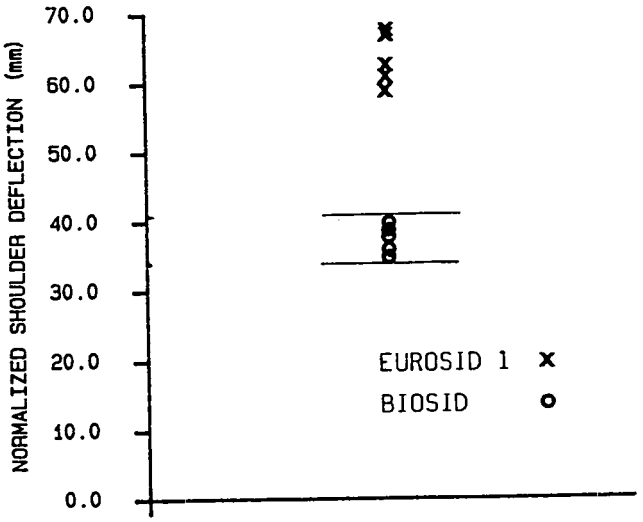

Figure 8. Normalized Shoulder Displacements: EUROSID 1 and BIOSID Responses Compared to ISO Requirements

As far as the impactor force is concerned, the EUROSID I response is well within the requirement [8] in terms of peak magnitude and pulse duration. On the other hand BIOSID response exceeds the corridor limit of about 46% and shows a short pulse duration. Results obtained in terms of shoulder displacement are opposite to those previously discussed. While the EUROSID I shoulder deflection is two times greater than the required upper limit (41 mm), the BIOSID response is within the ISO range.

EUROSID I AND BIOSID Shoulder Responses in 7G Sled Tests

In this section two types of dummy responses are considered. These are the lateral T1 displacement and the T1 lateral acceleration. These data are implicit since they were obtained from lateral sled tests involving mainly the neck segment (see Table 3). In this case the results are in favor of BIOSID, which shows a T1 displacement within the required limits.

EUROSID I AND BIOSID Shoulder Biofidelity Scores

Using equations given in appendix the dummies' scores were established on the basis of the 2 test conditions reported in this section. Table 6 summarizes the different factors and scores as obtained from Table 6 and Figure 7. It follows that biofidelity scores are, for the shoulder: B4 = 4.3 (EUROSID I); B4 = 5.7 (EUROSID I).

The ISO recommendations for the biofidelity test of the thorax, ISO/TR9790-3, are in the process of being revised and updated. This process is not yet finished, but a working document ISO/TC22/SC12/WG5-N249 exists. Its main proposals have been agreed upon, even if several details remain to be decided. In the tests presented here, TR9790-3 has been followed, but complemented by those parts of N249 which had been approved by WG5 at the time of testing during the first half of 1991.

Table 6. Weighing Factors and Scores for EUROSID I and BIOSID Shoulder Segments

TEST TYPE j	PARAMETERS k	WEIGHTING FACTORS $V_{4,j}$	$W_{4,j,k}$	$R_{4,j,k}$ EUROSID I	$R_{4,j,k}$ BIOSID
4.5 m/s Impactor - 1	Impactor force 1	6	8	10	0
	Shoulder deflection 2	6	6	0	10
7 G sled test - 2	T1 lat. acceleration 1	5	6	5	5
	T1 lat. displacement 2	5	6	0	10

The ISO tests of the biofidelity of the thorax comprise three different test modes. Number 1 is two drop tests, number 2 is three sled tests, and number 3 is two impactor tests. Of these, the drop tests were left out from this programme.

Requirement 2, sled test set-up. Tests were conducted according to requirement no. 2 of ISO/TC22/SC12/WG5-N249 (September 1989).

A seat with an instrumented side panel was mounted on an impact sled, transverse to the direction of travel. The side panel had two instrumented impact surfaces, one at the thorax and the other at the pelvis level. The dummy was placed at the end of the seat opposite to the instrumented panel. It remained at that position while the sled was accelerated to the prescribed impact velocity. The sled was then rapidly decelerated to zero velocity. At this instant the dummy slid towards the side panel, impacting it at almost the same speed as the sled had been travelling at. In order to facilitate a parallel lateral movement of the sitting dummy, the dummy was dressed and set on two plastic foils.

For each dummy six impacts were carried out at an impact velocity of 6.8 m/s. Three more impacts were then run at 8.9 m/s and with the instrumented side panels covered by 140 mm x 140 mm x 420 mm blocks of APR urethane foam.

Requirement 3, impactor test set-up. Tests were conducted according to requirement no. 3 of ISO/TC22/SC12/WG5-N249 (September 1989).

Each dummy, without its vest, was seated in an upright position and with its left arm raised. A 23.4 kg linear guided impactor with a flat surface of 150 mm diameter struck the left center of the rib cage at the speeds 4.3 and 6.7 m/s. Four tests at each speed were conducted for each dummy in these conditions.

Thorax Responses in Rigid and Padded Sled Tests

Measurements. Both dummies were instrumented according to the ISO requirements, i.e. measuring lateral accelerations at T1, T12 and at the 4th rib on the impacted side; and also lateral displacements of the impacted ribs relative to the thoracic spine.

In addition to these measurements a number of other transducers were also mounted into the dummies according to the designers' intentions. The instrumented side panels were attached to force load cells. High speed films were taken during all sled tests.

The thorax transducers were filtered by ISO-6487 CFC 180 Hz filters. The force signals from the instrumented side panels were filtered by FIR100 filters. After the filtering the signals were normalized as required by the ISO documents. The normalization was done assuming that the impact velocity V0 is the proper velocity to use; in certain test situations there is the alternative to employ a delta-V velocity calculated from an integrated accelerometer output. The latter method has not been used for the signals reported here.

Data. Figures 9 to 12 show the normalized force versus normalized time curves for the eighteen sled tests. The requirement corridors are copied from the ISO WG5-N249 document.

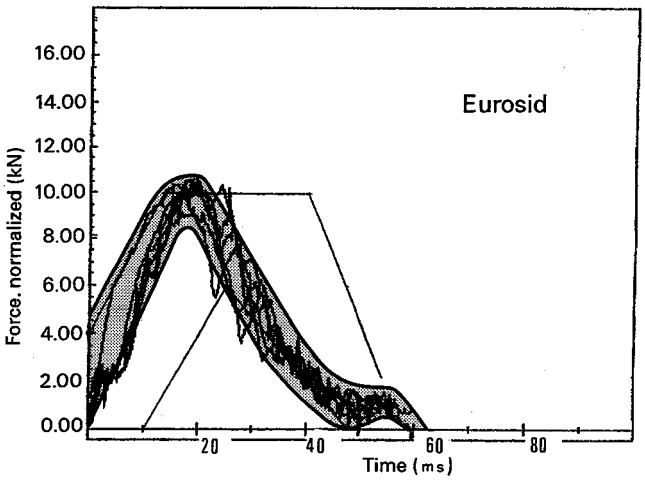

Figure 9. Tests nb 1-6 from Table 7: Normalized Impact Forces versus Normalized Time for EUROSID I in Rigid Impact at 6.8 m/s Sled Tests

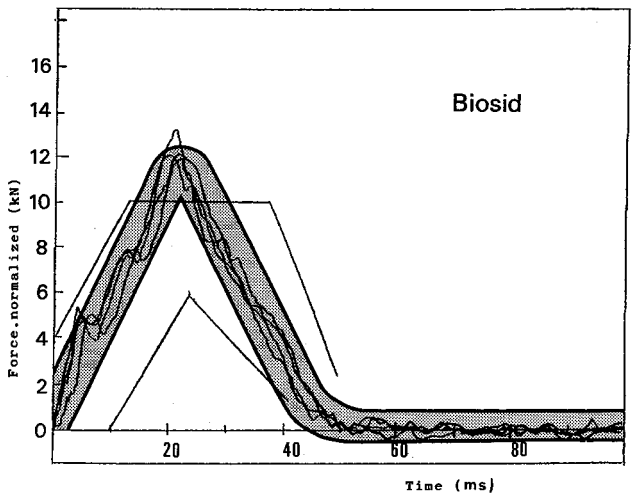

Figure 10. Tests nb 1-3 and 5 from Table 8: Normalized Impact Forces versus Normalized Time for BIOSID in Rigid Impact at 6.8 m/s Sled Tests

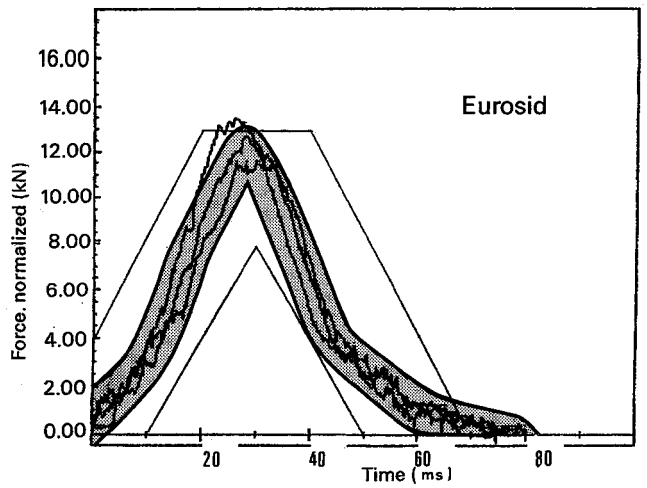

Figure 11. Tests nb 7-9 from Table 7: Normalized Impact Forces versus Normalized Time for EUROSID I in Padded Impact at 6.8 m/s Sled Test

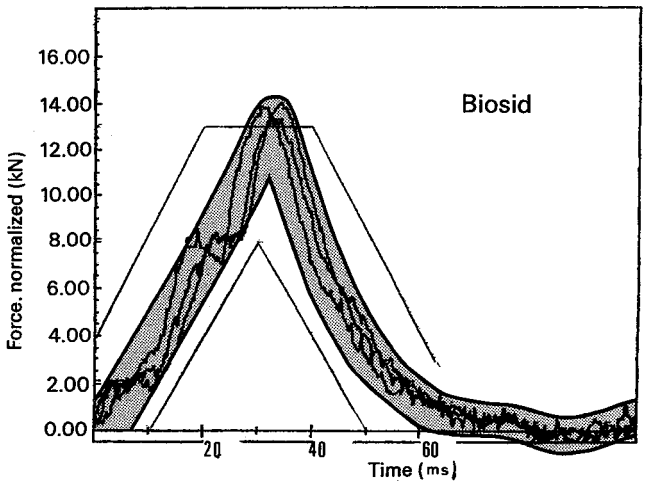

Figure 12. Tests nb 7-9 from Table 8: Normalized Impact Forces versus Normalized Time for BIOSID in Padded Impact at 6.8 m/s Sled Test

Tables 7 and 8 show the data relevant for an assessment of the biofidelity of the dummies. The large quantity of other data generated during these tests is still being analyzed and will be reported elsewhere.

Table 7. EUROSID I Sled Test Data

	LOW SPEED						HIGH SPEED		
TEST NUMBER	1	2	3	4	5	6	7	8	9
- Impact velocity (m/s)	6.76	6.78	6.83	6.80	6.73	6.76	8.93	8.97	9.01
- Spine angle (degrees)	10	10	14	9	17	4	8	8	4
- Effective mass (kg)	53.6	60.0	62.2	61.1	41.9	62.7	66.8	49.3	63.7
- Peak normalized shoulder impact force (kN)	9.33	10.4	10.4	10.3	10.3	10.6	11.8	13.5	12.7
- Peak normalized T1 acceleration (G)	48.2	43.6	36.9	37.8	36.6	45.8	57.8	48.1	60.8
- Peak normalized T12 acceleration (G)	44.6	51.0	49.4	49.5	39.2	58.5	78.0	68.9	84.2
- Peak normalized 4th rib acceleration (G)	94.4	101.0	102.2	97.2	82.8	115.4	81.5	74.3	137.8

Table 8. BIOSID Sled Test Data

	LOW SPEED						HIGH SPEED		
TEST NUMBER	1	2	3	4	5	6	7	8	9
- Impact velocity (m/s)	6.83	6.83	6.80	6.80	6.85	6.60	8.89	8.85	8.81
- Spine angle (degrees)	19	15	13	19	9	20	18	13	13
- Effective mass (kg)	72.9	73.2	72.7	74.5	70.5	74.6	72.8	72.0	73.0
- Peak normalized shoulder impact force (kN)	12.1	13.2	12.1	16.7	11.9	16.6	13.9	13.5	14.0
- Peak normalized T1 acceleration (G)	94.6	83.4	82.1	121.0	91.6	103.1	100.3	100.1	75.0
- Peak normalized T4 acceleration (G)	27.9	21.3	20.6	23.4	18.6	34.0	29.5	25.1	27.5
- Peak normalized T12 acceleration (G)	28.1	25.9	30.0	43.8	27.2	42.73	33.4	28.3	34.5
- Peak normalized 4th rib acceleration (G)	181.9	131.4	229.7	144.2	256.6	147.0	108.7	119.3	122.4

Analysis. After the tests an analysis of the high speed films showed that the dummies did not move exactly as prescribed in the ISO documents. At the instant of sled contact with its stopping device, the dummies started a sliding movement towards the instrumented impact side panel. During this movement the dummies also began a leaning movement towards their left side. This resulted in the dummies' spine not being vertical at the time of impact to the side panel. Instead the shoulder hit the panel some 10 - 20 ms before the pelvis. At impact velocities of 6.8 m/s and 8.9 m/s, respectively, this amounts to the shoulder being 7 - 14 cm ahead of the pelvis at the impact. The spine deviated several degrees from the vertical at the instant of impact. This angle is reported in Tables 7 and 8. The tables show that this angle is generally larger for the BIOSID than for the EUROSID I.

The reason for this movement might be attributed to the plastic foils between the dummy and the seat. The consequence is that the recorded data might be inappropriate for evaluation of the biofidelity of the dummy since the prescribed vertical position of the spine has not been maintained before the impact.

Analyzing the data in their present shape, and also comparing them with the recommended ISO values (see Table 11), one can see that both dummies show values outside the recommended intervals. In the case with rigid impacts the BIOSID has higher impact forces against the side panel than the EUROSID I. In the padded impact case both dummies are slightly outside the force corridor.

Irrespective of rigid or padded impact, one can also observe that the difference between the T12 acceleration and the rib acceleration is much larger for the BIOSID than for the EUROSID I.

As can be seen from Table 7, the peak normalized shoulder impact forces of tests no. 4 and 6 are abnormally high. These tests also exhibited a large spine inclination angle at the time of impact. They cannot be considered as recorded under such test conditions as are prescribed in the ISO documents. Therefore, these two signals will not be included in the further analysis.

Thorax Responses in Impactor Tests

Measurements. Accelerometers were fitted at the impactor, at locations T1 and T12 on the dummy's spine, and on each of the three ribs. The acceleration signals were filtered by a FIR100 filter. A displacement transducer was also fitted to each rib. The displacement signals were filtered by ISO-6487 CFC 600 Hz filters.

After the filtering the signals were normalized as required by the ISO documents. The normalized signals and their relations to the requirement corridors can be seen in Figures 13 to 15. Tables 9 and 10 show the normalized peak values of the signals.

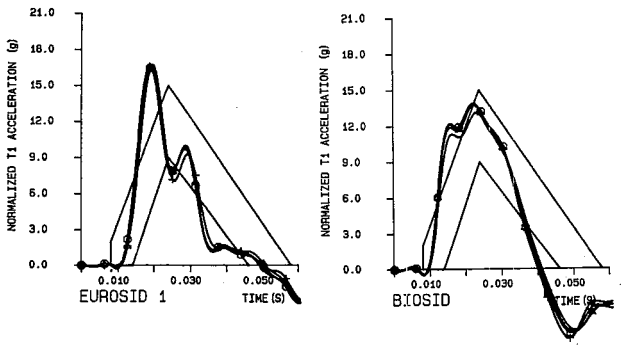

Figure 13. Normalized T1 Accelerations at 4.3 m/s

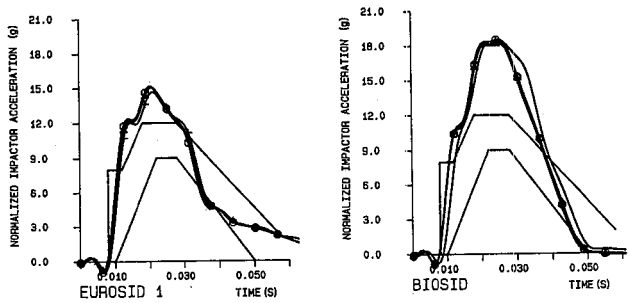

Figure 14. Normalized Impactor Accelerations at 4.3 m/s

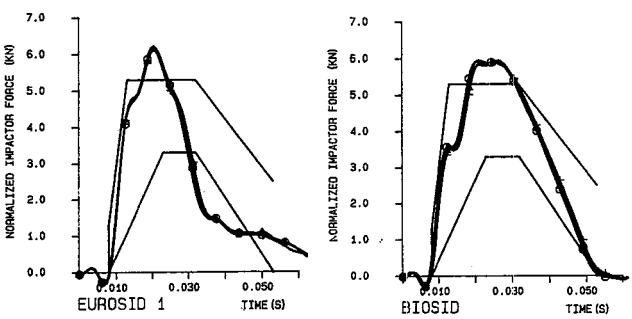

Figure 15. Normalized Impactor Forces at 6.7 m/s

Table 9. EUROSID I Impactor Test Data

	LOW SPEED			
TEST NUMBER	1	2	3	4
- Impact velocity (ms)	4.35	4.37	4.35	4.30
- Effective mass (kg)	26.83	26.66	26.82	26.66
- Max normalized impactor acceleration FIR 100 (G)	15	15	15	15
- Max normalized spine T1 acceleration FIR 100 (G)	17	16	17	17

	HIGH SPEED			
TEST NUMBER	5	6	7	8
- Impact velocity (ms)	6.78	6.72	6.78	6.72
- Effective mass (kg)	28.13	27.24	27.13	26.65
- Max normalized impactor force FIR 100 (kN)	6.2	6.2	6.2	6.1

Table 10. BIOSID Impactor Test Data

	LOW SPEED			
TEST NUMBER	1	2	3	4
- Impact velocity (ms)	4.35	4.37	4.35	4.32
- Effective mass (kg)	28.07	30.26	30.06	30.47
- Max normalized impactor acceleration FIR 100 (G)	18	19	18	18
- Max normalized spine T1 acceleration FIR 100 (G)	13	14	14	14

	HIGH SPEED			
TEST NUMBER	5	6	7	8
- Impact velocity (ms)	6.78	6.72	6.67	6.67
- Effective mass (kg)	29.67	29.57	29.21	29.37
- Max normalized impactor force FIR 100 (kN)	6.0	5.9	5.9	6.0

Data. Also for the impactor tests there is more data that is analyzed and which will be reported elsewhere. The following tables show the data relevant for an assessment of the biofidelity of the dummies.

Analysis. As can be seen from Figures 13 to 15 the response curves are slightly outside the prescribed corridors. An exception is the impactor acceleration for the BIOSID which shows a deviation larger than the width of the tolerance band.

The impactor tests indicate that the T1 and T12 accelerations are higher for the EUROSID I than for the BIOSID. For the rib accelerations the reverse is true, the BIOSID shows higher values than the EUROSID I. The rib displacements are about the same for both dummies at low speed, but become higher for the BIOSID than the EUROSID I at higher speed.

Biofidelity Scores for Thorax Segment

The recorded data from the thorax tests in Tables 7 to 10 are entered as averages into Tables 11 to 13 and give a total biofidelity rating for the thorax segment. All test data are used to calculate the averages, with the exception of the BIOSID low speed sled test (Table 8), where tests no. 4 and 6 were excluded for reasons stated previously.

Table 11. Biofidelity Rating of Thorax Sled Tests

SLED TEST	REQUIREMENT	EUROSID-1	BIOSID
LOW SPEED 6.8 m/s			
Impact Force	Corridor	Just Out	Slightly Out
T1 Acceleration	82 - 122	42	88
T12 Acceleration	71 - 107	49	28
Rib Acceleration	66 - 100	99	200
HIGH SPEED 8.9 m/s			
Impact Force	Corridor	Within	Just Out
T1 Acceleration	66 - 98	56	92
T12 Acceleration	82 - 124	77	32
Rib Acceleration	72 - 108	98	117

RESPONSE CONVERSION TO RATING NUMBERS	WEIGHTS	EUROSID-1		BIOSID	
		Response R	Rating RxW	Response R	Rating RxW
LOW SPEED 6.8 m/s					
Impact Force	W331 = 8	B = 5	40	A = 10	70
T1 Acceleration	W332 = 7	B = 5	35	C = 0	0
T12 Acceleration	W333 = 7	B = 5	35	C = 0	0
Rib Acceleration	W334 = 6	A = 10	60		
Weighted Rating B33		6.1		5.4	
HIGH SPEED 8.9 m/s					
Impact Force	W351 = 9	A = 10	90	B = 5	45
T1 Acceleration	W352 = 7	B = 5	35	A = 10	70
T12 Acceleration	W353 = 7	B = 5	35	C = 0	0
Rib Acceleration	W354 = 7	A = 10	70	B = 5	35
Weighted Rating B35		7.7		4.3	

Table 13 shows the calculation of the total biofidelity scores for the thorax segments. The results are:

- 3 (EUROSID I) = 5.9
- 3 (BIOSID) = 4.1.

Table 12. Biofidelity Rating of Thorax Impactor Tests

SLED TEST	REQUIREMENT	EUROSID-1	BIOSID
LOW SPEED 4.3 m/s			
Impactor Acceleration	Corridor	Slightly Out	Much Out
Spine Acceleration	Corridor	Slightly Out	Slightly Out
HIGH SPEED 6.7 m/s			
Impactor Force	Corridor	Slightly Out	Slightly Out

RESPONSE CONVERSION TO RATING NUMBERS	WEIGHTS	EUROSID-1		BIOSID	
		Response R	Rating RxW	Response R	Rating RxW
LOW SPEED 4.3 m/s					
Impactor Acceleration	W361 = 9	B = 5	45	C = 0	0
Spine Acceleration	W362 = 7	B = 5	35	B = 5	35
Weighted Rating B36		5		2.2	
HIGH SPEED 6.7 m/s					
Impactor Force	W371 = 9	B = 5	45	B = 5	45
Weighted Rating B37		5		5	

Table 13. Weighed Biofidelity of Thorax Segment

RESPONSE CONVERSION TO RATING NUMBERS	WEIGHTS	RESPONSE B	RATING BxV	RESPONSE B	RATING BxV
Sled 6.8 m/s	V33 = 7	6.1	42.7	5.4	37.8
Sled 8.9 m/s	V35 = 7	7.7	53.9	4.3	30.1
Impactor 4.3 m/s	V 36 = 9	5.0	45.0	2.2	19.8
Impactor 6.7 m/s	V 37 = 8	5.0	40.0	5.0	40.0
Weighted biofidelity for thorax	-	5.9	4.1	-	-

Repeatability Scores for Thorax Segment

Impactor Tests. For most of the recorded parameters one could state the repeatability of both dummies as typically exhibiting a coefficient of variation (c. v.) for four tests on the order of 1 to 4%. This includes the following analyzed eight parameters:

- Impactor deceleration
- T1 and T12 acceleration
- Rib peak deflection, three ribs
- TTI and VxC.

For the rib peak accelerations, however, odd data points did sometimes occur. This brought up the c.v. for the rib accelerations to a higher value. From a total of 48 recorded rib accelerations, about five occasional values contributed to c.v. values becoming between 5 and 15%. These are presumably cases when, for some unidentified reason, the set-up has deviated slightly from its nominal position. How large the set-up deviation has been is not possible to determine afterwards.

Sled Tests. As already noted, the sled test procedure was affected by a lack of stable vertical orientation of the spine during the last phases of the sled deceleration. This has contributed to large scatter in the data, and it would be difficult to separate this scatter into two contributions: one due to the repeatability of the test set-up and the other due to the repeatability of the responses of the dummies themselves.

At the present stage of analysis, it should be sufficient to present a brief account of the c.v. values for some dummy response parameters. The following fourteen parameters have been included in the analysis:

- effective thorax mass,
- shoulder impact force,
- accelerations at anatomic locations T1, T12 and rib 4,
- peak deflections for ribs 1, 2 and 3,
- TTI for dummy ribs, 2 and 3,
- Viscous Criterion for dummy ribs 1, 2 and 3.

These parameters are collected for the two series of rigid impacts and padded impacts, and they are summed up in the below table. The result is nearly independent of whether the suspect impacts nos. 4 and 6 are included or not. Therefore, we have 28 c.v. values distributed as follows:

COEFFICIENT OF VARIATION	EUROSID I	BIOSID
> 20 %	1 + 2 = 3	2 + 3 = 5
10-20 %	6 + 7 = 13	2 + 4 = 6
5-10 %	5 + 4 = 9	6 + 3 = 9
< 5 %	2 + 1 = 3	4 + 4 = 8

Analyzed so far and with the selected responses parameters, the conclusion is that the BIOSID thorax appears to be a more repeatable device in the sled test mode than the EUROSID I thorax.

Durability and Handling for Thorax Segment

For the impactor tests, no handling or durability problems were recorded for the thorax segments of the two dummies. For the more severe sled tests, however, several problems appeared.

EUROSID I. For this dummy the repeated impacts to the side deformed and twisted the upper arm. There also occurred a slight deformation of the left side of the ribs and the spring axis with a partly sideways displacement of the cup of the first rib. A recommended maximum number of severe impacts should therefore be defined between major checks of the condition of the chest.

BIOSID. For this individual dummy, which was more of a prototype, more problems were encountered. It has been said that these problems have also been observed elsewhere, and that redesign measures are underway.

The displacement potentiometer wires were difficult to handle.

The lumbar element appeared softer than that of the EUROSID I and the dummy easily tipped over sideways.

This has probably contributed to the non-vertical impact in the sled tests.The dummy thorax also turned left slightly before it impacted the side panel. Already in the first test this resulted in a permanent rearward deformation of the shoulder rib of about five mm. This deformation stayed at that value during the subsequent tests. However, there was a loosening and tear-off of rubber parts inside the back region of the left shoulder rib.

In test no. 6 (8.9m/s) the plate for the accelerator and potentiometer string attachment tore off (two screws were torn off). This could be repaired before the following tests. After the ninth test it was obvious that the lumbar element showed a higher mobility than it had at the beginning of the test series. At disassembly it was noticed that four screws had come loose at the lumbar pelvis interface.

The BIOSID, as tested, appears in need of improved robustness in several parts before it can be used in tests as severe as the rigid impact sled test.

Dummy Abdomen Performance

Reference Data

The response characteristics (see Figures 16 and 17) used to evaluate the abdominal segment are those prescribed by ISO in ref [9], and obtained with cadaver tests by APR [10], impacting against a rigid armrest. Test data of drop heights of 1 and 2 meters were normalized according to Mertz [9] and are reported in Table 14.

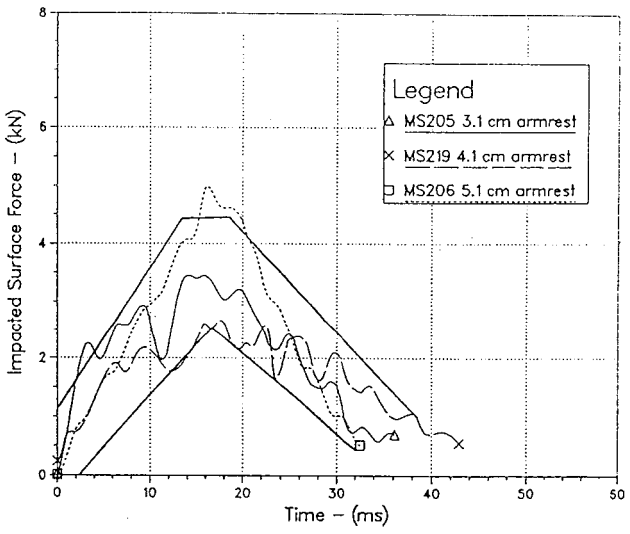

Figure 16. Normalized Lateral Abdominal Force-Time Curves and Proposed Corridor for a 1 Meter Drop onto a 4.1 cm Rigid Armrest

Test set-up, instrumentation and normalization. The dummies were suspended above the impact surface with their medial sagittal planes horizontal. The dummies were placed so that the armrest were centered on the abdominal region, including the "area of the 9th Rib." Except where both dummies are instrumented to measure loads in the abdominal region, only the data.required for the ISO evaluation were collected (see Figure 18).

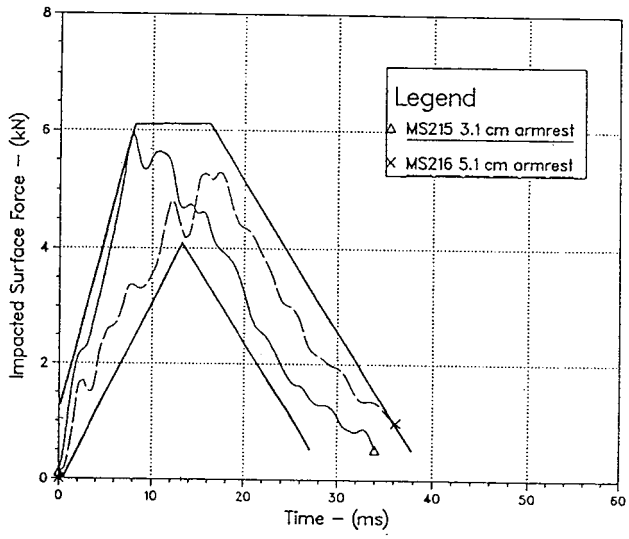

Figure 17. Normalized Lateral Abdominal Force-Time Curves and Proposed Corridor for a 2 Meter Drop onto a 4.1 cm Rigid Armrest

Table 14. Biofidelity Parameters and Limits for Abdomen

PARAMETERS	k	1 m DROP LIMITS	2 m DROP LIMITS	W5,j,k
- Armrest force	1	Corridor fig (a)	fig (b)	9
- T12 peak acceleration (g)	2	29-35	75-91	6
- 9th rib peak acceleration (g)	3	100-125	160-200	4
- Abdomen penetration	-	At least equal to the height of armrest (41 mm)		-

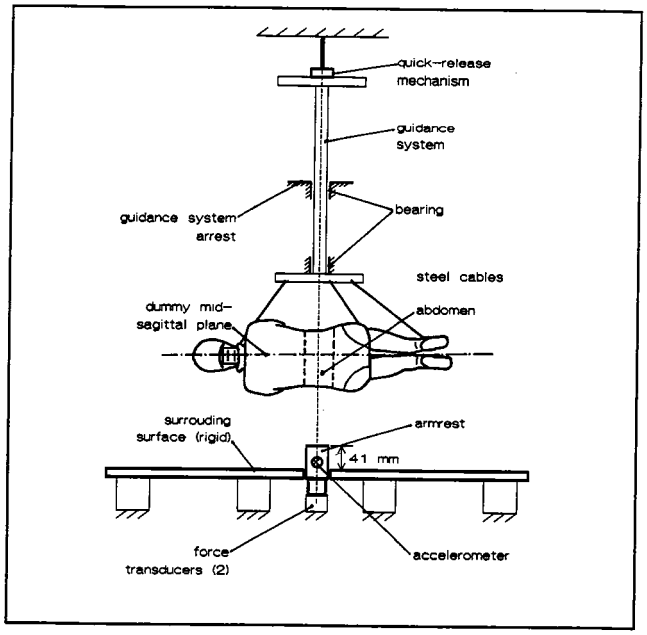

Figure 18. Test Set-Up Used in Abdomen Drop Tests

Furthermore,it was decided to perform only the 2 m drop test, this being the most severe condition. A total of 12 drop tests were performed, 6 tests each for both the EUROSID I and BIOSID.

The inertia compensated armrest force is calculated according to:

$$Fcomp = F1 + F2 + m * a\,dt$$

where:

F1 and F2 are the armrest forces measured with load cells,

m is the mass of the armrest,

a is the acceleration of the armrest.

Force, accelerations and time were normalized as required by ISO [9], with three normalizing factors: Rf, Ra, R.

Data Responses

The normalized values, for each parameter, are reported for each test and for each dummy.

- Normalized T_{12} and Rib Acceleration, Abdomen Penetration: The peak values are reported in Table 15, for each test, with mean value as SD, and in Figures 19 to 21, referring to the required corridors.
- Normalized Armrest Force: The time histories are reported in Figure 22, referring to the required corridor.

Table 15. Peak Normalized T12 Acceleration: Peak Normalized Rib 3 Acceleration - Abdominal Penetration

EUROSID I TEST NUMBER	1	2	3	4	5	6	Mean	SD
Me (Kg)	14.84	13.03	14.49	15.71	16.07	20.89	-	-
T12 acc. (g)	84.3	101.5	90.5	82.6	82.5	66.8	84.7	11.4
Rib 3 acc. (g)	242.7	214.3	174.8	191.2	285.8	304.5	235.6	51.8
Abd pentr (mm)	55.6	59.3	60.6	58.7	56.9	61.5	58.8	2.2

BIOSID TEST NUMBER	1	2	3	4	5	6	Mean	SD
Me (Kg)	16.02	15.13	15.58	15.21	13.63	14.27	-	-
T12 acc. (g)	53.2	58.0	72.0	68.2	58.0	62.8	62.0	7.1
Rib 3 acc. (g)	235.3	185.5	213.6	238.4	176.2	259.6	218.1	32.5
Abd pentr (mm)	94.4	86.2	92.3	86.3	93.5	96.5	91.5	4.3

Results Evaluation for Biofidelity

T12 Peak Acceleration. EUROSID I mean value is inside the corridor (4 of 6 test), while BIOSID is always lower.

Rib 3 Peak Acceleration. Both dummies' mean values are slightly outside the limits (higher), although BIOSID is the nearest to the corridor.

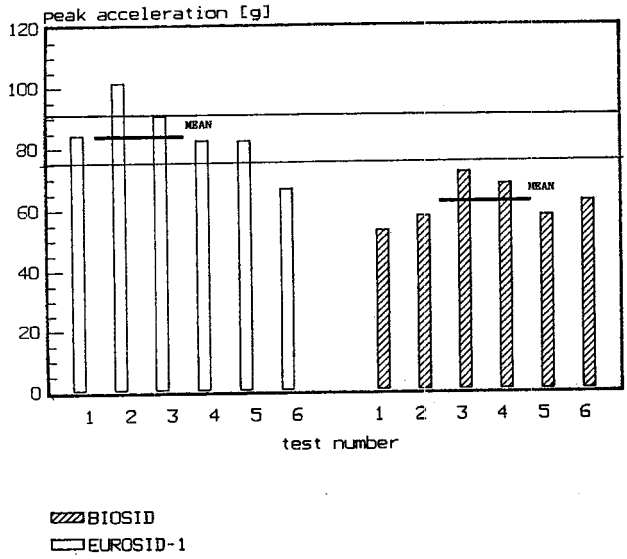

Figure 19. Peak Normalized T12 Acceleration in 2 m Drop Tests

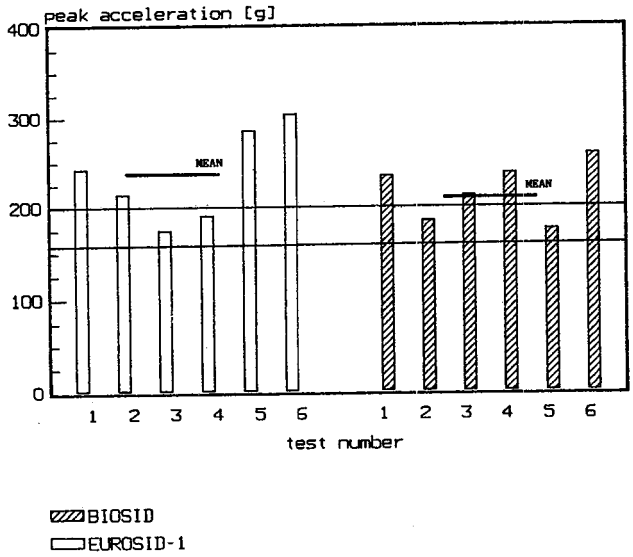

Figure 20. Peak Normalized Rib Acceleration in 2 m Drop Tests

Abdominal Penetration. Both dummies exceed the minimum required value,with BIOSID mean value being twice the minimum required. This seems to be in agreement with the lower acceleration levels.

Armrest Force. The behavior of the two dummies is quite different: EUROSID I shows a stiff behavior, with a narrow and too high force pulse. The peak value is considerably too high when compared to the ISO corridor, while the time duration (rising and falling edges) lies inside the corridor.

On the contrary, BIOSID shows a less stiff behavior, with a flat force pulse and a time duration higher than the corridor.This is in accordance with the lower acceleration levels and the higher penetration levels. Neverthe-

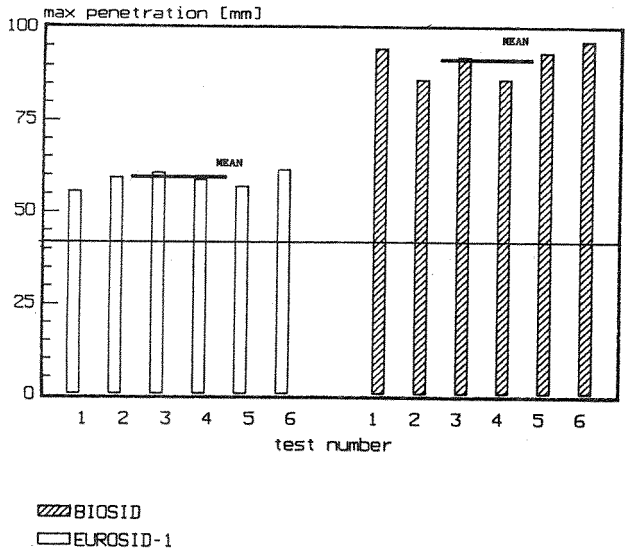

Figure 21. Peak Normalized Abdominal Penetration in 2 m Drop Tests

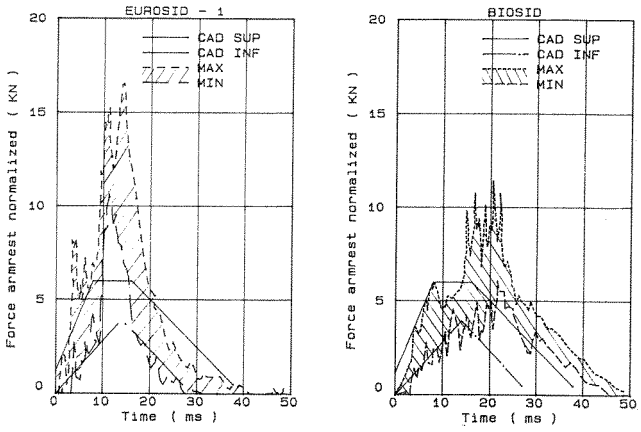

Figure 22. Normalized (and Inertia Compensated) Armrest Load for Abdomen Drop Tests: EUROSID I and BIOSID Responses Compared to ISO Corridor

less, such a behavior seems to be more "humanlike" than that of the EUROSID I.

Biofidelity Scores. Weighing factors, response scores, and biofidelity scores for the two dummies, established in accordance with [4, 7], are reported in Table 16.

Table 16. Weighed Factors, Response Score and Biofidelity Score for 2 m Drop Test

PARAMETERS	k	W5,2,k	REQUIREMENTS	EUROSID I Rk	BIOSID Rk
Armrest force	1	9	Corridor	0	5
T12 peak acceleration (g)	2	6	Min/Max	10	5
3th rib peak acceleration (g)	3	4	Min/Max	5	5
BIOFIDELITY SCORE B6	-	-	-	4.2	5

Repeatability

Repeatability is evaluated by means of the Coefficient of Variation CV (CV = [SD / mean value] * 100), and results are reported in Table 17.

Table 17. Repeatability of Tests

DUMMY	PARAMETERS		
	T 12	Rib 3	Abdomen Penetration
EUROSID I	13.4 %	20 %	3.7 %
BIOSID	11.4 %	15 %	4.6 %

Dummy Pelvis Performance

There are defined three pelvis response requirements by ISO in document [11]. Two from these requirements (Req.1 and Req.3) were chosen fort his programme for evaluating the biofidelity of EUROSID I and BIOSID pelvises.

The requirement 3 (sled tests) asks for normalized peak values of the impacted surface force and the pelvis acceleration.

The corresponding responses are based on impactor tests performed by Onser [12,13,14] and on cadaver sled tests carried out the University of Heidelberg [15].

Test set-up and measurement conditions, Requirement 1. The dummy was seated in an upright position on two sheets of Teflon. A 17,3kg impactor with a spherical segment face (120 mm in diameter, 150mm for the radius of curvature) stroke the pelvis in the great trochanter region. In fact, the impactor was centered on the energy absorbing block (see Figures 23, 24). Five impact tests were conducted with an impact velocity of 7m/s+ 2% and five with a velocity of 8m/s+ 2% for each dummy.

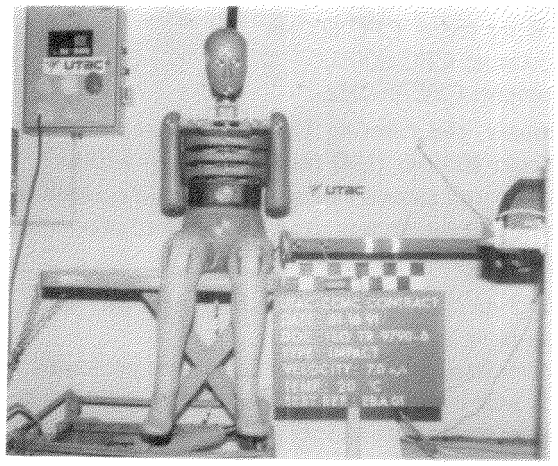

Figure 23. Test Set-Up Used in Impactor Tests Involving the Pelvis (EUROSID I)

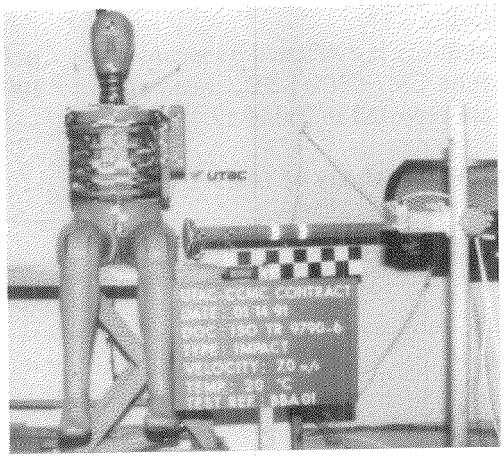

Figure 24. Test Set-Up Used in Impactor Tests Involving the Pelvis (BIOSID)

During the tests, the dummies were instrumented to obtain the following measurements:

Accelerations:
- Acceleration of the impactor,
- Acceleration of the thorax (T4 point),
- Acceleration of the pelvis.

Forces on BIOSID:
- Sacrum force,
- Iliac wing force (impacted side),
- Pubic force.

Forces on EUROSID I:
- Pubic force.

Moment on BIOSID:
- X moment on lumbar spine.

The signals were filtered at the following frequency classes (ISO-6487):
- impactor acceleration: CFC 180Hz
- pelvis acceleration: CFC 180Hz
- thorax acceleration: CFC 180Hz
- sacrum force: CFC 600Hz
- iliac wing force: CFC 600Hz
- pubic force: CFC 600Hz
- X moment: CFC 600Hz.

As previously, the filtering class of the impactor was lowered from 1000Hz (ISO requirement) to 180Hz.

Test set-up and measurement conditions, Requirement 3. The same test set-up was used as described above (see "Dummy Thorax Performance").

EUROSID I AND BIOSID Pelvis Responses in 7 and 8 M/S Impactor Tests

The normalized peak impactor forces are presented in Figure 25, where EUROSID I and BIOSID responses are compared to the ISO corridor.

The results are also reported in Table 18, where normalized peak impactor forces are listed. Test no. 8 for BIOSID shows an impactor force twice the values obtained during the other tests. This is due to the energy absorbing block for the pelvis, which had a stiffness out of tolerances.

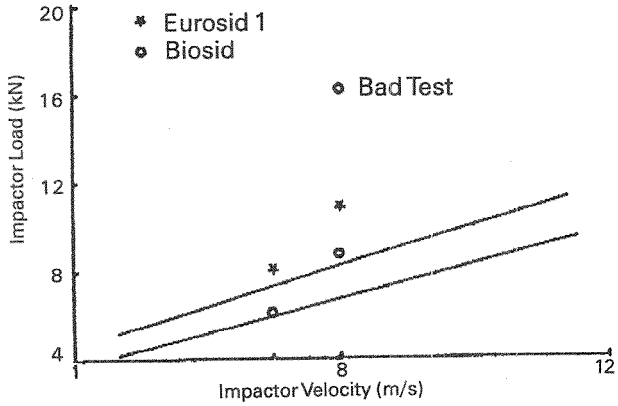

Figure 25. Normalized Impactor Versus Impact Velocity in Pelvic Tests

Table 18. EUROSID I and BIOSID Pelvis: Responses in 7 m/s and 8 m/s Impactor Tests

	EUROSID I					BIOSID				
Test Reference	**1**	**2**	**3**	**4**	**5**	**1**	**2**	**3**	**4**	**5**
Impact velocity (m/s)	7,10	7,03	6,97	6,97	7,03	7,03	7,03	6,97	6,97	7,03
Eff. Mass m_e (kg)	19,66	20,07	19,86	19,74	18,86	20,17	20,10	19,73	20,31	20,41
Nmlized peak impactor force (kN)	8,0	8,0	8,2	8,6	8,3	5,8	5,8	6,2	6,0	6,3
Test Reference	**6**	**7**	**8**	**9**	**10**	**6**	**7**	**8**	**9**	**10**
Impact velocity (m/s)	7,97	8,06	8,06	8,14	7,97	7,97	8,05	7,97	8,06	7,98
Eff. Mass m_e (kg)	21,18	19,98	20,05	19,25	20,11	18,99	18,79	13,99	18,27	18,72
Nmlized peak impactor force (kN)	9,9	11,0	11,1	11,5	10,6	8,1	8,2	17,9	8,7	8,2

Except of this test one can see the following:
- For the EUROSID I, the peak values of normalized force are slightly exceeding the limits set for the 7m/s tests, and considerably exceeding those for the 8m/s tests,respectively.
- For the BIOSID, they are comprised in the corridor for the 7m/s tests and little higher than maximum for 8m/s tests.

EUROSID I and BIOSID Pelvis Responses in Rigid and Padded Sled Test

The normalized peak impacted surface forces and the normalized peak lateral pelvis accelerations are reported in Table 19. The following conclusions can be drawn.

Table 19. EUROSID I and BIOSID Pelvis Responses in Rigid and Padded Sled Tests

	EUROSID I						BIOSID					
Test Reference	9101	9102	9103	9104	9105	9106	9101	9102	9103	9104	9105	9106
Impact velocity v_0= 6,5 m/s	6,76	6,78	6,83	6,80	6,73	6,76	6,83	6,83	6,80	6,80	6,85	6,60
Eff. Mass m_e (kg)	28,9	20,9	21,6	18,4	24,2	35,5	24,6	20,8	26,9	20,4	28,7	21,5
Nmlized peak impactor force (kN)	14,10	12,75	13,57	15,71	14,76	10,31	12,26	7,94	10,82	7,23	11,61	5,89
Nmlized peak lateral pelvis acceln. (g)	93,1	74,9	81,6	81,8	89,3	97,4	62,7	49,1	61,3	41,8	56,9	32,5
Test Reference	9107	9108	9109				9107	9108	9109			
Impact velocity v_0= 8,9 m/s	8,93	8,97	9,01				8,89	8,85	8,81			
Eff. Mass m_e (kg)	37,5	38,2	43,7				35,7	37,3	39,3			
Nmlized peak impactor force (kN)	9,23	9,96	10,57				8,62	9,23	9,47			
Nmlized peak lateral pelvis acceln. (g)	67,3	65,5	66,3				61,0	65,7	69,5			

EUROSID I. In the rigid sled tests, the normalized peak impacted surface forces are approximately twice as high as the ISO-specification whereas the mean values of the normalized peak lateral pelvis accelerations are only slightly too high.

In the rigid sled tests, the normalized peak impacted surface forces are approximately twice as high as the ISO-specification whereas the mean values of the normalized peak lateral pelvis accelerations are only slightly too high.

In the padded sled tests, the normalized peak forces on the impacted surface were slightly below, and the normalized peak lateral pelvis accelerations met, the ISO-specifications.

BIOSID. In the rigid sled tests, for both peak values there is a wide range of scattering (C.V.=23.5% and 28.1%). A possible explanation for this scattering may be obtained from the film analysis where one can observe, that the seating position of the dummy during the impact in test nos. 9104 and 9106 is not according to the upright seating position required by ISO. This phenomenon can be observed in all the tests, but it was most obvious in these two tests. Due to this anomaly, the load distribution on the dummy is not according to ISO requirement and so these two tests are not considered in the analysis.

Looking at the remaining four tests, the normalized peak forces on the impacted surface are considerably exceeding the ISO specifications in three cases, and only slightly in the last one.

The normalized peak lateral pelvis accelerations lay slightly below the ISO-specification.

In the padded sled tests, the scattering of both values cannot be detected. The normalized peak forces on the impacted surface are much too low compared with ISO specifications,while the normalized peak lateral pelvis accelerations meet the ISO specification.

EUROSID I AND BIOSID Biofidelity Scores for Pelvis Segment

Using the formulas from [4] and the weighing factors from [7] the dummies scores were established on the basis of the 4 test conditions described above. In Tables 20 and 21 there are the different factors and scores along with the requirements and dummies responses from which they were obtained. Therefore follows, that the dummies' biofidelity scores for the pelvis are:

- EUROSID I: B6 = 3.5
- BIOSID: B6 = 5.5 (* Except test nb 8)

EUROSID I and BIOSID) Repeatability in Pelvis Tests

Repeatability in 7m/s and 8m/s impactor tests. The EUROSID I offers a reasonable repeatability at the two impact velocities. The variations C.V. of the impactor accelerations, the pelvis accelerations and the pubic forces are 2.7%, 5.5% and 6.1% (7m/s-test) as well as 4.1%, 2.6% and 3.9% (8m/s-test).

Table 20. Weighing Factors and Scores for EUROSID I and BIOSID Pelvis Segment Obtained from Impactor Tests

TEST CONDITIONS V 6,j	V 6,1	W 6,1,1	Req. 1	EUROSID I	R 6,1,1	BIOSID	R 6,1,1
Impact Velocity 7 m/s	8						
Normalized peak impactor force vs impact velocity		9	Corridor	Outside	5	Inside	10
Biofidelity Score B 6,1				5		10	

TEST CONDITIONS V 6,j	V 6,2	W 6,2,1	Req. 1	EUROSID I	R 6,2,1	BIOSID	R 6,2,1
Impact Velocity 8 m/s	9						
Normalized peak impactor force vs impact velocity		9	Corridor	Far Outside	0	Outside	5
Biofidelity Score B 6,2				0		5	

Table 21. Weighing Factors and Scores for EUROSID I and BIOSID Pelvis Segment Obtained from Sled Tests (Except Tests nb 9104 and 9106)

TEST CONDITIONS	j	k	V 6,j	W 6,j,k	Requirement 3	EUROSID I - R 6,j,k	BIOSID* - R 6,j,k
Velocity Vo = 6.5 m/s		6	8				
Norm. peak impactor force (kN)	1			9	6.4 - 7.8	13.53 0	10.66 0
Norm. peak lateral pelvis acceleration (G)	2			7	63 - 77	86.4 5	57.5 5
Biofidelity score B 6,6						2.2	2.2
Velocity Vo = 8.9 m/s		8	8				
Norm. peak impactor force (kN)	1			9	11.6 - 13.6	9.92 5	9.11 0
Norm. peak lateral pelvis acceleration (G)	2			8	61 - 75	66.4 10	65.4 10
Biofidelity score B 6,8						7.4	4.7

The BIOSID shows also a relatively good repeatability at the 7m/s-tests for the peak values of impactor acceleration (C.V. 4.1%), pelvis acceleration (C.V. 3.6%), sacrum force (C.V. 4.1%); and spine X axis moment (C.V. 4.1%). Only the pubic force shows a greater scattering, with a C.V. of 17.3%.

At the 8m/s-tests the C.V. are very high due to the one test with the bad energy absorbing block (see above). But if one doesn't consider this test, the repeatability seems to be reasonable.

Repeatability in rigid and padded sled tests. The EUROSID I seems to show concerning the normalized peak lateral pelvis accelerations a very good repeatability in the padded sled tests (C.V. = 1.4%) but only a just acceptable repeatability in the rigid sled tests (C.V. = 9.7%).

A reasonable repeatability is to observe for the pubic symphysis forces (C.V.=6.1% in the rigid and 5.6% in the padded sled tests) and for the peak impacted surface forces in the padded tests (C.V.=6.8%). A poorer repeatability is given for these values in the rigid sled tests (C.V.=13.9%).

The BIOSID seems to have just an acceptable repeatability in the rigid sled tests concerning the pelvis accelerations (C.V.=10.6%) and also for the pubic forces (C.V.=9.6%) but a poor repeatability for the impacted surface forces (C.V.=17.9%). This analysis is to consider with the reservation of the discrepancy to ISO-specification of the seating position of the dummy during the impact as mentioned in chapter 2.6.2. Therefore the two worst tests nr. 9104 and 9106 are not regarded in this analysis. In the padded sled tests, the BIOSID shows a reasonable repeatability for the impacted surface forces (C.V. =4,8%) and the pelvis accelerations (C.V. =6.5%). Little poorer is the repeatability for the pubic forces (C.V.=10.8%).

Conclusions

The data from this project confirms earlier findings as regards the capabilities of mechanical surrogates of the human being in general, and of side impact dummies in particular. At the same time, it provides further indications towards the direction that ought to be taken if, at a future point of time, a valid tool capable of reasonably representing the biomechanical characteristics of vehicle occupants with sufficient accuracy shall become available.

To begin with the dummies' most prominent part, namely their heads, the study concluded that their repeatability appeared to be "excellent." This finding must, however be seen in comparison to the response limits defined by ISO. In the authors' view, an "excellent" repeatability of head responses that substantially exceed the upper limits of the ISO corridors (see above) has to be addressed as "poor" in terms of biofidelity.

The relative value of the biofidelity of a side impact dummy's head must further be judged against the results of previous evaluation projects and accident analyses, The available data base suggests that head contact with interior vehicle parts is in fact a rare occurrence in lateral impacts. When head contacts do occur in real accidents, they are in the majority of cases between the head and the object hitting or penetrating the vehicle. In such cases, it is of little relevance whether or not the dummy that may have been used to develop the vehicle type in question has had a good or an "excellent" head in terms of repeatability or *even* biofidelity. At any rate, preventing rigid obstacles from penetrating the struck vehicle's side structure in severe lateral impacts is, and probably will remain for the foreseeable future, beyond the state-of-the-art technology for the majority of cases. One possible conclusion in this particular area should therefore be that any further efforts aimed at improving side impact dummies should be focused on body segments that are of greater importance for the protection of vehicle occupants.

There is not much more to say about the relative biofidelity of the neck and shoulder segments than has already been said about the dummies' heads, with the exception that both dummies should possibly undergo a separate investigation into the response of their shoulders to oblique loads. It is recalled that the relative shoulder performance of the prototype EUROSID was quite different, depending on the direction of the load induced by a rigid impactor.

As regards the thoracic responses, one could again state that repeatability of either dummy was quite satisfactory, but that their biofidelity does still not appear to be sufficient. Although both dummies already constitute a certain improvement, in biofidelity terms, when compared to the prototype EUROSID or the NHTSA SID, respectively, more development work needs to be done if either of the new devices is to be used as element of any mandatory regulation. Again, it seems to be worthwhile to also consider the behavior of the dummies thoraces under oblique loading before a final decision on the implementation of a European side impact regulation is taken. In principle, all the above remarks can equally be applied to the two remaining, major body segments of importance, the abdomen and the pelvis.

Although one or the other of the two dummies shows better results in one or the other area of performance than its respective counterpart—*and predecessors*—neither of them can be said to be ready, on the basis of the present study, for use in a full-scale test procedure. Additional testing, covering other important areas such as sensitivity to velocity change and to padding effect, remains to be performed.

References

1. Bendjellal et al.,"Comparative Evaluation of the Biofidelity of EUROSID and US Side Impact Dummies" SAE Paper 881717. Proceedings of the 32nd Stapp Car Crash Conference, Atlanta, October 1988.
2. V.R. Hodgson, L.M. Thomas, "Head Impact Response" Vehicle Research Institute Report, V.R.I. 7.2, Society of Automotive Engineers, 1975.
3. "APR Lateral Cadaver Drop Tests Involving the Head" ISO/TC22/SC12/WG5, Document N165, June 1986.
4. ISO/TC22/SC12/WG5, "A Method to Calculate a Single, Weighted Biofidelity Value for a Side Impact Dummy" Doc. N253, March 1990.
5. ISO/TC22, "Road Vehicles—Anthropometric Side Impact Dummy. Lateral Neck Bending Response Requirements to Assess the Biofidelity of the Dummy" Nb TR 9790-2.
6. C.L. Ewing et al., "Dynamic Response of Human Head and Neck to +Gy Impact Acceleration" Proceedings of the 21st Stapp Car Crash Conference, New Orleans, October 1977.
7. ISO/TC22/SC12/WG5, "Proposed Weighing Factors for Rating the Impact Response Biofidelity of Various Side Impact Dummies" Document N278, June 1990.

8. ISO/TC22, "Road Vehicles—Anthropometric Side Impact Dummy. Lateral Shoulder Impact Response Requirements to Assess the Biofidelity of the Dummy" Nb TR 9790-4.
9. ISO TR 9790-5 first edition 1989-05-01 Road Vehicles—Anthropomorphic Side Impact Dummy, Part 5: Lateral abdominal impact response requirements to assess biofidelity of dummy.
10. G. Walfish, A. Fayon, C. Tarriere, J. Rosey, F. Guillon, C. Got, A. Patel, R. Stalnaker. Designing of A Dummy's Abdomen for Detecting Injuries in Side Impact Collisions. Fifth International Conference on the Biomechanics of Impact. September 1980.
11. ISO/TC 22/SC12, "Road Vehicles—Anthropomorphic Side Impact Dummy—Lateral Pelvic Impact Response Requirements to Assess the Biofidelity of the Dummy" TR 9790-6.
12. Cesari, D., Ramet, M., and Clair, P., "Evaluation of Pelvic Fracture Tolerance in Side Impact," SAE 801306, 24th Stapp Car Crash Conference, Oct. 1980.
13. Cesari, D., and Ramet, M., "Pelvic Tolerance and Protection Criteria in Side Impact," SAE 821159, 26th Stapp Car Crash Conference, Oct. 1982.
14. Cesari, D., Ramet, M. and Bouquet, R., "Tolerance of Human Pelvis to Fracture and Proposed Pelvic Protection Criterion to be Measured on Side Impact Dummies," 9th International Technical Conference on Experimental Safety Vehicles, Nov. 1982.
15. Kallieris, D., Mattern, R., Schmidt, G. and Eppinger, R., "Quantification of Side Impact Responses and Injuries," SAE 811008, 25th Stapp Car Crash Conference, Sept. 1981.

S8-O-06

Scaling HYBRID III and Human Head Kinematic Responses to Frontal Impact[1]

Marc S. Weiss, Sal Guccione
Naval Biodynamics Laboratory
Terry A. Watkins
University of New Orleans

Abstract

Injuries associated with impact acceleration forces are a major source of loss in both military and civilian transportation. The testing of impact protective devices under operational conditions is primarily done using anthropomorphic manikins such as the Hybrid III. As part of its Impact Injury Prevention program, the Naval Biodynamics Laboratory is studying human volunteer[2] and Hybrid III head-neck responses to whole-body acceleration. These data are being used to develop validated models, using Hybrid III responses, for predicting human head-neck responses at the full range of operational g-levels. For the -X directions, key linear and angular acceleration variables from selected sets of human experiments were fit using least-squares polynomial splines. The spline parameters are functions of the latency and amplitude of the peaks of the acceleration variables and are well-predicted from the initial head position and the sled acceleration profile. Similar functional forms were imposed on selected sets of Hybrid III data yielding equally good results. These common and consistent statistical models for human and Hybrid III data form the basis of a statistical scaling procedure between human and Hybrid III response for the -X direction. The results demonstrate an analytical approach for extrapolating human head/neck kinematics to levels and types of impact exposure where injury could occur. Currently, these results are being extended to include the +Y (lateral) and +Z (vertical) vector directions.

Introduction

The Naval Biodynamics Laboratory (NAVBIODYNLAB) is engaged in a long-term program to develop criteria for protecting aircrew from the potentially harmful effects of impact acceleration. As part of this program, predictive models for neck injury are being developed using the human head and neck response to whole-body acceleration. Over the past several years, a statistical regression approach has been used to develop a kinematic model for the head and neck response of human volunteers [1-4]. While this model is designed to address questions directly related to the prospect of injury in the hostile environment of military aviation, the techniques are broadly applicable to a range of biomechanical problems, including automotive crashes.

The statistical modelling approach differs fundamentally from a mechanistic model such as a mechanical linkage model or a finite element model. It is based first on sampling the response (human or manikin) and describing the sampled response with as few parameters as possible. A regression technique is then used to generate a statistical prediction of the response from the sled acceleration parameters. The goal of this procedure is to

[1]The interpretations and opinions in this work are the author's and do not necessarily reflect the policy and views of the Navy or other government agencies.
[2]Volunteer subjects were recruited, evaluated, and employed in accordance with procedures specified in the Department of Defense Directive 3216.2 and Secretary of the Navy Instruction 3900.39 series. These instructions meet or exceed prevailing national and international standards for the protection of human subjects.

predict the human response at potentially injurious high-G levels from measurements of the manikin response at the high-G level. This can be expressed schematically as follows:

Measure Manikin Response → Predict Human Response

In order to achieve this predictive model the following steps are taken:

Acceleration Parameters ⇆ Predict Manikin Response

Acceleration Parameters → Predict Human Response

These predictive equations are based on actual data obtained from measurements taken using manikins and human volunteers exposed to the same accelerations and in the same test configuration. The first step indicates that once the acceleration parameters are used to model the manikin response, the process can be reversed. That is, the manikin response can be used to predict the acceleration parameters. These predicted acceleration parameters can then be used to predict the human response. Thus, by appropriate analysis, the common regression on the acceleration parameters enables us to predict the unmeasured human response from the manikin response.

Methodology

Database

The data used in this analysis were obtained from 57 -Gx impact acceleration tests involving nine human volunteers and 30 -Gx tests using a 95th percentile Hybrid III manikin. All experiments were conducted at the NAVBIODYNLAB. The experimental and instrumentation details have been extensively reported elsewhere [5-8]. The human and manikin subjects were instrumented to measure head and neck displacement and linear and angular acceleration. They were seated with full torso restraint; the head and neck were allowed to move freely.

Figure 1 illustrates typical sled acceleration time traces for 7g to 20g. Volunteers were exposed to a maximum of 15.6g. The ranges of the sled acceleration parameters are listed in Table 1. These parameters are the: peak amplitude, endstroke velocity, onset (initial slope), peak duration (measured at 75% of peak amplitude), and overall length. All tests were run in the nominal neck-up, chin-up condition with the initial angular displacement close to zero radians. Representative human and HYBRID III head accelerations are shown in Figure 2 (angular acceleration) and Figure 3 (linear acceleration).

Analysis

To smooth the data, the head linear and angular acceleration curves were fitted with polynomial splines using least squares techniques [2-4]. For each curve, the times to peak and peak amplitudes for the first five peaks were determined from the fitted curve. These peaks are identified in Figure 2 and 3 by the numbers 1-5 for the human response (dotted curve) and the letters A-E for the manikin response (solid curve).

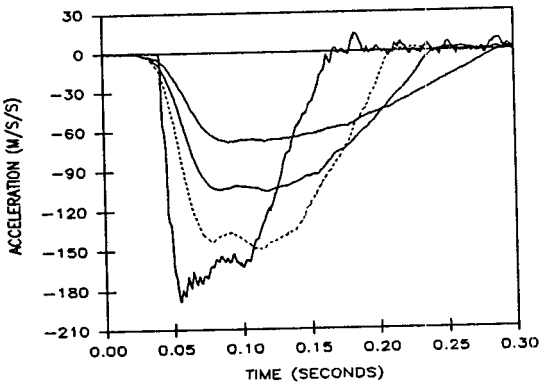

Figure 1. Typical Sled Acceleration Profiles

Table 1. Range of Sled Acceleration Parameters

PARAMETERS		HUMAN	MANIKIN
Peak	(m/s^2)	59.1 - 152.9	67.8 - 236.8
	(g)	6.0 - 15.6	6.9 - 24.2
End Stroke Velocity	(m/s)	9.8 - 17.6	10.8 - 20.5
	(km/h)	35 - 63	39 - 73
Onset	(m/s^3)	1314 - 5421	1427 - 17580
	(g/s)	134 - 554	146 - 1795
Duration	(ms)	87 - 122	64 - 117
Length	(ms)	200 - 301	128 - 273

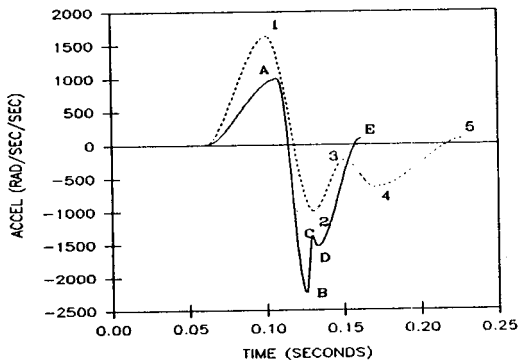

Figure 2. Representative Head Angular Accelerations About the Y-Axis for a -15Gx Test

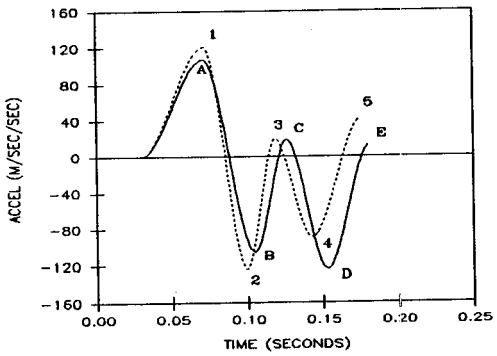

Figure 3. Representative Head Linear Accelerations About the X-Axis for a -15Gx Test

These computed values were then regressed against the peak sled acceleration, endstroke velocity and the initial head orientation in the X-Z plane. This resulted in a prediction model for peak values for each curve. Several SAS® regression programs (STEPWISE, RSQUARE, REG) were used in this process.[3] A simulation model was developed by adding appropriate normally distributed errors to the prediction model. The predicted curves are obtained by fitting the predicted peak values with cubic splines. Estimated upper and lower confidence bands for each curve were generated by simulating the predicted curve 100 times and determining the upper and lower boundaries.

Once the accuracy of the predictive modelling was established, a reverse prediction was used to estimate the human response using the measured manikin response. This was accomplished by estimating the sled acceleration parameters from the manikin response and then using these estimated parameters to predict the human response. This was first done for the range of accelerations in which there were human data to validate the procedures. The prediction model was then extended to higher accelerations using the manikin response at 19g and 24g.

Results

Excellent fits for the human and manikin head accelerations were obtained over the range of 6 to 16g. Figure 4 illustrates a typical simulation of a 10g -X human test with approximate 95% confidence bands indicated. This simulation uses the acceleration parameters to predict the head angular acceleration about the Y-axis. Figure 5 is a similar illustration for a manikin test. In both figures, the outer solid curves are the confidence bands. The inner dashed curve is the predicted mean response while the inner dotted curve is the measured mean response. These two figures demonstrate the first part of our modelling procedure. The narrow error band in Figure 4 indicates a highly accurate model for the human response. The broader error band in Figure 5 reflects the smaller sample size of five manikin 10g tests versus twelve 10g human tests. Nonetheless, the match between the predicted and measured mean responses is very good.

The second part of the modelling is illustrated in Figures 6-8. In these figures, the human response is predicted from the manikin response. The figures show, respectively, the predicted 8g, 12g and 15g -X human response (dotted curve), as well as the corresponding manikin response (solid curve). The average measured human response (dashed curve) is superimposed. These figures show an excellent fit between the predicted and observed angular accelerations. There is a slight increase in mismatch at the 15g level. Though not illustrated here, similarly good fits were obtained for the X and Z linear components of the head acceleration.

[3]SAS Institute, Inc., SAS/STATA, Release 6.01.

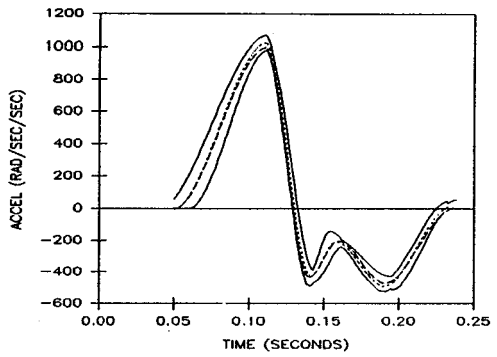

Figure 4. 10g Simulated Test: Human Head Angular Acceleration

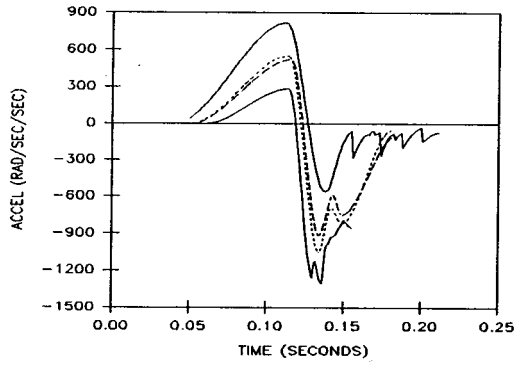

Figure 5. 10g Simulated Test: Manikin Head Angular Acceleration

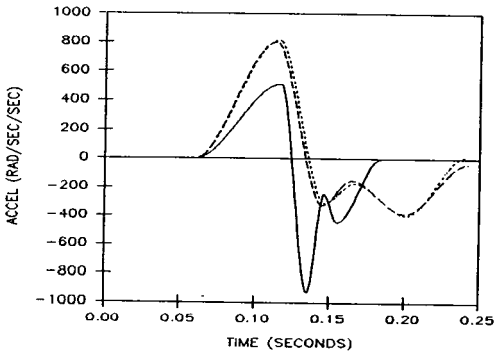

Figure 6. 8g Human Head Angular Acceleration Predicted by Manikin Response

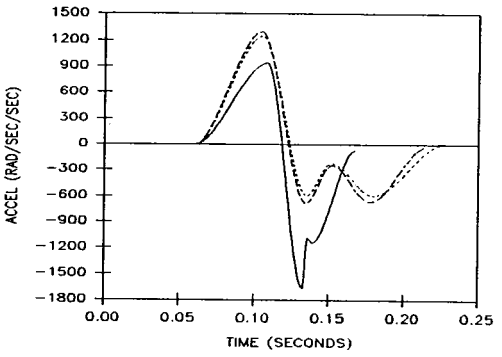

Figure 7. 12g Human Head Angular Acceleration Predicted by Manikin Response

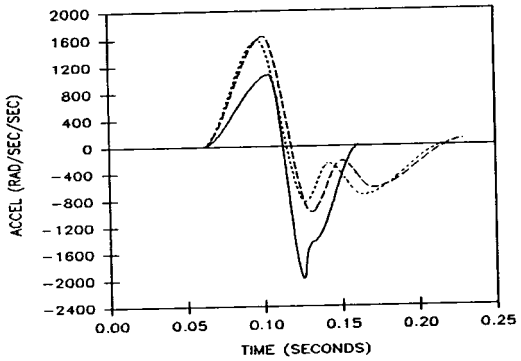

Figure 8. 15g Human Head Angular Acceleration Predicted by Manikin Response

Finally, Figures 9 and 10 illustrate the predicted 19g and 24g -X human response using the appropriate manikin response as the predictor. The manikin response is superimposed for illustrative purposes. Since no humans were tested at these levels, there is no direct validation of the simulation. Note that the manikin response shows a dramatic increase in the initial peaks of angular acceleration going from a 19g to a 24g input. Despite this, the model predicts a consistent change in the human response that is proportional to the increase in g-level.

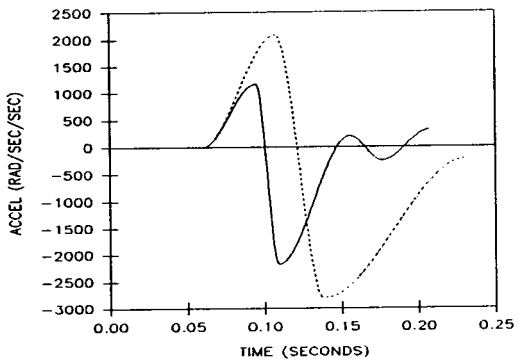

Figure 9. 19g Human Head Angular Acceleration Predicted by Dummy Response

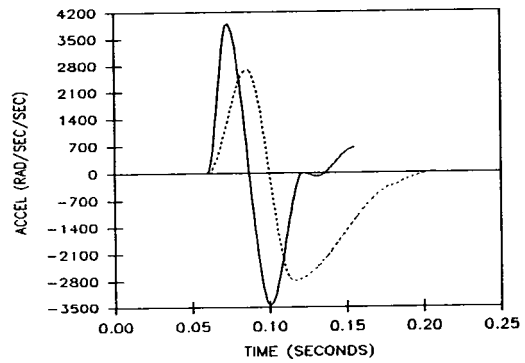

Figure 10. 24g Human Head Angular Acceleration Predicted by Dummy Response

Discussion

The problem of scaling human surrogate biomechanical responses to human responses is critical for valid testing of crashworthy vehicles and injury protective equipment. The results of this study are very encouraging in demonstrating a useful analytical approach towards addressing this problem. Using the HYBRID III as a human test surrogate, we have been able to extrapolate human volunteer head/neck kinematics to levels where injury might be expected. This reflects the fact that a similar analytic model describes both human and HYBRID III kinematics under conditions of similar seat and restraint configuration. These modelling techniques and procedures are general and broadly applicable to use of other surrogates such as animals [3] and cadavers. It is these biological surrogates which, when appropriately scaled, will generate the most useful information concerning the thresholds and mechanisms of acceleration induced injury. For the HYBRID III surrogate, this approach is currently being extended to include analysis of human impact acceleration response in the +Y (lateral) and +Z (vertical) vector directions.

Acknowledgements

The authors thank Mr. Ronnie Wilson of the Mathematical Sciences Division for his expert knowledge and tireless efforts in helping to produce the figures for this paper.

References

1. Watkins, T.A. and Guccione, S.J., Jr., "A Statistical Approach to Human Kinematic Response to Impact Acceleration." Presented at the 16th Annual International Workshop on Human Subjects for Biomechanical Research, Atlanta, GA, October 1988.
2. Watkins, T.A. and Guccione, S.J., Jr., "A Consistent Statistical Model for Human Kinematic Response to Impact Acceleration." Presented at the 17th Annual International Workshop on Human Subjects for Biomechanical Research, Washington, DC., October 1989.
3. Weiss, M.S., Guccione, S.J., Jr. and Watkins, T.A., "A Kinematic/Dynamic Model for Prediction of Neck Injury During Impact Acceleration," *AGARD Conference Proceedings No. 471*, Neuilly sur Seine, France, pp. 11:1-11:6, 1989.
4. Watkins, T.A., Weiss, M.S., Call, D. W., and Guccione, S. J., "A Kinematic Model for Predicting the Effects of Helmet-mounted Systems," *AGARD Conference Proceedings*, Neuilly sur Seine, France, (in press); 1991.
5. Ewing, C.L., Thomas, D.J., Lustick, L.S., Muzzy III, W.H., Willems, G.C. and Becker, E.B., "The Effects of the Initial Position of the Head and Neck on the Dynamic Response of Human Head and Neck to -Gx Impact Acceleration," *Proceedings of the Nineteenth*

Stapp Car Crash Conference, Society of Automotive Engineers, Inc., 400 Commonwealth Drive, Warrendale, PA, pp. 487-512, 1975.

6. Ewing, C.L., Thomas, D.J. Lustick, L.S., Muzzy III, W.H., Willems, G.C. and Majewski, P.J., "The Effects of Duration, Rate of Onset, and Peak Sled Acceleration on the Dynamic Response of the Human Head and Neck," *Proceedings of the Twentieth Stapp Car Crash Conference*, Society of Automotive Engineers, Inc., 400 Commonwealth Drive, Warrendale, PA, pp. 3-41, 1976.
7. Ewing, C.L., Thomas, D.J., Lustick, L.S., Muzzy III, W.H., Willems, G.C. and Majewski, P.J., "Dynamic Response of Human Head and Neck to + Gy Impact Acceleration," *Proceedings of the Twenty-First Stapp Car Crash Conference*, Society of Automotive Engineers, Inc., 400 Commonwealth Drive, Warrendale, PA, pp. 547-586, 1977.
8. Becker, E.B., "Stereoradiographic Measurements for Anatomically Mounted Instruments," *Proceedings of the Twenty-First Stapp Car Crash Conference*, Society of Automotive Engineers, Inc., 400 Commonwealth Drive, Warrendale, PA, pp. 475-505, 1977.

S8-O-07

Facial Fracture Probability Secondary to Steering Wheel Impact

Narayan Yoganandan, Anthony Sances, Jr., Frank Pintar, John Reinartz
Medical College of Wisconsin
Mark Haffner
National Highway Traffic Safety Administration

Abstract

Studies were conducted to evaluate the quasi-static and dynamic performance of an energy absorbing (EA) and a standard (STD) steering wheel at the lower spoke and rim (LSR) and at the center part of the unsupported rim (USR) locations. In addition, tests were conducted at the USR location of two steering wheels using intact fresh human cadaver heads. Using a custom designed impact drop test system, either zygoma was impacted at the USR location at velocities ranging from 1.73 to 6.71 m/s. Generalized force histories were recorded using a six-axis load cell under the hub of the steering wheel placed at 30 degrees to the horizontal to simulate restrained driver impact in collisions. Steering wheel deformations were recorded using a potentiometer. Accelerometers were placed on the specimen and under the wheel rim at the impact site, opposite to the impact site, as well as at locations 90 degrees from the USR. High speed photography documented wheel kinematics. Our previously published data at the LSR location on the EA wheel (32nd Stapp Conference) was combined with additional human cadaver tests (from this study) to obtain the facial fracture probability distribution at this location of the EA wheel. Facial trauma was assessed in all specimens using gross dissection, plain radiography, computed tomography, and defleshing techniques. Fracture severity was graded according to accepted techniques.

The interface force-time response at the wheel rim typically exhibits bimodal behavior. The first force peak appears to be a function of wheel rim inertia: it is coincident with maximum rim acceleration at the impact site, at a time when rim deflection is small. The second peak appears to be largely driven by the force-deflection behavior of the wheel since it occurs when rim deflection is approaching its maximum value and when rim velocity and acceleration have fallen to low values. However, the magnitude of the second force peak often exceeds the value which would be expected on the basis of quasi-static force-deflection behavior alone.

At low impact velocities, the first (inertial) peak is smaller than the second. However, at the higher impact velocities in this experimental series, the magnitude of the inertial peak can exceed the second peak value. Therefore, it is concluded that an understanding of both inertial and stiffness characteristics is necessary for optimal design of steering assemblies protective of the facial skeleton.

Data has been gathered and presented in four discrete sets: EA and STD wheels at LSR and USR locations. Additional biomechanical data was acquired for the EA wheel at the LSR location and combined with the previously reported information to permit a Weibull probability analysis. Results indicated that a force level of 1525 N corresponds to a 50% probability of facial fracture at the LSR location on the EA wheel. At the USR location on the EA wheel, no fractures were detected in seven tests conducted at velocities up to 6.7 m/s with peak forces up to 1335 N. Additional tests are necessary on the STD wheel to deduce probability distributions at both the USR and LSR locations.

Introduction

Maxillofacial trauma primarily affects our adult population, and is often quoted as an affliction of the young, mobile and aggressive portion of our community (10). Altercations and motor vehicle collisions account for a significant number of these injuries. Motor vehicle

crashes are responsible for a large number of mid-facial fractures and complex facial injuries involving multiple regions of the skeleton (10,17). A study conducted by Strakhammer and Olfsson reported that the zygomatic region of the face is involved in 42 percent of facial fractures from motor vehicle crashes (17). Substantial worldwide concern exists regarding facial injuries for unrestrained and restrained motor vehicle occupants (1,2,6-8,11,13,16,20,21,22,24,25). Recently, Zuby and Saul conducted a detailed examination of hardcopy National Accident Sampling System files to ascertain the nature of steering assembly induced facial trauma to restrained drivers. Maxilla, mandible, nasal, and zygomatic areas were identified as the most commonly injured regions. Approximately fifty percent of the steering wheel induced facial injuries occurred below speeds of 7 m/s (vehicle delta V) in seatbelted drivers (25). The unsupported portion of the rim accounted for 48 percent, the hub-spoke region accounted for 19 percent, and the junction of the spoke and rim accounted for six percent of the facial injuries.

Biomechanical data identifying the mechanisms of facial injury and tolerance information for facial impacts with automotive steering wheels is limited. In addition, a biomechanically validated human-like facial structure for a test dummy, based on facial injury data from steering wheel impacts, does not exist. Consequently, the Medical College of Wisconsin is developing studies in concert with the National Highway Traffic Safety Administration (NHTSA) of the U. S. Department of Transportation to investigate facial bone fracture secondary to steering wheel impact. In an earlier study, human cadaver studies were conducted by impacting the left or the right zygoma once at the junction of the lower spoke and rim (LSR) on both an energy absorbing (EA) and a commercially available standard (STD) steering wheel. The EA wheel was designed and developed by TRRL and Sheller-Clifford in the United Kingdom, and the STD wheel was obtained locally from a Ford Motor Company dealer. Results of this research were reported earlier (22); this project is a continuation of that research.

Purpose

The present study was undertaken to: a) evaluate the static and dynamic performance of the EA and STD steering wheels, b) to determine the differences, if any, between the injury mitigating characteristics of the steering wheel when the location of impact is the center part of the unsupported rim (USR) in contrast to the junction of the lower spoke and rim (LSR), c) to identify the likely biomechanical variables associated with facial fracture at both the LSR and USR locations on the two steering wheels, and d) to explore the possibility of a criterion for fracture applicable to wheel impact locations of varying area and stiffness. It is hoped that this series of investigations may lead to steering assembly designs more protective of the facial skeleton.

In this paper we will describe the techniques used to conduct quasi-static and dynamic tests on the steering wheel, and conduct intact fresh human cadaver head impact tests at the USR location on both the EA and STD wheels with the drop system designed earlier (22). Results of the additional tests conducted at the LSR location on the EA wheel will also be presented. An examination of these results together with the data from the previous study will be conducted.

Materials and Methods

Quasi-static Performance

The EA and STD steering wheels were loaded quasi-statically at a rate of 2.5 mm/s using an electrohydraulic testing device. Tests were conducted at the junction of the lower spoke and rim (LSR), as well as at the center of the unsupported rim (USR). The steering wheels were inclined at 30 degrees to the horizontal plane to simulate restrained driver impact in collisions. A six-axis load cell (Denton Inc., Rochester, MI) was placed directly under the hub of the steering wheel to record the generalized force histories. The loading surface attached to the piston of the testing device simulated the curvature of the human zygomatic bone. This fixture did not bind the steering wheel during loading.

Dynamic Evaluation

Vertical drop impact test system. The dynamic evaluation of the steering wheel performance was determined using the vertical drop impact test system which was specially designed to conduct head and facial impact injury studies (Figure 1). The system was validated by comparing the results with unconstrained, free fall, rigid headform experiments (22). Briefly, the device consists of a 7.6 m steel channel with a ground aluminum angle fixed to the outer edge. A vertically supported stainless steel monorail is centered on the channel with an attached cart assembly supported by two linear bearings and an outrigger. The linear bearings support the cart on the monorail as well as the outrigger. The outrigger bearing mechanism prevents the rotation of the cart about the vertical axis. The linear bearings constrain rotation about the other coordinate axes. A specially designed positioning fixture permitted the use of Z90.1 headforms as well as human cadaveric heads. The fixture was designed to allow for 360 degree rotation of the specimens in the lateral-lateral and superior-inferior directions to insure that the impact location is at a predetermined site. In all the studies the impact location was in the region of the malar eminence of either zygomatic bony complex.

Steering wheel instrumentation. Similar to the case of quasi-static performance studies described above, the steering wheel was inclined at 30 degrees to the horizontal and the six-axis load cell was placed directly

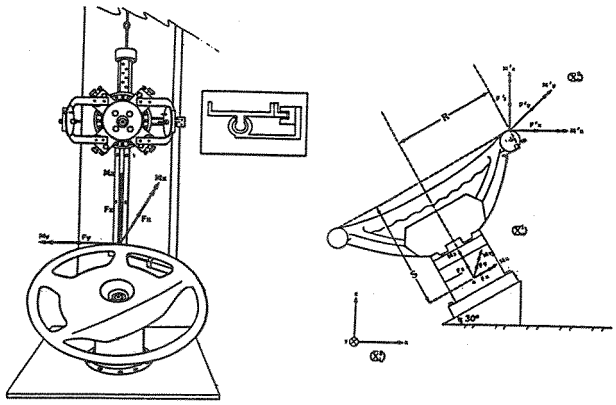

Figure 1. Diagram Illustrating the Vertical Drop Impact Testing Device (left) and a Section of the Steering Wheel with a Six-Axis Load Cell Placed Under the Hub. The steering wheel is inclined under at 30 degrees with respect to the horizontal.

under the hub to record the generalized force histories. In addition, a uniaxial potentiometer (Space Age Control Inc., Palmdale, CA) was placed normal to the steering wheel under the impact location to document the deformation of the rim impact site. A triaxial accelerometer (Endevco, San Juan Capistrano, CA) was rigidly fixed to the steering wheel under the impact site. Uniaxial accelerometers (Endevco, San Juan Capistrano, CA) were firmly fixed to the structure at a location opposite to the impact site as well as at both locations orthogonal to the impact site. All accelerometers were attached to the metal surface of the wheel by removing a small portion of the outer foam. Figure 2 illustrates the positioning of the wheel in the testing device for impact tests at the center of the unsupported rim. It also depicts the location of the instrumentation devices mounted on the steering wheel structure.

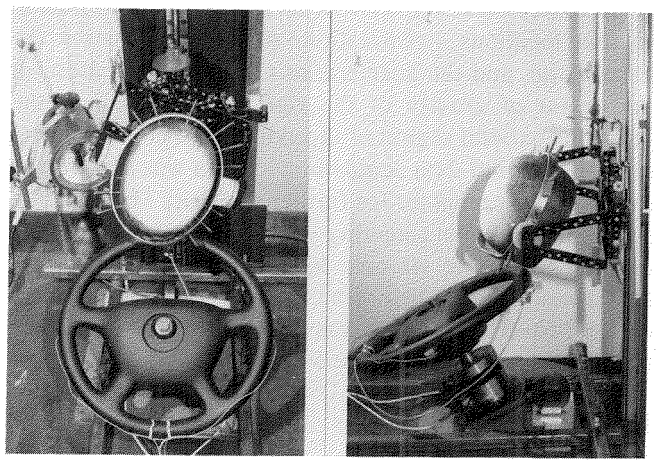

Figure 2. Photograph Illustrating the Positioning of the Steering Wheel and the Vertical Drop Impact Test System. Instrumentation on the steering wheel included accelerometers at the impact site (USR), opposite of the USR, and at bilateral locations (see Table 1). The six-axis load cell and the uniaxial potentiometer under the USR are clearly observable in the lateral projection (right).

Rigid headform (Z90.1) impact tests. The dynamic performance of the EA and STD wheels was initially evaluated using a rigid Z90.1 headform. The Z90.1 magnesium headform was mounted in a haloring and a triaxial accelerometer (Endevco, San Juan Capistrano, CA) was attached at the center of gravity. The headform was dropped using the vertical drop impact test system onto the center part of the unsupported rim of both EA and STD wheels. Tests were conducted at impact velocities ranging from 1.7 to 4.5 m/s with equivalent drop heights of 0.15 to 1.0 m. A new steering wheel was used for each experiment. Eighteen channels of data were gathered for each test (Table 1).

Table 1. Instrumentation Details for Dynamic Tests

TABLE 1: INSTRUMENTATION DETAILS FOR DYNAMIC TESTS

No.	Description	No. of Data Channels
1	Six-axis load cell underneath the hub	6
2	Uniaxial potentiometer under impact sit on the wheel	1
3	Triaxial accelerometer under the impact site on the wheel	3
4	Uniaxial/triaxial accelerometer opposite to impact site on the wheel*	3/1
5	Uniaxial accelerometer othogonal to triaxial accelerometers	2
6	Triaxial accelerometer at - C.G. of Z90.1 headform - posterior parietal region opposite to impact site on the specimen	3

* for rigid headform studies a triaxial accelerometer was used and for specimen tests a uniaxial accelerometer was used on the wheel.

Human cadaver head impact tests. A total of 18 fresh adult human cadaver heads were used in the study. The age, height, and weight of the specimens ranged from 51 to 83 years, 1.5 to 1.9 m, and 45 to 100 kg, respectively. All subjects (13 male and 5 female) had died secondary to cardiopulmonary complications (Table 2). Medical records were reviewed and routine radiography was done to select subjects without preexisting metastatic bone disease or any prevalent head and facial trauma. In addition, the criteria precluded selection of specimens with noticeable physical abnormalities. All specimens

Table 2. Details of Specimen Used in the Study

SPECIMEN IDENTIFICATION	AGE (years)	SEX	HEIGHT (m)	WEIGHT (kg)	CAUSE OF DEATH	STEERING WHEEL Type/Location
A	65	M	1.75	61	Myocardial ischemia	EA-USR
D	60	M	1.90	84	Sudden death	EA-USR
E	51	M	1.78	82	Heart failure	EA-USR
F	78	F	1.60	57	Heart failure	EA-USR
24	68	M	1.78	66	Heart failure	STD-LSR
21	68	M	1.83	59	Respiratory arrest	STD-LSR
G	67	M	1.70	45	Cardiopulmonary Failure	EA-USR
23	78	F	1.70	74	Heart attack	STD-LSR
22	83	F	1.60	82	Heart failure	STD-LSR
B	73	M	1.78	73	Pneumonia	EA-LSR
C	73	M	1.79	73	Pneumonia	EA-LSR
H	69	M	1.78	79	Heart Failure	EA-LSR
K	68	M	1.80	82	Renal Failure	EA-LSR
L	80	F	1.55	43	Cardiac Arrest	EA-LSR
M	58	M	1.78	100	Heart Failure	EA-LSR
N	71	M	1.83	54	Co Poisioning	EA-LSR
P	59	M	1.78	91	Cardio Respiratory Arrest	EA-LSR
Q	70	F	1.57	82	Heart Failure	EA-LSR

were isolated at the occiput-atlas level within one to three days after death and were double wrapped in plastic bags, sealed and kept deep frozen at -70 degrees Celsius. Two-dimensional computed tomography (CT) was done in axial and sagittal planes at overlapping 1.5 mm intervals using a CT scanner (General Electric, model 9800, Waukesha, WI). The specimens were thawed at room temperature for 12-20 hours in a humidity controlled environment before testing. Pretest radiographs of the specimen were taken.

A total of nine specimens were used to conduct USR tests (Table 2). Four of the nine specimens were impacted once at the USR location on the STD steering wheel. The remaining five specimens were used to conduct tests with the EA steering wheel; one preparation (specimen A) was tested at 1.73, 2.21, and 2.45 m/s velocity without any fracture, all other samples were tested once on either zygoma (right or left, randomly chosen). This resulted in a total of seven tests for the EA wheel. Physical data such as the chin to vertex distance, maximum circumference of head above the Frankfort plane, lateral-lateral measurement at the auditory meatus level, and nasion to occiput dimension were measured. In addition, the thickness of the skin at the impacting zygomatic area in the region of the malar eminence was recorded using a calibrated needle. The isolated weight of the cadaver head was also noted.

The head was mounted in a neurosurgical stainless steel haloring with fixation into the skull using eight to twelve screws. The specimen was then attached to the positioning fixture of the vertical drop impact test system described above. A triaxial accelerometer was firmly fixed to the skull with four stainless steel screws in the posterior parietal region opposite to the impact location. The z-axis of the accelerometer coincided with the vertical axis of the impact testing device. Other instrumentation used to record the biomechanical data are included in Table 1. A total of sixteen channels of data was collected in these tests. To achieve a standardized mass, all specimens including the weight of the fixtures such as haloring and screws were ballasted to 6.8 kg.

The specimens were suitably oriented in the positioning fixture so that the preparation was impacted normal to the malar eminence of the zygomatic bone. The specimens were dropped from a predetermined height (0.15 m to 2.29 m) at velocities ranging from 1.7 to 6.7 m/s for the USR tests. Additional tests at the LSR location on the EA wheel were conducted in the present study at velocities ranging from 1.41 to 5.59 m/s. The impact event was documented with high speed photography (Hycam II, Red Lake Laboratories, CA) at 1000 f/s. Immediately following the drop, contact areas were measured on the specimen and palpation was done. The zygoma-steering wheel rim contact areas were idealized as an ellipse and the major and minor axis dimensions were noted by determining the residual deformations of the tissue at the impact site. Following this, a gross dissection of the loaded region was performed to observe the macrolevel pathology. An area approximately spanning from the zygomatic arch to the lateral nasal region and from the lower orbit to the upper maxilla was carefully dissected for this purpose. Radiographs were taken and the specimens were imaged under the CT scanner. Specimens were then defleshed by immersing the preparation in a caustic liquid for 24-40 hours and thoroughly washing with a strong solution of hydrogen peroxide. Sufficient care was taken to preserve all the bony fragments of the preparation.

Biomechanical Data Collection and Analysis

The input force and steering wheel deflection data in quasi-static studies were gathered from a uniaxial force gage (Kistler Corp, Amherst, NY) and a linear variable differential transformer, respectively. The steering wheel deflection below the loading site was recorded using a potentiometer. These signals including the output six-axis load cell data were collected using a digital oscilloscope (Norland Corp., Fort Atkinson, WI) and a modular data acquisition system (Kaye Instruments Inc., Boston, MA) at appropriate sampling frequencies. From the force-deflection response, stiffness (defined as the slope of the curve in the most linear part of the response) and energy absorbing characteristics (integral of the force-deflection response) were computed.

All data during impact tests were collected according to NHTSA requirements using a digital data acquisition system (Kaye Instruments Inc., Boston, MA) with predesigned amplifiers and appropriate antialiasing filters. The sampling rate exceeded 8 kHz; in some instances a 24 kHz rate was selected. The signals were processed according to SAEJ211b specifications and class 1000 filtering was implemented. The data included the six-axis force and moment histories, accelerations of the wheel at various locations, deformations of the wheel under the impact site, and the accelerations of the preparation (at the center of gravity of the rigid headform or at the posterior parietal region of the skull). The collected data using the digital data acquisition system was transferred to a personal computer for further analysis. The dynamic forces at the zygoma steering wheel impact location were derived using the six-axis load cell histories and deformation histories according to the procedure described earlier (22). The resultant transformed peak forces (interface forces) were determined for each specimen.

Results

Quasi-Static Performance

Mechanical quasi-static responses of the EA and STD wheels indicated nonlinear characteristics (Figure 3). Predictably, the center part of the unsupported rim of both the wheels was not as stiff as the junction of the lower spoke and rim. In-addition, the EA wheel was less stiff than the STD wheel at both these locations. In the EA wheel, a maximum force of 1609 N was developed

when it was loaded at the junction of the lower spoke and rim; in contrast, a maximum force of 664 N was generated for the center part of the unsupported rim loading (Table 3). For the STD wheels, these forces were consistently higher (2989 N at the junction of the lower spoke and rim, 951 N at the center part of the unsupported rim). At the USR, the STD wheel was approximately twice as stiff as the EA wheel (stiffness of 41.3 N/mm vs. 21.4 N/mm).

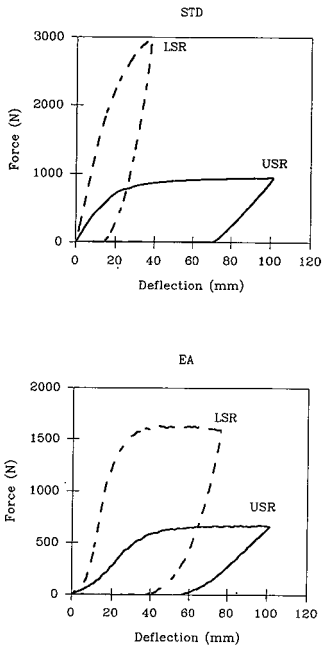

Figure 3. Quasi-static Response of the Steering Wheels Tested Using a Materials-Testing Device. Top: Standard wheel, and bottom: EA steering wheel. LSR and USR represent the junction of the lower spoke and rim and the center part of the unsupported rim of the steering wheel, respectively.

Table 3. Summary of Rigid Headform Impact Tests Conducted at USR

STEERING WHEEL	DROP HEIGHT (m)	IMPACT VELOCITY (m/s)	PEAK IMPACT Z FORCE (N)	WHEEL DEFORM-ATION* (mm)	HEAD ACCEL* (G)	HEAD INJURY CRITERIA	RESULTANT PEAK IMPACT FORCE (N)	MAXIMUM WHEEL DEFLECTION (mm)	MAXIMUM HEAD ACCEL (G)	MAXIMUM WHEEL RESULT ACCEL# (G)
EA	0.15	1.73	647.6	30.89	7.75	4.48	644.3	31.10	8.51	41.21
EA	0.23	2.12	728.4	38.65	8.40	6.14	758.4	38.98	10.03	49.57
EA	0.30	2.45	790.3	43.58	8.54	9.09	812.8	45.82	11.25	58.97
EA	1.00	4.47	1140.3	98.38	13.73	22.97	1194.9	98.46	14.89	80.28
STD	0.15	1.73	838.1	20.12	9.62	8.50	840.1	21.26	11.32	88.18
STD	0.23	2.12	925.4	25.93	11.68	9.67	935.1	27.66	12.78	84.31
STD	0.30	2.45	971.7	31.78	12.24	13.38	980.6	35.30	12.82	97.10
STD	1.00	4.47	1281.8	64.33	13.27	28.47	1275.4	88.35	17.34	237.81

NOTE:
* Wheel deflection and head acceleration values correspond to the peak impact Z force.
Wheel deflections were recorded from the uniaxial potentiometer placed underneath the impact site (USR) along the Z direction.
Maximum wheel resultant accelerations were recorded underneath the impact site (USR) on the wheel.

Rigid HeadForm Impact Tests

A summary of the results from the rigid headform tests conducted on the center part of the unsupported rim of the EA and STD steering wheels is included in Table 3. A comparison of the performance of the EA and STD wheels at the USR location at a velocity of 4.47 m/s is illustrated in Figures 4 and 5, respectively. In the interest of brevity, other (lower) velocities are not included. The maximum values of variables such as force, deformation, and acceleration are however, shown in Table 3 for all the tests conducted in the study. The interface force developed at the wheel rim typically exhibited bimodal characteristics. The first peak in the force-time response coincided with the peak wheel rim acceleration (Figures 4 and 5). This peak force corresponds in time to the occurrence of maximum wheel rim acceleration during the initial stages of impact. The rim deflections are small during this time. The force begins to rise again after the acceleration drops demonstrating that the inertial effects do not contribute significantly to the development of the subsequent increase in interface forces. Furthermore, the velocity also exhibits a gradual decrease while the force and the wheel rim deflection progressively increase towards their respective peak values. This suggests that rate effects do not significantly contribute to the development of the secondary peak force. However, the maximum interface force of 1141 N attained at a deflection of 98.4 mm for the EA wheel experiment, and 1282 N attained at a deflection of 64.3 mm for the STD wheel test exceeded the corresponding quasi-static values (see Section a. "Quasi-static performance" above).

Human Cadaver Head Impact Tests at the USR

Biomechanical findings. A summary of the salient biomechanical data from the EA and STD wheels is included in Table 4. Figure 6 illustrates a plot of the acceleration, transformed force, and dynamic wheel deformation histories for all the specimens tested. It should be noted that, the steering wheel deflections attain their absolute maximum values at or after the development of the peak impact force. Greatest displacements were recorded with the EA steering wheel. No facial lacerations were observed in either the EA or the STD wheel. Maximum permanent deformations occurred primarily at the loading site (center part of unsupported rim).

High speed film analysis. Results of the high speed film taken at 1000 f/s indicated the following: Immediately following impact, the steering wheel begins to deform principally in the vertical direction at the hub-ring as well as at the USR location. A gradual lateral displacement of the wheel rim will then ensue concomitant with vertical deflection. The lateral displacement will reach a maximum prior to the attainment of peak vertical deflection. Typically, the maximum lateral displacement occurred following the attainment of the first force peak (corresponding to the inertial effects) but well before the development of the ultimate maximum force. Following the gradual decrease of the lateral displacement from its peak value, the wheel deforms primarily as a curved beam partially constrained the two supported regions (entire unsupported rim portion) with maximum deformation at its center resulting in a wrapping around effect on the preparation.

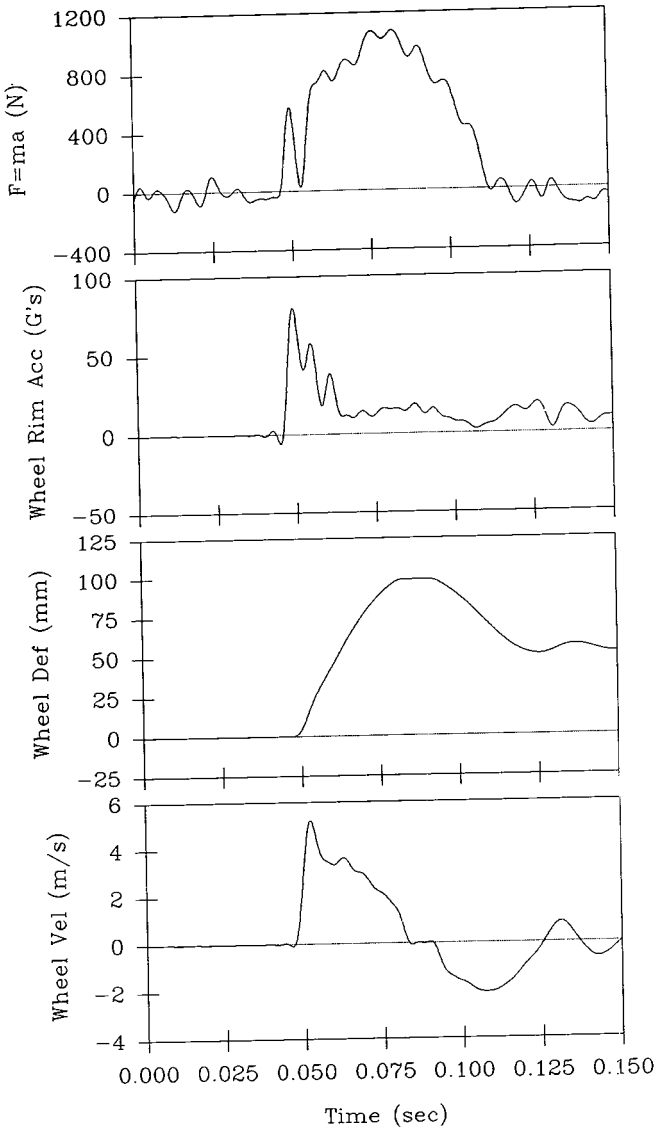

Figure 4. Dynamic Response of the EA Wheel Tested at the USR Location with Z90.1 Rigid Headform at a Velocity of 4.47 m/s. Top trace indicates the force computed from the rigid body mechanics principles, i.e., mass of the headform times the acceleration in the vertical (z) direction. Second from top: Acceleration response of the wheel rim at the impact site (USR) in the z-direction. Third from top: The deflection history of the wheel recorded by the uniaxial potentiometer placed underneath the impact site. Bottom. The velocity response of the wheel rim computed using the deflection history.

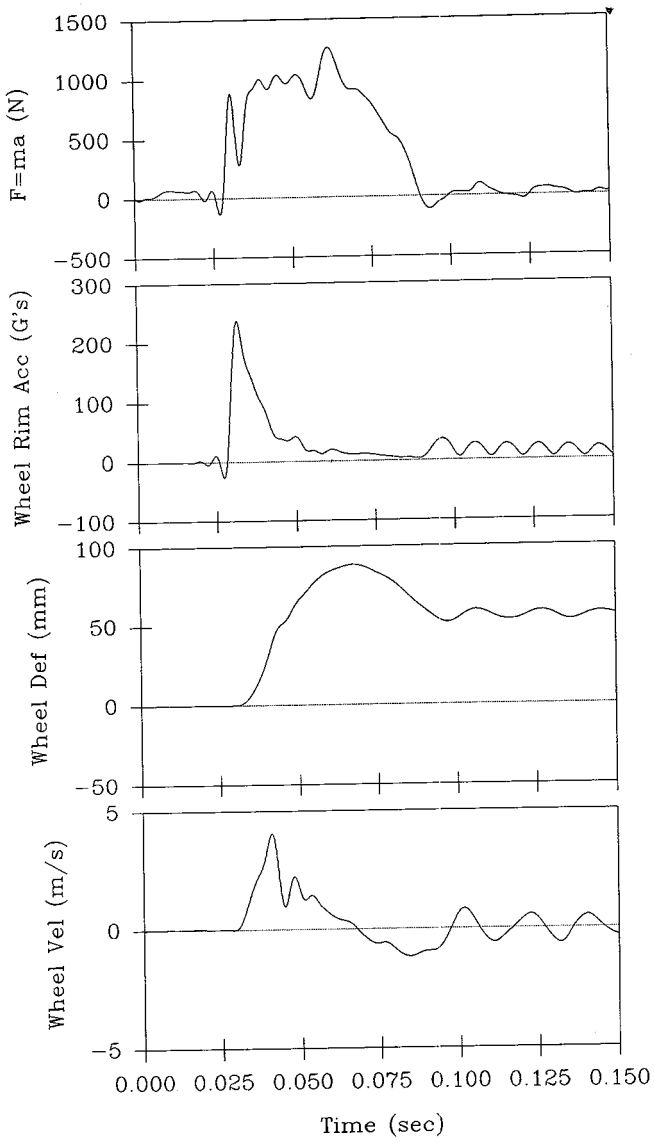

Figure 5. Dynamic Response of the Standard Wheel Tested at the USR Location with Z90.1 Rigid Headform at a Velocity of 4.47 m/s. Top trace indicates the force computed from the rigid body mechanics principles, i.e., mass of the headform times the acceleration in the vertical (z) direction. Second from top: Acceleration response of the wheel rim at the impact site (USR) in the z-direction. Third from top: The deflection history of the wheel recorded by the uniaxial potentiometer placed underneath the impact site. Bottom. The velocity response of the wheel rim computed using the deflection history.

Typically, for both EA and STD wheel tests, at the point where the maximum lateral displacement occurs, it is possible that the lateral wall of the orbit comes in contact with the wheel surface. The extent of bridging of the orbit structure depends on the magnitude of the lateral displacement. Furthermore, it is also possible that, at the time of the maximum lateral displacement, the wheel may not be in contact with the malar eminence of the zygomatic bone thus unloading the initial impact site. These factors may have contributed to the absence of bone fractures noted in the USR tests on the EA wheel.

Pathological observations. The pathological findings from the study which included the evaluation of displaced and foes fractures to the facial skeleton from palpation and gross dissection immediately following the impact, pre and post test radiography, CT, and defleshing techniques indicated no structural abnormalities for the EA wheel tests conducted at velocities up to 6.71 m/s.

Table 4. Summary of Biomechanical Data of Specimens Tested at USR Location

SPECIMEN I.D.	STEERING WHEEL	IMPACT SITE	IMPACT VELOCITY (m/s)	SPECIMEN (age/sex) (years/M-F)	RESULTANT PEAK IMPACT FORCE (N)	CONTACT AREA (mm²)	DEFORMATION* (mm)	RESULTANT HEAD ACCEL (G)	RESULTANT WHEEL ACCEL (G)	HEAD INJURY CRITERIA	FACIAL FRACTURE
A	EA	Right Zygoma	1.73	65/M	552.1	1244	31.59	7.24	34.63	3.81	NO
A	EA	Right Zygoma	2.12	65/M	657.0	1294	39.13	8.73	37.85	5.52	NO
A	EA	Right Zygoma	2.45	65/M	707.1	1354	46.49	9.78	43.91	7.78	NO
D	EA	Left Zygoma	4.47	60/M	1056.9	1875	107.72	13.69	124.08	22.31	NO
E	EA	Left Zygoma	5.59	51/M	1324.8	2120	140.15	16.24	153.29	35.20	NO
F	EA	Left Zygoma	5.59	78/F	1334.4	1984	138.73	19.31	173.97	32.60	NO
G	EA	Right Zygoma	6.71	67/M	1289.7	2081	199.79	27.98	231.03	53.40	NO
21	STD	Right Zygoma	4.47	68/M	1153.0	1099	88.96	38.05	226.68	40.20	NO
22	STD	Right Zygoma	4.47	53/F	1143.2	880	83.36	14.89	117.70	23.40	NO
23	STD	Right Zygoma	5.59	78/F	^1974.8	1484	92.07	38.46	191.66	90.01	
24	STD	Right Zygoma	5.59	68/M	#1668.2	1021	112.21	39.03		40.20	YES

*Steering wheel deformations for the EA wheel are exclusive of foam compressions.
^Apparatus malfunction; mounting fixture obstruction
#Force indicated is based on an extrapolation (see text for details)

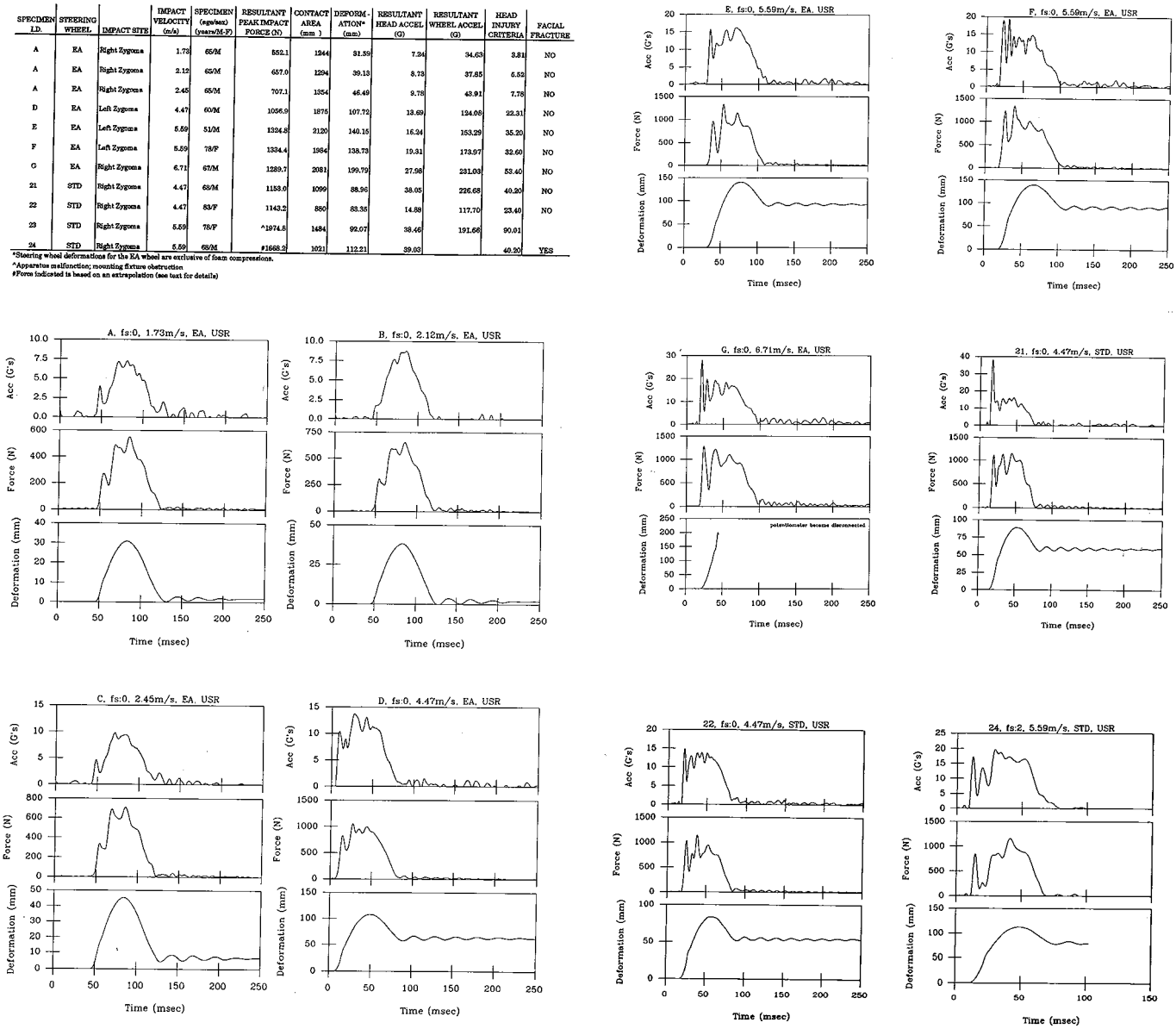

Figure 6a. Head Acceleration, Transformed Force, and Steering Wheel Deformation for all the Specimens Tested in This Study at the USR Location. Specimen identification, fracture severity (fs, on a scale of 0-4), impact velocity (m/s), wheel type (EA or STD), and the location (USR) is indicated on the top of the acceleration trace for each test.

Experiments with STD wheel also indicated no fractures up to 4.49 m/s; however, a velocity of 5.59 m/s produced foes fractures of the zygomatic arch and maxilla in one (specimen #24) of the two specimens tested on the USR. Based on an earlier classification of facial fractures (25), the injury severity for this pathology was estimated to be a 2. A peak transformed resultant force of 1668.3 N was calculated for this specimen because all the channels of data could not be gathered during the experiment. This force was extrapolated using the F_x signal recorded from the test. The following procedure was adopted: the ratio of the maximum transformed resultant force to the maximum F_x force was computed for all the tests conducted on the USR location of the STD wheel (mean: 1.44, SD: ± 0.10), and the ratio of the maximum transformed F_z force to the maximum F_x force was also calculated (mean: 1.44, SD: ± 0.11) for the same test. Using an extrapolation factor of 1.44, a peak force of 1668.3 N was estimated for this specimen.

Human Cadaver Head Impact Tests at the LSR

Table 5 includes a brief summary of the additional tests conducted at the LSR location on the EA wheel using nine cadaver heads. At velocities ranging from

1.41 to 5.59 m/s, peak forces at the impact site varied from 681.8 to 2290 N demonstrating fractures of varying severity. In the interest of brevity, the reader is referred to our previous publication on this topic (22) wherein detailed descriptions of the high-speed photographic analysis and the pertinent biomechanical characterizations are described. The additional specimen tests were performed to obtain a probability distribution at the LSR location on the EA wheel by combining the data from our earlier paper (22).

Table 5. Summary of Biomechanical Data of Specimen Tested at the LSR Location on the EA Wheel

Specimen I.D.	Impact Severity	Impact Velocity m/s	Peak Impact Force (N)	Fracture Severity
B	Right Zygoma	1.41	680.8	0
C	Right Zygoma	1.73	839.9	0
H	Right Zygoma	5.59	2290	3
K	Right Zygoma	2.91	1471	0
L	Right Zygoma	3.13	1652	2
M	Right Zygoma	2.79	1452	1
N	Left Zygoma	2.57	1492	0
P	Right Zygoma	2.79	1561	1
Q	Right Zygoma	2.68	1321	0

*: A total of 18 specimen tests were conducted at the LSR location on the EA wheel to obtain the facial fracture probability distribution. Nine of the 18 data points were obtained from our previous study (ref 22). In the present study, these additional tests using nine cadavers were conducted to give a total sample size of 18.

Discussion

Various biomechanical studies have been advanced in the past to understand the response of the human cadaveric facial structure under static and dynamic loads, to determine the mechanism of injury, and to establish tissue tolerances (3-5,9,11,12,18). The zygomatic region of the face has been an area of considerable research due to its involvement during motor vehicle related facial injuries. Consequently, this study was undertaken to determine the biomechanics of the zygomatic complex due to steering wheel loading.

Earlier facial injury studies of Foes, Foes, Nahum et al, and Foes et al using human cadavers have provided important baseline biomechanical and pathological data for the zygomatic bone (4,9,12,18). However, in these investigations, the loading surface did not include the characteristics of the steering wheel nor was the steering wheel used as the impacting object. Furthermore, evaluation of facial injuries in these studies was done using conventional radiographs and gross-dissection at the impact site. Plain films often miss clinically significant anatomical abnormalities. In addition, multiple impact tests were conducted on the same cadaver specimen (fresh and embalmed) which can confound the correlation of biomechanical data with the injury pathology. Due consideration of the possibility of bilateral propagation of fracture with unilateral, single impacts to the facial structure was also not provided in some studies. In a recent study, it has been documented that single high energy unilateral impact to the zygoma can result in propagated fractures to other regions such as maxilla and mandible as well as bilateral injuries (22). Therefore the present study was conducted using the entire steering wheel as the loading surface (in contrast to an artificial square or round impacting striker), thus incorporating the real curvature of the contacting surface. Controlled unilateral impacts were delivered to either zygoma of intact fresh human cadaver heads, thus eliminating the above confounding factors.

Foes in 1965 quantified the acceleration (G level) tolerances for different facial structures (18). In 1967, Foes suggested a temporal dependence for facial fracture based on impact duration (4). Impacts lasting beyond 4 ms produced fractures of the zygomatic bone around 880 N with a 28.7 mm diameter impactor (one square inch area). In contrast, forces of approximately 4450 N resulted in no fracture for impact durations of 3 ms or less. Furthermore, it was found that for impulses lasting longer than 4 ms, the tolerance was raised by a factor of 1.5 to 2.5 with a 65 mm diameter impactor (5.2 inch square area). It should be recognized that, increasing the impactor area to approximately five square inches may result in loading the neighboring bony complex (such as orbit) in addition to the zygomatic bone. From this viewpoint, the maximum forces reported in the study may not be directly applicable to the malar eminence region of the zygoma. Additionally, the maximum forces recorded by the impactor may not be the level at which fracture occurs. In 1968, Nahum et al indicated that oscillatory responses recorded from an accelerometer placed opposite to the impacting area of the face confounded the correlations between the impacting force and the force computed using rigid body mechanics principles (9). Further, the study contradicted the earlier suggestion made by Foes (4) regarding the temporal correlation for facial fracture. Zygomatic fractures were produced with a striker having a contact area of 645 sq mm (one inch square) and severe comminuted or depressed fractures occurred at forces ranging from 0.9 to 3.5 kN. Facial impact studies by Foes et al using a 25 mm diameter rigid cylindrical contact surface oriented across the front of the face to contact the nose at the level of the infra-orbital margin, suggested a tolerance of 3.0 kN for severe facial fractures (12). A summary of the biomechanical parameters associated with fracture of the human cadaveric zygomatic bone is included in Table 6. It is well documented in biomechanical literature that the strength of bone, particularly among women, and in the vertebral column and hip-femur complex, decreases with age. For the human facial bone however, this phenomenon has not been clearly demonstrated. The human cranial bone and the facial skeleton is primarily made of the cortical bone, and therefore, the effects of decreased bone strength due to degenerative diseases such as osteoporosis which principally affects the strength of the trabecular bony architecture may be minimal in the face. In our previous studies with 25 subjects of ages ranging from the fourth decade to the eighth decade, facial bone mineral content determined from ashing techniques did not demonstrate decreasing tendency with increasing age.

Table 6. Zygoma Fracture Forces in Literature

Investigator	Year	Fracture Parameters	Salient Experimental Features
Hodgson	(1964)	1441 - 6272 N 91 - 372 G	Rotary impactor at 1.27 to 9.51 m/s, 64-91 years of age, embalmed specimens with skin removed, multiple blows
Swearingen	(1965)	50 - 80 G	Specimens 28-74 years of age, tissue filled with gelatin, impact using a catapult
Hodgson	(1967)	1121 - 1663 N 1761 - 3363 N	Using 1 inch square impactor. With 5.2 inch square area using 2.56 inch diameter impactor, multiple blows to embalmed specimens 53-97 years of age at velocities 92.6 to 7.86 m/s
Nahum et al	(1968)	912 - 3470 N	With 1 inch square impactor specimen 55 to 81 years of age
Schneider & Nahum	(1973)	970 - 2850 N	Dropped 1.5 kg weight at velocities of 4.2 to 5.2 m/s specimens 45 to 80 years of age, multiple blows
Yoganandan et al	(1988)	1359 - 4604 N	Controlled unilateral impact tests with junction of lower spoke and rim of EA and STD steering wheels. One specimen and one steering wheel per test at velocities of 2.24 to 6.93 m/s. Specimens ranged from 57 to 71 years of age

To assess the biomechanical performance of the EA and STD steering wheels, the results obtained from this study on USR impacts with both wheels and additional tests on LSR impacts with the EA wheel, were compared with previous data for further analysis (22). A total of 25 data points for the EA wheel (18 at the LSR including 9 data points from the previous study and 7 at the USR) and 10 data points for the STD wheel (6 at the LSR from the previous study and 4 at the USR) were available. Plot of variation of impact velocity versus fracture severity for each specimen tested is shown in Figure 7. The fracture severity based on an earlier classification (22) was found to be zero (no fracture) for all the specimens tested on the EA wheel at the USR location at velocities ranging from 1.73 to 6.71 m/s. In contrast, specimens tested at the LSR location on the EA, and the LSR and the USR locations on the STD wheels demonstrated fractures of varying severity. Steering wheel deformation at the impact site did not correlate well with fracture severity although wheel deflections consistently increased with increasing velocity.

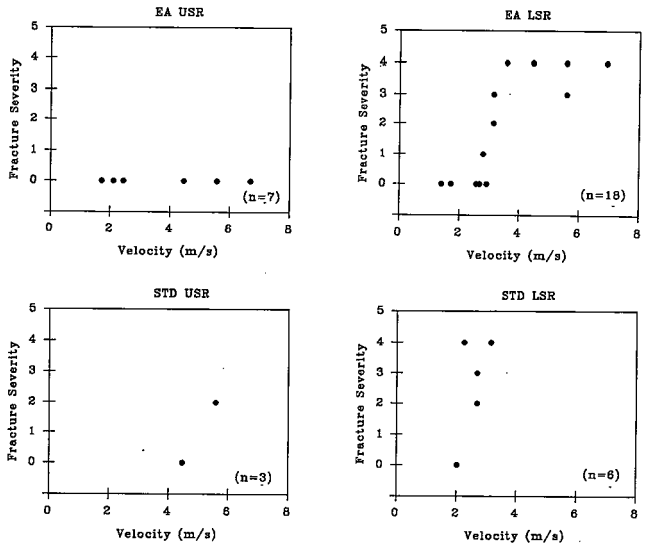

Figure 7. Fracture Severity vs. Velocity for the EA Steering Wheel at the USR (top left) and the LSR (top right) Location, and for the STD Steering Wheel at the USR (bottom left) and LSR (bottom right) Location

Because the lateral displacements may have resulted in an unloading of the zygomatic bone in the USR tests, the maximum interface force while the malar eminence region is in contact with the steering wheel was calculated as follows: based on the minimum one-half width of the zygomatic bone at the malar eminence region, the time at which the shear displacement exceeds this magnitude was determined; and from the interface force history, the maximum force developed prior to this time was obtained. Variation of this maximum interface force acting on the zygomatic bone with fracture severity is included in Figure 8. A close examination of the variation of the peak impact force with respect to velocity for the USR tests on the EA wheel with the rigid Z90.1 headforms and human cadaver preparations demonstrated striking similarities (Figure 9). This indicates that the rigid headform produces comparable peak forces at equivalent velocities. This suggests the plausible use of the Z90.1 to assess the performance of the wheel. However, similar tests have to be conducted at other locations (eg., LSR on the EA, USR and LSR on the STD wheel) to completely justify this approach.

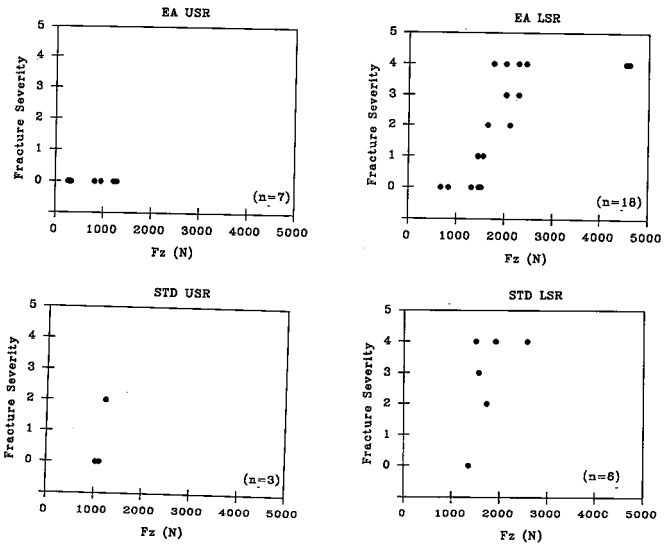

Figure 8. Fracture Severity vs. Peak Impact Force Developed at the Zygomatic Bone Contact for the EA Steering Wheel at the USR (top left) and the LSR (top right) Location, and for the STD Steering Wheel at the USR (bottom left) and LSR (bottom right) Location

The Weibull probability curve for LSR tests on the EA wheel shown in Figure 10 indicates that a force of 1525 N corresponds to a 50% probability of facial fracture at this location. At the USR location on the EA wheel, no fractures were detected in seven tests conducted at velocities up to 6.7 m/s with peak forces up to 1335 N. It should, however, be noted that it is not practical to conduct tests at the USR location on the EA wheel at higher velocities (more than 6.71 m/s) because of the limitations in the experimental design. Additional tests are necessary at the LSR and USR locations on the STD

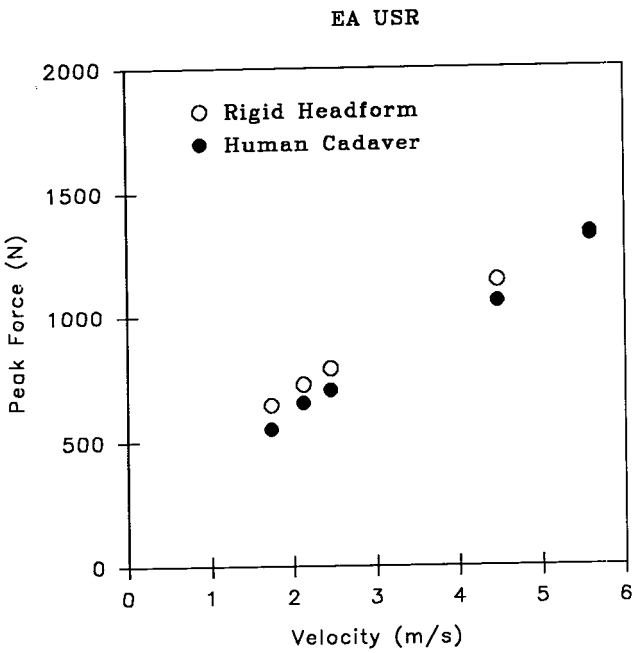

Figure 9. Comparison of the Variation of Peak Forces at the Impact Site with Impact Velocity for Human Cadaver Tests (solid circles) and Rigid Head Form (open circles). Note the similarities in the peak forces at a particular velocity. *: two specimen tests at a velocity of 5.59 m/s.

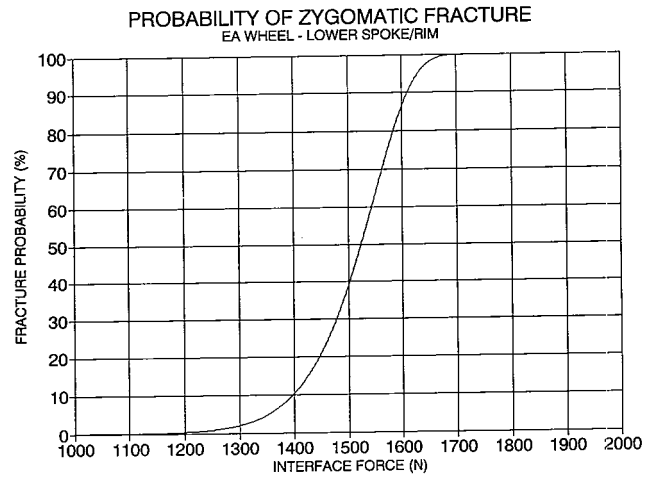

Figure 10. Weibull Probability Distribution for Facial Fracture at the LSR Location on the EA Steering Wheel

wheel to deduce probability distributions for facial fracture at these sites. Since one-fifth of steering wheel induced facial trauma to the restrained driver is associated with impacts at the hub-spoke region, tests are also warranted at this location of the wheel.

Conclusions

The following conclusions are drawn from the study.

1. The junction of the lower spoke and rim is stiffer than the center of the unsupported rim under quasi-static loading for both the EA and STD wheels.
2. The interface force-time response at the wheel rim typically exhibits bimodal behavior. The first force peak appears to be a function of wheel rim inertia: it is coincident with maximum rim acceleration at the impact site, at a time when rim deflection is small. The second peak appears to be largely driven by the force-deflection behavior of the wheel since it occurs when rim deflection is approaching its maximum value and when rim velocity and acceleration have fallen to low values. However, the magnitude of the second force peak often exceeds the value which would be expected on the basis of quasi-static force-deflection behavior alone.
3. At low impact velocities, the first (inertial) peak is smaller than the second. However, at the higher impact velocities in this experimental series, the magnitude of the inertial peak exceeded the second peak value. Therefore, it is concluded that an understanding of both inertial and stiffness characteristics is necessary for optimal design of steering assemblies protective of the facial skeleton.
4. Interface force was determined to be the most likely variable that correlates with zygomatic bone fracture. Within the limits of the ensemble, a force of 1525 N corresponds to a facial fracture probability of 50% for the EA wheel at the LSR location.
5. No fractures were documented at the USR location on the EA wheel at velocities up to 6.7 m/s. Peak interface forces up to 1334 N were recorded in these tests.
6. Additional tests are required to completely describe the probability distribution for the STD wheel at the LSR and USR locations.

Acknowledgement

We respectfully acknowledge the consultation and advice of Drs. Rolf Eppinger and Lee Stucki of NHTSA. Appreciation is extended to Shauna Barnes of Chi Associates for assistance in data processing. This research was supported in part by PHS CDC Grants R49CCR502508 and R49CCRT03640, DOT NHTSA Grant DTNH22-89-Z-07305, and the Department of Veterans Affairs Medical Research Funds.

References

1. Clemo KC, Penoyre S, White MJ: Safer steering wheels to reduce face bone fractures. *Proc 12th Intl Technical Conf Experimental Safety Vehicles*, Gothenburg, Sweden, May 29-June 1, 1989, pp 275-287.
2. Finkelstein MM: United States Status Report. *Proc 12th Intl Technical Conf Experimental Safety Vehicles*, Gothenburg, Sweden, May 29-June 1, 1989, pp.29-36.
3. Foes VR: Tolerance of the facial bones to impact. *Am J Anat* 120:113-122, 1967.

4. Foes VR, Nakamura GS: Mechanical impedance and impact response of the human cadaver zygoma. *J Biomech* 1:73-78,1968.
5. Foes VR, Patrick LM: Dynamic response of the human cadaver head compared to a simple mathematical model. *Proc 12th Stapp Car Crash Conf,* Society of Automotive Engineers, New York, 1968, pp 280-301.
6. Huelke DF, Compton CP: Facial injuries in automobile crashes. *J Oral Maxillofac Surg* 41:241-244, 1983.
7. Marcus JH, Blodgett R: Priorities of automobile crash safety based on impairment. *11th Intl Technical Conf Experimental Safety Vehicles,* Washington, D.C., May, 1987.
8. Melvin J, Shee T: Facial injury assessment techniques. *Proc 12th Intl Technical Conf Experimental Safety Vehicles,* Gothenburg, Sweden, May 29-June 1, 1989, pp 608-617.
9. Nahum A, Gatts J, Gadd C, Danforth J: Impact tolerance of the skull and face. *Proc 12th Stapp Car Crash Conf,* Soc of Automotive Engineers, New York, 1968, pp 302-316.
10. Neal DC, Wagner WF, Fiedler LD, Alpert B: The epidemiology of facial fractures. *J Ky Med Assoc,* June 1978, pp 275-278.
11. Newman JA, St Laurant A: *Head injuries resulting from automotive collisions,* Biokinetics and Associates, Ltd, March 1983.
12. Foes GW, Cavanaugh JM, Goldberg SJ, King AI: Facial impact tolerance and response. *Proc 30th Stapp Car Crash Conf,* Society of Automotive Engineers, Warrendale, PA, 1986, pp 379-400.
13. Otte, Dietmar: Residual injuries to retrained car-occupants in front and rear-seat positions. *11th Intl Technical Conf Experimental Safety Vehicles,* Washington, D.C., May, 1987.
14. Sances A Jr, Yoganandan N: Human head injury tolerance. In *Mechanisms of Head and Spine Trauma,* A Sances, Jr, DJ Thomas, CL Ewing, SJ Larson, F Unterharnscheidt, editors, Aloray Publisher, Goshen, NY, 1986, pp 189-218.
15. Schneider DC, Nahum AM: Impact studies of facial bones and skull. *Proc 16th Stapp Car Crash Conf,* Society of Automotive Engineers, New York, 1972, pp 186-203.
16. Status Report of The European Experimental Vehicles Committee (EEVC). *Proc 12th Intl Technical Conf Experimental Safety Vehicles,* Gothenburg, Sweden, May 29-June 1, 1989, pp 14-22.
17. Starkhammar H, Olofsson J: Facial fractures: A review of 922 cases with special reference to incidence and etiology. *Clin Otolarvngol* 7:405-409, 1982.
18. Foes JJ: Tolerances of the human face to crash impact. *Office of Aviation Medicine,* Federal Aviation Agency, Oklahoma City, OK, July 1965, 24 pp.
19. Viano D, Melvin JW, et al: Measurement in head dynamics and facial contact forces on Hybrid III dummy. *Proc 30th Stapp Car Crash Conf,* Society of Automotive Engineers, Warrendale, PA, Oct 1986.
20. Viano D: Cause and control of automotive trauma. *Bulletin of the New York Academy of Medicine,* 2nd Series, 64(5):376-421, 1988.
21. Welbourne ER, Ramet M, Zarebski M: A comparison of human facial fracture tolerance with the performance of a surrogate test device. *Proc 12th Intl Technical Conf Experimental Safety Vehicles,* Gothenburg, Sweden, May 29-June 1, 1989, pp 603-608.
22. Yoganandan N, Pintar FA, Sances A Jr, Harris GF, Chintapalli K, Myklebust JB, Schmaltz D, Reinartz J, Kalbfleisch J, Larson SJ: Steering wheel induced facial trauma. *Proc 32nd Stapp Car Crash Conf,* Society of Automotive Engineers, Warrendale, PA, 1988, pp 45-70.
23. Yoganandan N, Sances A Jr, Pintar FA, Harris GM, Mahadevappa M, Larson SJ: Three-dimensional computerized tomography analysis of steering wheel induced facial trauma. *Proc 12th Intl Technical Conf Experimental Safety Vehicles,* Gothenburg, Sweden, May 29-June 1,1989, pp 752-763.
24. Zuby D: Steering assembly induced facial injury. ASME Winter Ann Mtg, American Society of Mechanical Engineers, Boston, MA, Dec 13-18, 1987, 9 pp.
25. Zuby DS, Saul RA: Restrained drivers facial skeleton injuries resulting from steering assembly contact: A conspectus. *Proc 12th Intl Technical Conf Experimental Safety Vehicles,* Gothenburg, Sweden, May 29-June 1, 1989, pp 597-603.

S8-O-09

An Improved Finite Element Model of the Human Thorax

Gordon R. Plank
Volpe National Transportation Systems Center
Rolf H. Eppinger
National Highway Traffic Safety Administration

Abstract

An improved model of the human thorax, utilizing the 3-dimensional finite element computer code DYNA3D (1), is under development. Like the precursor (2) to this model, the thorax is represented by elastic bone, ligament and cartilage, viscoelastic muscle and interior elements, and a rigid body impactor. The current model is an accurate representation of a 50th percentile male with regard to skeletal anatomical structure, overall dimensions and mass. Mesh development and preparation for input to DYNA3D are discussed. The dynamic response of the model under impact conditions is compared to available cadaver data and strain in the interior thoracic volume under these conditions is examined. Plans for further model enhancement and applications are discussed.

Introduction

DYNA3D, the three-dimensional finite element structural analysis code and its pre- and post-processors INGRID and TAURUS, as well as DISPLAY, a mesh generator from the Engineering Mechanics Research Corporation (EMRC) are being used at the Volpe National Transportation Systems Center (VNTSC) to model various parts of the human body in order to examine their responses to various impact conditions. DYNA3D is appropriate for these simulations because of its ability to manage problems with very large deformation as experienced in thoracic impact tests. Earlier work at VNTSC in the area of modeling and analysis of the human thorax during crashes resulted in the development of a finite element model (Figure 1) that showed considerable biofidelity under PART 572[1] frontal impact conditions. The dynamic responses of this model were compared to data obtained in laboratory experiments and were found to show good fidelity (force-deflection characteristics) with the available test data. In addition, an extensive analysis of the sensitivity of the model dynamic response to variations in material properties was conducted.

The simulations are both qualitative and quantitative. The graphical output of the post-processor (TAURUS) presents the investigator with pictures that form important qualitative impressions that contribute to his ability to judge the reasonableness of the simulation and may suggest further changes in the model (e.g., mesh rezoning, changes in geometry, etc.) to improve its performance. Quantitative data is available in the form of element time histories of selected stresses and strains and nodal time histories of displacement, velocity and acceleration. In addition, the ability to plot stress and strain contours on selected cross sections of the model is also available.

Benefits from the use of these finite element models are numerous. The model may be used to define the strain fields within the thorax when subjected to impact forces and relationships may be derived among these data and trauma observed in laboratory testing. In this manner, the development of more representative injury criteria may be possible. The use of these models also represents considerable cost reduction when compared to physical tests on actual specimens in the laboratory. Parameters that are virtually impossible to measure in the laboratory can be examined in detail with these simulations. In addition, as a tool in the design of automotive interiors, anatomical models may be tested with simulations of automotive interiors to determine the injury mitigation characteristics of the interior contact surfaces.

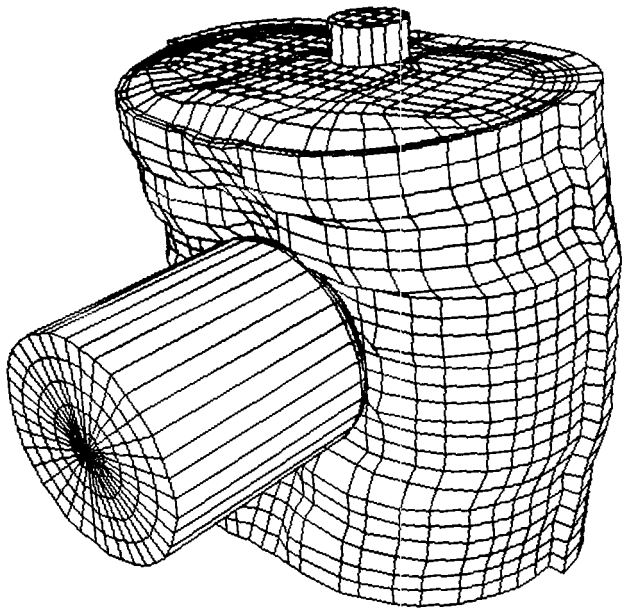

Figure 1. Early 7-Rib Model Under Impact

The objectives of the current effort are to develop a thorax model that is geometrically accurate and whose dynamic response shows good agreement with existing data. While clearly defined, these two objectives are

[1]Title 49, PART 572 of the United States Code of Federal Regulations.

often at odds. The unusual and asymmetric geometry of the thorax results in oddly shaped elements at numerous locations. Under the severe impact conditions imposed, elements become extremely distorted, presenting unacceptable conditions to the computational algorithms, often leading to a "crash" and program termination. The solution to these problems is judicious selection of material properties and element geometry appropriate for the specific test at hand.

Mesh Development

The structure of the current thorax model is based on geometry data reported by Roberts and Chen (3), Schneider et al (4), Robbins (5), and qualitative whole body cross-sectional anatomy (6), scaled to represent a 50th percentile male. The cross-sectional dimensions of the ribs (.42" x .21) were chosen to give the same bending characteristics as measured in the laboratory (3) on representative cadaver ribs about the two major cross sectional axes. The mesh generator DISPLAY (from the Engineering Mechanics Research Corporation) was used to develop the mesh. The current model uses symmetry in the mid-sagittal plane for frontal impacts to reduce the number of nodes required in the problem. For side impacts and as development continues and incorporates individual organs however, symmetry will be sacrificed.

The first phase of the current model development resulted in a 10-rib model without abdominal mass. As initial tests on this model showed it to be too compliant (see results), further improvement to the model was accomplished with the addition of ribs 11 and 12 as well as an abdominal mass. Since Roberts and Chen did not report data for ribs 11 and 12, the location and geometry of these ribs were estimated using data from other sources (4-6) to provide a smooth transition from the 10-rib model.

The current 12-rib model is considerably larger than the 7- and 10-rib models having 23,148 nodes and 20,758 elements compared to 7,213 nodes and 6,032 elements in the 7-rib model and 16,428 nodes and 14,378 elements in the 10-rib model. As in the earlier models, head and neck, arm and lower body masses in the 12-rib model are represented by high density parts attached to the basic thorax model and these parts are illustrated in Figure 2. The stiffness (elastic modulus, bulk modulus and Poisson's ratio) of these high density elements is chosen to match that of the adjacent elements in order to avoid large mismatches in material characteristics and point loading that can lead to unstable conditions. All of the elements in the current model are represented by 8-node solid brick elements. Early in the modeling process, fine tuning of several model regions was required to improve element aspect ratio, reduce distortion, and insure smooth transitions from one area to another. Typical of such fine tuning, the orientation of the cross-section of rib numbers 1, 2, 3 and 4 was improved considerably (Figure 3) before the addition of intercostal muscle elements. Similar exercises were required to improve the geometry of the costo-sternal cartilage elements and the costo-vertebral ligament elements.

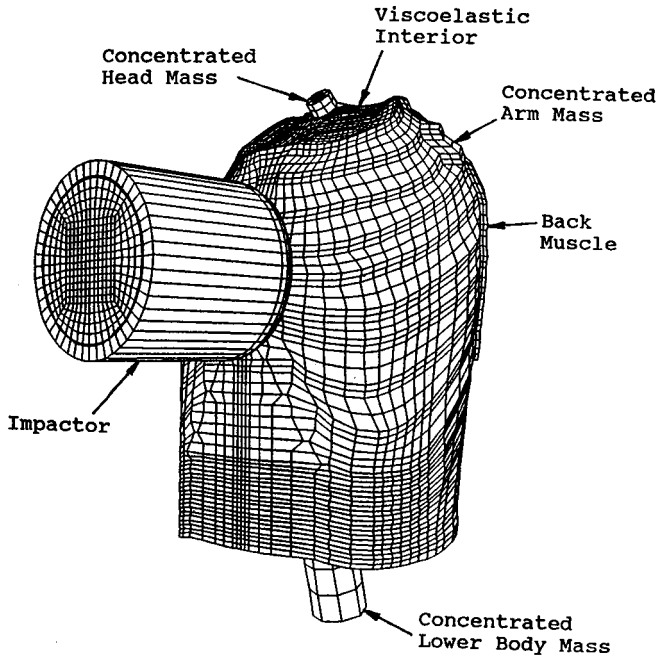

Figure 2a. True Geometry Thorax Model: 12-Rib Model with Impactor

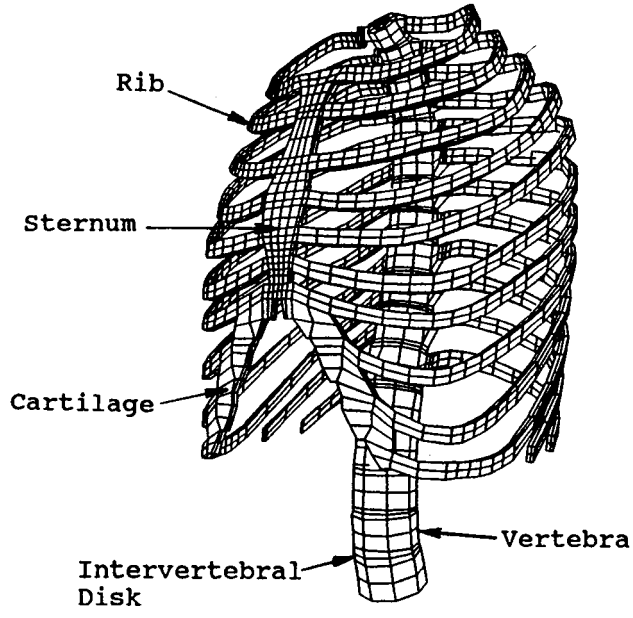

Figure 2b. True Geometry Thorax Model: Skeletal Portion

Mesh Conversion

Software required to convert DISPLAY output data to DYNA3D input data was acquired from EMRC and enhanced to suit the needs of the current model. Node coordinates and element connectivity are read from the DISPLAY output deck and converted to a format acceptable for input to DYNA3D. To include contact

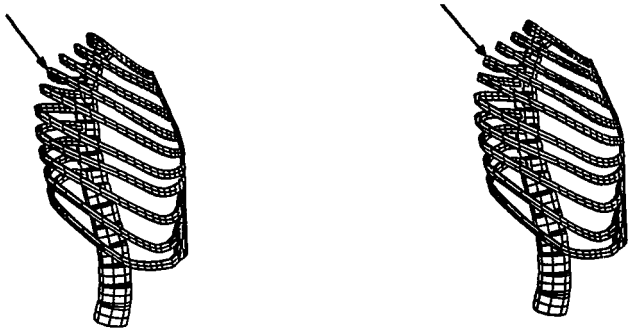

Figure 3. Adjustment of Rib Cross-Section Orientation: Before Adjustment (left) and After Adjustment (right)

interfaces in the model, the user designates pressure surfaces in the mesh developed in DISPLAY and the conversion software interprets these surfaces as contact interfaces and formats the information appropriately. Initial velocities for selected parts may also be specified. The current conversion software is capable of converting 4, 6 and 8-node solids as well as 4-node shell elements. It also recognizes model symmetry and places appropriate constraints on the nodes in the symmetry plane.

Material Properties

The materials used in the current model include elastic bone, ligaments, cartilage and disks, and viscoelastic muscle and interior volume. Information on the properties of these materials was gathered from available literature (7-11). As one might expect, there was more reliable information available on bone than any other material since it is easier to measure the constitutive properties of a hard, stiff material such as bone than to measure the properties of the softer, more compliant tissues. The viscoelastic material is represented in DYNA3D by the following relaxation formula:

$$G(t) = G_L + (G_S - G_L)e^{-(BETA)t}$$

where:

G_S = short term shear modulus
G_L = long term shear modulus
BETA = decay constant.

Information on the viscoelastic properties of biological materials is limited. In some studies, the function G is represented as a complex, frequency dependent variable and the interpretation of these data in the time domain can be difficult. Values for G_L, G_S and BETA used in the earlier study were based on limited information for these variables and estimates obtained from measures of elastic moduli and Poisson's ratio for the various materials in question. The three high density masses representing the head and neck, lower body, and arm have elastic, elastic and viscoelastic properties respectively. The density of the head and neck, arm, and lower body elements have been adjusted to yield a total body weight (representing a 50th percentile male) of 168 pounds. The geometry of the current model results in a more compliant dynamic response than the earlier 7-rib model when using the material properties of the earlier model (2). Because initial computer runs resulted in crashes due to the total collapse of thoracic elements in the vicinity of the impactor, the parameter values of the materials in the current model were modified in an effort to prevent this. The bulk modulus of the interior material was increased an order of magnitude from the original value of 4.17 to 41.7. This also served to make the model somewhat stiffer which was desirable as initial runs had shown it to be too "soft" (i.e., force too low, deflection too high). Changing the bulk modulus in this manner increases the incompressibility of the material and is equivalent to a change in Poisson's ratio from .460 to .496. A change of this magnitude is not an unreasonable solution to the problem of element collapse given the great difficulty in measuring the properties of these compliant biological materials and the resultant uncertainties in the published data. In addition, as a precautionary measure, the bulk modulus of the muscle material was increased from 33.3 to 66.6, the elastic modulus of the costo-sternal cartilage elements was increased from 1.74×10^3 to 3.00×10^3 and Poisson's Ratio for the cartilage elements was increased from .42 to .46. The latter three changes were shown to have little effect on the overall response of the 7-rib model developed earlier (2) and the effect on the current model was also expected to be small. The properties used in the current model are shown in Table 1.

Table 1. Model Material Properties for the 10- and 12-Rib Models (Units in Pounds, Inches and Seconds)

Bone (ribs, sternum and vertebrae) $E=1.75 \times 10^6$ Poisson's Ratio = .3 Density = 1.73×10^{-4}	Intervertebral Disks $E = 1.5 \times 10^3$ Poisson's Ratio = .2 Density = 1.0×10^{-4}
Viscoelastic Interior K = 41.7 G_S = 3.342 G_L = .3428 (computed) Density = 1.0×10^{-4} BETA = 100	Muscles K = 66.6 G_S = 10.170 G_L = 3.390 (computed) Density = 1.0×10^{-4} BETA = 100
Cartilaginous Elements $E = 3.00 \times 10^{-3}$ Poisson's Ratio = .46 Density = 1.0×10^{-4}	Ligamentous Elements $E = 1.74 \times 10^{-3}$ Poisson's Ratio = .42 Density = 1.0×10^{-4}

Impact Trauma

The real issue, of course, is determining the trauma experienced by the biological tissue during impact. It is of interest to examine particular areas of the thoracic interior as potential sites of serious injury. Such a representative location might be at the aortic arch where there are several small arteries that often suffer injury and occasional rupture as a result of blunt frontal thoracic impact. This point is represented by element number 17267 in the 12-rib model and strain was examined for this element.

Results and Discussion

Frontal Impact

The 10- and 12-rib models were run on the CRAY-2 computer at the U. S. Air Force Supercomputer Center

at Kirtland Air Force Base in New Mexico. A complete run required approximately five and one half hours of CPU time for the 10-rib model and seven and one half for the 12-rib model. Each model was subjected to a frontal impact with a six-inch diameter impactor in accordance with Part 572 requirements. The 12-rib model under impact conditions is illustrated in Figures 4 and 5. Force/deflection characteristics under these conditions are shown in Figures 6-8 and compared to the response corridors recommended by Neathery (12) (derived from previous recommendations by Kroell and others (13-15)) for a 50th percentile male dummy. It is seen that the force/deflection characteristics of the 12-rib model are somewhat closer to the recommended corridor than those for the 10-rib model, reflecting the influence of the additional two ribs and the abdominal mass. Figures 6 and 7 illustrate the response of each model to the higher velocity impact prescribed in Part 572 and Figure 8 shows the response of the 12-rib model to the lower velocity impact. In each case the models are too compliant, that is, the force/deflection characteristics exhibit too little force and too much deflection throughout the test. That these models were more compliant than the earlier 7-rib model could have been anticipated on the basis of geometry alone. The force of the impactor is no longer in the plane of the ribs as it was in the earlier model. The front of the ribs now experience downward movement during impact as well as the anticipated bending. In addition, the spacing between the ribs is greater and the cross-sectional area of the ribs is less in the current models than in the 7-rib model, insuring a more compliant response.

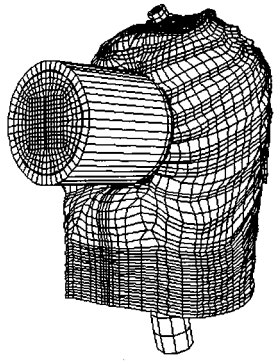

Figure 4. Current Model Under Impact (Oblique View)

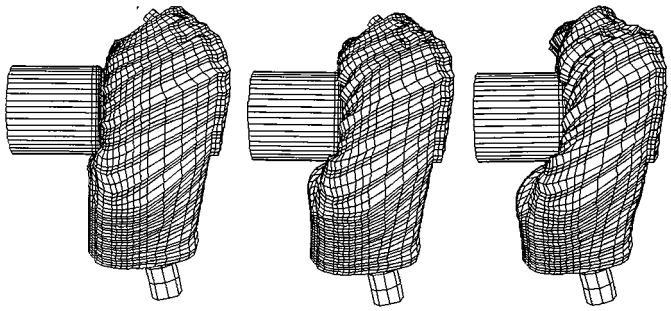

Figure 5. Current Model Under Impact (Side View)

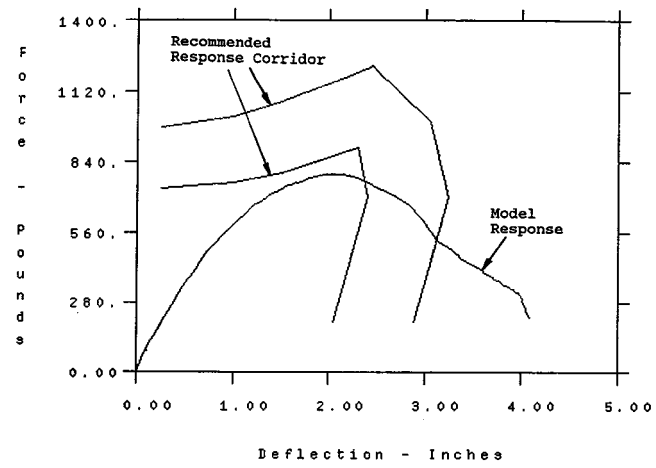

Figure 6. Force/Deflection Characteristics for the 10-Rib Model (Impactor Initial Velocity = 22 feet/sec.)

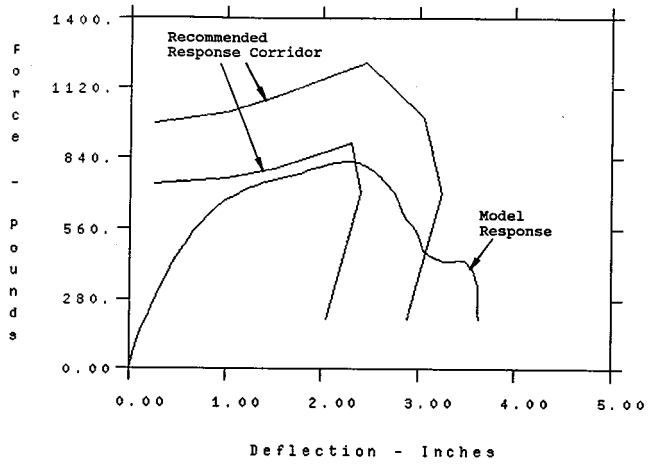

Figure 7. Force/Deflection Characteristics for the 12-Rib Model (Impactor Initial Velocity = 22 feet/sec.)

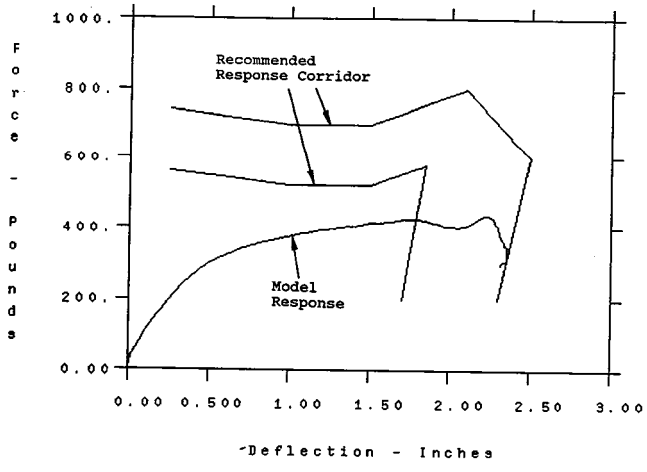

Figure 8. Force/Deflection Characteristics for the 12-Rib Model (Impactor Initial Velocity = 14 feet/sec.)

There are several potential ways to improve the dynamic response of the current model configuration. There is data (16) that suggests that the decay constant BETA may be decreased for the viscoelastic interior material. Varying BETA had minimal effect on the force/deflection characteristics of the 7-rib model, whose

response was dominated by the characteristics of the large ribs. In the current models, however, the decay constant for the interior viscoelastic material may play a much larger role in the shape of the force/deflection characteristics. In addition, the characteristics used for the viscoelastic materials were derived from data gathered in the laboratory on isolated specimens of lung, heart and muscle tissue. The impactor, on the other hand, is encountering these tissues in a different environment, as well as other large vessels, the trachea, bronchi, esophagus, connective and nervous tissue and other elements of the mediastinum. This presents a considerable argument for increasing the stiffness properties of the viscoelastic interior material. To a lesser extent, the argument holds true for the intercostal muscles.

Strain Time History

As mentioned earlier, strain in an area of potential serious injury was examined. X, Y and Z strain in element number 17267 which lies in the vicinity of the aortic arch is illustrated in Figure 9. It can be seen that while a large strain in the y-direction is anticipated, the z-direction exhibits even more strain. Part of this is due to the fact that the interior thorax material bulges out through the opening above the first rib. When a shoulder girdle enhancement is complete, this opening will be somewhat restricted by the clavicle and the tissue response at this point will change. It is also seen that, in the z-direction, the strain is still increasing at 30 milliseconds due in part to the overly compliant nature of the current model.

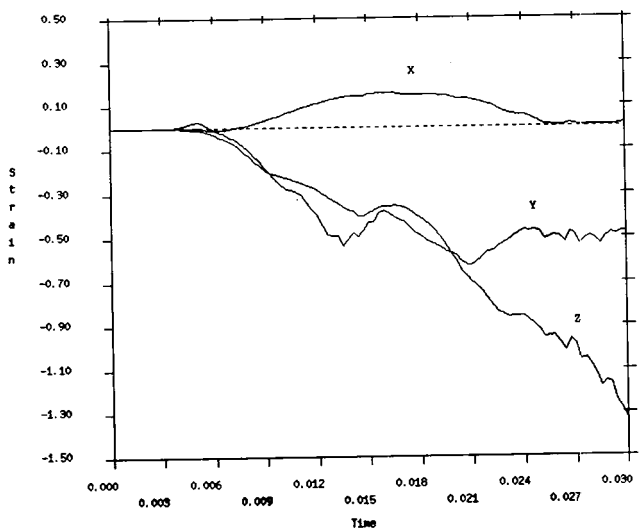

Figure 9. X, Y and Z Strain (Almansi) in Element Number 17267

Future Work

Immediate plans for the current thorax model include variation of the material properties (without straying significantly from published values) in order to optimize the dynamic response of the model with regard to the force/deflection corridor recommended by Neathery. Future enhancements and applications of the model include the development of discrete organs and the development of a shoulder girdle. There are plans to merge this model with head and neck models being developed at VNTSC and the NHTSA. The enhanced model will be used in tests with various interior contact surface models including seat belts, air bags, steering wheels and various tests of side impact into padded and unpadded surfaces. It will also be used in assessing data gathered with thoracic deformation instrumentation being developed at the NHTSA.

Conclusions

A geometrically correct model of the human thorax has been developed and in preliminary tests it shows promise of becoming a very useful analytical tool. Correct geometry opens up the opportunity to examine specific areas of the thoracic volume for impact effects and injury criteria development and creates the possibility of modeling specific organs and examining the response of these organs to various impact conditions. The current model appears to be too compliant or too "soft." Peak deflection is too large while force is too small. Potential solutions include increasing the bulk modulus K and/or decreasing the decay constant BETA for the interior material and the intercostal muscles. Various combinations of these parameter changes will be effected as development continues.

References

1. J. O. Hallquist and D. J. Benson, "DYNA3D User's Manual," Lawrence Livermore Laboratories, Report UCID-19592, Rev. 2, March, 1986.
2. Gordon R. Plank and Rolf H. Eppinger, "Computed Dynamic Response of the Human Thorax From a Finite Element Model," Twelfth International Technical Conference on Experimental Safety Vehicles, June, 1989.
3. S. B. Roberts and P. H. Chen, "Elastostatic Analysis of the Human Thoracic Skeleton," J. of Biomechanics, Vol. 3, pp. 527-545, Pergamon Press, 1970.
4. L. W. Schneider, D. H. Robbins, M. A. Pflug and R. G. Snyder, "Anthropometry of Motor Vehicle Occupants," Vol. 1, Report No. UMTRI-83-53-1, The University of Michigan Transportation Research Institute, Contract No. DTNH22-80-C-07502, December, 1983.
5. D. H. Robbins, "Anthropometry of Motor Vehicle Occupants," Vol. 2, Report No. UMTRI-83-53-2, The University of Michigan Transportation Research Institute, Contract No. DTNH22-80-C-07502, December, 1983.
6. D. R. Cahill and M. J. Orland, *Atlas of Human Cross-Sectional Anatomy*, Lea & Febiger, 1984.
7. S. H. Sundaram and C. C. Feng, "Finite Element Analysis of the Human Thorax," Journal of Biomechanics, Vol. 10, pp. 505-516.

8. David C. Viano, "Biomechanics of Bone and Tissue: A Review of Material Properties and Failure Characteristics," Paper No. 861923
9. L. Z. Shuck and S. H. Advani, "Rheological Response of Human Brain Tissue in Shear," Transactions of the ASME, Journal of Basic Engineering, ASME Paper No. 72-WA/BHF-2.
10. A. M. Nahum and J. Melvin, *The Biomechanics of Trauma*, Prentice Hall, 1985.
11. Y. C. Fung. *Biomechanics—Mechanical Properties of Living Tissues*, Springer-Verlag, New York, 1981, Chapter 12.
12. R. F. Neathery, "Analysis of Chest Impact Response Data and Scaled Performance Recommendations," Proceedings of the Eighteenth Stapp Car Crash Conference, December, 1974.
13. C. K. Kroell, D. C. Schneider, and A. M. Nahum, "Impact Tolerance and Response of the Human Thorax," Proceedings of the Fifteenth Stapp Car Crash Conference, November, 1971.
14. T. E. Lobdel, C. K. Kroell, D. C. Schneider, W. E. Hering, and A. M. Nahum, "Impact Response of the Human Thorax," *Human Impact Response—Measurement and Simulation*. Proceedings of Symposium at General Motors Research Laboratories, Oct. 2, 3, 1972, edited by W. F. King and H. J. Mertz, London: Plenum Press.
15. C. K. Kroell, D. C. Schneider, and A. M. Nahum, "Impact Tolerance and Response of the Human Thorax II," Proceedings of the Eighteenth Stapp Car Crash Conference, December, 1974.
16. J. G. Pinto and P. J. Patitucci, "Visco-Elasticity of Passive Cardiac Muscle," Journal of Biomechanical Engineering, Vol. 102, February, 1980.

S8-O-10

Analytical Trauma Research Using the Chest Band

Nopporn Khaewpong
Chi Associates, Inc.
Rolf H. Eppinger, Richard M. Morgan
National Highway Traffic Safety Administration

Abstract

This paper explores the potential for developing improved thoracic injury criteria using data derived from experiments using the chest band. The chest band is both a sensing device and an analytical process that determines the cross-sectional geometry of an object about which it is wrapped. In the process of determining the geometric shape of the object, the chest band process also provides both the local curvature and the time rate of change of the curvature of the object's peripheral surface. Thus the time histories of these variables at both fracture and non-fracture sites can be documented. A discussion of the rationale and the methodology for relating local curvature and other factors with thoracic skeletal injury is provided. Additionally, the rationale and processes of using the derived time varying contours from the chestband to establish the extent of internal thoracic injury are also explored by using a simplified finite element model of the chest. This model is a one-inch thick viscoelastic material in the shape of the measured thoracic contour. It is stimulated by using the time varying external contours obtained from the chestband as the inputs to calculate the stress and strain distribution throughout the model. Initial analysis indicates that the stresses and strains internal to the body are produced not only by the deformation of the periphery but are also influenced by the inertial conditions to which the entire body is exposed while being deformed.

Introduction

The External Peripheral Instrument for Deformation Measurement (EPIDM), or the more commonly called chest band, is both a sensing device and an analytical process that determines the cross-sectional geometry of a body about which it is wrapped. The sensing device consists of a urethane-encapsulated metallic strip to which a number of strain gauge bridges are attached at various locations along its length. These sensors are configured to sense local curvature of the band. The output from the physical chestband is the time histories of the curvature at multiple points on the periphery of the thorax around which the chestband is wrapped. Figure 1 shows a typical curvature time history during an impact event recorded by one of the strain bridges on the band. A continuous description of the curvature, K, around the periphery of the band (and body) at any instant in time, as shown in Figure 2, is approximated by an analytical fitting process, [1], that uses the multiply measured discrete curvatures obtained from the physical band. Typically, the bands used in the current experimental series have had either 16, 24, or 40 individual bridges around the periphery. The reconstruction of the

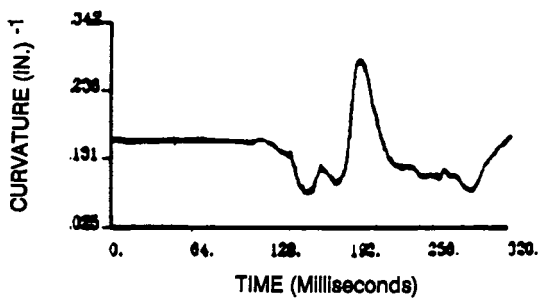

Figure 1. Curvature Time History

band's (and the body's) geometry is then performed using the continuous curvature information and an example of this process is shown in Figure 3.

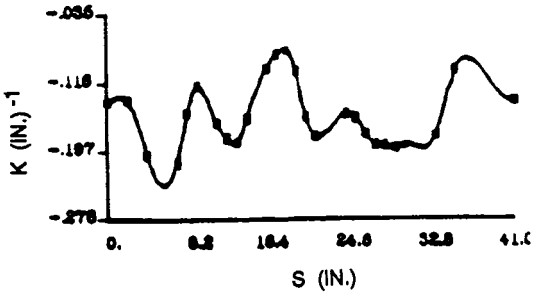

Figure 2. Distribution of Curvature Around Thorax

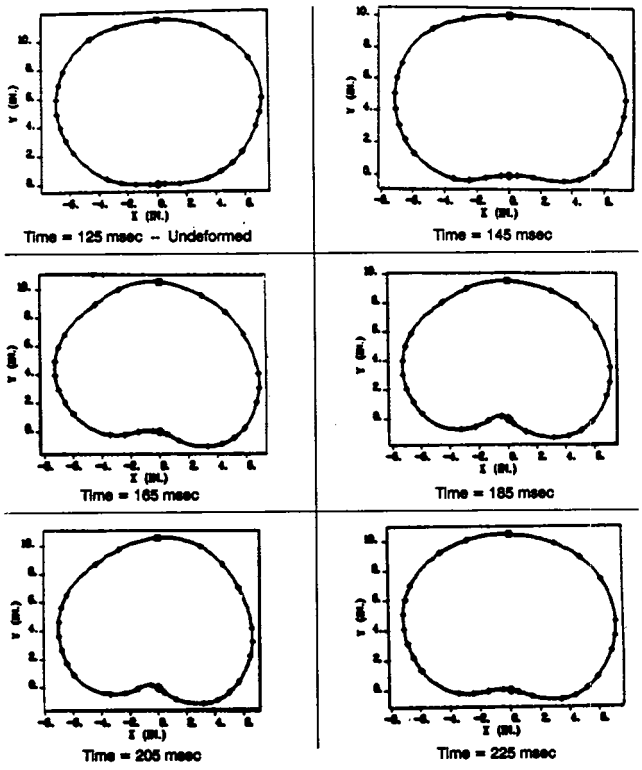

Figure 3. A Series of Chest Contours Captured by the Chestband

Thoracic Skeletal Injury

While skeletal injury can obviously occur throughout most of the body, detection and accurate prediction of the location and extent of skeletal injury in the highly deformable thoracic area has proven most elusive. Both field and laboratory studies have shown that thoracic skeletal injuries occur not only at sites where the crash forces are applied but at sites remote from the application of force. This evidence together with the observations that the thorax undergoes significant deformation during an impact suggests that rib failure is primarily a result of bending. Therefore, the following discussion develops a rationale and proposes a process that utilizes the time changing geometric information provided by the chest band to detect conditions of fracture on the thoracic structure. It is anticipated that the actual critical threshold values for fracture will be empirically derived from a series of laboratory experiments simulating frontal impacts using a variety of different restraint systems (Airbag, three-point belt, etc.) using the rationale and methodology discussed herein. An assessment of how the early experimental results support the proposed criterion is also presented. These early results were obtained using 16-gauge bands and further experimentation will be needed using higher-density gauge bands which have been shown to provide more accurate results. [8]

Proposed Thoracic Fracture Criterion

If one assumes that the ribs of the thorax are primarily vulnerable to failure in bending and that their geometric configuration prior to impact is strain free, then the prospect of failure at any point on a rib should be a function of the difference between the deformed curvature at that point and the original curvature at that point regardless of the type of external loading and the rib's material and failure properties. Since each location along the length of a rib could experience either a positive or negative change in curvature depending on the type of loading experienced during an impact and since it is highly likely that the ribs have a variety of nonuniformities, the critical change in curvature that identifies the onset of local fracture may be different for positive and negative changes of curvature. As a result, it is anticipated that both parameters will have to be monitored. If the influence of the nonuniformities is small, then the absolute value of the change in curvature may be a sufficient indicator of fracture potential. Additionally, since the architecture of the rib's cross-section varies both along its length and possibly in the vertical direction, the critical change in curvature values may also vary along the rib's length and as a function of elevation.

Since the ultimate objective is to predict rib fracture risk for an entire dynamic event, the maximum change in curvature, be it positive, negative, or absolute, over the entire event is proposed as the parameter that should be the most descriptive of fracture. Figure 4 illustrates a typical, complete distribution of curvature around the

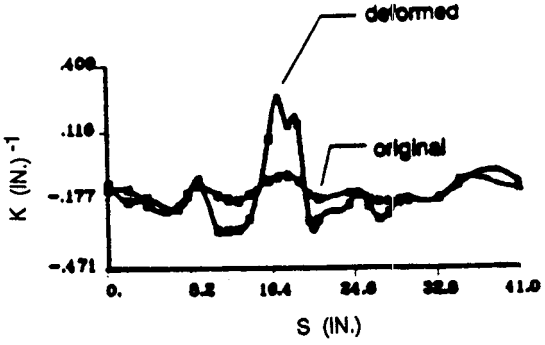

Figure 4. Thoracic Curvatures Associated with Original and Deformed States

thorax of a cadaver undergoing an impact test in a belt restraint at two different times: one just prior to the application of forces (at a time of 112.5 milliseconds on the event clock) and one 38 milliseconds later. The difference between these two curves, shown in Figure 5, represents the strain induced into a rib structure at that instant in time and, therefore, is the parameter that should be indicative of rib failure potential at that time.

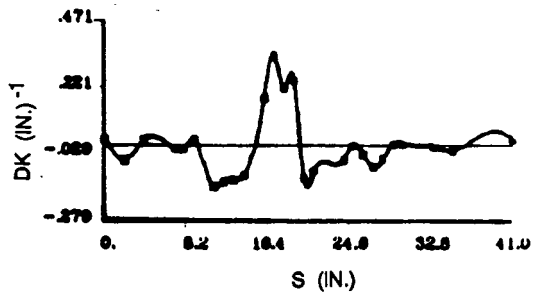

Figure 5. Change in Curvature Due to Deformation of Thorax

The absolute maximum change of curvature, Max. DK, along the total peripheral length of the structure for the entire event is shown in Figure 6a while the maximum positive and negative changes are shown in Figures 6b and 6c respectively.

A hypothesized fracture tolerance level for absolute maximum change of curvature is shown in Figure 7. In this figure, the curvature is depicted starting at the spine, S = 0 inches, and proceeding around the thorax to the left until coming to the sternum, s = 19 inches, and then continuing around to the right until the spine is again encountered, S = 40 inches.

To compensate for possible geometrical and material changes in the rib structure along its length, the critical change in curvature is envisioned to be different for three different regions, as depicted in Figure 8, around the thorax: Region A covers the area 5 inches on either side of the spine, region C covers the area approximately 4 inches on either side of the sternum and represents the cartilaginous portion of the thorax, and region B, the rib structure connecting the two other regions.

The curvature change for fracture onset is depicted as very small for Region A. The reasoning being that the greater section modulus in this area would cause critical tensile failure stresses to be reached with less curvature change than in region B. Region B has a somewhat higher critical value because of the expected smaller section modulus which requires a greater change in curvature to achieve the same surface stresses in the rib. Region C's very high critical value is reasoned to exist because of the cartilaginous nature of the material of the sternal area which would be very flexible and require a much greater change in curvature before failure would occur. In addition to the variation of the fracture threshold curvature in the circumferential direction, it is possible that the fracture threshold values of maximum change of curva-

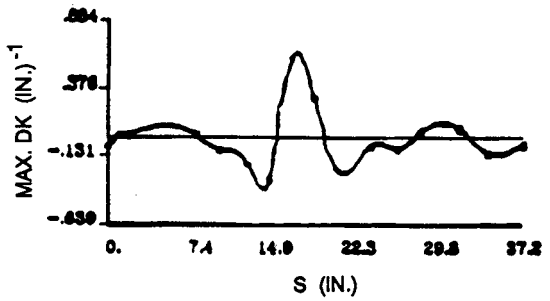

Figure 6a. Absolute Max Change of Curvature Along the Band Length S

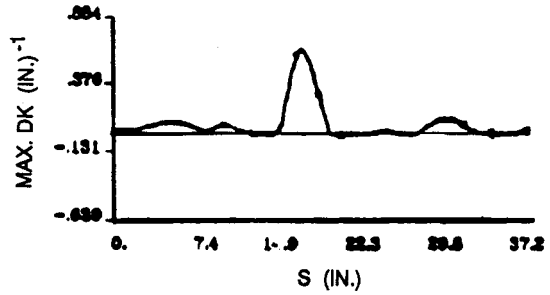

Figure 6b. Positive Max Change of Curvature Along the Band Length S

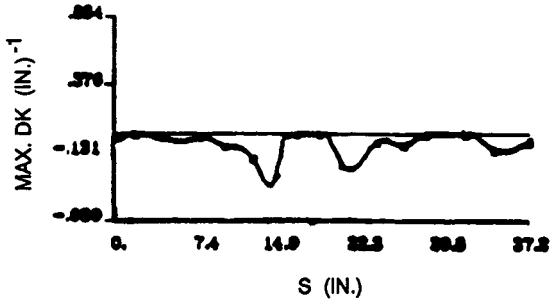

Figure 6c. Negative Max Change of Curvature Along the Band Length S

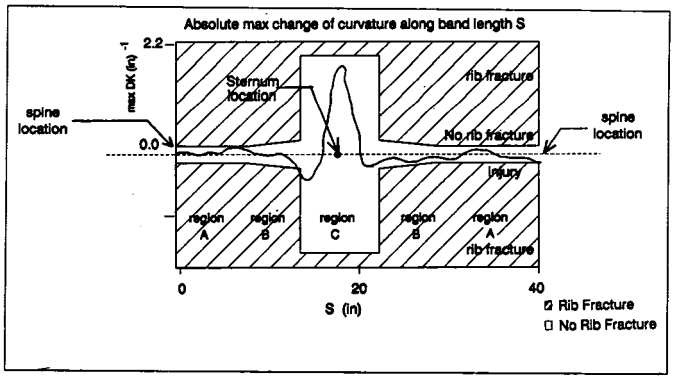

Figure 7. Hypothesized Fracture Tolerance Diagram at the Level of the 4th, 5th and 6th Rib

ture may also vary in the vertical direction. Strictly speaking, it should be assumed that the tolerance level of the maximum change of curvature would vary continuously in the vertical direction. As with the circumferential variation, it is probably necessary to simplify these vertical variations into a limited number of regions with common threshold values within each. In

this case however there are no obvious physical differences which would permit a reasonable ex ante classification to be made. Therefore, as a starting point, the threshold variation in the vertical direction could be explored by separating the thorax into possibly three vertical regions as shown in Figure 9, if the resulting experimental data allows.

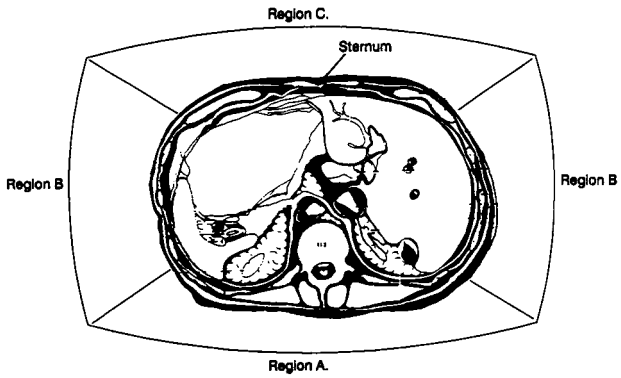

Figure 8. Subregions with Common Fracture Tolerance in the Circumferential Direction

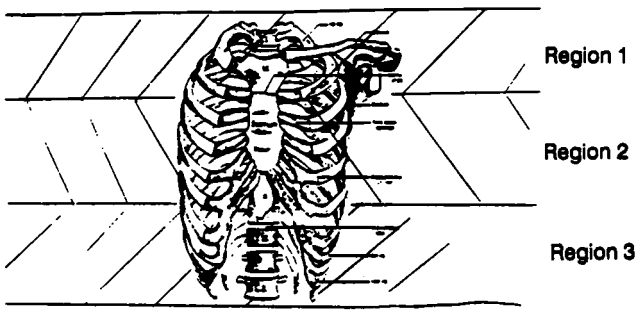

Figure 9. Subregions with Common Fracture Tolerance Level in Vertical (Superior Inferior) Direction

The material properties of the bone obviously have a significant influence on the condition at which failure occurs. Since the strength of human bones changes with age [2], it is reasonable to expect that the tolerance level of an older individual would be less than that of a young individual. How much the age factor contributes to the change in tolerance when considering curvature change is still unknown. It is possible that the standard deviation of the age factor is much less than those of the fracture location. In that case the age factor could be dropped from the criterion. But if the opposite is true then the tolerance level chart (similar to Figure 7) would become more complex. This would also be true for both the circumferential and vertical directions.

Experimental Results

Two frontal impact sled tests of cadavers restrained by three point-belt restraints have been conducted. The change in velocity of both tests was about 30 MPH. In the first test, performed by the Medical College of Wisconsin (MCW), the cadaver was 73 years old. A 36-gauge and a 16-gauge chest bands were used at level 5 and 7 respectively (see the diagram in Figure 10). The autopsy summary indicates that rib fracture occurred at ribs number 2, 3, 4, 5,7 ,and 8 at the midportion of the ribs. In addition rib 4 also had a second fracture at 3.5 cm lateral from midsternum. The absolute maximum change of curvature along the band length, i.e Max. DK vs. S curve, for both bands is shown in Figure 11. Figure 10 shows that the top band was located at the level of ribs 4 and 5 while the bottom band was at the level of ribs 7 and 8.

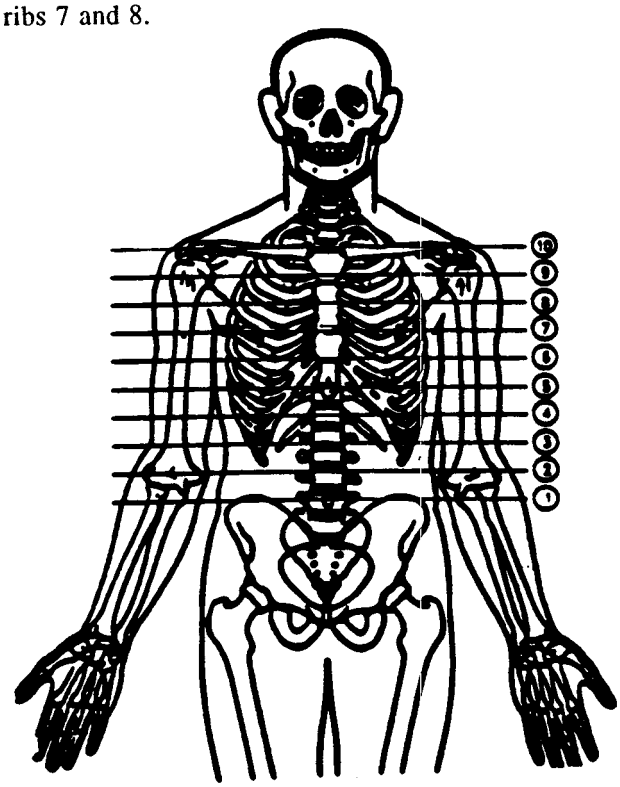

Figure 10. Possible Chest Band's Locations on the Human Thorax

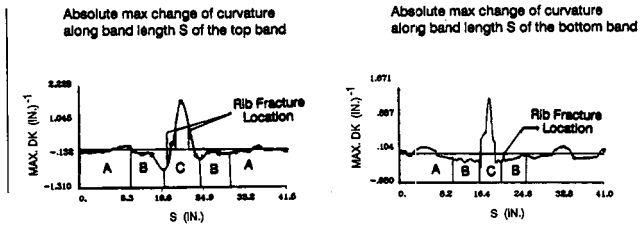

Figure 11. Fracture Location Mapping on the Absolute Change of Curvature from Medical College of Wisconsin Data

An attempt was made to try to map the location of the rib fractures on the Max. Dk vs. S curve in Figure 11. It shows that the rib fractures occurred in region B and C for the top band and only in region B for the bottom band.

The second test was performed by the University of Heidelberg (HDL). The cadaver was 36 years old. In this particular test only one 16-gauge chest band was used at level 7. The autopsy report indicates that there was no

rib fractures. The absolute maximum change of curvature along the band length for this test is shown in Figure 12.

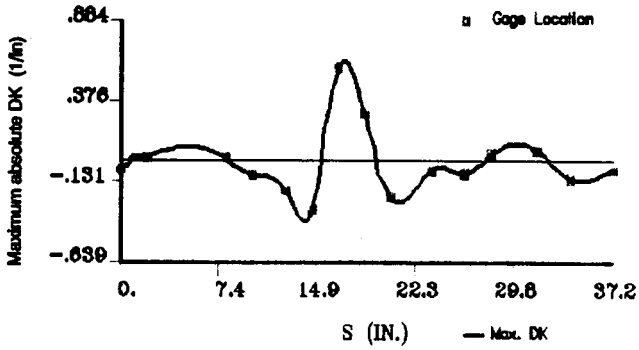

Figure 12. Maximum Change of Curvature of a No Rib Fracture Case (Heidelberg's Data)

Figure 13 compares the Max. DK vs. S curves of the corresponding top bands from each test. This shows that the magnitude of the max. DK in nearly all regions is much higher in the injury case than the no-injury one.

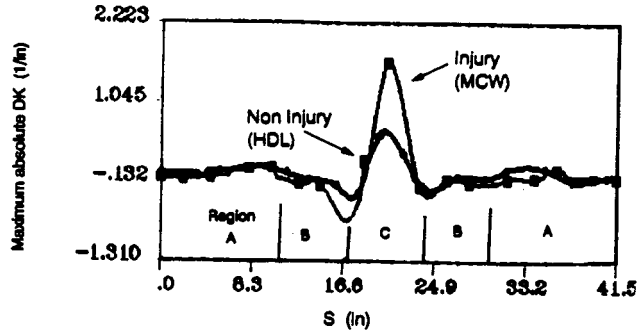

Figure 13. Comparison of Maximum Absolute Change of Curvature Between Injury (Medical College of Wisconsin) and Noninjury (Heidelberg) Cases

Developing a New Thoracic Internal Injury Criterion Using The Chest Band Data

In the past, analytical approaches to develop a thoracic injury criterion have been limited to used of either deformation, as implied in deflection based criteria [4, 5, 6, 7] or the inertial motion of the thorax, as indicated by the acceleration based criterion [3]. With the invention of the chestband by Eppinger [1], an instrument is now available which can accurately measure chest deformation so that it is no longer necessary to rely upon only one chest deflection measurement to characterize the deformation of the thorax. With the advantage of a complete peripheral description of deformation, a new and more complete way of developing an injury criterion can be pursued.

The Stress Analysis Methodology

The injury or failure of structures internal to the thorax experiencing an impact can be attributed to those structure experiencing conditions that exceed their individual critical stress or strain thresholds. Since the actual stresses and strains are a direct result of the deformations and motions that the surface of the thorax undergoes, it appears, at least theoretically, that if one has information about the deformation and motion of the surface of the body, that the internal stresses and strain can be determined and ultimately interpreted to predict the occurrence and extent of internal injuries.

The process proposed to accomplish this is to first create a finite element model of the thorax. Then simulate this model using the deformations as determined by the chestband and inertial motions as determined by accelerometry. The output of the model, local stress and strains, are then examined to establish correlation between them and observed injury and non-injury areas.

To establish the feasibility of this concept, a simplified model of the thorax was developed. This model represents the thorax as a one-inch thick viscoelastic material slab whose contours correspond to the actual undeformed thorax of the cadaver specimens as captured by the chestband instrument. The finite element mesh of this simplified chest model is given in Figure 14. It consists of 1805 nodes and 1360 three-dimensional 8-node shell elements. The model's constitutive properties are given in Table 1.

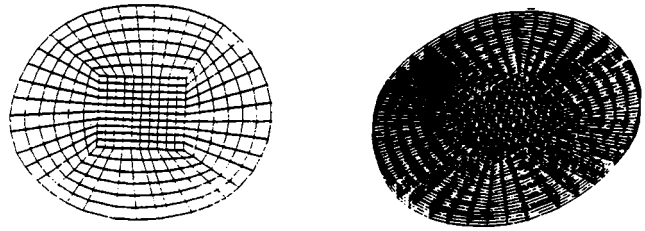

Figure 14. The Finite Element Mesh of a Simplified One Inch Thick Viscoelastic Chest Model

Table 1. Material Properties for Simplified One-Inch Thick Viscoelastic Thorax Model

The Viscoelastic model used in DYNA3D is represented by the following relaxation function:

$$G(t) = Gl + (Gs - Gl)e^{-(BETA)t}$$

where:

Gs = Short term shear modulus.
Gl = Long term shear modulus.
BETA = Decay constant.
t = Time

Material Properties Used in the Stress Analysis

Gs = 10.4 psi
Gl = 0.3425 psi
Beta = 100
Density = 0.75 x10.0e-4 Lb Mass / (in)**3
Bulk Modulus = 100.0 psi

Peripheral deformations and inertial motions as determined from the output of the chestband and accelerometers used in actual tests were processed to be compatible input to the finite element model. The model was then stimulated by these motions and the internal stress contours produced.

Conditions of the Analytical Simulations

Nodal boundary conditions for the chest model were generated for two reasons. First, to evaluate the feasibility of stimulating a finite element model using experimentally measured boundary deformations and, secondly, to investigate if experimentally measured deformation alone is sufficient to determine internal stresses or must the deformation be accompanied by the total inertial motions the body experiences. To simulate the first condition, the model was driven by the nodal deflection time histories measured experimentally. However, the inertial effects due to body motion are set to be negligible by making the sternum stationary with respect to inertial reference frame of the simulation. The nodal deflection time histories were computed from the times series of deformed contours of the subject thorax captured by the chestband instrument. The continuous nodal deflection time history function was derived by applying a cubic spline curve fitting technique to the discretized nodal displacement time history developed from the chest band. Because the DYNA3D program accepts only nodal velocity time histories, the nodal deflection time history were converted to velocity time histories by a simple derivative algorithm. Examples of both a nodal displacement and its corresponding velocity time history are shown in figure 15a and 15b.

To simulate the second case where the effect of measured inertial motion of the body is taken into account, the sternal velocity, derived from the experimentally measured sternal acceleration, was added to each previously derived nodal velocity. The total nodal velocity time history at each boundary node then consists of the summation of the nodal velocity from the deformation as computed in the first case plus the velocity derived from the sternum acceleration. An example of some of these nodal velocity time histories is given in Figure 15c.

As a result of this procedure, the thoracic model experiences exactly the same deformation pattern in both simulations and only the latter simulation experiences the additional of the gross inertial effects. The stress analysis on the two chest band data sets used in section one is carried out both with and without inertial effects.

Results From the Two Simulations

Relative Displacement and Velocity

Four node locations inside the chest model, two each in the vicinity of the spine and the sternum, are chosen from each simulation (See Figure 16). To analyze the relative displacement and velocity, each of the nodes

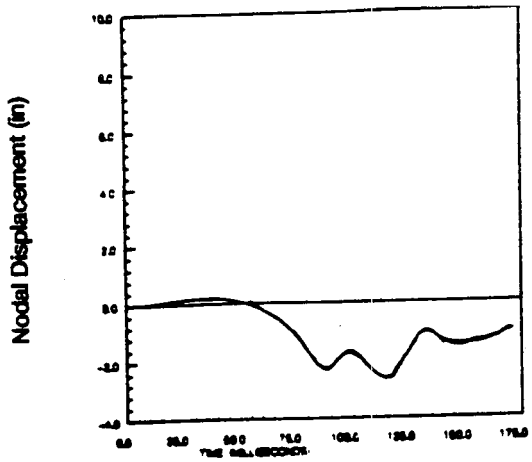

Figure 15. An Example of Nodal Displacement and Velocity Time History of Boundary Node Derived from Chest Band Data: (a) Nodal Displacement of a Boundary Node

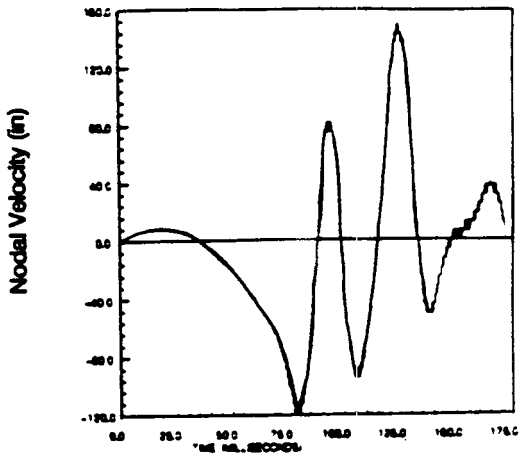

Figure 15. (b) Nodal Velocity of a Boundary Node Without Inertial Effect

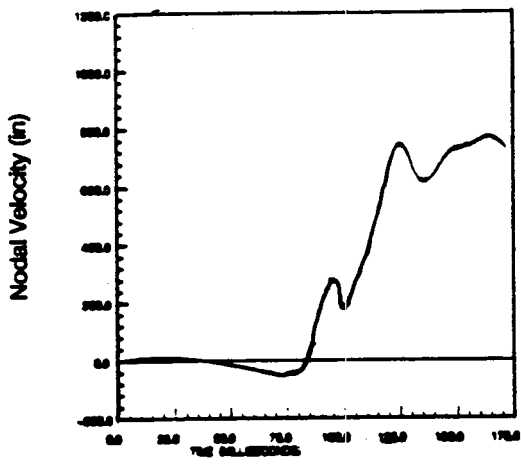

Figure 15. (c) Nodal Velocity of a Boundary Node With Inertial Effect

near the spine is paired with a node near the sternum which is closely aligned in the anterior-posterior direction. The relative displacement and velocity between the two nodes in each pair is then plotted for the time history of the event (See Figures 17 to 20). Each figure

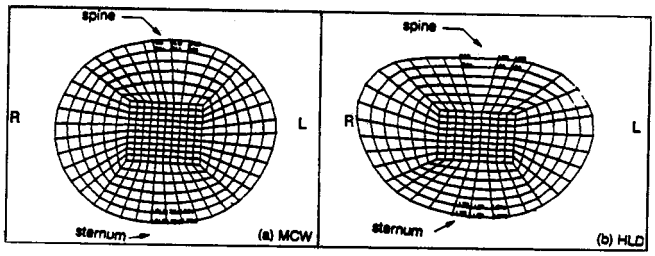

Figure 16. Peripheral Nodes Around the Spine and the Sternum (MCW = Medical College of Wisconsin, HDL = Heidelberg)

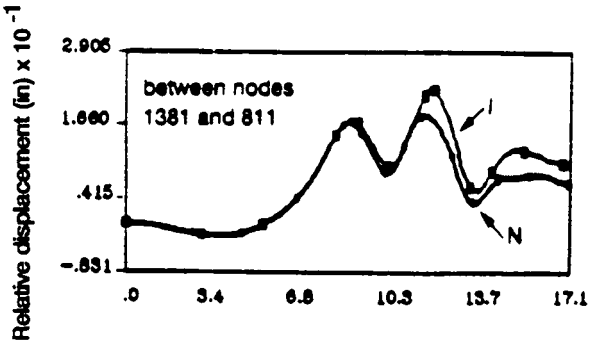

Figure 17. Relative Displacement Time History in Anterior-Posterior Direction. I = With Inertial Effect, N = Without Inertial Effect. (a) Injury Case, Medical College of Wisconsin Data

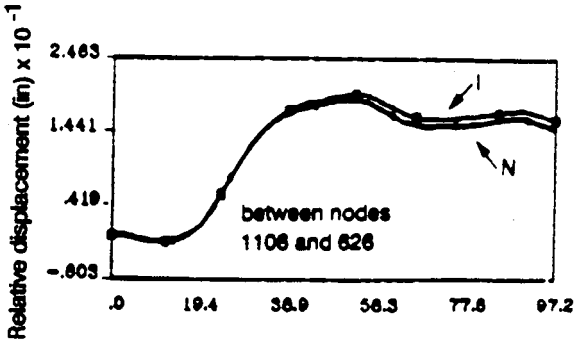

Figure 17. (b) Non-Injury Case, Heidelberg Data

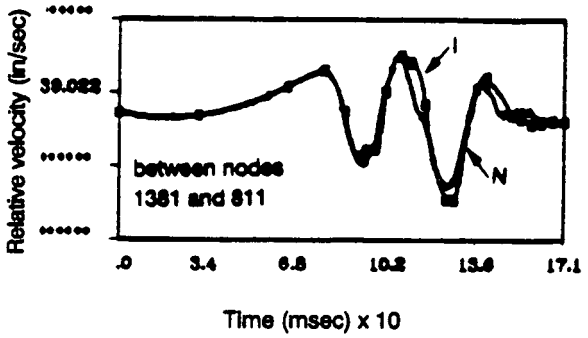

Figure 18. Relative Velocity Time History in Anterior-Posterior Direction. I = With Inertial Effect, N = Without Inertial Effect. (a) Injury Case, Medical College of Wisconsin Data

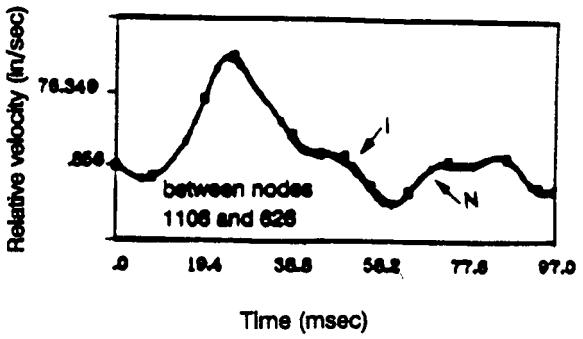

Figure 18. (b) Non-Injury Case, Heidelberg Data

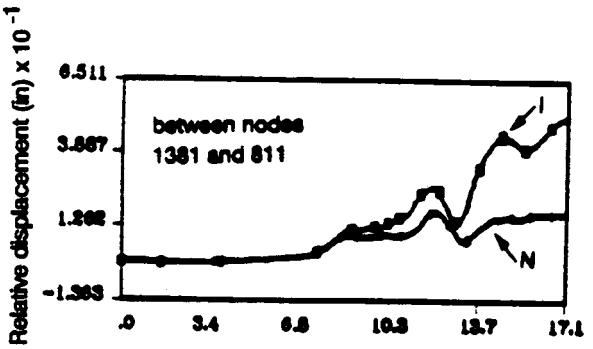

Figure 19. Relative Displacement Time History in Left-Right Direction. I = With Inertial Effect, N = Without Inertial Effect. (a) Injury Case, Medical College of Wisconsin Data

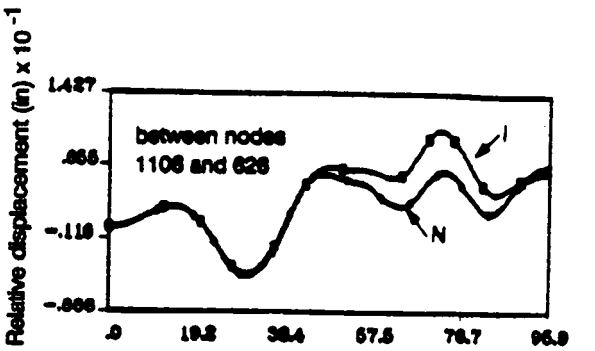

Figure 19. (b) Non-Injury Case, Heidelberg Data

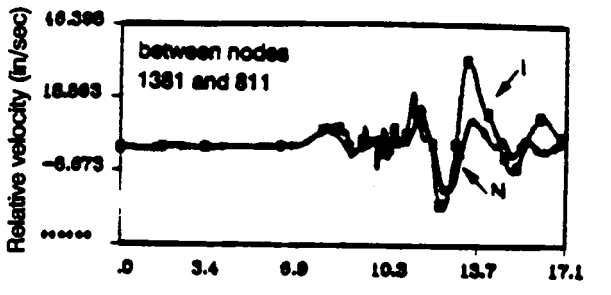

Figure 20. Relative Velocity Time History in Left-Right Direction. I = With Inertial Effect, N = Without Inertial Effect. (a) Injury Case, Medical College of Wisconsin Data

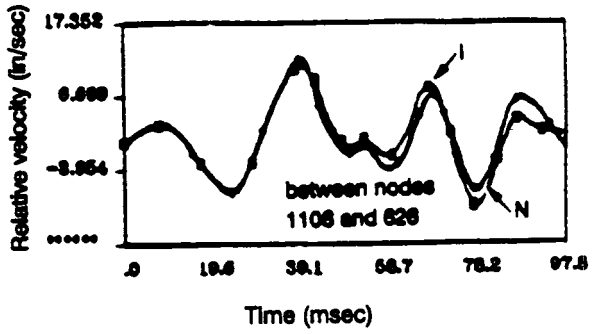

Figure 20. (b) Non-Injury Case, Heidelberg Data

shows the result both with and without inertial effects. In both cases, the displacement and velocity are higher when inertial effects are included. (It is also worth noting the difference between the two data sets. The results in the Wisconsin (injury) data show much larger differences than in the Heidelberg (non-injury) data.)

Maximum and Minimum Pressure

Figures 21a,b and 22a,b show the maximum and minimum pressure respectively. Each curve represents the maximum or minimum pressure at each time step irrespective of its location within the chest model. For each time step the location of the maximum/or minimum pressure between the two cases, namely with and without inertial effect, always occur at the same point inside the chest model. Once again the addition of the inertial effects results in higher maximum and minimum values.

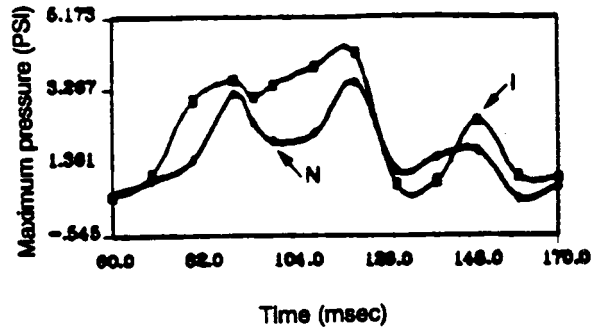

Figure 21. Maximum Pressure Inside the Chest Models. I = With Inertial Effect, N = Without Inertial Effect. (a) Injury Case, Medical College of Wisconsin Data

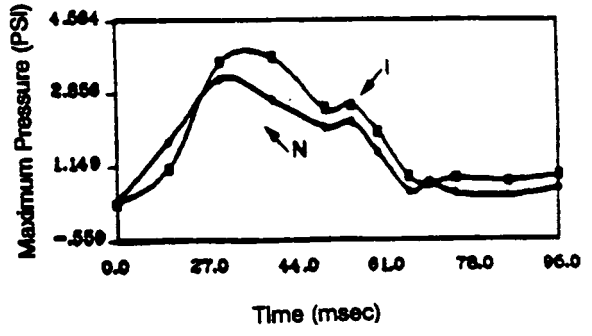

Figure 21. (b) Non-Injury Case, Heidelberg Data

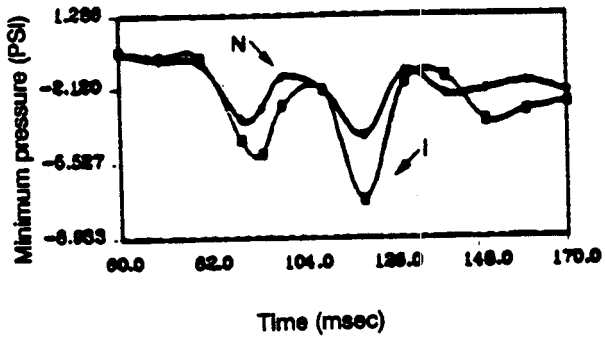

Figure 22. Minimum Pressure Inside the Chest Models. I = With Inertial Effect, N = Without Inertial Effect. (a) Injury Case, Medical College of Wisconsin Data

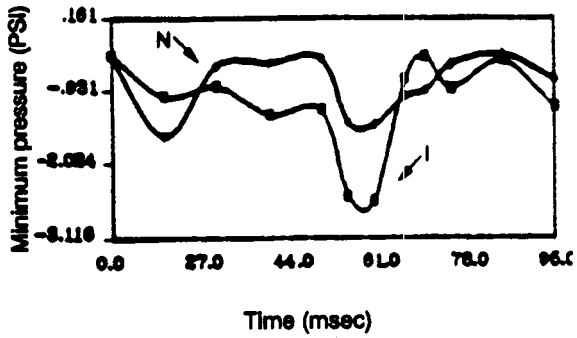

Figure 22. (b) Non-Injury Case, Heidelberg Data

Maximum Von Mises Effective Stress and Strain

Figures 23a,b and 24a,b show the maximum Von Mises [9] effective stress and strain respectively. As in the pressure plots each curve represents the maximum stress or strain at each time step irrespective of its location. But at each time step the location of its occurrence inside the chest model from both cases is always the same. Here also, the result of adding inertial effects is higher stress or strain values.

Conclusions

With the advent of the EPIDM chest band, a much more complete description of the mechanical effects of crash forces on the human thorax can be obtained. This more complete description has the potential of effecting development of more accurate injury predictive methodologies which utilize this information. It appears that the prediction of thoracic rib failure is the most straight forward to accomplish because parameters, local curvature, which are a direct output of the EPIDM process can be theoretically and experimentally linked to failure. Examples of how this would be accomplished have been presented and it now remains to acquire sufficient experimental data in order to establish the critical threshold values for the various areas of the chest.

The EPIDM process also appears to allow the development of a procedure which has the capabilities of predicting internal thoracic injuries. The process of analytically analyzing the effects of experimentally obtained deformational and inertial motions on a model

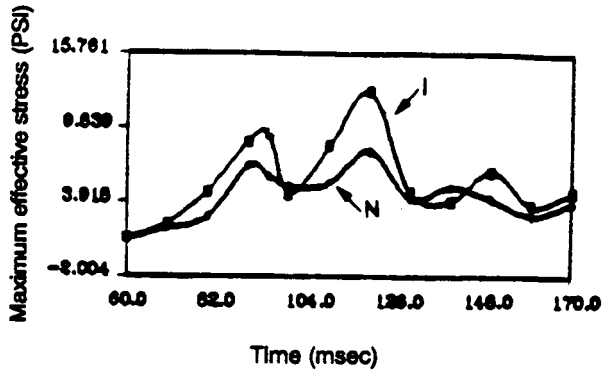

Figure 23. Maximum Von Mises Effective Stress Time History Inside the Chest Model. I = With Inertial Effect, N = Without Inertial Effect. (a) Injury Case, Medical College of Wisconsin Data

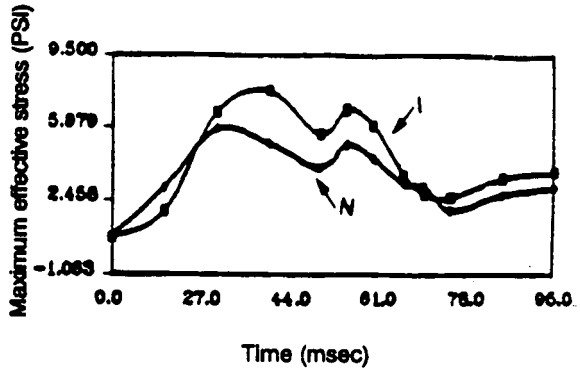

Figure 23. (b) Non-Injury Case, Heidelberg Data

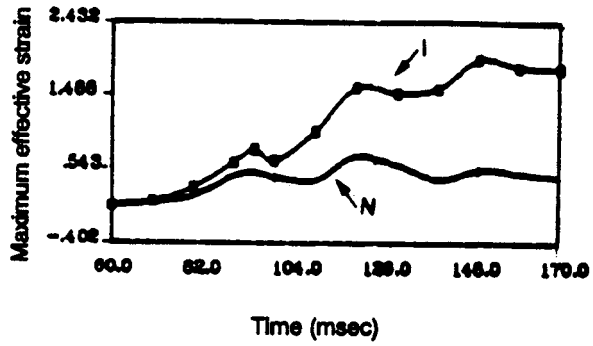

Figure 24. Maximum Von Mises Effective Strain Time History Inside the Chest Model. I = With Inertial Effect, N = Without Inertial Effect. (a) Injury Case, Medical College of Wisconsin Data

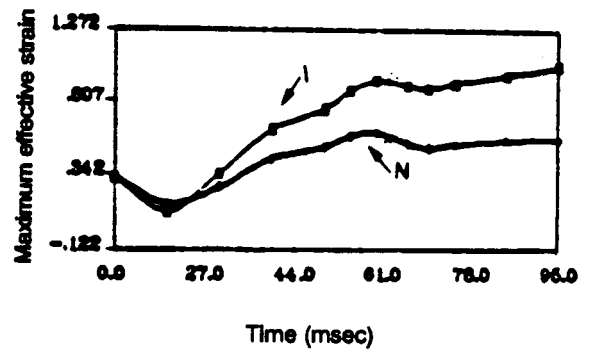

Figure 24. (b) Non-Injury Case, Heidelberg Data

of a thorax has been shown to be feasible and practicable. Initial investigations have strongly suggested that when additional experimental efforts are undertaken to establish the data base from which any criteria is to be developed, that both the deformation and inertial data are necessary to accurately predict the true stresses and strains, and therefore the injuries that are occurring within the thorax.

Disclaimer

The views presented are those of the authors and are not necessarily those of the National Highway Traffic Safety Administration, U.S. Department of Transportation.

References

1. Eppinger, R.H., On the Development of a Deformation Measurement System and Its Application Toward Developing Mechanically Based Injury Indices. Proceedings of the 33th STAPP Car Crash Conference. pp 21-28, 1989. Washington, DC.
2. Yamada, H., Strength of Biological Materials. Edited by F.G. Evans. The Williams & Wilkins Company, Baltimore 1970.
3. Eppinger, R.H., Marcus J.H., Morgan R.M., Development of Dummy and Injury Index for NHTSA's Thoracic Side Impact Protection Research Program. SAE Technical Paper Series # 840885.
4. Stapp, J.P., Voluntary Human Tolerance Levels. In Impact Injury and Crash Protection. Gurdjian, E.S., Lange, W.A., Patrick, L.M., Thomas, L.M., (Editors), Charles C. Thomas, Springfield, Illinois.
5. Kroell, C.K., Schneider, D.C, Nahum, A.M., Impact Tolerance and Response of the Human Thorax II. 18th STAPP Car Crash Conference SAE, Warrendale, PA 1981.
6. Neathery, R.F., An Analysis of Chest Impact Response Data and Scaled Performance Recommendations. Proceedings of the 18th STAPP Car Crash Conference.
7. Lau, I.V., Viano, D.C., The Viscous Criterion—Base and Applications of an Injury Severity Index for Soft Tissues. Proceedings of the 30th STAPP Car Crash Conference.
8. Hagedorn, A.V., Eppenger, R.H., Morgan, R.M., Pritz, H.B., Khaewpong, N., Application of a Deformation Measurement System to Biomechanical Systems. Proceedings of the 1991 International IRCOBI Conference, Berlin (Germany).
9. Fung, Y.C., Foundation of Solid Mechanics. Prentice-Hall International Series in Dynamics.

S8-O-11

3-D Anatomic Brain Model for Relating Cortical Strains to Automobile Crash Loading

F. Dimasi
Volpe National Transportation Systems Center
J. Marcus, R. Eppinger
National Highway Traffic Safety Administration

Abstract

This paper describes the development of a three-dimensional anatomic brain model using finite elements to estimate strains induced in soft cortical tissues of the brain in response to impact and non-impact loadings representative of the automobile collision environment. The upper cerebral cortex is modeled with longitudinal fissure to provide distinctive sagittal and coronal geometric features and the surrounding dura includes the falx anatomic partition. Sliding is permitted between cortical and dura/falx surfaces to simulate slip conditions at the perimeter of the human cortex. A relatively rigid skull-headpart with cranial cavity enclosing dura and cortex is also included for modeling direct contact events with upper interior structures. Simulated impacts with padded and unpadded A-pillars are made and first estimates of cortical strains resulting from these impacts are provided. Rigid body headpart acceleration responses are also estimated and discussed with soft tissue strains.

Introduction and Overview

The current head injury criteria (HIC) as specified in Federal Motor Vehicle Safety Standard (FMVSS) 208 evolved from the Wayne State Tolerance Curve [1] and provides a quantitative indication of the potential for serious head injury based on translational acceleration measurements at the center of gravity of a dummy head.

The Wayne State Tolerance Curve, which relates the probability of a head injury to a combination of time and acceleration was developed based on a number of tests in which the heads of human cadaveric subjects were dropped onto rigid and padded plates, and post test autopsies revealed the resulting injuries.

Because cadaveric subjects were used, it was not possible to evaluate functional impairments such as memory loss, paralysis, emotion changes, or intellectual impairments, nor could vascular injuries such as hematoma be evaluated because the vascular system was not perfused.

Thus, while HIC has been shown to be indicative of many forms of head injury, questions have been raised about its sensitivity to certain classes of brain injuries resulting from automobile crashes. These brain injuries, called Diffuse Axonal Injuries (DAI), do not have an identifiable lesion but result in neurological impairments. In addition, vascular injuries such as sub-dural hematomas may not be adequately predicted by HIC.

Results of recent experimental and pathophysiological studies performed by the University of Pennsylvania suggest that the functional impairment of a single nerve cell is directly related to the magnitude of strain imposed on the cell, and that the extent of injury to brain tissue is strongly related to both the magnitude and direction of applied loading [2].

These findings also indicate that strain levels developed in brain tissue and in bridging veins (the blood vessels between the top of the brain and the inside of the skull) are particularly sensitive to rotational acceleration. Bridging vein disruption is believed to be the cause of many brain hematomas. One can immediately imagine the difficulties involved in measuring and analyzing these quantities, even in laboratory experiments using relatively simple geometric shapes to simulate the complex geometry of the brain [3].

For these reasons, efforts have been directed at developing a first generation anatomic brain model using finite-elements as a predictive tool for estimating strains induced in the soft cortical tissues of the brain in response to dynamic forces and accelerations representative of the automobile collision environment.

Since rotational kinematics are known to have a strong influence on induced strains, and since directional effects are also of strong interest, a three-dimensional model with distinctive sagittal and coronal geometry is required. This paper describes the development of a first generation anatomic brain model which has been used for simulating impact with various upper interior surfaces and structures.

Specifically, this paper presents results of simulated impacts with padded and unpadded A-pillars (the forward post supporting the vehicle roof and holding the windshield on each side of the vehicle). These impacts are of concern because the heads of occupants located in the driver and front passenger positions frequently strike this structure during frontal or lateral crashes causing serious injury. We also wish to evaluate the potential injury mitigation resulting from the addition of foam padding to A-pillars.

The finite-element codes INGRID, DYNA3D and TAURUS [4,5,6] developed by the Department of Energy's Lawrence Livermore National Laboratory (LLNL) have been used for modeling, simulation and post processing respectively. These codes provide for the non-linear and large-deformation response of inelastic solids and structures in three dimensions.

Contact-impact algorithms make these codes particularly useful for simulating transient impact events

involving large displacements and sliding contact between impacting surfaces as well as for computing detailed physical quantities within the continuum. Prediction of such quantities will be required to develop a better understanding of collision mechanics and injuries to the brain which are responsible for so many of the devastating injuries sustained in automotive collisions.

The following paragraphs briefly describe the A-pillar model; and subsequently, the developmental process resulting in the first generation brain model is described. The impact scenarios described herein are a continuation of efforts to simulate laboratory tests wherein an instrumented Hybrid III headform was launched into free flight impacting padded and unpadded GM X-body A-pillars at various speeds.

Resultant accelerations from 25 mph simulated impacts with padded and unpadded A-pillars are compared with corresponding test data from free-motion headform laboratory tests. Simulated results include first estimates of strains induced in brain tissue in response to these impacts.

A-Pillar Model Structural Configuration and Modeling

The GM X-body A-pillar is a hollow curved structure, fabricated from three formed sheet stock sections. To provide an adequate model for the geometry and material properties of the A-pillar and the assembled structure, several X-body A-pillars were purchased from a recycled auto parts dealer and used for geometry, cross-section and material property measurements.

Figure 1 contains an "exploded-view" mesh plot of the three formed sheet metal sections comprising the A-pillar model to illustrate construction and modeling features. Although some minor variations in thickness and cross section were noted along the length of the A-pillar, these were considered insignificant and the pillar's cross section was modeled as uniform along its length. The sections are assembled by simulating a combination of spot welds and tack welds along the lengths of adjoining sections. The three-segment A-pillar is modeled with 550 shell elements.

Material testing of A-pillar coupons was conducted by MIT's Department of Material Science and Engineering. Measurement accuracy was 5% or better on yield strength and 10% or better for small strains beyond yield. Past yield, material behavior was characterized as linear strain hardening or perfectly plastic.

Material properties of the three sections comprising the A-pillar are shown below.

Section (ref. Fig 1)	Thickness (in.)	Yield Stress (psi)	Tangent Modulus (psi)
A	.063	33,000	1.5×10^6
B	.040	48,000	0.0 (perf. plastic)
C	.049	28,000	2.2×10^6

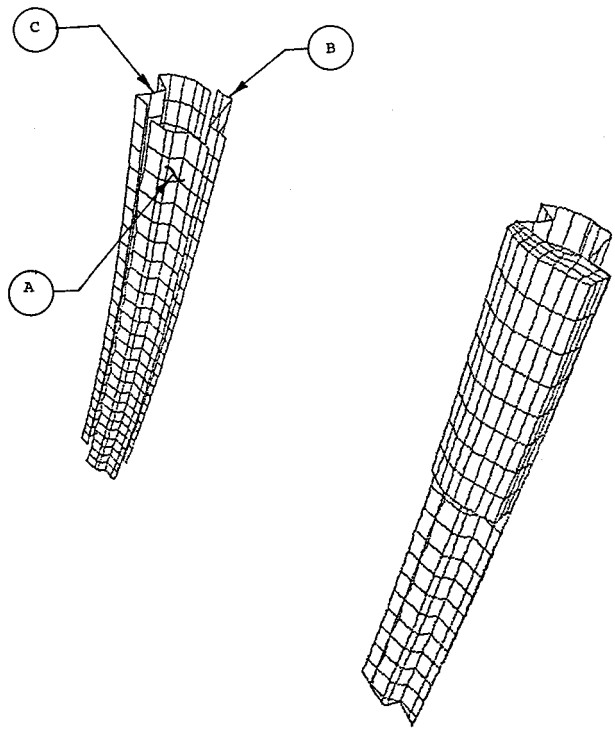

Figure 1. Exploded View of A-Pillar Components and Assembled A-Pillar/Cushion Mesh Model

Nodes located at the top and bottom extremities of the A-pillar were constrained in translation and free in rotation. Very good impact response was obtained with this configuration. Considering details of assembly, windshield and door components were judged to have minimal influence on A-pillar stiffness and were not modeled. A thin plastic finishing cover (not shown) was also disregarded for similar reasons.

For the padded simulation, a cushion was modeled to line the A-pillar using a soil and crushable foam material model. Since force-deflection data had been developed in laboratory tests to characterize the stiffness of various padding materials [7], material constants were defined by simulating the laboratory impact tests and adjusting stiffness parameters until similar force-deflection characteristics were provided by the simulated cushion. The simulated A-pillar padding component was modeled to conform with the general proportions of the cushion used in laboratory testing, using 311 solid elements.

First Generation Anatomical Brain Model

Recent experimental and pathophysiological results suggest excessive strain experienced by soft cortical tissues is a leading cause of brain injury and that the extent of injury to soft cortical tissue is strongly related to both the magnitude and direction of loading applied to the head.

These findings also indicate that strain levels developed in soft tissues and bridging veins are particularly

important in assessing the potential for injuries such as Diffuse Axonal Injury (DAI), and Sub Dural Hematoma (SDH). In DAI, axons (i.e., single nerve cells) experience excessive stretching causing the axon's membrane to lose its ability to maintain the internal/external calcium ion concentration ratio (approximately 50,000 times more calcium outside the cell). As the internal calcium level climbs, the axon loses its ability to function. Functional impairment occurs before mechanical destruction of the axon is realized.

The difficulties involved with measuring and analyzing detailed stress/strain distributions is readily apparent even in laboratory experiments using simple geometric shapes [e.g., 2,3] to simulate the complex geometry of the human brain. To provide an understanding of these strain distributions, a first generation anatomic brain model was developed to calculate strains developed in brain tissue.

Such a model will also be useful in studying the effects of directional loading, scaling or extrapolating injury data from primates to humans, and developing a better understanding of relationships between impact kinematics and injuries to soft cortical tissues. These injuries are responsible for many devastating brain injuries sustained in automotive collisions.

Before describing the model and impact simulations, it is important to note that additional research will be required before results from such a model can be related to injuries sustained by humans in the collision environment.

Most importantly, basic research is needed to provide: (1) a definition of damage tolerance limits in terms of maximum mechanical strains, strain rates and/or other physical quantities which can be related to various tissue failure, trauma and/or loss of function; and (2) improved constitutive relationships for various cortical tissues for modeling studies. Location of maximum strains is also of interest. Additional work will also be required to relate these quantities with neurological observations of impairment and dysfunction observed in humans for similar impact conditions.

Anatomic Features

The first step in developing a model was to consider anatomic features which are likely to affect strain fields throughout the brain. Principal anatomic features and basic geometry of the cranial cavity are illustrated in Figure 2. Features of known or suspected importance to anatomical modeling include the following:

1. Anatomic partitions such as the falx cerebri, tentorium and falx cerebelli;
2. Basic cortex geometry including the longitudinal fissure and distinctive sagittal and coronal geometry;
3. Constraint conditions at the base of the cerebral cortex where the brain stem and surrounding dura (the tough outer cover of the brain) enter into the upper cranial cavity after passing through the foramen magnum (the opening of the skull through which the spinal cord enters the brain) and tentorium;
4. Constraint (or slip) condition between the brain tissue and the dura as effected by pia and arachnoid membranes on the surface of the cortex; and
5. Potential directional stiffness effects due to what appears to be anisotropic material properties associated with the corpus callosum and corona radiata within the internal capsule.

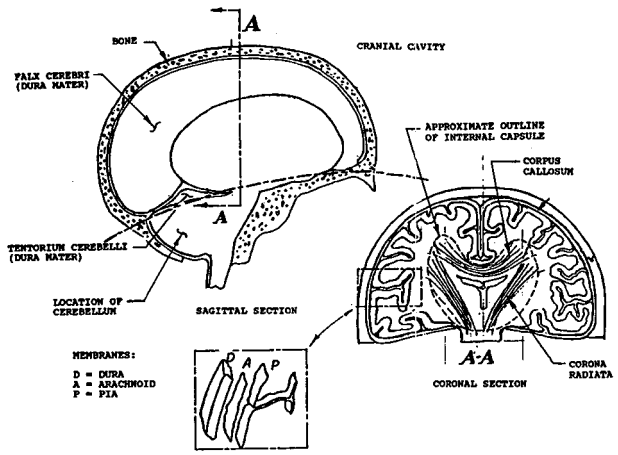

Figure 2. Principal Anatomic Features and Basic Geometry of Upper Cerebral Cortex and Cranial Cavity

Other factors which may be important include effects of the mennix (i.e. pia and arachnoid membranes) on local tissue stiffness at the outer perimeter of the cortex, vascular pressurization and cerebral spinal fluid (CSF) found in ventricles in interior regions and between mennix on the perimeter and in subdural and subarachnoid spaces.

Modeling Approximations

Since the main region of the brain is located in the upper cranium, the upper cerebral cortex was modeled using approximate but distinctive sagittal and coronal geometries including the longitudinal fissure which partitions right and left hemispheres and interfaces with the relatively thin, hard falx cerebri. The inferior surface was simplified and modeled with a cylindrical surface. The cerebellum was not included nor were details of brain stem egression, although an interior region of the inferior surface of the cortex was constrained to emulate brain stem egression. (The cerebellum, the falx tentorium and details of the internal capsule and brain stem egression will be considered in subsequent modeling.)

Figure 3A illustrates the cortex modeled with longitudinal fissure providing approximated sagittal and coronal geometry. The dura, which makes a double fold in the sagittal plane (the plane in the center of the body dividing right and left hemispheres) to form the falx anatomic partition, is a thick, tough membrane complete-

ly surrounding the cortex and brain stem. This was modeled using solid elements, and light friction was applied along the surface defined by the interior dural surfaces and the mating external surface of the cortex, to approximate slip conditions along this interface.

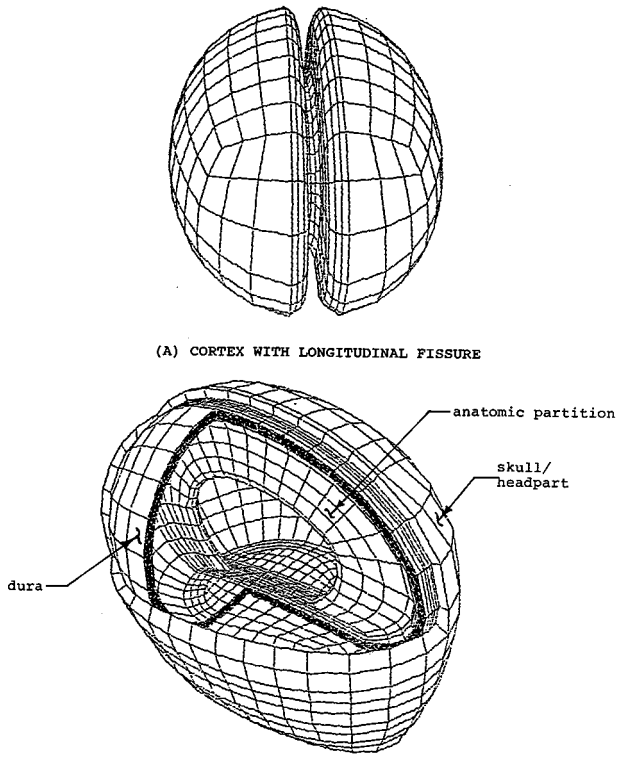

(A) CORTEX WITH LONGITUDINAL FISSURE

(B) CUTAWAY VIEW OF HEADPART AND DURA WITH ANATOMIC PARTITION

Figure 3. First Generation Anatomic Brain Model

The arachnoid and pia mater also lie along this interface, and the friction modeled in this region is intended to approximate the global behavior of a more complex interaction of tissues and membranes. This is tantamount to defining a slip condition between the external surface of the brain as it mates with the interior surface of the skull. Cerebral spinal fluid, vascular pressurization, and effects of mennix at the perimeter of the cortex/dura interface could not be estimated with any accuracy and were not fully considered.

Little is known about the tissue properties of the corona radiata and corpus callosum which constitute the internal capsule within the upper cerebral cortex. Since these are described anatomically as bundles of nerve fibers, it would not be surprising if these tissues exhibited directional stiffness effects. Representative material properties for dura and cortex were selected based on published data, [3,8] with consideration given to effects of mennix and potential directional stiffness effects.

A rate dependent visco-elastic material (Flugge) model was used for modeling the cortex. Shear relaxation behavior is described by initial and long-term shear modulii (2.5 and 5.0 psi, respectively) and a decay constant (100 sec.1) to describe the transition between static and dynamic behavior. The elastic modulus is described indirectly by specifying the material's bulk modulus. A value of 10,000 psi was used for the bulk modulus. A linear elastic material with a modulus of 1000 psi was used for modeling the dura. This value was reduced from published mechanical properties to account for the thicker falx used in this model.

In order to model contact events such as those described below, a skull with cranial cavity was modeled to house the soft dura and cortex components. An elastic modulus of 350,000 psi was selected from a range of mechanical properties provided in [8], resulting in a relatively rigid enclosure for the load applied in the impacts described below. A sectioned view of the assembled cortex/dura/skull-headpart model is shown in Figure 3B.

Although many details of the skull have been omitted at this time, the overall response of the headpart is believed to be very representative for the impact simulations discussed below. While the overall model should be suitable for relating soft cortical strains and dynamic loading, the skull as presently modeled is not appropriate for studying skull fracture and other details of the skull's response.

Simulated Impacts

To evaluate the potential effects of padding on strains induced in soft cortical tissue, the cortex/dura/headpart and A-pillar and cushion models described above were used to simulate 25 mph impacts with padded and unpadded A-pillars. Extensive laboratory testing conducted at speeds of 20 and 25 mph, has documented the benefits provided by cushioned A-pillars in the form of reductions in resultant head accelerations measured at the centroid of an instrumented Hybrid III headpart and corresponding values of HIC.

The headpart used in these tests had a modified posterior surface to permit the headform to be launched into free flight with controlled speed and direction using a hydraulically actuated impact accelerator. The headpart was instrumented with a nine-accelerometer package (NAP) for measuring translational and rotational headpart accelerations.

The headpart was positioned at the height of a normally seated 50th percentile occupant, facing the A-pillar. This resulted in a velocity vector of 45 degrees relative to the vehicle longitudinal axis and an impact location near the top of the pillar. Padded and unpadded A-pillars were impacted at speeds of 20 and 25 mph. A complete test description is provided in [9].

The model size and simulation times for unpadded and padded A-pillar simulations are as follows:

	Unpadded	Padded
Number of nodes	8,650	8,959
Number of solid elements	5,872	6,064
Number of shell elements	525	525
Length of time simulated (msec.)	12	16

The head described above was positioned and oriented relative to the A-pillar to simulate the laboratory tests referenced above. Both padded and unpadded simulations were conducted using a CRAY2 computer and required approximately 10 CPU min/simulated msec. Results are discussed below and compared with laboratory data.

Discussion of Results

Although interaction with the neck has a strong influence on headpart kinematics over the duration of the crash event, a comparison of headpart kinematics and resultant accelerations measured in fully instrumented dummies during impact vs. component level (i.e. headpart only) free-flight headpart impacts, indicates that the latter approach closely approximates full-dummy dynamic loading for short durations associated with impact of a stiff structure [9]. For these reasons, the headpart impact simulations described above should result in dynamic loads which are close approximations of the automobile collision environment.

To summarize, the kinematics associated with the padded vs. unpadded A-pillar impacts, the headpart/A-pillar relative positions at 12 msec. are shown in Figure 4. This figure gives a general indication of the relative displacements and rotations experienced in respective simulations. At 12 msec, the headpart in the padded simulation has barely rebounded from the A-pillar and experiences relatively little rotation. On the other hand, the headpart in the unpadded simulation experiences greater rotation about the pitch (i.e. lateral) axis and has clearly rebounded from the A-pillar at 12 msec.

While it is not obvious from these figures, roll motions (i.e., about longitudinal axis) are small but occur in opposite directions. This is probably related to the longer contact duration and smaller forces acting between the head and padded A-pillar, resulting in a different contact geometry and trajectory as the impact proceeds.

An approximation of the resultant acceleration at the centroid is provided for padded vs. unpadded simulations in Figure 5. These are approximations because a rigid body centroid technically does not exist for this model since the interior material undergoes some compression and flow between hemispheres, from one instant to the next.

The following procedure was used to approximate resultant accelerations about the centroid of the simulated headpart during impact. In post processing, rigid body velocities in the global X, Y, and Z axes were extracted for the cortex, dura, and skull components. These were then multiplied by the respective mass of each component and X, Y, and Z components were combined to provide total headpart momentum (at the centroid). This quantity was then divided by total headpart mass to provide an estimate of the centroidal velocities about the global X, Y, and Z axes. Finally, each component was differentiated and combined to provide the resultant accelerations shown in Figure 5.

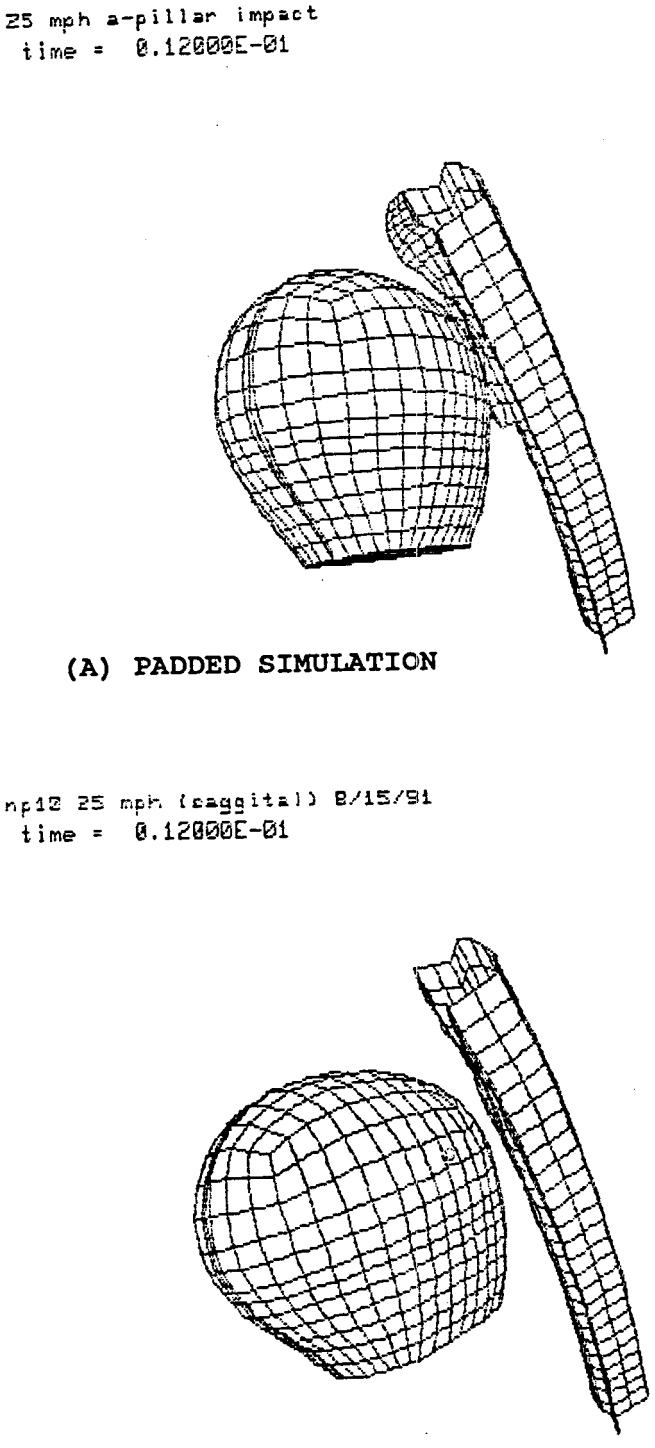

Figure 4. Comparison of Headpart Kinematics at 12 msec

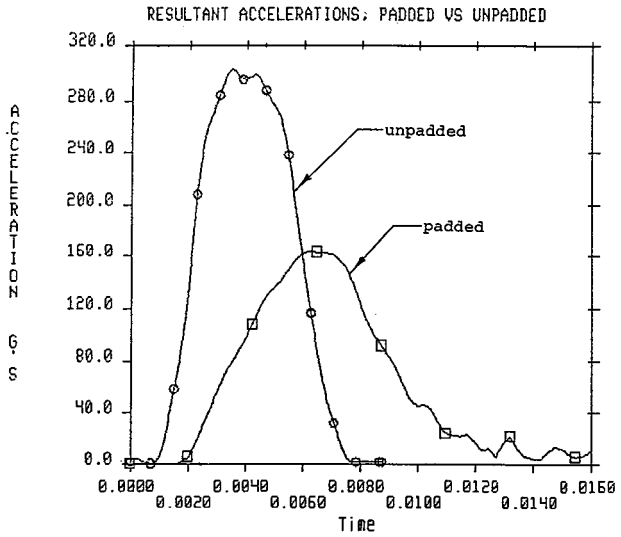

Figure 5. Resultant Accelerations (Approximated) at Centroid of Head Model

A comparison of resultant accelerations with test data for the free-flight laboratory impact tests is very good in terms of maximum accelerations and pulse shape for both padded and unpadded tests, although the width of the pulse for the unpadded simulation is somewhat wider than the corresponding test data. This is probably due to a difference in headpart mass, the simulated headpart being approximately 20% heavier than the headpart used in testing. A summary of resultant acceleration and HIC values follows:

	A-Pillar Configuration			
	Unpadded		Padded	
	Simulated	Test	Simulated	Test
Peak Res. Accel (G's)	303	312	165	164
HIC value	4431	2666	1085	973
Delta T (T2-T1), msec.	3.881	2.375	5.727	5.250

Contour plots of strain data were reviewed at each time state to determine values of maximum principal strain, maximum shear strain, general strain distribution, as well as the element containing the maximum strain. These strains are of interest since maximum principal strain is a good indicator of axonal injury, and shear strains are indicators of potential damage arising from rotational kinematics, particularly at the perimeter of the brain where bridging veins are located.

A comparison of maximum principal strains for selected elements experiencing high strains in the padded vs. unpadded simulations is provided in Figures 6A and 6B respectively. Corresponding values of maximum shear strain for padded vs. unpadded conditions are contained in Figures 7A and 7B. Values of maximum principal strain, maximum shear strain, and the time at which these strains occur are summarized below:

	Unpadded	Padded
Max. Principal Strain	75%	35%
Max. Shear Strain	60%	29%
Time of Max. Strains	4.2 msec.	7.0 msec.
Time of Max. Acceleration	3.5 msec.	6.3 msec.
Acceleration Amplitude	303 G's	165 G's

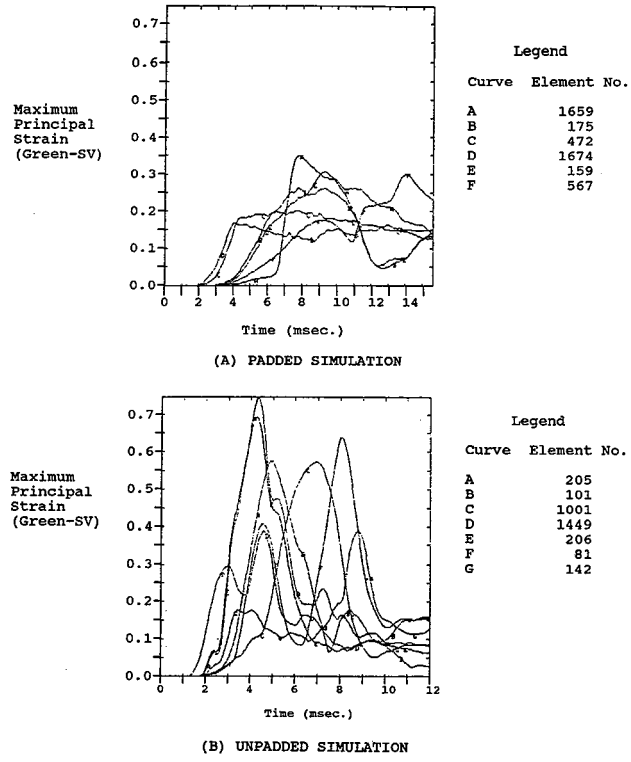

Figure 6. Time Histories of Maximum Principal Strain for Selected Elements

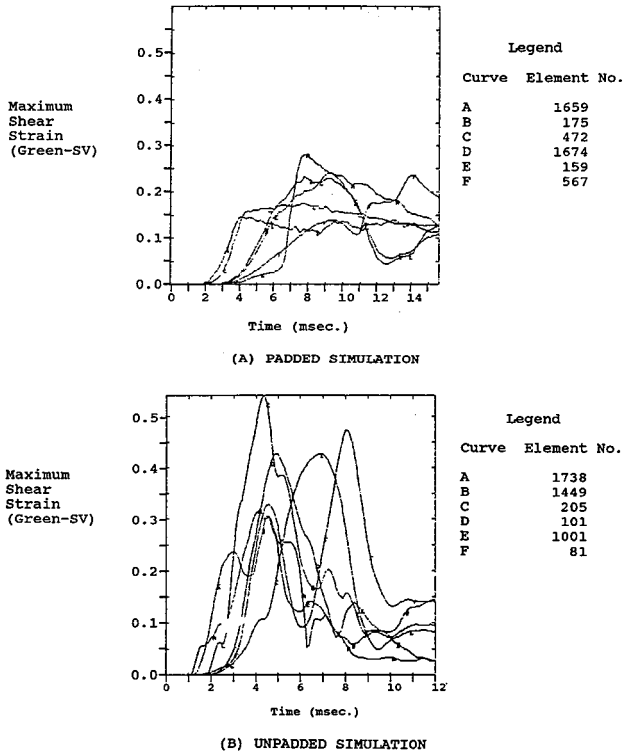

Figure 7. Time Histories of Maximum Shear Strain for Selected Elements

This data indicates that strains for the unpadded condition are approximately twice as large as corresponding strains in the padded condition and roughly proportional

to relative acceleration amplitudes, and that the maximum strains lag peak accelerations. It is also interesting to note that the square root of the ratio of HIC values is also proportional to the ratio of strains.

However, strain rates for elements in the unpadded simulation are generally much higher than in the padded condition, and the overall strain pattern in many high strain elements is very different. The unpadded response suggests the presence of a stronger pressure wave traveling through the brain material, whereas many high strain elements in the padded simulation have a more consistent, relatively stable response.

Figure 8 contains strain contours of effective plastic strain to provide a general indication of maximum strain locations at times close to peak acceleration. In the padded condition (Figure 8A), maximum strains occur both near the contact region and in the region directly opposite the point of impact. This is sometimes referred to as the contre-coup location, since it represents a counterblow or rebound effect resulting from an initial impact at an opposite location. The unpadded contour (Figure 8B) indicates high strains at the posterior location, on both left and right hemispheres.

Since a non-rigid headpart was used in these simulations, some small deformation of the skull occurs and is an influence on these strains. In addition to skull deformation, compression of the cortical material also occurs, primarily in the unpadded simulation, as indicated in Figure 9 (lower figure).

The upper illustration of Figure 9 is a sliced view cutting through the skull, dura, brain and A-pillar materials. The shaded area is a void which has developed between the dura and the brain material due to the brain material's compressibility. This compression occurs in the lower posterior region a short time after peak acceleration, and the compression and high strains in this region are related to the modeling of brain stem egression discussed above. Another interesting physical response is shown in Figure 10 which suggests some bending and/or twist occurring in the region occupied by the falx anatomic partition. The upper illustration of Figure 10 is a vertical slice through the mid-brain location and the lower illustration is from a superior-posterior viewing position.

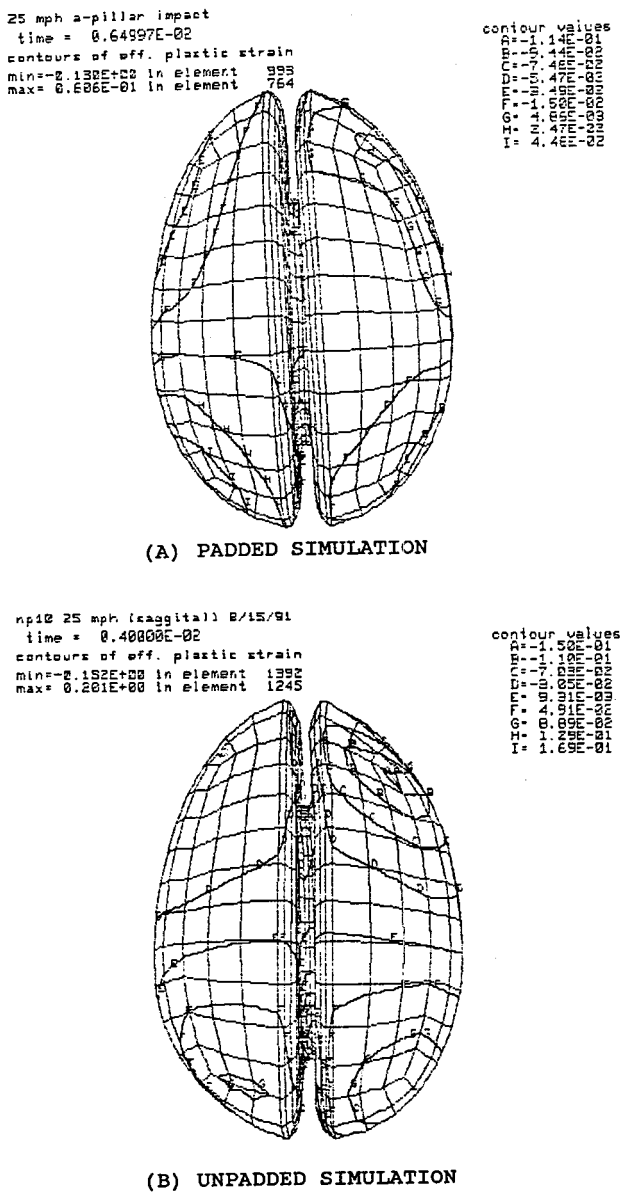

Figure 8. Strain Contour Illustrating High Strain Regions

Concluding Remarks

The above described simulations have provided first estimates of strains induced in the soft cortical tissue of the brain in response to impacts with padded and unpadded A-pillars which include generalized translational and rotational kinematic excitation. Comparison of estimated centroidal accelerations with laboratory data indicates that the dynamic loading applied in these simulations is representative of the automobile collision environment. The above results also indicate that soft tissue strains and strain rates are substantially reduced with the addition of padding, and that significant strains can develop after peak centroidal accelerations have occurred.

Although the anatomic brain model described herein includes many simplifying approximations and the brain is an enormously complicated structure, several important features have been included and the resulting strain data for these simulations suggests reductions in cortical strains and strain rates, and thus, brain injuries such as DAI may be provided by the addition of padding to A-pillars. The model is primarily intended for estimating strains in soft tissue and not for indicating brain injuries based on skull fracture. However, to evaluate directional loading effects through simulated impacts, additional work will be required in modeling the skull to provide representative mechanical behavior in various orientations.

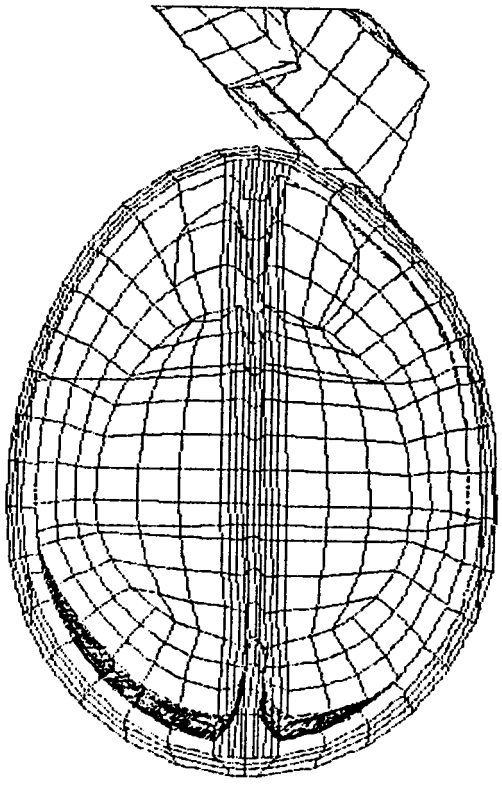

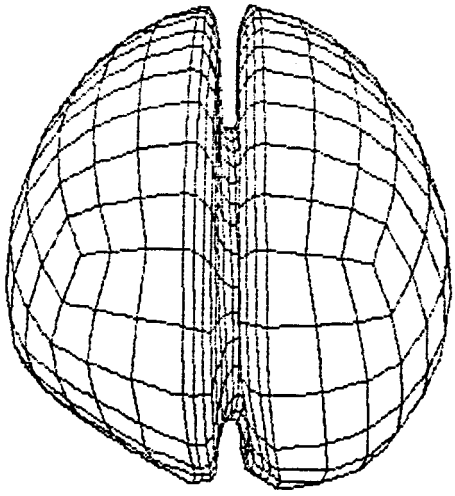

Figure 9. Compression of Cortex in Unpadded Simulation

Future modeling efforts will also include additional "real-geometry" features such as the cerebellum, tentorium cerebelli and details of the internal capsule and brain

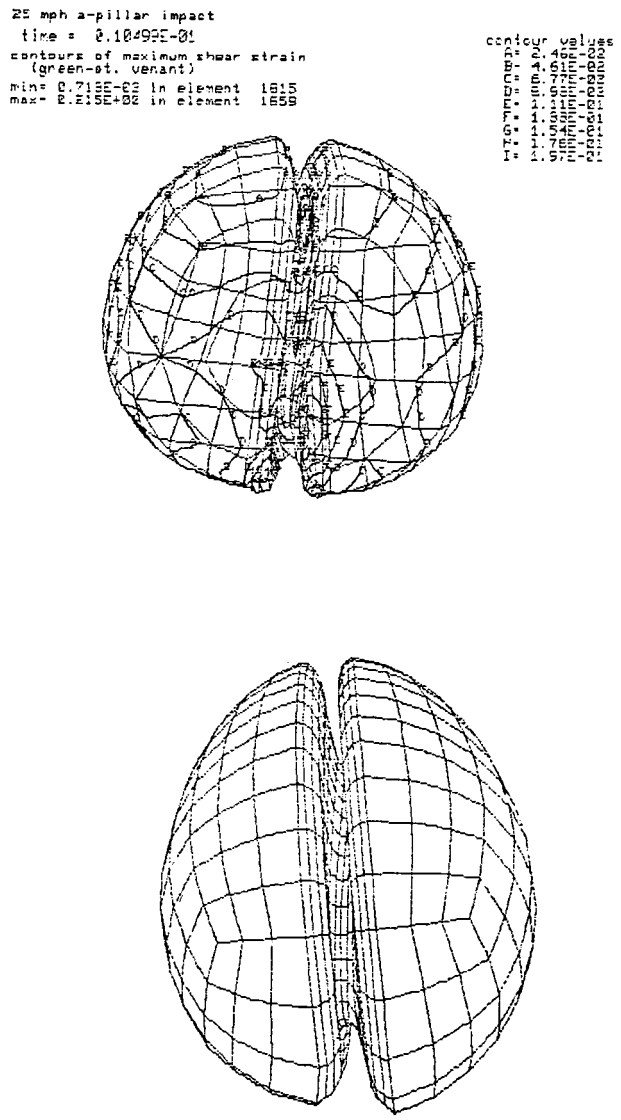

Figure 10. Bending and Twist of Falx in Padded Simulation

stem egression. Additional work will also be required to begin the process of relating strains predicted in various areas of the brain with neurological observations of impairment and dysfunction in humans for similar dynamic loadings, and to define damage tolerance criteria and limits for various soft tissues and/or fibers.

Many other complexities remain to be considered such as (a) the influence of the pia and arachnoid membranes and intervening cerebral spinal fluid on slip or traction along the perimeter of the cortex and adjacent to the falx anatomic partition, and (b) anisotropic effects associated with nerve fiber bundles comprising the corpus callosum and corona radiata. However, the inclusion of such effects awaits the development of more quantitative mechanical descriptions of these tissues and their interaction with surrounding tissues.

References

1. H.R. Lissner, M. Lebow, and F.G. Evans, "Experimental Studies on the Relation Between Acceleration and Intracranial Pressure Changes in Man," Surgery, Gynecology, and Obstetrics, Volume 113, 1960, pp. 329-338.
2. L. Thibault, T. Generelli, and S. Margolis, "Animal, Physical and Analytical Models for Use in the Development of Improved Head Injury Criteria," University of Pennsylvania, Department of Bioengineering and Department of Neurosurgery, DOT Report No. HS 807 481, Volume 1, March, 1989.
3. Susan S. Margolis, "Biomechanics of Traumatic Coma in the Primate," Doctoral Thesis, Department of Bioengineering, University of Pennsylvania, 1987.
4. D.W. Stillman, J.O. Hallquist, R. Rainsberger, Lawrence Livermore National Laboratory, "INGRID: A Three-Dimensional Mesh Generator for Modeling Nonlinear Systems," Revised July 1985, Report No. UCID-20506.
5. J. O. Hallquist, D.J. Benson, Lawrence Livermore National Laboratory, "DYNA3D User's Manual" (Non-Linear Dynamic Analysis of Structures in Three-Dimensions), Revised March 1986, Report No. UCID-19592.
6. B.E. Brown, J.O. Hallquist, R. Rainsberger, Lawrence Livermore National Laboratory, "TAURUS: An Interactive Post Processor For The Analysis Codes NIKE3D, DYNA3D, TACO3D, and GEMINI," Revised May 1984, Report No. UCID-19392.
7. M.W. Monk, L.K. Sullivan, NHTSA/Vehicle Research and Test Center, "Energy Absorption Material Selection For Head/A-pillar," Thirtieth Stapp Car Crash Conference Proceedings, San Diego, California, Oct 27-29, 1986, SAE P-189. (Paper Number 861887)
8. L. Thibault and T. Gennarelli, "Biomechanics of Craniocerebral Trauma." Central Nervous System Trauma Status Report, Edited by J.T. Povlishock. NINCDS, 1984.
9. R.A. Saul, M. Farson, D.A. Guenther "Development of a Component Level Head Impact Test Device," Thirtieth Stapp Car Crash Conference Proceedings, San Diego, California, Oct 27-29, 1986, SAE P-189. (Paper Number 861889).

S8-O-12

Dynamic Studies with Chest Contours

David Skrade, Narayan Yoganandan, Anthony Sances, Jr., John Reinartz, Frank Pintar

Medical College of Wisconsin

Abstract

The objective of the present study was twofold. First, to evaluate the External Peripheral Instrument for Deformation Measurement (EPIDM), and arrive at a methodology to be used in impact experiments. Second, was to conduct sled tests on an unembalmed human cadaver and a 50th percentile Hybrid III manikin to determine the thoracic deformation contours and, using these contours, to evaluate injury criteria such as normalized chest compression and viscous response. Initial evaluation of the EPIDM indicated the static drift over time to be minimal when the device is allowed an initial "warm up" time of 15 to 30 mts. The EPIDM methodology used in this study was based on three steps: (1) Prior to any testing, zero all gauges on a flat surface, (2) instrument the surrogate last before conducting the sled experiment, and (3) after the test, repeat the calibration procedure to ensure a proper working of all the gauges. A three-point belt restrained human cadaver and a Hybrid III manikin surrogate underwent sled tests at 48 kph velocities. These tests indicated that the EPIDM device can follow the dynamic thoracic deformations at impact. The deformation contours also permitted the computation of the following variables: Normalized compression histories, chest compressive velocities, as well as the viscous response (product of the normalized compression and the compressive velocity) characteristics. These studies suggest the potential of the EPIDM to derive injury criteria in an attempt to assess the crashworthiness of vehicular structures.

Introduction

The External Peripheral Instrument for Deformation Measurement (EPIDM) is a newly developed device which can monitor structural surface responses at predetermined locations. This device, also called the "chest band," is developed using the classical mechanics approach, i.e., describing the curve in terms of local curvature. The discrete local curvatures are computed by recording strains using strain gauges embedded appropriately in a non-frangible, steel band. Further data processing involves transformation of local curvatures over the entire surface into deformation contours. The operational theory, physical configuration, and initial tests on this EPIDM are reported elsewhere (6,7).

The EPIDM was developed to create surface deformation contours of the human surrogate thorax under simulated impact conditions. This device is noninvasive and maintains the structural integrity of the surrogate's body during impact. The purpose of the present paper is to examine the methodology which uses the EPIDM to

determine the thoracic surface contours of human surrogates. Details of the use of the EPIDM—e.g., initial calibration of the instruments, the temporal drift characteristics of the device, and the documentation of the temporal peak compressions from the computed contours—are reported. In addition, we also computed the displacement response characteristics of points on the surface of the surrogate's thorax using the deformation histories from the EPIDM.

Materials and Methods

Static Evaluation of EPIDM

The manufacturer of the EPIDM suggests four volts of excitation (Denton, Inc., Rochester Hills, MD, U.S.A.) to be used across each strain gauge bridge. In the laboratory, the EPIDM was used with three different voltages: 4V, 6V, and 10V. Six volts was selected arbitrarily, and the highest voltage represented the requirements of the data acquisition system used to collect data in our laboratory. To determine the amount of drift of the instrument under static conditions, the chest band was placed on a cylinder of 28 cm diameter (0.04167/cm curvature). The drift characteristics were recorded for 8 of the 16 gauges. Data were recorded at 5 to 20 minute intervals for a period of approximately 5 hours.

Following the drift tests, static calibration tests were conducted on all the 16 gauges. Eleven different curvatures (one flat surface and 10 cylinders with different diameters) were used with 4 volt and 10 volt excitation voltages. The EPIDM was tensioned slightly by hanging weights (22.2 N) at its ends so that the instrument follows the curvature of the cylinder (Figure 1). Data were collected for each strain gauge bridge and voltage versus curvature plots were constructed. Results were analyzed using linear regression analysis procedures. A protocol to be used in sled tests was developed from this data.

Deformation Contours with EPIDM

Using the methodology developed from the above tests, the EPIDM was used in simulated frontal impacts at 48 kph conducted with a deceleration horizontal sled. A 50th percentile Hybrid III anthropomorphic test device and an unembalmed human male cadaver (age 58 years, 178 cm overall height, 85 cm seated height, and 70 kg weight) underwent sled tests in a three-point belt restraint. Thoracic deformation contours were constructed from the chest band data on the two human surrogates. The human cadaver was selected based on medical history and radiography. It was also tested for the presence of antibodies to Human Immunodeficiency Virus and Hepatitis B before biomechanical testing. Even though the specimen was not infected, all precautions similar to that taken in a surgical environment were followed in the study. In addition, all precautions and guidelines suggested by the Centers for Disease Control, and others were followed during the test (3,4). Detailed

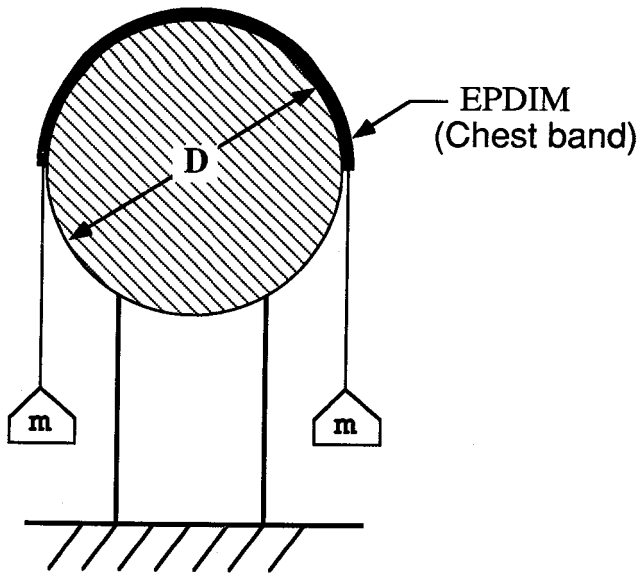

Figure 1. Diagram Illustrating the EPIDM Placed on a Cylinder of Known Diameter ("m" Denotes Hanging Weights)

anthropomorphic measurements according to the NHTSA guidelines were taken prior to test.

The cadaver was pressurized to approximate *in vivo* conditions. A balloon catheter was inserted into the femoral artery and inflated to prevent pressurization inferior to the abdominal region. A mixture of water and a thickening agent was pumped into the carotid artery to closely approximate the human vascular characteristics. In addition, the pulmonary system was pressurized prior to impact. All cadaver work, including radiography and pressurization, were done under the supervision of clinical personnel. The 50th percentile male Hybrid III manikin was used to compare its biodynamic response with the unembalmed human cadaver tissue. Two EPIDMs were placed at the mid-sternum region (approximately at the level of the fourth rib anteriorly) on the cadaver specimens, and at the level of rib 2 on the Hybrid III manikin (Figure 2). The deformation contours were computed by using the data from 24 channels of the EPIDM devices.

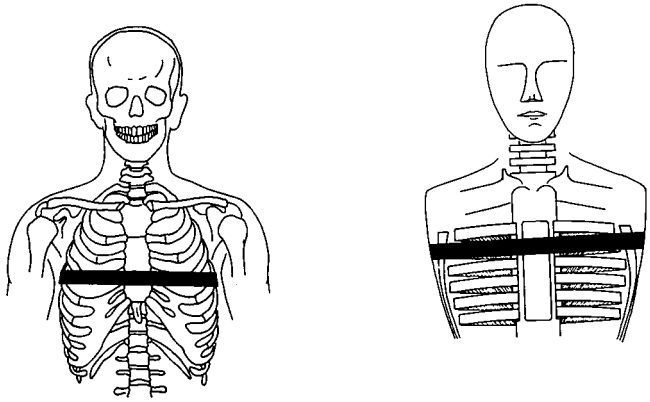

Figure 2. Placement of EPIDM on Human Cadaver (left) and Hybrid III Manikin (right)

All data were collected digitally with an Onboard Data Acquisition System (ODAS) according to SAE J211b specifications with a sampling rate of 12,500 Hz. Tension in the lap and shoulder belts, sled velocity, and acceleration data were gathered. Data processing included computation of the temporal thoracic deformation contours based on EPIDM signals (6,7). All data (EPIDM channels, from the internal potentiometer of the manikin, and seatbelt forces) were filtered at SAE class 1000. Sled acceleration data was filtered at SAE class 100. A second order digital two pass butterworth filter was used.

Deformation and Velocity Response Characteristics

Using the EPIDM data analysis routine, contours were computed at 1 ms intervals for the human cadaver and the Hybrid III manikin (Figure 3). An algorithm was developed to calculate chest compression along the anterior portion of the thorax. The following procedure was used to compute the viscous response. The software calculates the chest contours at every ms using the data from all of the EPIDM channels. In addition, the software has the ability to interpolate and provide deformations at discrete locations. Approximately 70 discrete points in the anterior region on each contour was selected and the deformation histories were examined at each of these points. At the particular discrete data point that resulted in the maximum chest compression, velocity of compression, and viscous responses were computed (9,10). The data from the Hybrid III internal chest potentiometer was also used to compute the velocity and viscous response according to previously suggested procedures (9,10). The viscous response was computed as the product of V and C, i.e. VC with C the chest compression normalized with respect to the surrogate chest depth. A chest depth of 229 mm was used for the Hybrid III manikin. The maximum value of the viscous response, i.e., $(VC)_{max}$ was noted.

Results

The voltage drift data as a function of time is illustrated in Figure 4. The greatest amount of drift occurs in the first 10 to 30 minutes, and then the instrument stabilizes, indicating that there is an initial "warm up" time for the instrument beyond which the drift is minimal. Furthermore, the pattern of drift did not have any particular bias with respect to any particular gauge or any particular voltage. The overall maximum drift for all the gauges, for all the three voltages, and at all intervals of time considered in this study, was within 1.2 percent. Consequently, the EPIDM protocol must allow for the initial stabilization process to take place in the instrument before it can be used to gather dynamic data. A linear relationship was found to exist between the curvature and voltage output of the strain gauges ($0.992 < R2 < 1.000$) for the two excitation voltages used in the study (Figure 5). Gradient of the plot indicates the gauge

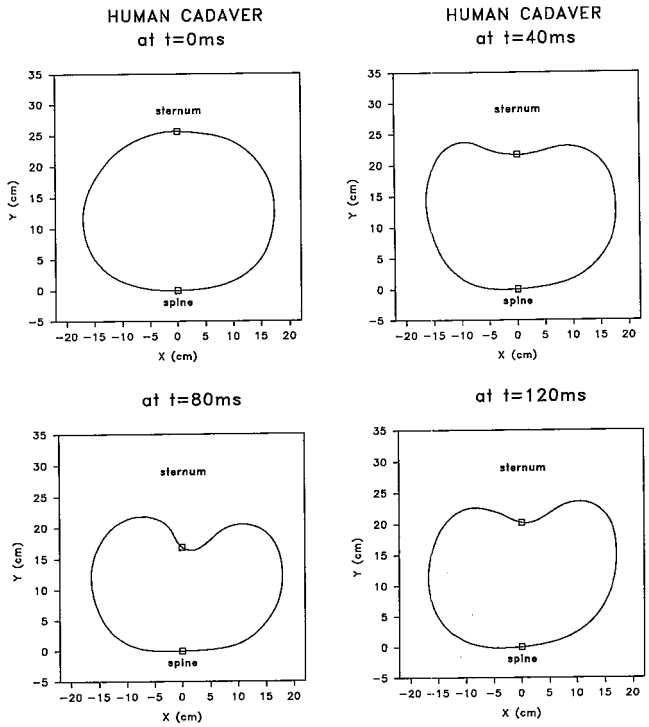

Figure 3. Thoracic Deformation Contours Computed from the EPIDM Data (Time Indicated on Each Contour: t=0, Undeformed State)

sensitivity. For a given curvature the output was high with 10 V of excitation in contrast to 4 V. The sensitivity per voltage of excitation, however, was not significantly different for 4 V or 10 V implying that either voltage can be used with EPIDM.

The pattern of chest deformation contours at the level of maximum deflection for the human cadaver and the Hybrid III manikin tests are depicted in Figures 6 and 7. The thoracic deformation contours are shown as viewed from head to toe, i.e., superior-inferior direction. The right side of the contour represents the right side of the human surrogate. Results for two pairs of representative tests are presented. The individual curvatures (and hence the deformations) recorded at discrete locations in the human cadaver and the Hybrid III manikin vary not only in magnitude, but also exhibit variations in the time domain. Therefore, comparison of the human cadaver with the Hybrid III manikin demonstrates regional differences in the deformation characteristics for these two tests. Bilateral rib fractures (R2-R11 on the right and R2-R5 on the left side) and a left clavicle fracture occurred in the human cadaver test. Flail chest did not occur. The specimen had a maximum AIS of 3 based on autopsy (1).

The EPIDM data computations resulted in normalized chest compressions of 0.38 for the human cadaver and 0.13 for the Hybrid III manikin. Peak chest compression velocities of 4.45 m/s and 2.32 m/s were obtained for the human cadaver and the Hybrid III manikin, respectively. In contrast, the internal sensor in the Hybrid manikin resulted in a peak compression velocity of 1.11 m/s. The

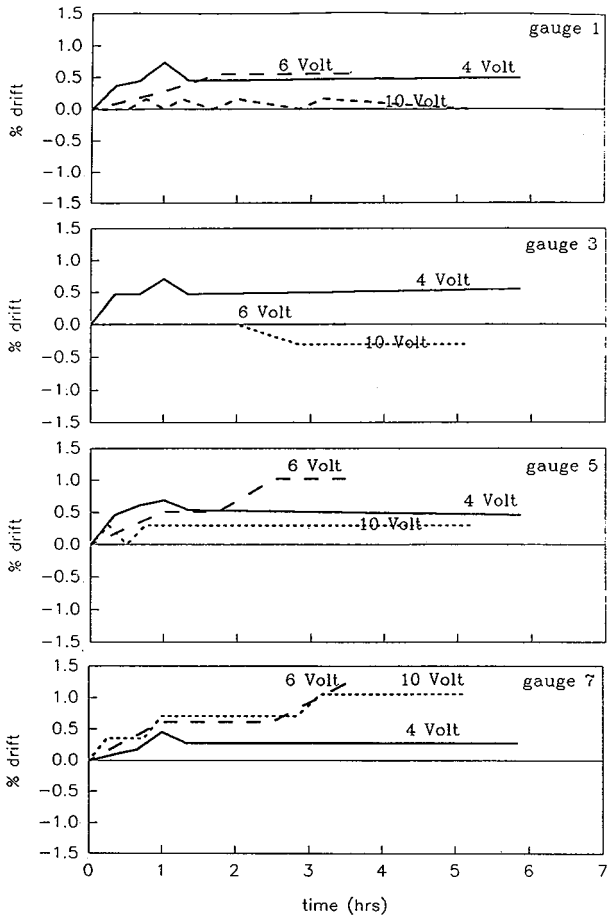

Figure 4a. Voltage Drift Variation in the Chest Band Strain Gauge Data (Gauges 1, 3, 5, 7) for Three Excitation Voltages

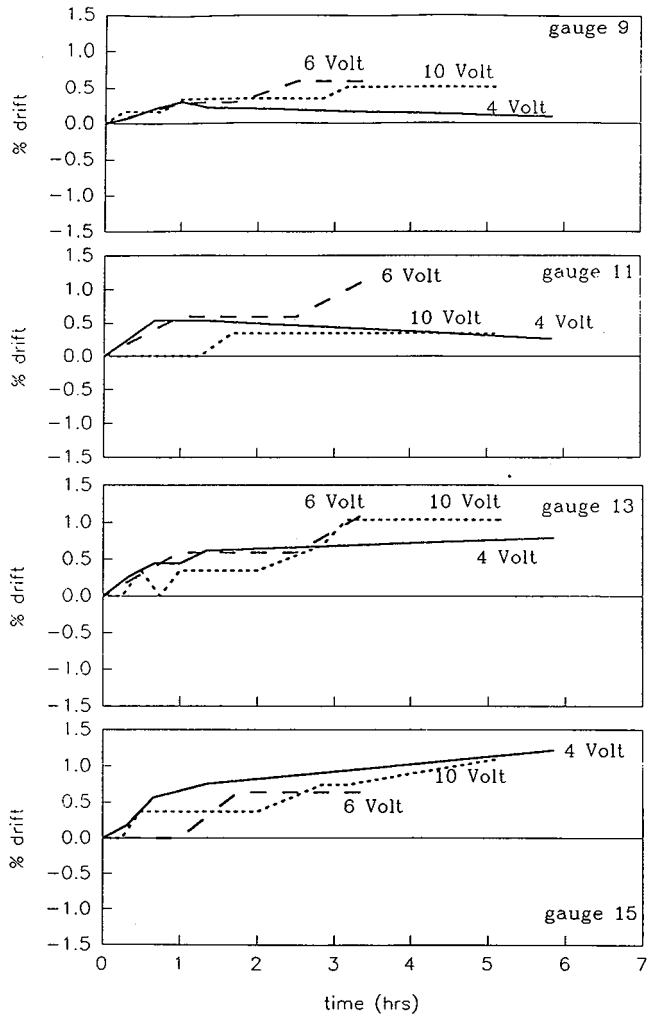

Figure 4b. Voltage Drift Variation in the Chest Band Strain Gauge Data (Gauges 9, 11, 13, 15) for Three Excitation Voltages

peak normalized chest compression computed using the sensor output agreed with the EPIDM data (Table 1). The viscous response (VC) computed as the product of the peak normalized chest compression and velocity, was 1.11 m/s for the human cadaver and 0.15 m/s for the manikin. A value of 0.09 m/s was obtained from the internal sensor data. A summary of these data is shown in Table 1. The normalized compression, chest velocity, and viscous response histories for the human cadaver and the Hybrid III manikin using the EPIDM are shown in Figures 8 and 9, respectively. Figure 10 illustrates the data obtained from the internal chest sensor of the manikin. In all cases, the peak chest velocity and peak viscous response preceded the occurrence of peak normalized chest compression.

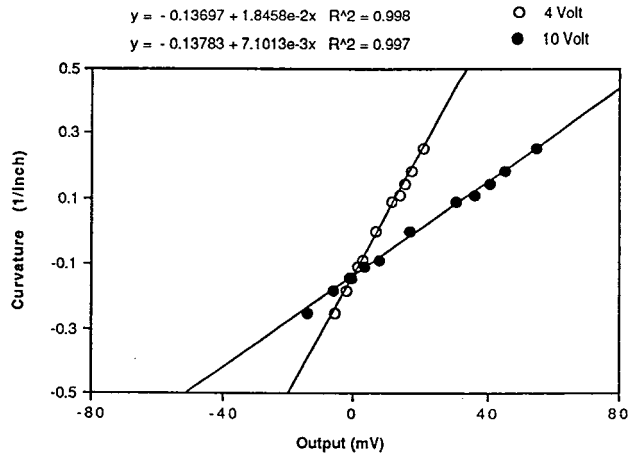

Figure 5. Linear Regression Plot Illustrating the Variation of Curvation with Output Voltage for Excitation Voltages of 4 V and 10 V for Strain Gauge #1 (Equations for Both Voltages Also Indicated in the Plot)

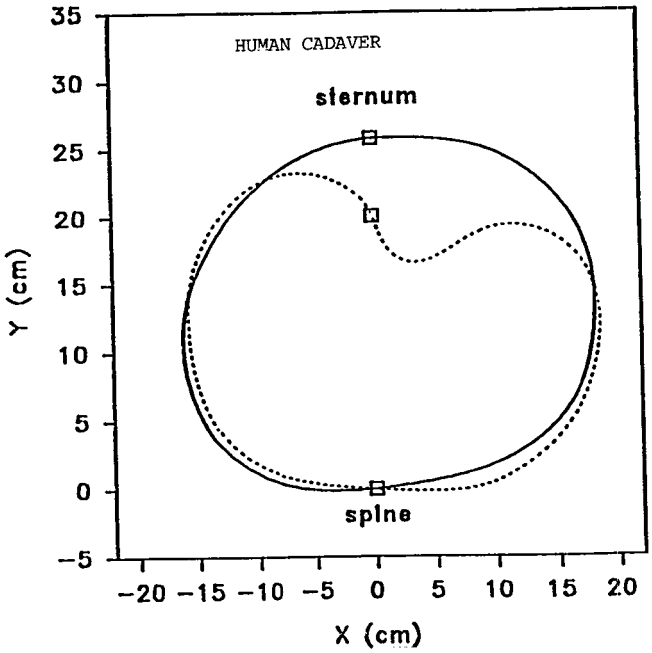

Figure 6. Thoracic Deformation Contours as Viewed from Head to Toe (Superior to Inferior Direction) (Solid lines, Initial Unloaded State; Dotted Lines, Deformed State)

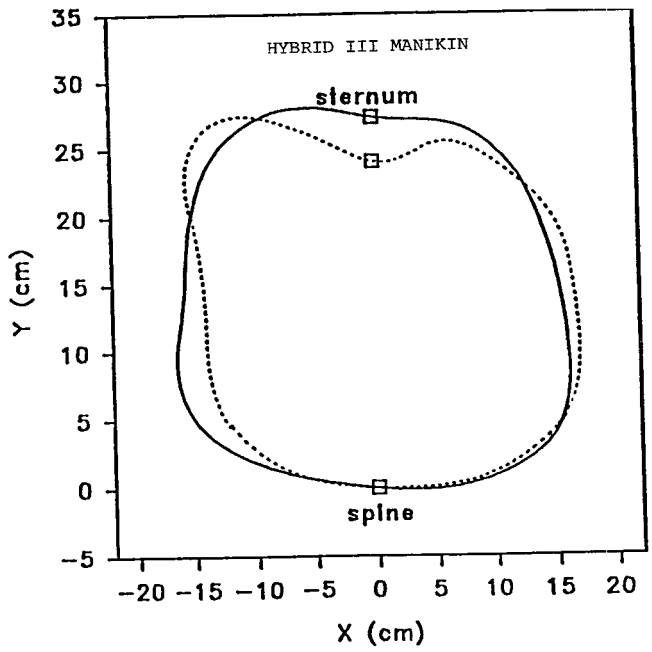

Figure 7. Thoracic Deformation Contours as Viewed from Head to Toe (Superior to Inferior Direction) (Solid Lines, Initial Unloaded State; Dotted Lines, Deformed State)

Table 1. Summary of Results

Specimen	EPIDM Data: Peak Normalized Compression	EPIDM Data: Peak Velocity (m/s)	EPIDM Data: VC (m/s)	Internal Sensor Data: Peak Normalized Compression	Internal Sensor Data: Peak Velocity (m/s)	Internal Sensor Data: VC (m/s)
Human Cadavers	0.38	4.45	1.11	--	--	--
Hybrid III Manikin	0.13	2.32	0.15	0.13	1.11	0.09

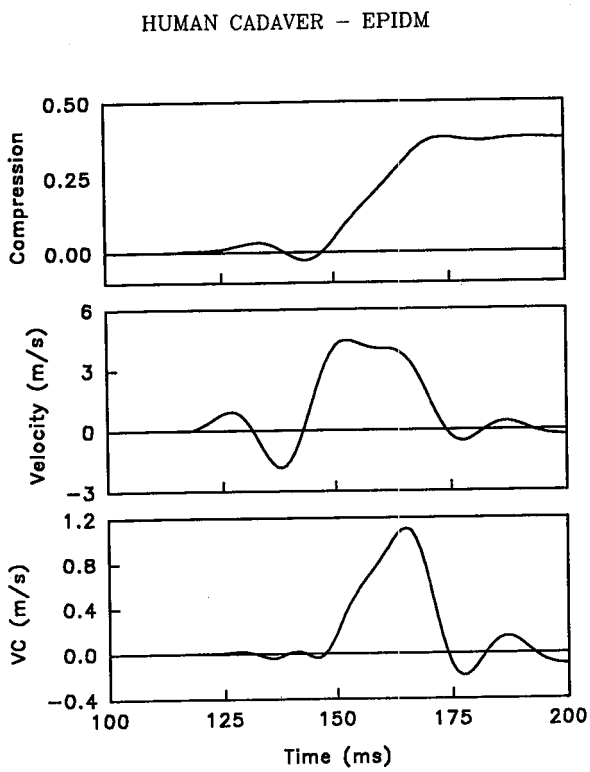

Figure 8. Normalized Compression (top), Chest Compressive Velocity (m/s) (middle), and VC (Viscous Response) (m/s) (bottom) Characteristics for the Human Cadaver Specimen (Data Obtained Using the EPIDM Device)

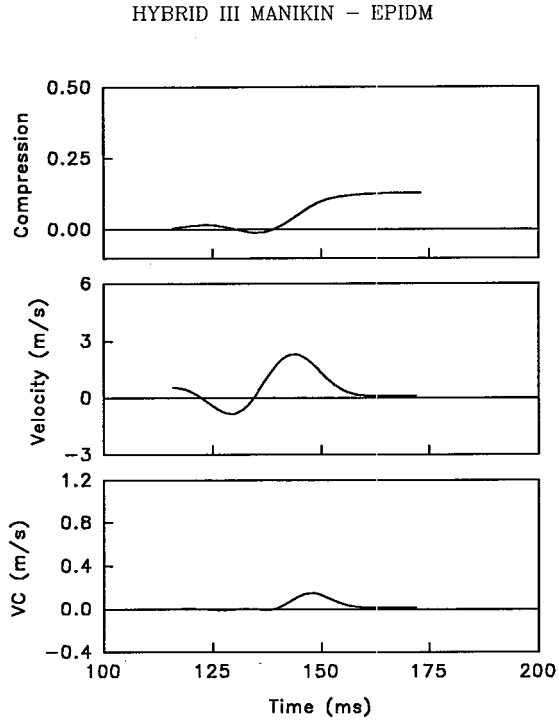

Figure 9. Normalized Compression (top), Chest Compressive Velocity (m/s) (middle), and VC (Viscous Response) (m/s) (bottom) Characteristics for the 50th Percentile Hybrid III Manikin (Data Obtained Using the EPIDM Device)

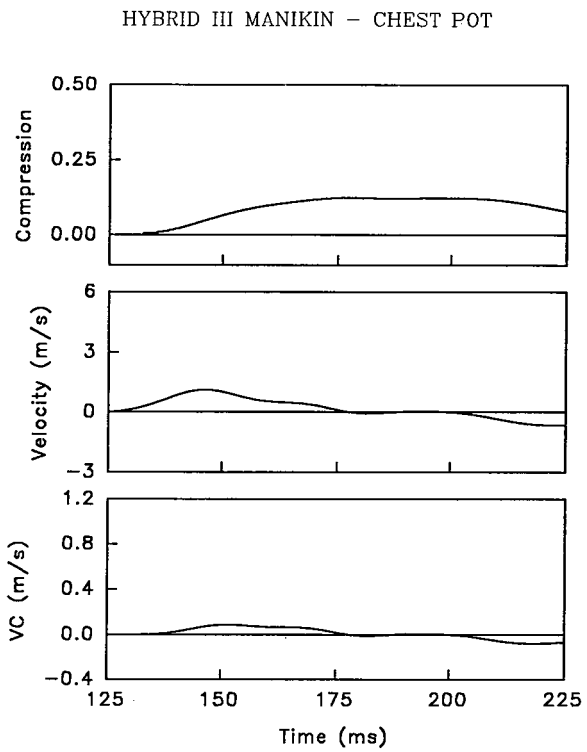

Figure 10. Normalized Compression (top), Chest Compressive Velocity (m/s) (middle), and VC (Viscous Response) (m/s) (bottom) Characteristics for the 50th Percentile Hybrid III Manikin (Data Obtained from the Internal Chest Potentiometer)

Discussion

The present study was undertaken to establish a methodology for using the EPIDM in sled impact studies. Initial experiments suggested the use of the following protocol for sled tests with the device. An excitation voltage of 10 V can be used instead of the 4 V excitation suggested by the manufacturer. The instrument needs an initial "warm up" time of 15 to 30 minutes before the voltage drift minimizes. It is suggested that one should zero all the gauges on a flat surface just prior to testing, and instrument the human surrogate last before conducting the sled test. As a precaution, following the dynamic test, one should repeat the static calibration procedures to ensure that the strain gauges in the EPIDM have not entered the plastic range.

The EPIDM was used to document the thoracic deformation contours for the two surrogates under frontal impact sled test conditions. The contours were computed from 24 channels of EPIDM. The overall similarities between the two surrogates—despite certain local differences—demonstrate the feasibility of using the device for calculating biomechanical variables. Although the original intent of the device was to obtain local surface chest deformations, in the present study, we explored the possibility of using temporal deformation contours to compute injury criteria such as the viscous response. To the best of our knowledge, no studies delineating the feasibility of using time varying surface chest deformations in sled tests to compute injury criteria have been reported. Because similar procedures were used to conduct both human cadaver and manikin tests under controlled laboratory conditions, comparison of secondary variables (such as viscous response) is appropriate. This data can also be used to assess the biofidelity of the manikin. It should, however, be noted that the objective of the present study was to illustrate—using a paired sample of one cadaver and one Hybrid III manikin—a procedure to compute the injury criterion. Results obtained from the tests should not be generalized to arrive at conclusions such as biofidelity of the Hybrid III thorax, applicability of the viscous criterion, etc. The apparent compatibility of the peak normalized chest compression and viscous response between the EPIDM and the internal sensor of the Hybrid III indicates that the potentiometer provides similar surface responses. In contrast, the observed differences in the chest compressive velocity between the sensor and the EPIDM may stem from the location of the two devices. The internal sensor responds subsequent to chest flesh compressions while the deformations by the EPIDM are recorded at the outer periphery. Deformation contours from the EPIDM are obtained by the interpolation of measured curvatures normal to the outside surface of the thorax, whereas, the data recorded by the internal potentiometer, connected to the sternum through a rod and slider mechanism, represent the skeletal deflections of the ribs. Compared to the manikin, human cadaver data indicated differences in the peak normalized chest compression, velocity, and viscous response (Table 1). Similar results have been reported in other studies (2,5,8,12). This may be due to the fact that the Hybrid III thorax is designed based on cadaver force-deflection response corridors due to blunt impact on the sternum at the fourth and fifth intercostal space. It should be noted that the manikin is nonfrangible, whereas, the occurrence of one or more rib fractures may accentuate changes in the local curvature/deformation in the human thorax. Consequently, it may also be appropriate to evaluate the biodynamic response of the cadaver tissue at sub-injury levels, and to compare with the Hybrid III manikin.

Conclusions

In this study, we have developed a methodology to conduct dynamic sled experiments with the EPIDM. Using a human male cadaver and a 50th percentile Hybrid III surrogate, we documented time-varying deformation histories of the thorax during impact. We have demonstrated the feasibility of using the EPIDM data to compute injury criteria such as viscous response characteristics. Due to the noninvasive nature of the device, as well as the practical feasibility to calculate the deformation histories at numerous locations on the surrogate chest, the EPIDM is potentially an important tool

for multidisciplinary teams interested in understanding the biodynamic response of the human thorax.

Acknowledgment

We respectfully acknowledge the assistance and support of Richard Morgan and Rolf Eppinger of NHTSA. This study was supported in part by DOT NHTSA Grant DTNH22-89-Z07305, PHS CDC Grant R499CCR703640, and Department of Veterans Affairs Medical Research Funds. All findings and views reported in this manuscript are based on the opinions of the authors and do not necessarily represent the consensus or views of the funding organizations.

References

1. *The Abbreviated Injury Scale,* 1990 Revision American Association for the Advancement of Automotive Medicine, IL, 1990.
2. Backaitis, S.H., St-Laurent, A., Chest deflection characteristics of volunteers and hybrid III dummies. *Proc 30th Stapp Car Crash Conf,* Society of Automotive Engineers, Warrendale, PA, 1986, pp 157-166.
3. Cavanaugh, J.M., King, A.I., Control of transmission of HIV and other bloodborne pathogens in biomechanical cadaver testing. *J Orthop Res* 8(2):159-166,1990.
4. CDC, Recommendations for prevention of HIV transmission in health-care settings. *MMWR* 36:3s-12s, 1987.
5. Cesari, D., Bouquet, R., Behaviour of human surrogates thorax under belt loading *Proc 34th Stapp Car Crash Conf,* Society of Automotive Engineers, Warrendale, PA, 1990, pp 73-81.
6. Eppinger, R.H., On the development of a deformation measurement system and its application toward developing mechanically based indices. *Proc 33rd Stapp Car Crash Conf,* Society of Automotive Engineers, Warrendale, PA, 1989, pp 21-28.
7. Hagedorn, A.V., Eppinger, R.H., Morgan, R.M., Pritz, H.B., Khaewpong, N., Application of a deformation measurement system to mechanical systems. *Proc 1991 Intl IRCOBI Conf,* Berlin, Germany, September 1991.
8. Katz, E., Groseh, L., Kassing, L., Chest compression response of a modified Hybrid III with different restraint systems. *Proc 31st Stapp Car Crash Conf,* Society of Automotive Engineers, Warrendale, PA, 1987, pp 246-249.
9. Lau, I.V., Viano, D.C., The viscous criterion—Bases and applications of an injury severity index for soft tissues. *Proc 30th Stapp Car Crash Conf,* Society of Automotive Engineers, Warrendale, PA, 1986, pp 123-142.
10. Viano, D.C., Lau, I.V., A viscous tolerance criterion for soft tissue injury assessment. *J Biomechanics* 21(5):387-399, 1988.
11. Yoganandan, N., Skrade, D., Pintar, F., Reinartz, J., Sances, A. Jr., Thoracic deformation contours in a frontal impact. *Proc 35th Stapp Car Crash Conf,* Society of Automotive Engineers, Warrendale, PA, 1991, (In Press).

S8-O-14

Crash Tests—One Element to Assess Passive Safety of Passenger Cars

A. Schmitz, B. Kraemer
TÜV Rheinland e.V., Institute of Traffic Safety

Abstract

To provide objective consumer information, concerning the interior safety of a passenger car, would give prospective car-buyers the chance of directly influencing road safety by selecting the safest cars. Several investigations have been carried out on this subject under different points of view. This paper will outline a first approach to a test method trying to assess the passive safety potential of passenger cars closely oriented to real-world accidents. The procedure should be suitable to point out deficiencies in vehicle safety design and to indicate methodical improvements in the passive safety performance. The results of several full scale impact tests are discussed referring to dummy response, structural behavior and safety performance of interior vehicle components. Furthermore additional component-tests are proposed which will be necessary to obtain an extensive assessment of the passive safety level of the tested vehicle.

Introduction

Considerable success has been achieved in the field of road safety to date as a result of various safety improvements. Despite the general increase in road traffic, the number of deaths in most countries decreased by about 30 to 50 percent from a maximum in the beginning seventies up to the year 1989 [1]. However, when one considers that there are about 50.000 road deaths in Europe each year, the price paid for mobility is still far too high. Approximately half of all fatalities are vehicle occupants.

There are many different reasons for the decrease in the number of road deaths, ranging from traffic-routing measures through driver training to automotive improvements. Up to now, however, it has been impossible to

perform isolated analyses of the decisive influencing factors for achieved safety goals due to the lack of practicable evaluation techniques. A common factor of all safety-improving parameters is that their effects only become apparent afterwards. Objective safety criteria on automotive safety improvements in particular, e.g. the design of deformation structures, are not available to prospective car-buyers today.

Valid EC Guidelines and ECE Regulations stipulate a number of statutory provisions and rules pertaining to the safety of vehicle occupants which must be observed and adhered to. In addition to existing technical codes and standards, various European draft regulations and proposals for discussion have been drawn up and should permit the integral evaluation of occupant protection in the future [2, 3]. In principle, however, only minimum requirements can be covered by statutory test methods for passive safety.

It has been estimated that a vehicle model designed solely on the statutory basis could not be successful on the market. On the other hand, passive safety still cannot be measured. It is a fact that the safety standards realized by vehicle manufacturers far surpass standardized test requirements. A retrospective consideration of the accident analysis leads to the conclusion that approximately 25% of all accident deaths and severe injuries could have been avoided if the persons involved in the accidents had used the safest vehicles available today [4].

Internationally discussed test and evaluation techniques for passive safety

- were introduced as proposals and are the subject of ongoing development
- still require a great variety of time-consuming adaptation processes
- and, finally, can only stipulate minimum standards.

However, road safety can be improved if comparable passive safety criteria are made available to prospective car-buyers. The results of opinion polls show that car-buyers now rank safety very highly [5]. On account of their greater safety-awareness, car-users have the chance to directly influence road safety by selecting the safest cars.

Test Method

The choice of a test configuration, suitable to assess the passive safety performance of passenger cars, should take into account that any test procedure can be representative for only a few real-world accident situations.

It should therefore be selected under consideration of the most frequent collision types and the severity of injuries sustained by the occupants. Various accident investigations have been carried out on this subject.

Assuming the fact that more than 50% of all car to car collisions are frontal impacts, Figure 1 [6] shows that only 21% of them occur with total overlapping of the involved cars frontal structures.

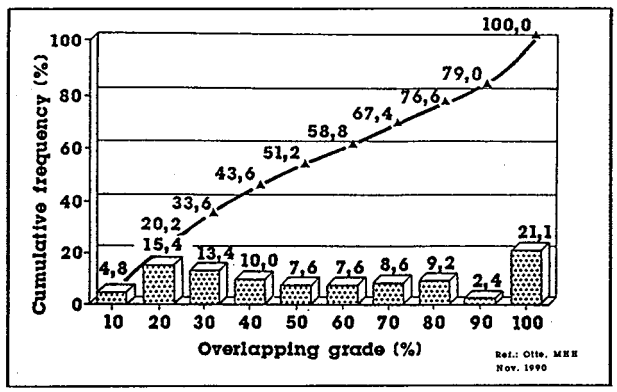

Figure 1. Overlapping Grades in Frontal Collisions

Far often a partial offset situation can be observed with overlapping grades up to 50%.

It was further established that for frontal collisions above a difference speed-level of 50 km/h the injury severity of the front seat occupants increases dramatically.

Derived from these observations, as a first step focussing on the frontal accident situation, the following laboratory test procedure is proposed:

- Frontal fixed barrier full-scale-crash test
- 50%-overlap on the driver's side, rigid impact block
- Impact speed 50 km/h.

Selection of Test Vehicles

The comparison of the obtained test data regarding passive safety characteristics is only acceptable for vehicles classified in the same mass category. Based on the actual European car fleet as a first estimation the following classification is proposed (according to unladen vehicle weight):

- Class 1 — < 800 kg
- Class 2 — 800-999 kg
- Class 3 — 1000-1199 kg
- Class 4 — 1200-1400 kg
- Class 5 — >1400 kg

To provide consumer information as early as possible after introduction of a new car model, the vehicles determined for an assessment test procedure should not be older than 6 months. Basic models should be chosen without optional equipment.

The above proposed test procedure has been carried out by T W Rheinland in three test series with a total of 24 vehicles.

For the investigation reported in the following 6 vehicles out of the class 2-category were selected with high sales figures on the German market in 1989/1990.

Test Conditions

Each of the tested vehicles was equipped with three instrumented 50th-percentile-Hybrid-II Dummies on the two front seats and on the left rear seating position, all belted with the standard restraints.

Vehicle preparation and dummy-positioning was performed according to the FMVSS 208 requirements.

The test weight was determined to be the unloaded vehicle weight plus the weight of dummies and instrumentation.

Dummy Measurements

Driver

- Head-, chest- and pelvis-accelerations
- Femur loads
- Lap and shoulder belt loads

Front passenger

- Head- and chest-accelerations

Rear seat passenger

- Head- and chest-accelerations
- Femur loads

Vehicle Measurements

- Impact speed
- Sill- and tunnel-accelerations
- Static deformation measurements

Film- and Photodocumentation

Each test was filmed with 7 high-speed-cameras from different positions. Still photos were taken before and after test covering all remarkable details.

Evaluation and Test Results

With the test results obtained it should be possible to assess how far the safety relevant structures of a passenger car are suitable to protect the occupants during an impact. Particular advantages and deficiencies should be pointed out and described for each tested vehicle.

From the measured and observed impact characteristics it was intended to establish a classification under consideration of the specific injury relevance of the single event.

For this purpose the following evaluation criteria were considered to be determinative:

- Structural Behavior
  - Front end deformation capability
  - Sill behavior
  - Roof behavior
  - Windscreen behavior
- Passenger compartment
  - Intrusion, longitudinal, lateral, vertical in different planes
  - Steering system behavior
  - Seat behavior
  - Behavior of the retention systems
  - Door opening behavior
  - Windows, glass
  - Danger of injury due to fracture/crack formation
  - Behavior of the control elements, pedals, switches, grips
- Occupant Loads
  - Head contact with parts of the passenger compartment
  - Head deceleration, biomechanical tolerance criteria HIC
  - Chest deceleration
  - Pelvis deceleration
  - Axial femur loads
  - Belt loads
  - Dynamic forward displacement of various parts of the body
  - Abdominal load as a result of submarining
- Other items
  - Battery behavior
  - Fuel system integrity
  - Loosening of parts
  - Rescue possibility

Structural Behavior and Passenger Compartment

Figure 2 gives an impression of the vehicles deformation characteristics when subjected to the proposed crash test, with an obvious effect of the offset impact configuration. After the maximum collapse of the vehicles front structures, the asymmetrical load causes further deformations of the left sill and roof area.

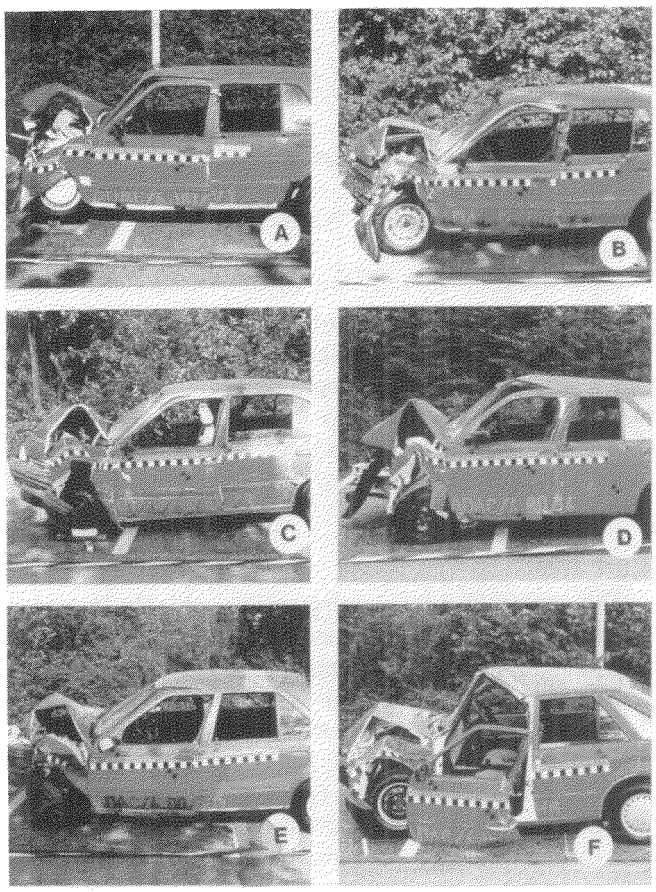

Figure 2. Deformation Characteristics

In 2 vehicles (D + F) the structure of the survical cell was not capable to withstand this loading, and buckling of a-pillar, roof side rail and left sill lead to great general intrusions into the driver side passenger compartment. Figures 3 and 4 show the maximum deformation values of the total vehicle and the a-pillar. The a-post displacement is causative for a problem concerning the occupant rescue possibility. After all doors of the tested vehicles remained closed during the test, the driver doors on the vehicles C, D and F were compressed afterwards between the hinges and the latch and could not be opened without the use of tools. In case of vehicle A both front doors were shifted behind the frontal edge of the rear doors and could only be opened after the rear doors were unlocked.

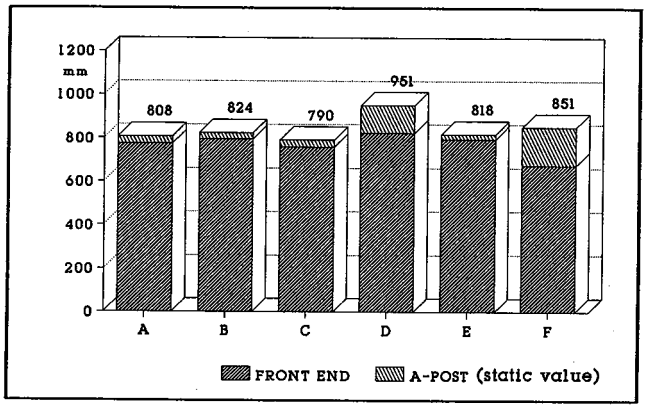

Figure 3. Dynamic Vehicle Deformation

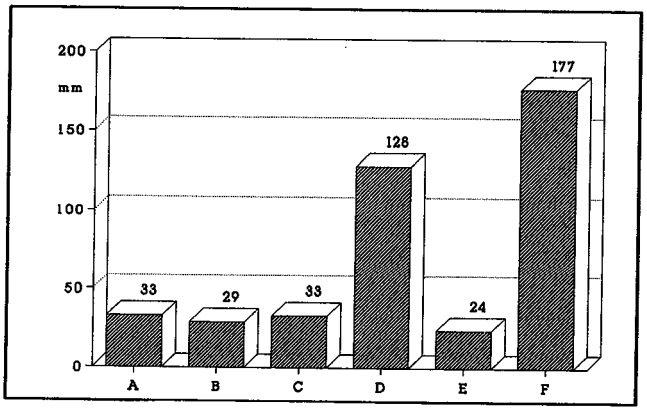

Figure 4. Left A-Post Displacement

Figure 5 shows the maximum static dashboard intrusion values. In vehicle A with a sufficient deformation behavior of the overall exterior passenger compartment it was observed, that the entire driver side instrument panel intruded into the survival cell. The high dashboard intrusion values of the vehicles D and F are due to the estimated general structural weakness.

Figure 6 shows the static horizontal steering wheel intrusions, also significantly high for the vehicles D and F. Additional steering column movement into the z-direction produces high relative head impact velocities on the steering wheel structure as it can be seen in figure 7. The impact speed was determined by evaluation of the high-speed-sequences up to the moment of head/steering wheel contact.

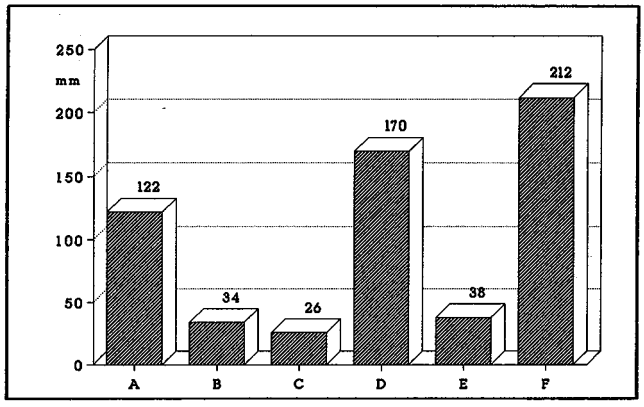

Figure 5. Dashboard Intrusion

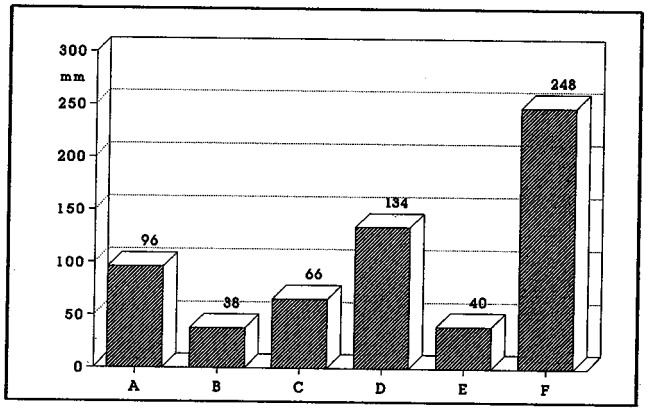

Figure 6. Horizontal Steering Wheel Intrusion

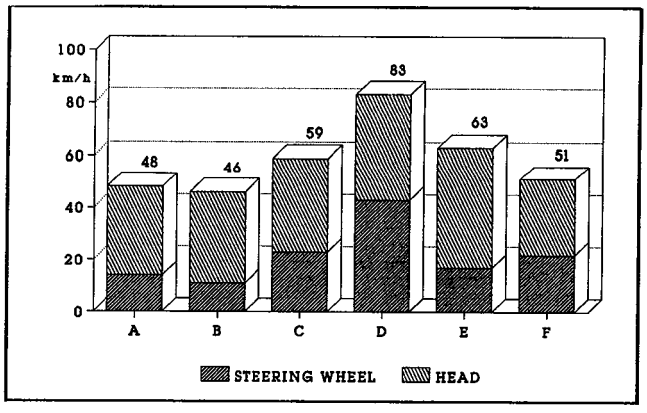

Figure 7. Relative Head Impact Velocity

Because of the frequency and severity of lower limb injuries observed in real accident situations which were suspected to be mainly due to lower facia contact and floor deformation, a footwell reduction value was established by calculating the footwell space on pedal level. The results are shown in Figure 8 also pointing out only poor deformation resistance for vehicle D and F.

Additional structural deficiencies could be observed for some vehicles which in real world accidents would

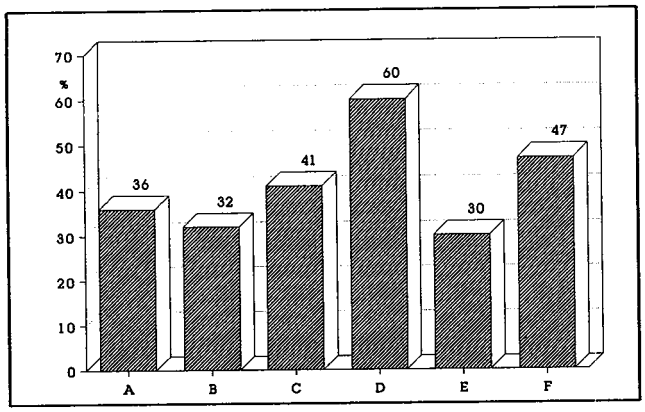

Figure 8. Footwell Reduction

be assumed to cause injuries to the occupants or at least to generate further risk potential:

- sharp-edged cracks in steering column covering, lower facia and center console (4 cars)
- sharp and rigid structures protruding in the knee impact zones (1 car)
- parts out of the panel region moving free in the passenger compartment (6 cars)
- insufficient windscreen retention (3 cars)
- downward deformation of the front seat structure, resulting in submarining of the occupants (1 car)
- opening of the glove box lid (1 car)
- cracks in the driver door panel (2 cars)
- forward downward deformation of the rear seat bench resulting in submarining of the occupants (4 cars)
- high head accelerations at the rear seated dummy from hitting the rigid unpadded rear sidewall structures during the rebound (4 cars)

Dummy Measurements

The reduction of survival space, due to the observed intrusions of steering wheel, dashboard and footwell, mainly endangers the driver, sitting closely to the impact area. The following discussion of the impact response is therefore focussed on the driver dummy. The measured values for front and rear passenger dummies are summarized in table 1.

Table 1. Head and Chest Values for the Front- (FSP) and Rear-Seated Passenger (RSP)

		A	B	C	D	E	F
HIC 36	FSP	196	443	244	149	287	467
	RSP	294	518	312	309	594	160
Head 3ms (g)	FSP	36	55	40	30	38	71
	RSP	44	93	42	52	56	31
Chest 3ms (g)	FSP	39	36	31	28	41	29
	RSP	35	37	33	24	35	26

Figure 9 shows the HIC 36 and 3ms-head acceleration values. No remarkable differences can be deducted in relation to the observed vehicle structural behavior. All values are fairly below the limits of biomechanical protection criteria.

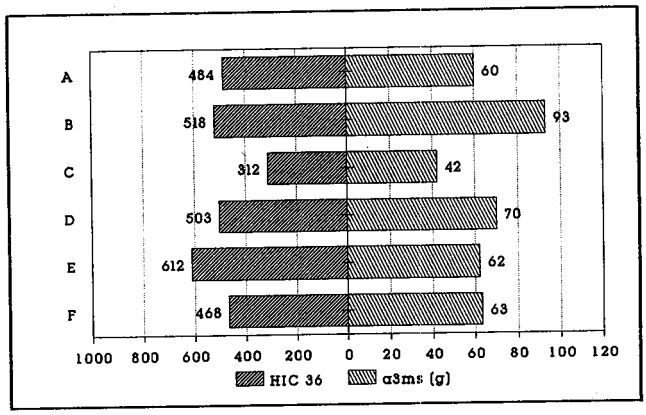

Figure 9. HIC 36 and Head Acceleration

Comparable outcome can be observed regarding chest and pelvis accelerations, presented in Figure 10. The comparatively higher values of the 3ms-pelvis acceleration for the vehicles A and B cannot be clearly related to vehicle deformation properties.

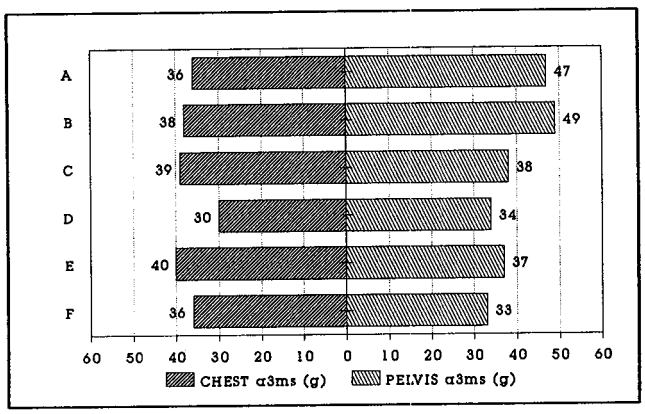

Figure 10. Chest and Pelvis Acceleration

The maximum longitudinal femur loads, shown in Figure 11, are higher for the driver's right knee but all below the tolerable threshold. This is considered to be due to the relative movement of the dummy to the left under the effect of the asymmetrical vehicle impact with the right knee suffering the first facia contact.

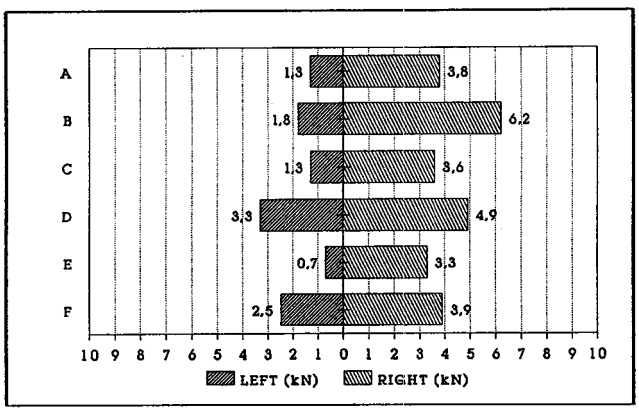

Figure 11. Femur Loads

Component Tests

To obtain a comprehensive assessment of the overall vehicle crashworthiness additional component tests are proposed.

Recent accident data have confirmed, that in frontal collisions the steering wheel is still an important injury relevant structure. Even for the restrained driver more than 50% of the head injuries are due to head contact with the steering wheel. Therefore in this paper the performance of additional component tests is focussed on the steering system.

As it could be derived from the full-scale-tests, due to the offset impact situation, the driver dummy's head trajectory was directed to the left, so that the head/ steering wheel impact occurred mainly on the steering wheel rim or in the left spoke/hub area.

This results generally in only slight glancing contacts with mostly moderate head acceleration values. So, even if the respective steering wheel does not offer sufficient energy absorption capability and the steering column shows inadequate intrusion properties, the calculated HIC values and the 3ms head acceleration level clearly cannot indicate this deficiencies.

If one considers, that in real-world accidents due to different impact situations, occupant size and out-of-position problems, many different impact points on the steering wheel are possible, the need of a separate component test to assess the steering wheel safety performance becomes obvious.

Figure 12 shows the results of two tests carried out in accordance to the energy-absorption test requirements adopted to the modified Council Directive 74/297/EEC [7] with two specimen (A+B) representative for serial type steering wheels which can be found on the market nowadays [8]. The steering wheels were mounted rigidly to a supporting structure and impacted on the central hub area. Major differences of the energy absorption capability are evident, indicating an important potential for optimization measures.

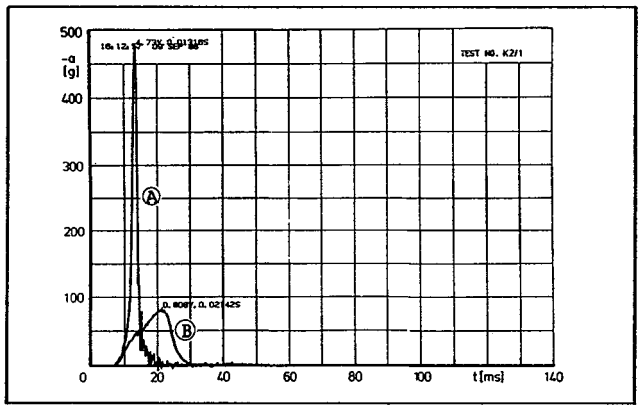

Figure 12. Steering Wheel Energy Absorption Capability

It should in addition be considered that the head impact velocities established during the vehicle crash tests, were more than 2 times higher than the required component test speed. To optimize a steering wheel structure only under consideration of the mandatory requirements could take the risk that the energy absorption quality would not be sufficient in a real world accident situation.

Furthermore it must be taken into account, that headform acceleration measurements during component tests, as well as dummy head acceleration recording in full-scale-test procedures, are not sufficient to indicate facial injuries due to high local pressures on the skin and bony structures. Several efforts have been made in the past developing procedures and instrumentation to provide detailed information about the pressure distribution over a dummy face and it should be further investigated if one of these proposals is suitable to be a tool for safety assessment.

Discussion and Conclusions

The proposed offset test procedure is suitable to identify specific advantages and deficiencies of the interior safety properties of passenger cars in case of a frontal impact situation.

The publication of the obtained findings is useful to provide differentiated consumer information to support the selection of a vehicle according to interior safety measures.

The problem of one-sided intrusion, which is often observed in real world accidents to be the main reason for severe injuries of the restrained front seat passengers can be covered with this test configuration.

The obtained dummy data must be evaluated under careful consideration of the reproducibility point of view, when carrying out only one single frontal test on each vehicle type. One information which variation range of dummy results due to scatter of test data and general repeatability characteristics of the procedure has to be taken into account, was given in [9], based on a test series with identical cars subjected to the same impact conditions.

The used 50% Hybrid-II dummies are representative of an only small average figure of car occupants in the real world accident scenario. Differences in body geometry, weight and constitution will lead to a widely varying impact response of a human being. Furthermore the Hybrid-II specific instrumentation only allows acceleration and force measurements. There is no sensitivity to indicate injuries due to high local pressure and/or penetration mechanisms.

In spite of ongoing investigations there is still a lack of objective, available information, concerning the determination of detailed causes of injury to occupants in car accidents. This data will be necessary to allow a linkage of construction and design features as well as of vehicle specific failure modes to the occurrence of specific patterns of injury.

On the background of the T.W. Rheinland experience with the application of the proposed test procedure it

seems therefore to be doubtful, whether any statements concerning the supposed injury severity a human being would have suffered in the specific vehicle during an equivalent accident, can be useful for consumer information purposes.

To obtain more detailed dummy results, for further projects the use of Hybrid-III dummies is proposed, equipped with additional instrumentation as there are for example available devices to measure neck loads and strain of the limbs. Existing techniques and proposals to determine pressure and penetration effects should be further developed and their applicability in the proposed test procedure should be examined.

The important problem of vehicle front- and side-structure-compatibility should also be taken into consideration in a suitable way. Optimization of a vehicle's front structure to ensure the highest possible level of protection to the occupants, may not lead to aggressive behavior in case of a car to car accident. One first step to solve this problem should be to provide data about the load distribution of the impacting structure.

For this purpose T W Rheinland intends to develop a segmented offset barrier to allow the registration of the impact load with an adequate degree of resolution. It must be further investigated, if this test method could be a sufficient tool to assess the compatibility features of a passenger car.

Outlook

With a frequency of more than 30 % the lateral collision is the second important accident configuration after the frontal impact. More than 20 % of all occupants subjected to a lateral impact suffer severe and fatal injuries.

To provide an extensive investigation of the passive safety qualities of a vehicle, it will be essential to adopt a dynamic side impact laboratory test to the assessment procedure.

Considering the different discussed side-impact test procedures [10, 11], from our point of view the proposed ECE-test configuration seems to be the best approach to the European traffic and accident situation and should be given preference.

Acknowledgements

The investigation described in this paper is based on a crash test series T W Rheinland carried out in 1990 by the order of ADAC. The results of these tests were made available by ADAC for further examination.

References

1. Brühning E.; von Fintel, K.-U., "Unfallgeschehen im internationalen Vergleich," Journal Internationales Verkehrswesen 40, Vol. 2, 1988.
2. Report of the ad hoc group ERGA-PASSIVE SAFETY.
3. Economic Commission for Europe, Principal Working Party on Road Transport, Working Party on the Construction of Vehicles, GRSP 8th session
4. Tingvall, C., Folksam-Report, 1990.
5. Journal "Absatzwirtschaft" 19/90.
6. Otte, D.: "Comparison and Realism of Crash Simulation Tests and Real Accident Situations for the Biomechanical Movements in Car Collisions," 34th Stapp Car Crash Conference, Proceedings Nov. 1990.
7. Commission of the European Communities, Draft, Council Directive 74/297/EEC, March 1991.
8. Felten, G.; Scheele, P., "Ermittlung der Schutzwirkung beim Lenkradaufprall," TÜV Rheinland, IVS-Kolloquium "Unfallschutz der Fahrzeuginsassen in Europa," Dezember 1988
9. Faerber, E.: "Streuung von Schutzkriterien in kontrollierten Aufprallversuchen gegen die 30°-Barriere," Federal Highway Research Institute (BASt), Accident Research Division, FP 8267.
10. NHTSA, Federal Register, Department of Transportation, FMVSS 214.
11. ECE-Proposal, TRANS/SC1/WP 29/GRSP/R.48.

S8-W-15

Analysis Method for External Forces Acting on the Dummy

Koushi Kumagai, Fumio Matsuoka, Hiroyuki Takahashi
Toyota Motor Corporation

Abstract

This paper describes a development of system for analyzing the external forces acting on a dummy. During frontal crash testing, various external forces act on a dummy. The dummy injury is caused by these forces. The dummy injury will be reduced by minimizing the external forces. If the external forces acting on dummy can be measured, the cause of dummy injury will be determined, which will be led to the way to reduce the dummy injury. For this reason, it is very important to measure them. However, in the past it was very difficult to measure them. In order to measure them, the following were developed:

(1) several force transducers to mount on head, chest and pelvis were developed and added to a dummy; and
(2) a computer software was developed, which was capable of obtaining the external forces acting on the dummy segments solving the motion equation of segments respectively.

The system was developed for the Hybrid III anthropomorphic test dummy. Using the Toyota-developed system, the followings could be obtained; external forces acting on head, chest and pelvis, and influences of these forces on the dummy injury. As a result, the developed system has become one of the most useful tools for developing the safer restraint system at Toyota.

Introduction

Various forces act on a dummy during a crash test, which cause the dummy injury. Such forces can be divided into external forces generated by the contact between the dummy and the restraint system and/or a part/parts in the vehicle compartment, and internal forces that act in the dummy itself. It was suggested that not only former but also the latter affect the severity of injury [3].

Hence, if the individual forces acting on the dummy can be measured, the cause of such an injury can be determined, which will be led to the reduction of injury. In this regard, measurements of such forces are effective and vital for the development of safer vehicles. Analysis on the external forces, however, have been absent due to difficulties involved in the measurements.

It may be considered to measure all forces acting on a dummy By means of force transducers, but it is extremely difficult, if not impossible, to measure contact forces between the dummy and the vehicle interior parts, which accounts for the absence of such measurement in practice. A simpler method would be to measure the force that acts from the neck to the head of dummy alone by means of a transducer, and to estimate contact forces between the dummy and interior parts by motion equations [1].

The authors have developed a System to determine forces that act not only the head but also on the chest and pelvis of the dummy, based on the method [1] mentioned above. Details of the system will be described in the following.

Development of External Forces Measuring System

Motions of dummies during front crash tests are two-dimensional in most cases, therefore, two-dimensional motions are assumed here.

A dummy is divided into three segments here—the head, chest and pelvis. Forces that act on the head, chest and pelvis consist of those that act among the three segments and those generated by direct contacts between the dummy and vehicle interior parts. For the measurement of the internal forces, transducers of a new type were developed and embedded into the dummy. Although similar transducers were available on market [4], it was decided to develop the new transducers, since the commercially available transducers had problems in mass and installation ease. For the external forces generated by the direct contacts between the dummy and vehicle interior parts, on the other hand, some other determination method was considered as described in the following, since such forces could not be measured by the transducers.

Method to Estimate External Forces

External forces are determined here by the expansion of the method to estimate the external force acting on the head [1]. Assuming a rigid model with several external forces acting on it as shown in Figure 1, a Newton's equation of motion can be established as expressed by Equation (1).

$$m_i A_i = \Sigma F_{ik} + \Sigma F_{ime} \quad (1)$$

Solving Equation (1) for ΣF_{ime}, Equation (2) is derived:

$$\Sigma F_{ime} = m_1 A_1 - \Sigma F_{1k} \quad (2)$$

By measuring each term on the right side of Equation (2), the resultant force ΣF_{ime} of unknown external forces can be obtained.

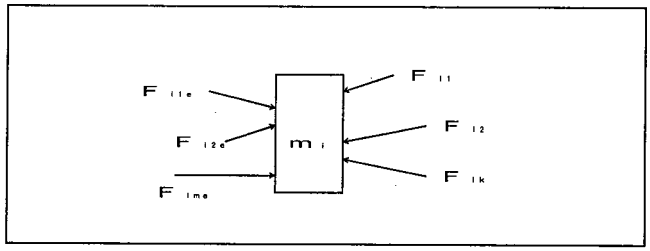

Figure 1. Mathematical Model

Development of Head Measuring System

The system is capable of measuring the force acting on the segment between the head and neck. but not capable of measuring other forces, such as the air bag reaction force caused by the contact between the air bag and the head , and the steering wheel reaction force due to the contact between the steering wheel and the head. The three-axial transducer of Hybrid III Dummy is used in the original form for the measurement of the force in the segment between the head and neck.

Development of Chest Measuring System

The system is capable of measuring the force acting on the segment between the chest and neck, and the force acting on the segment between the chest and pelvis, but not capable of measuring other forces such as reaction forces of the air bag, seat belt. and steering wheel as well as the external force acting from arms to the chest. An upper thoracic spine transducer was developed and installed above the thoracic spine of the dummy for the measurement of the force acting on the segment between the chest and the neck. and a lower thoracic spine transducer was also developed and installed below the thoracic spine for the measurement of the force acting on the segment between the chest and the lumbar spine.

Relative location of the transducer are as shown in Figure 2. The number of measuring items for the transducers is minimized, and their sizes and weight are also made as small/light as possible. High tensile aluminum alloy is used as the main material of fitting brackets so that the chest mass and other physical characteristic values would not change significantly By the crash test. The transducers are so made that they can be easily installed By boring holes through the thoracic spine of the dummy.

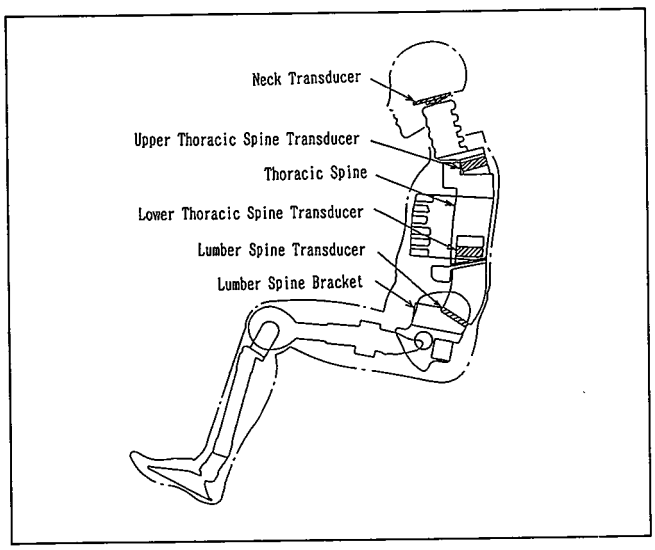

Figure 2. Instrumentation System

Development of Pelvis Measuring System

The system is capable of measuring the force acting on the segment between the lumbar spine and pelvis, but not capable of measuring other forces such as the external force acting from the seat belt to the pelvis. A lumbar Spine bracket and a lumbar spine transducer to be installed on top of the bracket are developed for the measurement of the force acting on the segment between the lumbar spine and the pelvis. Their relative locations are as shown in Figure 2. The transducer is so made that it can be installed easily without modifying the dummy.

Development of Computer Program

A computer program is developed for the analysis of measured data. Figure 3 shows the program flow chart.

Accuracy of Calculated Data

Head and chest impact tests were carried out for the verification of accuracy in results of analysis, by colliding impactors against the head and the chest of the dummy respectively. The external forces measured by the impactors and the values calculated by the developed computer program were compared, and the accuracy in the calculated values was verified.

Verified Results of Head Impact Force

The accuracy verification test for the head impact force was done by fixing the segment above the neck of the dummy to test board, and colliding the impactor

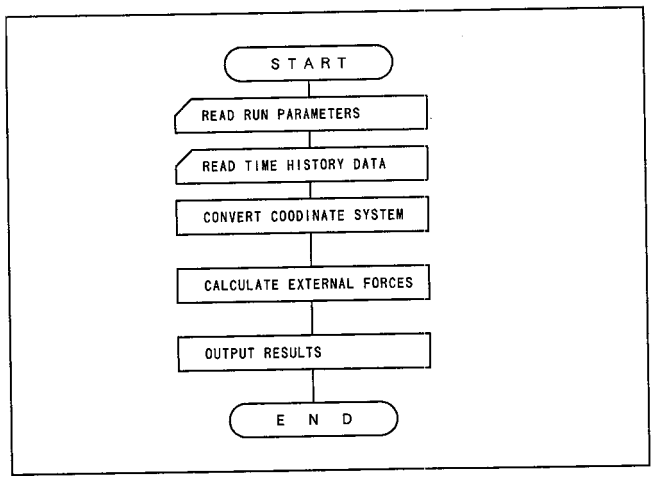

Figure 3. Flow of Analysis

against the forehead. The diameter and mass of the impactor were 76.2mm and 5kg, respectively. An accelerometer was adhered to the rear surface of the impacted surface, in order to calculate the impact load and the displacement. The impact Speed was set at 3m/sec. The results are shown in Figure 4, which verify extremely high accuracy of the calculated results.

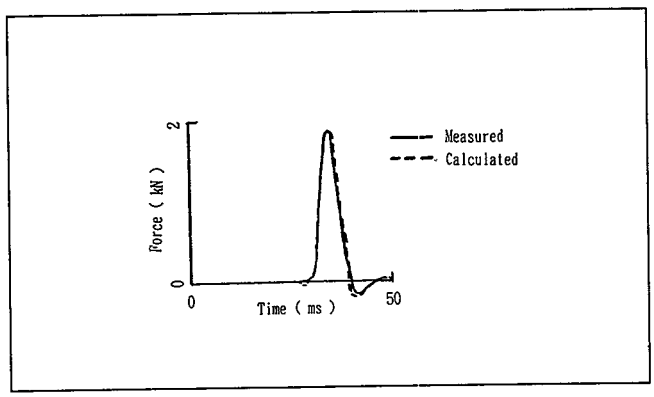

Figure 4. Comparison Between Measured Results (Solid Line) and Calculated Results (Dashed Line) of Head Impact Force

Verified Results of Chest Impact Force

The verification test for the chest impact force was done by colliding an impactor against the chest of the dummy in seated position. Arms of the dummy had been removed in advance, in order to exclude the external force that would act from the arms to the chest but could not be measured. The shape and the impact method of the impactor were the same as those of the dummy calibration test, while the impact speed was set at 4m/sec. The results are as shown in Figure 5, with a fairly close correlationship between the measured and calculated results of the maximum values of the force, but the calculated rise of the force lags behind that of the measured rise.

Application to HYGE Sled Test

The newly developed systems described in the foregoing were applied to the HYGE Sled test, with the

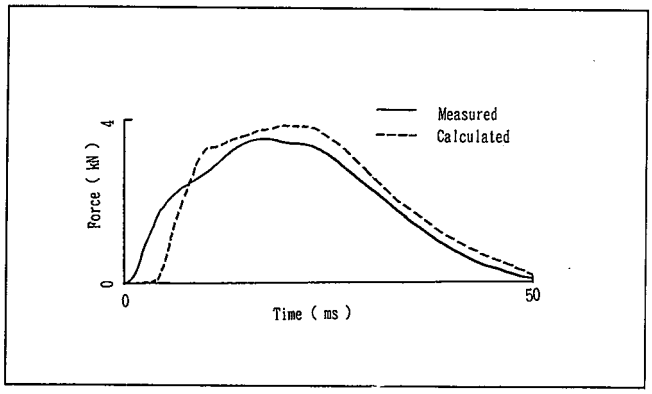

Figure 5. Comparison Between Measured Results (Solid Line) and Calculated Results(Dashed Line) of Chest Impact Force

air bag for the passenger seat installed. The test was carried out at the Speed of 30 mph. Figure 6 shows the results, with the contribution of the x-translational acceleration of the chest shown separately by each input path, which can be obtained by dividing values on both sides of Equation (1) by the mass of the chest. The solid line represents the chest x-translational acceleration. The conventional dummy measurement method is capable of obtaining this solid line alone. In reality, however, external forces acting on individual segments of the head, chest and the pelvis of the dummy account for about half of effects on the chest acceleration. It is hence deduced that about half of the chest acceleration does not have anything to do with the external forces acting directly to the chest.

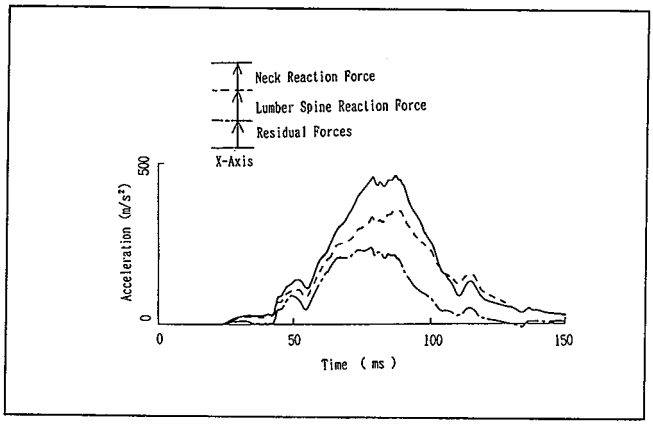

Figure 6. Effects of External Forces Acting on Chest for X-Translational Acceleration of Chest

Discussion

The reason for the delay in the rise of external force found by the chest impact verification test was the deformation of rib of the dummy occurred immediately after the collision of the impactor against the chest, which resulted in the relative displacement between the dummy rib front end (contacted with the impactor) and the thoracic spine where the acceleration was measured. The delay, however, does not exhibit a problem in practice, since the determination of the cause for the maximum injury value is the key issue in vehicle development.

In the HYGE sled test done on the passenger seat air bag, about half of the chest acceleration was attributable to the forces acting on the chest from the head and pelvis. In other words, effects of the external forces generated by the direct contact between the chest and vehicle interior parts account for only half of the chest acceleration, which means that such forces do not necessarily dominate the chest acceleration. Therefore, separate measurements of the forces acting on the chest by the direct contact and the forces acting among individual segments of the dummy (internal forces of dummy) are necessary to determine the cause of the chest acceleration, which is one of chest injury factors. In this regard, it is verified that the system developed under this study is effective because of the capability to determine such forces.

Conclusions

1. The development of the system, capable of determining external forces acting on the head, chest and pelvis of the dummy, has resulted in the creation of a useful tool for the determination of injury incidence mechanism.
2. Causes for the chest acceleration, which is one of chest injury factors, are determined by the application of this system to the HYGE sled test. It is thus verified that the system developed under this study is effective.

Acknowledgement

Appreciation is extended to staff of Kyowa Electric Company for the design and manufacture of the transducers.

References

1. David C. Viano, John W. Melvin, et al "Measurement of Head Dynamics and Facial Contact Forces In the Hybrid III Dummy," SAE Paper 861891.
2. John W. Melvin, T. Rex Shee, "Facial Injury Assessment Techniques." 12th International Technical Conference on E.S.V.
3. Hideo Takeda, Saburo Kobayashi, "Optimizing Knee Restraint Characteristics for Improved Air Bag System Performance of a Small Car" 9th International Technical Conference on E.S.V.
4. Robert A. Denton, Craig R. Morgan, "An Overview of Existing Sensors for the Hybrid III Anthropomorphic Dummy." 11th International Technical Conference on E.S.V.

S8-W-16

Brain Tolerance in the Frequency Field

R. Willinger, D. Césari
INRETS-LCB
C.M. Kopp
IMFS

Abstract

A recent study showed that, in case of impact, the brain followed the skull motion up to 200 Hz and was motionless over this frequency. A new mass-spring model which differentiated the brain mass from the other head components has been proposed. In the study presented in this paper, this model was used to calculate the skull to brain velocity ratios. This velocity ratio varied with frequency which showed a critical area ranging from 100 to 200 Hz. This result led us to analyze the tolerance curves given in the literature, in the frequency field. Expressing the total energy and energy ranging from 0 to 100 Hz for limit impacts, as a function of their spectrum maximal frequency, showed different injury mechanisms considered by various authors. This study yielded the first elements of a tolerance curve in the frequency field and for specific injuries.

Introduction

In this study, an attempt was made to better understand the injury mechanisms involved in case of cranial traumatisms. This research found applications in the development of test dummies used in vehicle or helmet approval tests. Various injury mechanisms are proposed in the literature from shock wave propagation to intracerebral shearing through the relative displacement between the brain and the skull or the different bone plates forming the skull.

No attempt to select one of these different mechanisms rather than another one has been made, we just tried to understand in which conditions or for which impact type a mechanism occurred rather than another one. Head kinematics under blow conditions led us to pay specific attention to possible analogies that might occur between head sudden translation and sudden rotation.

This research started from a previous study (Willinger et al., 1990) which enabled us to better understand the head dynamic behavior through a vibration analysis and during which the principle of a new head mathematical modeling has been adopted. This model was developed according to the Kirschoff laws and the results were related to brain matter dynamic mechanical properties.

Then experimental and theoretical studies led us to analyze in the frequency field, the curves of human tolerance to blows proposed in the literature. On the basis of energy contained in the acceleration signal, injury mechanisms and associated tolerance limits have been determined as a function of the maximum frequency included in the shock spectrum. The obvious analogy between sudden translations and rotations has also been demonstrated.

Head Dynamic Behavior

Modeling

The lumped model was aimed at describing the head dynamic behavior in case of sudden translation with or without impact. It was based on the head vibration analysis performed in a previous study. The mechanical impedance of physical models (box + bovin brain + water), and of in vitro and in vivo heads were then recorded using a striker and an accelerometer.

These experiments allowed the record of head natural frequency ranging from 400 to 600 Hz and showed a first natural frequency at about 100 Hz (Figures 1 and 2). Modal parameters relating to this natural frequency indicated the brain mass resonance with respect to the rest of the head. Thus a relative motion between the brain and the skull beyond a frequency of the order of 100 Hz was observed.

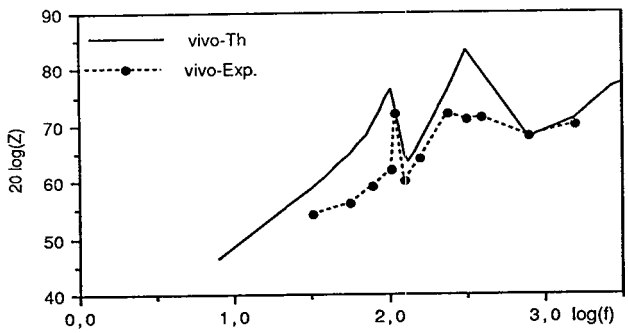

Figure 1. In Vivo Head Mechanical Impedance

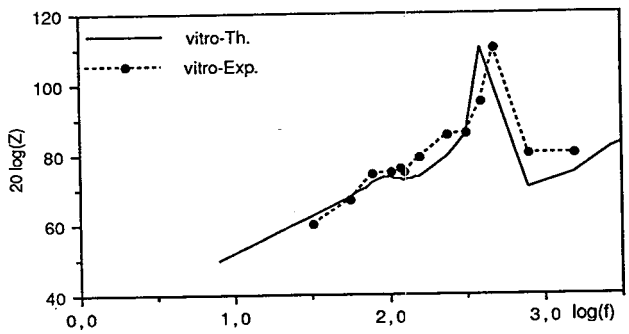

Figure 2. In Vitro Head Mechanical Impedance

From these recordings, a new mass-spring model which differentiated the brain mass from the other head components was proposed (Figure 3). A first equation of the assumed non damped model was proposed to identify head modal parameters. The expression for non damped impedance is:

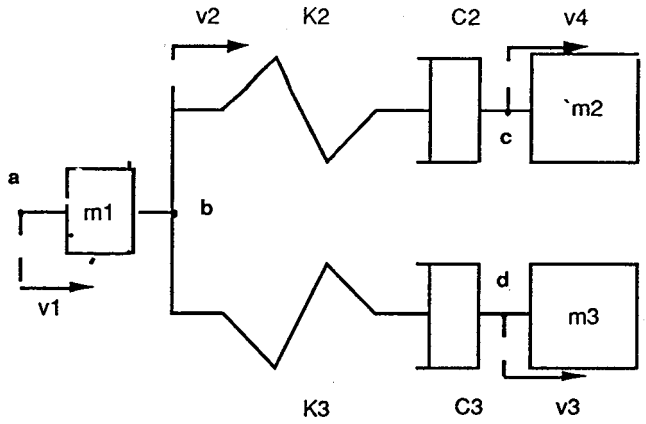

Figure 3. The Lumped Head Model

$$Z_n = j\omega \left(m_1 + \frac{K_2 m_2}{K_2 - \omega^2 m_2} + \frac{K_3 m_3}{K_3 - \omega^2 m_3}\right) \quad (1)$$

Stiffnesses and modal masses are given as a function of a_1, r_1, a_2 and r_2 read on the impedance curve and of mt, with respect to m_1, given by the curve position at low frequencies with respect to high frequencies. Damping was approximated from the logarithmic decrement at each of the two resonance frequencies. From Salter (1969), we have:

$$a_1 = \frac{1}{2\pi}\sqrt{\frac{K_2}{m_2}} \qquad a_2 = \frac{1}{2\pi}\sqrt{\frac{K_3}{m_3}} \quad (2), (3)$$

$$K_2 = (2\pi)^2 \frac{m_1 (r_1^2 - a_1^2)(r_2^2 - r_1^2)}{a_2^2 - a_1^2} \quad (4)$$

$$K_3 = (2\pi)^2 \frac{m_1 (a_2^2 - r_1^2)(r_2^2 - a_2^2)}{a_2^2 - a_1^2} \quad (5)$$

$$m_3 = \frac{K_3}{(2\pi a_2)^2} \qquad m_2 = m_t - m_3 - m_1 \quad (6), (7)$$

For heads in vitro and in vivo (Figures 1 and 2), calculations yielded the numerical values given in table 1.

Table 1. Model Parameters Identification

head	m1 kg	m2 kg	m3 kg	K2 N/m	K3 N/m	C2 Nm/s	C3 Nm/s
vivo	0.4	1.6	2.2	0.7E6	10E6	200	1500
vitro	0.8	1.7	3.6	0.7E6	25E6	600	70

The damped model equation allowed us to determine the brain to skull velocity ratio as well as its variations according to head excitation frequency. The damped model mechanical impedance is written:

$$Z = Z_1 + \frac{Z_2 Z_4}{Z_2 + Z_4} + \frac{Z_3 Z_5}{Z_3 + Z_5} \quad (8)$$

Kirschoff laws applied to points a, b, c, d and expressing the node equilibrium are written (Harris et al. 1988):

$$F - Z v_1 = 0 \quad (9)$$

$$(v_1 - v_2) Z_1 - (v_2 - v_3) Z_3 - (v_2 - v_3) Z_2 = 0 \quad (10)$$

$$(v_2 - v_4) Z_2 - v_4 Z_4 = 0 \quad (11)$$

$$(v_2 - v_3) Z_3 - v_3 Z_5 = 0 \quad (12)$$

When eliminating v_2 in equations (11) and (12), the v_3/v_4 ratio, i.e. the brain/skull velocity ratio can be expressed:

$$r(\omega) = \frac{v_3}{v_4} = \frac{Z_3 (Z_2 + Z_4)}{Z_2 (Z_3 + Z_5)} \quad (13)$$

Figure 4 shows the variations of this parameter as a function of excitation frequency. It can be observed that a relative velocity occurs at about 100 Hz and a change in the injury mechanism can be thus expected at these frequencies. When the impact energy is essentially located at low frequencies, stresses, strains and deformations are transmitted to the cerebral matter. When energy is concentrated at high frequencies, stresses are not transmitted any more and a skull-brain relative motion can be observed.

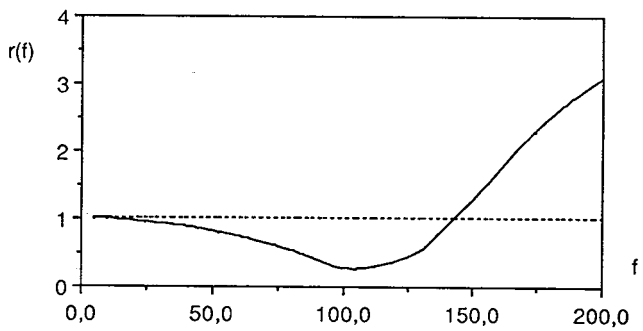

Figure 4. Skull-Brain Velocity Ratio as a Function of Excitation Frequency

Relative motion, even if the model provides a reliable description of the observations made, is certainly not due to the putting into motion of an undeformable solid fixed to the skull by springs. In real-world conditions, it is considered that brain "decoupling" is due to the dynamic mechanical properties of the cerebral matter. Indeed, owing to its complex receptance, the gel constituted by the brain matter does not transmit shearing stresses and behaves as a viscous fluid beyond 100-200 Hz.

Mechanical Properties of the Cerebral Matter

The assumption here above mentioned is confirmed by the Shuck and Advani study (1972), which gave the complex compliance of the cerebral matter under torsion-dependent shearing stresses. From the values obtained for real and imaginary parts, its modulus and phase have been calculated as a function of excitation frequency.

The result plotted in Figure 5 shows a "significant" receptance up to 60 Hz, a "mean" receptance between 60 and 200 Hz and a "low" receptance beyond 200 Hz. The phase changes corroborate what said above, as the phase is low at low frequencies and is close to 90° at high frequencies, which corresponds to an elastic solid behavior and then to a viscous fluid behavior following a viscoelastic phase between 60 and 200 Hz.

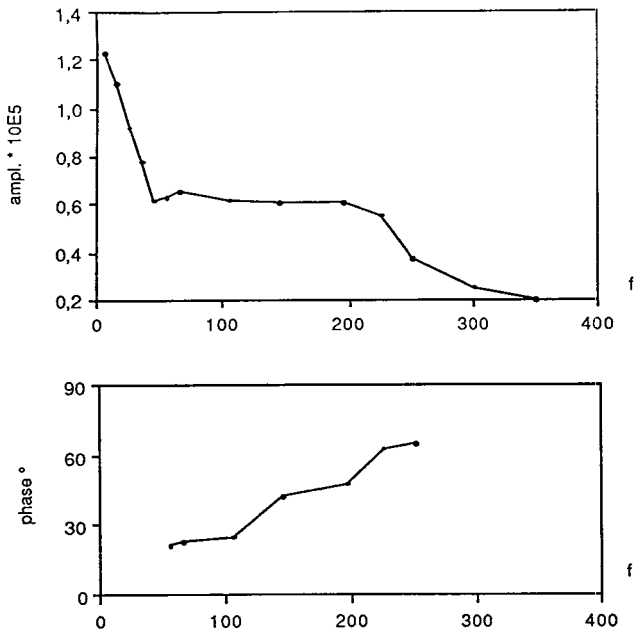

Figure 5. Complex Cerebral Receptance (Shuck 1972)

Shuck also noted that the behavior was linearly elastic at low frequencies only for angular strains under 3.5%. In the 60-200 Hz range, 1.3% angular strains already led to a brain irreversible mechanical behavior, and beyond 200 Hz, it was nearly impossible to cause strains generated by intracerebral shearing stresses.

Injury Mechanisms

The vibration approach of head behavior under blow conditions led us to suspect a change in injury mechanisms as a function of shock duration, therefore in spectrum-contained maximum frequency, i.e.:

- a mechanism implying shearing stresses and their related consequences, as well as angular strains when f_m maximum frequency was less than about 100 Hz. This mechanism results in diffuse brain injuries observed in "long-duration" impacts—for example an impact to a subject with a helmet or in case of sudden head rotation,
- a mechanism related to skull-brain relative motions in which impact energy is concentrated in the 100-800 Hz frequency range. This mechanism led to subdural hematomas and contusions or to hematomas located in the cortex periphery. It could typically be observed in case of so-called "hard" impacts, i.e. short-duration impacts.
- a mechanism for very short-duration impacts (less than 1 millisecond) or including very high frequencies (over 800 Hz) due to the propagation of a shock wave as also assumed by Kallieris et al. (1980). The model limits were thus reached and even when the r(ω) ratio presented very high values at high frequencies, low velocity amplitudes did not enable to give a physical significance to such a result.

This analysis led us to study brain tolerance curves in the frequency field. It is presented in the following section, but before presenting it, it seemed interesting to us to give the usually accepted distinction between the different injury mechanisms, based on the sudden head translation/rotation duality.

If for a sudden head rotation it is well established that shearing stresses lead to intracerebral injuries, the brain is assumed to be under compression in case of sudden translation. Under compression conditions, it should be noted that the complexity of the skull internal geometry, especially in the sagittal plane, ineluctably implies cerebral matter shearing stresses when the skull motion leads to the brain motion. In addition, even in areas subjected to a simple compression, significant shearing stresses can be observed in sections inclined at 45° with respect to the compression direction. This led to the conclusion that shearing is not an injury mechanism exclusively met in case of angular acceleration.

On the other hand, if experimental diffuse injuries are exclusively obtained with angular acceleration, this is essentially due to the shock duration which is too short to transmit stresses to the brain in case of linear impact. Owing to the head connection conditions, a long-duration rectilinear impact leads to a head rotation round cervical vertebras. In the same manner, a short-duration angular acceleration can be assimilated to the tangential acceleration it generates in first approximation as stresses are not transmitted to the brain. These observations are corroborated by the literature where no experiment of short-duration head rotation or long-duration rectilinear impact is reported.

We therefore propose to assimilate a linear acceleration X'' to an angular acceleration θ'' divided by the rotation motion radius of the order of 0.1 m, i.e:

$$\theta'' = 10X'' \qquad (14)$$

The validity of such an assumption is checked by a good superposition of rotation tolerance curves on translation tolerance curves by an approximate factor 10 (Figure 8). A factor 100 will be applied when energy contained in the input signal will be taken into account as this term includes the acceleration square.

Tolerance Curves in the Frequency Field

Observations and discussions of the 1st section encouraged us to introduce the notion of impact human tolerance into the frequency field. In general, frequency

analysis is well adapted to crash studies. In the present case, such an analysis can contribute to distinguish injury mechanisms as a function of input signal energy distribution in the frequency field.

To introduce this new approach, data found in the literature relative to cerebral tolerance in rotation as well as in translation have been used.

Data Origin and Processing

Tolerance curves in the time field conventionally express a limit acceleration (m s^{-2} or rd s^{-2}) as a function of shock duration. One of the first translation tolerance curves has been proposed by the Wayne State University (WSU) and was essentially based on experimentation (Figure 6). The tolerance curve in case of impact proposed by Stalnaker, relating to cerebral matter mean strain under compression (Mean Strain Criterium or msc (Stalnacker 1971) has been then considered. The curve given in Figure 6 gives a 0.6% allowable strain (McElhaney et al. 1976).

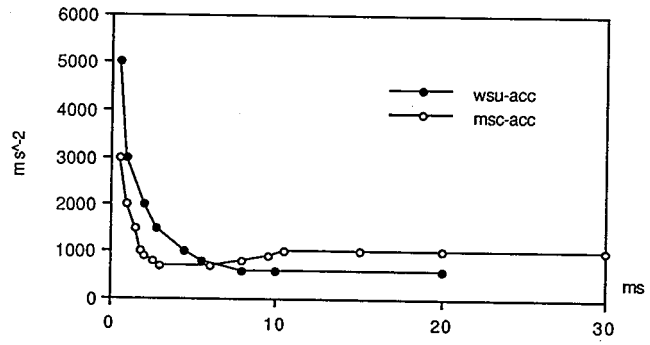

Figure 6. Translation Tolerance Curves

In the sudden rotation configuration, Bycroft (1973) gave a limit acceleration curve as a function of a prescribed duration (Figure 7). This curve considered an injury mechanism related to cerebral matter angular strains, with a 5% allowable value.

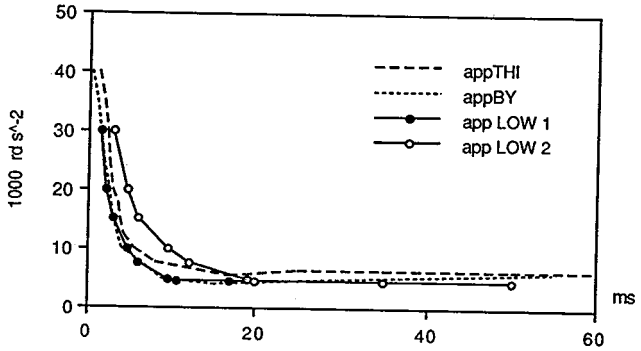

Figure 7. Rotation Tolerance Curves

Other authors gave the tolerance curve in terms of maximal acceleration as a function of angular velocity variation. For a prescribed impact, this velocity variation corresponded to the subtended area to the acceleration-duration curve ($\theta''=g(t)$). Consequently, for a given input signal (θ'', $\Delta\theta'$), duration t_0 will be given by:

$$\Delta\theta = \int_0^{t_0} g(t)\,dt \qquad (15)$$

Where g is the triangle, sinus or square function; t_0 is obtained from (15):
for the triangular signal:

$$t_0 = 2\Delta\theta'/\theta'' \qquad (16)$$

for the sinusoidal signal:

$$t_0 = \pi\Delta\theta'/2\theta'' \qquad (17)$$

for the rectangular signal:

$$t_0 = \Delta\theta'/\theta'' \qquad (18)$$

Löwenhielm and Thibault tolerance curves have thus been homogenized. Thibault (1990) considered the intracerebral injuries due to shearing ($\lambda = 1$), see Figure 7. Löwenhielm (1977) considered first the injury mechanism related to the bridging vein rupture (noted L1) and then took into account the brain mass displacement criterion (Löwenhielm 1973, noted L2) on Figure 7.

At this stage, it can be noted that it is difficult to make a distinction between the different tolerance curves and that some analogy can be observed between translation and rotation (Figure 8). Nevertheless, it can be observed that "msc" criterion is more severe for short-duration shocks and that Löwenhielm (L2) proposed a significantly higher limit for identical shocks.

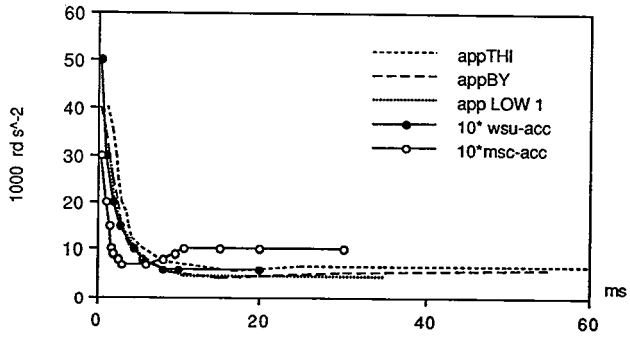

Figure 8. Time Tolerance Curves Superposition

Method

The expression of the time tolerance curves in the frequency field is based on the Fourier transform of an impact time signal (Max 1985). The method consists in taking various acceleration-duration curve points, in building up its input signal as a function of time and then in calculating the input signal Fourier transform. For a unit amplitude, the expression for these functions is:
for a rectangular impact:

$$A(f) = t_0 \frac{\sin(\pi f t_0)}{\pi f t_0} \qquad f_r = 1/t_0 \qquad (19)$$

for a sinusoidal impact:

$$A(f) = \frac{2t_0}{\pi} \frac{\cos(\pi f t_0)}{1-(2ft_0)^2} \qquad f_s = \pi/2t_0 \qquad (20)$$

for a triangular impact:

$$A(f) = \frac{t_0}{2} \frac{\sin(\frac{\pi}{2} f t_0)}{\frac{\pi}{2} f t_0} \qquad f_t = 2/t_0 \qquad (21)$$

The term f_r, f_s or f_t corresponds to maximum spectrum frequency for a duration to and a signal of rectangular, sinusoidal and triangular shapes respectively. This frequency is noted f_m.

The studies on the head dynamic behavior led to consider the total energy contained in the signal but also the energy contained in the 1-100 Hz range for a prescribed f_m frequency, i.e. for a given impact duration.

For each limit impact, values of B (total energy) and C (energy between 1 and 100 Hz) were calculated and plotted on the graph as a function of the associated f_m frequency. Thus a time tolerance curve (θ'',t_0) gave a family of 2 curves (B, f_m) and (C, f_m) in the frequency field with:

$$B(f_m) = 2\int_0^{f_m} A(f)^2\, df \qquad (22)$$

$$C(f_m) = 2\int_0^{100} A(f)^2\, df \qquad (23)$$

Signals are sinusoidal for the selected tolerance curves. Translation-related results are multiplied by 100 in accord with equation (14) to express them in equivalent rotation and analyze the analogies existing between rotation and translation.

Results and Discussions

The results relating to the six tolerance curves considered are plotted in Figures 9-a to 9-f. It can be observed:

- a superposition of B and C between 0 and 100 Hz, which is logical as for long-duration impacts, i.e f_m less than 100 Hz, equations (22) and (23) are identical,
- a minimum allowable total energy generally located at about 200 Hz but that can be located at about 600 Hz for the "msc" or close to 100 Hz for L2. This minimum will now be called "critical frequency f_c,"
- a quasi-constant value of allowable energy ranging from 0 to 100 Hz, as soon as the impact duration is short enough to introduce frequencies higher than the critical frequency (except for L2 and msc),
- a qualitative and quantitative analogy between translation and rotation (see curve "wsu" in Figure 10-a. Note that the "msc" curve differs due to the mechanism considered rather than to the translation shocks involved. This point will be thoroughly studied in the following part.

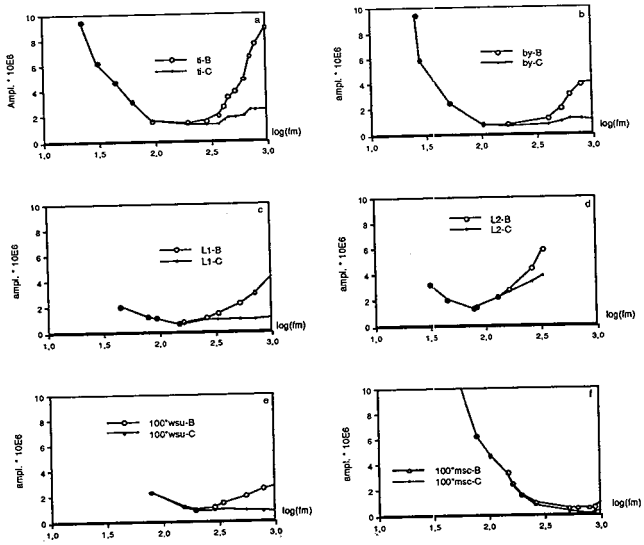

Figure 9. Change in Allowable Impact Energy as a Function of Maximum Frequency Contained in the Shock Spectrum. (B) total energy; (C) energy contained between 0 and 100 Hz. (a) Thibault, (b) Bycroft, (c) Löwenhielm 1 (d) Löwenhielm 2, (e) Wain State University, (f) Mean Strain Criterium

To better show the minimum in total energy B, as well as the notion of critical frequency, allowable total energy B changing has been plotted as a function of the reduced frequency logarithm (see Figure 10).

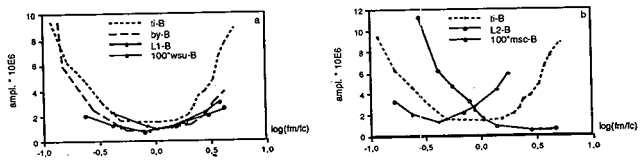

Figure 10. Allowable Total Energy as a Function of the Maximum Frequency Contained in the Shock Spectrum, Related to the 190 Hz Critical Frequency. (a) Brain Properties Related Mechanisms; (b) Other Injury Mechanisms

In our calculations we put f_c = 190 Hz, which represented the average of four critical frequencies close to 200 Hz (Thi, By, L1, wsu). In such a representation, the total energy is a parabolic function whose minimum abscissa corresponds to the injury mechanism considered. These total energy curves enabled to distinguish three classes of mechanisms:

- the first class (L2) presents a minimum at $\log(f_m/f_c)$ = -0.2, i.e. for a critical frequency of the order of 100 Hz (Figure 10-b). In his curve Löwenhielm considered the injury mechanisms related to the skull-brain friction. The 100 Hz critical frequency should certainly be related to the brain mass mechanical properties. For frequencies less than f_c, such a mechanism is not likely to occur as the brain follows the skull motion. On the other hand, as soon as f_m exceeds f_c, the mechanisms considered should be

taken into account as a relative skull-brain motion can occur,

- the second class presents a minimum at $\log(f_m/f_c) = 0.4$, i.e. for a critical frequency ranging from about 500 to 600 Hz (Figure 10-b). The mechanism considered takes into account the cerebral matter compression due to the relative motions of the bone parts forming the skull, in accord with the model developed by Stalnaker (1971). From this model, maximum motions occur at the first skull natural frequency at about 500 Hz. It is not therefore surprising to meet this critical frequency in the frequency analysis of the tolerance curves obtained using the "msc" criterion,
- Finally, the third class which presents a minimum at $\log(f_m/f_c) = 1$, i.e a minimum at 190 Hz (Thi, By, L1, wsu) takes into account an injury criterion which seems to be connected to the cerebral matter mechanical properties and the cerebral shearing (Figure 10-a). Indeed, the brain presents a decreasing resistance up to about 100 Hz. Beyond 200 Hz, the added energy is not transmitted to the cerebral mass and is therefore limited by other obviously more favorable conditions.

This assumption also explains the fact that allowable energy ranging from 0 to 100 Hz (Curve C) remains constant for short-duration impacts (f_m >200 Hz). Indeed, beyond this limit two conditions are likely to be required: the condition relating to C which is relatively restrictive and expresses the shearing risk in a brain presenting a low and constant receptance and that relating to the energy concentrated between 100 Hz and f_m given by the difference between B and C which could be the cause of the bridging vein rupture or other peripheral brain contusions or hematomas. This mechanism can possibly occur for shocks whose spectrum does not exceed a frequency of 1000 Hz. Beyond 1000 Hz, very short-duration impacts can be observed and thus this is the shock wave range. In our analysis, this led to a wide spread of the results beyond 800 Hz. These are the validity limits of the various models considered.

The detailed analysis of the intracerebral shearing tolerance is based on the impact energy part concentrated between 0 and 100 Hz. As a function of the shock duration, and therefore of the maximum frequency f_m contained in the shock spectrum, this frequency tolerance curve is determined by curve C for data relating to Thi, By, L1 and wsu (Figure 11) Between 0 and about 800 Hz, this energy expressed as a function of the reduced frequency logarithm and related to the average minimum value $C_{mini} = 9.\ 10^6$ (rd s^{-2})^2 can be approximated by the following power function:

$$\frac{C}{C_{mini}} = 1 - 0{,}45\log\frac{f_m}{f_c} + 4\left(\log\frac{f_m}{f_c}\right)^2 - 4{,}2\left(\log\frac{f_m}{f_c}\right)^3 \quad (24)$$

The equation plot to ± 15% is given in Figure 11, where the results recorded in the literature are also indicated. Equation (24) gives the tolerance expression to intracerebral injuries in the form of allowable energy ranging from 0 to 100 Hz, as a function of $C_{mini} = 9.10^6$ (rd s^{-2})^2 given in the literature, f_c given by Shuck and the maximum impact spectrum frequency. The validation range is 0 to 600 Hz.

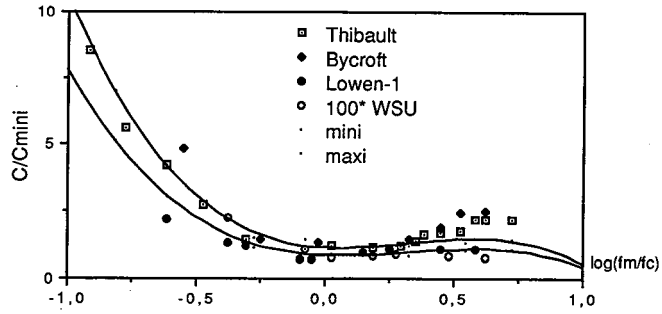

Figure 11. Frequency Tolerance Curves to Intra-Cerebral Lesions—Maximum energy contained between 1 Hz and 100 Hz

The evolution of the allowable energy ranging from 100 Hz to f_m is expressed by the term (B - C), as a function of maximum frequency contained in the shock spectrum. In Figure 12, this value is expressed as a function of the reduced frequency logarithm.

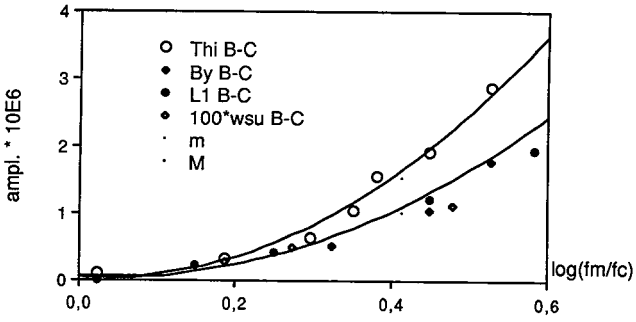

Figure 12. Frequency Tolerance Curve to Relative Motion Lesions—Maximum energy contained between 100 Hz and f_m

In the high frequency field, the brain does not follow any more the skull motions with a risk of sub-dural hematomas or of contusions due to the encephalon friction on the skull or its crushing on the skull walls. If this risk is likely to be avoided when f_m is less than 100 Hz; it becomes significant immediately beyond the critical frequency and then decreases again with f_m as allowable energy (B-C) increases with f_m up to 800 or 1000 Hz.

This change can be related to the viscoelastic properties of the brain-skull connections and the cerebral matter resonance. The curve equation which expresses the injury tolerance by relative motions as a function of the allowable energy in the shock spectrum can be written:

$$B - C = 8\left(\log\frac{f_m}{f_c}\right)^2 \qquad (25)$$

In Figure 12, the equation representation to ± 20% is superposed on the results given in the literature.

Conclusion

A new lumped head model based on the distinction between the cerebral mass and the other constituting elements enabled us to express the ratio of skull to brain velocities, as a function of excitation frequency in case of sudden acceleration.

The occurrence of a relative motion beyond 100-200 Hz led us to differentiate the injury mechanism related to the cerebral matter internal shearing and that generated by the brain motions within the skull.

The study showed that the main parameters leading to an injury were the energy introduced into the system as well as its distribution in the frequency field. In such a context, the acceleration vector orientation and the rotation-translation duality which are often mentioned in the literature, have more effect on the injury location than on its nature itself.

The results led us to analyze the tolerance curves proposed in the literature in the frequency field. For limit shocks from a time tolerance curve, allowable energy (B) and the allowable energy ranging from 0 to 100 Hz (C) are determined and these two values are plotted as a function of the maximum frequency contained in the shock spectrum (f_m).

Curves (B, f_m) present a parabolic shape whose minimum position is characteristic of the injury mechanism considered.

Curves (C, f_m) relating to frequencies where stresses can be transmitted to the cerebral matter show the injury risk due to intracerebral shearing (diffuse lesions).

Curves (B-C, f_m) relating to frequencies where a relative motion is observed between the brain and the skull, show the risk of injuries such as sub-dural hematoma or focal hematoma located in the encephalon periphery.

For very short-duration impacts including frequencies exceeding about 800 Hz in their shock spectrum, this model cannot be applied any more and it is the shock wave range.

If the results obtained can further be a guide to the development of new brain tolerances, they can up to now be applied in tests in vitro or using dummies. Indeed, it is suggested to add a frequency analysis of the results to the mathematical processing of the acceleration-time curve.

For such a type of tests, as Stalnaker did, it is recommended to develop dummy heads whose mechanical impedance is close to that recorded on living human subjects.

Acknowledgements

We do thank the "Ministere de la Recherche et de la Technologie" (the French Ministry of Research and Technology) for its support to the project.

Nomenclature

m_t overall head mass
m_1 frontal bone mass
m_2 brain mass
m_3 $m_1 - (m_1 + m_2)$
k_2, c_2 m_2 stiffness and damping
k_3, c_3 m_3 stiffness and damping
a_1, r_1 first head resonance and antiresonance
a_2, r_2 second head resonance and antiresonance
$j = (-1)^{0.5}$
ω angular frequency ($-2\pi f$)
Z_n head non damped impedance
Z head damped impedance
$Z_1 = j\,\omega\,m_1$
$Z_2 = c_2 + K_2/j\omega$
$Z_3 = c_3 + K_3/j\omega$
$Z_4 = j\,\omega\,m_2$
$Z_5 = j\,\omega\,m_3$
r(f) ratio of the skull to brain velocities
A(f) amplitude of the acceleration signal Fourrier transform
B total energy contained in an acceleration spectrum $(rd\ s^{-2})^2$
C acceleration spectrum energy contained between 0 and 100 Hz $(rd\ s^{-2})^2$
f_m acceleration spectrum maximum frequency
f_c critical frequency.

References

Bycroft, G.N., Mathematical model of a head subjected to an angular acceleration. J of Biomec. 1973, 487-497.

McElhaney, J.H., Roberts, V.L., Hilyard, J.F., Handbook of human tolerance, JARI, Tokyo 1976.

Harris, Shock and vibration handbook, Mc Graw-Hill, NY 1988.

Kallieris, D., Schmidt G., Hausler, E., Brain injuries under high speed loading. IRCOBI 229-240, 1980.

Löwenhielm, P., On the mechanism of cortical bridging vein rupture. IRCOBI conf., 1973,423-429.

Löwenhielm, P., Tolerance levels for bridging vein disruption calculated with a mathematical model. Univ. of Lund, Lund, Sweden 1977.

Max, J., Methodes et techniques de traitement du signal (tome 1). Masson, Paris 1985.

Salter, J., Steadystate vibration. Kenneth-Mason, London 1969.

Shuck, L.Z., Advani, S.H., Rheological response of human brain tissue in shearing. J Basic Eng., 905-911, 1972.

Stalnaker, R.L., Fagel, J.L., Driving point impedance characteristics of the head. J Biomec. 4, 127-139, 1971.

Thibault, L.E., Gennarelli, T.A., Margulies, S.S., The strain dependent pathophysiological consequences of inertial loading on central nervous system tissue. IRCOBI conf. 1990, 191-202.

Willinger, R., Cesari, D., Determination of cerebral motion at impact through mechanical impedance measurement. IRCOBI conf. 203-213, 1990.

S8-W-17

Development of a Sternum Displacement Sensing System for Hybrid III Dummy

Kenji Ogata, Masakazu Chiba
Toyota Motor Corporation
Hisashi Kawai, Fumio Asakura
Nippon Soken, Inc.

Abstract

A new "3D-MUSTERDS-Three Dimensional Multi-Point Sternum Displacement Sensing System" has been developed, in order to measure chest deflections of anthropomorphic dummy to be used in vehicle collision tests. The 3D-MUSTERDS consists of an optical position sensing system (which consists of light emitting diodes (LEDs) installed on the sternum and position sensing detector (PSD) cameras installed on the thoracic spine) to be placed in the rib cage, and an external system to calculate and control the coordinates. This new system is characterized by the ease in application to chest of Hybrid m dummy. It is also verified that its frequency response and the impact resistance are excellent, with sufficient capabilities as a practical system for the measurement of the sternum (chest) deflections in normal collision tests. This paper describes the outline of the system and some examples of its applications.

Introduction

Thoracic injuries of vehicle occupants in traffic accidents used to be discussed in terms of the thoracic spine accelerations, but the chest deflections have been noted in recent years as a new index for thoracic injuries in place of the accelerations (1).

Under such circumstances, a chest deflection measuring system has been incorporated in the Hybrid m dummy, and used widely as a useful tool for the evaluation of thoracic injuries.

The chest deflection measuring system is, however, capable of measuring only the deflection of a single point at the center of the sternum in the sagittal direction.

Therefore, a question still remained unsolved regarding the relationship between the deflection at this single point and deflections at other points.

The author et al., have carried out static compression tests on the dummy chest under various conditions to clarify the relationship. As a result, it is found that displacements at individual portions of the sternum are different, which can not be represented by the displacement of the single point at the center of the sternum alone.

It is also found that displacements may occur in directions other than the sagittal direction.

More accurate understanding of displacements at many portions of dummy sternum in collision tests is indispensable to the reduction of thoracic injuries of occupants in a traffic accident, that accounts for the decision to develop the 3D-MUSTERDS.

Chest Compression Tests

By using seatbelt and steering wheel, the static compression tests of the upper torso assembly (without flesh and skin) of Hybrid m dummy were conducted for the determination of displacements at many portions of the sternum.

The test conditions are shown in Figures 1 and 2.

Method and Locations of Load Applications

In the compression tests by means of seatbelt, the chest of dummy was pressed against a seatbelt through the jig attached to the thoracic spine.

There was two cases of seatbelt webbing location against the chest—namely, it passed over the upper portion of the sternum (rib No. 1) in one case, and over the lower portion (rib No. 6) in the other as shown in Figure 3.

In the compression tests by means of steering wheel, the chest of dummy was pressed in a similar manner against the steering wheel with the boss fixed. There were two cases of steering wheel rim location against the chest—namely, it was set against the center of sternum in one case, and against the lower portion in the other as shown in Figure 4.

In both cases, the initial angle between the wheel surface and the sternum was set at 25°.

Displacement Measuring Locations

Twelve points where ends of right and left ribs were fixed by bolts, and two more points out of twelve points where the potentiometer slider and right and left sides of sternum were bolted (corresponding to the displacement detection location of existing internal chest deflection

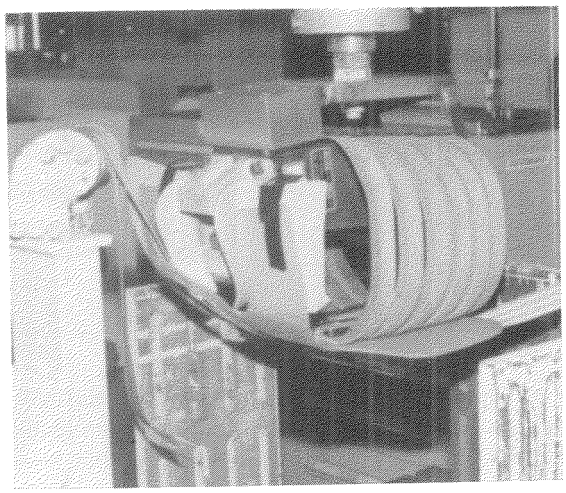

Figure 1. Test Condition of Chest Compression Tests by Seatbelt

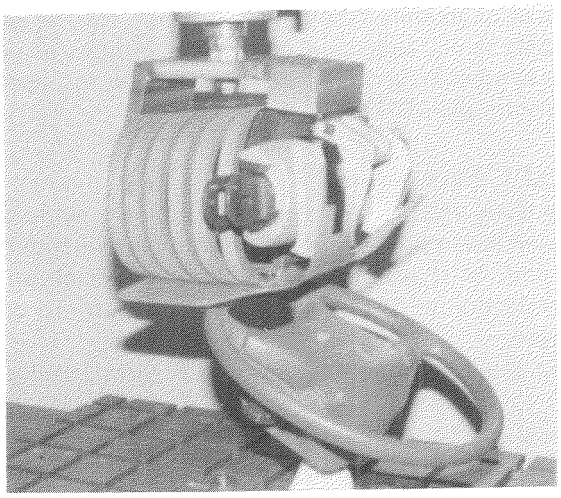

Figure 2. Test Condition of Chest Compression Tests by Steering Wheel

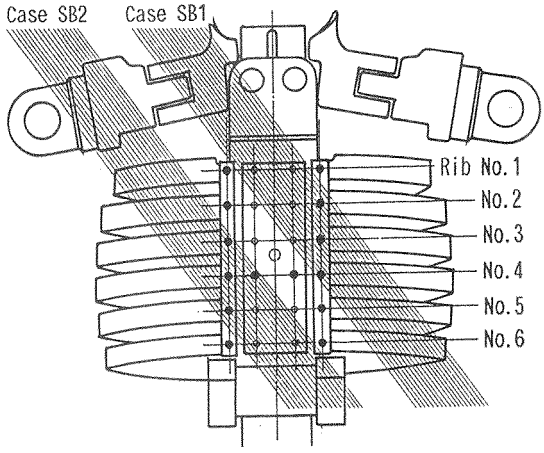

Figure 3. Shoulder Belt Locations Against the Chest (Sternum)

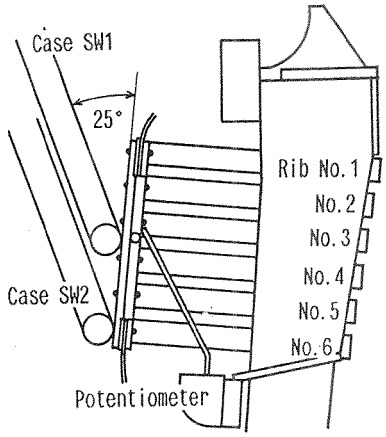

Figure 4. Steering Wheel Locations Against the Chest (Sternum)

measuring system) were selected as measuring locations for displacements.

The displacements in three directions against the thoracic spine were then measured respectively.

Locations and directions of the displacement measurements are shown in Figure 5.

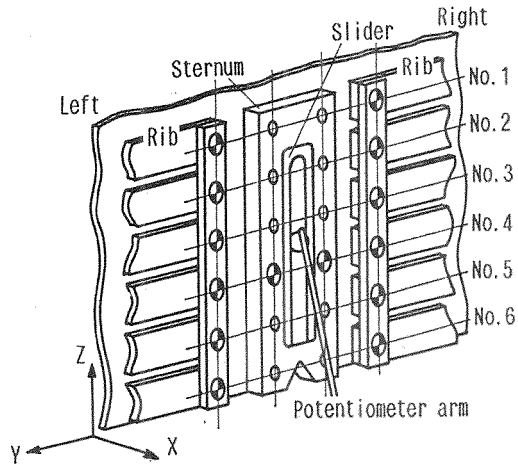

Figure 5. 14 Points Selected for Three Directional Displacements Measuring in Chest Compression Tests

Results of Measurements

Examples of measured results are shown in Figures 6 and 7, from which it may be said as follows.

Take a look at displacements in the X-direction first. In case where the load is applied by the seatbelt, the difference in displacement between upper and lower ribs is relatively small with a nearly uniform displacement of the entire sternum, whereas the difference between right and left ribs is quite large.

Therefore, it will be difficult to represent all displacements in the X-direction by the displacement of a single point alone at the center of the sternum.

In cases where the load is applied by the steering wheel, on the other hand, the difference between right and left ribs is small, while, in the case of lower sternum loading especially, the difference between upper and

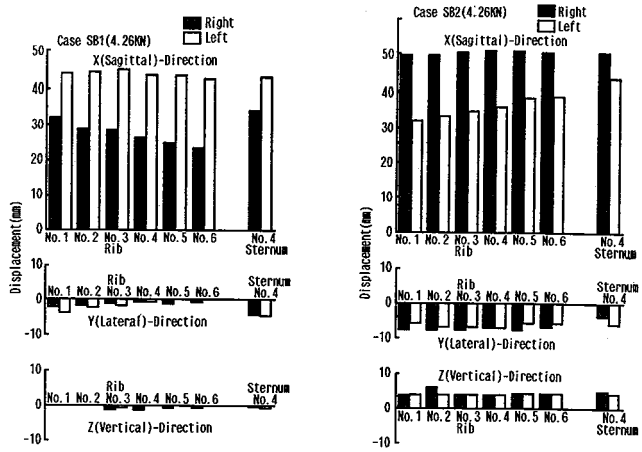

Figure 6. Results of Chest Compression Tests by Seatbelt

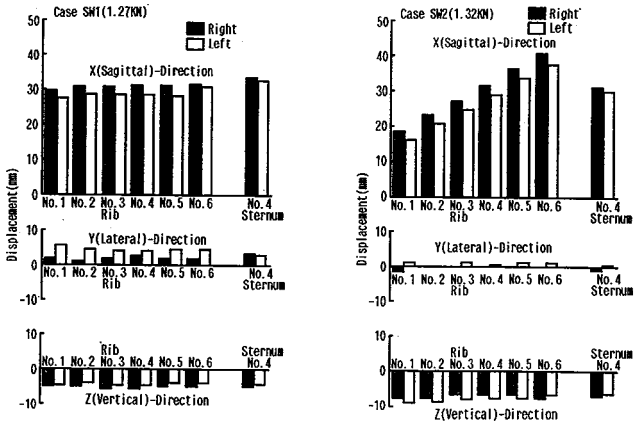

Figure 7. Results of Chest Compression Tests by Steering Wheel

lower ribs is large, contrary to the seatbelt loading conditions described above.

Hence, the displacement of the single point alone at the center of the sternum can not represent all displacements in the X-direction for this case as well.

In any event, displacements of individual ribs in the X-direction are characterized by the changes which are semi-linear to the longitudinal direction of the sternum.

This is presumably due to the high rigidity of the sternum of this type of dummy, as already pointed out (2).

Hence, it should be possible to estimate displacements of other points as long as displacements at two points on the upper and lower portions of the sternum are determined.

Next, displacements in Y and Z-directions are considered. In case of seatbelt loading, displacements tend to occur more easily in the Y-direction, whereas the steering wheel loading tends to show more significant displacements in the Z-direction.

It is found that such displacements provide important information for the determination of the difference in deflection of sternum caused by the difference in restraint system, though the displacement itself is as small as 20% of that of X-direction or so.

Development of 3D-MUSTERDS

Targets of Specifications and Performances

Following points were considered as requirements which the 3D-MUSTERDS must meet, and the development was initiated according to the targets.

(1) Displacement measuring points should be at least four on right and left sides respectively at the upper and lower portions of the sternum.
(2) The system must be capable of measuring three dimensional displacements of each measuring point continuously over a wide range with adequate accuracy.
(3) The installation in the rib cage of Hybrid m dummy (AM50) should be easy.
(4) Changes in specifications of the dummy upper torso should be minimized as much as possible.
(5) The system must sufficiently endure impacts in normal collision test environments.

Specific targets of specifications and performances to meet the requirements are shown in Table 1.

Table 1. Target Specifications and Performances for 3D-MUSTERDS

Displacement Measuring Range	X	0~76mm
	Y	−50~50mm
	Z	−20~20mm
Displacement Measuring Accuracy	X	less than ±2.5% of F.S.
	Y	less than ±5.0% of F.S.
	Z	less than ±5.0% of F.S.
Temperature Resistance (-10°C ~60°C)		less than ±2.5% of Displacement at 20°C
Frequency Response		more than 2KHz
Impact Resistance		more than 200G-3ms
Weight Increase		less than 1.69Kg*
Shift of Gravitational Center	X	less than ±10mm
	Y	less than ± 5mm
	Z	less than ±10mm

* 10% of weight of upper torso assembly (without flesh and skin)

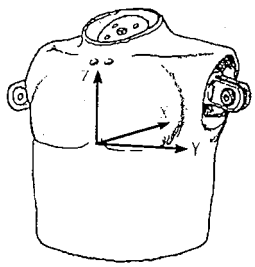

Three Dimensional Displacement Measuring Method and Principle

Various types of three dimensional displacement measuring methods known generally were studied first in order to come up with the optimum basic structure of the system for the attainment of the performance requirements stated above.

As a result, it was decided to use the triangulation method by means of binocular stereoscopic vision, because of the simple structure without moving parts, insusceptibility to the effect of external noise, high measurement/processing speed, high accuracy, etc.

This method is to project points concerned in the three dimensional space against two non-parallel planes, and to obtain the three dimensional coordinates of the points from the two dimensional coordinates on each plane.

The principle of the method is shown in Figure 8.

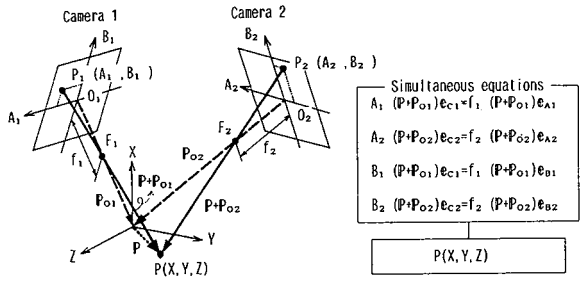

Figure 8. Principle of the Triangulation Method by Means of Binocular Stereoscopic Vision

Application to Sternum Displacement Measuring System

On application of the principle mentioned above to the sternum displacement measuring system, two cameras were fixed onto the thoracic spine in order to catch the light emitted from the LEDs installed on the sternum as shown in Figure 9.

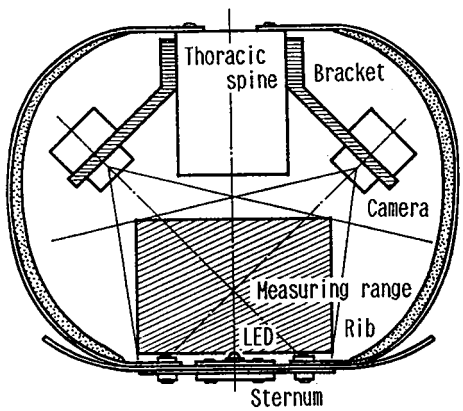

Figure 9. Basic Scheme of 3D-MUSTERDS

Development of Camera

In the displacement measuring system shown in Figure 9, appropriate performances of a camera itself, required to meet the range and accuracy of measurement shown in Table 1, were studied by the numerical calculations using simultaneous equations shown in Figure 8.

As a result, it was found that the accuracy required of two dimensional coordinates of the camera itself was ±1.2% of F.S. in order to satisfy the accuracy requirement of +2.5% of F.S. for the severest measurement in the X-direction, for example.

Cameras to be installed on the thoracic spine of a dummy should be as small and light as possible.

Hence, efforts were made to meet this accuracy requirement with the simplest structure, consisting basically of a filter, lens, image sensor and preamplifier as shown in Figure 10.

Selection of image sensor. Although various types of image sensors were already used in practice, the charge coupled device (CCD), one of the solid state image pickup devices, was considered first, since the image

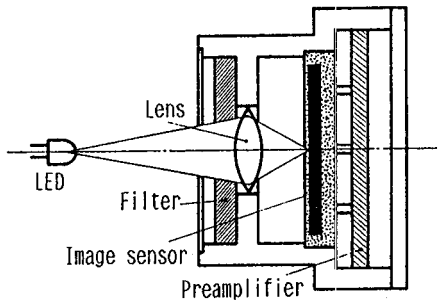

Figure 10. Basic Configuration of the Simplest Camera

pickup tubes represented by Visicon had problems in terms of size and impact resistance. It was found, however, that the CCD could not ensure the accuracy requirement stated earlier, due to the limitation in resolution power.

In the end, a position sensing detector (PSD), with a higher resolution power and frequency response performance, as well as the capability to generate continuous analogue outputs, was selected (3,4).

Such a PSD is capable of detecting the position of a given spot light on the light receiving surface, making use of the characteristic feature of the inverse proportional relationship between the generated current flowing through electrode by the spot light and the distance between the spot light and electrode, as shown in Figure 11.

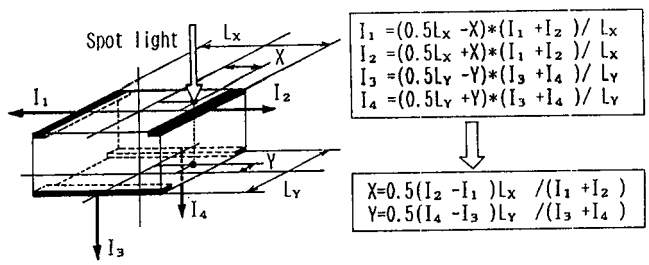

Figure 11. Principle of Two Dimensional Position Sensing Detector (PSD)

It is also characterized by the capability to recognize the position of the center of gravity of the luminous flux of the spot light.

The position resolution power of an ordinary two dimensional PSD is approximately 0.005 to 0.020mm.

Dark current. The effect of the dark current flowing through the PSD should be noted when considering the structure of a camera using a PSD. Since the dark current flowing through a PSD is equivalent to the light irradiated against the center of light receiving surface, the position of the center of gravity of luminous flux distribution including this deceptive light and the actual LED spot light will be detected. Therefore, some error is apt to occur against the actual position of the spot light, as shown in Figure 12.

In order to overcome this problem, the LED was provided with flashing signals by means of AC drive as shown in the same figure. Moreover, the PSD and the

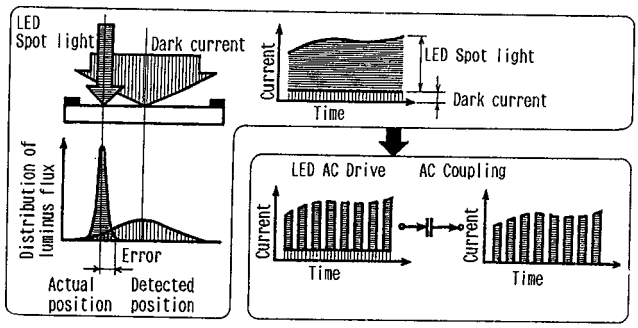

Figure 12. PSD Output Error Caused by Dark Current, and Measures for this Problem

preamplifier were connected by the AC coupling so that the DC current generated by the dark current could be eliminated.

The quantity of light in the rib cage of a dummy was measured under various conditions, since the position of the center of gravity of luminous flux could be subject to change by the quantity of disturbance light received by the PSD surface.

It was verified, however, that the disturbance light was negligible as its quantity was extremely small compared with that of LED.

Measures against optical/electric errors. Optical errors due to the refraction of light caused by the filter, aberration of lens, etc. and electric errors such as the nonlinearity of PSD and offset of preamplifier are inevitable for the configuration of such a camera as that shown in Figure 10, which are factors to reduce the accuracy in measurement.

Hence, the relationship between the actual position of the LED and the position of the LED spot light detected on the PSD light receiving surface was studied in advance.

Figure 13 shows the method and results of the study, from which it is evident that the farther becomes the LED position from the lens centerline, the lower becomes the sensing accuracy.

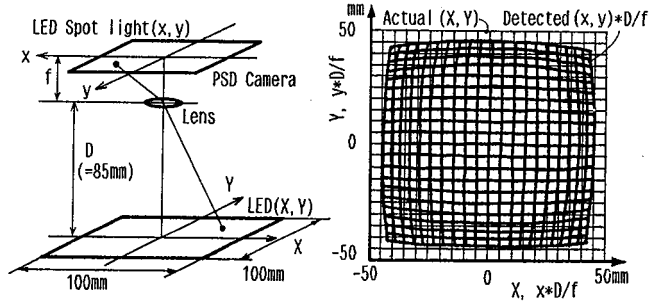

Figure 13. Test Method to Clarify the Relationship Between Actual LED Position and that Detected by PSD Camera, and Results

Making use of this relationship, the drop of accuracy is minimized by correcting PSD outputs accordingly.

Verification of measuring accuracy and range. After the measures were taken against the dark current and optical/electric errors, the total performance of the PSD camera itself was checked out. Figure 14 shows the method and the results, which verify that the accuracy of ±1.2% of F.S. required of the PSD camera itself for the two dimensional coordinates can be met if the distance between the camera and LED is about 80 to 200mm.

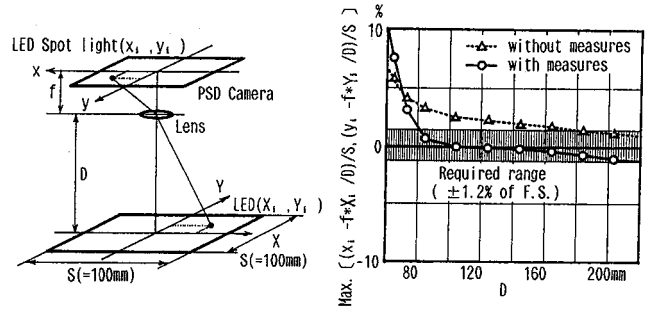

Figure 14. Test Method to Verify the Accuracy of PSD Camera (After Several Measures Were Taken), and Results

Impact Resistance

Impact tests for each direction were carried out with the combination of the PSD camera and LLD as shown in Figure 15, in order to check on effects of the distortion of camera body and minute motions of the components on the PSD outputs.

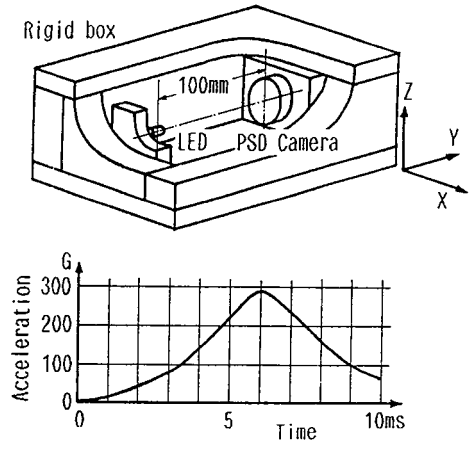

Figure 15. Impact Test Method and Applied Acceleration

As a result, it was verified that the impact was not a factor to deteriorate the measuring accuracy, because the rate of change in PSD camera outputs was practically zero even under the severe impact conditions, as shown in Figure 16.

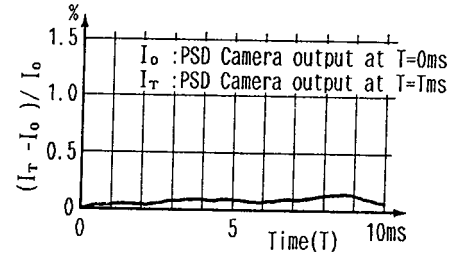

Figure 16. Rate of Change in PSD Camera Output During Impact Condition (X-Direction)

Some tests were also carried out on the PSD camera alone by the same way shown in Figure 15, in order to check on the deterioration of functions of the PSD camera by repeated impacts.

The relationship between the number of impact cycles and the PSD output change by the method shown in Figure 14 was also investigated. The results are shown in Figure 17.

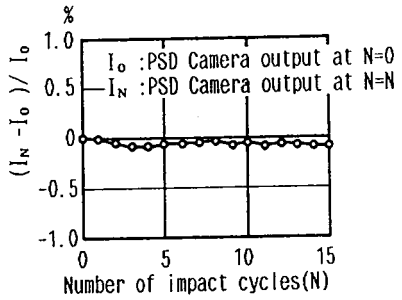

Figure 17. Rate of Change in PSD Camera Output Against the Repeated Impacts

Although a slight change was found in the PSD camera outputs, the rate of change was extremely small and stays nearly constant against the number of impact cycles repeated.

It is thus judged that the impact resistance of the PSD camera is sufficient.

Temperature Characteristic

The environmental temperatures for the dummy, when it is used in tests, are limited by the provisions of applicable standards, but the measuring accuracy of the PSD camera itself against the temperature change was also tested under this study.

As shown in Figure 18, the PSD cameras and LED were fixed to the jig and held in a thermostatic chamber to determine the LED positions (three representative points within the measuring range) through the cameras.

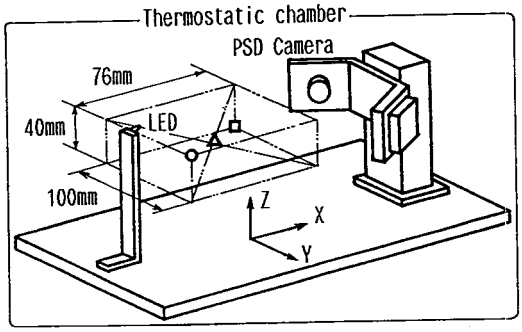

Figure 18. Test Method to Clarify the Relationship Between PSD Camera Outputs and Environmental Temperature

Figure 19 shows the results, from which it is verified that the accuracy stays quite stable against the temperature change, as the error is ±2.0% or less in the temperature range of -10°C to 60°C.

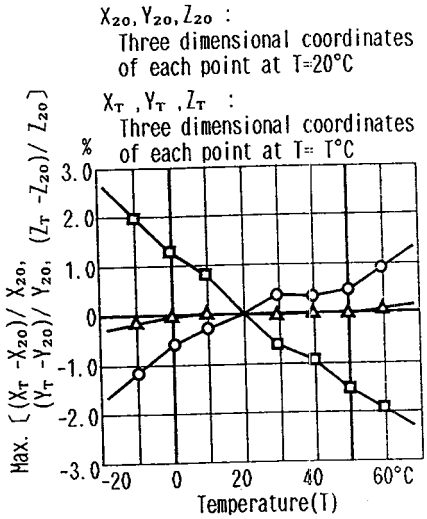

Figure 19. Rate of Change in PSD Camera Output Against the Temperature

Entire Configuration and Performances of 3D-MUSTERDS

The configuration of the 3D-MUSTERDS finally developed after various studies described above, and the flow chart of measurements are shown in Figure 20 through Figure 24.

Four LEDs in total were set as displacement measuring points—on right and left sides of the sternum by ribs No. 2 and No. 5 of the dummy.

Two PSD cameras (one pair) were set respectively on the upper and lower portions of the thoracic spine, and fixed by four bolts each through a bracket.

Both sides of the thoracic spine were cut off slightly to ensure the bracket installation accuracy to the spine.

The design of the bracket was considered from various points of view, such as the weight, installed rigidity and clearance from each rib.

As it was found that a mirror was indispensable to the bracket in order to provide a necessary distance between each LED and PSD camera shown in Figure 14, the method to install such a mirror was also considered, and the optimum specifications as a total system were thus selected.

It is necessary to identify individual LEDs in order for a pair of PSD cameras to read displacements of two LEDs, hence the time sharing lurninous control is provided with the LEDs for this purpose.

The controller is set outside the dummy, which consists of computation circuits to convert the PSD outputs into two dimensional coordinates on the light receiving surface of PSD, and timing controller (including the LED AC drive circuit).

Two dimensional coordinates of two cameras (PSDs) recorded in the data recorder are incorporated in the computer, which allows the determination of the three dimensional displacements of each LED-i.e., the sternum deflections—by solving simultaneous equations shown in Figure 8.

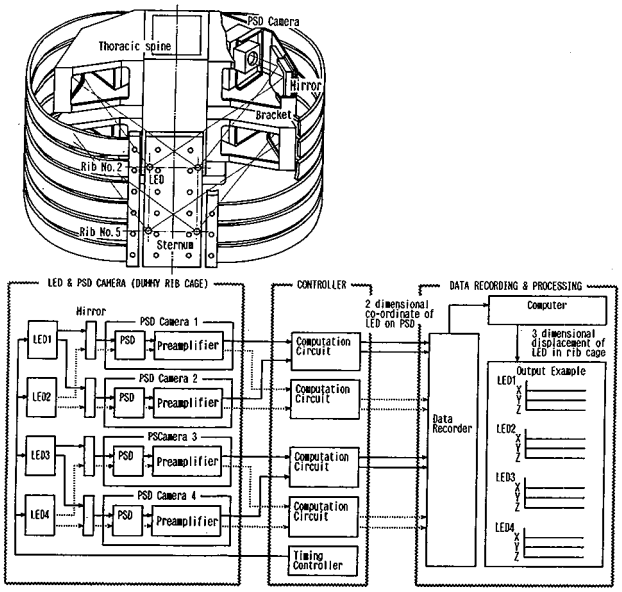

Figure 20. Final Configuration and Measurement Flow of 3D-MUSTERDS

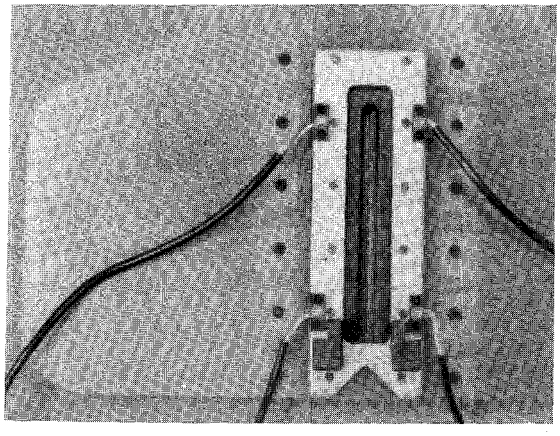

Figure 21. 4 LEDs Installed onto the Sternum

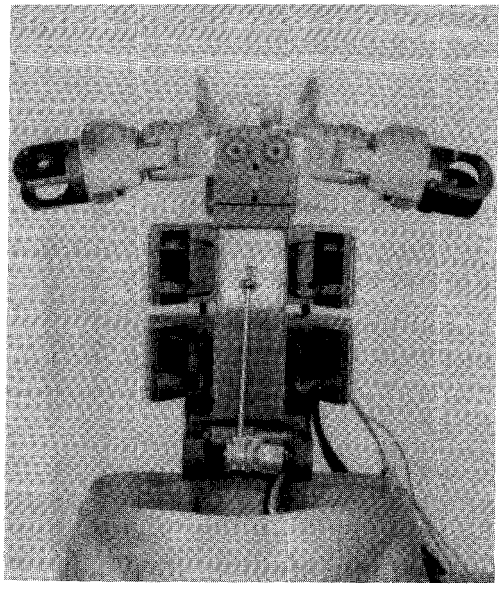

Figure 22. 4 (2 Pairs) PSD Cameras Installed onto Thoracic Spine Through Brackets (Front View)

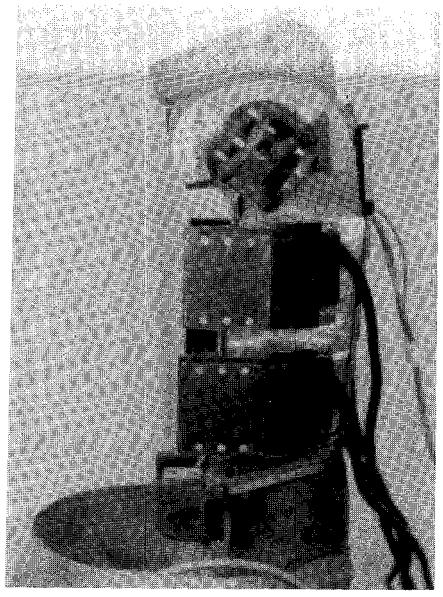

Figure 23. 4 (2 Pairs) PSD Cameras Installed onto Thoracic Spine Through Brackets (Left Side View)

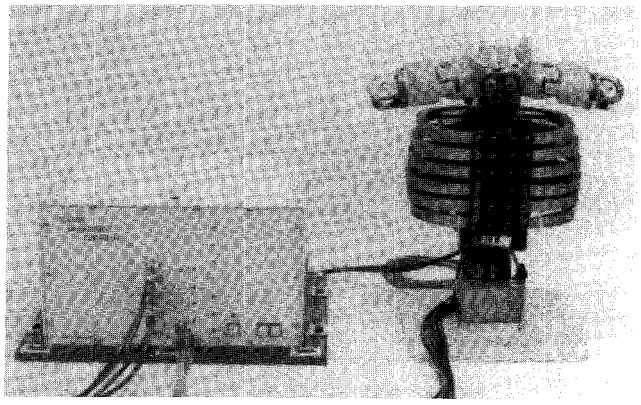

Figure 24. Upper Torso Assembly Equipped with 3D-MUSTERDS and Controller

Measuring Range and Accuracy

The LED measuring range and the accuracy in the conditions of 3D-MUSTERDS final assembly were checked by method shown in Figure 25.

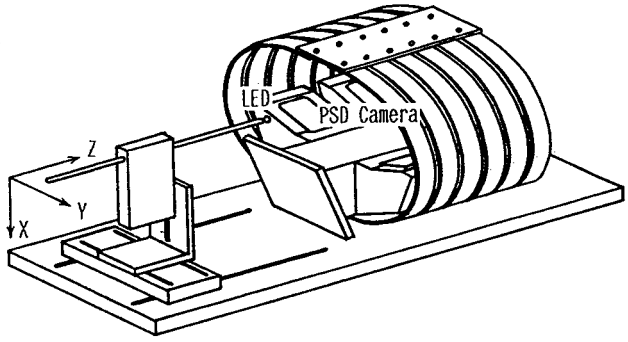

Figure 25. Test Method to Determine LED Measuring Range and Accuracy

Figure 26 shows the results of the determination for the LED measurable range. Although some small unmeasurable regions exist on the X-Y plane, the per-

formances appear to be adequate since the possibility of displacements of the measuring points set thereof into these regions seems to be low, even though the performance targets are not met completely.

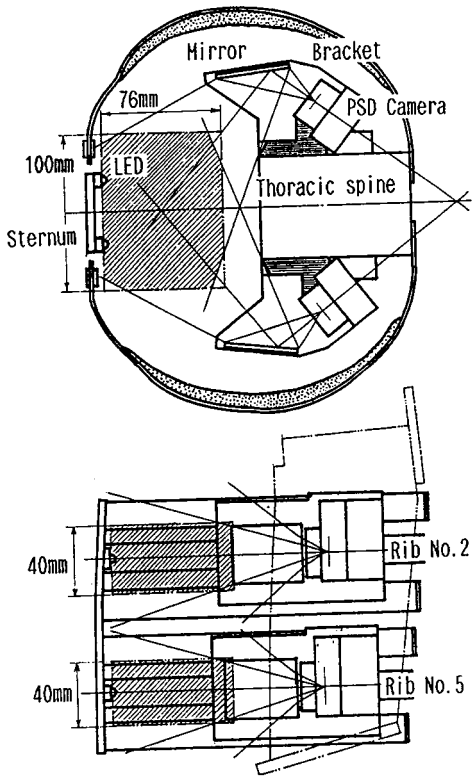

Figure 26. Required Measuring Range and Measurable Range

Figure 27 shows the measuring accuracy at each measuring point in the measurable range.

The measuring accuracy tends to drop as the distance between the measuring point and the thoracic spine becomes shorter for all displacements regardless of the direction, which makes it difficult to meet all performance targets, but it should not pose a serious problem in practice.

Impact Resistance of Bracket

Optical errors caused by relative displacements of camera brackets against the thoracic spine under impact conditions were studied.

Since it was difficult to measure minor displacements under actual conditions of impact, static load was applied to the bracket with the method shown in Figure 28, and estimated the errors by calculation according to displacements of portions where the mirror was installed.

As shown in Figure 29, the difference in displacement between the bracket front end and the rear end becomes 0.02mm or so where the load is 200 times the weight of bracket assembly (200G), which corresponds to 0.03° of the mirror angle change.

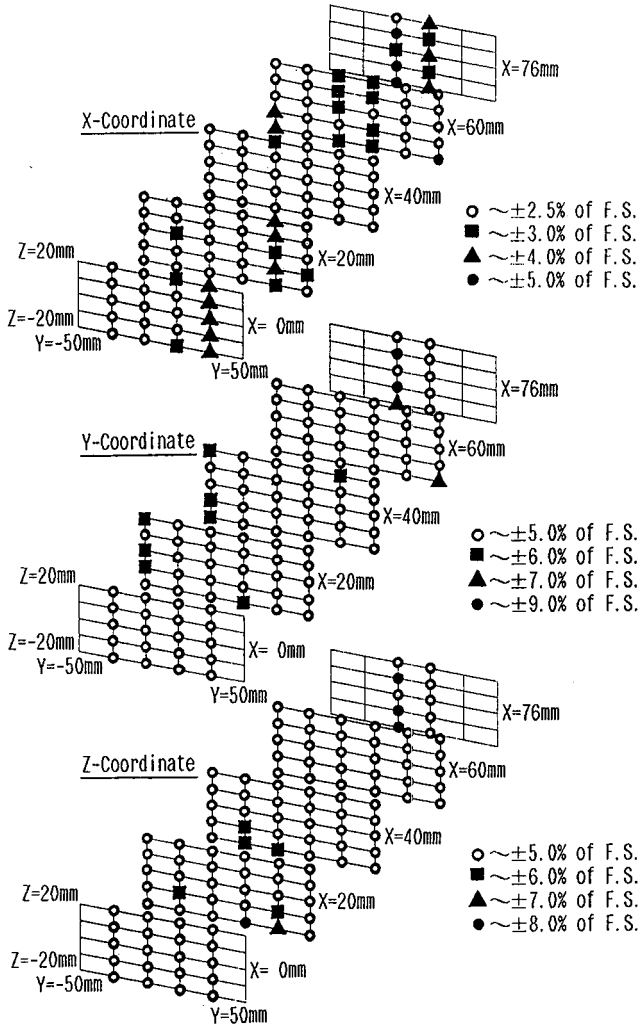

Figure 27. Measuring Accuracy (Error) at Each Point in Measurable Range

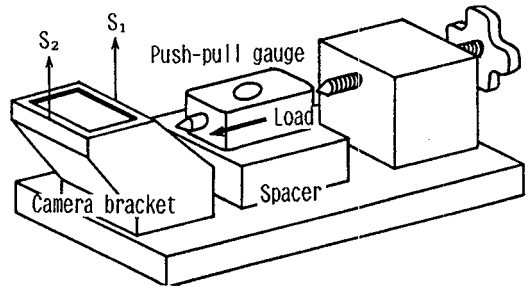

Figure 28. Static Loading Test Method to Determine the Rigidity of PSD Camera Bracket

From this value, it is verified that the bracket installation rigidity is sufficiently high, as the estimated measuring error at each measuring point is as small as 0.08mm or so.

Weight and Position of Center of Gravity of Upper Torso

The weight of upper torso assembly (without flesh and skin), including the LEDs, PSD cameras, etc., in the final condition was 18.5Kg, with the increase of 1.62Kg over the original weight.

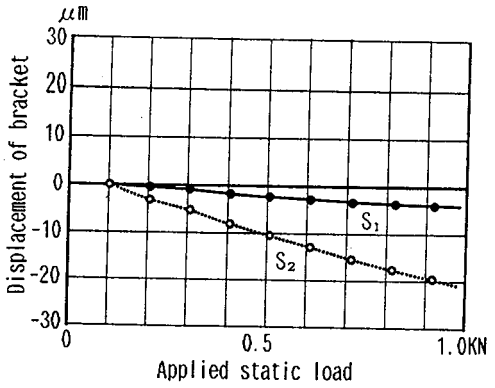

Figure 29. Displacements of PSD Camera Bracket

The center of gravity of the upper torso assembly was set rearward by 4.7mm and downward by 8.3mm respectively.

The basic performances and specifications of 3D-MUSTERDS are listed up as shown in Table 2, according to the foregoing data.

Table 2. Final Specifications and Performances of 3D-MUSTERDS

		Targets	Final Specifications & Performances
Displacement Measuring Range	X	~76mm	~76mm
	Y	−50~50mm	−50~50mm
	Z	−20~20mm	−20~20mm
Displacement Measuring Accuracy	X	less than ±2.5% of F.S.	less than ±2.5% (±5.0%*) of F.S.
	Y	less than ±5.0% of F.S.	less than ±5.0% (±9.0%*) of F.S.
	Z	less than ±5.0% of F.S.	less than ±5.0% (±8.0%*) of F.S.
Temperature Resistance (-10°C ~60°C)		less than ±2.5% of Displacement at 20°C	less than ±2.0% of Displacement at 20°C
Frequency Response		more than 2KHz	more than 10KHz
Impact Resistance		more than 200G-3ms	more than 210G-3ms
Weight Increase		less than 1.69Kg	1.62Kg
Shift of Gravitational Center	X	less than ±10mm	4.7mm
	Y	less than ± 5mm	0.0mm
	Z	less than ±10mm	−8.3mm

* Target performance could not be accomplished at some portions in measuring range.

Examples of Practical Applications of 3D-MUSTERDS

Sled tests (50Km/h frontal collision) were carried out using Hybrid III (AM50) dummy equipped with the 3D-MUSTERDS, while the dummy was restrained by three-point seatbelt to determine the displacements of individual portions of the sternum.

The seatbelt webbing locations against the chest were set in two different manners as shown in Figure 3, with reversed positions (on right and left sides) of the shoulder belt anchorage.

Conditions of the sled test are shown in Figure 30, while the examples of displacement measurement data are shown in Figure 31.

It is found that the sternum displacement in X-direction (sternum deflection), the most crucial index for chest injuries differs among different portions on the sternum as anticipated.

It is also found that the difference is particularly significant where the load is applied to the upper portion

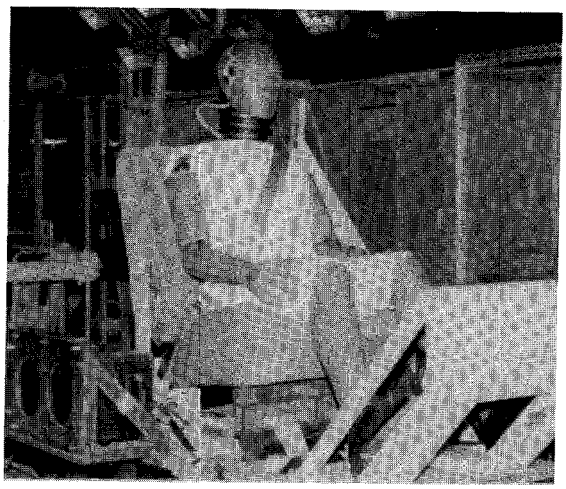

Figure 30. Sled Test Conditions with Hybrid III Dummy

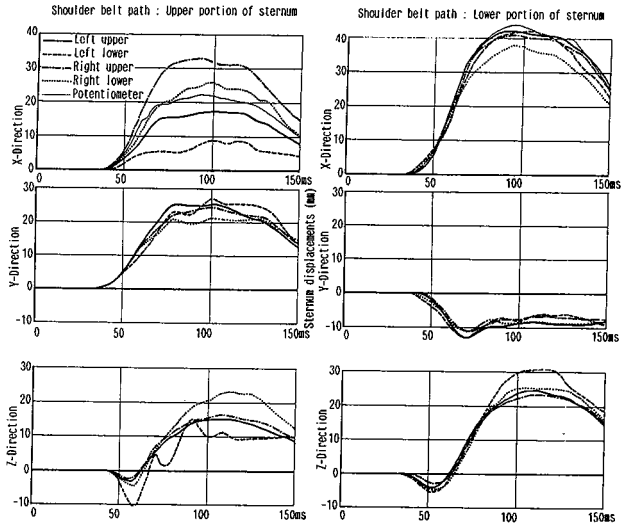

Figure 31. Sternum Displacements in Three Directions at Sled Tests Simulated 50 Km/h Frontal Collision

of the sternum, which does not agree at all with the displacement values measured by conventional potentiometer.

Displacements in Y and Z-directions, which were not determined in the past, are thus made measurable with this 3D-MUSTERDS.

It is verified that much larger displacements than those anticipated by static chest compression tests described earlier occur in dynamic tests.

It is also found that the sternum would displace to the left side by the load application to the upper portion, while it would displace to the right side by the load application to the lower portion, and that the sternum would displace downward first then displace upward in both cases.

Summary

The 3D-MUSTERDS, capable of measuring three dimensional displacements at individual portions of sternum, has been developed for more accurate deter-

mination of chest deflections of Hybrid m dummy in frontal collision tests.

This system detects the spot light of LEDs installed on the sternum of the dummy by means of two PSD cameras fixed to the thoracic spine, and calculates the three dimensional coordinates of the LEDs by using the principle of triangulation method with binocular stereoscopic vision.

This concept was generally used in past where the distance between the measuring point and the camera was sufficiently long, but the author et al. have succeeded in the application of this concept to the narrow space of the dummy rib cage through various studies.

The 3D-MUSTERDS has a simple structure, easy to be installed to a Hybrid m dummy, with excellent frequency response and impact resistance, as well as adequate measuring accuracy in practice.

A number of information on sternum displacements has been obtained through the sled tests carried out with the Hybrid m dummy equipped with this system. As a result, it is verified that the chest deflection alone measured by conventional potentiometer can not represent actual sternum displacements.

It is also found that the sternum makes considerable displacements in lateral and vertical directions also.

Verifications on effects of injury reductions in laboratory collision tests are indispensable to improvements in vehicle structures and occupant protection systems aimed at the reduction of the thoracic injuries of occupants in a traffic accident.

The utilization of 3D-MUSTERDS should provide one of useful means for that.

References

1. Ian V. Lau and David C. Viano, "The Viscous Criterion—Bases and Applications of Injury Severity Index for Soft Tissues;" 30th Stapp Car Crash Conference; SAE Paper 861882.
2. Lothar Grosch, Egon Katz and Lothar Kassing, "Chest Compression Response of Hybrid III with Combined Restraint;" 11th ESV Conference.
3. Takeshi Kasai, Toshiyuki Asahi, Takashi Yoshimori and Saburo Tsuji, "Measurement System of 3-D Motion Using a Pair of Position Sensing Detector Cameras;" Transactions of the Society of Instrument and Control Engineers Vol. 19-12.
4. Toshihiko Tomita, "Design and Product of Distance Sensor Using Position Sensing Detector;" Transistor Technology, Aug. 1990.

S8-W-18

Test Procedures for Defining Biofidelity Targets for Lateral Impact Test Dummies

A.K. Roberts, R.W. Lowne, M. Beusenberg, D. Cesari

European Experimental Vehicles Committee Working Group 9

Abstract

EEVC Working Group 9 published a comprehensive review of the lateral impact cadaver data base at the 1990 IRCOBI Conference in Lyon France. This paper provides a concise description of the test procedures and biofidelity targets which were included in that paper, modified in the light of test experiences. Minor changes have been made to the test procedures and test configurations as further information on the original cadaver tests has become available.

Introduction

Dummies are frequently designed and evaluated against cadaver data. EUROSID-1 dummy, the production version of the EUROpean Side Impact Dummy was based on published lateral impact cadaver data. EEVC Working Group 9 re-examined the available information on cadaver lateral impact response during 1990 and published a critical review of the data. From this review a general set of biofidelity design targets was developed for a lateral side impact dummy for the differing body areas.

The available information was very restrictive and encompassed only a small cadaver base. Unfortunately not all of the cadaver data or test conditions were appropriate for the specification of a crash test dummy. Some of the uncertainties in the data are due to difficulties in test reproducibility whilst others relate to the impact environment, such as impact velocity, test specification or body contact areas.

EEVC Working Group 9, first published their review and performance targets at the 1990 IRCOBI conference. Since the review was published further details of the concerning the original cadaver test procedures were discovered that affected the biofidelity test procedures, particularly with respect to the sled based rigid and padded wall tests. EEVC WG9 subsequently performed a wide ranging biofidelity test programme on the production EUROSID-1 dummy, based on the updated test procedures. During the course of the test programme several minor alterations to the test details were found to be necessary. This paper presents the test procedures and targets on which the EEVC WG9 biofidelity test programme was based. The results of this test programme were presented at the 1991 ESV conference.[1]

EEVC Review

General Review Conclusions

EEVC, having reviewed all of the cadaver data, test procedures and the types and severities of injury seen in accidents decided that some of the cadaver data were not appropriate for use in defining biofidelity targets. They also concluded that some body areas were more important than others and that the test procedures and body areas should be prioritized. WG9 concluded that the head, thorax, abdomen and pelvis should have a high priority rating based on the significance of injuries to these body areas. Although the abdomen is a high priority area based on injuries, the procedure for the biofidelity test based on the lateral drop of a cadaver or dummy, is considered to be poor in that it is very difficult to control the impact conditions precisely. Whilst the neck and shoulder injuries are not currently considered, their behavior may affect the kinematics and thus the impact conditions of other body areas. Therefore their biofidelity is considered but at low priority. It should be noted that ISO has also prepared a set of requirements for a side impact dummy. Although the objectives were the same the design targets are slightly different due to the inclusion and exclusion of different data and slight differences in the definition of effective mass. The Targets and test procedures are more closely defined in this document than the similar ISO documents.[2]

Biofidelity Design Targets

The data from the selected cadaver tests was used to determine a set of biofidelity targets for the dynamic performance of side impact dummies. The masses of the cadavers differ considerably. In order to reduce the scatter due to mass variation, the responses were normalized using a procedure similar to that proposed by Mertz and used by ISO.[2,3] The normalization procedure is summarized in the Appendix. As previously mentioned the targets were divided into two priority areas related to the risk and severity of injury and to the validity and quality of the cadaver data. The biofidelity test procedures closely follow the original cadaver tests and are specified in detail in the section on test procedures.

High Priority Targets

Head

One performance target is specified for the head, in a 200 mm rigid surface drop test based on tests performed by Hodgson and Thomas.[4] The resultant peak head acceleration should be 112g ± 29g.

Thorax

Impactor. This test is based on impactor tests performed on cadavers by HSRI.[5] Two targets are given; normalized impactor force-time response is shown in Figure 1 and Table 1, and normalized dummy T1 lateral acceleration-time response in Figure 2 and Table 2.

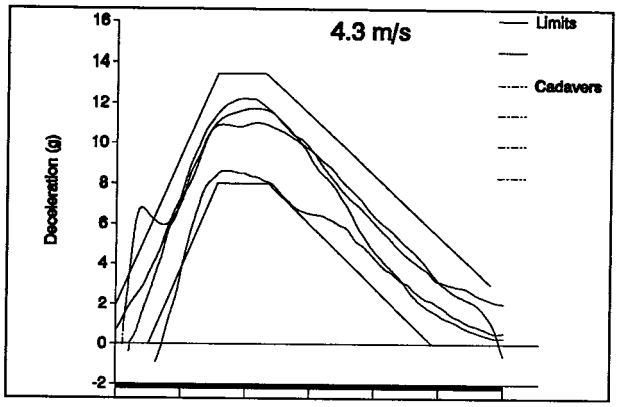

Figure 1. Thorax Impactor Acceleration Target

Table 1. Thorax Impactor Acceleration Corridor Coordinates

Time (ms)	Lower (g)	Upper (g)
0		2.0
5	0	
15.5	8	13.5
24		13.5
24.5	8	
50	0	
58		3.0

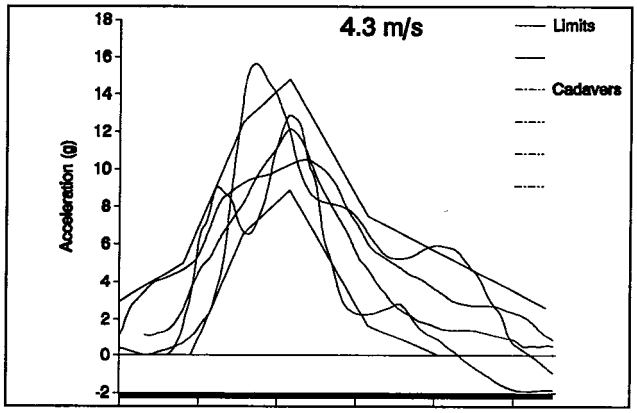

Figure 2. Thorax Impactor T1 Lateral Acceleration

Table 2. Thorax Impactor T1 Acceleration Corridor Coordinates

Time (ms)	Lower (g)	Upper (g)
0		3.0
8		5.0
9	0	
15.5	6.5	12.5
21.5	8.9	14.8
31.5	1.7	7.5
40.5	0	
54		2.7

Sled. These tests are based on sled tests performed at Heidelburg for NHTSA.[6] Targets are given for normalized wall forces for rigid and padded wall impacts. The impact velocities specified take into account the rebound velocities of the original tests.

a. Rigid Wall. The normalized thorax wall force-time target at 7.6 m/s is shown in Figure 3 and Table 3 and the normalized wall force-time target at 10.3 mls is shown in Figure 4 and Table 4.
b. Padded Wall. The normalized thorax wall force-time target at 10.3 m/s into the APR padding is shown in Figure 5 and Table 5.

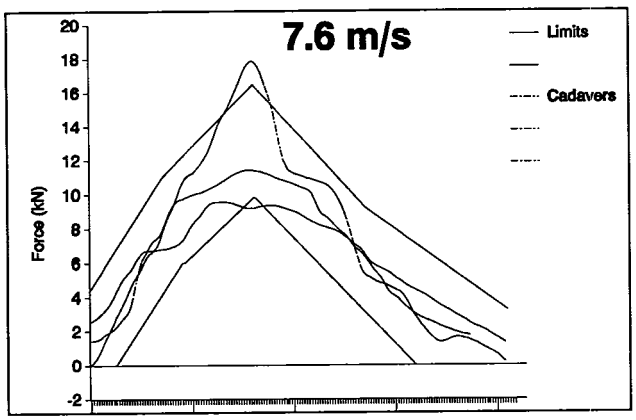

Figure 3. Thorax Rigid Wall Force (7.6 m/s)

Table 3. Thorax Rigid Wall Force Target Corridor Coordinates (7.6 m/s)

Time (ms)	Lower (kN)	Upper (kN)
0		4.5
2.5	0	
7		11.0
9	6.0	
16	9.8	16.5
27		9.25
32	0	
41		3.25

Abdomen

The abdomen target is based on free fall cadaver lateral drop tests performed by APR.[7] For the 1m drop tests on the abdomen, the normalized impact force-time target is shown in Figure 6 and Table 6.

Pelvis

Impactor. The pelvis test and target is based on impactor tests performed by INRETS.[8] A simple peak normalized force-impactor velocity target corridor is shown in Figure 7 and Table 7. The corridor is based on a least squares linear regression model of the results of impactor tests on cadavers:

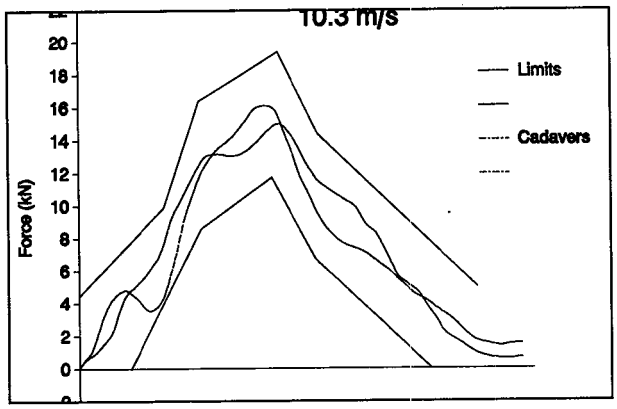

Figure 4. Thorax Rigid Wall Force (10.3 m/s)

Table 4. Thorax Rigid Wall Force Corridor Coordinates (10.2 m/s)

Time (ms)	Lower (kN)	Upper (kN)
0		4.5
6	0	
9.5		9.9
13.5		16.4
14	8.6	
22	11.75	
22.5		19.4
27	6.7	14.4
40	0	
45		5.0

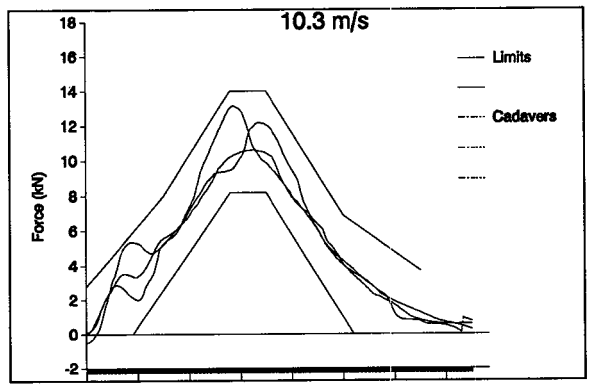

Figure 5. Thorax Padded Wall Force (10.3 m/s)

Force {KN} = -0.62 + 1.066 (Impactor velocity {m/s}.

No fixed impact velocity is prescribed for the tests except that the velocity must be between 6.0 m/s and 10.0 m/s.

Sled. As for the sled test conditions for the thorax, these tests are based on the sled tests performed for NHTSA at Heidelburg.[6] Targets for three configurations of sled test are given.

Table 5. Thorax Padded Wall Force Corridor Coordinates (10.3 m/s)

Time (ms)	Lower (kN)	Upper (kN)
0		2.8
9	0	
15		8.0
28	8.2	14.0
35	8.2	14.0
50		6.9
52	0	
65		3.7

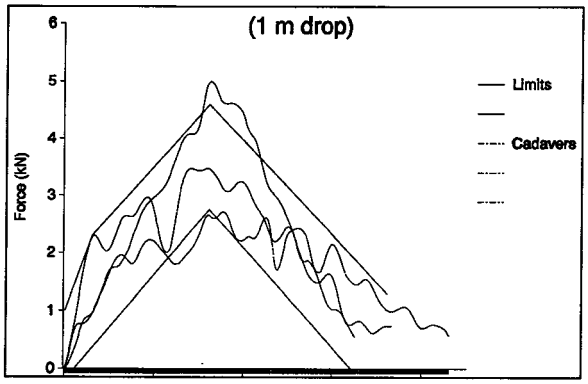

Figure 6. Abdomen Drop Test Force-Time Target (1m)

Table 6. Abdomen Drop Test Force-Time Target Corridor Coordinates (1m)

Time (ms)	Lower (kN)	Upper (kN)
0		1.0
1	0	
3		2.3
16	2.75	4.6
32	0	
36		1.3

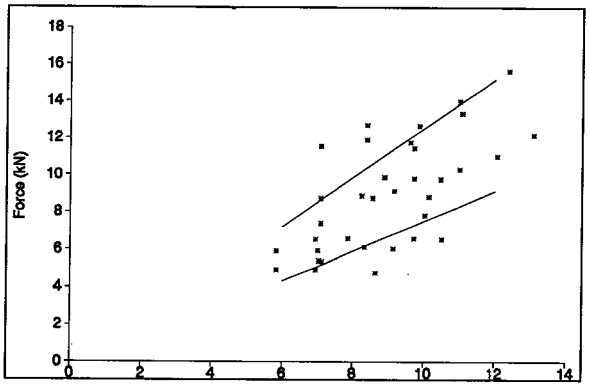

Figure 7. Pelvis Impactor Force-Velocity Target Corridor

Table 7. Pelvis Impactor Target Corridor Coordinates

Velocity (ms)	Upper (kN)	Lower (kN)
6	7.22	4.33
10	12.55	7.53

a. Rigid Wall. Normalized pelvic acceleration target range for impacts at 7.6 m/s and 10.3 m/s.

Normalized pelvis acceleration at 7.6 m/s: 52.7-87.9 g.
Normalized pelvis acceleration at 10.3 m/s: 79.5-132.5 g.

The normalized wall force-time target at 7.6 m/s is shown in Figure 8 and Table 8 and that at 10.3 m/s in Figure 9 and Table 9.

b. Padded Wall. The target range for normalized pelvis acceleration at 10.3 m/s is 65.8 - 109.7 g. The normalized wall force-time target at 10.3 m/s is shown in Figure 10 and Table 10.

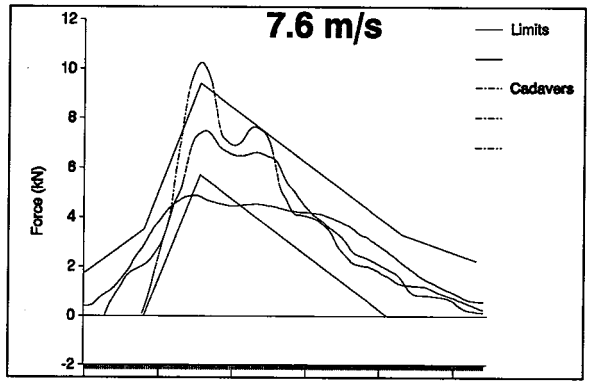

Figure 8. Pelvis Rigid Wall Force Target (7.6 m/s)

Table 8. Pelvis Rigid Wall Force Target Corridor Coordinates (7.6 m/s)

Time (ms)	Lower (kN)	Upper (kN)
0		1.75
8	0	3.5
15.5	5.7	9.4
41	0	3.3
53		2.25

Low Priority Targets

Neck

As the kinematics of the head/neck system are considered to be of some importance, flexion angles and trajectories of the head are defined as biofidelity targets. The test procedure is based on volunteer tests reported by Ewing.[9] Analysis of the original human volunteer data by Wismans et. al.[10] has shown that the response of the head and neck is principally determined by the T1 lateral acceleration and velocity change. Therefore the T1 acceleration is chosen as the main input requirement for neck biofidelity.

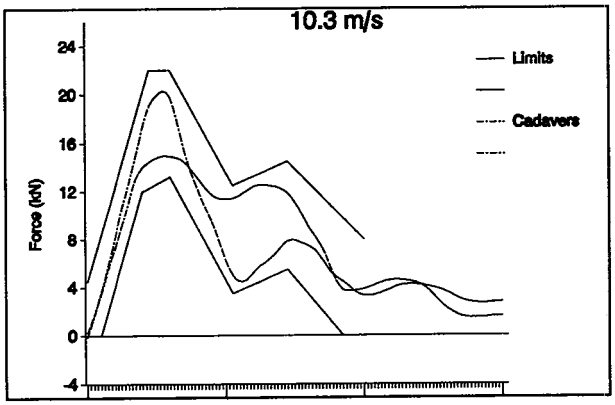

Figure 9. Pelvis Rigid Wall Force Target (10.3 m/s)

Table 9. Pelvis Rigid Wall Force Target Corridor Coordinates (10.3 m/s)

Time (ms)	Lower (kN)	Upper (kN)
0		4.5
1	0	
4	12.0	
4.5		22.0
6	13.25	22.0
10.5	3.2	12.5
14.5	5.5	14.5
17		11.0
18.5	0	
20		8.0

The targets for the neck performance are:

1. Maximum head flexion angle: between 44 and 59 degrees. (The head flexion angle is defined as the angle between the projection of the inferio-superior axis of the head in the plane of impact at t = O and the time to maximum head flexion).
2. Maximum horizontal displacement of the centre of gravity of the head: between 130 and 162 mm. (The horizontal displacement of the head centre of gravity is defined as the relative displacement of the centre of gravity of the head, projected in the plane of impact measured in the $T1_y$ direction, between t = O and the time of maximum horizontal displacement of head centre of gravity).
3. Maximum vertical displacement of the centre of gravity of the head: between 64 and 94 mm. (The downward vertical displacement of the head centre of gravity is defined as the relative displacement of the centre of gravity of the head, projected in the plane of impact and measured in the $T1_z$ direction, between t = 0 and the time of maximum horizontal displacement of head centre of gravity).

Note: $T1_z$ = Vertical direction, $T1_y$ = Lateral impact direction and $T1_x$ is the forward direction (perpendicular to the $T1_z$ and $T1_y$ directions).

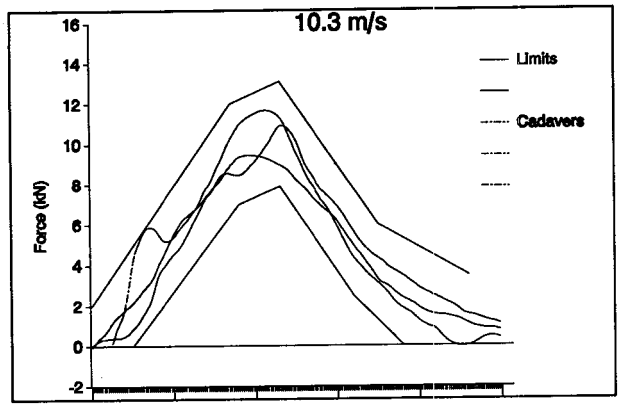

Figure 10. Pelvis Padded Wall Force Target (10.3 m/s)

Table 10. Pelvis Padded Wall Force Target Corridor Coordinates (10.3 m/s)

Time (ms)	Lower (kN)	Upper (kN)
0		2.0
5	0	
17		12.0
18	7	
23	7.9	13.1
32	2.5	
35		6.0
38	0	
46		3.5

Shoulder

Two test conditions for the shoulder are described; a dynamic test based on studies by APR,[11] and a quasi static test based on tests reported by Lowne et al.[12] For the dummy, the dynamic performance is more significant than the quasi static test, which is intended to ensure sufficient lateral displacement of the shoulder. Since clear, unambiguous dynamic displacement data are not available, a displacement-time target corridor is not specified. The targets for the shoulder are a normalized impactor force-time corridor and a minimum displacement requirement.

Dynamic target. The normalized shoulder force-time target corridor is shown in Figure 11 and Table 11. Normalized shoulder deflection: at least 32 mm.

Static target. Lateral displacement of the shoulder plunger relative to the spine under a 200 N lateral force: 55 mm.

Biofidelity Test Procedures

All of the biofidelity tests should be performed in a temperature controlled environment regulated between 20°C ± 2°C. It should be noted that some of the test

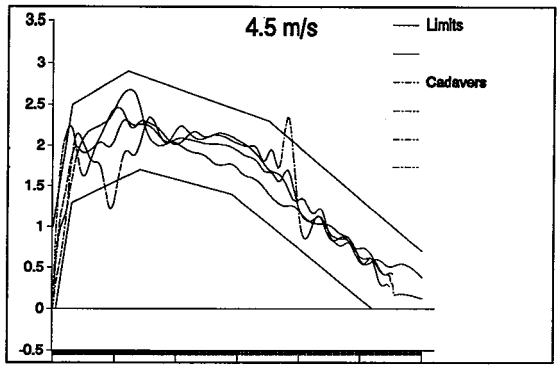

Figure 11. Shoulder Impactor Force-Time Target Corridor

Table 11. Shoulder Impactor Force Target Corridor Coordinates

Time (ms)	Lower (kN)	Upper (kN)
0		1.0
0.5	0	
3	1.3	2.5
12		2.9
14	1.7	
29	1.4	
35		2.3
52	0	
60		0.7

procedures may be different from those specified in the EUROSID Users' Manual used for dummy certification (eg: Impactor specification for the dynamic shoulder test). The procedures described in this paper are based as closely as possible on the original cadaver test procedures with appropriate setting up procedures defined for dummy evaluation.

Head Drop Test Procedure

Test description. The test is to be conducted using only the dummy's head. The head is to be positioned with a 200 mm ± 2 mm space between it and a flat, rigid impact surface. The impact surface is to be horizontal and the head oriented so that its midsagittal plane makes an angle of 35° with the impact surface and its anterior-posterior axis is horizontal. A quick release mechanism is required to drop the head onto the impact surface. The added mass of the support mechanism should not exceed 70 gm.

Test instrumentation. The dummy head is instrumented with a triaxial accelerometer located at its centre of gravity.

Data processing. Accelerations are to be filtered using to CFC 1000. No normalization procedures are defined for this configuration.

Neck Test Procedure

Test description. The sled acceleration should lie within the corridor specified in Figure 12 and Table 12. The measured T1 lateral acceleration must also meet the corridor specified in Figure 13 and Table 13. Since neck biofidelity is considered, the T1 lateral acceleration is of more importance than the sled deceleration. Therefore slight deviations in sled acceleration from the corridor specified in Figure 12 and Table 12 can be tolerated provided the T1 lateral acceleration meets the corridor specified in Figure 13 and Table 13. Sled velocity should be 6.9 ± 0.2 m/s.

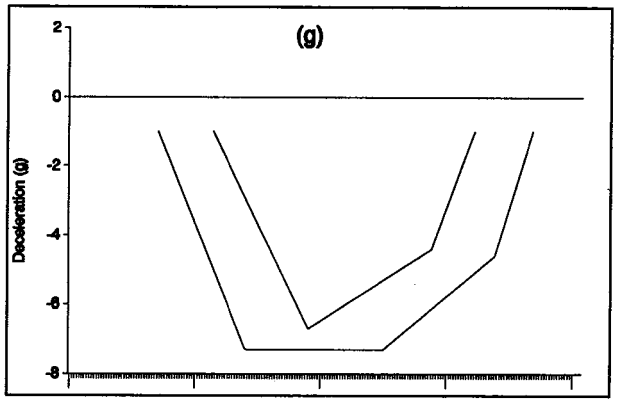

Figure 12. Sled Acceleration for the Ewing Neck Test

Table 12. Sled Acceleration Corridor Coordinates for the Ewing Neck Test

Time (ms)	Upper (g)	Lower (g)
35		-1.0
57	-1.0	
71		-7.3
95	-6.7	
125		-7.3
144	-4.4	
161	-1.0	
169		-4.6
184		-1.0

The complete dummy is to be seated in a nominally upright position in a test seat, functionally similar to the one used by Ewing. The test seat should be rigidly mounted on a sled, facing sideways (90°) to the direction of sled travel. A vertical, lightly padded side board is to be rigidly attached to the seat to restrict upper torso rotation and pelvis translation of the dummy. The top of the sideboard should extend to a level 40 to 50 mm below the top of the dummy's shoulder. The dummy should be positioned against the vertical side board such that the midsagittal plane of the dummy is vertical and perpendicular to the direction of sled travel. The thorax movement is to be restrained with a strap attached to the

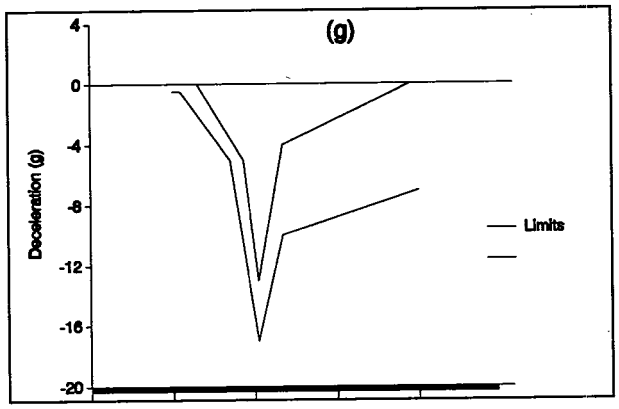

The time 't' for the T1 lateral acceleration is 50 ms after t = 0 of the sled acceleration corridor.

Figure 13. T1 Lateral Acceleration for Neck Test

Table 13. T1 Lateral Acceleration Corridor Coordinates for Neck Test

Time (ms)	Upper (g)	Lower (g)
t	0.0	-0.5
t+ 5		-0.5
t+ 15	0.0	
t+ 35		-5.0
t+ 43	-5.5	
t+ 52	-13.0	-17.0
t+ 67	-4.0	-10.0
t+145	0.0	
t+150		-7.0

back of the seat to limit shoulder forces. The pelvis is to be restrained by a lap belt and inverted 'V' pelvis strap tied to the lap belt. Both arms should be positioned alongside the thorax and restrained with suitable straps. The anterior-posterior axis of the head is to be horizontal.

Test instrumentation. The dummy is to be instrumented with a uniaxial accelerometer at the base of the neck (T1) with its sensitive axis directed laterally. Also the sled acceleration is to be measured. Photographic targets for measuring head c.g. translation in horizontal and vertical direction relative to T1, head rotation (angular rotation of the inferior-superior axis of the head relative to the vertical) and the horizontal translation of the base of the neck (T1) relative to the sled are necessary. Sufficient cameras are required to record all the relevant dummy and head displacements. Neck accelerations should be measured to CFC 180.

Data processing. No normalization procedures are defined for the neck test.

Shoulder Impactor Test Procedure

Test description. The shoulder impactor test shall be performed on a complete dummy using a linearly guided impactor. The impactor mass shall be 23.4 kg with a smooth flat face 6" diameter, the edge of the impact face being relieved with a 6mm radius. The dummy shall be seated upright with no additional lateral supports on a flat horizontal rigid surface with the legs straight and parallel. The arms shall be positioned parallel to the thorax. The axis of the impactor shall be aligned with the shoulder pivot ± 10 mm and at 90° to the mid sagittal plane. Impact velocity at the point of impact shall be 4.5 m/s ± 0.1 m/s.

Test instrumentation. For/aft impactor acceleration shall be measured according to CFC 180. Photographic targets should be fixed to the impactor and the dummy upper thoracic spine to calculate the shoulder deflection relative to the spine from high speed film. The external shoulder displacement is defined as the lateral displacement of the face of the impactor relative to the upper thoracic spine perpendicular to the anterior posterior axis of the dummy.

Data processing. Impactor acceleration shall be normalized according to the procedure described in the Appendix based on a thorax standard mass (M_s) of 20.5 kg.

Shoulder Quasi-Static Test Procedure

Rigidly support the thorax of the dummy in a vertical position to prevent lateral translation of the spine. Adjust the upper arm to a position of 40° forward of the torso line. Apply a lateral force to the outer extremity of the shoulder, adjacent to the arm pivot, with a 50 mm diameter plunger. Allow the shoulder and plunger to displace in any direction and record the maximum lateral displacement of the plunger with respect to the spine with an applied lateral force of 200N.

Thorax Impactor Test Procedure

Test description. The thorax impactor test shall be performed on a complete dummy using a linearly guided impactor. The impactor shall have a mass of 23.4 kg and a smooth flat face 6" diameter. The dummy shall be seated upright with no additional lateral support on a flat horizontal rigid surface with the legs straight forward and parallel. Both arms shall be positioned vertically upright above the head. The axis of the impactor shall be aligned with centre of the rib cage (vertically and laterally), at 90° to the mid-sagittal plane. The impact velocity shall be 4.3 m/s ± 0.1 m/s.

Test instrumentation. The fore/aft impactor acceleration and the T1 lateral acceleration shall be measured according to CFC 1000 and filtered with a 100 Hz Finite Impulse Filter (FIR). (The FIR filter programme is available to EUROSID users from TNO.)

Data processing. Impactor and dummy accelerations shall be normalized according to the procedure described in the Appendix based on a thorax standard thorax mass (M_s) of 29.6 kg.

Abdomen Drop Test Procedure

Test description. The dummy is to be suspended above the impact surface with its midsagittal plane horizontal and its abdominal region in line with the top surface of

the armrest. The armrest should contact the abdomen section just superior to the iliac crest and without interfering with the lower thoracic ribs. The simulated armrest is constructed of rigid hardwood. The armrest is 7 cm in width and should protrude 4.1 cm above the surrounding surface (Ref 7, Fig 1). The length of the armrest must be sufficient to prevent the dummy from striking the ends. The arm on the impact side is positioned 40° forward such that no contact with the arm takes place. The surrounding surface is made of hardwood and should be large enough to prevent the dummy from striking the edges. A quick-release mechanism is to be used to drop the dummy from a distance of 1 m measured between abdomen and armrest.

Test instrumentation. The simulated armrest is to be mounted on a piezoelectric load cell. If a piezoelectric load cell is not used the armrest must also be fitted with a uniaxial accelerometer, mounted vertically. Additionally lateral acceleration at T12 should also be recorded for normalization procedures. Forces and accelerations should comply with CFC 180.

Data processing. If a piezoelectric load cell is not used the load cell must be inertia compensated according to Equation 1. High speed camera coverage is required to determine abdominal penetration. Abdomen penetration is defined as the vertical displacement of the thoracic spine (directly over the armrest) relative to the top surface of the armrest measured from the time of first contact of the abdominal surface with the armrest. Impactor forces are to be normalized according to the procedure described in the Appendix based on an abdominal standard mass (M_s) of 16.4 kg.

Pelvis Impactor Test Procedure

Test description. The pelvis impactor test is performed on a complete dummy. The dummy should be sat on a fixed seat shown in Figure 14. The foam material used for the seat should be a polyethylene foam 40 mm thick having a density of 47.0 kg/m^3 or an alternative with similar properties. The upper arms should be positioned alongside the thorax (0°) and no addition lateral support to the dummy is to be given. The legs of the dummy shall be positioned perpendicular to the impact direction and parallel with each other. The linearly guided impactor shall have a mass of 17.3 kg and a smooth spherical impact face of radius 175 mm and a outer diameter of 120 mm. Impact velocity must be between 6.0 m/s and 10.0 m/s, the axis of the lateral impact being centred on the hip pivot point.

Test instrumentation. Impactor acceleration and pelvic acceleration shall be measured according to CFC 1000.

Data processing. The impactor acceleration shall be normalized according the procedure described in the Appendix based on a pelvic standard mass of (M_s) of 14.5 kg.

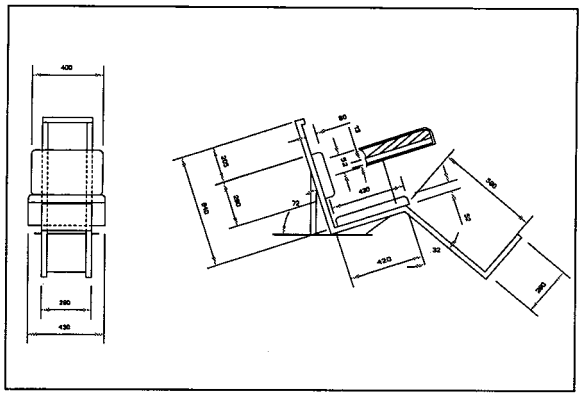

Figure 14. Pelvic Impactor Test Seat

Whole Body Sled Test Procedure

Test description. The whole body tests can be performed on either a standard deceleration impact sled or on a HYGE impact sled. The sled must be fitted with a rigid vertical impact wall onto which two force measuring plates are fitted. Perpendicular to the rigid wall a rigid low friction bench seat is attached in line with the motion of travel of the sled. The dimensions of the test seat and force measuring load cells are given in Figure 15. (The sliding test seat used by the University of Heidelberg for the cadaver tests was 1.5 m in length.) Since precise positioning of the horizontal slats is not available, the slats can be replaced by an alterative low friction surface for dummy testing. The dummy must be supported vertically on the non struck side during the acceleration phase of a non HYGE impact sled. The arms of the dummy are to be placed alongside the thorax (0°). Impacts are to be performed into the rigid wall at two impact velocities 7.6 and 10.3 m/s. One further test is to be performed at 10.3 m/s into the same wall onto which two foam blocks are mounted. Impact velocity tolerance shall be ± 0.1 m/s. The specified impact velocity includes any rebound velocity that may exist with a deceleration type sled. On both types of test sled the dummy must strike the wall at the prescribed velocity. The block specification is described in Section 3. The upper pad is to be located on the thorax force plate, the upper surface of the pad being in line with the top edge of the plate, parallel to the seat pan. The lower pad is to be located on the pelvis plate with the lower surface of the pad resting on the seat pan. Note: It is advisable to restrain the legs from excessive lateral articulation after the dummy strikes the wall in order to prevent damage to the knee joints.

Test instrumentation. Plate forces shall be measured CFC 1000 and lateral dummy accelerations at T1 and at the pelvis CFC 180. The force measuring plates are to be inertia compensated by placing an accelerometer in the centre of each force plate, its axis perpendicular to the surface of the plate.

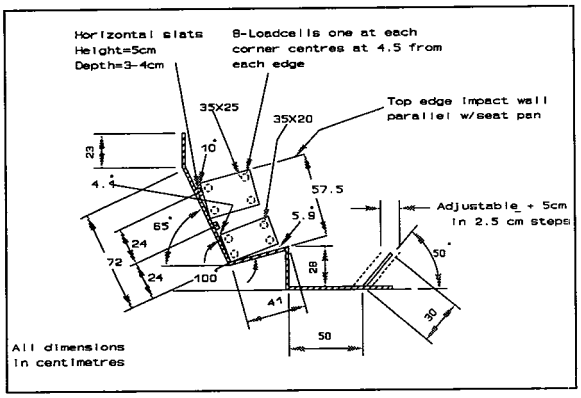

Figure 15. Heidelburg Impact Sled Seat

Data processing. The resultant, inertia compensated, forces derived using Equation 1.

$$F_i = \sum F_{plate} + (M_{plate} A_{plate}) \quad (1)$$

Where

F_i = Inertia compensated plate force

F_{plate} = Plate force

M_{plate} = Mass of plate

A_{plate} = Acceleration of plate, where acceleration is positive in the direction of impact of the dummy.

All forces and dummy accelerations must be normalized according to the procedure described in the Appendix to a standard mass (M_s) of 37.0 kg for the thorax and a standard mass M_s of 24 kg for the pelvis, and both filtered with a 100 Hz FIR filter.

Appendix

Data Processing and Normalization

To permit comparisons between cadaver and dummy tests and dummy to dummy tests common data processing procedures must be adopted. The following sections detail the methods that should be used to enable valid comparisons to be made.

Instrumentation and Data Processing

All instrumentation and filtering is to meet the ISO standard—ISO 6487:1987[13]—and recommended Channel Filter Classes (CFC). Wall forces for the sled impacts and impactor forces for the thorax impactor tests must be filtered using a 100hz Finite Impulse Filter (FIR). (A copy of a recommended FIR Fortran filtering programme called 'THRXINJ' is available to EUROSID users from IW-TNO, the suppliers of the dummy.)

Time zero does not exist for most of the biofidelity assessment tests, therefore all responses should be time shifted by eye to give the best match to the overall shape of the target corridors.

Normalization Procedures

To reduce variations in cadaver output and test conditions all data channels for the targets have been normalized according to a procedure developed by Mertz and Lowne and detailed in the ISO requirements.[2,3] For the biofidelity tests all of the data must be normalized in a similar way to reduce scatter due to test setup variability. Normalization procedures are defined for the appropriate test condition. Impactor normalization is based on a two mass spring model while the sled and drop tests on a single mass spring model, since the effective mass of the striking object is infinite.

To perform normalization a standard effective mass for the associated body part is required. In this analysis the effective mass for each cadaver has been derived from the original transducer records. As the effective mass of the body varies during the period of the test, a decision has to be made regarding the time at which the effective mass should be defined. For normalization, this is not too critical provided the same definition is used for the dummy tests. For the thorax impactor tests this was selected to be when the impactor velocity was at a common velocity with the lateral velocity of the spine. For the shoulder and pelvis this was taken to be at the end of the main pulse as there was no means of determining the time of common velocity in the base cadaver tests. In the sled tests the effective mass is taken at the end of the main wall force pulse. The standard body part mass was then determined for each group of cadavers in the test—Equation 2. In determining the standard masses for the thorax and pelvis in the wall tests an average standard mass for all three test conditions has been taken although the data suggests that different values for the three different test conditions would be appropriate.

Table 14 gives the standard masses derived from this analysis. These standard masses should be used for the dummy normalization procedures. For cadaver-to-dummy comparisons to be made, normalization of the cadaver and dummy data must be based on the same standard mass. The body part standard masses used in this analysis will in some instances be different from those of other analyses as the cadaver sample on which this study is based may differ.

$$M_s = 76 * \left(AVERAGE \left[\frac{Effective\ body\ part\ mass}{Total\ cadaver\ mass} \right] \right) \quad (2)$$

Table 14. Normalization Standard Effective Masses

Test Procedure	Body Part Standard Effective Mass (kg)
Shoulder impactor	20.5
Thorax impactor	29.6
Abdomen drop	16.4
Pelvis impactor	14.5
Rigid and Padded wall	
Upper force (thorax)	37.0
Lower force (pelvis)	24.0

Single spring-mass system. For the purposes of normalizing the results of the sled impacts and the drop tests, the cadaver and dummy can be considered to be modelled by a single mass-spring system impacting an infinite mass.

Under these conditions the equations of motion of the mass are:

$$x = V_0 \sqrt{\frac{M}{k}} \sin\left(\sqrt{\frac{k}{M}}\, t\right) \tag{3}$$

$$\ddot{x} = -V_0 \sqrt{\frac{k}{M}} \sin\left(\sqrt{\frac{k}{M}}\, t\right) \tag{4}$$

Where

V_0 is the impact velocity

M is the effective body mass, and

k is the spring stiffness.

Displacement, force, acceleration and time can then all be normalized to a standard (s) set of values from the observed value in the 'i'th test (i). Thus

$x_s = x_i * R_x$ (Displacement normalization)

$F_s = F_i * R_f$ (Force normalization)

$\ddot{x}_s = \ddot{x}_i * R_a$ (Acceleration normalization)

$t_s = t_i * R_t$ (Time normalization)

Where M_s and K_s are the standard effective mass and standard stiffness.

$$R_x = \sqrt{\frac{M_s}{M_i}} * \sqrt{\frac{K_i}{K_s}} \tag{5}$$

$$R_f = \sqrt{\frac{M_s}{M_i}} * \sqrt{\frac{K_s}{K_i}} \tag{6}$$

$$R_a = \sqrt{\frac{M_i}{M_s}} * \sqrt{\frac{K_s}{K_i}} \tag{7}$$

$$R_t = \sqrt{\frac{M_s}{M_i}} * \sqrt{\frac{K_i}{K_s}} \tag{8}$$

M_i and K_i are the effective mass and stiffness for test 'i'.

These factors were used to normalize the cadaver data using characteristic cadaver body dimensions as a substitute for stiffness (see Ref 3).

The same equations are used to normalize the dummy test results. Under these conditions, $K_i = K_s$, M_s is the standard effective mass from the cadaver tests and M_i is the effective mass determined in each test with the dummy.

Thus the normalizing factors for the sled and drop tests with the dummy become:

Displacement:

$$R_x = \sqrt{\frac{M_s}{M_i}} \tag{9}$$

Force:

$$R_f = \sqrt{\frac{M_s}{M_i}} \tag{10}$$

Acceleration:

$$R_a = \sqrt{\frac{M_i}{M_s}} \tag{11}$$

Time:

$$R_t = \sqrt{\frac{M_s}{M_i}} \tag{12}$$

Spring—two mass system. For the impactor tests, the normalization is based on a spring and two mass model (Figure 16).

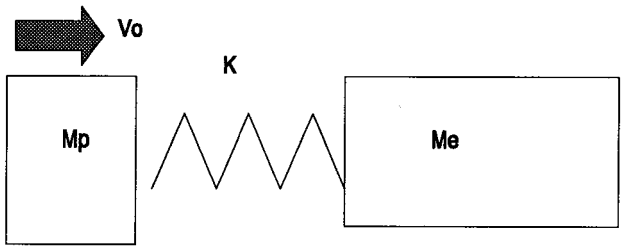

Figure 16. Two Mass—Spring Model

The relevant equations of motion for this system are:

$$x_p = \sqrt{\left(\frac{M_p}{K}\right)} \left(\frac{M_e}{M_p+M_e}\right)^{\frac{3}{2}} \sin\sqrt{\left(\frac{K(M_p+M_e)}{M_pM_e}\right)} t + \left(\frac{M_pV}{M_p+M_e}\right) t \tag{13}$$

$$\ddot{x}_p = \sqrt{\left(\frac{K}{M_p}\right)} \sqrt{\left(\frac{M_e}{M_p+M_e}\right)} \sin\sqrt{\left(\frac{K(M_p+M_e}{M_pM_e}\right)} \cdot t \tag{14}$$

$$x_b = \sqrt{\left(\frac{M_e}{K}\right)} \left(\frac{M_p}{M_p+M_e}\right)^{\frac{3}{2}} \sin\sqrt{\left(\frac{K(M_p+M_e)}{M_pM_e}\right)} t + \left(\frac{M_pV}{M_p+M_e}\right) t \tag{15}$$

$$\ddot{x}_e = -\sqrt{\left(\frac{K}{M_e}\right)} \sqrt{\left(\frac{M_p}{M_p+M_e}\right)} \sin\sqrt{\left(\frac{K(M_p+M_e}{M_pM_e}\right)} \cdot t \tag{16}$$

Where x_p, $\ddot{x}_p$ and M_p are the displacement, acceleration and mass of the impactor and x_b, $\ddot{x}_b$ and M_e are the displacement, acceleration and effective mass of the body part.

Impactor force and acceleration can be normalized according to the equations:

$F_{p(s)} = F_{p(i)} * R_p$ (Impactor force normalization)

$\ddot{x}_{p(s)} = \ddot{x}_{p(i)} * R_p$ (Impactor acceleration normalization)

and the body part response can be normalized according to:

$\ddot{x}_{b(s)} = \ddot{x}_{b(i)} * R_b$ (Cadaver or dummy acceleration normalization)

The time can be normalized using:

$$t_{(s)} = t_{(i)} * R_t$$

where the (s) suffix refers to the results normalized to the standard mass, the (i) suffix to the result of the 'i'th test, the 'p' suffix refers to impactor readings while the 'b' suffix refers to responses measured on the cadaver or dummy.

The normalizing factors are given by:

$$R_p = \sqrt{\left(\frac{K_s}{K_i}\right)} \cdot \sqrt{\left(\frac{M_e(s)}{M_e(i)}\right)} \cdot \sqrt{\left(\frac{M_p + M_e(i)}{M_p + M_e(s)}\right)} \quad (17)$$

$$R_b = \sqrt{\left(\frac{K_s}{K_i}\right)} \cdot \sqrt{\left(\frac{M_e(i)}{M_e(s)}\right)} \cdot \sqrt{\left(\frac{M_p + M_e(i)}{M_p + M_e(s)}\right)} \quad (18)$$

$$R_t = \sqrt{\left(\frac{K_i}{K_s}\right)} \cdot \sqrt{\left(\frac{M_e(s)}{M_e(i)}\right)} \cdot \sqrt{\left(\frac{M_p + M_e(i)}{M_p + M_e(s)}\right)} \quad (19)$$

These equations have been used to normalize the cadaver responses for the impactor tests using a characteristic cadaver body dimension to represent K.

These equations are used also to normalize the dummy data, but here $K_i = K_s$ and the equations reduce to:-

$$R_p = R_t = \sqrt{\left(\frac{M_e(s)}{M_e(i)}\right)} \cdot \sqrt{\left(\frac{M_p + M_e(i)}{M_p + M_e(s)}\right)} \quad (20)$$

$$R_b = \sqrt{\left(\frac{M_e(i)}{M_e(s)}\right)} \cdot \sqrt{\left(\frac{M_p + M_e(i)}{M_p + M_e(s)}\right)} \quad (21)$$

For dummy response normalization, the effective mass for the body part in the test, $M_{e(i)}$, should be established as described below, while the standard effective mass, $M_{e(s)}$, is taken from Table 14.

Impactor Normalization

Shoulder. a) Determine the effective mass of the shoulder area using Equation 22. The effective mass should be evaluated by integration to the end of the initial impactor pulse.

$$M_e = \frac{\int F_p \, dt}{V_0} \quad (22)$$

Where

M_e = Effective mass of the body part (kg)
F_p = Impactor force (N)
V_0 = Lateral impact velocity (m/s)

b) Normalize the impactor force and time using Equation 20.

Thorax. a) Determine the effective mass of the dummy part using Equation 23. The effective mass should be determined when the impactor and dummy are at a common velocity by integrating to the time when the velocity of the impactor equals that of T1. (On the first occasion if two should exist.)

$$M_e = \frac{\int M_p \ddot{x}_p \, dt}{\int \ddot{x}_b \, dt} \quad (23)$$

Where

M_e = Effective mass of the body part (kg)
M_p = Mass of the impactor (kg)
x_p = Impactor acceleration (m/s^2)
x_b = Body part lateral acceleration at T1 (m/s^2)

b) Normalize the impactor acceleration and the time using Equation 20 and the thorax acceleration using Equation 21.

Pelvis. a) Determine the effective mass of pelvis area of the dummy using Equation 24. The effective mass should be evaluated by integration to the end of the initial impactor pulse.

$$M_e = \frac{\int F_p .dt}{V_0} \quad (24)$$

Where

M_e = Effective mass of the body part (kg)
F_p = Impactor force (N)
V_0 = Lateral impact velocity (m/s)

b) Normalize the impactor acceleration and the time using Equation 20 and the thorax acceleration using Equation 21.

Abdomen drop test. a) Determine the effective mass of the abdomen part using Equation 25. The effective mass should be evaluated by integration to the end of the initial impactor pulse.

$$M_e = \frac{\int F_a .dt}{\int \ddot{x}_{T12} .dt + (T*g)} \quad (25)$$

Where

M_e = Effective mass of abdomen (kg)
F_a = Force on the armrest (N)
x_{T12} = Lateral acceleration of T12 (m/s^2)
T = Pulse length (s)
g = gravity (m/s^2)

b) Normalize the armrest force using Equation 10, time using Equation 12 and displacement by Equation 9.

Sled Normalization

a) Determine the effective mass of the dummy part (thorax and pelvis) using Equation 26. The effective mass should be taken at the end of the initial wall force for the appropriate body part.

$$M_e = \frac{\int F .dt}{V_0} \quad (26)$$

Where

M_e = Effective mass of the body part (kg)
F = Compensated impact wall force (kN)
V_0 = Initial impact velocity (m/s)

Note: V_0 should be taken to be the same as for the thorax, even though the profile of the seated dummy will cause the pelvis to impact the wall after the shoulder/thorax complex. It should be assumed that at the time of impact of the pelvis the dummy-to-wall velocity has not decreased.

b) Normalize the wall forces using Equation 10, dummy acceleration using Equation 11 and time using Equation 12.

Specification of Impact Padding

The sled test padded wall padding was developed by APR. The polyurethane foam blocks were 140mm x 140mm x 420mm with a density of 135 → 150 gm/l. The quasi-static force/deflection characteristics (with a loading rate of 100 mm/min) are shown in Ref 2.

Acknowledgements

Participating members of EEVC Working Group 9 are: M. Beusenberg, D. Cesari, K-P. Glaeser, E.G. Janssen, R.W. Lowne (Chairman), A. Pastorino, A.K. Roberts (Secretary).

References

1. Roberts A.K. The Biofidelity of the Production Version of the European Side Impact Dummy EUROSID-1 Thirteenth ESV Conference. Paris France. 1991.
2. ISO Technical Reports 9790 1-6. (a) ISO/TC22 Road Vehicles—Anthropomorphic Side Impact Dummy—Lateral Head Response Requirements to Assess the Biofidelity of the Dummy. ISO/DTR 9790-1 Ref No ISO/TC22/SC22/WG5 N1554 E. (b) ISO/TC22 Road Vehicles—Anthropomorphic Side Impact Dummy—Lateral Neck Response Requirements to Assess the Biofidelity of the Dummy. ISO/DTR 9790-2 Ref No ISO/TC22/SC22/WG5 N1554 E. (c) ISO/TC22 Road Vehicles—Anthropomorphic Side Impact Dummy—Lateral Shoulder Response Requirements to Assess the Biofidelity of the Dummy. ISO/DTR 9790-3 Ref No ISO/TC22/SC22/WG5 N1554 E. (d) ISO/TC22 Road Vehicles—Anthropomorphic Side Impact Dummy—Lateral Thoracic Response Requirements to Assess the Biofidelity of the Dummy. ISO/DTR 9790-4 Ref No ISO/TC22/SC22/WG5 N1554 E. (e) ISO/TC22 Road Vehicles—Anthropomorphic Side Impact Dummy—Lateral Abdominal Response Requirements to Assess the Biofidelity of the Dummy. ISO/DTR 9790-5 Ref No ISO/TC22/SC22/WG5 N1554 E. (f) ISO/TC22 Road Vehicles—Anthropomorphic Side Impact Dummy—Lateral Pelvic Response Requirements to Assess the Biofidelity of the Dummy. ISO/DTR 9790-6 Ref No ISO/TC22/SC22/WG5 N1554 E.
3. Mertz H J. A Procedure for Normalizing Impact Response Data. SAE paper 840884, Warrendale, PA. USA. 1984.
4. Hodgson V R and L M Thomas. Head Impact Response. Wayne State University School of Medicine. Vehicle Research Institute Report VRI 7.2 SAE. 1975.
5. Robbins D H, R J Lehman and K Augustyn. Prediction of Thoracic Injuries as a Function of Occupant Kinematics. Proc. 7th. ESV Conf. Paris, 1979.
6. Eppinger R H, K Augustyn and D H Robbins. Development of a Promising Universal Thoracic Trauma prediction Methodology. Proc. 22nd Stapp Car Crash Conf. SAE paper 780891. 1978.
7. Walfisch G, A Fayon, C Tarriere, J Rosey, F Guillon, C Got, A Patel and R Stalnaker. Designing a Dummy;'s Abdomen for Detecting Injuries in Side Impact Collisions. Proc 5th IRCOBI Conf. Birmingham, 1980.
8. Cesari D, M Ramet and R Bouquet. Tolerance of Human Pelvis to Fracture and Proposed Pelvic Protection Criteria to be Measured on Side Impact Dummmies. Proc Ninth ESV Conf. 1982.
9. Ewing, C L, D J Thomas, P L Majewski, R Black and L Lustik. Measurement of Head, T1 and Pelvic Response to -Gx Impact Acceleration. Proc 21st Stapp Car Crash Conf. Oct. 1986. SAE paper 861893.
10. Wismans, J., H. van Oorchot, H.J. Woltring, Omni-Directional Human Head-Neck Response. 30th Stapp Car Crash Conference, San Diego, California USA, Oct. 1986. SAE paper 861893.
11. Bendjellal, F, G Walfisch, A Fayon and C Tarriere. APR Biomechanical Data. APR, Nanterre, France 1984.
12. Lowne R W and A K Roberts, Design of t he MIRA Side Impact Dummy (Appendix). Page 357, Biomechanics of Impacts in Road Accidents—Proceedings of the seminar held in Brussels 21-23 March 1983.
13. ISO 6487:1987 Roads Vehicles—Techniques of measurement in impact tests—Instrumentation.

S8-W-19

Influence of the Seat and Head Rest Stiffness on the Risk of Cervical Injuries in Rear Impact

J.Y. Foret-Bruno, F. Dauvilliers, C. Tarriere, P. Mack
Renault

Abstract

A seat with an integral seat belt is a means by which the occupant can be restrained more effectively in the case of frontal impact. This of course involves stiffening the seat back whose current relative fragility limits the risk of cervical injury to occupants involved in rear impact at impact speeds over 20 - 25 km/h. This study addresses the question of what solutions exist which guarantee adequate protection against cervical injury in the case of rear impact with a stiffened seat, while still ensuring the higher restraint effectiveness desired in the case of frontal impact. The study consists of the following:

- accidentology study of the frequency and severity of injuries to occupants in rear impact accidents, taking into account the presence or absence of a head rest and the seat's resistance upon impact.
- definition of the accident conditions in which the greatest risk of cervical injury occurs so as to relate this risk to neck load measurements carried out on a Hybrid III dummy.
- tests carried out using a Hybrid III dummy, manipulating the following variables—the horizontal head/head rest distance, head rest stiffness, seat back elasticity, and impact speed, in order to study the influence of these variables on dummy neck measurements.
- presentation of the response limitations of the Hybrid III dummy.
- recommendations for obtaining adequate protection in current and future vehicle models.

Accidents Involving Injuries—The Current Situation

The Peugeot S.A./Renault Laboratory of Accidentology and Biomechanics currently has accident data involving 8,000 vehicles and approximately 15,000 occupants. Detailed data analysis of impact severity, occupants' condition, and injury types has made it possible to better describe rear impact and its consequences.

Rear Impact Compared to Other Impact Types

Rear impact is statistically less frequent and less severe than frontal or side impact. It represents 7% of those involved in accidents, 3 to 4% of serious injuries and 1 to 2% of fatalities.

The risk of being seriously injured in the case of rear impact is approximately 5 times less than in the case of frontal impact. In fatal rear impact accidents, 20% of the striking vehicles are cars while 65% are heavy trucks, the remaining 15% are due to stationary obstacles.

The Frequency of Cervical Injury

Cervical injuries (all levels of severity) are the most frequent in the case of rear impact as they are seen in 27% of the cases whether the occupant was wearing a seat belt or not.

In frontal and side impacts the percentage of cervical injuries is respectively 10% and 8% for occupants wearing seat belts.

Cervical Injury Severity

Two categories of cervical injuries can be determined:

- serious injuries such as fractures of the cervical vertebrae with or without neurological consequences (AIS ≥ 2). It is important to emphasize that such injuries are present in only 1% of cases.
- minor injuries (strains, pain: AIS = 1) which make up the majority of this injury type (99%).

However, this sort of abrupt cervical hyperextension with no contact being made to the head or neck is a recent and poorly understood injury.

Kahane (1) has noted that, according to NCSS accident data, victims of cervical hyperextension take sick leave from work for, on the average, 4 days. Our figures are of the same magnitude. Thus, if it were not for after effects experienced by accident victims, this problem would be of little importance. However, many with such injuries experience headaches, neck pain, perceptual problems, and tingling sensations in the hands some years after the accident.

Toussaint and Fabeck (2) have described cervico-encephalic disorders which have psychic symptoms, among others, rather similar to those that can be observed in past concussion victims.

According to Fournier (3), 90% of the after effects of isolated injuries to the cervical rachis disappear after 18 months to 2 years.

Animal study results have shown that muscle and ligament tearing, muscular bleeding and encephalic or nervous system disorders result from efforts transmitted by the upper part of the spinal cord. Using high speed X-ray analysis on cadavers, Nelson (4) revealed the abnormal changes in cervical spine movement due to injuries to the soft cervical tissues after hyperextension.

We can therefore see that these injuries are far from minor in the case of certain accidents.

Influence of Occupant Sex on the Frequency of Cervical Injuries

All accidentology teams have observed that women are more susceptible to cervical injuries than men. The following percentages illustrate this fact well (Table 1).

Table 1. Frequency of Cervical Injuries as Function of Impact Type

Impact Type	Women	Men
Rear	42%	21%
Side	13%	6.5%
Frontal	17%	7.5%

The difference in cervical morphology between women and men clearly explains this heightened susceptibility. States (5) puts forward the hypothesis that the difference stems from the fact that women have lesser cervical musculature than men. Using data obtained from anthropometry studies carried out by the American army, the author compares head volume to neck cross-sectional area using the following formula.

$$\frac{(Head\ circumference)^3}{(Neck\ circumference)^2}$$

For men and women in the 50th percentile, the ratios are respectively:

- 1/135 for men,
- 1/151 for women.

This ratio illustrates that women have less neck musculature than men given the same head size.

Head Rest Effectiveness

There are no texts stating that the head rest is effective against severe cervical injuries.

Many studies after 1980 have dealt with this subject. In the case of minor injuries half the authors concluded that the head rest was not effective at all, while the other half agreed that the head rest is 0 to 20% effective.

The Peugeot SA/ Renault Laboratory wrote (6) in 1980 that the head rest was almost completely ineffective for men and only slightly effective for women (= 10%). It was also noted that seat breakage seemed more effective than the presence of a head rest.

Only Volvo attributed a high 55% effectiveness to the head rest (7).

It was therefore interesting to learn 10 years later whether the Peugeot S.A./Renault Laboratory's conclusions would be the same when given the data from twice the number of accident victims (almost 800). Table 2 shows that head rests are effective in reducing the risk of cervical injury by 30% for men and women.

Results analysis. Accident research, started in 1970, was carried out using a high percentage of older vehicles. Therefore it is interesting to try to understand the causes behind such an advance in head rest effectiveness which, if only the most recent vehicles are looked at, can reach 60% effectiveness.

Table 2. Frequency of Cervical Injury as a Function of Sex and Presence or Absence of a Head Rest

	With Head Rest	Without Head Rest	Head Rest Effectiveness
Men	15.3%	23.2%	34%
Women	30.3%	45.4%	33%

This 60% figure can justifiably be considered not only due to a better head rest design in recent vehicles but as well to other contributing factors.

In order to study this development, three vehicle categories were specified based on vehicle age (< 1971, 1971 to 1976, > 1976) and for each of these vehicle categories, the impact severity (D V) observed was taken into account. This was necessary as the risk of injury decreases when the impact speed increases because the seat breaks after a certain impact severity threshold is passed:

- cervical injury frequency by D Velocity:
  - < 15 km/h 36%
  - > 15 km/h 20%
- seat breakage frequency for impacts at >25 km/h:
  - < 1971 87%
  - > 1976 55%

Table 3, which takes into account the remarks above, answers the question of whether other factors contribute to higher head rest effectiveness.

Table 3. Cervical Injury Frequency by Vehicle Age, Seat Condition and Head Rest Presence

Seat condition	Head rest	< 1971	1971 - 1976	> 1976
Intact	No	25	28	37
	Yes	30*	21	13
	Effectiveness	0%	25%	63%
Broken	No	21	24	31
	Yes	20*	24	15
	Effectiveness	0%	0%	51%
Total	---	24	22.5	19.5

* small sampling (only 5% had head rests)

It can be seen by looking at figures for the different vehicle ages, that cervical injury frequency increases considerably for newer vehicles when there is no head rest, whether or not the seat breaks. However the risk of cervical injury decreases regularly for newer vehicles when there is a head rest.

Therefore, despite the fact that head rest effectiveness goes from 0 to 60% and that the percentage of occupants using head rests is increasing (5%, 40%, and 63% respectively for the three vehicle age categories) the overall risk of cervical injury is reduced by relatively little (24% to 19.5%).

The only explanation is the frequency of seat breakage at different impact speeds as a function of vehicle age. Thus, at the same average speed, seat breakage is much more frequent in older vehicles (61%) than in recent vehicles (36%) (Table 4).

Table 4. Frequency of Seat Breakage as a Function of Vehicle Velocity and Age

Δ Velocity	<1971	1971 to 1976	> 1976
< 15 km/h	19	14	3
16 to 25 km/h	61	48	38
> 25 km/h	87	62	55
Total	36	43	36

In recent vehicles seats broke at the seat back adjuster mechanism in 70% of the cases, while in older vehicles seat breakage took place at the guide rail level in 70% of the cases observed.

Conclusions. The head rest has become effective simply because seats have become stiffer. Before, seat breakage took place in the majority of cases before the head rest could come into play.

It can be concluded therefore, that given this high effectiveness, the systematic installation of head rests in all vehicles was a good initiative.

Future seat back stiffening (seats with 3 in-board belt anchorages) therefore requires the use of an optimum head rest.

Definition of Accident Conditions to Be Duplicated in Which the Risk of Cervical Injury is Greatest

Table 3 shows that the risk of cervical injury in current seat types is highest without head rests mainly when the seat back does not break (probability of .37).

These accident conditions have thus been chosen as the accident conditions to be duplicated using the Hybrid III dummy. The speed and deceleration pulse were inferred from the accidentology collisions studied.

The speed chosen was 15 km/h (sled impact speed against barrier) and the deceleration distance chosen was approximately 300 mm.

Seat models from a production vehicle were used in all testing. Static testing demonstrated that seat back elasticity and the load level at which the seat adjuster mechanism breaks were relatively similar for different seats (Figure 1).

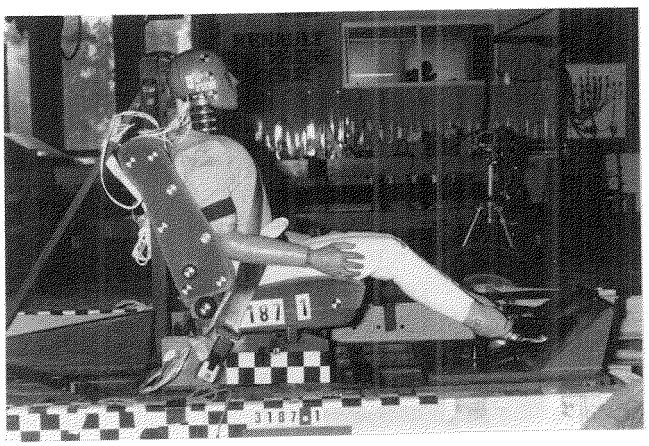

Figure 1. Reference Test (N1)

Tests with the Hybrid III Dummy

For all tests, the Hybrid III dummy was equipped with a neck load measurement device located in C1. The following were measured: My (torque), Fx (shearing force), Fz (pull force), maximum head extension angle in relation to the thorax, and head and thorax acceleration.

Comparison of Measurements Taken for Various Tests with the Cervical Injury Risk Observed in Real Accidents (Table 5)

Table 5. Results Obtained from Dummy Tests with Standard Back Seat

Back seat	Sled Speed = 15 km/h						
	Standard						
Head rest	Without	Experimental	Without	Bad behavior		Good behavior	
Test Number	N1	N2	N3	N4	N5	N6	N7
							
Stopping Distance (mm)	279	275	195	294	283	287	281
Shear Force (N) max	280	130	170	140	100	160	900
Tension Force (N) max	300	100	240	330	320	350	260
Extension Torque (Nm) max	23	8	8	7	10	5	5
Flexion Torque (Nm) max	3	8	3	4	7	3,5	5
Head/Thorax Angle (deg) max	49	0	0	12	8	16	5

The first series of tests allowed the verification of what is observed in real accidents. Thus, compared to the reference crash (Test #1, Figure 2) which gives the neck load levels, loads which can be used as "criteria" to predict .40 probability of cervical injury. The following were the important results obtained:

- Seatback breakage (Test #2 and #3, Figure 3) results in the division by 2 and 3 of certain loads such as Fx and My (Figure 4). Moreover the rotation of the head in relation to the thorax is almost non-existent compared to a 49° rotation in the reference test. The presence of a head rest, under these conditions, results in only slight changes from those values observed without a head rest. Only the pull force, which varied very little from the first to the second test, was clearly less.

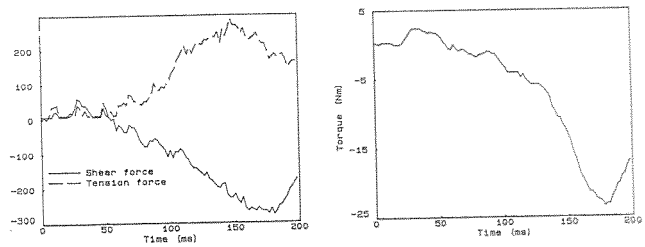

Figure 2. Forces and Bending Torque for the Reference Test N1

In this test a head rest equipped with pre-compressed foam, placed in contact with the head and not movable even under exerted head force (no rotational movement nor vertical movement) was used. This head rest was called the "experimental" head rest throughout testing (Figure 5).

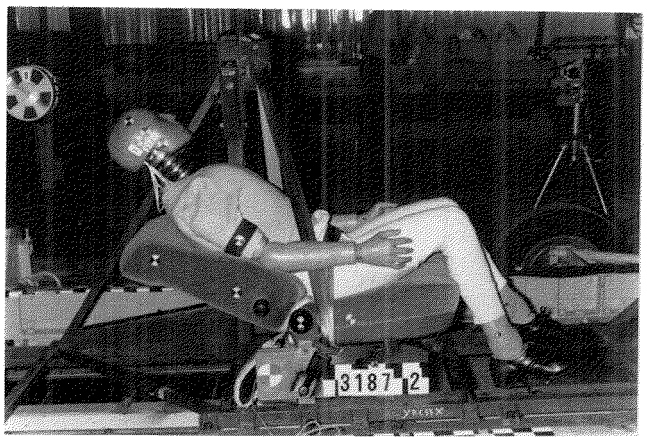

Figure 3. Seatback Breakage (Test N3)

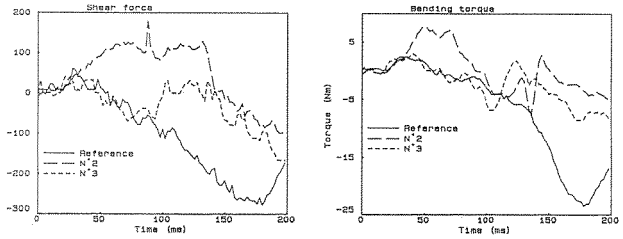

Figure 4. Shear Forces and Bending Torques for the Tests N1, N2, and N3

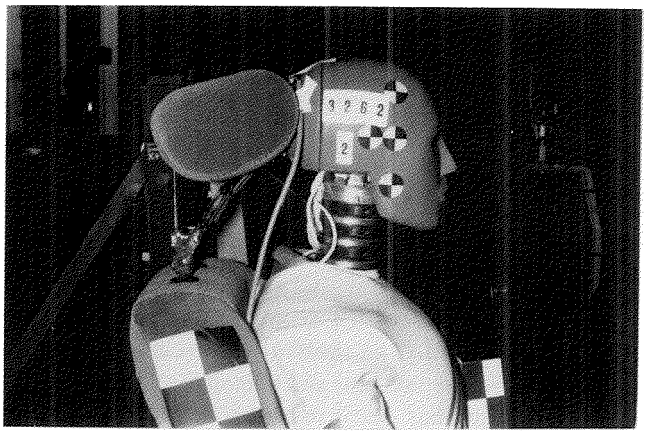

Figure 5. Experimental Headrest

- Tests in which the seat back did not break (Tests #4, 5, 6, and 7) show that the head rest, no matter what its position in relation to the head, and no matter whether it held under the force exerted by the head, reduces the most predictive criteria of cervical injury (Figure 6). Its observed effectiveness in road conditions is therefore upheld with Hybrid III.

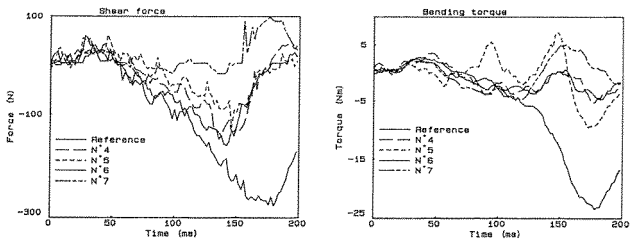

Figure 6. Shear Forces and Bending Torques for the Tests N1, N4, N5, N6, and N7

These four tests also indicate the following:

- a head rest with two positions, in order to be as effective as possible, should stay in contact with the head and not pivot too easily under the force exerted by the head (Tests #4 &5).
- the wider the distance between the head and the head rest, the greater the shearing force and the rotation of the head in relation to the thorax (comparison of Test #4/5 and #6/7).
- the best results are observed when the head rest, in contact with the head, cannot pivot (Test #7).

It can be hypothesized that testing with the above-mentioned "experimental" head rest would further improve these results.

Test #3, designed to test this hypothesis ended in seat back breakage, the seat back's adjuster mechanism having reached its breaking point.

Influence of Seat Back Stiffness (Table 6)

Table 6. Results Obtained from Dummy Tests with Standard Rigidified Back Seat

Sled Speed	15 km/h			30 km/h			65 km/h
Back Seat	Standard	Standard Rigidified					
Head Rest	Without	Without	Experimental	Without	Good Behavior	Experimental	Experimental 2
Test Number	N1	N8	N9	N10	N11	N12	N13
							
Stopping Distance (mm)	279	285	300	530	520	500	1020
Shear Force (N) max	280	210	90	400	350	270	580
Tension Force (N) max	300	250	150	660	1080	680	960
Extension Torque (Nm) max	23	18	7	40	30	6	18
Flexion Torque (Nm) max	3	7	12	34	23	25	66
Head/Thorax Angle (deg) max	49	33	0	62	26	14	0

In all previous tests, the seat back tilted backwards 8° to 12° and then returned to its initial position (Test #1, 4, 5, 6, and 7).

Making the seat back stiffer (Figure 7), which eliminates this "elastic tilting," gives the following results at the same 15 km/h speed (Figure 8):

- when there was no head rest there was a decrease in loads and head rotation in relation to the thorax compared to the reference test (Test #8).
- when using the "experimental" head rest (Test #9), the same load measures as in Test #7, which had the best results, were observed. Only the pull force was divided approximately in 2.

Analysis of film data, as well as the analysis of a test with cadaver under very similar conditions (speed of 10 km/h), show that the beginning of the rebound of the seat back tilt (seat back from a production line seat) takes place at the point where the head begins to rotate backwards (Figure 9). Thus the beginning of the backward movement of the head and the forward return of the thorax take place simultaneously. This explains the additional loads observed compared to the loads observed in the case of the stiffened seat back.

When there is a good head rest in contact with the head, these observed differences are eliminated.

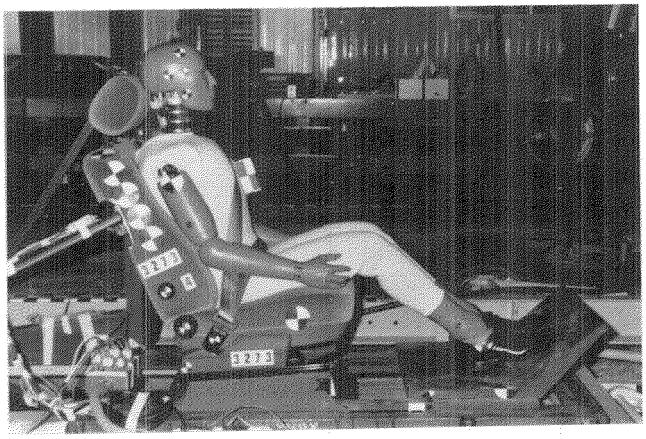

Figure 7. Seatback Stiffer (Test N11)

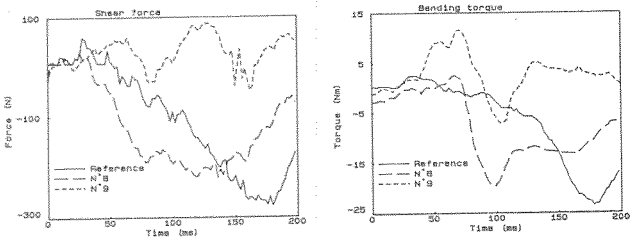

Figure 8. Shear Forces and Bending Torques for the Tests N1, N8, and N9

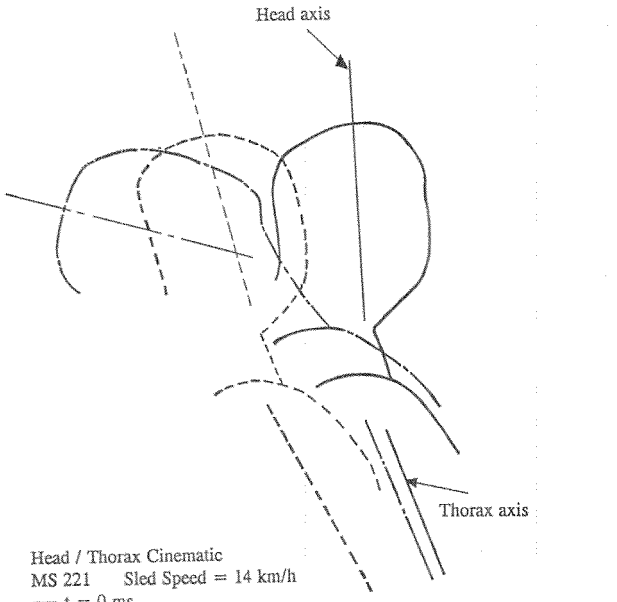

Head / Thorax Cinematic
MS 221 Sled Speed = 14 km/h
— t = 0 ms
--- t = 100 ms maximum backward movement of the head, no head rotation
— t = 200 ms maximum extension of the head

Figure 9. Cadaver Test

Influence of Speed (Table 6)

Tests at higher speeds were necessary in order to evaluate the additional risks to an occupant, in the case of rear impact, which are attributable to a stiffer seat back. Three tests were therefore carried out at 30 km/h with a deceleration distance of 500 mm.

- Test #10 was carried out without a head rest. In this test it was observed that loads continued to be very high, much higher than those in Test #1 which was the reference test (Figure 10). The head rotation in relation to the thorax reached 62°.
- Test #11 was carried out with a production line head rest. In this test the shearing force and the torque force were noticeably reduced and, above all, head rotation in relation to the thorax was the most reduced in comparison to test #10. These two loads (Fx and My), however, were still of the same magnitude as in the reference test. It can therefore be supposed that given this configuration, a risk of cervical injury exists in so far as the diminished head rotation (from 49° to 26°) is not sufficient to lessen this risk.
- Test #12 was carried out with an "experimental" head rest. In this test the best results were obtained since the torque measured was the lowest, and the head rotation angle only reached 14°. Only the shearing force still remained high (270 N compared to 280 N in the reference test).

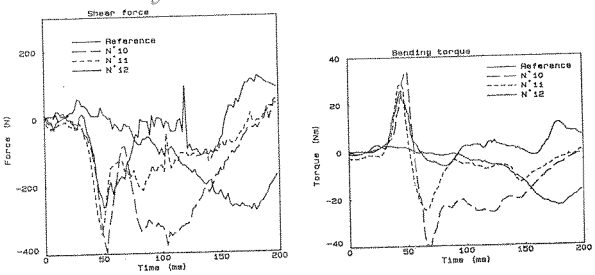

Figure 10. Shear Forces and Bending Torques for the Tests N1, N10, N11, and N12

Hybrid III Dummy Response Limitations

Of the three criteria (torque, shearing force and head/thorax angle) which seem to predict the risk of cervical injury, only the shearing force cannot be greatly diminished in the last test and remains at the load limit. Does this mean that, because of this value which is close to the limit, the risk of cervical injury still exists?

In an attempt to answer this question, a comparative test was carried out on a cadaver and the Hybrid III dummy under very severe crash conditions (speed 65 km/h, deceleration distance 930mm, a_m = 18g). The seat had a stiffened seat back and a stiff head rest in contact with the head (Figures 11 and 12).

Head movement in relation to the thorax is almost non-existent in both tests. The autopsy of the cadaver showed no injury to neck tissue or ligaments. As well it can be noted that there were no injuries to other body areas.

The test with the Hybrid III dummy however resulted in high measurements at the neck level (Test #13). The shearing force reached 590 N, that is to say 2 times higher than in the reference test, and the torque measured 18 Nm, slightly lower than in the reference test.

So, considering this shearing force, the risk of cervical injury would be high. Whereas the test with a cadaver

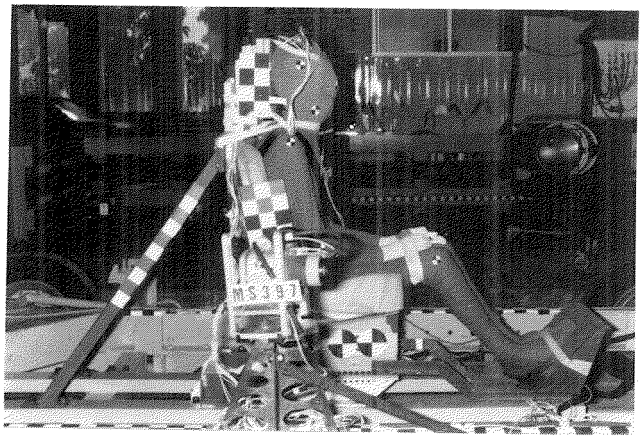

Figure 11. Test with Cadaver and Dummy (N13)

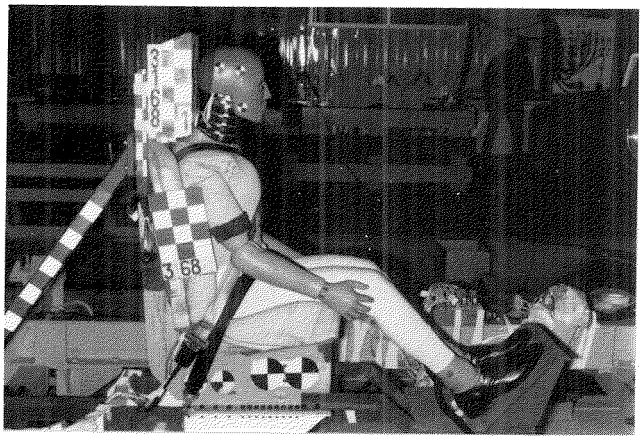

Figure 12. Test with Cadaver and Dummy (N13)

indicated no injury. Furthermore, it is logic dictates that without any relative movement between the head, the neck and the thorax there is no risk of injury.

Therefore it would seem that this shearing force measured at the neck load measurement device level does not signify a risk of injury when there is violent contact between the head and the head rest but is rather due to the law of action-reaction. The strong force exerted by the head rest on the head leads to a proportional reaction force measured between the head and the neck. Should then, under these conditions, only the torque and angle of head rotation in relation to the thorax be used as criteria when there is head contact?

The answer to this question would seem to be yes, given that the biofidelity of the Hybrid III in extension is only based on tests with cadavers without head support.

Furthermore, dummy neck design is such that any relative movement of the head in relation to the neck, however small, leads directly to shearing forces. The dummy does not have, as the human spinal column does, the possibility of natural movements which do not lead to stress.

Therefore it is important to be careful in interpreting load measures in the case of head contact.

Recommendations for Obtaining Adequate Protection in Current and Future Vehicle Models

We have seen that the elastic rebound of the seat backs backward tilt increased the neck load given the same impact speed.

Therefore it seems of the utmost importance that, before seat back breakage occurs, these elastic rebounds be as weak as possible in current vehicle seats in order to limit the risk of injuries, in particular when there is no head rest. It is also important to point out that all French vehicles have been equipped with front seat head rests since last year.

We have also demonstrated that in order to be the most effective possible, the head rest should be in contact with the head. Thus it is necessary to have two settings with sufficient swivel angles. Furthermore:

- the optimal head rest position for the occupant should not be easily knocked out of adjustment when a force is exerted on the head rest, the actual case for many head rests.
- though head rest padding is associated with comfort and security, too soft padding can result in too great of a head rotation.

From head acceleration and force measurements it has been possible to set, given different impact speeds and seat back stiffness, specifications for a very effective head rest. Such a head rest, when placed against the back of the head, should be able to stand the following loads without any change in position:

- longitudinal force 750 N
- vertical force 250 N
- torque 70 Nm.

These recommendations should make it possible, for occupants of future vehicles, to benefit from better protection with 3 in-board belt anchorage seats in the case of rear impact, as well as to obtain optimal protection in the case of frontal impact.

Acknowledgements

This study was partially sponsored by the French Ministry of Research and Transportation (Paris).

References

1. C.J. Kahane, "An Evaluation of Head Restraints—FMVSS 202" NHTSA Technical Report. DOT HS 806-108, February 82.
2. J. Toussaint et P. Fabeck, "Le Syndrome Cervical Traumatique" Acta Orthopedica Belgica 1966 32 N° 1 12-50.
3. Fournier et collaborateurs, "Sequelles des Traumatismes du rachis cervical. Resultats de l'enquete efffectuee par 120 medecins conseils au cours de l'annee 81 et approche clinique" 21-22 mai 1982,

Deauville, France, Revue Francaise du Dommage Corporel Edition J.B. Baillere, Paris.
4. C.L. Nelson, "Detection of Soft-Tissue Injuries of the Cervical Spine" Proceedings of 14th A.A.A.M., November 19-20, 1970 Ann-Arbor, Michigan USA.
5. J.D. States, "The Effectiveness of Head Restraints in Rear End Impacts" Rochester University, PB 221682, June 1973. Distributed by National Technical Information Service. US Department of Commerce.
6. C. Thomas and Co., "Protection against Rear-End Accidents" IRCOBI, Cologne September 1982.
7. N. Bohlin, H. Norin and A. Anderson, "Reports on Traffic Accident Research," AB Volvo, Gothenburg, 1973 (DOT HS-013 622).

S8-W-20

Improvements in the ATB/CVS Body Dynamics Model

John T. Fleck
J & J Technologies Inc.

Abstract

The ATB/CVS (Articulated Total Body Model/Crash Victim Simulator) is a three dimensional model used to study human and/or dummy biomechanics in various crash situations. The model was originally developed under the joint sponsorship of the National Highway Traffic Safety Administration (NHTSA) and the Motor Vehicle Manufacturers Association (MVMA). Various improvements in the model were sponsored by NHTSA and the Armstrong Aerospace Medical Laboratory at Wright Patterson Air Force Base. Since that time J & J Technologies Inc. has developed a new version of the model which has some significant new capabilities. These new features include an increase in the number of segments, a mass-flow inflation algorithm for the airbag and an automatic point generator for the harness (seatbelt) routines. These features allow one to model, for example, an airbag attached to a collapsible steering column. This paper gives a short description of the new features.

Introduction

The Crash Victim Simulator (CVS) program development began in the early seventies under the joint sponsorship of the National Highway Traffic Safety Administration (NHTSA) and the Motor Vehicle Manufacturers Association. In 1975 the Aerospace Medical Research Laboratory at Wright-Patterson Air Force Base sponsored the development of an improved joint routine, a harness routine and the inclusion of aerodynamic forces. This modified program was called the Articulated Total Body (ATB) Model. Since that time, various modifications have been made to the programs. In most cases changes to either of the programs were included in the other hence one may refer to the CVS/ATB Model. The latest version is entitled ATB IV.2.

The CVS/ATB Model is a three-dimensional dynamic model designed to compute the motion and forces acting on a "victim" in a crash situation. The National Highway Traffic Safety Administration's interest is primarily in the development of safety standards for vehicles to minimize the injuries to occupants of motor vehicles. The Air-Force's interest is to minimize injury to pilots during ejection from an airplane.

The CVS/ATB Model differs from most other models in that it allows the user the freedom to define the "victim" and or the "vehicle" as disjoint sets of connected rigid segments. For example, the program can be used to model two occupants interacting with each other and/or one or more vehicles. There is no restriction on the number of segments used to define the occupants ("victims") or the vehicles other than storage limitations of the computer used. The program (CVS/ATB Model) is written in FORTRAN hence is easily installed on most medium or large-scale computers. Recently, it has been converted to run on a micro-computer.

It is assumed that the reader has some familiarity with the program. A description of the basic ATB Model is contained in the reference cited at the end of this paper.

Improvements in ATB IV.2

The new version of the ATB model has many more tests on the consistency of the input data. In particular it checks whether any dimension statements are violated and whether any program restrictions are violated. For example, if a segment has a prescribed motion, it checks the consistency of the initial positions and velocities as given in the data for the prescribed motion with the data as supplied on the initial position cards. If an inconsistency is detected the program outputs an appropriate message and stops. A listing of the program stops are contained at the end of the input description listing. The current listing contains over 100 program stops which are checks on the input.

This new version allows a prescribed motion to be relative to another prescribed motion, i.e. the user may wish to model a vehicle where a door moves with respect the vehicle. The relative door motion can be inputted in the same fashion as the vehicle and the program will add the motion of the door to the motion of the vehicle.

In previous versions where the input option to set the initial linear and angular velocities to the initial velocity of the vehicle was used, the initial linear velocity of the segments did not consider the relative position of the

segments with respect to the vehicle. This has been corrected both in the initial calculations of the linear velocities and in the output routine which calculates the time history of a segment's linear velocity with respect to a different segment.

Modifications

J & J Technologies Inc., offers a version of the ATB model with added optional features. The model can be tailored to the user needs. New features that are available are:

Computer. A version of the program is available that runs on an 80386 or 80486 (or equivalent) micro computer with an 80387 or 80487 coprocessor.

Units. In the standard version of ATB the unit of force must equal the unit of weight. In the enhanced version, if the unit of weight is kilograms the unit of force may be kilograms, kilo-Newtons or Newtons.

Increased dimensions. The standard version of ATB has limits of 30 segments, 40 ellipsoids, 30 planes and 50 functions. A modified version can be assembled with these and/or other dimensions tailored to a user's need.

Airbag enhancement. The standard version of ATB uses a high pressure gas bottle to supply the gas to the bag and only allows the bag to be deployed from an ellipsoidal panel attached to the primary vehicle.

A mass-flow option is available where the user inputs the mass flow rate and the temperature of the gas source as functions of time and the program computes the pressure, temperature, and volume of the gas in the bag using the appropriate thermodynamic equations.

An option to attach the deployment panel to any segment is available, i.e., the bag may be deployed from a collapsible steering wheel.

Harness algorithm enhancement. The standard version of ATB requires that the user prescribe a set of possible contact points of the belts in a harness with the segments to be contacted. The program will select, from this prescribed set, a subset of points which are consistent with the current geometry, during the course of a run. Since the contact points must lie on an ellipsoid and since the initial configuration of selected points usually lie in a plane, the computation of these prescribed points is a chore for the user.

An option is available that will automatically generate sets of points with the user supplying just a few points. For example, for the torso belt the user may supply the upper and lower anchor points and one point on the upper torso and ask the program to select ten more points which lie in the plane of the three inputted points and lie on the torso.

If the user specifies a zero coefficient of friction for the belt along the belt line the current ATB may or may not produce equal tensions in the belt segments as would be expected. This has been corrected so that zero friction will produce equal tensions in the modified harness routines.

Another problem that has been corrected in the modified routines is the fact that if the user inputs the reference points in a reverse order, i.e. from anchor point B to anchor point A instead of from A to B, the program may produce significantly different results. With the corrected version the results will be within computational accuracy.

An option is also available which allows a harness to be dropped and remain dropped from consideration once it no longer contacts a body segment (when the harness contains only one belt and the selected points are only the two anchor points). This option has been found useful in side impact simulations.

Flexible segment. The flexible segment option allows the user to constrain the relative angular orientation of the internal segments of a string of segments to be a prescribed quadratic function of the relative yaw, pitch and roll of the terminal segments. For example, the user may wish to model the neck by one or more segments and prescribe the relative angular orientation of these segments using the upper torso and the head as the terminal segments.

The current version of ATB requires that segments used in the flexible segment option have principle inertias that are along the geometric axis, i.e., the option to rotate the principle axes with respect to the geometric axes cannot be used. The modified version corrects this deficiency and has a option which simplifies the input of the prescribed quadratic functions.

Function input and use. A modification allows the user to specify a scale factor and an offset for a function which is specified by a table. This feature is useful in a parameter study where the user may wish to run a data set where particular functions are increased or decreased by, say 10%, without having to change the table.

It has been found that the routine, which updates the functions used by contact routines and which have specified energy recovery (R) factors and specified offset (G) factors which affect the computation of loading and unloading curves, can produce a new function definition which will compute a force which exceeds the value of the base curve when reloading. This has been corrected in the modified version. Also the modified version allows the user to specify a straight line unload-reload slope. This slope may be a function of the deformation if desired.

Belt algorithm. In the current version of the belt algorithm the user specifies two anchor points and a fixed point on a segment. The routine forms a plane containing these three points and computes the tangent points to the ellipse formed by the intersection of this plane with the ellipsoid containing the fixed point. It has a zero friction option and an infinite friction option. In the zero friction option the fixed point is treated as a loop through which the belt passes and the tension is computed from the total belt length. The tensions will be equal at all points of the belt. In the infinite friction

option the belt is assumed pinned to the segment at the fixed point and each section (from fixed point to anchor point) is treated separately. Also the anchor points must be attached to the same segment (usually the vehicle). If the segment containing the fixed point rotates such that fixed point is not contained on the arc between the tangent points the routine may produce erroneous results. When the tangent points coincide with the fixed point, which is an indication that the belt should no longer be active (such as in a side impact or submarining situation), the current routine will continue to compute a tension and apply a force and torque to the segment.

A modified version of the belt routines automatically repositions the fixed point, allows finite non-zero friction and allows the belt to be dropped when the tangent points coincide with the fixed point (which is no longer fixed). The anchor points may be attached to different segments.

Other modifications. Allow the user to select each time history of a plane-segment or a segment-segment contact to be printed during the current run, not printed during the current run and printed later, or not printed at all. The current version of ATB has only the options to print or not to print all of plane-segment and/or segment-segment contacts with no option to recover the information if it is not printed.

For each of the plane-segment and/or the segment-segment contacts, the user may instruct the program to stop a specified number of time intervals after first contact is made. This feature is useful in testing data sets.

Currently hyper-ellipsoids may have different powers only for the plane-segment contacts where the edge-effect option is not specified. A version of the hyper-ellipsoid routines is being developed which removes this restriction. This will allow the user to define surfaces such as cylinders which intersect with each other.

All known errors in the ATB IV.2 program as originally released have been corrected.

Special versions of the program with added features have been created for some users to fit their specific needs.

Associated Program

A 'bubble man' plot routine is available which plots front, side and top views of the model. The routine is written to drive an Hewlett Packard 8 pen plotter (specifically an HP-7550A), but can be modified for other plotters. As an option, it can produce a file which can be viewed directly on the screen using a companion program. The routine has a hidden line option, it plots planes, ellipsoids, hyperellipsoids, airbags, airbag panels, springs, belts, harnesses and constraints (such as fixed point and fixed distance). The user has the option of selecting different colors and/or the option to suppress the plotting of various elements.

Summary

Since ATB-IV.2 has been released, J & J Technologies Inc. has made many enhancements to the model which greatly increases its usefulness. The new versions of the restraint-system routines can be used for side-impact situations where the old versions may fail. The mass-flow option for the airbag routines can be used to simulate current inflation techniques.

J & J Technologies Inc. continues to work on the model to improve its performance.

Reference

"Articulated Total Body Model Enhancements," Volume 2: User's Guide. Louise. A. Obergefell, Thomas. R. Gardner, Ints Kaleps and John T. Fleck. January 1988, AAMRL-TR-88-043.

Technical Session 9
Frontal Crash Protection

Chairperson: S. Christopher Wilson, Canada

S9-O-01

Influence of Rigid Wall Impact Speed on Dummy and Vehicle Loadings

Eberhard Faerber
Federal Highway Research Institute (BASt)

Abstract

The objective of the investigation was to determine the influence of 0° rigid wall impact speed on dummy and vehicle loadings by testing three different types of vehicle at speeds of 30 km/h, 40 km/h, 45 km/h, 50 km/h and 55 km/h. The test vehicles were subcompact, compact and full-size vehicles. During the initial testing stage, a total of fifteen tests was conducted, in other words, one test for each constellation. The front seats were occupied on each occasion by two hybrid III dummies.

Introduction

The BASt chose to conduct this investigation into the influence of rigid wall impact speed on dummy loadings for various reasons. A bibliographical study revealed that there are no publications available in respect of such an investigation.

As a matter of routine, the American Traffic Safety Administration (NHTSA) subjects all available vehicle models to 0° rigid wall testing at a speed of 56.3 km/h and publishes the test results. In comparison with the 48 . 3 km/h test prescribed by law (FMVSS 208), the impact energy at 56.3 km/h is almost 40 % higher. The car industry complains that as a result of this practice, they are forced to adopt more robust vehicle construction designs than required by law.

No legislation requiring full-scale testing of total passive vehicle safety has yet been introduced in Europe. At the beginning of 1991, the European Experimental Vehicles Committee (EEVC) established the WG 11 working group to investigate the possibility of improving existing legislation and, if appropriate, introducing full-scale testing as a means of increasing passive safety in the event of frontal impact. During the course of the investigations of WG 11, the question arose of whether there are any types of vehicle which might register higher dummy loadings at low test speeds (< 50 km/h, for example) than at high test speeds.

An investigation conducted by BASt into the main areas of emphasis of the WG 11 study revealed that 30° 50 km/h rigid wall impacts impose only minimum safety requirements on both larger and smaller vehicles. For this reason, the UK in particular suggested raising the impact speed of this configuration to 55 km/h.

In order to conduct a thorough investigation into the influence of rigid wall impact speeds, it was accepted that it would be necessary to carry out forty-five impact tests (and three repeat tests) at five different test speeds on vehicles of three different weights. During the initial stage, three types of vehicle were subjected to a single test at the various applicable speeds.

The remainder of this paper presents the results of these first fifteen impact tests.

Test Method

The vehicles were subjected to 0° frontal impact testing at impact speeds of 30 km/h, 40 km/h, 45 km/h, 50 km/h and 55 km/h. The following vehicle types were selected:

- subcompact car: FORD Fiesta
- wheel base 2292 mm, curb weight 750 kg
- compact car: Volkswagen Golf Rabbit) II wheel base 2475 mm, curb weight 855 kg
- mid-size/large car: Audi 100 (4000) wheel base 2687 mm, curb weight 1,110 kg.

The vehicles were tested in a roadworthy condition without luggage using a petrol substitute. On each occasion, the two front seats were occupied by hybrid III dummies wearing seatbelts.

The vehicles were tested in respect of the following values:

- wall force on 10 elements and total force
- vehicle accelerations
  - c.g.: triaxial (tunnel) left-hand and right-hand sill: x - axle
- belt forces
  - lap belt: 2 points (left and right) shoulder belt: 2 points (top and bottom).

The dummies were comprised of the following parts of the body:

- head, upper neck
  - acceleration: triaxial
  - longitudinal force (FNZ)
  - shearing force (FNX)
  - bending moment (MNY)
- chest
  - acceleration: triaxial
  - chest deflection
- pelvis
  - acceleration: triaxial
- femur
  - longitudinal force

In order to put meat on the bones of the values, the tests were also filmed using up to eight high-speed cameras each taking 1000 pictures a second.

Test Results

For the purpose of recording the results, the signal traces were calculated using both time and conventional criteria (such as maximum and 3ms values) in respect of all the measurement channels. The signal traces were obtained from the 10 kHz digitalized data and filter by means of software conforming to SAE 211. The values are reproduced in tables 1 to 6 in the appendix.

What result could be expected in respect of the influence of impact speed on the course of the measurement curves?

Three basic assumptions are possible, see Figure 1.

- rising impact speed produces greater impact duration without significantly increasing the loading level;
- rising impact speed alters the shape of the signal traces;
- rising impact speed alters the maximum amplitude of the signal traces without significantly increasing the impact duration.

The correlation between impact speeds and characteristic values is usually determined by means of regression calculation. The following two formulations were selected:

linear regression:

dummy/vehicle loading = $a_i + b_i \cdot v$, and

power regression:

dummy/vehicle loading = $a_j \cdot v \exp b_j$

The graphs contained in Figures 2 and 3 confirm the accuracy of the last of these assumptions. In all the measuring curves of a vehicle, impact duration and signal trace shape are practically identical. In consequence, it is possible to arrive at fairly accurate loading characterizations at the various impact speeds solely by means of the maximum and 3ms values. Important measurement plots in respect of the tests conducted on the compact car (VW Golf) have been reproduced to illustrate this point. As no belt forces were recorded for this vehicle, the total belt force values are those of the subcompact car (FORD Fiesta).

The correlation was calculated using the following formulas:

linear regression:

$$a_i = \frac{\Sigma y - b_i \cdot \Sigma x}{n}$$

$$b_i = \frac{n\Sigma xy - \Sigma x \cdot \Sigma y}{n\Sigma x^2 - (\Sigma x)^2}$$

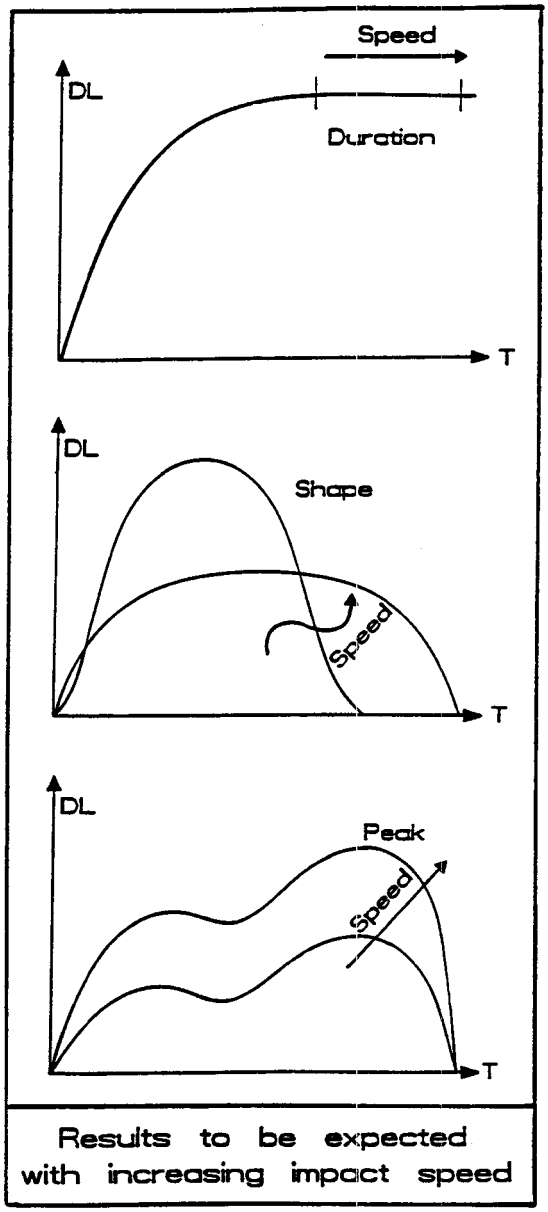

Figure 1. Results to be Expected with Increasing Impact Speed

$$COR_i = \frac{n\Sigma xy - \Sigma x\Sigma y}{\sqrt{(n\Sigma x^2 - (\Sigma x)^2 \cdot (n\Sigma y^2 - (\Sigma y)^2)}}$$

(correlation coefficient)

power regression:

$$a_j = e \exp \frac{\Sigma \ln y - b_j \cdot \Sigma \ln x}{n}$$

$$b_j = \frac{n\Sigma \ln x \cdot \ln y - \Sigma \ln x \cdot \Sigma \ln y}{n\Sigma (\ln x)^2 - (\Sigma \ln x)^2}$$

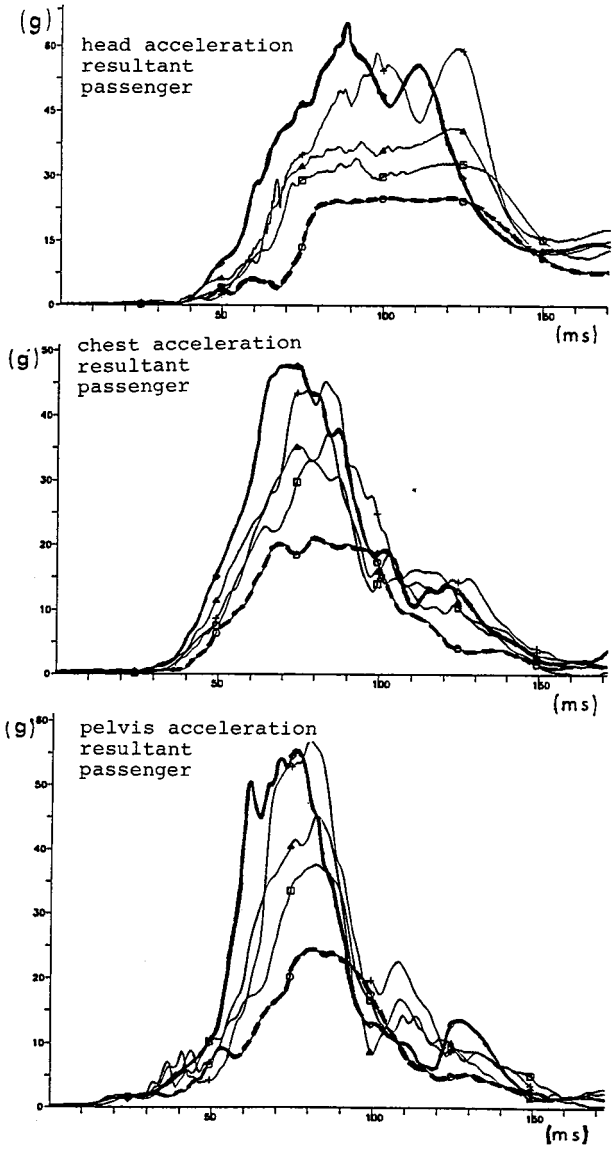

Figure 2. Dummy Loading of Compact Car Tests (VW Golf), Each for 5 Test Speeds (- - - Test Speed 30 km/h, — Test Speed 55 km/h)

$$COR_j = \frac{n\Sigma \ln x \cdot \ln y - \Sigma \ln x \cdot \Sigma \ln y}{\sqrt{n\Sigma(\ln x)^2 - (\Sigma \ln x)^2) \cdot (n\Sigma(\ln y)^2 - (\Sigma \ln y)^2)}}$$

(correlation coefficient)

Linear and power regressions were calculated for all the values contained in tables 1 to 6, see tables 7 to 24 in the appendix.

A selection of regression curves is reproduced in Figures 4 to 6 in order to illustrate the correlation between dummy and vehicle loading values and impact speed.

In order to increase the amount of data for the regression calculations, consideration was given to the possibility of normalizing and, where appropriate, collating various values, such as those of the dummies and the test vehicles, and subsequently calculating joint regressions for such collated normalized values. However, particularly due to the broad span of dummy loading values available in respect of parts of the body and also especially due to the fact that the range of the values in relation to the protection criteria is too high, this possibility was rejected on methodological grounds.

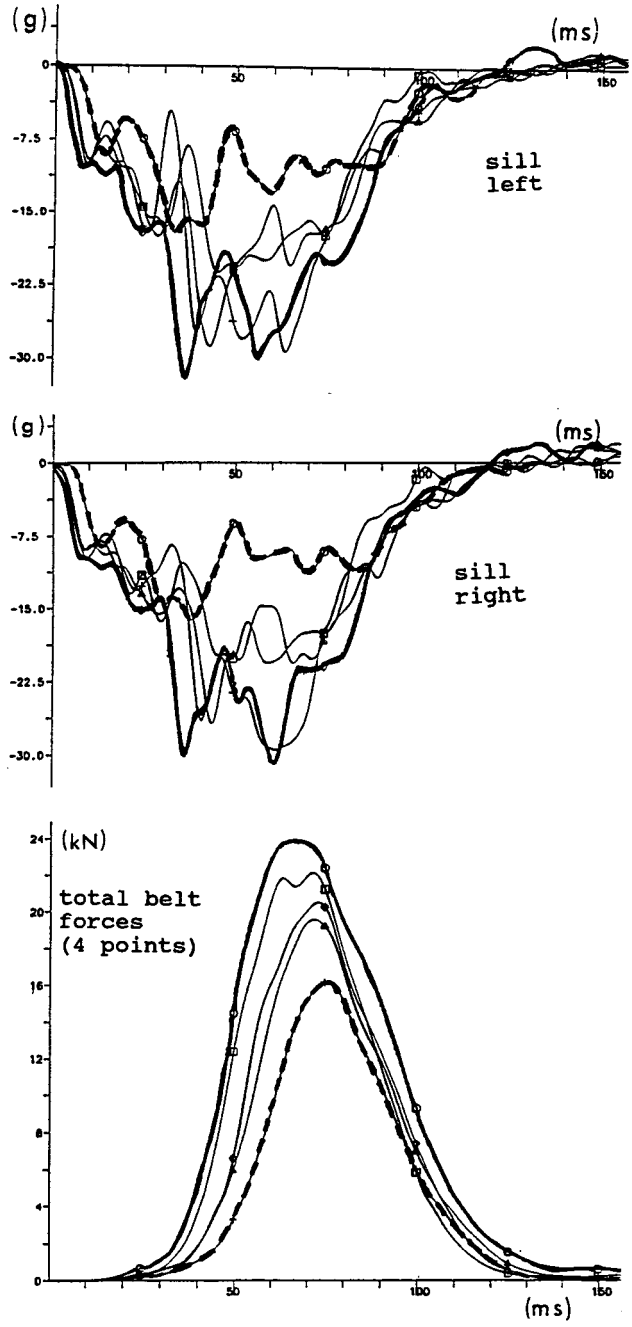

Figure 3. Door Sill Accelerations of Compact Car (VW Golf) Total Belt Forces of Subcompact Car (Ford Fiesta, Not Measured for Compact Car), Each for 5 Test Speeds (- - - Test Speed 30 km/h, — Test Speed 55 km/h)

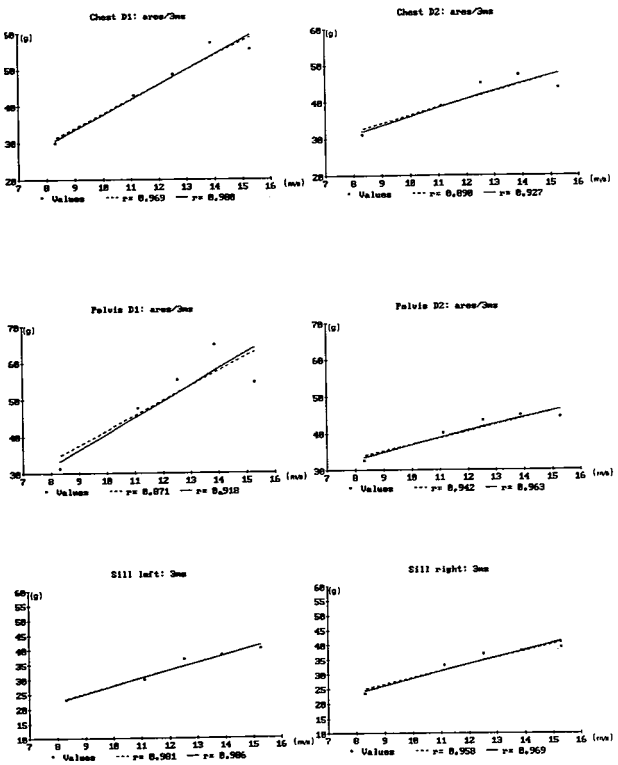

Figure 4. Selected Regression Curves—Ford Fiesta (- - - Linear, — Potential, D1 = Driver Dummy, D2 = Passenger Dummy)

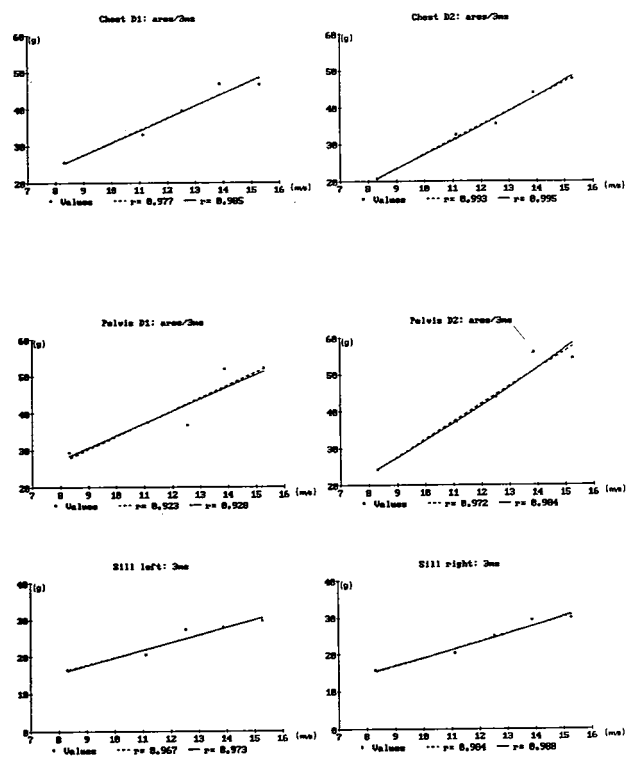

Figure 5. Selected Regression Curves—Volkswagen Golf (Rabbit) (- - - Linear, — Potential, D1 = Driver Dummy, D2 = Passenger Dummy)

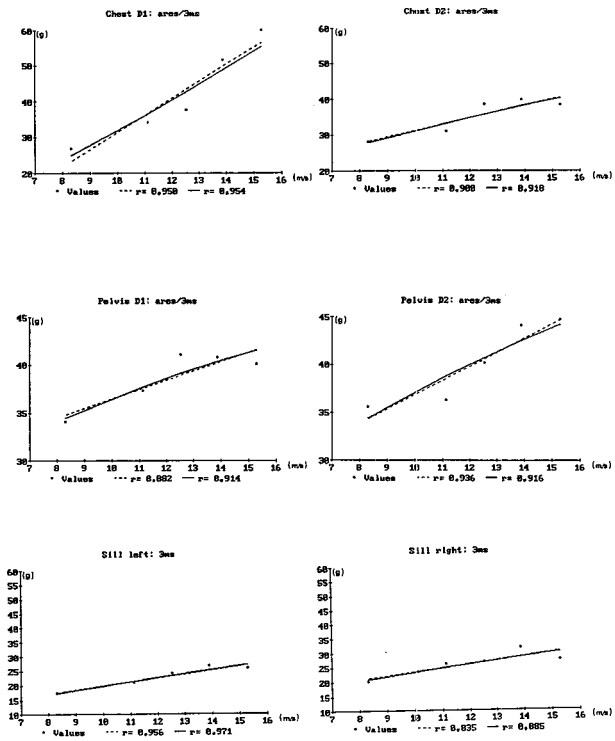

Figure 6. Selected Regression Curves—Audi 100 (4000) (- - - Linear, — Potential, D1 = Driver Dummy, D2 = Passenger Dummy)

Conclusions

During the initial stage of this test, only one test was conducted per vehicle at the five impact speeds. For this reason, only a comparatively limited amount of data is available for statistical analyses. Therefore, the regression equations should initially be interpreted with caution.

In some instances, the correlation equations with the constants a_i,j and b_i,j (linear and power, Tables 7 to 24 in the appendix) would indicate the existence of major differences in respect of the individual values and the various vehicle types. However, a glance at the measurement data and, in particular, at the correlation curves (Figures 4 to 6) reveals that in terms of results, the differences between the linear formulation and the power formulation are only minor. Or, in other words:

> the linear and power regression curves in respect of the various values are practically congruent.

The "classical" measurement data, the 3ms values of head, chest and pelvis accelerations, produced higher correlation factors than the other measurement data. One reason for this is the fact that the calculation of the 3ms values represents a kind of filter. No correlation exists between either dummy neck values or chest deflections and impact speed. In the case of the dummy values, the power regressions produce slightly higher correlation factors than in the case of the linear correlation.

The head impacts of the driver dummies produced higher head accelerations with higher exponents in the case of power regression. On the other hand, the regression coefficients were lower. The exponents were even higher in the case of the HIC values, a reflection of the HIC calculation procedure—raising "effective" head acceleration to the power of 2.5.

In respect of the tests conducted on the FORD Fiesta, the driver head, chest and pelvis and the passenger head 3ms power regression values are progressive in character (power indices > 1 and between 1.08 and 1.4). All belt forces and the passenger chest and pelvis values are degressive in character (power indices < 1 and between 0.44 and 0.67).

In contrast to the subcompact car (FORD Fiesta), the compact car (Volkswagen Golf), produced higher power indices in respect of head loadings, but degressive regression curves for the passenger dummy chest and pelvis values. The full-size vehicle (Audi 100) produced even higher power indices in respect of head loading values. In this case, the power regressions produced progressive correlations only for the chest loading values. All other dummy values were degressive in character.

The vehicle values reveal as little tendency towards uniformity as the dummy values: the calculation of the correlation equations produced the same correlation factors in respect of both linear and power regression. In respect of the subcompact car, the power regressions produced exponents between 0.9 and 1.1. The values are similar in the case of the compact car, but it is obvious that particularly low exponents were calculated in respect of the tunnel accelerations. In the case of the full-size vehicle, particularly low exponents were calculated in respect of the door sill accelerations.

Although, as mentioned above, only a small number of tests was conducted, the statistical analyses permit some cautious conclusions to be drawn. In the case of the dummy values, the power correlations produced only minimally higher correlation factors than the linear correlations. It was not established that certain dummy values at low impact speeds produce higher values than at high speeds. In respect of vehicle data, both formulations and the linear and power regression produced approximately equal regression values. In respect of the speed range tested, the linear and power regression curves are practically congruent. This leads to the conclusion that it is sufficiently safe to assume the existence of a linear correlation between impact speed and dummy and vehicle loadings.

Summary

The correlation between impact speed and dummy and vehicle loading was investigated in fifteen impact tests. Three different-sized vehicles were tested at five different impact speeds.

The form and the impact duration of all measurement courses remained practically unchanged, regardless of impact speed. On the whole, only maximum amplitude height was affected by an increase in impact speed. Linear and power regression calculations were performed in respect of the various values. Both formulations produced almost identical regression curves, leading to the conclusion that it is sufficiently safe to assume the existence of a linear correlation between impact speed and dummy and vehicle loading levels.

Appendix

Table 1. Dummy Data, Driver, Head, Chest

		Driver Dummy						
		Head				Chest		
Car Type	Impact Speed (km/h)	res. max g	res. 3 ms g	HIC	HIC 36	res. max. g	res. 3 ms g	deflect. max (mm)
FORD FIESTA	30	34	33	259	195	31	30	27
	40	121	69	579	512	44	43	37
	45	*223	85	580	574	51	49	36
	50	*82	74	715	703	63	57	41
	55	*165	75	846	847	58	55	44
VW GOLF	30	29	29	242	147	26	26	25
	40	58	56	413	337	34	33	53
	45	100	92	845	836	42	40	34
	50	72	69	943	809	48	47	51
	55	*105	100	1317	1317	49	47	42
AUDI 100 (4000)	30	*29	28	196	108	28	27	29
	40	*113	86	449	449	35	34	29
	45	*153	113	783	783	38	38	24
	50	*144	126	949	949	57	52	31
	55	*147	114	1245	1245	72	61	29

* Head hits steering wheel

Table 2. Dummy Data, Passenger, Head, Chest

		Passenger Dummy						
		Head				Chest		
Car Type	Impact Speed (km/h)	res. max g	res. 3 ms g	HIC	HIC 36	res. max. g	res. 3 ms g	deflect. max (mm)
FORD FIESTA	30	55	40	321	256	32	31	-
	40	100	56	627	518	39	39	-
	45	108	90	1034	942	46	45	-
	50	104	68	1002	945	48	47	-
	55	82	75	965	908	45	44	-
VW GOLF (Rabbit)	30	25	25	174	109	21	21	26
	40	34	33	388	206	33	33	39
	45	41	41	527	322	37	36	37
	50	60	59	1035	739	45	44	38
	55	65	61	1043	802	48	48	48
AUDI 100 (4000)	30	27	26	199	116	28	28	37
	40	36	35	347	227	31	31	33
	45	43	43	525	372	39	39	-
	50	47	46	636	470	40	40	-
	55	67	59	799	671	40	38	40

Table 3. Dummy Data, Driver, Neck, Pelvis, Belt Forces

		Driver Dummy										
		Neck			Pelvis		Belt forces					
Car Type	Impact Speed (km/h)	x-force kN	z-force kN	Moment y Nm	res. max. g	res. 3 ms g	Shoulder upper kN	Shoulder lower kN	Lap left kN	Lap right kN	Total Force kN
FORD FIESTA	30	1.3	1.1	89	32	31	5.3	2.9	3.1	3.1	15.8
	40	1.1	1.6	50	53	48	7.5	4.2	4.0	4.0	21.4
	45	1.0	2.3	35	60	55	7.7	5.6	4.1	4.1	22.7
	50	-	-	-	74	65	7.5	3.6	3.7	3.7	20.1
	55	1.1	1.6	23	60	55	7.4	4.2	3.7	3.7	20.8
VW GOLF (Rabbit)	30	1.1	0.8	84	30	29	-	-	-	-	-
	40	0.9	1.1	43	38	37	-	-	-	-	-
	45	1.4	1.6	43	38	37	-	-	-	-	-
	50	1.2	1.7	33	53	52	-	-	-	-	-
	55	1.3	2.4	38	55	52	-	-	-	-	-
AUDI 100 (4000)	30	1.1	0.8	72	34	34	5.8	4.1	3.4	5.2	17.6
	40	1.0	1.2	35	38	37	7.0	5.5	3.9	5.8	21.6
	45	0.8	1.1	81	43	41	5.3	5.8	4.4	6.2	21.1
	50	0.6	1.8	47	41	41	8.0	3.6	4.5	6.8	22.1
	55	0.7	3.9	171	42	40	7.8	5.3	4.9	6.6	23.6

Table 4. Dummy Data, Passenger, Neck, Pelvis, Belt Forces

		passenger Dummy										
		Neck			Pelvis		Belt forces					
Car Type	Impact Speed (km/h)	x-force kN	z-force kN	Moment y Nm	res. max. g	res. 3 ms g	Shoulder upper kN	Shoulder lower kN	Lap left kN	Lap right kN	Total Force kN
FORD FIESTA	30	1.5	1.2	99	34	33	5.4	5.1	3.4	2.5	16.2
	40	1.6	1.9	134	42	40	6.6	6.1	4.2	3.1	19.6
	45	2.0	2.3	146	46	43	7.7	5.3	4.7	3.4	20.5
	50	-	-	-	46	45	7.7	3.5	4.8	6.6	22.1
	55	1.3	1.7	74	46	44	7.7	5.9	4.2	6.9	23.9
VW GOLF (Rabbit)	30	-	-	-	25	24	-	-	-	-	-
	40	-	-	-	38	37	-	-	-	-	-
	45	-	-	-	45	44	-	-	-	-	-
	50	-	-	-	57	56	-	-	-	-	-
	55	-	-	-	56	54	-	-	-	-	-
AUDI 100 (4000)	30	1.0	0.8	80	36	36	5.3	4.8	3.6	2.8	16.1
	40	1.1	3.0	29	38	36	5.7	2.7	3.7	3.1	14.7
	45	1.0	0.9	59	42	40	6.9	4.4	4.8	6.4	20.6
	50	1.0	1.0	62	45	44	7.7	6.0	4.8	6.7	24.2
	55	1.4	2.1	88	46	45	6.0	4.4	3.8	6.5	19.8

Table 5. Vehicle Data, Accelerations, Tunnel, Sill

		Vehicle								
Car Type	Impact Speed (km/h)	Tunnel res. max. g	Tunnel res.3ms g	Tunnel res.50ms g	Door sill left max. g	Door sill left 3ms g	Door sill left 50ms g	Door sill right max. g	Door sill right 3ms g	Door sill right 50ms g
FORD FIESTA	30	29	27	8.1	24	23	6.5	24	24	7.1
	40	32	31	15.2	31	30	9.7	35	33	9.5
	45	44	42	15.6	38	37	14.4	38	37	11.5
	50	42	41	15.5	40	38	16.2	40	38	13.5
	55	48	45	17.9	42	40	16.1	43	39	15.8
VW GOLF (Rabbit)	30	29	26	10.1	17	16	9.5	16	16	9.2
	40	25	24	14.1	21	21	12.8	21	20	12.7
	45	35	33	14.7	29	27	14.4	27	25	14.4
	50	37	34	14.9	29	28	13.4	30	29	11.8
	55	39	36	19.8	32	30	18.1	31	30	17.5
AUDI 100 (4000)	30	26	22	11.3	18	17	10.4	21	20	10.2
	40	39	34	15.4	22	21	14.1	28	26	13.8
	45	32	30	18.6	26	24	15.1	28	27	16.6
	50	59	53	27.8	29	27	14.6	35	32	14.9
	55	47	41	27.8	27	26	17.9	29	28	16.8

Table 6. Vehicle Data, Wall Force, Deformations, Displacements

		Vehicle				
Car Type	Impact Speed (km/h)	Wall Force max. kN	Deformation Film mm	Displacement Tunnel * mm	Displacement Sill left * mm	Displacement Sill right * mm
FORD FIESTA	30	251	276	365	361	358
	40	353	390	485	457	453
	45	415	411	539	537	527
	50	460	471	610	570	570
	55	479	578	707	670	650
VW GOLF (Rabbit)	30	130	400	402	413	420
	40	145	505	508	531	526
	45	-	554	593	605	617
	50	208	649	682	685	695
	55	254	710	711	720	735
AUDI 100 (4000)	30	264	410	448	458	445
	40	447	547	587	600	584
	45	436	572	820	831	788
	50	521	765	-	789	757
	55	589	841	876	903	855

* Via double integration of acceleration

Table 7. FORD FIESTA, Driver Dummy, Linear Regression Equations

FORD FIESTA driver dummy		
Measuring Parameter	Potential Regression	Correlation Factor
Head result max.	-62.0 + 15.3 ·v	0.56
Head result 3 ms	-6.78 + 6.05 ·v	0.81
HIC	-424 + 82.4 ·v	1.0
HIC 36	-544 + 90.7 ·v	0.99
Chest result max.	-5.45 + 4.47 ·v	0.95
Chest result 3 ms	-1.92 + 3.99 ·v	0.97
Chest deflection max.	8.70 + 2.31 ·v	0.97
Neck x-force max.	1.49 - 0.03 ·v	-0.71
Neck z-force max.	0.59 + 0.09 ·v	0.53
Neck moment y max.	161 - 9.45 ·v	-0.96
Pelvis result max.	-3.47 + 4.86 ·v	0.86
Pelvis result 3 ms	1.10 + 4.06 ·v	0.87
Belt forces total max.	12.39 + 0.64 ·v	0.65

v = impact speed

Table 8. FORD FIESTA, Driver Dummy, Potential Regression Equations

FORD FIESTA driver dummy		
Measuring Parameter	Potential Regression	Correlation Factor
Head result max.	0.37 ·v exp 2.27	0.74
Head result 3 ms	1.97 ·v exp 1.40	0.87
HIC	4.63 ·v exp 1.92	0.99
HIC 36	1.38 ·v exp 2.38	0.98
Chest result max.	2.61 ·v exp 1.17	0.97
Chest result 3 ms	3.06 ·v exp 1.09	0.98
Chest deflection max.	5.57 ·v exp 0.76	0.97
Neck x-force max.	2.46 ·v exp -0.32	-0.75
Neck z-force max.	0.23 ·v exp 0.79	0.66
Neck moment y max.	10040 ·v exp -2.22	-1.0
Pelvis result max.	2.76 ·v exp 1.20	0.91
Pelvis result 3 ms	3.38 ·v exp 1.08	0.92
Belt forces total max.	6.80 ·v exp 0.44	0.74

v = impact speed

Table 9. FORD FIESTA, Passenger Dummy, Linear Regression Equations

FORD FIESTA passsenger dummy		
Measuring Parameter	Linear Regression	Correlation Factor
Head result max.	34.4 + 4.51 ·v	0.55
Head result 3 ms	0.80 + 5.30 ·v	0.75
HIC	-481 + 104 ·v	0.90
HIC 36	-590 + 107 ·v	0.91
Chest result max.	14.4 + 2.26 ·v	0.90
Chest result 3 ms	14.78 + 2.16 ·v	0.89
Chest deflection max.	-	-
Neck x-force max.	1.79 - 0.02 ·v	-0.16
Neck z-force max.	0.82 -0.08 ·v	0.51
Neck moment y max.	148 - 2.90 ·v	-0.25
Pelvis result max.	21.9 + 1.72 ·v	0.91
Pelvis result 3 ms	19.07 + 1.80 ·v	0.94
Belt forces total max.	7.17 + 1.09 ·v	1.0

v = impact speed

Table 10. FORD FIESTA, Passenger Dummy, Potential Regression Equations

FORD FIESTA passenger dummy		
Measuring Parameter	Potential Regression	Correlation Factor
Head result max.	11.8 ·v exp 0.80	0.68
Head result 3ms	3.95 ·v exp 1.12	0.84
HIC	5.13 ·v exp 1.99	0.94
HIC 36	2.08 ·v exp 2.31	0.95
Chest result max.	7.67 ·v exp 0.68	0.94
Chest result 3 ms	7.77 ·v exp 0.67	0.93
Chest deflection max.	-	-
Neck x-force max.	2.00 ·v exp - 0.10	-0.14
Neck z-force max.	0.31 ·v exp 0.70	0.65
Neck moment y max.	225 ·v exp - 0.29	-0.24
Pelvis result max.	12.2 ·v exp 0.5	0.94
Pelvis result 3 ms	10.51 ·v exp 0.55	0.96
Belt forces total max.	4.27 ·v exp 0.63	1.0

v = impact speed

Table 11. FORD FIESTA, Vehicle Data, Linear Regression Equations

FORD FIESTA		
Measuring Parameter	Linear Regression	Correlation Factor
Tunnel res. max. Tunnel res. 3 ms	3.15 + 2.92 ·v 4.75 + 2.64 ·v	0.94 0.94
Sill left max. Sill left 3 ms	2.81 + 2.62 ·v 2.12 + 2.58 ·v	0.98 0.98
Sill right max. Sill right 3 ms	3.25 + 2.66 ·v 6.06 + 2.31 ·v	0.98 0.96
Wall force max.	-27.7 + 34.28 ·v	0.99
Deformation max. 1)	-90.3 + 41.7 ·v	0.98
Displace tunnel. 2)	-57.4 + 48.6 ·v	0.99
Displace sill left	-9.30 + 43.2 ·v	0.99
Displace sill right	3.80 + 41.5 ·v	1.0

1) Maximum value from film evaluation
2) Maximum value from double integration of acceleration

v = impact speed

Table 12. FORD FIESTA, Vehicle Data, Potential Regression Equations

FORD FIESTA		
Measuring Parameter	Potential Regression	Correlation Factor
Tunnel res. max. Tunnel res. 3 ms	4.18 ·v exp 0.89 4.29 ·v exp 0.86	0.93 0.94
Sill left max. Sill left 3 ms	3.42 ·v exp 0.93 3.09 ·v exp 0.95	0.98 0.99
Sill right max. Sill right 3 ms	3.30 ·v exp 0.95 3.87 ·v exp 0.87	0.98 0.97
Wall force max.	24.24 ·v exp 1.11	0.99
Deformation max. 1)	22.51 ·v exp 1.17	0.98
Displace tunnel 2)	36.6 ·v exp 1.07	0.99
Displace sill left	43.5 ·v exp 0.99	0.99
Displace sill right	45.13 ·v exp 0.97	1.0

1) Maximum value from film evaluation
2) Maximum value from double integration of acceleration

v = impact speed

Table 13. VOLKSWAGEN, Driver Dummy, Linear Regression Equations

VW GOLF driver dummy		
Measuring Parameter	Linear Regression	Correlation Factor
Head result max. Head result 3 ms HIC HIC 36	-52.3 + 10.2 ·v -47.9 + 9.6 ·v -1143 + 155 ·v -1304 + 163 ·v	0.87 0.89 0.96 0.95
Chest result max. Chest result 3 ms Chest deflection max.	-3.25 + 3.51 ·v -2.43 + 3.33 ·v 12.5 + 2.33 ·v	0.99 0.98 0.53
Neck x-force max. Neck z-force max. Neck moment y max.	0.72 + 0.04 ·v -1.16 + 0.22 ·v 130 - 6.69 ·v	0.53 0.96 -0.88
Pelvis result max. Pelvis result 3 ms	-3.78 + 3.82 ·v -1.12 + 3.49 ·v	0.94 0.92
Belt forces total max.	-	-

v = impact speed

Table 14. VOLKSWAGEN, Driver Dummy, Potential Regression Equations

VW GOLF driver dummy		
Measuring Parameter	Potential Regression	Correlation Factor
Head result max. Head result 3 ms HIC HIC 36	0.41 ·v exp 2.05 0.47 ·v exp 1.97 0.53 ·v exp 2.86 0.06 ·v exp 3.64	0.92 0.93 0.98 0.98
Chest result max. Chest result 3 ms Chest deflection max.	2.53 ·v exp 1.1 2.61 ·v exp 1.07 4.65 ·v exp 0.86	0.99 0.98 0.65
Neck x-force max. Neck z-force max. Neck moment y max.	0.48 ·v exp 0.36 0.02 ·v exp 1.75 1533 ·v exp -1.42	0.49 0.97 -0.93
Pelvis result max. Pelvis result 3 ms	3.20 ·v exp 1.03 3.60 ·v exp 0.97	0.94 0.93
Belt forces total max.	-	-

v = impact speed

Table 15. VOLKSWAGEN, Passenger Dummy, Linear Regression Equations

VW GOLF passenger dummy		
Measuring Parameter	Linear Regression	Correlation Factor
Head result max. Head result 3 ms HIC HIC 36	-28.72 + 6.04 ·v -25.3 + 5.66 ·v -1053 + 138 ·v -895 + 109 ·v	0.96 0.96 0.94 0.92
Chest result max. Chest result 3 ms Chest deflection max.	-11.3 + 3.95 ·v -11.84 + 3.92 ·v 5.12 + 2.66 ·v	0.99 0.99 0.91
Neck x-force max. Neck z-force max. Neck moment y max.	- - -	- - -
Pelvis result max. Pelvis result 3 ms	-15.9 + 4.91 ·v -15.0 + 4.75 ·v	0.98 0.97
Belt forces total max.	-	-

v = impact speed

Table 16. VOLKSWAGEN, Passenger Dummy, Potential Regression Equations

VW GOLF passenger dummy		
Measuring Parameter	Potential Regression	Correlation Factor
Head result max.	0.78 ·v exp 1.61	0.97
Head result 3 ms	0.86 ·v exp 1.56	0.97
HIC	0.22 ·v exp 3.13	0.98
HIC 36	0.06 ·v exp 3.49	0.97
Chest result max.	1.18 ·v exp 1.37	0.99
Chest result 3 ms	1.13 ·v exp 1.38	0.99
Chest deflection max.	4.28 ·v exp 0.87	0.92
Neck x-force max.	-	-
Neck z-force max.	-	-
Neck moment y max.	-	-
Pelvis result max.	1.17 ·v exp 1.44	0.99
Pelvis result 3 ms	1.18 ·v exp 1.43	0.98
Belt forces total max.	-	-

v = impact speed

Table 17. VOLKSWAGEN, Vehicle Data, Linear Regression Equations

VOLKSWAGEN GOLF		
Measuring Parameter	Linear Regression	Correlation Factor
Tunnel res. max.	11.3 + 1.77 ·v	0.79
Tunnel res. 3 ms	10.1 + 1.68 ·v	0.85
Sill left max.	-2.22 + 2.28 ·v	0.97
Sill left 3 ms	-0.72 + 2.05 ·v	0.97
Sill right max.	-3.18 + 2.29 ·v	0.98
Sill right 3 ms	-3.36 + 2.24 ·v	0.98
Wall force max.	-31.0 + 17.7 ·v	0.95
Deformation max. 1)	12.94 + 45.0 ·v	0.99
Displace tunnel 2)	3.55 + 47.07 ·v	0.99
Displace sill left	28.9 + 45.9 ·v	1.0
Displace sill right	17.9 + 47.9 ·v	0.99

1) Maximum value from film evaluation
2) Maximum value from double integration of acceleration

v = impact speed

Table 18. VOLKSWAGEN, Vehicle Data, Potential Regression Equations

VOLKSWAGEN GOLF		
Measuring Parameter	Potential Regression	Correlation Factor
Tunnel res. max.	7.52 ·v exp 0.59	0.72
Tunnel res. 3 ms	6.59 ·v exp 0.61	0.81
Sill left max.	1.64 ·v exp 1.10	0.97
Sill left 3 ms	1.76 ·v exp 1.05	0.97
Sill right max.	1.42 ·v exp 1.14	0.98
Sill right 3 ms	1.35 ·v exp 1.15	0.99
Wall force max.	12.1 ·v exp 1.09	0.95
Deformation max. 1)	52.9 ·v exp 0.95	0.99
Displace tunnel 2)	49.3 ·v exp 0.98	0.99
Displace sill left	55.4 ·v exp 0.95	1.0
Displace sill right	54.4 ·v exp 0.96	0.99

1) Maximum value from film evaluation
2) Maximum value from double integration of acceleration

v = impact speed

Table 19. AUDI, Driver Dummy, Linear Regression Equations

AUDI 100 driver dummy		
Measuring Parameter	Linear Regression	Correlation Factor
Head result max.	-94.7 + 17.3 ·v	0.90
Head result 3 ms	-72.7 + 13.6 ·v	0.92
HIC	-1132 + 152 ·v	0.99
HIC 36	-1297 + 164 ·v	0.99
Chest result max.	-28.7 + 6.11 ·v	0.92
Chest result 3 ms	-17.16 + 4.85 ·v	0.95
Chest deflection max.	26.8 + 0.14 ·v	0.14
Neck x-force max.	1.69 - 0.07 ·v	-0.83
Neck z-force max.	-2.84 + 0.38 ·v	0.80
Neck moment y max.	-49.2 + 10.3·v	0.51
Pelvis result max.	26.2 + 1.09 ·v	0.87
Pelvis result 3 ms	26.71 + 0.98 ·v	0.88
Belt forces total max.	11.62 + 0.78	0.94

v = impact speed

Table 20. AUDI, Driver Dummy, Potential Regression Equations

AUDI 100 driver dummy		
Measuring Parameter	Potential Regression	Correlation Factor
Head result max.	0.11 ·v exp 2.76	0.91
Head result 3 ms	0.17 ·v exp 2.49	0.93
HIC	0.28 ·v exp 3.10	0.99
HIC 36	0.02 ·v exp 4.08	0.99
Chest result max.	1.10 ·v exp 1.48	0.93
Chest result 3 ms	1.53 ·v exp 1.32	0.95
Chest deflection max.	26.1 ·v exp 0.03	0.08
Neck x-force max.	9.19 ·v exp -1.00	-0.82
Neck z-force max.	0.01 ·v exp 2.22	0.86
Neck moment y max.	7.79 ·v exp 0.86	0.34
Pelvis result max.	17.1 ·v exp 0.34	0.91
Pelvis result 3 ms	18.0 ·v exp 0.31	0.91
Belt forces total max.	6.97 ·v exp 0.45	0.95

v = impact speed

Table 21. AUDI, Passenger Dummy, Linear Regression Equations

AUDI 100 passenger dummy		
Measuring Parameter	Linear Regression	Correlation Factor
Head result max.	-23.0 + 5.49 ·v	0.93
Head result 3 ms	-12.1 + 4.4 ·v	0.98
HIC	-564 + 87.1 ·v	0.99
HIC 36	-585 + 78.2 ·v	0.97
Chest result max.	12.7 + 1.88 ·v	0.92
Chest result 3 ms	13.4 + 1.78 ·v	0.90
Chest deflection max.	30.74 + 0.52 ·v	0.48
Neck x-force max.	0.63 + 0.04 ·v	0.60
Neck z-force max.	0.75 + 0.07 ·v	0.19
Neck moment y max.	44.4 + 1.58 ·v	0.19
Pelvis result max.	22.4 + 1.54 ·v	0.96
Pelvis result 3 ms	22.1 + 1.48 ·v	0.94
Belt forces total max.	7.32 + 0.96·v	0.68

v = impact speed

Table 22. AUDI, Passenger Dummy, Potential Regression Equations

AUDI 100 passenger dummy		
Measuring Parameter	Potential Regression	Correlation Factor
Head result max.	1.20 ·v exp 1.43	0.96
Head result 3 ms	1.79 ·v exp 1.25	0.98
HIC	1.39 ·v exp 2.33	0.99
HIC 36	0.24 ·v exp 2.89	0.99
Chest result max.	7.33 ·v exp 0.63	0.93
Chest result 3 ms	7.64 ·v exp 0.61	0.92
Chest deflection max.	26.7 ·v exp 0.13	0.38
Neck x-force max.	0.47 ·v exp 0.34	0.55
Neck z-force max.	0.19 ·v exp 0.80	0.32
Neck moment y max.	35.5 ·v exp 0.21	0.12
Pelvis result max.	14.4 ·v exp 0.42	0.94
Pelvis result 3 ms	14.4 ·v exp 0.41	0.92
Belt forces total max.	4.46 ·v exp 0.58	0.68

v = impact speed

Table 23. AUDI, Vehicle Data, Linear Regression Equations

AUDI 100		
Measuring Parameter	Linear Regression	Correlation Factor
Tunnel res. max	-4.26 + 3.67 ·v	0.77
Tunnel res. 3 ms	-5.96 + 3.42 ·v	0.79
Sill left max.	5.76 + 1.51 ·v	0.92
Sill left 3 ms	6.31 + 1.37 ·v	0.96
Sill right max.	10.3 + 1.46 ·v	0.77
Sill right 3 ms	10.5 + 1.30 ·v	0.84
Wall force max.	-89.8 + 44.2 ·v	0.97
Deformation max. 1)	-142 + 62.9 ·v	0.97
Displace tunnel 2)	-92.9 + 65.6 ·v	0.95
Displace sill left	-79.9 + 65.1 ·v	0.95
Displace sill right	-48.8 + 60.0 ·v	0.96

1) Maximum value from film evaluation
2) Maximum value from double integration of acceleration

v = impact speed

Table 24. AUDI, Vehicle Data, Potential Regression Equations

AUDI 100		
Measuring Parameter	Potential Regression	Correlation Factor
Tunnel res. max.	2.55 ·v exp 1.10	0.82
Tunnel res. 3 ms	1.85 ·v exp 1.18	0.85
Sill left max.	3.44 ·v exp 0.78	0.95
Sill left 3 ms	3.75 ·v exp 0.73	0.97
Sill right max.	5.28 ·v exp 0.67	0.84
Sill right 3 ms	5.58 ·v exp 0.62	0.88
Wall force max.	18.8 ·v exp 1.27	0.97
Deformation max. 1)	32.33 ·v exp 1.18	0.97
Displace tunnel 2)	37.0 ·v exp 1.18	0.96
Displace sill left	40.5 ·v exp 1.15	0.96
Displace sill right	43.2 ·v exp 1.1	0.97

1) Maximum value from film evaluation
2) Maximum value from double integration of acceleration

v = impact speed

S9-O-02

Full Size Semi-Frontal Crash Simulations with Passenger Cars at 55 km/h Against Rigid Barrier

Florian Schueler
Insitute for Forensic Medicine,
University of Heidelberg
Peter Hupfer, Lothar Wech
TÜV BAYERN

Abstract

Beginning April 1990 frontal collision simulations with middle- and compact-class cars have been performed. For these crash tests a new experimental technique—using Electronically Controlled Vehicles—was developed. All tests were conducted at a collision velocity of 55 km/h and 50% offset against a rigid barrier. The main task of this test series was to achieve an estimation on the vehicle-specific injury potential (crashworthiness). In the vehicles, dummies of type Hybrid II/50% male were positioned on the driver's and co-driver's seats. The measured vehicle and dummy data (accelerations, forces, deformations) and injury criteria were used to calculate this injury potential. The results as well of the high-speed films as of the vehicles' structure behaviour gave further basic data. Finally, results of Heidelberg long-term investigations gave basic knowledge for the injury mechanisms. Another future aim of this collision series is to discuss the problems of rating individual passive safety levels of different vehicles in accordance to realistic main accident types and with respect to optimized injury criteria in dummies.

Introduction

Recently, vehicle safety has become an essential criterion for the decision on the purchase of a car, apart from comfort and economy. But what objective safety criteria are available to the prospective customer?

First of all, one has to distinguish between active and passive safety. While active safety is intended to prevent accidents, passive safety contributes to the reduction of the injury consequences of an accident. This includes measures for the reduction of acceleration, forces and deflections endured by the driver and the passengers. Furthermore it includes measures for securing sufficient survival space as well as effective rescue after accidents by proper function of the required car components.

The prospective car purchaser may gain a first impression of the active safety of a car, for instance, during a test drive. To obtain helpful and realistic information and basic knowledge concerning the passive safety of a car, i.e. crahworthiness, objective data must be available for the purchaser.

For this sake, TÜV BAYERN—the Technical Control Board of Bavaria—has developed a new test method, the ECV Crash (ECV stands for Electronically Controlled Vehicle).

To give the consumer information about passive car safety, the german automotive magazine "auto motor und sport" started a large scale comparative test series, performed by TÜV BAYERN in cooperation with the Institute for Forensic Medicine at the University of Heidelberg.

Test Procedure

The whole test procedure consists of test preparations, performance of the test run according to the ECV Crash System and the evaluation of all test data including the high-speed film analysis and the examination of the tested vehicle.

Description of the ECV Crash System

Contrary to the crash testing equipment used so far, the vehicle to be tested is driven by its own engine; steering adjustments are made by an electric motor. The entire measuring and control systems including a board-computer are placed inside the vehicle. In this way, the ECV Crash System permits crash tests under realistic conditions. The ECV Crash Test differs from usual tests by

- the drive through the engine of the vehicle under realistic operating conditions, including the activated electric network of the car;
- the electronic control systems of the car, which permit utmost precision regarding longitudinal and transversal guide of the free-running vehicle;
- the data logging equipment integrated in the test vehicles, which records all measurement data;
- complete mobility, which means that the ECV Crash System is universally applicable everywhere;
- maximum flexibility regarding crash configurations and vehicle combinations (for instance, vehicle-vehicle crash).

Operation of the vehicles without driver is possible due to the control unit which is integrated in the test vehicle. An electric pilot cable either in or on the driveway serves for tracking. The actual vehicle's position during the approach is reported to the control unit via an electronic receiving antenna attached to the front bumper. The necessary steering corrections are continuously and automatically calculated and performed by means of an electric motor at the steering linkage, which will automatically be separated before the crash.

The velocity is coordinated by the control unit in a similar way. For this purpose, a precision speedometer hub reports the vehicle's actual speed to a computer, which compares it with the previously entered set value.

The speed corrections calculated on this basis are performed by means of a control element via engine control (see Figure 1). In this way the desired conditions can be met with a precision not reached before: this results in a speed tolerance less than 1% at a speed of approximately 50 km/h and a lateral deviation of only a few milimetres.

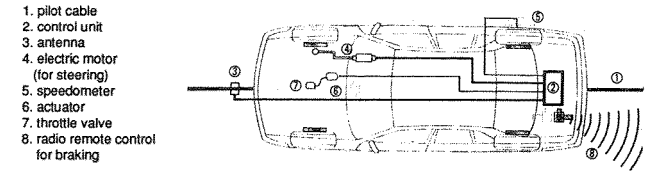

Figure 1. Operating Schematic Diagram of the ECV Crash System

The control unit in the trunk also controls automatic starting and braking of the test car. Different braking maneuvers are possible via radio remote control at any time (see Figure 2).

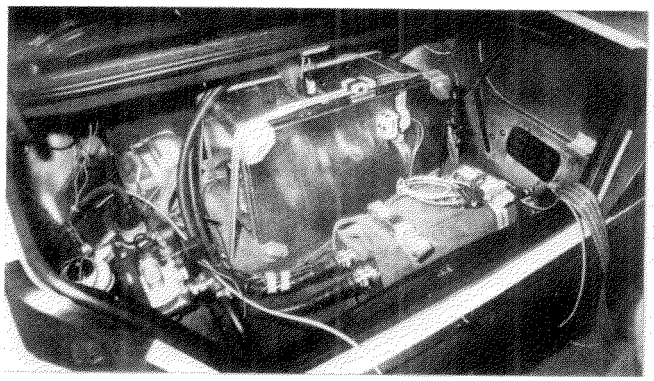

Figure 2. Test Equipment, Installed in a Test Vehicle

Special Features of the ECV Crash System

TÜV BAYERN set up this ECV Crash System on its test site at Jesenwang near Munich for the first time in spring 1990. Since that time, a series of tests has been performed with this equipment. Upper middle-class and compact-class cars were crashed against concrete barriers at half-side offset ("offset crash"). As these tests were of comparative nature, the test conditions had to be identical for all "candidates." This could be reached by means of the ECV system.

Apart from that, almost all accident configurations may be simulated by the ECV Crash System of TÜV BAYERN. A concrete barrier with exchangeable barrier-crash-head is available for crashes against rigid obstacles. Different offset percentages are possible using this electronic tracking system by simple transversal displacement of the vehicle antenna or the pilot cable. Furthermore the system is able to perform tests involving obstacles and crash configurations of greater proportion than often could be simulated in a test lab. These tests include:

- Cross-positioned trucks, etc.,
- High-speed crash tests (v > 100 km/h),
- Multi-car crashes (simulation of pile-ups),
- Collisions of two vehicles freely running into each other at any angle and offset configuration.

Data Acquisition

Measuring data is available from the car and from both properly positioned (according to FMVSS 208) front passenger-dummies.

Whereas the car data is measured at three points which aren't subjected to deformations (the lower left and right side of the B-pillar and a solid structure in front of the back seats), the measuring points on the dummies are standardized as for the dummy type Hybrid II (head-, chest- and pelvis accelerations in 3 axis and the forces in both femora). Finally, the belt forces are registered via special belt force transducers, positioned on the belt near the dummy's shoulder.

All transducer signals—time histories—are stored in the measuring unit, contained in the car s trunk. Immediately after the test, the measuring unit is saved and taken out of the car, so all measuring data can be read, i.e. time histories are plotted, special values (for example resulting accelerations, 3 ms values, etc.) are listed and deduced injury criteria(first of all the Head Injury Criterion) will be calculated.

Other crash data, like vehicle deformations and high-speed cinematography are mentioned below.

Test Evaluation

The crash test results are evaluated in several steps. Vehicle geometry and positional change of the car itself and certain components of the vehicle s structure due to the crash are registered before and after the crash.

All measurement data of both dummies, as well as the car deformations are scaled.

Especially the scaling of the dummy data is based on the present, established Injury Tolerance limits—also given in the FMVSS 208—whereas the different injury-severity levels are defined according to the Abbreviated Injury Scale (AIS, Rev. 85) and derived from the different levels of the special acceleration- and force-measurement values.

In addition to these measurement values, (see Table 1) the results of the cinematographic analysis of the high-speed film material (with frequencies ranging from 500 pps up to 2000 pps) are taken into account.

The correlation of the acceleration- and force-time histories of the dummies and the dynamic behaviour of the car during the crash (i.e. the maximum dynamic deformation, special dummy body-to-car structure contact points and induced motions of the dummy's body) round off the estimation base of the degree of regional and overall injury severity of the tested vehicle (see Table 2).

Discussion

First of all, the crash test configuration was defined by "auto motor und sport" magazine in accordance with several car manufacturers and is designed to examine the "worst case" of common accident situations.

Table 1. Basic Data of ECV Tests

		Dummy	Injury Criteria		Accelerations (g) 3 ms M			Forces (daN) Femur			Intrusion
No.	Mass / Length	Position	HIC35	SI	Head	Thorax	Pelvis	Belt	left	right	Class
2	M 1599	Driver	880	364	88	45	46	852	176	134	3
	L 4720	Co-Driver	196	190	34	32	39	977	109	136	2
3	M 1519	Driver	1697	520	102	63	47	748	255	218	5
	L 4685	Co-Driver	872	253	87	36	47	619	170	159	3
4	M 1486	Driver	1349	377	115	43	45	704	440	105	4
	L 4810	Co-Driver	441	278	53	38	43	729	168	72	3
5	M 1459	Driver	1238	549	83	64	50	821	88	148	3
	L 4748	Co-Driver	< 200	226	<35	36	49	838	214	150	2
6	M 1492	Driver	905	575	82	58	68	748	565	280	4
	L 4780	Co-Driver	< 650	mv	<80	(65)	(57)	683	486	82	3
7	M 1341	Driver	1364	402	117	45	44	508	126	215	6
	L 4500	Co-Driver	1381	218	135	34	51	643	673	156	5
10	M 1145	Driver	551	322	65	42	49	384	326	426	5
	L 3985	Co-Driver	579	242	92	31	57	649	203	109	4
11	M 1555	Driver	502	269	61	41	52	667	195	318	4
	L 4433	Co-Driver	200	218	34	34	42	741	176	54	2
12	M 1675	Driver	468	290	49	40	51	660	117	176	3
	L 4790	Co-Driver	260	240	39	36	44	633	186	69	3

mv: missing value; "<": value not greater than ...; (...): reconstructed signal

Table 2. Estimated Degree of Regional and Overall Injury Severity

Run-No.	Head and Neck					Thorax / Abdominal region				Pelvis / Femur / Feet				Overall Prognosis
	a-Value	HIC	Neck impact	Neck torsion	Prognosis	a-Value	Belt force	Th/Abd.-impact	Prognosis	a-Value	Femur force	Leg-room deformation	Prognosis	
2	+	+	./.	./.	fair	++	0	./.	fair	+	++	+	fair	fair
3	0	--	0	./.	poor	+	0	./.	fair	+	++	-	accept.	poor
4	-	0	0	./.	accept.	++	0	0	fair	+	+	0	fair	acceptable
5	+	+	./.	./.	fair	+	0	./.	fair	+	++	++	fair	fair
6	+	+	./.	./.	fair	+	0	-	accept.	-	+	0	accept.	acceptable
7	-	0	-	--	poor	++	+	--	poor	+	++	--	poor	poor
10	++	++	./.	--	fair	++	++	--	accept.	+	+	-	accept.	acceptable
11	++	++	./.	./.	fair	++	+	moderate	fair	0	++	0	accept.	fair
12	++	++	./.	./.	fair	++	+	./.	fair	0	++	+	fair	fair

However, all concluding statements and finally the quality of vehicles tested in regard of passive safety are restricted entirely to this test particular configuration at 50% offset and 55 km/h impact velocity.

The dummy, type Hybrid II, was chosen because he is commonly used by car manufacturers (also according FMVSS 208) and most of all because he was applicated in the development of the tested vehicles. On the other hand, a more advanced version, especially the dummy type Hybrid III is not yet reliable enough and therefore isn't recommended from official side.

Estimating the test results, it must furthermore be taken into account that variation of the measurement values in one and the same test type (with identical car types) and the variation caused by the measuring system leads to a whole result variation, that could be minimized by performing several identical tests. This procedure is limited by costs.

During the crash test series it was apparent that further development of dummies as well as of injury criteria seems to be most important. From the point of view of biomechanics, there is a need for advanced injury prediction concerning different head and neck injuries on the one side and for lower leg and foot on the other side.

Finally, new aspects transferring technological biomechanics could be seen in new criteria for car construction. For example: the elimination of elastic behaviour (overload by rebound), the degree of mass concentration in the deformation zone of the vehicle or "intelligent deformations" even behind the passenger compartment and hereby a diminution of crash impact active mass of the car.

Acknowledgements

The authors would like to express their gratitude to the publishers of "auto motor und sport," Stuttgart for releasing the data for this paper.

S9-O-03

Test Procedure Comparison in Frontal Impact

Gilles Vallet, Dominique Cesari, Yves Derrien, Seán ó Ríordáin
INRETS

Abstract

If it is agreed that it is appropriate that Europe accepts an evaluation procedure for frontal impact protection, there must be agreement on the procedure to be retained. The three possible procedures are the orthogonal frontal impact (of the type in force in the USA), an impact against 30° angled barrier and a 45% offset impact. Theoretically, each procedure has its advantages and its disadvantages. This paper compares the three procedures taking particular note of injury tolerance criterion.

Introduction

It is very difficult to assess the protection provided by a vehicle to its occupants in case of frontal impact. There are three crash configurations commonly used in different laboratories. Each procedure has specific advantages as well as shortcomings. The three configurations selected by the LCB laboratory and its industrial partners are the following ones:

- 90 degree angled dynamometric barrier at an impact velocity of 57 km/h,
- 30 degree angled barrier with respect to the vehicle axis at an impact velocity of 57 km/h
- 90 degree angled offset barrier where the overlap is 45%, at an impact velocity of 50 km/h.

These crash configurations have been used for testing several vehicles of different makes and models. The results of the various tests are presented. They compare the influence of the test procedure on the level of protection.

Description of the Different Configurations

First, it is worth noting that all the vehicles studied have been identically instrumented whatever the obstacle

type. Instrumentation is detailed. Each vehicle included a number of accelerometric measurement points. These were:

- longitudinal acceleration (with respect to the vehicle horizontal axis) measured at two engine points, at the cylinderhead and crankcase levels.
- longitudinal acceleration on the gearbox.
- three-axis acceleration (longitudinal, transversal and vertical) at six points in the passenger compartment:
  - on the lower side-rail, at the B pillar level, left-side and right-side,
  - on the lower side-rail, 200 mm behind the previously mentioned points, left and right
  - at the rear of the vehicle, on the centreline (rear trunk)
  - on the center line, between the R points of the two dummies on the central tunnel.

These accelerometric measurements were complemented by an analysis of the films taken during the tests. Films were taken by 9 high speed cameras (from 500 to 1000 frames/sec.), located perpendicular to the vehicle, on each side of the vehicle, underneath and above.

Finally, the interior structures of the passenger compartment were entirely removed before and after the test in order to take accurate measurements of the characteristic points structure. Two HYBRID II dummies belted in the front seats were used. They were fully instrumented.

A 90° angled dynamometric barrier included 6 measurement zones equipped with force meters. Six forces and their sum were available. The impact velocity was 57 km/h. A 30° angled barrier were equipped with a lateral stop aimed at avoiding any sliding movement across the barrier. The following diagram illustrates the system used. The impact velocity was 57 km/h.

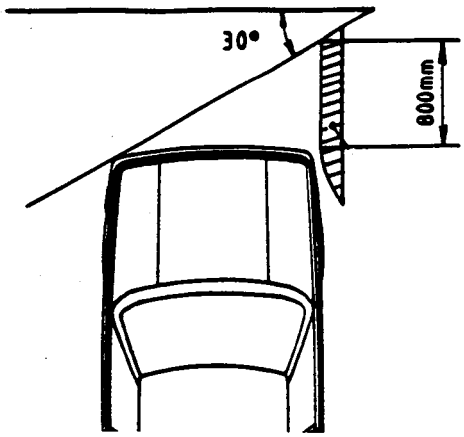

The following diagram shows the modus operandi of the 45 % offset barrier.

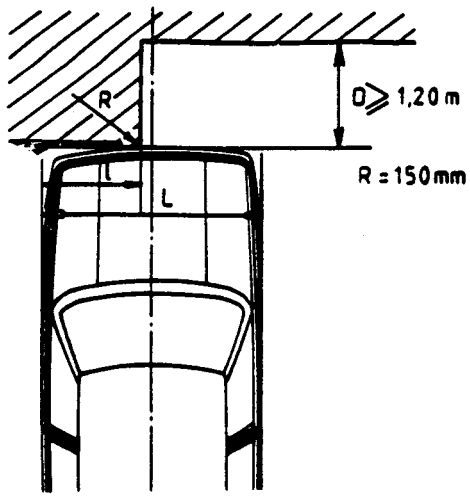

Influence of the Crash Configuration on Different Vehicles

A two-level comparison was made: with respect to the vehicle (structure) and to its occupants.

Occupants

The criteria selected were as follows:

- HIC
- SI
- Resultant thorax acceleration
- Compression stresses on femurs.

The figures in appendix 1 show the results obtained for 5 different vehicles.

First, let's consider the HIC value. It should be noted that, for the drivers of two vehicles, comparable HIC values have been recorded in dynamometric and 30° angled barrier configurations at an impact velocity of 57 km/h, with a slightly higher severity for the 30° barrier. In both cases, the HIC value almost exceeded 1000. But two other cases showed a significantly higher severity for the dynamometric angled barrier with a similar behaviour for non symmetrical obstacles. If for these two vehicles, the results obtained with a dynamometric barrier were more severe, the severity level differed significantly from the previous one as the HIC value was doubled. Finally, the last vehicle tested showed poor results globally with a lesser severity for the offset barrier. In this case it should be noted that for the driver, the HIC value was always greater than 1000, which is generally agreed to be the limit not to be exceeded.

Considering the front seat passengers, for which head impact was less direct and significant, the grouping differs slightly. Three vehicles showed severe results least the dynamometric barrier, but the severity levels reached were so high that the only evident constatation was that the less aggressive configuration was the offset barrier at an impact velocity of 50 km/h with a 45% overlap.

Another important body segment, the HYBRID II thorax, provided three accelerations of which the resultant should not exceed a tolerance limit of 60 g on 3 ms. SI levels, which were directly calculated from acceleration, are also shown in the enclosed figures. For this criterion, a different result distribution can be observed. Globally, a close similarity should be noted for the dynamometric barrier and the 30° angled barrier, without any marked predominance of one or the other, with the exception of vehicle 5 which did not show such good results against the dynamometric barrier. Nevertheless, the threshold was most often exceeded for the 0° barrier configuration at an impact velocity of 57 km/h. When considering all the vehicle occupants and two injury severity criteria—HIC value and thorax acceleration—it should be noted that the HIC limit value was 5 times exceeded for the 0° barrier and the 30° barrier. On the other hand, the THORAX resultant acceleration never exceeded the 60 g limit over 3 ms. For the driver, despite the thorax contact with the steering wheel, it should be observed that the steering wheel columns correctly collapsed, as collapse ranging from 25 to 85 mm was recorded.

To decide between these two crash configurations, the average of HIC values exceeding 1000 has been calculated for each case. The dynamometric barrier gives us an average of 1396 and the 30° barrier gives us an average of 1326, but with no significant difference between the two. If the average HIC is calculated for all cases, then we obtain averages of 1125 and 996 respectively for the dynamometric barrier and 30° barrier. However, on this small sample we are unable to conclude statistically that these population are different.

Doing the same calculations on the resultant of the thorax acceleration we obtain 50.3 g and 43.7 g for the dynamometric barrier and the 30° barrier. Respectively, again the two populations cannot be said to be different.

Turning to femur compressions, analysis shows that when looking at the driver and passenger together, the 30° barrier is slightly more severe. However taking drivers and passengers separately we found no difference between driver and passenger on the same barrier.

Therefore these criteria do not separate the dynamometric barrier and the 30° barrier. The lesser severity obtained in the offset impact test led us questioning the impact velocity value selected for such a configuration. Indeed, preliminary studies showed that such a test performed at an impact velocity of 57 km/h would be far too severe and that the increase in impact velocity from 50 km/h to 57 km/h would yield an energy variation of 30%. Thus this test could be conducted at an impact velocity of 53 km/h.

Vehicles

The tables in appendix 2 show the main results obtained from the vehicle accelerometric measurements. Within the scope of this study, two main measurement points have been used: point R and the left-hand rear side rail. Only maximum values have been considered.

Longitudinal acceleration was taken into account. The R point was chosen because of its nearness to the dummy's, and it is hopefully more representative of the accelerations the dummy's undergo. The selection of the second point is due to the good quality of the signal at this point as it is a "hard" point of the structure, with a low noise level due to support vibration. In addition, this point is always located on the maximum deformation with, and by double integration, it gives the structure crush depth with time. Finally, the structure was deformed at this point in only one case, while for the other accelerometers, significant rotations were recorded which precluded any valid conclusion as regards the directions given by the axes.

Calculating the average maximum acceleration at the R point and at the rear left side rail we found no significant difference between configurations. However there was significantly lower results for the offset impact when compared with the 30° impact at the R point.

Finally, interior deformations were measured. These deformations were assessed by measuring the backward movement of 25 points defined by adhesive plastic targets on the front part of the interior of the passenger compartment under the dashboard previously removed. These 25 points formed a regular mesh whose horizontal lines were the:

- lower edge of the windscreen
- window lower cross-member
- front apron beam bottom
- front apron/toeboard joint
- toeboard/floor pan joint

and the vertical lines were on the left and right sides by the A pillars, on the centreline and 300 mm on each side of the centreline. These different parallel planes were named A to E from the left pillar.

For one of the vehicles studied, the appendix 3 gives the measurement point displacements for the three crash types. The vehicle front is shown on the left of the curves. The same vertical planes for the three configurations are given in parallel.

It should be first noted that asymmetric impacts led to a slightly greater deformation on the collision side. Right-side deformation in these two cases was extremely limited. It should also be observed that impact deformations into an offset barrier were smaller than into a 30° barrier, but the difference was not significant. But it worth noting that the largest deformation on the centreline (noted C) occurred when using a dynamometric barrier. Note that all the sampled vehicles had a transversal engine with. This type of engine there is generally less engine intrusion as compared to with a longitudinal engine-gearbox unit. Nevertheless, the maximum crush depth recorded during the tests did not exceed 250 mm at the toeboard/front-apron junction.

External vehicle deformations were also studied. The following figure shows the vehicle 2 outline before and after the three different tests. Note that in the dynamometric barrier where the entire car front is brought into play, there is still significant deformation.

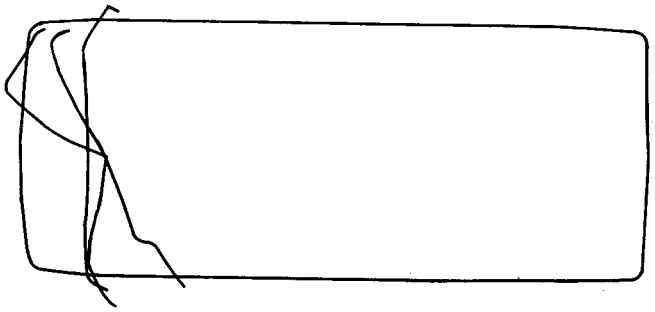

Figure 1. External Deformations

For all five tests against the dynamometric barrier the mechanical elements (engine, gearbox, etc...) contacted the bulkhead which deformed accordingly. However for the offset barrier, the engine came to rest just before the bulkhead.

Conclusion

The crash into a 90° dynamometric barrier, associated with an impact velocity of 57 km/h, allowed the study of current vehicle limits without severity levels high that any observation could just as well lead to opposite conclusions. The advantage of such a test is that the structure deforms in a symmetrical manner and we obtain additional information of interest such as the impact force. In association with dynamic measurement of the crush depth, obtained either through the double integration of acceleration or by film analysis, it is possible to obtain the deformation energy. With reference to accidentology, the deformations corresponding the closest with those obtained in real-world crashes are those obtained with the 30 and offset barriers. At every level the results from the 30° barrier and the dynamometric barrier appear very similar. Consequently, because of its closeness to real world accidents; this configuration is useful.

As regards the offset barrier, it seems that the impact velocity selected was too low. Indeed, the engine compartment deformation limits were generally not reached. But at an impact velocity of the order of 53 to 54 km/h, which increases kinetic energy by 12 to 17%, the same severity level as found on the other two configurations will be reached for the driver while obtaining completely different structure deformations.

Appendix 1

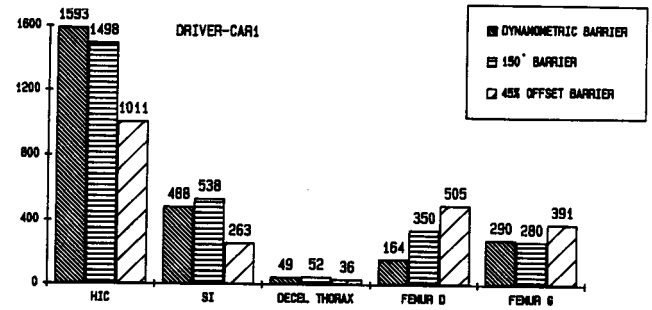

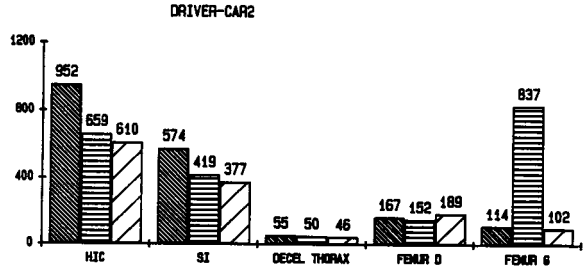

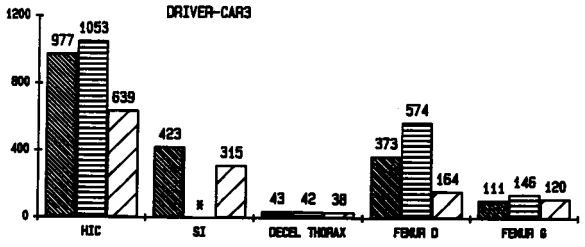

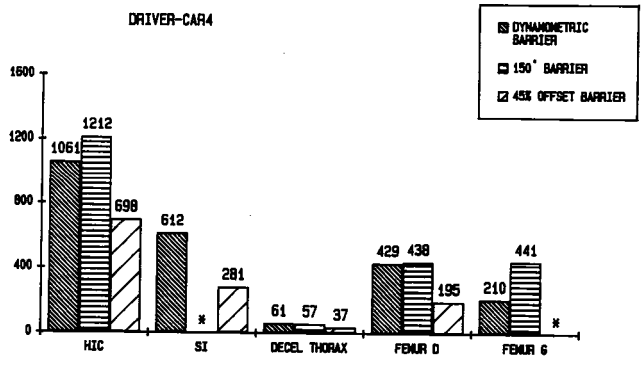

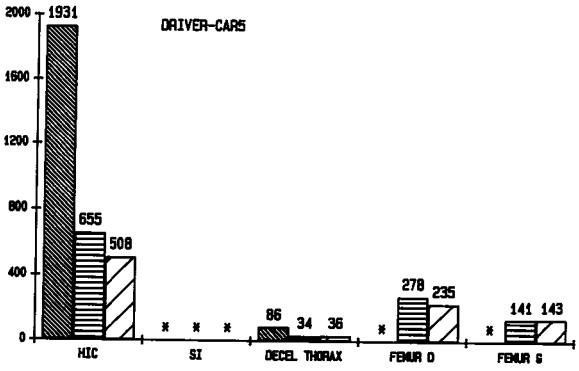

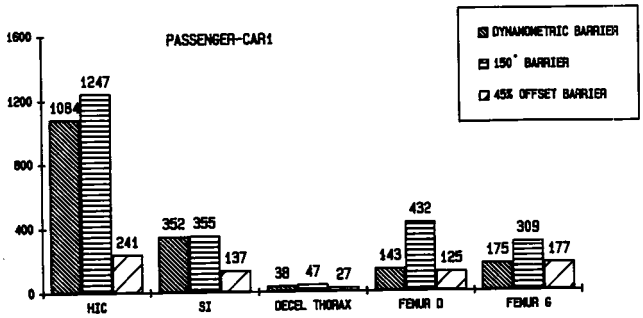

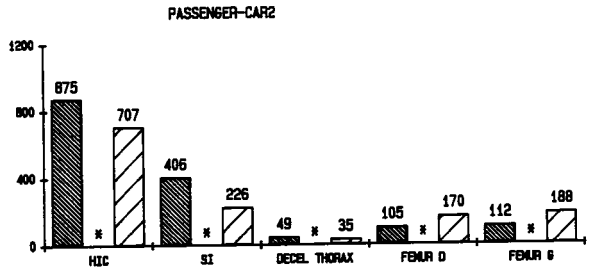

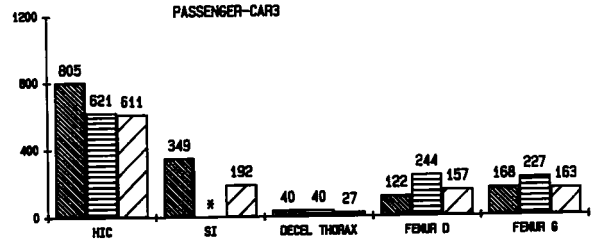

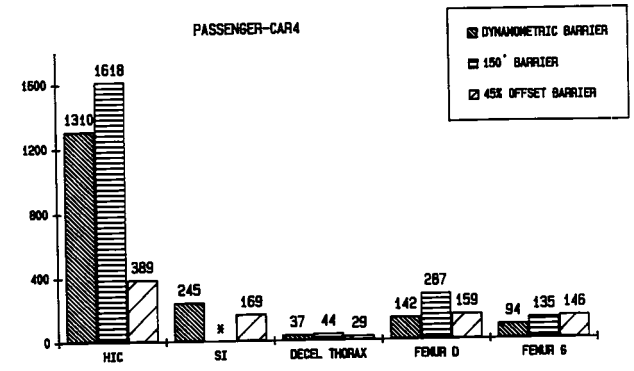

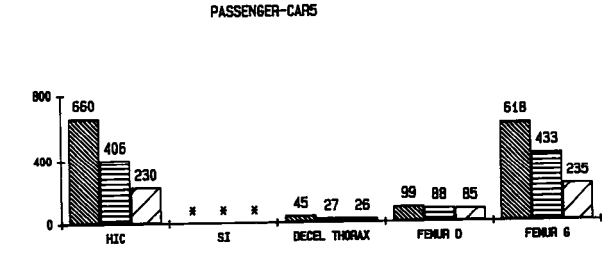

Appendix 2

car	car 1	car 1	car 1
crash test	offset barrier	30° barrier	dynamo barrier
lower side-rail right	38/ 18 / 11 / 38	40/30/13/48	41 / 17 / 14 / 43
lower side-rail left	30 / 27 /42 / 49	39/24/27/44	42 / 14 / 17/ 43
B pillar right	33 / 32 / 14 / 39	37/16/16/39	43 / 14 / 25 / 46
B pillar left	32 / 23 /22/ 39	52/28/28/53	34 / 21 / 26/ 40
center (point R)	45 / 30 / 32 / 49	41/44/31/44	50 / 26 / 36 / 55
car	car 2	car 2	car 2
crash test	offset barrier	30° barrier	dynamo barrier
lower side-rail right	29 / 20 / 11 / 35	44 / 20 /25 / 45	30 /8 /9 /31
lower side-rail left	28 / 6 / 6 / 28	41 / 34 /25 / 52	30 /10 /11 /31
B pillar right	30 / 8 / 8 / 31	48 / 20 /12 / 51	33 /10 /15 /36
B pillar left	32 / 20 / 11 / 34	30 / 16 /20 / 34	39 /12 /12 /39
center (point R)	37/16/20/38	42/42/29/51	42/17/33/44
car	car 3	car 3	car 3
crash test	offset barrier	30° barrier	dynamo barrier
lower side-rail right	28 /14 /11 /29	29 /15 /13 /31	52/29/ /
lower side-rail left	26 /14 /8 /27	30 /24 /16 /35	45/32/ /
B pillar right	28 /16 /10 /31	37 /14 /25 /38	59/54/ /
B pillar left	28 /19/12 /33	29 /16 /12 /32	69/67/ /
center (point R)	39 /14 /26 /42	57 /9 /19 /58	*
car	car 4	car 4	car 4
crash test	offset barrier	30° barrier	dynamo barrier
lower side-rail right	27 /15 / 9 /29	36/11/17/37	34/13/ /
lower side-rail left	26 /13 /10 /29	44/8/15/46	43/18/ /
B pillar right	29 /19 /11 /34	49/25/21/51	44/30/ /
B pillar left	22 /13 /12 /26	53/14/24/54	37/37/ /
center (point R)	41 /22 /18 /43	66/14/39/67	*
car	car 5	car 5	car 5
crash test	offset barrier	30° barrier	dynamo barrier
lower side-rail right	30	*	41
lower side-rail left	28	40/26	66/
B pillar right	28	33/24	37/
B pillar left	38/14	31/21/*/33	43/
center (point R)	32/	61/	*

Appendix 3

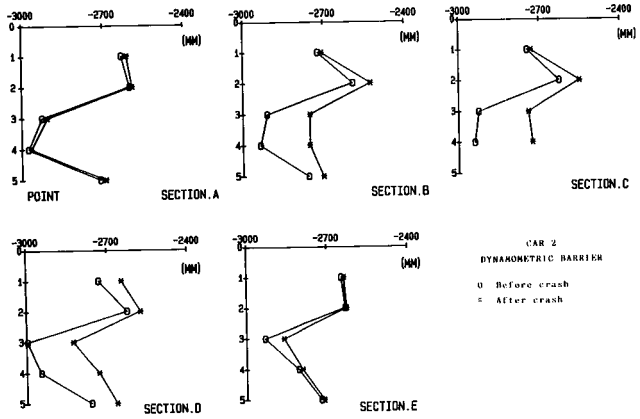

Appendix 3 (Continued)

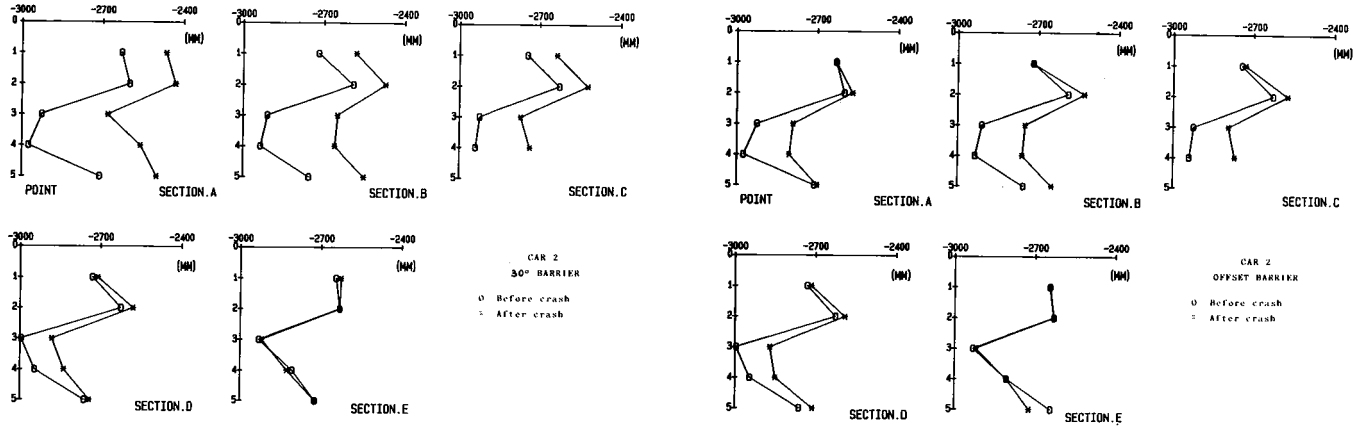

S9-O-04

The Effects of FMVSS No. 208 and NCAP on Safety as Determined from Crash Test Results

James R. Hackney
National Highway Traffic Safety Administration

Introduction

In 1978, the National Highway Traffic Safety Administration (NHTSA) began the crashworthiness assessment of new cars by conducting high speed 35-mph frontal barrier crash tests. This New Car Assessment Program (NCAP) has primary goals to provide consumers with a measure of the relative safety potential of automobiles and to establish market forces which encourage vehicle manufacturers to design higher levels of safety into their vehicles.

NHTSA has now conducted NCAP crash tests of 304 different makes and models of passenger cars (PCs) and 50 light trucks and vans (LTVs). The data from the driver and passenger dummies are regularly released as part of NHTSA's Consumer Information Program as required by Title II of the Motor Vehicle Information and Cost Savings Act (15 U. S. C. 1942 et seq.).

With model year (MY) 1987 automobiles, the mandatory passive safety requirements of Federal Motor Vehicle Safety Standard (FMVSS) No. 208, "Occupant Crash Protection," were phased in. Prior to 1987, only a few vehicles had been voluntarily produced with passive restraint systems. These included GM, Ford, and Mercedes airbags and VW and Toyota passive belts. Beginning in MY 1987, the manufacturers selected either passive belts (2 or 3 point, non-motorized or motorized) or airbags to meet the FMVSS No. 208 requirements. In NHTSA's Enforcement program since then, approximately 20 PCs have been crash tested each year at 30 mph into a fixed rigid barrier to evaluate certification.

The objectives of this report are (1) to examine and compare the results from these two test programs, (2) to assess the improvements in vehicle safety which have resulted from NCAP and FMVSS No. 208, (3) to examine manufacturers response to NCAP and the public awareness of vehicle safety, and (4) to apply data from the crash programs to evaluate safety differences between vehicle weight classes.

Test Conditions

The test conditions for both test programs are based on years of development work conducted by NHTSA, the automobile industry, and others to develop the test devices and test procedures used in measuring compliance to the passive restraint requirements of FMVSS No. 208. For these requirements, certain injury criteria, as measured by the anthropomorphic dummies, are not to be exceeded in a 30 mph frontal barrier crash. The injury criteria apply to the head (as measured by a composite of acceleration values known as the Head Injury Criterion, or HIC), chest (as measured by chest deceleration, chest gs), and upper leg (as measured by femur axial compression loads). These criteria are used to evaluate the compliance of vehicles to the safety standard and to assess the performance of the vehicles in the NCAP tests.

The major differences between the FMVSS No. 208 tests and the NCAP tests, which have been conducted for MY 87 through MY 91 PCs, are (1) the nominal speed at which the tests are conducted (i. e., 30 versus 35 mph) and (2) the use of all available restraint systems in the NCAP tests as compared to only the use of the passive restraint systems in the FMVSS No. 208 tests (note: the exception to this is the condition in which the vehicle has a driver airbag and a manual safety belt system for

the right front passenger. In the FMVSS No. 208 test, the vehicle is then tested with the airbag as the restraint for the driver and the manual system for the passenger).[1] Other minor variations between the two test conditions include; for the NCAP tests, dummies are not calibrated as often as in the FMVSS No. 208 tests, a load cell barrier is attached to the fixed rigid barrier and additional instrumentation is used (i. e., load cells on the safety belts).

NCAP Tests. The NCAP crash tests are conducted at 35 mph in order to provide a level of impact severity sufficiently higher than the 30 mph FMVSS No. 208 test speed so that possible differences in frontal crash safety performance can be observed. As calculated from the kinetic energy, a 35 mph crash is about one-third more severe than a crash at 30 mph.

In these 35 mph crash tests the vehicle experiences a total change in velocity, including rebound from the barrier, of approximately 40 mph. In a 30 mph crash test the change in velocity is approximately 33 mph. From examination of the National Accident Sampling System (NASS) files, the fatality and injury rates for restrained front seat occupants are two to three times greater in a crash with a 40 mph change in velocity than in a crash with 33 mph change in velocity. For events in which crash severity is determined, the NASS files also show that more than 40 percent of the life-threatening (AIS 4 and greater) injuries and fatalities of occupants in frontal collisions occur in crashes with a change in velocity greater than 33 mph.

NCAP and FMVSS No. 208 Databases

In the late 1970's, NHTSA Research and Development established an electronic database on a VAX mini-computer for the storage of agency-conducted crash test data. Since that time, more than 1,500 crash tests have been conducted with complete data sets stored and maintained in this vehicle crash test database. These tests include all tests through MY 1991 which have been conducted in NCAP and in support of FMVSS No. 208.

In 1985, extensive studies were conducted on the NCAP data [1]. To support these studies, a list of parameters which were judged to be important in evaluating vehicle safety performance was developed and analyses of the electronic measurement data were performed to extract these parameters for each vehicle which had been tested in the NCAP. A DBASE III file and a SAS file which contain these parameters were established in 1986. These files have been updated through MY 1991 vehicles and are maintained by engineering support staff at the Volpe National Transportation Systems Center. A similar DBASE III file has recently been completed on the PCs which have been tested in FMVSS No. 208. Fifty two parameters (38 for FMVSS No. 208) on each test are included in these files (see Table 1).

The availability of these parameters and the actual vehicle and dummy response curves in the Vehicle Crash Test Database establish the feasibility to conduct extensive comparisons between the two test programs and in-depth analyses of vehicle structures and restraint systems.

Comparisons of Results from FMVSS No. 208 and NCAP Tests

For MYs 1987 through 1991, 98 PCs have been tested in FMVSS No. 208 and 127 PCs have been tested in NCAP. Listings of the automobiles and the responses from dummies in these tests are given in Table 2 for the FMVSS No. 208 tests and in Table 3 for the NCAP tests.

Overall Comparisons

From the data in Tables 2 and 3, the averages and standard deviations are calculated. These are given in Table 4. Significant differences in average HIC values are noted, with the average NCAP HICs approximately twice those from the FMVSS No. 208 tests. These higher HIC values are indicative of the much greater probability of head to steering assembly and head to instrument panel contacts which occur in the higher severity NCAP tests. However, the average chest Gs are only marginally higher (4 to 5 Gs) in the NCAP tests. In examining the femur loads, the use of all available restraint systems in the NCAP tests is reflected in lower average values for the more severe crash tests. The lap belt which is not part of the passive restraint system in many of the vehicles, but which is used in the NCAP tests, prevents or decreases the knee contacts with the steering assembly and instrument panel. The standard deviations and ranges indicate approximately twice the absolute variation for the HIC values in the NCAP tests than in the FMVSS No. 208 tests (i.e., 400 versus 200). When compared to the average values, however, these deviations are almost identical (approximately 40 percent of the average).

Distributions of dummy response results from FMVSS 208 tests and NCAP tests are shown in Figure 1. Over 92 percent of the HICDs and 97 percent of the HICPs are below 750 in the FMVSS 208 tests. In NCAP, only 41 percent of the HICDs and 67 percent of the HICPs are below 750. For the NCAP, more than 49% of the HICDs and almost 27% of the HICPs fall between 750 and 1250. Almost 17% of the HICDs and 8.5% of the HICPs in these more severe tests exceed 1250.

Although the averages and distributions of the HICs indicate the much higher responses of the dummies in

[1]It should also be noted that NHTSA will test the "worst case" condition in FMVSS No. 208, based on manufacturer-supplied certification data. Theoretically this could include the use of both the active and automatic restraints furnished with the vehicle. Through MY 1991, no PCs have been tested in FMVSS No. 208 with both restraint systems employed.

Table 1. Parameters in DBASE Files

Parameter	Description
TESTNO	Number which identifies test in NHTSA Vehicle Data Base
MODYR	Vehicle Model Year
MAKE	Vehicle Make
MODEL	Vehicle Model
BODY	Vehicle Body Type
WHLBAS	Vehicle Wheelbase (inches)
TESTWT	Vehicle Test Weight (pounds)
WTCLSS	Vehicle Weight Class
SPEED	Vehicle Test Speed (mph)
HICD	Driver HIC
HAISD	Driver AIS Estimated From HIC
CGD	Driver Chest Acceleration (g's)
CAISD	Driver AIS Estimated From Chest Acceleration
HICP	Passenger HIC
HAISP	Passenger AIS Estimated From HIC
CGP	Passenger Chest Accelerations (g's)
CAISP	Passenger AIS Estimated From Chest Acceleration
LFEMD	Driver Left Femur Force (pounds)
RFEMD	Driver Right Femur Force (pounds)
LFEMP	Passenger Left Femur Force (pounds)
RFEMP	Passenger Right Femur Force (pounds)
PEAKG	Peak Deceleration of Vehicle Compartment when Filtered to 30 Hz (g's)
TPEAKG	Time at which PEAKG Occurs (msec)
TPULSE	Duration of the Vehicle Crash Pulse
BARFOR *	Maximum Total Barrier Force (pounds)
DISBF *	Vehicle Dynamic Displacement at BARFOR Computed from 100 Hz Filtered Crash Pulse Data (inches)
STFBF *	Vehicle Linear Stiffness Derived from BARFOR and DISBF (pounds/inch)
MAXDIS	Maximum Vehicle Dynamic Crush Derived from 100 Hz Filtered Crash Pulse Data (inches)
HEADT1	Estimated Starting Time of Head Impact with Steering Assembly (msec)
HEADT2	Estimated Ending Time of Head Impact with Steering Assembly (msec)
VELCHG	Change in Driver Head Velocity due to Contact With Steering Assembly (mph)
RESTRD	Driver Restraint System
RESTRP	Passenger Restraint System
BELT1D *	Time at which the Driver Torso Belt Force Reaches 200 Pounds (msec)
BELT2D *	Time at which the Driver Torso Belt Force Reaches BELTLD (msec)
BELTLD *	Driver Torso Belt Force Nominally Set at 1,000 Pounds
BELTRD *	Driver Torso Belt Loading Rate (pounds/msec)
BELTPD *	Peak Driver Torso Belt Force (pounds)
BELT1P *	Time at which the Passenger Torso Belt Force Reaches 200 Pounds (msec)
BELT2P *	Time at which the Passenger Torso Belt Force Reaches BELTLD (msec)
BELTLP *	Passenger Torso Belt Force Nominally Set at 1,000 Pounds
BELTRP *	Passenger Torso Belt Loading Rate (pounds/msec)
BELTPP *	Peak Passenger Torso Belt Force (pounds)
HHD	Distance from Driver Head to Windshield Header (inches)
HWD	Distance from Driver Head to Windshield (inches)
CSD	Distance from Driver Chest to Hub of Steering Wheel (inches)
KDD	Distance from Driver Knees to Lower Dash Panel (inches)
HHP	Distance from Passenger Head to Windshield Header (inches)
HWP	Distance from Passenger Head to Windshield (inches)
CDP	Distance from Passenger Chest to Dash Panel (inches)
KDP	Distance from Passenger Knees to Dash Panel (inches)

* Parameters available only for NCAP tests.

Table 2. Results from FMVSS No. 208 Crash Tests

VEHICLE IDENTIFICATION				DUMMY RESPONSE PARAMETERS							
MAKE	MODEL	DRS	MY	HICD	CGD	LFEMD	RFEMD	HICP	CGP	LFEMP	RFEMP
AMC	ALLIANCE	2	87	970	43	446	1252	599	41	1232	880
VOLKSWAGEN	GOLF	4HB	87	883	44	1291	847	406	41	1222	1066
MAZDA	626	4	87	702	39	667	1379	459	37	1581	1284
CHRYSLER	LEBARON	2	87	691	39	806	1738	263	27	1206	964
OLDSMOBILE	CALAIS	2	87	681	36	1022	1575	383	34	455	874
BUICK	LESABRE	2	87	664	35	1126	883	366	30	733	607
TOYOTA	CAMRY	4	87	527	41	1393	1959	469	43	1429	1547
HYUNDAI	EXCEL	4HB	87	485	44	1975	1930	303	48	1571	1076
YUGO	GVS	2HB	87	436	40	1169	1392	291	36	1179	1736
MERCURY	LYNX	4HB	87	416	41	1031	913	526	40	1132	1011
SUBARU	SUBARU	2	87	353	34	949	783	292	32	490	444
HONDA	ACCORD	2HB	87	315	46	1590	278	374	39	435	471
PUEGEOT	505	4	88	903	44	1658	907	218	37	1146	1332
VOLKSWAGEN	JETTA	4	88	678	50	1072	1421	656	43	822	1213
NISSAN	MAXIMA	4	88	658	45	1163	1361	662	51	1071	1013
DODGE	SHADOW	4	88	647	45	1496	1623	409	38	853	1141
OLDMOBILE	CUTLASS SUP	2	88	631	34	909	723	507	38	856	291
CHEVROLET	BERETTA	2	88	543	37	428	1604	502	36	493	632
VOLVO	740	4	88	459	54	1500	2010	167	42	778	1048
FORD	TEMPO	4	88	456	44	1144	1209	561	45	668	521
HONDA	PRELUDE	2	88	452	43	597	1025	315	34	911	574
CHRYSLER	EAGLE PREM	4	88	429	50	1580	1703	473	42	1488	1381
TOYOTA	CRESSIDA	4	88	381	42	1504	1187	387	41	1094	1294
ISUZU	IMPULSE	2	88	336	37	1258	1066	243	32	880	788
MITSUBISHI	STARION	2	88	320	48	1819	1686	710	57	1172	1360
FORD	TEMPO	4	88	318	47	1464	1560	327	41	661	612
ACURA	LEGEND	4	88	284	45	1548	1651	387	37	659	1235
DODGE	DAYTONA	2	88	194	28	677	1439	319	28	991	825
CHEVROLET	CORSICA	4	89	872	42	509	1451	615	40	1122	959
BUICK	SKYLARK	2	89	724	46	1283	1734	527	45	485	913
MERCEDES	190E	4	89	599	50	1857	1969	454	40	544	436
PONTIAC	GRAND PRIX	2	89	598	42	1250	1079	542	44	671	695
PONTIAC	BONNEVILLE	4	89	578	36	751	1208	346	30	530	444
MITSUBISHI	PRECIS	4	89	524	39	2367	1300	253	40	1544	1138
NISSAN	SENTRA	2	89	509	49	1370	1355	653	40	1000	1190
SUBARU	GL	4	89	496	48	1270	1034	720	44	634	821
CHRYSLER	CONQUEST	2	89	490	54	1753	1700	420	44	1316	1894
AUDI	200	4	89	463	58	2263	1375	185	34	392	259
FORD	TEMPO	4	89	435	45	1636	1077	390	41	749	616
LINCOLN	CONTINENTAL	4	89	421	46	1572	1391	305	43	1100	1468
HYUNDAI	SONATA	4	89	420	42	1764	1570	298	37	1264	1054
NISSAN	PULSAR	2	89	408	50	1363	2030	304	35	559	
TOYOTA	CRESSIDA	4	89	359	39	1371	1616	441	41	1266	1057
SAAB	9000	4	89	323	46	1235	1601	232	36	503	
SAAB	900S	2	89	289	40	986	1548	223	35	1327	1840

Table 2. Results from FMVSS No. 208 Crash Tests

VEHICLE IDENTIFICATION				DUMMY RESPONSE PARAMETERS							
MAKE	MODEL	DRS	MY	HICD	CGD	LFEMD	RFEMD	HICP	CGP	LFEMP	RFEMP
DAIHATSU	CHARADE	2	89	272	45	2045	1386	233	40	1503	1507
FORD	ESCORT	2	89	244	38	1444	1080	437	34	989	1007
DODGE	DIPLOMAT	4	89	106	29	1366	1341	460	37	196	115
CHEVROLET	LUMINA	4	90	921	50	815	1288	579	40	285	508
CHEVROLET	LUMINA	4	90	921	50	815	1288	579	40	285	508
SUBARU	JUSTY	2	90	769	45	297	622	626	48	352	717
SUBARU	LEGACY	4	90	711	40	1570	1799	452	46	1014	1376
CHEVROLET	CAPRICE	4	90	632	46	194	105	513	39	251	401
NISSAN	AXXESS	4	90	624	41	1104	1004	572	43	1310	1342
NISSAN	STANZA	4	90	595	50	1481	1499	383	43	823	913
MITSUBISHI	PRECIS	4	90	573	41	2147	1393	286	38	1349	990
VOLKSWAGEN	FOX	2	90	572	38	1350	1310	305	36	810	1226
TOYOTA	COROLLA	4	90	524	45	1540	1668	582	41	1024	1208
MAZDA	323	4	90	459	44	2323	2038	481	39	1225	1385
TOYOTA	CELICA	2	90	435	55	1692	1332	473	38	710	949
FORD	MUSTANG	2	90	433	41	1737	1328	262	25	250	175
DODGE	SPIRIT	4	90	414	49	1261	1263	282	40	280	898
PLYMOUTH	LASER	2	90	406	28	731	738	496	33	670	629
LEXUS	ES-250	4	90	397	51	1530	1513	364	46	847	1137
HONDA	CIVIC	4	90	385	54	1066	1554	866	43	619	1309
DODGE	DYNASTY	4	90	352	45	1027	1142	287	34	620	764
VOLKSWAGEN	PASSAT	4	90	326	40	1352	1306	336	41	1063	1284
HYUNDAI	EXCEL	2	90	310	40	1447	1201	504	44	1323	1207
ACURA	INTEGRA	4	90	275	39	1135	1729	518	44	805	1692
FORD	LTD CROWN V	4	90	268	45	1410	932	219	33	817	651
FORD	TAURUS	4	90	249	53	1491	1999	192	36	591	323
FORD	THUNDERBIRD	2	90	208	35	1983	1148	222	33	1885	1175
PONTIAC	FIREBIRD	2	90	197	37	981	1042	442	35	208	524
PLYMOUTH	SUNDANCE	4	90	138	32	1056	1226	222	31	358	357
OLDSMOBILE	DELTA 88 RO	4	90	88	26	1006	1208	183	35	337	160
MAZDA	MIATA	CV	91	790	46	1262	1160	326	39	549	1008
TOYOTA	TERCEL	4	91	671	39	964	1048	406	38	874	942
PONTIAC	LEMANS	2	91	647	50	2115	1762	588	48	1288	1821
GM	SATURN	4	91	636	40	755	1068	633	39	1109	1076
GEO	METRO	CV	91	616	51	1817	1977	852	54	385	235
MITSUBISHI	GALLANT	4	91	603	40	1290	1103	496	38	999	1094
VOLKSWAGEN	CORRADO	2	91	540	59	1474	1343	486	48	1338	1650
TOYOTA	CELICA	2	91	514	59	1622	1263	417	40	343	647
TOYOTA	MR2	2	91	433	63	1622	1677	305	42	234	390
BMW	318i	2	91	431	62	1739	2136	227	36	473	613
AUDI	100	4	91	407	48	2272	1362	214	32	610	276
NISSAN	STANZA	4	91	382	45	1272	1669	707	46	958	1265
MERCURY	CAPRI	CV	91	335	52	1655	1940	148	36	874	1227
FORD	ESCORT	2	91	315	31	1215	963	457	33	1059	930
CHRYSLER	LEBARON	CV	91	306	52	913	1634	214	27	310	474

Table 2. Results from FMVSS No. 208 Crash Tests

VEHICLE IDENTIFICATION				DUMMY RESPONSE PARAMETERS							
MAKE	MODEL	DRS	MY	HICD	CGD	LFEMD	RFEMD	HICP	CGP	LFEMP	RFEMP
ISUZU	STYLUS	4	91	290	43	1517	1695	903	44	273	382
FORD	PROBE	2	91	270	37	1485	1451	173	32	973	944
CHEVROLET	CAPRICE	4	91	267	39	1516	1590	563	40	401	394
HONDA	ACCORD	4	91	247	46	2092	1312	500	43	784	1151
CHRYSLER	5TH AVE	4	91	225	47	932	1118	203	31	536	661
DODGE	SHADOW	CV	91	201	48	1378	1232	260	44	646	678
CHEVROLET	BERETTA	2	91	172	52	1317	1371	383	33	291	202
BUICK	PARK AVE	4	91	158	29	1064	1372	647	33	935	908

Table 3. Results from NCAP Crash tests for MY 87 through 91

VEHICLE IDENTIFICATION				DUMMY RESPONSE PARAMETERS							
MAKE	MODEL	DRS	MY	HICD	CGD	LFEMD	RFEMD	HICP	CGP	LFEMP	RFEMP
NISSAN	SENTRA	4	87	2034	61	803	615	799		304	415
YUGO	GV	2HB	87	1855	45		585	379	41	701	172
PEUGEOT	505	4	87	1831	60	300	546	1786	50	535	176
ISUZU	I-MARK	4	87	1809	53	351	747	1042	51	365	225
VOLKSWAGEN	FOX	2	87	1801	52	484	723	2140	52	924	450
DODGE	SHADOW	2HB	87	1488	49	1003	748	653	36	529	486
SUBARU	GL	4	87	1339	58	1016	694	884	44	485	309
NISSAN	200SX	4	87	1226	53	1390	740	664	37	103	89
MITSUBISHI	STARION	2HB	87	952	48	1260	1752	377	46	1369	2323
PLYMOUTH	SUNDANCE	4HB	87	873	52	717	832		41	467	540
TOYOTA	CAMRY	4	87	871	51	1380	1200	973	46	1160	1167
MAZDA	626	4	87	846	52	820	1300	801	46	1487	1255
PONTIAC	GRAND AM	2	87	846	44	879	1848	601	41	497	529
CHRYSLER	LE BARON	2	87	791	62	1008	1863	1698	82	1776	853
HONDA	ACCORD	2HB	87	769	46	863	695	382	36	1244	558
HYUNDAI	EXCEL	4	87	757	54	2408	1794	345	46	1187	1006
MERCURY	TOPAZ	4	87	743	64	585	1277	626	40	957	455
CHEVROLET	CAMARO	2HB	87	733	39	736	961	660	39	353	144
HYUNDAI	EXCEL	2HB	87	716	55	790	345	1003	43	1360	775
SUBARU	JUSTY DL	2HB	87	611	42	529	1256	547	38	595	426
PONTIAC	SUNBIRD	4	87	603	36	428	1079	404	37	483	211
ACURA	INTEGRA	2HB	87	599	35	791	387	597	34	262	354
SAAB	9000	4HB	87	584	37	120	346	440	35	435	638
FORD	ESCORT	2HB	87	551	42	1146	1053	418	40	465	619
FORD	MUSTANG LX	2HB	87	479	42	580	1589	301	34	921	290
OLDSMOBILE	CALAIS	4	87	405	70	1085	1737	328	40	1435	555
PEUGEOT	505	4	88	1701	60	1657	930	1457	45	751	328
RENAULT	MEDALLION	4	88	1656	57	205	617	873	38	411	1193
BUICK	PARK AVENUE	4	88	1467	54	712	479	794	37	1366	686
CHRYSLER	NEW YORKER	4	88	1362	55	730	1580	424	43	1102	454
NISSAN	PULSAR	2HB	88	1134	40		122	430	31	226	1742
VOLKSWAGEN	FOX	2	88	1114	55	344		1424	44	663	478

Table 3. Results from NCAP Crash tests for MY 87 through 91

VEHICLE IDENTIFICATION				DUMMY RESPONSE PARAMETERS							
MAKE	MODEL	DRS	MY	HICD	CGD	LFEMD	RFEMD	HICP	CGP	LFEMP	RFEMP
NISSAN	SENTRA WAG	4W	88	1047	53	880	686	526	42	1030	853
FORD	FESTIVA	2HB	88	1014	52	976	876	822	43	747	251
TOYOTA	TERCEL	2HB	88	1005	40	1245	572	398	42	367	261
MAZDA	RX-7	2HB	88	921	39	186	1135	614	48	268	650
NISSAN	MAXIMA	4	88	907	64	1422	1500	861	49	885	1049
BUICK	REGAL	2	88	880	50	996	686	535	33	642	526
CHEVROLET	BERETTA	2	88	864	50	1692	1731	559	42	1052	796
PONTIAC	LE MANS	2	88	819	57	1263	792	897	44	378	389
HONDA	CIVIC DX	2HB	88	787	37	767	816	533	38	471	184
DAIHATSU	CHARADE	2HB	88	768	43	574	1188	642	37	598	388
FORD	TEMPO	4	88	721	47	1113	1773	470	50	1037	702
SAAB	900S	2HB	88	718	46	1776	1395	1250	35		1535
MERCURY	SABLE	4	88	712	51		1512	410	35	862	913
OLDSMOBILE	DELTA 88	4	88	710	51	1350	2119	539	38	520	593
FORD	TAURUS	4	88	707	38		775	359	47	455	438
TOYOTA	COROLLA	2HB	88	593	42	719	1162	397	40	300	393
VOLVO	740 GLE	4	88	519	42	1143	1793	445	42	723	634
ACURA	LEGEND	4	88	435	50	926	730	618	41	708	722
MAZDA	929	4	88	273	51	1093	774	859	49	450	450
CHEVROLET	CORSICA	4	88		44	1293	614	752	40	737	845
PEUGEOT	505S	4	89	1983	64	966	839	2192	77	1024	554
DODGE	SPIRIT	4	89	1421	47	672	1295	537	45	772	707
CHEVROLET	CAPRICE	4	89	1328	64	406	260	1365	42	493	495
HYUNDAI	SONATA	4	89	1196	54	869	603	937	53	1717	293
GEO	METRO	4	89	1075	56	805	244	840	46	465	1002
TOYOTA	COROLLA	4	89	994	49	1101	894	546	45	451	681
MITSUBISHI	GALANT	4	89	971	50	1613	1229	998	40	584	526
FORD	PROBE	2HB	89	970	46	691	870	496	35	579	187
MITSUBISHI	MIRAGE	4	89	960		827	1367	772	42	1218	1078
GEO	METRO	2	89	951		789	671	1177	33	458	571
MERCURY	TRACER	4HB	89	940	48	2073	733	425	38	658	581
EAGLE	PREMIER	4	89	877	46	742	1011	868	44	765	685
LINCOLN	CONTINENTAL	4	89	863	48	314	1326	492		1247	1090
NISSAN	MAXIMA	4	89	808	51	611	664	736	44	1409	1043
TOYOTA	CRESSIDA	4	89	790	51	1632	1554	544	51	1246	1107
VOLKSWAGEN	FOX	2	89	787	64	139	738	818	58	1019	508
CHRYSLER	FIFTH AVE	4	89	786	43	1132	766	682	43	667	575
HONDA	CIVIC CRX	2HB	89	750	39	361	903	520	37	791	375
EAGLE	MEDALLION	4	89	745	41	1721	1738	589	39	1574	1670
PLYMOUTH	ACCLAIM	4	89	663	46	1201	1552	810	50	840	873
AUDI	80	4	89	600	49	168	324	515	39	1871	245
FORD	THUNDERBIRD	2	89	541	44	1224	1138	496	40	1264	776
NISSAN	240SX	2HB	89	407	41	1234	656	525	44	687	854
DODGE	DAYTONA	2HB	89	399	39	729	795	297	32	908	457
AUDI	100	4	89	185	35	998	571	710	31	894	757

Table 3. Results from NCAP Crash tests for MY 87 through 91

VEHICLE IDENTIFICATION				DUMMY RESPONSE PARAMETERS							
MAKE	MODEL	DRS	MY	HICD	CGD	LFEMD	RFEMD	HICP	CGP	LFEMP	RFEMP
HONDA	PRELUDE	2	90	1279	59	770	674	854	48	681	733
CHEVROLET	LUMINA	4	90	1200	58	782	935				
VOLKSWAGEN	PASSAT	4	90	1182	59	1104	1154	604	46	1436	2474
NISSAN	STANZA	4	90	1105	59	1404	1205	629	47	813	744
NISSAN	AXXESS	4HB	90	1051	46	919	1266	654	46	1257	1143
BMW	325i	2	90	1036	56	865	853				
GEO	PRISM	4	90	1030	47	1341	1549	1141	53	455	447
SUBARU	LEGACY	4	90	1007	52	1957	1899	675	44	842	1121
LEXUS	ES250	4	90	992	55	1102	1689	630	47	1012	1075
MAZDA	MIATA	2CV	90	920	59	1026	796	531	42	911	763
TOYOTA	CELICA	2	90	834	50	1071	1190	685	37	906	609
MERCEDES	190E	4	90	800	60	705	1028	833	58	582	331
MITSUBISHI	ECLIPSE	2HB	90	772	44	1152	1033	612	40	499	413
CHEVROLET	CAVALIER	4	90	770	49	775	1749	485	37	531	890
FORD	TAURUS	4	90	735	46	1219	1261	609	40	581	318
HYUNDAI	EXCEL	2HB	90	696	41	1385	1921	419	39	1682	964
FORD	MUSTANG	2CV	90	651	42	1353	1707	438	50	1063	408
ACURA	INTEGRA	4	90	585		1545	1684	637	42	1301	1877
CHRYSLER	IMPERIAL	4	90	517	43	767	862	2132	56	979	863
LINCOLN	TOWN CAR	4	90	471	40	1768	883		36	855	844
INFINITI	M30	2	90	466	43	936	1132	443	45	844	716
CADILLAC	DEVILLE	4	90	423	39	541	764		46	1629	1113
CHRYSLER	LEBARON	2CV	90	298	40	332	1119	2043	46	611	769
BUICK	LESABRE	2	90		35	1049	669	426	32	908	903
TOYOTA	COROLLA	4	91	1238	54	1375	917	613		1342	1469
TOYOTA	TERCEL	4	91	1138	57	945	1325	729	51	778	948
HONDA	CIVIC	4	91	1068	50	1002	2158	601	47	771	625
MITSUBISHI	GALANT	4	91	1024	61	1243	1395	711	53	906	1232
SATURN	SL2	4	91	918	44	1009	1326	1018	46	1178	974
HYUNDAI	SCOUPE	2	91	870	45	2532	967	618	42	1296	332
BUICK	CENTURY	4	91	815	47	1340	1014	1144	40	315	179
MAZDA	PROTEGE	4	91	779	57	1718	853	612	51		1087
NISSAN	300ZX	2	91	765	54	1495	1415		47	1668	1552
PLYMOUTH	ACCLAIM	4	91	761	55			446	43		
HONDA	ACCORD	4	91	750	50	1361	1452	378	40	1214	900
CHEVROLET	CAMARO	2HB	91	585	39	717	627	583	42	150	174
NISSAN	SENTRA	4	91	583	46	1117	1210	681	45	475	
ISUZU	STYLUS	4	91	580	57	1021	859		46	439	717
HONDA	ACCORD	4W	91	562	45	519	1015	539	43	892	562
FORD	PROBE	2HB	91	550	42	1051	1592	418	45	1501	1033
NISSAN	STANZA	4	91	546	56	1803					
CHEVROLET	CAPRICE	4	91	533	54	1529	1527	1101	48	613	626
CHRYSLER	NEW YORKER	4	91	511	55	709	1133			958	793
DODGE	SHADOW	4HB	91	503	42	1234	739	457	39	647	781
CHEVROLET	CORSICA	4	91	493	41			956	44		

Table 3. Results from NCAP Crash tests for MY 87 through 91

VEHICLE IDENTIFICATION				DUMMY RESPONSE PARAMETERS							
MAKE	MODEL	DRS	MY	HICD	CGD	LFEMD	RFEMD	HICP	CGP	LFEMP	RFEMP
FORD	TAURUS	4W	91	480	44	1900	1593	258	38	327	207
FORD	ESCORT	2	91	434	42	1403	1055	450	39	2152	1119
GEO	STORM	2	91	417	47	393	507	981	45	478	555
CHEVROLET	BERETTA	2	91	343	37	659	910	739	35	523	230

Table 4. Averages, Deviations, Minimums and Maximums from FMVSS No. 208 and NCAP Test Results

Parameter	HICD	HICP	CGD	CGP	LFEMD	RFEMD	LFEMP	RFEMP
208 Average	465	418	44	39	1332	1366	829	911
208 Std Deviation	197	166	7	6	447	370	386	421
208 Minimum	88	148	26	25	194	105	196	115
208 Maximum	970	903	63	57	2367	2136	1885	1894
NCAP Average	864	726	49	43	1010	1065	834	715
NCAP Std Deviation	365	383	8	7	460	444	414	421
NCAP Minimum	185	258	35	31	120	122	103	89
NCAP MAXIMUM	2034	2192	70	82	2532	2158	2152	2474

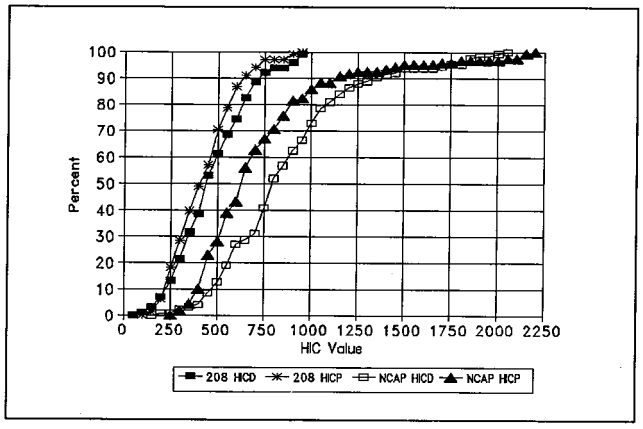

Figure 1. HIC Distributions—FMVSS No. 208 Compared to NCAP

NCAP, a large number of the PCs meet the FMVSS requirements in the higher speed crash test. Examination of the data in Table 3 indicates that more than 60 percent of the PCs (where all data are available) meet FMVSS No. 208 criteria.

Specific Comparisons

Of the 98 PCs tested in FMVSS No. 208 and the 127 PCs tested in NCAP for MYs 1987 through 1991, sixty one can be considered as nearly identical (i.e., in a few cases, variations may exist in drive train configurations and/or sheet metal design). These 61 PCs are listed in Table 5.

In making comparisons between dummy results from these "identical" vehicles, the following outcomes should be expected; (1) a vehicle which performs well (i.e., low dummy HIC and chest G response values) in the 35 mph NCAP test is expected to perform relatively as well in the 30 mph FMVSS 208 test, (2) a vehicle which performs poorly (i. e., high dummy response values) in the NCAP test may or may not perform poorly in the FMVSS 208 test, and (3) little correlation between dummy responses other than as stated in (1) and (2) will occur.

These expected outcomes are based on differences in the test conditions. Both manual and automatic restraint systems are used in the NCAP test. In most cases, only automatic restraint systems are used in the FMVSS test. The higher speed NCAP test requires the vehicle to dissipate approximately one-third more crash energy than in the FMVSS No. 208 test. The greater crash energy in an NCAP test is dissipated in approximately the same time as the crash energy in FMVSS No. 208 test (see discussion of crash pulses in Section 4). This higher severity crash causes much greater intrusion and higher acceleration in the occupant compartment. The steering assembly, instrument panel, and floorpan may experience significant erratic motion and deformation in the NCAP test. These effects will alter the dummy kinematics and dummy contact points when compared to the FMVSS No. 208 test. In addition, the protective capability of some safety belt systems may be approached or exceeded in the higher severity tests. The amount of belt stretch and "spool out" is often much higher in the NCAP test and may allow excessive excursion of the dummy.

By examining the crash test data of the "identical" cars in Table 5, statements can be made relative to the above discussions. In Table 5, the dummy responses are given (parameters are defined in Table 1). After the HICD in this table, rankings (RK) within the test group (i.e., FMVSS No. 208 or NCAP) are given. Very little consistency is found between the rankings for HICD. By applying the method of least squares, regression between the driver HICs indicates little correlation with an R-squared of 0.17. For the other three parameters, chest Gs and passenger HICs, even less correlation is found. Based on the data from these 61 comparisons, it can be concluded that this lack of correlation between the two vehicle test groups does not allow the prediction of an NCAP test result from the FMVSS No. 208 test result.

However, it is observed that the good performing vehicles in the 35 mph test also perform well in the 30 mph test. In fact, it may be concluded from these data that a passenger car that meets the FMVSS No. 208

Table 5. FMVSS No. 208 & NCAP Test Results from Similar Vehicles

TEST	VEHICLE IDENTIFICATION			DUMMY RESPONSE PARAMETERS								
TYPE	MAKE	MODEL	MY	HICD	RK	CGD	LFEMD	RFEMD	HICP	CGP	LFEMP	RFEMP
COMP	ACURA	INTEGRA	90	275	12	39	1135	1729	518	44	805	1692
NCAP	ACURA	INTEGRA	90	585	18		1545	1684	637	42	1301	1877
COMP	ACURA	LEGEND	88	284	13	45	1548	1651	387	37	659	1235
NCAP	ACURA	LEGEND	88	435	6	50	926	730	618	41	708	722
COMP	AUDI	100	91	407	27	48	2272	1362	214	32	610	276
NCAP	AUDI	100	89	185	1	35	998	571	710	31	894	757
COMP	BUICK	LESABRE	87	664	52	35	1126	883	366	30	733	607
NCAP	BUICK	LESABRE	90			35	1049	669	426	32	908	903
COMP	BUICK	PRK AVE	91	158	1	29	1064	1372	647	33	935	908
NCAP	BUICK	PRK AVE	88	1467	57	54	712	479	794	37	1366	686
COMP	CHEVROLET	BERETTA	88	543	41	37	428	1604	502	36	493	632
NCAP	CHEVROLET	BERETTA	88	864	36	50	1692	1731	559	42	1052	796
COMP	CHEVROLET	BERETTA	91	172	2	52	1317	1371	383	33	291	202
NCAP	CHEVROLET	BERETTA	91	343	3	37	659	910	739	35	523	230
COMP	CHEVROLET	CAPRICE	90	632	47	46	194	105	513	39	251	401
NCAP	CHEVROLET	CAPRICE	89	1328	55	64	406	260	1365	42	493	495
COMP	CHEVROLET	CAPRICE	91	267	9	39	1516	1590	563	40	401	394
NCAP	CHEVROLET	CAPRICE	91	533	10	54	1529	1527	1101	48	613	626
COMP	CHEVROLET	CORSICA	89	872	59	42	509	1451	615	40	1122	959
NCAP	CHEVROLET	CORSICA	88			44	1293	614	752	40	737	845
COMP	CHEVROLET	LUMINA	90	921	61	50	815	1288	579	40	285	508
NCAP	CHEVROLET	LUMINA	90	1200	52	58	782	935				
COMP	CHRYSLER	5TH AVE	91	225	5	47	932	1118	203	31	536	661
NCAP	CHRYSLER	5TH AVE	89	786	27	43	1132	766	682	43	667	575
COMP	CHRYSLER	LEBARON	87	691	54	39	806	1738	263	27	1206	964
NCAP	CHRYSLER	LEBARON	87	791	30	62	1008	1863	1698	82	1776	853
COMP	CHRYSLER	LEBARON	91	306	16	52	913	1634	214	27	310	474
NCAP	CHRYSLER	LEBARON	90	298	2	40	332	1119	2043	46	611	769
COMP	DAIHATSU	CHARADE	89	272	11	45	2045	1386	233	40	1503	1507
NCAP	DAIHATSU	CHARADE	88	768	25	43	574	1188	642	37	598	388
COMP	DODGE	DAYTNA	88	194	3	28	677	1439	319	28	991	825

Table 5. FMVSS No. 208 & NCAP Test Results from Similar Vehicles

TEST	VEHICLE IDENTIFICATION			DUMMY RESPONSE PARAMETERS								
TYPE	MAKE	MODEL	MY	HICD	RK	CGD	LFEMD	RFEMD	HICP	CGP	LFEMP	RFEMP
NCAP	DODGE	DAYTNA	89	399	4	39	729	795	297	32	908	457
COMP	DODGE	SHADOW	88	647	50	45	1496	1623	409	38	853	1141
NCAP	DODGE	SHADOW	91	503	8	42	1234	739	457	39	647	781
COMP	FORD	ESCORT	89	244	6	38	1444	1080	437	34	989	1007
NCAP	FORD	ESCORT	87	551	14	42	1146	1053	418	40	465	619
COMP	FORD	ESCORT	91	315	19	31	1215	963	457	33	1059	930
NCAP	FORD	ESCORT	91	434	5	42	1403	1055	450	39	2152	1119
COMP	FORD	MUSTNG	90	433	31	41	1737	1328	262	25	250	175
NCAP	FORD	MUSTNG	87	479	7	42	580	1589	301	34	921	290
COMP	FORD	PROBE	91	270	10	37	1485	1451	173	32	973	944
NCAP	FORD	PROBE	91	550	13	42	1051	1592	418	45	1501	1033
COMP	FORD	TAURUS	90	249	8	53	1491	1999	192	36	591	323
NCAP	FORD	TAURUS	90	735	22	46	1219	1261	609	40	581	318
COMP	FORD	TBIRD	90	208	4	35	1983	1148	222	33	1885	1175
NCAP	FORD	TBIRD	89	541	11	44	1224	1138	496	40	1264	776
COMP	HONDA	ACCORD	87	315	18	46	1590	278	374	39	435	471
NCAP	HONDA	ACCORD	87	769	26	46	863	695	382	36	1244	558
COMP	HONDA	ACCORD	91	247	7	46	2092	1312	500	43	784	1151
NCAP	HONDA	ACCORD	91	750	23	50	1361	1452	378	40	1214	900
COMP	HONDA	CIVIC	90	385	25	54	1066	1554	866	43	619	1309
NCAP	HONDA	CIVIC	91	1068	46	50	1002	2158	601	47	771	625
COMP	HONDA	PRELUDE	88	452	33	43	597	1025	315	34	911	574
NCAP	HONDA	PRELUDE	90	1279	54	59	770	674	854	48	681	733
COMP	HYUNDAI	EXCEL	90	310	17	40	1447	1201	504	44	1323	1207
NCAP	HYUNDAI	EXCEL	90	696	20	41	1385	1921	419	39	1682	964
COMP	HYUNDAI	EXCEL	87	485	35	44	1975	1930	303	48	1571	1076
NCAP	HYUNDAI	EXCEL	87	757	24	54	2408	1794	345	46	1187	1006
COMP	HYUNDAI	SONATA	89	420	29	42	1764	1570	298	37	1264	1054
NCAP	HYUNDAI	SONATA	89	1196	51	54	869	603	937	53	1717	293
COMP	ISUZU	STYLUS	91	290	15	43	1517	1695	903	44	273	382
NCAP	ISUZU	STYLUS	91	580	15	57	1021	859		46	439	717

Table 5. FMVSS No. 208 & NCAP Test Results from Similar Vehicles

TEST	VEHICLE IDENTIFICATION			DUMMY RESPONSE PARAMETERS								
TYPE	MAKE	MODEL	MY	HICD	RK	CGD	LFEMD	RFEMD	HICP	CGP	LFEMP	RFEMP
COMP	LEXUS	ES250	90	397	26	51	1530	1513	364	46	847	1137
NCAP	LEXUS	ES250	90	992	42	55	1102	1689	630	47	1012	1075
COMP	LINCOLN	CONT.	89	421	30	46	1572	1391	305	43	1100	1468
NCAP	LINCOLN	CONT.	89	863	35	48	314	1326	492		1247	1090
COMP	MAZDA	626	87	702	55	39	667	1379	459	37	1581	1284
NCAP	MAZDA	626	87	846	34	52	820	1300	801	46	1487	1255
COMP	MAZDA	MIATA	91	790	58	46	1262	1160	326	39	549	1008
NCAP	MAZDA	MIATA	90	920	40	59	1026	796	531	42	911	763
COMP	MERCEDES	190E	89	599	44	50	1857	1969	454	40	544	436
NCAP	MERCEDES	190E	90	800	31	60	705	1028	833	58	582	331
COMP	MITSUBISHI	GALANT	91	603	45	40	1290	1103	496	38	999	1094
NCAP	MITSUBISHI	GALANT	91	1024	44	61	1243	1395	711	53	906	1232
COMP	MITSUBISHI	STARION	88	320	20	48	1819	1686	710	57	1172	1360
NCAP	MITSUBISHI	STARION	87	952	41	48	1260	1752	377	46	1369	2323
COMP	NISSAN	AXXESS	90	624	46	41	1104	1004	572	43	1310	1342
NCAP	NISSAN	AXXESS	90	1051	45	46	919	1266	654	46	1257	1143
COMP	NISSAN	MAXIMA	88	658	51	45	1163	1361	662	51	1071	1013
NCAP	NISSAN	MAXIMA	88	907	38	64	1422	1500	861	49	885	1049
COMP	NISSAN	PULSAR	89	408	28	50	1363	2030	304	35	559	
NCAP	NISSAN	PULSAR	88	1134	48	40		122	430	31	226	1742
COMP	NISSAN	SENTRA	89	509	37	49	1370	1355	653	40	1000	1190
NCAP	NISSAN	SENTRA	91	583	16	46	1117	1210	681	45	475	
COMP	NISSAN	STANZA	90	595	43	50	1481	1499	383	43	823	913
NCAP	NISSAN	STANZA	90	1105	47	59	1404	1205	629	47	813	744
COMP	NISSAN	STANZA	91	382	24	45	1272	1669	707	46	958	1265
NCAP	NISSAN	STANZA	91	546	12	56	1803	970		46	413	558
COMP	PEUGEOT	505	88	903	60	44	1658	907	218	44	1146	1332
NCAP	PEUGEOT	505	88	1701	58	60	1657	930	1457	45	751	328
COMP	PONTIAC	LEMANS	91	647	49	50	2115	1762	588	48	1288	1821
NCAP	PONTIAC	LEMANS	88	819	32	57	1263	792	897	44	378	389

Table 5. FMVSS No. 208 & NCAP Test Results from Similar Vehicles

TEST	VEHICLE IDENTIFICATION			DUMMY RESPONSE PARAMETERS								
TYPE	MAKE	MODEL	MY	HICD	RK	CGD	LFEMD	RFEMD	HICP	CGP	LFEMP	RFEMP
COMP	SAAB	9000	89	323	21	46	1235	1601	232	36	503	
NCAP	SAAB	9000	87	584	17	37	120	346	440	35	435	638
COMP	SAAB	900S	89	289	14	40	986	1548	223	35	1327	1840
NCAP	SAAB	900S	88	718	21	46	1776	1395	1250	35		1535
COMP	SATURN	SL2	91	636	48	40	755	1068	633	39	1109	1076
NCAP	SATURN	SL2	91	918	39	44	1009	1326	1018	46	1178	974
COMP	SUBARU	GL	89	496	36	48	1270	1034	720	44	634	821
NCAP	SUBARU	GL	87	1339	56	58	1016	694	884	44	485	309
COMP	SUBARU	JUSTY	90	769	57	45	297	622	626	48	352	717
NCAP	SUBARU	JUSTY	87	611	19	42	529	1256	547	38	595	426
COMP	SUBARU	LEGACY	90	711	56	40	1570	1799	452	46	1014	1376
NCAP	SUBARU	LEGACY	90	1007	43	52	1957	1899	675	44	842	1121
COMP	TOYOTA	CAMRY	87	527	40	41	1393	1959	469	43	1429	1547
NCAP	TOYOTA	CAMRY	87	871	37	51	1380	1200	973	46	1160	1167
COMP	TOYOTA	CELICA	91	514	38	59	1622	1263	417	40	343	647
NCAP	TOYOTA	CELICA	90	834	33	50	1071	1190	685	37	906	609
COMP	TOYOTA	COROLLA	90	524	39	45	1540	1668	582	41	1024	1208
NCAP	TOYOTA	COROLLA	91	1238	53	53	1375	917	612		1342	1469
COMP	TOYOTA	CRESSDA	89	359	23	39	1371	1616	441	41	1266	1057
NCAP	TOYOTA	CRESSDA	89	790	29	51	1632	1554	544	51	1246	1107
COMP	TOYOTA	TERCEL	91	671	53	39	964	1048	406	38	874	942
NCAP	TOYOTA	TERCEL	91	1138	49	57	945	1325	765	51	778	948
COMP	VW	FOX	90	572	42	38	1350	1310	305	36	810	1226
NCAP	VW	FOX	89	787	28	64	139	738	818	58	1019	508
COMP	VW	PASSAT	90	326	22	40	1352	1306	336	41	1063	1284
NCAP	VW	PASSAT	90	1182	50	59	1104	1154	604	46	1436	2474
COMP	VOLVO	740	88	459	34	54	1500	2010	167	42	778	1048
NCAP	VOLVO	740	88	519	9	42	1143	1793	445	42	723	634
COMP	YUGO	GV	87	436	32	40	1169	1392	291	36	1179	1736
NCAP	YUGO	GV	87	1855	59	45		585	379	41	701	172

criteria limits (i.e., HICs<1000, Chest Gs<60, and femur loads<2250) in the NCAP test should meet the requirements in the 30 mph test. This appears to be true even though in most FMVSS No. 208 tests, only the automatic restraint systems are used. Thirty-seven of the 61 PCs (61 percent) have no available dummy response data (some have missing data) which exceed the 208 criteria.

The data indicate that quite often even the worst performing vehicles in the NCAP tests still easily meet the FMVSS No. 208 requirements in the 30 mph test. For example, the 1987 Chrysler Le Baron, which had a high passenger HIC (1698) and high chest Gs (62 and 82) did well in the FMVSS No. 208 test. Similarly, the 1987 Yugo GV, the 1989 Hyundai Sonata, and the 1990 Nissan Stanza did not do very well in the NCAP tests, but performed quite well in the FMVSS No. 208 tests.

In contrast, there are some marginal situations. The Hyundai Excel (femur loads), the Peugeot 505 (driver HIC), and the Chevrolet Lumina (driver HIC) had high dummy responses in the NCAP tests. These same vehicles, although meeting FMVSS No. 208 requirements, could be considered marginal performers in the 30 mph tests. It should be noted that only seven of the 61 cars in the FMVSS 208 tests had HIC values which exceeded 750. These vehicles were the Peugeot 505, the 1990 Chevrolet Lumina, the 1989 Chevrolet Corsica, the 1991 Mazda Miata, the 1991 Isuzu Stylus, the 1990 Subaru Justy, and the 1990 Honda Civic. In NCAP, 41 of the PCs had HIC values which exceeded 750.

It should also be noted that there are some reversals (i.e., higher responses in the lower speed tests). For the HICs, these reversals usually occur when both values are low and small changes in the response curves result in a shift in the HIC values (Hyundai Excel MY 90 and Ford Escort). For the chest Gs, these reversals are usually associated with airbag equipped vehicles where the belt system are not used in the FMVSS No. 208 tests (Volvo 740, Toyota Celica, and Ford Taurus).

In Figure 2, the average values normalized to FMVSS No. 208 requirements are shown for these specific comparisons. These data show the large differences in the HIC values (approximately a factor of two) in the different test groups, very little difference in average chest Gs, and slightly higher femur loads in the lower speed tests due to not using the manual belts. These higher average HICs correspond to the much higher probabilities of fatalities and injuries as reflected in the real world NASS crash data.

Section 1—Summary and Conclusions

From examining and comparing the FMVSS No. 208 and NCAP test data, the following general observations can be made:

(1) HIC values on the average are much greater in the NCAP tests due to compartment intrusion and restraint system performance in the higher severity crashes.

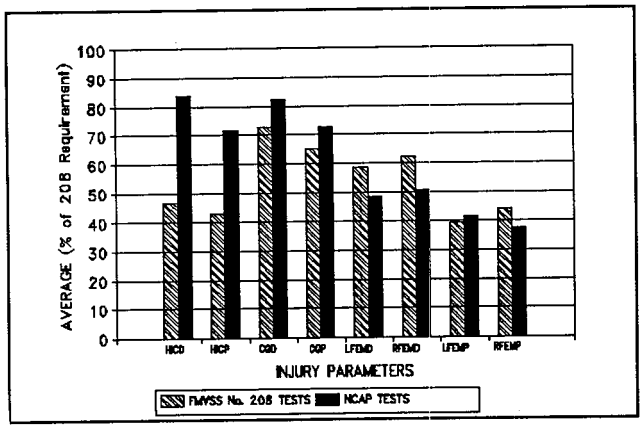

Figure 2. Average Values for 61 PCs—Comparison of FMVSS No. 208 and NCAP Test Results

(2) Standard deviations indicate much greater absolute variations (2:1) for HIC in the NCAP tests.

(3) When comparing HIC distributions, NCAP data provide much clearer distinction between vehicle safety performance than observed from FMVSS 208 data. More than 90% of the HICs in the FMVSS tests are below 750 and more than 50% are below 500.

(4) The much larger dummy response values which are often seen in the NCAP tests as compared to the FMVSS tests are also reflected in the real world crash results. When compared to a crash near the delta V of the FMVSS No. 208 test condition, the fatality rate from NASS is 2 to 3 times greater in a crash of the NCAP test severity.

(5) Little correlation exists when ranking "identical" vehicles in the two different crash test groups. The data indicate, that for a specific PC, test results from one program cannot be used to predict the test results that may occur in the other program.

(6) The good performing vehicles in the 35 mph test also perform well in the 30 mph test. Vehicles which meet FMVSS No. 208 requirements at 35 mph are likely to easily meet the requirements at 30 mph. Sixty percent of the "identical" vehicles met the FMVSS requirements in *both* test groups (see Table 4) and approximately 60 percent of *all* passenger cars which have been tested in NCAP since 1986 (see Table 3) have met these requirements.

(7) Poor performing vehicles in the 35 mph test often perform very well in the 30 mph test. However, poor performance of vehicles in the 35 mph tests may be indicative of marginal performance in the 30 mph tests.

Effects of NCAP and FMVSS No. 208 on Vehicle Safety

A goal of NCAP is to establish market forces which encourage vehicle manufacturers to design higher levels of safety into their vehicles. Initially, to be effective in generating these market forces which may influence vehicle manufacturers to improve the potential occupant

protection of their passenger cars, NCAP needed to determine if substantial differences in frontal crash safety performance existed between vehicle makes and models. If significant safety performance differences are found, how do the consumers and the manufacturers respond?

In this section, data which have been collected from the crash tests during the thirteen years of NCAP are analyzed to determine the range of vehicle performance and the safety performance trends in the 35 mph barrier crash tests. In addition, dummy response data from 30-mph tests which were conducted from 1977 through 1980 are compared to the recent (1987 through 1991) FMVSS No. 208 data to estimate the effects of NCAP on the safety of vehicles in the lower crash speed tests.

Range of Performance

The tests conducted in NCAP indicate that there are significant differences in the measured frontal safety performance among passenger cars. These differences may be illustrated by examining the distribution of maximum HIC values (the higher value from the driver or passenger is selected) which have occurred in the tested vehicles. (Note: the HIC injury parameter is chosen because the widest variations in dummy responses are found in these data and because head injuries tend to be the most debilitating).

In Figure 3, the HIC distributions for all passenger cars which have been tested in NCAP are shown. The HIC values in this figure are the maximum values from the driver or the right front seat passenger dummies and, except for 1991, are grouped by combining two model years of NCAP results (i. e., in the figure, model year 80 includes results from 79 and 80, model year 82 includes results from 81 and 82, etc.). The distributions in this figure indicate the substantial variations in measured safety performance which occur in the tested passenger cars. In the early years of NCAP, 1979 through 1984, a wider distribution of responses is noted with values ranging from a low of 408 to high of 4513. Since 1984, some decrease in this dispersion has occurred; however, the range in 1989-91 is still quite substantial with a low value of 399 and a high value of 2192.

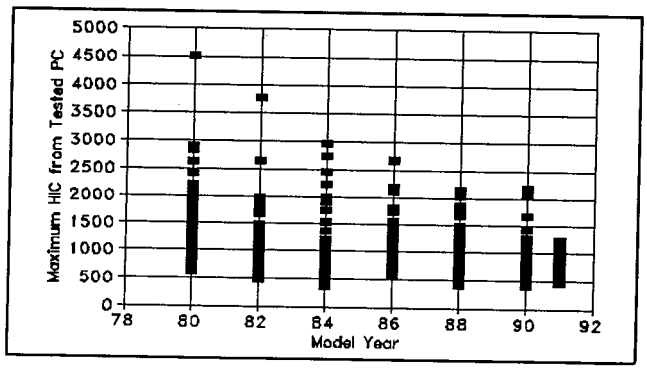

Figure 3. NCAP Test Results—Range of HIC Values by MY

Since it is often more appropriate to compare the performance of vehicles within weight classes, these distribution data are further separated into four weight classes in Figure 4 for MYs 1987 through 1991. The weight classes are subcompact (curb weight less than 2450 lbs.), compact (curb weight 2450 to 2949 lbs.), intermediate (curb weight 2950 to 3450 lbs.), and large (curb weight over 3450 lbs.). Substantial variations are found within each weight class for these last five MYs.

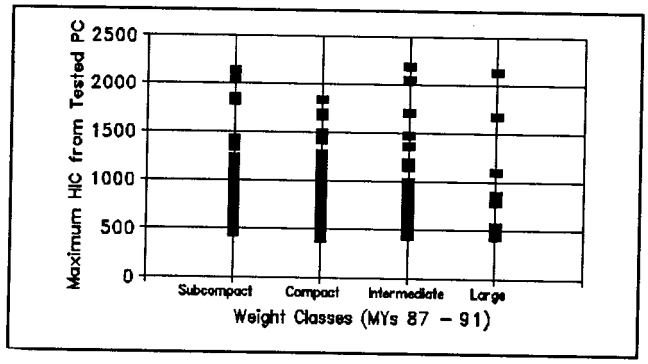

Figure 4. NCAP Test Results—Range of HIC Values by Weight Class

Figures 4 illustrates that the potential for occupant protection varies substantially within various vehicle market classes. These data indicate that NCAP has and continues to provide safety information to consumers which may be used in their vehicle purchasing decisions.

Safety Improvements and NCAP

With frontal crash test data on 304 passenger cars over thirteen MYs, trends of vehicle safety performance in the 35 mph barrier crashes can be examined. In the following two sections, analyses of these trends are presented by using the individual dummy response data (HICs and Chest gs) and then by grouping the vehicles in two performance categories.

These analyses are performed by using both the individual MY averages and the cumulative averages. Analyses are conducted for both unweighted and weighted data sets.

It should be noted that the average for an individual MY is a function of the passenger cars which are selected for that MY and how those selected cars happened to perform in the NCAP tests. The selection of the passenger cars for a MY is based on new models which are introduced by the manufacturers, significant safety changes which have been incorporated into existing models, and cost and budget considerations. This selection process does not necessarily lead to a statistical cross-section of the new car fleet for a particular MY. With this type of selection process, it would be expected that fluctuations may occur in the individual MY averages. However, if substantial safety improvements are being incorporated into the PCs by the manufacturers, a general downward trend in these individual MY averages should be expected.

The cumulative average is defined as an average of the data for all MYs through the MY of interest (i.e., the cumulative average of the driver HIC for MY 1985 is the average of the driver HIC values for all PCs tested beginning with MY 1979 through MY 1985). The cumulative average reflects the safety performance of the fleet of the tested PCs.

As appropriate, analyses in the following sections are conducted with both the unweighted and weighted NCAP data. The unweighted data are the data from the actual vehicles which have been tested. The weighted data are these data which have been weighted by the estimated distribution of the tested vehicle in the fleet for a given year. This estimate is derived from Polk's Annual National Vehicle Population Profiles and from vehicle sales reported in Automotive News. The use of the unweighted data may be the more accurate method for assessing potential safety performance since weighing of the test data does not consider variations in vehicle models (e.g., drive train and optional equipment). Regardless of these shortcomings, the weighted data do provide additional information relative to the NCAP data fleet trends.

For ease of comparison in many of the following discussions, the NCAP data are presented in terms of percentage of FMVSS 208 criteria.

Dummy Response Trends. In Figure 5, trends of NCAP dummy HICs and chest gs are shown for all tests which have been conducted during the thirteen years of the program. Both the averages by model year and the cumulative averages for the unweighted and weighted fleet are shown. Significant downward trends are noted for each of the injury parameters. The most notable improvements, however, are seen in the reduction in driver and passenger HICs. The driver HIC unweighted cumulative average has decreased from a high of almost 1300 in 1980 to slightly over 1000 in 1991. The passenger HIC unweighted cumulative average has dropped from near 1300 in 1980 to about 900 in 1991. The weighted cumulative averages also show large decreases since 1979. However, weighing the data by the vehicle registrations indicates that some of the PCs with the higher dummy responses had the lower sales volumes.

The data as shown in Figures 6 and 7 give additional insight as to how manufacturers and which vehicle weight classes have contributed to this downward trend. In Figure 6, cumulative averages of driver and passenger HICs are given by place of vehicle origin. For the NCAP test conditions, these data indicate the difference in safety performance which existed between the domestic (USA) and foreign (Europe and Japan) manufacturers in the late 1970s and early 1980s. The Japanese manufacturers made significant and rapid improvements to their vehicles and, by the late 1980s, the Japanese passenger car safety performance as measured by the cumulative averages was approximately the same as the domestics'. The European manufacturers have responded with some

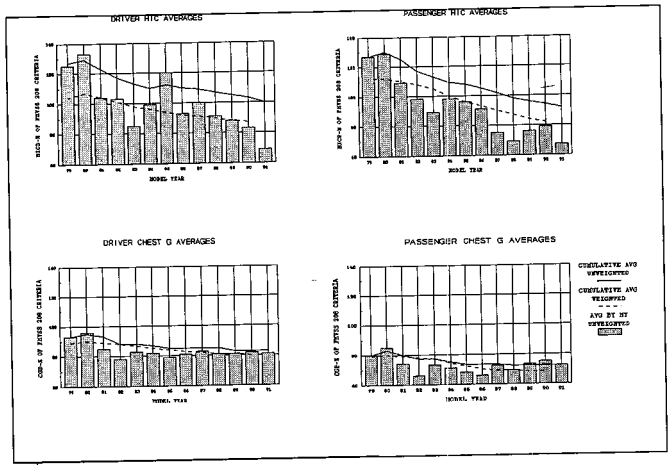

Figure 5. NCAP Dummy Response Trends

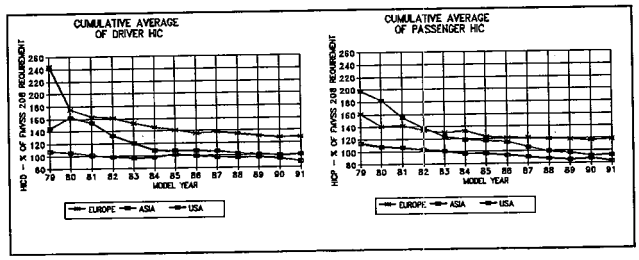

Figure 6. NCAP Safety Performance Trends by Place of Origin

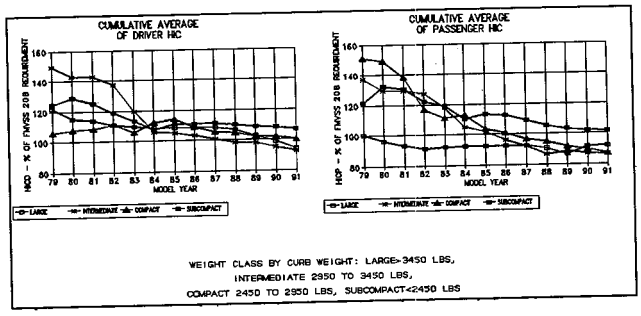

Figure 7. NCAP Safety Performance Trends by Weight Class

improvements; however, as a group, the cumulative averages of their models are higher than the others. The domestic manufacturers, although beginning with a relatively good average safety performance in 1979, have lowered the average HICs by 20 to 30 percent by 1991.

In Figure 7, cumulative averages of driver and passenger HICs are given by passenger car weight class. These data also indicate some large differences in safety performance between weight classes during the early years of NCAP. However, since about MY 1986, these differences have essentially disappeared except for the subcompact weight class. The subcompact weight class, although substantially improved since MY 1979, as shown by the cumulative averages, may not provide the same level of safety as the other weight classes in the barrier type crashes. Section 4 of this paper presents a definitive study of safety differences between lighter and heavier weight PCs.

Vehicle Performance Groups. In addition to providing the data for examining dummy performance trends, the NCAP results can also be used to examine overall vehicle safety potential by placing each vehicle in a specific performance group. Two performance groups will be used. The first group, which will be referred to as the lower risk group, will be composed of the vehicles which meet all requirements of FMVSS 208 in the 35 mph crash test.

The second group, which will be referred to as the higher risk group, will be composed of the vehicles which have a driver and/or passenger HIC which exceeds 1250, and/or a chest acceleration which exceeds 60 gs, and/or a femur load which exceeds 2250 lbs. This second group is based on the higher probabilities of life-threatening injuries as estimated from risk function curves which have been developed by GM and others [2, 3]. These risk function curves, which are used in this section and later in section 4, can be considered as examples of many such injury probability curves which can be derived from existing biomechanical data by various analytical methods. These curves are shown in Figures 8, 9, and 10.

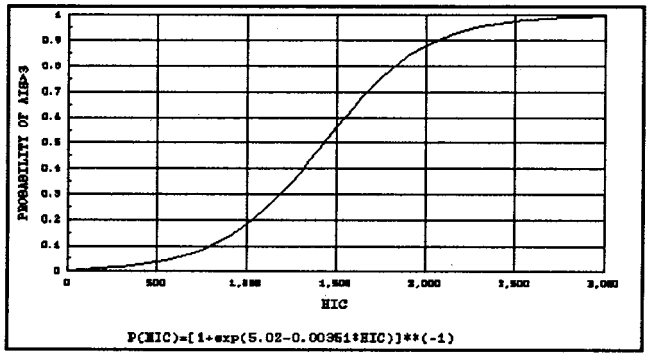

Figure 8. Injury Risk Function—HIC

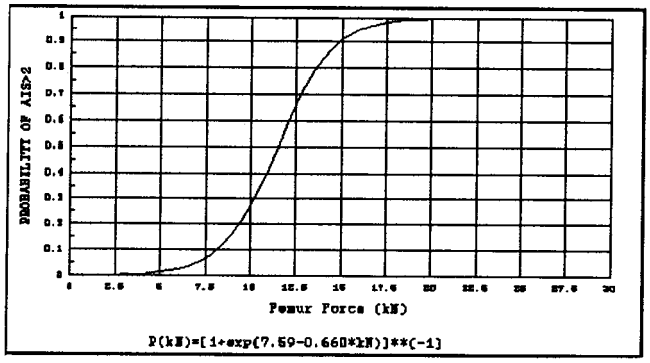

Figure 9. Injury Risk Function—Chest g

In Figure 11, the cumulative percents and the percents by model year are given for these two performance groups. For the lower risk group, a notable increase in the percentage of passenger cars which meet FMVSS No. 208 criteria in the 35 mph crash test is seen. The cumulative percentage has increased from approximately

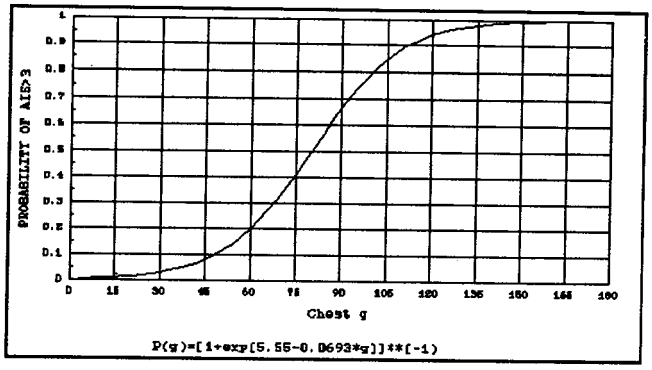

Figure 10. Injury Risk Function—Femur

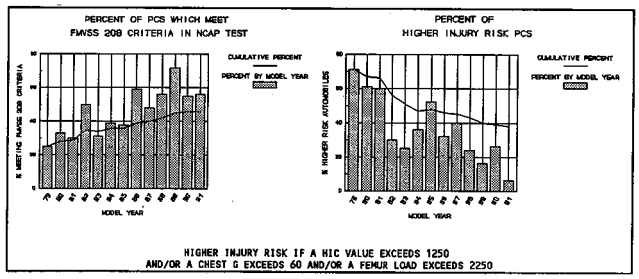

Figure 11. NCAP Safety Performance Trends

25 percent in 1979 to over 45 percent in 1991. Since MY 1986, approximately 60 percent of all passenger cars tested in the NCAP have met the FMVSS 208 requirements. This indicates; (1) that the vehicle manufacturers have the knowledge and capability to design passenger cars which provide exceptional safety in the severe 35 mph crash, and (2), that with the phase in requirements of passive restraints beginning with MY 1986, the vehicle manufacturers may have become more diligent in the design of improved occupant protection.

Also, as shown in Figure 11, the cumulative percentage of passenger cars in the higher risk group has significantly declined from the early years of NCAP. In MY 1979, more than 70 percent of the passenger cars were in this higher risk group. In MY 1991 the cumulative percent is less than 40 percent. The percentages by model year show that, in the last five MYs, less than 25 percent of the tested passenger cars were in the higher risk group. These data show that the vehicle manufacturers have greatly reduced the number of passenger car models which have very poor safety performance in severe frontal crash events.

Safety Improvements and FMVSS No. 208

By using existing average dummy response values from 30 and 35 mph crash tests which were conducted from 1977 through 1980, comparisons were made with the MY 1987 through 1991 FMVSS 208 and NCAP test results. These comparisons are shown in Figure 12. Very significant improvements are noted in the HICs. The average HIC values in the recent NCAP tests are approximately equal to the average HIC values of the 30 mph tests in the late 1970s. These are substantial reductions from approximately 1300 to well below 1000.

Similarly, the average HIC values in the recent FMVSS No. 208 30 mph tests reflect almost a 50 percent reduction when compared to the 30 mph tests results of the late 1970 vehicles. These data reflect the impact of both the NCAP and FMVSS No. 208 on the vehicle manufacturers approach to passenger car safety[2].

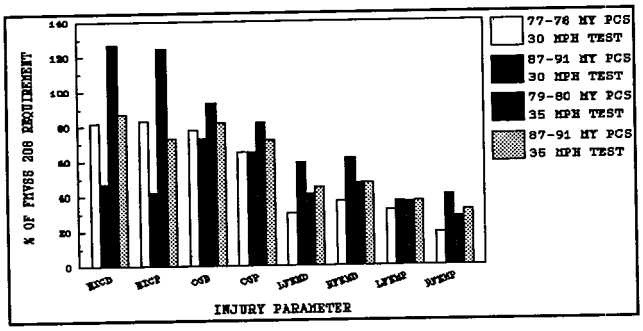

Figure 12. Trends in PC Safety from 30 and 35 Mph Barrier Crash Test Results

Section 2—Summary and Conclusions

Since the beginning of the NCAP in 1978, NHTSA has conducted 35 mph crash tests of 304 different makes and models of passenger cars. Analyses of data from these tests indicate:

(1) There are significant differences in the potential safety performance among passenger cars. Although these differences have been reduced in recent years, HIC values still ranged from a low of 399 to a high of 2192 in MYs 89,90, and 91. The NCAP tests continue to provide consumers with occupant protection information which may be used in purchasing decisions.

(2) Since 1979, significant measurable improvements have occurred in passenger car safety. The cumulative average for HIC has decreased by approximately 30 percent from a high of almost 1300 in 1980 to about 1000 in 1991.

The cumulative percentage of passenger cars in the lower risk group has increased from approximately 25 percent in 1979 to over 45 percent in 1991. Since MY 1986, approximately 60 percent of all passenger cars tested in the NCAP have met the 30 mph crash test requirements of FMVSS No. 208.

The cumulative percentage of passenger cars in the higher risk group has significantly declined from the early years of NCAP. In MY 1979, more than 70 percent of the passenger cars were in this higher risk group. In MY 1991 the cumulative percent is less than 40 percent.

(3) Comparisons of MY 1977 through 1980 crash test results to recent FMVSS No. 208 and NCAP test results reflect the very positive impact of both the NCAP and FMVSS No. 208 on the vehicle manufacturers approach to passenger car safety.

Manufacturers Response to NCAP and the Public's Awareness of Vehicle Safety

Specific Examples

In addition to the overall trends, as given in Section 2, which have shown the influence of NCAP in improving vehicle safety performance, many specific examples of vehicle makes and models which were improved after initial NCAP tests can be cited. In Table 6, a list of several of these specific examples is given. This list contains data which illustrate how manufacturers have reacted to initial NCAP test results.

Two early examples in the program occurred with Volvo and Mercedes models. Each of these manufacturers have traditionally advertised the safety aspects of their vehicles. In 1979, a Volvo 244 DL and, in 1980, a Mercedes 240D, were tested in NCAP. Surprisingly, both of these vehicles had high driver and passenger HIC values. Examination of the safety belts of these vehicles indicated unsatisfactory belt reel-out from the retractors due to excessive belt lengths. This condition allowed severe head contacts to occur between the driver dummies and the steering assemblies and between the passenger dummies and the instrument panels. Both manufacturers made significant design changes to eliminate these safety problems. Results of their models in succeeding years, as shown in Table 6, indicate the success of their changes.

Notable examples occurred when initial tests of several Japanese models resulted in very high dummy responses. These models included; Honda Civic and Prelude, Mazda 626 and RX-7, and Toyota Celica, Corolla, and Cressida. Factors which contributed to the poor performance of these models in these initial tests may have included; inadequate energy management of the crash forces (i. e., poor structural design), excessive intrusion and inappropriate collapse characteristics of the steering assembly and instrument panels, and inferior safety belt parameters. The data in Table 6 indicate the manufacturers' positive reactions to improve the safety performance of these models. In some cases, the manufacturers modified the existing model and in other cases the improved safety was incorporated in a complete redesign of the model. Relative to the improvements in potential occupant protection, the results, as shown in the table, were exceptional. HIC values were reduced by as much as 75 percent and chest gs and femur loads were reduced by 50 percent or more.

Other interesting examples have occurred with the beginning of the New Car Assessment "Optional Test" Program in 1986. This program gives to the manufactur-

[2]Other factors such as increased liability litigation, advances in technology, and recognition that improved safety can provide a competitive sales advantage may also have contributed to these trends.

Table 6. NCAP Examples of Vehicle Safety Improvements

VEHICLE IDENTIFICATION			DUMMY RESPONSE PARAMETERS							
MAKE	MODEL	MY	HICD	HICP	CGD	CGP	LFEMD	RFEMD	LFEMP	RFEMP
VOLVO	DL	79	1782	1889	52	61	320	900	700	320
VOLVO	DL	82	550	381	45	35	154	1147	892	227
VOLVO	DL (SW)	85	621	262	33	31	100	1005	630	615
VOLVO	DL	85	651	310	36	25	350	1020	590	
MERCEDES	240D	80	1262	1369	54	44	674	1687	666	1449
MERCEDES	300SD	84	890	734	63	44	1410	1150	295	490
MERCEDES	190E	90	800	833	60	58	705	1028	582	331
DODGE	COLT	82	932	1730	72	44	517	782	506	276
DODGE	COLT	85	787	741	42	32	480	460	1090	370
RENAULT	MEDAL.	88	1656	873	57	38	205	617	411	1193
EAGLE	MEDAL.	89	745	589	41	39	1721	1738	1574	1670
FORD	GRANADA	79	1442	1279	61	56	1750	350	390	570
FORD	GRANADA	82	860	1050		52	980	800	460	340
FORD	TAURUS	86	1209	695	53	37	828	1485	566	502
FORD	TAURUS	88	707	359	38	47		775	455	438
FORD	TEMPO	84	2955	1104	63	45	750	480	675	370
FORD	TEMPO	85	1207	932	52	40	870	580	440	310
FORD	TEMPO	88	721	470	47	50	1113	1773	1037	702
HONDA	CIVIC	79	2030	2093	93	46	1080	838	1520	1460
HONDA	CIVIC	80	2626	1506	54	47	1006	3118	418	218
HONDA	CIVIC	81	607	492	41	35	200	500	1100	540
HONDA	CIVIC	84	563	846	37	43	1067	602	1566	1275
HONDA	PRELUDE	80	2904	1759	52	45	445	1057	465	277
HONDA	PRELUDE	84	659	475	43	31	600	510	690	980
HYUNDAI	EXCEL	86	999	2662	73	55	2248	785	1597	520
HYUNDAI	EXCEL	87	757	345	54	46	2408	1794	1187	1006
HYUNDAI	EXCEL	87	716	1003	55	43	790	345	1360	775
HYUNDAI	EXCEL	90	696	419	41	39	1385	1921	1682	964
MAZDA	626	82	969	1693	47	50	575	1215	550	250
MAZDA	626	83	1196	1087	45	56	450	350	260	360
MAZDA	626	87	846	801	52	46	820	1300	1487	1255
MAZDA	RX-7	85	921	1345	40	42	369	476	604	809
MAZDA	RX-7	88	921	614	39	48	186	1135	268	650
MERCURY	SABLE	86	1237	680	48	44	1039	1780	671	465
MERCURY	SABLE	88	712	410	51	35		1512	862	913
PONTIAC	FIREBIRD	79	965	1297	42	47	582	472	503	717
PONTIAC	FIREBIRD	83	408	376	34	32	900	480	100	125
SAAB	9000	86	773	1443	71	46	484		541	421
SAAB	9000	87	584	440	37	35	120	346	435	638
TOYOTA	CELICA	79	849	1862	61	59	2920	435	400	520
TOYOTA	CELICA	82	702	530	36	45	456	448	360	359
TOYOTA	CELICA	86	627	430	42	40	382	721	439	593
TOYOTA	CELICA	90	834	685	50	37	1071	1190	406	609
TOYOTA	COROLLA	80	838	1162	69	92	740	775	200	270
TOYOTA	COROLLA	82	842	828	59	40	1400	1178	888	507
TOYOTA	COROLLA	84	630	611	41	42	1320	730	340	395
TOYOTA	COROLLA	89	994	546	49	45	1101	894	451	681
TOYOTA	COROLLA	84	432	602	37	47	1100	450	580	300
TOYOTA	COROLLA	88	593	397	42	40	719	1162	300	393
TOYOTA	CRESSIDA	81	1980	771	55	50	1710	1982	1644	1807
TOYOTA	CRESSIDA	85	883	914	50	58	1725	1820	1355	1820
TOYOTA	CRESSIDA	89	790	544	51	51	1632	1554	1246	1107
VW	JETTA	81	1210	1272	68	52	1276	1191	1559	1286
VW	JETTA	85	898	1008	50	51	362	396	711	516
AUDI	4000	80	1322	1428	70	45	408	353	1030	527
AUDI	5000	85	2105	557	39	31	362	357	292	326
AUDI	100	89	185	710	35	31	998	571	894	757

ers the option to request a test or retest of a particular vehicle model, based on design changes to a previously tested model or the introduction of innovative safety features. This optional test is sponsored by the manufacturer but conducted by following the NCAP test procedures under NHTSA control at a NHTSA approved test site.

The Mercury Sable, the Ford Taurus, and the Audi 100 are examples of models which have been tested in this optional program. For the Sable and the Taurus, the manufacturers incorporated design changes after the initial NCAP tests were conducted. The retests indicate the potential for improved occupant protection.

For the Audi 100, the manufacturer requested the optional test because of innovative safety features, which included a driver airbag and unique safety belt pretensioning devices. All dummy responses were low in the Audi 100 test with the driver HIC of 185 being the lowest HIC ever recorded in the NCAP 35 mph test. The manufacturer (Audi) has used these data extensively in advertising campaigns to inform consumers of the occupant safety provided by the Audi 100. Data are shown in Table 6 of other Audi models. These data show the inferior NCAP performance of previously tested Audi models. The comparison between the previous Audi models and the new Audi 100 and the use of the Audi 100 NCAP results in the advertising campaigns may represent a change in philosophy by the manufacturer toward NCAP safety performance.

Table 6 contains several other examples from different manufacturers which illustrate the capabilities to introduce improvements in safety performance in particular makes and models.

Automobile Manufacturers' Reactions

The positive actions by the manufacturers are illustrated by overall trends in Section 2 and by the above discussions on specific examples. Manufacturers, including GM, Ford, Honda, Toyota, Volvo, Mercedes, and others, conduct 35 mph crash tests on some or all of their passenger cars during the developmental phases.

Goals have been established within the individual companies to develop vehicles which perform well in the NCAP tests. For example, Ford states that, beginning in the late 1980s, their policy has been to meet FMVSS No. 208 criteria in a 35 mph barrier crash test. In fact, of the 17 Ford models that have been tested in NCAP since MY 1986, fifteen have met all the FMVSS No. 208 criteria. The other two were very close with a driver HIC of 1014 and a driver chest g of 64. The average HIC and chest g values for the Ford models during these last four years are; 680 for the driver HIC, 470 for the passenger HIC, 45 for the driver chest gs, and 41 for the passenger chest gs. These data certainly substantiate Ford's goal to design passenger cars which perform well in the NCAP tests.

Further evidence of the importance that manufacturers are now placing on good safety performance in the NCAP tests was displayed when Audi requested the optional test on the Audi 100 as discussed previously. Until that request, Audi had shown reluctance to designing their vehicles to perform well in the higher severity NCAP test. This was evident from examining test results from earlier Audi models. However, it appears that most manufacturers, not only Audi, are convinced that the consumer is very interested in the potential safety that a passenger vehicle provides and that the consumer will use safety information about a vehicle during the selection and purchasing process.

Use and Availability of the NCAP Results

A primary goal of NCAP is the effective dissemination of the test results so that consumers are aware of the data and so that the consumer may properly utilize the data in vehicle purchasing decisions. Each year the Agency conducts approximately 30 crash tests in NCAP to generate these comparative crashworthiness data for consumer information. These data are made available through regular press releases as the tests are completed. These press releases are distributed to all the major news services, consumer groups, magazines, and many other associations. Over 1000 different organizations with readership in the tens of millions receive these press releases. These data are then used by many of these organizations in their programs and publications to inform the public of the potential safety of the tested vehicles.

Consumer Reports, a popular publication of Consumers Union (CU), annually uses the NCAP data in a special issue on automobiles. The April 1990 issue contains an extensive article, "Which Cars Do Better in a Crash," based on the 35 mph crash test results and CU's judgments on passenger car crash protection. In a discussion with Robert Knoll of CU, it was verified that this annual automotive issue is consistently the most popular issue published by CU. The sales of the 1990 issue exceeded over five million copies, with approximately 4.6 millions subscriptions and more than one-half million counter sales. Mr. Knoll also stated that CU receives extensive consumer response to the automotive safety articles. Consumer Reports represents the single most effective distribution source for the NCAP data.

The "Car Book," originally published by the Department of Transportation in 1980, is now published each year by Jack Gillis of the Consumer Federation of America. This publication also uses the crash test data from NCAP tests as the principle source of safety information. Sales of the "Car Book" average approximately 75 thousand per year.

The United Services Automotive Association (USAA) Foundation, the nation's sixth largest insurer of motor vehicles, publishes a very comprehensive booklet, "The

Car Guide," which provides its members with information regarding passenger safety, damageability, theft risk, and insurance experience of various vehicles. The safety information is based on the NCAP test results. "The Car Guide" is distributed annually to USAA's approximately two million members.

The exposure to the public of the NCAP data through the different media also results in many individual inquiries to NHTSA. The Agency responds to approximately 15 thousand telephone calls each year through the NHTSA Hot Line regarding the crashworthiness test results.

From recent indications, these data are now often used by consumers in making their vehicle purchase decisions. A survey of Washington-area automobile dealers, conducted by the Insurance Institute for Highway Safety (IIHS) and reported in the Washington Post Business Magazine, indicates that "safety ranks near the top of new-car buyers' shopping lists...." Of 227 Washington area dealers interviewed, 68 percent said buyers rated safety as one of their "most important" concerns in a new-car purchase and another 28 percent said buyers saw safety as "fairly" important...."

The vehicle manufacturers seem very aware of the consumer interest in occupant protection. As recently reported in the Orlando Sentinel:

> *In a recent Ford survey of potential customers, safety came in second only to vehicle reliability as the main requirement in buying a new car . . . . "Consumers have forever put to rest that safety doesn't sell," Ford's Joyce Stinson said.*

This awareness of consumer attitude is reflected by the expansion by the vehicle manufacturers of their advertisements into the safety arena. Volvo and Mercedes, always leaders in advertising the safety of their vehicles, have been enthusiastically joined by many other manufacturers. Chrysler, Ford, GM, Audi, Subaru and others use both printed and TV commercials in which safety aspects of their vehicles are highlighted. Occasionally, such as for Audi, Fiat, and GM, actual NCAP results may be used in the advertisements.

Section 3—Summary and Conclusions

An encouraging aspect of NCAP has been the positive actions by the manufacturers to institute significant improvements in passenger car safety performance. Many of the manufacturers conduct 35 mph crash tests on some or all their passenger cars during the developmental phases. Often goals have been established within the individual companies to develop vehicles which perform well in these severe crash tests. It appears from recent advertising that most manufacturers are convinced that the consumer is very interested in the potential safety that a passenger vehicle provides and that the consumer will use safety information about a vehicle during the selection and purchasing process.

Many specific examples of vehicle makes and models which were improved after initial NCAP tests can be cited. In some cases, the manufacturers modified the existing model and in other cases the improved safety was incorporated in a complete redesign of the model. Changes incorporated into specific makes and models by the manufacturers reduced dummy responses by as much as 75 percent.

A primary goal of NHTSA's NCAP is the effective dissemination of the crash test results so that the consumer may properly utilize the data in vehicle purchasing decisions. These data are made available to more than 1000 organizations through regular press releases. Many of these organizations use the data in their programs and publications to inform the public of the potential safety of the tested vehicles. Major publications, such as "Consumer Reports," "The Car Book," and the USAA "Car Guide," reach up to 7 million households each year. From a recent survey, it is indicated that the consumer may often use available safety data in making their vehicle purchase decisions.

Application of Data from the Crash Programs to Evaluate Safety Differences Between Vehicle Weight Classes

Several studies by NHTSA of real-world crashes have concluded that occupants of lighter (smaller) passengers cars are at greater risk of injury and death than occupants of heavier (larger) passenger cars [4, 5]. The laws of physics strongly support this conclusion for multiple vehicle crashes since the lighter vehicle would be exposed to a higher change in velocity. However, the NHTSA studies have indicated that even in single vehicle crashes and when controlling for crash severity in multiple vehicle crashes the injuries and fatality risks are still greater for the occupants in the lighter vehicles. The purpose of this section is to present an analysis of the structural characteristics of the passenger car fleet which may clarify the conclusions of the NHTSA real-world studies.

Scope of Study

The main emphasis of this study is to examine and analyze the differences between the potential safety performance of lighter and heavier passenger cars in frontal crashes as can be determined from NCAP and FMVSS No. 208 test data. This Initial study will be limited to an engineering examination of representative vehicles and a determination of the distribution of structural parameters which may affect safety performance. Data from crash tests from FMVSS No. 208 and NCAP through MY 1990 will be used. Further statistical analyses of these data will be conducted in a later report.

The NCAP and FMVSS No. 208 files are divided into two groups: Group *Lwt* consisting of passenger cars with test weights below 3000 pounds and Group *Hwt*

consisting of passenger cars with test weights above 3200 pounds. As defined by the vehicle size classes in Reference 4, Group *Lwt* passenger cars include mini-compact and subcompact classes and Group *Hwt* passenger cars include compact, intermediate, fullsize, and luxury classes. A 200 lb. weight gap is included between the two groups to provide a minimum separation. For vehicles tested in NCAP, these two groups provide comparison of nearly the same number of vehicles (120 in Group *Lwt* and 127 in Group *Hwt*). From the FMVSS No. 208 tests, there are 20 passenger cars in Group *Lwt* and 38 passenger cars in Group *Hwt*.

For each group, potential safety performance is assessed for restrained and unrestrained front seat occupants in two crash severities (i.e., a 40 mph change in velocity in NCAP and a 33 mph change in velocity in FMVSS No. 208). Two methods are used for assessing the potential safety performance.

Parameters of the crash pulses are examined and the differences between Group *Lwt* and Group *Hwt* are presented. A single mass approach and a multiple degree of freedom model [7] are used to determine the effects of these differences on the potential for unrestrained occupant injuries.

For the restrained occupants, the average dummy response data for Group *Lwt* and Group *Hwt* are compared. Injury probabilities are estimated from curves developed by General Motors and others [3, 4] from available cadaver data. In addition, the multiple degree of freedom model is used to assess the effects of the crash pulse differences on restrained occupants.

Crash Pulse Parameters

Three crash pulse parameters which are tabulated in the NCAP and FMVSS No. 208 databases are the peak g's, times to peak g's, and duration of the crash pulse. (Note: All crash pulses are filtered with SAE class 30 Butterworth filters prior to determination of these parameters.) Typical crash pulses for Group *Hwt* and *Lwt* are shown in Figures 13 and 14. The three parameters are depicted in these figures.

Comparisons of the distributions of these parameters for Groups *Lwt* and *Hwt* are shown in Figures 15, 16, and 17 for NCAP vehicles and in Figures 18, 19, and 20 for FMVSS No. 208 vehicles. Average values for the two groups are also given in these figures.

NCAP Crash Pulses. For the cars tested at 35 mph in NCAP, the average peak g's for the two groups are approximately the same (29.9 for Group *Lwt* and 29.3 for Group *Hwt*). Some differences in the distribution may, however, be significant (see Figure 15). 30 percent of the peak g's for Group *Hwt* are below 26 g's. Only 18 percent of Group *Lwt* are below 26 g's.

The averages and distributions for time to peak g and for the crash pulse duration are significantly different for the two groups (see Figures 16 and 17). The averages for time to peak g's are 60 msec for Group *Hwt* and 49 msec

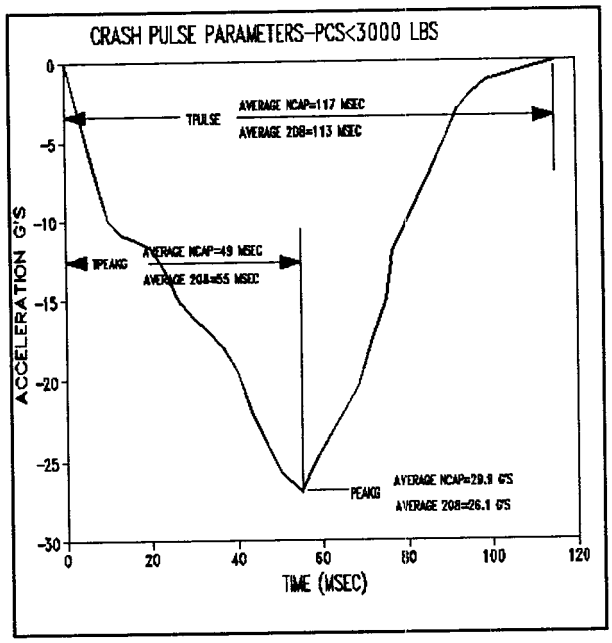

Figure 13. Crash Pulse Parameters for PCs < 3000 Pounds

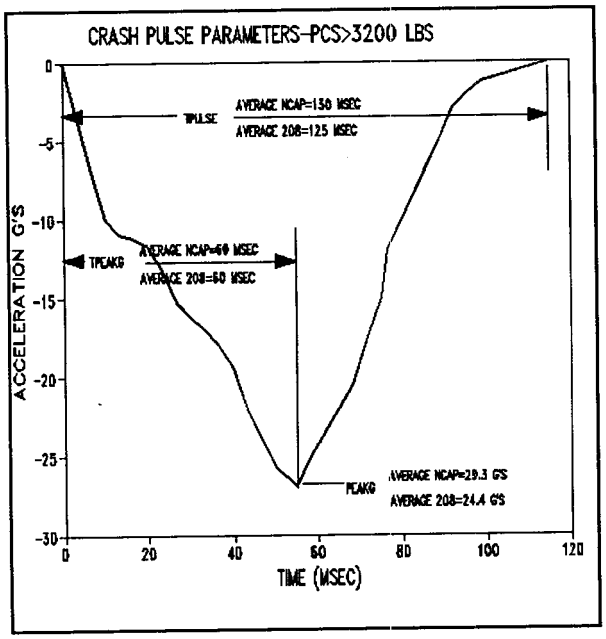

Figure 14. Crash Pulse Parameters for PCs < 3200 Pounds

for Group *Lwt*. The averages for the crash pulse duration are 130 msec for Group *Hwt* and 117 msec for Group *Lwt*. More than 52 percent of the Group *Lwt* times to peak g are below 50 msec. Only 24 percent of Group *Hwt* are below 50 msec. More than 63 percent of the crash pulse durations for Group *Lwt* are below 120 msec. Only 32 percent of Group *Hwt* durations are below 120 msec.

FMVSS No. 208 Crash Pulses. For the cars tested at 30 mph in FMVSS No. 208, the average peak g's for the two groups are 26.1 for Group *Lwt* and 24.4 for Group *Hwt*. Differences in the distribution are shown in Figure

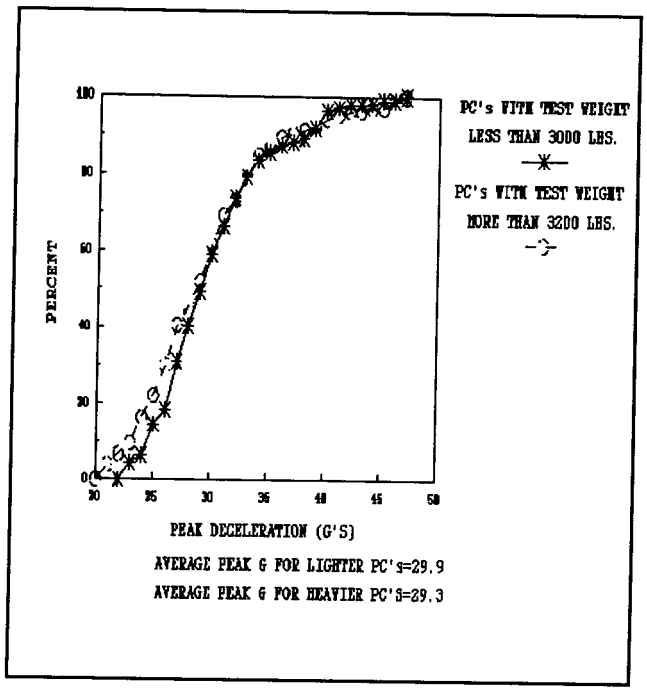

Figure 15. Distribution of Peak g—NCAP Data

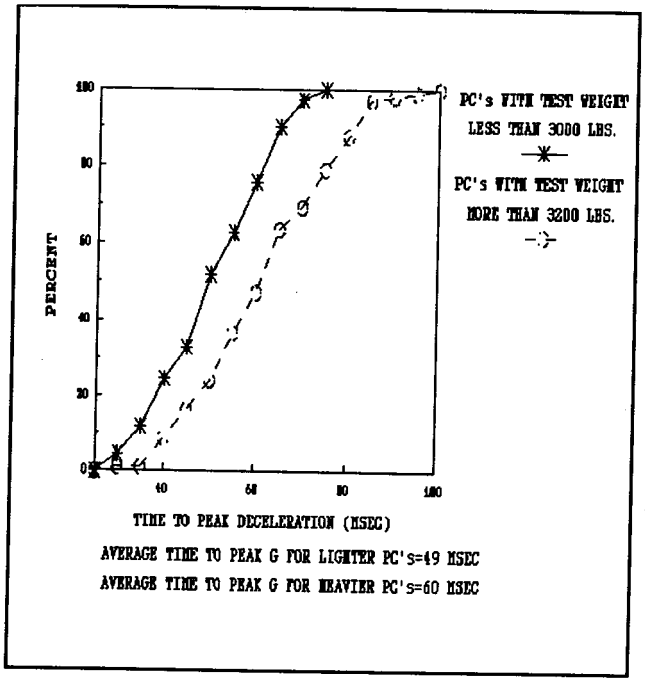

Figure 16. Distribution of Time to Peak g—NCAP Data

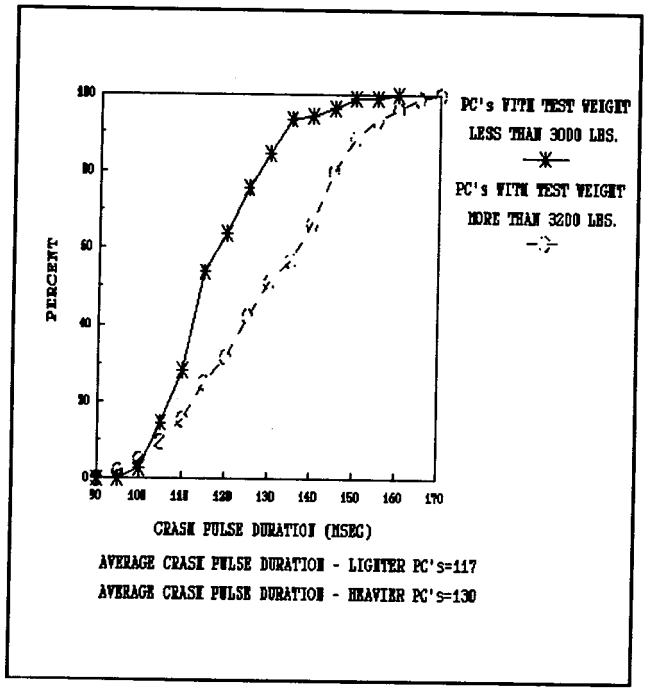

Figure 17. Distribution of Crash Pulse Duration—NCAP Data

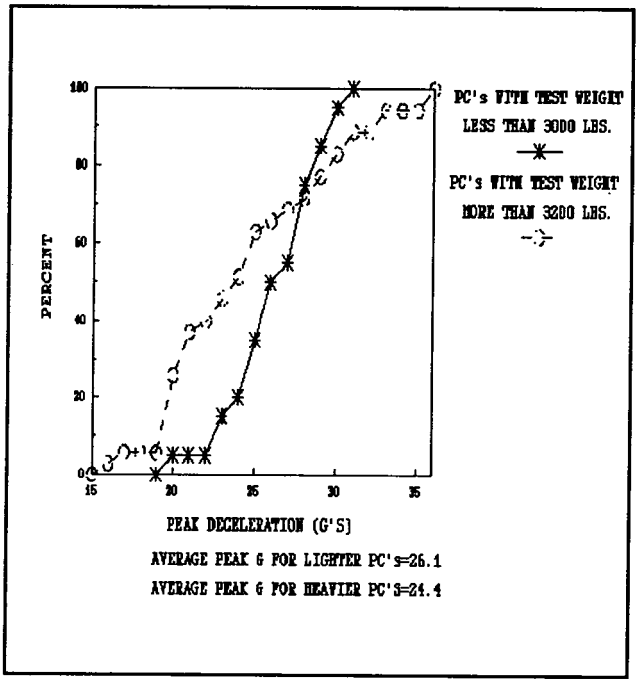

Figure 18. Distribution of Peak g—FMVSS No. 208 Data

18. 66 percent of the peak g's for Group *Hwt* are below 26 g's. 50 percent of Group *Lwt* are below 26 g's.

As for the NCAP results, the averages and distributions for time to peak g and for the crash pulse duration may be significantly different for the two groups (see Figures 19 and 20). The averages for time to peak g's are 60 msec for Group *Hwt* and 55 msec for Group *Lwt*. The averages for the crash pulse duration are 125 msec for Group *Hwt* and 113 msec for Group *Lwt*. More than 50 percent of the Group *Lwt* times to peak g are below 55 msec. Only 37 percent of Group *Hwt* are below 55 msec. Seventy five percent of the crash pulse durations for Group *Lwt* are below 120 msec. Only 49 percent of Group *Hwt* durations are below 120 msec.

Effect of Crash Pulse Differences on Injury Probability for Unrestrained Occupants

Single Mass Approach. In this simple approach, a single independent mass represents each relevant body part (i. e., head, chest, and femur) of the unrestrained occupant. In a crash, the single mass moves forward at a constant velocity equal to the striking velocity of the

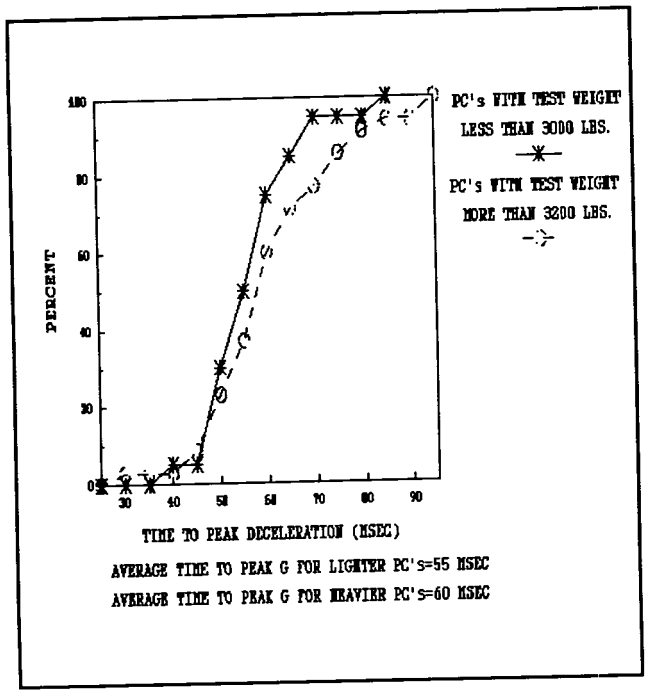

Figure 19. Distribution of Time to Peak g—FMVSS No. 208 Data

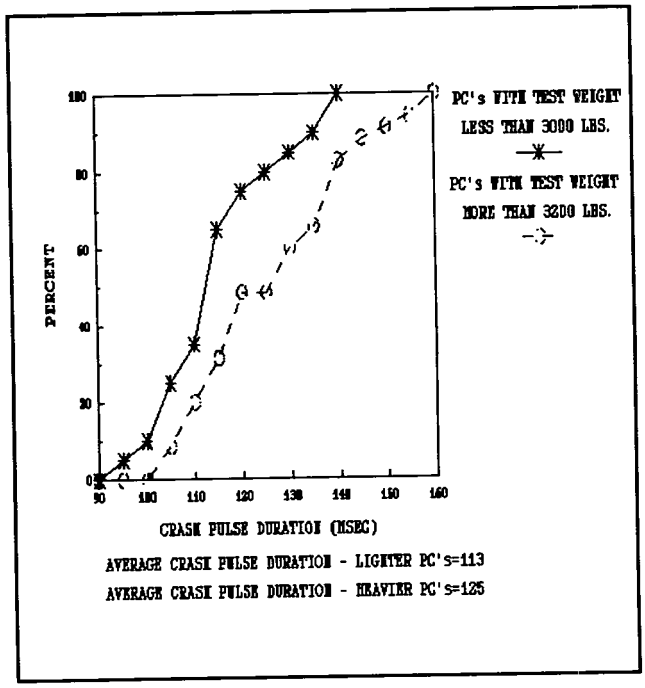

Figure 20. Distribution of Crash Pulse Duration—FMVSS No. 208 Data

vehicle until contact occurs with some interior surface. For the head, the more common contact surfaces are the windshield and the header. The chest of the driver strikes the steering assembly. The chest of the passenger strikes the instrument panel. Femurs are loaded due to knee contacts with the lower instrument panel or dash.

Tabulated data in the databases locate the initial position of a 50th percentile dummy with respect to these contact surfaces. In Table 7, the average values of the distances from the body part to the relevant surfaces are given. (Note: See Table 1 for definition of parameters. The parameters are shown graphically in Figure 21.)

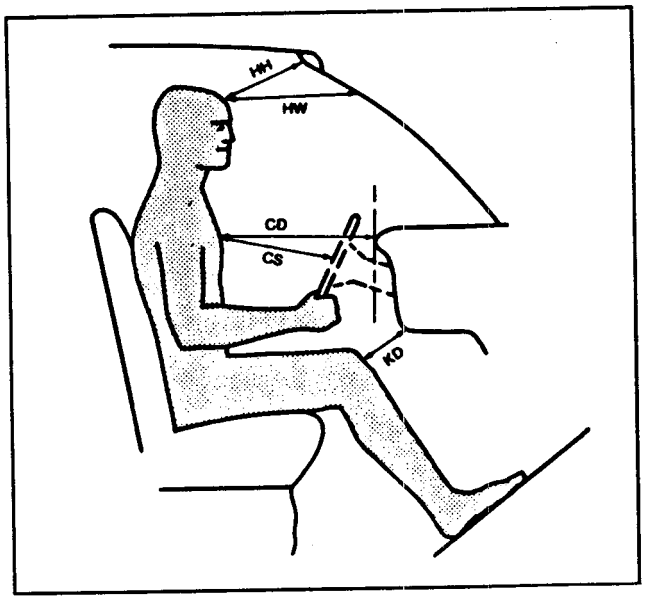

Figure 21. Occupant Location Relative to Vehicle Interior

Table 7. Dummy Locations in Crash Tests

Parameter	Average Measurement (inches)			
	Group Lwt		Group Hwt	
	NCAP	208	NCAP	208
HHD	14.1	15.7	14.5	14.3
HWD	19.5	20.5	20.0	19.8
CSD	14.8	15.0	14.2	13.4
KDD	6.0	5.1	6.0	4.6
HHP	14.0	15.9	14.5	14.6
HWP	19.3	20.4	19.1	20.0
CDP	22.8	23.7	22.6	22.1
KDP	6.5	5.6	6.7	5.2

As seen from these data, the average sitting positions in Groups *Lwt* and *Hwt* are very nearly the same for the NCAP vehicles. These values are also similar for the FMVSS No. 208 vehicles, however, the dummies in the Group *Lwt* vehicles tend to be located slightly farther from the potential contact surfaces than those in the heavier vehicles. Any variations between NCAP and 208 dummy locations are attributed to the different distribution of car makes and models and model years.

As noted above, significant differences exist in the crash pulses of the two vehicle groups. To illustrate how these crash pulse differences can affect the injury potential in the two groups for unrestrained occupants, contact velocities for the single mass to interior surfaces are determined. The single mass is located at 5, 10, 15, 20, and 25 inches from the interior surfaces. These locations span the average seating position distances as given in Table 7.

In NCAP, two vehicles which illustrate the wide variations that may occur in contact velocities are the 1984 Pontiac T1000 for Group *Lwt* and the 1983 Chevrolet Caprice for Group *Hwt*. The crash pulse, velocity, and displacement curves for these two vehicles are shown in Figures 22, 23, and 24.

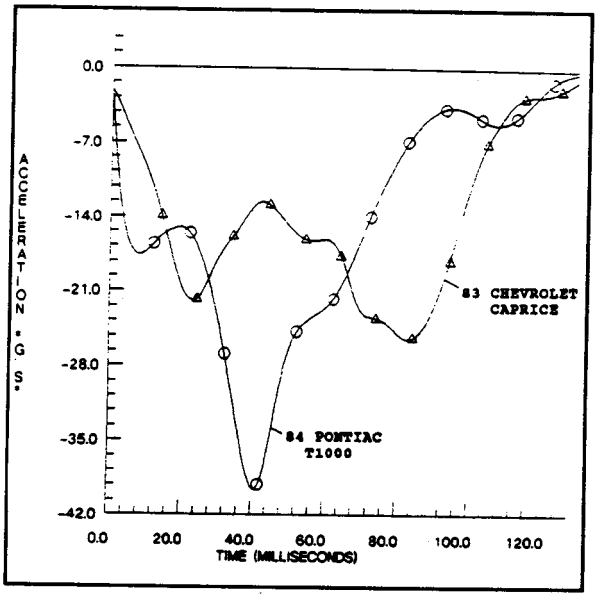

Figure 22. NCAP Crash Pulses—Caprice and T1000

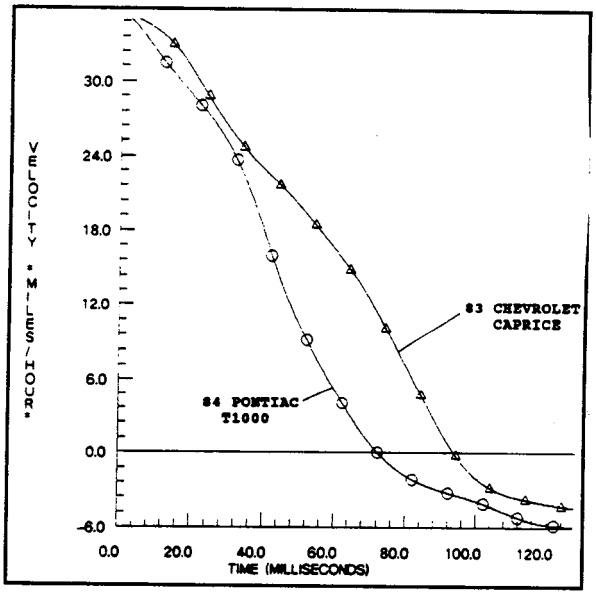

Figure 23. NCAP Delta V's—Caprice and T1000

Similarly, in FMVSS No. 208, two vehicles which have very different crash pulses and which illustrate the wide variations that may occur in contact velocities are the 1990 Honda Civic for Group *Lwt* and the 1989 Lincoln Continental for Group *Hwt*. The crash pulse, velocity, and displacement curves for these two vehicles are shown in Figures 25, 26, and 27.

For an impact velocity of 35 mph, the single mass will move .616 inches each msec. For an impact velocity of 30 mph, the single mass will move .528 inches each

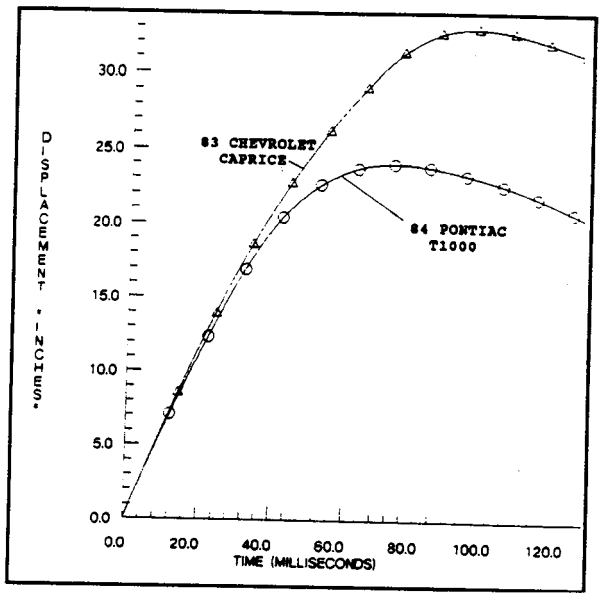

Figure 24. NCAP Dynamaic Crush—Caprice and T1000

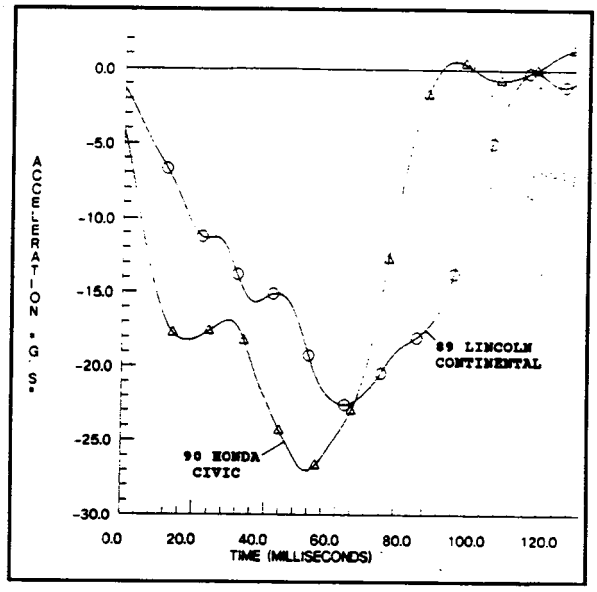

Figure 25. FMVSS No. 208 Crash Pulses—Continental and Civic

msec. The interior surfaces are assumed to displace as shown in Figures 24 and 27. Tables 8 and 9 give the times of contact, interior surface velocities, and the relative contact velocities for the single mass at the 5, 10, 15, 20, and 25 inch locations.

In the 35 mph NCAP crash tests, the contact velocities in the Group *Lwt* vehicle (the Pontiac T1000) exceed those of the Group *Hwt* vehicle (the Chevrolet Caprice) by 1.4 to 6.3 mph. In the 30 mph FMVSS No. 208 crash tests, the contact velocities in the Group *Lwt* vehicle (the Honda Civic) exceed those of the Group *Hwt* vehicle (the Lincoln Continental) by 0.4 to 3.1 mph. These higher contact velocities are indicative of the potential for more serious injuries to unrestrained occupants in the lighter Group *Lwt* passenger cars at the 35 and 30 mph crash speeds.

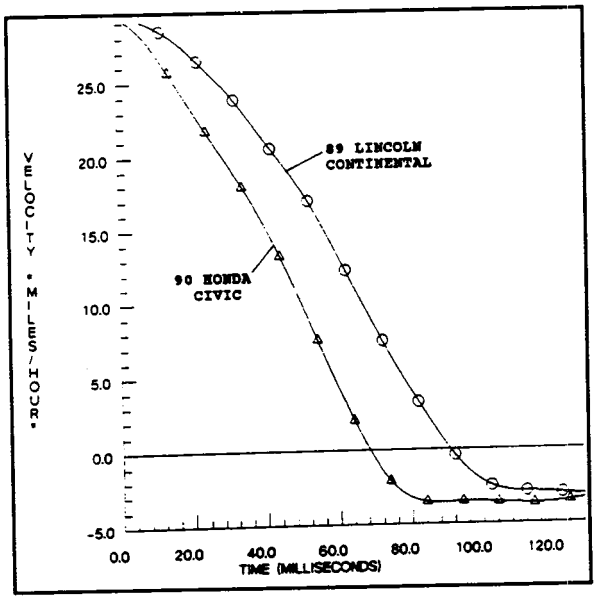

Figure 26. FMVSS No. 208 Delta V's—Continental and Civic

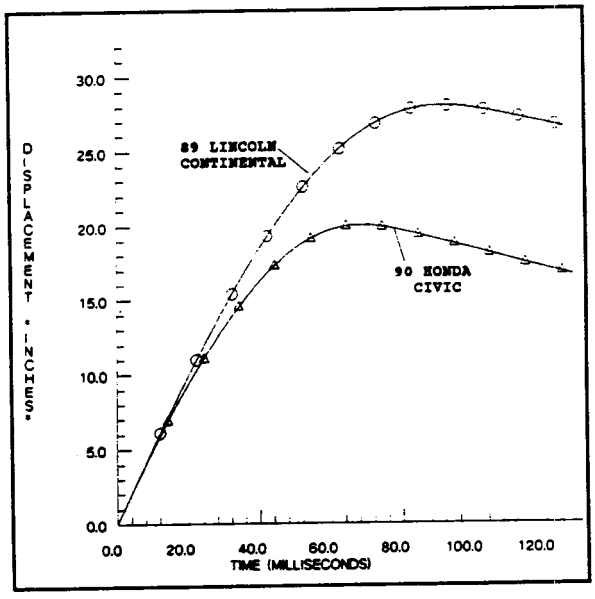

Figure 27. FMVSS No. 208 Dynamic Crush—Continental and Civic

Multiple Degree of Freedom Approach. To further examine the crash pulse effects on the unrestrained occupants, multiple degree of freedom crash victim simulations with the Passenger and Driver Simulation Model (PADS) were conducted. The PADS model includes mathematical simulations of the steering assembly, instrument panel, header, and windshield. For this analysis, all parameters were held constant except for the crash pulses. In Table 10, data from PADS are given for four passenger cars which were tested in the NCAP; a 1984 Pontiac T1000 and a 1985 Dodge Colt which are Group *Lwt* vehicles, and a 1983 Chevrolet Caprice and a 1980 Chrysler LeBaron which are Group *Hwt* vehicles. Crash pulses for these four vehicles are shown in Figures 22 and 28. (Note: Major differences

Table 8. Results of Single Mass Analysis for NCAP Vehicles

Vehicle	Distance of Mass from Surface (in.)	Contact Time (msec)	Velocity of Surface at Contact (mph)	Contact Velocity (mph)
Pontiac T1000 (Group Lwt Vehicle)	5	41	17.2	17.8
	10	53	9.0	26.0
	15	61	4.6	30.4
	20	71	0.6	34.4
	25	79	-1.6	36.6
Chevrolet Caprice (Group Hwt Vehicle)	5	46	21.5	13.5
	10	63	15.3	19.7
	15	75	9.5	25.5
	20	86	3.9	31.1
	25	95	0.2	34.8

Table 9. Results of Single Mass Analysis for FMVSS No. 208 Vehicles

Vehicle	Distance of Mass from Surface (in.)	Contact Time (msec)	Velocity of Surface at Contact (mph)	Contact Velocity (mph)
Honda Civic (Group Lwt Vehicle)	5	41	16.5	13.5
	10	55	6.9	23.1
	15	66	0.9	29.1
	20	76	-2.8	32.8
	25	84	-3.6	33.6
Lincoln Continental (Group Hwt Vehicle)	5	53	16.9	13.1
	10	68	9.1	20.9
	15	81	3.7	26.3
	20	91	-0.3	29.7
	25	100	-2.2	32.2

Table 10. Results of Multiple Degree of Freedom Analysis for NCAP Vehicles

Vehicle	Knee Contact Velocity (mph)	Chest Contact Velocity (mph)	Head Contact Velocity (mph)
Pontiac T1000	16.5	31.3	39.8
Chevrolet Caprice	9.8	26.7	33.7
Dodge Colt	14.6	28.1	38.2
Chrysler LeBaron	11.4	26.9	36.3

are evident between crash pulses of the T1000 and Caprice. The Colt and LeBaron crash pulses are similar.)

Similarly, for two passenger cars which were tested in FMVSS No. 208; a 1990 Honda Civic (a Group *Lwt* vehicle) and a 1989 Lincoln Continental (a Group *Hwt* vehicle), PADS runs were conducted and the data are presented in Table 11.

Again, as for the single mass analysis, higher contact velocities are seen for the Group *Lwt* vehicles. In the 35 mph NCAP crash tests, the contact velocities from PADS for the Group *Lwt* vehicles (the Pontiac T1000 and the Dodge Colt) exceed those of the Group *Hwt* vehicles (the

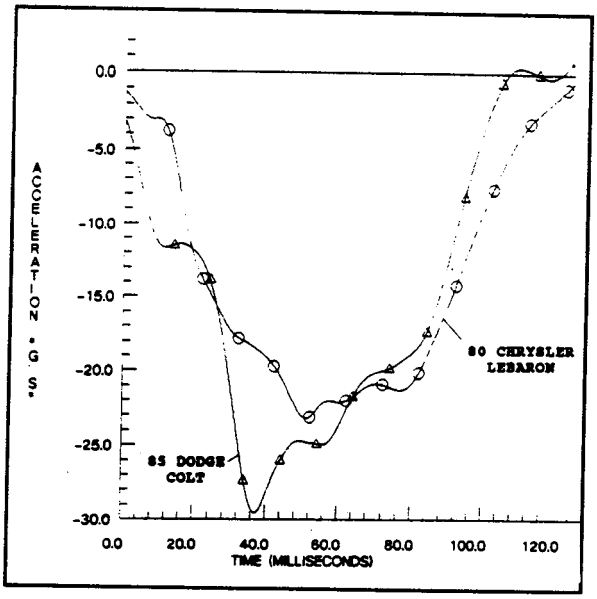

Figure 28. NCAP Crash Pulses—LeBaron and Colt

Table 11. Results of Multiple Degree of Freedom Analysis for FMVSS No. 208 Vehicles

Vehicle	Knee Contact Velocity (mph)	Chest Contact Velocity (mph)	Head Contact Velocity (mph)
Honda Civic	13.5	26.3	37.3
Lincoln Continental	9.7	26.0	33.7

Chevrolet Caprice and the Chrysler LeBaron) by 0.9 to 6.7 mph. In the 30 mph FMVSS No. 208 crash tests, the contact velocities from PADS in the Group *Lwt* vehicle (the Honda Civic) exceed those of the Group *Hwt* vehicle (the Lincoln Continental) by 0.3 to 3.8 mph.

HIC and chest g's were significantly higher as calculated by PADS for the Pontiac T1000 when compared to the Caprice. The HIC for the T1000 was 1474 and chest g's were 107. For the Caprice, the HIC was 1077 and chest g's were 72. (Note: Other PADS models became unstable soon after occupant contacts occurred and HICs and chest g's were not obtained).

Both the single mass analysis and the PADS analysis indicate that the differences in crash pulses between Group *Lwt* and Group *Hwt* vehicles may result in contact velocities as much as 6 mph greater in the smaller vehicles in crashes similar to the 35 mph NCAP crash tests and as much as 4 mph in crashes similar to the 30 mph FMVSS No. 208 crash tests.

Differences in Injury Probability for Restrained Occupants

Assessment of Dummy Response Values from NCAP and FMVSS No. 208 Tests. When examining all Group *Lwt* and Group *Hwt* passenger cars from NCAP and FMVSS No. 208 tests, the average dummy injury response values indicate that restrained occupants in the lower weight vehicles may be at greater risks of injury than those in the heavier vehicles, especially in the higher speed crashes as simulated by NCAP. These average values are given in Table 12 and graphically shown as percentages of FMVSS No. 208 requirements in Figures 29 and 30.

Table 12. Average Injury Response Values from Restrained Dummies for Group *Lwt* and Group *Hwt* Vehicles

Parameter	Average Values from NCAP		Average Values from FMVSS No. 208	
	Group Lwt	Group Hwt	Group Lwt	Group Hwt
HICD	1,094	966	504	480
CGD	50	49	44	44
LFEMD	938	889	1,305	1,295
RFEMD	820	995	1,206	1,320
HICP	1,032	886	473	398
CGP	44	43	40	39
LFEMP	764	808	1,024	798
RFEMP	650	639	1,049	868

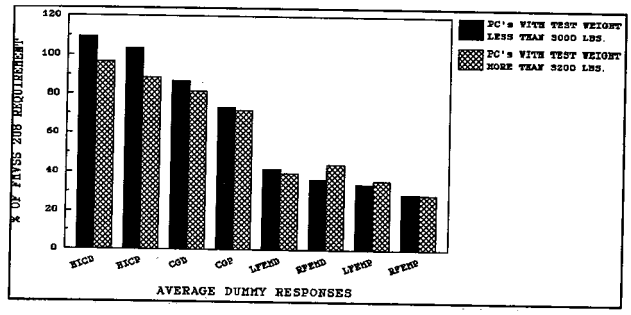

Figure 29. Dummy Response Averages—NCAP Data Comparisons of Light Weight to Heavy Weight PCs

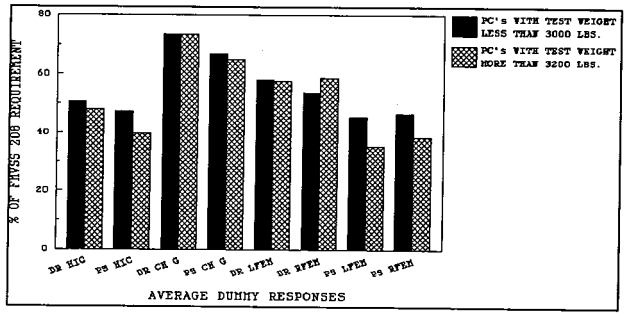

Figure 30. Dummy Response Averages—FMVSS No. 208 Data—Comparisons of Light Weight to Heavy Weight PC

Logistic curves of injury risk functions are shown in Figures 8, 9, and 10. From these functions, the probabilities of injuries are estimated for the average dummy response values which are given in Table 12. These probabilities are shown in Figures 31 and 32. These data indicate that, in the NCAP test conditions, the probability of a life threatening head injury is approximately 50 percent greater for the restrained occupants of the lighter Group *Lwt* vehicles than for the restrained occupants of the heavier Group *Hwt* vehicles (increasing from 16 to 23 percent for the driver and from 13 to 20 percent for the passenger). In the FMVSS No. 208 test conditions, only minor increases in the probability of severe head injuries for the restrained

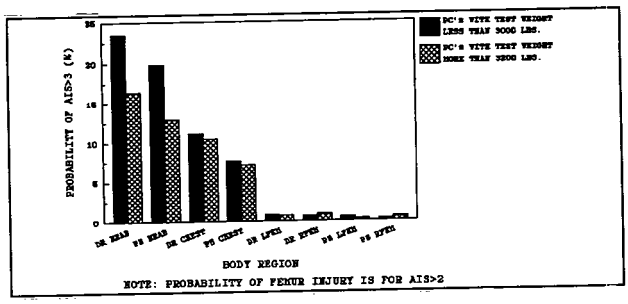

Figure 31. Injury Probability Based on GM Risk Functions—Average Risks in NCAP Crash Test

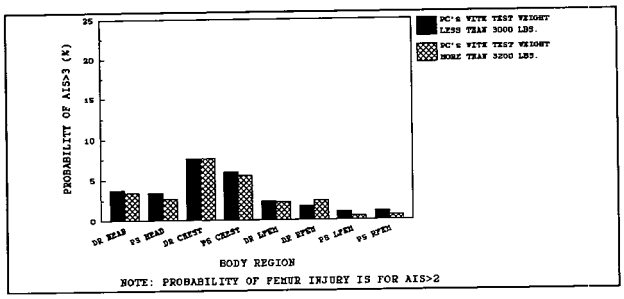

Figure 32. Injury Probability Based on GM Risk Functions—Average Risks in FMVSS No. 208 Crash Test

occupants of the Group *Lwt* to the Group *Hwt* vehicles are noted.

Multiple Degree of Freedom Analysis for Restrained Occupants. PADS runs for belt restrained drivers using the crash pulses from the NCAP tests of the Pontiac T1000 and the Chevrolet Caprice were also completed. Data from these simulations indicate the higher injury probability for the restrained occupants of the Group *Lwt* vehicles. For the Pontiac T1000 driver, the HIC is 1,248 and the chest g's are 65 due to steering assembly contacts. These are much higher than for the Chevrolet Caprice in which head contact did not occur and the resulting HIC was only 673. The driver chest did strike the steering assembly in the Caprice. However, the contact was much less severe than in the T1000 and resulted in chest g's of 37.

The Effect of Weighting the NCAP Data by Vehicle Registrations

In the above paragraphs, analyses were presented which used the unweighted data from the actual vehicles which have been tested. The effects of using the previously-defined vehicle registration weightings on the principal parameters which were used in the above unweighted studies are given in Table 13.

By applying these weightings to the NCAP tested vehicles for the 1990 fleet, approximately 18 million passenger cars are contained in the *Lwt* Group and approximately 23 million passenger cars are in the *Hwt* Group.

Examination of these weighted data indicates that for the crash pulse parameters (PEAKG, TPEAKG, and TPULSE) no significant differences are observed between the weighted and unweighted values. Therefore, the effects of the crash pulse differences on the injury probability for unrestrained occupants are the same for the weighted data as for the unweighted data.

Table 13. Comparison of the Average Principal Vehicle and Dummy Parameters—Weighted and Unweighted

Parameter	Group Lwt		Group Hwt	
	Weighted	Unweighted	Weighted	Unweighted
PEAKG	28.6	29.9	29.4	29.3
TPEAKG	49	49	66	60
TPULSE	119	117	133	130
HICD	889 (13%)	1,094 (23%)	838 (11%)	966 (16%)
HICP	876 (13%)	1,032 (20%)	776 (9%)	886 (13%)

(Numbers in parentheses indicate the percent probability of life-threatening head injury as predicted from risk curves when using the average HIC values.)

For the NCAP dummy response parameters (HICD and HICP), it is noted, as in the previous study [8], that the potential safety performance of the weighted fleet is better than the unweighted fleet. The differences between lighter and heavier vehicles are also reduced when the NCAP data are weighted by vehicle registrations. However, the data continue to indicate that the average estimate of probability of life threatening head injuries are greater for the lighter Group *Lwt* vehicles (approximately 20% greater for the driver and approximately 45% greater for the passenger).

Section 4—Summary and Conclusions

Recent agency studies of real-world crashes have concluded that occupants of lighter cars are at greater risk of injury than occupants of heavier cars even in crashes of the same severity. Crash test data from NCAP and FMVSS No. 08 tests strongly support these conclusions for unrestrained occupants.

This study shows that the crash pulse parameters of the lighter cars will expose the unrestrained occupants to more severe environments, especially in single vehicle crashes. As an average, the crash pulses for lighter vehicles reach the peak decelerations much earlier in the crash events than the heavier vehicles and have significantly shorter durations. These differences result in contact velocities for the unrestrained occupants which may be as much as 6 mph higher than those experienced in the heavier vehicles.

Average dummy response data indicate that, for all passenger cars which have been tested in NCAP and FMVSS No. 208, the restrained occupants are also at greater risk of injury in the lighter vehicles. From risk function curves, restrained occupants in the higher speed NCAP crashes may be as much as 50 percent more likely to suffer serious head injuries in the lighter vehicles.

References

1. Hackney, J. R., and Carlin Ellyson, "A Review of the Effects of Belt Systems, Steering Assemblies, and Structural Design on the Safety Performance of

Vehicles in the New Car Assessment Program," Proceedings of the Tenth International Technical Conference on Experimental Safety Vehicles, July 1985, Oxford, England.
2. Prasad, P., Ford Motor Company, and Harold Mertz, General Motors Corp., "The Position of the United States Delegation to the ISO Working Group 6 on the Use of HIC in the Automotive Environment," SAE Paper 851246, presented at the SAE Government/Industry Meeting and Exposition, Washington, D.C., May 1985.
3. Viano, D. C., and Sudhakar Arepally, "Assessing the Safety Performance of Occupant Restraint Systems," General Motors Research Laboratories, Research Publication GMR-7093, July 1990.
4. "Effect of Car Size on Fatality and Injury Risk in Single-Vehicle Crashes," U. S. Department of Transportation, National Highway Traffic Safety Administration, Washington, D.C., August 1990.
5. "Effect of Car Size on Fatality and Injury Risk in Multiple-Vehicle Crashes," U. S. Department of Transportation, National Highway Traffic Safety Administration, Washington, D.C., To be published.
6. "Recommended Definitions for Passenger Car Size Classification by Wheelbase and Weight," Final Report by the Passenger Car Classification Subcommittee of the Transportation Research Board, August 1984.
7. "The Development and Use of PADS (Passenger/Driver Simulation) Computer Program," Final Report, National Highway Traffic Safety Administration, Contract No. DTNH 22-82-R-07017, March 1984.
8. Hackney, J. R., W. T. Hollowell, and D. S. Cohen, "Analysis of Frontal Crash Safety Performance of Passenger Cars, Light Trucks and Vans and an Outline of Future Research Requirements," Proceedings of the Twelfth International Technical Conference on Experimental Safety Vehicles, May 1989, Goteborg, Sweden.

S9-O-05

Avoiding Sub-optimized Occupant Safety by Multiple Speed Impact Testing

Hans Norin, Clas Jernström, Magnus Koch, Stephan Ryrberg, Sven-Erik Svensson
Volvo Car Corporation

Abstract

Car manufacturers carrying out crash tests at only one speed and with only one occupant size run the risk of sub-optimizing their safety systems. This is discussed occasionally, but often in such all-embracing terms that a car designer is often left without any advice as to how the sub-optimization can be reduced. This risk will be illustrated through an assumed case. An existing belt system is compared with some new, hypothetical designs. Depending on which test strategy is chosen, the safety properties of one of the new designs can be found to be either better, or worse, than the existing system. This shows that the consequences of an inadequate test strategy for new safety systems can be, that instead of achieving a reduction in injuries, the result might be an increase in the number of injuries out in the real traffic environment. The illustration is done using a method whereby accident injury statistics can be correlated with dummy responses from crash tests in the laboratory and with dummy responses in the MADYMO Simulation Program. Different collision speeds and variations in occupant size should therefore be considered when test strategies for occupant protection systems are defined. Also, legislators and consumers should pay more attention to safety performance in different circumstances.

Introduction

The purpose of this paper is:

- To show how a limited test strategy and some unfortunate characteristics of a belt system might lead to sub-optimization of the occupant protection system.
- To introduce a new tool which permits us to demonstrate the risk of sub-optimization. By using this tool it is also possible to optimize protection systems. The result will then be a minimizing of the expected total injuries over a wide spectrum of traffic speeds and occupant sizes.
- To spread knowledge about the importance of a well-optimized crash protection system for a whole range of crash speeds.

Background

There exists an opinion that the performance requirements in the motor vehicle standards will imply a threshold between the level of no injuries and the level where a certain injury or fatality may occur, regardless of occupant size, age and general physical condition. This is truly not the case.

If, for example, the standards require that vehicles comply with certain performance requirements for any speeds up to 30 mph, this should imply that the vehicle should give full protection for its occupants up to that particular speed. Using this logic, by requiring the vehicles to comply with the same performance requirements for a higher test speed, the protection of the

occupants would be improved. However, the performance requirements in the standards only indicate a certain probability of an occupant escaping injury during a crash.

Over the years, several authors have pointed out that impact tests carried out at only one speed run the risk of leading to sub-optimization. Many interesting contributions have been made, of which Horsch's (1) and Korner's (2) are two of the most detailed studies to have been carried out in recent times.

This paper continues the discussion by showing that there exists a risk of sub-optimizing safety systems if the crash performance of the vehicles is optimized towards a single high crash speed and a single occupant size.

The risk becomes higher the more the test speed is raised. This is due to the fact that the vast majority of crashes occur at an impact speed that is lower than the maximum speed in the safety standards, e.g. 30 mph in FMVSS 208.

The problem becomes even more emphasized when considering the rating programs performed by government agencies, consumer organizations and the media. These ratings are normally carried out using only one test speed that is higher than the speed in the safety standards. The test results from the ratings have received extensive attention from the media and from the car-buying public.

A good rating result is normally perceived as being an indication of a well-performing and well-optimized occupant protection system, considering ALL crash speeds, occupant sizes, etc, up to and including the speed used in the rating. Although this may be the case, this paper shows that the rating results may be deceiving if an occupant protection system of a car that has performed well in a rating test is optimized towards only ONE impact speed and ONE occupant size.

However, few test methods have been developed and carried out at lower speeds. Do the companies and organizations concerned believe, perhaps, that these accident situations are taken care of by a demonstrated protection at high speeds?

In Volvo's opinion this is unsatisfactory. Through several years of following up accidents (3) we have revealed a picture of a large quantity of personal injuries at crash speeds way below the test speeds which are often used. The normal tests do not give enough indication of the risk of injury and the protection effects at the speeds at which the majority of injury-producing accidents occur.

There is, admittedly, a technical international discussion regarding safety at other speeds than those prescribed in the authorities' test methods. However, the conclusions from the debate have primarily been indicative, and without sufficient substance for the development of practical design tools for our car design engineers.

That is in contrast to this paper, where we demonstrate a case of sub-optimization risk with the aid of a helpful tool—the Injury Prediction Model.

The Injury Prediction Model

The Model has been developed over several years at Volvo (2, 4). Comments on the development will follow in the section of the paper entitled Discussions and Conclusions. Figure 1 shows the different stages of the Model. Each stage will be described in detail in the following sections. The description will use some of the data from the sub-optimization case.

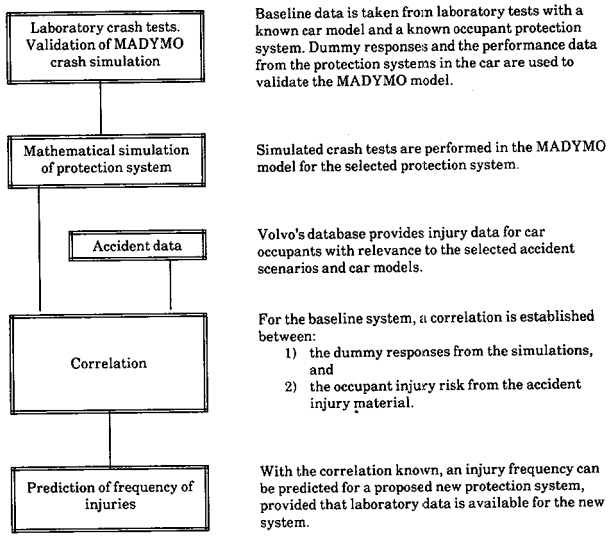

Figure 1. The Injury Prediction Model and Its Stages

Laboratory Crash Tests and Validation of MADYMO Crash Simulation

Crash tests in the form of full-scale impact tests and Hyge sled tests were run in the laboratory in order to achieve the required input data to validate the simulation model. A large quantity of data was recorded and used for the validation. For this paper, we will only make use of the dummy protection responses, in other words HIC36 [i.e., HIC with 36 ms limit (5)] and Cr [i.e., the resultant chest acceleration].

In order to connect the laboratory tests with the greatest possible amount of data from real crashes in the field, the Volvo model 240, European version, was chosen for the crash tests.

Four cars were crashed, in frontal collisions against a fixed barrier. The crashed cars were equipped with three-point retractor belts, and were as identical as possible in all other aspects. Two 50 percentile Hybrid III (Part 572E) dummies were placed in the cars according to FMVSS 208, in the driver's and passenger's positions. The crash speeds chosen were: 15, 25, 35 and 40 mph.

Using our knowledge from other tests with 240 cars, it was considered that the measurement results now ob-

tained were representative and could be used as a basis for our conclusions in this study.

In addition to the full-scale tests, two Hyge sled test series were run to further study the movement of the dummy and protection criteria during a crash. These were carried out with 50 percentile and 5 percentile Hybrid III dummies. The tests were only run at two crash speeds, 25 and 35 mph, but in general with the same conditions as in the full-scale tests, i.e. the same vehicle type, crash pulse, belts, etc. Some of the tests were run with the dashboard and steering wheel fitted in the body shell. In the tests, those parts were placed in the most rearward position they assumed during the corresponding full-scale tests.

The compatibility between the full-scale tests and the sled tests is judged as being very good.

Validation of MADYMO Crash Simulation. A MADYMO model (6) of the crashing Volvo 240 car and its restrained occupants was set up. Three different occupant sizes were modelled.

- M50, the male 50th percentile Hybrid III dummy. Data according to (7) was used.
- F5, the female 5th percentile Hybrid III dummy. Data was based partly on a scaling of the M50 dummy, and partly on data obtained by measurements on one of Volvo's dummies. C.f. Figure 2.
- M95, the male 95th percentile Hybrid III dummy. Data was based on a scaling of the M50 dummy.

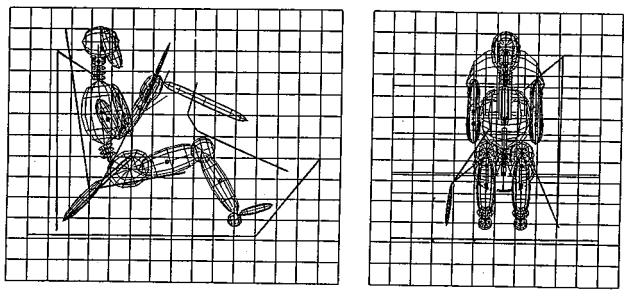

Figure 2. The MADYMO 3D Model of the Female 5th Percentile Hybrid III Dummy in the Driver Position of a Volvo Model 240

The MADYMO model was validated against the crash and sled tests. Figure 3 shows an example of the correlation between two dummy response signals recorded in one of the laboratory crashes at 35 mph and MADYMOs simulation of the same crash.

Mathematical Simulation of Protection System

Several crash tests were then performed in the MADYMO model for the baseline belt system. In this case the simulated tests were made at crash speeds of 15, 25, 25 and 40 mph and with the three occupant sizes. The output was 24 groups of dummy responses: three dummy sizes, four crash speeds and two front seat positions.

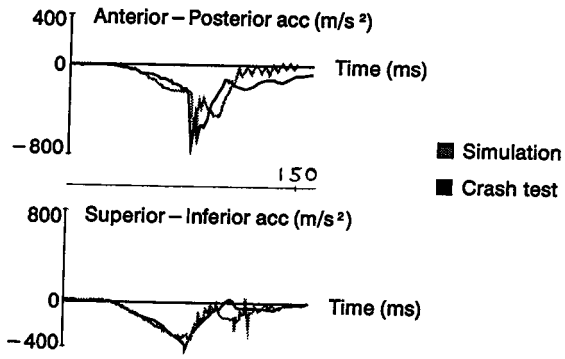

Figure 3. Acceleration Signals in the Centre of Gravity of the Head of the 5th Percentile Dummy During Crash Tests

Accident Data

From the statistical material on accidents—2547 frontal collisions with Volvo 240 cars where the driver and front seat passenger used a seat belt—we obtain the statistical distribution of crash severity (i.e. crash speed) and occupant height and information regarding the range of injuries for these occupants. An injury risk (8, 9) can be calculated from the material for each crash speed, position in the car and passenger size for every relevant body part and injury type. For our purpose here, we chose the level AIS2+ as the threshold between non-significant and significant injuries. If, instead, the analysis is done for AIS3+ or AIS4+, very similar results are obtained.

Correlation

The next stage in the Injury Prediction Model is to establish a correlation between the accident injury data and the dummy response numbers from the MADYMO simulations. Such a correlation is valid under conditions which Korner (2) has formulated: "Provided that the crash mode of the laboratory tests is equivalent to the real life accident type, and that a valid crash severity parameter is used, and that the protection criterion is a valid measure of injury production, then this correlation is generally applicable."

The correlation is determined with the aid of the SAS statistical software (10). The dummies' protection criteria from the MADYMO simulations are correlated with the injury risk from the accident material. All the occupant sizes and crash speeds are included in the correlation. The correlation implies, for example, that a certain HIC36 value in laboratory crashes is related to a certain head injury risk in a corresponding crash situation in traffic.

Prediction of Frequency of Injuries

The final stage in the Injury Prediction Model is then to determine an injury risk. With the known correlation between laboratory data and injury risk, an injury frequency can be predicted for a proposed new protection system, provided that crash test performance in some form is available for the new system.

The procedure is to multiply the statistically established joint distribution of accident crash speeds and occupant sizes by the injury risks from the simulated crash data. The result will be a predicted total injury frequency for the proposed protective system.

Study of Possible Sub-Optimization

Choice of Belt Systems

For our study of the sub-optimization we need to select some alternative variants of belt systems. The variants shall, taking into consideration that we are working with a demonstration example, have properties that are clearly different from the base system.

In order to find "good" variations of the belt system's technical design, a sensitivity analysis on the baseline belt system was carried out in the MADYMO model. Five system parameters were varied, namely the stiffness of the belt itself, mechanical features such as pre-tensioner and force limiter, different belt feeds using slack or belt locking. Two other parameters, the softness of the seat cushion and the car crash pulse, were also varied. Customary dummy responses in the computer-simulated crashes were determined for the driver as well as the passenger. A factorial design of experiments (11, 12) was utilised in order to systematically combine and vary the seven parameters without requiring too much work.

As a result of the sensitivity study, and taking into account the purpose of our investigation, three belt systems were chosen for further study.

- The first system, designated **STD**, is the baseline system. It corresponds to the standard three-point belt system in the Volvo 240, with belt elongation of 10%. (The elongation is determined at 10kN tensile force.) This was the system used in the laboratory crash tests.
- The second system, designated **FLM** (for Force Limiter), has a 4% belt elongation and 8 kN force limiter. This combination should, according to the sensitivity study, give good performance at crash speeds of around 35 mph.
- The third system, designated **PRT** (for Pretensioner), is a standard belt with 10% elongation, but modified by the addition of a pyrotechnical pretensioner. This combination should, according to the sensitivity study, give good performance for a wide spectrum of crash speeds.

Study of Chosen Belt Systems

Simulated crash tests were performed in the MADYMO model for the two newly defined systems. The test parameters were the same as for the baseline system. The output was 48 groups of dummy responses: three dummy sizes, four crash speeds, two front seat positions and two belt systems. See Tables 1 and 2.

Some of the tabulated results from the simulations at 35 mph are presented in the bar chart in Figure 4.

Table 1. Passenger Dummy Response Data for the Simulated Crashes with the Three Belt Systems

Speed mph	Dummy size	Cr m/s² STD	Cr m/s² PPT	Cr m/s² FLM	HIC_{36} sg$^{2.5}$ STD	HIC_{36} sg$^{2.5}$ PPT	HIC_{36} sg$^{2.5}$ FLM
15	M50	266	213	317	65	80	86
15	F5	255	172	240	98	76	100
15	M95	168	154	185	26	41	14
25	M50	299	246	355	116	146	159
25	F5	252	208	239	186	144	168
25	M95	221	189	238	320	96	213
35	M50	540	402	405	1159	377	369
35	F5	303	299	337	397	269	375
35	M95	347	304	328	912	733	859
40	M50	555	596	553	1817	1452	1727
40	F5	421	379	385	680	440	614
40	M95	440	358	406	1969	1264	1510

Table 2. Driver Dummy Response Data for the Simulated Crashes with the Three Belt Systems

Speed mph	Dummy size	Cr m/s² STD	Cr m/s² PPT	Cr m/s² FLM	HIC_{36} sg$^{2.5}$ STD	HIC_{36} sg$^{2.5}$ PPT	HIC_{36} sg$^{2.5}$ FLM
15	M50	265	213	317	151	118	151
15	F5	261	182	250	101	77	102
15	M95	168	154	186	72	67	53
25	M50	299	246	355	396	328	396
25	F5	276	217	257	295	164	252
25	M95	191	191	239	176	225	165
35	M50	441	471	442	692	679	563
35	F5	341	307	327	318	280	362
35	M95	376	378	378	1031	783	918
40	M50	573	583	528	1890	928	1383
40	F5	487	445	452	824	440	914
40	M95	424	400	419	1622	1400	1508

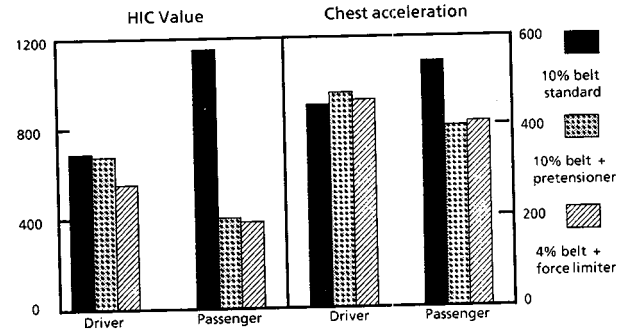

Figure 4. Simulated Crash Test Results: HIC36 Values and Chest Acceleration for Analysed Belt Systems, 50th Percentile Dummy, Driver and Front Seat Passenger, 35 mph

Looking at the driver's HIC36 values in Figure 4, we can see that there has been a reduction for the **PRT** and **FLM** systems compared with the **STD** system.

For the passenger, the **STD** version's HIC36 value is high (due to an adverse impact against the dashboard) whilst the two alternative belt systems have considerably reduced HIC36 values. With regards to the chest acceleration for the driver, the change from the base version is marginal (slight increase), whilst we can see a clear improvement in the values for the passenger.

Analysis of Performance at 35 mph. The conventional evaluation of a safety system is a single crash test and analysis of the performance at the legally prescribed 30 mph. Some presume that meeting the requirement at an

increased crash speed implies an increased occupant protection. Such an evaluation of the data from the three simulated belt systems is possible from Figure 4. It indicates that both the pretensioner **PRT** and the stiff belt **FLM** could contribute towards an increased level of safety. If we had to choose between these two systems, the **FLM** alternative has slightly lower dummy responses throughout.

The **FLM** system is probably also, from a technical point of view, a simpler design solution. These factors can be arguments for choosing the **FLM** system before the **PRT** system.

Analysis of Injury Outcome. As an alternative to the conventional test at 35 mph we can, thanks to the Injury Prediction Model, evaluate the belt systems in terms of predicted injuries in accidents. Using the correlation between dummy response numbers and injury risk for the baseline **STD** belt system, the dummy responses for the alternative belt systems **FLM** and **PRT** can likewise be translated to injury risk for these systems. The result is a predicted total injury frequency for each of the alternative belt systems. This is presented in the bar chart in Figure 5.

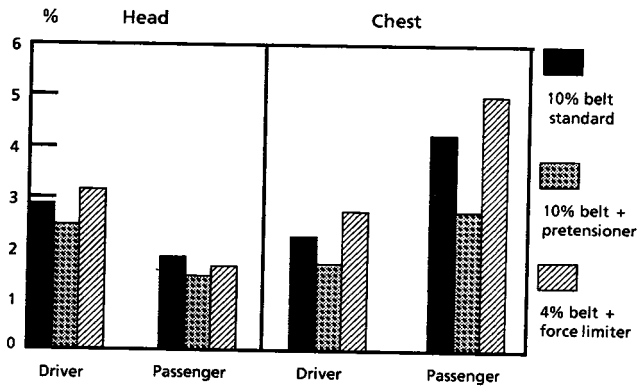

Figure 5. Predicted Head and Chest Injury Frequencies for Standard and Modified Belt Systems, Driver and Front Seat Passenger, All Speeds, All Occupant Heights

We can see from Figure 5 that the alternative pretensioner **PRT** has a lower injury frequency in relation to the base version **STD** for both head and chest injuries (AIS 2+) for the driver and front seat passenger. The stiff belt **FLM** alternative, however, has resulted (except for the passenger's head injury frequency) in an increase in the risk of injury. The alternative which, from the simulated crash test results involving a 50 percentile dummy at 35 mph, appeared to be the best solution, has, when we take into consideration the distribution of crash severity and occupant height, a much higher injury frequency for head and chest than the base version **STD** and the pretensioner alternative **PRT**.

The relative increase and reduction of the injury frequency for the two alternative belt systems is evident from Figure 6.

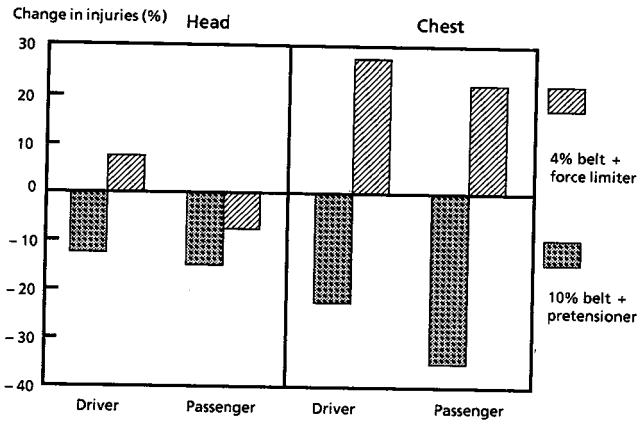

Figure 6. Percent Changes in Predicted Head and Chest Injuries Between the STD Belt System and the Alternative Systems

Compared with the **STD** belt,we can see that the **PRT** reduces the head injuries by approximately 12% for the driver and 14% for the front seat passenger. Corresponding reductions for the chest injuries are approximately 22% and 36% respectively.

For the alternative **FLM** versus **STD**, however, we can see an increase in the head injuries for the driver of approximately 8% and for the passenger there is a reduction of 8%. Regarding the risk of chest injuries, there is a marked increase for both the driver and front seat passenger of 26% and 23% respectively.

Tests at One Speed versus Tests in Several Scenarios. It can be seen clearly from the above analyses that a test strategy confined to laboratory testing at the standardized 35 mph will give quite a different picture of the relative merits of the three belt systems than that obtained from tests performed at several speeds and with several occupant sizes. This fact should affect future test strategies for occupant protection systems.

Discussions and Conclusions

Optimized Performance

We have shown that tests carried out at only one speed mean a risk of sub-optimizing the car's safety properties. Figure 7 shows clearly that a system (**FLM**) can be designed which has good performance at high speeds, but not at low speeds. It is also evident that it is possible to design a system (**PRT**) which produces improvements within a large range of speeds. Corresponding effects can be achieved for all occupant heights.

If crash safety properties at several speeds are not taken into consideration during development work, there is a risk of investing large resources into incorrect measures, and instead of achieving a reduction in injuries, the result is an increase in the number of injuries out in the real traffic environment.

Using the method described in this paper it is, however, possible to study the effect of future design

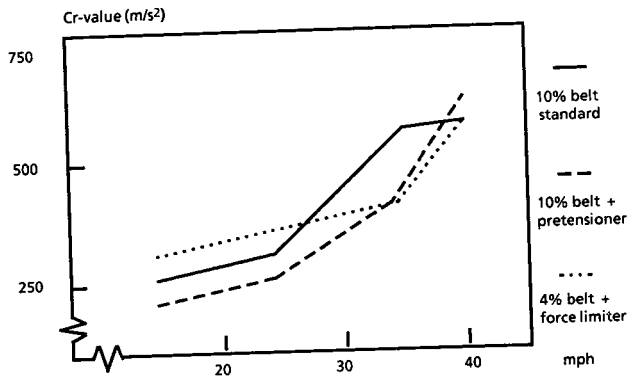

Figure 7. Chest Acceleration as a Function of Crash Speed for the Three Different Systems, 50th Percentile Passenger Dummy

and legislative proposals, through which it is possible to concentrate on correct measures at an early stage.

With an accuracy which up until now has not been possible, our example shows the magnitude of the sub-optimization which crash tests at only one speed can lead to.

There are, admittedly, several approximations and uncertainties in the data and the models used. However, many of these errors are probably of a systematic nature. So if, for instance, the calculated chest injury frequencies in Figure 5 have a systematic error making them 20% too high, *the difference between the calculated injury frequencies should to a large extent be free from such errors.* And it is the *differences,* which are plotted in Figure 6, that we use for judging the relative merits of the three analyzed belt systems.

Other shortcomings and errors in the models and the data are more difficult to determine. As described in the next section, work is underway to improve the quality in these areas.

Even if it is difficult today to give an accurate assessment of the magnitude of the errors involved, an engineer's reflection on Figure 7 leads to a conviction that there are actual differences between the belt systems. The relationship between their performance data is presumably a reality which has consequences for car manufacturers as well as for motorists.

Development of the Model

The Injury Prediction Model has now become a tool at Volvo in the evaluation and design of new occupant protection systems.

The method is also applicable for comparison of more different types of protection systems, e.g. airbag versus belt. It can also be applied for different types of accidents, e.g. side collisions and rear end collisions. Design parameters which can then be analyzed are, for example, the stiffness of the padding and the structure.

It is therefore important that corresponding methods are developed for other types of accidents, e.g. side collisions (2), and that the way of thinking becomes generally used by car manufacturers and legislators.

The method's usability means that there is a need for better computer programs for the simulation of accidents.

More accurate accident data needs to be collected, e.g. better parameters for crash severity and injury mechanisms should be developed and put into use.

It could also be of great value to simplify the described method so that a rough estimate of the injury reduction for a given design proposal is obtained quickly by using a relatively simple mathematical expression. This assumes that the system's performance at various speeds is known. This can be very useful, for example, for manufacturers who do not have access to their own databases regarding speed and occupant size distribution, etc. Here, the authorities can play a crucial role by developing the necessary basic information and spreading the acquired knowledge.

When discussing laboratory tests for new safety systems, the MADYMO simulations and the Injury Prediction Model are also helpful aids in the selection of test parameters and testing matrixes. They also form a complement to crash tests which cannot be performed in the laboratory for capacity reasons.

For the Readers to Consider

There is a tendency to consider any opposition from the automotive industry to high crash speeds in the safety standards and safety ratings as an unwillingness to cooperate towards improving traffic safety. This is generally not true. It is in the interests of all parties that the level of occupant safety is raised. That must be a top priority.

Volvo is deeply committed to safety. We therefore feel under obligation to optimize the occupant protection systems in our cars towards real world crashes and their effect on occupants. For this reason, we perform crash tests at a range of speeds in order to find the optimum safety design properties of the vehicles. Publicity-wise, this attitude may not be very rewarding, since it will not necessarily give the best results in rating tests. But it is what we believe in.

The purpose of this paper is to spread the knowledge about the importance of a well-optimized crash protection system for the whole range of crash speeds. We urge the readers to consider the facts presented in this paper in future discussions about crash ratings, safety standards, etc.

Acknowledgements

The authors would like to recognize Jan-Inge Eliasson, Irene Isaksson-Hellman, Björn Lundell, Mats Moberg and Anders Öhlund, who have been directly involved in the testing and analysis behind this report. We also wish to recognize Anders Eugensson and Johnny Korner for their helpful comments and suggestions.

References

1. J.D. Horsch; Evaluation of Occupant Responses Measured in Laboratory Tests, SAE 870222.
2. J. Korner; A Method for Evaluating Occupant Protection by Correlating Accident Data with Laboratory Test Data, SAE 890747.
3. H. Norin, J. Korner; Volvo Traffic Accident Research, 1985.
4. H. Norin, I. Isaksson-Hellman; Prediction of Injury Potential of a Safety Design Feature. A Theoretical Method Based on Mathematical Simulations and Traffic Accident Data. Report to be published, 1992.
5. Federal register; Vol 50, No 71, pages 14590-14592; Vol 51, No. 201, pages 37030-37033.
6. MADYMO, User's manual 3D version 4.3, TNO the HAGUE, the Netherlands, 1990.
7. MADMYO, Databases version 4.3, TNO the HAGUE, the Netherlands, 1990.
8. M. Koch; Recent work with a Method for the Fitting of Injury versus Exposure Data into a Risk Function, 1988 International IRCOBI Conference, Cologne.
9. S.H. Walker, D.B. Duncan; Estimation of the Probability of an Event as a Function of Several Independent Variables. Presented in Biometrika, 1967.
10. SAS STAT User's Guide, Version 6, 4th Edition, Cary NC; SAS Institute Inc., 1990.
11. G.E.P. Box, W.G. Hunter and J.S. Hunter; Statistics for Experimenters, J. Wiley 1978.
12. M. Phadke; Quality Engineering Using Robust Design, Englewood Cliffs. 1989.

S9-O-06

Improving the Protection of Restrained Front Seat Occupants in Frontal Crashes

D.J. Dalmotas, E.R. Welbourne
Transport Canada

Abstract

The principles that underlie Transport Canada's policy on occupant restraints are restated. Those principles require both improvements in the protection of the individual occupant and increases in benefits to society through the more general use of restraint systems. Progress in seat belt use in Canada is summarized. The effectiveness of current three-point seat belts in preventing fatalities in frontal collisions is briefly reviewed. The residual injury problem in frontal collisions of equivalent or lower severity to the standard 48 km/h frontal barrier test is then defined with reference to recent accident data. Performance of current systems in actual collisions and in the frontal barrier test is compared. It is concluded that requiring all occupant restraint systems to meet the alternative set of performance criteria, recently proposed by Transport Canada for automatic seat belts, would significantly improve their performance. Requiring only the use of available technology, the primary effect of those criteria would be virtually to preclude injurious head and facial contacts with the vehicle interior in collisions of the regulated collision severity. Objective methods of defining seat belt fit are still required, in particular to reduce the incidence of belt-induced abdominal injury.

Introduction

Two principles, first enunciated in 1981 [1], underlie Transport Canada's policy on occupant restraints:

- maintaining and improving the protection afforded to the individual occupant by the restraint system; and
- maximizing social benefit by promoting the increased use of restraint systems in collaboration with provincial governments.

Progress in improving the protection of the individual restrained occupant is the main subject of this paper. To provide some context, it is however useful briefly to review the progress that has been made in Canada in promoting seat belt use.

All Canadian provinces and the two territories now have laws requiring the use of available seat belts by all occupants, subject to minor exceptions. Prior to the introduction of the first provincial seat belt legislation in 1976, only about 14 percent of car drivers were restrained. The most recent survey of seat belt use in Canada, conducted in June 1991, [2] showed that 85.1 percent of car drivers were using available seat belts. The corresponding figures for passenger vans and light trucks were 80.2 and 70.2 percent respectively.

In three provinces, Newfoundland, Quebec and Saskatchewan, more than 90 percent of car drivers are now restrained. The rates achieved in those provinces are among the highest in the world. The lowest rate of seat belt use is 74.7 percent, in Canada's smallest province. In 1990, all provinces, the territories and the federal government endorsed the National Occupant Restraint Programme, which includes initiatives in education, enforcement and evaluation. Its aim is to attain 95 percent use of seat belts by 1995, a goal that is clearly now within reach. An earlier goal of 80 percent use by 1983 was missed by a wide margin.

Figure 1 summarizes the progress that has been made since 1980. That figure shows the percentage of Canadian drivers using available shoulder belts, with the corresponding highest and lowest provincial use rates. From 1982 to 1989, annual total traffic deaths in Canada remained essentially constant at about 4200±150 over a period in which traffic increased by some 20 percent. In 1990, however, the figure fell to 3957; it is the first year since 1962 in which fewer than 4000 people have died in road accidents. While it is difficult to separate the effect of increasing belt use from other factors, such as the reduction in impaired driving, it has undoubtedly contributed to that achievement.

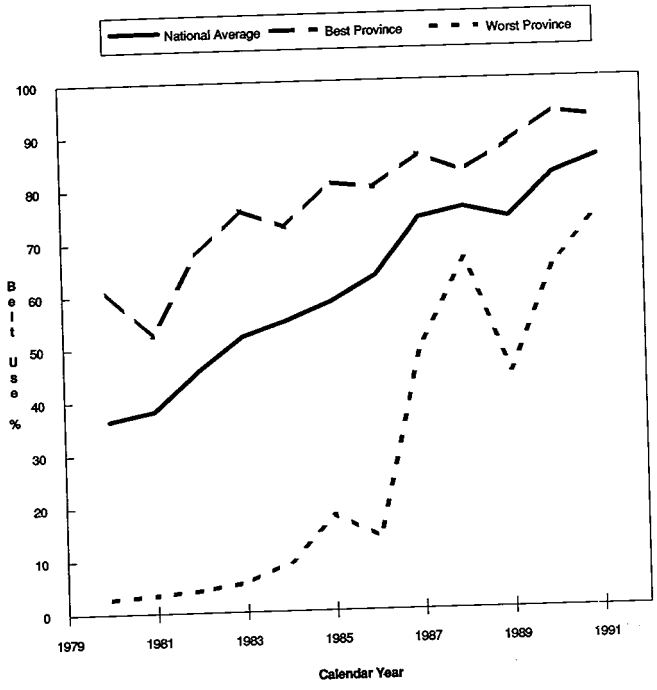

Figure 1. Percentage of Car Drivers Wearing Shoulder Belt—National Roadside Seat Belt Surveys: 1979-1991

Current and Proposed Requirements for Frontal Crash Protection

In Canada, the only passenger cars that must be subjected to a 48 km/h frontal barrier collision are those equipped with automatic seat belt systems. Canadian standards do not at present require that the performance of vehicles equipped with three-point seat belts, alone or in combination with a supplementary air bag, be subjected to such a dynamic test. The protection afforded by three-point manual seat belts is determined indirectly by requirements relating to the design of the ensemble and to the design and performance of its components and attachments to the vehicle structure.

The current performance requirements applicable to automatic seat belt systems consist of a maximum value of the Head Injury Criterion (HIC) of 1000, a peak chest acceleration not exceeding 60 g for more than 3 ms and a maximum femur load of 10 kN, all measured on either a Part 572 or Hybrid III dummy.

An alternative set of performance requirements for automatic seat belt systems, which requires the use of a Hybrid III dummy, has recently been proposed. The alternative set consists of a peak resultant head acceleration not exceeding 80 g, regardless of the pulse duration, and a maximum chest deflection at mid-sternum of 50 mm. The existing 10 kN limit on maximum femur load is retained. Extending these requirements to all occupant restraint systems, regardless of type, is presently under consideration.

Performance of Three-Point Belts in Frontal Collisions

Estimated Effectiveness

As many have previously noted, the effectiveness of seat belts in preventing injury consists of two distinct components. The first, mainly attributable to the lap portion of the belt, is the prevention of occupant ejection when primary containment provided by the vehicle structure has failed. Door opening or failure of glazing are the most usual events. The second component of effectiveness is the prevention or mitigation of occupant contact with surfaces interior to the vehicle.

In frontal collisions, Evans' median estimate [3] of the effectiveness in preventing driver fatalities of three-point belts is 43 percent, of which 9 percent is attributable to preventing ejection. The corresponding figures for right front passengers are 39 and 8 percent respectively. The low indicated effectiveness against ejection does not imply that three-point belts are ineffective in preventing ejection. Canadian and other data show that manual three-point belts are virtually 100 percent effective in that respect; the low estimated effectiveness simply reflects the relatively low rate of ejection of unrestrained occupants in frontal collisions. The balances of 57 and 61 percent of driver and passenger fatalities in frontal impacts, against which the three-point belt is ineffective, are almost entirely attributable to contacts with the vehicle interior, deformed or undeformed.

Dalmotas and Krzyzewski [4] estimated the overall effectiveness of three-point belts in preventing serious, non-fatal injuries from Canadian mass accident data. They noted the effect on such estimates of the uncertain reliability of police reporting of the belt use of uninjured occupants. For that reason, if for no other, there do not appear to be any reliable, systematic estimates of the effectiveness of three-point belts in preventing or mitigating non-fatal injuries to front seat occupants in frontal crashes. Detailed data from studies of injuries to restrained occupants do, however, allow the residual injury problem to be specified more precisely.

Injury Experience of Restrained Occupants in Frontal Collisions

Canadian accident studies. Two sources of data on the injury experience in Canada of front seat occupants restrained by three-point belt may be cited. In the Fully

Restrained Occupant Study (FROS) [5], a convenience sample of injured front seat occupants, who were wearing three-point belts, was collected and analyzed. Each occupant experienced at least one injury of AIS 2 or greater severity, as defined in the 1975 edition of the Abbreviated Injury Scale [6]. The data were collected in several defined geographical areas of Canada which were not necessarily representative of the whole country. The investigative procedures were however similar in all essential respects to those being used in the continuing Passenger Car Study (PCS).

In that study, data are collected by ten teams located in universities across Canada. Each team investigates a representative sample of the collisions that occur in a prescribed local geographical region. Specific data are collected on a wide range of human, vehicular and environmental factors associated with each such collision. Transport Canada combines the data collected by all teams into a master database. National estimates of the incidence of particular variables are then derived by means of an appropriate weighing scheme.

The teams review the motor vehicle collisions reported to the police in the prescribed regions on a frequent basis. Collisions that meet the study criteria are identified and a subset of those are selected, according to a defined sampling plan, for further investigation. Collisions meeting the study criteria involve at least one passenger car and are reported by the police as having resulted in at least one fatal or non-fatal injury.

Where possible, the teams inspect all involved vehicles within a day or two of the collision. Information on vehicle damage and occupant contact points is recorded and the accident site is also inspected. Team members interview vehicle occupants and other persons involved in the collisions. As far as possible, data on injuries are confirmed by the admitting hospital. The data presented in this paper relate to accidents that occurred in the four-year period from 1984 to 1987.

Gross comparisons of FROS and PCS data. In the data available to date from the PCS, 15.2 percent of occupants suffered at least one injury of AIS 2 [7] or greater severity in frontal collisions, regardless of collision severity. Of those occupants 74.9 percent were drivers and 25.1 percent, right front passengers. The corresponding figures in the FROS data were 75.2 and 24.8 percent respectively.

Of occupants represented in the PCS data who were injured at AIS 2 or higher severity, 66.1 percent incurred those injuries in collisions of extent 3 or less according to the SAE Collision Deformation Classification [8]. In the Fully Restrained Occupant Study, the corresponding percentage was 71.9.

Injury experience of drivers. Among drivers in FROS, the most frequently injured body region was the head and face, followed by the chest and lower extremities. The PCS data show a similar ranking for injuries at AIS 3 or higher severity. Most such injuries (73.7%) occurred in collisions of CDC extent greater than 3. That result is consistent with the FROS data, in which serious to fatal head injuries were usually associated with intruding vehicle structure, such as the A-pillar. The majority of the facial injuries (77.0%) observed in the PCS occurred in collisions of CDC extent 3 or less. In the FROS, facial injuries almost invariably resulted from simple contacts with the steering assembly, not exacerbated by intrusion.

The most evident difference between the data from the two studies is in the incidence of injuries to the lower extremities at AIS 2 or higher severities. Whereas lower extremity injuries constituted only 21.5 percent of injuries in that severity range in the FROS, they accounted for 33.9 percent of injuries at AIS 2 or more in the more recent PCS.

Injury experience of right front passengers. The highest incidence of serious to fatal injuries (AIS 23) to passengers in PCS was to the abdomen, followed closely by the incidence of chest injuries. These body regions were also the most frequently injured in the Fully Restrained Occupant Study. The majority of injuries to the chest and abdomen at AIS22 occurred in collisions of CDC extent 3 or less in both studies.

Injury Frequencies in Single-Event Frontal Collisions

The somewhat different bases of the two studies compared above dictate caution in drawing conclusions from their results. There is, however, little evidence to suggest that a significant improvement has occurred in the protection of restrained occupants during the 8 to 10 years between the two studies. In respect of the incidence of injuries to the legs and feet of drivers, there is at least a suggestion of the opposite trend.

To form some idea of what might be accomplished by more stringent standards for occupant protection in frontal collisions, two subsets of the 1984-87 PCS data have been extracted. The first relates to all single-event frontal impacts to passenger cars, regardless of severity. The second subset is further limited to those frontal impacts resulting in damage of CDC extent 3 or less. In both subsets, the only injuries considered are those incurred by restrained drivers or right front passengers aged 16 or more, for whom complete injury data were available. A few injuries not directly associated with the impact, e.g., burns, have been excluded.

The second subset is limited to collisions of CDC extent 3, since that is approximately the extent of the deformation that results from a standard 48 km/h frontal impact with a flat rigid barrier. It should however be borne in mind that in real collisions falling in the designated group, the vehicle deformation is almost never as uniformly distributed. In consequence, the peak acceleration of the occupant compartment tends to be less and the probability of localized intrusion is greater than in the standard frontal barrier test.

Summary data from the PCS database on occupant injuries are presented in Tables 1 to 3. Each table

contains four sections. The upper sections relate to drivers and the lower to right front passengers. The sections at the left give simple percentages and those at the right give cumulative percentages.

Table 1 shows the percentages of drivers and passengers incurring injuries of the stated maximum AIS level to the designated body region in all frontal collisions regardless of severity.

Table 1. Distribution of Injured Occupants by Body Region Injured and AIS Injury Severity Rating—Front Seated Three-Point Restrained Car Occupants Over the Age of 15 Years—Single Event Frontal Impacts/All Collision Severitites

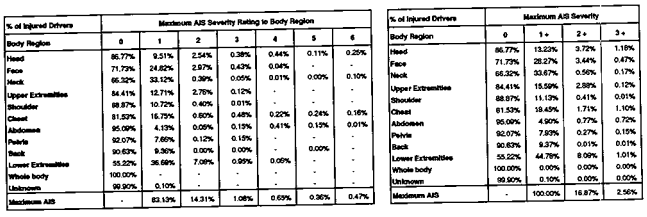

% of Injured Drivers	Maximum AIS Severity Rating to Body Region						
Body Region	0	1	2	3	4	5	6
Head	86.77%	9.51%	2.54%	0.38%	0.44%	0.11%	0.25%
Face	71.73%	24.82%	2.97%	0.43%	0.04%	-	-
Neck	66.32%	33.12%	0.39%	0.05%	0.01%	0.00%	0.10%
Upper Extremities	84.41%	12.71%	2.76%	0.12%	-	-	-
Shoulder	88.87%	10.72%	0.40%	0.01%	-	-	-
Chest	81.53%	16.75%	0.60%	0.48%	0.22%	0.24%	0.18%
Abdomen	95.09%	4.13%	0.05%	0.13%	0.41%	0.15%	0.01%
Pelvis	92.07%	7.60%	0.12%	0.15%	-	-	-
Back	90.63%	9.30%	0.00%	0.00%	-	0.00%	-
Lower Extremities	55.22%	36.68%	7.09%	0.95%	0.05%	-	-
Whole body	100.00%	-	-	-	-	-	-
Unknown	99.90%	0.10%	-	-	-	-	-
Maximum AIS	-	83.19%	14.31%	1.08%	0.69%	0.36%	0.47%

% of Injured Drivers	Maximum AIS Severity			
Body Region	0	1+	2+	3+
Head	86.77%	13.23%	3.72%	1.16%
Face	71.73%	28.27%	3.44%	0.47%
Neck	66.32%	33.67%	0.56%	0.17%
Upper Extremities	84.41%	15.59%	2.88%	0.12%
Shoulder	88.87%	11.13%	0.41%	0.01%
Chest	81.53%	18.45%	1.71%	1.10%
Abdomen	95.09%	4.90%	0.77%	0.72%
Pelvis	92.07%	7.93%	0.27%	0.15%
Back	90.63%	9.37%	0.01%	0.01%
Lower Extremities	55.22%	44.78%	8.09%	1.01%
Whole body	100.00%	0.00%	0.00%	0.00%
Unknown	99.90%	0.10%	0.00%	0.00%
Maximum AIS	-	100.00%	16.87%	2.56%

% of Injured F.R. Pass.	Maximum AIS Severity Rating to Body Region						
Body Region	0	1	2	3	4	5	6
Head	86.47%	12.65%	0.37%	0.36%	0.03%	0.09%	0.02%
Face	77.80%	22.01%	0.11%	0.05%	0.04%	-	-
Neck	84.53%	15.09%	0.28%	0.02%	0.05%	-	0.03%
Upper Extremities	78.50%	13.12%	8.17%	0.21%	-	-	-
Shoulder	81.55%	17.56%	0.87%	0.02%	-	-	-
Chest	73.76%	23.55%	1.88%	0.11%	0.22%	0.20%	0.28%
Abdomen	89.32%	9.71%	0.08%	0.33%	0.37%	0.21%	-
Pelvis	91.20%	8.44%	0.34%	0.02%	-	-	-
Back	94.56%	5.29%	0.15%	0.01%	-	0.05%	-
Lower Extremities	58.85%	40.53%	0.10%	0.52%	0.01%	-	-
Whole body	99.85%	0.15%	-	-	-	-	-
Unknown	99.98%	-	0.02%	-	-	-	-
Maximum AIS	-	88.28%	10.03%	0.43%	0.45%	0.49%	0.32%

% of Injured F.R. Pass.	Maximum AIS Severity			
Body Region	0	1+	2+	3+
Head	86.47%	13.53%	0.87%	0.50%
Face	77.80%	22.20%	0.19%	0.09%
Neck	84.53%	15.47%	0.38%	0.10%
Upper Extremities	78.50%	21.50%	8.38%	0.21%
Shoulder	81.55%	18.45%	0.89%	0.02%
Chest	73.76%	26.23%	2.68%	0.81%
Abdomen	89.32%	10.69%	0.98%	0.09%
Pelvis	91.20%	8.80%	0.36%	0.02%
Back	94.56%	5.45%	0.22%	0.06%
Lower Extremities	58.85%	41.15%	0.63%	0.53%
Whole body	99.85%	0.15%	0.00%	0.00%
Unknown	99.98%	0.02%	0.02%	0.00%
Maximum AIS	-	100.00%	11.72%	1.69%

Table 2 gives the corresponding data for frontal collisions of CDC extent 3 or less.

Table 2. Distributed of Injured Occupants by Body Region Injured and AIS Injury Severity Rating—Front Seated Three-Point Restrained Car Occupants Over the Age of 15 Years—Single Event Frontal Impacts/ CDC Damage Extent 3 and Under

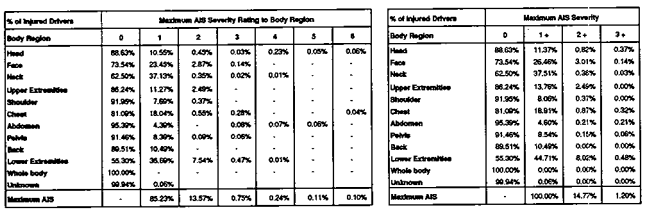

% of Injured Drivers	Maximum AIS Severity Rating to Body Region						
Body Region	0	1	2	3	4	5	6
Head	88.63%	10.55%	0.43%	0.03%	0.23%	0.05%	0.06%
Face	73.54%	23.45%	2.87%	0.14%	-	-	-
Neck	62.50%	37.13%	0.35%	0.02%	0.01%	-	-
Upper Extremities	86.24%	11.27%	2.49%	-	-	-	-
Shoulder	91.95%	7.80%	0.27%	-	-	-	-
Chest	81.09%	18.04%	0.55%	0.28%	-	-	0.04%
Abdomen	95.39%	4.36%	-	0.09%	0.07%	0.06%	-
Pelvis	91.46%	8.36%	0.09%	0.06%	-	-	-
Back	89.51%	10.49%	-	-	-	-	-
Lower Extremities	55.30%	36.99%	7.54%	0.47%	0.01%	-	-
Whole body	100.00%	-	-	-	-	-	-
Unknown	99.94%	0.06%	-	-	-	-	-
Maximum AIS	-	85.23%	13.57%	0.75%	0.24%	0.11%	0.10%

% of Injured Drivers	Maximum AIS Severity			
Body Region	0	1+	2+	3+
Head	88.63%	11.37%	0.82%	0.37%
Face	73.54%	26.46%	3.01%	0.14%
Neck	62.50%	37.51%	0.36%	0.03%
Upper Extremities	86.24%	13.76%	2.49%	0.00%
Shoulder	91.95%	8.06%	0.31%	0.00%
Chest	81.09%	18.91%	0.87%	0.32%
Abdomen	95.39%	4.60%	0.21%	0.21%
Pelvis	91.46%	8.54%	0.15%	0.06%
Back	89.51%	10.49%	0.00%	0.00%
Lower Extremities	55.30%	44.71%	8.06%	0.48%
Whole body	100.00%	0.00%	0.00%	0.00%
Unknown	99.94%	0.06%	0.00%	0.00%
Maximum AIS	-	100.00%	14.77%	1.20%

% of Injured F.R. Pass.	Maximum AIS Severity Rating to Body Region						
Body Region	0	1	2	3	4	5	6
Head	85.41%	13.84%	0.38%	0.25%	-	0.11%	-
Face	84.01%	15.94%	-	0.05%	-	-	-
Neck	82.41%	17.44%	0.10%	-	0.05%	-	-
Upper Extremities	84.84%	14.33%	0.65%	0.18%	-	-	-
Shoulder	91.58%	7.70%	0.73%	-	-	-	-
Chest	71.22%	26.29%	1.90%	0.11%	0.17%	0.02%	0.20%
Abdomen	92.20%	7.13%	-	0.22%	0.23%	0.22%	-
Pelvis	98.50%	1.32%	0.18%	-	-	-	-
Back	93.71%	6.04%	0.18%	0.01%	-	0.06%	-
Lower Extremities	62.86%	36.93%	0.06%	0.14%	-	-	-
Whole body	99.82%	0.18%	-	-	-	-	-
Unknown	100.00%	-	-	-	-	-	-
Maximum AIS	-	96.00%	3.03%	0.16%	0.26%	0.35%	0.20%

% of Injured F.R. Pass.	Maximum AIS Severity			
Body Region	0	1+	2+	3+
Head	85.41%	14.58%	0.74%	0.36%
Face	84.01%	15.98%	0.05%	0.05%
Neck	82.41%	17.59%	0.15%	0.05%
Upper Extremities	84.84%	15.16%	0.83%	0.18%
Shoulder	91.58%	8.43%	0.73%	0.00%
Chest	71.22%	28.78%	2.49%	0.59%
Abdomen	92.20%	7.81%	0.69%	0.68%
Pelvis	98.50%	1.50%	0.18%	0.00%
Back	93.71%	6.29%	0.25%	0.07%
Lower Extremities	62.86%	37.15%	0.22%	0.14%
Whole body	99.82%	0.18%	0.03%	0.00%
Unknown	100.00%	0.00%	0.00%	0.00%
Maximum AIS	-	100.00%	4.00%	0.97%

Table 3 gives the percentages of all injured occupants who received those injuries in collisions of CDC extent 3 or less.

The sources of these injuries and their prevention or mitigation are considered in more detail in subsequent sections of the paper.

Table 3. Percentage of Injury Problem Accounted by CDC Damage Extent 3 and Under Collisions—Front Seated Three-Point Restrained Car Occupants Over the Age of 15 Years—Single Event Frontal Impacts

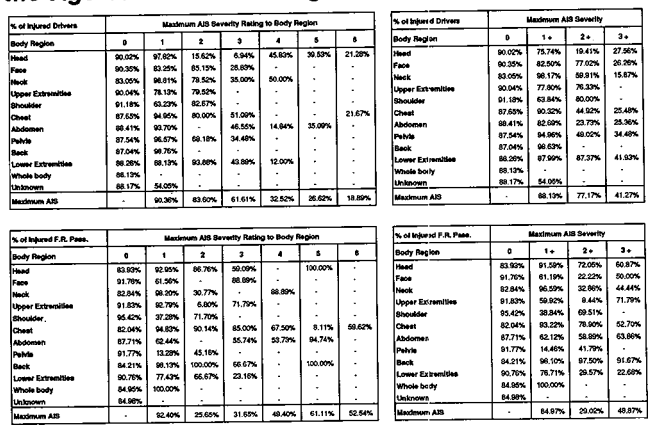

% of Injured Drivers	Maximum AIS Severity Rating to Body Region						
Body Region	0	1	2	3	4	5	6
Head	90.02%	97.92%	15.62%	6.94%	45.83%	39.58%	21.28%
Face	90.35%	93.25%	85.13%	28.89%	-	-	-
Neck	83.05%	98.81%	79.52%	35.00%	50.00%	-	-
Upper Extremities	90.04%	78.13%	79.52%	-	-	-	-
Shoulder	91.18%	93.23%	82.67%	-	-	-	-
Chest	87.63%	94.95%	80.00%	51.09%	-	-	21.67%
Abdomen	98.41%	99.70%	-	46.55%	14.84%	35.09%	-
Pelvis	97.54%	96.57%	69.18%	34.48%	-	-	-
Back	97.04%	99.76%	-	-	-	-	-
Lower Extremities	86.28%	98.13%	93.88%	43.89%	12.00%	-	-
Whole body	98.13%	-	-	-	-	-	-
Unknown	98.17%	94.05%	-	-	-	-	-
Maximum AIS	-	90.36%	83.60%	61.61%	32.52%	26.62%	18.89%

% of Injured Drivers	Maximum AIS Severity			
Body Region	0	1+	2+	3+
Head	90.02%	75.74%	19.41%	27.56%
Face	90.35%	82.50%	77.02%	26.26%
Neck	83.05%	98.17%	59.91%	15.87%
Upper Extremities	90.04%	77.80%	76.33%	-
Shoulder	91.18%	93.84%	80.00%	-
Chest	87.63%	90.32%	44.92%	25.48%
Abdomen	98.41%	82.69%	23.79%	25.36%
Pelvis	97.54%	94.96%	49.02%	34.48%
Back	97.04%	99.63%	-	-
Lower Extremities	86.28%	97.99%	87.37%	41.93%
Whole body	98.13%	-	-	-
Unknown	98.17%	94.06%	-	-
Maximum AIS	-	98.19%	77.17%	41.27%

% of Injured F.R. Pass.	Maximum AIS Severity Rating to Body Region						
Body Region	0	1	2	3	4	5	6
Head	83.93%	92.95%	86.76%	50.09%	-	100.00%	-
Face	91.76%	61.56%	-	88.89%	-	-	-
Neck	82.84%	98.20%	30.77%	-	88.89%	-	-
Upper Extremities	91.83%	92.79%	6.80%	71.79%	-	-	-
Shoulder	95.42%	37.28%	71.70%	-	-	-	-
Chest	82.04%	94.83%	90.14%	85.00%	67.50%	8.11%	98.62%
Abdomen	87.71%	62.44%	-	55.74%	53.79%	94.74%	-
Pelvis	91.77%	13.28%	45.16%	-	-	-	-
Back	94.21%	98.19%	100.00%	66.67%	-	100.00%	-
Lower Extremities	90.76%	77.43%	66.67%	23.16%	-	-	-
Whole body	84.95%	100.00%	-	-	-	-	-
Unknown	84.98%	-	-	-	-	-	-
Maximum AIS	-	92.40%	25.65%	31.55%	48.40%	61.11%	52.54%

% of Injured F.R. Pass.	Maximum AIS Severity			
Body Region	0	1+	2+	3+
Head	83.93%	91.59%	72.05%	50.87%
Face	91.76%	61.19%	22.22%	50.00%
Neck	82.84%	96.59%	32.86%	44.44%
Upper Extremities	91.83%	59.92%	8.44%	71.79%
Shoulder	95.42%	38.84%	69.51%	-
Chest	82.04%	93.22%	78.90%	52.70%
Abdomen	87.71%	62.12%	58.89%	63.66%
Pelvis	91.77%	14.46%	41.79%	-
Back	94.21%	98.10%	97.50%	91.67%
Lower Extremities	90.76%	76.71%	29.57%	22.66%
Whole body	84.95%	100.00%	-	-
Unknown	84.98%	-	-	-
Maximum AIS	-	84.97%	29.02%	48.87%

Closed Head Injury

In the voluminous material that has been written about the mechanisms of closed head injury and measures of human tolerance, one point is very clear: in the automotive crash environment, closed head injury is invariably associated with an impact to the head. The instances in which closed head injury may have occurred without contact are few while the evidence linking head impact and brain injury is both massive and unequivocal. In an automobile collision in which no occupant head contact occurs, the probability of brain injury is extremely small.

Intrusion evidently limits the potential for reducing fatal head injuries by improving the performance of the occupant restraint system, unless parallel improvements in the vehicle structure are also made. Nonetheless, when the performance of current seat belt systems is measured in the standard 48 km/h frontal collision, they are by no means consistently effective in preventing injurious head contact with vehicle interior surfaces.

Despite the fact that there has, for many years, been no substantive change in performance requirements relating to head injury protection, some progress has nonetheless been made. A very rough indication can be obtained by comparing the incidence of driver and passenger head contacts in 44 frontal barrier crashes of 1976-78 model year passenger vehicles at 48 km/h reported by Dance and Enserink [9] with more recent data obtained under similar though not identical conditions. In the original 44 tests, the head of the Part 572 dummy driver struck some part of the steering wheel in 41 instances or 93 percent of the tests. In 18 of the same 44 tests (41%), the similar passenger dummy struck the dash panel.

Those results may be compared with data obtained from 61 tests on passenger cars and light trucks of model years 1986 to 1991. They included 3 tests using a barrier face inclined at 30° to the transverse axis of the vehicle. The majority of the tests employed Hybrid III dummies in both driver and passenger seats. Some of the Hybrid IIIs were equipped with an experimental frangible face system, and a few Part 572 dummies were also used.

The head of the dummy driver hit some part of the steering wheel in 55 of the 61 tests (90%). In four, it hit an inflated airbag and in the remaining two, there was no head contact. For passengers in the front outboard position, a larger reduction in the incidence of head contact was observed. In 46 cases (75%), the passenger dummy did not hit the vehicle interior during the initial impact. Of the remaining 15 events, nine consisted of soft contacts on rebound with the seat or side of the vehicle, four consisted of grazing contacts with the dashboard, while two were contacts with flying debris.

The foregoing comparison suggests that the progress made in reducing potentially injurious head contacts is confined to the right front passenger. The seat belt systems in most passenger cars for the North American market are still designed so that the driver's head hits some part of the steering wheel during a 48 km/h frontal barrier test. The lack of progress in reducing driver head contacts is attributable in part to the lack of a dynamic performance requirement for vehicles equipped with manual seat belts. To the extent that seat belt design has been influenced by dynamic testing, that lack of progress may also be ascribed in part to using a value of HIC of 1000 as the *de facto* goal for head injury protection.

The effect of using HIC as the basis for assessing the probability of closed head injury can be seen by considering the distributions of 93 HIC values shown in Figure 2. They were measured on Hybrid III driver and passenger dummies in a subset of the 61 tests cited above. The different shadings within each bar correspond with an unlimited integration interval and maxima of 36 and 15 ms. The 93 data shown are all those from the 61 tests cited above that involved either no dummy head contact or the head of the dummy hitting some part of the steering wheel or dashboard. Non-contact events are grouped at the left of the figure and the impact events at the right. Excluded are values associated with three other classes of event, contact with an air bag, contact on rebound from the primary impact and contact with flying debris.

The most obvious feature of Figure 2 is that regardless of the integration interval, the ranges of HIC values for the 41 events in which no dummy head contact occurred, and the 52 events involving head contact with steering wheel or dashboard, exhibit substantial overlap. In the U.S. regulations, the introduction of a 36 ms maximum integration time for HIC reflects an attempt to improve its power to distinguish between hard contacts and less harmful events. It can be seen, however, that even with a 15 ms maximum interval, 19 of the 52 contact events yield HIC values less than the highest non-contact HIC. Regardless of the integration interval, no single value of HIC provides adequate discrimination of harmless non-contact events from potentially injurious impacts to the head.

It is nonetheless clear that, as the integration interval approaches zero, the distinction between contact and

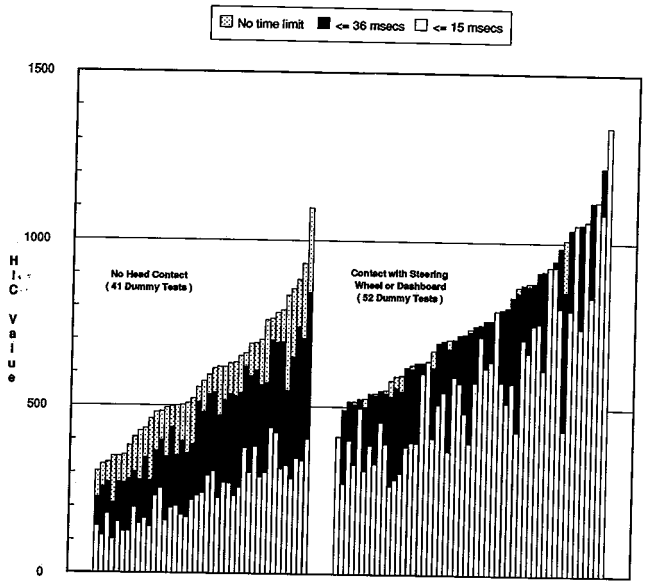

Figure 2. HIC Values as a Function of Head Contact and Time Interval of HIC Calculation—Hybrid III(E) ATD/49 Km/h Frontal Barrier Crash Tests

non-contact events becomes sharper. However, for a constant maximum value of HIC, it is also the case that the permitted peak and average head accelerations increase without limit. A simple way out of that dilemma is to abandon HIC and use the peak resultant head acceleration directly as the measure of performance.

In Figure 3, the peak resultant head accelerations measured in the same 93 events are presented in a similar format to that of Figure 2. No minimum pulse duration is specified. It can be seen that whereas all of the non-contact events produce peak resultant head accelerations of less than 80 g, 44 of the 52 contact events exceed that level. Moreover, the eight events that produced peak accelerations of less than 80 g would have been very unlikely to have caused more than superficial injury to a human occupant. All consisted of grazing contacts with the steering wheel rim or hub, or in the case of the dummy passenger, the dashboard.

The data presented in Figures 2 and 3 show that a simple 80 g limit on peak resultant head acceleration is considerably more effective than HIC in distinguishing harmless (non-contact) events from those that are associated with a high probability of head injury ("hard" contacts).

The basic rationale for using a simple 80 g limit on peak resultant head acceleration to reduce the incidence of closed head injury may be summarized in three points:

- In actual motor vehicle collisions, closed head injury is extremely rare in the absence of head contact. When head contact does occur, the associated injuries range in severity from minor to lethal.
- In 48 km/h frontal barrier tests, Part 572 and Hybrid III dummies experience peak resultant head accelerations in the absence of contact that are invariably

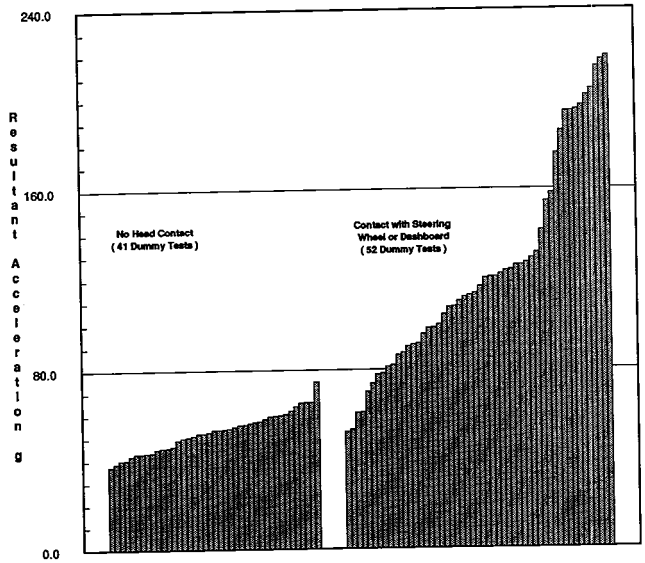

Figure 3. Peak Resultant Head Acceleration Values as a Function of Head Contact—Hybrid III(E) ATD/48 Km/h Frontal Barrier Crash Tests

less than 80 g. Under the same conditions, a human occupant would not be expected to experience any type of head injury.

- In 48 km/h frontal barrier tests, all but the softest contacts with an interior surface of the vehicle generate a peak resultant head acceleration exceeding 80 g. Under the same conditions, a human occupant would be exposed to some risk of incurring a head injury of indeterminate but probably low severity.

It should be noted that the proposed 80 g limit does not purport to be a biomechanical tolerance level for closed head injury in the conventional sense. It is simply a kinematic measure that enables a quite reliable distinction to be made between harmless and harmful events in tests simulating motor vehicle collisions.

Implications of an 80g Head Acceleration Limit

Closed Head Injury

Effect on vehicle design. Insofar as the front outboard passenger is concerned, recent crash test data show that an adequately designed three-point seat belt is sufficient to preclude dummy head contact in frontal barrier collisions at 48 km/h. Such systems currently produce peak resultant head accelerations in the range from 40 to 75 g, though poorly designed systems can be envisaged which might produce non-contact head accelerations exceeding 80 g. For example, the combination of belt webbing of high modulus with slow locking response of the retractor might generate such head accelerations. However, there seems to be no good reason to accommodate such systems, since the maximum tensile forces developed in the necks of restrained occupants are rather closely correlated with peak resultant head acceleration. (That issue is briefly discussed below.) Hence, unless manufacturers choose to carry over improvements in the performance of the driver's restraint system to the passenger, the 80 g limit is not expected to induce any significant change in passenger restraint systems.

A primary objective of the 80 g limit is to eliminate injurious driver head contacts in the standard 48 km/h barrier collision. If head contact occurs, it will necessarily be with a highly compliant object such as an inflated air bag or a well padded and compliant steering wheel.

To achieve the requisite performance, the preference of the major North American manufacturers would likely be the use of a supplementary air bag. The highest peak resultant head acceleration observed by Transport Canada in four frontal barrier tests of restraint systems comprising three-point belts with supplementary air bags is 58 g, clearly well within the proposed limit.

Two vehicle-to-vehicle frontal crash tests have also been conducted by Transport Canada on vehicles equipped with three-point belts and drivers' air bags. The lateral overlap between the vehicles at impact was 50 percent and the velocity change for the target vehicles was approximately 48 km/h. In each collision, the target vehicle was stationary, with its longitudinal axis directed 15 degrees away from the path of the striking vehicle. The relevant dummy responses for the target vehicle occupants are shown in Table 4. It can be seen that the responses of both passenger and driver dummies were well within proposed limits.

Table 4. Dummy Response in Vehicle-to-Vehicle Offset Frontal Impacts

Test Number	Seating Position	ATD Type	Restraint System	Peak Resultant Head Acceleration (g)	Peak Chest Deflection (mm)	Peak Femur Load (kN)
TC90-127	Driver F. R. Pass.	Hybrid III Hybrid III	Manual 3-Pt. w/ ACRS Manual 3-Pt.	30 36	28 28	4.50 1.04
TC90-128	Driver F. R. Pass.	Hybrid III Hybrid III	Manual 3-Pt. w/ ACRS Manual 3-Pt.	31 59	32 29	6.83 2.10

An alternative to the use of a supplementary air bag for the driver is the use of a three-point belt system that provides effective restraint of the upper torso. The two vehicles cited previously in which no driver head contact at all occurred in a 48 km/h frontal barrier test, were equipped with automatic two-point seat belts and manual lap belts. A major factor in the effectiveness of the upper torso restraints was the nature and the location of the shoulder belt anchorage. The belt was attached to the door frame at shoulder height, which maximized the effective stiffness of the belt. Moreover, since the end of the belt was attached directly to the door frame, the belt stretch and spool-out generated by the conventional D-ring and floor-level retractor were eliminated. A less desirable feature of the design was its primary reliance on compressive loads in the femurs to restrain the lower torso. Nonetheless, a similar basic approach to controlling the kinematic behaviour of the occupant could be

used in designing a manual three-point belt system. Other options include the use of locking D-rings or, at considerably higher cost, belt pretensioners.

Effect on occupant injuries. The PCS data for passengers are basically consistent with the observed restraint system performance in barrier tests. In frontal collisions of CDC extent 3 or less, the incidence of passenger head contact is low, with only 0.36 percent of exposed passengers experiencing head injury at AIS 3 or higher level. The unweighted data are too sparse to support any general conclusions on the sources of the more severe injuries. However, of the five passengers that experienced head injury at AIS 3 or more, only one in fact exceeded that level, suffering a concussion at AIS 5 from impact to the windshield.

Since the 80 g limit would not *require* significant changes to the design or performance of the passenger's restraint system, no direct benefits in reduced passenger injuries are directly attributable to it. Some may nonetheless accrue from a further reduction in the incidence of passenger head contacts in those vehicles in which improved belt restraints are provided to both driver and passenger.

The incidence of head injuries to drivers at AIS 3 or greater levels in Table 2 is essentially the same at 0.37 percent as for passengers (0.36 percent). The average severity of driver injuries is however markedly higher than that for passengers. Driver injuries are associated with impacts to the steering assembly, various other parts of the vehicle structure and intruding objects. Given the diversity of contact points observed in a relatively small sample of accidents, it is not feasible to estimate the benefits of the 80 g limit with any precision. It is not, however, unreasonable to expect reductions in both the frequency and severity of driver head injuries to flow from an 80 g limit. Such benefits may be expected whether improved belt design or a supplementary air bag is used to achieve the required performance.

The discussion in this and subsequent sections of the paper has, for reasons of brevity, been limited to the more severe injuries that occur in collisions of severity equal to or less than the standard 48 km/h barrier collision. It should also be noted, however, that reductions may also be expected in the severity of injuries in more severe frontal collisions and in the incidence of minor and moderate injuries.

Facial Injury

Effect on vehicle design. Limiting the permissible peak resultant head acceleration to 80 g may be expected to reduce the incidence of driver facial contact with the steering assembly, very substantially, if not to eliminate it, in frontal collisions with velocity changes up to 48 km/h. As noted above, the most probable industry response to such a requirement is the use either of a supplementary air bag or an improved seat belt to preclude driver head (and hence facial) contact.

In principle, manufacturers could meet an 80 g limit by such means without affecting the potential of the steering wheel to cause facial injury in other circumstances that are not directly regulated. Examples are collisions resulting in velocity changes exceeding 48 km/h and unfavourable combinations of driver size and seat position. It is therefore desirable that the steering assembly be designed to mitigate contact injuries in circumstances other than those simulated in the test collision. The preferred approach would be the use of a separate component test that encouraged the use of steering wheels that were both compliant (to reduce peak forces on the face) and well padded (to distribute those forces). One possible means of establishing performance levels would be the use of the frangible face system developed by Biokinetics and Associates for Transport Canada [10].

Effect on occupant injuries. For the reasons noted in the section on closed head injury, no direct benefit in reduced facial injuries to passengers is expected. Some indirect benefits may, however, carry over to the passenger in vehicles in which required improvements in the driver's belt are also made to the passenger's.

Table 2 indicates that the current incidence of facial injuries of AIS 2 or greater severity is about 3 percent, while for passengers the equivalent figure is only 0.05 percent. The markedly lower incidence of facial contact with the steering assembly, resulting from the 80 g limit on peak resultant head acceleration, is therefore expected to produce a substantial reduction in the incidence of facial injuries to drivers. The incidence of such injuries may be expected to approach the level currently observed for passengers.

Neck Injury

There does not currently exist an adequate biomechanical basis for specifying a general criterion for neck injury under arbitrary loading conditions. However, limiting the resultant head acceleration to 80 g has the additional effect of limiting the forces and moments induced in the neck to quite modest levels. Under non-contact conditions, a frontal impact induces primarily tensile forces in the neck. On the basis of estimates obtained by accident reconstruction, Mertz [11] has suggested that the maximum tensile force tolerable without neck injury is 3.3 Kn.

In Figure 4, peak tensile forces measured in the necks of Hybrid III dummies in 48 km/h frontal barrier crashes which did not result in head contact are plotted against the peak resultant head acceleration. It can be seen that the trend of the results suggests that the 3.3 Kn limit on neck tension is broadly consistent with the 80 g limit on peak resultant head acceleration.

The PCS data suggest that, in frontal crashes of CDC extent 3 or less, and in the absence of head contact, neck injury occurs quite infrequently to either drivers or passengers. Those injuries that do occur, consist almost

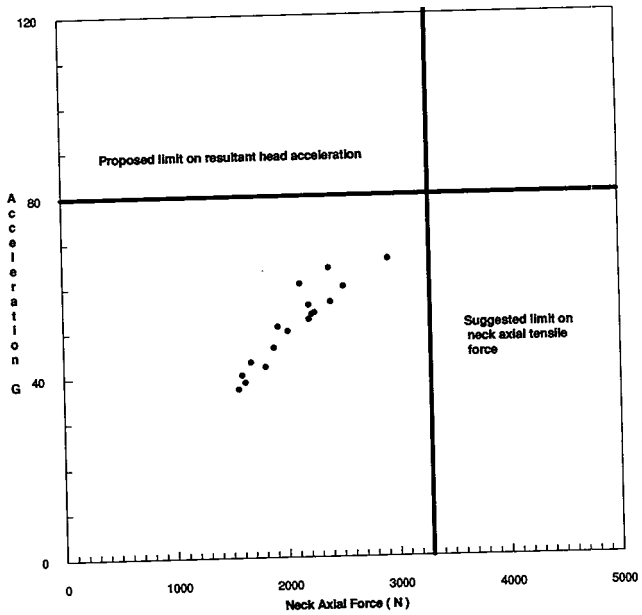

Figure 4. Cross-Plot of Peak Resultant Head Acceleration vs Maximum Neck Axial Tensile Force—Hybrid III(E)/ No Head Contact

exclusively of strained neck muscles (AIS 1). In the absence of contact between head or neck and something other than the seat belt webbing, the incidence of more severe neck injuries is very low. To the extent that driver neck injury is associated with head contact, some reduction may be expected as a result of the 80 g limit.

Thoracic Injury

Incidence and Severity of Injuries

Table 2 indicates that an estimated 0.32 percent of restrained drivers and 0.5 percent of passengers injured in frontal collisions of CDC extent 3 or less experienced serious to fatal injuries to the thorax. If uninjured occupants are also included, the corresponding rates are 0.13 and 0.26 percent respectively. A front seat passenger is thus about twice as likely as a driver to experience a serious or fatal chest injury in a frontal collision of the specified severity.

The drivers' injuries are predominantly associated with impacts to the steering assembly. For restrained front seat passengers, the seat belt itself is the primary source of injury. In the absence of exacerbating factors, principally loading by an unrestrained rear seat occupant, the severity is minor to moderate in collisions up to CDC extent 3.

Controlling Thoracic Injury

Fractures of the ribs, clavicle and sternum are possible consequences of restraining the upper torso by a diagonal belt, alone or in combination with a supplementary air bag. While a single rib fracture is considered only a minor injury (AIS 1), more serious injuries of the internal organs are almost invariably preceded by rib fractures. Maintaining the integrity of the rib cage thus greatly reduces the probability of serious injury to the internal organs of the thorax.

The incidence of rib fracture depends on the age, sex and seating position of the occupant, with elderly female passengers being particularly at risk. If injurious contacts between the driver's chest and the steering assembly can be prevented, the residual problem for both driver and passenger restraints is to minimize the incidence of rib fractures induced by the restraint system.

The relevant North American standards, currently set a limit of 60 g on the peak acceleration measured at the centre of gravity of the dummy thorax. As a measure of the potential for chest injury, a limit on chest acceleration limit is unacceptable. The primary mechanism of chest injury that is of concern is the fracture of one or more ribs. Peak acceleration gives no information on the probability of rib fracture, which depends crucially on how the forces producing the acceleration are distributed over the rib cage.

As earlier noted, if a Hybrid III dummy is used, the current standards require also that the chest compression be measured at the mid-sternum. Unlike acceleration, compression of the chest has been recognized as a measure strongly associated with the occurrence of rib fracture since the earliest investigations of thoracic injury mechanisms. In defining the limit to be placed on the chest compression of the dummy, the relations between the geometrical and stiffness characteristics of the dummy chest and some representative human chest must be taken into account.

Work on thoracic injury tolerance, summarized by Melvin and others [12], reflects an early consensus, based on cadaver tests, that compression of the human chest in the 30-35 percent range is associated with serious chest injury (AIS 3). An analysis by Neathery et al. [13] of an earlier set of data on male cadavers, including adjustment of the data to an average driver age of 45, led to the figure of 75 mm for the mid-sternal deflection of a 50th percentile male dummy. It should be noted however, that the dummy was assumed to have "substantial biofidelity" under the blunt thoracic impact loading used in the cadaver tests.

Translating that result to the Hybrid III dummy, loaded either by a diagonal belt or such a belt and an air bag requires a number of assumptions. A first observation must be that the Hybrid III chest is substantially stiffer than the chests of comparable young live males. Backaitis and St-Laurent [13] reported that under loading by a diagonal belt, the chest of the Hybrid III was 10 to 25 percent stiffer than the chests of tensed and relaxed male volunteer subjects respectively. Even if an injury severity of AIS 3 were acceptable as the target level for restraint system performance, some downward adjustment of the 75 mm deflection figure would still be indicated.

However, the geometry and deflection response of the Hybrid III thorax differ significantly from those of the

live human. There is accordingly a strong argument for choosing the permitted level conservatively, pending the availability in the longer term of a dummy with a more human-like thorax. On the basis of the quite limited data currently available, a 50 mm limit on mid-sternal compression appears to be both readily attainable and to offer a higher level of protection against serious injury to the thorax.

Implications of a 50 mm Chest Deflection Limit

Effect on vehicle design. Figure 5 shows a histogram of maximum chest deflections measured in 105 tests on Hybrid III dummies restrained by three-point belts. Four of the driver dummies were also restrained by supplementary airbags. As may be seen in the figure, 9 of the 105 tests resulted in chest deflections exceeding 50 mm. Of those, 2 exceeded only marginally (<1 mm) while the largest deflection measured was almost 60 mm. As may be seen in the figure, the modal deflection range is from 35.01 to 40.00 mm for the chosen 5 mm intervals. It may be concluded that a maximum chest deflection of 50 mm is readily attained by current three-point belts, with or without a supplementary air bag.

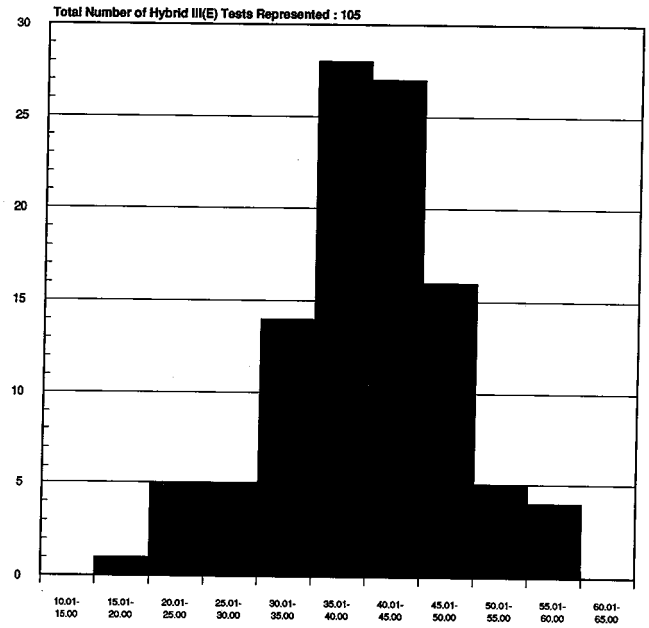

Figure 5. Distribution of Hybrid III Sternal Deflection Values Observed in 48 Km/h Frontal Barrier Crash Tests

Effect on occupant injuries. Since all but a few current three-point systems produce chest deflections of less than 50 mm, only a minor improvement in the current injury experience of restrained occupants may be expected from a regulated limit on chest deflection. The accident data suggest that serious chest injuries resulting from belt loading alone occur infrequently to younger passengers. The incidence of such injuries increases rapidly with the age of the occupant. Means of accommodating the limited injury tolerance of the chest in elderly occupants or in more severe collisions are not immediately evident.

Abdominal Injury

Incidence and Severity

The incidence of serious to fatal abdominal injuries differs significantly for drivers and passengers in collisions of CDC extent 3 or less. Table 2 shows that while only 0.21 percent of injured drivers experienced abdominal injuries of AIS 3 or greater severity, the equivalent figure for passengers was more than three times as great (0.68%). Including the uninjured occupants involved in the same collisions, the corresponding figures are 0.08 and 0.35 percent respectively. Moreover, while both the steering assembly and lap belt are involved in about half the cases of driver abdominal injury, passenger injuries are almost exclusively associated with the lap belt.

Provided that the lap belt remains below the iliac crests (anterior superior iliac spines or ASIS) the risk of injury to the abdominal organs is minimal. There are only two possible ways for the lap belt to intrude upon the soft tissue of the abdomen: either it was improperly worn or it moved above the ASIS during the collision.

Improper wearing does not necessarily imply carelessness on the part of the wearer. The current Canadian standard governing seat belt geometry evidently provides no guarantee that an occupant can place the lap belt in an anatomically correct position with respect to the pelvis or maintain it in such a position. One aspect of the abdominal injury problem is therefore poor initial geometry of the seat belt system.

Movement above the ASIS of a belt that was initially correctly positioned is a consequence of the phenomenon of "submarining." [14] It is characterized by forward displacement and rotation of the pelvis under the belt. Such motion may result from the use of an excessively compliant seat cushion, which compresses under the occupant as he moves forward during the collision. It is also associated with seat belt systems that use both the femurs and the lap belt to restrain the lower torso. Though in such cases the peak loads in the belt are considerably reduced, it remains undesirable to load the abdomen except over the pelvis.

Precluding Loading of the Abdomen by the Lap Belt

There are several difficulties in trying to prevent loading of the abdomen by the lap belt by means of the standard frontal barrier test. Apart from other considerations, it is doubtful that any existing dummy adequately simulates the kinematic response of a human subject to the conditions favouring submarining.

For this reason, Transport Canada has focussed its efforts on providing an objective method of quantifying lap belt fit with respect to the generally accepted anatomical constraints. The Belt-fit Test Device (BTD) consists essentially of 50th percentile male lower torso and chest forms mounted on the SAE H-point machine. Scales graduated in millimetres are provided on the lower torso form, passing vertically through the positions of the two ASIS. The origins of the scales coincide with

the ASIS. The position of the upper edge of the lap belt with respect to either ASIS may therefore be read directly from the scale. Systematic data on some 50 current production vehicles are presently being assembled. The first results indicate that the geometry of current seat belt systems varies over a wide range.

The major objection to controlling only the initial fit of the lap belt is that it does not preclude the dynamic problem of submarining. While that is true, inadvertent submarining is easily avoided by proper design of the seat. Hence, unless other considerations in the design of the seat or restraint system intervene, there is no reason for a vehicle manufacturer to subvert the intent of a requirement for good initial fit of the lap belt.

At the time of writing, there are no systematic data that would allow an estimate of the proportions of current abdominal injuries that are attributable respectively to initially poor belt fit and to submarining. The causes of inadvertent submarining are now well recognized and the observed variability in current lap belt geometry is considerable. There is accordingly a strong presumption that most of the current problem is attributable to anatomically incorrect initial fit.

Injuries to the Lower Extremities

Incidence and Severity

The limit of 10 kN on the compressive load in the femur is the only current requirement for protection of the lower extremities in the standard frontal crash test. Femur loads in 48 km/h frontal barrier tests are typically less than half of the regulated maximum.

In the accident data for frontal collisions of CDC extent 3 or less, fractures of the femur or patella appear relatively infrequently, except for elderly occupants or in the presence of intrusion. Even so, Table 2 shows that 0.48 percent of drivers injured in collisions of CDC extent 3 or less experience serious injuries to the lower extremities. Fractures of the tibia and fibula, dislocations of the ankle and fractures of the bones of the foot are observed.

Injuries to the lower extremities have quite reasonably received less attention than life-threatening injuries to the head, chest and abdomen. The permanent disability that often results from such injuries may justify their receiving more attention in the future. The available accident data suggest that the injury mechanisms are quite varied and may be difficult to control through the medium of the current standard frontal barrier collision.

Conclusions

A review of data from frontal barrier tests and accident investigations undertaken by Transport Canada suggests that significant improvements are possible in the level of protection provided to front seat occupants restrained by seat belts. Current requirements for restraint system performance in the standard frontal barrier test are not sufficiently demanding nor are they applied to all relevant vehicles and restraint systems. In addition, an objective requirement for anatomically correct lap belt geometry is needed.

Potentially injurious but preventable head and facial contacts with the steering assembly are observed in the standard frontal barrier test and commonly experienced by restrained drivers in real collisions of equivalent and lower severity. Placing a simple 80 g limit on peak resultant head acceleration offers a reliable means of distinguishing potentially injurious head impacts from harmless non-contact events in the standard frontal barrier test. Such a limit is readily met either by improvements in the design of seat belts and steering assemblies or the use of a supplementary air bag. Reducing the incidence of facial fractures among drivers may require the use of supplementary measurements of the impact performance of the steering assembly.

Limiting the acceleration of the chest in the standard barrier test provides no control of the initial injury mechanisms of most importance. Limiting chest compression to 50 mm is greatly preferable. That limit is readily attainable and would maintain the level of protection available from current three-point belts.

Abdominal injuries induced by the seat belt could be appreciably reduced if anatomically correct initial seat belt geometry were required by the relevant standards. The use of a test device providing an objective measurement of belt fit is proposed.

Acknowledgment and Disclaimer

The authors are pleased to acknowledge the contributions made by Robert Malo, Jean Beaulieu, Yves Bourdon and other colleagues at Transport Canada's Motor Vehicle Test Centre. They set and maintained exceptionally high standards in preparing and instrumenting vehicles and dummies and in performing and reporting the crash tests cited in this paper.

The conclusions reached and opinions expressed in this paper are solely the responsibility of the authors. Unless otherwise stated, they do not necessarily represent the official policy of Transport Canada.

References

1. Campbell, G.D. & Welbourne, E.R. Transport Canada's policy on occupant restraints. *Proceedings of the International Symposium on Occupant Restraints*, 1981, 135-14g. Morton Grove: American Association for Automotive Medicine.
2. Estimates of shoulder seat belt use from annual surveys 1980-1991, Road Safety Leaflet CL 9104(E), August 1991, Transport Canada.
3. Evans, L. Restraint effectiveness, occupant ejection from cars and fatality reductions. *Accident Analysis and Prevention*, 1990, 2, 167-175. Oxford: Pergamon Press.
4. Dalmotas, D.J. & Krzyzewski, J. Restraint system effectiveness as a function of seating position.

Restraint Technologies: Rear Seat Occupant Protection, 1987, SP-691, 75-95. Warrendale: Society of Automotive Engineers.
5. Dalmotas, D.J. Mechanisms of injury to vehicle occupants restrained by three-point seat belts. SAE Technical Paper 801311, 1980, Society of Automotive Engineers.
6. The Abbreviated Injury Scale (1975 Revision). *Proceedings of the 19th Conference of the American Association for Automotive Medicine*, 1975, 438-466. Morton Grove: American Association for Automotive Medicine.
7. *The Abbreviated Injury Scale 1980 Revision*, 1980. Morton Grove: American Association for Automotive Medicine.
8. Collision Deformation Classification, SAE Recommended Practice J224, March 1980, Society of Automotive Engineers.
9. Dance, D.M. & Enserink, B. Safety performance evaluation of seat belt retractors. SAE Technical Paper 790680, 1979, Society of Automotive Engineers.
10. Newman, J.A. & Gallup, B.M. Biofidelity improvements to the Hybrid III headform. *Proceedings of the Twenty-Eighth Stapp Car Crash Conference*, 1984, 87-99. Warrendale: Society of Automotive Engineers.
11. Mertz, H.J. Injury assessment values used to evaluate Hybrid III response measurements. NHTSA Docket Submission VSG 2284, Part III, Attachment 1, Enclosure 2, 1984, General Motors Corporation.
12. Melvin, J.W. & Weber, K. (Eds.) Review of biomechanical impact response and injury in the automotive environment, Chapter 3: Thorax. In: *Advanced Anthropomorphic Test Device (AATD) Development Program, Phase 1 Reports: Concept Definition*, DOT HS 807 224, 1988. Washington: National Highway Traffic Safety Administration.
13. Neathery, R.F., Kroell, C.K. & Mertz, H.J. Prediction of thoracic injury from dummy responses. *Proceedings of the Nineteenth Stapp Car Crash Conference*, 1975, 295-316. Warrendale: Society of Automotive Engineers.
14. Backaitis, S.H. & St-Laurent, A. Chest deflection characteristics of volunteers and Hybrid III dummies. *Proceedings of the Thirtieth Stapp Car Crash Conference*, 1986, 157-166. Warrendale: Society of Automotive Engineers.
15. Adomeit, D. Seat design—a significant factor for safety belt effectiveness. *Proceedings of the Twenty-Third Stapp Car Crash Conference*, 1979, 39-68. Warrendale: Society of Automotive Engineers.

S9-O-07

Upper Interior Head Impacts: The Safety Performance of Passenger Vehicles

Hampton C. Gabler, Donald T. Willke
National Highway Traffic Safety Administration
J. Joseph Wagner
Automated Sciences Group, Inc.

Abstract

Each year in the U.S., it is estimated that 4000 persons are killed and another 9300 sustain serious head injury due to impacts with vehicle upper interior structures. The safety performance of passenger vehicles in occupant head impacts with the upper interior is examined in this paper. The upper interior is defined as the A/B/C-pillars, the side roof rails, the front header rail, and the rear header rail. The results of a recent NHTSA fleet characterization effort involving over 220 free motion headform (FMH) impact tests on fourteen passenger cars, light trucks, and minivans are presented in this paper. The effects of variations in impact angle, impact location, and contact velocity on FMH responses are explored in this test series. Localized hard spots and protrusions (e.g. motorized seat belt tracks) were identified and tested to determine design-specific head impact hazards. The conclusions are that head impact injury potential is a strong function of vehicle design, and that upper interior head impact protection varies widely from vehicle to vehicle.

Background

In the United States in 1989, estimates are that 4000 occupants of passenger cars, light trucks, and vans died as a result of head to upper interior impact [1]. Another 9300 occupants survived these impacts, but were left with a serious head injury. Survival of a head to upper interior impact is frequently debilitating: the National Highway Traffic Safety Administration (NHTSA) disability studies show that approximately 50% of the medium term cognitive impairment in frontal crashes are due to contact with the A-pillar and roof rails [2].

As a result of increasing restraint usage, increasing numbers of restrained occupants are exposed to the national traffic accident environment each year. As shown in Figures 1-2, the number of fatally injured belted occupants who suffered at least one serious head injury from head to upper interior impact has grown over

the last 10 years. Belted occupants are not injured as a result of wearing their safety belts, but rather are injured *despite* wearing their safety belts. In fact, safety belts provide some degree of protection against injuries from head impact with the upper interior.

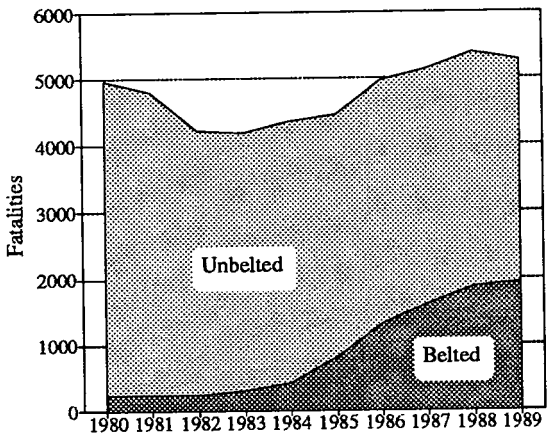

Figure 1. Upper Interior Head Impacts—Car Fatals with Serious Head Injury

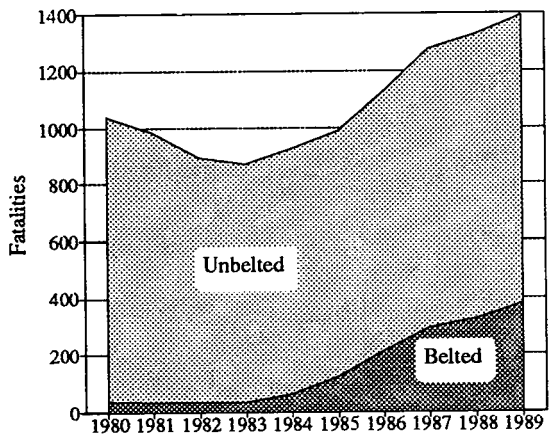

Figure 2. Upper Interior Head Impacts—LTV Fatals with Serious Head Injury

The distribution of serious injuries among the primary upper interior components is shown in Figure 3 [1]. Note that for belted occupants serious injury from impacts with the front header and the A-pillar are greatly reduced. However, as would be expected, belts apparently have little effect on injuries from head impacts with the side components including the side roof rail, B-pillar, or side window frame.

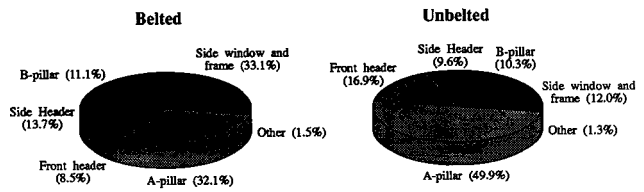

Figure 3. Upper Interior Head Impacts Serious Head Injury by Component

The recent widespread introduction of airbags promises to further mitigate this situation to some extent in frontal accidents, but data on airbag deployments are still too sketchy for the national accident statistics to allow an estimate of airbag effectiveness at preventing head to upper interior contact. While airbags may reduce head injuries in frontal accidents, airbags are not expected to prevent head to upper interior impacts in side and rear impacts or rollovers. In fact, even in frontal impacts, airbags are not guaranteed to prevent head contact with the upper interior. A preliminary investigation of the NHTSA Special Study of Airbag Deployments has shown a number of head to upper interior contacts of moderate severity, for occupants restrained by airbag.

To alleviate the head to upper interior impact problem, NHTSA research efforts have focused on the evaluation of promising upper interior paddings as a countermeasure for all occupants—regardless of restraint type, lack of restraint, or accident mode. Earlier NHTSA studies [3] have shown that in sled tests using full vehicle bodies, the application of 1" of padding to upper interior surfaces can reduce HIC by as much as half. Note that NHTSA countermeasure tests are conducted using add-on pads. Integral design of the padding and underlying structure could improve the effectiveness in a production upper interior design.

The upper interior, as defined in this paper, includes all components of the roof support structure. This grouping includes the A-pillar, the B-pillar, the C-pillar, the front header rail, the side roof rails, the rear header rail, and the side door window frames. For this paper, passenger vehicles refers to both passenger cars, light trucks, vans, and utility vehicles under 10,000 pounds. When the paper refers to head hereafter, this term will refer to both the head and the face.

Objective

The primary objective of this paper is to present the results of an investigation of head impact injury potential as a function of vehicle upper interior designs currently in the U.S. passenger vehicle fleet. The second goal is to present an evaluation of the effectiveness of padding as a countermeasure for reducing head injury potential.

Approach

In Reference 3, an initial research test procedure for upper interior testing was presented, along with the results of tests conducted on twelve baseline passenger cars. Nearly all the HIC responses from these tests were below 1000, seeming to indicate that head to upper interior impacts are not likely to produce serious head injuries. In fact, according to accident statistics [1], many people are seriously injured and killed from these types of impacts. Therefore, the test procedure used in those tests did not result in impacts that were of the severity representative of those that produce serious head injuries in real accidents.

An investigation was then initiated to explore appropriate test procedure modifications. There were two main

goals for this revision of the procedure. The first was to develop a research test procedure that results in laboratory impact severities that are more representative of real world severities. This would be done largely through the adjustment of approach angles and/or impact speed. The second goal was to develop a research test procedure that allowed for a thorough evaluation of the injury causing potential of a vehicle's upper interior structures. This would be done by defining ranges for impact locations and approach angles, rather than defining specific values for these parameters, as in the initial research procedure.

The following is a summary of the revised research test procedure used in the testing presented later in this paper. A more detailed description of the investigation that lead to the revisions is in Reference 4.

Headform. A free-motion headform (FMH) was selected for use in this program. A series of twenty-two sled tests was conducted in which the head of a full Hybrid-III dummy impacted lengths of rectangular tubing, simulating upper interior structures. Both 15 and 20 mph tests were performed on unpadded and padded simulated structures, in which the tubing stiffness and impact angle were varied. An identical series of tests was also conducted using the FMH, rather than the full dummy. A linear regression between the HIC responses of the two surrogates was performed, and a strong correlation was found. The regression produced a coefficient of determination, r_2, of 0.969.

There are two distinct advantages of the FMH over the more traditional guided impactor. First, and most importantly, the FMH can simulate the more realistic glancing impacts, while guided headform tests are conducted normal to the structure. Since the two approaches may lead to the selection of different countermeasures, it is important to conform to reality as much as is practical to increase the chances that the most beneficial countermeasures are used. Second, since the FMH is free to rotate after impact, head rotational motion can be measured. Therefore, the FMH may be a viable headform when rotational head injury criteria are developed, allowing a more complete evaluation of the head injury causing potential of upper interior structures.

Impact Zone on the FMH. Since the FMH is essentially a Hybrid-III head, it was developed for use in forehead impacts. The biofidelity of the Hybrid-III head in impacts to the lower face and jaw areas has not been established. Therefore in this procedure, the first contact between the FMH and the structure must occur within a specified impact zone on the FMH. This zone consists of the area within a 5" wide strip, centered on the head's midsagittal plane, extending from the top most point of the head, down to the bridge of the nose (note that the nose is removed for FMH testing).

Impact Zones on the Structures. Since accidents of all modes (front, side, oblique, rollover, etc.) occur on the roadways, occupants can strike their heads on essentially any exposed interior structure or surface. This is especially true for the upper interior structures. Since all these structures are candidate for head impacts, all must provide protection.

The impact location on each structure must fall within the structure impact zones as described below. Impact location is defined as the location of first contact between the structure and the FMH. All zones include only those interior surfaces which can be contacted by the FMH.

- *Roof rails (front and rear headers, side rails)*—The impact zones on these structures consist of the areas along the entire length of the roof rails, from the lowest portion of the rails, up six inches into the roof, along the contour of the roof.
- *A-pillar*—The impact zone on this structure consists of the area along the length of the structure, from the instrument panel to the roof rail juncture.
- *B, C and D-pillars*—The impact zones on these structures consist of the areas along the length of the structures, from the side door window level to the roof rail junctures.

Approach Angles—Horizontal Plane. Similar to the concept used to define impact zones on the structures, an occupant's head can strike the upper interior structures from nearly any angle interior to the vehicle. Although the most severe cases should usually occur from nearly perpendicular angles, certain designs could produce severe impacts from other angles. Following this philosophy, approach angles in the horizontal plane were selected to encompass all interior angles. They are as follows (0° is forward and positive angles are clockwise):

- Front header: -90° to 90°
- Side rails: left: -180° to 0°, right: 0° to 180°
- Rear header: 90° to -90°
- A-pillar: left: -90° to 0°, right: 0° to 90°
- B-pillar: left: -180° to 0°, right: 0° to 180° (unless rearmost pillar)
- C-pillar: left: -180° to 0°, right: 0° to 180° (unless rearmost pillar)
- D-pillar (or rearmost pillar): left: -180° to -90°, right: 90° to 180°

Note: For any particular structure, it may not be possible to test throughout the entire range of listed approach angles and also achieve impact within the specified impact zones on the structure and FMH.

Approach Angles—Vertical Plane. The limits for the ranges of approach angles in the vertical plane were selected based on a survey of 5th percentile female seated positions and FMH test results [4]. The female dummy was used to find head-to-structure angles for a variety of vehicles, since it represents the "worst case" adult position for these angles. Means and standard deviations were found for each measurement, weighted to represent the 1989 sales fleet.

To represent a large percentage of small adult females, the upper limits (positive angles) were chosen as the

mean plus one standard deviation (to the nearest 5°). Since a distinction between the front header and side rail was not easily made, the statistics from the combination of these two structures were used. The A and B-pillars were treated separately. The chosen ranges are as follows (0° is horizontal and positive angles are up):

- Roof rails (front and rear headers, side rails): 0° to 50°
- A-pillar: -30° to 30°
- B, C, and D-pillars: -45° to 45°

Note: Once again for any particular structure, it may not be possible to test throughout the entire range of listed approach angles and also achieve impact within the specified impact zones on the structure and FMH.

Impact Speed. To reduce the complexity of the test procedure, it was decided that a uniform impact speed would be used for tests on all structures. From the analysis of Reference 5, it was determined that median values for Δv for serious to fatal head injury accidents varied from 21 to 28 mph. This was analytically determined to correspond to head contact speeds in the range of 10 to 23 mph. To collect data for this selection, two series of fleet characterization tests were conducted at the NHTSA's Vehicle Research and Test Center (VRTC). One used an impact speed of 15 mph, while the other used 20 mph. These test series are described later in this paper.

Vehicle Selection

20 mph Testing. Using 1989 sales figures [6], a fleet sample of twelve light passenger vehicles was selected for testing of upper interior structures. Based on the sales ratio, eight of these were passenger cars, while the other four were light trucks or vans (LTV's).

For the passenger cars, the individual models were combined by body type (eg. GM A-body) and then ranked by body type sales. Only the top 46 selling body types (sales over 50,000 units) were considered for use in this program (85% of total passenger car sales). This group was then broken down into five weight categories, and the number of cars tested from each category was selected based on sales percentages as shown below in Table 1.

Table 1. Passenger Car Selections for 15 mph Testing

Weight Category	Curb Weight Range (pounds)	Percent of Sales (%) *	Vehicles Tested
1	< 2250	20.3%	Ford Escort Honda Civic
2	2250-2525	18.4%	VW Golf
3	2525-2750	22.0%	Ford Tempo Toyota Camry
4	2750-3000	10.4%	Ford Taurus
5	over 3000	28.9%	Mercury Grd Marquis Buick Electra
Total		100.0%	8
* percentage of top 46 selling body types only			

The top 46 selling body types were then listed, in order of sales, for each weight category. From these lists, the appropriate number of body types from each category was selected for testing, based on their availability to the VRTC. The 8 passenger car models tested are listed in Table 1.

For the LTV's, a small and a full sized pickup were selected, as well as a van and an all purpose vehicle. The models chosen were as follows:

Chevrolet S-10 Pickup
Ford F-150 Pickup
Chevrolet Astro Mini-van
Ford Bronco II

15 mph testing. The 15 mph tests were conducted after the 20 mph tests, so some of the vehicles listed above were not re-usable, due to damage. Therefore, only five passenger cars were tested, one from each of the five weight categories. The models were as follows:

Ford Escort
Volkswagen Golf
Toyota Camry
Ford Taurus
Mercury Grand Marquis

Three of the LTV's were re-usable, and two additional models were also tested. These were as follows:

Chevrolet S-10 Pickup
Chevrolet Astro Mini-van
Ford Bronco II
Dodge Caravan
Dodge B-150 Van

Test Procedure

As described above, this project tested vehicle upper interiors at two distinct impact velocities, 15 mph and 20 mph, in order to bracket the range of median impact speeds. Not all vehicles were tested at both speeds. Each vehicle in our fleet sample was subjected to FMH tests of the four primary components—(1) A-pillar, (2) B-pillar, (3) side roof rail, and (4) the front header. As an aside to the main program, some vehicles were subjected to additional testing of the C-pillar, rear header, and roof The results of these auxiliary tests are not presented in this paper.

Two FMH tests were conducted for each of the four major upper interior components. In the 20 mph series, the first tests were conducted at "standard" impact locations and approach angles. The locations were chosen based on the position of a normally seated 50th percentile male Hybrid III dummy. For the front header, this location was centered vertically on the header directly forward of the dummy head c.g., the approach angle in the horizontal plane was 0°, and the approach angle in the vertical plane was 50°. For the side roof rail, the location was centered vertically on the rail directly lateral to the dummy head c.g., and approach

angles in the horizontal and vertical planes were 90° (or -90°) and 20°, respectively. On the A-pillar, the location was at the same height as the dummy head c.g., with horizontal and vertical approach angles of 35° (or -35°) and 20°, respectively. Finally, for the B-pillar, the location was centered longitudinally on the pillar at the same height as the dummy head c.g., with horizontal and vertical approach angles of 90° (or -90°) and 5°, respectively. Also in the 20 mph series, the second tests were conducted at alternate locations and approach angles. In these tests, the impact locations were subjectively chosen at hard spots (eg. weld overlaps or stiffeners), when present, and a variety of approach angles were used. In some cases, the standard location was a hard spot, so the alternate location was selected at a second hard spot, if present.

The standard and alternate impact locations for the 15 mph series were chosen in the same manner as for the 20 mph series. "Standard" approach angles were not used in this series, though. Instead, each test was conducted at the most severe approach angle allowed by the research test procedure outlined in the APPROACH section of this paper.

The nominal test matrix for a single vehicle is shown in Table 2.

Table 2. Nominal Test Matrix for a Single Vehicle

Upper Interior Components	15 mph		20 mph	
	Standard Location	Alternate Location	Standard Location	Alternate Location
A-Pillar				
B-Pillar				
Side Rail				
Front Header				

Measures of Safety Performance

The central goal of this study was to determine the safety performance of current passenger vehicles in head impacts with the upper interior. This evaluation was performed in tests of the upper interiors of production vehicles. This baseline evaluation was then followed up with an evaluation of the safety performance of upper interiors with add-on pads.

To evaluate vehicle upper interiors, this study used two measures of safety performance—both related to the potential for head injury. The first was the Head Injury Criterion (HIC) used by the NHTSA to assess the safety of vehicles in frontal-barrier impacts. The second was the Head Injury Risk function developed by GM and others [7,8]. This risk function curve is an example of many such injury probability curves which can be derived from existing biomechanical data by various analytical methods.

The Head Injury Risk Function has been proposed as a relationship between HIC and Probability of AIS 4+ Brain Injury [7]. The function may not directly apply to other types of head injury, e.g. functional impairment, which may also be present with brain tissue injury at a given HIC level. In addition, the risk function is strictly applicable only to frontal head impacts. The function may not apply, for example, to HICs measured when the side of the head impacts a component. The reader should keep these restrictions in mind when reading this paper. When the paper refers to "probability of AIS 4+ head injury" and "head injury risk," these terms will refer to the probability of AIS 4+ brain injury in impacts between the forehead of the headform and the component of interest.

The head injury risk can be computed from the Logist probability function shown below, and is shown in Figure 4.

$$p(x) = [1 + e^{\alpha - \beta(HIC)}]^{-1}$$

where $\alpha = 5.02$ and $\beta = .00351$

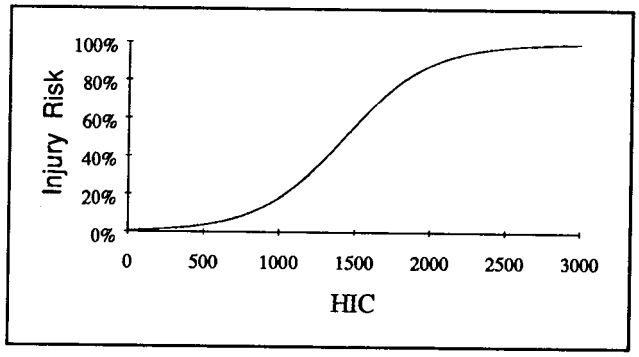

Figure 4. Injury Risk Function Based on HIC and Serious Head Injury

Fleet Characterization Results

The primary goal of this study was to assess the safety performance of a sample of the current passenger vehicle fleet in head to upper interior impacts. The results of the baseline fleet characterization are tabulated in Table 3. The HIC responses resulting from the 15 mph tests are presented in Figures 5-8. The Probability of AIS 4+ head injury for the 15 mph tests are presented in Figures 9-12. The HIC responses resulting from the 20 mph head impact tests are presented in Figures 13-16. The Probability of AIS 4+ head injury for the 20 mph tests are presented in Figures 17-20.

In the discussion below, p(4+) refers to the probability of AIS 4+ injury. Also, the term "worst HIC" refers to the highest HIC response measured for a structure of a particular vehicle, between the standard and alternate impact locations. Also, the probability of injury, padding effectiveness, and reductions in HIC are based on FMH HIC responses. If these responses are transformed to full dummy HIC responses, these probability of injury, HIC

Table 3. Results of Baseline Characterization

HIC											Injury Risk							
15 mph Vehicle	A-pillar Standard	A-pillar Worst	Vehicle	Front Header Standard	Front Header Worst	Vehicle	Side Rail Standard	Side Rail Worst	Vehicle	B-pillar Standard	B-pillar Worst	A-pillar Standard	A-pillar Worst	Front Header Standard	Front Header Worst	Side Rail Standard	Side Rail Worst	B-pillar Standard	B-pillar Worst
Escort	524	823	Camry	483	801	Escort	439	590	Bronco II	744	905	4	11	3	10	3	5	8	14
Golf	652	985	Escort	539	726	Golf	557	756	Escort	925	1029	6	17	4	8	4	9	15	20
Camry	707	1225	S-10 Pickup	541	600	B-150 Van		953	Astro Van	954	1008	7	33	4	5		16	16	19
Taurus	780	907	Golf	634	868	Taurus	729	1431	Camry	1068	1068	9	14	6	12	8	50	22	22
G. Marquis	1002	1080	G. Marquis	652	925	Bronco II	897	1029	G. Marquis	1180	1180	18	23	6	15	13	20	29	29
S-10 Pickup	1028	1749	Caravan	687	934	Astro Van	924	1352	B-150 Van		1237	20	75	7	15	14	43		34
Bronco II	1289	2373	Taurus	687	687	S-10 Pickup	1006	1006	Caravan	1341	1511	38	96	7	7	18	18	42	57
Astro Van	2180	2557	Astro Van	730	1311	Caravan	1207	2304	Golf	1362	1385	93	98	8	40	31	96	44	46
Caravan	2586	2606	Bronco II	747	747	G. Marquis	1251	2182	Taurus	1500	1642	98	98	8	8	35	93	56	68
B-150 Van		2752	B-150 Van		2077	Camry	1434	1434	S-10 Pickup	1867	1867		99		91	50	50	82	82
20 mph	**Standard**	**Worst**		**Standard**	**Worst**		**Standard**	**Worst**		**Standard**	**Worst**	**Standard**	**Worst**	**Standard**	**Worst**	**Standard**	**Worst**	**Standard**	**Worst**
VW Golf	1220	1529	F-150 Pickup	993	993	Civic	833	2015	Bronco II	1198	1472	32	59	18	18	11	89	31	54
S-10 Pickup	1314	3544	S-10 Pickup	1000	1416	S-10 Pickup	916	1604	Civic	1458	1698	40	100	18	49	14	65	52	72
Camry	1339	1595	Civic	1020	1532	Escort	1286	1447	Taurus	1615	2912	42	64	19	59	38	51	66	99
Bronco II	1546	1546	Taurus	1140	1140	G. Marquis	1329	3968	Camry	1642	2311	60	60	27	27	41	100	68	96
Escort	1564	1564	Tempo	1178	1178	Tempo	1849	2310	Electra	1861	1983	62	62	29	29	81	96	82	87
Civic	1594	2214	Bronco II	1210	1712	Bronco II	2063	2902	G. Marquis	1922	1922	64	94	32	73	90	99	85	85
G. Marquis	1817	2123	Camry	1215	1561	Taurus	2092	2282	F-150 Pickup	2119	2219	80	92	32	61	91	95	92	94
Electra	2009	3556	VW Golf	1264	1910	Electra	2112	2408	Tempo	2307	2617	88	100	36	84	92	97	96	98
Tempo	2041	2403	Escort	1359	1533	VW Golf	2147	2147	Escort	2383	2383	90	97	44	59	93	93	97	97
F-150 Pickup	2249	2249	G. Marquis	1465	2178	Camry	2181	2887	Astro Van	2693	3039	95	95	53	93	93	99	99	100
Taurus	2462	3298	Astro Van	1742	2389	Astro Van	2671	2914	VW Golf	2746	3460	97	100	75	97	99	99	99	100
Astro Van	4908	4996	Electra	2980	2980	F-150 Pickup	3075	3075	S-10 Pickup	3113	3113	100	100	100	100	100	100	100	100

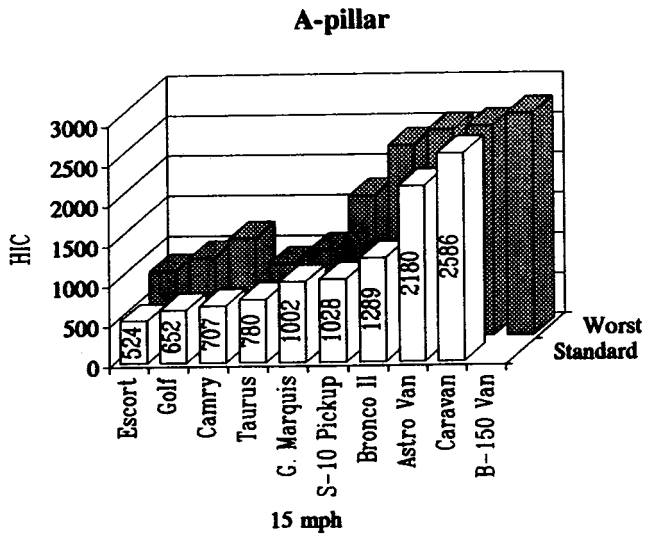

Figure 5

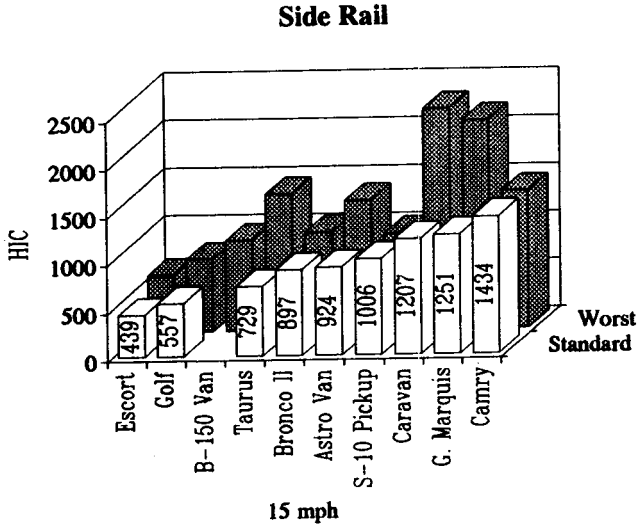

Figure 7

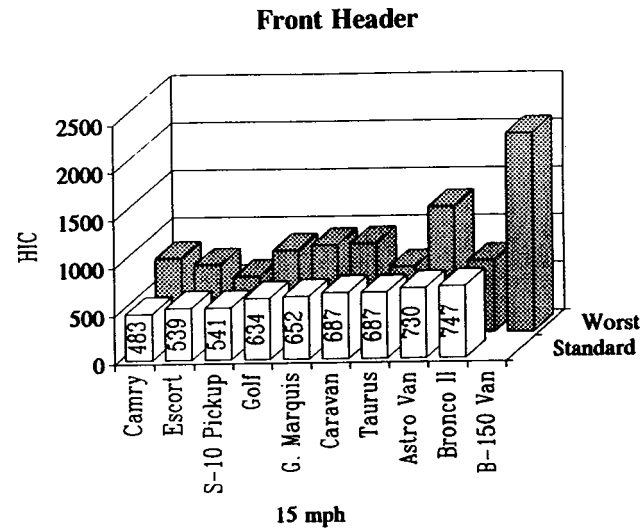

Figure 6

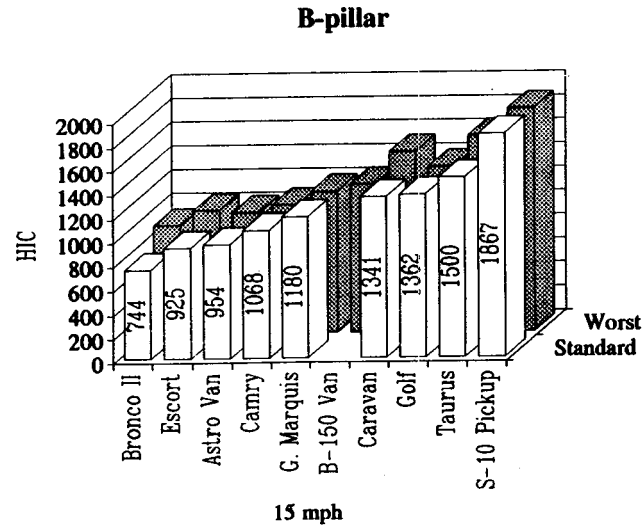

Figure 8

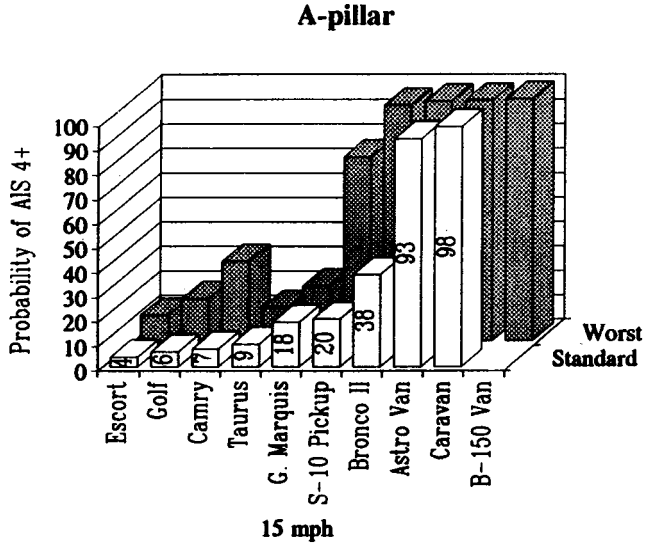

Figure 9

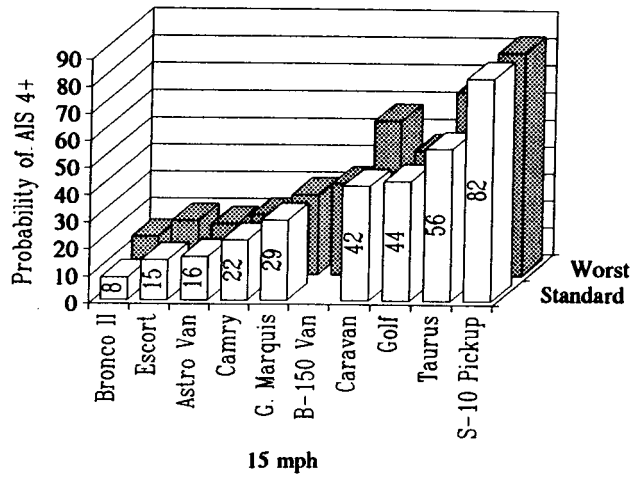

Figure 12

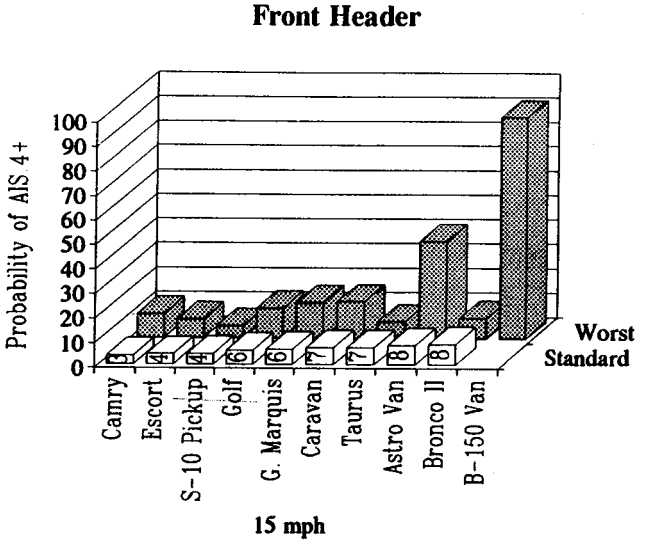

Figure 10

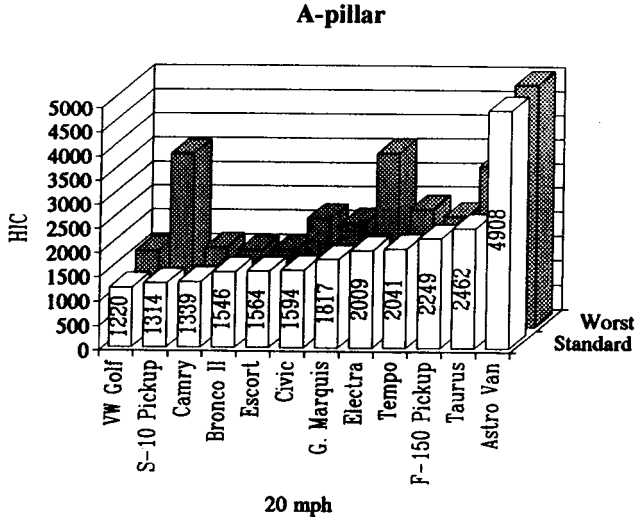

Figure 13

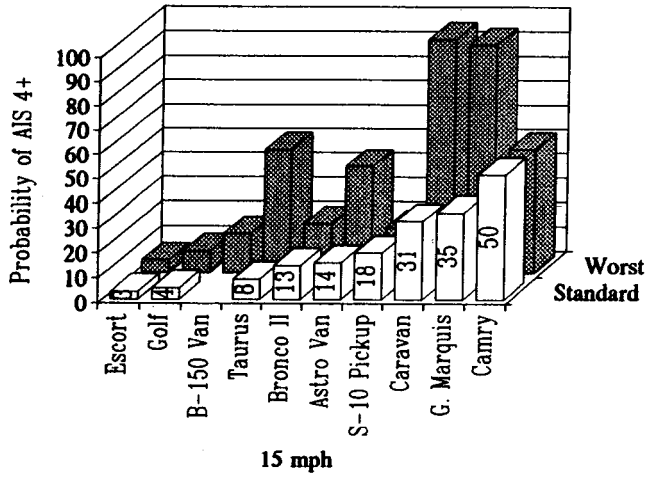

Figure 11

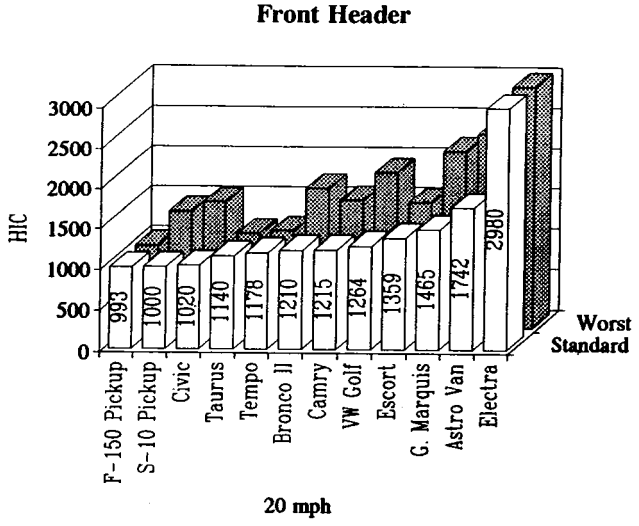

Figure 14

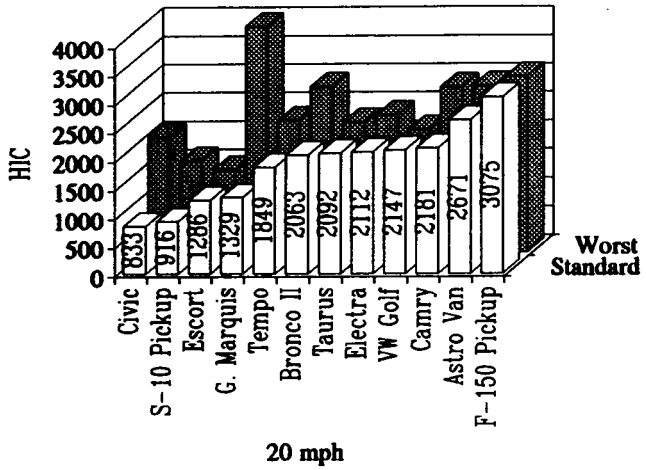

Figure 15

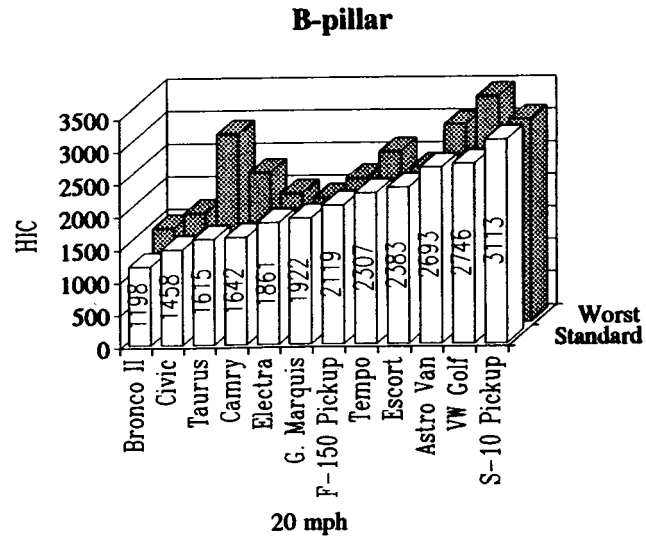

Figure 16

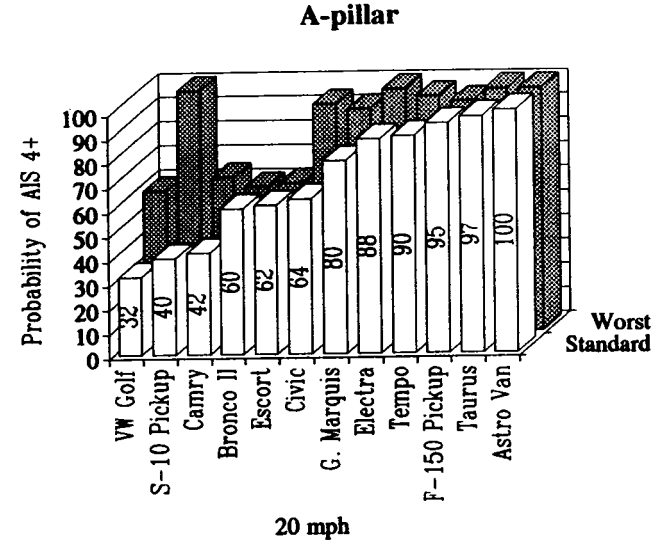

Figure 17

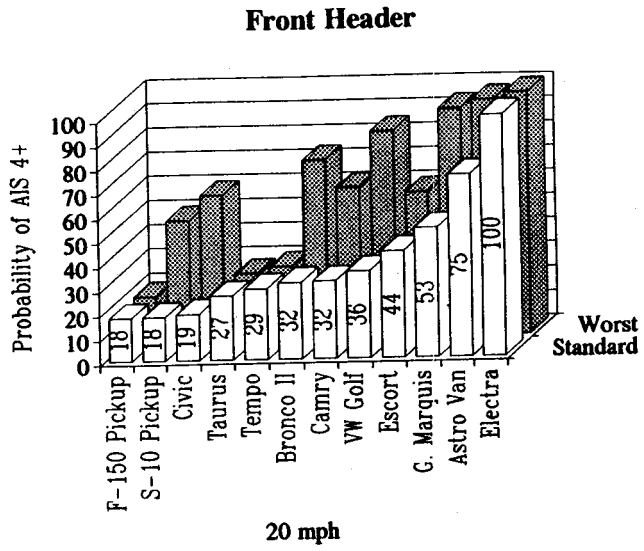

Figure 18

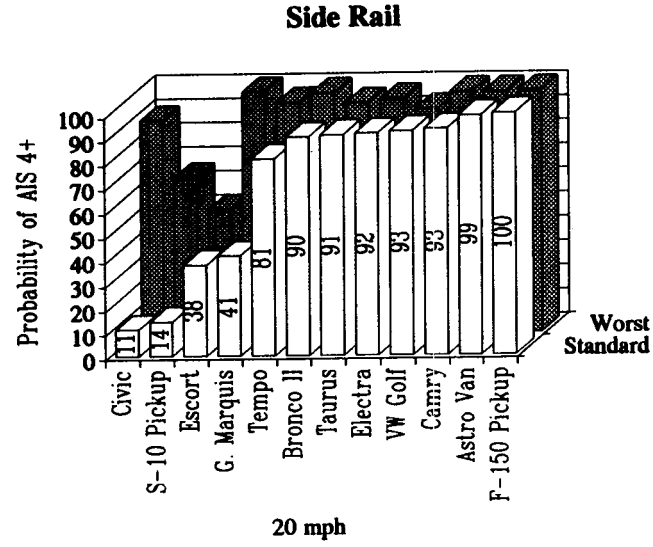

Figure 19

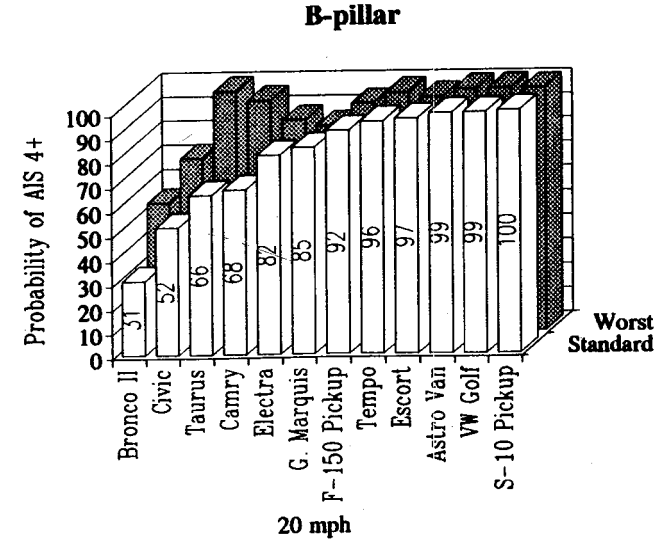

Figure 20

reductions, and padding effectiveness values may change.

In 15 mph head impacts with the A-pillar, HIC in impacts at the standard location varied from a minimum of 524 for the Ford Escort to 2586 for the Dodge Caravan. This corresponds to a Head Injury Risk ranging from $p(4^+)=4\%$ to $p(4^+)=98\%$. In 20 mph head to A-pillar impacts, HIC at the standard location ranged from a low of 1220 for the VW Golf to an unsurvivable 4908 for the Chevrolet Astro, or a Head Injury Risk ranging from $p(4^+)=32\%$ to $p(4^+)=100\%$. The maximum worst HIC in 15 mph impacts was recorded for the Dodge B-150 Van (HIC=2752); the highest worst HIC in 20 mph impacts was recorded for the Chevrolet Astro (HIC=4996).

In head impacts with the front header, all 15 mph HIC responses measured at the standard impact locations were under 1000 and showed little variation from vehicle to vehicle. The maximum worst HIC was recorded when an overlap in the Dodge B-150 Van front header was impacted, resulting in a HIC of 2077. An impact to an overlap on the Chevrolet Astro front header was the only other 15 mph front header impact to result in a HIC over 1000 (HIC=1311). At 20 mph, all HIC responses measured at the standard locations were very near to or above 1000. The maximum worst HIC of 2980 was measured in the Buick Electra, once again at a header overlap.

Side roof rail 15 mph impact tests at the standard locations showed HIC varying from 439 for the Ford Escort all the way to 1434 for the Toyota Camry. The largest worst HIC recorded at 15 mph was on the Dodge Caravan (HIC=2304), a nearly 50% jump from its standard location 15 mph HIC of 1207. The Mercury Grand Marquis also displayed a very severe worst HIC (HIC= 2182). In 20 mph impacts to the standard locations, HIC ranged from 833 for the Honda Civic to 3075 for the Ford F-150 Pickup. The highest worst HIC at 20 mph was again on the Mercury Grand Marquis, with a HIC of 3968.

B-pillar 15 mph impact tests to the standard locations showed HIC varying from 744 for the Ford Bronco II to 1867 for the Chevrolet S-10 Pickup. The HIC at the standard location for the Chevrolet S-10 pickup was also the maximum worst HIC recorded. In the 20 mph standard location impacts, HIC ranged from 1198 for the Ford Bronco II to 3113 for the Chevrolet S-10 Pickup. The highest worst HIC at 20 mph was recorded on the VW Golf, with a HIC of 3460.

Discussion

The fleet characterization tests show a wide vehicle to vehicle variation in HIC for each upper interior component. With the exception of the B-pillar, there was a slight trend toward lighter vehicles producing lower HIC responses, although the correlations were not strong. If such a relationship does exist, it may result from the need to provide adequate roof support in the event of a rollover. Presumably, heavier vehicles would require a stronger, possibly stiffer, roof support structure to meet FMVSS No. 216 and to prevent roof collapse in rollovers.

One surprising finding was the severity of HIC responses recorded in tests on minivans and vans. In 15 mph head impacts with the A-pillar, the three vans in this study, a Dodge Caravan, a Chevrolet Astro mini-van, and a Dodge B-150 full-sized van, resulted in HIC responses higher than any other vehicle tested. In 20 mph head impacts with the A-pillar, the Chevrolet Astro resulted in HIC=4908 (standard location) and HIC=4996 (worst HIC), which were the highest HIC responses recorded in this test series. The reasons for HIC responses are unclear, but may indicate that upper interior designs in vans and minivans are unlike those found in either passenger cars or light trucks.

It was also interesting to note the effect that the presence of tracks for motorized passive shoulder belts had on the resulting HIC responses. Two of the vehicles tested had such passive belts, the Toyota Camry and the Ford Escort. The HIC responses from all the tests conducted on the Ford Escort seat belt track are listed in Table 3 and are as follows:

- 15 mph
  - A-pillar/standard: HIC= 524
  - Side roof rail/standard: HIC= 439
  - B-pillar/standard: HIC= 925
  - B-pillar/worst: HIC=1029
- 20 mph
  - A-pillar/standard/worst: HIC=1564
  - Side roof rail/standard: HIC=1286
  - Side roof rail/worst: HIC=1447
  - B-pillar/standard/worst: HIC=2383

The HIC responses from all but two of the tests conducted on the Toyota Camry seat belt track are also listed in Table 3, and are as follows:

- 15 mph
  - A-pillar/not listed: HIC= 881
  - Side roof rail/not listed: HIC=1398
  - B-pillar/standard/worst: HIC=1068
- 20 mph
  - A-pillar/worst: HIC=1595
  - Side roof rail/worst: HIC=2887
  - B-pillar/standard: HIC=1642
  - B-pillar/worst: HIC=2014

A comparison of these HIC responses to those from impacts on structures without seat belt tracks indicate that the presence of the track did not generally seem to cause unusually high HIC responses. In fact, the HIC responses from the seat belt track tests were in the upper half of all worst HIC responses (for a structure) in only the 20 mph Toyota Camry side roof rail and the Ford Escort B-pillar tests. In some cases, the HIC from the impact on the track was lower than the HIC response from the non-track impact (eg. 15 mph Ford Escort A-pillar).

The Effectiveness of Padding

A major goal of this study was to determine the effectiveness of padding as a countermeasure for reducing head injury potential in our fleet sample. Earlier NHTSA full dummy tests have shown that 1 inch of properly chosen padding can reduce HIC by as much as half. To evaluate this head injury countermeasure in the fleet sample, a subset of the vehicles was chosen for additional tests with padding. To evaluate the padding under severe conditions, the padding was usually applied to that spot on each component identified as the "worst HIC" impact location. Note that the "padded" tests were conducted using add-on pads in order to evaluate feasibility. Integral design of the padding and underlying structure could improve the effectiveness in a production upper interior design.

The objective in this study was to simply determine the feasibility of lowering HIC in our fleet sample. Hence, the padded tests varied both padding material and their thickness in order to achieve HIC < 1000 where possible. In the tables below, the computation of padding effectiveness is based on a comparison of the baseline vehicle and that particular padding design which met the design goal of minimum HIC. That is, it is 100% minus the probability of receiving an AIS 4+ head injury in the padded test, given a head injury would have occurred in the baseline test.

To limit the effect on driver field of vision, the design target was to limit A-pillar and frontal header paddings to 1 inch of thickness. For the B-pillar and side rail, two components outside of the driver's forward field of vision, the design target was to limit padding thickness to 1.5" inches. In some instances where these padding thicknesses were not sufficient to reduce HIC responses below 1000, additional tests were conducted with thicker paddings. The results of the padding effectiveness tests are presented for 15 mph impacts in Table 4 and for 20 mph impacts in Table 5.

As shown in Table 4, a 1" thickness of Dytherm padding (manufactured by the ARCO Chemical Company) was sufficient to reduce HIC responses below 1000 in all but one of the 15 mph impacts. The single exception was the Dodge Caravan A-pillar, which required 1.25" of padding to achieve this reduction. In these tests, padding was found to reduce HIC by 17% to 73%. Effectiveness of padding was a dramatic 42% to 94%.

At the much more severe impact speed of 20 mph, the target thicknesses of padding were generally not sufficient to reduce HIC responses below 1000, although several just slightly exceed this criterion (note that a test with 1" of padding was not conducted on the VW Golf front header). Even with an additional 0.25" to O.5" of padding, some of HIC responses were still above 1000. These tests did show nearly the same impressive percent reductions in HIC observed at 15 mph. Added padding reduced the HIC responses by 32% to 59%, and the effectiveness of padding was 36% to 85%.

Table 4. Effectiveness of Padding in 15 mph Head to Upper Interior Impacts

Upper Interior Component	Vehicle	Padding	HIC			Probability of AIS 4+ Injury (%)		
			No Pad	Pad	% Diff	No Pad	Pad	% Eff
A-Pillar	Gd. Marquis	1" Dytherm-3	1080	627	41.9%	23	6	75.1%
	Golf	1" Dytherm-3	985	682	30.8%	17	7	61.1%
	S-10 Pickup	1" Dytherm-4	1749	884	49.5%	75	13	83.0%
	Bronco II	1" Dytherm-4	2373	780	67.1%	96	9	90.4%
	Astro Van	1" Dytherm-4	2557	811	68.3%	98	10	89.6%
	Camry	1" Dytherm-4	1225	864	29.5%	33	12	63.2%
	Caravan	1" Dytherm-2 1.25" Dytherm-2	2606	1106 912	57.6% 65.0%	98	24 14	75.3% 85.8%
	B-150 Van	1" Dytherm-3	2752	891	67.6%	99	13	86.8%
Front Header	Camry	1" Dytherm-2	801	390	51.3%	10	3	74.4%
	Gd. Marquis	1" Dytherm-2	925	637	31.1%	15	6	59.9%
	Astro Van	1" Dytherm-2	1311	707	46.1%	40	7	81.6%
	Caravan	1" Dytherm-2	934	719	23.0%	15	8	48.9%
	B-150 Van	1" Dytherm-3	2077	876	57.8%	91	13	86.2%
Side Rail	Gd. Marquis	1" Dytherm-3	2182	633	71.0%	93	6	93.8%
	Caravan	1" Dytherm-3	2304	626	72.8%	96	6	94.1%
	Astro Van	1" Dytherm-2	1352	628	53.6%	43	6	86.9%
	Camry	1" Dytherm-3	1434	711	50.4%	50	7	85.3%
B-Pillar	Camry	1" Dytherm-3	1068	612	42.7%	22	5	75.5%
	Gd. Marquis	1" Dytherm-2	1180	981	16.9%	29	17	41.7%
	Astro Van	1" Dytherm-2	1008	704	30.2%	19	7	60.8%
	Taurus	1" Dytherm-2	1642	944	42.5%	68	15	77.3%
	Golf	1" Dytherm-3	1362	823	39.6%	44	11	75.9%
	Caravan	1" Dytherm-2	1511	980	35.1%	57	17	70.1%
	B-150 Van	1" Dytherm-2	1237	660	46.6%	34	6	81.4%

Table 5. Effectiveness of Padding in 20 mph Head to Upper Interior Impacts

Upper Interior Component	Vehicle	Padding	HIC			Prob. of AIS 4+ Head Injury		
			No Pad	Padded	%diff	No Pad	Padded	%eff
A-Pillar	VW Golf	1" Dytherm-4 1.25" Dytherm-4	1529	1039 1005	32.0% 34.3%	59	20 18	65.5% 68.7%
	Civic	1" Dytherm-4	2214	906	59.1%	94	14	85.4%
	Taurus	1" Dytherm-4	3298	1504	54.4%	100	56	43.5%
Front Header	Civic	1" Dytherm-2 1.5" Dytherm-2	1532	1044 862	31.9% 43.7%	59	20 12	65.2% 79.6%
	VW Golf	1.5" Dytherm-2	1910	1280	33.0%	84	37	56.0%
Side Rail	Civic	1.5" Dytherm-3 2" Dytherm-2	2015	1035 896	48.6% 55.5%	89	20 13	77.4%8 5.0%
	VW Golf	1.5" Dytherm-3 2" Dytherm-2	2147	1156 990	46.2% 53.9%	93	28 18	70.1%8 1.0%
	Taurus	1.25" Dytherm-4	2282	1048	54.1%	95	21	78.2%
B-Pillar	Civic	1.5" Dytherm-2	1698	1081	36.3%	72	23	68.4%
	VW Golf	1.5" Dytherm-2 2" Dytherm-2	3460	1592 1466	54.0% 57.6%	100	64 53	36.1%4 6.8%
	Taurus	1.5" Dytherm-2	2912	1546	46.9%	99	60	39.6%

Tables 4 and 5 above report the results of padded tests using three types of Dytherm foam--Dytherm-2, Dytherm-3, and Dytherm-4. The numeric designation after the Dytherm trade name refers to the foam density. Dytherm-2, for example, refers to a Dytherm foam of density 2 pounds / cubic foot. The denser foams, e.g. Dytherm-4, tend to be stiffer than the less dense foams, e.g. Dytherm-2.

These tests suggest that padding the upper interior is a feasible and extremely effective method of reducing head injury potential. These padding tests should not be

viewed an upper bound on improvements that can be made to the upper interior. The countermeasure tests only explored the use of padding: even higher countermeasure effectiveness may be possible by softening or otherwise redesigning the underlying metal pillars and rails.

Conclusions

This paper has presented the research test procedure and the results from a recent NHTSA fleet characterization effort to examine the safety performance of fourteen passenger cars, light trucks, and minivans in head to upper interior impacts. The test series explored the effect of variations in impact angle, impact location, and contact velocity on FMH responses. A test series was also conducted in which the upper interiors of a subset of the baseline vehicles were padded, and then subjected to FMH tests. The conclusions from this study are as follows:

- Head impact injury potential is a strong function of vehicle design, and upper interior head impact protection varies widely from vehicle to vehicle. In 15 mph FMH impacts to baseline structures, HIC responses varied from 439 to 2752, while those from 20 mph impacts varied from 833 to 4996.
- The minivans and vans tested in this program appear to have upper interior designs which yield severe HIC responses. In 15 mph FMH impacts with the A-pillar, the three vans in this study resulted in HIC responses higher than any of the other vehicles tested. The highest HIC response recorded in this test series were measured in 20 mph FMH impacts with a mini-van A-pillar.
- Padding the upper interior is a feasible and exceptionally effective method of reducing head injury potential. Padding effectiveness was dramatic (varying from 36% to a high of 94%), and regularly exceeded 50% (i.e., in 35 of 41 tests). Note that the NHTSA padded tests were conducted using add-on pads. Integral design of the padding and underlying structure could improve the effectiveness in a production upper interior design. [Note: Padding effectiveness is defined here as 100% minus the probability of receiving an AIS 4^+ head injury in the padded test, given a head injury would have occurred in the baseline test.]

Disclaimer

References

1. Partyka, Susan C.; "Serious Head Injury in Light Passenger Vehicles from Rail, Header, and Pillar Contact;" June 27, 1991. NHTSA Docket 88-06-GR-003.
2. Marcus, Jeffrey H., and Robert Blodgett; "Priorities of Automotive Crash Safety Based on Impairment;" Proceedings of the Eleventh International Technical Conference on Experimental Safety Vehicles; May 1987.
3. Willke, Donald T., and Hampton C. Gabler, "Upper Interior Head Protection: A Fleetwide Characterization;" NHTSA; paper number 89-SA-0-010, presented at the 12th International Technical Conference on Experimental Safety Vehicles; May 1989.
4. "Development of a Research Test Procedure for Upper Interior Head Protection Testing;" NHTSA; Event report for project VRTC-89-0140; January 1991.
5. Monk, Michael W., Hampton C. Gabler, Lisa K. Sullivan; "Subsystem Testing for Head to Upper Interior Safety;" NHTSA; presented at the 11th International Technical Conference on Experimental Safety Vehicles; May 1989.
6. Automotive News: December 11, 1989 and December 25, 1989 issues.
7. Prasad, P., Ford Motor Company, and Harold Mertz, General Motors Corp., "The Position of the United States Delegation to the ISO Working Group 6 on the Use of HIC in the Automotive Environment," SAE Paper 851246, presented at the SAE Government/Industry Meeting and Exposition, Washington, D.C., May 1985.
8. Viano, D.C., and Sudhakar Arepally, "Assessing the Safety Performance of Occupant Restraint Systems," Proceedings of the 34th Stapp Car Conference, SAE Paper 902328, November 1990.

S9-O-08

A Study of the Safety Performance of Production Vehicles Equipped with Driver Air Bags in the NHTSA Test Programs

William T. Hollowell, Fabienne J. Frey
National Highway Traffic Safety Administration

Abstract

In issuing Federal Motor Vehicle Safety Standard (FMVSS) No. 208, "Occupant Crash Protection," the

National Highway Traffic Safety Administration (NHTSA) has encouraged the installation of driver air bags with its provision that each car manufactured with these devices would be counted as one unit toward the manufacturer's calculation of its phase-in requirements. With this incentive, a number of manufacturers have installed driver air bags in selected vehicles in their productions lines. The consumer acceptance and preference for air bags have prompted the manufacturers to quickly expand the availability of air bags over many car lines. In its crash testing programs, the NHTSA has conducted tests in which a variety of occupant restraint conditions are available. The restraint conditions include the belt systems (three point and two point systems), the air bag system, and combined belt/air bag systems. This paper presents an analysis of the safety performance for vehicles equipped with these various restraint conditions from the crash test results obtained in the FMVSS No. 208 compliance test program and from the New Car Assessment Program (NCAP). Additionally, a summary is presented of the results obtained from a test program of static deployments of selected production driver air bag systems.

Introduction

Since the enactment of FMVSS No. 208, "Occupant Crash Protection" and through the completion of the model year 1990 test program, the National Highway Traffic Safety Administration has conducted crash tests of sixty seven (67) different makes and models of passenger cars (PC's) for evaluating the vehicle's compliance to the standard's performance requirements. Each of these vehicles was crashed into a rigid barrier at a test speed of 30 mph with instrumented 50th percentile Part 572 Hybrid II or Hybrid III dummies positioned in the driver and right front seat passenger locations. The dummies are restrained only by those devices which provide the automatic protection as required by FMVSS No. 208. In the driver location of these tested vehicles, twenty one (21) dummies were restrained with an air bag, thirty two (32) dummies were restrained with a two point automatic belt (torso belt), and fourteen (14) dummies were restrained with a three point automatic belt (lap and torso belts).

Additionally, between 1979 and through the model year 1990 test program, the NHTSA has conducted crash tests of 281 different makes and models of PC's in NCAP. Each of these vehicles was crashed into a rigid barrier at a test speed of 35 mph. This is five mph faster than the prescribed speed for compliance with FMVSS No. 208. The NCAP is an experimental consumer information program which develops data on frontal crashes. In this program, a given vehicle is tested once at the nominal test speed of 35 mph with instrumented 50th percentile Part 572 Hybrid II or Hybrid III dummies in the driver and right front seat passenger locations. The dummies are restrained by all available automatic and manual protection devices. The crash tests are designed to indicate, for vehicles within the same weight class, the relative levels of occupant protection and vehicle safety in this crash condition. In the driver location of these tested vehicles, two hundred and twenty eight (228) dummies were restrained with a manual three point belt restraint, twenty (20) dummies were restrained with an air bag and manual three point belt restraint, twenty one (21) dummies were restrained with a two point automatic belt (torso belt) and manual lap belt, and twelve (12) dummies were restrained with a three point automatic belt (lap and torso belts).

At the Twelfth International Technical Conference on Experimental Safety Vehicles, a review of the data from the NCAP vehicles which had been tested was presented [1]. At that time, 233 passenger cars and 41 light trucks and vans (LTV's) had been tested. In addition to presenting similar tables and charts as in the 1985 paper [2], the report provided trends and analyses based on fleet weighted observations and provided comparisons of PC to LTV parameters. The fleet of tested vehicles estimated to be on the roads in 1988 consisted of over 37 million PC's and almost 9 million LTV's. Comparison of the performance of the tested 1981 PC fleet to the tested 1988 PC fleet showed a considerable improvement in potential safety performance for restrained occupants in high speed frontal crashes. Comparisons of specific late model (MY 1986 to 1988) vehicles within each weight class indicated the potential for significant safety improvements for the future vehicle fleet. In examining the LTV dummy responses and comparing them to the PC performance, HIC's and Chest G's for the LTV's were found to be approximately 10 to 20 percent higher than for the PC's. Even though LTV's have higher dummy responses than PC's, the manufacturers have demonstrated the capability to provide improved performance since 28 percent of the tested LTV's meet FMVSS No. 208 requirements in the NCAP test conditions.

In issuing FMVSS No. 208, the NHTSA has encouraged the installation of driver air bags with its provision that each car manufactured with these devices would be counted as one unit toward the manufacturer's calculation of its phase-in requirements. With this incentive, a number of manufacturers have installed driver air bags in selected vehicles in their productions lines. The consumer acceptance and preference for air bags have prompted the manufacturers to quickly expand the availability of air bags over many car lines. The restraint conditions include the belt systems (three point and two point systems), the air bag system, and combined belt/air bag systems. The aforementioned papers did not consider the restraint system types in their review of the safety trends. This paper presents an analysis of the safety performance for vehicles equipped with these various restraint conditions from the crash test results obtained in the FMVSS No. 208 compliance test program and

from the NCAP test program. While the comparisons are given by restraint type, it should be noted that the performance reflects the total system (i.e., the vehicle structural design, the steering assembly/intrusion, and the restraint system). Additionally, a summary *is* presented of the results obtained from a test program of static deployments of selected production driver air bag systems.

Results from the Anthropomorphic Dummy Responses

For each of the FMVSS No. 208 compliance tests and the NCAP tests, Part 572 Hybrid II or Hybrid III anthropomorphic dummies were positioned in the driver and right front passenger seats of the vehicles. Standard instrumentation included triaxial accelerometers in the head and chest, and load cells in the right and left femurs. The head injury criteria (HIC) and three millisecond clip chest accelerations (Chest G's) in G's are derived from the accelerometers, and the femur loads are obtained from the load cell outputs as specified in FMVSS No. 208. The data from these tests provide NHTSA with the most extensive set of frontal crashworthiness information ever assembled on production vehicles.

The analyses of the dummy responses are done for both unweighted and fleet weighted data. The unweighted data are the responses measured from the vehicles which have been tested. The weighted data are these data weighted by the estimated distribution of the tested vehicles in the fleet for calendar year 1990. This estimated distribution is derived from the total vehicle registrations obtained from the Polk's National Vehicle Population Profiles and from the vehicle sales reported by Automotive News.

Table 1 contains both unweighted and fleet weighted average and median values of the HIC, Chest G's, and femur loads for the driver dummies as measured in the New Car Assessment Program tests. The values are tabulated by restraint system types. Figures 1-3 provide the fleet weighted cumulative distributions of these dummy responses in graphical form, while Figures 4-6 provide the corresponding unweighted cumulative distributions. In reviewing the tabulated results, the best performance in the HIC measurement is provided by the vehicles utilizing the combined air bag and three point belt restraint system. This is consistent for both the unweighted and the fleet weighted averages and medians. This tendency is clearly depicted in the cumulative distributions for both the fleet weighted and unweighted HIC's (See Figures 1 and 4). Overall, the vehicles with the automatic restraint systems (i.e., the air bag/three point belt system and the automatic two-point and three point belt systems) provided the better performance in the HIC measurements. However, it should be noted that improved performances have been obtained in the vehicles with the manual belt systems in the later model years. The improvements were achieved by modifications to the steering assemblies, safety belt characteristics, anchor point locations, and front end structures. These same improvements have been incorporated into the vehicles with the automatic restraints. In contrast, it is seen that vehicles with the manual three point belt system provided the lowest femur loadings. In reviewing the test results, it was found that the distance from the knee to the dash panel was an average of one inch further away in these vehicles as compared to the vehicles equipped with automatic restraint systems. This difference resulted from the older vehicle designs and from the use of knee bolsters that have been incorporated as part of the changes to implement the automatic restraint systems in the newer vehicles. The knee bolsters were purposely designed to engage the knees in order to provide occupant kinematics that are compatible to the automatic restraint systems. For the vehicles with the automatic restraint systems, the femur loads were similar. The air bag equipped cars had slightly lower readings. It should be noted that the overall knee loadings are well below the requirements established for the FMVSS No. 208 injury tolerances.

Table 1. NCAP Test Results: Driver HIC's, Chest G's, and Femur Loads Passenger Cars at 35 MPH

Restraint System Type(s)	Unweighted Results						
	HIC		Chest G's		Femur Load		Vehicles Tested
	Ave	Med	Ave	Med	Ave	Med	
ABG/3PT	662	709	48	43	1261	1132	20
3PT	1079	932	50	49	1070	955	228
PS2/LAP	851	790	50	48	1485	1540	21
PS3	975	863	54	50	1486	1276	12
Restraint System Type(s)	Fleet Weighted Results						
	HIC		Chest G's		Femur Load		Fleet Size
	Ave	Med	Ave	Med	Ave	Med	
ABG/3PT	669	708	49	47	1416	1268	1,698,088
3PT	888	781	48	46	1120	1050	40,501,097
PS2/LAP	751	790	49	48	1419	1334	3,498,013
PS3	915	828	54	50	1575	1740	2,464,280

Note: ABG = Air bag, 3PT = manual three point belt, LAP = manual lap belt
PS2 = Automatic shoulder belt, PS3 = Automatic lap and shoulder belt

Table 2 contains both unweighted and fleet weighted average and median values of the HIC, Chest G's, and femur loads for the driver dummies as measured in the FMVSS No. 208 compliance tests. The values are tabulated by restraint system types. Figures 5-7 provide the fleet weighted cumulative distributions of these dummy responses in graphical form, while Figures 9-12 provide the corresponding unweighted cumulative distributions. In reviewing the tabulated results, the best performance in the HIC measurement is provided by the vehicles equipped with the air bag restraint systems. This is consistent for both the unweighted and the fleet weighted averages and medians. This trend is clearly depicted in the cumulative distributions for both the fleet weighted

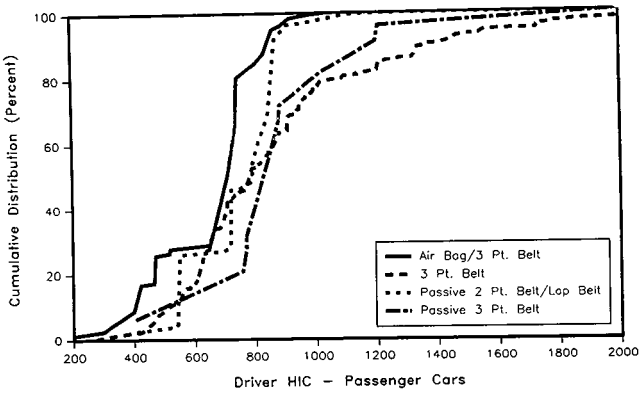

Figure 1. Comparison of NCAP Driver HIC's by Restraint System Type (Fleet Weighted)

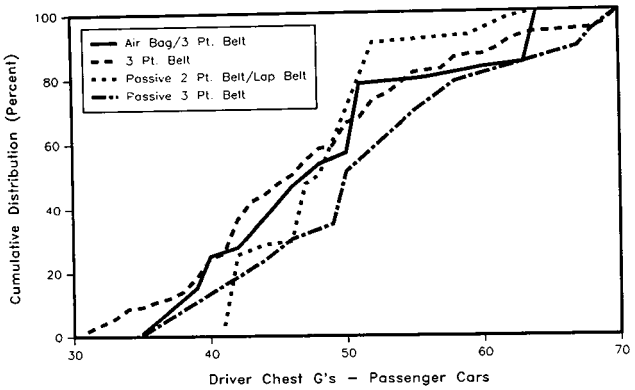

Figure 2. Comparison of NCAP Driver Chest's G by Restraint System Type (Fleet Weighted)

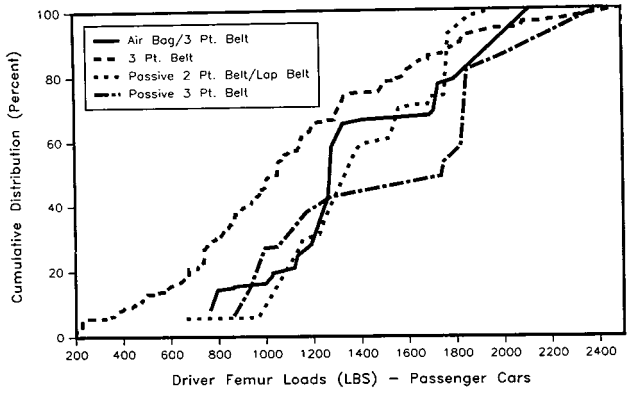

Figure 3. Comparison of NCAP Driver Femur Loads by Restraint System Type (Fleet Weighted)

and unweighted HIC's (See Figures 7 and 10). In contrast, it is seen that the vehicles equipped with automatic three point belt systems provided the lowest femur loadings. As mentioned previously, the compliance tests were conducted without the manual belts. The low readings for the vehicles equipped with the three point automatic belts resulted from the use of the lap belt portion of the restraint system. It is interesting to note that the femur loads in the 30 mph compliance tests without the lap belts were higher than those in the corresponding 35 mph NCAP teats with the same restraint system and a lap belt (i.e., in the comparisons of air bag to airbag/three point

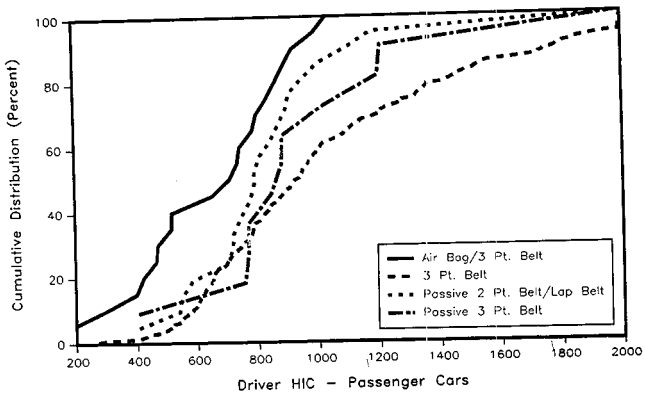

Figure 4. Comparison of NCAP Driver HIC's by Restraint System Type (Unweighted)

Table 2. Compliance Test Results: Driver HIC's, Chest G's, and Femur Loads—Passenger Cars at 30 MPH

Restraint System Type	Unweighted Results						
	HIC		Chest G's		Femur Load		Vehicles Tested
	Ave	Med	Ave	Med	Ave	Med	
ABG	333	338	44	46	1567	1557	21
PS2	494	459	43	42	1584	1548	32
PS3	668	632	42	42	1202	1250	14
Restraint System Type	**Fleet Weighted Results**						
	HIC		Chest G's		Femur Load		Fleet Size
	Ave	Med	Ave	Med	Ave	Med	
ABG	336	338	45	44	1578	1605	1,846,030
PS2	518	525	43	41	1652	1618	3,085,899
PS3	630	595	40	37	1315	1348	2,377,507

Note: ABG = Air bag, PS2 = Automatic shoulder belt, PS3 = Automatic lap and shoulder belt

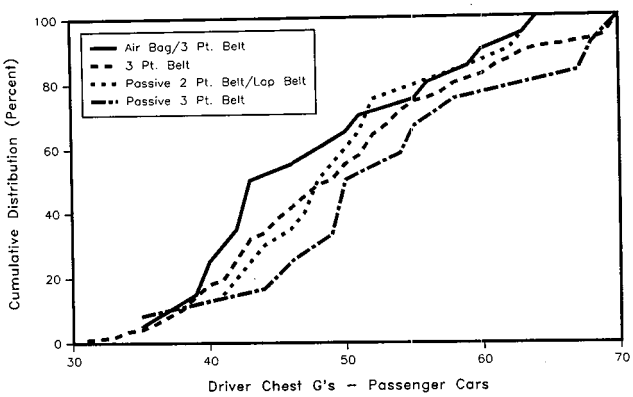

Figure 5. Comparison of NCAP Driver Chest G's by Restraint System Type (Unweighted)

belt and in the comparisons of the automatic shoulder belt to the automatic shoulder belt/manual lap belt). As in the NCAP tests, the femur loadings are significantly below the requirements established for FMVSS No. 208.

Performance of Air Bags in Static Deployment Tests

In the preceding section, the performance of vehicles equipped with driver air bag systems was analyzed in terms of the NCAP and FMVSS No. 208 crash test results. These tests were conducted at crash severity

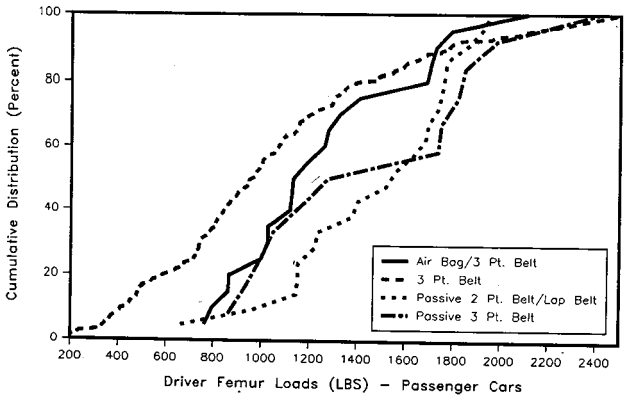

Figure 6. Comparison of NCAP Driver Femur Loads by Restraint System Type (Unweighted)

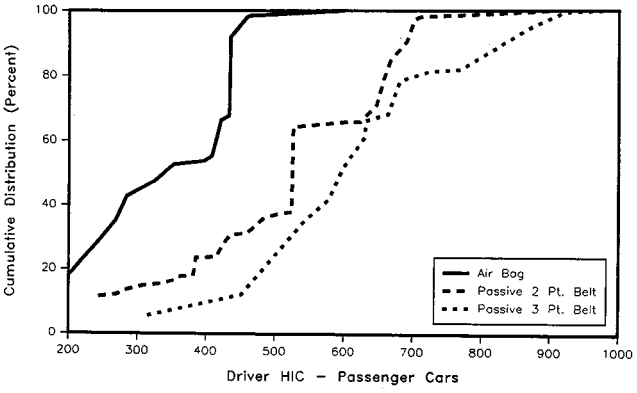

Figure 7. Comparison of Compliance Driver HIC's by Restraint System Type (Fleet Weighted)

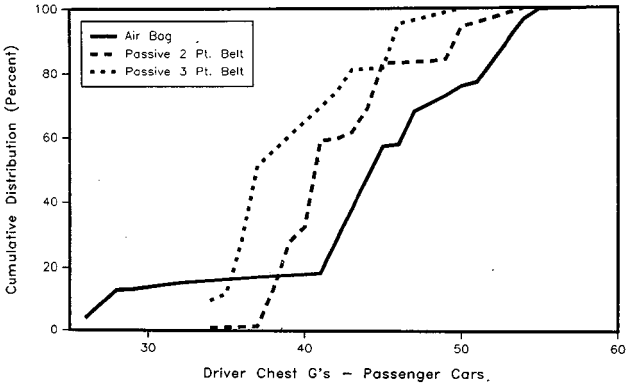

Figure 8. Comparison of Compliance Driver Chest G's by Restraint System Type (Fleet Weighted)

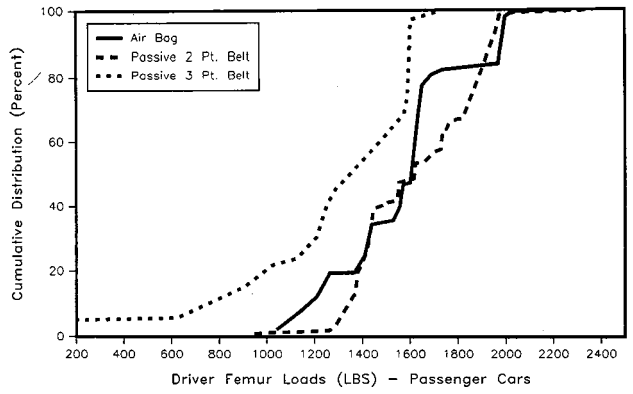

Figure 9. Comparison of Compliance Driver Femur Loads by Restraint System Type (Fleet Weighted)

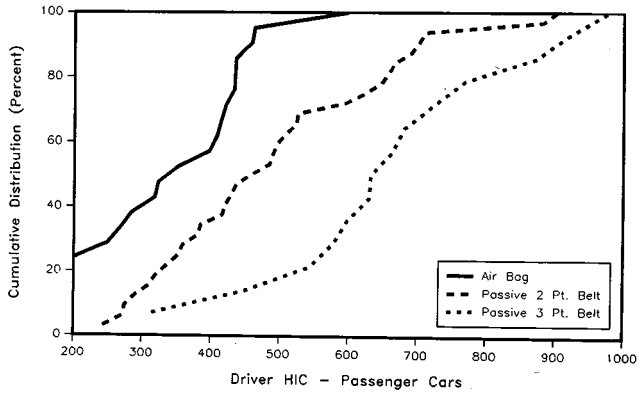

Figure 10. Comparison of Compliance Driver HIC's by Restraint System Type (Unweighted)

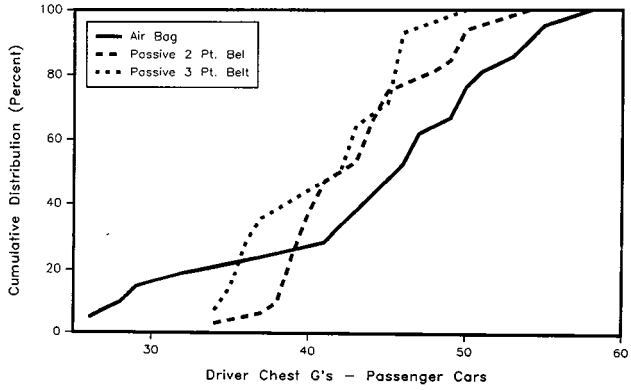

Figure 11. Comparison of Compliance Driver Chest G's by Restraint System Type (Unweighted)

levels in which life-threatening injuries are observed in the real world accident field experience. The automatic safety belt systems and the combination belt/air bag systems are very effective in reducing the serious injuries and fatalities. However, the elimination of all injuries may not be feasible. Injuries may occur in crashes that are beyond the performance envelope of the restraint systems, e.g., crashes where the occupant compartment has extensive intrusion or crashes where the restraint is not intrinsically effective. Also, secondary injuries may occur as a result of loadings from the vehicle and/or occupant protection systems. Examples of this type include abdominal and spinal injuries resulting from the occupant submarining the lap belt; facial injuries resulting from belted drivers contacting the steering wheel; thoracic, head, and neck injuries resulting from belt loadings in high severity crashes; and arm, neck, and facial injuries resulting from air bag inflation. Although the restraint systems are very effective in reducing the serious injuries and fatalities, the remaining injuries are still a concern. Many research efforts are underway to develop systems that have fewer residual injuries. One particular study was undertaken to examine air bag inflation.

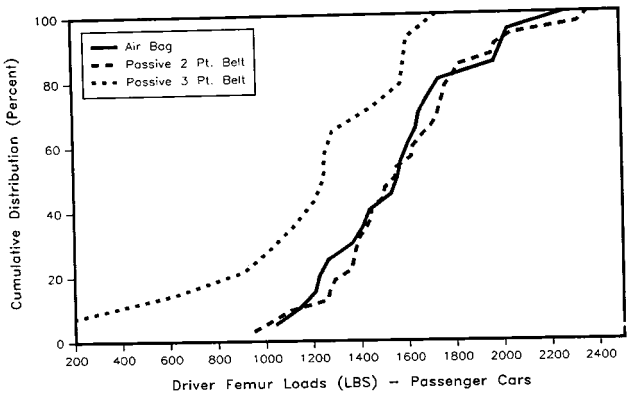

Figure 12. Comparison of Compliance Driver Femur Loads by Restraint System Type (Unweighted)

The aforementioned study was undertaken to investigate factors that may contribute to the likelihood of injuries during air back inflation. The majority of these injuries involve facial, neck, and forearm abrasions as well as burns on the hands. It is possible that trade-offs in design factors can be made between air bag deployment characteristics and high speed protection. For example, the possibility of injuries during air bag inflation can be minimized by reducing the air bag size and inflation time; but, these changes could reduce the occupant protection afforded in severe crashes. It should be noted, however, that changes have been observed in production vehicles and have not resulted in any degradation in the vehicles' crash test performance. The reader should also note that the findings in this study should not be used to produce specific design changes in air bag systems without including the effects of crash dynamics and the overall system performance This paper reports the findings to date of this study.

A test series of static air bag deployments was conducted to quantify the deployment characteristics of several production driver air bag systems and to examine the interactions between the deploying air bags and dummies seated in relatively close proximity to the deploying air bag system. The testing was performed in two phases. Phase I was conducted to determine the deployment characteristics, and Phase II was conducted to study the deployment interaction with fifth percentile female dummies.

During both phases, the test configuration consisted of a base frame bolted to the floor and an angled beam simulating the steering column. High speed film (5,000 fps) was used at three viewing angles for each test. The angle of the beam during Phase I testing was 90 degrees. A backboard grid was used to assist in the determination of the air bag displacement during the film analysis. Nine air bag systems were tested in Phase I. Four of these were selected for the Phase II testing. The Phase II selections were based on the prevalence of the systems in the 1990 model year fleet, the type of folding pattern, the inflation time, and on providing systems with and without tethers.

Four of the nine air bags tested in Phase I had tethers, and there were a total of four distinct folding patterns. Seven air bags had vents at the 3 and 9 o'clock positions, one had vents at the 11 and 1 o'clock positions, and one had a 6" wide arc extending from a 10 to 2 o'clock position. The arc shaped vent had a Kevlar covering over the vent, which served as a filter. None of the other bags' vents were covered. Seven of the bags were nylon 840 denier weave; the other two had a finer 420 denier weave.

The high speed filming in Phase I testing provided overhead, side, and full frontal views. Film analysis was undertaken to digitize and determine the peak displacement of the leading edge of each air bag as a function of time. The peak velocity of each air bag system was also calculated in this manner. Peak velocities of the air bags in Phase I testing ranged from 98 to 211 mph and had an average of 144 mph. Peak displacements ranged from 12 to 20 in. and had an average of 16.4 in. The presence of tethers had a significant effect on the amount of peak displacement. Particularly, the peak displacement for untethered bags averaged 19 in. compared to an average peak displacement of 14 in. for the four tethered air bags. The velocity at which facial contact would have occurred (based on a 15 in. nose to hub distance) was calculated for the untethered systems and sound to range from 39 to 184 mph, averaging 92 mph. See Table 3 for a summary of these measurements.

Table 3. Phase I—Static Air Bag Deployment Test Results

Air Bag System	Tethered (Yes/No)	Peak Velocity (MPH)	Peak Displacement (IN)	Velocity at Facial Impact (MPH)	Inflation Time (MSEC)
I	Yes	120	12	NC	25
II	No	157	20	95	30
III	No	116	19	98	28
IV	No	98	17	46	46
V	No	112	17	39	47
VI	Yes	167	14	NC	29
VII	Yes	167	14	NC	23
VIII	Yes	150	15	NC	21
IX	No	211	20	184	21

1. NC: Noncontact--Facial contact is assumed to take place at 15 inches.

During the Phase II tests, a fifth percentile female Hybrid III dummy was positioned in a generic seat on the seat frame. The seat positions used were determined by (1) positioning the dummy in each of the respective test vehicles at the FMVSS No. 208 seating position, (2) moving the seat to the full forward track pop-uptown, and (3) measuring the relative positions between the dummy and the steering wheel. The tests were filmed at high speed (5,000 fps) from two side views (90 and 45 degrees) and an overhead view. The steering wheel was mounted on the beam bolted to the base frame at predetermined angles (using shims), based upon the steering column angle of the test vehicle. Two of the four systems were then tested 3 in. closer to determine

the effect of an even closer seating position on a tethered and an untethered air bag system. Table 4 contains a summary of the measurements used and calculated values of head acceleration and HIC of Phase II tests.

Table 4. Phase II—Static Air Bag Deployment Test Results

Air Bag System	Head Accel. (G's)	HIC	Chest to Hub (IN)	Nose to Hub (IN)	Pelvic Angle (DEG)	Chalk Disturbance	
						Jawline	Face
I	10.35	2.3	7.00	11.25	20.0	Extensive	None
I	12.95	3.1	4.25	10.25	20.0	Slight	None
II	*	**	7.50	9.50	15.0	Extensive	Extensive
IV	18.13	8.7	8.00	12.00	20.0	Slight	Extensive
IV	NA	NA	5.00	10.25	19.5	Extensive	Extensive
IX	23.50	2.9	8.25	13.25	20.5	Slight	Extensive

* Head Acceleration in X axis exceeded scale value of 50 G.
** Not computed due to head acceleration exceeding scale.

The purpose of Phase II was to investigate the interaction of a smaller stature dummy seated in relatively close proximity with a deploying air bag, concentrating on facial contact. In order to qualitatively study facial impact, a standard powdered chalk solution was painted on the dummies faces in a tricolor scheme. The chalk disturbances caused by the dummy's face contact with the air bags were photographed and noted.

For System I, a slight facial contact occurred initially with the center of the inflating air bag. The dummy again made facial contact with the air bag while the lower half of the bag finished inflating. This second interaction produced significant chalk disturbance along the jawline and lower chin. System I was tested again with the dummy 3 in. closer to the center of the steering wheel. This closer position increased the area in which facial contact occurred, but seemed to reduce the intensity of the chalk disturbances.

System II produced very significant chalk disturbances on the chin, lips, nose, and cheeks. Also, a sliding motion appeared to occur over most of the contact area. The air bag was still unfolding at the time that facial contact occurred.

Significant chalk disturbances occurred in System IV on the chin, lips, and nose areas. A bag imprint found in the chalk on the cheeks and brow indicated a slapping motion occurred on those areas. In a second test run on System IV, with the dummy seated 3 in. closer to the center of the steering wheel, significant chalk disturbances were found on the chin, lip, cheek, nose and brow. The second test showed an increase in the slapping motion that occurred in the first test and an increased sliding motion.

Air bag system IX produced significant chalk disturbances on the chin, lip, nose, cheek, and brow of the dummy. Slight chalk disturbances occurred along the jawline to the chin.

The presence of tethers and the type of folding had a significant effect on a bag's peak displacement which in turn affected the type and amount of chalk disturbance which occurred. The tethers reduced the peak displacement of the bag and allowed the bag to be more fully inflated before facial contact occurred. This reduced the incidence and amount of sliding of the bag on the dummy's face. If the bag was not fully inflated at the time of facial impact, the type of folding pattern employed also affected the type and amount of chalk disturbance. A modified accordion folding pattern produced a smoother surface (i.e., a less creased surface) at the time of facial impact, decreasing the amount of sliding motion that occurred while the bag completed inflating.

Summary

This paper presents an analysis of the safety performance for vehicles with the various restraint conditions from the crash test results obtained in the FMVSS No. 208 compliance test program and from the New Car Assessment Program. The major observation from the analysis is that the vehicles equipped with driver air bag systems provided the overall best performance in terms of the HIC criteria for the FMVSS No. 208 compliance tests, and the vehicles tested with the combined driver air bag and manual three point belt restraint system provided the corresponding overall best performance in the NCAP tests. The findings were reflected in both the calculated averages and medians and in the cumulative distributions.

Additionally, a summary is presented of the results obtained from a test program of static deployments of selected production driver air bag systems. The presence of tethers and the type of folding was found to have a significant effect on the amount of facial chalk disturbance which occurred. The tethers reduced the peak displacement of the bag and allowed the bag to be more fully inflated before facial contact occurred. This reduced the incidence and amount of sliding of the bag on the dummy's face. If the bag was not fully inflated at the time of facial impact, the type of folding pattern employed also affected the type and amount of chalk disturbance. A modified accordion folding pattern produced a smoother surface (i.e., a less creased surface) at the time of facial impact, decreasing the amount of sliding motion that occurred while the bag completed inflating.

Acknowledgments

The test series of static air bag deployments, conducted to quantify the deployment characteristics of several production driver air bag systems and to examine the interactions between the deploying air bags and dummies seated in relatively close proximity to the deploying air bag system, was directed by Mr. Jerome Rossar of the Office of Crashworthiness Research and by Ms. Lisa Sullivan of the Vehicle Research and Test Center.

References

1. Hackney, James R., Hollowell, William T., and Cohen, Daniel S.,"Analysis of Frontal Crash Safety Performance of Passenger Cars, Light Trucks and Vans and an Outline of Future Research Requirement," Proceedings Twelfth International Technical Conference on Experimental Safety Vehicles, pp. 233-241, 1989.
2. Hackney, James and Ellyson, Carlin, "A Review of the Effects of Belt Systems, Steering Assemblies, and the Structural Design on the Safety of Vehicles in the New Car Assessment Program," Proceedings Tenth International Technical Conference on Experimental Safety Vehicles, pp. 380-413, 1985.

S9-O-09

Supplemental Air Bag Restraint Systems: Successes and Challenges

Robert H. Munson, Joseph C. Marsh
Ford Motor Company

Abstract

The success of air bag systems is clear. Air bag systems are now practical and effective as supplemental restraints for reducing the risk of injury in certain classes of vehicles and in certain collisions, but several key challenges remain. For example, the air bag inflator supply base is still fragile. There are also a number of customer misconceptions resulting from differences between customer beliefs about air bag systems and actual air bag system operation and field performance. Field investigation will continue to be critical to the automotive industry and the research community's understanding of real-world occupant restraint system performance. Field experience has demonstrated that the combination of safety belts and air bags now provide the best overall risk reduction, but only if safety belts are used, and used properly. Hence, there will continue to be a critical need to promote the proper use of safety belts.

Overview

The automotive industry is experiencing a major challenge of continuing to meet our own goals and the customers' growing demands, particularly in the safety arena. We have to continue to monitor the customer's perceptions and how these relate to the performance of our products in the real world.

This leads to a primary challenge in the field today. It is important that we vigorously pursue the investigation and analysis of real-world field experience, especially in light of the wide diversity of new restraint systems and other safety features being introduced. A safely performing vehicle is the result of careful design and analysis, considerable testing, careful manufacturing and, of course, responsible drivers who are aware of and fulfill their obligations to themselves and to others.

While Ford conducts extensive sled and crash tests, beyond the levels needed to demonstrate compliance with the Federal Motor Vehicle Safety Standards, these tests can only be surrogates for experience in actual field operation. Consequently, the critical importance of the field crash experience is clear.

The following sections of the paper provide some insights into a crash safety topic that is receiving wide attention air bag supplemental restraint systems (SRS). The paper will also discuss the critical need to continue the promotion of safety belt usage and a glimpse of what "tomorrow" may bring.

Supplemental Restraints

National Highway Traffic Safety Administration (NHTSA) concluded in 1984 that the combination of air bags and safety belts in use was the most effective restraint system for reducing overall risk of fatalities and injuries (1). (See Table 1.) However, before a Ford supplemental air bag program could be pursued, the feasibility of a reasonably safe, reliable, effective and practical system had to be established and, we had to be confident of greatly increased belt usage.

Table 1. NHTSA Restraint System Effectiveness Estimates for Front Seat Occupants of Cars

Restraint System	Injury Level	
	Fatal	AIS 2-5
Lap and Shoulder Belt	40-50%	45-55%
Automatic Belt	35-50	40-55
Air Bag only	20-40	45-55
Air Bag and Lap/Shoulder Belt	45-55	50-60

Based on the massive research and testing done by Ford and others at the time, Ford believed that reasonable air bag practicability would be established. Ford also was hopeful that the vast majority of the U.S. population would be covered by safety belt Mandatory Use Laws. Both of these in fact occurred.

Phase-In

To gain early on-road experience with air bag systems that differed in several ways from earlier generations of experimental systems, Ford signed a contract to install air bags in a General Services Administration (GSA) fleet of 5,000 cars. As a result, Ford began installing a supplemental driver-side air bag system in a GSA fleet of 1985 Tempo vehicles. GSA, NHTSA, and Ford all closely monitored the fleet. Ford gained extensive practical experience in installations, operations, replacements, and field performance.

Ford's passive restraint phase-in program is outlined in Table 2. Each line of the table indicates when a new passive restraint system was first introduced to each car line. In 1985, the Tempo and Topaz cars equipped with a driver-side supplemental air bag system were sold to various government and private fleets. In 1989, Ford introduced a dual driver- and passenger-side supplemental air bag system as standard on the Lincoln Continental. In 1990, the dual air bag system was also standard on the Town Car, that is, until an interruption occurred in the supply of air bag modules.

Table 2. Ford Passive Restraint Phase-In by Model Year

Year	Vehicle Lines	Passive Restraint System Introduction
1985	Tempo/Topaz	Driver Air Bag*
1987	Escort/Lynx	Motorized Torso Belt
1988	Tempo/Topaz	Motorized Torso Belt
1989	Thunderbird	Motorized Torso Belt
	Cougar	"
	Continental	Driver & Passenger side Air Bag
1990	Taurus/Sable	Driver-side Air Bag
	Crown Victoria	"
	Grand Marquis	"
	Mustang	"
	Mark VII	"
	Town Car	Driver & Passenger side Air Bag
	Probe	Motorized Torso Belt
	Festiva	"
1991	Capri	Driver-side Air Bag
1992	Taurus/Sable	Driver & Passenger* side Air Bag
	Crown Victoria	
	Grand Marquis	"
1992	Aerostar	Driver-side Air Bag
	Econoline 150/250	"

* Optional equipment

Supply

As you may know, there was an incident in March, 1990 at the supplier facility that temporarily suspended production of passenger-side air bag modules for the Continental and Town Car. Maintaining a consistent air bag supply base has been a key industry challenge. Air bag manufacturing has been, and continues to be, a developing industry. Air bag propellant manufacturing is not risk-free because sodium azide, while not an explosive, can form sensitive explosives, if proper precautions are not adhered to. By the last count, the manufacturers of air bag propellant for the U.S. automotive industry have had a dozen sodium azide-related fires since February, 1988, resulting in a number of interruptions and injuries (2). Fortunately there have been no fatal injuries. The issues that caused these interruptions have been addressed, and as of June, 1991 the supply lines were being refilled with passenger-side air bag modules. Replacement modules are available both for repairs and for a dealer "kit" installation program.

Current Models

For the 1991 model year Ford has equipped nine car lines with a driver-side supplemental air bag. These vehicles include: the Ford-Crown Victoria, Taurus, Mustang; the Mercury-Grand Marquis, Sable, Capri; and the Lincoln-Mark VII, Continental, and Town Car. The driver-side air bag continues as an option on Tempo and Topaz vehicles. Over half of the cars we sell today are equipped with air bags.

For the 1992 model year a passenger-side air bag is standard on the Lincoln Continental and Town Car, and optional on the Crown Victoria, Grand Marquis, Taurus, and Sable. Ford is also installing a driver-side air bag as standard equipment on 1992-model Aerostar mini-vans and full-size E-150 and E-250 Econoline vans. Ford plans to install both driver- and passenger-side supplemental air bags as standard equipment on all cars sold in North America beginning in the mid-1990's.

Today there are two million Ford Motor Company vehicles equipped with supplemental air bags on the road. We estimate that they have travelled about 32 billion miles, and been involved in some 140,000 crashes, including 16,000 severe enough to activate the air bags.

Misconceptions

Now let's take a look at the air bag system itself, and a fairly common misconception that exists about supplemental air bag systems. The Ford air bag supplemental restraint systems have many components (Figure 1), that can be grouped into three basic subsystems:

- The air bag modules with inflators;
- The crash sensors and associated wiring harness; and
- The diagnostic module with readiness indicator lamp.

Since the basic elements of an air bag system are common for most vehicle designs, many people conclude that *all air bag systems are alike*. But air bag systems are not all alike; in fact, they are quite different. They use:

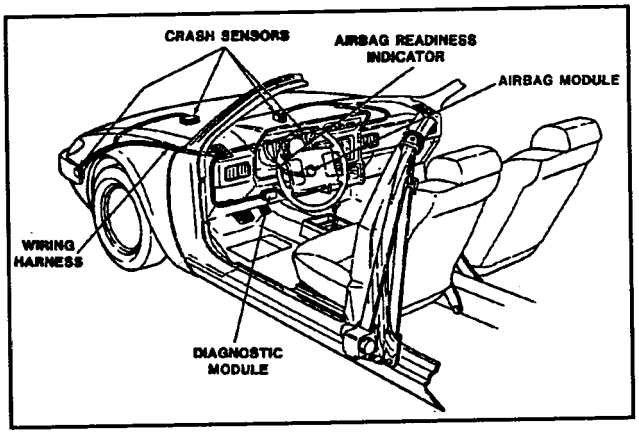

Figure 1. Supplemental Air Bag Restraint System Elements

- Different crash sensors and locations;
- Different gas generation chemicals, filters, and inflation rates;
- Different air bag materials, tethers, and vents;
- Different electronic module designs and diagnostics; and
- Different crash speed and mode requirements for deployment.

For example, the current Ford deployment system is always operational, independent of the ignition key position. Turning the ignition key OFF will not deactivate it. And, the Ford diagnostic module checks for circuit faults while the ignition is ON. It warns the driver that service is required and *disables* the air bag system if certain faults are detected. To date, no other systems have these features.

Complaints

The point is that, because of their distinctive design approaches, different air bag systems generate different field experience. Sometimes, these system differences are reflected in customer complaints. The NHTSA Hot-Line file of customer complaints provides a good example of the contrasts between customer perceptions and what actually happened, for two types of air bag systems: one with a relatively high severity deployment threshold and one with a relatively low severity deployment threshold (Figure 2).

Let's digress a moment to explain "threshold." The level of frontal crash severity required for an air bag deployment is called the "deployment threshold." In the Ford design, for example, air bags are designed to deploy at impact speeds over approximately 14 mph in a head-on collision into a solid barrier under normal ambient conditions for crash test facilities. Some manufacturers design their air bag systems to deploy at other crash severity thresholds—some at lower and others at higher levels than Ford's.

As seen in Figure 2, vehicles designed with a higher deployment threshold are more likely to have complaints about non-deployments in what customers judged to be

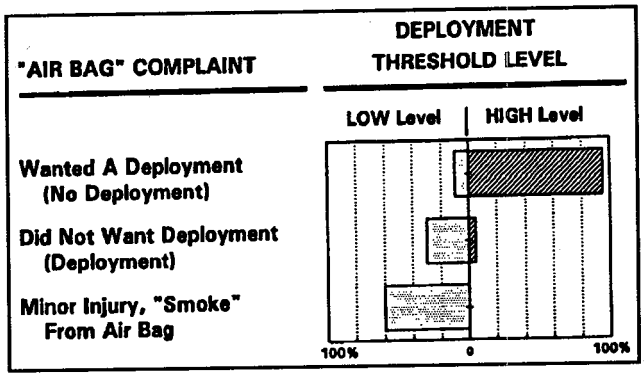

Figure 2. NHTSA Hot Line "Air Bag" Complaints

a serious crash. The system performed as designed, but customers complained that the bag should have deployed. In a way, these are "success stories" . . . the air bag system did not deploy when it was not needed, and the safety belts protected the driver.

Air bags are not designed to deploy in every crash. The air bag system is not designed to deploy in side, rear, rollover or lower-severity frontal crashes. In our experience, the air bag deploys in about 12% of the crashes—those involving moderate to higher-severity frontal impacts.

In contrast, vehicles with a lower deployment threshold have more customer complaints because the bag did deploy. Again, the system performed as designed, but not consistent with some customers' incorrect expectations. They did not expect an air bag deployment in what they judged to be a minor crash; or they were upset by a minor injury or by seeing "smoke" from an air bag deployment. In fact, minor abrasions can occur, and some "smoke" (visible particulate matter or powder) is produced in all air bag deployments.

This observation leads to another key reason for using safety belts in air bag equipped vehicles. Along with the protection they afford in all accident modes, the use of safety belts helps to keep the occupant in position and away from a deploying air bag. The occupant also should sit as far away as practicable from the air bag module. This can reduce the risk of injuries, e.g., abrasions, from the air bag.

So, it is clear that some customers' incorrect perceptions of air bags can differ from "real world" operations. We all face the challenge of recognizing and helping to dispel these misunderstandings. Air bag systems will present fresh challenges for all field investigators as they observe new and unique restraint systems, occupant complaints, and injury patterns.

Field Experience

Since it may be a few years before solid statistical studies of air bag effectiveness are completed, there is an immediate need for the clinical investigation and analysis of air bag field experience. The value of clinical field investigations is exemplified by contrasting some of our specific on-road air bag experience with some customer

perceptions, in terms of non-survivable crashes and non-deployment crashes.

Clearly, one should not expect to avoid all injuries in every crash with an air bag deployment. The Tempo in Figure 3 and a large truck collided head-on. As you can see, the passenger compartment was not intact after the crash. The incident was judged by experts at the scene not to be survivable under any circumstances.

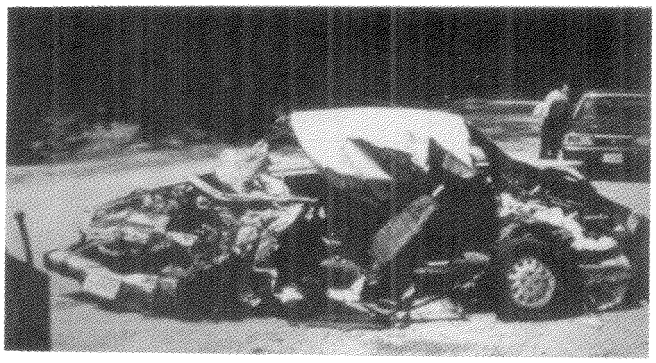

Figure 3. Catastrophic Intrusion

As noted earlier, "Non-Deployment" complaints usually occur after lower severity frontal crashes, where an air bag was not advisable or designed to supplement the protection provided by an active 3-point belt. The "Non-Deployment" in Figure 4 was a minor severity, angle-impact. Note that in angle impacts the sensors are designed to respond to the forward component, not the full impact force. Reports like these are, in a way, success stories, because they demonstrate the unlikeliness of inadvertent deployments.

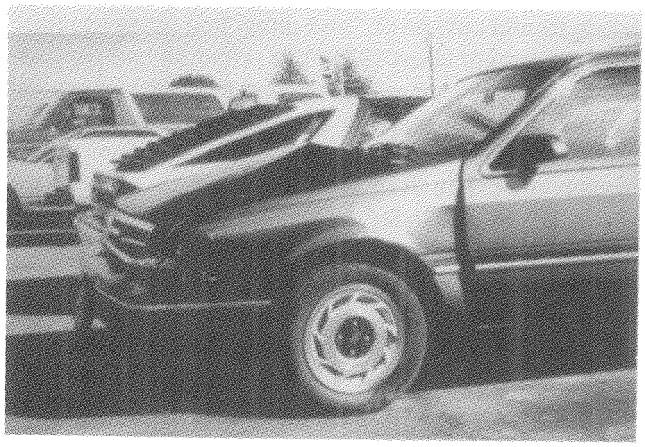

Figure 4. Non-Deployment Impact

Emergency Rescue

The perceptions of some emergency rescue crews provides the strongest example yet of how out-of-hand situations can get with misunderstanding. Following a Union City, New Jersey collision in July, 1990 the headlines read: "Air Bag Bursts, Contaminates 20 More at Scene."

Newspapers asserted that an apparently malfunctioning air bag "exploded" during a minor car accident, spewing a skin-burning chemical onto the driver and contaminating 20 other onlookers and police officers. A shower was set up in the middle of the street. Anyone who had touched the chemical was isolated. Their clothing was removed, and they were showered before being transported to a hospital. Their clothes and other personal articles that were believed to have been contaminated were confiscated. The air bag was cut from the car, placed in a plastic bag, and transported as hazardous waste. Police also cordoned off the block for about four hours to prevent others from being "infected." Unfortunately these extreme precautionary measures were taken based on misinformation about air bag systems.

Residue—In fact, the powdery residue the local authorities thought was toxic usually consists of corn starch or talcum powder; and sodium compounds, like baking soda—accompanied by minute deposits of sodium hydroxide. They may be a slight irritant to the skin and eyes, but pose no long-term health hazard. This powder is NOT considered toxic.

Rescue—Without going into specifics it should be emphasized that: occupants and rescuers are NOT exposed to harmful levels of chemicals with deployed or undeployed air bag modules. In fact, deployed air bags are not dangerous and there is no reason to delay emergency medical treatment following an air bag deployment. And further, undeployed air bags are unlikely to deploy during a rescue. To further reduce the risk, rescuer's should disconnect the battery before cutting into the steering column.

In response to such misunderstandings, NHTSA has published Rescue Guidelines for Air Bag Equipped Cars (3). We have also prepared a "Rescuer's Guide," that is specific to Ford and is easy for readers to copy (4). Ford also participated in a new ACTS (American Coalition for Traffic Safety) video, "Air Bags—A Crash Course for Rescue Personnel" (5). Clearly, there is a critical need to continue our efforts to combat misinformation among these important safety personnel.

Safety Belts and Air Bags

Deployments

Let's consider the subject of safety belts by looking at the results of collisions where it is known that air bags did deploy. In fact, the air bag deployment in the prior New Jersey case was normal and the driver was wearing the active 3-point safety belt system and sustained only minor injury.

The value of individual field collision investigations is best exemplified in a dramatic air bag deployment success story from another New Jersey collision that NHTSA is evaluating. NHTSA's report indicates that the crash involved a full overlap head-on collision of a Crown Victoria (Figure 5) and a full size GMC pickup truck, with a 50 mph Delta-V, or change in velocity, for each vehicle. That is twice the crash energy of a 35 mph barrier impact.

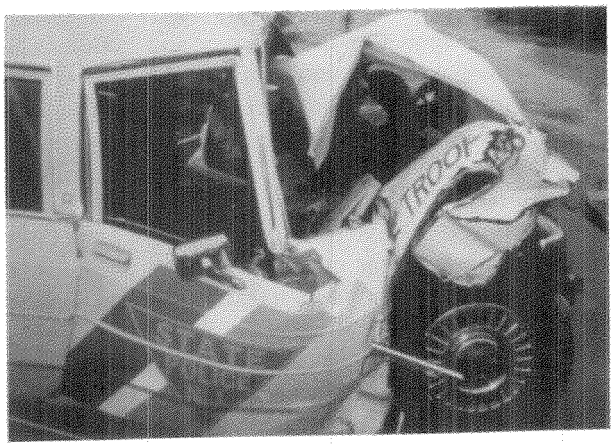

Figure 5. Crown Victoria Head-On

The driver of the Crown Victoria, a New Jersey trooper, was wearing his 3-point belt when the air bag deployed, and survived with only a broken kneecap and belt loading marks. Unfortunately the unbelted driver of the pickup truck died at the scene. This exceptional case underscores the potential effectiveness of supplemental air bags and properly-worn belts.

Belt use in the early GSA fleet of Tempo/Topaz air bag deployments was an exceptional 87%. As observed in Figure 6, there were fewer moderate or higher injuries to belted drivers than to unbelted drivers in the air bag deployment cases. Both these experiences make one thing very clear: Today's air bags, combined with properly worn safety belts, do provide discernable injury risk reduction.

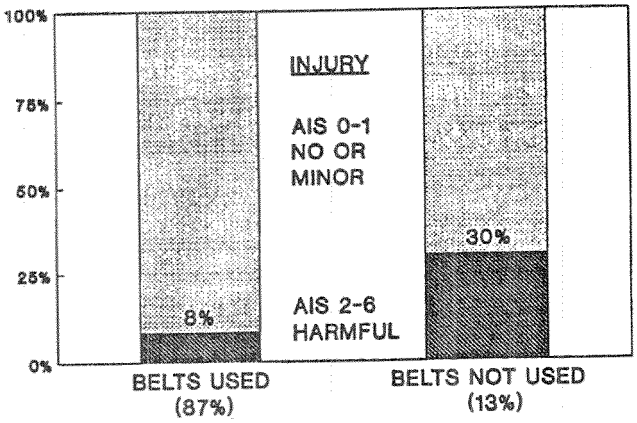

Figure 6. Tempo/Topaz Air Bag Deployments, Belt Usage and Injury Severity

Belt Usage

But will customer perceptions of air bag systems affect safety belt usage? To address this question, we compared the observed belt usage rates in the 1988 model year Continental, without air bags, and the 1989 model year Continental equipped with air bags. Obviously, we would like to see safety belt usage rates maintained or increased in cars equipped with air bags. We observed belt use in 1988 Continentals and then the 1989 air bag equipped Continentals in the same locations, one year later. There was no drop in active belt usage with air bags.

Researchers at the University of North Carolina (UNC) and Insurance Institute for Highway Safety (IIHS) have also found encouraging results to-date (6,7). The results shown in Table 3 confirm our initial observation that belt usage has not been lower in air bag equipped cars.

Table 3. Air Bag Installation and Safety Belt Usage

Air Bag Equipped	Belt Usage Rate		
	UNC	IIHS	Ford
Yes	74%	66%	73%
No	76	63	73

Although these were limited studies, the data provided do not support the conclusion that the addition of air bags will lead to a decline in the usage of safety belts. It is important to underscore the critical need to continue the promotion of proper safety belt usage. This will continue to be a key challenge for the automobile industry, and the entire safety community.

Recall that the installation of air bags was predicated on two factors: the development of safe, reliable and effective air bag restraint systems, and the increase in safety belt usage. Millions of air bag equipped cars are now on the road. According to the crash statistics and reports received by NHTSA: "Air bags are performing as expected, protecting motorists from injury and death in serious frontal collisions," and safety belt usage has risen over 300 percent since 1984. The retention and continuous improvement of safety belt usage rates is a critical need. We can not let down our guard on this issue.

Passenger-Side Air Bag

Now lets turn to today's passenger-side Supplemental Restraint System. We do have one early passenger air bag "success" story. A Continental and GMC "Jimmy" met in a head-on crash. Both the driver and passenger in the Continental were women in their 70's and both were using their active 3-point safety belts. Neither occupant had any moderate or higher injuries to the head, face, neck or torso. While both ladies did sustain arm and leg fractures—both are very thankful for the dual air bag system.

What have we seen in our field experience to-date? We have some information on 30 front seat passengers in passenger-side air bag deployments to-date. While there are too few cases to form definitive conclusions, almost half of the passengers reported minor air bag contact injuries, such as abrasions. This is very similar to driver air bag experience. Of the moderate-to-serious injuries, most involved side interior or unknown contact

areas. One child was reported to have been briefly unconscious following air bag contact—there were no reported after-effects. We know of two passenger fatalities. In one, the right-side of the car struck a bridge pillar. The other crash is still under investigation by NHTSA.

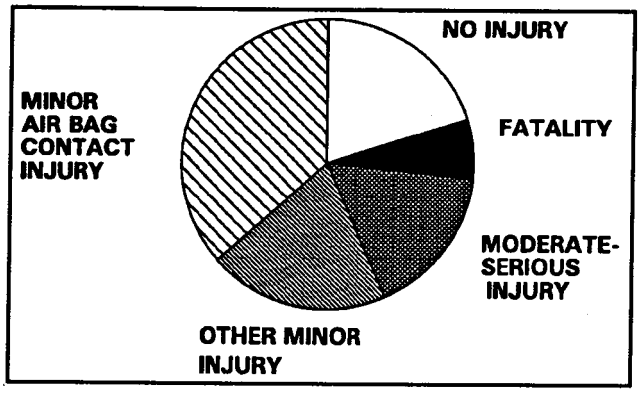

Figure 7. Thirty Front Seat Passengers in Passenger Air Bag Deployment Crashes

Obviously the passenger seat will contain a wider range of occupant age, stature, and posture than the driver's seat. The thirty passengers reported to-date have ranged from four children (under 5) to four elderly (over 70). One case involved an uninjured 9 month infant on the passenger's lap. This diversity will present a special challenge for the evaluation process.

Most of the 30 passengers were using safety belts. The use of safety belts is also critical for right front-seat passengers, who are more likely to be out-of-position than drivers when the air bag deploys.

Future

The largest and most dramatic change in the future will be the inclusion of driver and passenger air bags in ninety percent of all new cars in the U. S. by 1995, according to a recent NHTSA analysis (8). As the benefits of air bags become more widely known and accepted, and as the strength of the supply base increases, broader application beyond North America can also be expected.

At the same time there will be an evolution in the design of air bag systems as sensor systems are simplified and the air bag modules become smaller and lighter—without compromising the level of performance. Less process-critical air bag inflation schemes will be developed and applied. Computer simulations of air bag subsystems and the modeling of the interaction of a crash test dummy and an inflating air bag also will be further developed.

There will be continuing work on experimental side air bags and built-in child seats by the automotive and supplier industries and by the research community. Finally, there will be continued product evolution and improvements as further technology developments and field performance information become available.

Summary

In summary, the industry has clearly been engaged in rapid growth in safety technology with many new challenges, including a new era of passive occupant restraint systems. Ford suppliers have gone from producing 70,000 air bags for the 1989 model year to over one million for the 1991 model year. And that is only a fraction of the Ford long-term projected air bag production volumes for both driver- and passenger-side air bags in automobiles, light trucks, and vans. The magnitude of these changes has been challenging for our assembly operations and suppliers. The supply base is still fragile and will be for some time.

Safety is clearly a key purchase factor for our customers. Consequently, our challenge is to make new safety technology available as soon as practicable. Still, it is important that we continue to strive to discover and understand different vehicle/highway system experiences. There has never been a stronger need for safety research with an emphasis on pre-crash and crash field experience. And all the technology in the world will not soon overcome the danger of an alcohol impaired driver, an improperly restrained occupant, an unsafe highway condition, or an improperly maintained vehicle.

There is still a CRITICAL need to promote safety belt usage and driver responsibility. Both technology and behavior advances are needed. And we need the participation of all the organizations concerned with safety. It will take everyone, working together, to continuously improve the vehicles and the way they are operated. We are agreed—highway safety has to be improved. Using our common skills, resources, and technologies we can make real progress on the many aspects of traffic safety.

Again, Ford looks forward to a continuing and effective working relationship with all the organizations participating in this ESV conference. Working together, we can make a difference.

Acknowledgment

The authors wish to acknowledge the U.S. National Highway Traffic Administration, Accident Investigation Division for its extensive support of the special accident investigation program.

References

1. "Occupant Crash Protection; Final Rule," NHTSA Docket 74-14, Notice 36, July, 1984.
2. "Motor Vehicle Safety—Information on Accident Fires in Manufacturing Air Bag Propellent," U.S. General Accounting Office, R2CED-90-230, September, 1990.
3. "Emergency Rescue Guidelines for Air Bag Equipped Cars," U.S. NHTSA, 1990. Call (800) 424-9393 for a copy.
4. "Rescuer's Guide for Ford Motor Company Air Bag Supplemental Restraint System," Ford Automotive

Safety Office, October, 1990. Call (800) 392-3673 for a copy.
5. "Air Bags—A Crash Course for Rescue Personnel," ACTS (American Coalition for Traffic Safety) video; January 1991. Call (202) 775-8377 for a copy.
6. "Usage Patterns and Misuse Rates of Automatic Seat Belts by System Type," Reinfurt, D. W., Cyr, C. L., Hunter, W. W., Highway Safety Research Center, University of North Carolina. In 34th Proceedings of the Association for the Advancement of Automotive Medicine, pages 163-179, October, 1990.
7. "Surveys Show Driver Belt Use Does Not Drop in Cars Equipped With Air Bags," *IIHS Status Report*, Volume 25, No. 6, page 3, Insurance Institute for Highway Safety, June 30, 1990.
8. "NEWS: NHTSA Projects Lives Saved by Air Bags Through 1995," U.S. Department of Transportation, Office for Public Affairs, January 30, 1991.

S9-O-10

Seat Belt Pretensioners to Avoid the Risk of Submarining—A Study of Lap-Belt Slippage Factors

Yngve Håland
Electrolux Autoliv AB
Gert Nilson
Chalmers University of Technology

Abstract

Submarining occurs when the lap-belt, under load generated by the occupant, in a car collision slips up over the iliac crests and compresses the abdomen. The process has been found injurious if it occurs before the lab-belt force has dropped below 3kN. Most of the severe cases have been found in high violence crashes. By a series of sled tests followed by mathematical simulations of typical front seat and rear seat belt geometries and with a seat comprising of a homogenous cushion on a flat steel plate it has been shown that:

- Occupants are more likely to submarine if the upper belt anchorage is far behind their shoulder (as in a rear seat or in a front seat in a two-door car).
- The closer to the seat the occupant's feet are placed, the more likely submarining is to occur.
- Belt slack increases the risk of submarining.
- A pre-tensioner that operates on the buckle, significantly reduces the risk of submarining.

It is also shown that the angle between the lap-belt and the pelvis, measured when the belt force has peaked and dropped to 3 kN, well can predict the risk of submarining.

Introduction

The term submarining is used to describe the process where the lap-belt, under load generated by the occupant, in a car collision slides up over the iliac crests and compresses the abdomen. Submarining may in severe cases result in liver and spleen injuries and lumbar vertebra fractures. Injuries to the colon and the messentary as well as lower member fractures are also common (Leung et al., 1982). Kramer (1991) estimates the costs due to submarining injuries to be one sixth of the total cost for hospital care of victims in car to car accidents in Germany, which makes submarining one of the leading causes of harm.

The frequency and severity of abdominal injuries induced by submarining have been the focus in several investigations. The majority of the severe cases have been observed in high violence crashes, $\Delta v > 50$ km/h (Leung et al., 1982; Otte, 1990). Both investigations show that about 60-70 % of the serious (AIS 2 3) abdominal and pelvis injuries are caused by the belt in frontal collisions. Otte (1990) found 10% AIS 3-4 injuries to abdomen and pelvis in frontal collisions at a Δv of 51-70 km/h, but only 1% at a Δv of 31-50 km/h. Leung et al. (1982) show somewhat higher figures; 12% of all seriously injured drivers had sustained severe abdominal and dorsolumbar fractures. The corresponding figure for the passengers was 16%.

Several attempts have been made to predict submarining. Adomeit (1979) proposes that the angle formed by the lap-belt and the x-axis in the horizontal plane from a side view should be 50-70° to avoid submarining. Leung et al. (1982) show that also the angle formed by the lap-belt (from the anchorage) and the x-axis in a view from above affects the risk of submarining. Horsch and Hering (1989) have demonstrated, by a series of tests, that submarining takes place when the "critical" belt to pelvis angle reaches a typical value of 30°. In a recent investigation performed by O'Connor and Rao (1990), the importance of the initial lap-belt position in relation to the anterior superior iliac spine (A.S.I.S.) has been demonstrated; a difference in position of 15 mm upwards in the z-axis direction was in some cases enough to cause submarining.

Leung et al. (1982) found that if the lap-belt slips off the iliac crest wings before the average force (measured in both straps) has dropped below 3 kN, injury is likely.

Kramer (1991) shows that there is a strong correlation between the lap-belt force at the time of submarining and the severity of injuries sustained. He proposes two pelvic acceleration limits to prevent abdominal and pelvic injuries; max 83 g for a pelvis rotation angle below 20° and max 20 g for an angle of more than 26°.

Also other factors that can influence the tendency to submarining have been addressed by different investigators, such as belt slack (Leung et al., 1982), seat design (Adomeit, 1979; Lundell et al., 1981), and leg (foot) position (Horsch and Hering, 1989).

The aim of this study is to complement earlier investigations and demonstrate different design factors effect on submarining by sled tests and mathematical simulations. The work is focused on three factors; the position of the pillar loop (the D-ring), the leg (foot) position and belt slack. The hypothesis is that submarining takes place when a critical angle between the lap-belt and the pelvis has been reached. A consequence of the hypothesis is that the belt-to-pelvis angle becomes a continuous variable to determine the risk of submarining.

Methods

Sled Tests

Dynamic tests were performed at the Electolux Autoliv sled test facility in Vargarda, Sweden (Figure 1).

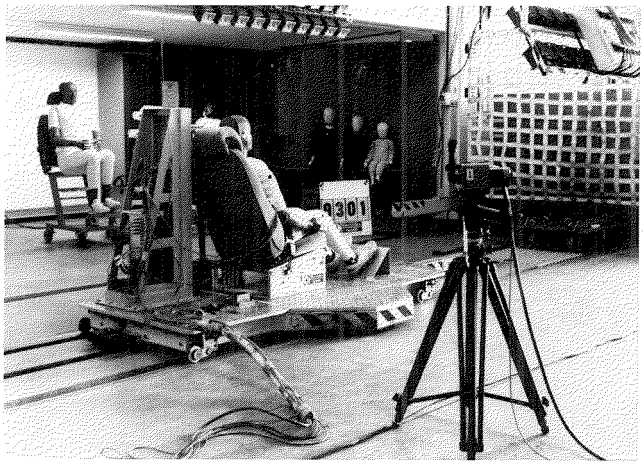

Figure 1. The Electrolux Autoliv Sled Test Facility in Vårgårda, Sweden

One high speed video camera (Kodak) was used to record the dummy movements during the crash sequence. The camera operated with 1000 frames per second. The video recordings were used for test analysis and documentation.Two views, one from the side and one from the front, of a typical test configuration can be seen in Figure 2. A special seat was designed for the test.

The seat cushion was made of polyether foam with a thickness of 120 mm and a density of 50 kg/m^3. The cushion was covered by a typical car seat fabric and the sub-structure was a stiff steel plate. The plate was angled 7° with respect to the horizontal plane, except for its frontal part, which was horizontal. The reasons for using this configuration were to simulate a comfortable seat without any anti-submarining device, as well as to simplify the transference of the test into a mathematical model. The back of the seat was angled 23°. Figure 3 is a stylistic picture of a test configuration. The y-axis in the coordinate system coincides with the centerline

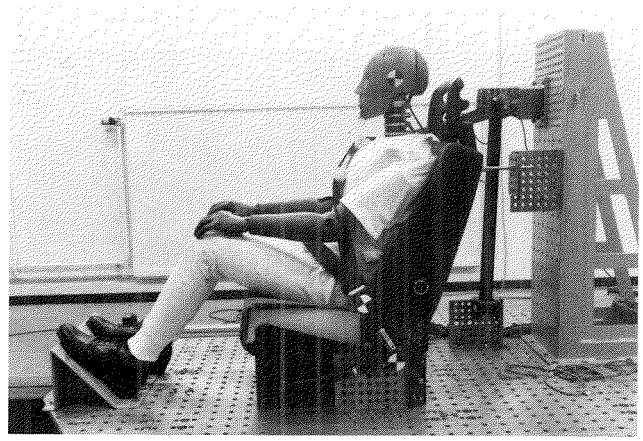

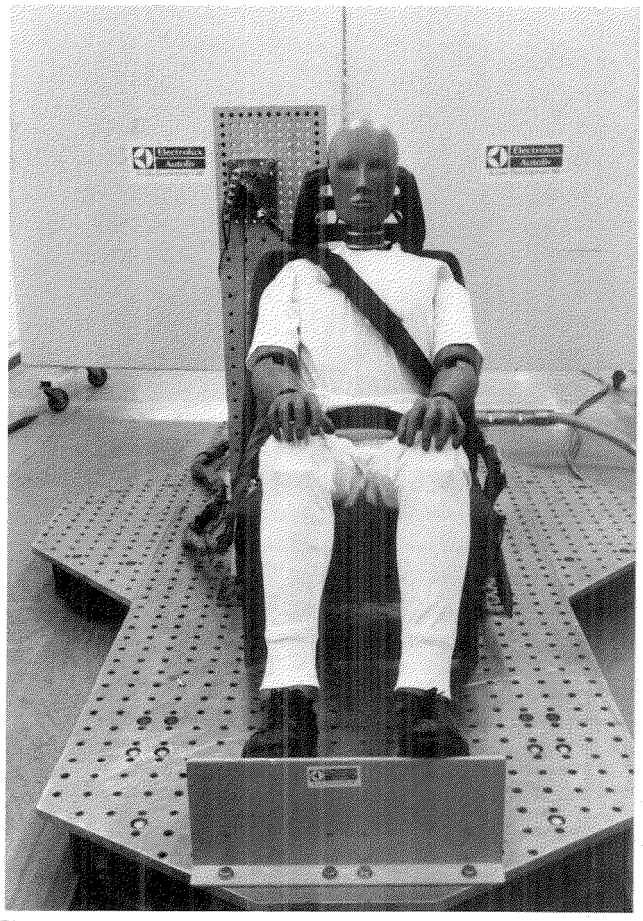

Figure 2. Side and Front Views of a Typical Test Configuration

through the hip joints. The reference system represents a front seat belt system in a four-door car. The geometrical data are summarized in Table 1.

The initial lap-belt angle was approximately 64°. The sled tests were run at 50 km/h. A crash pulse was chosen according to ECE R16. Figure 4 shows the pulse. The average deceleration was about 25 g.

From an initial series of sled tests, where several parameters (belt geometry, with and without belt slack and pretensioner) were varied, four different configurations were selected for further tests in the mathematical

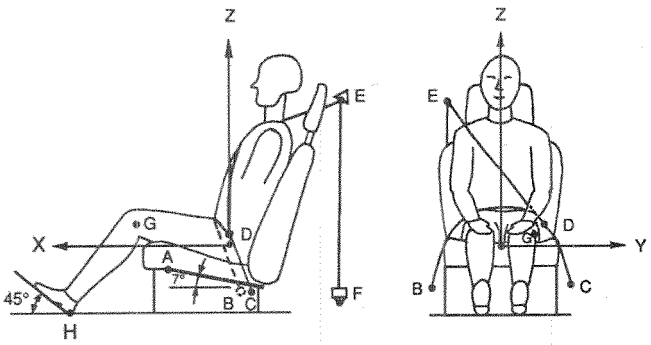

Figure 3. Test Configuration

Table 1. Geometrical Data of the Reference Test Configuration ("Front Seat")

Position (fig.3)	x (mm)	y (mm)	z (mm)
A	+300	-	-130
B	-80	-265	-135
C	-105	+265	-135
D	0	+250	+60
E	-340	-275	+560
F	-385	-300	-210
G	+330	+175	+110
H	+705	-	-310

Note: A = Point where the seat sub support goes from 7° to horizontal
B = Lower outer attachment point for the lap-belt
C = Attachment point for the bucklebracket (or the pretensioner)
D = Midpoint of belt passage through the buckle tongue
E = Mid position of webbing through the D-ring
F = Retractor attachment point
G = Left outer side of knee joint
H = Position of the foot plate

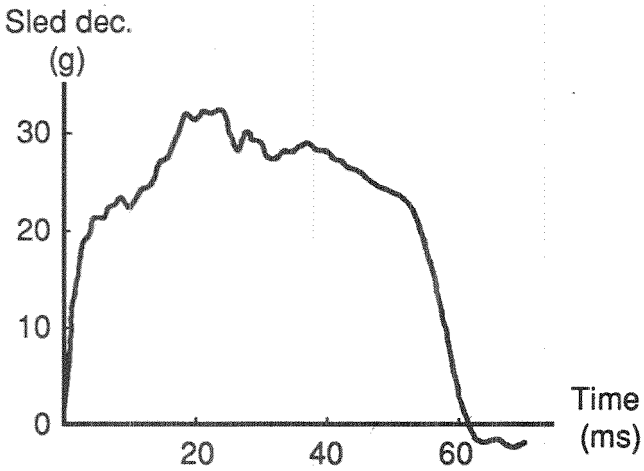

Figure 4. Sled Deceleration Pulse

model. The first two represents a typical four-door car front-seat belt geometry. The other two represents a typical rear seat belt geometry, which is similar to a two-door car front-seat or a belt-in-seat geometry, where the D-ring was positioned 200 mm further behind the dummy shoulder (With reference to point E in Figure 3, x= -540 mm instead of -340 mm).

All configurations were run with 100 mm slack, split 50/50 between shoulder-and lap-parts of the belt, since this case well represents real wearing conditions. In order to maintain constant conditions between the tests, the slack was introduced by putting soft foam between the lap-belt and the abdomen as well as between the shoulder belt and the chest. The seat belt webbing was "low friction-treated" and had an elongation of 10 % at 10 kN. The amount of webbing on the retractor reel was 400 mm.

For each belt geometry, tests were performed both with and without a mechanical buckle pretensioner of a type manufactured by Electrolux Autoliv (Figure 5). In a crash, the pretensioner pulls the buckle rapidly downwards. The process is completed before an unrestrained mass has moved 20 mm (Håland and Skånberg, 1989). The initial pulling force, generated by a coil spring, is 1500 N. Maximum stroke is about 80 mm. The buckle pretensioner eliminates slack in the lap-belt as well as in the shoulder belt. The buckle tongue used had one slot for the webbing passage. This type of tongue permits an easy transport of webbing between the two belt segments compared with two-slot tongues.

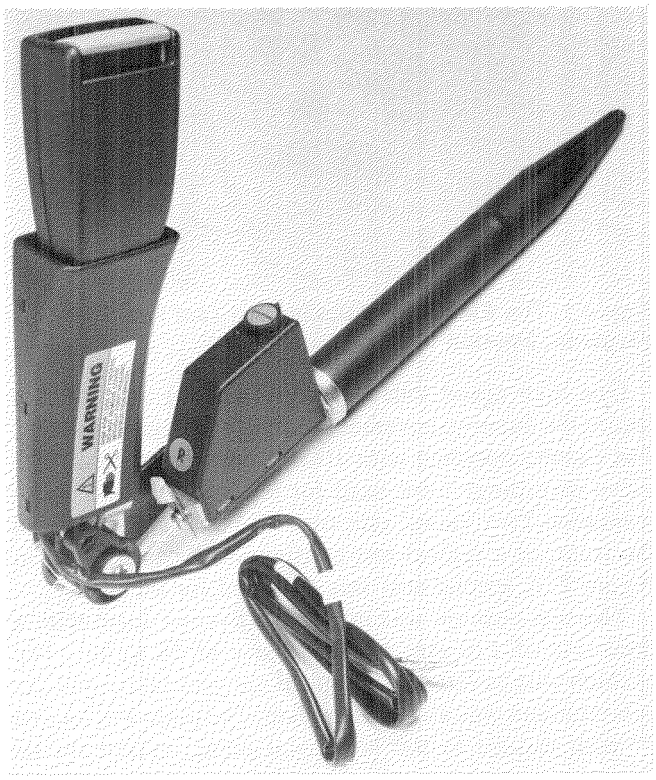

Figure 5. Mechanical Buckle Pretensioner with Coil Spring

Table 2 describes the four different test configurations. Each configuration was run twice.

Table 2. The Four Different Test Configurations (Ref. as in Figure 3 and Table 1)

No.	Configuration	Slack	Pretensioner
I	Front seat (ref.)	100 mm	No
II	Front seat (ref.)	100 mm	Yes
III	Rear seat (D-ring -200 mm)	100 mm	No
IV	Rear seat (D-ring -200 mm)	100 mm	Yes

The Hybrid III dummy, instrumented with tri-axial accelerometers in head, chest and pelvis, was used. The shoulder belt force was measured between the D-ring and the shoulder and the lap-belt force close to the lower anchorage point (B in Figure 3). The dummy pelvis was instrumented with three force sensors, so called "load bolts," below the Anterior Superior Iliac Spine (A.S.I.S.) on each side,to detect belt slippage on the pelvic surface. The upper load bolt is located about 10 mm below the A.S.I.S. and the middle bolt another 26 mm below. The lap belt was positioned about 25 mm below the A.S.I.S. on each side of the pelvis.

Mathematical Simulations

Occupant Model

The mathematical model used in the study was MADYMO 3D, release 4.3 (TNO Road-Vehicles Research Institute, 1990; Lupker and Fraterman, 1990). In order to duplicate the sliding of the lap-belt over the pelvic structures, the standard description of the Hybrid-III lower torso (TNO Road-Vehicles Research Institute, 1990) was changed in the following way: To the single outer contour, which describes the shape of an unloaded Hybrid-III lower torso, was added a stiff inner contour, describing the actual pelvis (Figure 6). The frontal part of the pelvis was modelled by a number of planes, as suggested by Bosio (1990). The part that interacts with the seat was modelled by two small ellipsoids. The geometry was obtained from published drawings of the Hybrid-III (General Motors Corporation, 1984).

Also the contour of the lower torso itself was changed. The almost circular cross-section suggested in the database was replaced with a hyperelliptical cross-section (third degree), for two reasons: Firstly the new shape was in better agreement with the shape prescribed by General Motors Corporation (1984), secondly the dummy response was much more in agreement with the reference sled tests when the new contour was used. The part that interacts with the belt was modelled as a relatively soft plane in front of the pelvis (Figure 6).

The lap-belt was attached to two small elements, which were put in the belt's position in the xz-plane and in the position of the iliac crests in the y-direction. The elements were prevented from sliding off the pelvis in the lateral direction by two so called point-restraints, which strongly resisted outward motion. The point-restraints also transferred some load from the belt to the lower torso in the other plane-parallel direction, to compensate for the fact that the planes only transferred the plane-perpendicular component of the load.

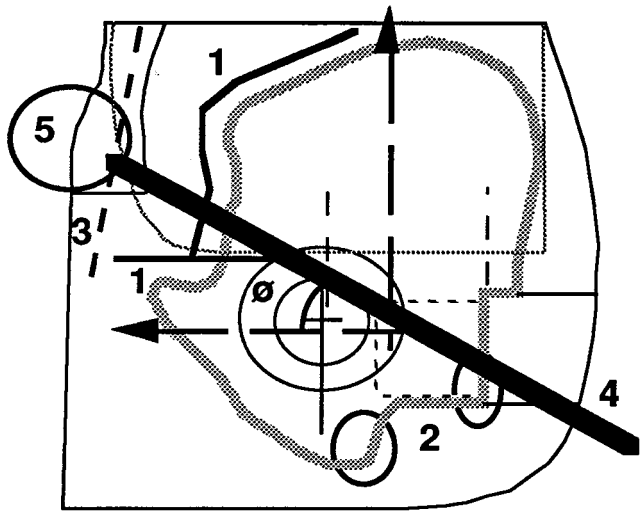

The grey contour represents the dummy pelvis. The solid contours show the pelvis' representation in the mathematical model—both the frontal (1) and the lower (2) parts. The dashed line (3) shows the plane that represents the frontal soft parts of the lower torso. Also one of the belt-straps (4) and the "ball" to which is attached (5) are shown, as well as the belt-to-pelvis angle (ø).

Figure 6. Stylistic Picture of a Hybrid III Lower Torso

Parametric Study

Altogether 32 simulations with different initial conditions were carried out, the four sled test configurations included. In half the number of tests the D-ring was located close to the dummy's shoulder, representing a four-door car front-seat geometry, in the other 16 runs the D-ring was moved 200 mm backwards to model a rear seat (or a two-door car front-seat) geometry. The other independent variables tested were initial belt load (slack/pretensioning) and initial foot position. Table 3 shows the test matrix, which was the same for each D-ring position.

Table 3. Test Matrix for the Mathematical Simulations

Belt conditions / Foot position	+50	0	-50	-100
Normal (20 mm slack)	x	x	x	x
Slack (extra 100 mm)	x	x	x	x
Normal with pre-tensioning	x	x	x	x
Slack with pre-tensioning	x	x	x	x

The 16 configurations shown were simulated twice, first with the D-ring close to the dummy's shoulder (front seat geometry), then with the D-ring moved 200 mm backwards (rear seat geometry).

Four different initial belt conditions were tested, these being 1) properly adjusted belt (referred to as "normal" and in the mathematical model set to 20 mm slack), 2) belt with slack (100 mm extra slack, distributed equally in the lap- and shoulder belt parts) 3) and 4) the same as 1) and 2), respectively, with the addition that a belt pre-

tensioner was considered to operate on the buckle. Thus, in the two last cases an initial belt force of approximately 500 N was applied to both the lap- and the shoulder strap. The difference between the tests was the initial position of the buckle, since, in the sled tests, the agent pulls the buckle a longer distance to tighten the belt when there is slack in the straps. Also four different initial positions of the dummy's feet were tested, being "reference," +50 mm, -50 mm and -100 mm.

Measurements

In the mathematical model it is possible to measure the angle ϕ between the lap-belt and the normal to the pelvic frontal surface (Figure 6) as a function of time. The belt slips off the pelvis (the A.S.I.S) and into the abdomen if the component of the belt force parallel to the pelvic frontal surface is directed upwards in the pelvic coordinate system and larger than the motion-resistive force. On the outer side a major part of the upward directed force can be derived from the belt force times tan ϕ. ϕ is measured when the average belt-force (measured on both sides) is 3 kN (negative flank). According to Leung et al. (1982) injury is unlikely if submarining occurs when the belt force has dropped below this value. Tan ϕ was then used as a measure of the likelihood of (an injurious) submarining.

Results

Sled Tests

The signals from the accelerometers and the webbing force transducers were used to validate the mathematical model, which then was used to study the influence of different parameters on the risk of submarining (see below).

The force sensors below the A.S.I.S. on each side of the dummy pelvis indicated if submarining had occurred. Figure 7 shows the forces for the mid and upper load bolts on the buckle side for the front seat configuration with 100 mm belt-slack. The belt slips from the middle load bolt to the upper at t=60 ms. Then, 8-10 ms later, there is a sudden drop in the load on the upper bolt, which indicates that the belt has slipped over the A.S.I.S. (submarining). The lap belt force at that time is approximately 5 kN. The test results of the four configurations are summarized in Table 4.

The Figures 8, 9, 10 and 11 show pictures (from high speed film) of the four configurations at 0, 40 and 80 ms.

Mathematical Simulations

Results from the mathematical simulations are presented in Figures 12-14. The first figure shows the tangent of the angle between the outer lap-strap and the pelvis, measured at 3 kN average belt force (negative flank), for each of the four sled-test configurations. In the sled tests, the dummy clearly submarined in the case "rear-seat geometry with slack," barely submarined in the case

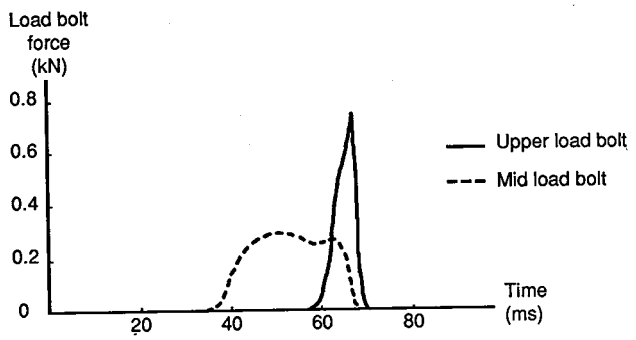

Figure 7. Forces Measured by the Mid and Upper Load Bolts on the Buckle Side for the Front Seat Belt Configuration with 100 mm Slack

Table 4. Tests Results of Four Seat Belt Configurations

No. Configuration	Submarining	Lap belt force at the time of subm.
I Front seat w. 100 mm slack	Yes[1]	5 kN
II Fr. seat w. 100 mm slack + pret.	No	
III Rear seat w. 100 mm slack	Yes[1]	8 kN
IV R. seat w. 100 mm slack + pret.	No	

[1] *On the buckle side of the lapbelt.*

"front seat geometry with slack" while it did not submarine in the two cases where a pre-tensioner was used. The results obtained thus establishes a "transition zone," for the value of the tangent of the belt-to-pelvis angle, in which the probability of submarining increases from zero (below the value obtained in the rear seat with pretensionercase) to one (above the value obtained in the front seat without pretensioner-case). This zone is marked in Figures 13 and 14, where the results from all the runs in the study are plotted.

As can be seen the risk of submarining increases when the initial foot-position is moved backwards. With the particular belt- and seat properties used in this study and the D-ring in the rearward position ("rear-seat" geometry) the risk for submarining would be negligible only in the case with almost straight legs and a buckle pretensioner, while submarining would be very probable in all cases where no pretensioner is acting.

The situation is apparently better in the "front-seat" cases, where the results indicate that the risk for submarining will be small to moderate if the belt is properly adjusted and the legs kept in a relatively straight manner ("driver's pose"). However, the introduction of a buckle-pretensioner still decreases the probability of submarining significantly.

Discussion

When occupant restraint systems are being developed for new car models, the problem of submarining may be underestimated and neglected for various reasons.

Official requirements, as stipulated for example in FMVSS 208, are valid for front seat occupants only. There are no requirements for rear seat occupants.

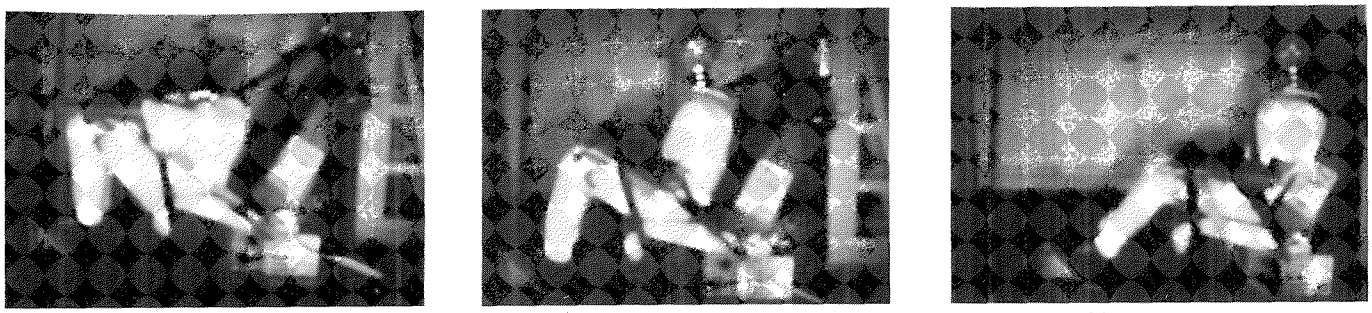

0 ms 40 ms 80 ms

Figure 8. Front Seat Belt with 100 mm Slack

0 ms 40 ms 80 ms

Figure 9. Front Seat Belt with 100 mm Slack + Pretensioner

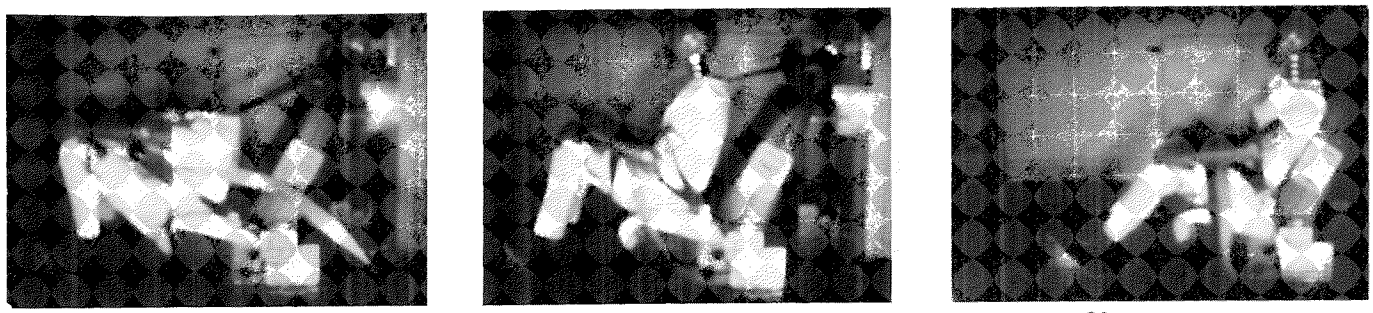

0 ms 40 ms 80 ms

Figure 10. Rear Seat Belt with 100 mm Slack

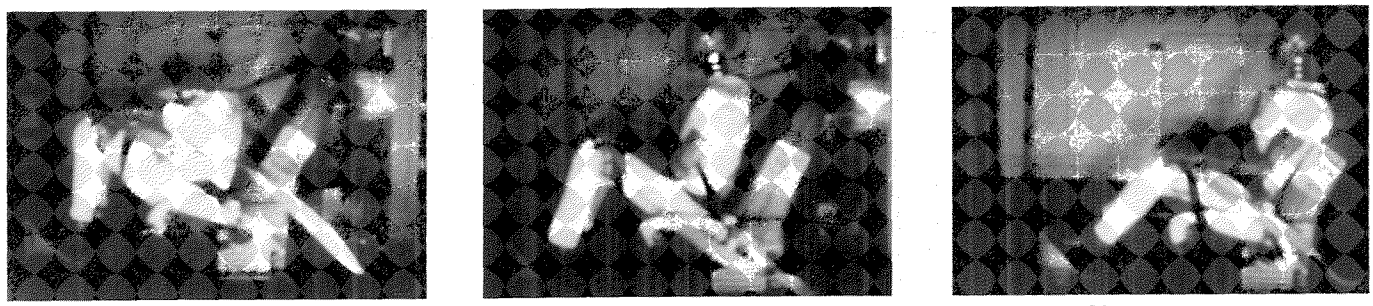

0 ms 40 ms 80 ms

Figure 11. Rear Seat Belt with 100 mm Slack + Pretensioner

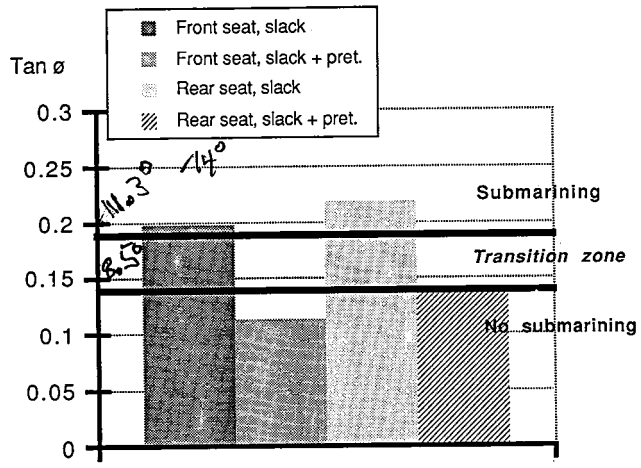

Figure 12. The Tangent for the Angle Between the Lap-Belt and the Pelvis, Measured when the Belt Force is 3 kN, Obtained in the Mathematical Duplication of the Four Sled Tests

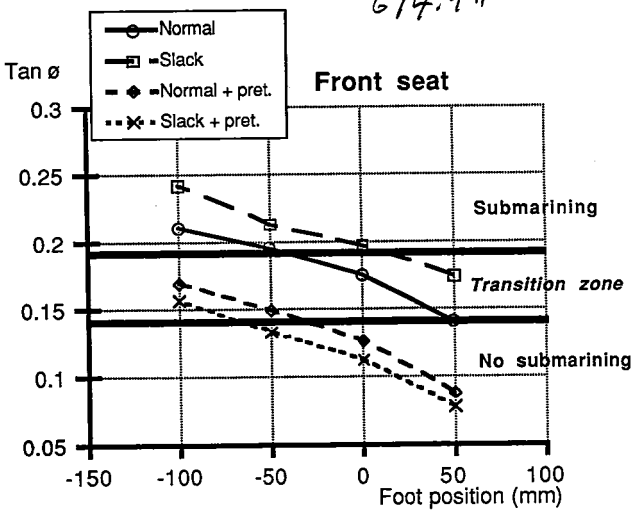

Figure 13. The Tangent for the Angle Between the Lap-Belt and the Pelvis, Measured when the Belt Force is 3 kN, for Different Initial Belt Conditions and Foot Positions in the Front Seat Geometry

Dynamic tests are performed with the human substitutes (Hybrid II or III) dressed in thin cotton clothes. The belt system slack is then small, compared to the conditions in the daily use in a car, especially in the wintertime, when people are wearing a lot of clothes.

One problem is the lack of official abdominal injury criteria in frontal impacts. The interest is many times focused on the head and chest loads, thus neglecting the potential problem of loads to the abdomen.

Accident investigations indicate that submarining is a greater problem for belted rear seat occupants than for front seat occupants. However, since compulsory use of seat belts in the rear seat has been introduced only recently in many countries, statistically significant conclusions cannot yet be drawn.

Partly due to some of the facts presented above, the knowledge about the mechanisms that cause submarining

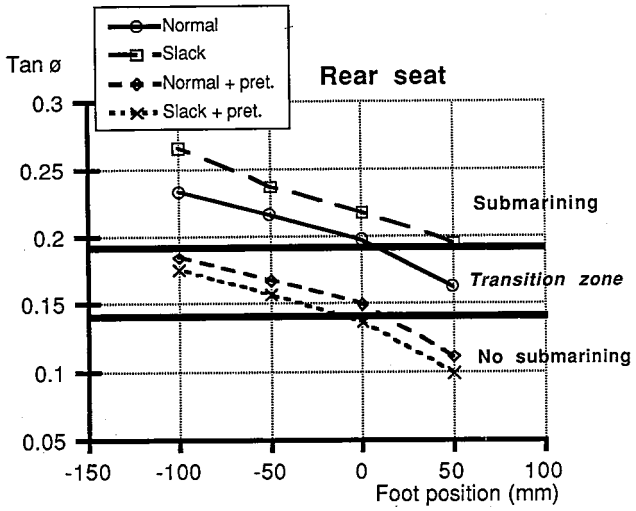

Figure 14. The Tangent for the Angle Between the Lap-Belt and the Pelvis, Measured when the Belt Force is 3 kN, for Different Initial Belt Conditions and Foot Positions in the Rear Seat Geometry

is poor. One important reason could be that in mechanical experiments only a yes/no result is obtainable, which is insufficient since it requires a (too) large number of tests to evaluate the influence, or even the relevancy, of different design parameters.

One advantageous feature of a mathematical model is the possibility to measure virtually anything found desirable to measure. Horsch and Hering (1989) state that the angle between the normal to the pelvic surface upon which the lap-belt normally acts and the belt (here called ϕ) determines the probability of submarining. Thus, one part of this work has been to transfer a number of mechanical experiments into a mathematical model, to enable high-resolving measurements of the angle ϕ. In order to simplify the transference a relatively simple seat design—a homogeneous cushion on top of a rigid steel plate—and a belt with known dynamic properties were used. With all geometric data carefully measured it was straightforward to make the mathematical model respond in very good agreement with experimental results.

Since the reference tests contained cases both with and without submarining it was possible to obtain a "least value" of the belt-to-pelvis angle over which submarining is certain, as well as a "largest value" under which submarining is unlikely. The range of values in between becomes a "transition zone," in which the probability of submarining goes from zero to one. The assumption that there in fact is a relation between tan ϕ and the risk of submarining is supported by the fact that, in the mathematical simulations of the four sled-tests, higher ϕ values were obtained for the two submarining cases than for the two non-submarining cases. In addition, the more pronounced the (tendency for) submarining—according to the signals from the load-bolts and the high-speed video analysis—the higher the ϕ value obtained, which indicates that the relation is monotone.

It should be pointed out that the belt's sliding off the pelvic structures is in itself a physical phenomenon, which properties are independent of, for instance, the belt geometry or the seat structure. Thus, no change in an independent variable, except belt surface friction, would affect the range of angles defining the transition zone, even though the change might strongly affect the outcome of the test.

The measurements could have been made the other way around, that is, the belt force could have been measured at a specified belt-to-pelvis angle, for instance the angle ϕ for which $\tan \phi = \mu$, where μ is the coefficient of friction between the belt and the dummy. The main argument for doing it the way it was done, is that the belt-force drops very rapidly in the critical range, which means that a steep force-curve cuts a smooth angle-curve. The results would not change a lot if the angles were measured at a belt-force of, for instance, 2 kN or 4 kN. If doing it the other way, the results would very strongly depend on the choice of critical angle value, which in turn could be chosen anywhere in the transition zone.

One other reason for measuring the belt-to-pelvis angle at 3 kN is the strong evidence presented by Leung et al (1982), this belt force being critical.

Throughout the study the angle of the belt strap, that is attached to the floor, has been measured, instead of that of the strap attached to the buckle. It could be argued that since car occupants first slide under on the buckle-side, and—like in our reference sled tests—sometimes there only, this angle ought to be the most relevant to measure. One reason for not doing so is that it is hard to precisely model the trajectory of the buckle, not least because of the strong influence from the lower torso belt-strap. Another reason is that there ought to be a reasonably simple relation between the probability of a complete submarining and the probability of a "one-side submarining," so that an increase in the former should indicate an increase in the latter. This is supported by the fact that in the two sled-tests where submarining occurred, the signals from the load bolts show that the belt was "climbing" upwards also on the outer side, and the effect was more pronounced in the case with the higher belt-to-pelvis angle value.

The conclusion is that in a mathematical model a continuous parameter that evaluates the likelihood of submarining is obtainable, namely $\tan \phi$, where ϕ is the angle between the structure-anchored lap-belt strap and the upper, frontal part of the pelvis.

The results obtained in the study show four things:

1) Occupants are more likely to submarine if the upper belt is anchored far behind their shoulder, like it is in a rear seat or in a front seat in a two-door car, than if the strap is anchored close to their shoulder.
2) The closer to the seat occupants' feet are placed, the more likely submarining will occur.
3) Belt slack increases the risk of submarining.
4) The introduction of a belt pre-tensioner that operates on the buckle, significantly reduces the risk of submarining.

The reason a rear seat geometry increases the risk for submarining is plausibly that with such a geometry the upper part of the body is restrained at an earlier stage, in comparison with a front seat geometry. The upper belt forms a loop around the occupant's upper torso, and the main interaction between the occupant and the belt takes place near the occupant's shoulder. This means that the restraint, at the same time as it holds back the upper torso, introduces a downwards directed force. When the upper torso is held back early this downwards directed force will enhance the pelvic rotation more in comparison with the case when the upper torso restraint comes into action later thus allowing the body to jack-knife over the lap-restraint.

The dependency on the foot-position could be explained in the following way: In all simulations the feet rest against a support, which means that the centres of mass of the upper legs can only be translated forwards by pivoting around the knee joints. The straighter the legs, the more the inertial force trying to translate the upper legs and lower torso will be met by the foot support, via the knee joints. This in turn will hinder the rotation of the lower torso, since the legs and the lower torso interact at a point below the latter's centre of rotation.

Slack increases the risk for submarining since the impulse into the seat and thus the energy available to rotate the pelvis will be higher. This is in agreement with the findings of, for instance, Leung et al. (1982) and Otte (1990), which show that the risk of submarining increases with impact severity.

The pre-tensioner, finally, helps to prevent from submarining in two ways: Firstly it reduces the slack. Secondly it pulls the buckle downwards, which brings the lap-belt clasp closer and narrows the opening for the pelvis to slide through. The findings that a better restrained upper torso increase the risk of submarining indicate, however, that a pre-tensioner acting on the retractor would do less good and in fact could increase the risk for submarining, especially if there is a high friction in the tongue, which would hinder the pre-tensioner tighten the lap-belt.

It is important to note that, due to the more limited space, rear seat occupants generally sit with a narrower knee angle than front seat occupants, which means that two of the mechanisms found to increase the risk for submarining interact in a standard rear seat. Another complicating matter is that few present rear-seat design concepts allow the introduction of devices that would help to prevent from submarining, such as a submarine-beam or a steep ramp, even though such solutions have been suggested in the literature (Lundell et al., 1981).

The cushion is, in addition, normally close to the bottom plate of the car, which limits the possibilities to lower the buckle position.

Conclusions

There is a higher risk of submarining in the rear seat than in the front seat. The introduction of a buckle pretensioner improves the situation significantly.

Also the front seat designer ought to consider the effects on risk of submarining introduced by the D-ring position and the foot position, since these factors interact when the front seat occupant adjusts the seat forwards. Due to the strong influence of the D-ring position alone, special attention must be paid to the risk for submarining in the front seat in a two-door car or in a car where all the belt anchorage points are in the seat structure.

This work also shows that tan ϕ, where ϕ is the angle between the structure-anchored lap-belt strap and the upper, frontal part of the pelvis, is a measure of the risk of submarining and thus could be a helpful tool to evaluate new design concepts.

References

Adomeit, D., "Seat Design—A Significant Factor for Safety Belt Effectiveness," SAE Technical Paper No. 791004, in proceedings of the 23rd Stapp Car Crash Conference (1979).

Bosio, C., "Simulation of submarining with MADYMO," in proceedings of the Second International MADYMO Users' Meeting (1990).

General Motors Corporation, "Hybrid-III—An Advanced Anthropometric Crash Test Dummy," National Highway Traffic Research Safety Administration, Washington D. C., USA (1984).

Horsch, J. D., and Hering, W. E., "A Kinematic Analysis of Lap-Belt Submarining for Test Dummies," SAE Technical Paper No. 892441, in proceedings of 33rd Stapp Car Crash Conference (1989).

Håland, Y. and Skånberg, T., "The Mechanical Buckle Pretensioner to Improve the Three-Point Seat-Belt," in proceedings of the Twelfth International Conference on Experimental Safety Vehicle (ESV) (1989).

Kramer, F., "Abdominal and Pelvic Injuries of Vehicle Occupants Wearing Safety Belts Incurred in Frontal Collisions—Mechanisms and Protection," in proceedings of 1991 International Conference on the Biomechanics of Impact (IRCOBI) (1991).

Leung, Y. C., Tarriere, C., Lestrelin, D., Got, C., Guillon, F., Patel, A., Hureau, J., "Submarining Injuries of 3 Pt Belted Occupants in Frontal Collisions-Description, Mechanisms and Protection." SAE Technical Paper No. 821158, in proceedings of the 26th Stapp Car Crash Conference (1982).

Lupker, H.A. and Fraterman, E., "Status MADYMO Program (1990)," in proceedings of the Second International MADYMO Users Meeting (1990).

O'Connor, C.S. and Rao, M.K., "Dynamic Simulations of Belted Occupants with Submarining," SAE Technical Paper No. 901749, in proceedings of Passenger Car Meeting and Exposition (1990).

Otte, D., "Comparison and Realism of Crash Simulation Tests and Real Accident Situation for the Biomechanical Movement in Car Collisions," SAE Technical Paper No. 902329, in proceedings of the 34th Stapp Car Crash Conference (1990).

TNO Road-Vehicles Research Institute, "MADYMO Databases, Version 4.3," The Netherlands (1990).

TNO Road-Vehicles Research Institute, "MADYMO User's Manual 3D, Version 4.3," The Netherlands (1990).

S9-0-11

A Preliminary Field Analysis of Chrysler Driver Airbag Effectiveness

W. Randall Edwards
Chrysler Corporation

Abstract

Over a period of 17 months from April 1988 to September of 1990 Chrysler Corporation converted all its U.S. built passenger cars to equip them with a driver airbag supplemental restraint system. In an effort to evaluate the driver airbag effectiveness from early data in reducing frontal crash driver fatalities, the driver fatality rates for each of the converted vehicles before and after the introduction of the driver airbag are compared. Without enough fatality data to statistically quantify the effectiveness of the driver airbag, a methodology for assessing the effectiveness is demonstrated which will quantify it when more data are available. Driver airbags show directional improvement in reducing driver fatalities but the magnitudes are not statistically reliable at this time.

Introduction

The driver airbag has long been touted as a safety device that would save the lives of drivers and reduce the severity of head and chest injuries of drivers in frontal automobile crashes. Ever since the first patents for an inflatable restraint system (Hetrick, USA, 1953), claims and analyses of their injury and fatality reduction potential have been the subject of debate. They have also been the motivation for automatic crash protection regulations in the United States for passenger cars because

voluntary seat belt usage rates were so low (≈10% in 1980).

After a prolonged regulatory impasse, phased-in passive restraints became a U.S. regulation for the 1987 model year. While Chrysler was not the first to introduce inflatable restraints to the U.S. market (G.M., Ford, and Daimler Benz marketed airbag equipped vehicles earlier), it made a swift conversion of all its U.S. built passenger cars to a driver airbag with a manual lap-shoulder belt between April of 1988 and September of 1989. In every case, an existing production passenger car was equipped with a driver airbag supplemental restraint system. This rapid conversion provides a sharp demarcation opportunity to evaluate the effectiveness of the driver airbag because gradual changes in demographics, driving behavior, seat belt usage, roadway environment, and fatality rate can be assumed constant for the purpose of evaluating the vehicle crashworthiness improvement via the driver airbag.

Up to now, anecdotal field studies of driver and passenger airbag systems have provided the only available feedback as to their crash protection performance. A companion paper at this conference, by Huelke, Roberts & Moore (91-S1-W-19), documents the largely positive perception the public, safety advocates, and the U.S. automobile industry have regarding inflatable supplemental restraint systems. One would think that after a period of time that these accumulated events would demonstrate a statistically quantifiable reduction in the driver fatality rate.

Methodology

Using fatality data from the U.S. Department of Transportation Fatal Accident Reporting System (FARS), driver fatality rates of Chrysler cars built without and then with the driver airbag are compared to determine its effectiveness. While the driver airbag is intended to supplement lap-shoulder seat belts to reduce fatalities and serious injuries, only fatalities will be studied here because the National Accident Sampling System (NASS) data base which deals with both is much smaller than the FARS data base for making comparisons (5700 accident records/yr. vs 41000 accident records/yr.). Secondly, insurance industry casualty data are not collected in a format that is useful at this time for determining the effectiveness of the airbag.

Table 1 shows all Chrysler produced passenger carlines between 1987 and 1991 (imports and joint venture vehicles are omitted). Chrysler markets similar cars under more than one name and dealership network. For example, Dodge Spirit, Plymouth Acclaim, and Chrysler LeBaron Landau (M Body), are built from the same platform and for the purpose of this study, carlines from the same platform are combined. The vehicles included in this study are outlined in Table 1. One or two model years of fatality data are analyzed on either side of the introduction of driver airbags. A yearly production summary for U.S. sales is shown in Table 2. The vehicle exposure is computed from the monthly production and delayed two months to compensate for an assumed 60 day sales inventory. Because of the 60-day inventory, no 1991 model year vehicles built after 10/31/90 are included in the exposure computation.

Table 1. Chrysler Corporation Passenger Carlines by Model Year

Body Code	1987	1988	1989	1990	1991
AA			Dodge Spirit Plymouth Acclaim	Dodge Spirit Plymouth Acclaim Chrysler LeBaron	Dodge Spirit Plymouth Acclaim Chrysler LeBaron
AC		Chrysler New Yorker Dodge Dynasty	Chrysler New Yorker Dodge Dynasty	Chrysler New Yorker Dodge Dynasty	Chrysler New Yorker Dodge Dynasty
AE	Chrysler New Yorker Dodge 600 Plymouth Caravelle	Chrysler New Yorker Dodge 600 Plymouth Caravelle			
AG	Dodge Daytona	Dodge Daytona (1)	Dodge Daytona	Dodge Daytona	Dodge Daytona
AH	Chrysler LeBaron GTS Dodge Lancer	Chrysler LeBaron GTS Dodge Lancer	Chrysler LeBaron GTS Dodge Lancer		
AJ	Chrysler LeBaron	Chrysler LeBaron (1)	Chrysler LeBaron	Chrysler LeBaron	Chrysler LeBaron
AK	Chrysler LeBaron Chrysler Town & Country Dodge Aries Plymouth Reliant	Chrysler LeBaron Chrysler Town & Country Dodge Aries Plymouth Reliant	Dodge Aries Plymouth Reliant		
AL	Dodge Omni Plymouth Horizon Dodge Charger Plymouth Turismo	Dodge Omni Plymouth Horizon	Dodge Omni Plymouth Horizon	Dodge Omni Plymouth Horizon	
AM	Chrysler Fifth Ave. Dodge Diplomat Plymouth Gran Fury	Chrysler Fifth Ave. (1) Dodge Diplomat (1) Plymouth Gran Fury (1)	Chrysler Fifth Ave. Dodge Diplomat Plymouth Gran Fury		
AP	Dodge Shadow Plymouth Sundance	Dodge Shadow Plymouth Sundance	Dodge Shadow Plymouth Sundance	Dodge Shadow Plymouth Sundance	Dodge Shadow Plymouth Sundance
AY				Chrysler Fifth Ave. Chrysler Imperial	Chrysler Fifth Ave. Chrysler Imperial
BB		Eagle Premier	Eagle Premier	Eagle Premier Dodge Monaco	Eagle Premier Dodge Monaco

(1) Mid-Year Driver Airbag — 100% Driver Airbag — FARS Study Vehicles

Table 2. Driver Airbag Vehicle Production

Body Code	Driver Airbag	U.S. Market Production Model Year 1987	1988	1989	1990	1991 (1)	Total Vehicles	Vehicle (2) Exposure (Veh.*Yr.)	Relative Vehicle Size ~Curb Weight (KG.) (#)	Length (MM) (IN.)	Width (MM) (IN.)
AM	Without	145802	66987	0	0	0	212789	786779	1700	5250	1840
	With	0	7608	27233	0	0	34841	75108	3750	206.7	72.4
AC	Without	-	127153	208893	0	0	336046	717953	1391	4918	1741
	With	-	0	0	135809	43583	179392	115646	3066	193.6	68.5
AA	Without	-	-	131384	0	0	131384	214783	1282	4602	1730
	With	-	-	0	211197	91955	303152	184851	2827	181.2	68.1
AJ	Without	83531	63682	0	0	0	147213	485444	1300	4696	1740
	With	0	24769	91163	59236	16496	191664	283500	2875	184.9	68.5
AG	Without	33197	43944	0	0	0	77141	247254	1280	4552	1760
	With	0	22869	70388	38752	10937	142946	222488	2822	179.2	69.3
AP	Without	-	-	166767	0	0	166767	298371	1200	4361	1710
	With	-	-	0	134512	60246	194758	119149	2645	171.7	67.3
AL	Without	-	-	84943	0	0	84943	84943	1042	4146	1682
	With	-	-	0	32579	0	32579	32502	2296	163.2	66.8

(1) Production Through 10/31/90
(2) Vehicle Exposure Through 12/31/90

The FARS search was based on vehicle identification numbers (VIN) of the subject vehicles which are encoded with the make, model, model year, and type of restraint system on the vehicle.

Since airbags are primarily intended and assumed to offer supplemental protection in frontal accidents, this study will concentrate on their effectiveness in frontal and near frontal type accidents. These are represented in the FARS data as 11 o'clock to 1 o'clock principal impacts. All rollover first and most harmful events, as described in FARS, are deleted as well as all 2 o'clock to 10 o'clock principal impacts, top impacts, submersions and fires. The FARS search began with the 1986 calendar year to capture any fatalities in early 1987 model year vehicles built, sold and crashed in 1986, extended through 12/31/90, and includes some early is determined by summing the fatalities for each model before and after airbags, and dividing by the vehicle

years of exposure. The resultant driver fatality rate percentage change determines the driver airbags effectiveness for frontal accidents at the assumed constant seat belt usage rate.

The driver fatality rate is a function of vehicle crashworthiness, vehicle crash avoidance, the roadway environment, driver demographics and behavior, seat belt usage, and time period of study.

In this study it is assumed that the only significant change to these vehicles that would affect crashworthiness of each body style is the addition of a driver side airbag so that the change in fatality rate is attributable only to the driver airbag. There were no significant structural changes made to these vehicles which would affect the crashworthiness to accommodate the driver airbag.

In support of this premise, vehicle crash avoidance for every vehicle studied was unchanged over the period of study. Antilock brakes, traction control, crash avoidance radar, or drunk driver interlocks were neither introduced nor deleted from any of these vehicles during the period of study.

It is assumed that the roadway environment is essentially unchanged throughout the study. All fatalities occurred on U.S. roads. Comparisons are not being made between the U.S. and Spain or Peru, for example, and seasonal traffic and weather effects have been cancelled by including the entire calendar year.

Since Dodge Daytonas are being compared with Dodge Daytonas and Chrysler New Yorkers with Chrysler New Yorkers, demographic shifts are assumed to be negligible.

Data from the Insurance Institute for Highway Safety and the U.S. National Highway Traffic Safety Administration indicate that seat belt usage nationwide was relatively constant (1) at ≈47% (Figure 1) throughout the time period of study, and seat belt usage has been observed to be independent of driver airbag installation (2).

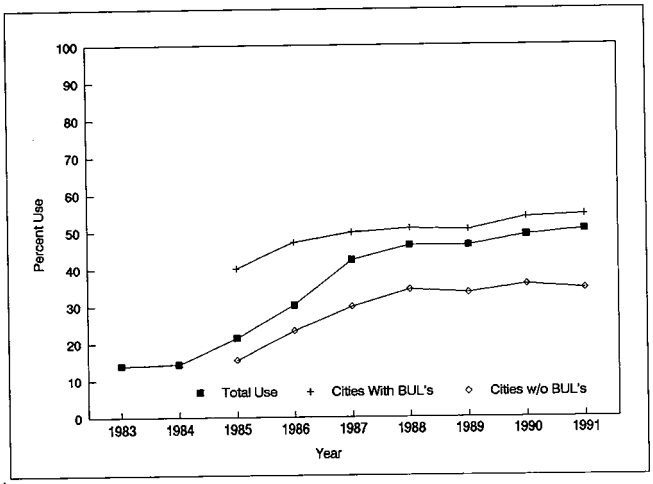

Figure 1. U.S. Driver Safety Belt Use: NHTSA 19 City Survey

Finally, overall motor vehicle fatality rates are assumed constant throughout the period of study, despite slight year-to-year improvement. Essentially all vehicles included in the study are exposed to the same highway environment at the same time. Comparisons between 1990 and 1960 are not being made.

Data Analysis

The FARS data sort produced 628 occupant fatalities for the seven models involved over the five calendar years studied (Table 3). Of these, there were 416 driver fatalities; 313 in non-airbag vehicles and 103 in airbag-equipped vehicles.

Table 3. 1986-1990 FARS Data—All Occupant Fatalities

Body Code	Without Driver Airbag Seating Position							With Driver Airbag Seating Position							
	Front			Rear			Un-	Front			Rear			Un-	
	Left	Center	Right	Left	Center	Right	Known	Left	Center	Right	Left	Center	Right	Known	
AM	88	0	31	4	1	9	4	3	0	0	0	0	0	0	
AC	40	1	15	1	1	1	0	6	0	0	1	0	1	0	
AA	15	0	7	1	0	0	0	14	0	6	2	0	1	1	
AJ	54	1	17	2	0	4	0	20	1	9	1	0	2	0	
AG	50	0	23	2	0	0	1	33	1	15	0	0	3	2	
AP	44	1	18	4	0	2	0	22	0	7	0	0	0	0	
AL	22	0	2	1	0	1	0	3	0	2	0	0	0	0	
Total	313	3	113	15	2	17	5	103	2	41	4	0	7	3	628

Since driver airbags are not intended to offer protection in non-frontal crashes, rollover accidents (as first harmful event and most harmful event in FARS terminology) are eliminated. Rollover fatality is frequently caused by ejection or impact with interior components for unbelted occupants. Similarly side, rear, and top impact most harmful events are removed from the data set along with fires and submersions. The resultant data set was reduced to 178 driver frontal crash fatalities (139 in non-airbag equipped vehicles and 39 in those with a driver airbag).

Because of the small sample sizes, the probability of fatality for each driver was equated to that of a 20 year-old male being fatally injured. This technique has been used by others (3)(5) to compensate for inevitable demographic differences on fatal injury susceptibility.

Table 4 is a summary of the data analysis for each body style with and without a driver airbag. Included in the summary are the number of vehicles produced, their exposure in vehicle years on U.S. highways, the number of driver fatalities, average driver age, age range, ratio of the males to females, seat belt use, and the equivalent number of 20 year-old male fatalities. Finally the "normalized" frontal fatality rate is computed and a percentage change determined for each body style.

Because of the small sample sizes, there is considerable sensitivity and variability in the fatality rate percent change. As one can see, the percent change in fatality rate ranges from -61.7% (AL Body) to a +60% (AC Body). Figure 2 illustrates the fatality rate variability and inconsistencies between body styles.

One would rather not have to make an estimate of the effectiveness of the driver airbag on data with such a high degree of variability, but that was one of the

Table 4. 1986-1990 FARS Data Analysis for Chrysler Cars—11 O'Clock-1 O'Clock Frontal Collisions Only

Without Driver Airbag

Body Code	U.S. Vehicles	Vehicle Exposure (Veh*Yr)	Driver Fatals	Driver Frontal Fatality Rate (Million Veh*Yr)	Drivers Average Age (Yr)	Age Range (Yr)	Male-Female	Seat Belt Use Yes-No-Unknown	20 Year Old Male Equiv. Fatals	Normalized Driver Frontal Fatality Rate (Million Veh*Yr)		R.F. Passenger Fatals
AM	212789	786779	36	45.76	61.6	29-81	21-15	11-24-1	14.29	18.16		15
AC	336046	717953	20	27.86	55.1	31-77	15-5	9-10-1	8.70	12.12		7
AA	131384	214783	9	41.90	52.2	30-83	6-3	4-5-0	4.70	21.88		6
AJ	147213	485444	22	45.32	40.0	16-83	12-10	5-13-4	13.56	27.93		11
AG	77141	247254	15	60.67	32.2	17-78	9-6	3-12-0	11.04	44.65		7
AP	166767	298371	21	70.38	37.1	16-74	13-8	6-11-4	14.17	47.49		8
AL	84943	148925	16	107.44	42.9	19-78	13-3	5-9-2	9.96	66.88		0
Total	1156283	2899509	139				89-50	43-84-12	76.42			54

With Driver Airbag

Body Code	U.S. Vehicles	Vehicle Exposure (Veh*Yr)	Driver Fatals	Driver Frontal Fatality Rate (Million Veh*Yr)	Drivers Average Age (Yr)	Age Range (Yr)	Male-Female	Seat Belt Use Yes/No/Unknown	20 Year Old Male Equiv. Fatals	Normalized Driver Frontal Fatality Rate (Million Veh*Yr)	Normalized Driver Frontal Fatality Rate Percent Change	R.F. Passenger Fatals
AM	34841	75108	2	26.63	41.0	38-44	2-0	1-1-0	1.16	15.44	-15.0	0
AC	179392	115646	5	43.24	53.6	28-79	2-3	1-4-0	2.25	19.41	60.2	0
AA	303152	184851	5	27.05	44.0	24-65	2-3	3-2-0	2.78	14.93	-31.8	4
AJ	191664	283500	5	17.64	35.2	19-56	4-1	1-2-2	3.38	11.92	-57.3	3
AG	142791	222488	12	53.94	32.6	18-69	7-5	5-7-0	8.68	39.01	-12.6	5
AP	194758	119149	8	67.14	31.1	16-69	8-0	4-3-1	6.46	54.39	14.5	1
AL	32579	32502	2	61.53	59.5	46-73	2-0	1-1-0	0.83	25.63	-61.7	2
Total	1079177	1033244	39				27-12	16-20-3	25.54			15
Average											-14.8	

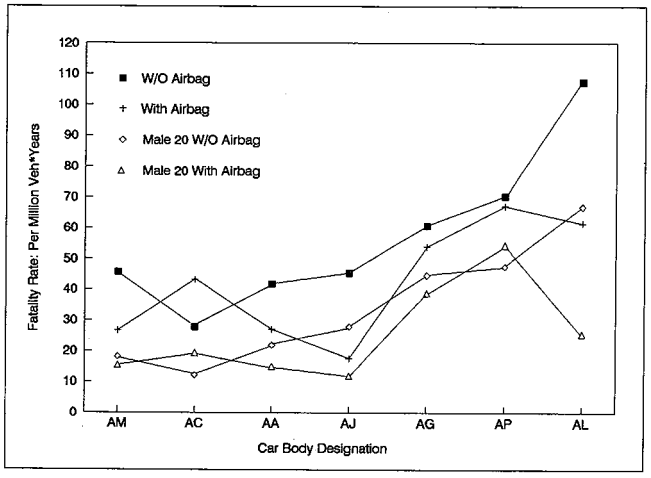

Figure 2. Carline Frontal Fatality Rates With and Without Driver Airbag

compromises recognized initially with this study. To have abundantly adequate data might require several more years of exposure thus delaying any early quantitative feedback estimate.

There are several choices one can make in combining the carline driver fatality rate changes for a single effectiveness estimate. Using either an exposure-weighted or vehicle-weighted average misrepresents the airbag fleet versus the non-airbag fleet because some cars were introduced with airbags earlier than others. Specifically, the vehicle exposure volume fractions by body style are not equivalent for the before and after airbag installation. Similarly, a vehicle-weighted comparison is biased. Once again the volume fractions by body styles are not equal for the non-airbag fleet and the airbag fleet because of the way the FARS data were chosen to surround the introduction of the driver airbag. As a result, a simple average of the body style fatality rates was used to compare the fatality rates before and after airbags and determine an average driver airbag effectiveness of 14.8% for a seat belt usage of 47%.

In an alternative analysis to this aggregate seat belt use analysis, each seat belted and unbelted driver fatality is used to compute a driver airbag effectiveness. One reasons that the driver fatality rate for any body style before and after the driver airbag should be identical if all drivers were unrestrained by seat belts or airbags. What this amounts to is adjusting the fatality data upward based on the restraint systems effectiveness as if they were disconnected. Since the fatality rates between the airbag and non-airbag vehicles are not equal, the effectiveness of the driver airbag must account for the difference, all other fatality rate factors being equal.

For example, we know that some people wear seat belts and some of them unfortunately are killed in frontal accidents. If none wore seat belts, many more would have died.

Adding the un-seat-belted fatalities to the seat-belted fatalities, and estimating how many more would have died had no one worn seat belts, leads to an unrestrained fatality rate when divided by the vehicle exposure. (Eq. 1 and 2).

$$NAUDFFR = \frac{NAUDF + \frac{NABDF}{(1 - SBE)}}{VENA} \quad (1)$$

where

NAUDFFR = non-airbag unrestrained driver frontal fatality rate
NAUDF = non-airbag unbelted driver fatalities
NABDF = non-airbag belted driver fatalities
SBE = seat belt effectiveness
VENA = vehicle exposure—non-airbag vehicle

Similarly

$$AUDFFR = \frac{\frac{AUDF}{(1 - AE)} + \frac{ABDF}{(1 - (SBE + IAE))}}{VEA} \quad (2)$$

where

AUDFFR = airbag unrestrained driver frontal fatality rate
AUDF = airbag unbelted driver fatalities
ABDF = airbag belted driver fatalities
AE = airbag effectiveness without seat belts
IAE = incremental airbag effectiveness with seat belts
VEA = vehicle exposure—airbag vehicle

Setting equation 1 equal to equation 2, and substituting normalized fatality data for each carline and a generally accepted seat belt effectiveness, one can estimate the driver airbag effectiveness for an assumed incremental effectiveness of seat belts with airbags (Eq. 3).

$$AE = 1 - \frac{\frac{ABDF}{1 - (SBE + IAE)} + AUDF}{VEA \times NAUDFFR} \quad (3)$$

Assuming that there is no incremental effectiveness from airbags (IAE = 0) for the seat belted driver, in equation

3, one can see that this assumption maximizes the airbag effectiveness estimate for the unbelted driver. For no incremental effectiveness, unbelted driver airbag effectiveness ranges from 60% for AL body to -42% for AC body with an average of 10.5%. At five percent incremental effectiveness, the unbelted effectiveness ranges from 58% for AL body to -46% for AC body with an average of 6.1%.

Discussion of Results

Both methods of assessment show similar body style effectiveness trends and variability. While the effectiveness of the driver airbag can be body style dependent because of weight, size and demographic differences, it should not be negative and the distribution of effectiveness should take some familiar pattern (e.g., normal, uniform or lognormal, etc.) unless there is too little data (i.e., small sample sizes). Because of expected differences in body style to body style driver airbag effectiveness, the overall absolute effectiveness will then be sales mix dependent.

As one can see in Table 4 and Figure 2, the fatality rates for drivers of AC and AP bodies are higher with airbags than without, which is unexpected and not what anyone wants to believe. Besides the small sample size explanation, the seat belt use of AC body driver fatalities with an airbag (≈20%) and without an airbag (≈50%) runs counter to most other body styles and the all body averages. As for the AP body, the male-to-female ratio is considerably different for the airbag and non-airbag vehicles which may explain this unexpected change. Both of these vehicles will be particularly interesting to follow-up on when more FARS data are available.

Similarly, the unexpected large fatality rate reductions for AJ and AL bodies can be explained by small sample sizes and the average age differences for the AL body drivers with and without an airbag.

One data set that correlates well with the initial assumptions is that for the AG body (Dodge Daytona). For the airbag and non-airbag equipped vehicles, the vehicle exposure, average age, age range, and gender ratio are very similar. As one would expect, the ratio of unbelted to belted fatalities is lower for the airbag equipped vehicles, and this time that is true for the AG body too. If an overall effectiveness could be estimated from just one of the body styles studied, the AG body (Dodge Daytona) would be best one to choose with its 12.6% reduction and its intuitive correlation with the basic assumptions.

For the second analysis method, where belted and unbelted driver fatalities are recombined as totally unrestrained occupants, the body style to body style percent effectiveness estimate is plagued by the small sample size and demographic factors as discussed earlier. AC and AP bodies show large negative effectiveness. Even the AG body data, favored because of its data consistency with the original assumptions, has now projected a slightly negative effectiveness. (Remember, a negative percent change in fatality rate is a positive effectiveness and vice versa). An interesting aspect of this approach is that the seat belt use rate is not an explicit factor, however one must contend with the accuracy of FARS seat belt data, seat belt effectiveness and assumptions of the incremental seat belt-airbag system effectiveness.

As mentioned earlier, as the incremental effectiveness assessment increases, the unbelted driver airbag effectiveness assessment decreases. If a 5% incremental airbag effectiveness is assumed, for the *belted* driver (as estimated by Evans (4)), based on the limited current fatality data the effectiveness of the driver airbag in reducing *unbelted* driver fatalities reduces to an average 6.1%. This incremental system effectiveness may be better estimated when more data are available through a comparison of the ratios of unbelted driver fatalities to belted driver fatalities for vehicles with and without an airbag through the double pair comparison process.

Also in Table 4, the far right column shows the right front passenger fatalities for these vehicles and demonstrates the insufficiency of these data for a double pair comparison at this time. Ratios with zeros in the denominator are meaningless.

In conclusion, every effort has been made to honestly and objectively present the early indications of driver airbag effectiveness based on limited exposure of only Chrysler Corporation products on U.S. roads. In dealing with small sample census data, no claim of statistical significance is made for the estimated effectiveness, but these preliminary results provide no reason to question the credibility of driver airbag effectiveness estimates by NHTSA, Evans, Huelke et al., and Wilson and Savage ranging from 17% to 40% (4). Because of certain unsurvivable frontal impacts, a growing more-fragile older population, and unbelted drivers, a driver airbag cannot be expected to guarantee immortality for all drivers in all frontal collisions. Although a statistically significant reduction in driver fatalities due to the driver airbag performance has not been proven in this evaluation, it has demonstrated that there is life saving potential in the driver airbags performance.

From the scarcity of fatality data, and especially injury data, it has been a challenge to determine the overall effectiveness of the driver airbag to prevent any fatalities, much less the incremental life saving benefit to the belted driver. More data over the next couple years will allow analysis to converge on the true effectiveness of airbags in preventing fatalities as well as serious injuries for both the belted and unbelted driver. It is reasonable to believe that a substantial degree of the overall effectiveness will be in the mitigation of serious injuries.

Acknowledgements

The author wishes to recognize the following for their contributions to this paper: My Chrysler management for its encouragement to undertake the project. Mr. Terry Klein and Ms. Judith Hilton of NHTSA for providing the FARS data requested. Mr. Yunyong Hongsakaphadana, of Chrysler's technical computer center, who sorted the FARS data at the author's direction. Mr. Al Slechter and Mr. Howard Willson of Chrysler for their critical reviews. Ms. Maxine Farley (Chrysler) for typing the manuscript with its interminable editorial refinements.

References

1. NHTSA, Office of Driver and Pedestrian Research, "Occupant Protection Trends in 19 Cites," May 1991.
2. "IIHS Status Report," Vol. 25, No. 6, June 30,1990.
3. *Traffic Safety and the Driver*, Leonard Evans, 1991, Van Nostrand Reinhold, pp. 25-28.
4. Ibid., pp. 241-245.
5. "The Effectiveness of Automatic Seat Belts in Reducing Fatality Rates in Toyota Cressidas," Carl E. Nash, NHTSA, June 1989.

S9-O-12

The Need for Improved Structural Integrity in Frontal Car Impacts

C. Adrian Hobbs
Transport and Road Research Laboratory

Abstract

Despite the use of seat belts, frontal impacts pose the greatest accident threat to car occupants. The major cause of serious and fatal injuries arises from occupant contact with intruded parts of the car structure. Relevant legislation, to control passenger compartment intrusion, is limited to a rigid block impact, at 50 km/h. In Europe the only mandatory requirement, in this test, relates to rearward displacement of the steering wheel. Research is showing the need for a test which is both offset and uses a deformable impact face. A list of proposed criteria for a new test procedure is presented and details of one such offset deformable impact test are given.

Introduction

Even in Great Britain, where seat belt wearing rates are high, car occupants involved in frontal impacts account for the largest group of road accident casualties. The major cause of their injuries is contact with intruding parts of the car's structure. The current 50 km/h block impact test has frequently been criticized as being inadequate (1,2,3). Modern cars suffer little or no intrusion in this test, even when carried out at 60 km/h. However, in accidents the same cars suffer substantial intrusion at similar or lower impact speeds. If the intrusion problem is to be addressed, a new test procedure is required which will require the car's structure to absorb energy in the test in the same way that it does in accidents.

Accident Analysis

Car occupant accidents account for more than half (56%) of the 340,000 road accident casualties each year in Great Britain (4), even though seat belt wearing rates, amongst front occupants, exceed 90 percent (5). In-depth accident investigations have shown that about two-thirds of these car occupant casualties occur in impacts with another car and just over two-thirds are involved in frontal or oblique-frontal impacts (6). Usually, only part of the car's front is involved. In about 45 percent of cases only the outer third of the car's front is impacted and in a further 33 percent the impact involves up to two-thirds of the front. The whole front is involved in only about 17 percent of cases. Even then the loading on the car is usually asymmetric.

The wearing of seat belts has done much to reduce injuries in frontal impacts. However, belt wearers are still being injured. These injuries occur either because of direct seat belt loading or because the seat belt is unable to prevent the wearer from hitting parts of the car's interior. The occurrence of passenger compartment intrusion increases the likelihood of such occupant contact, if the seat belt ride down space is infringed. About two thirds of all serious (AIS≥3) injuries suffered by belted occupants have been shown to be caused by contact with intruding parts of the car structure. In contrast, the incidence of serious injuries from seat belt loading is very small. More than ninety percent of all seat belt induced injuries are minor (AIS 1) bruises.

There would be no benefit in adopting measures to limit intrusion if deceleration forces alone would produce injuries of similar severity. Analysis of impact test data shows that asymmetric impacts result in very similar decelerations on both sides of the car (Fig 1). Consequently, seat belt loads are also similar for both front seat occupants. Accident cases where passenger compartment intrusion has been limited to only one side of the passenger compartment have been used to study further the relative importance of intrusion and deceleration. In the majority of such cases, where two belted front seat occupants were present, the injuries to the occupant exposed to intrusion were more severe than for the other occupant. The UK Co-operative Crash Injury Study (7) has investigated accidents involving over 9000 occupants. In the study there were 238 cases where the above comparison was possible. In 49 cases at least one of the

front seat occupants was seriously injured (MAIS≥3). In 44 (90%) cases the occupant exposed to intrusion suffered greater injury than the occupant not exposed to intrusion. In only four cases was the reverse true and in one case the injury severity was the same. There were five cases where occupants sustained critical or greater injury (MAIS≥5) on the intruded side and the occupant on the other side suffered minor or no injury (MAIS≤1). In a further 27 cases, serious or severe injuries (MAIS ≥3) were suffered by the occupant exposed to intrusion where again the occupant not exposed to intrusion escaped with minor or no injury (MAIS≤1). In over a third of these cases (36%) the intrusion was on the passenger's side. So the difference in injuries could not be due solely to the presence of the steering assembly.

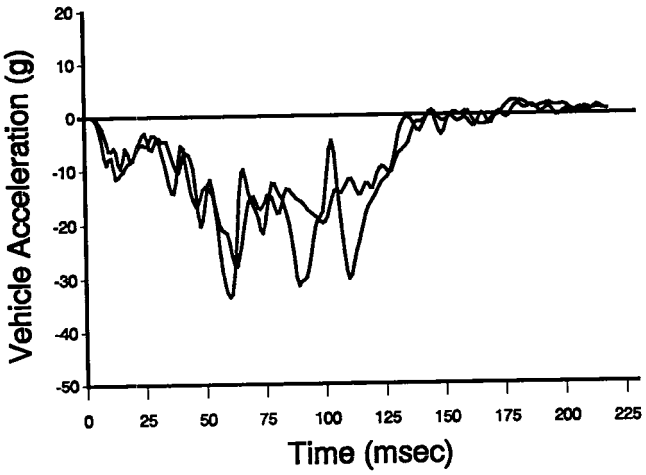

Figure 1. Fore/Aft Acceleration of Left and Right Outboard Seat Belt Mounts in 40 Percent Offset Impact Against a Deformable Block

The overwhelming predominance of intrusion and contact related injury strongly suggests that benefits would arise from its reduction, even at the expense of greater deceleration and consequently higher seat belt loads.

Fatality Study

A detailed fatal accident injury analysis is being carried out, using recent UK crash injury data. In order to avoid confusion over injury mechanisms, only 'simple' frontal impacts are being studied. Simple impacts have been defined as ones in which only one noteworthy impact occurred, without the car overturning. Improving protection in such impacts should also improve protection in more complex accidents.

Of the 52 fatal cases studied so far, six (12%) involved frontal impacts with an angled approach and 45 (87%) had impacts which were purely frontal. One case could not be determined. Car to car impacts accounted for 32 (62%) of cases. Five (10%) cases involved impacts with a roadside object, five (10%) involved a light goods vehicle and eight (15%) involved a Heavy Goods Vehicle. One impact was with a horse and one was unknown. Two (4%) cases involved under-run and three (6%) were sideswipes. The whole front of the car was involved in 12 (23%) of cases, compared with 14 (27%) having up to 1/3 overlap and 19 (37%) having between 1/3 and 2/3 overlap. In one case, only the central third of the car's front was involved. Even for this small sample, these statistics are very similar to those reported from other analyses.

Vehicle Damage. In a front engine car, the involvement of the structure on either side of the engine compartment affects how the impact energy is absorbed by the car's structure. In this fatal accident sample, only one side was involved in 33 (63%) cases and both sides were involved in 15 (29%) cases. However, in five of these fifteen cases, one side was loaded substantially more than the other.

What happens to the main longitudinal box sections, which form part of these side structures, is also important. In only eight (15%) cases were both longitudinals involved and in three of these cases the loading was primarily on one of them. In 29 (56%) cases only one longitudinal was involved, and in four of these the longitudinal was only partly involved. In 14 (27%) of the cases neither longitudinal was involved and one case was unknown.

In all of these accidents, only part of the front structure has been used to absorb the impact energy. Even within the structures involved, the loads were frequently not directed into the stiff longitudinals, which have the greatest energy absorption capability.

Passenger Compartment Intrusion. Passenger compartment intrusion occurred in all but nine (17%) of these fatal cases. The intrusion was extensive or very extensive in 29 (56%) cases, moderate in ten (19%) cases and light in three (6%) cases. The extent of the intrusion was not simply dependent upon impact severity but was much more dependent upon how the structure had been loaded. Most frequently the intrusion was confined to the impacted side of the car.

Occupant Details. Thirty five (67%) of the fatally injured occupants were drivers, 14 (27%) were front seat passengers and three (6%) were rear seat passengers. Seat belts were worn by 42 (86%) of the fatally injured front seat occupants. In seven (14%) cases, fatally injured front seat occupants were subjected to additional loading from behind. Five of these cases involved loading from unrestrained rear seat occupants. Thirty three (63%) of the fatal casualties were male compared with 19 (37%) being female.

The fatal casualties were rather older than might have been expected in the car user population. Nineteen (37%) were over sixty compared with 26 (50%) being aged between thirty and fifty-nine and only seven (13%) were below twenty. It is not clear to what extent this is because of the increased susceptibility of the elderly to injury.

Occupant Injuries. The majority of fatal injuries were to the head, thorax or abdomen. The 52 fatalities

sustained 24 AIS≥3 injuries to the head, 38 AIS≥3 injuries to the thorax and 22 AIS≥3 injuries to the abdomen. It was not always possible to determine precisely how many injuries caused death but an attempt was made. It appears that 31 (60%) deaths resulted from a single fatal injury, seven (13%) resulted from two injuries, three (6%) from three injuries, two from four injuries and one from five injuries. One case could not be determined. There were some injury complications, six (12%) were probably related to old age, seven (13%) to poor health and four (8%) to some post injury complication.

Remedial Measures. Although difficult, an attempt has been made to determine what remedial measures could prevent the serious and fatal injuries.

- HEAD: Of the 26 casualties with moderate or greater (AIS≥2) head injury, 13 (50%) might have benefitted from reduced intrusion alone, seven (27%) from reduced intrusion in combination with other improvements, three (12%) from improved restraints alone and three from other improved features such as to the steering assembly. In 17 (65%) cases it was thought that protection against the injury was very probable or certain. In a further five cases it was assessed as probable, with one case possible and two cases unlikely. One was unknown.
- THORAX: In the 41 cases of thorax injury (AIS ≥2), intrusion reduction alone might have benefitted 13 (32%) cases and reduced intrusion with other improvements, including improved restraints, might have benefitted a further 13 (32%) cases. Improvements to the restraint system alone might have helped in eight (20%) cases and improved restraints, with other improvements, including reduced intrusion, might have benefitted a further 11 (27%) cases. Protection was thought to be very probable or certain in 21 (53%) cases, probable in five (12%) cases, possible in eight (20%) cases and unlikely in six (15%) cases. One was unknown.
- ABDOMEN: Abdominal injury (AIS≥2) was seen in 22 cases. Seven (32%) of these might have benefitted from reductions in intrusion alone, seven (32%) from reductions in intrusion with other improvements. Six (27%) would have benefitted from improved restraints alone and seven (32%) from improved restraints, in combination with other changes. In 18 (82%) cases protection was thought to be very probable or certain, in two cases it was possible and in two cases it was unlikely.

In accordance with earlier findings, this analysis confirms that the priority for reducing the number of fatalities in frontal impacts is to reduce passenger compartment intrusion. It is recognized that the analysis is based on a relatively small sample of fatally injured occupants using a necessarily subjective assessment technique.

Energy Absorption and Passenger Compartment Intrusion

In a frontal impact, the passenger compartment collapses when insufficient impact energy is absorbed by the structure ahead of it. This may be because the impact is so severe that it is beyond the capability of any acceptable frontal structure to absorb all the energy. However, in the majority of cases inadequacies in the car's design have resulted in the front structure being incapable of absorbing sufficient impact energy. In some cases the passenger compartment collapses in preference to the front structure, because its 'dynamic stiffness' is lower. In other cases, structures which are capable of absorbing the impact energy do not have the forces directed into them.

With manufacturers using legislative impact tests in the development of new cars, it is essential for these tests to reflect adequately what is required for protection in real accidents. Currently the only European requirement which addresses passenger compartment integrity is the 50 km/h perpendicular block impact (8). Primarily, this test controls the extent of steering wheel intrusion. Further requirements exist for passenger compartment intrusion, but they are not mandatory (9) in most countries.

In the United States a similar impact test is required but in this test the assessment is made using an anthropometric dummy (10). The US requirement also calls for compliance at approach angles of up to ±30°. A more severe perpendicular block test, at 35 mile/h, is used for the US New Car Assessment Programme (11).

Even in Europe, many manufacturers use the 30° angled block impact for 'in house' testing. Usually, they aim to comply with the 'non-mandatory' European intrusion requirements. Despite this, car structures do not perform in accidents as well as they do in block impact tests. Most current production cars survive perpendicular or 30° angled block tests with little or no passenger compartment intrusion. Even when impacted at 60 km/h intrusion levels are usually low (Fig 2). However in typical accident impacts, these same cars suffer excessive levels of intrusion at similar or lower impact speeds (Fig 3).

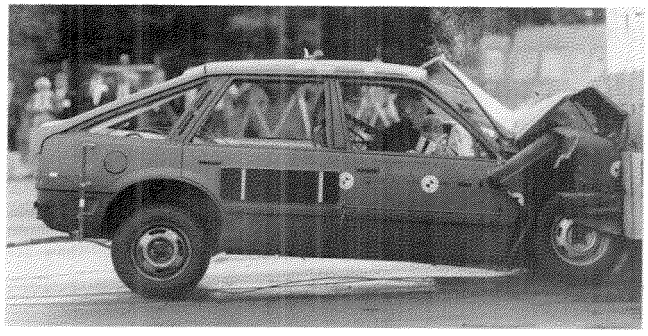

Figure 2. Perpendicular Rigid Block Impact, at 60 km/h, Showing Little Intrusion

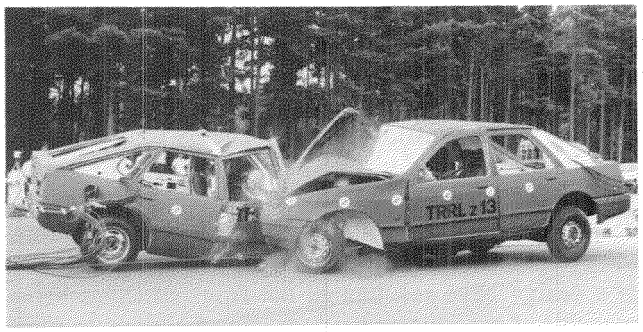

Figure 3. Forty Percent Overlap Car-to-Car Impact, at 50 km/h, Showing Passenger Compartment Intrusion

Comparison of Accident and Block Impacts

Greater levels of intrusion are seen in accident impacts, compared with block impacts, because of differences in how the car's structure is loaded. This in turn gives rise to differences in the way the impact energy is absorbed. The main differences so far identified are related to:

1. Force distribution across the car's width
2. Force transfer into main longitudinal box sections
3. Forces imposed on the engine
4. Failure initiation of longitudinal box sections
5. The presence of non-axial loads

Anything which reduces the capability of the front structure to absorb the impact energy increases the likelihood of passenger compartment collapse. This is because any energy which cannot be absorbed within the front structure must be absorbed by deformation of the passenger compartment behind it.

Force Distribution Across the Car's Width

In a perpendicular block impact, the front structure of the car is evenly deformed across its entire width (Fig 4). However, in the majority of accidents the structure on just one side of the engine compartment takes most of the load (Fig 5). With little compressible structure within the engine compartment, or ahead of it, little energy can be absorbed in the central part of the car's front. If intrusion is to be avoided, it is necessary for virtually all the impact energy to be absorbed within a single side of the frontal structure.

Force Transfer into Main Structural Box Sections

Within a frontal side structure there are both stiff and weak components, with the main longitudinal box sections usually being the stiffest parts. If these deform in axial collapse they can absorb substantial amounts of impact energy; but for this to happen it is necessary for the impact loads to be directed into them. This is not a problem in a rigid block impact, as the block ensures that both stiff and weak parts are constrained to deform equally.

In a typical accident impact, it is unusual for the stiff structures on each car to line up. Usually these small

Figure 4. Full Width Perpendicular Block Impacted Car, Showing Uniform Deformation

Figure 5. Car After 40 Percent Overlap Car-to-Car Impact, Showing Asymmetry and Weak Structure Deformed More Than Stiff Structure

areas of stiff structure line up with areas of weaker structure on the other car. As a result, the weak structures deform in preference to the stiff structures. The stiff box sections may not deform very much or their collapse may be delayed.

A delay in the collapse of the stiff structures has another effect. In most cars, the front structure is weak towards the top and stiff lower down. This delay can cause the top part of the front structure to deform earlier than the bottom part and may lead to more intrusion at facia level. This differential collapse also generates vertical bending forces within the front structure, which may further reduce its energy absorption capability, by promoting bending rather than axial collapse.

Computer simulation models have been used to study impacts into rigid and deformable faced blocks. In an impact with a rigid block, the stiff lower structure and the weak upper structure are constrained to deform

together. In impacts into a deformable face, differential motion can occur between the upper and lower parts of frontal structures (Fig 6). In such cases, the collapse of the weak top structure precedes that of the stiff lower structure. Further into the impact, the lower structure collapses more rapidly, being loaded more as the stiffness of the lower part of the deformable face increases. In the example shown, the upper and lower parts eventually end up with about the same extent of deformation, which is similar to that seen after an impact. This differential rate of collapse may explain why facia level intrusion is more pronounced in car to car impacts than in rigid offset block impacts.

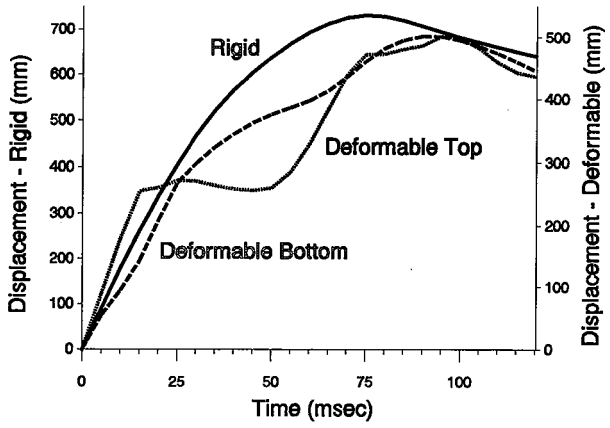

Figure 6. Displacement of Car Front in Simulation of Rigid and Deformable Impacts

Forces Imposed on the Engine

When a front-engine car hits a rigid block, its engine must stop very rapidly. For this to happen, very high forces have to be generated within the structure ahead of the engine. These high forces lead to substantial amounts of impact energy being absorbed by small deformations within this structure.

When brought to rest, the engine transmits loads onto the firewall. This part of the firewall is relatively stiff, being supported by the floor tunnel, and again substantial amounts of energy may be absorbed within small amounts of deformation. In full width rigid block impacts, about half of all the impact energy may be absorbed in this way.

In typical accident impacts, the structure of the other car is incapable of generating these high forces, so comparatively little energy is absorbed in this manner. Consequently, other parts of the car body have to absorb much more energy.

Computer simulation models have shown how the motion of the engine in the car differs when rigid and deformable impacts are compared. With the rigid block, the engine moves forward for a short time while the structure immediately in front of it crushes. It is then rapidly decelerated. This shows up as rearward motion relative to the car body (Fig 7). With a deformable face on the block the engine continues to move forward in the body for a long time, before the forces generated by the deformable face are sufficient to drive it backwards into the car body.

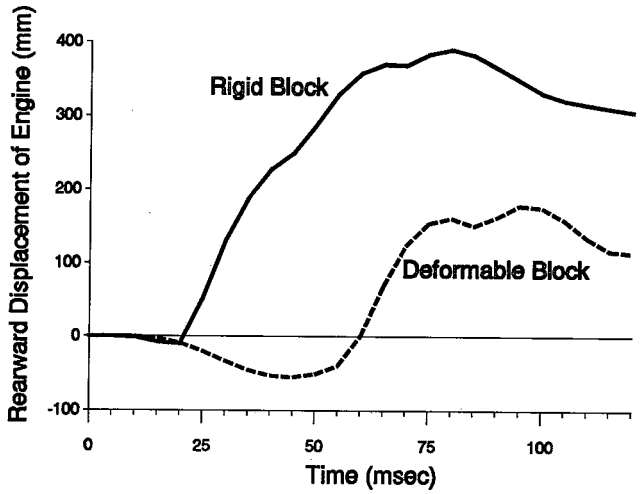

Figure 7. Engine Displacement Within Car, in Rigid and Deformable Impacts

Failure Initiation of Structural Box Sections

The front longitudinal box sections are relatively stiff structures which fail in axial collapse. Usually, substantial forces are needed to initiate their failure. When they do collapse, they can absorb large amounts of energy, in the form of strain energy. They will not absorb energy if they do not collapse or if they are simply displaced backwards, crushing the structure behind them (Fig 8).

In a rigid impact, the front of a longitudinal box section is brought to rest almost instantaneously. This generates very high inertial forces within it, which can be used to initiate failure. In a non-rigid impact, this rapid deceleration does not occur and the high inertial forces are absent. In such impacts, the box section may not collapse or again the collapse may be delayed.

The Presence of Non-Axial Loads

In about 15 percent of frontal impacts, the impact loads are not directly parallel to the longitudinal axis of the car. This may be because the approach direction is slightly oblique or because of rotation during the impact. Such non-axial loads generate horizontal bending moments in the frontal box sections which try to bend them sideways. Where this causes longitudinal box sections to fail in bending, rather than axial collapse, their energy absorption capacity can be substantially reduced. Testing into an angled block does not guard against structures which fail in this way as the main forces, which are due to inertia, still act longitudinally along the car.

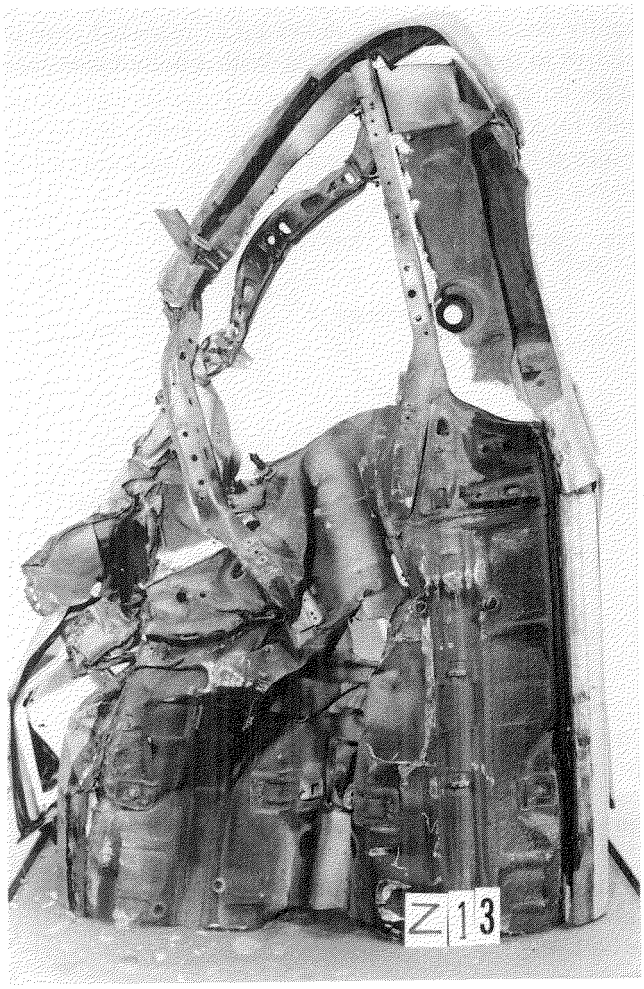

Figure 8. Car Underside After 40 Percent Overlap Car-to-Car Impact, Showing Uncollapsed Box Section on Impact Side

Requirements of an Improved Frontal Test Procedure

If future car structures are to be developed with better intrusion resistance in accidents, a more realistic test is required. Such a test does not have to be 'representative' of any particular impact type, but it does need to be capable of guiding car design towards structures which can perform adequately over a range of accident impact types. To do this it must require the car to absorb the impact energy in a realistic manner. The desirable characteristics of such a test, which have so far been identified, are:

1. Offset impact, primarily to load one side of the car's structure.
2. Non-rigid impact, so that the car must be designed to direct loads into the main energy absorbing structures.
3. Impact which cannot generate unrealistically high loads on the engine.
4. Impact which will not generate unrealistically high inertial loads to help initiate failure of energy absorbing structures.
5. Presence of non-axial forces, to guard against structures designed for purely axial loading.

Frontal Impact Testing at TRRL

Recent frontal impact testing at TRRL has provided information about the behavior of vehicle structures in different types of impact. Much has been learnt about how impact energy is absorbed with a view to understanding how passenger compartment intrusion may be prevented.

Over twenty full scale crash tests have been carried out, using different impact configurations. These tests have included offset and angled car to car impacts, perpendicular, offset and angled rigid block impacts. In order to overcome most of the problems listed above, a new test configuration is being studied. This involves a 40% overlap impact into a block fitted with a deformable face (Fig 9). This test configuration goes a long way towards meeting the requirements set out above. However, it does not take into account the requirement for non-axial forces. It is not yet clear how this particular requirement can be incorporated into a simple test procedure. It could be incorporated with a mobile deformable barrier test, which will be examined in the future.

Figure 9. Forty Percent Overlap Impact into Deformable Faced Block

Tests with this configuration have indicated that it uses mechanisms for energy absorption which are similar to those observed in car to car impacts. The tests have also produced much more realistic damage patterns than those seen with other configurations. Comparison with in-depth accident studies has shown that the car deformation is similar to that most frequently occurring in accidents.

Conclusions

Accident investigations have revealed that the structural collapse of car passenger compartments is the major cause of serious and fatal injuries to belted occupants in frontal impact accidents. Passenger compartment collapse is seen in accidents at impact speeds less than the 50 km/h of the legally required frontal block impact test, in which intrusion seldom occurs. These differences have been shown to be due to differences in the way impact energy is absorbed.

A set of requirements has been proposed for an improved test procedure. A partial overlap impact test into a deformable faced block meets most of these requirements, producing damage patterns which closely match those commonly seen in accidents, and absorbing the impact energy in a realistic manner.

Research is continuing to develop the test method further, study the behavior of car structures in impacts, and to identify legislative requirements which can best achieve improvements in car occupant protection.

Acknowledgement

The work described in this paper forms part of the programme of the Transport and Road Research Laboratory. It was commissioned by the Vehicle Standards and Engineering Division of the Department of Transport. The paper is published by permission of the Director.

References

1. Thomas, C., S. Koltchakian, C. Tarriere, C. Got and A. Patel, *Inadequacy of 0° Barrier Test With Real World Frontal Accidents*, Proceedings of the Twelfth International Technical Conference on Experimental Safety Vehicles, Gothenburg, 1989.
2. Pletschen, B., R. Herrmann, I. Kallina and F. Zeidler, *The Significance of Frontal Offset Collisions in Real World Accidents*, SAE International Congress and Exposition, Detroit, 1990.
3. Hobbs, C. A., *Essential Requirements for an Effective Full Scale Impact Test*, SAE International Congress and Exposition, Detroit, 1990.
4. Road Accidents Great Britain 1989, Department of Transport, HMSO, London, 1990.
5. Broughton, J., Restraint Use by Car Occupants, 1982-1989, TRRL Research Report 289, Crowthorne, 1990, The Transport and Road Research Laboratory.
6. Hobbs, C. A., Car Occupant Injury Patterns and Mechanisms, Proceedings of the Eighth International Technical Conference on Experimental Safety Vehicles, Wolfsburg, 1980.
7. Mackay, G. M., S. J. Ashton, M. D. Galer and P. D. Thomas, *The Methodology of In-Depth Studies of Car Crashes in Britain*, SAE International Congress and Exposition, Detroit, 1985.
8. ECE Regulation 12, *Uniform Provisions Concerning the Approval of Vehicles with Regard to the Protection of the Drivers Against the Steering Mechanism in the Event of Impact*, United Nations, Geneva, 1975.
9. ECE Regulation 33, *Uniform Provisions Concerning the Approval of Vehicles with Regard to the Behavior of the Structure of the Impacted Vehicle in a Head on Collision*, United Nations 1975.
10. NHTSA, FMVSS 208, *Occupant Crash Protection*, United States Department of Transport.
11. Hackney, J. and V. Quarles, *The New Car Assessment Program—Status and Effect*, Proceedings of the Ninth International Technical Conference on Experimental Safety Vehicles, Kyoto, 1982.

S9-O-13

Frontal Impact Protection Requires a Whole Safety System Integration

C. Tarriere, C. Thomas, X. Trosseille
Renault

Abstract

Beyond the generalization of the belt wearing, the improvement of the frontal impact protection is one of the most efficient action to reduce the number of the severe road victims. However, the attempt to evaluate the potential gains shows some important limitations to this efficiency and indicates the necessity of complementary actions. Among them:

- the front-end of the trucks needs to be modified to avoid underide and too severe decelerations of car occupants,
- due to the interaction between the protection in frontal and in lateral impact, the gain in frontal could be lost by an increase of the aggressiveness of the impacting car in side collisions,
- in car-to-car head-on collisions, the gain would be reduced by the increasing aggressiveness of the heavier car.

The author presents the quantification of the expected gains for the most prioritary countermeasures, discusses the major interactions between them, and tries to define the required conditions to optimize the whole safety system.

Introduction

Achieving the most substantial benefits in secondary safety requires a two-pronged approach aimed both at improving the performance of the "structure/restraint systems" combination in asymmetric frontal impacts for a broad-enough range of velocities (delta-V from 55 to 60 km/h), and at reducing frontal aggressiveness against other vehicles, particularly in the case of side-impact crashes.

In addition, such an approach cannot ignore the inescapable fact that cars are getting lighter in order to cope with environmental demands (better fuel economy, less CO2 and pollution).

In the final analysis, the search for safety benefits will necessarily involve a broad, systemic approach based on the following indicators:

- protection criteria, measured on instrumented dummies,
- criteria for reducing aggressiveness, measured on a dynamometric barrier,
- and criteria for reducing fuel consumption and the production of C02, which will need to take into account a reduction in the power/weight ratio in order to control and then reduce the death rate in single-vehicle crashes.

Why Is Improving Protection Against Frontal Impact the Number 1 Priority?

Bureaucratic Truth vs. Scientific Proof

There are already so many regulations on frontal impact, some say, that the new priority should be introducing regulations aimed at improving side impact protection. This line of thinking is purely bureaucratic and simply ignores the scientific facts. According to our own assessment, the benefits to be expected from the side impact regulations that are being contemplated in Europe—and that were recently introduced in the U.S.—would be 6 times less effective than those expected from improvements in frontal impact protection.

Conditions Required for Achieving the Best Gains in Frontal Impact

Selecting a test that matches as closely as possible the deadliest front impact configurations. Such a test will be deemed representative of global frontal impacts if its configuration agrees with the characteristics of real-life accidents, therefore ensuring that test results will eventually translate into better highway safety.

Investigating actual collisions provides a basis for designing a suitable configuration with the most appropriate velocity.

The asymmetric configuration:

This configuration is the one used most widely in studies relating to overlap, deformation and resultant trajectories.

Based on 413 cars involved in front-end crashes (all severities of injuries combined) that were investigated in the region of Hanover (Germany), Otte (1) reports that 79% of them showed no evenly-distributed frontal deformation. The same author notes that in frontal impact the resultant trajectory of the forces is exactly parallel with the longitudinal axis of the car in only 23.7% of the cases.

Zeidler et al. (2) reports that 84% of the 822 cars they analyzed that were involved in injury-inducing frontal crashes were not symmetrically and evenly deformed along the front end.

Gloyns et al. (3) reports that 90% of the fatal frontal crashes they investigated could not be represented by the full frontal barrier test.

Lastly, the results from a survey conducted by the Peugeot-Renault Association involving 1831 belted front seat occupants confirm these findings. Figure 1 gives the state of these occupants according to the type of frontal overlap with the obstacle and the type of deformation for one sample, all brands and models combined. The number of occupants was reduced to 1000 for easier reading. Only 23 out of the 126 fatally and seriously injured (MAIS 3+)—i.e. 18%—had the front ends of their cars evenly and symmetrically deformed. Before making any comparisons with the full frontal barrier test, it may be useful consider the mean acceleration sustained by these occupants. For 7 out of the 23 seriously injured reported under these conditions, the obstacle crashed against most often was the door of another car. In these cases, the estimated mean acceleration is much below that recorded in tests against an inflexible barrier. These cases appear in the "Symmetric (low deceleration)" category in Figure 1.

		SEVERITY OF INJURIES FOR 1,831 BELTED FRONT OCCUPANTS (N = 1,831 occupants reduced to 1,000 for this table)				
		M.AIS 0	M.AIS 1-2	M.AIS 3+5	Killed	TOTAL
(1/4 track)	All cases	64	79	9	2	154
(1/3 track)	All cases	54	54	9	2	119
(1/2 track)	Rectangular deformation	6	7	1	-	14
	Oblique deformation	59	102	18	6	185
(2/3 track)	Rectangular deformation	9	10	2	1	22
	Oblique deformation	52	87	21	7	167
(distributed)	Rectangular deformation (low mean acceleration)	48	54	6	1	109
	Rectangular deformation (high mean acceleration -impacts related to 0° test)	9	33	13	3	58
	Oblique deformation (impacts related to 30°test)	13	27	10	4	54
(pinpoint)	All cases	10	10	2	-	22
	Overhanging obstacle with passenger compartment intrusion (all types of overlap)	5	9	2	4	20
	Above or below the frame No passenger compartment intrusion (all types of overlap)	38	35	3	-	76
	TOTAL	367	507	96	30	1000

Figure 1. Frontal Real-World Accidents—M.AIS of Belted Front Occupants According to Type of Overlap and Type of Deformation

All in all, the full frontal barrier test represents only 13% (16/126) of the belted front seat occupants who were seriously or fatally injured in frontal crashes.

Figure 1 also shows the types of overlap and deformation observed in the other cases. The data show that the deformation equivalent to the 30° angled barrier test resulting from frontal impact with a 50 to 100% overlap covers:

- 41% of the belted front seat occupants, all injuries combined,
- 52% (66/126) of the seriously and fatally injured,
- and 57% (17/30) of the fatalities alone.

Other tests such as the corner impact (1/2 overlap) can also cause asymmetric front-end deformations, but at a right angle. However, this type of deformation is rarely observed in actual crashes.

Selecting a priority-type asymmetric frontal test configuration—such as the 30° angled barrier on the driver's side—also requires estimating the force of the impact sustained by the belted occupants.

Force of the impact:

The force involved in actual frontal crashes is traditionally estimated in terms of the instantaneous velocity variation of the occupant (delta-V) and the mean acceleration of the vehicle (Am).

Figure 2 shows the cumulative delta-V percentages for belted front seat occupants that were not subjected to additional loading from rear seat passengers, according to various severities of injury. A delta-V value of 53 km/h covers half of the 169 severely and fatally injured for whom the force of the impact could be evaluated.

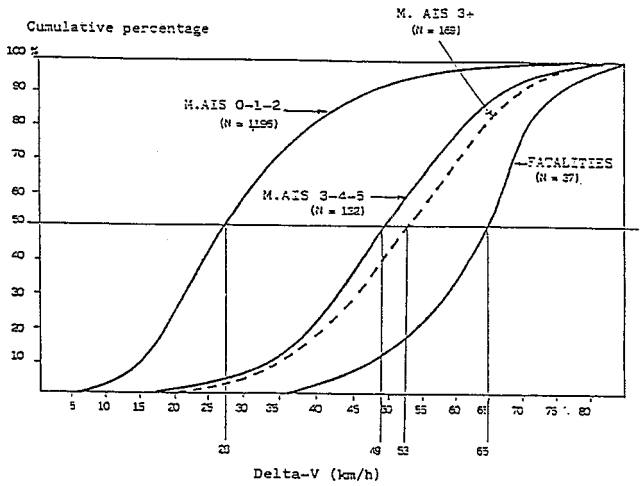

Figure 2. Frontal Impacts—Cumulative Percentages of Belted Front Occupants (Without Rear Occupant Overload) According to Delta-V and Severity of Injuries (N=1,365)

Another way to quantify the most representative velocity consists in examining the overall severity of the lesions in each delta-V category (see Figure 3). The data show that one out of two belted front seat occupants is

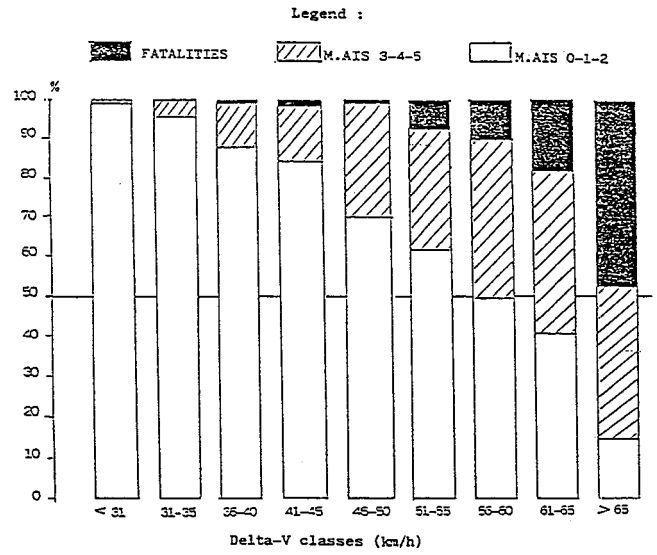

Figure 3. Frontal Impacts—Breakdown of Severity of Injuries for Belted Front Occupants (Without Rear Occupant Over Load) by Delta-V Classes

seriously or fatally injured in the delta-V category ranging between 56 and 60 km/h.

Thomas et al. (4) investigated the estimated mean acceleration in actual frontal crashes equivalent to the 30° angled barrier test with delta-V values on the order of 55 km/h. Based on 320 actual frontal crashes that could be assimilated to that test, the data show that the majority of the mean acceleration values for delta-V values between 50 and 60 km/h fall between 10 and 13 g (4). Most of the mean acceleration values measured in 30° barrier tests for this same range of velocities fall between 11 and 15 g (4). One may conclude that the 30° barrier test simulates rather faithfully the mean acceleration sustained by car occupants involved in crashes between 50 and 60 km/h.

In addition to delta-V and mean acceleration, intrusion is yet another factor that may bear on the risk incurred by belted front seat occupants. Table 1 shows the distribution of 403 such occupants broken down into delta-V categories according to the intrusion level inside the passenger compartment. The data show that for delta-V values ranging from 51 to 60 km/h, intrusion involves one fourth (25/101) of the belted front seat occupants, and most of all, 46% (17/37) of the seriously and fatally injured.

Table 1. Distribution of 403 Belted Occupants by Classes of Delta-V in Relation to the Intrusion

Level of Intrusion (inward displacement of the lower edge of the windshield)	Overall severity	Delta-V (in km/h)			
		40-50	51-60	61-70	TOTAL
Null or moderate (< 250 mm)	M.AIS 0-1-2	208	56	11	275
	M.AIS 3-4-5	26	19	19	64
	Killed	1	2	2	4
	Total	235	32	32	343
Critical (> 250 mm)	M.AIS 0-1-2	7	8	2	17
	M.AIS 3-4-5	7	13	7	27
	Killed	0	4	12	16
	Total	14	25	21	60

Figure 4 provides a distribution of the severities of injury according to the delta-V, mean acceleration and intrusion for actual crashes equivalent to the 30° angled barrier test, although no information is given on the resultant trajectory of the occupant.

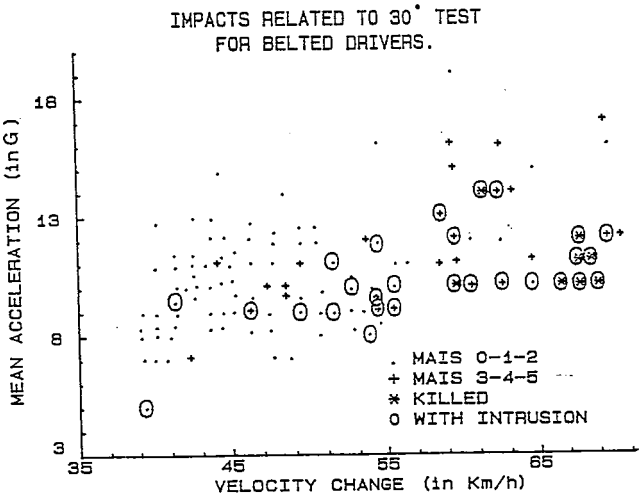

Figure 4. M.AIS of Belted Drivers According to Velocity Change, Mean Acceleration of Cars and Intrusion for Frontal Real-World Accidents Related to the 30° Angled Barrier Test

Otte (1) reports that the mean resultant of the forces is located to the left of the longitudinal axis, forming an angle estimated to be about 5°. The frequency of head impacts against the steering wheel also provides some indication as to the drivers' trajectories.

P. Thomas (5) observes that for values of delta-V between 50 and 59 km/h, 56% (56/99) of the belted drivers experience head/wheel impact. G. Walfisch et al. (6) report a similar frequency in the same delta-V category, based on the crash sample investigated by the PSA/Renault Association.

From an experimental standpoint, these authors note that in the delta-V category from 46 to 60 km/h, the impact of the head of the belted dummy driver is almost systematic in 0° or 50% offset tests, which is not the case in real life.

At any rate, the problem is elsewhere. In frontal crash tests—run as part of car design, regulation compliance or even car rating—the reference to a single head-wheel impact is unacceptable. In real life, there are not one but many conditions under which head-wheel impacts can occur, depending on the size of the occupant, the kinematics of the occupant, the characteristics of the frontal crash, the way the steering column moves, and the exact location of the impact against the steering wheel.

Therefore, a specific test needs to be designed that can measure the protection to the head (face, brain, skull, neck) provided by the steering wheel, and at various locations thereof. Such a test is the necessary complement to any overall frontal barrier test, whatever that test may be.

In the last analysis, any representative frontal test should restitute the parameters that govern the risks incurred by the maximum number of belted front seat occupants, i.e. it needs to provide for:

- a delta-V of at least 55 km/h,
- a mean acceleration on the order of 13 g,
- an asymmetric deformation of the front end of the car giving rise to a potential risk of intrusion on the driver's side,
- and a slightly oblique occupant trajectory that provides for the possibility that the head of the driver dummy will hit the left hand side of the steering wheel.

It should be specified however that such a test will not, of course, be sufficient to predict how safe a car is in all frontal crash situations. The test described above only seems the one most appropriate at present to cover close to half the seriously and fatally injured belted front seat occupants of cars involved in frontal crashes.

Selecting the tool for predicting the risk of lesions. This means designing a biofaithful dummy that can help scientists avoid making errors when they interpret test results. The base for such a dummy already exists: Hybrid III. It has a thorax, neck and head that are much improved compared with its predecessor's—Hybrid II—and that gives dynamic responses which are more closely related to those of human beings.

But although Hybrid III represents a significant step forward, further improvements are still needed in the following areas:

- collar bone stiffness,
- face biofidelity,
- pelvic behavior in submarining,
- chin/sternum contact,
- and adding asternal rib simulation.

In addition to progress in terms of biofidelity, Hybrid III makes it possible to measure several parameters that can be used to assess the risk of lesions in various body regions. A thorough analysis of all the parameters—both technical and medical—for a large number of actual crashes can help scientists clearly specify the risks facing car occupants: Accidentology can thus determine the types of impact encountered, their force, the body regions that are most at risk, and the types of lesions that are observed.

Based on the data, the role of biomechanics is to translate the physical parameters measured on dummies into protection criteria, and to set the various thresholds beyond which lesions may occur. That is the only way the risk of bodily injuries to the occupants involved in actual crashes can be predicted. Table 2 sums up the criteria proposed for frontal impact.

Table 2. Criteria Synthesis Suggested for the Frontal Test

	US CRITERIA	RENAULT CRITERIA : Proposal
SKULL	HIC < 1000	HIC<1000 If direct head impact. To be calculated during head contact
BRAIN		w<25000 rd/s2
FACE		F1<500 daN (forehead on rim) F2<250 daN (below forehead, with deformable face and on a large area)
NECK		My<250 Nm) Fx <250 daN) without head impact with impact : under determination
CHEST	a < 60 g	Deflection < 50 mm a < 60 g
ABDOMEN		F < 150 daN in case submarining is detected
FEMUR	F < 1000 daN	F < 1000 daN

Why Is It Important Both to Improve Protection Against Frontal Impact and to Reduce Frontal Aggressiveness Against Other Vehicles, Particularly in Side-Impact Crashes?

At present, car safety policies vary from country to country, but the one feature they share is that they only address the issue of protection inside the vehicle being certified. they ignore the risks that such a vehicle may pose to other users.

This void is that much more serious that there is no other truly effective means of protecting these users. Accordingly, a car's frontal aggressiveness cannot be effectively compensated by a regulation aimed at making an impact against for instance the doors of another vehicle tolerable by its occupants. Of course, the overall number of injuries can be lowered by making specific design changes to the side of cars, but the effectiveness of such changes is too limited to affect the number of serious injuries and fatalities (7, 8). Effective protective measures—measures that could cut down that number in half—are technically and economically unfeasible, as shown by the evaluation program for the Renault COVER (9 to 11). Naturally, such inability to compensate reaches 100% in the case of road users that are most vulnerable, i.e. pedestrians and two-wheelers.

Charges against the aggressiveness of certain cars were levelled over fifteen years ago (12 to 17). Its components were identified: weight, architecture and stiffness. Spectacular demonstrations were made, such as Philippe VENTRE' s to the 3rd International Conference on ESV (18) in a communication entitled: "A Homogeneous Safety in a Heterogeneous Fleet." The author clearly demonstrated that a small Renault 5 weighing 660 kg could offer the same protection as that of a standard-sized American car weighing twice as much, but whose aggressiveness would have been reduced. The case was made using a front-end collision between the two vehicles (Figure 5).

To date, such studies have not prompted any new regulatory developments. Could it be for lack of quantifying the influence on highway fatalities? If so, the void is now filled: we know for instance that the risk is 5 times higher in the most aggressive car category (over

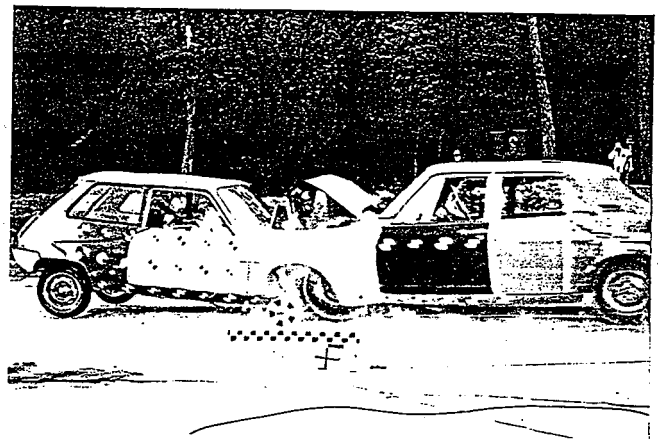

Figure 5. Head-On Crash Test Between Two Cars Weighing Respectively 660 kg and 1320 kg Running Each at 70 km/h (Source: from Ventre (18))

1000 kg) than in the least aggressive one (under 800 kg) (Figure 6). And these are but averages by weight category. The risk runs probably from 1 to 20 between the least and the most aggressive car.

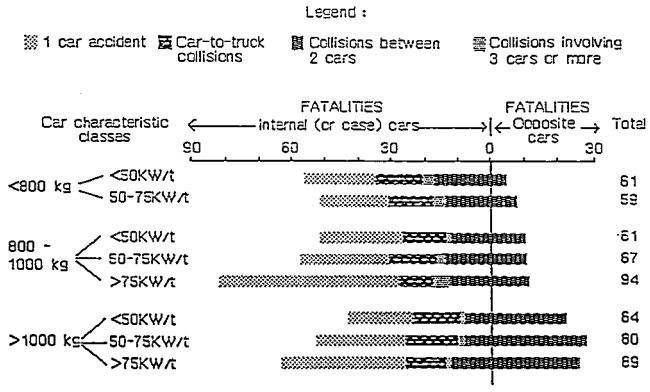

Figure 6. Distribution of Fatalities Among 1,000 Drivers in Each Car Class of Weight and "Power/Weight" Ratio According to Obstacle Type (Source: Sample of 41,944 Drivers, France 1989, Gendarmerie File)

The stakes are high, even higher when pedestrians and two-wheelers are taken into account—and justifiably so—since here again the risk varies in relation with the aggressiveness of the vehicle (Figure 7).

It is often said, particularly in the United States, that safety inside a car drops as the car gets lighter. This indeed complies with the laws of mechanics. The velocity variation of car occupants wearing seat belts anchored to the non deformed section of their cars is proportional to weights ratio. For example comparing two cars involved in a frontal collision, one weighing 700 kg and the other 1400 kg, with a closing speed of 100 km/h, delta-V will be 67 km/h for the lighter car and 33 km/h for the heavier one. Turning now to the statistics on actual crashes, the death rate is 25 per thousand drivers of cars under 800 kg, compared to 10 for cars over 1000 kg. Therefore, the death rate indeed increases as cars get lighter, but the ratio is still below 2.5. Accordingly, the

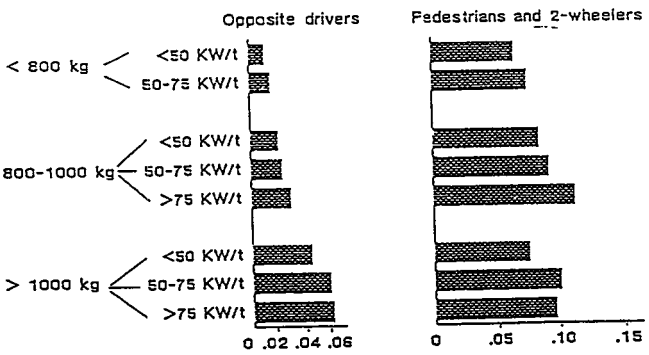

Figure 7. Fatality Rates of Opposite Car Drivers and Pedestrian or Two-Wheelers According to the Striking Car Weight Class and "Power/Weight" Ratio (Source: Sample of 50,710 Car Drivers, France 1989, Gendarmerie File)

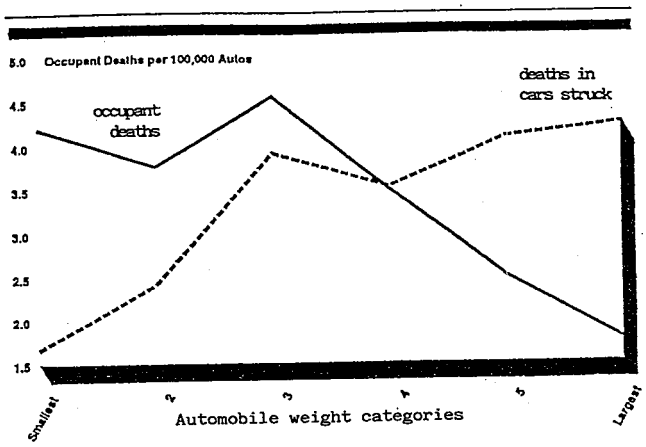

Figure 8. Deaths in Two Cars Accidents—USA, FARS 1975-1988 File (Source: From Chelimsky (19))

increased safety inside the heavier cars does not offset, by far, the risk they pose to the outside since, as indicated above, the corresponding ratio is 1 to 5 when comparing the average for cars under 800 kg and that for cars over 1000 kg.

Figure 6 clearly illustrates the results drawn from a data base on 40,000 drivers involved in injury-inducing traffic accidents which occurred in France in 1989. Our findings are in good agreement with those published recently in the United States (19). The author, E. Chelimsky, points out that " ... the safety provided to the occupants of a large car must be considered together with the risk posed by that same car to passengers in other automobiles.... (I)t is not true that cars become more dangerous simply by getting lighter."

Our findings are in full agreement with C. Thomas's paper (20) presented and discussed 6 months earlier at the AAAM Conference held in Scottsdale (USA) in October 1990. The author shows that although the death rate is higher inside lighter-than-average cars in the French automobile fleet, overall, the heavier cars are more dangerous. The number of victims in the struck cars (only 2-car collisions are studied) increases faster with weight than their number decreases inside these same vehicles.

The results obtained in the US regarding only 2-car accidents relate to crashes that occurred in the 1978-1988 period. These crashes are broken down into six equal-sized categories of car weights, from category 1 (smallest cars) to category 6 (largest cars).

It is noteworthy that the risk inside the cars (as opposed to the risk outside, in cars that are struck) is highest in the 3rd weight category, and not in the two lightest car categories (Figure 8).

The same figure also shows (dashed line) the effect of car size as an initiator of force. The risk of fatalities in the "other" car increases dramatically starting from the 3rd heaviest car category.

It is clear that when you add the two categories of fatalities (inside and outside) in each weight category, the lightest car category is the least dangerous overall. For the rest, the results differ slightly from those recorded in France, and such for various reasons including the lower seat belt use rate in the US.

Thus, on the basis of two very different samples, the French one representing 90% of all traffic injuries sustained in that country, one can better understand why there is an imperative need to tie in the search for better frontal protection with a limit on the aggressiveness of vehicles. Any improvement to frontal protection alone is likely to cause more heterogeneity in the fleet, particularly between the heaviest cars—that would be made even stiffer to meet the new requirements—and the existing fleet. Accordingly, there is an urgent need to introduce objective means of measuring aggressiveness, such as those proposed hereinbelow.

Analysis of the Influence of the Power/Weight Ratio

In this comparative study of risk in each weight category of cars in the fleet, there is yet another important parameter beside weight: the power/weight ratio.

The above-mentioned US study also investigates one-car accidents (Figure 9). For this type of crashes the sample only includes recent—one to two-year old—passenger cars involved in fatal accidents from 1986 to 1988 grouped in the same six weight categories as above.

Here, the most dangerous cars are in the fourth weight category, where the risk is much higher than that in the three lower weight categories. The risk is lowest in the sixth category, which is comprised of the heaviest cars. These cars also have the lowest risk of rollover.

The author offers no explanation for the fact that cars in the fourth category are more dangerous.

Referring to our own results, we submit that an additional parameter plays an important role in one-car accidents: the power/weight ratio.

The influence of the power/weight ratio is felt across all the weight categories (see Figure 6). For a same category of power to the ton, this influence tops out in the

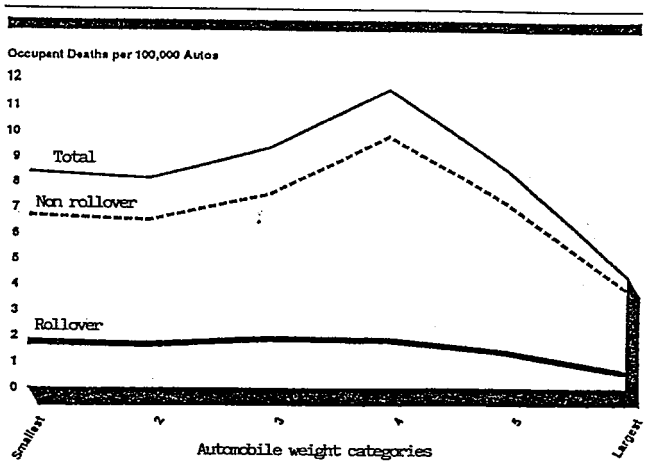

Figure 9. Deaths in One Car Accidents—USA, FARS 1975-1988 File (Source: From Chelimsky (19))

cars of average or below average weight. For example in cars weighing between 800 and 1000 kg with a power/weight ratio of 75 kW/ton, there is a sizable excess risk that represents 66% of the "inside" fatalities and 59% of all the fatalities ("inside" + "outside") associated with that category. Loss of control is the major cause, particularly going off the road round a curve and crashing against a fixed obstacle. But the power/weight ratio also translates into more aggressiveness toward the most vulnerable users (Figure 7).

One can see how important it will be to limit the power/weight ratio in the near future, when the average weight of cars tends to drop in order to meet environmental requirements.

Proposals on How to Estimate the Aggressiveness of Car Structures

Several approaches can be imagined to estimate the aggressiveness of cars. But rather than choose a specific test, we suggest that the most cost-effective solution consists in tying in this estimate with the future frontal impact test.

Indeed, would it not suffice to measure the forces applied to the barrier in dynamic tests to get a good description of their maximum values and distribution? The side members and the engine/gearbox unit transmit the brunt of the forces, and it needs to be accurately recorded by the selected frontal impact test configuration. Among the asymmetrical impacts, the so-called "overlap higher than 1/3" impacts do not adequately account for the engine/gearbox unit forces. However, the asymmetrical impact against a 30° angle barrier, shown above to be quite representative, would be acceptable to estimate the aggressiveness involving the quasi instantaneous impact of one side member and the engine/gearbox unit and, at high speed, of the whole front end of the car.

How feasible is estimating a car's aggressiveness using the 30° angle barrier test? Instrumenting the 30° angle barrier using force cells has already been done (21). Measurement platforms divide up the barrier area into several sectors, each sector corresponding to one of the vehicle's structural components involved in the impact (engine block, side members, wheels, hood, and so on); each platform is made up of a stiff plate mounted onto four piezoelectric sensors with two or three components. The way in which the forces normal to the surface are distributed between the cells of the same platform helps determine the location of the point where the resultant of these forces is applied on that platform. A measurement is therefore technically feasible.

What needs to be agreed on next is how many cells there should be and how they should be distributed. Indeed, the spatial measurement of the forces must be accurate enough so that the authorized limits—which are yet to be determined—depending on the location are compatible with an actual decrease in side impact aggressiveness.

Some may think that running additional tests is not cost effective so long as the full front impact test remains a mandatory requirement.

With respect to this type of impact, we have a picture of the French car fleet in the 80s as given by the moving deformable barrier test proposed by UTAC (22). For impacts at 35 km/h covering 20 representative vehicles, mean overall stiffness values ranging from 500 kN/m to 5000 kN/m (!) and peak forces from 179 kN to 510 kN were recorded. In a first step, it would be interesting to get a new picture of the fleet in 1991. This picture would help define specifications based on the least aggressive vehicle, making sure that the vehicle that is selected offers good protection against frontal impacts.

However, such initial approach to the 0° barrier test should not prevent us from considering the feasibility of estimating aggressiveness using the 30° angle barrier test, a potentially fruitful path for the future.

Conclusion

In the light of these findings, it should be obvious that the problems at hand are highly complex.

Gone are the times when simplistic proposals such as "Improving vehicle safety merely requires better side impact protection" or "Improving vehicle safety merely requires tougher regulations in terms of passive safety, and running tests at a higher speed" could be made.

Before making users pay for implementing such proposals, let's first ascertain what benefit they would derive in terms of a diminished risk on the road.

As concerns protection against side impacts for instance, our estimates show that the benefit would indeed be very small, due to the shape—thinness of the side wall—and to the highly unfavorable ratio between the stiffness of the front end of cars and that of the side wall.

Increasing protection against frontal impacts is a much higher priority since the expected benefits are five times higher than in side impacts. Nevertheless, such benefits should be attained using the "softest" methods, i.e. those

that improve protection inside the vehicle without increasing its aggressiveness outside. This means putting a priority on optimizing the effectiveness of protection systems inside the passenger compartment.

Such optimization should be applied to each seat in the vehicle: indeed, the requirements are different for the driver, the front seat passenger and the rear seat passengers depending on whether they are seated next to a door or in the middle, and whether they are adults or children. And for the latter the demands are still different for each age group.

There is still a lot of work to be done in this area, and the "COVER" experimental vehicle presented by RENAULT provides many useful applications.

Progress in the area of frontal impacts can and must be sought by improving the behavior of car structure. This does not mean stiffening, as stiffening fails to deliver better overall protection. Recent examples show that cars that are too stiff transmit forces to the occupants through the restraint system, forces that exceed human tolerance particularly in the thoracic region.

To improve structural behavior means getting better control over this parameter with a view toward maximizing the dissipation of energy while at the same time avoiding unacceptable deformation of the passenger compartment. The criteria measured on instrumented dummies can be used to predict the risk of injury, and hence to assess any improvement to the "structure-restraint system" couple.

It should also be stressed that the damage to a car (its deformation) does not provide—in and by itself—any pertinent measurement of safety.

But there is yet another imperious reason not to increase structural stiffness. In addition to the risk stiffness poses to the occupants in crashes against fixed obstacles—i.e. 39% of all the frontal impacts involving fatalities in France—it also constitutes a considerable danger on the road by increasing the aggressiveness of striking vehicles. Let's not forget that any car on the road is as much a potentially struck vehicle than a potentially striking one.

Limiting front end aggressiveness is an imperious necessity. This objective can only be reached if one acts simultaneously to improve protection against frontal impacts—a desirable goal—and to limit aggressiveness.

The aggressiveness of vehicles is highly dependent on their weight. One can easily conceive how dangerous it would be to let the heterogeneity of cars on the road in terms of weight and stiffness further increase without controlling their aggressiveness.

Studies have also shown that the weight-safety relationship is not a linear one. There is an excess risk related to the power/weight ratio that comes into play independently and that primarily manifests itself in the form of loss of control of the car in a curve (one car accidents).

In the final analysis, it is becoming ever more obvious that safety can only be served by a systemic approach.

Frontal impact protection of course remains the number one priority in passive safety, but it needs to be considered by curbing the evolution of weight and by limiting the aggressiveness of cars against one another.

Overall highway safety will advance as the heterogeneity of the fleet decreases. This goal has to be reached in the context of an inescapable drop in weight in order to lower both fuel consumption and pollution.

The stakes thus appear in an overall perspective where safety imperatives are confronted with those of the environment.

Safety benefits can be expected in spite of—or thanks to—lighter cars, but two conditions need to be fulfilled:

- fleet heterogeneity must be fought against and reduced,
- and power must decrease as cars become lighter. In other words, the power/weight ratio must not increase, it must go down.

Fulfilling these conditions requires a clearly stated political will. Indeed, the natural trend in the past decades has been toward more power and heavier cars, and specifically, more weight in cars that are among the heaviest in the existing fleet.

Finally, it is on purpose that this report has only addressed those issues that concern secondary safety. In fact, safety as a whole is a much more complex matter. A coherent road safety policy cannot avoid comparing the cost effectiveness of the various proposals being made, according to whether they relate to injury prevention (so-called passive or secondary safety) or accident prevention (so-called active or primary safety). The fact that protection against side impacts is not very effective does not mean that nothing should be done. It only shows that lives should be saved by other, more cost effective means, i.e. crash avoidance. Measures of the highest priority need to be taken to improve the road infrastructure. For instance:

- a traffic circle in place of an intersection cuts down the risk of accidents involving serious injuries twenty-fold;
- and putting up guardrails along roads lined with trees would likely cut almost in half the number of killed against trees recorded in FRANCE in 1990 by the state police force.

Accident prevention will account for the great majority of the lives saved in the future (23, 24). Broadening the analysis to all the safety issues and integrating them into a comprehensive system should not be used as an alibi to do nothing. Measures designed to improve frontal impact protection constitute a priority that is that much less arguable that they form an overall system coupled with support measures that give it a clearly established coherence and effectiveness.

References

1. D. Otte, "Comparison and Realism of Crash Simulation Test and Real Accidents Situations for the Biomechanical Movements in Car Collisions" SAE paper 90 23 29.
2. F. Zeidler, H. H. Schreier and R. Stadelmann, "Accident Research and Accident Reconstruction by the EES-Accident Reconstruction Method" Proceedings of SAE Congress, Detroit, Michigan, February 25-March 1, 1985 P. 159. SAE Paper 850256.
3. P.F. Gloyns, S.J. Rattenbury and I.S. Jones, "Characteristics of Fatal Frontal Impacts and Future Countermeasures in Great Britain" Proceedings of 12th ESV Conference, Goteborg-Sweden May 29-June 1, 1989.
4. C. Thomas, S. Koltchakian, C. Tarriere, C. Got and A. Patel, "Inadequacy of A 0° Degree Barrier with Frontal Real-World Accidents" Proceedings of 12th ESV Conference, Goteborg-Sweden, May 29-June 1, 1989.
5. P. Thomas, "Head and Torso Injuries to Restrained Drivers From the Steering System" Proceedings of IRCOBI Conference, Birmingham-U.K., September 8, 9, 10, 1987.
6. G. Walfisch, D. Pouget, C. Thomas and C. Tarriere, "Head Risks in Frontal Impacts: Similarities and Differences Between Tests and Real-Life Situations" Proceedings of 12th ESV Conference, Goteborg-Sweden, May 29-June 1, 1989.
7. D. Viano, "Estimates of Fatal Chest and Abdominal Injury Prevention in Side-Impact Crashes" Journal of Safety Research, Vol. 20, pp 145-152, 1989.
8. C. Henry, C. Thomas and C. Tarriere, "Side Impacts: Expected Benefits of Planned Standards" Proceedings of 12th International ESV Conference, Goteborg, Sweden, May 29-June 1, 1989.
9. N. Casadei, "VSS—Safety Synthesis Vehicle" Proceedings of 13th International ESV Conference, Paris-France, November 4-7, 1991.
10. G. Walfisch, "Renault VSS Safety Vehicle: Occupant Safety in Frontal Impacts" Proceedings of 13th International ESV Conference, Paris-France, November 4-7, 1991.
11. J. Rio, "Renault VSS Safety Vehicle: Occupant Safety in Lateral Impacts" Proceedings of 13th International ESV Conference Paris-France, November 4-7, 1991.
12. G. Chillon, "The Importance of Vehicle Aggressiveness in the Case of a Transversal Impact" Proceedings of 1st International ESV Conference, January 25-27, 1971.
13. H. Appel, "Optimum Deformation Characteristics for Front, Rear and Side Structures of Motor Vehicles in Mixed Traffic."
14. E. Chandler, "Car-to-Car Compatibility" Proceedings of 4th International ESV Conference, Kyoto, Japan, March 13-16, 1973.
15. P. Ventre, "Proposal for Test Evaluation of Compatibility Between Very Different Passenger Cars" Proceedings of 4th International ESV Conference, Kyoto, Japan, March 13-16, 1973.
16. U. Seiffert, "Compatibility on the Road" Proceedings of 5th International ESV Conference, London, England, June 4-7, 1974.
17. P. Ventre, "Compatibility Between Vehicles in Frontal and Semi-Frontal Collisions" Proceedings of 5th International ESV Conference, London, England, June 4-7, 1974.
18. P. Ventre, "Homogeneous Safety Amid Heterogeneous Car Population?" Proceedings of 3rd International ESV Conference, Washington, D.C. May 30-June 2, 1972.
19. E. Chelimsky, "Automobile Weight and Safety" Statement to the Senate Committee on Commerce, Science and Transportation, Subcommittee on Consumer, Washington D.C., April 11, 1991. TECH-91-229.
20. C. Thomas, G. Faverjon, C. Henry, J.Y. Le Coz, C. Got and A. Patel, "The Problem of Compatibility in Car-to-Car" Proceedings of 34th AAAM Conference, Scottsdale, Arizona, October 1-3, 1990.
21. Kistler, Technical information: crash Dynamometer System.
22. E. Chapoux, J.C. Jolys, R. Dargaud, "An Approach for the Design of a Deformable Mobile Barrier to Evaluate the Protection Afforded to Occupants of a Passenger Car Involved in a Side Collision" Proceedings of IXth ESV, Kyoto, Japan, 1982.
23. D.C. Viano, "Limits and Challenges of Crash Protection" In Accident Analysis and Prevention, Vol. 20, No 6, pp 421-429, 1988.
24. C. Thomas, S. Koltchakian, C. Tarriere, B. Tarriere, C. Got and A. Patel "Primary Safety Priorities in View to Technical Feasibility Limits to Secondary Automotive Safety" Proceedings of 23rd FISITA Congress, Torino, Italy, 7-11 May 1990.

S9-O-14

Occupant Protection in Coaches

Ross Dal Nevo, Paul Duignan, Michael Griffiths
Roads and Traffic Authority of NSW

Abstract

In 1989, New South Wales, experienced the two worst coach crashes in Australia's history. First, a coach to truck crash with a closing speed of approximately 200 km/h where 19 died. Two months later, a coach to coach crash with again a closing speed of approximately 200 km/h, in which 35 died. Australia had reviewed world wide research just prior to these crashes and was about to adopt a regulation similar to ECE 80. Following the first crash the NSW Road Safety Bureau's Crashlab considered what protection ECE 80 would have offered had it been in place. The review found little, if any potential gain. Accordingly, work commenced to refine the development of a seat incorporating a 3-point seat belt which offered protection to 20 g's. In subsequent crashes, it was confirmed that passive 10 g protection would not offer adequate protection. The crashes also verified the belief that a total coach safety package incorporating roll-over strength, emergency exits and 3-point seat belt occupant protection was required. This paper summarizes the findings of five coach accidents, the research conducted on the adequacy of ECE 80, and the future direction of coach safety in Australia.

Introduction

During the past four years Australia has endured five of the most serious road accidents in its history. The common factor to all five accidents were that they each involved a coach. In all 66 people were killed and 136 injured.

As a result of investigations and findings of each of these accidents, questions were raised with regards to

- the strength of seat anchorages,
- the role of lap/sash seat belts and,
- improved roll-over strength.

This paper provides a brief description of each accident, the protection systems and structural strength required to survive coach accidents, a review of the adequacy of the ECE 80 standard for coach seats and the future direction of bus occupant protection in Australia.

The Crashes

The first accident, Bass Highway, Anderson, February 1987, involved a coach colliding with a small car, subsequently leaving the carriage-way and colliding head-on with a tree. The accident killed 5 of the coach occupants including the driver. A further 17 were injured including the two car occupants. The carriage way was a single lane and undivided.

Inspection of the coach showed that one seat assembly became totally detached from its anchorage points with another 13 either showing broken or distorted mountings. Four of these seats had broken welds at the footplates (1).

The second crash, Grafton/Cowper, October 1989, claimed the lives of 20 people and seriously injured 15. The accident was a side swipe involving a fully laden semi-trailer and an interstate coach. Both vehicles were travelling on a single lane carriageway at approximately 100 km/h. There was massive intrusion into the side of the coach by the leading edge of the trailer.

All but two of the 19 coach passenger fatalities were seated on the right (off-side) of the coach. The seats on this side, and several from the other, were effectively all detached from their mountings. The detachment of the seats from both the floor mountings and the wall mountings contributed to the occupants being thrown into the "crush zone" and subsequently receiving fatal injuries. The injuries from intrusion were gross.

The third crash, Kempsey, December 1989, was Australia's worst road accident and claimed the lives of 35 people and seriously injured another 40. This accident involved two interstate coaches approaching at speeds of approximately 100 km/h each and colliding head on with an approximate 90 percent overlap.

20 of the 23 seats in one coach and a similar number in the other coach, detached from their mountings and "stacked" at the front of the coaches. Injuries to the occupants were exacerbated by this and were essentially of a crushing nature caused by both the initial impact with the back of the seat in front and an impact to the back by the seat behind. Sharp edges on the fractured cast aluminum seat mounts caused laceration injuries. There were numerous complete traumatic leg amputations.

The fourth accident, Mt Tamborine September 1990, claimed the lives of 11 people and seriously injured a further 38. It involved a coach leaving the road while negotiating a turn and subsequently rolling 270 degrees down a two metre embankment. The speed of the coach before leaving the road was estimated to be 55 km/h (2). The coach came to rest against a substantial tree.

The injuries sustained were either from ejection (3 people) and contact with the interior of the coach from the initial deceleration and then the roll-over. Examination of the coach showed that 19 of the 22 seats suffered fractures to the mounting points. The coach structure also dynamically deformed approximately 30-35 degrees to the side during the roll-over and as a consequence reduced the occupant survival space (3).

The fifth accident, Talbingo, May 1991, injured 26 children. The coach had travelled down 5.8 km of a 6.5 km single lane carriageway with gradients reaching 4 percent. The driver of the coach lost control and the bus subsequently left the road and rolled 540 degrees, 360 degrees without contact with the ground. The coach came to rest on its roof at the bottom of a 5 metre embankment.

The important characteristic of this accident is that the coach roof structure, from bottom of the windows up, was completely dislodged. All the occupants were ejected from the vehicle.

Findings

Structural

The most interesting component of the five crashes reported was that four different accident modes were experienced (side-swipe, full frontal, offset and, roll-over). The common element in each accident was the inadequacy of the seat anchorages to withstand the impact.

In the first three accidents there was a substantial forward component involved in the deceleration. This deceleration allowed the occupants to contact the seat in front and thus add to the inertial forces already being applied to the anchorage points and seat legs. The most common failure mode was fracturing of the footplates and bolts.

In the frontal impacts the coach structures performed adequately considering the severity of the impact. The estimated average deceleration in the Kempsey crash was 16 g's and the coach structures were essentially undeformed behind the crumple zone.

In the roll-over accidents the coach's structure was considered to have performed poorly. In the Mt Tamborine accident the dynamic deflection of the structure above floor level was estimated to be approximately 35 degrees. This is compared to the new Australian Design Rule 59 (ADR) requirements shown in Figure 1 where the structure should not deform more than approximately 11 degrees. In the Talbingo accident the entire roof structure was removed to the bottom of the windows, thus leaving the interior of the coach exposed and offering no protection to the occupants.

Injuries

In most cases the inadequacy of the seat anchorages to withstand the impact force of the accident contributed to the severity of the injuries. Injuries were sustained by contact with the seat in front as well as contact by the seat immediately behind. In the case of the Mt Tamborine accident the lack of occupant restraints allowed some occupants to be ejected from the coach and others to contact the luggage racks or roof structure. The major injuries suffered in this accident were in the thoracic region. This accident highlighted the inadequacy of using

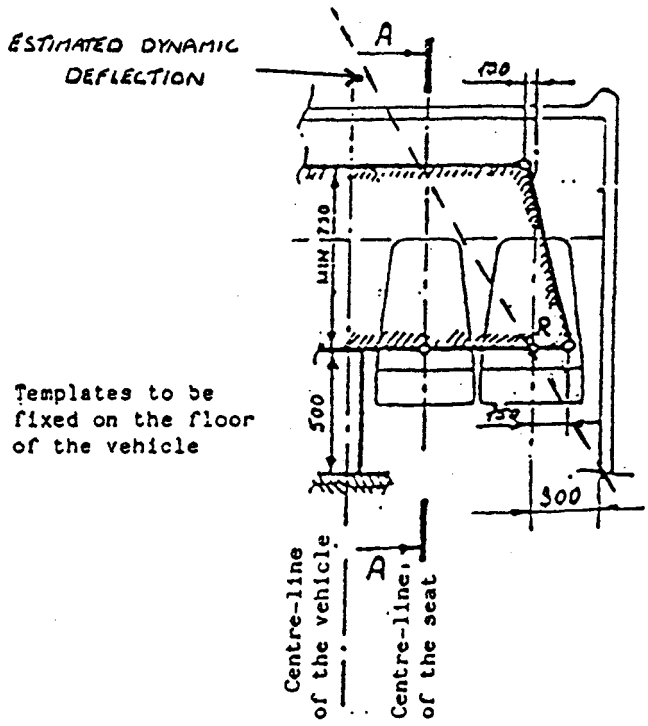

Figure 1. Dynamic Deflection of Coach Structure (Reproduced from ADR59/00)

the seat in front as a passive restraint system. The severity of the injuries in this accident were also increased by the age of the passengers (all over 55 years) (3).

The Talbingo accident highlighted that if seat belts alone were used it would have led to an increased injury severity, thus the need for a total safety package which includes not only the incorporation of 3-point (lap/sash) seat-belts, but improved roll-over strength. During the roll-over stage of the accident all the passengers (majority under 16 years) were thrown from the bus structure.

In all accidents there was extensive intrusion into the residual occupant space by either the external bus structure or interior components which became dislodged during impact.

Emergency Exits

During the rescue operations of the accidents, particularly the two night accidents, Grafton and Kempsey, confusion existed over the location of the emergency exits. Those bus occupants, who were still partially mobile, didn't know where the emergency exits were. At least one occupant received serious lacerations smashing through a window. Another occupant who managed to find a roof exit, broke his leg whilst leaping from the bus roof.

The rescuers could not find the emergency exits and even if they had, the exits were not suitable for stretcher access. This indicated the need for exits to be identifiable in the dark, by occupants and rescuers. The exits need to be towards the middle of the coach on both

sides. They need to large enough to accommodate a stretcher and if they are high off the ground, steps are required.

Seat Strength Test Program

Prior to the Grafton and Kempey crashes, Australian Design Rule (ADR) 66/00; *Seat Strength Seat Anchorage Strength & Padding in Omnibuses* was issued in draft form with a proposed implementation date of 1st July 1992. The technical requirements of ADR 66/00 are based on ECE Regulation No. 80.

ECE 80 and ADR 66/00 specify both static and dynamic test procedures for evaluating the strength and performance of seat structure, anchorages and padding.

Following the Grafton bus crash, which resulted in 19 fatalities, an evaluation of the strength of current production coach seats was conducted to the requirements of ECE 80 by the New South Wales Roads and Traffic Authority, Crashlab.

Test Program Objectives

The objectives were; 1) to assess the performance of current production coach seats against both the static and dynamic tests specified in ECE 80; 2) to establish the correlation between the static and dynamic tests and the real life crash performance of coach seats.

The program was conducted in four stages:

- Stage 1. Static testing to ECE Regulation 80.
- Stage 2. Dynamic testing to ECE 80 using non-instrumented TNO 10 test dummies.
- Stage 3. Dynamic testing to ECE 80 using instrumented Hybrid III anthropomorphic test dummies.
- Stage 4. Dynamic testing of a prototype seat incorporating a retractable lap and sash seat belt.

Stage 1. Static Tests (1)

ECE 80 Static Test. The static strength test specified in ECE 80 attempts to simulate the loads applied to the rear of a seat by the knee and chest contact from an unrestrained rearward occupant(s). This is achieved by the simultaneous application of two loads in a horizontal longitudinal direction at each seating position. All of the seats tested were of a dual occupant design, therefore, this necessitated the simultaneous application of four test loads.

ECE 80 Test Rig. A static test rig was constructed to the requirements of ECE Regulation 80. The rig comprised a rigid base frame and an adjustable bulkhead to which four hydraulic loading rams were mounted (Figure 2). The coach seat modules, (representative sections of the coach floor/wall structure incorporating the seat attachments), mounted to the base frame while the bulkhead accommodated independent vertical and lateral adjustment for each ram. The test loads were applied to the seats via body blocks attached to the end of each ram.

Figure 2. ECE 80 Bus Seat Static Test Rig

The loading rams were mounted between sets of rollers which constrained the application of load to the longitudinal axial direction. The reaction force between each ram and the bulkhead was monitored with a force transducer. Each ram was powered by a separate hydraulic circuit which incorporated a pressure control servovalve. The servovalve was driven by an electronic controller card which monitored the output of the force transducer and increased or decreased the hydraulic pressure to the ram, as required, to achieve the pre-set test load. The displacement of each body block was monitored with a string potentiometer displacement transducer.

Test Seats. Ten separate seat models were supplied from five manufacturers for evaluation in the static test program. Nine of the seats represented current production models. The tenth seat, which was no longer in production, was included as it was represented in one of the fatal coach crashes. Six of the seats used a combination of wall and floor mounting attachments while the remaining four (4) were designed with floor mounts only.

Assessment Criteria. The ECE 80 static test assessment criteria are based on the energy absorption and structural strength of the seat. The criteria includes:

- displacement of the upper body block is not to be less than 100 mm and not more than 400 mm.
- displacement of the lower body block is not to be less than 50 mm.
- no part of the seat, seat mountings or accessories is to become completely detached during the test.
- one or more of the seat anchorages may become partially detached if the seat remains firmly held and all locking systems remain locked.
- no structural part of the seat or accessories has any fracture or sharp pointed edges or corners likely to cause any bodily injury.

Test Results. Of the ten seats tested, nine (9) clearly failed to meet the static test pass criteria. The remaining seat demonstrated the capacity to meet the test loads, although, was unable to sustain all four loads simultaneously for the required duration of 0.2 seconds.

The nine seats which failed the static test were equally represented by three modes of failure. These modes were: 1) collapse of the seat squab; 2) penetration of the seat squab by the lower body blocks (Figure 3); 3) separation of the seat structure at the floor anchorage points.

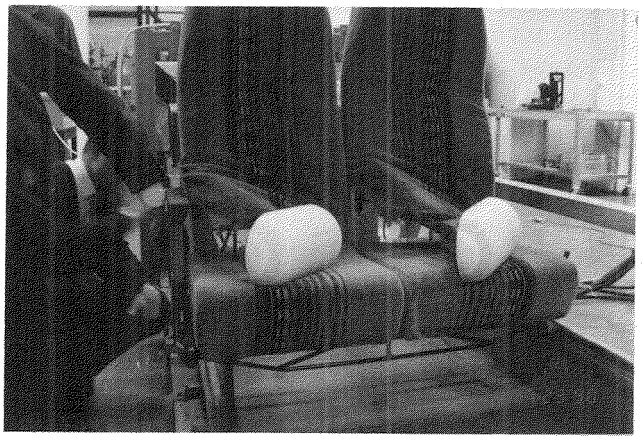

Figure 3. Seat Squab Failure by Body Block Penetration

The collapse of the seat squab resulted in failure through excessive displacement of the upper body blocks. The penetration of the squab by the lower body block resulted in failure from the seat's inability to sustain the test load. The separation of the seat anchorage structure resulted in forward rotation of the seat assembly and failure by excessive displacement of the upper loading blocks.

The seats which failed by squab collapse and structural separation demonstrated performance limits which would e hazardous in a real accident situation. In contrast, seat failure by squab penetration was not a conclusive indication of how the seats would perform in a real accident situation. In these cases the anchorages were not subjected to the full test loads and the loading method was not able to give an effective representation of actual impacts.

A point of concern raised from the squab penetration mode of failure was that it may encourage the relocation or fitment of additional lateral members to the squab. Such modification to prevent penetration would prove detrimental with respect to the mitigation of leg injuries to the occupant behind the seat.

The overall impression from the static test results was that the failure modes exhibited were not truly representative of those present in the Grafton or Kempsey coach crashes. In both coach crashes there was evidence of the anchorage attachments both on the seat and in the floor separating under impact. In the static tests, in which the actual vehicle attachment systems were replicated, no structural floor anchorage failures occurred.

Stage 2. Dynamic Tests—TNO Dummies (2)

Dynamic Test. This series of tests assessed the structural strength of bus seats when subjected to the dynamic test conditions of ECE Regulation 80.

The test method involved impacting the seat under evaluation from the rear with a test dummy in each seating position provided. The dummies were positioned unrestrained on a auxiliary seat identical to, and to the rear of, the one under evaluation. The test and auxiliary seats were attached to the coach floor modules. The modules were mounted on the Crashlab Monterey Crash Simulator (rebound sled) which produced the required impact deceleration specified in ECE Regulation 80.

Each dynamic test was filmed with three high speed cine-film cameras. One camera was mounted on the sled provided a side-on view. Two stationary cameras were used to obtain side-on and over-head views of the impact. All three cameras were operated at a film speed of 500 frames per second.

Test Dummies. TNO 10 anthropometric dummies were used in the Stage 2 tests. ECE 80 specifies the use of Hybrid II anthropomorphic test dummies (ATD's) which accommodate instrumentation to measure the head and chest accelerations and the femur leg forces. This data enables calculation of the head, thorax and femur injury acceptability criterion values. However, as all six seats in the dynamic test program had previously failed the static strength test, TNO dummies were selected as an intermediate step due to concern of serious damage to the more expensive Hybrid ATD's.

Test Conditions. The sled was calibrated to a deceleration pulse meeting the requirements of ECE 80. This pulse produced an impact velocity change of 31.3 km/hr and a peak deceleration of 11.1 G. The duration of the pulse above 8.0 G was 70.2 ms. and the rise time from 0.0 G to 8.0 G was 19.8 ms. The average deceleration of the test pulse was 7.94 G.

Dynamic Test Criteria

The pass criteria for the ECE 80 dynamic test are based on the forward movement of the test dummy(s), the biomechanical response of the dummies and the strength of the seat and seat mountings.

Evaluation of the biomechanical response was not possible in Stage 2 as the TNO's did not accommodate suitable instrumentation. The evaluation was subsequently based on the seat and seat anchorage strength criteria, which are the same as for the static test, and the forward movement criteria.

The forward movement criterion is satisfied if the any part of the head and trunk of the test dummy does not pass beyond a transverse plane situated 1.6 m from the seating reference point of the auxiliary seat on which the dummy was originally seated.

Dynamic Test Results. All six seats were successful in restricting the forward movement of the test dummies to less than 1.6 meters. One seat, however, sustained a failure of the inboard anchorages even though the dummies were restrained.

The six seats in the dynamic test program represented identical models to those tested in the static test

program. In the static tests all six seats failed by one of the three modes previously described. The only mode of failure which was represented in the dynamic tests was the separation of the seat structure at the anchorage attachments.

The correlation between the static and dynamic test results was very poor. Two of the three failure modes exhibited in the static tests were not reproduced in the dynamic tests. The overall seat deformation was also much less severe in the dynamic tests.

Analysis of the high speed film shows that the application of load to the rear of the seat squab occurs in two distinct stages in the dynamic tests. The initial stage of loading being produced by the lower leg/knee of the dummy impacting the seat squab. The second stage of impact occurs latter when the upper torso/thorax area of the dummy impacts the upper portion of the squab. The trajectory of the thorax prior to impact is in a forward and downwards arc due to the upper torso of the manikin pivoting about the hips. In contrast, the static test loads are applied simultaneously to both the upper and lower portions of the squab at a fixed height and in a forward horizontal direction.

The main conclusion drawn from Stage 2 was that the dynamic test is not as severe as the static test and that the correlation of seat performance between the two tests is very poor. The mode of failure obtained in the dynamic tests was representative of that from the real life coach crashes, albeit to a much lesser degree, indicating that the nominal 8.0 G deceleration pulse of ECE 80 is much lower than that experienced in both the Grafton and Kempsey crashes.

Stage 3. Dynamic Tests—Hybrid III Dummies (3)

Dynamic Test and ATD's. The results of Stage 2 indicated that the Hybrid ATD's would not be at risk of serious damage in the dynamic tests. Thus, Stage 3 was essentially a repeat of Stage 2 using instrumented Hybrid III ATD's. The Hybrid III was substituted in place of the Hybrid II on the basis of availability and justified on the grounds of representing improved biofidelity.

The Hybrid III ATD's accommodated instrumentation to measure the resultant triaxial head and chest accelerations and the axial femur leg forces. This data was used to assess the ATD's responses against the biomechanical acceptability criterion.

Test Seats. Nine pairs of dual occupant seats were supplied for testing. Four sets were representative of the models included in Stage 2. The other five sets were representative of models not previously tested. All of the seat assemblies were designed with combined floor and wall mounting attachments.

Evaluation Criteria. The test evaluation criteria included the forward movement of the ATD's and the seat and seat anchorage strength requirements as for the previous tests.

The biomechanical evaluation criteria required that; 1) the head acceptability criterion (HAC) be less than 500; 2) the thorax acceptability criterion (ThAC) be less than 30 G except for periods totalling less than 3 ms; 3) the femur acceptability criterion (FAC) be less than 10 kN and the value of 8 kN not be exceeded except for periods totalling more than 20 ms.

Dynamic Test Results. Seven of the seat assemblies were successful in meeting the strength criteria for the seat structure and seat mounts. One seat which did not meet the strength criteria (M5) suffered separation of the inboard anchorage attachment from the adjustable mounting track. This seat subsequently failed to restrict the forward movement of the ATD's to within the allowable displacement.

Figures 4 to 7, show the biomechanical responses obtained in the tests. These results indicate a wide variation in the performance of the seats tested. The Head Acceptability Criteria (HAC) ranged from a lowest value of 36 to a highest value of 489. The Thorax Acceptability Criteria (ThAC) values ranged from 6.35 G to 30 G and the Femur Acceptability Criteria (FAC) values ranged from 2.0 kN to 6.5 kN.

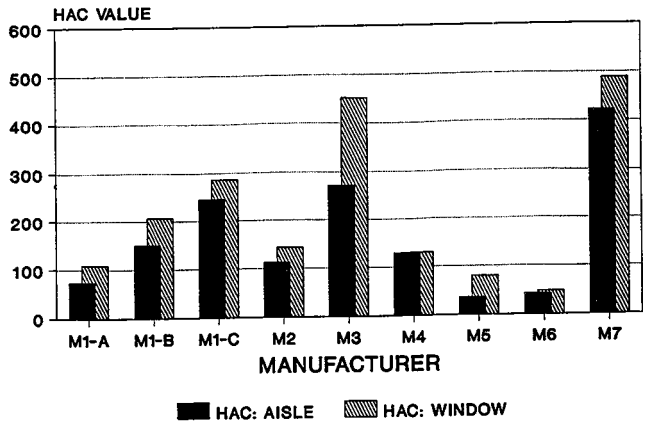

Figure 4. Hybrid III Head Acceptability Criterion (HAC) Responses

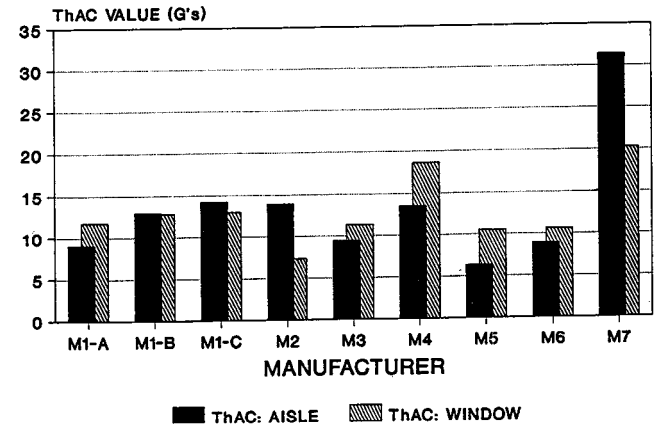

Figure 5. Hybrid III Thorax Acceptability Criterion (ThAC) Responses

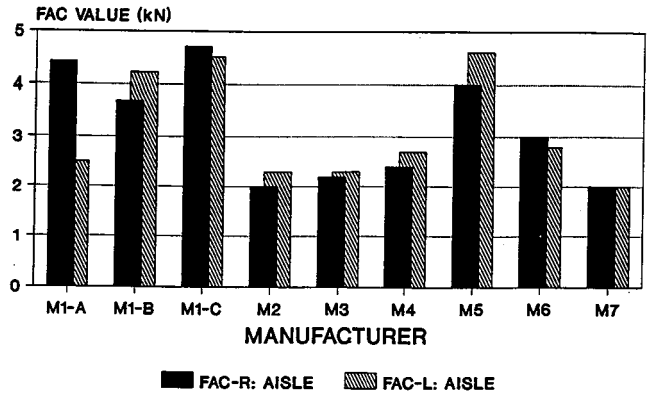

Figure 6. Hybrid III Femur Acceptability Criterion (FAC) Responses for Aisle Seating Position

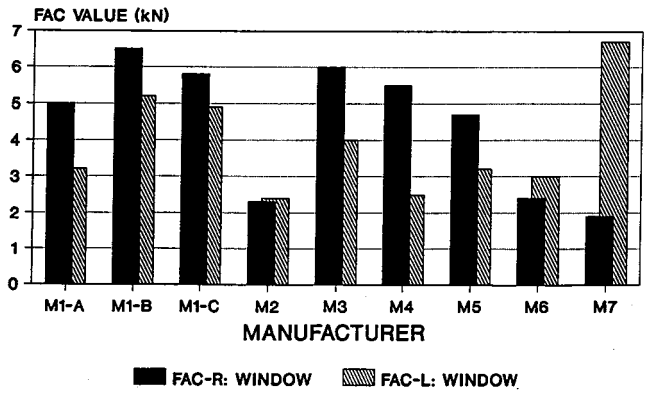

Figure 7. Hybrid III Femur Acceptability Criterion (FAC) Responses for Window Seating Position

The results indicated that the aisle seating position generally yields the lower overall biomechanical injury response. This corresponds with the aisle seating position being more compliant, exhibiting larger deformation after impact. This was illustrated in test M5 (seat supplied by manufacturer 5) where the aisle seat anchorages separated on impact, resulting in the lowest HAC and ThAC values obtained in the test series.

The trend for more compliant seats to produce lower biomechanical injury values was also demonstrated by the tests on seats M1-A, M1-B and M1-C. These seats were all of the same basic design and model but incorporated various modifications designed to improve their static test performance. The basic seat design (M1-A) experienced the largest deformation but yielded the lowest values for HAC (74) and ThAC (9.1). Seat M1-B with modifications to strengthen the base produced HAC values which were approximately double that obtained for the M1-A seat and also marginally higher ThAC values. Seat M1-C which experienced the least deformation incorporated structural modifications to the base as well as redesigned and strengthened inboard anchorages. This seat produced a HAC value of (286) which is almost four times that of the basic unstrengthened seat.

The Stage 3 results again highlighted the lack of compatibility between the Static and Dynamic tests specified in ECE 80. The modifications made to the Ml seats were in response to the perceived need to increase structural strength for the static test. However, these modifications resulted in a more aggressive seat with a less favourable dynamic performance.

Seat M6 was representative the seats installed in the coach involved in the mount Tambourine accident. The performance of the seats in the crash, in terms of strength and ability to mitigate injury, was much less than that implied by the laboratory tests. This raises serious doubts as to the adequacy of the ECE 80 dynamic test requirements in terms of pulse severity and the concept of using the seat squab as the sole means of (passive) occupant restraint.

Stage 4. Dynamic Tests on Seats With Integrated Seat Belts (4)

Test Seat. The first three stages of testing established the performance level of current production model coach seats against the static and dynamic requirements of ECE 80. In Stage 4, tests were conducted on a prototype twin occupant coach seat which incorporated a separate lap and sash (3-point) emergency locking seat belt for each occupant. The seat belt assemblies and anchorages were fully integrated into the seat frame structure.

In earlier development tests the seats demonstrated the ability to provide restraint to two 75 Kg occupants (ATD's) at impacts up to 24 G. The tests conducted in Stage 4 were in response to concern that a seat strong enough to withstand the forces imposed by integrated seat belts would present a serious threat of injury to any unrestrained passengers seated behind them. Also in question, was the capacity of the seat to remain intact under the combined loading produced by a restrained belted occupant and an unrestrained rear occupant bearing on the back of the seat, under crash conditions.

Test Configuration. Three test configurations were investigated; 1) test seat impacted from rear by two unrestrained Hybrid III ATD's at ECE 80 dynamic deceleration pulse; 2) test seat occupied by two restrained TNO 10 dummies and impacted from the rear by two unrestrained Hybrid III's at ECE 80 pulse; 3) test seat occupied by two restrained TNO 10 dummies and impacted from the rear by two unrestrained Hybrid III's at 20 G.

Test Results. Configuration 1: The results from the first test, on the unoccupied seat, were that the HAC and Femur criteria were met, while the ThAC values exceeded the allowable limit. The inboard dummy registered a ThAC value of 35.1 G and the outboard dummy a value of 37.0 G, both of which exceeded the allowable 30 G maximum.

Configuration 2: In the second test, with restrained dummies in test seat, the ThAC and Femur response of the ADT's met the pass criteria where as the HAC criteria was exceeded. The HAC values obtained for the inboard and outboard ATD were 1,897 and 2,195 respectively. The increase in HAC was due to a lower

head strike site on the test seat which had deflected forwards as a result of the loading produced by its restrained occupants.

Configuration 3: The results of the third test, conducted with restrained dummies in the test seat at 20 G, were essentially the same as for configuration 2. The ThAC and Femur values were within the allowable limits while the HAC values were again excessive. The HAC values obtained from the inboard and outboard ATD were 1,653 and 1,791 respectively. In subsequent tests which were conducted using the same configuration, HAC values of less than 1,000 were obtained through the crude application of polystyrene foam sheet to the rear of the seat squab.

In addition to not meeting the HAC criteria, the rear inboard seat anchorages pulled free of the mounting track during impact.

The results indicate that, in the configuration supplied, the test seat had the potential to injure unrestrained occupants. However, the results also showed that the seat and anchorages were capable of restraining the combined loads of four test dummies at 20 G while remaining essentially intact. This also demonstrated that the level of protection provided for restrained occupants would not be compromised by other occupants who choose not to use their seat belts.

Another feature of the test seat which complements its dynamic performance, is that there is not a significant weight or cost penalty associated with the additional structural strength and safety provided.

Conclusions

The following is a brief summation of the conclusions drawn from the coach accident investigations and the seat strength tests presented in this paper:

- Four distinct accident modes were represented in the five fatal coach crashes investigated.
- It is necessary to have a total safety package which incorporates 3-point (lap/sash) seat belts, improved coach structures for roll-over and intrusion, and more identifiable emergency exits.
- The correlation between the dynamic and static performance requirements of ECE 80 is very poor.
- The ECE 80 static test produced modes of seat failure which were not representative of those experienced in actual coach crashes.
- The use of the ECE 80 static test as a design tool may result in coach seats which do not perform well in mitigating occupant injuries.
- The ECE 80 dynamic test is not severe enough to replicate the severity of real world crash experiences.
- Test have shown it possible to manufacture a coach seat incorporating a 3-point seat belt that will offer occupant protection at impacts up to 20g's without incurring significant cost or weight penalties.
- Seats can be manufactured incorporating 3-point seat belts for improved safety for seat belted occupants without further compromising the safety of unrestrained occupants.

Future Direction of Coach Safety

In response to the findings of the coach accident investigations and the seat strength evaluations, Australia is proceeding towards the adoption of a total coach safety package incorporating roll-over strength, emergency exits and 3-point seat belts.

Coach roll-over strength is to be addressed by Australian Design Rule (ADR) 59/00 which has an implementation date of July 1992. The technical requirements of ADR 59/00 are based on ECE Regulation 66 "Super Structure Strength of Large Passenger Vehicles."

The requirements for emergency exits are covered in Australian Design Rule 58/00 which has a proposed implementation date of July 1993.

Proposed Australian Design Rule SBASS, which has an intended implementation date of July 1993, specifies the requirements for seats, seat anchorages and three point seat belts in coaches. The basis of this rule is that the restraint system shall provide 20g crash protection.

Postscript

Since this paper was presented, a further coach crash has occurred in Australia involving a double decker coach and resulting in five fatalities. The most severe injuries occurred from direct penetration of the coach occupant space. A detailed investigation is underway.

References

1. Ackerman C., Middlehurst J., Report on Fatal Bus Crash, Bass Highway, Anderson, February 1987. Road Traffic Authority of Victoria. Internal Report.
2. Ruller J., Report into the investigation of Fatal Traffic Incident Henri Robert Drive, Mt Tamborine 25th September 1990., Report to Coroner, Traffic Accident Investigation Squad, Queensland Police Depot, Alderly.
3. Duignan P, Dowdell B, Brown J., Study of Injury Mechanisms of Mount Tamborine Coach Crash, September 1990. Research Note 2/91. Available from Crashlab, RTA Library P.O. Box 110, Rosebery 2018 NSW Australia. FAX 61-2-662 4118.
4. Dal Nevo R., Report on Static Testing of Coach Seats to the Requirements of ECE Regulation 80. Crashlab Report SR 90/189 1990. Available from Crashlab, RTA Library P.O. Box 110, Rosebery 2018 NSW Australia. FAX 61-2-662 4118.
5. Dal Nevo R., Report on Dynamic Testing of Coach Seats to the Requirements of ECE Regulation 80. Crashlab Report SR 90/231 1990. Available from Crashlab, RTA Library P.O. Box 110, Rosebery 2018 NSW Australia. FAX 61-2-662 4118.

6. Dal Nevo R,. Wong H.L., Report on Series Two Dynamic Testing of Coach Seats to ECE Regulation 80. Crashlab Report SR 91/144 1991. Available from Crashlab, RTA Library P.O. Box 110, Rosebery 2018 NSW Australia. FAX 61-2-662 4118.

7. Dal Nevo R., Report on Dynamic Testing of Stratos Safe-T-Seat. Crashlab Report SR 91/244 1991. Available from Crashlab, RTA Library, P.O. Box 110, Rosebery 2018 NSW Australia. FAX 61-2-662 4118.

S9-O-15

Are Air Bags Compatible with Child Restraint Systems and Roadside Safety Features?

Thomas Turbell
Swedish Road and Traffic Research Institute, VTI

Abstract

For about 20 years rearward facing child seats have been used in Sweden for children up to the age of 3 years. These seats are usually mounted in the front seat passenger position leaning against the dashboard. The protection performance has been shown to be excellent (90-95% injury reduction) and this concept is now being adopted in other countries. A passenger air bag can obviously be dangerous in combination with this type of child seats and some dynamic tests have been done with different combinations. These tests show that the dummy accelerations will reach very high levels and that some child seats will disintegrate. This paper will present these results and discuss possible countermeasures. The new requirements for roadside safety features that are now being developed in Europe and the USA are based on the assumption that passengers are not using seatbelts. These requirements will encourage the development of systems with a low g-level at the beginning of the collision in order to let the unbelted occupants hit the dashboard with a low impact speed. During this phase the air bag will probably not deploy. When the passenger is in contact with the instrument panel the g-levels will be allowed to increase and the air bag will deploy. This is obviously a dangerous situation. This paper will discuss the present state of these requirements and the problems with air bag use in these situations.

Introduction

Air bags are now being introduced on a large scale, especially in the USA. The European market is a couple of years behind, but air bags are already offered in some cars. In order to work properly the air bag must be fully inflated within 50 ms after sensing a severe crash pulse. In order to do that a significant amount of emergency has to be released in a short time. If a car occupant or any other object is obstructing the path of the air bag during inflation, a dangerous situation might occur.

The problem with Out-of-position car occupants has been studied before [1,2,3] and is at present discussed in the ISO working group ISO TC 22/SC 10/WG 3. Several research projects are also in progress, especially within the industry.

This paper will deal with the problem of rearward facing child restraints in combination with passenger air bags. During the last two years, an SAE Task Force, Child Restraint Air Bag Interaction CRABI, has developed test procedures and suitable dummies on this subject. These dummies are now being evaluated and it can be expected that it will take at least another year before those test procedures will be incorporated in any legislation.

The potential risk of combining air bags with rearward facing child seats was first reported in 1976. [4] Since then this has been a special concern of the Swedish researchers in child safety. The only type of child restraint used by Swedish toddlers aged 1-3 is the rearward facing seat supported by the dashboard. [5] This concept is now being considered also in other European countries since a number of serious neck injuries have been found in forward facing child seats. The other type of rearward facing child seats is the infant carrier, which is used worldwide. This system is not dependent on the dashboard as a support, but a front passenger seat installation is often preferred because of the good possibilities of supervising the child.

The introduction of passenger air bags in cars in Sweden and the possibility of obtaining currently representative air bags for testing, was the initial impetus for this project.

The second part of this paper deals with the risk of out-of-position passengers in collisions with roadside safety devices. At the moment the US test procedures are being revised and a European standard is being developed. In both cases the question of the air bags has not been considered.

Dynamic Tests

Test Procedures

The dynamic frontal crash test procedure according to ECE-Regulation 44 [6] was used. The air bags, supplied by AUTOLIV AB, as used in all tests were of a type that is expected to come into use in a couple of years. Air bag volume was approximately 150 l and the triggering

time was set to 15 ms after impact. In the first 3 tests the air bags were installed at the instrument panel position on the Reg. 44 test rig in a "mid-mount" configuration with a 5° upward orientation of the blow-up direction. In the last test the air bag was installed in a "top-mount" configuration with a blow-up direction of 60° to the horizontal.

Head acceleration was recorded in addition to the required measurements in Reg. 44. The "typical" values given below indicate results from earlier tests without air bags.

Results

Test #: B959
Date: 900606-2
Air bag position: Mid-mount 5° upwards.
CRS used: Akta Loveseat, Hard shell infant carrier for group 0, approval no. E5 02006. This device is representative of most of the current infant carriers. When installed, the distance to the dashboard is approx. 30 cm.
Dummy: TNO P3/4 9 kg
Impact speed: 50,0 km/h
Stopping distance: 650 mm
Observations from highspeed film: The CRS is hit by the AB and assumes a vertical position.
Dummy acceleration data:
Chest resultant/3 ms: 38 g (Typical <50 g)
Head resultant/3 ms: 121 g (Typical <50 g)
Comments: Although there is no direct contact with the air bag in the beginning of the deployment the membrane force of the inflating bag is enough to produce high head acceleration in the dummy.

Test #: B956
Date: 900601-1
Air bag position: Mid-mount 5° upwards.
CRS used: Folksam Mini, Hard shell rearward facing CRS for group 0+1, approval no. E5 02051. This seat is representative of the "hard shell" seats available on the Swedish market.
Dummy: TNO P3 15 kg
Impact speed: 50,3 km/h
Stopping distance: 660 mm
Observations from highspeed film: The CRS is pushed away from the AB approx. 10 cm. The AB then goes downwards. There is no damage to the CRS.
Dummy acceleration data:
Chest resultant/3 ms: 131 g (Typical <50 g)
Head resultant/3 ms: 79 g (Typical <40 g)
Comments: In this, and the following cases, the punch out force of the air bag acts directly on the child seat. Even if this seat is intact after the test the accelerations in the dummy are quite high.

Test #: B957
Date: 900605-1
Air bag position: Mid-mount 5° upwards.
CRS used: Akta Duo + Baby, EPS-shell rearward facing CRS for group 0+1 approval no. E5 02022. This type of EPS-shell seats have been popular in Sweden for a couple of years.
Dummy: TNO P3 15 kg
Impact speed: 50.1 km/h
Stopping distance: 665 mm
Observations from highspeed film: The seatback of the CRS is completely destroyed when hit by the AB.
Dummy acceleration data:
Chest resultant/3 ms: 126 g (Typical <50 g)
Head resultant/3 ms: 78 g (Typical <40 g)
Comments: The high accelerations and the complete collapse of the CRS indicate a high injury risk for the child. The child is also unprotected in any secondary collision.

Test #: B960
Date: 900607-1
Air bag position: Top-mount 60° upwards
CRS used: Akta Duo + Baby, EPS-shell rearward facing CRS for group 0+1 approval no. E5 02022.
Dummy: TNO P3 15 kg
Impact speed: 50,0 km/h
Stopping distance: 660 mm
Observations from highspeed film: The top of the CRS is immediately blown away and the CRS collapses completely. The dummy is displaced downwards and ends up under the instrument panel.
Dummy acceleration data:
Chest resultant/3 ms: 69 g (Typical <50 g)
Head resultant/3 ms: 185 g (Typical <40 g)
Comments: The high accelerations and the complete collapse of the CRS indicates a high injury risk for the child. The child is also unprotected in any secondary collision.

Comments

The tested infant carrier and child seats do not seem to give adequate protection to its occupants under these circumstances. There is no reason to believe that rearward facing child restraints of other makes would behave differently.

Due to these results and some other incidents the "soft-shell" child seats are no longer in production in Sweden. They now have a hard cover on the outside of the EPS-shell. However, approx. 500.000 of these seats have been sold and will be used for many years to come.

The Time Bomb

Even if we should be successful in warning the owners of new cars not to use rearward facing child seats in combination with passenger air bags a "time bomb" is built into the system. We can expect that the second owners of these vehicles, more likely to be parents of small children, will not be reached by the warning messages. Even if they are, it is very likely that some will ignore the warnings and use their approved infant seats in the dangerous position. We must not forget that there are millions of infant seats available worldwide.

These seats have a long lifetime and are re-used many times.

Roadside Safety Features

In order to protect motorists from injury, several roadside safety features have been developed. Among these devices are median barriers, guardrails, yielding signs and light supports and crash cushions. These objects are developed and approved by crash tests.

For several reasons dummies are not used in these tests. The occupant risk is evaluated from the accelerations measured in the vehicle center of gravity.

Occupant Impact Velocity (OIV)

This approach has been used in the NCHRPR 230, Recommended procedures for the safety evaluation of highway appurtenances, published in 1981. [7] A popular name for this method is "the Flail Space Method." A very similar method was also published in Sweden in 1980 [8]. The main features of these evaluation procedures are the following:

- *Assume that the car occupants are not using any seat belts.* Even with a high general usage rate of seat belts it can be assumed that a large part of the occupants in roadside crashes are not belted.
- *Keep the impact speed of the occupants into the dashboard at a minimum level.* This is calculated by integration of the vehicle acceleration assuming that the occupant is a free mass that will move 0.6 m before impact. The NCHRPR is at present subject to an update where the "Flail Space" model probably will be kept. The proposed limit value for the impact to the dash is 9 m/s (32 km/h).
- *When the occupant is in contact with the dashboard the acceleration may rise to a higher level.* This phase is called the Occupant Ridedown. It is assumed that the acceleration may rise to 20 g during this phase without posing any serious threats to the occupant.

Theoretical Head impact Velocity (THIV) and Post-Impact Head Deceleration (PHD)

This evaluation procedure [9] has been proposed and will probably be used in the European Standard that is now being developed within CEN (European Committee for Standardization). Although this is a more sophisticated, two dimensional, model the main principles are the same as in the US requirements.

Intentional OOPO?

The problem of the Out-Of-Position Occupant (OOPO) has been discussed for a long time. The main concern is that an OOPO will be too close to the deploying air bag and that serious to fatal injury can occur.

The design goals for roadside safety features as described above may well encourage this out-of-position situation. The goal is in fact to position the occupant in contact with the dashboard or the steering wheel.

Conclusions

The introduction of passenger air bags poses a serious injury risk to small children using rearward facing child restraints in the front seat of the car.

There are several solutions to the problem that ought to be given a high priority in the development of air bags, child restraints and regulations.

- Mandatory warning labels in the cars and on the child restraints.
- The position of the air bag on the dashboard. Top- or low-mounted air bags may be safer.
- The deployment phase of the air bag might be altered in order to create a less aggressive situation.
- A detection device that will provide early deployment, before the impact starts, would allow for enough time of deployment at a lower intensity.
- Proximity sensors or switches might disconnect the air bag when a child restraint is installed. The ISOFIX [10] concept now discussed in the ISO working group (ISO/TC 22/SC 12/WG 1) may include devices available to disconnect the air bag.
- The rearward facing child restraints may be designed so that they can reduce the forces from the deploying air bag.

The present design criteria for roadside safety features may encourage designs that can induce an unwanted out-of-position situation. A careful evaluation of this problem ought to be made. For some roadside objects it might be feasible to ensure the deployment of the air bag at the first contact. This will, however, probably be unfavorable to unrestrained passengers in cars without air bags.

References

1. Mertz, H., Driscol, G., Lenox, J., et al., Response of Animal Exposed to Deployment of Various Passenger Inflatable Restraint System Concepts for a Variety of Collision Severities and Animal Positions. 9th International Technical Conference on Experimental Safety Vehicles, 1982.
2. Mertz, H., Restraints Performance of the 1970-76 GM Air Cushion Restraint System. SAE International Congress and Exposition. SE Paper 880400, 1988.
3. Horsch, J.D., Lau, I.V., Andrzejak, D.V., et al., Assessment of Air Bag Deployment Loads. 34th Stapp Car Crash Conference. SAE Paper 902324, 1990.
4. Aldman B., et al., Possible Effects of Airbag Inflation on a Standing Child. AAAM 18th annual conference, 1974.
5. Turbell, T., The Future of Child Restraints in Europe, Eurotraffic-91, Alborg, 1991.
6. United Nations, Economic Commission for Europe, ECE, Uniform Provisions Concerning the Approval of Restraining Devices for Child Occupants of

Power-Driven Vehicles ("child restraint systems") (E/ECE/324/E/ECE/TRANS/505) Regulation No. 44 Geneva, 1981.
7. Michie, J.D., Recommended procedures for the safety performance evaluation of highway appurtenances. National Cooperative Highway Research Program Report (NCHRPR) 230, Washington, 1981.
8. Turbell, T., Eftergivliga belysningsstolpar. VTI Report 204, 1980.
9. Laker, I.B., A Guide to the Measurement of Theoretical Head Impact Velocity (THIV) and Post-impact Head Deceleration (PHD). TRRL Reference 3.691, Farley Hill, 1991.
10. Turbell, T., ISOFIX Status report, May 1991. ISO/TC 22/SC 12/WG1 N220.

S9-O-16

Enhanced Airbag Model for the ATB Program

Tariq Shams, Nagarajan Rangarajan
GESAC, Inc.

Abstract

An enhanced airbag model has been developed for the Articulated Total Body (ATB) Crash Victim Simulation program. It consists of a number of new features and some features of the existing bag model have been modified. The new model can be implemented on minicomputers, workstations and 80386/80486 based microcomputers. Features of the enhanced airbag model discussed in this paper are, 1) a revised thermodynamic model which allows for gas flow to be input as a mass rate table and an optional temperature table for the temperature of the inflator, 2) an enhanced bag deployment model that allows for several input options to describe the bag shape during deployment, 3) general bag shape algorithm that allows modelling of an elliptical cylinder with ellipsoidal caps, 4) a revised model to describe impact between the airbag and the occupant during the unfolding of the bag, 5) allowance for the input of bag shape during deployment as a time-history table, 6) a simple folding model to calculate the effects of the bag impact during deployment, 7) a revised contact force calculation between the bag and external segments and planes which includes an explicit calculation of the contribution of bag tension. Results of theoretical validation of the model for impact of the bag with simple shapes will be presented. Initial validation based on data from sled tests will also be presented.

Introduction

The Articulated Total Body program (ATB) is a widely used crash victim simulation program [1]. The airbag model originally available in this program suffers from a number of limitations such as restrictions in the way gas inflow is modelled, numerical instability, restrictions in the shape of bags that can be modelled, etc. These limitations made the bag model cumbersome to use and an unreliable design and modelling tool.

Airbags are becoming standard equipment in cars and therefore restraint system engineers and other researchers need a more efficient tool to model bags. Recognizing this, engineers at the General Motors Corporation have undertaken an effort to enhance the airbag model using the Cal-3D program which is their proprietary version of the ATB program [2]. Following the same argument, we have developed a number of enhancements to the airbag model which have been implemented in ATB and in our commercial occupant simulation model "DYNAMAN."

This paper describes the enhancements developed to make the ATB airbag model capable of modelling currently available airbags. The simplicity of the model and input data, the reasonable correlation between simulation and test results, and the short duration it takes to exercise this model even on microcomputers suggests that it is a good design tool which can be used to carry out parametric tests as a part of the overall design process.

The enhancements to the bag model will be described in the next few sections. In each section, we will start off by giving a brief description of the limitation of the old airbag model and follow it up with a description of the enhancements.

Enhanced Model Development

Bag Thermodynamics

Limitations of the old airbag model. The mass flow rate is determined from a fixed volume gas supply, based on the theory of compressible fluid flow. It is difficult to convert the data from tank tests into the required characteristics of the gas supply.

Enhanced thermodynamics model. In the new model, the mass flow rate is provided as a time-history table. Mass flow rates can be obtained from manufacturers or by converting standard tank test results (which provide pressure histories within a constant volume tank). Gas temperature in the generator can be input as a constant or as a temperature-time history table.

The thermodynamic state variables (pressure, temperature, and volume) are computed at each instant of time based on the laws of conservation of energy and assuming [2,3,4]:

- Isentropic flow.

- The gas behaves as an ideal gas with constant specific heats.
- The processes of gas flow into the bag and of airbag deformation is adiabatic.
- The temperature and pressure are uniform within the bag at each instant of time. This means that the relaxation times of the thermodynamic variables are much shorter than rates of local deformation and mass flow.

Using the above assumptions, the following bag thermodynamic calculations are made during the time the bag is filling up and after complete deployment when additional mass flow is responsible for increasing pressure.

- During deployment, at each time step:
  - calculate total mass in bag
  - determine bag volume or pressure depending on deployment input
  - determine contact volume
  - determine temperature in bag
- After full deployment, at each time step:
  - calculate total mass in bag
  - determine contact volume
  - determine total bag volume and pressure, including expansion due to optional bag stretch
  - determine temperature in bag

Bag Deployment

Limitations of the old airbag model. The bag is modelled as an ellipsoid and during deployment the axes of the ellipsoid are scaled in the ratio of the current volume to the final bag volume. The initial pressure in the bag during inflation is taken to be at atmospheric pressure until the effective volume (current volume + penetration volume) equals user defined volume of the bag, at which point, bag pressure can rise above atmospheric. No work is done in inflating the bag to its full volume.

Enhanced deployment model. The new bag model allows the user to define the expansion time history of the bag in the following ways:

- No input—it is assumed that the bag fills at atmospheric pressure and the bag geometry is determined by scaling from current volume as in the old bag model.
- Bag volume-time history is specified—pressure is calculated based on the perfect gas equations and current dimensions of the bag axis are calculated by assuming scaling with respect to final bag shape.
- Bag axes-time history is specified—volume is calculated and then pressure calculated.

Regardless of the input options, if there are interactions during deployment, then the geometry that the bag would have if there was no contact is used to determine the intersections with the contacting segments.

With the modified deployment input, gauge pressures within the expanding bag may be positive before the effective volume reaches the geometric volume, and contacts with impacting segments will generate forces. Thermodynamic calculations were also modified so that the effective volume during deployment was based on the current bag geometry.

A sample procedure to obtain deployment data. As a part of this work, a procedure was developed to determine bag deployment data from film analyses of an airbag viewed through two orthogonal projections, namely a side view and a plan view. In order to test this procedure, digitized data from films of a mid-mount airbag deployment sequence were obtained from the National Highway Transportation Safety Administration (NHTSA). The digitized data were processed to obtain contour dimensions of the bag during deployment. The contour dimensions provided data for calculating the velocity and acceleration of the leading edges of the bag in any of the three principal directions. Also, a simple integration scheme was used to estimate the bag volume from the data defining the contours in two orthogonal views.

A computer program was also developed to analyze the digitized bag configuration data during deployment obtained from film analysis. This program can visually display the evolution of the bag in the two cross-sections for which film data were available. The program determines the maximum extents of the bag in two orthogonal directions for each view at each time in the deployment sequence. It assumes that these two extents represent approximately the axes lengths of an equivalent elliptical section. For each view, the program estimates the area of the bag section using a simple Simpson's integration over the contour of the bag section.

Once the area of the bag in each view is estimated, the program estimates the volume of the bag, by assuming elliptical cross-sections across the common axis between the two sections and then again numerically integrating the area of these sections over the common axis. Since the times at which the two views are measured are usually different, the cross-section values at common times were estimated by a simple linear interpolation of the original cross-sections.

Once the axes lengths at different instants of time were determined then these values can be input into the new airbag model to describe the unhindered deployment of the bag. This deployment history has been utilized in a trial simulation with the new bag model. Since no dynamic information for this bag was available from the test, it has not been possible to utilize the data in an impact simulation.

Figures 1 and 2 show the side and plan views of the bag deployment as obtained from the digitized film data.

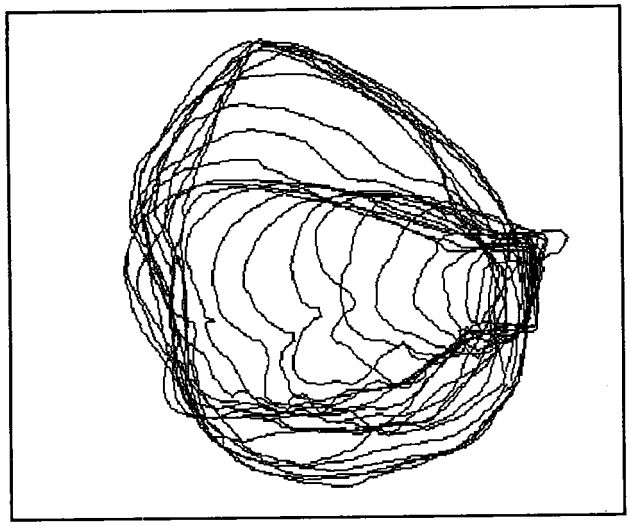

Figure 1. Side View of Bag Deployment

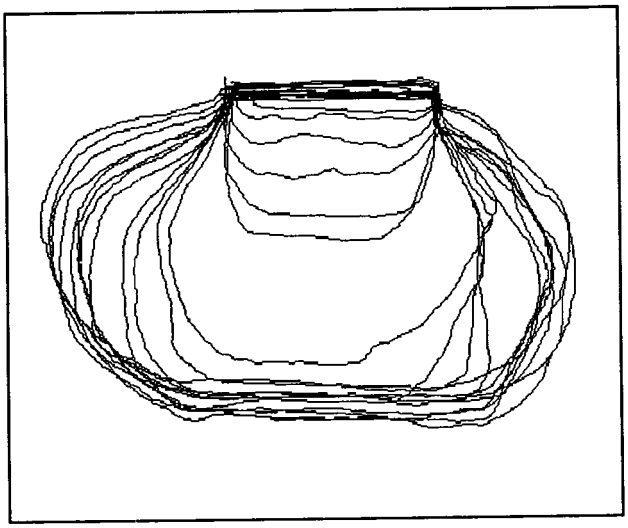

Figure 2. Plan View of Bag Deployment

Bag Dynamics During Deployment

Limitations of old bag model. The original bag model did not have a model of the bag dynamics during inflation.

Model of bag dynamics in enhanced model. In order to determine the effect of the expanding bag on occupants who may interact with it at the early stages of deployment, some estimates of the energy transfer is necessary. In order to arrive at this estimate, it was assumed that gas flow through the inflator orifice was sonic and this flow propelled the leading surface of the bag against an intruding segment. The force due to impact of such a moving surface is determined from a simple energy transfer mechanism where the momentum of the leading surface is completely transferred to the contacting segment and hence the force acting on the surface may be estimated.

Some preliminary research was carried out in assessing the suitability of a model of the initial gas flow into the uninflated bag. It was assumed that during the earliest deployment phase, the flow will resemble an unbounded turbulent jet through an orifice. For a cylindrical jet, the fall in the maximum jet velocity is inversely proportional to the distance from the orifice [5]. In such a jet, the total momentum across a section remains constant and can be taken to be the momentum at the orifice.

The folding pattern is modeled approximately as being rolled into a cylinder or linearly in an accordion pattern. The gas jet will cause the bag to unfold and initially the bag will expand only in the direction of the jet. As a first approximation, the bag will continue expansion in the deployment direction till the maximum geometric extent is reached. At that point the bag will begin to expand in the other two directions. These models of folding patterns are being currently evaluated.

Bag Contact and Penetration

Limitations of old airbag model. The interaction between an occupant and the bag is modeled as the intersection of two ellipsoids, which then provides a geometrically based calculation of the deformed volume. The forces acting on occupant segments are estimated from the active contact area and the current pressure.

Enhanced contact and penetration models. As the bag shape has been generalized to include more than one section, with both cylindrical and ellipsoidal geometries, a new penetration algorithm described below has been developed.

The procedure for calculating the contact forces are built up of several algorithms. These are:

- Algorithm for detecting penetration. The ATB routine for detecting penetration has been generalized to allow for penetrations between an ellipsoidal segment with an ellipsoid, a cylinder or a semi-ellipsoid.
- Algorithm for calculating of maximum penetration. Existing ATB routine was generalized to account for penetration with a bag with a cylindrical section or an ellipsoidal cap.
- Calculation of penetration volume and area of intersection. Because of the somewhat arbitrary nature of the individual bag segments, the volume and area are being calculated by integrating over the portion of the occupant ellipsoid and bag segment that have penetrated one another. Simpson's method is being used to integrate in 2 and 3 dimensions.

After enhancing the ATB routines as described above, the algorithms were tested by comparing results yielded by them with analytic computations of area of contact and the direction vector for two intersecting spheres. The numerical integration scheme developed to calculate the volume of intersection between the segments, and the area of contact (including the resultant direction of the area) was found to be reasonably accurate (between .1 and 1%). The calculations appeared to be stable over a variety of ellipsoid shapes (from spherical to highly

oblate and prolate spheroids with major to minor axis ratio of 10 to 1). Figure 3 shows an example of an intersection of an ellipsoid B with a bag A. Figure 4 shows the method by which the numerical integration of the penetration volume is calculated, i.e. by subdividing the penetrated volume into small wedges.

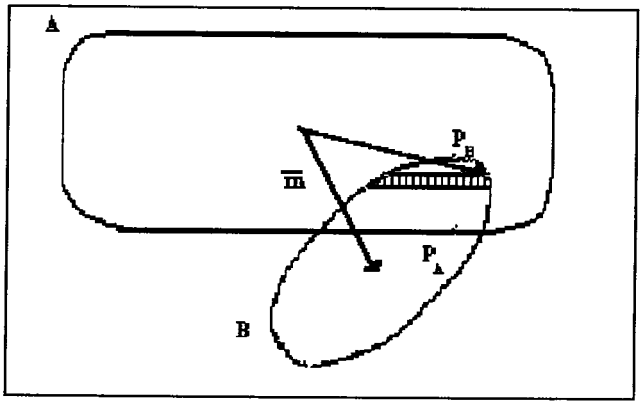

Figure 3. Penetration of Bag by Ellipsoid

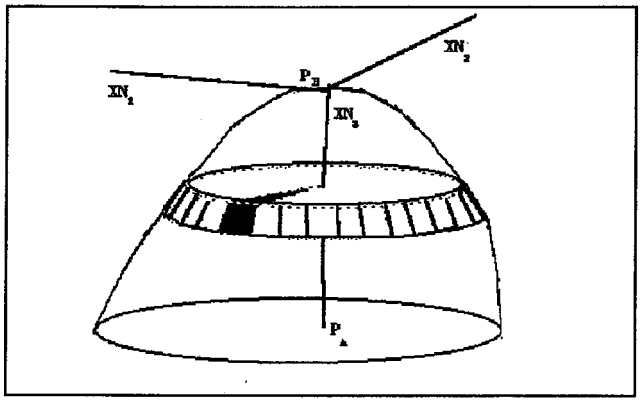

Figure 4. Calculation of Penetration Volume Using Numerical Integration

Bag Tension Calculations

Limitations of the ATB airbag model. There is no independent calculation of the bag tension. The bag itself is assumed to be stretchless. This can cause problems in situations such as when the rise of pressure in the bag due to penetration cannot by itself support the penetrating segment.

Enhanced bag tension calculations. The calculations being made for the deformation due to tension, are based on the following assumptions:

- There is no local deformation of the bag due to stretching. This assumption should hold for the typical materials involved with airbags.
- Equilibrium is maintained at any moment while the bag is being penetrated.
- Tension is uniform over latitudinal planes and it varies slowly over the entire bag. This assumption should hold fairly well when the relative velocity of the segment is less than the speed of elastic waves in the bag. This assumption will not be true for bags with sharp contours, e.g. a cylindrical section with flat sides stitched on. Also, for highly elliptical bags the tension must vary over the surface for positive gauge pressure within the bag, if the pressure is assumed to be uniform. But for large, smoothly curved bags the assumption of uniform tension is reasonable for those sections where there is no direct contact with the segment. In general, in the absence of an external force, the tensions at a point along two orthogonal directions on the bag are related by the equation:

$$\frac{T_1}{r_1} + \frac{T_2}{r_2} = p$$

where
T_i = tension in each direction
r_i = radius of curvature of the bag in a plane section containing direction i
p = pressure in the bag

A set of equations describing equilibrium conditions for the pressure and tension and excluding inertial and stretch effects was derived. This equation was then used to relate the change in tension along each of the two coordinate directions on the surface of the bag in the region where there is no contact. A numerical algorithm estimates the deformed contour by integrating these equations over the section of the bag which is not in direct contact with any segment. Since contact is made with ellipsoids, the two natural orthogonal directions are one measuring an azimuthal angle and one measuring a polar angle.

The total force acting on the segment is found from the force due to pressure acting over the area of contact and the total tension force integrated over the contour. In Figure 5, the area on which the pressure force is acting is denoted by A, and the effective area supported by the tension is denoted by B. The total force, for the situation depicted in the figure, where both the segment and the bag shapes are spherical is given by:

$$F = \pi r^2 p + 2\pi r T \sin\theta$$

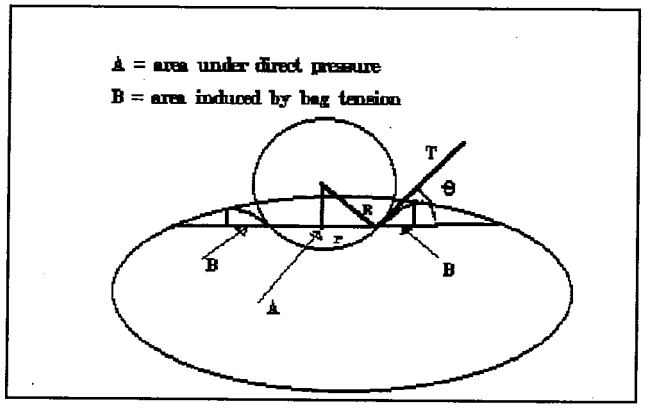

Figure 5. Pressure and Tension Contributions to Total Force

Validation of New Airbag Model

Simulations of Simple Ellipsoid Impact

New algorithms in the modified ATB program were tested in phases. The new thermodynamic model with the mass flow table as input, was tested first and this thermodynamic model was also tested with a user specified deployment history as input. Mass flow tables used in tank tests were used as input and the total mass and pressure in the bag matched well with the test results.

The new algorithms for measuring the penetration of the bag were tested using ellipsoids with different shapes impacting a bag pressurized to a specified level. Checks were made to see if the law of conservation of energy was obeyed, i.e., the impactor should rebound from an unstretchable bag (without vents) with the same speed. Approximate penetration distances and penetration volumes were also be estimated using simple equations and these were compared with the results of the simulations.

The airbag used for the simulation tests, had an ellipsoid shape with x, y, z semiaxes of 6.0, 12.0, and 12.0 inches respectively. It was inflated to a gauge pressure of 5 lbs/sq. in. A mass of 20 lbs was used as the impactor in the simulations. It was given an initial longitudinal velocity of 100 in/sec. Four simulations were performed with the impactor having different semiaxes in each simulation. The dimensions were selected primarily to vary the aspect ratio of the face of the intruding segment. The following dimensions for the ellipsoids were used:

Table 1. Ellipsoid Dimensions Used for Simulations

Simulation	Shape	x (in)	y (in)	z (in)
1	sphere	3.5 in	3.5 in	3.5
2	oblate spheroid	1.0 in	5.0 in	5.0
3	prolate spheroid	5.0 in	2.0 in	2.0
4	large spheroid	1.0 in	12.0 in	12.0

The results for these simulations are summarized in Table 1. It shows the maximum penetration of the ellipsoid in each simulation the corresponding force. It also shows the distribution of pressure and tension forces for the maximum force and the rebound velocity after the impact is completed.

As can be seen from these results, the depth of penetration is a function of the aspect ratio of the penetrating segment. Object 3 which most resembles a thin, long segment of the body is balanced mostly by tension forces as can be seen from the relatively high ratio between tension and pressure forces for this object. One would then expect object 4 which is a large (size comparable to the bag) flat object, would be predominantly balanced by the pressure. A perusal of the results in Table 2 seems to contradict this expectation. The reason for this is that even though the tension force itself is low, the contour in contact is so big, that the final contribution is nearly the same as that of the pressure force.

Table 2. Results of Simulation

Simulation	Max. Penet (in)	Max. Force (lbs)	Press. Force (lbs)	Tension Force (lbs)	Rebound Vel. (in/s)
1	2.70	228	187	42	100.0
2	1.66	409	384	25	100.9
3	5.24	92	82	10	100.0
4	1.10	466	261	205	101.0

Validation Using Sled Test Data

Two sets of sled test data were used. A Hybrid III 50% dummy seated on a hard seat in the driver side position was used to simulate the occupant in these full frontal crash tests. Crash pulses represented initial speeds of 30 to 35 mph. In the first test, the dummy did not have any belt restraints and was restrained by the airbag and dash panel. In the second test, the dummy had was restrained by lap and shoulder belts in addition to the airbag.

Figure 6 shows the comparison of the upper torso resultant accelerations of the simulation and the first test. Figure 7 is a similar comparison of the resultant head accelerations. There is good correlation in the values of the peak resultant accelerations for both cases. For the head acceleration, there is an appreciable lag in the timing of the peak. We are looking into this discrepancy further by analyzing the film from the test to compare the kinematics more thoroughly. Figures 8 and 9 are similar graphs for the test with the dummy restrained by belts. In these simulations, there is good correlation with test results for both the magnitude and the time of the peaks.

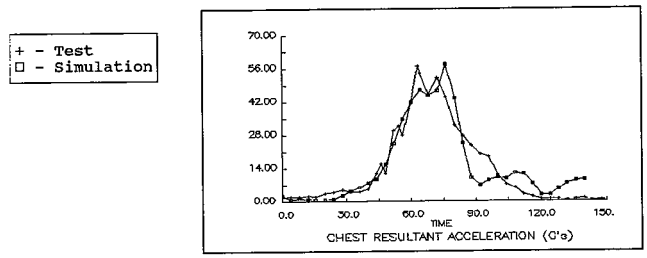

Figure 6. Comparison of Upper Torso Resultant Accelerations for Unbelted Driver

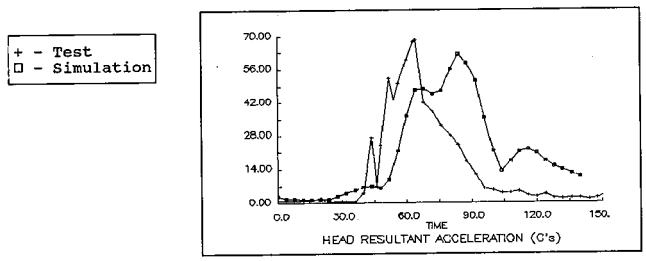

Figure 7. Comparison of Head Resultant Accelerations for Unbelted Driver

Conclusions

A model to carry out a more realistic analysis of airbag interaction with a vehicle occupant has been developed. The new model allows for the input of the

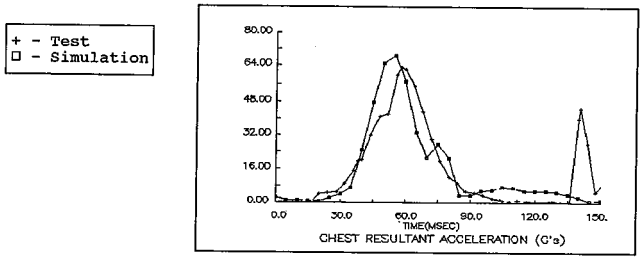

Figure 8. Comparison of Upper Torso Resultant Accelerations for Belted Driver

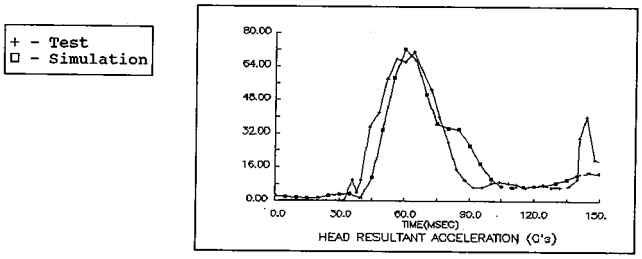

Figure 9. Comparison of Head Resultant Accelerations for Belted Driver

gas as a flow rate table, thus allowing for testing of designs with different mass flow rates. The deployment history of the airbag may also be input, thus allowing for various methods for inflating the airbag, depending on folding patterns and different rates at which the airbag inflates in different directions. The airbag shape has also been generalized to allow for cylindrical as well as ellipsoidal bags. The thermodynamic calculations have also been modified to allow for the generalization in the gas flow and in airbag shape. The contact force calculations have also been modified to allow for calculations of the generalized shapes.

Recommendations for Future Efforts

Further validation of the dynamics of the bag itself and the behaviour of the bag in impact situations during deployment is necessary. The methodology for such validation would include experimental testing of airbag deployment motion without impact with an external object, of airbag deployment motion with impact with external object in the path. Experimental testing and comparison with simulation results of contact forces arising from impact with variously shaped external objects moving at different speeds and possibly different directions is also needed.

Several future enhancements are being considered. One is a more detailed contact routine which uses dynamic equations for the airbag membrane rather than assuming a quasi-static equilibrium condition. Another is a more accurate modeling of the initial bag deployment, where the gas jet interaction with the bag material is followed locally rather than assuming a gross motion of the bag face and the accompanying folded bag. A third is modeling of the firing time by using an algorithm for detecting the deceleration level or change of velocity or a similar logic that may be used by the sensor system. A fourth enhancement is generalizing the bag shape, and finally, modeling of internal tethers as tension elements (which cannot support compression).

Acknowledgements

Part of the work described in this paper was carried out under funding from the NHTSA and under an SBIR award from the Armstrong Aerospace Medical Research Laboratory (AAMRL).

References

1. J.T. Fleck, F.E. Butler, N.J. DeLeys, "Validation of the Crash Victim Simulator," NHTSA Report Nos. DOT-HS-806-279 through 282, 1982, Vols 1-4.
2. J.T. Wang, Donald Nefske, "A New CAL3D Airbag Inflation Model," SAE Technical Paper Series 880654, 1988
3. T. Shams, W. Mahmud, "Passenger Airbag Model of Deployment and Occupant Interaction," Contract No. DTNH22-88-C-07477, January 1990.
4. I.G. Currie, "Fundamental Mechanics of Fluids," McGraw Hill Book Company, 1974.
5. H. Schlichting, "Boundary Layer Theory," McGraw Hill Book Company, Seventh Ed., 1979.

S9-O-18

Finite Element Simulation of Airbag Deployment and Interactions With an Occupant Model Using DYNA3D

T.B. Khalil
General Motors Corporation
R.J. Wasko
Motor Vehicle Manufacturers Association of the U.S.A.
J.O. Hallquist, D.J. Stillman
Livermore Software Technology Corporation

Abstract

Analytical modeling of airbag inflation is desirable in automotive design, particularly when the technique encompasses the airbag, occupant and vehicle structure in an integrated system. This paper reviews the development of nonlinear finite element (FE) technology to simulate airbag deployment and its interaction with an articulated occupant model. The technology is being developed in the dynamic large deformation DYNA3D

code which has been successfully used in vehicle crashworthiness simulations. During the project evolution, a number of technical issues have become quite clear and dictated specific developments.

A fabric material model which treats wrinkling has been developed. An algorithm to determine the airbag volume during the inflation process was added. A simplified gas model based on assuming uniform thermodynamic properties (pressure, density, temperature and internal energy) throughout the airbag deployment was coupled to the airbag structure. Early in the development, the problem of air bag unfolding was determined to be important, so a new contact algorithm was developed to properly simulate unfolding. This led into identifying a need for generating a folded mesh of an airbag, so this too was developed; since no meshing algorithms were available to generate tightly folded fabrics. Finally, work was done to simulate an occupant by a system of jointed ellipsoidal rigid bodies. These new capabilities have been brought together into a framework, MVMA/DYNA3D; that can be used in a system's approach to mathematical simulation of occupant response in a vehicle crash environment.

This paper summarizes these developments with emphasis on validating inflation of an unfolded airbag, predicting its deployment kinematics and identifying its contact and interactions with several spherical and flat surfaces. The predicted bag deformations and contact forces compared favorably with corresponding experimental data. In addition, a preliminary attempt was made to simulate the deployment and interactions of a folded airbag with a hybrid III dummy model.

Introduction

Public and government interest in transportation safety, and in particular public demand for better protection against potential harm in motor vehicle crashes has been intensifying throughout the industrialized and developing countries. Accordingly, occupant protection has been, and continues to be, a primary design consideration in the automotive industry. Lately, vehicle manufacturers have accepted the fact that vehicle safety, embodied in structural crashworthiness and occupant protection systems, provide a measure of product superiority and a competitive advantage in the market place.

The subject of occupant protection is truly multidisciplinary, encompassing many fields: structural mechanics, material science, biomechanics, mathematics, numerical analysis, etc. There are two extreme approaches to vehicle design: totally analytical, relying primarily on computational techniques, and completely empirical based on trial and error experimental procedures. Obviously, neither extreme is desirable; a combination of rational analysis with well thought of testing offers the greatest potential in cost and time benefits.

This paper summarizes the development of basic analytical finite element technology to simulate airbag inflation and interaction with an occupant model. The developed technology can be used in conjunction with experiments to mathematically simulate the response of an occupant in a vehicle crash environment; where both the influence of vehicle crashworthiness and restraint systems: airbag, belts, knee bolster can be evaluated for occupant protection

Background

It is commonly acknowledged by engineers and scientists charged with occupant protection that human harm and injuries can be dramatically reduced by minimizing occupant movement and subsequent collision (second collision) with the vehicle interior. Several seat belt systems have been introduced to keep the occupant in his (her) seat should a crash occur. In recent years a combination of a lap belt, airbag (lately has been called supplemental inflatable restraint device), and a knee bolster has emerged as a favored supplemental "passive" restraint system. The effectiveness of such a system in minimizing or reducing injury severity from second collision impacts is evidenced by the recent activity of major automotive manufacturers to incorporate it (or plan to in the near future) in virtually all their vehicles.

The heart of this supplemental passive restraint system is a prefolded fabric sack, stowed away in the passenger side of the dashboard and/or in the steering wheel hub, that can be filled with pressurized inert gas in a short time (approximately 20-40 ms). The development of such a device dates back to early 1950's [1,2]. Over the past 20 years considerable research has been conducted to bring the airbag from an experimental laboratory device to a mass produced reliable restraint system.

As with many engineering systems, early airbag research was predominantly experimental. Analytical studies of airbag deployment and its potential protection of vehicle occupants, in the event of crash, followed shortly [3,4]. Several analytical models have been developed to simulate airbag inflation and subsequent interactions with an occupant model. The majority of these models were developed as part of "Crash Victim Simulators" (CVS); where the occupant is typically represented by an assemblage of articulated rigid bodies.

An overview of these models and their shortcomings is provided in a recent study [5]; sponsored by the Motor Vehicle Manufacturers Association (MVMA) of the United States of America. Limitations of current airbag models include: simple two-dimensional geometry, bag elasticity may not be accounted for, bag shape is unaffected by the occupant and vehicle interior geometry and the use of "tuneable parameters" raises questions about the model's truly predictive capability. It is generally acknowledged, even by the developers of such huerstic models [5], that their capabilities are inadequate for simulating impact and interactions with an occupant. This particular capability is extremely important in vehicle design, not only for the normally seated adult but also for the forward positioned child.

Recent progress in nonlinear Finite Element (FE) technology together with the availability of continually increasing power in computer hardware have allowed for the successful simulations of vehicle crashes where the structure is represented with sufficient detail [6]. This success has provided an impetus to safety engineers to apply FE technology to airbag modeling [7,8,9].

In 1989, as part of MVMA's continuing research effort in occupant protection by analytical techniques, a need was identified to develop a state-of-the-art FE technology to simulate airbag deployment and interactions with an articulated rigid (or deformable) occupant model. This technology should not be limited to the previously discussed shortcomings. It also should provide MVMA with the necessary source codes so its members can adapt it to their specific requirements. A decision was made to develop this technology within the framework of the public domain code (Circa 1989), DYNA3D [10]; which is widely used in crashworthiness analysis [11].

Overview of DYNA3D

The development of the DYNA3D code began in 1976 [12] at the Lawrence Livermore National Laboratory and was originally developed to study crashworthiness of bombs dropped from aircraft.. The code formulation is Lagrangian based and utilizes an explicit integration scheme in time. Early in the development of airbag modeling, it became apparent that given the requirement of reasonable mesh densities, large deformation three-dimensional calculations could be achieved only if the software was highly optimized, vectorized, employed element technology that would permit as fewer calculations as possible and provided a robust treatment of contact impact problems.

To achieve the goal of cost effective elements, it became necessary to use under integrated elements with some means of controlling the zero energy modes, called "hour-glassing" that get excited during the calculations. Fortunately, it was found that this could be easily accomplished by introducing appropriate mesh constraints to rid the deformations of the spurious modes without influencing the actual deformations. Several techniques have since developed [13,14] which largely overcame the hour-glassing problem for most applications. We noted in our airbag development, however, that triangular elements were the most stable elements and that hour-glassing still exists in some of the shell elements in DYNA3D. In an attempt to provide a cost effective quadrilateral shell element for treating the membrane behavior of the airbag material, we have implemented a recently developed element [15] which appears to be less susceptible to hour-glassing.

Objectives

The objectives of this effort then were to develop the theoretical basis and all necessary coding in DYNA3D to:

- Model airbag inflation,
- Incorporate the gas dynamics of the inflation process,
- Develop technology to generate a folded airbag FE grid,
- Develop a single surface contact algorithm to model airbag unfolding,
- Model the dynamics of an articulated occupant model and
- Simulate the contact and interaction process between a deploying airbag and an occupant model.

Approach

To achieve these objectives, we first considered the airbag modeling problem and developed the necessary capabilities to solve it. This included modeling of the fabric behavior, the "control volume" approximation and the equation of state for the gas. Next we incorporated in DYNA3D a gas inflation model [16] to treat the gas flow during the inflation process. An inflator model is also added to determine the mass and energy flow rates into the airbag from the inflator. Then, we developed an airbag folding algorithm to fold FE meshes of unfolded airbags into their initial folded geometry. This folding algorithm is embedded in the INGRID [17] mesh generator code.

The airbag contact problem was also considered and a new single surface contact algorithm was developed especially to treat inflation of a folded airbag although much additional work remains to be done in this area. We have also developed a lumped mass occupant model using rigid bodies and joints available in DYNA3D. To treat the contact between the occupant and the airbag "contact entities" were developed which can attach to rigid bodies to provide a very cost effective contact treatment. The contact entity is an analytical representation of the contact surface that allows for closed form solutions of the contact problem.

In this paper we present the highlights of these developments incorporated in MVMA/DYNA3D. We believe that much research remains to be done; and hope to report on it in future meetings.

Airbag Modeling

Three aspects of airbag modeling are described in this section. First, the treatment of the fabric is considered. secondly, modeling of the interior of the airbag is outlined where we used a "control volume" to avoid the necessity of modeling the air with solid elements. Finally, we describe the equation of state model that provides the gas pressure as a function of temperature and density.

Fabric Material Model

The most obvious feature in fabrics is that they have almost no bending strength and compressive loads immediately result in buckling plus an inability to develop compressive stresses. The inability to support compressive loads introduces a strong non-linearity into

any attempt to approximate fabrics as isotropic or orthotopic continua. An additional complicating factor is that the fibers which makeup a fabric interact in a complex manner which can deviate considerably from continuum behavior.

Several approaches are available to simulate the compressive behavior of fibers [18-21]. In MVMA/DYNA3D, we followed the approach described in reference [18] for treating the non-linearity in fabric behavior. The airbag fabric model is based on an orthotopic elastic material model which can be used in conjunction with several shell elements in DYNA3D. The shell element can be represented by a multi-layered laminate as shown in Figure 1. To allow for an arbitrary orientation of the finite elements within the mesh, each ply in the fabric may have a unique orientation angle (ß) which measures the offset angle (Θ) from some reference determined by the angle (ψ), defined for each element.

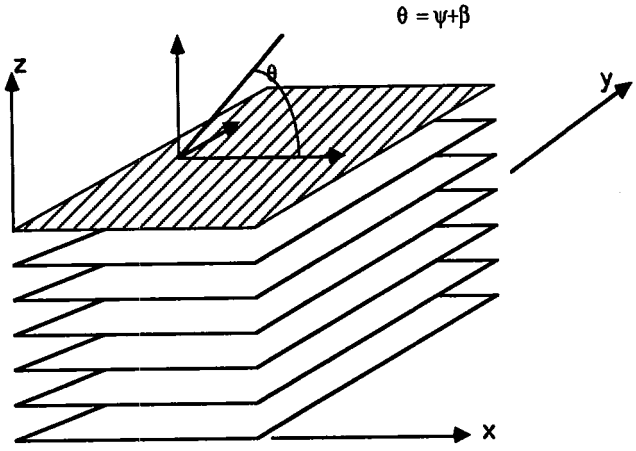

Figure 1. Multi-Layer Fabric Defined (Angle ß, Measured from a Reference Determined by the Angle ψ for Each Element, is Defined for Each Lamina)

The fabric material model differs from an elastic orthotopic model in two important ways:

- compressive stresses are inadmissible,
- there exists initial "slack", i.e. only low levels of stresses are developed in the fibers until the material is stretched taunt.

This behavior can be modelled by representing the modulus of the fiber as a function of fiber strain. Figure 2 illustrates an idealized modulus-strain relation for a fabric material. The idealized model produces a zero modulus for compressive strains (segment a-b in Figure 2) and piece wise linear modulus for tensile strains (segments b-c-d). The zero compressive modulus simulates the inability of the fibers to carry compressive stresses and the piece wise tensile modulus simulates the initial slack in the fabric.

In addition to the previous material model, a second model has been implemented into DYNA3D based on truncating the stresses such that no compression is allowed.

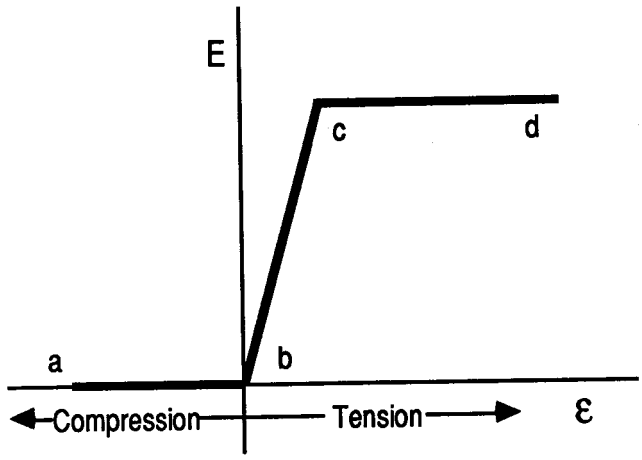

Figure 2. Idealized Young's Modulus as a Function of Fibre Strain

Control Volume Modeling

A direct approach for modeling the contents of the airbag would be to discretize the interior of the airbag using solid elements. The total volume and pressure-volume relation of the gas would then be the sum of all elemental contributions. Although this direct approach could be applied in a straight forward manner to an inflated airbag, it would become very difficult to implement during the inflation phase of the airbag deployment. Additionally, as the model is refined, the solid elements would quickly overwhelm all other computational costs and make the numerical simulation prohibitively expensive.

An alternative approach for calculating the airbag volume, that is both applicable during the inflation phase and less computational demanding, treats the airbag as a "control volume". The control volume is defined as the volume enclosed by a surface. In the present case the "control surface" that defines the control volume is the surface modeled by membrane elements comprising the airbag fabric material.

Because the evolution of the control surface is known, i.e. the position, orientation and current surface area of the airbag elements, we can take advantage of these properties of the control surface to calculate the control volume by applying Green's theorem. This leads to:

$$v = \oint x n_x d\Gamma \approx \sum_{i=1}^{N} \bar{x}_i n_{ix} A_i \qquad (1)$$

where,
V = control volume,
N = number of elements,
x = average x coordinate for each element i,
n = direction cosine between the element normal and the x coordinate and
A = the surface area of the element.

The previous equation is implemented in MVMA/DYNA3D with the direction of integration chosen to be parallel to the maximum principal moment of inertia of

the surface. Numerical experiments have shown that this choice of integration direction produces more accurate volume than in selecting a coordinate direction or other principal inertia directions. A special treatment was also included to account for airbag venting holes.

Equation of State (EOS) Model

At each time step in the calculation the pressure in the airbag corresponding to the control volume can be determined from an EOS that relates the pressure to the current gas density (volume) and the specific internal energy of the gas. The EOS for airbag simulations is the usual 'Gamma Law Gas Equation of State' used in reference [5], which follows from thermodynamic considerations of adiabatic expansion of an ideal gas. This equation can be written as:

$$P = (\gamma - 1)\rho e \tag{2}$$

where P is the pressure, γ is the ratio of specific heats, ρ is the density and ε is the specific internal energy of the gas. The specific internal energy evolution equation corresponding to two states is given by:

$$e_2 = e_1 \left(\frac{V_2}{V_1}\right)^{(1-\gamma)} \tag{3}$$

The control volume equation (1) together with the EOS *(2)* and the specific internal energy equation (3) completely define the pressure-volume relation for an inflated airbag

Airbag Inflation Model

An airbag inflation model based on reference [16] formulation was coded and implemented in MVMA/DYNA3D. The model considers the mass flow due including the vents and leakage through the bag. This model requires as input the mass flow rate and gas temperature going into the bag from an inflator, provided as functions of time.

Also, an airbag inflation capability was incorporated into MVMA/DYNA3D; which permits the addition of a user subroutine to determine the mass and energy flow rates into the bag. This development closely parallels those reported in reference [16], and assumes that the control volume of the inflator is constant and that the amount of propellant reacted can be defined as a tabulated curve of fraction reacted versus time.

Airbag Model Validation

The airbag modeling capability in MVMA/DYNA3D is validated by comparing the model response of a generic driver side airbag with experimental data from reference [5]. In the experiments, the airbag shown in Figure 3 was inflated to a volume of 60 liters at a pressure of 4000 Pa. The mass of the airbag including the straps was 405.6 gm. Tests were conducted by launching different shaped projectiles at varying velocities into a supported airbag. The time history of the projectile displacement, velocity and acceleration along with the airbag pressure history were recorded.

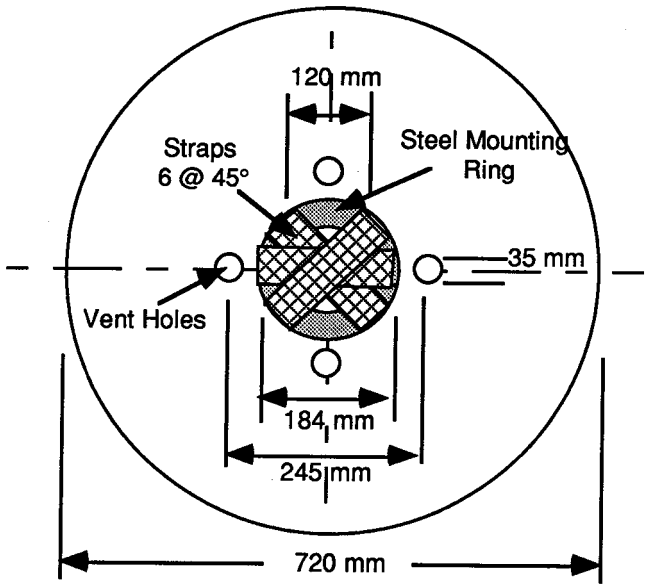

Figure 3. Schematic of Deflated Generic Airbag Used in Reference [5]

In this paper, we present a comparison between model predictions and experimental results for a hemispherical projectile (165 mm in diameter and 7.85 kg mass) with an initial velocity of 5.2 m/s impacting an airbag supported on a flat plate. Although similar models were developed for all of the experiments described in reference [9], no additional results are presented here due to the qualitative similarity among all the results and space limitations. The FE model (Figure 4) simulated the airbag with membrane quadrangular elements. Two additional models with a coarse and refined meshs (3969 and 14840 elements) were also developed and used in our analysis. The fabric material properties were taken as provided in reference [9].

The modeling proceeded in two steps. In the first step dynamic relaxation was used to obtain the static equilibrium configuration for the inflated bag. In the second, a full model restart assigned an initial velocity to the impactor and initialized all elemental and nodal variables. The calculation CPU time on a CRAY-YMP was roughly 20 minutes with the dynamic relaxation phase requiring about one-third of the total. The simulation was carried out to 110 ms. Triangular shell elements were used because convergence during the dynamic relaxation proved to be very difficult due to the zero energy modes and resulting hour-glassing. Only recently when we added a new shell element [15] we were able to achieve convergence with the quadrilateral shell element.

Results and Discussion

Figures 5 and 6 show configurations of impactor interactions with the inflated airbag using the standard DYNA3D composite material model with coarse and fine

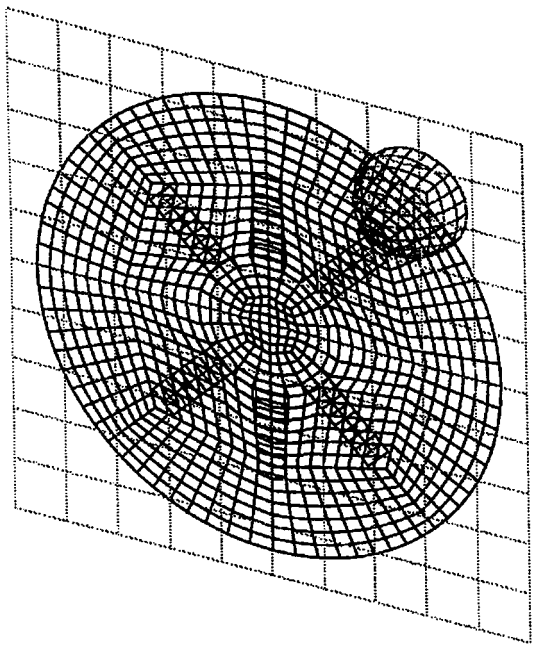

Figure 4. Finite Element Model of Hemispherical Impactor and Airbag Including Tethers and Flat Plate Support

mesh calculations. Figure 7 shows similar results for the coarse mesh with the fabric material model. The results obtained with the fine mesh and fabric material models are in close agreement. Table 1 shows calculated airbag volumes for the two mesh densities and three material models. Using the fabric model, we were able to capture the proper airbag volume of 60 liters with the coarse mesh density.

Table 1. Calculated Inflated Airbag Volumes

Volume	Material Model	# of Elements
56.9 liters	Isotropic elastic	4592
56.8 liters	Orthotopic elastic	4592
56.8 liters	Isotropic elastic	18368
60.1 liters	Fabric	4592

Figures 8 through 10 compare MVMA/DYNA3D results for impactor displacement, velocity and acceleration with corresponding experimental data. In general, the model results compared quite well with the experimental data during the impact phase of the test, i.e. up to 45 ms. In the rebound phase, however, the comparisons are not as favorable due to impactor rebound in the experiment, and subsequent contact with the launching ram via a coil spring. This second contact changes the acceleration history of the impactor by virtue of changing its mass as evident in Figure 10, where an acceleration spike occurred at about 55 ms in the experimental results.

Figure 11 compares the predicted impactor force versus displacement with corresponding experimental data. The computed result is in good agreement with its

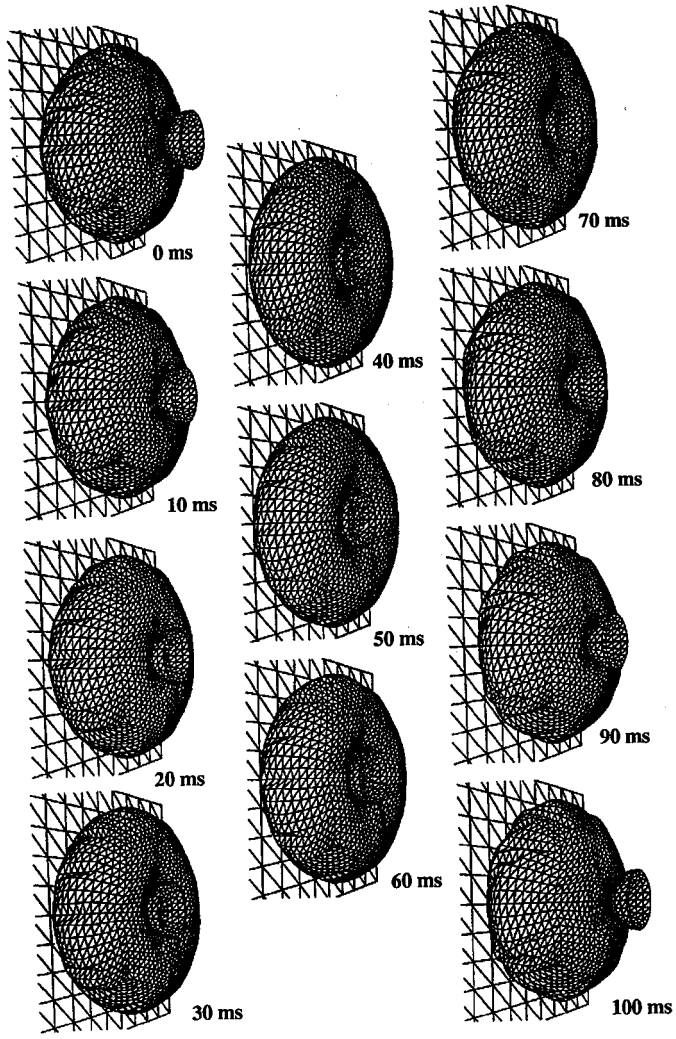

Figure 5. Deformed Shapes at 10 ms Intervals Using Composite Material Model in DYNA3D with Coarse Mesh (3696 Elements in the Airbag)

experimental counterpart during the impact phase. However, in the rebound phase the experimental result diverge dramatically from both the computed result and the impact phase of the test. The discrepancy is not just from the large acceleration spike, noted previously, but the entire rebound phase in the test differs from the impact phase.

The measured rebound phase is suspect, as it is expected that the rebound phase should be similar to the impact phase as indicated by the computed response shown in Figure 11. The reason for to believe this should be similar can be seen by observing the sinusoidal shape of the displacement history in Figure 8, i.e., the impactor and airbag act like a one-degree-of-freedom spring-mass system. A simple analysis of its equation of motion yields 170 ms period of oscillation which fits the computed displacement history in Figure 8 quite well. In the experiment, displacements and accelerations were measured independently [9]. It seems reasonable to ignore the rebound phase of at least the acceleration response when comparing the model prediction with test data.

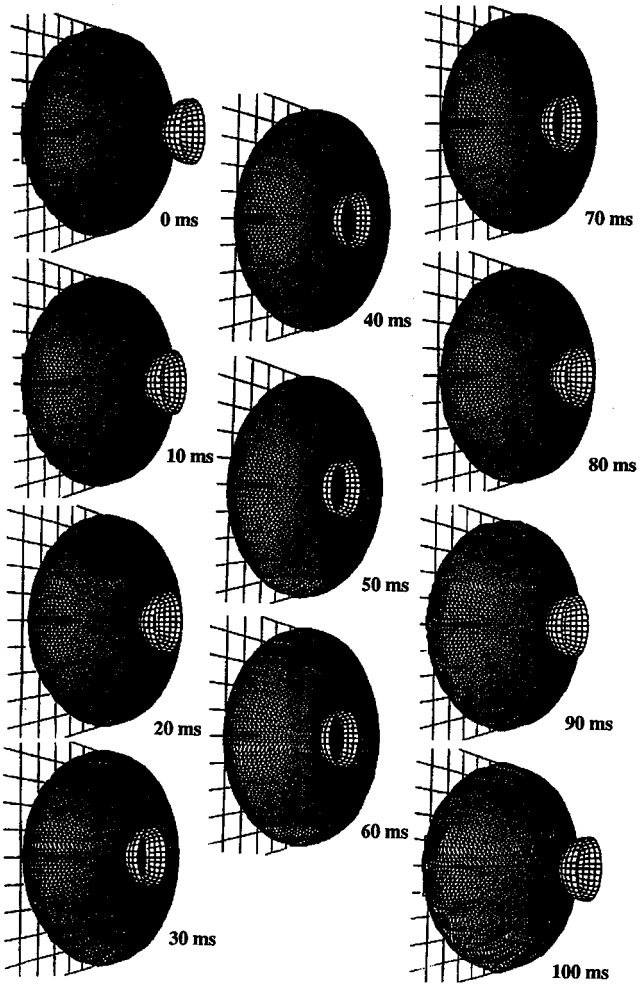

Figure 6. Deformed Shapes at 10 ms Intervals Using Composite Material Model with Fine Mesh (14784 Elements in the Airbag)

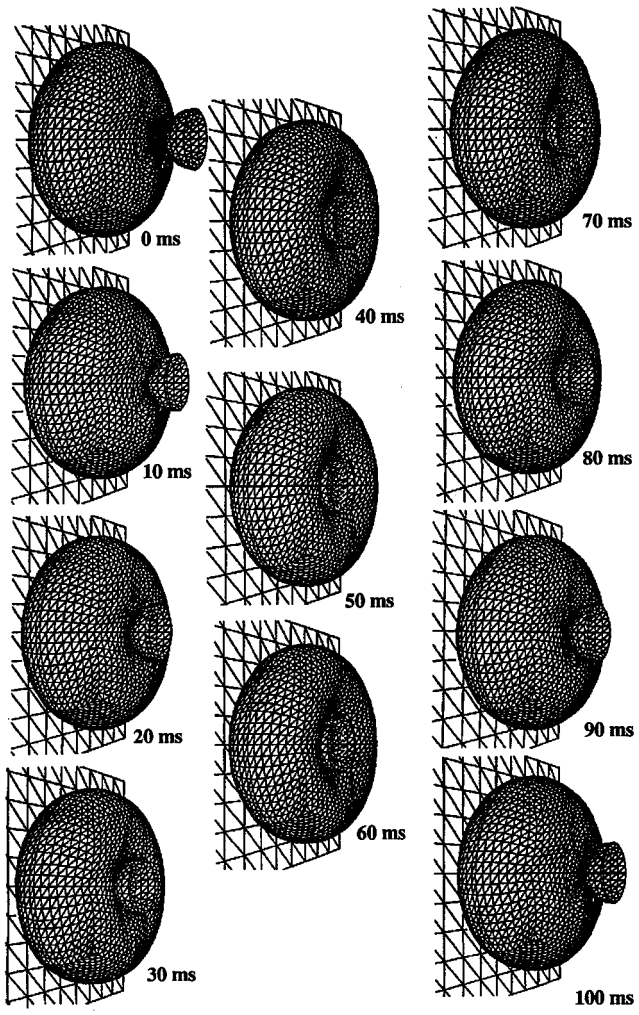

Figure 7. Deformed Shapes at 10 ms Intervals Using Fabric Material Model with Coarse Mesh

A further question remains concerning the validity of the measured impactor displacement duration shown in Figure 8. The increase is believed to be due to spring contact with the impactor which persisted after the maximum displacement is reached. It appears that the spring/impactor contact lengthens the contact duration rather than increasing the maximum displacement as might be expected without knowing when the second contact with the ram occurs.

Figure 12 shows a comparison between the computed and measured pressure history. Similar to the previous results, good agreement was noted only during the impact phase. The longer duration in the measured pressure history is consistent with the longer displacement period observed in Figure 8. The agreement between the measured and calculated peak pressures is quite good.

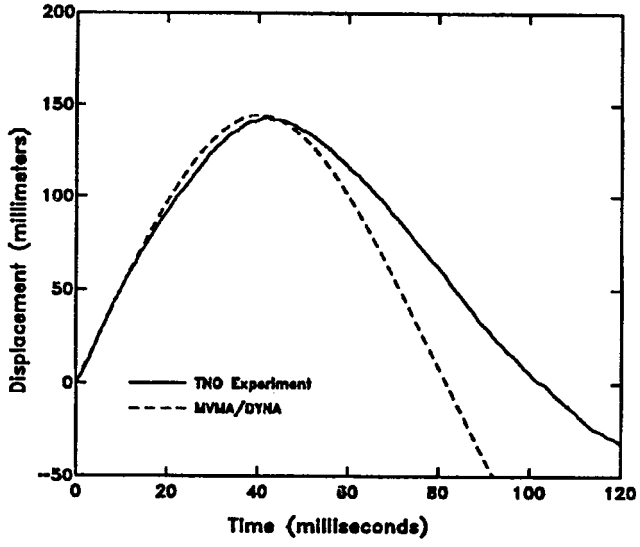

Figure 8. Comparison of MVMA/DYNA3D Calculated Displacement History with Experimental Results from Ref. [5]

Airbag Folding Algorithm

An airbag folding algorithm is necessary for proper airbag simulations for the following reasons:

- The pressure history needed to inflate an airbag depends on its initial configuration. It can be easily

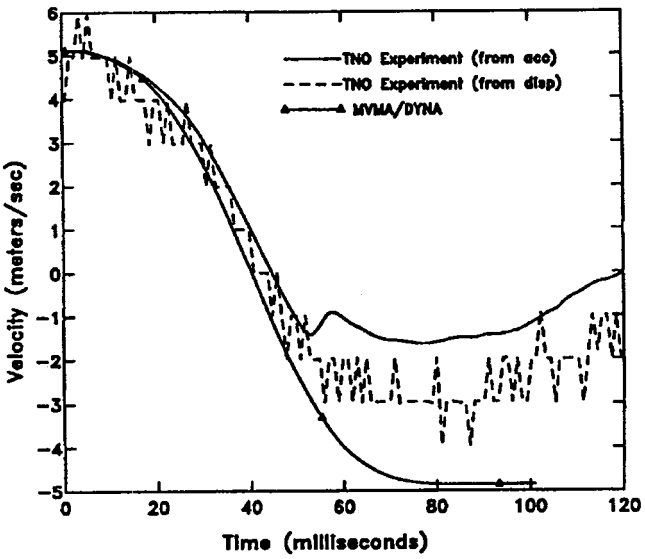

Figure 9. Comparison of MVMA/DYNA3D Calculated Velocity History with Experimental Results from Ref. [5]

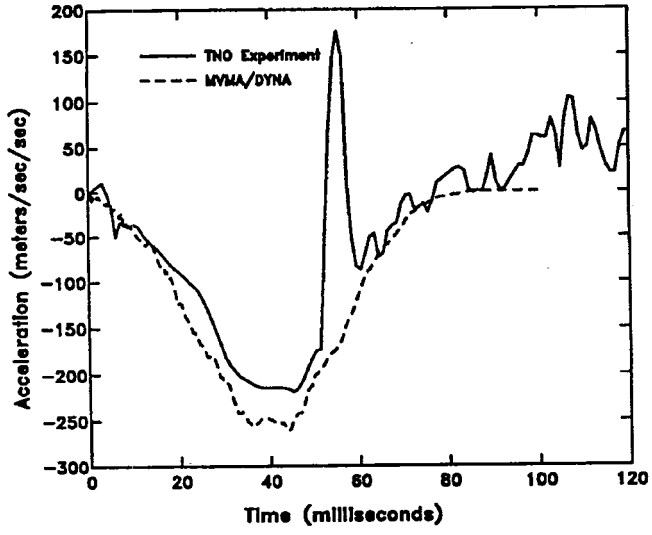

Figure 10. Comparison of MVMA/DYNA3D Calculated Acceleration History with Experimental Results from Ref. [5]

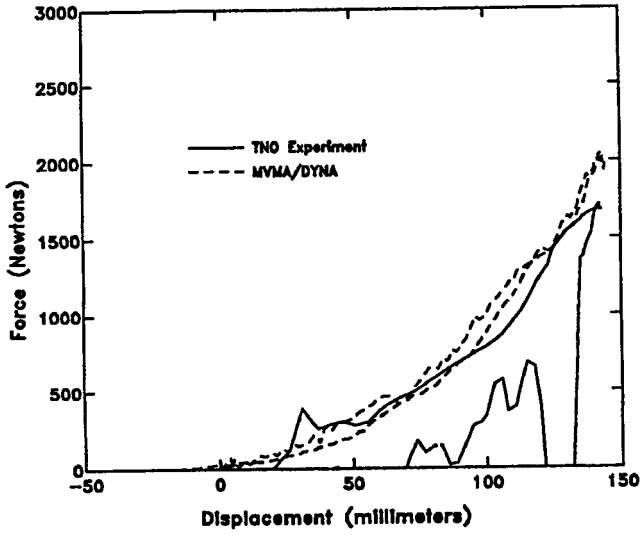

Figure 11. Comparison of MVMA/DYNA3D Calculated Impactor Forces Versus Displacement with Experimental Results from Ref. [5]

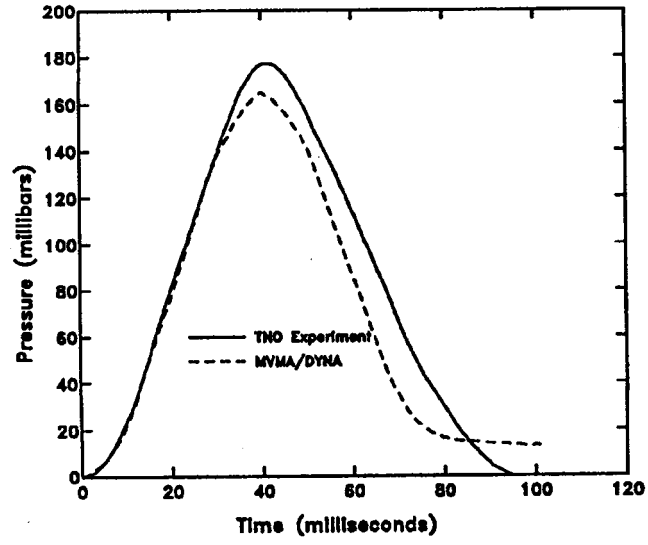

Figure 12. Comparison of MVMA/DYNA3D Calculated Airbag Pressure History with Experimental Result from Ref. [5]

demonstrated that much higher pressure would be required to inflate a folded airbag than would be needed to inflate an unfolded or partially unfolded bag.

- The driver side airbag' s anchor points are behind the plane of the steering wheel. This makes placing an unfolded airbag model into a vehicle model more difficult (geometrically) than similarly placing an initially folded airbag model.
- The folded airbag is initially confined by the steering wheel cover. The resistance of this cover to airbag expansion can alter the pressure history and deployment of the airbag.
- Perhaps the most significant additional capability that results from including an initially folded airbag is the ability to model the interactions of the vehicle's interior with a deploying airbag. In particular, the interaction of vehicle occupants for both normal and out of position cases with a deploying bag can be studied with the folded airbag capability.

We have developed an airbag folding algorithm as part of the DYNA3D mesh generator INGRID [17] to create FE models of folded airbags. The algorithm treats two types of folds: small radius folds, where the radius of the fold is less than the element size, and large radius folds where the radius of the fold is larger than the element size. The mesh generator allows for the following necessary attributes for airbag analysis: determination of surface normals, initialization of orthotopic angles, accounting for fabric thickness and creating models with triangular or quadrilateral elements of roughly uniform size to maximize the time step increment.

Producing a mesh of a folded airbag mimics the actual folding procedure used to assemble an airbag into a steering wheel. We start with an unfolded unpressurized airbag as the initial geometry for defining the airbag grid (Figure 13). Then a series of planar reflections are performed. Figure 13 shows the 6 locations of small radius folds. This step is followed by large radius folds which ultimately produce a folded airbag mesh as shown in Figure 14.

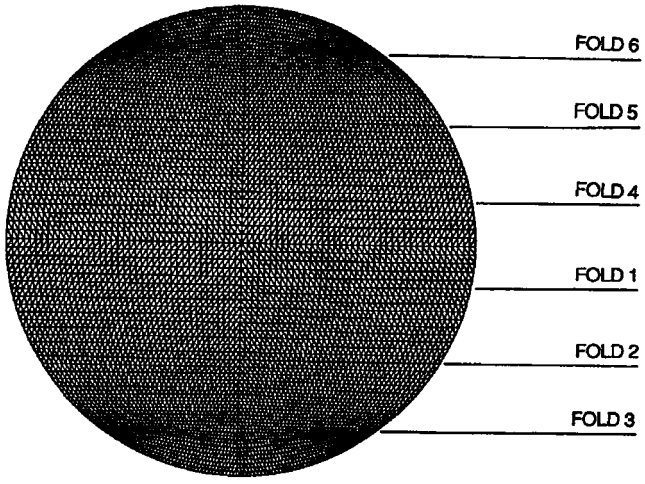

Figure 13. INGRID Mesh of Deflated Airbag Showing the Locations of the First Six Folds (Small-Radius Folds)

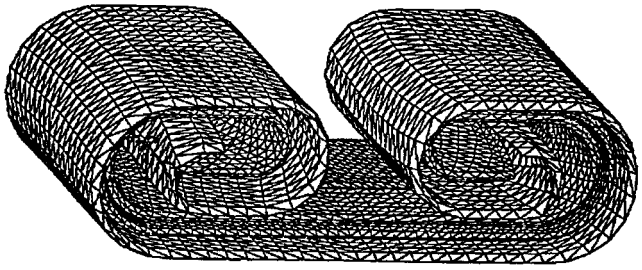

Figure 14. INGRID Model of a Folded Airbag

Occupant Modeling and Interactions with Airbag

Contact Considerations

To model deployment of a folded airbag and its subsequent contact and interactions with an occupant it is necessary to first treat interactions among the folded layers of the airbag as the pressurized gas flows into the airbag and second to account for fabric contact with the occupant. Contact treatment during airbag unfolding can conceptually be accomplished by the single surface contact algorithm in DYNA3D [22]. This contact algorithm has been successfully used in many crashworthiness simulations. Its initial application to airbag unfolding however,was not totally successful because it lacked the extensive searching capability that is necessary for a reliable solution.

Accordingly, we have developed and implemented a new single surface contact algorithm in MVMA/DYNA3D especially designed for use in folded airbag calculations. Figure 15 shows a sequence of an unfolding bag configurations in time, and clearly demonstrates the contact algorithm robustness and capability in treating contact in a multilayered bag without penetration. The bag was modeled by 1752 triangular elements and initially had 20 folds. The calculation time was two CPU hours on a MIP work station to inflate the bag to 24 ms.

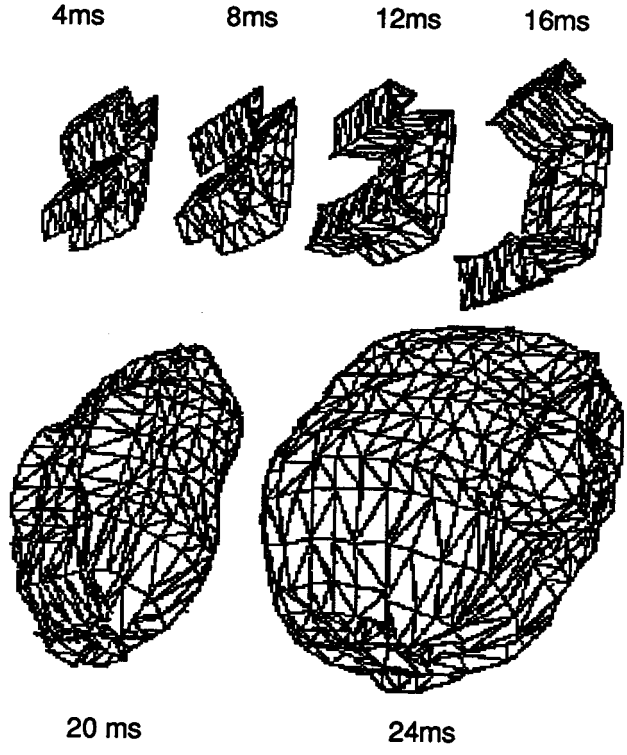

Figure 15. A Sequence of Unfolding Airbag Configurations at 4 ms Intervals (the Airbag Model Includes 1752 Triangular Elements)

Occupant contact with the inflating airbag fabric can be simulated by the surface-to-surface contact algorithm in DYNA3D. This however requires simulation of the occupant by a fine mesh to accurately capture the contact forces. The drawbacks of this procedure are: large storage requirements, more computation cost and longer mesh generation time. Therefore, geometric contact entities were added as an alternate method to model contact among curved rigid bodies impacting deformable surfaces.

The geometric contact entities are developed by using standard solids modeling approach where the geometric entity is defined by a scaler function G(x,y,z). The location of a nodal point (x,y,z) is determined relative to the contact target. If the point is found to be outside the solid, then there is no contact, otherwise the point penetrated. In the latter case, contact has occurred and a restoring force is applied to bring the nodal point to the surface of the geometric entity. To accomplish this, the penalty method was used because it is the simplest and

most efficient technique in such calculations. The restoring force is proportional to the penetrated distance into the solid and acts along the normal direction. Currently contact entities are implemented for an infinite plane, a cylinder, and a sphere and an ellipsoid. The ellipsoid is intended to be used with rigid body occupant modeling. Figure 16 demonstrates ellipsoid impact from an initial velocity on a flat plate. The simulation captured quite well the contact and interactions between the rigid ellipsoid and the deformable plate.

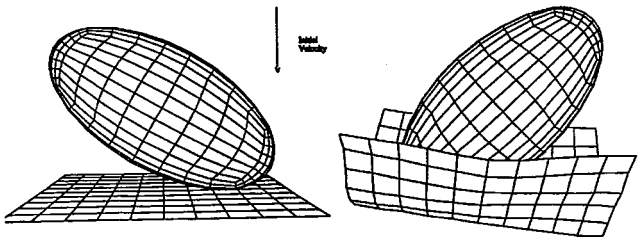

Figure 16. Rigid Ellipsoid Impact on a Flat Plate by MVMA/DYNA3D Contact Entities

Occupant Modeling

A MADYMO-3D model of the hybrid III dummy [23] has been converted into DYNA3D format using the mesh generator INGRID [17]. All of the geometric details and joint definitions, as given in reference [23] are included in the model (Figure 17). Representative joint stiffness and damping properties are yet to be incorporated in the model. Currently, the individual rigid bodies are permitted to rotate freely about their joints.

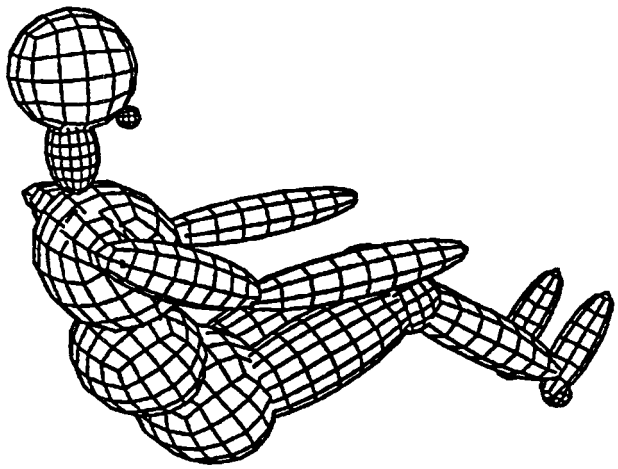

Figure 17. Hybrid III Dummy Model Represented in MVMA/DYNA3D by a Combination of Ellipsoids Connected by Appropriate Joints

Figure 18 shows the initial configuration of a seated occupant model restrained by a 3-point belt system. The model also includes a schematic steering wheel with a folded driver side airbag. This model was run using MVMA/DYNA3D to simulate occupant interactions with a deploying airbag. The airbag was inflated with a simple pressure-time curve. Ellipsoidal geometric entities were used to model contact between the dummy and the bag, whereas single surface contact was used in the airbag unfolding phase. A sequence of deformed configurations is shown in Figure 19 which illustrate the kinematics of airbag deployment and its interactions with the dummy. A number of remaining details need to be included in this model before it represents a practical airbag-occupant simulation in a crash event. These include realistic modeling of the vehicle interior: seat, belts, knee bolster, steering system, dash board, windshield, etc.. This additional modeling needs to be followed by validating the model using experiments from sled tests prior to incorporating the dummy and restraint system into a full vehicle system model which ultimately could be used for modeling crash tests.

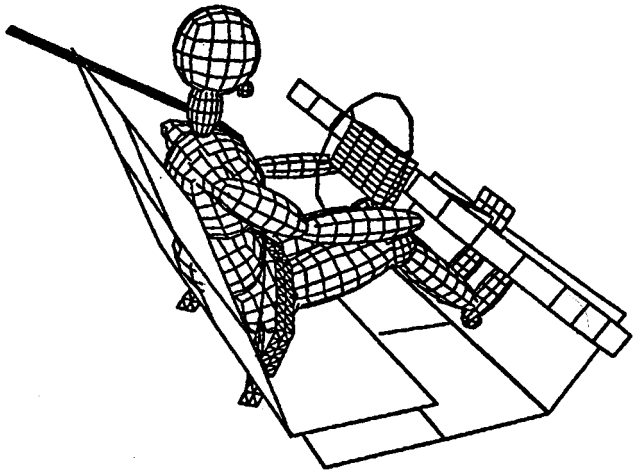

Figure 18. Initial Configuration of a Driver Dummy Model with a 3-Point Belt and Folded Airbag

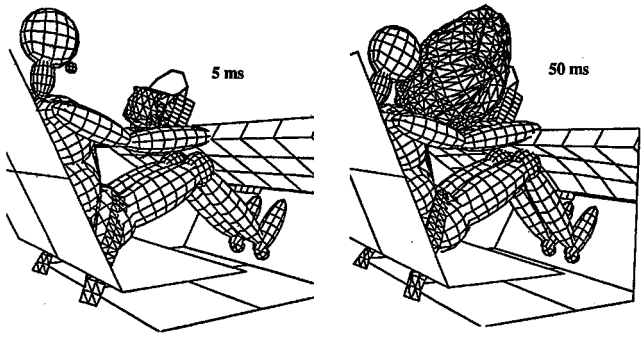

Figure 19. Kinematics of Dummy Interactions with a Deploying Airbag at 5 ms and 50 ms

Summary

- MVMA has sponsored the development of a FE based technology to simulate airbag inflation and interactions with an occupant model. The research, conducted by Livermore Software Technology Inc., involved adding various capabilities to the 1989 public domain version of DYNA3D. The new capabilities (in MVMA/DYNA3D) are: a wrinkle free fabric material model, an airbag inflation model, inflator model, a single surface contact algorithm for

unfolding a prefolded airbag and contact entities. Also, the rigid body and joint simulation capabilities were improved so that occupant dynamics modeling can, and has been, accomplished in DYNA3D. Further a mesh generator was incorporated into INGRID to generate folded airbag models.

- The predictions of the FE airbag model response agreed quite well with published experimental data involving a hemispherical impactor launched into a stationary pressurized airbag.
- While much progress has been made to numerically simulate airbag deployment and interactions with an occupant model, there are still a number of issues that need to be addressed in future work. These include: improving the computational speed and robustness of the single surface contact algorithm, validating an airbag-dummy system model corresponding to a realistic crash environment and addressing the passenger side airbag.

Acknowledgment

The authors would like to thank G. Kostyniuk and P. Prasad, members of MVMA Analytical Model Simulation Task Group, for their support and guidance of this project.

References

1. Clark, C. et. al., "Impact Protection with the "Airstop" Restraint System," Proceedings of 8th. Stapp Car Crash Conference, SAE Publication, 1964, pp. 79-113.
2. Campbell, D. D., "Air Cushion Restraint Systems Development and Vehicle Application," SAE Publication No. 720407, 2nd. International Conference on Passive Restraints, 1972.
3. Nefske, D. J., "A Basic Airbag Model", SAE Publication No. 720426, 2nd. International Conference on Passive Restraint, 1972.
4. Wu, H., "Interaction Dynamics of an Inflating Air Bag and a Standing Child," SAE Paper No. 730604, 1973.
5. De Coo, P. J. A. et. al., "Computer Simulation of Driver Airbag with Rigid Body," TNO Report to MVMA, 1989.
6. Johnson, J. J. and Skynar, M. J., "Automotive Crash Analysis using the Explicit Integration Finite Element Method," Proceedings of Symposium on Crashworthiness and Occupant Protection in Transportation Systems, Khalil, T. B. and King, A. I. Eds., AMD-Vol. 106 and BED-Vol. 13, ASME, WAM, 1989 pp. 27-33.
7. Nieboer, J. J. et. al., "Status of MADYMO 2D Airbag Model," Proceedings of 32nd. Stapp Car Crash Conference, SAE Publication, 1988, pp. 223-235.
8. Hoffmann, R. et. al., "Finite Element Analysis of Occupant Restraint System Interactions with PAM-CRASH," Proceedings of 34th. Stapp Car Crash Conference, SAE Publication, 1990, pp. 289-301.
9. Nieboer, J. J. et. al., "Airbag Modeling Techniques," Proceedings of 34th. Stapp Car Crash Conference, SEA Publication, 1990, pp. 243-259.
10. Hallquist, J. O. and Stillman, D. W., "Modeling of Airbags Using MVMA/DYNA3D," LS Report to MVMA, 1990.
11. Benson, D. J. and Hallquist, J. O., "The Application of DYNA3D in Large Scale Crashworthiness Calculations," Proceedings of 1986 ASME International Computers in Engineering Conference, 1986.
12. Hallquist, J. O., "Preliminary User's Manuals for DYNA3D and DYNAP (Nonlinear Dynamic Analysis of Solids in Three Dimensions)," University of California, Lawrence Livermore National Laboratory, Rept. UCID-17268, 1976.
13. Flanagan, D. P. and Belytschko, T. B., "A Uniform Strain Hexahedron and Quadrilateral and Orthogonal Hourglass Control," Int. Numer. Meths. Eng., 17, 1981, pp. 679-706.
14. Belytschko, T. B. and Tsay, C. S., "A Stabilization procedure for the Quadrilateral plate Element with One-Point Quadriature," Int. J. Num. Methods. Eng, 19, 1983, pp. 405-419
15. Englmann, B. E. et. al., "A Simple Shell Element Formulation for Large Scale Elastplastic Analysis," Analytical and Computational Models of Shells, CED-Vol. 3, Eds. Noor, Belytschko and Simo, ASME, New York, 1989, pp. 399-416.
16. Wang, J. T. and Nefske, D. J., "A New CAL3D Airbag Inflation Model," SAE Paper No. 880654, 1988.
17. Stillman, D. W. and Hallquist, J. O., "INGRID: A Three-Dimensional Mesh Generator for Modeling Nonlinear Systems," University of California, Lawrence Livermore National Laboratory, Rept. UCID-20506, 1985.
18. Lloyd, D. W., "The Analysis of Comolex Fabric Deformations," in Hearle. J. W. S., et. al. Eds., Mechanics of Flexible Fibers Assemblies, Sijthoff & Noordhooff, The Netherlands, 1980, pp. 311-342.
19. Leech. C. M., "The Dynamics of Flexible Filaments Assemblies," in Hearle, et.al., Eds., Mechanics of Flexible Fibers Assemblies, Sijthoff & Noordhoff, The Netherlands, 1980, pp. 343-390.
20. Roddman, D. G., "Force Transmission in Wrinkled Membranes," Ph. D. Dissertation, Technical University, Eindhoven, 1988.
21. Berkowitz, H. M. et. al., "Flexible overlays for Inflatable Decoys, Vol. I-Analytical Model Development and Experimental Verification," Final Report to Norton Air Force Base, 1989.
22. Benson, D. J. and Hallquist, J. O., "A Single Surface Contact Algorithm for the Postbuckling Analysis of Shell Structures," Comp. Meths. Appl. Mechs. Eng., 78, 1990, pp. 141-163.
23. Wisman, J. and Hermans, J. H. A.,"MADYMO3D Simulations of Hybrid III Dummy Sled Tests," SAE Paper 880654, 1988.

S9-O-19

Modelling the Occupant in a Vehicle Context—An Integrated Approach

R.M.V. Sturt, B.D. Walker, J.C. Miles
Ove Arup & Partners
A. Giles, N. Grew
Rover Group Limited

Abstract

Numerical simulation plays a key role in design for crashworthiness. Analysis of vehicle structure performance, occupant motion and restraint systems, and occupant/structure interaction are currently tackled by different methods in design offices, using different software and, often, different analysts. However, this paper demonstrates that it is now feasible to adopt a single unified approach. The argument is developed with particular reference to occupant modelling and is supported by quantitative correlations between sled tests and simulation.

Introduction

There currently exist several different analytical approaches to crashworthiness simulation. Traditionally, lumped parameter, framework, finite element continuum and occupant models are developed using different software packages. Frequently, different expert analysts are needed to drive each code and there is no means of establishing continuity or comparability between the different types of model.

Where occupants and structure are treated separately, a more fundamental difficulty exists: the two systems interact in reality, and it is technically incorrect to model them separately. This is particularly true of side impact, in which the occupant interacts with the interior of the door structure. In frontal impact, knee bolster design requires careful consideration of how the legs of the occupant influence the deformation of the bolster. Airbags provide a further example: the loading on the occupant arises from complex interactions with the bag.

The purpose of this paper is to illustrate how one single computer program, OASYS DYNA3D, can now be used in a realistic fashion to address all of the important aspects of vehicle impact in one single fully three-dimensional simulation. Extensive quantitative correlation has been carried out against sled tests and the results are summarized in this paper.

OASYS DYNA3D (Ref 1) is based on the LS-DYNA3D program developed by Dr J O Hallquist (Ref 2). Dr Hallquist's pioneering work with LS-DYNA3D has been adopted by automotive manufacturers worldwide for crashworthiness applications. OASYS DYNA3D is Quality Assured and contains a number of unique features purpose-written for occupant-related analyses, e.g. the new seat belt algorithms.

Occupant Models

Occupants are typically represented as a series of rigid bodies representing head, neck, upper torso, etc, linked together to form a mechanism. The bodies are commonly ellipsoidal.

It is straightforward to reproduce this type of analysis using OASYS DYNA3D, since all the requisite features (rigid bodies, joints, and rotational springs and dampers) are present. However, the bodies need not necessarily be ellipsoidal. Figure 1 shows a more representative HYBRID III model which has been developed by the authors using data digitized from the dummy itself. The principal advantage of representing the true shape of the dummy lies in improved modelling of interaction with the restraint systems: for example the belt may slide over the chest or off the shoulder. Using the ellipsoid representation the belt would slide off too easily or get stuck in the 'valley' between two ellipsoids.

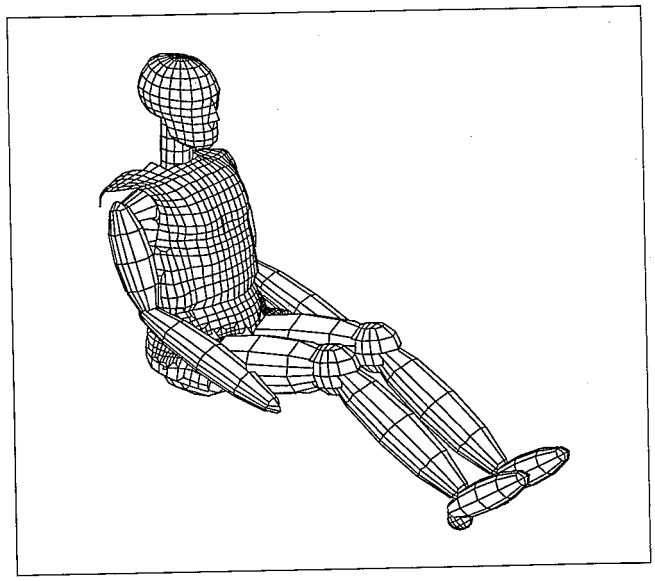

Figure 1. Hybrid III Dummy Model

The geometry, masses and inertias have been taken from published data (Ref 3). Joint stiffness and damping characteristics are derived from Rover data.

Seat Belt Models

New algorithms have been written for OASYS DYNA3D to represent seat belt systems including slip-rings, retractors and pretensioners. These features can be included in simulations with negligible increase in CPU requirements. This section describes the new features.

Belt Webbing

The belt webbing is represented by a series of one-dimensional tension only elements, with user defined force-elongation characteristics for loading and unload-

ing. The characteristics used (shown in Figure 2(a)) were derived from dynamic tests performed in the laboratory.

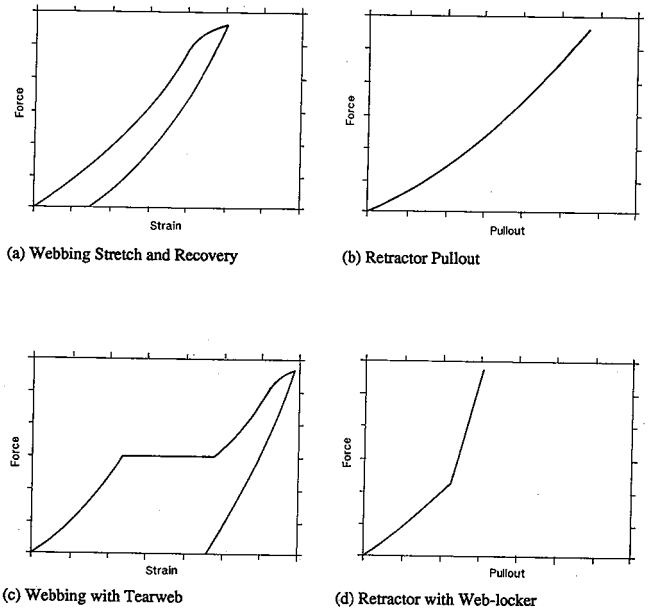

(a) Webbing Stretch and Recovery (b) Retractor Pullout

(c) Webbing with Tearweb (d) Retractor with Web-locker

Figure 2. Belt and Retractor Input

Sliprings

Sliprings play an important part in the performance of the belt. Material feeds through from the retractor section into the shoulder section, and from the lap section into the shoulder section, so motion at shoulder level results in tensioning of the whole belt including the lap section. For this reason it is inadequate to model the belt simply as a spring element attached to the D-ring and shoulder; the process of feed-through must be included. A slipring feature has been added to OASYS DYNA3D to represent this: belt elements can pass through the slipring, resisted by friction (see Figure 3(a)).

Retractors

The retractor adds significant compliance to the belt system: even when an inertia-reel retractor locks, webbing can still be drawn off the drum due to film spool effect.

The retractor feature in OASYS DYNA3D allows material to be fed from the retractor into the belt or reeled back into the retractor from the belt—see Figure 3(b). Before locking, material is reeled in under constant tension; this allows initial form-finding to take place. Once locked, webbing may be pulled out according to a user-defined force vs pull-out curve. Figure 2(b) shows the characteristics derived from dynamic laboratory tests that have been used for the analyses.

Pretensioners

Pretensioners tighten the seat belt during the initial phases of a crash. There are two main types: those that act to rotate the reel of the retractor, and those that act to move the stalk anchorage rearwards.

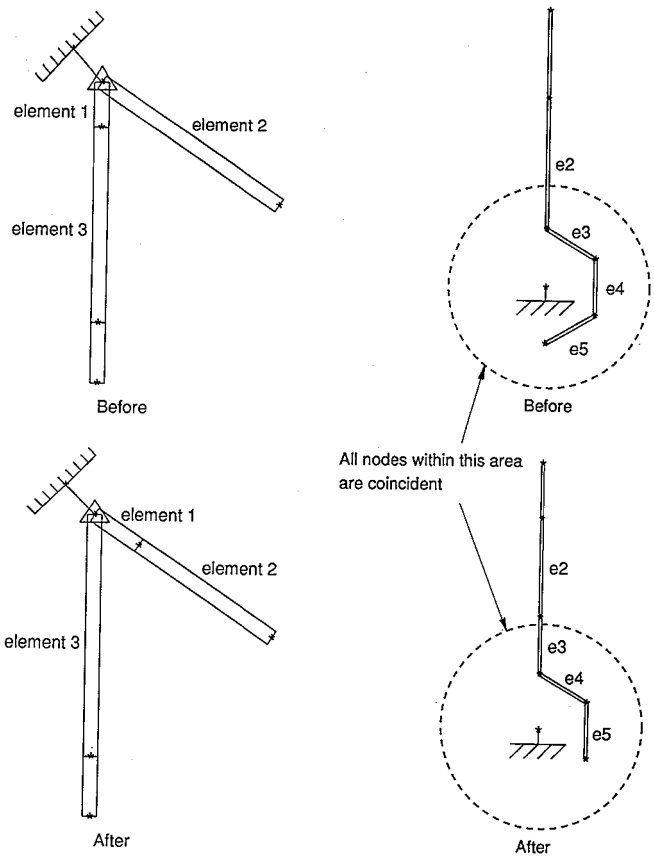

(a) Slipring Feed-through (b) Retractor Pullout

Figure 3. OASYS DYNA3D Slipring and Retractor Implementation

In OASYS DYNA3D, both types can be represented. The retractor type is simulated by entering a pull-in vs time curve, while the stalk anchorage can be moved using a preloaded spring.

Weblockers

A pair of toothed cams grip the belt near the retractor to limit compliance due to spool-out. These devices are simulated by entering a stiffer characteristic for retractor pull-out (see Figure 2(d)).

Tearwebs

A length of belt is sewn up concertina-style; when the force reaches a given level the threads pull out, resulting in a controlled dissipation of energy. These features may be modelled by adjusting the stretch characteristics of the belt elements at the tearweb (see Figure 2(c)).

Interaction with Occupant

Contact between belt and occupant is achieved using the standard OASYS DYNA3D contact algorithms. In this way, sliding of the belt over the chest or off the shoulder can be represented. Surface stiffnesses are adjusted to represent the compliance of the different body regions of the dummy.

Airbag Models

This section describes the approach to airbag modelling that has been adopted.

The principal concern has been to avoid excessive computer run times: since the models are intended to be used as a design tool, fast turn-around time is a big advantage. The number of elements used to represent the airbag must be limited to a few hundred, and consequently the unfolding process (which typically requires several thousand elements) cannot be simulated. However, in the majority of cases interaction between bag and occupant does not commence until the bag is fully inflated so the unfolding process need not be modelled. The approach employed by the authors has been to use a coarsely meshed pre-inflated airbag. Figures 4 and 5 show the models of Driver and Passenger side airbags. These contain 384 and 600 shell elements respectively.

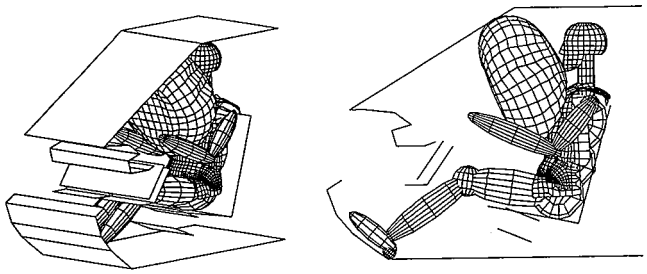

Figure 4. Driver Side Airbag Model

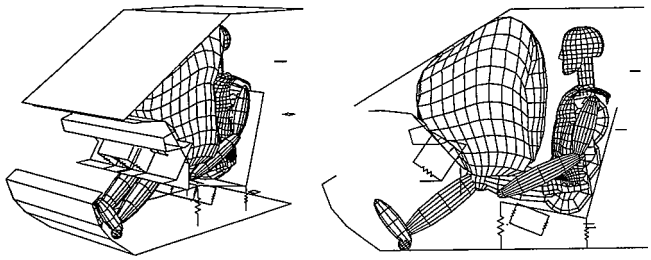

Figure 5. Passenger Side Airbag Model

When the occupant is out of position and interacts with the airbag as it unfolds, a finer mesh is required. Hallquist (Ref 5) is currently refining the very complex contact algorithms which are required if this is to be done properly.

Bag Material

An isotropic 'smeared wrinkle' material model has been written to represent the bag. This adopts a simple but robust algorithm which has been found to work well. Although differences in warp and weft stiffnesses are ignored, the level of accuracy is appropriate to the level of modelling of the occupant.

Gas Representation

The presence of gas inside the bag is represented by pressure applied over the inner surface. Although OASYS DYNA3D contains the gas law algorithms developed by Hallquist (Ref 2), at this stage simple pressure vs time curves have been used. The curves were derived from pressure histories measured during actual sled tests and are reproduced in Figure 6.

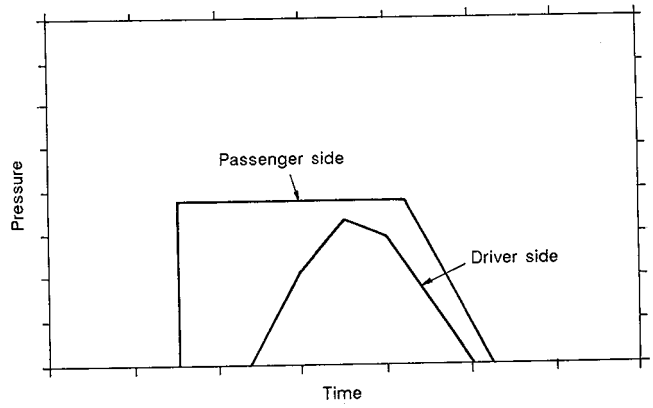

Figure 6. Airbag Pressure Input

Sled Models

The dimensions of the sled model (Figure 7) are taken from drawings of the Hyge rig. A small number of rigid elements are used to provide contact planes. The whole sled is treated as rigid, except that the seat is free to translate vertically relative to the sled and the seat pan and knee bolsters can translate normal to their surfaces. All of these motions are resisted by non linear spring elements providing the 'ride-down' characteristic. The crash pulse is applied as a velocity input.

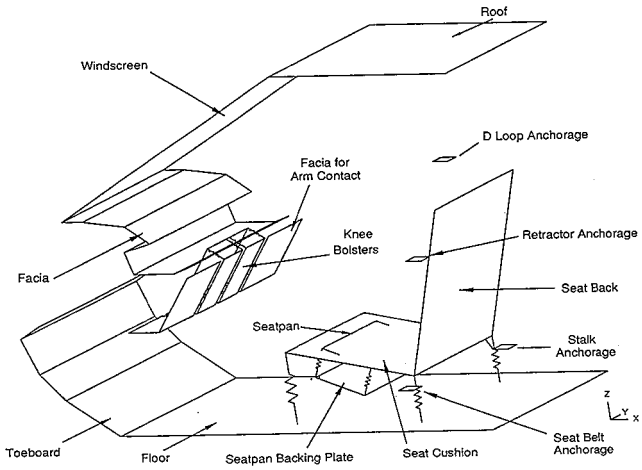

Figure 7. Sled Model

Correlation with Test

Correlations have been carried out with sled test data for the following cases:

- 30mph Belted
- 35mph Belted
- 30mph Driver side Airbag
- 30mph Passenger side Airbag

In each case results from two sled tests were available.

Belted Tests

Figure 8 shows a sequence of elevations on the sled at 0, 60ms, 90ms and 120ms for the 30mph test. Correlation with test results is given in Figure 9 for chest and

head resultant accelerations, head trajectories, and forces in the shoulder belt, lap belt and retractor. The equivalent plots for the 35mph test are given in Figures 10 and 11.

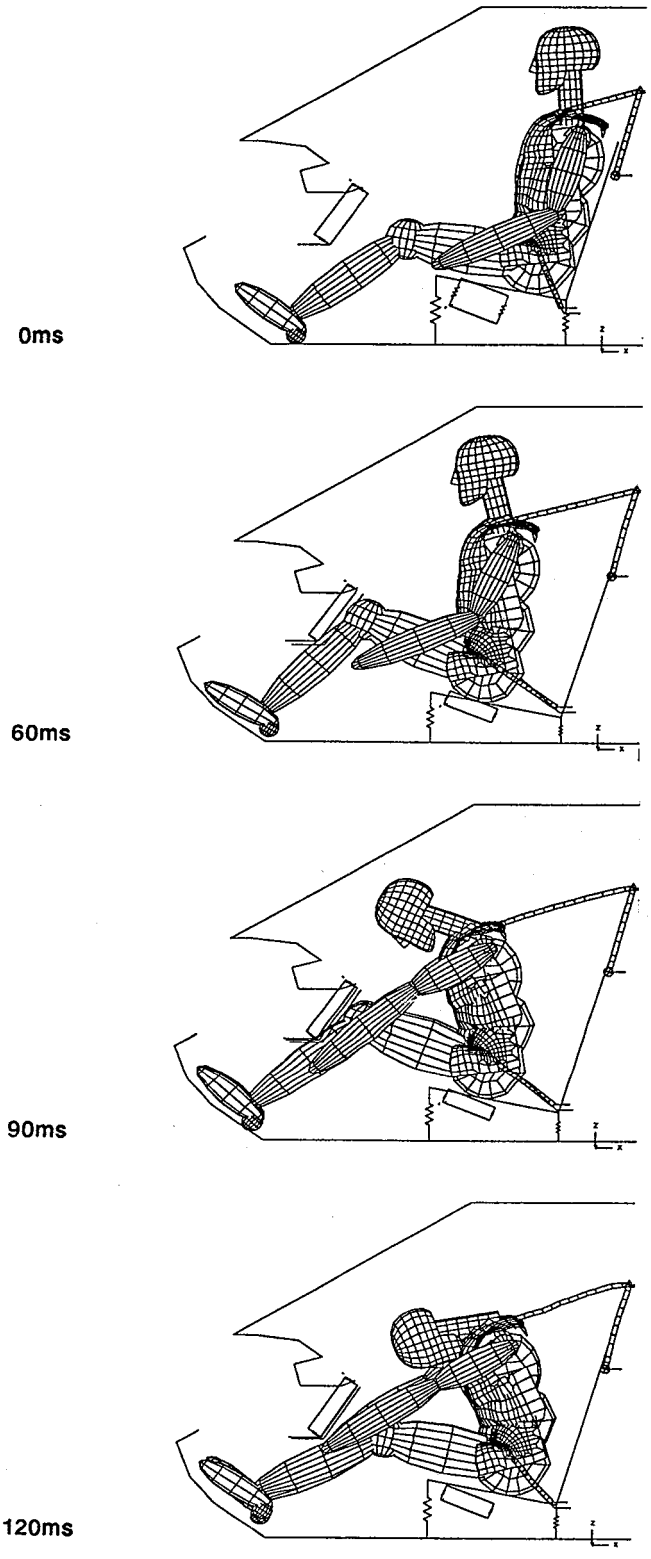

Figure 8. 30mph Belted Sled Test Simulation

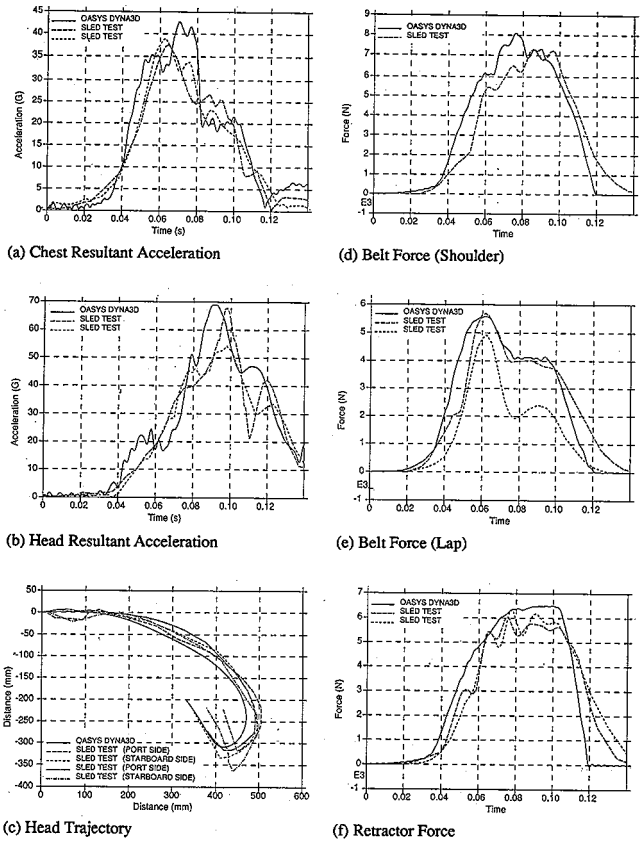

Figure 9. 30mph Belted Sled Test Correlation

In general results show good agreement. The discrepancies which arise may be partly due to the following factors:

- the chest compliance may be underestimated thus reducing the forward motion of the head.
- contact between arms and facia at 70ms is probably too severe. In reality the arms strike the edges of the foam which used in the sled as a knee bolster.
- the foot to floor contact is unrealistically stiff, causing spikes in the acceleration traces at around 40ms, particularly in the pelvis.

The time history post-processor OASYS T-HIS allows filtering of results to standard specifications (e.g. Channel filter Class 180), and calculation of HIC and 3ms Clip values. For example the 30mph simulation showed HIC of 807 (against 710 and 652 from test) and Chest 3ms Clip of 41 (against 37 from both tests). Given the well-known variability of HIC values these results are considered satisfactory.

Run time was 55 minutes on a CONVEX C210 computer for a 140ms simulation.

Driver Side Airbag

Elevations of the sled are shown in Figure 12. Chest and head accelerations are compared with test in Figure 13.

Correlation is good for all quantities including head acceleration. The analysis took 1.5 CPU hours to run to 140ms on a CONVEX C210 computer.

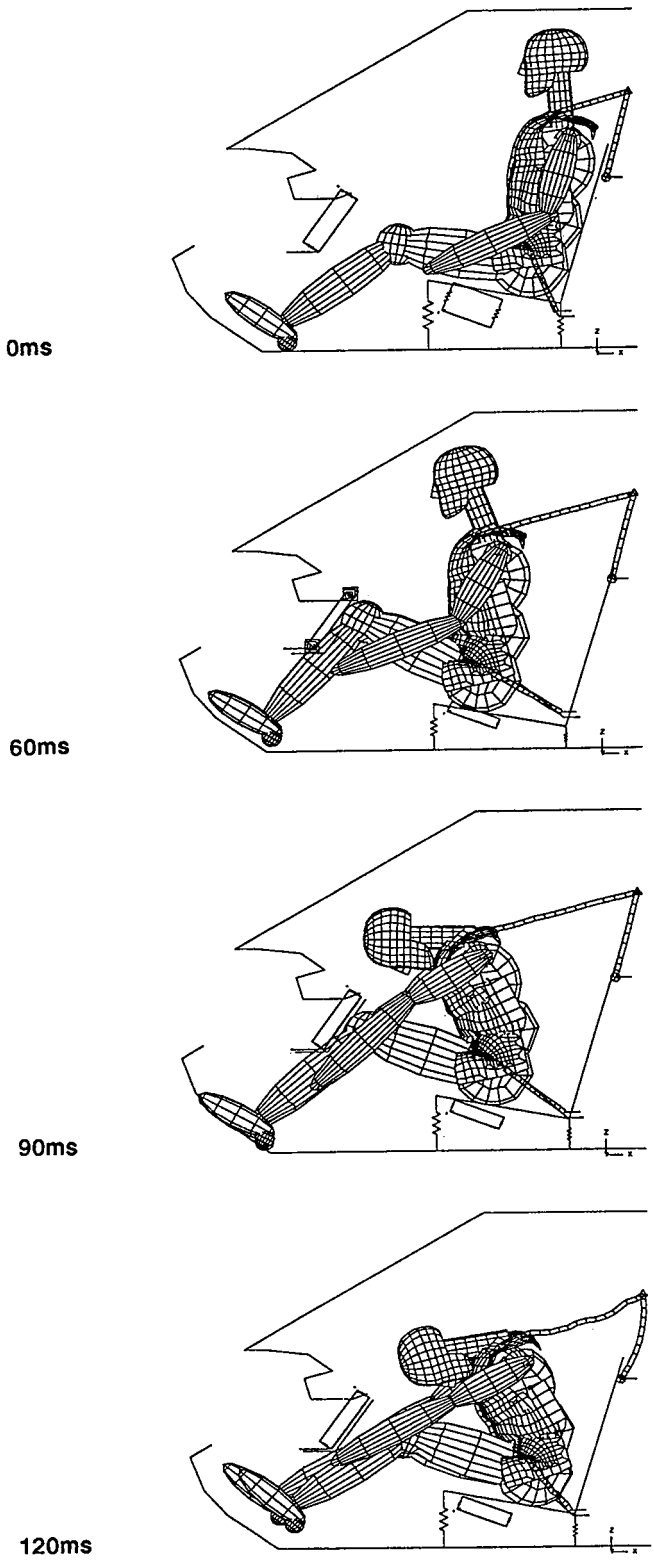

Figure 10. 35mph Belted Sled Test Simulation

Passenger Side Airbag

Figure 14 shows elevations of the sled at 0, 60ms, 90ms and 120ms. Chest and head accelerations are compared with test in Figure 15.

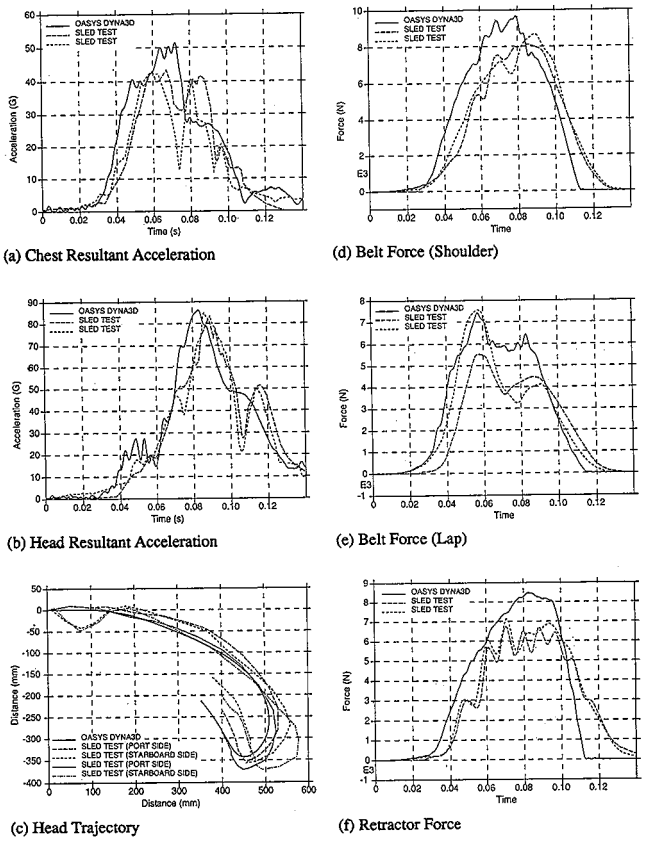

Figure 11. 35mph Belted Sled Test Correlation

The displaced shapes and chest accelerations are predicted within the range of experimental error. However, head accelerations have been over-predicted (23% on peak resultant). The reasons for this are not fully understood but it is believed that the representation of the neck may be partly responsible. It is modelled as a rigid entity with spherical joints at top and bottom, whereas in reality the neck can also undergo axial and shear deformations. It is also unclear whether the moment-rotation characteristics used for the neck joints are realistic when large rearward rotations occur.

The analysis took 2.5CPU hours to run to 140ms on a CONVEX C210 computer.

Further Demonstrations

Some further analyses have been undertaken to demonstrate the effect of weblockers and pretensioners and the possibilities of the integrated approach to occupant/structure interaction. These have not been correlated with test due to unavailability of data.

Effect of Web-Lockers

The presence of a web-locker on the retractor of the 35mph belted sled test has been simulated by alterations to the retractor characteristic as per Figure 2(d). The effect on head trajectory is shown in Figure 16. Forward motion is reduced by 50mm.

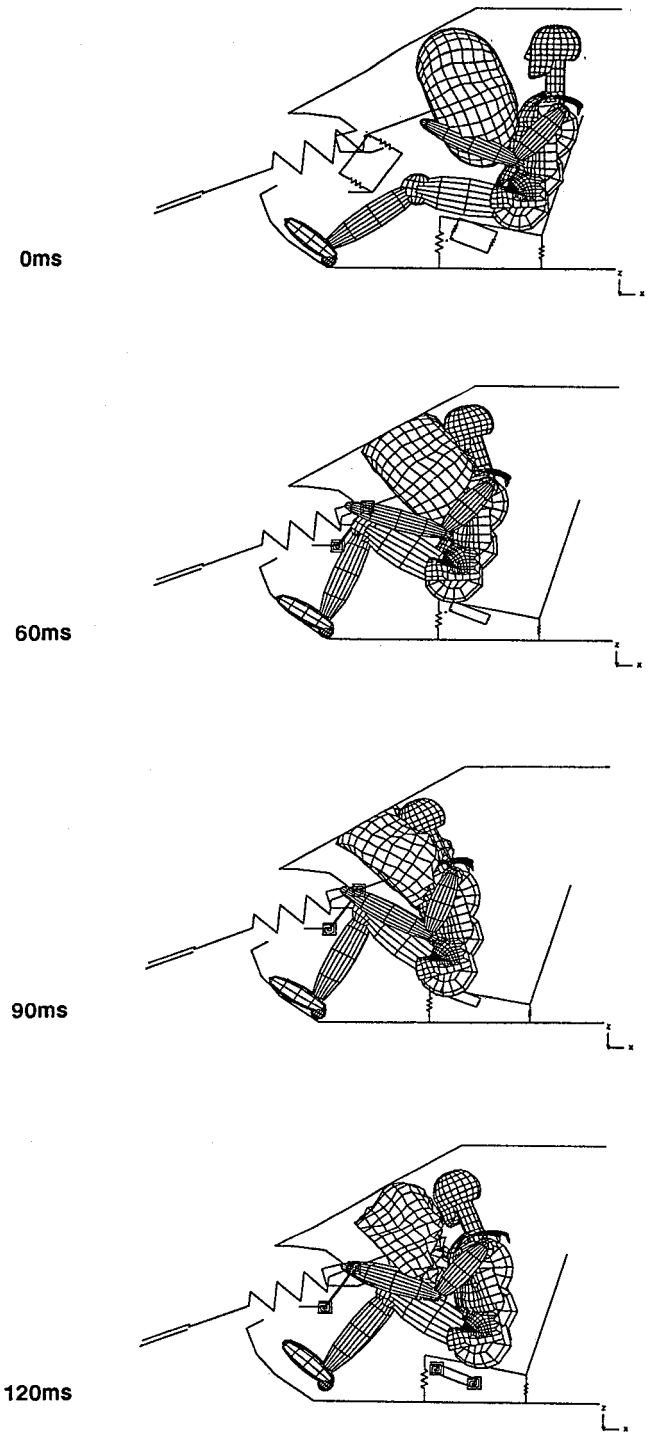

Figure 12. Driver Side Airbag Sled Test Simulation

Effect of Pyrotechnic Pre-Tensioner

A pyrotechnic pre-tensioner causing the retractor to reel in 60mm of belt over a 15ms period has been simulated. The effect on head trajectory is shown in Figure 16. The effect is more marked than that arising from the web-locker: the forward travel of the shoulder is much reduced, leading to a lower head trajectory with 130mm less forward travel. Despite this, peak head accelerations are reduced from 85 to 65g.

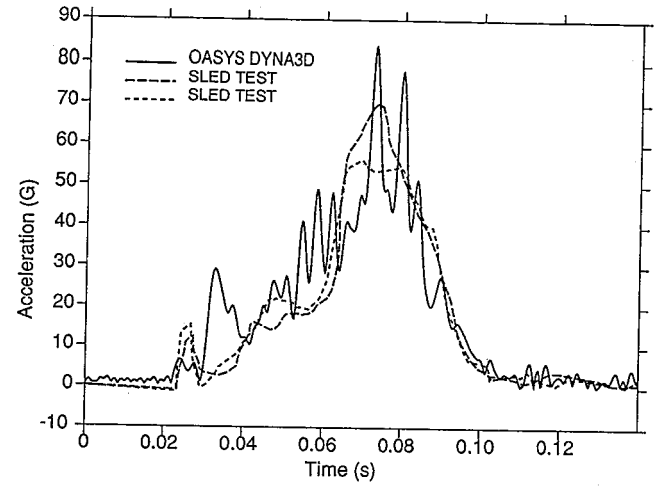

(a) Chest Resultant Acceleration

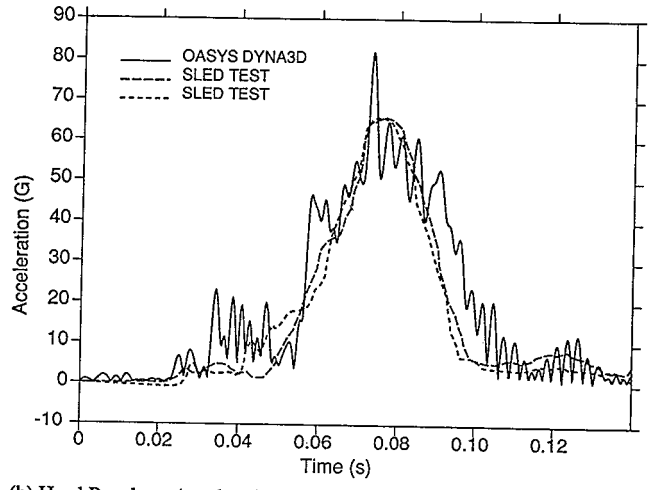

(b) Head Resultant Acceleration

Figure 13. Driver Side Airbag Sled Test Correlation

Effect of Torsion Bar Pre-Tensioner

The device in question is a mechanism which pulls the buckle stalk 60mm downwards, thus tightening the belt over the occupant. This has been simulated using pre-loaded spring elements and the effects on head trajectory are shown in Figure 16. Because less restraint is applied to the shoulder the trajectory shows a more open path to that caused by the pyrotechnic retractor. Peak head acceleration is 77g, compared to 65g for the pyrotechnic device and 85g for the standard belt system.

Demonstration Occupant/Structure Analysis

Figure 17(a) shows an analysis which demonstrates the possibilities of the integrated approach to occupant/structure interaction. The velocity input to the sled has been replaced by a lumped parameter representation of the front of the vehicle, while the single rigid plane knee bolster has been surplanted by a detailed shell element representation.

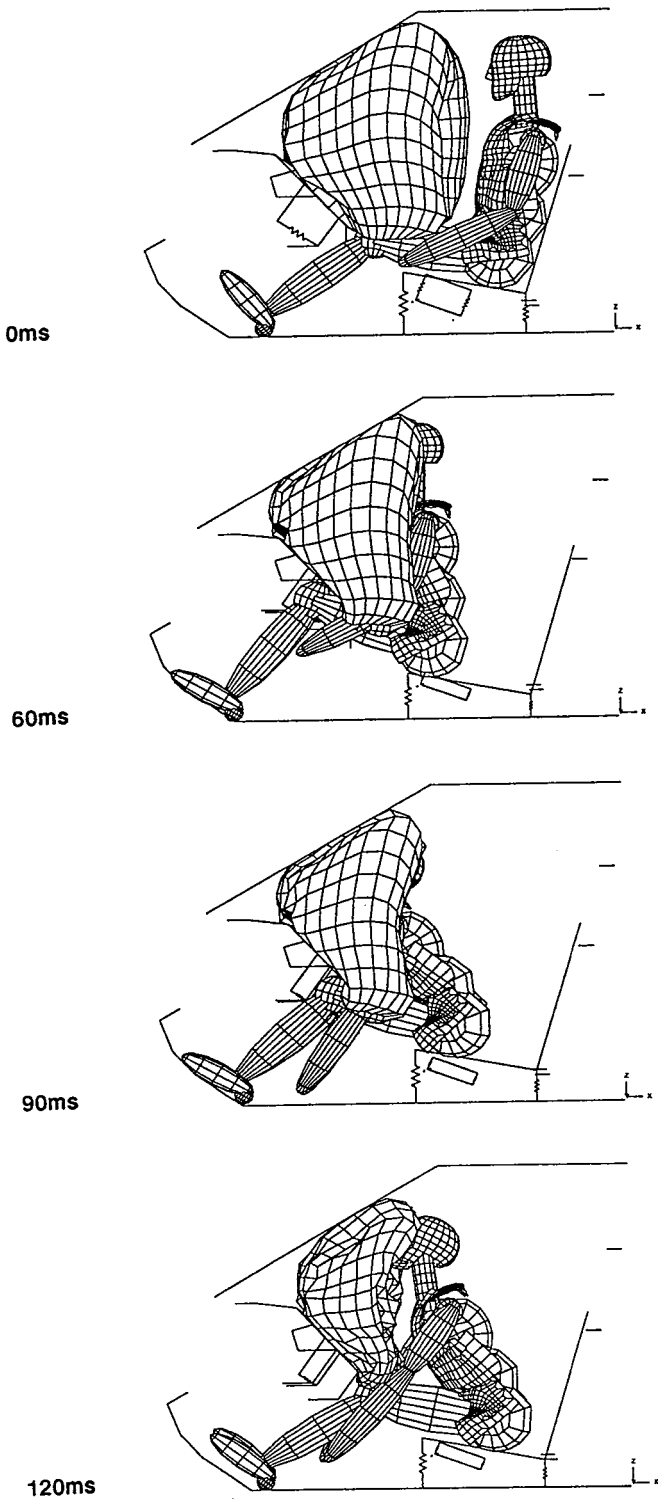

Figure 14. Passenger Side Airbag Sled Test Simulation

In Figure 17(b) this has been taken further: the belted occupant has been placed in a structural model of a vehicle.

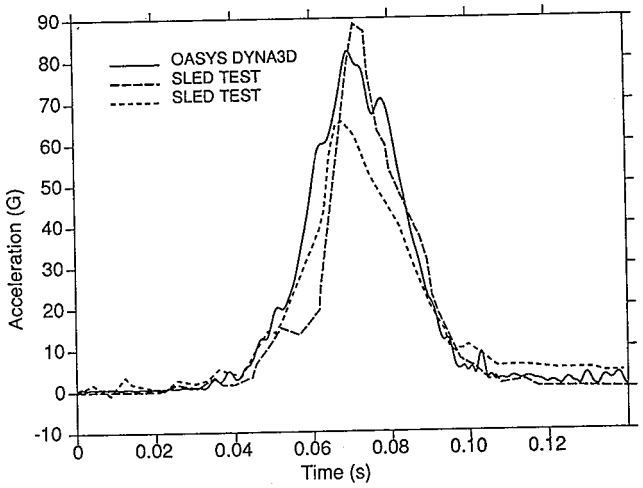

(a) Chest Resultant Acceleration

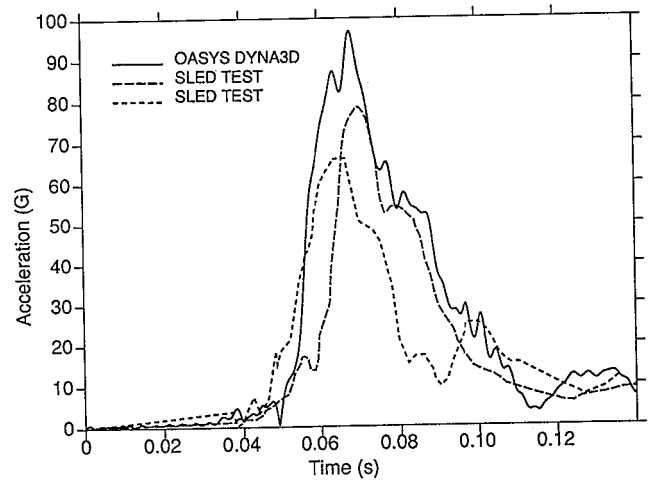

Figure 15. Passenger Side Airbag Sled Test Correlation

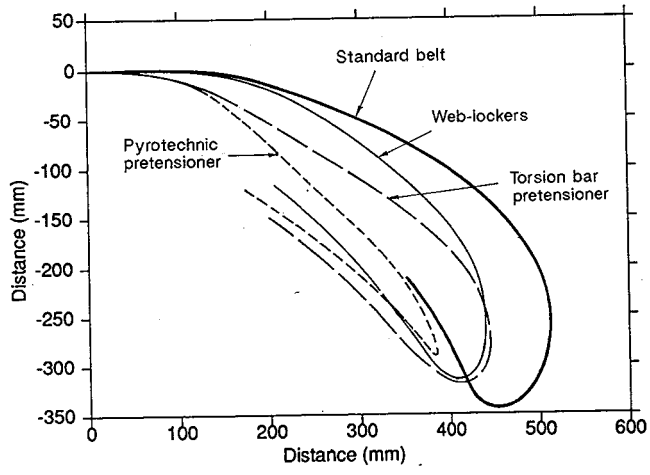

Figure 16. Belt System Variants—Head Trajectory

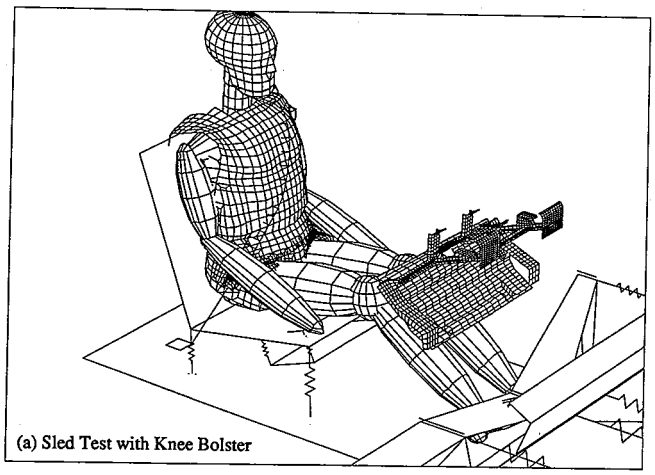

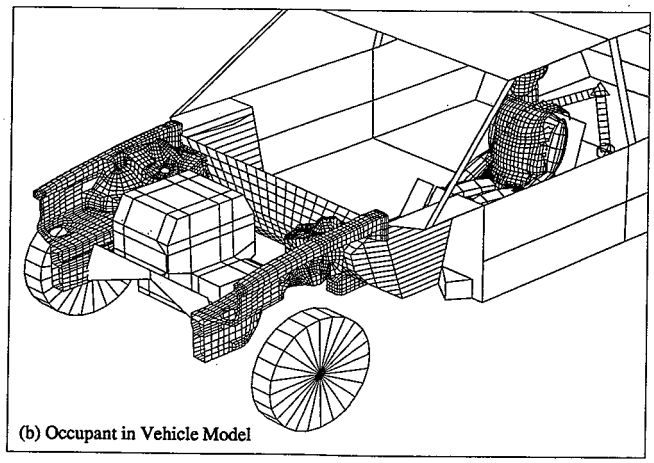

Figure 17. Occupant/Structure Models

Conclusions

- A single code, OASYS DYNA3D, which is already in use for vehicle structure analysis, has been shown to be capable of delivering realistic fully three-dimensional occupant simulations.
- Correlations with sled test results are good for belt and airbag restraint systems.
- Good results can be achieved using simple models which take relatively little computer time, even when airbags are involved.
- The software can also be used to demonstrate the effect of features such as pre-tensioners and web-lockers.
- A fully integrated calculation is possible, in which occupant, vehicle structure, restraint system, and the interactions between these items are present.

Acknowledgement

The authors wish to thank Rover Group Limited for permission to publish the material contained in this paper.

References

1. OASYS DYNA3D 5.1 User Manual; OASYS Ltd, 13 Fitzroy Street, London, W1P 6BQ, England.
2. Hallquist J.O.; LS-DYNA3D 902 User Manual.
3. J Kaleps, J Whitestone; "Hybrid III Geometrical and Inertial Properties," SAE 880638, 1988.
4. B.D. Walker and P.R.B. Dallard (Ove Arup and Partners),"An Integrated Approach to the Simulation of Vehicle Crashworthiness and Occupant Protection Systems," SAE 910148, 1991.
5. Hallquist, J.O. Private Communication.
6. J.H. Leach; "Practical Tools for Vehicle Impact Simulation Part 1: Vehicle Impact Simulation in Rover Group," Proc. Instn Mech Engrs, Vol 205, 1991.
7. J.C. Miles, R.M.V. Sturt and J.H. Leach; "Practical Tools for Vehicle Impact Simulation Part 2: An Integrated Approach Using OASYS DYNA3D," Proc Instn Mech Engs, Vol 205, 1991.

S9-O-20

Advances in Problem-Adaptive Occupant Modelling with PAM-SAFE

X. Ni, D. Lasry, E. Haug
Engineering Systems International S.A
R . Hoffmann
Engineering System International GmbH

Abstract

The wide variety of dummy/structure interactions encountered in current occupant safety simulations necessitates problem-adaptive occupant modelling. This can be achieved by extending existing rigid body occupant models towards deformable finite element models. In this paper modelling aspects for the inclusion of linked rigid and deformable segment occupant models into an explicit finite element crash simulation code is described. The realistic modelling of dummy joints is crucial for the numerical simulation of occupant kinematics and dynamics during impact. Different models for dummy joints are available in programs based on Rigid Body Dynamics. A new approach for the modelling of joints in an explicit finite element code is presented. It combines the effectiveness of the rigid body joints with the advantages of uncoupled system equations. Examples are given to illustrate the function of the different joints. Comparisons with results from standard crash victim simulation programs, as well as correlations of actual sled tests results with preliminary simulation results serve as a basis for validating the FE-joint models.

Introduction

The mathematical modelling of vehicle occupants under the influence of impact loads has been under steady development since more than 25 years. A variety of models has been developed and is being used extensively for research and development in the automotive safety environment [1]. The standard technique that has been applied, is to treat the occupant as a system of rigid segments, interconnected by joints.

Recently dynamic finite element techniques have been applied to tackle specific problems in the passive occupant safety field which could not be analyzed satisfactorily by the standard Crash Victim Simulators. The analysis of the airbag unfolding and deployment is a prime example [2]. Other applications include kneebolsters, collapsible steering columns, steering wheels and vehicle side structures. Common to all these areas is the strong interaction of structural parts with the occupant and the resulting large deformations. Moreover finite element methods have in recent years become the standard tool for numerical crashworthiness analysis of automobile structures.

The integration of these finite element techniques into the occupant simulation process was achieved by dynamically coupling the finite element code with the rigid body code. In the coupling the finite element structure serves the purpose of a sophisticated contact model. Forces generated upon contact between an occupant segment, i.e., a rigid body and a finite element structure, lead to motion of the rigid body and deformation of the FE-structure. An example of this coupling technique is the program PAM-CVS which couples the explicit FE-code PAM-CRASH with the rigid body programs MADYMO and CAL3D [3].

In this paper, recent advances in the PAM-SAFE occupant modelling approach are presented. They are intended to expand the capabilities of currently used simulation techniques by providing a methodology to adapt the surrogate model itself to the problem-specific needs. The approach covers a wide range of models and applications of increasing complexity, from simplified dummy models with linked rigid segments, detailed full finite element deformable models of frontal and side impact dummies, to models of the human anatomy. This in effect renders the numerical tool applicable to automobile safety design as well as to dummy development.

The paper is organized as follows. First, the modelling of joints in an explicit FE-code is discussed. Examples of multiple joint systems are given and compared to the classical rigid body dynamics approach used in Crash Victim Simulators. Validation results are then presented, illustrating the use of integration of dummy models based on these flexible nonlinear joints into the framework of an industrial crashworthiness and occupant safety program. In the last section the adaptivity aspect of the approach is discussed, in particular the evolution of the models to more detailed ones for specific analyses needs in both frontal and side impact.

The PAM-SAFE Joint Models

Joints are elements which connect different parts of a structure. They allow an articulation of different structural parts under the condition that certain relative translational motions are restricted. Constraint conditions may be imposed on the open relative translational and/or rotational motions of the structural part around the joint. Usually these conditions impose forces or moments on the joint which resist the relative motion. The structural parts connected by a joint may be rigid or deformable or a combination of both. In the case that the two parts of the structure are deformable, the classical FE-technique of a Nodal Constraint [4] can be used to rigidly link the displacements of two nodes belonging to the different parts. However if one of the parts of the structure or both are modelled as rigid bodies, the principle of the nodal constraint cannot be directly applied to the joint nodes. The reason is that the motion of all nodes belonging to a rigid body is completely defined by the rigid body's center of gravity, and moreover, the rigid body is generally connected to other rigid bodies or deformable structures by other joints. An exact way of solving this problem is to couple the governing equations of all interconnected rigid bodies in a system by generating a set of coupled system equations. These system equations then would also take into account the constraint conditions imposed by the joints. This is the classical approach used in rigid body dynamics. However it will eliminate the advantage of an explicit program where the governing equations are uncoupled.

An alternative approach has been taken in the PAM-SAFE joint models. Penalty springs are introduced to constrain the translational degrees of freedom of the two nodes defining the joint. With this the advantage of having an uncoupled system is preserved. However particular attention has to be paid in the program to the numerical stability [5] of this system which is composed of rigid bodies and springs.

In the following different types of joints that are currently available in the PAM-SAFE code are discussed. Being kinematically equivalent, the main differences between the elements presented lay in the way of handling of the rotational degrees of freedom for these articulations in the three-dimensional space.

The Spherical Joint

The spherical joint has characteristics which are similar to the so-called 'Cardan Joint' or 'Euler Joints' in Rigid Body Dynamics programs [6,7]

A spherical joint is defined between two nodes N1 and N2, located initially at the same physical point in space. The constraint that the translational movements of these two points remain the same is enforced by means of penalty translational springs.

The relative orientation of structures linked by a spherical joint is achieved by the three successive rotations ϕ, Θ, ψ also called Bryant angles. The joint mechanism is illustrated in Fig. 1. Fig. 2 shows the initial joint coordinate systems r,s,t connected to N1, defined by means of two additional reference nodes M1 and M2. The first relative rotation ϕ is carried out about the r-axis and results in a rotated system r, s', t'. The second rotation around s' by Θ yields the rotated system r', s', t" and the third rotation is performed about the t" axis with the angle ψ. Nonlinear moment-rotation curves for loading and unloading may be specified for each of the three rotation. Damping and friction may also be specified.

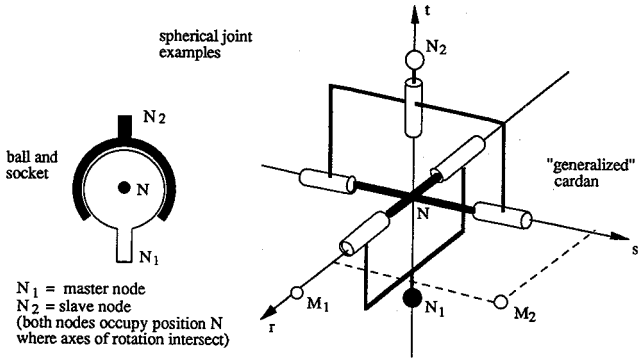

Figure 1. Schematic Examples of the Kinematic Mechanism for the Spherical Joint

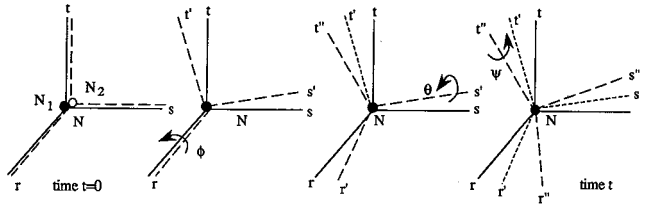

Figure 2. Successive Rotations and Coordinate Systems of Spherical Joint Model

The Flexion-Torsion Joint

A flexion-torsion joint is defined between two nodes N_1 and N_2 that must be located initially at the same physical point. The translational degrees of freedom are penalized as for the spherical joint described above. In order to be able to compare the behaviour of this element with similar joints familiar to the safety engineer, a specialized version of this flexion-torsion element was developed. Its notations are similar to those found in flexion-torsion joints in Rigid Body Dynamics codes. In the flexion-torsion joint element, the joint position is determined by two successive rotations called bending (angle α) and torsion (angle β). In particular, the bending moment depends now on the angle γ which indicates the direction of flexion. Fig. 3 illustrates the successive rotations for this joint.

The bending moment is a function of both a and y by the following law

$$M_b = - C(\gamma)\, M(\alpha)\, u,$$

Where u is the unit vector perpendicular to the t and t" axes, and $C(\gamma)$ is the directional dependency curve given in the input.

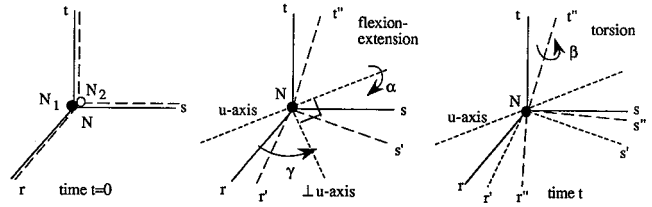

Figure 3. Successive Rotations and Coordinate Systems of the Flexion-Torsion Joint

Non-linear moment-rotation load curves for loading and unloading are given for the α (bending) and β (torsion) rotations. Damping and constant friction with ramping are available for α and β rotations.

The Six-Degree-of-Freedom Spring (6-dof spring)

Nonlinear translational and rotational spring-dampers have also been developed, in the form of a general 6-dof spring. It is the most versatile element to constrain the relative motion of different structural parts in an arbitrary way. It applies user specified non-linear forces and torques on the local degrees of freedom of two nodes depending on their relative translational and rotational motion. The local system is moving with one of the two constrained nodes. These nonlinear springs are used to model different kinds of rotational and translational connections in safety applications, such as simplified deformable chest models, collapsible steering assembly, etc., and in structural crash analysis for the early design phases of crashworthy car components.

Validation of Simple Assembly of Rigid Bodies and Joints

The purpose of this example is to validate the spherical and flexion-torsion joints of PAM-SAFE on a simple case consisting of 3 rigid bodies and 2 joints. No exact analytical solution exists for this problem, so the results are validated by comparison with the results obtained using leading rigid body dynamics programs used in the automotive industry, such as MADYMO-3D and CAL3D.

The model, illustrated in Fig. 4, consists of three rigid bodies RB1, RB2, and RB3, connected by 2 flexible joints J1 (between RB1 and RB2) and J2 (between RB2 and RB3). Rigid body RB1 is fixed, and on the center of gravity of RB3, an initial translational and angular velocity is imposed. The example model was analyzed for two different cases:

- case 1: J1 and J2 are spherical joints
- case 2: J1 and J2 are flexion-torsion joints.

For both cases, the moments computed at the joints by PAM-SAFE are compared with results obtained with rigid body programs.

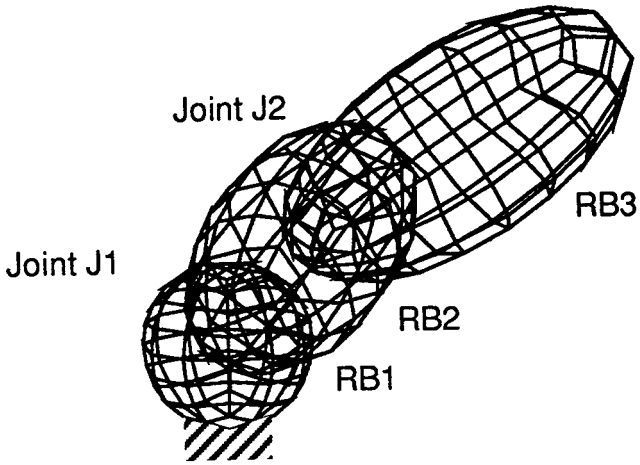

Figure 4. Setup of Two Joint Example Problem

Case 1: Spherical Joint

In Figures 5 and 6, the moment around ψ for both joints J1 and J2 is compared to the result obtained with the rigid body program. As can be seen the two results are identical, and the two curves can be exactly superimposed.

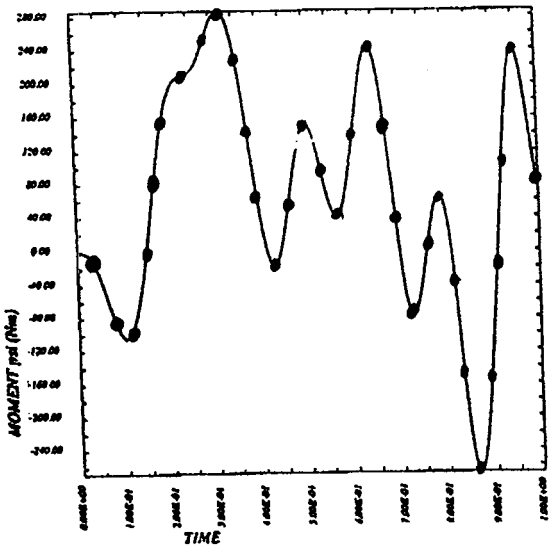

Figure 5. Two Joint Example (Spherical Joint) Moment About ψ for Joint J1: (a) PAM-SAFE Joint Model (solid line) (b) MADYMO Rigid Body Model (dots)

Case 2: Flexion-Torsion Joint

The flexion moment (around α) and the torsion moment (around ß) for joint J2 are compared to the results obtained with the rigid body program in Fig. 7 and Fig. 8. Here again the two results are identical, and the two curves can be exactly superimposed.

In a fashion similar to this simple joint assembly, a finite element model of the standardized Hybrid III neck pendulum test was developed to simulate the nonlinear flexion and extension portions of the test [12]. The results of the simulations were in good agreement with those obtained using rigid body codes, as well as with actual test data [8]. This model is currently being

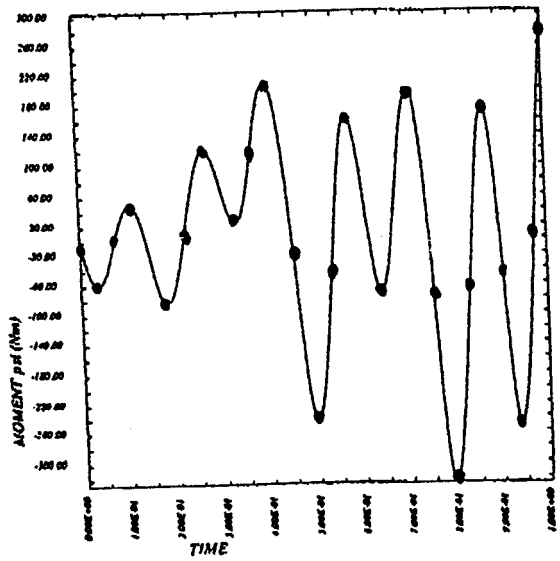

Figure 6. Two Joint Example (Spherical Joint) Moment About ψ for Joint J2: (a) PAM-SAFE Joint Model (solid line) (b) MADYMO Rigid Body Model (dots)

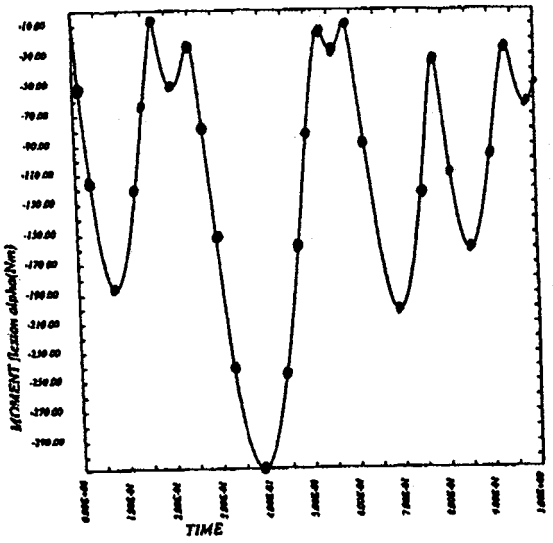

Figure 7. Two Joint Example (Flexion-Torsion Joint) Flexion Moment for Joint J2: (a) PAM-SAFE Joint Model (solid line) (b) MADYMO Rigid Body Model (dots)

improved with 5 joints in series in order to capture more accurately the behavior of the Hybrid III neck formed of alternate rubber and metal disks, and will be reported elsewhere.

Dummy in Car Interior and Dummy/ Passenger Side Airbag Interaction

Dummy in Car Interior

The next step consists in generating a rigid body type dummy model within PAM-SAFE. It represents the 50th percentile Hybrid III dummy and is based on data published earlier [9,10]. Ellipsoidal surfaces were used in PAM-SAFE to represent and visualize the rigid bodies of the dummy which represent its segments. The rigid bodies are connected by the new PAM-SAFE joints. An

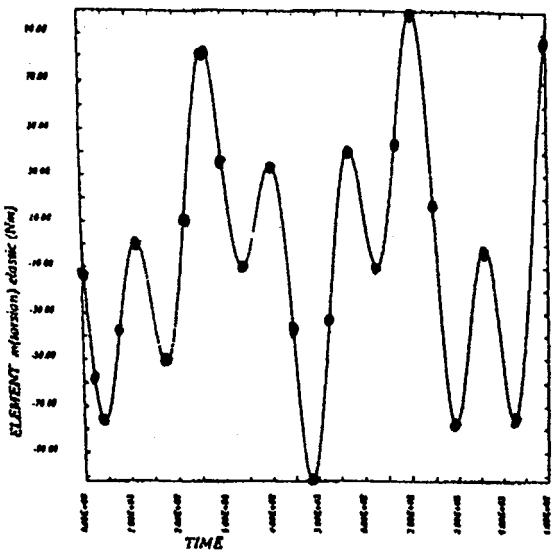

Figure 8. Two Joint Example (Flexion-Torsion Joint) Torsion Moment for Joint J2: (a) PAM-SAFE Joint Model (solid line) (b) MADYMO Rigid Body Model (dots)

equivalent MADYMO model was generated. The dummy, illustrated in Fig. 9, consists of rigid bodies joined by flexible joints: nine spherical joints (equivalent to the cardan joints in MADYMO) and five flexion-torsion joints. The initial position of the dummy is somewhat different from that of the data published in [10], it corresponds more to the reality of a dummy sitting in an actual car interior.

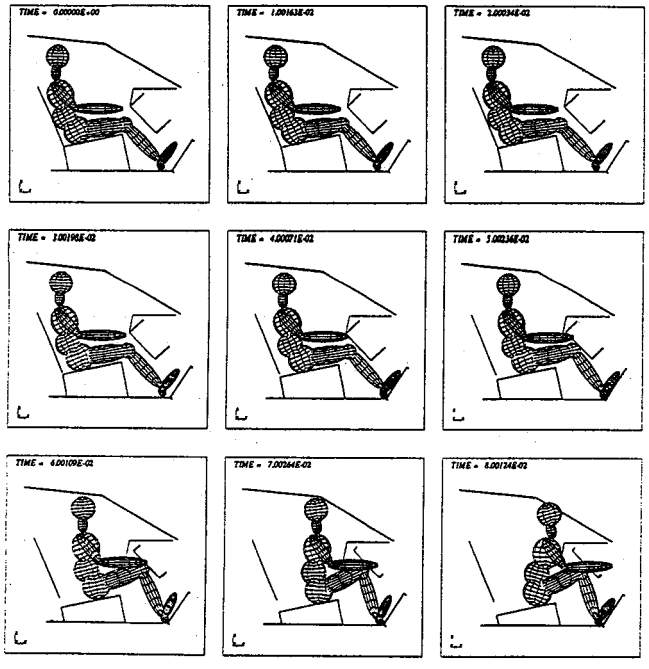

Figure 9. Dummy Simulation: Kinematics Predicted by Explicit FE Code PAM-SAFE

In PAM-SAFE the contacts dummy/car seat and dummy/kneebolster are modelled in a simple way: the seat, represented by a simple rectangular plate is mounted on nonlinear springs with stiffness equal to the stiffness of the MADYMO dummy/seat interaction, and similarly for the kneebolster. An acceleration field consisting of the gravitational acceleration and the crash pulse was applied to the dummy segments.

The results obtained with PAM-SAFE and MADYMO for this simulation are found in Fig. 9 and 10 respectively, where it is seen that the gross motions of the dummy obtained with both programs are very similar. The CPU time on an SGI work station for this 150 ms PAM-SAFE simulation involving the dummy and the simplified car interior model (no coupling with rigid body code) was less than 7 minutes.

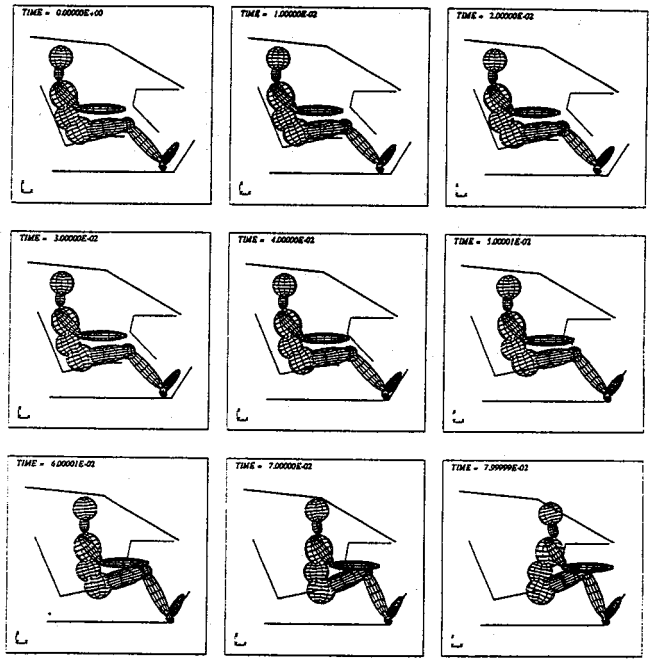

Figure 10. Dummy Simulation: Kinematics Predicted by Rigid Body Code MADYMO-3D

Dummy/Passenger Side Airbag Interaction

A complete simulation involving the dummy was modelled and is being validated by ASL/TAKATA in PAM-SAFE with the newly developed joints (no coupling with rigid body code) and a passenger side airbag as presented in Figure 11. The model corresponds to an actual 35 mph sled test. In Figure 12, time history plots for the normalized head, chest and pelvis accelerations show a very good correlation between preliminary simulation results and test results. Note that the chest model used was totally rigid, as opposed to the actual dummy, which explains the discrepancy in the chest plots. This can be easily improved by adding a one dimensional spring dashpot system in the chest model as is done in rigid body codes ("double ellipsoid chest"), or, to obtain much more detailed information on the chest deformation, by using a fully deformable chest model such as discussed in the next section.

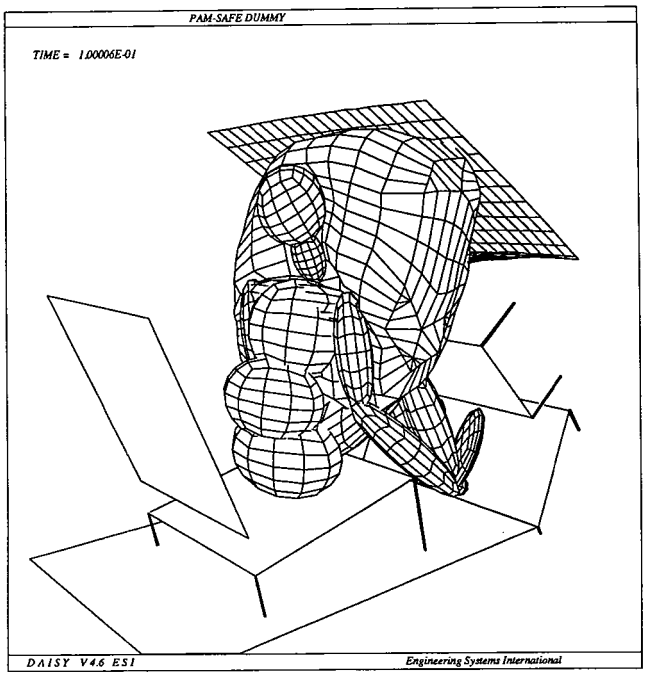

Figure 11. Validation Test: Dummy Interaction with Passenger Side Airbag and Kneebolster (PAM-SAFE)

Problem-Adaptivity: Occupant Models of Increasing Complexity

One of the key features in the approach adopted in PAM-SAFE is its problem adaptivity. Occupants are considered as a *modular* assembly, interconnected by joints, of segments that may be of different levels of complexity:

- rigid segments,
- "quasi-rigid" segments, where all the deformation effects are lumped together in one-dimensional non-linear spring dampers (such as in Lobdell type models),
- fully deformable segments; an example of such a fully deformable chest model, constituted of an assembly of shell and brick finite elements in PAM-SAFE is the Hybrid III Thorax model in Fig. 13 developed by Wayne State University and described in [11].

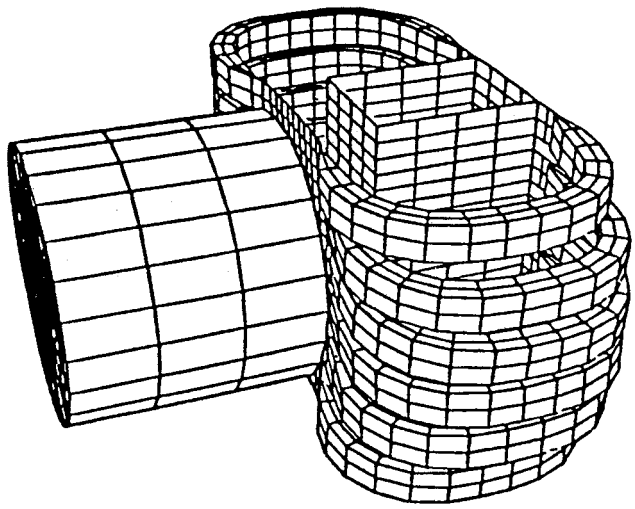

Figure 13. Hybrid III Deformable Thorax Model (Skin Vest Removed)

The occupant model used for a particular simulation is constructed interactively in the recently developed PAM-SAFE STATION graphical integrated environment [13] from a segment database including these 3 types of segments, so that it is exactly adapted to the level of detail and confidence expected from the simulation. An example of such "mixed" or "hybrid" dummy models in PAM-SAFE is illustrated in Figure 14. A fully deformable model of the chest of the EUROSID European Side Impact Dummy, where the embedded in a dummy where the other segments are rigid and interconnected by flexible joints.

Conclusion

Different models for the simulation of joints in an explicit finite element program have been developed and have been validated on test applications. The results of

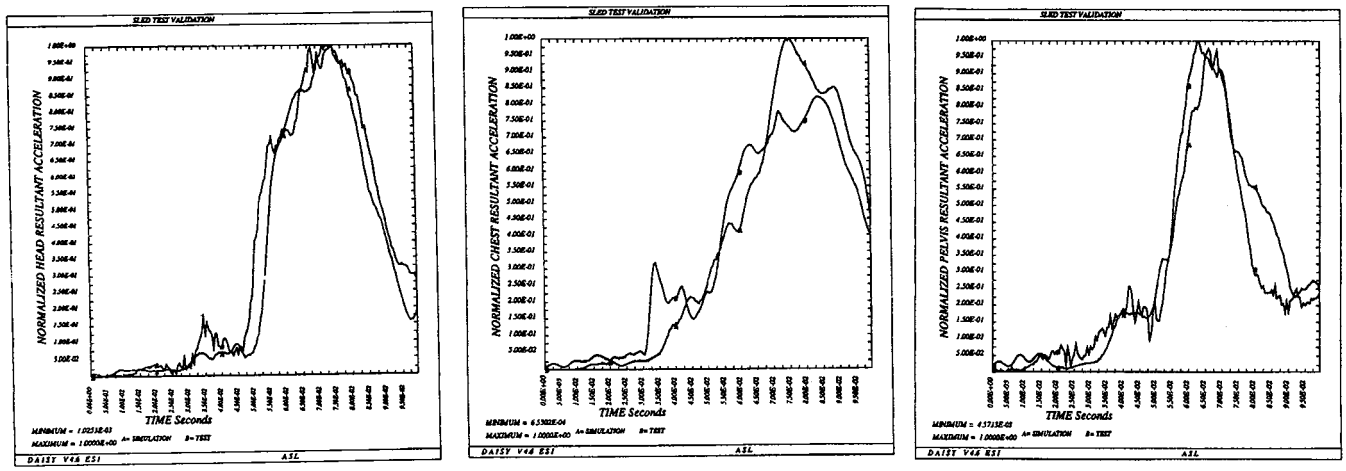

Figure 12. Normalized Head, Chest and Pelvis Accelerations, Simulation and Experimental Results (PAM-SAFE, Plots Courtesy of ASL/TAKATA)

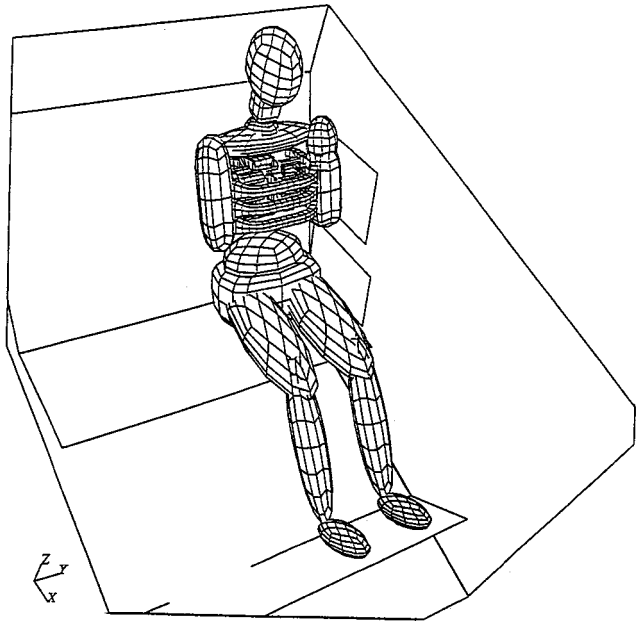

Figure 14. EUROSID Thorax Model Implemented in a Full Dummy Model (PAM-SAFE)

simulations show that the FE-element joints give the same results as joints in Rigid Body Dynamics codes. A validation of a sled test including a dummy formed of rigid body segments, articulated by these joints, exhibits excellent correlation between computed and measured accelerations.

The validated FE-joint models are a crucial step towards a fully integrated crash analysis. Together with the existence of deformable submodels of dummy segments, it is now possible to adapt the dummy model to the specific problem under investigation, i.e., the dummy model may be detailed in areas of interest, whereas other areas use the classical and economical rigid body approach. Moreover this finite element dummy can easily be integrated with a restraint system model, e.g., a FE-airbag, or even with a full structural crash model.

Acknowledgements

The authors would like to thank P. Chalons, J. Ruckert, P. Marcault and A. Leroy for their valuable assistance in the modelling and simulation of the test examples. The sled model by T. Subbian and the support and advice of G. Narwani, both from Automotive Systems Laboratory (ASL) are gratefully acknowledged. The EUROSID chest model validation is being conducted as part of a joint project between ESI and INRETS, with the encouragement of Dr. Cesari.

References

1. Prasad, P., Chou, C.C. "A Review of Mathematical Occupant Simulation Models" ASME Annual Winter Meeting, San Francisco, 1989.
2. Hoffmann, R., Pickett, A.K., Ulrich, D., Haug, E., Lasry, D., Clinckemaillie, J. "A Finite Element Approach to Occupant Simulation: The PAM-CRASH Airbag Model" SAE Paper 890754, 3/89.
3. Hoffmann, R., Ulrich, D., Protard, J.B., Wester, H., Jaehn, N., Scharnhorst, T. "Finite Approach Analysis of Occupant Restraint System Interaction with PAM-CRASH" 34th Stapp Car Crash Conf., SAE Paper 902325, November 1990.
4. PAM-CRASH, Theoretical Manual, ESI SA, Rungis, 1989.
5. Ni, X. "Numerical Stability for Dummy Modelling using an explicit code (PAM-SAFE)," ESI Internal Report, 1991.
6. MADYMO 3D User Manual, TNO, Delft, 1989.
7. Fleck, J.T., Butler, F.E. "Validation of the Crash Victim Simulator, Volume 1, Part 1: Analytical Formulation" Final Report, 1981.
8. Paver, J.G., Khatua, T.P., Pizialli, R.L., Whitestone, J., Kaleps, I., Taylor, C. "The Prediction of Hybrid III Manikin Head-Neck Kinematics and Dynamics" SAE Paper 900450, 1990.
9. Kaleps, I., Whitestone, J. "Hybrid III Geometrical and Inertial Properties" SAE Paper 880638, 1988.
10. Wismans, J., Hermans, J.H.A. "MADYMO3D Simulations of Hybrid III Dummy Sled Tests" SAE Paper 880645, 1988.
11. Pan, H., Yang, K., Lasry, D., Hoffmann, R. "Finite Element Modelling of the Hybrid III Dummy Chest" to be presented at the 35th Stapp Car Crash Conf. 1991.
12. P. Marcault, A. Leroy, "Modelisation Numerique de Mannequin pour Crash Automobile," Rapport de travail de fin d'etudes, Ecole Centrale de Lyon, 1991.
13. PAM-SAFE.STATION User's manual, Engineering Systems International, Rungis, 1991.

S9-O-21

Design Considerations of the Passenger Airbag System

Kazuhiro Seki, Kanichi Fukuda, Kiyoshi Honda
Honda R&D Co., Ltd.

Abstract

As a major part in the design processes of an airbag for use in the front passenger seat, airbag specifications defining the bag deployed shape, bag deployment direction, module location and bag storage methods were

prepared based on various tests. The tests were conducted by taking into consideration the parameters specific to the passenger seat, i.e. wide range of age, physical size and weight of passengers, and seating conditions such as position, direction and posture. This paper analyzes the test results to find ways to obtain an effective protection capability of the airbag while reducing its impact on the passenger during deployment.

Introduction

Design of an airbag module for the passenger side requires a different approach than that for the driver side due to the fact that any occupant in the passenger seat may have various postures at various positions.

In order to effectively protect the passenger of various builds and postures with minimum impact from the deployed bag, design considerations for bag shape and mounting position are more important for the passenger side than for the driver side.

The two elements of protection capability and deployment impact have opposite effects on the passenger. Balancing between these elements are key points in designing the passenger airbag.

This paper describes how we studied theses elements in the course of our airbag design.

Considerations of Airbag Shape and Inflator Characteristics

The shape of the deployed airbag must be determined by taking into account elements that enable the airbag to have effective protection capability under various passenger conditions (passenger's physical size, weight, seating posture with and without a seat belt, etc.) with minimum injury to the passenger as mentioned above.

In this section, we concentrate on how to exclude such undesirable elements from the airbag design specifications.

Conditions Restraining Passenger after Airbag Deployment

First, to identify problems associated with the installation of an airbag, the occupant being restrained must be defined in terms of physical size, weight, posture and seat belt usage. The basic concept of the airbag is to act as a supplemental restraint system for the seat belt. Nevertheless, it should be considered to reduce injuries when the seat belt is not used.

Figure 1 shows cross sections of the same type of airbags (pillow type) deployed in different ways inside the cabin.

The bags were deployed, each with the same inflator, in 30mph frontal barrier crash tests with unbelted dummies.

Examples of the test data are shown in Table 1, which shows that both types of airbags work well and meet requirements of FMVSS 208.

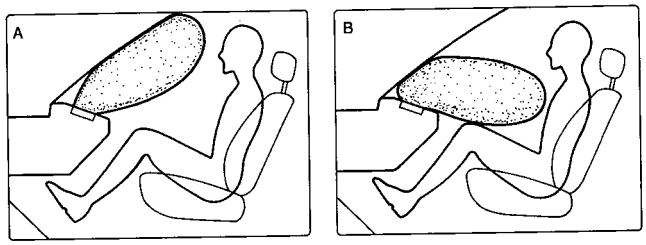

Figure 1. Bag Shapes During Initial Stage Development

Table 1. Frontal Crash Data for Two Types of Bags

Data \ Type	A	B
HIC	204.3	108.3
Chest G	44.5G	26.5G

In the case of A in Figure 1, behavior of the passenger not wearing a seat belt must be given attention; case A has a problem for the neck. In a collision, first the head of the passenger contacts the bag and then stops its movement while the rest of body is moving forward because the airbag restrains only the head. A backward bending moment of the neck is caused. This may not occur if the airbag is not installed and should be considered an additional injury.

Table 2 shows examples of backward bending moments measured at the neck.

Table 2. Neck Bending Moment Data for Two Types of Bags

	A	B
Neck Bending Moment (Backward)	130.4 N•m (Not including rebound)	0.0 N•m

The possibility of injury due to installation of an airbag must be minimized. Case B indicates a low level of injury but it is only for the 50th percentile male dummy (AM50). Its design is not favorable. Therefore the most stable bag shape for the passenger in the normal position is triangular, in order to restrain all parts of the passenger's body evenly.

Conditions During Airbag Deployment

To evaluate the adverse effects of airbag deployment (i.e. its impact on the passenger), it is necessary to take into account for the occupant, not only in the normal

position, but also out of normal position. To determine the effects of airbags due to different shapes, the size is measured in three directions; width, depth, and height.

The minimum width of the airbag should be one which assures coverage of the entire width of the passenger. Balancing between the increased protection capability and the decreased impact of airbag deployment must be considered by using an airbag greater than this width limit. The height of the airbag is to be determined to achieve proper protection capability, with the car ceiling as the upper limit. The depth will be described later in this paper.

The Effects of Airbag Width Variations

First, the relationship between the bag width and its impact on the passenger was analyzed. To achieve the same protection capabilities during head-on collisions among bags of various widths, the output tank pressures of the inflators were adjusted according to airbag volume capacity (Table 3).

Table 3. Four Kind Width Bag and Crash Test Data

Data \ Type	I	II	III	IV
Bag Width (mm)	400	500	600	700
Bag Volume (Liter)	116.8	134.8	154.8	169.0
Inflator Maximum Pressure (KPa) (60 L. Tank)	332	385	445	485
Inflator Max.Press. / Bag Vol.	2.84	2.86	2.87	2.87
Frontal Crash Data (Chest G)	51.1	47.3	47.7	50.5

Figure 2 shows the tank pressure curve of the inflator used. The maximum values of the inflator in Table 3 were measured at point (f) at fill time (the bag is fully inflated to the design form). Maximum inflator output capacity refers to the inflator output per unit volume of the bag at fill time and is almost a equal in all cases (i.e. the inflator output depends on the bag capacity).

Four modules, each made to specification I, II, III, and IV respectively, were prepared. Static deployment tests were performed accordingly. Figures 3 and 4 show the impact from bag deployment on the passenger sitting in and out of normal position.

The 5th percentile female (AF5) dummy was used to represent a passenger sitting in normal position. The seat position was set to bring the dummy as close as possible to the module (i.e. seat position and recline were set to frontmost positions). Furthermore, the dummy was placed at the position equal to the distance it would

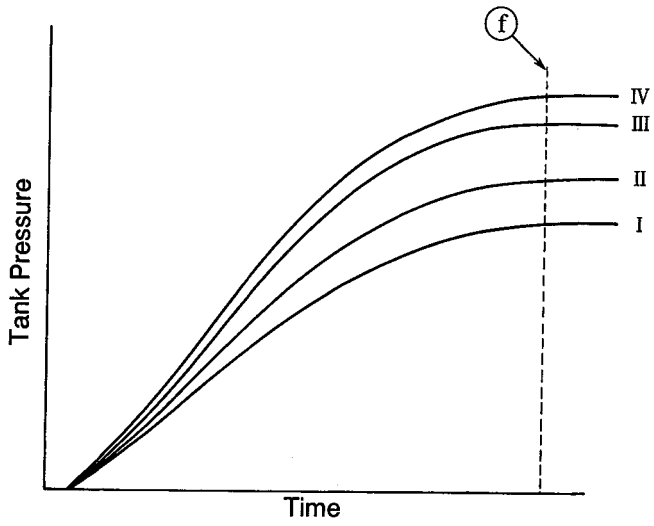

Figure 2. Four Types of Inflator Tank Pressures

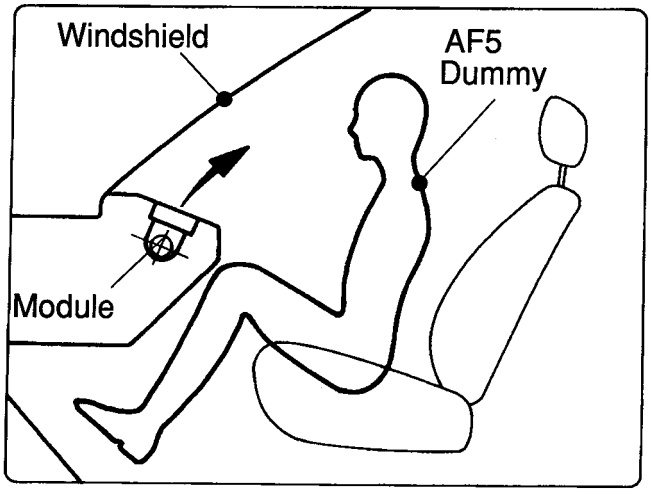

Figure 3. Deployment Impact Test Position (AF5 Dummy)

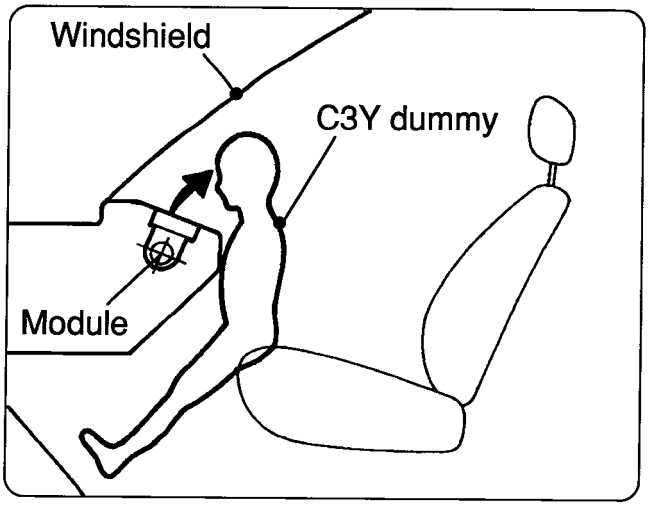

Figure 4. Deployment Impact Test Position (C3Y Dummy)

move before the airbag sensor senses the collision. Position of this dummy is illustrated in Figure 3.

As a representative of a passenger sitting out of normal position, the lightest, 3 year old child (C3Y)

dummy was used. Its sitting position data is presented as SAE J1980 No.1 in Figure 4. These test results are shown in Figures 5 and 6.

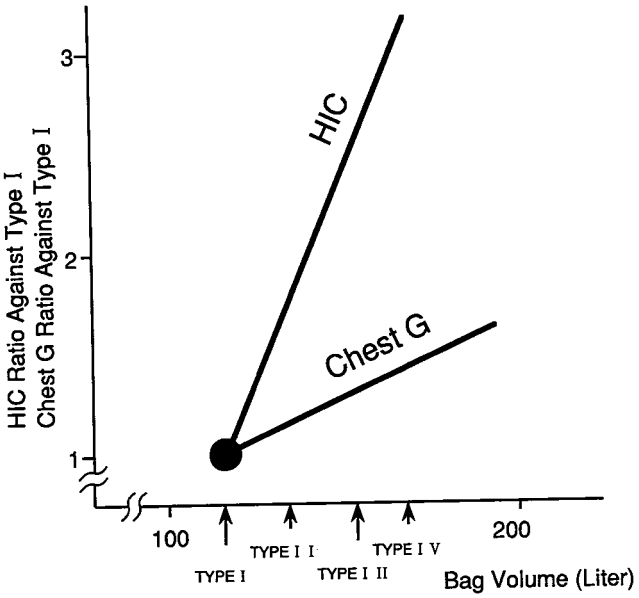

Figure 5. Deployment Impact Test Result (AF5 Dummy)

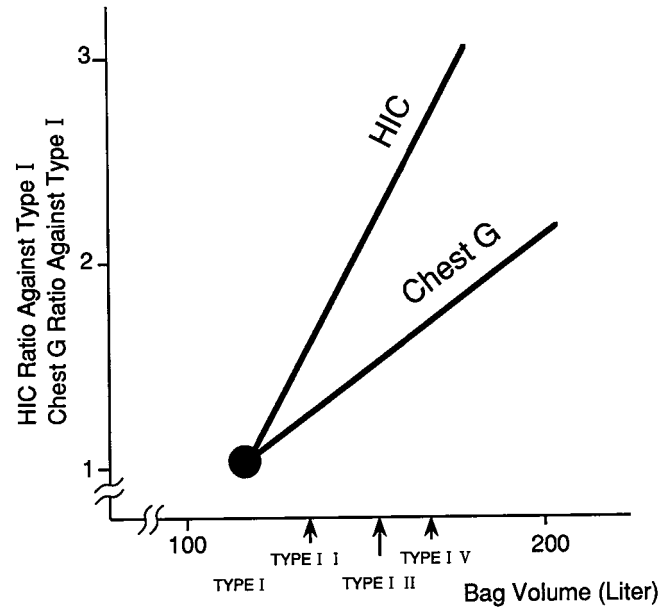

Figure 6. Deployment Impact Test Result (C3Y Dummy)

From the results it can be seen that the impact from the deployment of the airbag on the passenger linearly increases as its width increases, provided that the passengers have the same energy absorption characteristics. This is applicable to passengers in both normal and out of positions. This is because (1) the maximum deployment stroke of a wider bag (S in Figure 7) deployed by a higher capacity inflator is larger than those of a narrow bag (2) initial pressure rise of the tank pressure curve becomes faster as the inflator capability increases (Figure 2) and consequently, bag deployment speed increases.

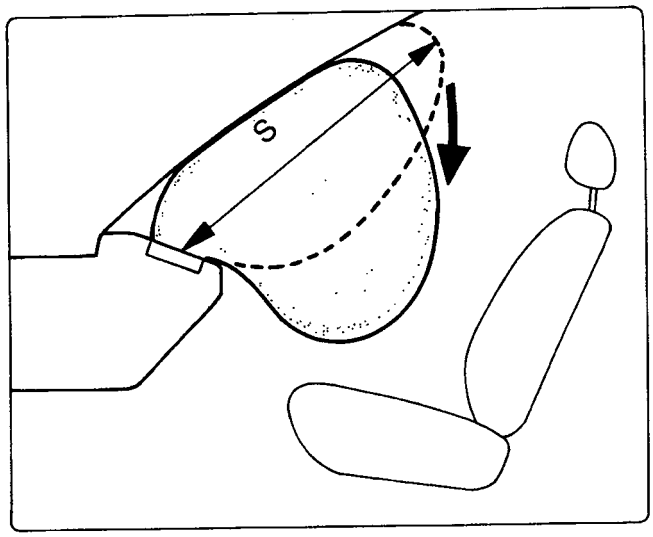

Figure 7. Bag Deployment Process

The Effects of Airbag Depth Variations

When bags of varying depth are set to have the same load characteristics of restraint, the deeper bag will make a greater impact on the passenger because they have a higher bag deployment speed and a longer maximum deployment stroke.

Although the wider bag and the deeper bag have similar increased impacts, their effects on passenger protection are slightly different from each other: the starting time of restraint depends on the airbag depth variations.

As seen in Figure 8, bag (α) has stroke 'a' and bag (ß) has a shorter stroke 'b'. When bags (α) and (ß) have the same load characteristics, bag (α) can absorb energy a/b times that of bag (ß). And when the same energy is encountered, bag (α) can protect the passenger with a load b/a times that required by bag (ß). These comparisons are made on the assumption that both bags are now fully deployed and ready for generating a load to protect the passenger.

Also, these comparisons are made on the basis of bag energy absorption capacity: effects on the passenger will greatly vary as the position and load of the bag changes.

In the next test the larger capacity bag (α) was deployed by the same inflator as the small capacity bag (ß). This combination, called bag (α'), is somewhat different from that of bag (ß). The load characteristic (load vs stroke) of bag (α') is somewhat different from that of bag (α). That is, the initial load curve is lower than that of bag (α) becomes closer to the curve of bag (α) as the passenger moves forward (in this case, bags (α) and (α') have the same vent hole characteristics).

Table 4 shows the impacts upon the passenger by bag (α') (test was conducted in the same way as with the C3Y).

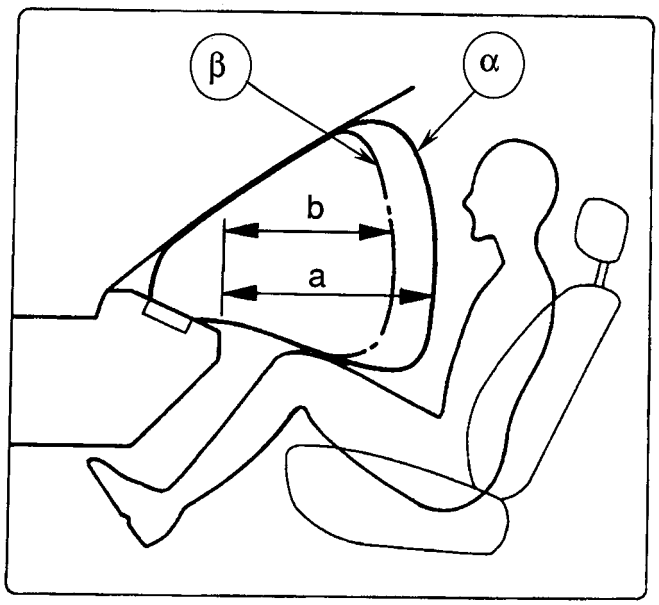

Figure 8. Comparison of Two Types of Bag Shape (Type α and ß)

Table 4. Deployment Impact Test Result (Three Types of Bag and Inflator Combinations)

	α	β	α'
HIC	351.8	200.7	140.7
Chest G	30.4	22.5	12.5

These test results show that bag (α) has a smaller impact than not only bag (α) but also bag (ß). This is due to the fact that the larger bag (α), insufficiently deployed by the smaller capacity inflator, wraps around the passenger in front of the module, and the tension of the bag at fill time is small (Figure 9). But the peak impulse G caused by bag (α') contacting the passenger after the bag deploys is larger because the larger bag (α') has larger mass using the same inflator.

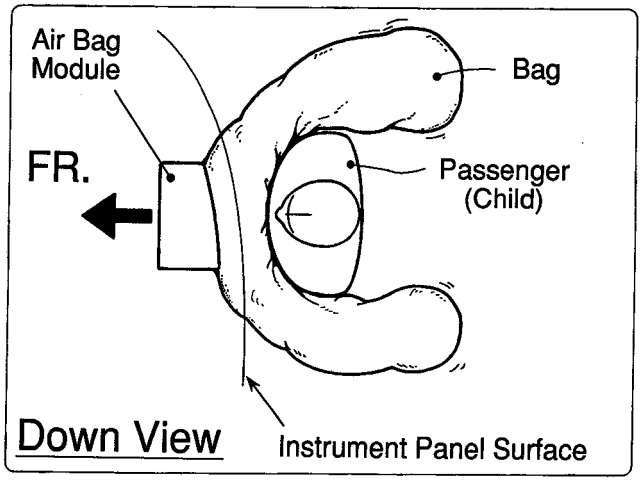

Figure 9. Bag Deployment Shape with Standing Child

Next, the passenger protection capabilities of these bags are compared. Table 5 compares the capability of the bags for a passenger wearing a seat belt to those for a passenger not wearing a seat belt. The values in Table 5 are with respect to bag (α) which is given a base value of 100 (a smaller value means high performance). The type (α) good for a passenger without a seat belt and type (α')is good for one with a seat belt.

Table 5. Frontal Crash Test Results (Three Kinds of Bag and Inflator Combination, With and Without Seat Belt Occupant)

	With Seat Belt			W/O Seat Belt		
	α	β	α'	α	β	α'
HIC (Ratio)	100	108	78	46	—	105
Chest G (Ratio)	100	85	90	89	—	145

The tests on various bag sizes proved that when airbag specifications and inflator characteristics are determined, it is important to identify the kinds of protective effects that the bag can offer to various kinds of passengers (while wearing and not wearing a seat belt). Bag selection affects the type and amount of impact from the deploying bag to the passenger. The final design must be made after considering the trading offs.

Module Layout for the Best Location

Location of the module and direction of the bag deployment must be determined by taking into consideration the elements mentioned in the bag shape section. This is to provide the most effective protection for the passenger and minimize the impact on the passenger given by the deploying bag.

This section reviews the location of the airbag and deploying direction of the bag.

Deploying Direction of Bag

First, assume that the bag is deploying in either of the directions shown in Figure 10.

We then evaluated the passenger protection capability. The tests show that the bag offers the same protection independent of deployment direction when it is completely inflated after the fill time.

In Figure 11, both bags deploy toward the passenger and windshield in the similar formation at fill time, t3.

During the time period t1 to t2, before fill time (Figure 11), the two bags deploy in different ways and in different shapes. The covered area and stroke toward the passenger of two bags differ from each other.

The balancing between these characteristics and impact on the passenger must be taken into considerations during the design phase.

Next, a discussion is made about the airbag deployment impact.

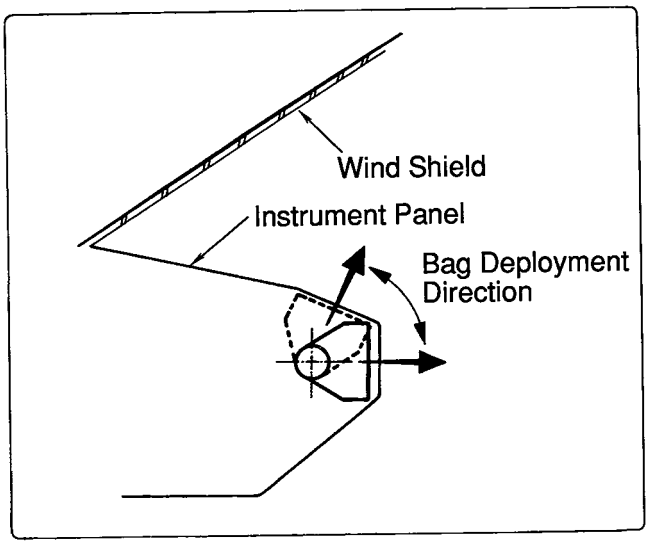

Figure 10. Angle Deployment Test

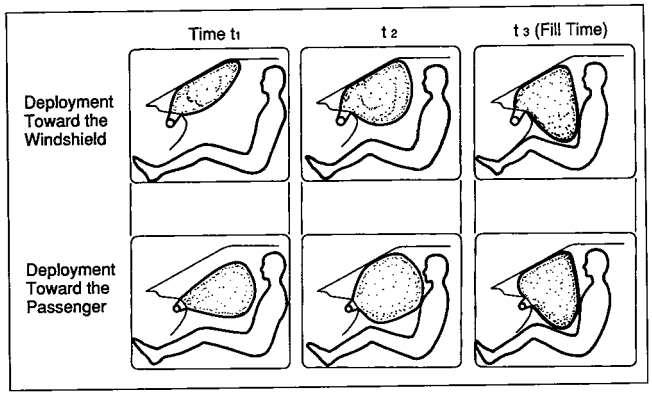

Figure 11. Comparison of Two Types of Bag Deployment Directions

Impacts from the deploying bag were measured while the dummies were placed in (AF5, Figure 3) and out of normal position. (C3Y, Figure 4). These are the same positions that were used for the bag shape effect test on AF5.

During the test the bag was deployed in three directions: horizontally to the chest of the dummy (H, 0°) to the face of the dummy (M, 35°) and to the top of the head (U, 70°), (Figure 12).

The result is shown in Figure 13. Changes in HIC and chest G are expressed as a ratio to that of H direction which is 1.0. Both HIC and chest G are small for deployments in the upper direction.

The tests were continued, using a 6 year old child (C6Y) dummy which represented a taller passenger whose head is in contact with the windshield (dotted circle in Figure 12).

The result is shown in Figure 14 which is the same one that obtained from the C3Y test. The bag, when deploying to the dummy's face, U direction offers a better result than when it is deploying in the other directions, H and M.

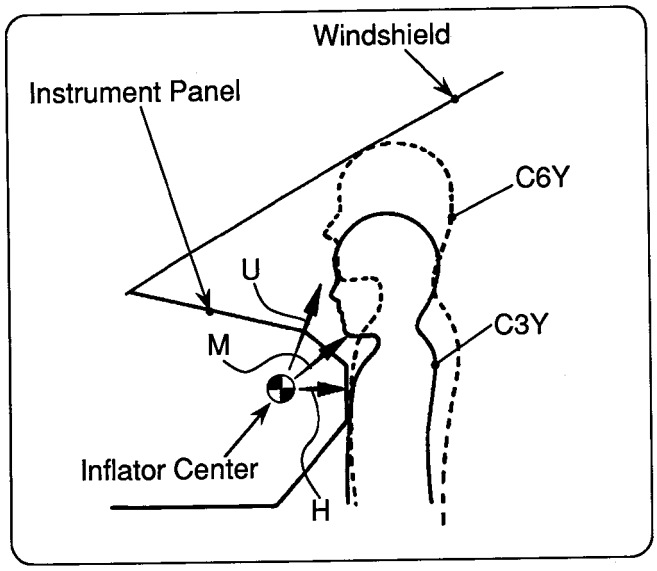

Figure 12. Angle Deployment Test for C3Y and C6Y

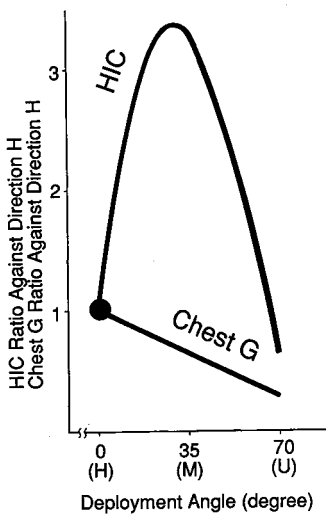

Figure 13. Angle Deployment Test Result (C3Y)

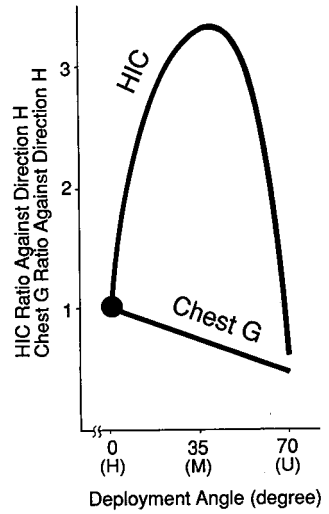

Figure 14. Angle Deployment Test Result (C6Y)

Module Position

The module was relocated to a position approximately 150mm closer to the windshield from the previous position and tested. The test data taken with C6Y dummy is in Table 6. The bag was deployed at 70°, the same as U before (Figure 15). (HIC and chest G when deploying at U', compared to those (defined 100 at U).

Table 6. Deployment Impact Test Results (With Module Moved Closer to Windshield)

	HIC(Ratio)	Chest G(Ratio)
U	100	100
U'	41	71

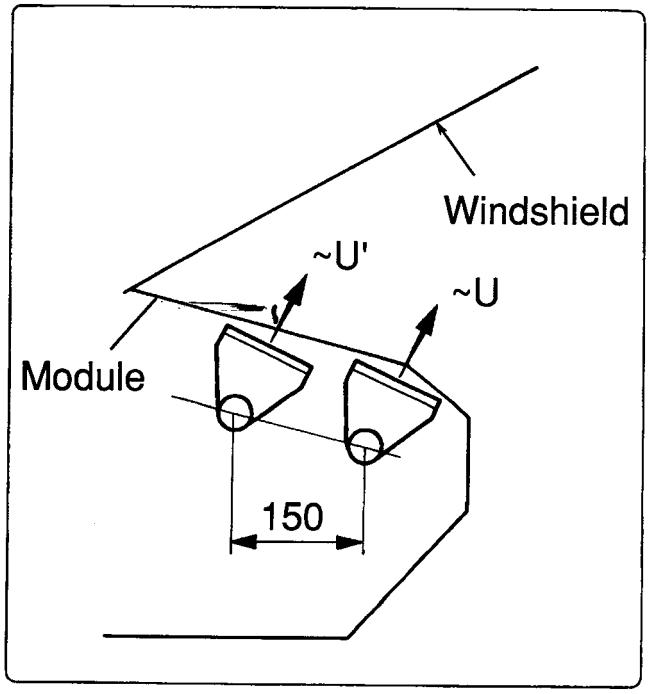

Figure 15. Deployment Impact Test with Module Moved Closer to Windshield

The impact from the bag further decreases as the distance between the module and the passenger increases.

These tests suggest that to minimize impact from the deploying bag, the bag is to be installed closer to the windshield and to be deployed along the windshield. When reviewing the point of passenger protection ability, differences in deployment directions and deployment modes (Figure 11) offer different passenger protection capabilities. These two parameters should be analyzed further.

The deployment mode of a bag can be fine tuned by modifying the internal design of the module as described below.

Controlling Bag Deployment Mode by Module Design

When the bag is deployed along the windshield (arrow (1) Figure 16), it is deployed at a high rate to form the shape (A) in Figure 16. Then the bag is deployed in arrow (2) and finally forms shape (B). It is desirable that the bag forms the shape (B) as quickly as possible to accommodate the passenger during crash. For faster formation of (B) in Figure 16, the bag must quickly deploy in direction (2). The following technique ensures the bag to deploy effectively in this manner.

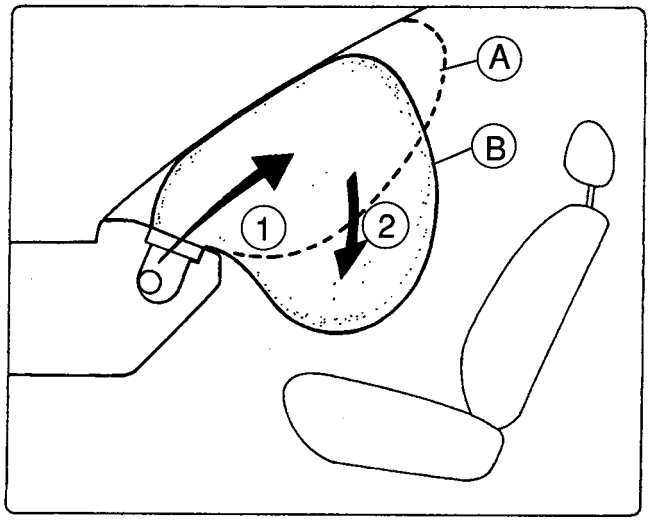

Figure 16. Bag Deployment Process

Modifying the Bag Storing Configuration

Figure 17 is an example of bag storage. There is an offset (a) between the physical center of the inflator and the center of gravity bag.

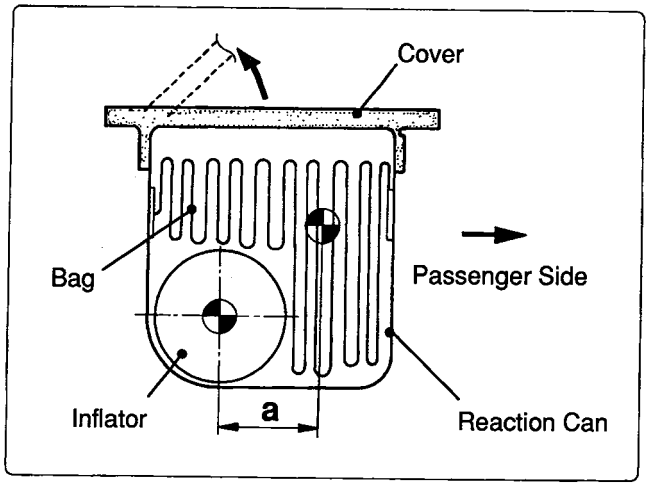

Figure 17. Example of Bag Storage

This configuration generates rotation during deployment of the bag. The rotating force increases as the distance (a) is increased.

Modifying the Folding Configuration of the Bag

Figure 18 shows how the bag is folded to generate rotation. The bag is last folded over in the passenger direction when it is stored.

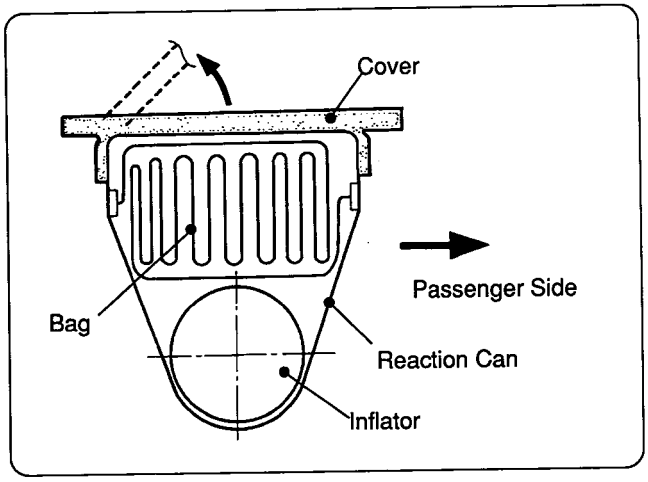

Figure 18. Example of Bag Fold Pattern

The dispositioned tension T generates rotation power during deployment. Because the bag is folded like a bellow, its deployment direction upon ejection from the module disperses in four directions with decreasing speed (1) in Figure 16.

Others

The deployment mode of the bag can be controlled by other ways such as the use of a strap and modification of the inflator characteristics, which are not covered in this paper.

Conclusion

A study is presented from the view point of "balancing between the protection capability of airbags and their impact during deployment" of the larger, passenger airbags.

A study about designing an airbag, more particularly an airbag having a larger bag deployment volume for front seat passenger, is presented from a view point of "balancing the occupant protection capability and the impact against the front seat passenger by the deploying airbag."

As the number of airbag-equipped cars is rising, automotive collision safety engineers are expected to continue their effort to study the airbag which well balances afore-said two conflicting elements so that motorists can benefit from the airbag.

S9-O-22

Achievable Optimum Crash Pulses for Compartment Sensing and Airbag Performance

Russel Brantman
Breed Automotive

Abstract

Realistic achievable 30 mph (48 kph) vehicle to frontal barrier crash pulses (in the Delta-V domain) are defined for optimum single-point occupant compartment sensing, and total airbag performance. These optimum Delta-V pulse shapes are established through airbag system computer modeling, but are based on examination of many vehicle to barrier crash pulses to insure realistic achievability. To be useful, not only do "optimum" airbag crash pulses need to be defined, but also "upper and lower bounds" within which good performance can be achieved. Through computer modeling, upper and lower bounds are established that provide acceptable compartment sensing times (including allowance for sensor manufacturing tolerance bounds), and that should limit airbag injury measures to 350 HIC and 40 Chest G. Although established for a 30 mph frontal barrier crash, knowledge and experience have been used in defining the Delta-V pulse shapes such that good sensor performance would also be expected in the mid speed range. In accordance with this objective, undesirable Delta-V pulse shapes that are within or near the above optimum pulse boundary are also shown.

Introduction

Since an occupant's FMVSS-208 injury measures are essentially governed by his relative velocity during the application of restraint, evaluation of a vehicle's crash pulse performance should take place in the Delta-V domain. Within this domain, candidate 30 mph (48 kph) frontal barrier optimum crash pulse shapes and bounds were defined based upon knowledge of airbag system performance, and upon examination of many vehicle to barrier crash pulses to insure realistic achievability. For simplicity, the candidate Delta-V pulse shapes were expressed as piecewise linear segments.

Pulse shape optimization was performed for an unbelted driver restrained by an FMVSS-208 driver airbag system. However, deployment time constraints were imposed that should make the results applicable also for a passenger airbag system.

The optimization methodology that was employed was as follows: Candidate pulse shapes were divided into three regions—sensor trigger, airbag seating, and occupant ridedown—each of which was then optimized sequentially using sensor and airbag simulation models, and experience. A fixed airbag system design was used throughout, except for a scale factor on the column stroking force that was tuned to the crash pulse. Thus, the only variable affecting the predicted sensor trigger

times and occupant injury measures was essentially the shape of the crash pulse.

For establishing the optimum crash pulse bounds, the optimization criteria were to limit airbag injury measures to 350 HIC and 40 Chest G. Within these bounds, optimum pulse shapes were defined by minimization of Chest G. A maximum Pulse Duration (time to zero car velocity at maximum crush) of 90 ms was used, as being the largest duration that was both reasonably and widely achievable.

The computer simulations were performed using Breed Automotive's SENSOR and VODS (Vehicle Occupant Dynamic Simulation) proprietary computer programs. The sensor parameters used were those of our current production passenger compartment AMS (All-Mechanical Sensor). The airbag system parameters used were those of a validated existing airbag system design, including steering column and knee bolster, with a high output inflator.

Airbag Optimum Crash Pulse and Bounds

Figure 1 summarizes the results of the optimization study. The Upper and Lower Bounds shown, for a 30 mph front barrier crash, will limit airbag injury measures to 350 HIC and 40 Chest G. The Optimum Targets shown will further reduce these injury measures to about 250 HIC and 32 Chest G. (Note again that the maximum of a 90 ms Pulse Duration was chosen only because it was the longest duration that was reasonably and widely achievable.)

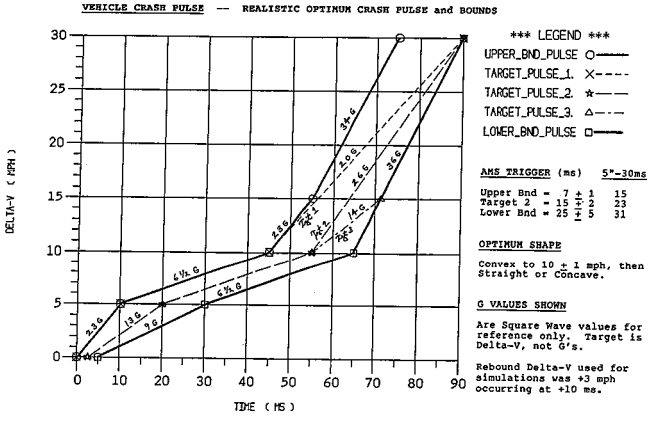

Figure 1. Realistic Delta-V Targets and Bounds—30 mph Barrier Crash Pulse—For Optimum Compartment Sensing and DS/PS Airbag Performance

Of these Optimum Targets, the Optimum Pulse is Target 1, followed by Target 3, and then Target 2. Even though Target 3 has a 10 G higher ridedown than Target 2, its reduced relative velocity during the initial airbag restraint (when the airbag is stiffest) produces somewhat better injury measures.

The pulse shapes are divided into three regions: Sensor Trigger (the initial bumper impact pulse that triggers the sensor); Airbag Seating (the time in which the airbag is deploying and coming up to positive pressure); and Occupant Ridedown (during which the occupant rides down the crash pulse, coupled to the car through the airbag and steering column).

The pulse shape requirements on these three regions for optimum compartment sensing and airbag performance are described below.

Sensor Trigger Region

The Sensor Trigger Region is generally the first 10 to 25 milliseconds of the 30 mph frontal barrier pulse. For an occupant compartment sensor, this pulse is governed by the stiffness and available deflection of the bumper and its support structure before it fails under the impact.

For optimum compartment sensing, this initial front-end structure should be very stiff, and should have an appropriate available deflection to extend the duration of the pulse sufficient for sensor trigger.

For a 30 mph frontal barrier crash with a good car front-end structure, the passenger compartment sensor (over its manufacturing tolerance band) will trigger in the range of 3 to 4 mph Delta-V. However, in order to ensure timely sensor trigger on moderate speed crashes, it is desirable for the bumper impact pulse at 30 mph to produce a Delta-V of 5 mph.

The AMS trigger times shown in Figure 1 show that the higher the initial impact G level, the more optimum the sensor trigger, and the lower the variation over the manufacturing tolerance band. (The sensor trigger values shown correspond to the design mid calibration, with the ± times corresponding to the manufacturing high and low calibration tolerance.)

The 5"-30ms time is the usual guideline for required sensor trigger time in high speed impacts. (That is, the sensor should have triggered at least 30 ms prior to the time it takes for a free-mass occupant to travel 5 inches.) Thus we see that even down to the level of Target 2, excellent sensor trigger times are achieved, with very small variation over the manufacturing tolerance band. However, at the Lower Bound crash pulse, we are approaching the limit of acceptable sensor performance.

Airbag Seating Region

The Airbag Seating Region is the time during which the airbag is deploying and coming up to positive pressure. During this time, an unbelted occupant would still be without restraint. Thus, it is highly desirable for the vehicle to experience only a low deceleration during this time.

This portion of the crash pulse is governed by the crush distance between the bumper support and the engine, and by the initial stiffness of the engine support structure.

If the occupant experiences high Delta-V during this Airbag Seating Time, two very detrimental effects occur. First, the deploying airbag will not have sufficient time to unfold and seat itself properly. Due to rapid travel, the occupant will interfere with the unfolding airbag and can

cause it to roll upwards, which will severely compromise its restraint effectiveness. The second effect is that if the occupant's relative velocity is high at the time when the airbag is first capable of providing restraint, then this will produce high penetration into the airbag, with a large spring-mass type overshoot, at the time when the airbag is stiffest.

For a driver airbag, this Airbag Seating Time will usually be about 30 ms. However, for a passenger airbag, one should allow for a 40 ms pressurization time. For optimum airbag restraint performance, the Delta-V should increase to only 10 mph by the end of this time.

This optimum Airbag Seating Delta-V was established by creating a junction point on the crash pulse Delta-V at 40 ms after sensor trigger, and then varying the Delta-V at this junction point (while keeping all other junction points fixed) until the driver injury measures were minimized.

The interesting aspect of this part of the optimization study, is that the 10 mph Airbag Seating Delta-V is truly optimum for the Bounds and Targets shown on Figure 1. Lower Delta-V values did not improve driver injury measures, and in fact, made them worse. In addition, actual car crash pulse investigation shows that this 10 mph Airbag Seating Delta-V is achievable.

Occupant Ridedown Region

The Occupant Ridedown Region is the remaining portion of the crash pulse (after Airbag Seating), during which the occupant's torso rides down the crash pulse, by being coupled to the car through the airbag and steering column.

This portion of the crash pulse is governed by the front-end side rails, the engine, and its main supporting structure.

Obviously, the longer the duration for this portion of the crash pulse, the lower the G level that can be achieved, and the better it is for the occupant. Thus, of the Optimum Targets shown on Figure 1, Target 1 is the Optimum Pulse for a crash pulse limited to a duration of 90 ms.

However, because the occupant is coupled to the car through a restraint system, subtle nuances can exist. In particular, it turns out that a concave shape for the ridedown portion of the pulse is usually better than a straight line Delta-V, since it reduces the occupant's Delta-V during the initial airbag restraint when the bag is stiffest. Thus, Target 3 is somewhat better than Target 2, even though it has a 10 G higher ridedown.

In summary then, the best overall Delta-V pulse shape is convex to 10 mph and then straight or concave to the end of the pulse. The initial portion of the pulse to 5 mph should be as steep as possible for best sensor trigger, and then the next 5 mph should be drawn out over 35 ms (to allow 40 ms from sensor trigger) for passenger airbag seating.

Airbag Optimum Crash Pulse Performance Tables

Table 1A shows the Dynamic Crush for the Optimum Targets and Bounds, which ranges from 24 to 33 inches (61 to 84 cm).

Table 1A. 30 Mph Frontal Barrier Airbag Optimum Crash Pulses (Crash Pulse Duration and Vehicle Dynamic Crush)

CRASH PULSES	PULSE DURATION (milliseconds)	DYNAMIC CRUSH (inches / cm)	ENERGY MANAGEMENT
o Upper Bnd	75	24 / 61	Good
o Target 1	90	27 / 69	Excellent
o Target 2	90	30 / 76	Very Good
o Target 3	90	31 / 79	Very Good
o Lower Bnd	90	33 / 84	Good

1) "Pulse Duration" = Time to Zero Velocity at Maximum Crush.

2) The choice of 90 ms Pulse Duration for the Airbag Optimum Crash Pulses was based on this being the largest duration that was reasonably and widely achievable.

However, large dynamic crush does not necessarily mean good crash performance—it is how you manage the energy absorption that is more important than the total crush. In this regard, Target 1 with 27 inches Crush) provides better airbag results than Target 3 (with 31 inches Crush), which in turn is much better than the Lower Bound (with 33 inches Crush). And the Upper Bound with only 75 ms Pulse Duration and 24 inches Crush is about equivalent in airbag protection performance to the Lower Bound with its 90 ms Pulse Duration and 33 inches Crush.

However, while good energy management can optimize what you have, you are still limited in what you can achieve by what is the maximum Pulse Duration and Vehicle Crush that is available.

Table 1B shows typical Crash Pulse Duration and Vehicle Dynamic Crush for American Cars, categorized by size, with good to excellent 30 mph frontal barrier crash pulses. These results compare favorably with our Optimum Targets and Bounds, and support the claim that the Optimum Crash Pulse Targets and Bounds are realistically achievable.

Table 1B. American Cars With Good 30 Mph Frontal Barrier Crash Pulses (Typical Crash Pulse Duration and Vehicle Dynamic Crush)

CAR SIZE	PULSE DURATION (milliseconds)	DYNAMIC CRUSH (inches / cm)	ENERGY MANAGEMENT
o Luxury	105	33 / 84	Selected Cars Were All Good To Excellent
o Full	95	30 / 76	
o Mid	88	27 / 69	
o Compact	80	24 / 61	

In particular, in terms of available Pulse Duration and Vehicle Crush, our most Optimum Crash Pulse (Target 1) should be achievable down to the level of a good Mid-Size American Car. And even a good Compact American Car should be able to remain within our Upper Bound Crash Pulse.

Table 2 shows the VODS airbag injury measure predictions for the Upper and Lower Bound Pulses. As was mentioned, the simulations were conducted using a fixed airbag system design, except for a scale factor on the column stroking force that was tuned to the crash pulse.

Table 2. Optimum Crash Pulse Boundary VODS Predictions

UPPER BND PULSE			
HIC	250	25% *	(65 TO 105 MS)
CHEST G'S	40	65% *	(71 MS)
FEMUR LOAD	1750	80% *	(74 MS)
UPPER BND PULSE	(AND 85% COLUMN FORCE)		
HIC	360	35% *	(80 TO 105 MS)
CHEST G'S	40	65% *	(89 MS)
FEMUR LOAD	1750	80% *	(74 MS)
LOWER BND PULSE			
HIC	300	30% *	(80 TO 120 MS)
CHEST G'S	40	65% *	(88 MS)
FEMUR LOAD	1750	80% *	(92 MS)
LOWER BND PULSE	(AND 85% COLUMN FORCE)		
HIC	400	40% *	(95 TO 120 MS)
CHEST G'S	43	70% *	(88 MS)
FEMUR LOAD	1750	80% *	(92 MS)

Sensor Trigger = 7 ms for Upper Bnd Pulse, and 25 ms for Lower Bnd Pulse.

* = % (rounded to nearest 5%) of FMVSS-208 Allowables: 1000 HIC, 60 Chest G, 2250 lbs (10 kn) Femur Load.

VODS = Breed Automotive "Vehicle Occupant Dynamic Simulation" proprietary computer program.

Simulations were conducted using a fixed airbag system design, except for a scale factor on the column stroking force.

The results on Table 2 indicate that these Pulse Bounds should limit airbag injury measures to 350 HIC and 40 Chest G. They also show that, for the Pulse Bounds, the standard column performed best, and that the results were not very sensitive to moderate changes in column stroking force.

Table 3 shows the VODS airbag injury measure predictions for the Optimum Target Pulses. These Targets should reduce the airbag injury measures to about 250 HIC and 32 Chest G. They also show that, with these pulses, the column stroking force needs to be reduced; but that this must be done carefully for Targets 2 & 3 in order to avoid impulsive bottoming out of the column.

The extreme sensitivity shown by Targets 2 & 3 to small changes in the level of the column stroking force indicates that the existing airbag system design is not optimum for these pulses, and that an adjustment beyond a simple scale factor on the column stroking force is needed. Thus, a parametric sensitivity study varying the airbag venting and the shape of the column stroke force-deflection curve should be conducted to optimize the total airbag system design.

Table 3. Target Crash Pulse VODS Predictions

TARGET 1 PULSE	(AND 85% COLUMN FORCE)		
HIC	190	20% *	(60 TO 115 MS)
CHEST G'S	32	55% *	(67 MS)
FEMUR LOAD	1290	55% *	(72 MS)
TARGET 1 PULSE	(AND 75% COLUMN FORCE)		
HIC	210	20% *	(85 TO 115 MS)
CHEST G'S	30	50% *	(96 MS)
FEMUR LOAD	1290	55% *	(72 MS)
TARGET 2 PULSE	(AND 85% COLUMN FORCE)		
HIC	290	30% *	(75 TO 120 MS)
CHEST G'S	32	55% *	(74 MS)
FEMUR LOAD	1500	65% *	(83 MS)
TARGET 2 PULSE	(AND 75% COLUMN FORCE)		
HIC	350	35% *	(95 TO 115 MS)
CHEST G'S	39	65% *	(101 MS)
FEMUR LOAD	1500	65% *	(83 MS)
TARGET 3 PULSE	(AND 85% COLUMN FORCE)		
HIC	220	20% *	(70 TO 120 MS)
CHEST G'S	32	55% *	(105 MS)
FEMUR LOAD	1310	60% *	(91 MS)
TARGET 3 PULSE	(AND 75% COLUMN FORCE)		
HIC	290	30% *	(100 TO 120 MS)
CHEST G'S	37	60% *	(105 MS)
FEMUR LOAD	1310	60% *	(91 MS)

Sensor Trigger = 7 ms for Target 1, and 15 ms for Targets 2 & 3.

Undesirable Delta-V Pulse Shapes

Although the Optimum Pulse Bounds are intended to serve as a band in which good airbag crash performance can be achieved, not all pulse shapes that lie within or near these bounds are desirable.

Figure 2 shows Undesirable Delta-V Pulse Shapes that are within or near the Optimum Pulse Bounds. Three distinct undesirable limiting conditions are shown: a Cross Bound Pulse, a Plateau Pulse, and a Linear Delta-V Pulse.

Table 4 shows the VODS airbag injury measure predictions for these pulses. The results, their reasons, and additional detrimental features of these pulse shapes are discussed below.

The Cross Bound Pulse

The Cross Bound Pulse starts at the Lower Bound and then crosses over to the Upper Bound, thus seeing a relatively slow sensor trigger followed by a rapid Delta-V rise. The airbag injury measures jump to 500 HIC and 45 Chest G.

The Cross Bound Pulse represents the most usual deficiency seen in the average stiffer vehicle crash pulses.

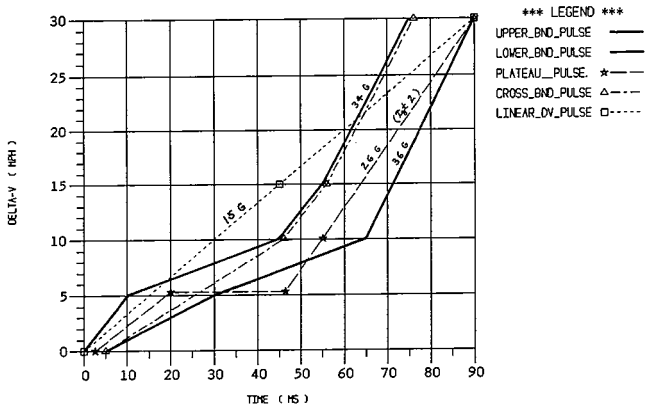

Figure 2. Undesirable Delta-V Pulse Shapes Within/Near Optimum Pulse Boundary

Table 4. Undesirable Crash Pulse Shape VODS Predictions

CROSS BND PULSE

HIC	500	50% *	(85 TO 100 MS)
CHEST G'S	45	75% *	(72 MS)
FEMUR LOAD	1780	80% *	(79 MS)

PLATEAU PULSE (AND 85% COLUMN FORCE) **

HIC	250	25% *	(90 TO 120 MS)
CHEST G'S	38	65% *	(84 MS)
FEMUR LOAD	1750	80% *	(87 MS)

PLATEAU PULSE (AND 75% COLUMN FORCE)

HIC	350	35% *	(95 TO 120 MS)
CHEST G'S	39	65% *	(103 MS)
FEMUR LOAD	1750	80% *	(87 MS)

** This pulse can also cause very late sensor trigger on mid speed and angle barrier crashes.

LINEAR DELTA-V (MIN CONSTANT G) (AND 85% COLUMN FORCE)

HIC	260	25% *	(50 TO 105 MS) **
CHEST G'S	37	60% *	(62 MS)
FEMUR LOAD	1570	70% *	(64 MS)

** Actual injury measures will be substantially higher than this prediction, since model does not simulate the poor airbag seating that will occur due to high occupant velocity during bag deployment.

Sensor Trigger = 20 ms for Cross Bnd Pulse,
15 ms for Plateau Pulse, and
13 ms for Linear Delta-V Pulse.

The Plateau Pulse

The Plateau Pulse shown is a modification of Target 2, such that instead of a gentle rise to 10 mph during Airbag Seating, the pulse drops to zero G, and plateaus at a constant 5 mph until it intersects the extension of the Target 2 Ridedown Pulse. The Chest G jumps from 32 to 38, and Femur Loads increase from 65% to 80% of allowable. Thus, as discussed previously, a gentle rise in Delta-V during Airbag Seating is more optimum than having no pulse during this time.

However, the most detrimental feature of the Plateau Pulse is that if there is insufficient impulse to trigger the sensor in the Sensor Trigger Region (as might be the case in mid speed or angle barrier crashes), then the sensing element returns to its starting condition during the zero G plateau, and has to start over again from the very beginning after the plateau is completed; thus creating a very late sensor trigger.

This same scenario can occur even if the pulse does not have a true plateau, but the Delta-V rise during Airbag Seating is too low, with insufficient G's to overcome the sensor bias (which typically for a passenger compartment sensor with damping is about 4 to 5 G's).

The Plateau Pulse (or low Delta-V after bumper collapse) represents the most usual deficiency seen in the average softer vehicle crash pulses.

The Linear Delta-V Pulse

The Linear Delta-V Pulse corresponds to a minimum constant G (square-wave acceleration) pulse. Since the vehicle sees only 15 G's on such a 90 ms pulse, it might be thought that this would be the best pulse for the occupant. However, we see that the predicted airbag injury measure for the occupant is 37 G's, as compared to 30 G's for Optimum Target 1.

The reason for this is that the occupant is not coupled to the car until the airbag is capable of producing positive pressure; and at that point in time (approximately 40 ms for this pulse), he has achieved a considerable relative velocity, much higher than he would have with the Target Pulse curves. As has been discussed, this high relative velocity will produce high penetration into the airbag, with a large spring-mass type overshoot, at the time when the airbag is stiffest.

In addition, the actual airbag injury measures that will occur will be substantially higher than the predicted values, since the model does not simulate the poor airbag seating that will take place due to the high occupant velocity causing adverse interaction with the deploying airbag.

Conclusion

In summary, realistic achievable 30 mph (48 kph) vehicle to frontal barrier crash pulses (in the Delta-V domain) have been defined for optimum single-point occupant compartment sensing, and total airbag performance. Along with these airbag optimum crash pulses, upper and lower pulse boundaries have been established within which good airbag protection performance can be achieved. However, there are undesirable pulse shapes that can lie within or near these bounds. These pulse shapes have been identified, and their detrimental features discussed.

Acknowledgment

The fundamental work for this study was sponsored by Jaguar Cars Limited. The work was performed at the request of Mr. David Lees, Manager Occupant Protection, at Jaguar Cars.

S9-O-23

The MADYMO Finite Element Airbag Model

H.A. Lupker, H.B. Helleman, E. Fraterman, J. Wismans
TNO Road-Vehicles Research Institute

Abstract

Simple as well as more sophisticated empirical airbag models have been developed since the early seventies. By discretization of the fabric skin of the airbag in finite elements the motion of the different parts of the fabric and contacts with penetrating objects is described more accurately than by the empirical models. This is particularly useful for oblique and out-of-position impacts. Moreover the fabric material behaviour is described in a more realistic way allowing the calculation of the stress distribution in the airbag fabric. The newly developed MADYMO finite element airbag model is optimized for airbag simulations in a crash victim simulation environment. The software implementation resulted in a flexible and user-friendly simulation tool. The approach and theory of the MADYMO finite element airbag and the results of two out-of-position simulations and tests are presented. The agreement between the measured and calculated results is good while computing times are quite reasonable.

Introduction

The rapid increase in car usage after the second world war led to a stronger emphasis on reducing the harm due to car accidents. The first regulations concerning seat belts were drawn up by the US government in 1963. Despite the introduction of retractors, seat belts are frequently not worn, especially in the USA. The recently introduced Federal Motor Vehicle Safety Standards (FMVSS) therefore require all passenger cars to be equipped with a passive restraint system for both front-seat occupants. This led to the installation of automatic belt systems and airbag restraints in new passenger cars. Another US requirement is that airbags must operate correctly with and without seat belts. In Europe seat belts are worn more frequently and airbags are designed to operate in combination with seat belts.

Historically, the development process for the restraint design of passenger vehicles has relied heavily on physical testing of components and restraint systems. The use of simulation models can save much time during the early phases of the design process. Back in 1963 McHenry proposed a 2D numerical model to describe the motion of a vehicle occupant in a collision event (1). In 1970 a 3D occupant model was published by Robbins (2). These initial developments were followed by a number of more general occupant simulation tools (3). In 1983 the first commercially available version of MADYMO was released. The most recent MADYMO version, version 4.3, was released in 1990 (4).

Due to their limited CPU load and short turn around time the occupant simulation programmes have proven to be very suitable tools for sensitivity analyses and design optimization studies. Systematic analysis of parameter effects can be carried out using for instance Design of Experiments methods (5). Due to the continuous implementation of extensions and improvements, models for both the crash dummies and the protection devices, such as seat belts and airbags, are becoming more and more realistic and versatile.

Obviously the simulation model must contain all the relevant aspects. For frontal car crashes the occupant, the car interior and the restraint system must be modelled. Contacts must be defined between the occupant and the seat and the interior surfaces that the occupant may contact. To account for the collapse of the car frontal structures it is sufficient to apply an acceleration pulse to the occupant and to prescribe the overall motion of vehicle interior parts, i.e. the steering column, the instrument panel, the floor and the toepan, to account for the crash of the car frame.

The purpose of this paper is to present the MADYMO finite element airbag as a first implementation of the recently developed MADYMO finite element module. First a brief discussion on airbag modelling techniques will be presented. This is followed by a description of the approach and theory used for the MADYMO finite element airbag module. To illustrate the potential of this module the results of two out-of-position simulations and tests will be compared. A discussion on current and future finite element developments concludes this paper.

Airbag Modelling Techniques

The three most important components of an airbag system are the bag itself, the inflator and the sensors. The sensors determine whether a sufficiently strong impact occurs to activate the airbag system. To be able to determine this for different impact locations a combination of several sensors is usually required. Due to the sudden change in car motion one or more sensors are triggered and some logic is used to combine these to form a criterion for the activation of the inflator. After the inflator is activated it produces hot gas. Due to the pressure build-up in the airbag compartment the airbag module cover breaks and the airbag starts unfolding. To resist the high temperature and tensile loading, two layers of fabric are often used for that part of the bag that is in the gas flow during the unfolding.

The trigger time and inflator characteristics should be tuned so that for most situations the occupant comes in contact with the airbag only after full deployment. Straps (also called tethers) are often used to limit the deployment range of the airbag which postpones the moment of contact between occupant and airbag. Tear

seams can be used to control the deployment and to reduce the inflation rate in order to minimize bag slap effects.

After unfolding and complete deployment of the airbag, an over-pressure is built up inside the airbag and the whole bag is stressed. During the contact between occupant and the fabric skin, gas flows out of the airbag through exhaust orifices, pores in the fabric skin and/or seams. During this phase the airbag can be considered as a viscous damper that restrains the forward motion of the occupant to prevent him from hitting the steering wheel or dashboard. The gas permeability of uncoated fabrics is of great importance for the overall performance of the airbag and thus thermal ageing has to be controlled by using special finishing conditions for the fabric or some aftertreatment process.

In the last two decades several empirical airbag models have been developed among which is the MADYMO 2D model, Figure 1, (6). These models use rather simple approximations for the contact interaction between the occupant and the fabric skin. The properties of the gas inside the airbag are determined by using a lumped parameter approach. During deployment the bag pressure is taken identical to the atmospheric pressure and bag inertia forces are neglected. Although the current MADYMO 2D empirical airbag model has proved itself in many situations to be a valuable tool in the design process of airbag systems, it has its limitations. The results for out-of-position situations, where contact already occurs during deployment, have less value than the results for in-position situations due to the fact that during deployment no forces are exerted on objects penetrating the airbag. Moreover due to the assumed axial symmetry, oblique impacts can not be simulated correctly.

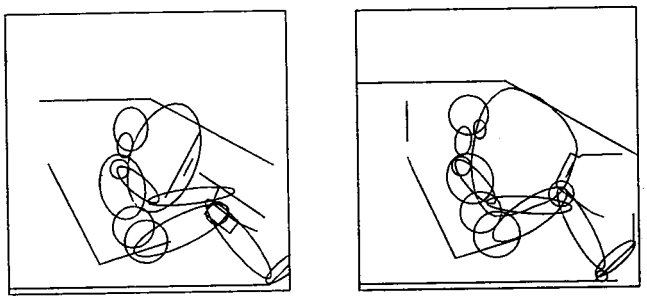

Figure 1. MADYMO Empirical Airbag Model: Driver Side Airbag (left), Passenger Side Airbag (right)

In 1987 several potential methods for airbag modelling were already under investigation at TNO (6). Using finite elements was found to be the most promising option. For use of the finite element airbag models in occupant protection studies a coupling or integration with a crash victim simulation model was proposed. In 1988 the coupling strategies were studied (7) which resulted in the coupling between MADYMO and the finite element code PISCES 3D-ELK in 1989 (8-9). More recently interfaces between MADYMO and the explicit finite element codes PAM-CRASH (10-12) and DYNA3D (13-14) have been realized. The recently released MADYMO finite element airbag model is fully integrated in the MADYMO multibody program and optimized for airbag simulations in a crash victim simulation environment.

With discretization of the fabric skin of the airbag in finite elements the motion of the different parts of the fabric and the contacts with penetrating objects are described more accurately than with the empirical models. Moreover the fabric material behaviour is modelled in a more realistic way allowing the calculation of the stress distribution in the airbag fabric. Also the mass distribution of the fabric material is accounted for by the discretization of the fabric skin. Thus inertia effects (bag slap) and pressure forces on penetrating objects will be accounted for also during deployment of the airbag. Mostly similar thermodynamics, i.e. a lumped parameter approach, to those in the empirical models are used. The most important disadvantage of the finite element approach, especially for parameter optimization and sensitivity studies, is the relatively long computer run time required for each simulation.

MADYMO Finite Element Module

In the finite element method the instantaneous values of the unknown state variables are approximated by a linear combination of assumed functions which are only non-zero in an elementary volume. Based on this approximation the finite element method reduces the continuous system to a discrete numerical system. The actual continuum is divided into finite volumes, surfaces or line segments representing an assemblage of finite elements. The continuum is then analyzed as a complex system, composed of relatively simple elements where compatibility should be ensured along all boundaries between elements. These elements are interconnected at a discrete number of nodal points, the nodes. The deformation of a finite element is defined by the motion of the nodes. Therefore the nodes corresponding to each element, the connectivity, the initial nodal positions and velocities as well as the element properties, i.e. the material behaviour, must be specified by the user. In the present version of the MADYMO finite element module only constant strain triangular membrane elements, Figure 2, and contacts without friction are implemented which limits its present use to airbag modelling or comparable systems which can be described as membranes.

A combination of the MADYMO multibody techniques with finite element techniques allows a more detailed description of the contact interactions with car interior parts or restraint systems than by using only the contact ellipsoids and planes as implemented in MADYMO. Moreover the structural behaviour of the interior parts, restraint systems and critical dummy parts can be analyzed while maintaining the advantages of a multibody approach. Two kinds of interactions generate forces

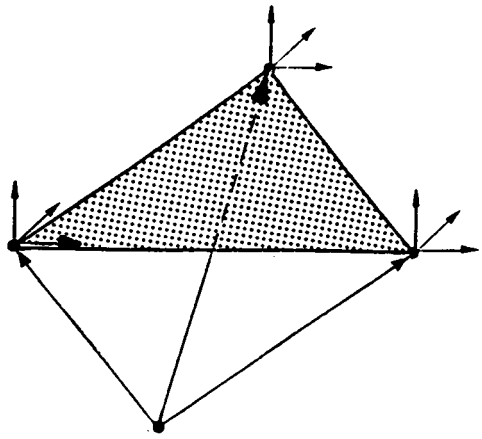

Figure 2. Constant Strain Triangular Membrane Element

between the finite element structures and the multibody systems, i.e. supports and contacts. Supports are rigid connections between the nodes on one hand and a multibody element, system with prescribed motion or inertial space on the other. Contacts can be defined between the nodes and contact surfaces, i.e. planes and ellipsoids. Mutual contacts between finite elements cannot be accounted for in this version.

The approach of the interactions between the multibody elements and finite elements outlined above (Figure 3), allows the use of different time integration methods for the equations of motion corresponding with the finite element module (Central Differences method) and the multibody module (Runge Kutta method). The selected explicit integration methods are conditionally stable and therefore put limitations on the time step that can be used. Due to the often needed fine finite element spatial discretization, the finite element module needs a much smaller time step than the multibody module. To increase the efficiency of the entire analysis the finite element module is being subcycled with respect to the multibody module using a different constant time step for each module. In the next sections only the model assumptions and simulation possibilities of the finite element airbag module are presented. A more thorough description is included in the MADYMO user's manual.

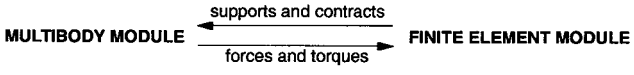

Figure 3. Interaction Between Multibody and Finite Element Module

Airbag Skin and Strap Model

The skin of the bag used in airbag systems consists of fabric sheets, often with venting holes, sewed together. These sheets possess almost no bending stiffness and can therefore be modelled using membrane elements. The material properties of technical fabrics used for airbag manufacturing are directional dependent. However, two perpendicular principal material directions can be defined which coincide with the warp and weft direction of the fabric. Due to the kinematic interaction between the warp and weft threads and their undulation in the unstressed state the stiffness increases with the loading for uniaxial tension tests (15). Since this effect is small under biaxial tension a linear orthotopic material behaviour is assumed to be sufficient for most applications. During compression wrinkling prevents the build-up of stresses to counteract this deformation. Using membrane elements in combination with linear material models would require several elements per wrinkle to achieve a realistic model which will lead to meshes with several thousand elements. Therefore tension only material models (only stiffness against elongations) have also been implemented.

For the thermodynamics the airbag is treated as a "control volume" bounded by the bag with gas flowing through. This "control volume" is continuously monitored and taken to be equal to the volume enclosed by the membrane elements used to model the fabric skin. The volume thus calculated only equals the volume inside the airbag skin if the triangular elements form a closed contour. Therefore an element mesh of the airbag fabric in the deflated state must be made that also covers the venting holes with membrane elements. A special material type with negligible stiffness against elongation or compression has been implemented for the modelling of the venting holes.

In order to limit the deployment range of the airbag straps are often used which form a connection between the back and front of the airbag. A strap is modelled as a massless linear spring between two nodes. Forces are only calculated in the straps when the actual length is longer than the untensioned length. A relative elongation at which rupture occurs can be specified.

Using finite element preprocessors it is possible to make a finite element mesh of the fabric skin in the initial folded configuration. As long as the occupant only interacts with the airbag after unfolding, the initial configuration is expected to have a limited influence on the occupant motion. The laborious creation of a folded airbag configuration is than superfluous. A finite element model can be made in the inflated state first. A pre-simulation must then be conducted during which the volume enclosed by the airbag will be reduced to a volume comparable to that of the folded airbag by creating an under-pressure. Contact ellipsoids or planes are used to direct the finite element motions. The finite element mesh of the fabric skin resulting from this pre-simulation must then be included in the input data for the actual model.

Airbag Inflation Model

The airbag inflation process is modelled as an expanding volume of gas, mass and heat, flowing into and out of the volume bounded by the airbag skin. Gas is blown into the airbag by the inflators and flows out through venting holes and pores in the fabric. The inflation process is treated as adiabatic, i.e. apart from

the heat in the gas flows there is no heat transfer between the expanding volume and its surroundings. The pressure difference between the "control volume" and the surrounding atmosphere is acting on the membrane elements used to model the fabric tissue resulting in a change of motion of the nodes. After full deployment the fabric tissue will be stressed due to this pressure build-up in the "control volume."

The mass inflow of each inflator must be specified by the user by means of a mass flow rate versus time characteristic. The heat supply, or rather the enthalpy, is determined by the temperature and the gas species in the gas mixture delivered by the inflators. A temperature versus time characteristic and the supplied gas mixture, using mole fractions, must be specified by the user for each inflator. The supply mechanism of each inflator can be activated by one or more sensors. The orientation of the sensor and the acceleration of the multibody element to which the sensor is connected at the sensor position, determine the triggering of the sensor based on a user defined condition. If the inflator is activated by more sensors the triggering of the different sensors are combined as specified by the user, using the logical functions AND and OR.

Gas can flow out of the airbag through venting holes and pores in uncoated fabric. The mass flow through venting holes is approximated by a one-dimensional, quasi-steady, isentropic flow model (16). If the pressure in the airbag exceeds the critical pressure (approximately 1.85 times the pressure of the surrounding atmosphere) choked or sonic flow will occur in the venting holes. For such cases the pressure of the surrounding atmosphere is replaced by the critical pressure in the relation for the mass flow rate through the venting holes. A discharge coefficient is used to account for the non-isentropic flow effects. No pressure forces are working on the elements used to cover the venting holes resulting in a force deficit that leads to a more realistic motion of the whole airbag. Due to the deformations of the membrane elements surrounding the venting hole the flow area varies in time, resulting in a more realistic mass outflow calculation.

Leakage through porous airbag fabrics is calculated using an equation for the gas flow through a flat screen placed perpendicular to the flow direction (17). The model is based on a resistance coefficient which is assumed as only a function of the quotient of the free and total area which is a realistic assumption for larger Reynolds numbers (Re>>0.01). The free area is calculated using a porosity coefficient which can be specified for each membrane element separately. Thus for leakage through the fabric the flow area varies in time as was the case for the venting holes. It is also possible to account for the extra gas flow through seams by specifying a higher porosity coefficient for those membrane elements overlapping the seams.

The gas inside the airbag is treated as a mixture of ideal gases and the state variables, pressure and temperature, are assumed to be uniform throughout the bag interior (lumped parameter approach). A linear temperature variation of the constant pressure heat capacity is assumed. The constant pressure heat coefficients and the molecular weight have been predefined as default value for eleven gases that could be of interest for airbag inflation. The properties of user defined gases can be specified if only values for the gas mixture are available. The average heat capacities of a mixture of gases are determined using the Amagat-Leduc rule of partial volumes (18). The ideal gas law and the energy conservation equation for unsteady gas flow (19) are used to calculate the pressure and temperature of the gas mixture inside the airbag.

Out-of-Position Tests and Simulations

As stated before, the empirical airbag models have less value for out-of-position situations than for in-position situations. To illustrate the potential of the MADYMO finite element airbag model for such situations, two out-of-position tests have been simulated. In these tests a driver side airbag comes into contact during inflation with an initially stationary pendulum or 50th percentile Hybrid III dummy, Figure 4. A detailed description of the experimental setup can be found in (9).

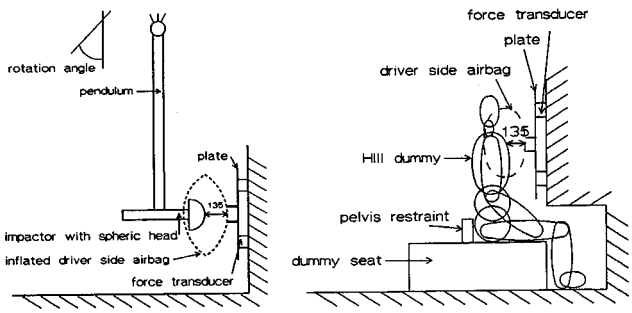

Figure 4. Global Set-Up Driver Side Airbag Tests: Pendulum (left), Hybrid III Dummy (right)

For both tests similar 60 litre driver side airbags were used. The airbags are made of nylon 66 and are neoprene-coated. They have four identical venting holes at the back. Six straps connect the front with the back. The airbag dimensions are given in Figure 5.

The airbags were unfolded before the tests and fixed to a plate, which in turn was fixed to a rigid wall with three force transducers. For the experiment with the pendulum, the pendulum was fixed to the surroundings in such a way that only a rotation about an horizontal axis parallel to the backplate was possible. The distance between the rotation axis and the centreline of the impactor is 1310 mm. The spherical impactor head has

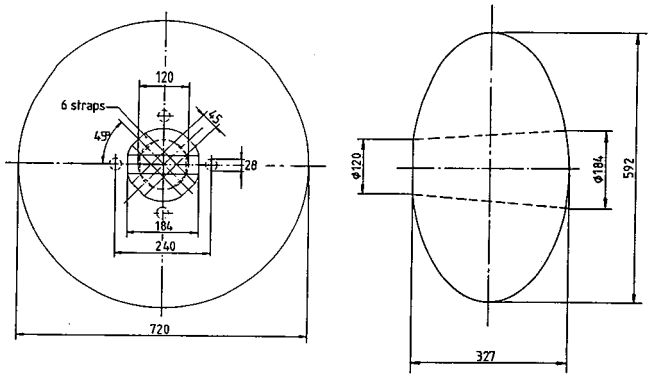

Front view (uninflated) Side view (inflated)

Figure 5. Diagram of the Driver Side Airbag: Front View, Uninflated (left) and Side View, Inflated (right)

a diameter of 82 mm. The total mass of the pendulum is 10.9 kg. The mass moment of inertia with respect to the centre of gravity of the pendulum, located 245 mm above the centreline of the impactor, is 2.07 kg.m^2. The reaction force on the wall was recorded using three identical load cells. The rotation angle of the pendulum was recorded using a potentiometer.

For the experiments with the 50th percentile Hybrid III dummy, the dummy was seated in a stationary upright position. A pelvis restraint was fixed to the dummy seat in order to prevent the dummy from sliding over the dummy seat. Next to the reaction force on the wall the acceleration of the head and chest of the dummy were also recorded using a triax of accelerometers.

The driver side airbag is modelled as two flat disks connected at the outer rim using 1024 three node triangular membrane elements. A linear elastic isotropic material behaviour is assumed.

The material properties used are:

Young's modulus: 60 N/mm^2
Density: 620 kg/m^3
Poisson ratio: 0.3
Thickness: 0.5 mm

The straps are modelled as massless springs. The strap material is assumed to be the same as the airbag skin material, resulting in a stiffness of 4500 N/m for each strap. The untensioned length of the strap is equal to 275 mm.

No outflow of gases through the coated fabric and seams is assumed, i.e. the porosity factor is zero for all elements used to represent the fabric skin. The total area of the exhaust holes is 2740 mm^2. Based on experience the discharge coefficient is assumed equal to 0.625.

The heat capacity coefficients and molecular weight of the gas mixture delivered by the inflator are used as input for the simulation. The constant pressure heat capacity is modelled as a linear function of the absolute temperature T according to:

$$C_p = 29.135 + 0.004825\ T$$

The molecular weight is 0.028014 kg/mol. The mass flow and the temperature of the gas mixture delivered by the inflator are modelled according to Figure 6. The inflator is activated at the start of the simulation.

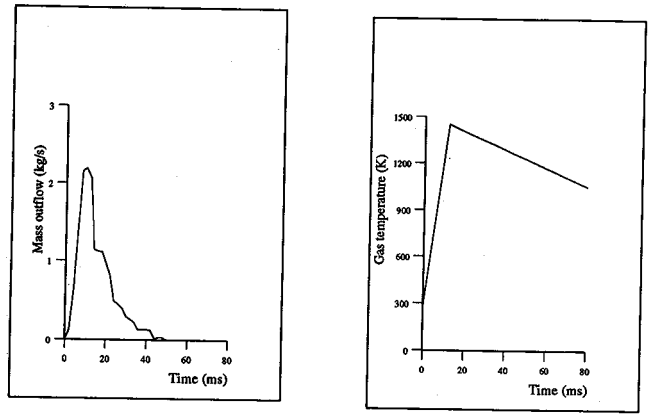

Mass outflow Gas temperature

Figure 6. Inflator Characteristics: Mass Outflow (left), Gas Temperature (right)

The pendulum is modelled by a single element multi-body system with three ellipsoids connected to it. The first ellipsoid is a sphere representing the impactor face that contacts the airbag. The two other ellipsoids are only added for visualisation. The connection of the pendulum with the surroundings has been modelled with a point-restraint with such high spring stiffnesses that the translational motions are negligible. The rotation angle of the impactor has been determined by integrating the calculated angular velocity. The reaction force of the support plate has been determined by summing the forces due to contacts and rigid connections. The dummy has been modelled using the 50th percentile Hybrid III dummy database as provided by MADYMO version 4.3.

The most important calculated time histories are presented together with the experimental results. The pendulum rotation angle and reaction force, perpendicular to the support plate, time histories are presented in Figures 7 and 8 respectively. The kinematics are presented in Figure 9. The resultant acceleration for the dummy chest and head, and the reaction force time histories are presented in Figures 10, 11 and 12 respectively. The kinematics are presented in Figure 13.

As can be seen in the figures there is a good agreement between the results for the calculations and experiments. Deviations in the contact force can be explained by the way in which the contact force is determined. The numerically determined reaction force is the force of the airbag on the support plate, while the measured reaction force is the force of the support plate on the wall.

The calculation CPU time for the simulation with the 50th percentile Hybrid III dummy database, using 1024 membrane elements for the airbag, is roughly one hour on a Silicon Graphics IRIS 4D/210S.

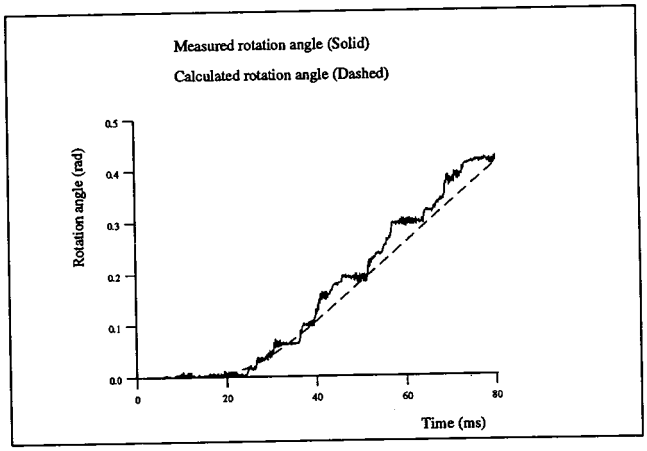

Figure 7. Pendulum Rotation Angle Time History

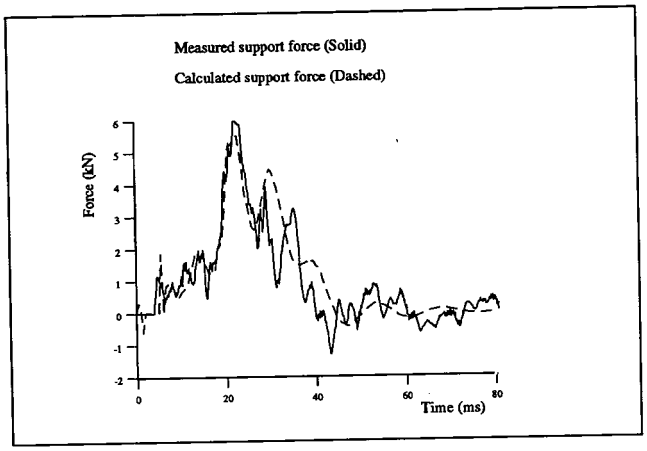

Figure 8. Reaction Force Time History for the Experiment with Pendulum

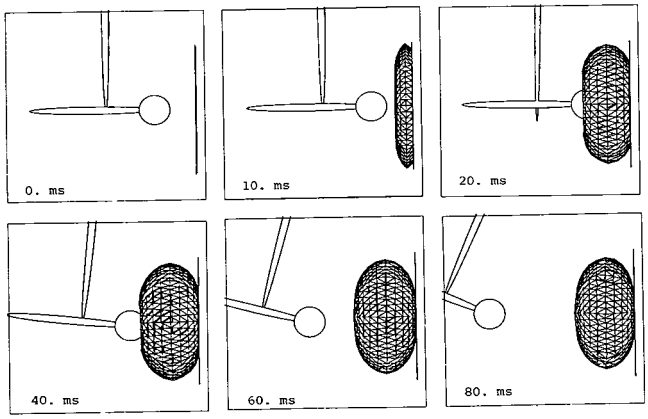

Figure 9. Pendulum and Airbag Motions

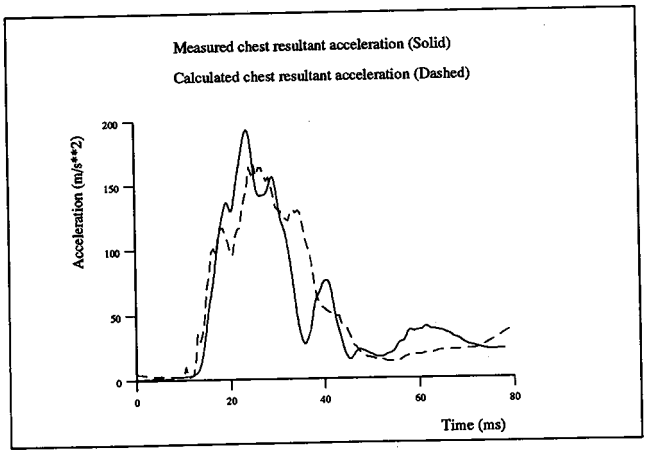

Figure 10. Chest Acceleration Time History

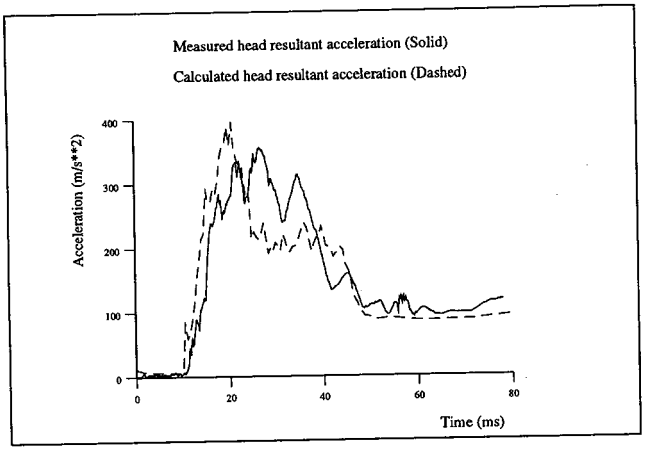

Figure 11. Head Acceleration Time History

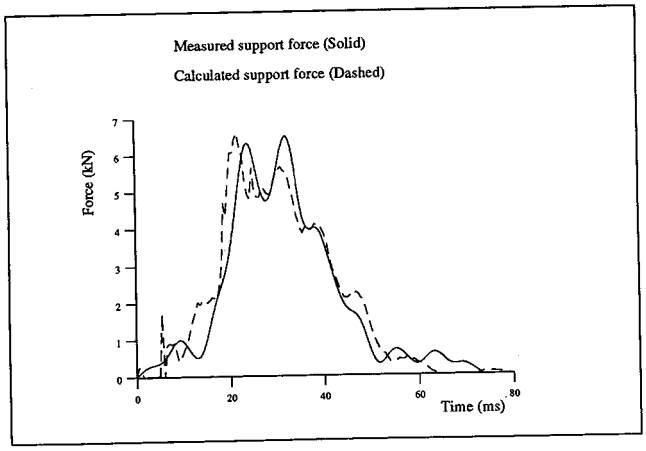

Figure 12. Reaction Force Time History for the Experiment with Dummy

Discussion and Conclusion

The developed finite element airbag model presented here is fully integrated in the MADYMO multibody program and optimized for airbag simulations in a crash victim simulation environment. The software implementation resulted in a flexible and user-friendly simulation tool which poses few limitations upon the user with respect to the geometrical complexity of the individual models. This is certainly true for the thermodynamics due to the predefined gases and the different models for gas outflow through venting holes and porous fabric. The agreement between the measured and calculated results for the presented out-of-position simulations is good while the computing times even for work stations are quite reasonable. Simulations for both driver, Figure 14, and passenger side airbag systems, Figure 15, in a car environment as well as for a motorcycle airbag system,

Figure 16, have been performed and compared with tests. The results obtained for the motorcycle airbag system will be published in the proceedings of this conference (20). A selection of the results for the airbags in a car environment is planned to be presented in a future publication (21).

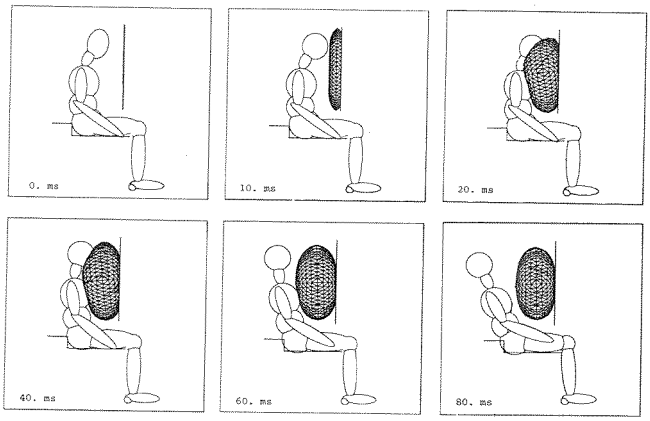

Figure 13. Dummy and Airbag Motions

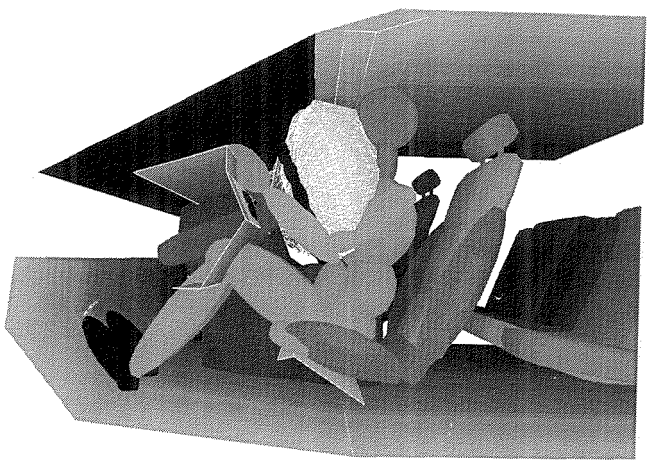

Figure 14. Finite Element Model of a Driver Side Airbag

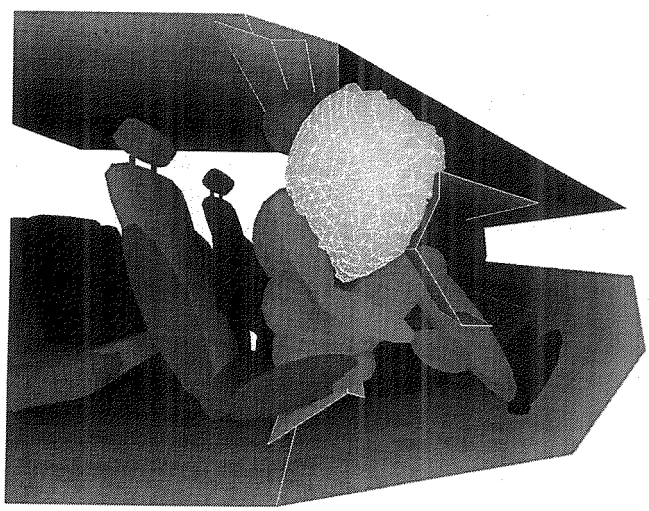

Figure 15. Finite Element Model of a Passenger Side Airbag

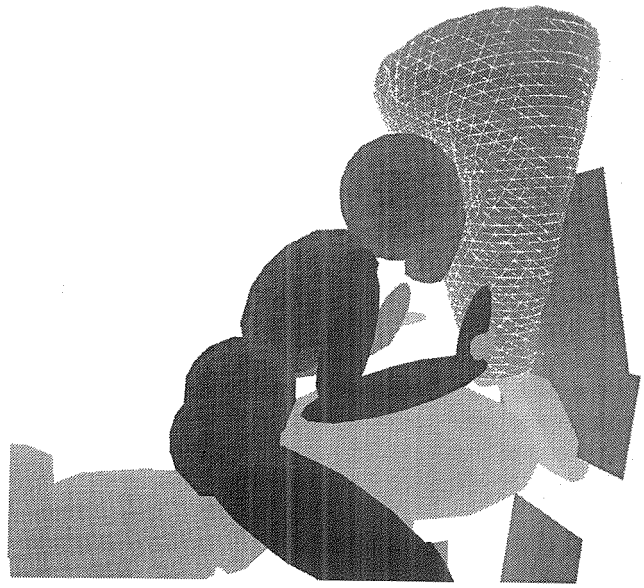

Figure 16. Finite Element Model of a Motorcycle Airbag

For certain situations like an out-of-position simulation with a passenger side airbag a complication can arise if the gas flow coming out of the inflator is directed towards the occupant. In such a case the inertia effects of the gas jet can have a significant influence on the occupant motion. This effect can be accounted for by using an Eulerian discretization for the gases inside the airbag instead of the lumped parameter approach. The MSC/DYTRAN code, a currently partly integrated version of PISCES and MSC/DYNA being developed towards a full integration of both, has the option of mixed analyses, using a Lagrangian discretization for the airbag fabric, an Eulerian discretization for the gases inside the airbag and a multibody occupant model using the coupling with MADYMO. An accurate description of the gas behaviour using a three dimensional Eulerian finite element mesh will however require very long computer run times. A relatively simple analytical model to account for the gas jet effects is anticipated for the next release of the MADYMO finite element airbag model. This model will hardly influence the computer run times required but will be based on some limiting assumptions, i.e. at the outlet the velocity of the outflowing gas is constant and has the same density as the gas in the airbag. The question of accuracy should however be considered in the knowledge that real airbags differ from each other due to manufacturing tolerances, through ageing and as the environmental temperature and pressure change.

As long as the occupant only interacts with the airbag after unfolding, the initial configuration of the airbag will have a limited influence on the occupant motion. However if there is contact before complete unfolding, significant contact forces could be generated during unfolding of which the magnitude largely depends on the airbag initial folding pattern and unfolding mechanism. By using tear seams and well designed folding patterns

the bag slap effects should be minimized to prevent injuries, especially to the passenger's face, as much as possible. The unfolding of the airbag itself depends mainly on the pressure build-up in the airbag folds, the interaction between these folds and contacts with car interior surfaces. Therefore besides making an initial folded mesh and applying a correct treatment of the contact between the folds, the gas flow through the folded airbag should also be modelled. This requires a very fine three dimensional Eulerian mesh resulting in numerical models requiring supercomputers.

Since its appearance on the market the MADYMO program has been continuously modified and improved (4). In its present form the program appears to be a very useful tool to users all over the world for crash victim simulations. Due to the recently released finite element module and the more advanced multibody module in the next release of MADYMO, even more simulation possibilities arise. The multibody module is most suitable for the modelling of the crash dummy or human body behaviour during a crash or impact. Those parts that undergo large deformations, e.g. the ribcage and the neck, can be replaced by finite element models allowing a more detailed analysis of those parts. Using finite elements for car interior parts or restraint systems allows a more detailed description of the contact interactions. Shell and volume elements in addition to the membrane elements are planned to be included in the MADYMO finite element module in order to be able to model critical dummy parts with finite elements in some future dummy databases.

References

1. R.R. McHenry, Analysis of the dynamics of automobile passenger-restraint systems, 7th Stapp Car Crash Conference, 1963.
2. D.H. Robbins, Three-dimensional simulation of advanced automotive restraint systems, International Automotive Safety Conference Compendium, paper no. 700421, 1970.
3. P. Prasad and C.C. Chou, A Review of Mathematical Occupant Simulation Models, pp 95-112, Crashworthiness and Occupant Protection in Transportation Systems AMD-Vol. 106, The winter annual meeting of the American society of mechanical engineers, San Francisco, December 1989.
4. H.A. Lupker et al., Advances in MADYMO Crash Simulations; SAE 910879, International Congress and Exposition, Detroit, February 1991.
5. A.C. Bosio and H.A. Lupker, Design of Experiments in Occupant Simulation, SAE 910891, International Congress and Exposition, Detroit, February 1991.
6. J.J. Nieboer et al., Status of the MADYMO 2D Airbag Model; SAE 881729, 32nd Stapp Car Crash Conference, Atlanta, October 1988.
7. P.J.A. De Coo et al., Integrierte Kollisionssimulation mit FE- und Insassenmodellen, VDI Congress Berechnung im Automobielbau, Würzburg 1988.
8. A.M.A. van der Heijden et al., Numerical Simulation of Airbag Behaviour; Proceedings Susi Conference, Cambridge, July 1989.
9. W.E.M. Bruijs, Subcycling in Transient Finite Element Analysis; PhD Thesis Eindhoven University of Technology, ISBN 90-9003684-9.
10. R. Hoffman et al., A Finite Element Approach to Occupant Simulation: The PAM-CRASH Airbag model; SAE 890754, International Congress and Exposition, Detroit, February 1989.
11. R. Hoffmann et al., Finite Element Analysis of Occupant Restraint System Interaction with PAM-CRASH, SAE 902325, 34th Stapp Car Crash Conference, Orlando, November 1990.
12. D. Lasry, R. Hoffmann and J.B. Protard, Numerical Simulation of fully Folded Airbags and their Interaction with Occupants with Pam-Safe, SAE 910150, International Congress and Exposition, Detroit, February 1991.
13. J.O. Hallquist et al., Modelling of Airbags using MVMA/DYNA3D, Internal Report to MVMA, Livermore Software Technology Corp., Livermore (1990).
14. D.W. Stillman and J.O. Hallquist, Interfacing LS-DYNA3D with MADYMO3D for coupled simulations, Livermore Software Technology Corp., Livermore (1990).
15. J.J. Nieboer, J.Wismans and P.J.A. de Coo, Airbag modelling Techniques, SAE 902322, 34th Stapp Car Crash Conference, Orlando, November 1990.
16. J.T. Wang and D.J. Nefske, A New CAL3D Airbag Inflation Model; SAE 880654, International Congress and Exposition, Detroit, February 1988.
17. I.E. Idelchic, Handbook of Hydraulic Resistance. Heidelberg etc. Springer Verlag. ISBN 3-540-15462-2, Berlin, 1986.
18. F.F. Huang, Engineering Thermodynamics, Collier Macmillan Publishers, London, 1976.
19. M.M. Abbot and H.C. van Ness, Thermodynamics, Schaum's Outline Series, McGraw-Hill Book Company, New York, 1976.
20. J.J. Nieboer et al., Computer Simulation of Motorcycle Airbag Systems, 13th International Technical Conference on Experimental Safety Vehicles, Paris, November 1991.
21. W.E.M. Bruijs et al., Simulations with the MADYMO FEM airbag model, To be published at the International Congress and Exposition, Detroit, February 1992.

S9-O-25

The Development of a Computer Program to Enhance the Fit of Seat Belts —

Doug Kendall
Crash Protection Centre
Motor Industry Research Association

Abstract

To the vehicle occupant a correctly fitting seat belt system is important in maximising both the comfort and convenience in normal use, and the dynamic performance in the event of an accident. A series of research projects has been carried out at MIRA to develop a mathematical model to aid vehicle designers in the configuration of seat belts with the aim of ensuring comfort and convenience to as great a percentage of the population as possible. This model is incorporated into a computer program called BELTFIT. The analysis technique takes into account any combination of anchorage locations, stalk characteristics, seat position and seat angles. The program predicts the belt paths on a wide range of occupant sizes and carries out a series of checks against comfort and safety criteria. Using dynamic programming techniques the path of the belt across the occupant is predicted by calculating the shortest route over the body surface. Rapid assessment of seat belt installations is possible without the need for lengthy subjective wearer trials. In addition to checks of fit on human wearers, the program can also be used to predict the fit on anthropomorphic test devices prior to impact test evaluations. This paper illustrates the development of the program and also describes the latest enhancements including restraint system design for rear seat occupants, which have been introduced with the aim of widening the application of the program.

Introduction

The international trend towards the introduction of safer vehicles has led vehicle manufacturers to put increasing emphasis on the safety, comfort and convenience of seat belts. Legislation in virtually all markets ensures that the use of seat belts greatly increases the safety of most wearers in the event of an impact.

In the past manufacturers have designed seat belt installations first and foremost to conform with legislation, making adjustments on an empirical basis using prototype seating bucks to accommodate a selection of wearers chosen in-house. This has always been a lengthy and variable process since it is difficult to explore the full range of dimensional possibilities offered by even the most basic seat belt installation.

In order to provide a more analytical solution to this problem MIRA has developed BELTFIT, a predictive computer program for testing and improving seat belt layouts at the drawing board stage.

This paper aims to illustrate some of the background to the development of the software and to give practical examples of the use of the program.

Background

The original method for predicting the path a seat belt follows across the wearer was developed several years ago by MIRA (1) using the theory of developable surfaces. This theory was applied to highly simplified human shapes assembled from cylindrical and conical surfaces.

Experience of this first technique soon showed that the limitation to simple geometric shapes did not produce sufficient accuracy when compared to human forms because belt lie is altered quite significantly by anatomical detail.

The first version of BELTFIT was based on the "Golden Shell" anthropomorphic dummies, adapted using information provided by NHTSA. Three body shapes were chosen, representing the extremes and the midpoint of the range of adult occupants, namely the 5th percentile female, the 95th percentile male and the 50th percentile male. Few people actually conform to the dummy dimensions in all respects, the limitless variability of human shapes presenting difficulties in checking against all wearers.

The original data, used for Versions 1 to 3 of the program, was not felt to give a true representation of the real slumped torso shape of the human in a typical car seat. In particular the data gave a dummy with a very straight back, which rotated simply about the hip. For this reason MIRA carried out a programme of research to identify the true slumped shape of a range of car occupants.

This study involved detailed measurement of the surface contours of a range of individuals representing the target profiles identified above plus other selected groups of wearers who were thought to have particular problems with seat belt fitting. In addition to the measurement of surface contours the study also examined the variation in contours as a function of seating angles in order to develop an algorithm for defining the slump characteristics. These, more realistic, body shapes were incorporated into Version 4 of the program.

Since early development days up until 1990 the BELTFIT program was run only on main frame computers. However, with the increasing power and widespread availability of the desk top PC it was decided to re-write the coding and re-structure the operating environment to provide a more user friendly graphical user interface available on a wide platform of machines. These enhancements were incorporated into Version 5 of the program.

Principle of Operation

BELTFIT functions by calculating the minimum path of the belt across the body surface, based on the observation that a belt wearer manually shortens the belt webbing on a static system in the same way as the automatic tightening and hence shortening effect of an inertia reel or automatic system (2). The body models within the program comprise a number of contour lines representing a three dimensional map of the body surface. An optimisation technique, known as dynamic programming, is used to calculate the shortest route across the body surface given the start and finish points of the belt hardware.

Having calculated the lie of the belt across the occupant the program then performs a series of checks of the belt lie against a set of pre-determined comfort criteria. These criteria will be discussed later.

Accuracy of Calculation Process

In order to carry out an analytical check of the accuracy of the belt plotting routines a comparison was made of the BELTFIT calculated belt lengths and belt contact points with a number of three dimensional surfaces for which analytical solutions could by found.

These models were as follows:

- Model 1 was a simple rectangular box with dimensions similar to a human subject.
- Model 2 was a L-shaped box, used to test the accuracy of the curve fitting procedures by forcing the torso and lap belts to pass through the region where the surface of the body changes from vertical to horizontal.
- Model 3 was a semi-cylinder, used to test the ability of BELTFIT to approximate a continuous curved surface by a model with a number of flat surfaces.
- Model 4 was as for Model 3 but with a seat belt stalk, used to test the accuracy of predicting the position of a rigid stalk on a curved surface modelled by flat facets.

For each analysis a set of anchorage locations was chosen which would cause unsuitable tangent lines to the body, i.e., worst case. The following was found:

Table 1. Calculation Accuracy, Errors (mm)

Model	Torso Belt Length		Lap Belt Length	
1	0.0278	(0.0018%)	0.0311	(0.0023%)
2	0.3900	(0.0275%)	0.0000	(0.0000%)
3	0.9250	(0.1530%)	0.9250	(0.1530%)
4	1.2500	(0.2710%)	1.2500	(0.2710%)

The above table demonstrates that the shortest path across a variety of shapes can be calculated with sufficient accuracy by the software.

Body Shapes

In addition to the 3 basic body shapes discussed earlier, a further 3 models have been incorporated, chosen to represent groups of wearers thought to have difficulty with seat belt comfort. The full list of body models is described below, with corresponding stature and weight data.

Table 2. List of Body Models

Model	Stature, mm	Weight, kg
1. 50th percentile male	1740	72.6
2. 95th percentile male	1848	97.0
3. 5th percentile female	1533	49.8
4. Short heavy female	1540	64.7
5. Tall light female	1736	58.5
6. Tall heavy female	1719	71.5

Notes

Model 1 is 50th percentile for both stature and weight
Model 2 is 95th percentile for both stature and weight
Model 3 is 5th percentile for both stature and weight
Model 4 is 5th percentile for stature and 75th percentile weight for that stature group
Model 5 is 95th percentile for stature and 25th percentile weight for that stature group
Model 6 is 95th percentile for stature and 75th percentile weight for that stature group

All percentiles based on the MIRA survey of UK car drivers (3). Each body model has two options: driver and passenger. The earlier study on body posture had shown that the shoulder profile of the passenger differed from that of the driver and hence this is reflected in the body models.

In addition to these models the program also incorporates child models, representing 3 year old and 6 year old children. Due to a shortage of data on these body sizes these models are actually scaled down versions of the adult models, a pro-rata scaling process being undertaken to reduce the relevant limbs and torso dimensions compared with the adult. Whilst accepting this to be not a truly valid method of representing child occupants, due to a shortage of applicable data it is the best currently achievable.

Comfort/Fit Criteria

The principle aim of BELTFIT has always been to aid the designer in the production of well-fitting, comfortable seat belts, therefore it has been necessary to have an exact definition of what is and what is not comfortable.

The criteria of acceptability for seat belt fit were established round common-sense rules based on the three areas of belt contact on the body, namely the shoulder, chest and pelvis. These rules are as follows:

- *Fit on shoulder.* The edge of the belt should not touch the neck. The centreline of the belt should be in-board of the acromion process. The belt should not press on the top of the shoulder. This should be a stable solution with no alternative fit off the shoulder.
- *Fit on chest.* This check is only applied to the female models. Since many women find the belt uncomfortable if it presses on the breast, the program checks whether the belt contacts the underside of the inner breast.
- *Fit on pelvis.* The program checks whether the stalk/buckle lies in front of a pelvic reference point. The belt must lie with the centreline below the ASIS

points on the pelvis. (ASIS—Anterior Superior Iliac Spines, the bony protuberances on the upper point of the pelvis).

In addition to the checks on occupant comfort the program also provides information on belt lie, such as whether the belt touches the clavicle or is deflected by the seat.

Finally the program gives the user a listing of belt lengths, in total and on the body, lap belt angles and torso contact relative to the mid-sternum or to the torso centre of gravity.

All these features have been introduced over the development period through input and requests from program users, with the aim of making the program as relevant and useful as possible.

Legislation Checks

In addition to the analysis of belt comfort the program can also perform a check of the acceptability of installations with respect to international legislation. The zonal acceptance limits are overlaid onto the output and errors messages are displayed if appropriate, thus enabling the user to see easily where the fault lies.

Since there are several regulations governing anchorage position, for example FMVSS 210 and EEC 82/318, each can be analysed separately. Care has been taken to ensure that the analysis of regulations is comprehensive, for example the design seat back angle may be different from the seat back angle under investigation for comfort analysis, or the user may wish to use the EEC alternative for upper anchorage location.

The development of user options such as these benefitted greatly from input by experienced users resulting in a program which permits full flexibility.

Vehicle Hardware Features

As discussed earlier the program in its Version 1 phase was simply a routine for plotting belt route across the body. Through development into the current Version 5, the program has added a great many features which allow the engineer to more accurately model the true vehicle characteristics.

The first feature to be added was the representation of stalk bending. Version 1 of the program only allowed the stalk to be modelled as a fixed link. This was enhanced firstly to allow the stalk to be modelled as a completely flexible component, representing the webbing typically used in rear seats. The second enhancement was to allow the modelling of a semi-rigid stalk, typically the steel braided cable used in the front seats. A later refinement has allowed the stalk to be modelled as a link which is laterally stiff but free to rotate, within user-defined limits, in a longitudinal plane.

Given that it is possible to model stalk bending it then also became necessary to represent the seat outline, since the lie of the belt on the wearer can be significantly affected by deflection of belt and stalk due to contact with the seat. From study it was concluded that a simple representation of the seat outline in those areas where belt or stalk contact might occur would be sufficient. Therefore a basic outline comprising data defining the top corners, the base/back intersection and the seat angles in these areas was employed. By limiting the data to this simple format it was felt that data entry could be kept straightforward without compromising accuracy.

A further enhancement has been to allow front and rear seats to be modelled differently. On the front seat, the belt is basically routed round the seat outline whereas on the rear seat the designer can additionally allow the belt to route through the base or the back if required.

Since many seats now have one or more anchorages attached to the frame the program was modified to allow any or all of them to move with the seat when the seat was moved forwards and upwards.

The program was further enhanced to allow input of an upper anchorage strap guide since many manufacturers are now using this technique. This guide is simply defined by the x y z co-ordinates of the end points and the belt is diverted appropriately by the program.

It is believed that at the moment all current seat belt installations can be modelled accurately, however undoubtedly designers will come up with further variations on the theme of three point belt plus stalk. Recent additions to the program have dealt with the latest vehicle developments. It is expected that the program is robust enough to manage future vehicle developments.

Method of Operation

The program in its latest form has been designed to allow for easy use by the inexperienced user without compromising speed for the more practised operator. The program follows the current trend of menu-driven data entry, with defaults at every stage to allow the inexperienced user to progress. The more practised user still has the option of modifying all the variables to suit his own requirements.

For a very basic, initial assessment the user only requires the three dimensional coordinates of each anchorage, relative to the Seating Reference Point (SRP) or to a vehicle co-ordinate system, plus the length of the stalk if any. These co-ordinates are all input in an intuitive manner in response to program prompts. For example, the program requests "Upper Anchorage *above* SRP?" and "Lower Inner Anchorage *below* SRP" rather than just asking for the z co-ordinate and forcing the user to remember the + and - signs.

Having input the basic data the program prompts the user to select a body model from the range of menu options, giving default hip offsets for each body, which the user could change if required.

The program then prompts the user to check the installation against international regulations, if required.

Finally the program calculates the fit of the belt across the body. At the end of the calculation the installation is presented in the form of front and side views with the

calculated belt lengths and angles plus the error messages, if any, relating to comfort and legislation.

At this stage the user can either plot the results, modify the anchorage positions or add further data, such as a seat outline, a different stalk, a strap guide or a change in seat travel.

This method of operation has been developed through the use of trials on both experienced and inexperienced users. Through this technique a number of traps have been built into the software to prevent program problems through the inexperienced user entering obviously erroneous data, for example a seat angle of 250° instead of 25°, or an anchorage 5011mm from the SRP instead of 501.1mm.

The mode of use has been adopted to follow an intuitive path without imposing an over elaborate logic route onto those users who do not require full guidance.

Examples

The following illustrations show an example of the use of the program to solve one particular problem for one wearer in one seating position. Of necessity the full implications of the solution of one problem for one wearer on the fit of the belt on other wearers are not explored here. However, the solution of this simple problem does illustrate the potential for use of the software in the exploration and solution of complete vehicle installations for a range of wearers. In the following example the basic data for run 1 is as follows:

Table 3. Run 1 Data, Anchorage Locations Relative to SRP

Anchorage	Behind, mm	Left, mm	Above, mm
Upper	380	250	620
Lower Outer	90	270	-210
Lower Inner	130	-220	-232

Stalk length: 150mm, semi-flexible
Seat travel: 50mm
Track angle: 7°
Occupant: 50th percentile male

Figure 1 shows the results of the BELTFIT calculation.

It can be seen from the scowl on the wearers face and the error message on the output that there is a comfort failure here. The solution to this problem would appear to be to move the belt lie lower down the torso. Hence by moving the upper anchorage down 50mm and outboard 30mm to follow the B pillar curvature and the lower inner anchorage forward by 40mm, the new input data for these anchorages is as follows:

Table 4. Run 2 Revised Anchorage Locations, Relative to SRP

Anchorage	Behind, mm	Left, mm	Above, mm
Upper	380	280	570
Lower Inner	90	-220	-232

All other input data remains as for Run 1.

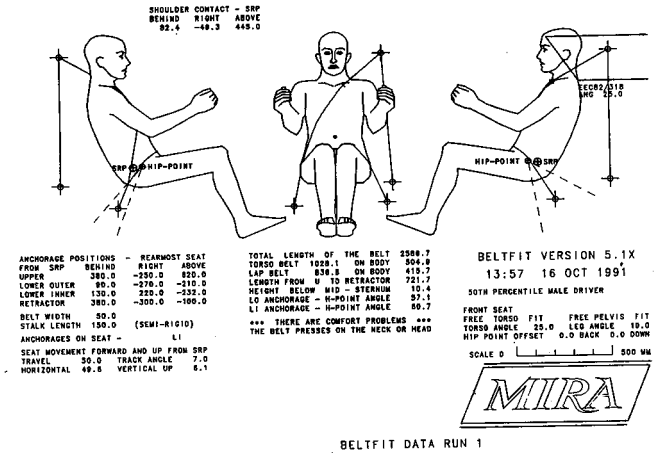

BELTFIT DATA RUN 1

Figure 1. BELTFIT Data Run 1

The resulting calculated fit for the revised data is shown in Figure 2.

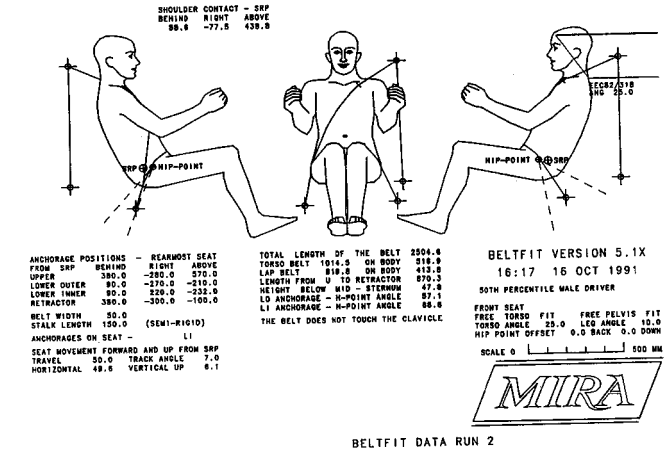

BELTFIT DATA RUN 2

Figure 2. BELTFIT Data Run 2

It can be seen that the wearer is now smiling and that there are no longer any comfort failure messages.

As discussed earlier this example has demonstrated a solution for one wearer only. The user would now evaluate solutions for other wearers in other seating positions in order to develop a range of anchorages which are suitable, or indeed a range of adjustment which must be made available in order that all wearers could be made comfortable.

Future Developments

User Options

As discussed earlier the child models represented in BELTFIT do not correspond fully to any true anthropometric profile; therefore it is anticipated that further development of these models will be taking place. These models will also interact with a child restraint system.

In addition to the child models the program will be further enhanced by the addition of data defining anthropomorphic test devices, for example Hybrid II, Hybrid III and 95th percentile Hybrid III. This will allow the crash test engineer to accurately set up belt lie prior to impact testing.

To take into account the changing stature of the population as a whole it is anticipated that the basic models in the program will be modified to simulate the expected target percentile groups for the year 2000. This will require data defining exactly the morphology of the expected groups for this year. However, once this is derived the input of new body models will be achievable.

A further development is expected to be the incorporation of an Optimisation feature, whereby the program will choose the optimum position, for example for an upper anchorage, given a range of positions defined by start and end points, plus a radius of curvature. Early development on this work has suggested that an algorithm will need to be developed which defines the weighting to be applied to the belt lies at various body contact points.

An ongoing development is the introduction of versions for non-English language users. A German version is to be introduced in the third quarter of 1991, followed by a French version in early 1992.

Hardware Features

The current version is configured to run on a PC operating DOS 3.0 or higher; this allows easy portability between computers. A requirement exists however to develop the program into the UNIX operating system, perhaps under XWindows. This will allow linking to other workstation software plus on-site networking.

Conclusions

The BELTFIT program has been developed by MIRA to allow easy and reliable design of seat belt installations in terms of occupant comfort. The program has been developed in conjunction with end-users and adapted to their own requirements.

Modification to the graphical user interface, subsequent to user trials, has led to a program which allows the inexperienced user to progress without recourse to a user manual. However, the needs of the experienced user have also been considered so that full functionality is maintained.

The program has been extensively developed following the latest modifications in seat belt hardware and is in the process of on-going evolution to allow accurate and reliable modelling of any future developments.

References

1. Searle, J A, "The Geometrical Basis of Seat Belt Fit," Ergonomics, Vol 171974.
2. Sheppard, D J, "The BELTFIT Program for Making Seat Belts Safer and More Comfortable," Passenger Car Meeting, Troy, Michigan, 1982. SAE 820795.
3. Haslegrave, C M, "An Anthropometric Survey of British Drivers," Ergonomics, Vol 22, 1979.

S9-W-17

Validation and Description of "PASSIM-PLUS" Passenger Airbag Model

Michael U. Fitzpatrick, Kelly E. Thompson
Fitzpatrick Engineering

Abstract

A description and most recent validation of PASSIM-PLUS, a multi-element passenger side airbag model for analyzing airbags of complex shape, is discussed. This model has the capability of simulating passenger interaction with a three dimensional airbag of completely arbitrary, user defined shape. Further, this model actually simulates the instantaneous shape of the airbag as determined by the various contact surfaces encountered by the airbag. Therefore, the shape of the contact surface presented to the passenger is not constant and can accommodate large deflection penetrations by the passenger. Because of the multi-element airbag approach, the effect of instantaneous vent blockages on porous airbag materials may be evaluated. Up to 3000 airbag elements can be used to configure the desired airbag geometry. Airbag mass and its effect on airbag deployment rate and the subsequent bagslap forces are computed. Because of this, the model is capable of simulating forward positioned children as well as normally seated adults. The model is fully supported by various menu driven pre- and post-processors for creating the input files as well as evaluating the output. A special, menu driven, interactive pre-processor structured to receive User input in a format compatible with conventional airbag drawing coordinates and dimensions facilitates rapid creation of the 3-D airbag "mesh." Because of this, the multi-element mesh, for even the most complex airbag shapes, may be quickly obtained. Another pre-processor computes the inflator mass flow and gas temperatures from tank test data. All FMVSS-208 injury measures are computed and summarized. Post-processors provide full graphic output in curve overlay (for comparing test vs. simulation or simulation vs another simulation) and kinematic format. The most recent validation of the model is discussed. This validation situation involves a normally seated, adult passenger. The results show that the model is not only easy to use but also very accurate in its predictive ability.

Introduction

The goal of a simulation program should be to provide its user with a means of obtaining accurate information both quickly and easily. This paper will look closely at the latest version of the new simulation computer model, PASSIM-PLUS and its most recent validation. Following

this validation the following topics will be covered: General Model Description, Feature Highlights, Key Features in Detail, and MFP- PLUS: Airbag Creation.

Validation

PASSIM-PLUS has been validated in a previous publication (1), however improvements and enhancements have been made since that time. The most recent validation is included here.

This validation was conducted under contract to the U.S. Department of Transportation with NHTSA sponsorship (2). We wish to especially thank Mr. Jerry Kossar of NHTSA for his valuable assistance in obtaining the necessary input data for this validation. Due to manufacturer request, the actual type of car, vehicle manufacturer and suppliers will remain anonymous. The purpose of this validation was to study the correlation of the actual crash results with the results of a corresponding PASSIM-PLUS simulation.

The dummy used in this crash was a Hybrid 11. The airbag utilized in this validation is depicted in Figure 1. The airbag was constructed of a porous nylon weave of 7.4 cubic feet in volume. The effective vent area for the porous material was 16.3 square inches. After setting up the input file for this validation, the configuration generated by PASSIM-PLUS is shown in Figure 2. Figure 2 also shows dummy placement and the fully inflated, unobstructed shape of the airbag.

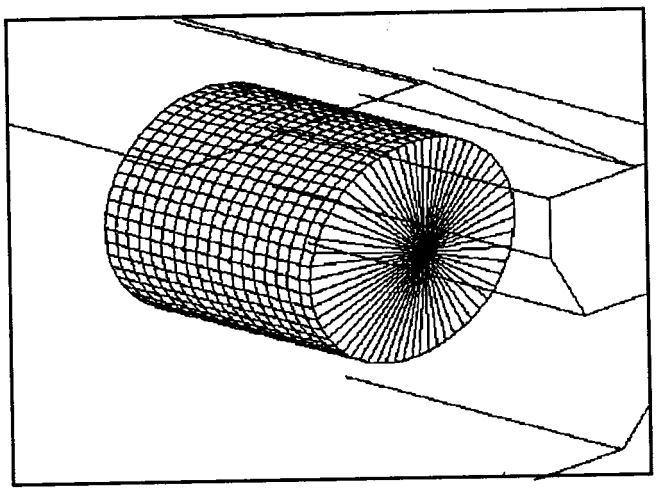

Figure 1. Airbag Used in Validation

The program "GENFLOW" was used to get the input values for the inflator primary gas flow and the gas flow and gas stagnation temperatures. After GENFLOW was run, the computed results were compared to actual flow measurements as shown in Figure 3. As can be seen, the correlation was excellent.

The validation is described follows:

Crash: 29.5 m/hr Frontal
Dummy: 50th Percentile Hybrid II
Car Size: Full Size
Simulation Date: July 8, 1991

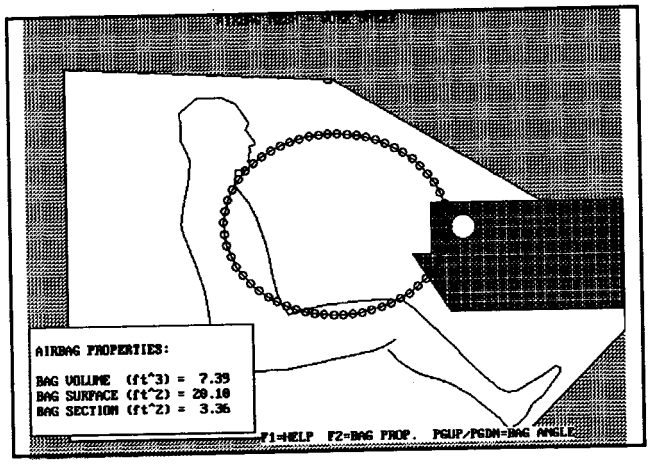

Figure 2. Compartment Graphics Showing Dummy Placement

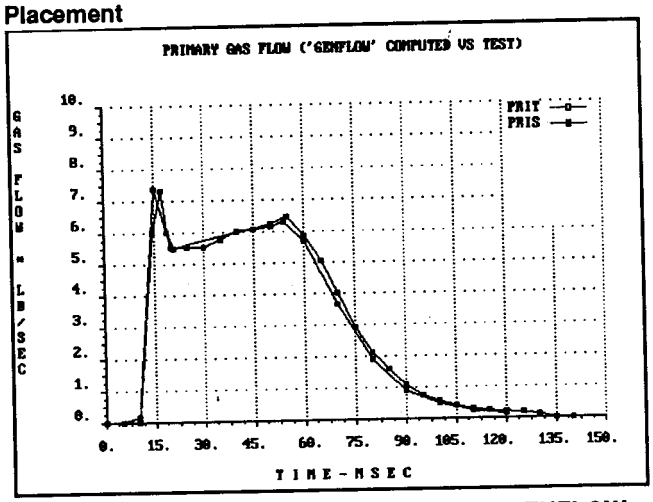

Figure 3. Primary Gas Flow Measurements, GENFLOW vs TEST

Curve plot overlays of the resultant Head G's, Chest G's and Femur Loads of simulation vs. test are shown in Figures 4, 5 and 6, respectively. This type of comparison yields the most information since both phasing and magnitude may be readily compared. The correlation between predicted and computed injury measures was very good.

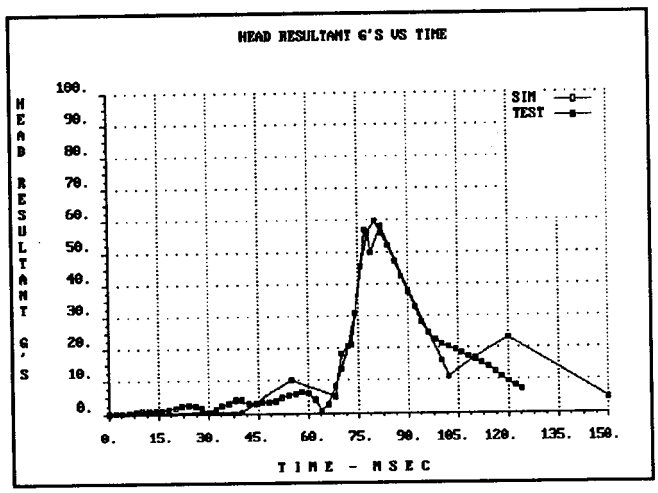

Figure 4. Validation: Resultant Head G's vs. Time

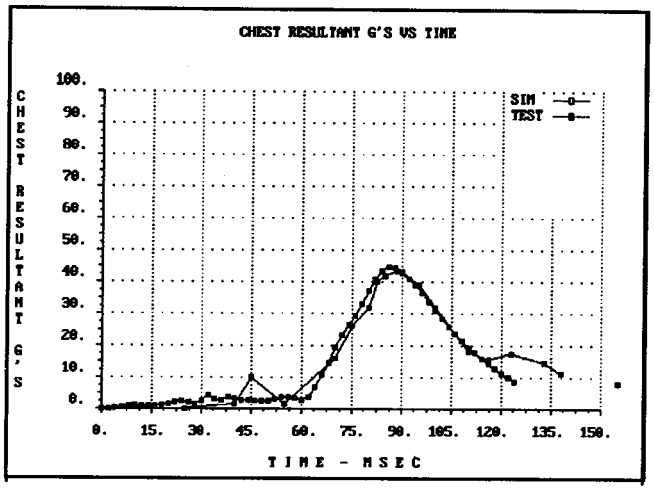

Figure 5. Validation: Resultant Chest G's vs. Time

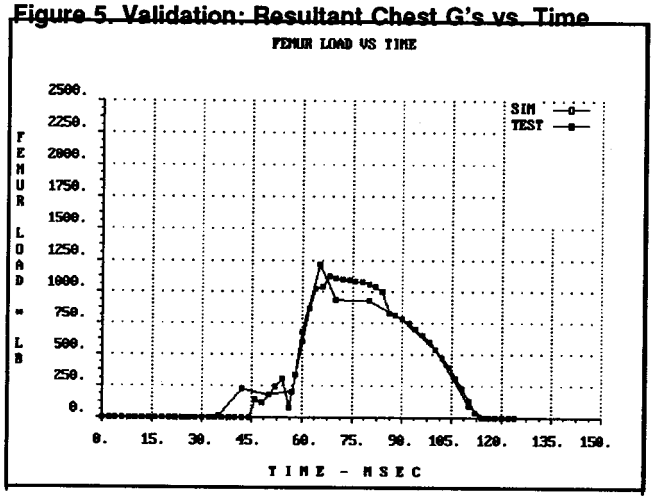

Figure 6. Validation: Femur Load vs. Time

Figures 7 and 8 are kinematic graphics of the validation.

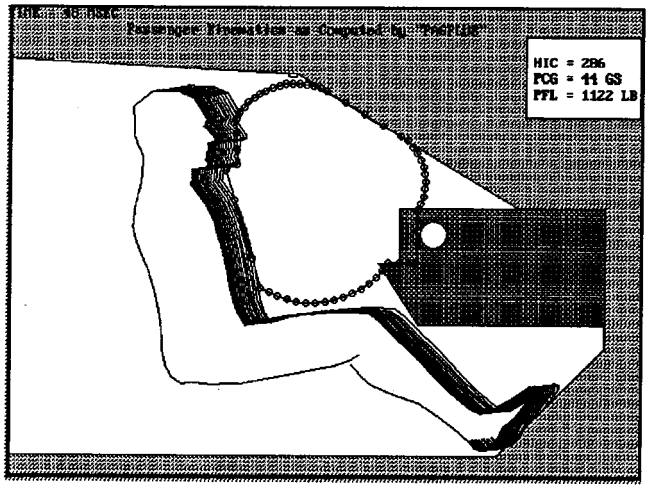

Figure 7. Validation Kinematics at 48 msec

Now, the PASSIM-PLUS model will be discussed.

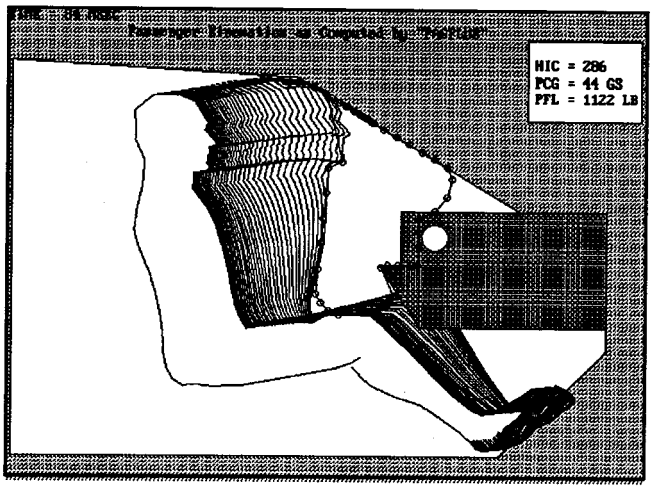

Figure 8. Validation Kinematics at 84 msec

General Model Description

The original Passenger Simulation Program first written and marketed by Fitzpatrick Engineering was PASSIM. "PASSIM" is an acronym for "Passenger Simulator." This earlier model is limited to airbags of right cylindrical shape with ellipsoidal cross-section. PASSIM remains an efficient and reasonably accurate model for uncomplicated airbag shapes in crash situations which involve normally seated passengers.

PASSIM-PLUS is a new simulation program which was built on the framework of the PASSIM model. PASSIM-PLUS has been extensively modified to include many more capabilities which provide even greater accuracy in situation involving more complicated airbag shapes, or the out of position child, for example. PASSIM-PLUS is a two dimensional, lumped mass computer model of a vehicle passenger interacting with a deploying and then fully deployed three dimensional airbag and/or belt restraint system. This passenger model includes five masses.

The masses which describe the passenger are the head mass, the main torso mass, the sternal mass (useful for those cases where "bagslap" is of interest), the lower body mass (pelvis and upper legs), and the lower leg mass. In addition, the airbag masses are composed of the mass which impacts the passenger and is restrained in its deployment by interference with the chest, and the mass that surrounds the passenger that is relatively unrestrained as it deploys.

The passenger airbag is simulated by a user-selected airbag shape into which programmed amount of gas flows. By adjusting the airbag vent size, the airbag shape, and the flow profile of the gas entering the airbag, one may design the airbag restraint system to achieve lowest injury measures in a given crash environment.

In a similar fashion, a two or three point belt system may be optimized by selecting belt elongation and anchor point locations such that injury is minimized. This may be done for a belt system acting as the primary restraint or in combination with the airbag.

Highlighted Capabilities

This program is designed to describe the interaction between the passenger of the vehicle and his airbag and/or belt restraint system in a crash situation. In the past, other programs have been written to describe such an interaction, but to date, none incorporates the combination of useful features which PASSIM-PLUS has.

The following are brief descriptions of some of the capabilities of PASSIM-PLUS. Those capabilities which primarily enhance accuracy are listed first, and those whose primary benefit is in the area of user convenience follow.

Accuracy

- PASSIM-PLUS simulates the entire deployment sequence of the rapidly expanding airbag from its initial stowed configuration through full deployment.
- Because of (1), the program can compute the detailed interaction of the unfolding airbag with the passenger chest. This is especially useful in computing the injury associated with a forward positioned passenger, such as the out-of-position child, being impacted by the deploying airbag.
- If windshield impact with the head occurs, the appropriate injury measures are computed.
- Airbag stretch is taken into account by the user specifying the bag stretch coefficient. The amount of stretch is a function of the instantaneous airbag pressure.
- Chest deflection due to combined action of airbag and belts is computed (including "bagslap" effects).
- PASSIM-PLUS computes all of the common injury measures such as:
  - Head Injury Criterion (HIC)
  - Chest Acceleration vs time
  - Head Acceleration vs time
  - Femur loads vs time
  - Peak Chest Acceleration with "3 msec clip"
  - Sternal and chest deflection, velocity and acceleration
  - Chest Viscous Criterion.
- PASSIM-PLUS is versatile enough that the user may:
  - specify the deployment angle the bag is to take upon inflation,
  - specify the airbag fabric weight,
  - specify the up-down, fore-aft location of the gas generator relative to the seated passenger,
  - specify the gas flow properties for the particular gas generator being simulated,
  - specify the belt elongation and anchor point locations,
  - specify the pelvic girdle, and torso, compliance properties for belt interaction and sternal and chest compliance properties for airbag interaction,
  - specify either two or more "driver type" gas generators staged in their firing by a user specified amount of time or, specify a conventional cylindrical gas generator,
  - specify the position of the passenger relative to the position of bag stowage so that the detailed interaction and degree of injury to the passenger sternum, chest and head due to impact with the deploying airbag may be determined,
  - specify the force-deflection properties of the knee bolster, and the frictional properties of the seat bottom,
  - model an aspirated inflator.

User Convenience

- Both Metric and English versions are now built into all Fitzpatrick Engineering's (FE) programs.
- More than one type of restraint system may be simulated with a single input file. With this capability, the user has a choice of simulating:
  - passenger airbag only,
  - 3-point continuous loop belt system only,
  - 3-point continuous loop belt system in combination with passenger airbag,
  - 3-point separate belts (not continuous loop) in combination with passenger airbag,
  - 2-point belt systems or lap belt only systems in combination with the airbag. These can be simulated by using option "d" with the force characteristics of the appropriate belt set to zero.
- A second gas generator staged in its firing sequence by a user specified amount can be simulated.
- Knee Restraint strain rate effects can be included. The user specifies the knee restraint strain rate factor in the input file.
- Belt pretensioning may be simulated. At the sensing time selected, the belts are tightened a user specified amount. Any combination of lap, torso, or lap and torso belts may be pretensioned.
- The program is able to compute the energy loss from any airbag due to heat transfer from the bag to the surroundings.
- The user may select from two possible bag folding methods ("accordion" or "rolled under").
- As with FE's previous programs, PAS-SIM-PLUS is able to be comfortably run on microcomputers.
- As a user convenience, several input files may be linked to run in "batch mode" without user intervention. This mode will automatically save the appropriate information for the later (or simultaneous) printing and plotting of run output.
- Output may be obtained in the form of tables, curves, run summaries and kinematical representations.

While developing PASSIM-PLUS, FE has worked hard to maintain the balance between User Convenience and Accuracy. PASSIM- PLUS is designed to be simple to use while still having the capability to be an accurate aid in either designing and optimizing a restraint system

or predicting the design performance of a given restraint system.

As a design tool, the program is oriented toward the hardware actually encountered in most design situations. In addition, the software modules that describe the performance of the various hardware components are designed to be complementary one to the other. For example, some computer programs may model the passenger anthropometric properties very well, but might not simulate nearly as well the bag shape actually used or the interaction of the airbag with the passenger chest and head during the deployment process. PASSIM-PLUS, on the other hand, is structured to provide balanced treatment of all the various restraint and passenger components which make up the total model.

Key Features in Detail

The following are more detailed descriptions of-a few of the very important features of PASSIM-PLUS:

Arbitrary User Defined Shape

PASSIM-PLUS has the capability of simulating virtually any three dimensional airbag shape. The PASSIM-PLUS airbag is defined by the user as a series of elements of user selected size. The intersection of any two line elements is called a "node." A typical PASSIM-PLUS airbag shape is usually composed of 500 to 3000 nodes. This flexibility allows the user to simulate virtually any bag shape desired. Figure 9 shows the mesh creation worksheet with one possible PASSIM-PLUS airbag shape. Figure 10 shows a 3-D view of the airbag created in the worksheet shown in Figure 9.

Airbag Conformity

PASSIM-PLUS, because of its multi-element construction composed of hundreds of tiny airbag fabric elements, will conform to the shape of any contacted surfaces automatically. This means that the contact areas, and the resulting contact forces with the passenger and compartment are computed much more accurately. This capability is extremely beneficial for situations which involve a forward positioned passenger such as the out-of-position child because now, when the airbag contacts the passenger early in the deployment sequence, the airbag will first impact and, then "flow," all the while conforming to the contacted surface.

Figures 11 and 12 show PASSIM-PLUS simulating a forward positioned, 3 year old seated child and a deployment angle of 60 degrees at two different times in the bag deployment sequence (18 and 60 msec.) As may be seen in these figures, the PASSIM-PLUS airbag correctly conforms to the contacted surfaces.

Many Airbag Reaction Surfaces

Airbag reaction surfaces at the head, neck, torso, femur, knee, tibia, instrument panel (top and front), knee bolster, floor, windshield, header and roof have been added.

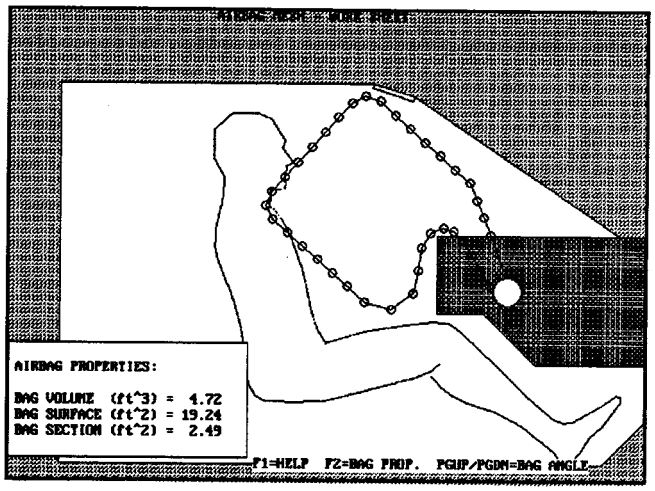

Figure 9. Mesh Creation Worksheet, Sample Airbag

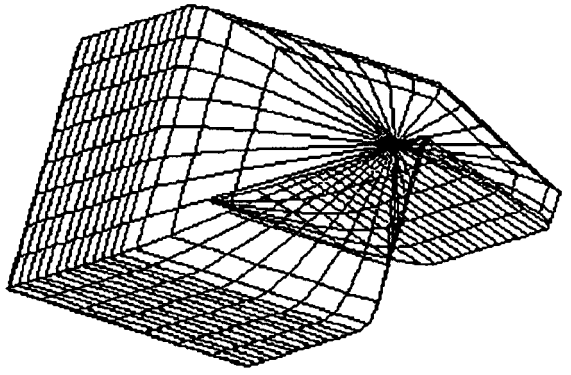

Figure 10. A Different 3-D View of the Same Airbag

Vertical Deployment Angles

With PASSIM-PLUS, the airbag may be deployed in a vertical or near vertical direction and "bounced off" the windshield by selecting a near vertical deployment angle. Figures 13 and 14 show a graphic representation at two different times for a forward positioned, 3 yr old seated child, with a vertical airbag deployment angle of 90 degrees.

Calculation of Instantaneous Venting Due to Airbag Porosity

A new area of enhanced flexibility is the capability of addressing porous bags. In the past, porous bags presented a particular problem in that it was difficult to estimate the overall porosity and effective vent area of the airbag. This was due to the fact that the porosity of the airbag was constantly changing as various parts of the airbag became blocked by doors, windows, windshield, instrument panel, knee bolster and the passenger himself. With PASSIM-PLUS this is no longer a problem as the location of each small airbag segment may be individually accounted for and venting either not allowed or allowed depending on whether it is in contact with a blocking surface or not. The program can then subtract the blocked surface area from the total surface available for

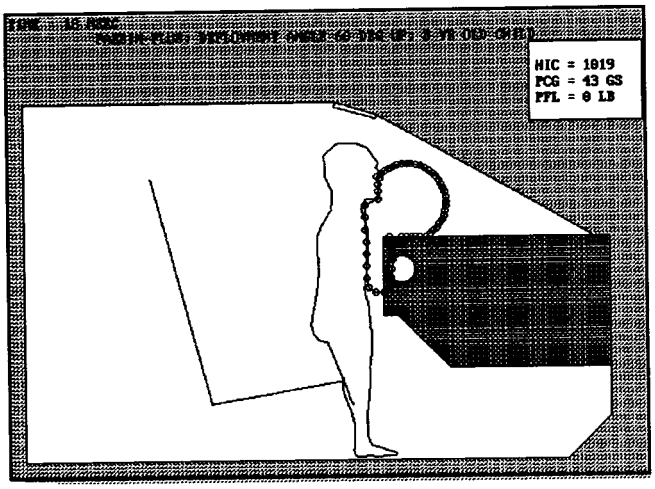

Figure 11. Standing Child, dep. angle 60 deg., 18 msec.

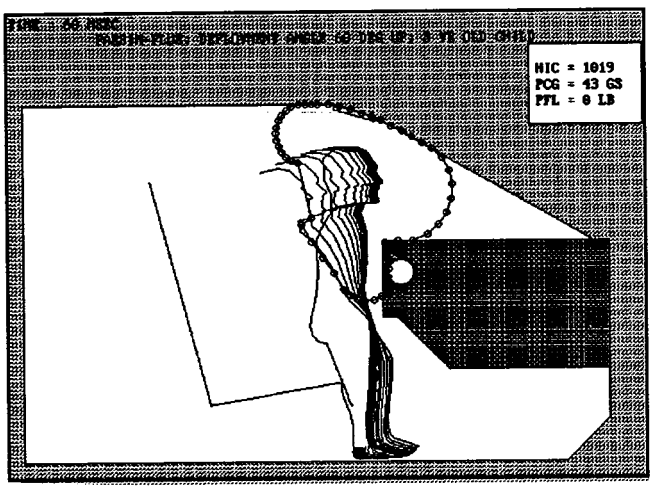

Figure 12. Standing Child, dep. angle 60 deg., 60 msec.

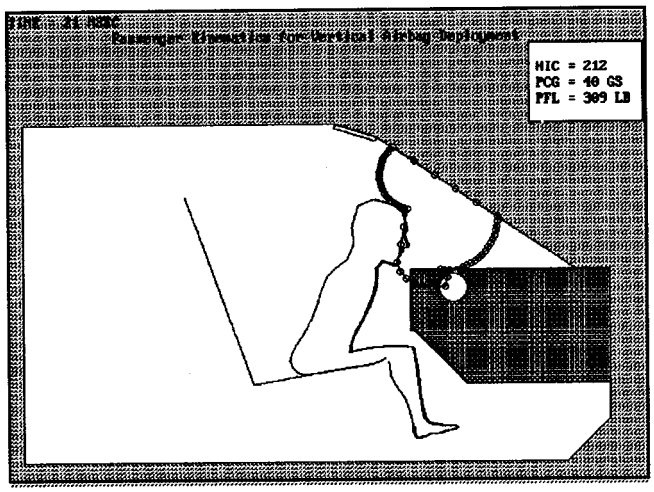

Figure 13. Vertical Deployment, 21 msec.

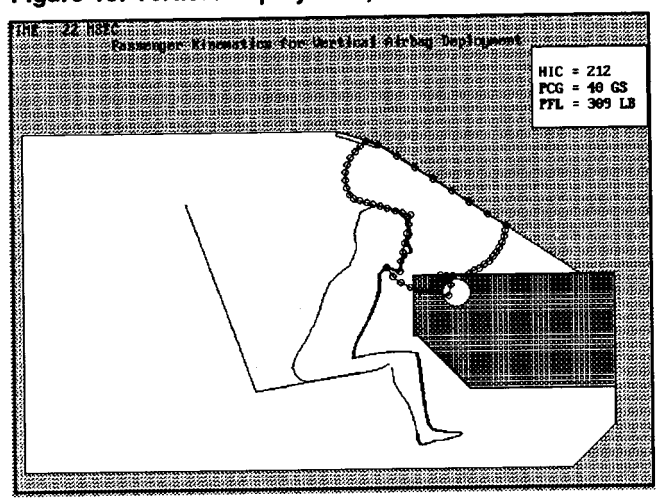

Figure 14. Vertical Deployment, 22 msec.

venting at each instant in the computational process. By knowing, at each instant the area available for venting, the bag pressure and the fabric porosity; PASSIM-PLUS can accurately compute the venting from the porous bag.

Seat Back and Bottom

The seat back and seat bottom are modeled in detail in PASSIM-PLUS so that impact due to the small, forward positioned child being propelled rearward into the seat back and bottom (including the forward edge of the seat bottom) is modeled more accurately. The seat bottom front edge was modeled so that impact with the lower leg and subsequent upward leg rotation is accurately computed.

In addition, the passenger is not constrained to remain in contact with the floor of the compartment. This allows the forward positioned child trajectory to be modeled accurately as his trajectory often includes leaving contact with the floor with subsequent impact with the seat front edge and back.

Evaluation of Structural Intrusion

Time histories of the intrusion of the toeboard, knee bolster and instrument panel have been added as input. As a result of this important enhancement, the effect of intrusion of any or all of these components on injury may be evaluated. In addition, the user can see a visual display of these intrusions in animated sequence on screen with the use of the post-processor PAG-PLUS.

Microcomputer Compatibility

One of the most beneficial features of PASSIM-PLUS is its ability to efficiently run on microcomputers. A typical run completed on a 33 MHZ, 80386 based machine takes approximately three minutes.

MFP-PLUS: Airbag Creation

In keeping with FE's dedication to User Convenience, a pre- processor has been developed which enables the user to create airbags and set up input files for PASSIM-PLUS with ease. For example, the program is completely menu driven and contains a special subroutine for interactively generating the airbag surface mesh.

There are many useful options with this program such as:

- MFP-PLUS has several very convenient ways of creating the mesh input for PASSIMPLUS. One way that is especially useful if a drawing of the airbag exists is to select the "drawing option." In this case,

the program will request the input for the desired final airbag shape by asking the user to specify either interactively or by access from disk the airbag dimensions in the same format as exist on the drawing of the airbag. By merely specifying radii lengths, points of radii origin, degrees of radii arc, etc; the user can watch as the final airbag shape is created on screen in the context of the vehicle compartment with the passenger in place. The program then creates the multi-element airbag mesh to the user specified "density" in terms of nodes per slice and number of slices.

- At any time, the user may request to see a 3-D view of the airbag which has been created. This 3-D view has a user option of being seen in the vehicle context or simply by itself. The 3-D airbag may be rotated about any axis, translated up or down, or "zoomed-in" upon at user selected increments of change.
- MFP-PLUS also has the ability to "grab nodes" on a specific "bag slice" and drag them to other locations in order to specify local indentations or other local surface irregularities due to bag tethers, doublers, or other localized effects.
- One may also toggle between slices to quickly see the shape of the various airbag sections which have been created.
- Once a specific slice has been fine tuned to a final shape, that slice may be scaled and/or copied to another slice location making it unnecessary to recreate the shape or a similar shape again. In this way, libraries may be created of various airbag shapes. In addition, the final airbag volume, cross sectional area, perimeter in two planes and surface area is instantaneously computed on screen for each change in slice or node geometry. At no time does the user have to calculate or input any mesh dimensions himself. This is automatically done by the computer after the user has answered a few simple questions. The slices may be scaled in various ways relative to each other to obtain many complex spherical and ellipsoidal based shapes. Virtually any airbag shape may be created with the one constraint that, for now, the bag must be symmetrical about the centerline of the passenger.
- High resolution hard copies of anything seen on screen may be made at any time on virtually any printer (including color on color printers). Before printing, the image may be rotated, cropped, scaled, color or gray shadings of each component adjusted, and even saved in various formats (.TIF, .PCX, .IMG, etc.) for inclusion into various desktop publishing and graphics based word processing programs. Post-processors for comparative (overlay) curve plotting and high resolution, animated, color graphics are also available.

In short, the PASSIM-PLUS program with its associated pre- and post-processors makes it possible for the user to have a comprehensive, self contained package for the complete, detailed design and evaluation of virtually any type of inflatable or belt restraint system for the passenger.

Conclusions

PASSIM-PLUS provides the user with the necessary tools for automotive restraint computer simulations for the right front passenger. The easy to use, menu driven user interface makes convenient the changes which are necessary in restraint system optimization. The new 3-D airbag of completely arbitrary, totally user defined shape which is composed of thousands of tiny fabric elements allows the user to have the flexibility needed in ACRS design work.

PASSIM-PLUS has proved effective as a tool used to optimize and/or develop passenger airbag and belt restraint systems. PASSIM-PLUS' ability to run on microcomputers and microcomputer networks makes the resulting information accessible to an extremely wide range of users and applications.

References

1. Michael U. Fitzpatrick,"PASSIM-PLUS, A Multi-Element, Passenger Airbag Model," SAE Technical Paper Series #910151, February, 1991.
2. Michael U. Fitzpatrick, "User's Manual for and Validation of "PASSIM-PLUS" Automobile Restraint System Simulation Model," U. S. Department of Transportation, Mr. Jerry Kossar (Contract Technical Monitor), Contract Number: DTNH2289-C-07147, July 5, 1991.

S9-W-26

Performance Evaluation of Crash Test Data Acquisition Systems

Randa Radwan
National Highway Traffic Safety Administration
John Nickles
Research and Special Programs Administration
U.S. Department of Transportation

Abstract

This paper provides an update of the system implemented by the National Highway Traffic Safety Administration for evaluating the performance of data acquisition systems at crash test facilities actively conducting testing for the agency. The system provides overall evaluation from sensor interface to delivered digital tape,

including data reduction. Specialized signal generator hardware is combined with customized signal processing software, and an evaluation test procedure to assure conformance to SAE and ISO recommended instrumentation practices. Reference signals with known characteristics are injected into the data acquisition system under evaluation. Time, amplitude and frequency performance measures, based on the SAE and ISO specifications, are computed and analyzed.

Introduction

As early as 1979, the National Highway Traffic Safety Administration (NHTSA) has been conducting vehicle and component crash tests to study and rate the crashworthiness of motor vehicles. Other tests are also conducted to enforce compliance to several Federal Motor Vehicle Safety Standards (FMVSS) in the United States. In practice, several crash test facilities perform the tests under contract to the NHTSA. The accuracy and correctness of the collected data is critical for both the valid comparison of data from several crash test sites, and for performing analyses utilizing the data collected at different test sites. Moreover, these data serve as a basis for numerous NHTSA published reports, and the corresponding analyses support existing and new safety standards.

In this paper, an evaluation test system to determine and improve the accuracy of the data acquisition process is described. The goal is to minimize differences due to data acquisition in test data acquired at different vehicle and sled crash test facilities. A parallel objective is to assure compliance of the test facilities with the Society of Automotive Engineers Recommended Instrumentation Practice, SAE J211 [8], as required by NHTSA contract specifications. Evaluation test results at certain active test facilities are also presented. Performance evaluation of data acquisition is now performed every six months at facilities actively conducting tests for the NHTSA under the New Car Assessment Program (NCAP), and the vehicle to barrier compliance testing, FMVSS 208.

Data Acquisition System (DAS) Evaluation Test System Overview

The DAS evaluation test process is conducted separately from the crash, sled, or component test event. The test facilities are required to setup their DAS systems in the same manner as in the actual test event. A NHTSA furnished and certified signal waveform generator (SWG) is placed at the sensor interfaces to provide the input signal source, a precise waveform sequence with known characteristics. These signals, one per DAS channel, are conditioned, recorded, filtered, and detrended, etc. employing the facility's regular practices. The digitized data are then written to magnetic tape per NHTSA specifications for crash tests. A block diagram of the test setup is shown in Figure 1. Once at NHTSA, the evaluation test data are loaded into a custom database and are processed using a specialized signal processing software. The database has the same format as the NHTSA vehicle crash test database. Time, amplitude, and frequency performance measures are computed and analyzed for each channel; failures to meet the requirements are indicated. The current performance requirements, outlined in Table 1, are based on the recommended instrumentation practices of the Society of Automotive Engineers, SAE J211, and of the international standard ISO 6487. The evaluation results are analyzed by the NHTSA staff and feedback is provided to the facilities on problem areas. Sufficient details are provided in the processing results to aid in the diagnosis and troubleshooting of problem areas.

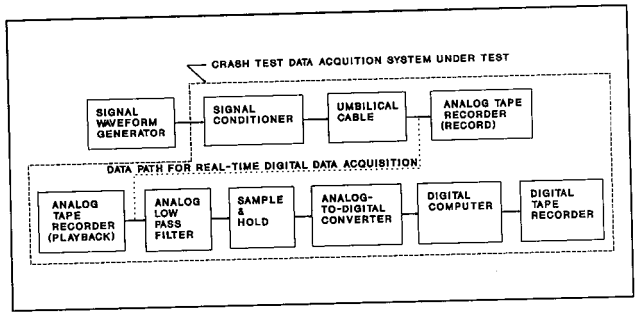

Figure 1. Test Configuration

Table 1. Current NHTSA DAS Performance Requirements

steady state amplitude deviation	2.5 %
amplitude linearity	2.5 %
amplitude offset error	2.5 %
amplitude overshoot	13 %
time zero offset	1 ms
time deviation	1 ms
component channel to channel time difference	0.1 ms
HIC deviation	6 %
dynamic response	SAE J211 CLASS 1000 frequency response corridor

The DAS evaluation process does not require detailed knowledge of data acquisition hardware components nor of the SWG hardware by the test facility personnel. The SWG, fully described in a later section, has simple connectors and is intended for use as a "black" box. Moreover, the same process for data recording and digitization is used as in a regular crash test event.

DAS Test System Development

The main development of the SWG hardware and the corresponding Signal Processing SoftWare (SPSW) was conducted by MGA Research Corporation, under contract to the NHTSA entitled "Test Site Instrumentation Study" [1]. This study was motivated by the New Car Assessment Program (NCAP) program which required detailed, overall comparison of 35 mph vehicle to barrier crash

tests, conducted at several test facilities. The NCAP program, begun in 1979, is conducted to provide consumers with comparative crashworthiness of motor vehicles.

The test site instrumentation study was divided into three phases. Under Phase I, in 1980, a survey of equipment and characteristics at 15 crash and sled facilities was conducted [2]. A prototype signal waveform generator, a solid state and digital based device with three output analog signals, was developed. Six different waveforms were stored in the generator's memory. This prototype was compatible with the facilities' data acquisition characteristics, and was used to inject the same signals into the data acquisition systems of the facilities participating in the survey. The data were recorded and digitized, and a preliminary analysis of the facilities' response characteristics was performed. Significant variations were found among the test facilities in this early period:

- up to 20% differences in the Head Injury Criteria (HIC) values,
- up to 10 msec time shifts,
- up to 10% deviation in amplitude at low frequencies (under 100 Hz), up to 30% deviations in amplitudes at the high frequencies (around 1000 Hz),
- and only 6 out of the 16 facilities were digitizing the analogue data fast enough to meet the antialiasing sampling criteria.

In phase I, the feasibility of an SWG based approach for systematic data acquisition system evaluation testing was established.

Under phase II, the SWG was refined and designed for field deployment [3]. The field SWG was designed with three self testing features: tests on the stored waveforms, tests on the output voltage, and tests on the time accuracy. It had sixteen output signals, each composed of 6 component waveforms, to be injected at the sensor interface of a facility's DAS. The following component waveforms were selected to determine specific DAS performance measures: a rectangular and staircase waveform, x, y, and z component of dummy head accelerations from a 35 mph vehicle to barrier test representing more typical head impact condition, a half sine pulse representing a severe crash pulse, a summed sine waveform, and a waveform consisting of white noise.

In the second phase, the specialized processing software was also primarily developed. The program, fully described in the following section, is written in FORTRAN, and resides on the NHTSA VAX cluster under VMS. It is composed of algorithms that compute performance measures of a given DAS based on the characteristics of the recorded SWG waveforms and the expected theoretical traces stored in the SWG memory.

Under phase II, further analysis of the phase I survey results was conducted. This resulted in the recommendations, outlined in Table 2, which are NHTSA current practices.

Table 2. Current NHTSA Data Acquisition Practices

Crash test facility's DAS performance based on SAE J211 and ISO 6487
Facilities supply consistent "raw" CLASS 1000 data to NHTSA
Data comparison by NHTSA based solely on results from NHTSA crash test databases
Facilities use NHTSA supplied software/algorithms for injury measure calculations

The development of the SWG which is presently in use was completed in phase III. In 1984, the hardware was refurbished and the panel redesigned since the phase II SWGs did not survive shipment by common carrier. The timing accuracy was improved by using only one crystal clock for timing of both the waveform and time reference output signals. Moreover, under phase III, the signal processing software was applied and enhanced.

Signal Waveform Generator (SWG) Hardware

Description

The Phase III SWG, shown in Figure 2, is 12.7 X 10.1 X 9.2 inches in size, weighs 12 pounds, and is designed to be used at crash test facilities by facility personnel. The SWG is powered from a 117 VAC 60 Hz power source. Instructions are provided in the SWG operator's manual [4] for changing the power supply input to accept 230 VAC 50 Hz power. Ten SWGs were fabricated by MGA Research Corporation. At present five SWGs are deployed at NHTSA crash test contractor test sites.

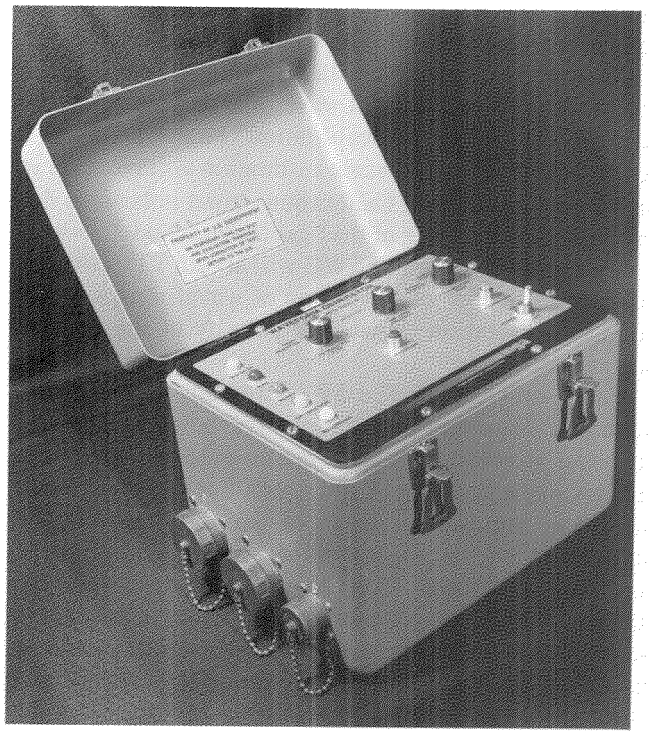

Figure 2. Phase III Signal Waveform Generator

The SWG functions by storing the precision waveforms digitally in erasable programmable read-only-memory (EPROM). When a test is performed, the waveform data is read out of EPROM under microprocessor control, converted to analog form by a digital-to-analog converter (DAC), and scaled by a resistive, operational amplifier network for transmission to the SWG output jacks. Every 30.5 microseconds (μs) a new data sample is processed by the DAC and made available at the SWG outputs. The SWG is described in greater detail in the SWG operator's manual.

The SWG provides a total of 20 output channels. Sixteen of the output channels provide precision waveforms at signal levels and source impedances representative of bridge circuit transducer outputs. These 16 channels are called "data" channels in this paper. Two of the output channels provide the same waveforms at relatively high voltage signal levels for SWG check-out use and are called "check-out" channels in this paper. Two output channels provide a time reference signal and are called "time reference" channels in this paper.

SWG Output Levels. Signal output levels from the data channels are switchable between a high level, ±100 mV, labeled "piezo electric" and a low level, ±10 mV, labeled "strain gage" on the SWG control panel. The check-out channels have corresponding full scale output voltage levels of ± 5.0 volts and ± 0.5 volt. The time reference channels are transistor-transistor-logic (TTL) compatible.

The 16 data channels each present an equivalent source impedance of approximately 350 ohms and provide a symmetrical, non-grounded ("floating") output. The two check-out channels provide "single ended" outputs.

Calibration Output. After the SWG is powered up and it completes its self test, all waveform outputs are at the zero level. Pressing the "calibration" button produces a positive or negative full scale calibration voltage level at each waveform output. Calibration output polarity is determined by the setting of the "calibration mode" switch.

Remote Operation. The SWG will accept TTL compatible signals to control generation of waveforms, generation of a calibration signal, and polarity of the calibration signal.

Waveform Outputs. The SWG provides two precision waveform sequences simultaneously, shown in Figure 3. Each test waveform sequence is available on eight of the data channels and one of the check-out channels. Each waveform sequence consists of the following, in the order specified: rectangle, half-sine, stair, sum-of-sines, and crash waveforms. The Group 1 waveform sequence contains the X components of the half-sine and crash waveforms and the Group 2 waveform sequence contains the Z components of these waveforms. The rectangle and stair waveforms are used to measure channel time accuracy, amplitude accuracy, and amplitude overshoot. The half-sine pulse waveform is used to measure channel-to-channel time differences. The sum-of-sines waveform is used to measure channel frequency response. The half-sine and crash waveforms are used to determine if any characteristic of the data acquisition channel is degrading the HIC values that would be calculated from the crash data recorded on that channel.

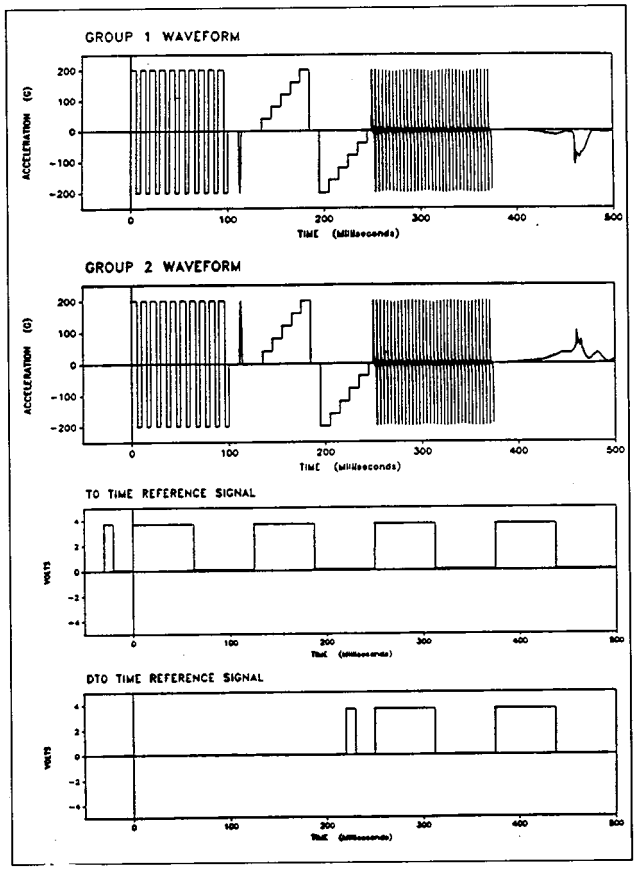

Figure 3. SWG Waveform Outputs

The rectangle waveform consists of a square wave that alternates between the plus and minus full scale levels for ten complete cycles. The exact timing of each cycle in the rectangle waveform is shown in Figure 4. The tenth cycle of the rectangle waveform is 61 μs shorter than the other nine. Thus, the length of the rectangle waveform is 99.979 ms. The exact timing of all of the waveforms has been incorporated into the SWG SPSW.

The peak value of each half sine pulse, shown in Figure 5, is the corresponding full scale level. The two half-sine pulse components are synchronized in time. The half-sine pulse waveform was designed to simulate a short duration impact which is often found in actual crash test data.

The stair waveform, shown in Figure 6, measures amplitude linearity. The Phase III stair waveform has steps of twice the height and duration but approximately half the number as the Phase II stair waveform.

The sum-of-sines waveform, the first two cycles shown in Figure 7, is a sinusoidal composite consisting of the sum of 14 sinusoids. The frequencies of the sinu-

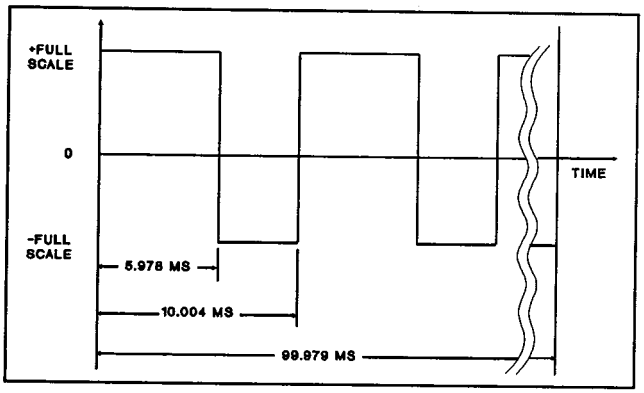

Figure 4. Rectangle Waveform Timing

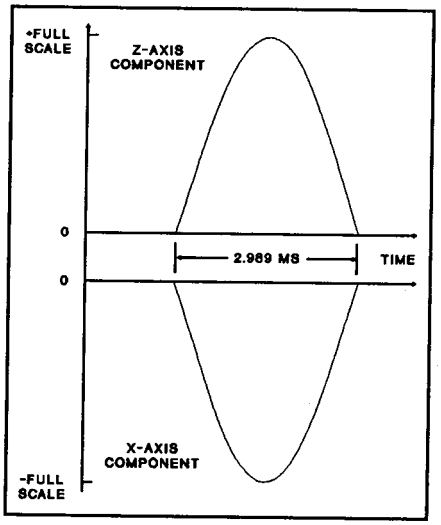

Figure 5. Half-Sine Pulse Waveform

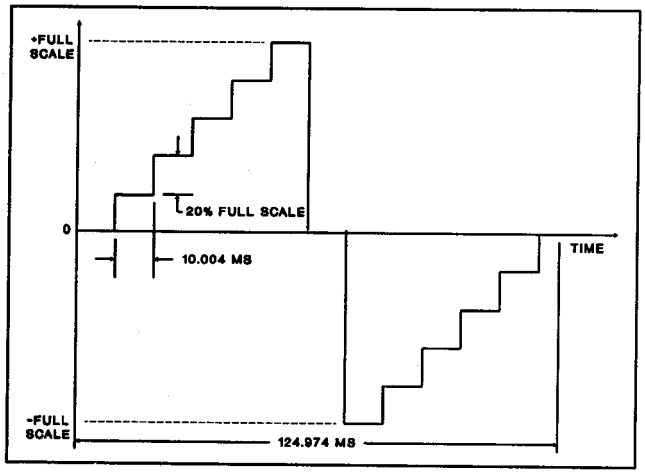

Figure 6. Stair Waveform

soids are the 14 consecutive integer harmonics of the lowest (fundamental) frequency. Each sinusoid in the summation has the same amplitude. The fundamental signal frequency is 273.4375 Hz. Therefore, the signal frequencies are 273.4375, 546.875, ..., 3828.125 Hz. The peak values of the sinusoidal composite signal are the full scale level. The duration of the sinusoidal composite is 124.2265 ms. This provides approximately 34 full cycles of the lowest frequency signal. These signal frequencies coincide with 14 of the output frequencies of the analyzing 2048 point discrete Fourier transforms when the data being analyzed are sampled at intervals of 75, 100, and 125 microseconds. These same sampling intervals are currently used by the NHTSA crash and sled test contractors.

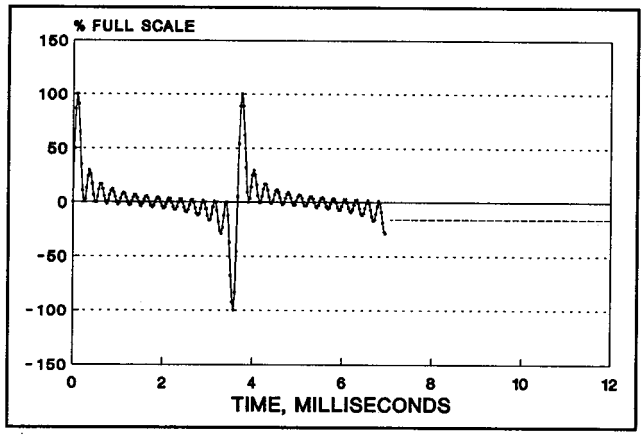

Figure 7. Sum-of-Sines Waveform

The crash pulse waveform, shown in Figure 8, consists of the "X" and "Z" components of actual dummy head acceleration crash pulse data from a vehicle to barrier crash test. The "X" component is in the same test waveform sequence as the "X" component of the half-sine pulse and the "Z" component is in the other test waveform sequence. The HIC value of the resultant pulse achieved by the vector summation of the "X" and "Z" components is 929.54.

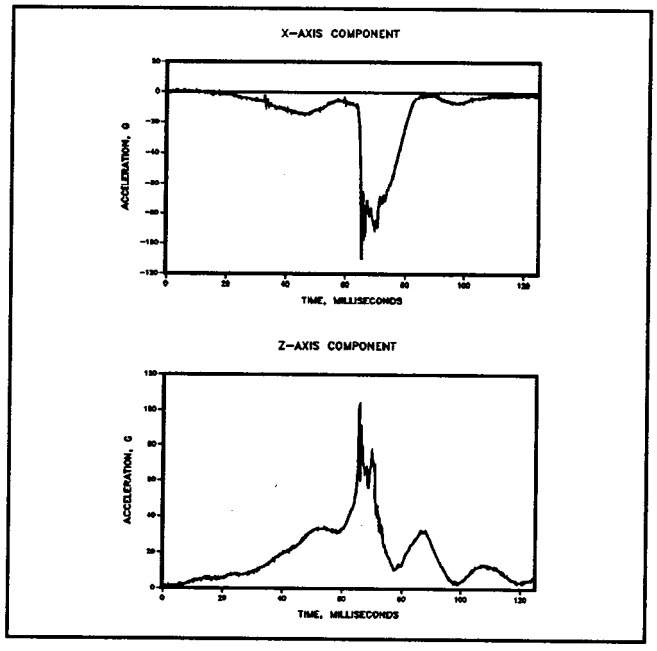

Figure 8. Crash Pulse Waveform

Time Reference Outputs. The time reference outputs, shown in Figure 3, are used to test facility sampling

frequency and time shifts between "time-zero" (T0) and data channels. The time reference output is also used to separate each waveform from the input data stream. The T0 time reference signal consists of five positive pulses. The first is a pre-time-zero pulse approximately 10 ms wide. This pulse starts when the "record" switch on the SWG control panel is pressed and can be used by digital data acquisition systems to start data recording. The leading edges of the first through the fourth T0 pulses after the pre-time-zero pulse correspond to the beginnings of the rectangle, stair, sum-of-sines, and crash waveforms, respectively.

The "delayed time zero" (DT0) time reference signal provides the same time reference information for situations where only the last two waveforms in the sequence are recorded. The duration of each pulse in the T0 and DT0 outputs have been measured to within ±2 μs and incorporated into the SPSW.

Measuring SWG Performance

The performance of the SWG was measured to assure the quality of its outputs for testing crash test data acquisition systems. Furthermore, the exact timing of the SWG outputs had to be known and incorporated into the SWG SPSW to achieve correct analysis of the DAS test data. The methods developed for testing the performance of the SWG were subsequently used in the certification testing that is performed on every SWG annually. The precise timing and the amplitude accuracy of the SWG outputs were determined by testing five SWGs. The most exhaustive testing, the performance test, was performed on SWG S/N 6, for which the precise timing of the SWG outputs was determined. Since the SWG functions under microprocessor control, and it is reasonable to assume that all ten SWGs have identical programs and waveforms stored in their EPROMs, once the timing of the outputs of one SWG are determined, the relative timing of the outputs of the other nine should be the same. The only variant in SWG timing would be the frequency of the crystal clock oscillator that provides the time reference for the SWG. Clock frequency, amplitude accuracy, and frequency response were tested during the certification testing of the other four SWGs.

Method of Test. The following paragraphs describe the testing methods used to test SWG performance and the instrumentation used for this testing.

Timing Accuracy. The test for timing accuracy is a test of each of the five factors which contribute to SWG timing accuracy. The first is the actual frequency of the SWG crystal clock oscillator. The second is the timing accuracy of the time reference signals from the SWG. The third is the precision with which the SWG time reference pulses coincide with the SWG waveform data. The fourth is the precision with which the group 1 and group 2 waveforms are synchronized with each other. The fifth is the timing accuracy of the individual waveforms.

The frequency of the SWG crystal clock oscillator time reference was measured using a Hewlett-Packard 5386A-004 frequency counter, which is accurate to 0.5 Hz when measuring frequencies near 4.0 Mhz.

The actual times of occurrence of the T0 and DT0 transitions within the 30.5 μs SWG DAC output sample interval were measured using the precision data acquisition system (PDAS), purchased for this test. The sampling of the PDAS was synchronized to the SWG DAC strobe pulse. Consequently, all time measurements over intervals greater than 30.5 μs are relative to the SWG crystal clock oscillator reference. Sample timing within one 30.5 μs interval was controlled by the PDAS crystal clock oscillator. These measurements were made on SWG S/N 6 only.

The coincidence of the initial rising edges of the first T0 time reference pulse after the pre-T0 pulse and the rectangle waveform was measured to determine the timing accuracy of the waveform data relative to the time reference. The time difference between these two leading edges was measured using a Hewlett-Packard 54200D dual trace digital storage oscilloscope. The details of the rectangle waveform leading edge were determined using the PDAS. This measurement was performed on SWG S/N 6 only.

The difference in time-of-occurrence between the two half-sine pulses from the SWG is measured by the SWG SPSW developed to analyze the recorded waveforms.

The software used to process SWG waveform data performs a test to determine the times at which recorded changes in level of the rectangle and stair waveforms occur. If the recorded waveform changes levels at times that are different from those that the software uses as a reference, a time difference error is calculated. These data provide a measure of waveform timing accuracy. The results of this analysis were confirmed by a detailed examination of the raw data printout for SWG S/N 6.

Amplitude Accuracy. The accuracy of the waveform amplitudes was determined by two methods. The SWG SPSW, as modified to accept the longer data sets recorded for this test, was used to analyze the waveform data recorded by the PDAS. Then, to verify the results of the software analysis, the recorded raw data printouts were examined at critical points for SWG S/N 6. The amplitude accuracy measures determined are SWG full scale amplitude accuracy using the positive calibration signal from the SWG as a reference, amplitude linearity, and zero offset.

The zero, positive, and negative calibration voltages at both "piezo resistive" and "strain gage" settings from all SWG output channels were measured with a Fluke 8050A digital multimeter to confirm that each channel output is providing the correct calibration voltage level. The Fluke 8050A has an accuracy for DC voltage measurements of ±(0.03% of reading + 2 digits).

To establish the zero and calibration levels for scaling the PDAS, averages were computed of the SWG zero

output level and the SWG positive calibration output level, using the PDAS software. At first single 100,000 point averages of each level were computed. Later it was found that better estimates of the true averages could be determined by repetitively computing 16,000 point averages and plotting them. A 30.5 μs sampling interval was used for recording the zero and calibration level data. Finally, the average value of the zero offset that precedes the waveform was subtracted from each point in the waveform data set.

To determine amplitude accuracy from the recorded test data, the SWG SPSW compares the average values of the constant portions of the recorded rectangle and stair waveforms with the theoretical values for these waveforms at those levels. The peak values for the half-sine waveforms reported by the SPSW were verified by examining the scaled raw data printouts.

The PDAS used to measure waveform accuracy was a Model DAP 2400/5, manufactured by Microstar Laboratories of Redmond, WA. Some of the capability of the DAP 2400/5 is outlined in Table 3.

Table 3. PDAS Features

Analog inputs	16 channels, single ended or differential
Input ranges	±2.5 V, ±5 V, ±10 V, or 0 to 5 V
A/D converter	12 bit resolution
Accuracy	±0.025% full range
Programmable gain amplifier	Gains 1, 10, 100, 1000
Sample interval	4.25 μs to 10 ms
On-board RAM	512K bytes
16 MHz clock	±30 PPM accuracy ±50 PPM stability, -20°C to +70°C 5 PPM per year drift
Start of sampling	On software command or external trigger
Records data	16 channels before and after trigger
Sampling a sequence of channels	External pulse starts sampling a sequence of up to 16 channels once per external clock pulse
Host computer	IBM PC compatible

To match the ±10 Mv and ±100 Mv outputs of the SWG to the ±2.5 V input of the PDAS, two Burr-Brown INA110/SG integrated circuit amplifiers were used external to the PDAS to provide the required gain. To synchronize the PDAS sampling to the SWG DAC strobe pulse, the SWG was modified to make the DAC strobe pulse accessible through one of the SWG output connectors and digital logic was designed and fabricated to gate the DAC strobe pulse to the PDAS starting at the first rise of the pre-time zero pulse.

Frequency Response. The frequency response of a data acquisition system is determined by processing the sum-of-sines waveform from the SWG with the SPSW. The SWG amplitude frequency response should be 0 Db ("flat") at all sum-of-sines signal frequencies.

Measured Performance. The measured performance of the SWG is outlined in Table 4.

Table 4. Measured SWG Performance

Time reference (data clock) accuracy	7 PPM, -10°C to +50°C implies max time reference error = ±3.5 μs for the 0.5 s waveform duration
Time reference signal accuracy	Timing measured to ±2 μs and incorporated into SPSW
Coincidence of time reference pulses to start of waveform	time reference pulse rises 14 μs after rectangle waveform time reference pulse coincides exactly with stair waveform time reference pulse lags start of sum-of-sines waveform by 28 μs
Coincidence of group 1 and group 2 waveforms	Exactly synchronized
Waveform timing accuracy	Waveform timing measured to the exact DAC sample number and SPSW edited to conform to measured values
Amplitude accuracy	±0.06% full scale at "piezo resistive" level ±0.5% full scale at "strain gage" level
Output noise	<0.05% full scale rms at "piezo resistive" level <0.15% full scale rms at "strain gage" level
Amplitude frequency response	0, ±0.02 dB

Operational Problems

Occasionally, after being shipped to a new location by common carrier, the SWG will not pass its own self test. In many instances, this situation can be remedied by disassembling the SWG to the extent of removing the printed circuit cards from the card cage and reinserting them. When SWGs are tested for certification, the tinned copper foil PC card edge connectors are cleaned. This clears up many of the self-test problems.

At the low ("strain gage") output level, all SWG output waveforms exhibit an offset that differs from the zero offset measured before and after the waveform transmission is complete. In at least one instance this waveform offset has been of sufficient magnitude to compromise the DAS test results. To minimize this offset effect, current practice is to use the high ("piezo resistive") output level for all measurements and install resistive shunts at the instrumentation interface to reduce the signal voltage level to the full range of the channel under test, where this is necessary.

Phase III SWG Signal Processing Software (SPSW)

Waveform Processing Method

Waveform data from up to 18 channels can be processed during one processing run. First the time reference data for the set of data to be processed during one run is read by the SPSW. This establishes the array index values that correspond to each leading edge of the time reference waveform. Then the waveform data to be processed is read by the SPSW. As the data from each channel is read it is separated into arrays that contain the data for each waveform.

Rectangle Waveform Processing

The rectangle waveform is used to check the following characteristics of a data channel:

a. "Time-zero" offset
b. Time deviation from theoretical time
c. Full-scale steady-state amplitude response
d. Amplitude overshoot in response to a step input

"Time-Zero" Offset. The time=0 or "time-zero" (T0) reference for the data is established by the first data sample in the time reference waveform that exceeds 50% of the maximum value of that waveform. Similarly, the first sample of the rectangle waveform that exceeds 50% of the nominal maximum of the rectangle waveform, determines the actual time of the first rise in the rectangle waveform. The difference between these two times is defined as the time-zero offset for the channel being tested. A time-zero offset less than or equal to 1.0 millisecond is acceptable.

Time Deviation from Theoretical Time. The actual time of the zero crossing of the recorded rectangle waveform is measured to determine the variations in the data time base. Each zero of the rectangle waveform crossing subsequent to T0 is supposed to occur at 5.978, 10.004, 15.982, 20.008, 25.986, 30.012, etc. milliseconds after T0. The measured time of each subsequent zero crossing of the rectangle waveform is determined by each data sample in the sequence that has a sign change. The time deviation is the difference between the measured and the theoretical zero crossing times.

Steady-State Amplitude Deviation from Theoretical Amplitude. The steady-state amplitude deviation from theoretical amplitude is determined by comparing the steady state average for each of the 20 occurrences of the extremes throughout the entire rectangle waveform to the theoretical full scale values. The steady-state amplitude is calculated by averaging the data values over the closed intervals from B to C and from E to F shown in Figure 9. Points B and E are the centers of the constant amplitude levels and points C and F are one millisecond before the next expected zero crossing. The duration of the averaging is approximately 2 milliseconds for the positive amplitude levels and 1 millisecond for the negative amplitude levels. Deviation from the theoretical full scale amplitude is expressed as a percentage of the theoretical full scale level.

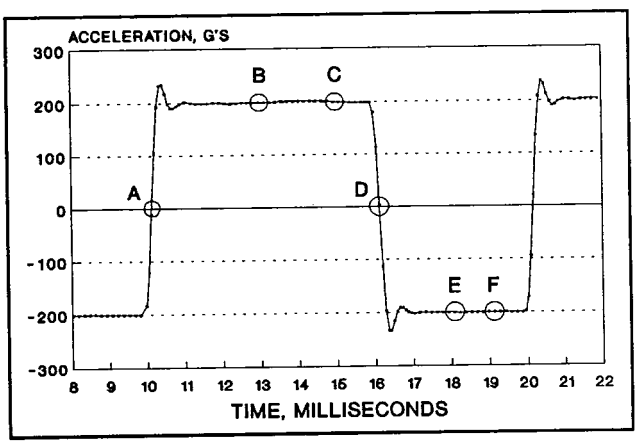

Figure 9. Analysis Intervals

Amplitude Overshoot Relative to the Calculated Steady-State Amplitude. The relative overshoot is determined by obtaining the data value extreme which occurs over the closed interval from A to B for the positive intervals and from D to E for the negative intervals, shown in Figure 9. The value of relative overshoot is expressed as a percentage of the change in measured steady-state amplitude by dividing the calculated overshoot by the change in measured steady-state amplitude.

Half-Sine Waveform Processing

Channel-to-Channel Time Difference. The calculated times of occurrence of the magnitude peaks of the X and Z components are utilized to determine the channel-to-channel time difference. The times of the peak magnitudes are determined by calculating the two times at which each waveform crosses a level which is 20% of full scale by linear interpolation between the two samples that are on either side of the 20% level. It is then assumed that the peak magnitude occurs at the time which is exactly halfway between the two 20% level crossings. The difference between the X-axis and Z-axis time-of-peak-magnitude values is the channel-to-channel time difference. The tolerance allowed for this difference is ±0.1 millisecond.

HIC Deviation. The HIC deviation is determined by comparing the HIC value determined from the resultant of the recorded X and Z components to a theoretical value. The theoretical HIC reference value is determined from half-sine data sets that are created by generating the plus and minus full scale half-sine pulses produced by the waveform generator and sampling these data sets at the test data sampling frequency. The resultant of these data sets is calculated and the HIC reference value of this resultant data set is computed by the HIC36 subroutine. HIC errors should be less than 6%.

Stair Waveform Processing

The stair waveform is used to check the following characteristics of the data channel:

a. Time deviation from theoretical
b. Steady-state amplitude deviation from theoretical levels
c. Steady-state amplitude deviation from best "least-squares" fit straight line
d. Amplitude linearity
e. Amplitude offset
f. Amplitude overshoot for different amplitude levels

Time Deviation from Theoretical. The time deviation from theoretical is determined by subtracting the theoretical time of each rise in the stair waveform from the actual time at which the recorded waveform response first exceeds 50% of the change in levels between two steps in the waveform. For example, 10.004 milliseconds is subtracted from the measured time of occurrence of the first sample to exceed 10% of full scale, 20.008 milliseconds is subtracted from the measured time of occurrence of the first sample to exceed 30% of full scale, etc.

Steady-State Amplitude Deviation from Theoretical Amplitude. The data used to determine the steady-state amplitude for each step in the waveform occurs in the interval from approximately two ms after a rise in the stair waveform to approximately one ms before the next rise. The steady-state amplitude for each step is calculated by taking the average of the amplitude values in this interval. Once the actual steady-state value is determined, it is then compared to the theoretical steady-state value. The difference between the theoretical and actual values is divided by the full-scale amplitude in order to express the deviation from theoretical amplitude as a percentage of the full-scale amplitude.

Amplitude Deviation From Best Least-Squares Fit Straight Line. A best least-squares fit straight line is fit to the data whose X and Y coordinates are the following: The X coordinates are the theoretical amplitudes that are supposed to be reported by the data acquisition channel. The Y coordinates are the amplitude deviations from theoretical described above. The amplitude deviation from the best fit straight line is the difference between the amplitude deviation from theoretical and the corresponding "Y" value on the best fit straight line. The tolerance for these deviations is ±2.5%.

Amplitude Linearity. The amplitude linearity reported in the STAIR summary report is the slope of the best fit straight line described in the preceding paragraph.

Amplitude Offset. The amplitude offset is the Y value of the best fit straight line described above, that corresponds to X=0.

Amplitude Overshoot Relative to Calculated Steady-State Value. The maximum level in the first two ms after a rise in the stair waveform is used to determine the relative amplitude overshoot by comparing the value of this peak level to the calculated (average) steady-state amplitude following the step. The difference between the maximum and the steady-state value is divided by the difference between the steady-state levels occurring before and after the step and expressed as a percentage of the step height. The tolerance for overshoot is 13%.

Sum-of-Sines Waveform Processing

The frequency response analysis starts by reading the recorded sum-of-sines data into an array. Then, an array of theoretical sum-of-sines data is created, sampled at the same interval as the recorded data. Next, the recorded data and the computed data are each multiplied by a Gaussian data window. A 2048 point discrete Fourier transform (DFT) of each of the windowed data sets is computed. The index of each DFT element whose frequency corresponds to a signal frequency is computed. The magnitude of each DFT element whose frequency corresponds to a signal frequency is determined. The ratio of the DFT of the theoretical data set to the DFT of the recorded data set, at the lowest signal frequency, is used as a scaling factor. The ratio of the DFT of the recorded data to the DFT of the theoretical data, at each signal frequency, multiplied by the scale factor, is the numeric amplitude ratio at that signal frequency. A description of this algorithm and its source program listing are provided in greater detail in the SPSW documentation [5].

Crash Waveform Processing

The crash waveform HIC deviation is determined by computing the HIC value of the resultant of the recorded X and Z components and comparing it with the HIC value of 929.54 that was computed for the original crash data. The allowable HIC deviation is ±6% or less.

Reporting and Tabulating Processed Data

During each processing run, report files are written that contain the results of processing the data from each channel included in that run, one report file for each waveform. Also a table is assembled and written to a disk file, which presents a summary of the most significant values of the processed data from that run.

DAS Evaluation Test Results

Historical Trend in Performance in Active NCAP and FMVSS 208 Crash Test Sites

A brief history of DAS evaluation testing, using the SWG, at NCAP crash testing sites is provided in Table 5. During 1986, 1987, and 1988 DAS evaluation testing was confined to occupant channels. This explains the relatively small number of data channels tested during those years. In 1990 the requirement to perform a DAS evaluation test on all channels to be used in testing for the New Car Assessment Program (NCAP), and the vehicle to barrier compliance testing program, under FMVSS 208, was made a part of the test contracts for those programs. As demonstrated in Table 5, the ratio of # of defective channels to the # of channels tested has declined in recent testing. At present, there are no known significant deficiencies in the DAS facilities at the three contractors listed in Table 5 below and the new NCAP contractor site (SITE4) whose results are presented in the next section. Analysis of the detailed processing results for each of the defective channels in the latest tests has indicated that the failures are marginal and mainly attributed to system noise. In all cases, defective channels were corrected before actual crash tests were performed.

Diagnosis and Troubleshooting of Problem Areas

Analyses of the detailed processing results have provided a tool for diagnosis and troubleshooting of DAS problem areas at the test site facilities. Generally, throughout this evaluation testing activity, whenever a serious deficiency was discovered and brought to the attention of the facility, the facility personnel moved quickly to correct the deficiency. For example, while SITE2 was digitizing the data from the 1986 test, it was

Table 5. Historical DAS Evaluation Test Results

SITE1		
Date	# Defective/# Tested	# & Type of Failure
16-Jul-87	2/26	2 ctctd
17-Jul-87	6/26	5 ad, 2 ctctd
18-May-90	41/69	5 ad, 36 fr, 4 ctctd
10-Sep-90	0/69	none
SITE2		
Date	# Defective/# Tested	# & Type of Failure
21-Oct-86	9/16	7 os, 1 fr, 2 ctctd
25-Feb-88	1/16	1 fr
11-Sep-89	3/31	3 fr, 1 ctctd
12-Sep-90	2/79	1 ad, 1 fr
SITE3		
Date	# Defective/# Tested	# & Type of Failure
12-Aug-87	24/28	24 HIC
11-Apr-90	15/23	3 noise, 12 HIC
29-Nov-90	2/83	2 noise

ad - amplitude deviation
fr - frequency response
os - overshoot
HIC - HIC error
ctctd - channel-to-channel time difference

pointed out to them that the even numbered channels had excessive overshoot. At that time, they could digitize two channels at a time. They replaced the one defective anti-aliasing filter after digitizing the first fourteen data sets. That corrected the situation. In September 1989, the SITE2 results indicated excessive channel-to-channel time difference in one pair of driver chest channels. The detailed processing output indicated a slow analogue to digital (A/D) conversion rate. SITE2 was advised to run their A/D at a faster rate and to digitize all signals from channels from the same sensor location in the same run. In May of 1990, the SITE1 results showed that the frequency response of the 36 barrier load cell channels had a much lower cutoff frequency than that required by J211. This was traced to band limiting by the instrumentation amplifiers used for those channels. These amplifiers were replaced by wider band instrumentation amplifiers and a satisfactory frequency response was obtained. The four channel-to-channel time difference deficiencies were traced to one misaligned tape head on one of their analog tape recorders. This recorder was retired from service. The five amplitude deviation deficiencies were traced to five on-board instrumentation amplifiers. All instrumentation amplifiers of that model were replaced by instrumentation amplifiers of a different model.

Performance versus Requirements in Current NCAP and FMVSS 208 Test Sites

Results Summary. After the completion of all of the processing runs for a single test, software is available that can combine the processed results for the data channels from several processing runs into one summary table. The data contained the summary table are the sensor normally connected to the channel tested (SENSOR), the NHTSA data file number for the data, T0 offset, the average of the ten steady-state amplitude deviations computed for the positive levels of the rectangle waveform (AMPDEVPOS), the average of the ten steady-state amplitude deviations computed for the negative levels of the rectangle waveform (AMPDEVNEG), the average of the amplitude overshoots calculated for the 20 step changes of the rectangle waveform (OVRST), the maximum of the absolute values of the steady-state amplitude deviations from theoretical amplitude of the stair waveform (AMPLINREF), the maximum of the absolute values of the amplitude deviation from the best least-squares fit straight line to the amplitude deviations of the stair waveform (AMPLINBFSL), the amplitude frequency response at 1640 Hz in Db scale (AR1640), HIC error in the acquired half-sine pulse waveform (HSHIC), the channel-to-channel time difference between the two channels paired to provide HIC data (CTCTD), and HIC error in the acquired crash pulse data (CRSHIC). Summary results for current NCAP test sites are provided in Tables A-1 through A-4. HIC results and channel-to-channel time differences are blank for the channels that are used as the reference channel for each triad of channels. In 1990, SITE4 was a new crash test site under contract to the NCAP testing program.

Simple statistics for the above-mentioned performance measures for the occupant channels at the four NCAP sites are provided in Tables 6 through 9. Similar tables for the corresponding vehicles channels are provided in Appendix A, Tables A-5 through A-8. The LR1640 measure is the AR1640 value in linear scale.

Table 6. SITE1—Simple Statistics of Occupant Channels Performance Measures

Variable	N	Minimum	Maximum	Mean	Std Dev
TOFF	16	0	0	0	0
ADEVPOS	16	-0.3610000	-0.2400000	-0.3062500	0.0367850
ADEVNEG	16	0.2700000	0.4440000	0.3745000	0.0517983
OVRST	16	9.6520000	10.0760000	9.8450000	0.1332246
ALINREF	16	0.3810000	0.5200000	0.4558125	0.0349022
ALINFS	16	0.0540000	0.1920000	0.1016250	0.0346235
LR1640	16	0.6910349	0.7063176	0.6986437	0.0037042
HSHIC	8	-0.2100000	-0.0400000	-0.1212500	0.0535690
CTCTD	8	-0.0050000	0.0010000	-0.0020000	0.0022678
CRSHIC	8	-0.0500000	0.5600000	0.1925000	0.2122499

Table 7. SITE2—Simple Statistics of Occupant Channels Performance Measures

Variable	N	Minimum	Maximum	Mean	Std Dev
TOFF	30	0	0.1000000	0.0533333	0.0507416
ADEVPOS	30	-0.6500000	1.1310000	-0.0994333	0.4064600
ADEVNEG	30	-1.0370000	1.4620000	0.3345667	0.4652238
OVRST	30	2.9020000	3.5810000	3.1146000	0.2011232
ALINREF	30	0.3930000	1.4650000	0.7173000	0.2326424
ALINFS	30	0.1600000	0.5140000	0.2812000	0.0942866
LR1640	30	0.6546362	0.6910349	0.6744664	0.0114133
HSHIC	16	-1.4400000	1.2900000	-0.0962500	0.5895295
CTCTD	16	0.0070000	0.0420000	0.0296875	0.0110798
CRSHIC	16	-0.4600000	2.5200000	0.9312500	0.7892518

As can be observed from the Tables, the maximum deviation for the T0 offset for the occupant channels in all the sites is 0.25 msec, the maximum absolute deviations for AMPDEVPOS and AMPDEVNEG are 0.65% and 1.462%, the maximum for OVRST is

Table 8. SITE3—Simple Statistics of Occupant Channels Performance Measures

Variable	N	Minimum	Maximum	Mean	Std Dev
TOFF	28	0.1250000	0.2500000	0.2187500	0.0551198
ADEVPOS	28	-0.2290000	0.1660000	-0.0035714	0.0953028
ADEVNEG	28	-0.2920000	0.3340000	0.0181786	0.1422093
OVRST	28	5.7230000	7.3770000	6.7557857	0.4739733
ALINREF	28	0.0710000	0.3980000	0.2013929	0.0725567
ALINFS	28	0.0520000	0.4490000	0.1380000	0.0725672
LR1640	28	0.7227698	0.8016781	0.7709060	0.0159786
HSHIC	12	-5.5200000	-0.2100000	-3.5525000	2.3826499
CTCTD	12	-0.0070000	0.0090000	0.000583333	0.0049810
CRSHIC	12	-4.3000000	0.0600000	-2.7775000	2.0162257

Table 9. SITE4—Simple Statistics of Occupant Channels Performance Measures

Variable	N	Minimum	Maximum	Mean	Std Dev
TOFF	16	0	0.1220000	0.0152500	0.0416709
ADEVPOS	16	-0.2320000	-0.0030000	-0.1486875	0.0491714
ADEVNEG	16	-0.1810000	0.0230000	-0.1118125	0.0546458
OVRST	16	8.9990000	9.3800000	9.1316250	0.1080326
ALINREF	16	0.1200000	0.2380000	0.1695000	0.0358311
ALINFS	16	0.0500000	0.1940000	0.1120625	0.0475205
LR1640	16	0.6760830	0.6942246	0.6814218	0.0047281
HSHIC	8	-0.8200000	-0.3500000	-0.6775000	0.1477208
CTCTD	8	0.0090000	0.0220000	0.0150000	0.0052915
CRSHIC	8	-0.2000000	0.1800000	-0.0762500	0.1329809

10.076%, the maxima for AMPLINREF and AMPLINBFSL are 1.465% and 0.514%, the maximum absolute deviations for HSHIC and CRSHIC are 5.52% and 4.3%, and the maximum absolute deviation for CTCTD is 0.042 ms. The frequency response measurement at 1640.625 Hz ranges between 0.6546 (-3.68 Db) and 0.8017 (-1.92 Db). For SAE J211 class 1000 data, a range of frequency response of -0.5 to -3.9 Db is acceptable at 1640 Hz. The maximum frequency response variation in the four sites can be seen in Figure 10. In this figure, the two channels that show the greatest and least attenuation at 1640 Hz for each site are plotted. Therefore, with the worst case deviations, the performance measures of the DAS at the four sites are within the performance requirements outlined in Table 1.

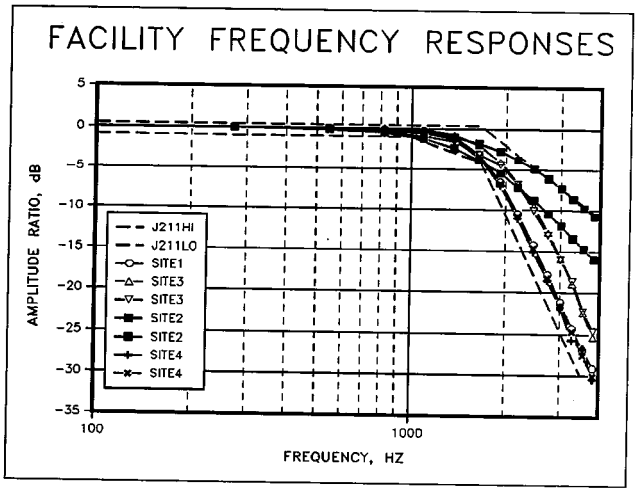

Figure 10. Maximum Frequency Response Variations at the NCAP Sites

Table 10 demonstrates the vast reduction in test data variations due to data acquisition in the last decade. It contrasts the deviations from the 1980 facility survey with the worst case Mean performance of current NCAP facilities.

Table 10. Worst Case Data Deviations Due to Data Acquisition

	1981 Facility Survey	1990 NCAP Facilities
time shifts	10 ms	0.219 ms
amplitude deviations	20-30 %	0.375 %
HIC computations	20 %	3.55 %
SAE J211 frequency response corridor	only 6 out of 16 met sampling requirements	all passed

Figures 11 through 20 portray the variations in a given performance measure amongst the four sites. An interesting feature is that for each performance measure, the range of deviation was very narrow for at least one site. This demonstrates the capability of any given crash site to further minimize the differences in each of the time, amplitude and frequency measures. Given the advances in the data acquisition technology and given that the data acquisition process is the most controlled part of a crash test event, this supports the authors' belief that even very small differences in the test data amongst sites due to the acquisition process should not be tolerated.

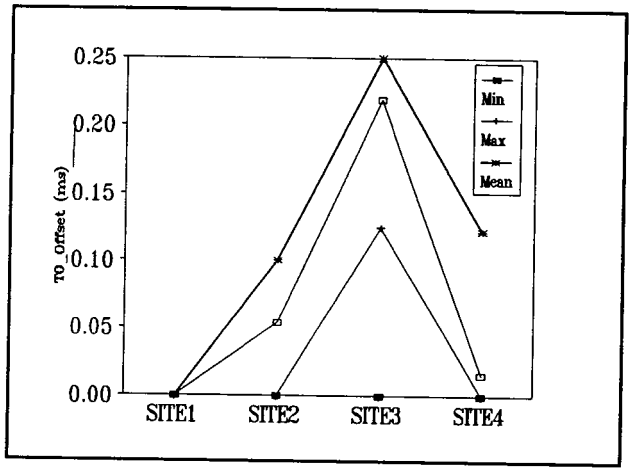

Figure 11. Occupant Channels—Time Zero Offset Performance

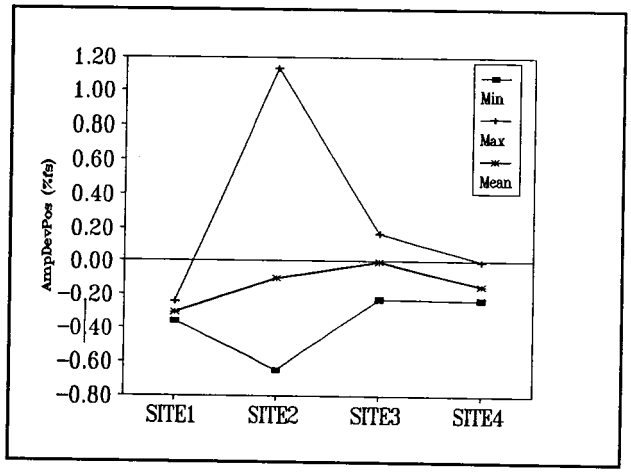

Figure 12. Occupant Channels—Positive Amplitude Deviation

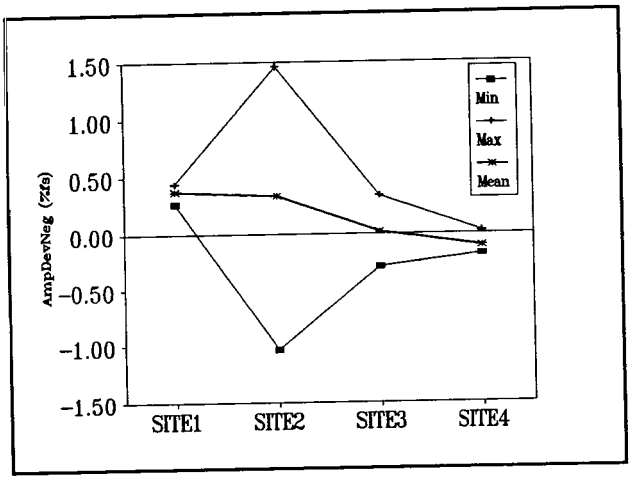

Figure 13. Occupant Channels—Negative Amplitude Deviation

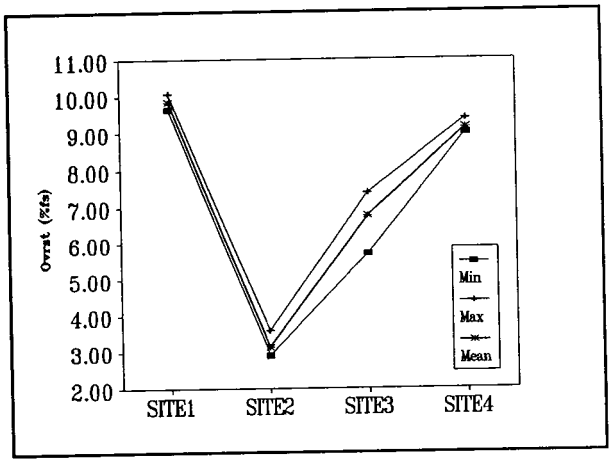

Figure 14. Occupant Channels—Overshoot Performance

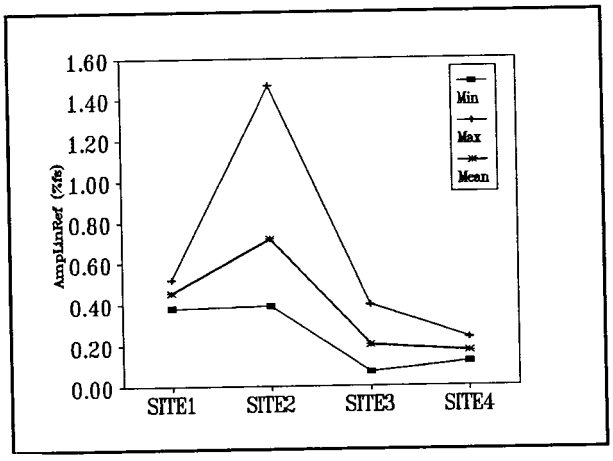

Figure 15. Occupant Channels—Amplitude Linearity to Theoretical Value

Statistical Analysis. Analysis of variance (ANOVA) on the mean values of each of the performance measures for the four sites was conducted. The results showed there is significant evidence that there are differences between the means of all the measures amongst the four sites. For all of the measures, the p-value was 0.0001 or less with exception of ADEVPOS for which p-value was 0.0019.

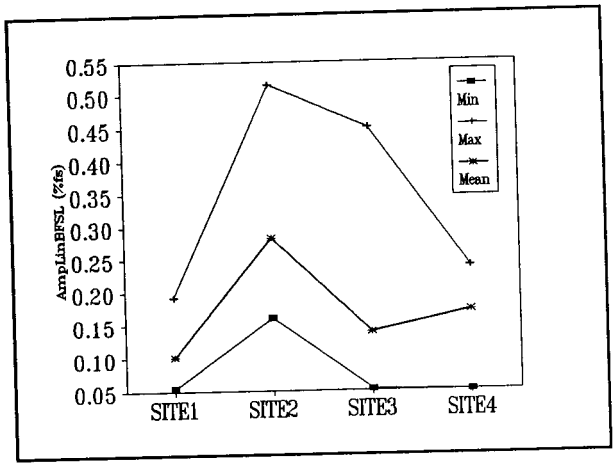

Figure 16. Occupant Channels—Amplitude to Best Fit Line Linearity

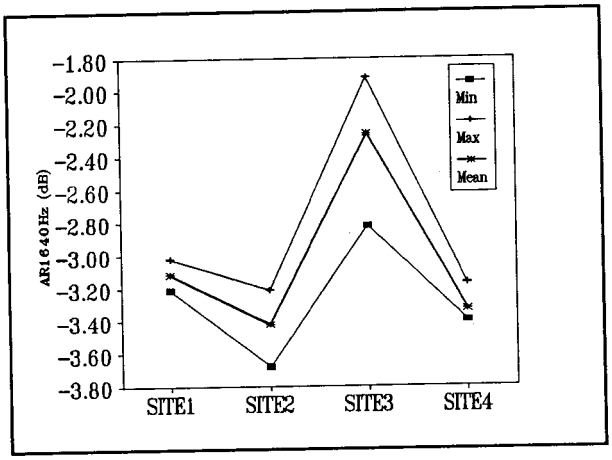

Figure 17. Occupant Channels—Frequency Amplitude Response at 1640 Hz

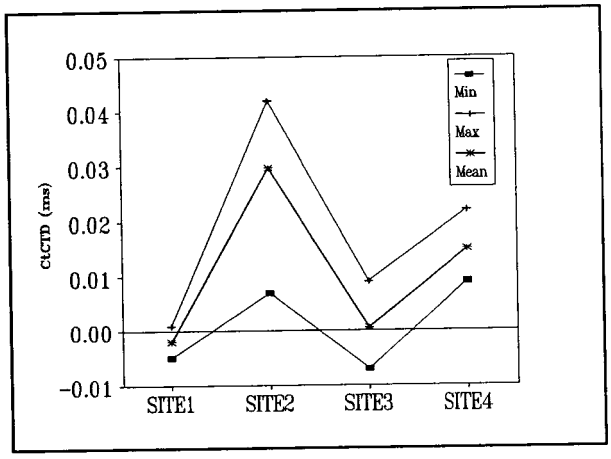

Figure 18. Occupant Channels—Channel to Channel Time Difference

The p-value is the probability of obtaining a given test statistics as a result of pure chance, i.e. chance in 1 the results are random or plain wrong. As such, the hypothesis that there is no difference between the mean values for a given performance measure at different sites is rejected.

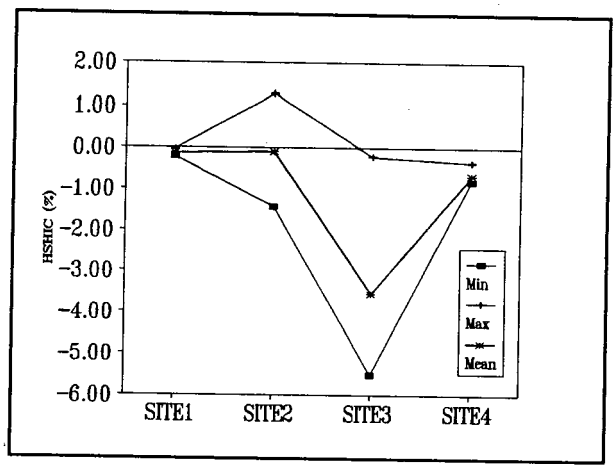

Figure 19. Occupant Channels—Half Sine HIC Deviation

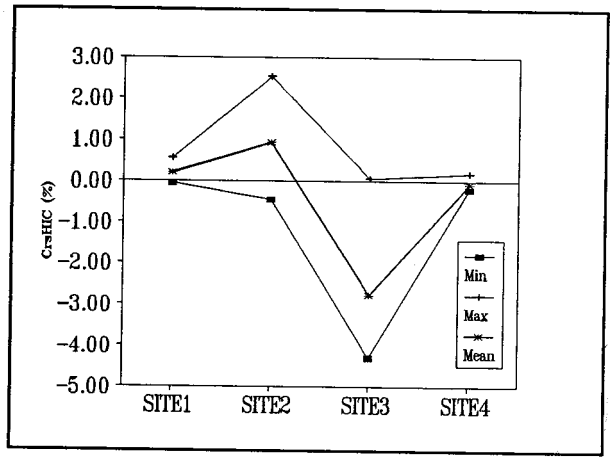

Figure 20. Occupant Channels—Crash Pulse HIC Deviation

A multiple range comparison test was conducted on the means of each measure. Based on the means and the variance, the procedure grouped the sites into subsets whose means were not significantly different. The analysis was conducted using the SAS General Linear Model (GLM) procedure [6]. The results of this analysis are summarized in Table 11 for each of the performance measures. The classification is the following: given the variance, means of the same letter are not significantly different. Although the same letters are used, the classes for the different measures are separate. The letters designate a ranking of size: A, largest value; ...; D, smallest value (including negative values). For example, Table 11 shows that for the HSHIC and CRSHIC measure, SITE3 was the only site with significantly different mean values.

For each of the four sites, correlation between the performance measures for both the occupant channels were also computed. The measures for which R, the Pearson correlation coefficient is greater than 0.7 and the probability the hypotheses that the measures are not correlated is less than 0.01 are presented in Table 12. R^2 is a measure of the variance accounted for by the linear relationship between the two measures. The probability of the designated magnitude presents significant evidence

Table 11. Multiple Range Comparison Test for the MEANS of the Performance Measures

Variable	SITE1	SITE2	SITE3	SITE4
T0_Offset	C	B	A	C
AmpDevPos	B	A	A	A
AmpDevNeg	A	A	B	B
Ovrst	A	D	C	B
AmpLinRef	B	A	C	C
AmpLinBFSL	B	A	B	B
LR1640	B	C	A	C
CTCTD	C	A	C	B
HSHIC	A	A	B	A
CRSHIC	A	A	B	A

Table 12. Occupant Performance Measures Correlation

SITE4	HSHIC	CRSHIC	CTCTD
OVRST	0.927/0.0009	0.881/0.0038	n/a
LR1640	n/a	n/a	0.924/0.001
HSHIC	n/a	0.861/0.006	
SITE1			
	Ovrst		
LR1640	0.782/0.0003		
SITE2			
	HSHIC	CRSHIC	
AmpDevPos	0.817/0.0001	n/a	
AmpDevNeg	0.923/0.0001	0.748/0.0009	
AmpLinRef	n/a	0.720/0.0017	
HSHIC	n/a	0.715/0.0018	
SITE3			
	HSHIC	CRSHIC	
LR1640	0.881/0.0002	0.870/0.0002	
CTCTD	0.831/0.0008	0.834/0.0008	
HSHIC	n/a	0.997/0.0001	

to reject the hypothesis that the two measures are uncorrelated. The analysis was conducted using the SAS CORR procedure [7]. Table 12 indicates a strong correlation between the HIC deviation measures and the frequency response at 1640 Hz (LR1640) and the channel-to-channel time difference (CTCTD) for SITE3.

Conclusions and Future Directions

In summary, a system has been established and applied to evaluate the data acquisition process from

sensor interface to delivered digital tape at crash test sites conducting tests under the auspices of the U. S. National Highway Traffic Safety Administration (NHTSA). This evaluation testing is currently conducted every six months at crash test sites performing tests under the NHTSA NCAP and vehicle to barrier FMVSS 208 testing programs. It is also carried out at NHTSA biomechanics and components test facilities on an as needed basis. Moreover, the associated hardware and signal processing software can be made available to crash test sites outside of NHTSA.

Current evaluation testing results indicate that all the active NHTSA NCAP and FMVSS 208 crash sites satisfy the present performance requirements. As demonstrated in the previous section, the reduction in test data variations due to data acquisition has been more than an order of magnitude within the last decade. The performance measures for the data acquisition systems of the above-mentioned facilities are well inside the performance requirements for all the amplitude and time performance measures. This is underscored by the fact that there have been significant advances in the data acquisition technology in the last decade.

Additional performance requirements such as phase delay and time linearity are planned to be incorporated into the processing software. Also, for improved maintenance and reliability, off-the-shelf boards and units are being investigated as possible replacements for the current SWG hardware. The new hardware will provide basically the same waveform signals.

Overall, a study of representative NHTSA crash and biomechanics test site facilities to assess test environment and capabilities is planned for 1992. The purpose is to identify other data quality and integrity issues related to the sensors and the dynamic test events that need to be addressed. Given that data acquisition is the most controlled aspect of the crash testing process, the emphasis of this study will be on sensors, calibration practices, test procedures, film/video data collection, and quality control practices etc.

Appendix A

Table A-1. Occupant Channel Processed Data Summary for Site1 Data Acquisition Test of 10 Sep 1990

SENSOR	FILNO	TO_OFFSET MSEC	AMPDEVPOS %FS	AMPDEVNEG %FS	OVRST %FS	AMPLINREF %FS	AMPLINBFSL %FS	AR1640 dB	HSHIC %	CTCTD MSEC	CRSHIC %
HEDX1	0018.001	0.000	-0.361	0.300	10.076	0.460	0.147	-3.08	-0.11	0.000	-0.01
HEDY1	0018.002	0.000	-0.351	0.270	9.764	0.430	0.092	-3.16	-0.21	0.000	0.01
HEDZ1	0018.003	0.000	-0.281	0.409	9.930	0.470	0.192	-3.13			
HEDX2	0018.014	0.000	-0.240	0.367	10.075	0.444	0.130	-3.07	-0.04	-0.001	-0.05
HEDY2	0018.015	0.000	-0.285	0.367	9.788	0.475	0.084	-3.13	-0.10	0.001	0.31
HEDZ2	0018.016	0.000	-0.335	0.405	9.949	0.486	0.086	-3.08			
CSTX1	0018.005	0.000	-0.316	0.294	9.755	0.381	0.054	-3.13	-0.13	-0.004	0.33
CSTY1	0018.006	0.000	-0.358	0.325	9.974	0.410	0.077	-3.06	-0.16	-0.004	0.11
CSTZ1	0018.007	0.000	-0.301	0.419	9.686	0.439	0.063	-3.16			
CSTX2	0018.018	0.000	-0.292	0.375	9.780	0.446	0.079	-3.12	-0.07	-0.003	0.56
CSTY2	0018.019	0.000	-0.255	0.369	9.976	0.435	0.097	-3.02	-0.15	-0.005	0.28
CSTZ2	0018.020	0.000	-0.293	0.418	9.730	0.452	0.109	-3.12			
LF1	0018.004	0.000	-0.318	0.410	9.788	0.520	0.127	-3.12			
RF1	0018.008	0.000	-0.336	0.403	9.835	0.458	0.082	-3.15			
LF2	0018.017	0.000	-0.261	0.444	9.762	0.478	0.091	-3.10			
RF2	0018.021	0.000	-0.317	0.417	9.652	0.509	0.116	-3.21			

Table A-2. Processed Data Summary for Site4 Acquisition System Test of 12 April 1991

SENSOR	FILNO	TO_OFFSET MSEC	AMPDEVPOS %FS	AMPDEVNEG %FS	OVRST %FS	AMPLINREF %FS	AMPLINBFSL %FS	AR1640 dB	HSHIC %	CTCTD MSEC	CRSHIC %
HDCG1X	0022.014	0.122	-0.104	-0.101	9.230	0.120	0.066	-3.26			
HDCG1Y	0022.015	0.000	-0.186	-0.166	9.125	0.133	0.079	-3.39	-0.66	0.009	0.05
HDCG1Z	0022.016	0.000	-0.192	-0.166	9.181	0.159	0.083	-3.34	-0.69	0.019	-0.03
CHST1X	0022.017	0.000	-0.173	-0.133	8.999	0.159	0.065	-3.28			
CHST1Y	0022.018	0.000	-0.142	-0.116	9.002	0.129	0.073	-3.38	-0.82	0.011	-0.16
CHST1Z	0022.019	0.000	-0.127	-0.136	9.011	0.134	0.070	-3.32	-0.78	0.022	-0.17
FMRR1	0022.020	0.000	-0.165	-0.057	9.174	0.135	0.050	-3.37			
FMRL1	0022.021	0.000	-0.160	-0.032	9.141	0.174	0.066	-3.17			
HDCG2X	0022.026	0.122	-0.141	-0.119	9.277	0.238	0.194	-3.30			
HDCG2Y	0022.027	0.000	-0.135	-0.139	9.074	0.209	0.168	-3.39	-0.79	0.009	-0.20
HDCG2Z	0022.028	0.000	-0.144	-0.149	9.102	0.187	0.165	-3.35	-0.64	0.018	-0.16
CHST2X	0022.029	0.000	-0.141	-0.066	9.057	0.199	0.143	-3.32			
CHST2Y	0022.030	0.000	-0.003	0.023	9.380	0.156	0.130	-3.35	-0.35	0.012	0.18
CHST2Z	0022.031	0.000	-0.154	-0.181	9.038	0.160	0.139	-3.31	-0.69	0.020	-0.12
FMRR2	0022.032	0.000	-0.232	-0.105	9.226	0.219	0.133	-3.40			
FMRL2	0022.033	0.000	-0.180	-0.148	9.089	0.201	0.169	-3.38			

Table A-3. Occupant Channel Processed Data Summary for Site2 Data Acquisition Test of 12 Sep 1990

SENSOR	FILNO	TO_OFFSET MSEC	AMPDEVPOS %FS	AMPDEVNEG %FS	OVRST %FS	AMPLINREF %FS	AMPLINBFSL %FS	AR1640 dB	HSHIC %	CTCTD MSEC	CRSHIC %
HEDX1	0015.001	0.100	-0.499	0.385	3.465	0.832	0.383	-3.28	-0.12	0.042	1.65
HEDY1	0015.002	0.100	0.218	0.492	3.249	0.944	0.328	-3.68	0.08	0.026	0.77
HEDZ1	0015.003	0.000	-0.373	0.363	3.051	0.846	0.391	-3.41			
HEDX2	0015.009	0.100	-0.648	-0.311	3.287	0.727	0.360	-3.30	-1.44	0.042	-0.46
HEDY2	0015.010	0.100	-0.292	0.265	3.011	0.805	0.514	-3.67	-0.56	0.032	1.04
HEDZ2	0015.011	0.100	-0.650	-0.242	3.028	0.816	0.402	-3.45			
CSTX1	0015.004	0.100	-0.090	-0.029	3.484	0.490	0.369	-3.24	-0.34	0.031	0.40
CSTY1	0015.005	0.000	0.001	0.544	3.110	0.953	0.369	-3.56	0.15	0.015	2.51
CSTZ1	0015.006	0.000	0.010	0.356	2.920	0.723	0.280	-3.34			
CSTX2	0015.012	0.100	-0.187	0.232	3.133	0.538	0.344	-3.29	-0.36	0.033	0.30
CSTY2	0015.013	0.100	1.131	1.462	2.988	1.465	0.452	-3.62	1.29	0.007	2.52
CSTZ2	0015.014	0.100	-0.206	0.329	2.984	0.617	0.353	-3.38			
FMRL1	0015.007	0.100	-0.209	0.564	3.348	0.628	0.178	-3.28			
FMRR1	0015.008	0.100	-0.113	0.214	2.921	0.511	0.229	-3.62			
FMRL2	0015.015	0.000	-0.281	0.526	2.965	0.612	0.163	-3.42			
FMRR2	0015.016	0.000	-0.191	0.521	3.356	0.671	0.213	-3.39			
NECX1	0015.030	0.000	-0.132	0.569	3.231	0.697	0.268	-3.22	0.30	0.037	1.27
NECY1	0015.031	0.000	-0.104	0.450	2.902	0.516	0.302	-3.60	0.10	0.016	0.88
NECZ1	0015.032	0.000	-0.085	0.667	2.941	0.800	0.249	-3.38			
NCMX1	0015.033	0.100	-0.070	0.655	3.318	0.640	0.248	-3.21	0.49	0.040	1.24
NCMY1	0015.034	0.100	-0.169	0.479	2.964	0.507	0.160	-3.59	0.31	0.036	0.24
NCMZ1	0015.035	0.100	-0.109	0.708	3.018	0.628	0.240	-3.34			
NECX2	0015.036	0.000	-0.117	0.482	3.247	0.461	0.180	-3.29	-0.34	0.036	0.54
NECY2	0015.037	0.000	-0.155	0.531	2.941	0.563	0.180	-3.60	-0.17	0.013	0.75
NECZ2	0015.038	0.000	-0.280	0.663	2.908	0.654	0.206	-3.45			
NCMX2	0015.039	0.000	-0.214	0.334	3.283	0.393	0.171	-3.21	-0.40	0.038	0.41
NCMY2	0015.040	0.000	-0.464	0.227	2.919	0.592	0.215	-3.60	-0.53	0.031	0.84
NCMZ2	0015.041	0.000	-0.416	0.476	2.907	0.639	0.196	-3.48			
DSPL1	0015.042	0.025	1.071	-1.037	2.998	1.265	0.268	-3.37			
DSPL2	0015.043	0.018	0.640	-0.838	3.581	0.986	0.227	-3.39			

Table A-4. Occupant Channel Processed Data Summary for Site3 Data Acquisition Test of 29 Nov 1990

SENSOR	FILNO	TO_OFFSET MSEC	AMPDEVPOS %FS	AMPDEVNEG %FS	OVRST %FS	AMPLINREF %FS	AMPLINBFSL %FS	AR1640 dB	HSHIC %	CTCTD MSEC	CRSHIC %
HEDX1	0019.002	0.125	-0.129	0.147	6.290	0.207	0.077	-2.26	-5.06	0.001	-4.09
HEDY1	0019.003	0.125	-0.058	0.120	6.342	0.254	0.139	-2.19	-4.96	0.000	-4.15
HEDZ1	0019.004	0.125	0.128	-0.030	6.304	0.186	0.105	-2.23			
HEDX2	0019.018	0.250	-0.229	0.099	7.356	0.243	0.104	-2.23	-5.37	-0.003	-4.26
HEDY2	0019.019	0.250	-0.206	0.068	7.252	0.272	0.124	-2.21	-5.52	-0.005	-4.30
HEDZ2	0019.020	0.250	0.038	-0.113	7.201	0.157	0.124	-2.29			
CSTX1	0019.006	0.125	0.119	0.001	6.413	0.161	0.118	-2.15	-4.83	-0.007	-4.11
CSTY1	0019.007	0.125	0.005	-0.269	6.012	0.398	0.449	-2.32	-4.90	-0.003	-4.05
CSTZ1	0019.005	0.125	0.005	0.334	6.016	0.241	0.156	-2.24			
CSTX2	0019.021	0.250	-0.159	0.211	7.067	0.262	0.087	-2.38			
CSTY2	0019.022	0.250	0.061	0.007	7.377	0.183	0.122	-2.25	-5.31	0.001	-4.21
CSTZ2	0019.023	0.250	-0.001	-0.168	7.039	0.226	0.182	-2.32	-5.32	-0.002	-3.95
LF1	0019.009	0.125	0.003	0.087	6.352	0.136	0.123	-2.50			
RF1	0019.010	0.250	0.016	-0.044	6.642	0.232	0.246	-2.37			
LF2	0019.025	0.250	0.031	0.197	7.108	0.151	0.149	-2.43			
RF2	0019.026	0.250	0.054	0.029	7.130	0.123	0.076	-2.17			
NEFX1	0019.011	0.250	-0.060	-0.036	6.627	0.116	0.106	-2.27	*		
NEFY1	0019.012	0.250	-0.024	-0.101	6.465	0.101	0.091	-2.37	*		
NEFZ1	0019.014	0.250	-0.061	0.094	5.723	0.303	0.186	-2.82	*		
NEMX1	0019.013	0.250	0.035	0.008	6.510	0.116	0.092	-2.39	*		
NEMY1	0019.016	0.250	-0.033	-0.292	6.594	0.299	0.155	-2.40	*		
NEMZ1	0019.015	0.250	-0.068	-0.178	6.379	0.071	0.052	-2.39	*		
NEFX2	0019.027	0.250	0.031	0.037	7.214	0.178	0.170	-2.07	-0.57	0.008	-0.27
NEFY2	0019.028	0.250	0.017	-0.013	7.243	0.167	0.134	-2.07	-0.25	0.009	-0.05
NEFZ2	0019.029	0.250	0.166	0.164	7.081	0.255	0.105	-2.10			
NEMX2	0019.030	0.250	0.055	0.068	7.307	0.210	0.138	-1.96			
NEMY2	0019.031	0.250	0.030	-0.035	6.987	0.152	0.136	-2.03	-0.33	0.003	0.05
NEMZ2	0019.032	0.250	0.134	0.117	7.131	0.239	0.120	-1.92	-0.21	0.005	
0.06											

* All three channels from neck force sensor were provided group 1 waveform and all three neck moment channels were provided group 2 waveform so that HIC analyses could not be performed on these channels.

Table A-5. SITE1—Simple Statistics of Vehicle Channels Performance Measures

Variable	N	Minimum	Maximum	Mean	Std Dev
TOFF	53	0	0	0	0
ADEVPOS	53	-0.3650000	-0.0840000	-0.2258302	0.0945135
ADEVNEG	53	-0.0140000	0.4700000	0.2676604	0.1314761
OVRST	53	9.6960000	10.1350000	9.8951887	0.1020415
ALINREF	53	0.1130000	0.4990000	0.2690189	0.1081832
ALINFS	53	0.0380000	0.2060000	0.0908491	0.0328729
LR1640	53	0.6934258	0.7063176	0.7006559	0.0033208

Table A-6. SITE2—Simple Statistics of Vehicle Channels Performance Measures

Variable	N	Minimum	Maximum	Mean	Std Dev
TOFF	49	0	0.1200000	0.0346939	0.0530370
ADEVPOS	49	-1.7410000	1.6370000	0.4652041	0.5264503
ADEVNEG	49	-2.4560000	0.9720000	-0.3724490	0.6708323
OVRST	49	1.4450000	3.7270000	2.7526735	0.6343538
ALINREF	49	0.4430000	2.2030000	0.8108980	0.3558828
ALINFS	49	0.0480000	0.3160000	0.1386327	0.0692886
LR1640	49	0.6486344	0.8241381	0.6982243	0.0547784

Table A-7. SITE3—Simple Statistics of Vehicle Channels Performance Measures

Variable	N	Minimum	Maximum	Mean	Std Dev
TOFF	55	0.1250000	0.2500000	0.2045455	0.0606849
ADEVPOS	55	-0.3290000	0.3340000	0.0171273	0.1299507
ADEVNEG	55	-0.3060000	0.3750000	0.0645273	0.1320784
OVRST	55	5.8710000	7.5640000	6.6779636	0.4386953
ALINREF	55	0.0940000	0.9090000	0.2631636	0.1715741
ALINFS	55	0.0670000	0.5350000	0.1901273	0.1276716
LR1640	55	0.7087613	0.7952433	0.7657625	0.0124962

Table A-8. SITE4—Simple Statistics of Vehicle Channels Performance Measures

Variable	N	Minimum	Maximum	Mean	Std Dev
TOFF	44	0	0.2450000	0.0638182	0.0721182
ADEVPOS	44	-0.6190000	0.1250000	-0.1530227	0.1804157
ADEVNEG	44	-0.3070000	0.3200000	-0.1020682	0.1712189
OVRST	44	8.8440000	9.3430000	9.1110455	0.1144113
ALINREF	44	0.0920000	0.7200000	0.2651591	0.1891344
ALINFS	44	0.0570000	0.4150000	0.1662273	0.1036878
LR1640	44	0.6691138	0.6854882	0.6789842	0.0040024

Appendix B. Abbreviations and Acronyms

DAC: digital-to-analog converter
DAS: data acquisition system (In this report, DAS primarily refers to a crash test data acquisition system.)
DFT: discrete Fourier transform
DT0: delayed time-zero
EPROM: erasable programmable read-only memory
HIC: head injury criterion (a number computed to indicate the severity of head injury)
Mhz: megahertz
ms: milliseconds
Mv: millivolts
PDAS: precision data acquisition system (refers to the data acquisition system used for testing a SWG)
PPM: parts per million
SAE: Society of Automotive Engineers
S/N: serial number
SPSW: signal processing software (refers to software developed to analyze SWG output waveforms)
SWG: signal waveform generator
T0: time-zero
TTL: transistor-transistor-logic
μs: microseconds

References

1. Hollowell, W. T., Arendt R. H., "Data Integrity Assessment of the New Car Assessment Program," Proceedings of the 9th International Technical Conference on Experimental Safety Vehicles, Kyoto, Japan, November 1982.
2. Arendt, R. H., Miller P. M., "Test Site Instrumentation Study," U.S. Department of Transportation, National Highway Traffic Safety Administration, Washington, DC, DOT HS-805-979, June 1981.
3. Arendt, R. H., Voytovich G. L., Mcgrath M. T., Miller P. M., "Test Site Instrumentation Study-Phase II," U.S. Department of Transportation, National Highway Traffic Safety Administration, Washington, DC, DOT HS-805-979, June 1981.
4. MGA Research Corporation, *Operator's Manual for Waveform Generator Model RPG-6236-A*, U.S. Department of Transportation, National Highway Traffic Safety Administration, Washington, DC, February 1988, DOT-HS-807-218, 36 p.
5. MGA Research Corporation, *Waveform Generator Signal Processing Software*, U.S. Department of Transportation, National Highway Traffic Safety Administration, Washington, DC, September 1988, DOT-HS-807-312, 172 p.
6. SAS Institute Inc. (1990), *SAS/STAT User's Guide*, Version 6, 4th Ed., Volume 2, Chapter 24.
7. SAS Institute Inc. (1988), *SAS Procedures Guide*, Release 6.03 Edition, Chapter 13.
8. Society of Automotive Engineers, Inc., "Instrumentation for Impact Tests," SAE J211OCT88, October 1988, 21 p.

S9-W-27

New Technique Used by P.S.A. for Creating Dynamic Test Apparatus Enabling Crash Simulation in Accordance with Programmed Laws

G. Mauron, F. Bocaly, F. Laurent
PSA Peugeot - Citroen
A. Depret-Bixio, A. Grenier
Domange-Jarret

Abstract

The originality of the technique used, developed by the Domange-Jarret company, is based on the compression of visco-elastic fluids (gums, silicones) by appropriate mechanical or hydraulic means. The fundamental principle of this technique consists of primarily using the pasty viscosity of this fluid, which is far greater than other fluids, as a shock absorbing function; with its compressibility characterizing a spring or accumulator function. The results obtained are developed and a statement is presented in terms of performance and reliability being the main advantages of using this technique.

Introduction

Greater research into the area of safety has led to developments in dynamic experiments and appropriate measurement techniques. A crash simulation is carried out by an experiment on a trolley to determine the characteristics and performance of the means of protection. This simulation is achieved by representing the deceleration of the vehicle occupants and the essential quality of the simulation must be the possibility of faithfully reproducing it. In fact, a one-off test proves nothing. Only by working on the tests of repeatable and comparable tests can the aim of improving the product be pursued.

This deceleration representation was obtained in our laboratories by various procedures which have evolved over the years, in order to constantly improve test repeatability and reproduction. In the 1960's trolley deceleration was achieved by layers of lead tubes; towards the 1970's by collapsing metal tubes, then by the forced movement of an olive-shaped metallic device creating radial deformation of polyurethane cones. This technique was used and recommended in the ECE 16 and 44 regulations. Since 1988, the use of trolley-mounted hydrostatic deceleration programmers (Figure 1) has been a beneficial replacement of the polyurethane impact absorbers both in terms of results and ease of use.

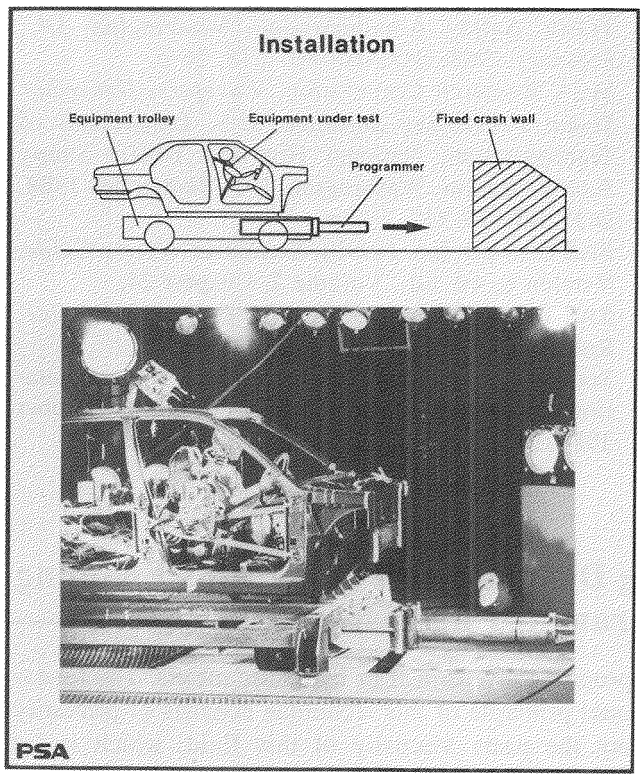

Figure 1. Impact Test Bed Deceleration Programmer

The latest stage has been to install an acceleration test bed which enables the study of the behavior under impact of specific components without requiring the vehicle to be destroyed as the impact sequence is simulated by the acceleration of a trolley on which an automobile body is mounted (Figure 2), (Figure 1, Figure 2).

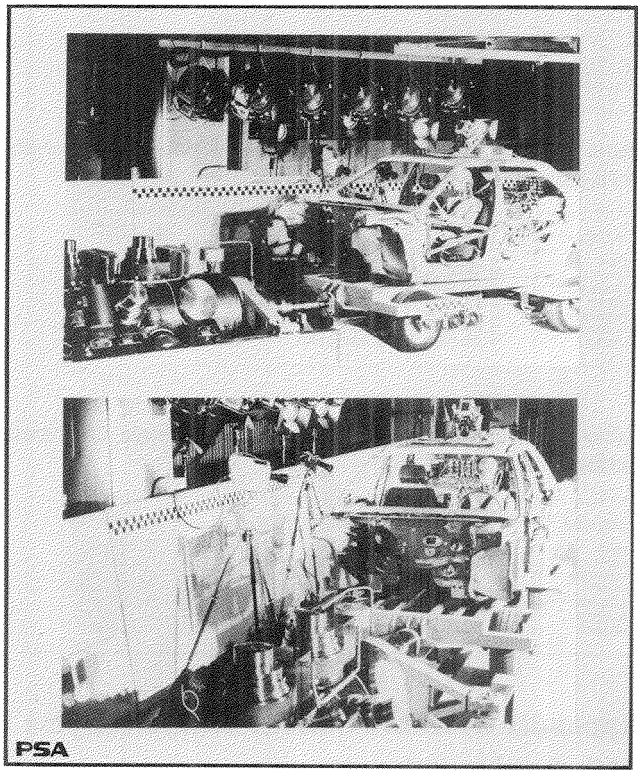

Figure 2. Crash Simulation on the Acceleration Test Bed

Acceleration Test Bed or Inverted Acceleration Catapult

Function

When a vehicle collides with an obstacle, the impact is comparable to that of spontaneous acceleration from an initial rest position. Once the required speed has been reached, impact occurs and the trolley can be gently braked by mechanical means over a long distance. The goal to be attained with the launcher being to accelerate a mobile mass of between 1.5t and 2t in accordance with a defined law of acceleration. The effort/displacement diagrams produced correspond to the ECE 44 and 16 regulations (Figure 3) for a mobile mass of up to 2,000 kg. Other profiles can be envisaged, in particular representing the deceleration laws noted during vehicle impacts at speeds of up to 60 k.p.h. The speed with which the test can be set up enables it to be run several times in the same day.

Catapult Assembly

The test method comprises 3 distinct parts (Figure 4):

The propulsion shaft. On arming, the shaft moves the mobile trolley via a magnetic coupling and, on firing the shaft accelerates the trolley (coupling unlocked). The propulsion shaft is a long metallic rod which can be finely adjusted, directly operated by the main energy

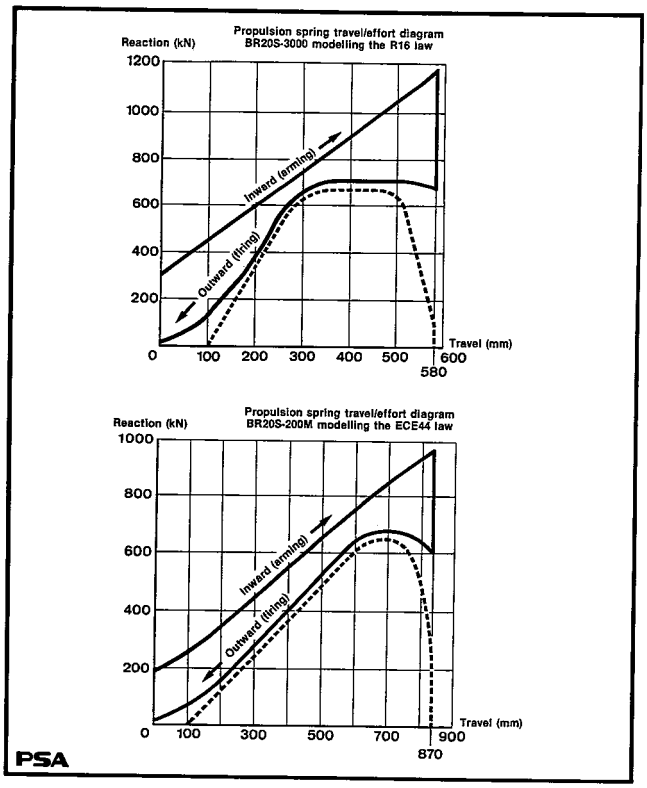

Figure 3. Travel/Effort Diagram

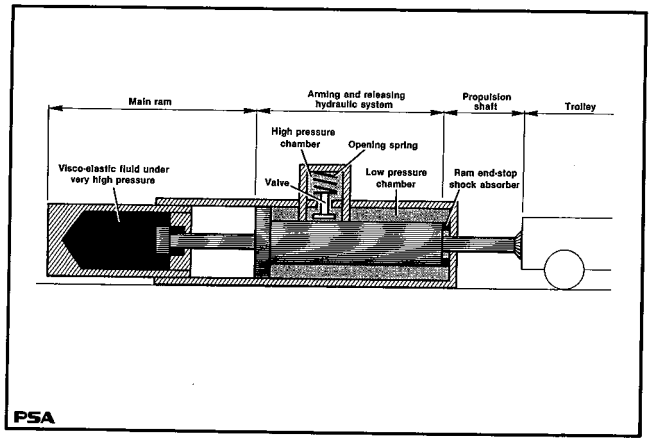

Figure 4. Representation in the "Unarmed" Position

accumulating spring. This precisely machined and ground shaft constitutes the only link between the calculated effort spring and the test trolley. It is therefore the longest part of the catapult. It enables the ironing out of slack inherent in the gears and other moving parts which could influence the trolley's law of acceleration.

The hydraulic arming system. This is the most complex part of the catapult. This system comprises: an hydraulic power unit, a frame enclosing the propulsion shaft, and nine relief valves mounted on the frame.

The hydraulic power unit arms the main ram and the valve springs. Its characteristics are: a pressure of 350 bar, an electrical power of 30 kW at 1,500 R.P.M., an output of 4.51/min., and a 600 litre capacity tank. It is installed in a ditch behind the catapult.

The frame is the largest mechanical part of the catapult and represents the main body. Briefly, it comprises a 5m long, 800 mm diameter cylinder. Everything is arranged around this element. The propulsion shaft crosses it from end to end, and around it are set the nine valves in three rows and at 120 degrees from each other. The frame is rigid enough to restrain the nine eccentric 300 kg weights and to withstand the shock of the catapult release. It also houses the main ram low pressure chamber.

The valves form the trigger which sets off the main ram. They are mounted on the frame. The valves are closed by high pressure (320 bar) hitting the piston and pushing the valve down onto its seat. An elaborate mechanism ensures that valve opening, taking 10 ms., is almost instantaneous (Figure 3, Figure 4).

In order to reduce the time required to evacuate the oil from the high pressure chamber, this evacuation is activated simultaneously on all nine valves and is achieved via an hydraulic system with drilled blocks forming three successive levels of opening slide mechanisms. The valve is then pushed by the spring.

This spring is of a design similar to that of the main ram. Its operation is based on hydrostatic compression of silicon gum. The gum is submitted to very high pressure: 3,000 bar. The spring pushing the valve has a take-up movement of 1mm for a compression travel of 43mm. The effort applied is 530 kN at the beginning of travel going to 190 kN at the extent of travel, the variation being linear. As the valves are of 120 mm diameter, the total area available to evacuate low pressure oil when the catapult is fired is 1,000 cm2. Such a surface area was considered necessary to guarantee proper oil evacuation: it was imperative to ensure that when the oil is escaping it in no way hinders correct propulsion shaft travel.

The main ram is an energy absorbing spring operating by compressing visco-elastic fluid under a very high pressure (above 3,000 bar). It catapults the trolley following a given acceleration law. The originality of the technique used, a technique which is patented, is based on the hydrostatic compression using suitable mechanical devices, of visco- elastic elastomers. These elastomers are silicones obtained by the synthesis of organic silicium compounds. They are in the form of gum which are polycondensed with a very high molecular weight. If an elastomer is subjected to a sufficiently high variation in volume, this material undergoes an increase in pressure, the value of which is similar to that of liquids. For example, for a volume reduction of 13%, the pressure can pass from 1 to 3,000 bar. This compressibility characterizes the spring function. The given travel/acceleration functional diagram is created here by judicious adjustment of sliding pistons inside a tank of silicone gum.

Operating Phases (Figure 5)

Arming. The hydraulics compress the main energy-absorbing spring ram and retain it cocked until firing. The arming sequence starts with the closure of the nine valves. The pressure increases in each valve to tighten each spring. In fact, the valves operate in the opposite way to car engine valves. Once the valves are closed by the 320 bar high pressure, the hydraulic power plant output is directed to the low pressure chamber. By increasing the pressure in the main body the propulsion shaft is pushed in and the main ram is armed. The circuit is not perfectly sealed and oil leaks from around the main ram in the catapult body. An arrangement of organized leakage has been preferred as opposed to one with seals as they would have to be large in diameter (300 mm) and would be submitted to violent and wearing shocks which would mean that the seal could not be guaranteed. Once the main ram (i.e. the energy absorbing spring ram) is compressed to the point determined for the test, the firing sequence can begin (Figure 5).

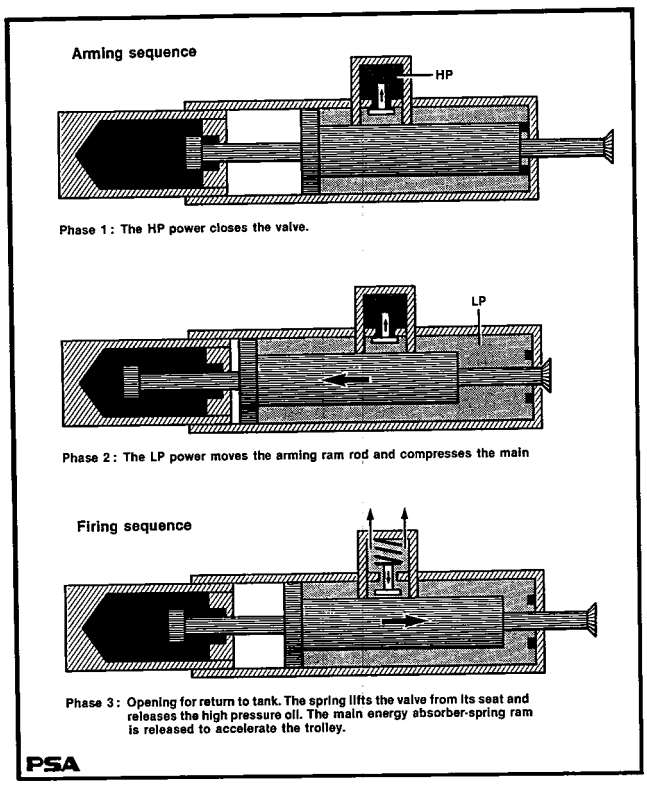

Figure 5. Operating Principle Diagrams for Both Sequences

The firing. The rapid firing accelerates the mobile trolley in a very short time—about 10 ms. The firing sequence is activated by electric relays which simultaneously energize the drilled valve blocks.

A cascade of slide mechanisms free the fluid in the high pressure chamber and the springs can then push the valves and they open. In turn they cause the fluid in the main body to be released (low pressure chamber) and the main ram is activated. Releasing this energy absorber-spring ram catapults, according to the pre-determined law of deceleration, the propulsion shaft which is pressed against the trolley. At the end of the shaft travel, as the trolley has no mechanical link with the ram, it is propelled towards the braking area.

For safety reasons, if one wishes to stop the firing sequence at the end of the arming sequence, a manually operating valve enables the pressurized oil to be freed, causing a very slow firing of the apparatus and then the progressive opening of the nine valves.

Optical and Physical Data Collection

The measurement equipment which can be fitted for impact is modular and does not require any electrical connection to the outside during the test. This equipment consists of completely autonomous data acquisition boxes which can be placed simultaneously at different points. Each box enables complete data acquisition on 16 or 32 channels according to the type. The maximum recording time is 6 seconds per channel. The sampling frequency is 10 kHz with 12 bit resolution. The operating autonomy of each box is about 15 minutes for the vital functions (sensor supply, internal control, Ethernet communication...) and 2 hours for memory storage. This equipment has been designed to withstand repeated impacts of 70g half-sine for 11 ms. The internal logic automatically advises the VAX central computer of the identity of the sensors fitted for the test thus preventing any possible wiring errors. During the complete preparation phase the one or more data collection boxes are linked to the computer system via the Ethernet network. At the moment of firing, the outside electricity supply is automatically disconnected and, from the initial moment of impact the measurements are stored in the internal memory of the fitted boxes. Just after the test, the power supply is reconnected in the vehicle to the computer network and the collected data is transferred. These measurements are then validated and stored in the central computer.

High speed 16mm cameras are mounted on the trolley and on the ground. Two high speed, 400 frames per second, color VHS video recorders are also installed. It is thus possible to quickly verify the initial visual tests using the high speed video trajectography software.

After developing and by using a high resolution (1250 x 2592 pixels) black and white scanner, the numerized images are stored on a high capacity hard disc (capacity 3 gigabytes). A detailed software programme enables 256 different points in the frame to be automatically logged (special lines of sight or random points) by using contrast and shape recognition analysis techniques. The same programme, in its analysis mode gives very quick access to the main graphic and calculation results by using a high resolution work station (Figure 6), (Figure 7, Figure 8).

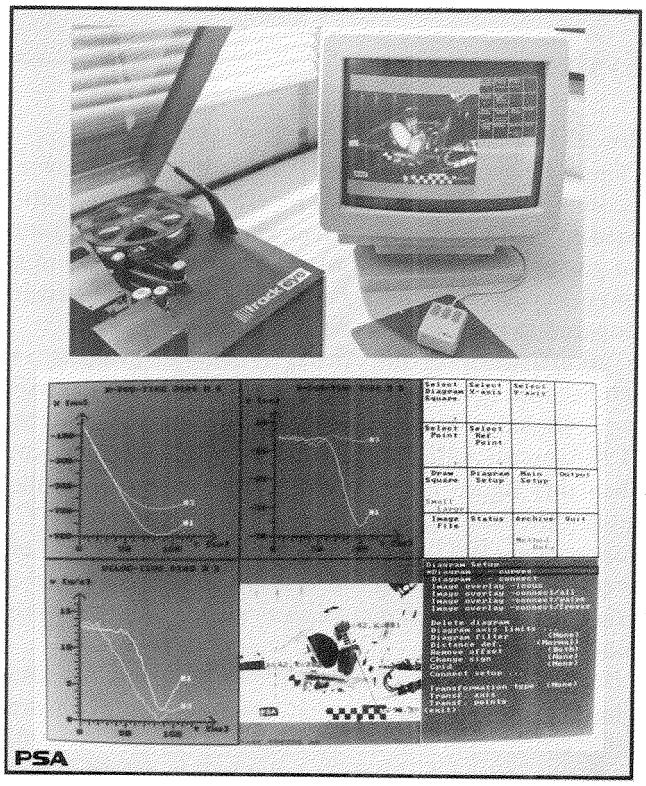

Figure 6. Numerized Image Automatic Analysis

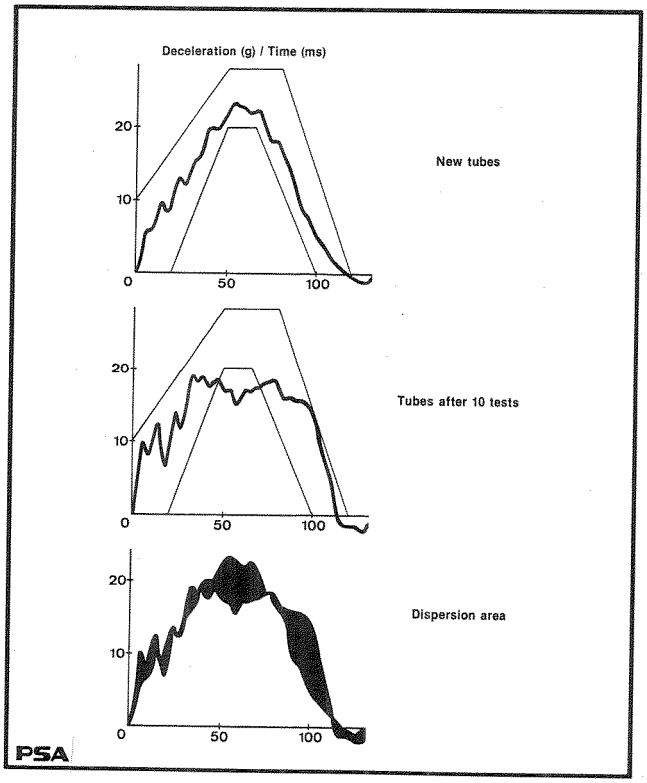

Figure 7. Dispersion Registered with Polyurethane Tubes on the Deceleration Curve of Regulation 44

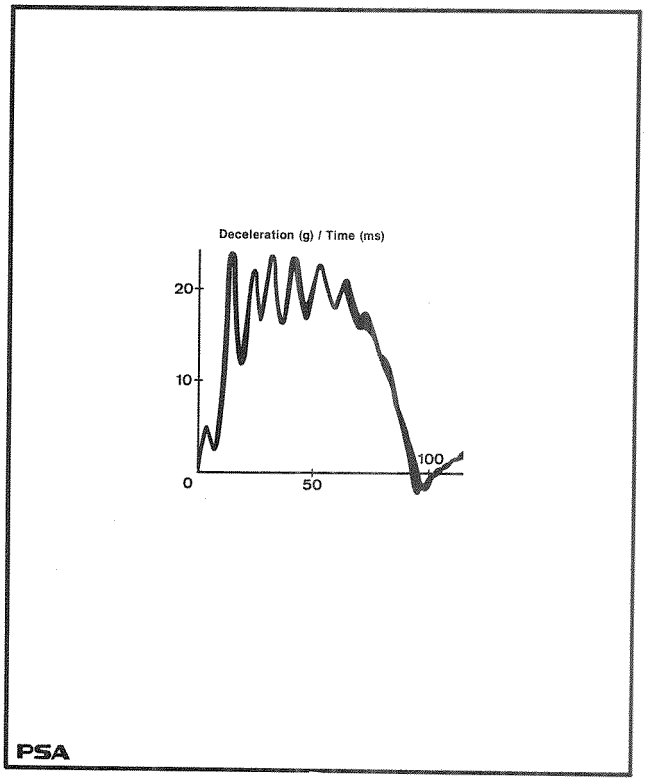

Figure 8. Dispersion Area Obtained with Hydrostatic Deceleration Programmer

Crash Simulation Reliability

To validate the feasibility and repeatability of a firing, the work has essentially focussed on interpreting the results obtained in the field of the trolley acceleration curve and by comparing these results over several successive firings.

This methodology has enabled us to evaluate the dispersions, quantify them and graphically reproduce them on an area chart. Thus, we have been able to note that the polyurethane tubes dispersion area (Figure 7) used for trolley deceleration was far greater than that of the hydrostatic deceleration programmers (Figure 8).

The acceleration test bed uses the same technique as the programmers, thus giving the similar low dispersion rates, and with no wear or ageing affecting the test reliability and repeatability is almost permanently guaranteed; and this for each deceleration law defined by a specific visco-elastic spring.

Conclusion

An acceleration test bed, with the aim of carrying out dynamic experiments simulating vehicle crash deceleration, based on visco-elastic fluid technology, produces very good repeatability and representation of the law being studied.

This technique, more compact and less costly than the Hyge test beds is an attractive solution for the technological development of crash simulation and experimental laboratories.

S9-W-29

A New Compact European Driver Airbag System

Michel Kozyreff
Autoliv Klippan
Dieter Schaper
Autoliv GmbH

Abstract

The use of the 3 points safety belt has saved a great number of human lives. Head impacts onto the steering-wheel still cause deaths but, moreover, a lot of face injuries. Airbags are good answers to the problem. When the bag dimension is limited to 30 1, the protection function is achieved and most of the drawbacks are avoided. This makes low cost design possible. Some of the functions need optimization, while the inflator requires a complete change of technology as proposed by Autoliv and Livbag.

Introduction

Airbags are now part of the daily life in the North American car industry. This is due to the system efficiency but also to the powerful incentive of the FMVSS 208 standard.

In this context, Airbags are one of the answers to the requirement of passive restraint; the consumers have rapidly preferred this solution rather than the passive belts and an increasing majority of cars are now so equipped in the United-States (Figure 1).

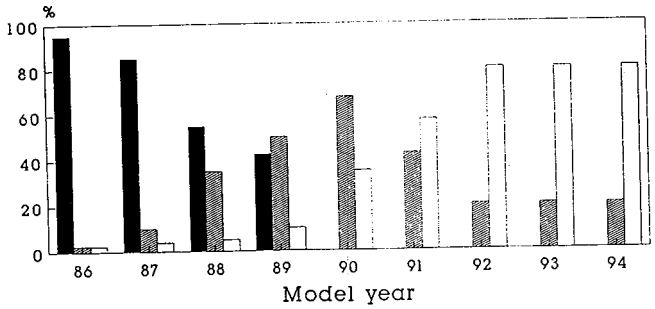

Figure 1. Market Share of the Various Restraint System for Front Seat in the United States

The first result of this situation is that Airbags developed for this market have many features which are not required for the basic function of the Airbag: a system purely supplementary to the seat belt.

In Europe, there is no legal support to help the Airbag market to increase; on the other hand this allows the industry to focus on the real function of the Airbag and to implement them at a considerably lower cost compared to their American counterparts.

The Efficiency of the Airbag

The efficiency of the three point belt is well known. According to D. Viano (1990) its efficiency can be estimated to be 42 % for the driver and 39 % for the front seat passenger. In other words, the risk to be killed in a frontal impact is reduced by 42 % for a belted driver compared to an unbelted one.

The efficiency of the Airbag is hard to evaluate as such because its introduction started together with "belt laws." Globally, D. Viano estimates its efficiency to be a 4 % increase with the three point belt as a reference. When this figure is compared to the system cost, the global efficiency appears even lower as shown by C. Chillon et al (1987). A conclusion is that the number of saved lives is not enough to justify the existence of the Airbag which is much more expensive than a usual three point belt.

However, the efficiency of a restraint system has also to be evaluated considering non lethal injuries which are highly costly from human and social standpoint. According to this criterion, the three point belt is definitely not the ultimate restraint system because the user's face and head are the most exposed part of the body in an accident.

The United-Kingdom provides very interesting data on this problem: the enforcement of belt use is relatively recent and has resulted in usage rate of about 95 %.

The investigation conducted by P. Harms et al (1983, 1987) shows that, for belted drivers involved in a frontal impact (see Figures 2, 3, 4):

- head injuries caused by an impact onto the steering-wheel are met in 30 % of the considered cases when the impact velocity is between 30 kph and 50 kph
- when the velocity is above 50 kph, the head injuries are met in more than 65 % of the cases
- among the entire sample, 25 % of the head injuries are caused by an accident occurring with a velocity change less than 27 kph, the proportion raising up to 50 % when the velocity change is less than 34 kph
- 97 % of the head injuries are AIS 1 or 2 but many are physically or psychologically painful. For instance, 21 % of the injuries are nose or teeth fractures
- head impacts onto the steering-wheel are responsible for 1 % of the deaths

Equivalent data are resulting from research conducted in France and Germany as explained by D. Danner et al (1987).

It appears clearly that despite the very high efficiency of the three point belt as far as the number of fatalities is concerned, some cases are still observed that are caused by head impact onto the steering-wheel. The

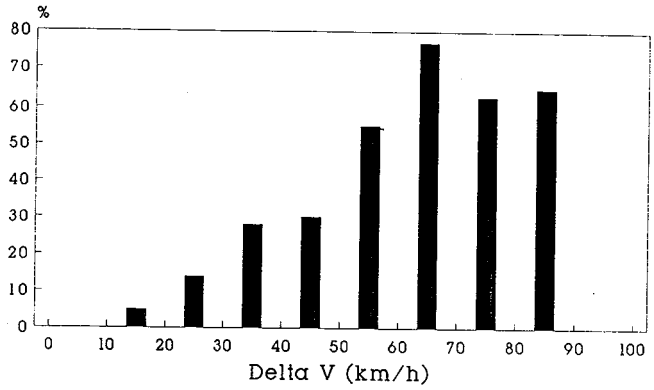

Figure 2. Frequency of Injuries Due to a Head to Steering-Wheel Impact for Different Vehicles of Front Impact

AIS	Head injuries	
	No	Percent
1	403	73
2	130	24
3	1	0
4	11	2
5	3	1
6	0	0
Total	548	100

Figure 3. Distribution of Head Injuries as a Function of Their Severity

Injury type	Percent
Damages soft tissues	59
Fractures	27
Unconsciousness	14

Figure 4. Head Impacts on Steering-Wheel (Injury Types Versus Frequency)

injuries resulting of such impacts are met in a very high number; they are unacceptable. This is the reason why steering-wheels are the main target for restraint system developers in countries where the usage of the three point belt is mandatory.

Recent improvements of the energy absorbing characteristics of the steering-wheels are only partial answers. I. Myklebust et al show that face fractures occur when the transmitted load exceeds 1 kN and when it is concentrated on a small area. No steering-wheel, even equipped with an energy absorbing padding, can induce lower values when the head impact velocity exceeds 9 m/s.

It appears that the Airbag is the solution to the problem; but it has to be optimized in order to be a purely supplementary system protecting the driver's head from impact onto the steering-wheel: this is the Eurobag concept.

Required Characteristics for the Protection Function

Electrolux-Autoliv used all available techniques in order to select the optimal size of the Eurobag with a result confirming L. Johansson et al work (1987).

Intensive computer simulation using Drisim and Madymo gave minimum HIC values with bag volumes below 35 liters. No advantage was found in using larger bag volumes.

Sled tests and full size car crashes with different car models confirmed the computer simulation whatever the criterion: HIC, contact pressure, laceration. The Figure 5 is comparing head resultant accelerations and HIC 36 when 70 liter and 30 liter Airbags are added to a three point belt in a 50 kph sled test. As a reference, data are provided for the Hybrid 2 dummy wearing only the three point belt. The effectiveness of the Airbag is clear as well as the advantage of the 30 liter bag in terms of HIC.

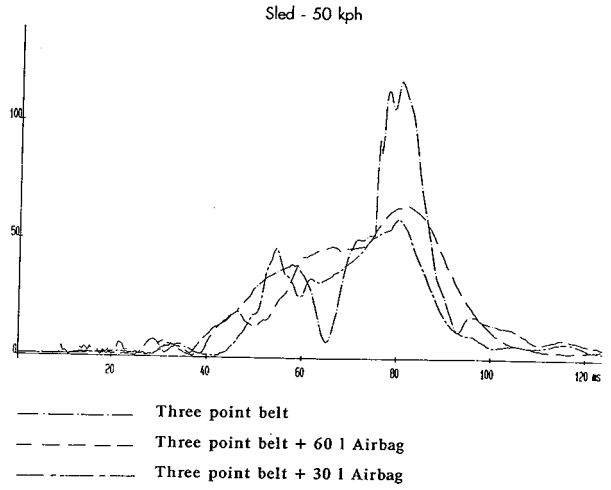

Figure 5. Head Resultant Acceleration and HIC

Computer simulation and crash tests confirmed an important underestimated effect of the Airbag: when a large bag is used combined to a belt, the resultant acceleration of the thorax is higher than when the same belt is used without an Airbag. Pretensioners are used to solve this problem on many cars sold in the United States. K.H. Digges et al (1981) and many others have explained the reasons of this phenomenon that does not exist when a 30 liter bag is used. The Figure 6 shows thorax resultant acceleration measured in four sled tests conducted at 50 kph using different restraint systems. The conclusion is that a 30 liter bag can be used with an excellent thorax injury criterion without the help of a pretensioner.

The Airbag deployment can be the cause of injury by itself in case of an out of position occupant. This concern appears in many papers like the one by H.J. Mertz (1988).

Very simple and comparative test results are mentioned here. The tests, carried out with Renault as mentioned by G. Walfisch (1991) consisted of deployments directly onto the Hybrid III dummy's head; various distances between head and steering-wheel were investigated. The head resultant acceleration, the shear force on the neck, the bending moment on the neck and

the maximum head-torso angle were measured (see Figure 7).

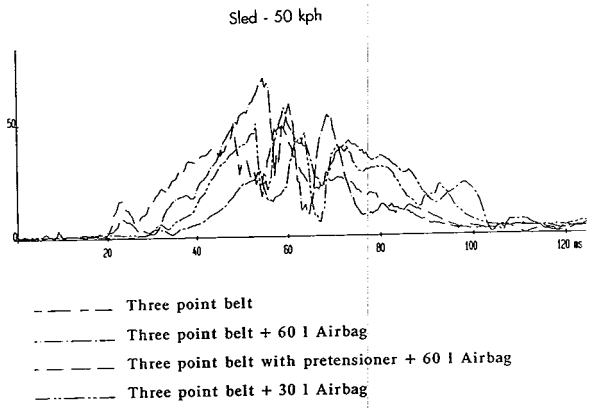

Figure 6. Thorax Resultant Acceleration

Bag type	Head resultant acceleration (g)	Neck shear force (daN)	Neck bending moment (Nm)	Head torso angle (degrees)
30 liters 1 vent hole	< 20	< 67	< 50	< 51
30 liters no vent hole	< 50	< 83	< 53	< 54

Test were conducted with head to steering-wheel distance varying from 75 mm to 125 mm

Figure 7. Eurobag Deployment with "Out of Position" Driver

All the data show that a 30 liter bag is safe even in these "out of position" conditions, whatever its "hardness." Such conclusions can hardly be drawn when a large bag is used.

The conclusion of this part is that a 30 liter bag can provide the desired protection to a belted driver experiencing a frontal impact. It also reduces some of the main undesirable effects associated with the use of a large volume Airbags, as it is the case in the United States.

Discussion of the Existing Technology

Although different functions are expected from an Eurobag (purely supplementary) and from a US Airbag (passive restraint) it cannot be avoided to refer to the latter for the technical solutions. Some of the existing solutions can be transferred to the Eurobag concept, some cannot for technical and economical reasons.

It is interesting to analyze the cost of a present typical US Airbag system; it is proposed to identify each subsystem and to determine its contribution to the system cost. Within the said subsystem, it is also possible to quantify what is the part of the cost which is really induced by the primary function (head protection in supplement to the belt), the part induced by the passive restraint requirement and, finally, the one due to the "State of the Art;" this expression is used to identify technical features which cannot be questioned in the United States mainly for product liability reasons, and that remained identical and unchanged in all systems produced today.

This exercise was conducted and Figure 8 shows the cost breakdown of a typical US driver Airbag system.

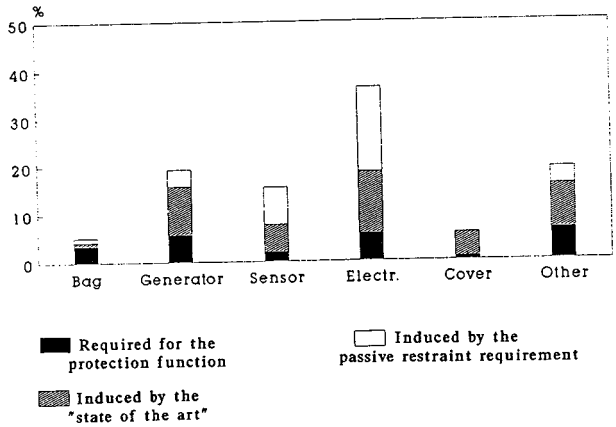

Figure 8. U.S. Airbag (Cost Per Function)

Function	Features required by FMVSS 208	State of the Art characteristics
Bag	Volume 60 liters	. Thick, coated fabric for compatibility with inflator
Inflator	. Generant load adopted to 60 liters	. Sodium Azide based generant
Sensor	. Multiple sensors spread in vehicle (see also wiring harness) . Severe environmental conditions	. Sensible technology, few suppliers
Electronics	. Warning in case of failure	. Full diagnostic capability with interface . Crash data recording . Reinforced PU foam or similar
Cover	. Steering-wheel capable to stand high loads	
Others	. Wiring harness to link spread out functions	

Figure 9

In Europe, the target is to eliminate all cost related to "passive restraint" or to "State of the Art."

For some items, this step can be accomplished just by simplification. This is the case of the sensor and igniting system. For other items, this step is only possible if drastically different technologies are used. The inflator is the best example of this approach.

The Eurobag Inflator

All inflators designed for driver side Airbags presently used in the United-States have very similar characteristics. Even their physical interface and their dimensions are comparable. The gas is the result of the combustion of a Sodium Azide based generant. This choice was made twenty years ago when it was believed that very large Airbags were necessary. Several hundred liters of gas had to be produced in a car and Nitrogen was the only gas that would cause no hazard linked to toxicity.

At that time, this choice was reasonable. It can be questionable when the bag size is only 30 liters.

As a matter of fact, Sodium Azide based generant have a major weak point: the gas output to generant mass ratio is low with only 45 % of the generant mass converted into gas. The 55 % remaining are combustion residues that must be kept inside the inflator by means of filters.

Beside their cost, package and weight, filters are also reducing the gas temperature. The gas temperature is not a problem as such unlike hot solid particles that can cause burns to the bag.

The lower gas temperature resulting from the use of filters means also a lower specific volume with, as a result, another need to increase the generant load. Typical figures for Sodium Azide loads are 80 g for a 70 liter bag and 50 g for a 30 liter bag (Eurobag).

The inflators using this technology are big, heavy and expensive. The filters being not perfect, dust and smoke are common in US Airbag deployments. They are assumed not to be toxic; however very few persons can stay in a car after such a deployment without severe coughing and eye irritation. This situation became a real concern for all car manufacturers proposing Airbags.

In the Autoliv Eurobag, the generant is no longer based on Sodium Azide. This choice was the start of the development of the Euroflator by Livbag (an Autoliv-SNPE venture). The main features are a 100 % gas output to generant mass ratio (no solid residues) and a higher combustion temperature. Less than 10 9 of generant are used to deploy a 30 liter bag. No dust is observed.

The reduced generant mass makes possible a simple and compact structure, greatly helping the integration of all the sub-functions into the steering-wheel.

Figure 10 is comparing the overall dimensions of the new inflator to Sodium Azide based units. Figure 11 is comparing the main features of the two technologies when adapted to the 30 liters Eurobag.

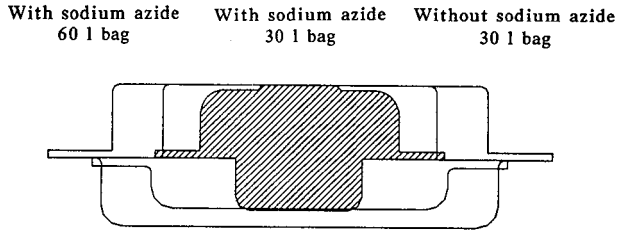

Figure 10. Comparison of Gas Generator Dimensions

Crash Sensor and Ignition

The crash sensor sub-function does not require a technology change to implement the wanted optimization.

In the United States, more than 95 % of the systems are using electrical igniting system, triggered by an electromechanical sensor linked to a capacitor.

The elimination of the features due to the passive restraint requirement and to the State of the Art results firstly in a complete integration of the sub-functions into the steering-wheel. For the crash sensor, this is made possible by the fact that a higher threshold is desired in terms of crash severity because the Eurobag is purely supplementary.

	Traditional technology	New technology (LIVBAG)
Generant	Sodium Azide based	Nitrocellulose based
Toxicity	High	No
Recyclability	No	Full
Gas output	45 %	100 %
Gas T° (1)	"Cold"	"Hot"
Generant load	45g	< 10g
Solid residues	25g	-
Filters	Yes, weight from 100g to 150g	No
Dust, smoke	Yes	No
Output variation between -40°C and +85°C	> 40 %	< 20 %
Life duration	> 10 years	> 10 years

(1) The words "cold" and "hot" are used with a purely comparative meaning

Figure 11. Comparison of Gas Generator Characteristics for Eurobag Systems

Immediate benefits are less sensors, wires, connectors and a simpler and less expensive rotating connector because all the igniting circuitry is situated "after" it. Also important are the environmental conditions which are much less severe in the steering-wheel than in the engine compartment for instance. (Most of the sensors are located in the engine compartment in US Airbags).

This rapid discussion shows that a simple electromechanical sensor mounted in the steering-wheel together with the igniting circuit is a most efficient choice. A big advantage is to keep the electrical igniter that is used in almost all existing systems with a demonstrated very high reliability. Another advantage is to make the use of an all-electronic system possible for cases where the discrimination between "non fire" and "all fire" events requires the use of a silicon sensor.

Conclusion

The interest of the Eurobag as a supplementary system was demonstrated. Not only the offered protection is adequate, but drawbacks of larger bags are avoided.

The cost of such a system should be such that it will be largely used.

To reach this target, design efforts must be concentrated on items requiring new technologies. The inflator is such a case: Livbag Sodium Azide-free inflator is one of the most important features of the Autoliv Eurobag.

References

1. P.L. Harms, M. Renouf, P.D. Thomas: "Injuries to restrained Car Occupants; What are the outstanding problems ?"; ESV Conference 1987.

2. Dr. C. Viano: "Effectiveness of Safety Belts and Airbags in preventing Fatal injury" SAE paper 910901, 1991.
3. C. Chillon, G. Brutel, G. Mauron, F. Hartemann, C. Henry, C. Thomas: "Comparison between the Three Point Belt and the Air cushion; Evaluation and Discussion of this Cost efficiency ratio;" ESV Conference 1987.
4. L. Johansson, J. Billig, H. Mellander: "The Development of an advanced Airbag Concept;" ESV Conference 1987.
5. I. Myklebust et al: "Steering-wheel induced Facial Trauma;" Stapp Conference 1988.
6. P. Thomas: "Head and Torso Injuries to restrained Drivers from the Steering-wheel;" IRCOBI 1987.
7. K.H. Digger, V. Roberts, J. Morris: "Residual Injuries to Occupants protected by Restraint Systems;" Passenger Car Meeting and Exposition, Dearborn 1989.
8. H.J. Mertz: "Restraint Performance of the 1973-76 GM," "Air Cushion Restraint System;" SAE paper 880400.
9. M. Danner, K. Langwieder, Th. Hummel: "Experience from the analysis with a high belt usage rate and aspects of continued increase in passenger safety;" ESV Conference 1987.
10. G. Walfisch, N. Casadei, D. Pouget: "Cover—Véhicule de synthèse sécurité, Protection des occupants en choc frontal et arrière;" ESV Conference 1991.

S9-W-31

Overlap Car-to-Car Tests Compared to Car-to-Half Barrier and Car-to-Full Barrier Tests

Carl Ragland, Gayle Dalrymple
National Highway Traffic Safety Administration

Abstract

In issuing Federal Motor Vehicle Safety Standard (FMVSS) No. 208, "Occupant Crash Protection," the National Highway Traffic Safety Administration (NHTSA) has established requirements for crash protection with automatic restraints at up to 30 mph in frontal impacts into a barrier. The lives and injuries which will be saved are substantial. However, it is estimated that, even after full implementation of this standard, frontal impacts will account for approximately 10,900 passenger car and light truck fatalities per year. Due to this continued safety problem, the NHTSA has added the improvement of frontal crash protection to its priority plan (1). Research has been initiated to investigate concepts to mitigate this problem including the evaluation of advanced restraints, improved structural integrity, and improved energy absorbing interiors. A detailed definition of the safety problem for frontal impacts subsequent to the implementation of FMVSS No. 208 has been initiated. Based on this safety problem definition, a comprehensive research program is being designed to identify mitigation concepts. The research program will utilize real world crash data, laboratory crash test data, and computer simulations to arrive at countermeasures. This paper presents some preliminary analyses of the laboratory crash tests for exploring possible test procedures that can be used to further evaluate structural integrity countermeasures. Particularly, a series of baseline car-to-car tests were conducted to provide comparisons of crash responses between full frontal barrier, car-to-barrier overlap and car-to-car overlap impacts. These tests were useful to provide a better understanding of the crash kinematics by crash mode. They were conducted at 63.5% overlap and 90% overlap and were compared to previously conducted full frontal barrier and 50% overlap barrier tests at 25 mph and 35 mph.

Introduction

A series of tests were conducted to compare crash responses between full frontal barrier, car-to-barrier overlap and car-to-car overlap impacts. This series of tests used two vehicle models that have been extensively tested in NCAP, steering assembly research tests, and structural crashworthiness research tests. The tests were used to better understand the crash kinematics by crash mode for different frontal test conditions. This research supports one of NHTSA's high priority programs as contained in the agency's 1991-1993 priority plan (1), and forms one part of the work supporting an advanced frontal crash program as discussed at the previous ESV (2,3).

Background

The subject vehicles in this test series were Toyota Celicas and Hyundai Excels. The model years used were 1987 and 1989, but there were no structural differences between these model years. The first tests on these cars were 1987 NCAP tests. During NCAP testing, the Toyota was observed to prevent intrusion better than the Hyundai, although both cars had similar crash pulses. A research program (4) was conducted using these same vehicle models and model years, because of their similarity in crash pulse and dissimilarity in intrusion characteristics. That program was conducted as a baseline exercise to review the potential for improvement in

steering assembly characteristics for unrestrained occupants. Those research tests were conducted in full frontal barrier and 50% overlap barrier modes at 25 mph and 35 mph to better understand crash kinematics in those crash modes.

In 1989, the program was altered to use restrained occupants due to the increasing use of air bags and seat belts (both manual and passive) as a result of Federal Motor Vehicle Safety Standard No. 208, "Occupant Crash Protection." Vehicle manufacturers have selected to install air bags in a variety of their production lines and some have committed to install air bags in all future production. To date, the accident field experience has been very promising with respect to the efficacy of these devices. While significant gains have been achieved, much remains to be accomplished. Toward this goal NHTSA began examining frontal test configurations as a means of upgrading frontal crash protection.

In the latest completed test series, four car-to-car tests using eight 1989 model Toyotas and Hyundais were conducted at 63.5% overlap and 90% overlap (i.e. 63.5% and 90% of the front fender-to-fender width was engaged upon impact). Both cars were moving at approximately 35 mph. Each test used a driver dummy in one car and a passenger dummy in the other. These tests were conducted to determine similarities and differences between car-to-barrier tests previously conducted and the car-to-car overlap tests. Table 1 shows the matrix of the test series used in this study.

Table 1. Test Matrix of Car-to-Car and Car-to-Barrier Tests

	TEST SPEEDS (Miles/hour)			
	VSB 100%	VSB 50%	VTV 63.5%	VTV 90%
TOYOTA	35.4	34.7	35.5	34.8
HYUNDAI	34.8	34.7	35.3	34.2

NOTATION: VSB 100% - Vehicle-to-stationary barrier, 100% engagement
VSB 50% - Vehicle-to-stationary barrier, 50% overlap
VTV 63.5% - Vehicle-to-vehicle, 63.5% overlap
VTV 90% - Vehicle-to-vehicle, 90% overlap

Dummy Response

Figures 1 through 4 compare the dummy responses for the restrained drivers and passengers only. Figure 1 shows the HIC comparisons between the 35 mph tests using restrained dummies. Note that the Hybrid II dummy was used in the NCAP tests and the Hybrid III dummy was used in the research tests. The driver and passenger of the Celica and the driver of the Hyundai all show consistent trends, with the 63.5% overlap car-to-car and the full barrier tests producing almost identical HIC's. Substantially higher HIC's (1.5 to 2.1 times greater) are observed for the 90% crash mode. This difference can be attributed to higher intrusion combined with a relatively severe crash deceleration pulse (discussed in the next section). The only inconsistent response was the Hyundai passenger exhibiting a much higher HIC in the full barrier test than in either of the other two crash conditions. This is probably due to the dummy's head striking his own knee in the NCAP test, but not in the other tests. Observations from these crash test results indicate that HIC is influenced similarly by crash pulse and intrusion. Intuitively, one would expect higher intrusion, as seen in the 63.5% overlap tests, to cause higher HIC's than the full barrier tests. The reason this was not true is that the dummy trajectory was off center to the left of the stiffer portion of the wheel in all offset testing, particularly in the 63.5% overlap. In a real world crash in which the trajectory of the vehicle may be lateral as well as frontal, the occupant might easily have impacted the center of the hub with fatal consequences.

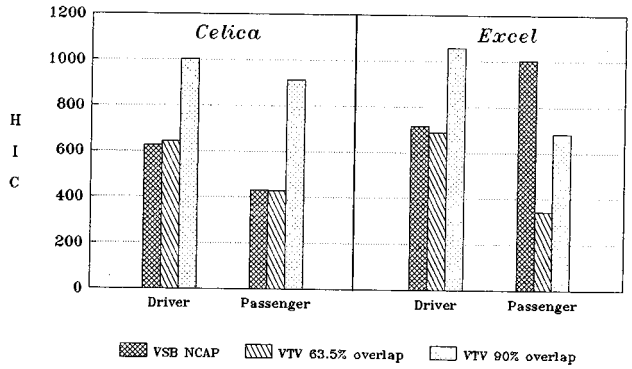

Figure 1. Comparison of Head Injury Criterion (HIC)

Figure 2 shows the chest responses for all four dummies and three crashes. The chest responses also show a clear and consistent trend for the Toyota driver and passenger and the Hyundai driver. The response for these three dummies was highest in the 90% overlap car-to-car and lowest in the full barrier with the 63.5% car-to-car dummy response falling between the two. This suggests a correlation between chest response and intrusion, as well as crash pulse, with intrusion dominant. This is because in the 63.5% overlap crash, intrusion (to be discussed in following sections) was only slightly higher than the 90% overlap crash, yet the crash pulse (see next section) was much softer than the other crashes. The exception to the consistency is again the Hyundai passenger. In this car the 63.5% overlap car-to-car yields the highest dummy chest response with the 90% only slightly lower and the full barrier producing the lowest response. This slight deviation is of little concern, since the chest response still appears to be strongly influenced by intrusion and crash pulse.

Figure 3 shows the left femur maximum force and Figure 4 shows right femur maximum force. While this data is not as consistent across the board as the head and chest responses, the average of the right and left Femur force is consistently higher for the 63.5% overlap test, with the 90% next and the full barrier lowest with the exception of the Toyota passenger. The Toyota femur forces are very low (less than 600 pounds) and all crashes are similar, possibly indicating no intrusion or no

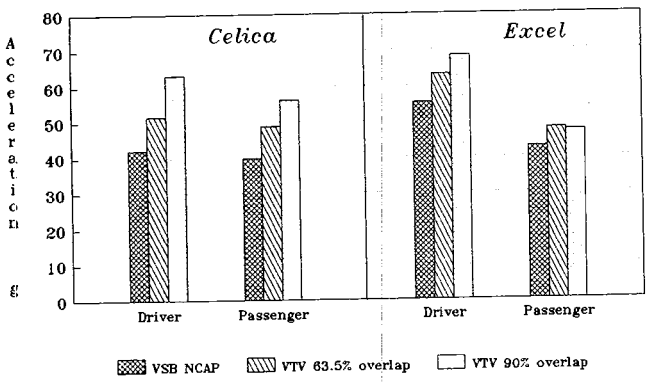

Figure 2. Comparison of Chest 3ms Clip

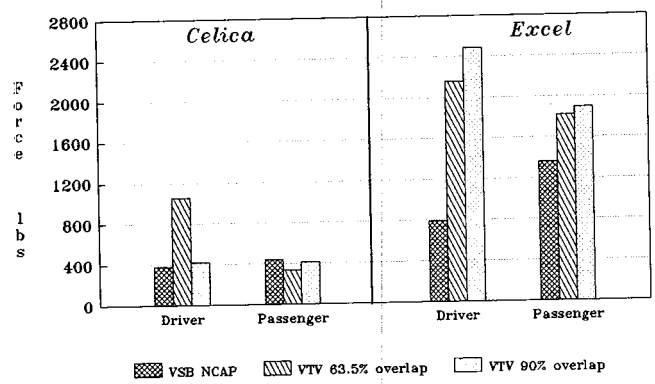

Figure 3. Comparison of Left Femur Force (Pounds)

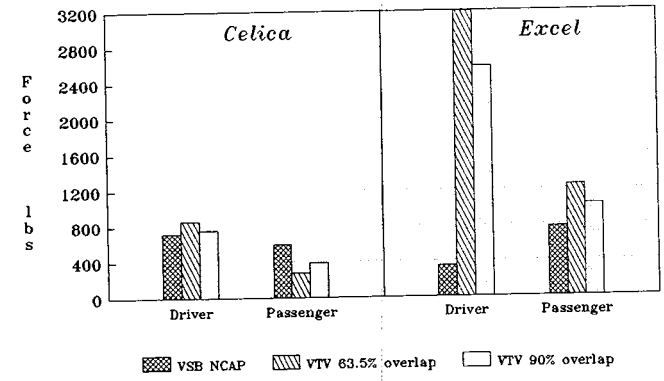

Figure 4. Comparison of Right Femur Force (Pounds)

knee contact. These data indicate a strong correlation between femur force and intrusion with very little, if any, dependence on crash deceleration pulse severity.

Deceleration Response of Vehicle Structure

Four crash conditions are compared to evaluate crash deceleration responses (crash pulses). These are all approximately 35 mph delta V (ignoring restitution). Two crashes were car-to-car, conducted at 63.5% and 90% overlap and the other two were fixed barrier tests conducted at 50% and 100% (full barrier) overlap. Table 1 shows the test matrix.

Figure 5 shows the crash pulses for the four Celica tests. Note that the highest peak deceleration occurs in the 50% overlap fixed barrier test, followed closely by the full barrier test. The 90% car-to-car is next with the 63.5% overlap car-to-car crash representing the "softest" crash pulse. Peak acceleration alone is not the only indicator of crash pulse severity, but perhaps equally important is the duration of impact. For this study, duration is calculated from time zero to the time at which the velocity curve first reaches zero. The vehicle may still be under deceleration at this time (spring back of the structure), but forward motion over ground has stopped, the vehicle motion has begun to reverse and the dummy has already contacted the interior. Figure 6 shows the velocity curves. From this figure it can be seen that the shortest crash pulse is the full barrier test, followed by 90% overlap and 50% fixed barriers, which are fairly close together. Finally the test with the longest duration is the 63.5% overlap car-to-car test. Figure 7 shows another measure of crash pulse severity, dynamic displacement. Looking at maximum dynamic displacement from this figure, the order of the crash pulses from softest (most dynamic displacement or crush) to stiffest is the 63.5% overlap, the 50% overlap, the 90% overlap and the full barrier impact. This order is the same as obtained when ranking by duration, except for one minor difference. The four tests are grouped in pairs with the full frontal and 90% overlap grouped together and the 50% and 63.5% grouped together. By duration/velocity ranking the 50% and 90% were grouped together near the middle of the other two extremes, 63.5% (longest duration) and full barrier (shortest duration).

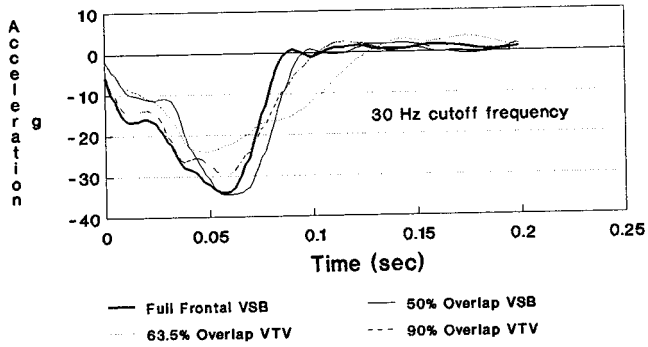

Figure 5. Crash Pulses for Celica Tests

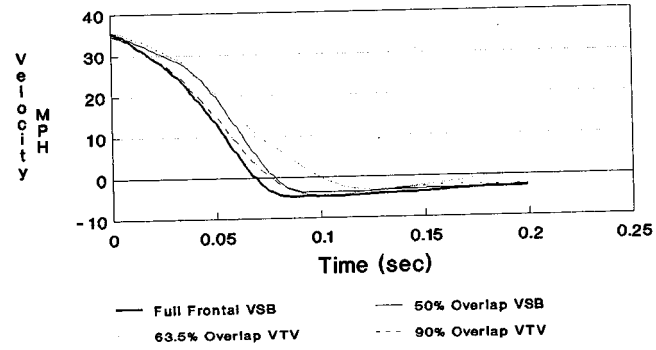

Figure 6. Velocity-Time Curves for Celica Tests

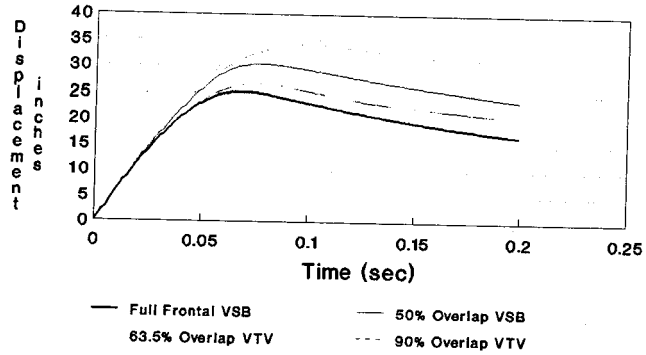

Figure 7. Displacement-Time Curves for Celica Tests

Looking at the Hyundai crash pulses, Figures 8-10 show very consistent results. All three measures of crash pulse severity show their decreasing order as: 1) full barrier 2) 90% overlap 3) 50% overlap and 4) 63.5% overlap. This order was expected prior to testing and was the same as resulted from two out of the three measures for the Toyota. Further inspection of the four crash pulses in these figures reveals similarity between the 50% and 63.5% tests, and an almost identical match between the full barrier and the 90% overlap test. The similarity between the 50% and 63.5% begins to deviate at approximately 50 milliseconds. At this point in the car-to-car test the structures begin to disengage by lateral motion induced by the non-symmetrically deformed front bumpers and the forces imposed by the engines.

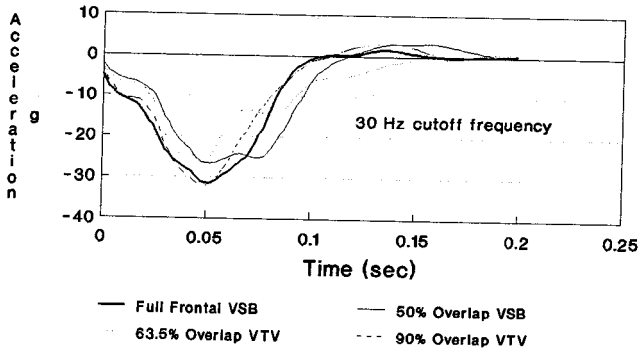

Figure 8. Crash Pulses for Excel Tests

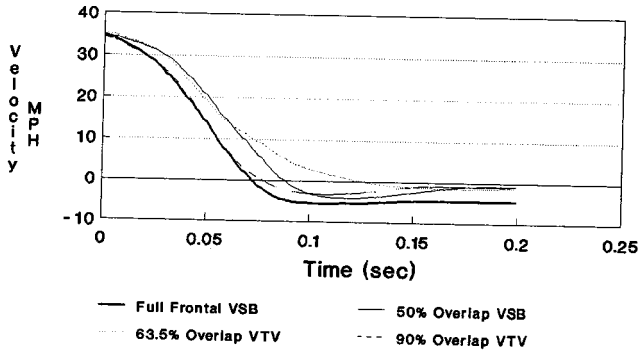

Figure 9. Velocity-Time Curves for Excel Tests

It can be concluded for the Celica that the 63.5% and the 90% impacts produce similar shape crash pulses of different severity inversely proportional to their percentage of overlap. The 50% and full barrier pulses also bear some resemblance. In terms of peak acceleration, the 50% barrier appears to be an anomaly, producing the highest peak. The other measures of crash pulse severity are in the order expected with the full engagement more severe than the 50% overlap. By two out of three of the measures of crash pulse severity, the 50% fixed barrier lies between the 63.5% and 90% overlap car-to-car barriers. This was as expected when the test conditions were chosen. However, the 50% barrier produces the highest peak acceleration. This may be explained by the fact that the compartment experiences more crush in the 50% overlap car-to-barrier test than in the 90% overlap car-to-car test. This compartment crush difference is caused by a very stiff suspension link between the lower A-arm and the compartment floor pan. This link adds tremendous rigidity between the compartment and either tire during a crash. The rigid barrier forces the tire rearward during impact, whereas a striking car yields and crushes to conform to the excessive stiffness of the tire contact area. Any advantage gained by this method of reducing intrusion in a car-to-car impact is somewhat offset by allowing intrusion from other sources, such as rearward movement of the engine. Intrusions, which will be discussed in the next section may be compared in Figures 11-14.

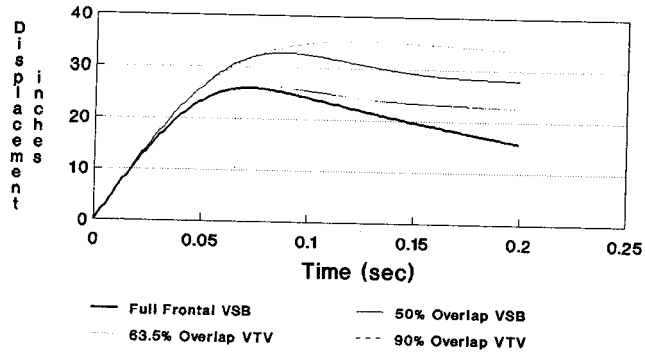

Figure 10. Displacement-Time Curves for Excel Tests

Intrusion

Figures 11-14 show comparisons of intrusion parameters for the two barrier and two car-to-car impacts. Figure 11 shows maximum displacement rearward with respect to the rest of the compartment as measured dynamically by film analysis. The value of horizontal intrusion shown in this figure is the maximum value recorded before the dummy contacted the steering wheel rim or hub with his head (usually 1-5 milliseconds before contact). In the car-to-car overlap tests the intrusion continued after initial dummy head contact occurred. In the car-to-barrier tests this phenomenon was not observed since the unrestrained dummies continued loading the steering column causing more stroke and less observable intrusion. The time of maximum intrusion is shown in Figure 12. Note the similarities in maximum intrusion time even though the fixed barrier tests used

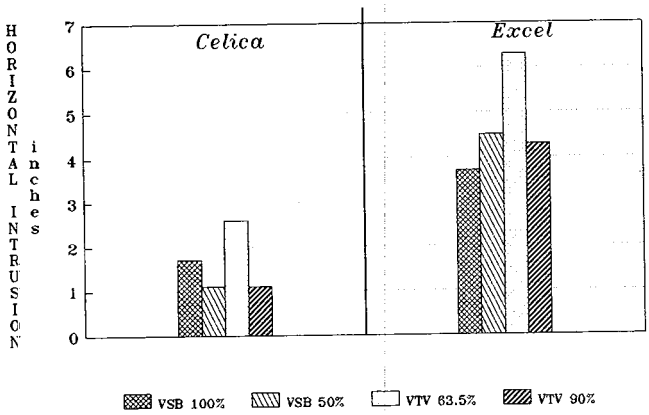

Figure 11. Maximum Rearward Horizontal Dynamic Displacement of Steering Wheel

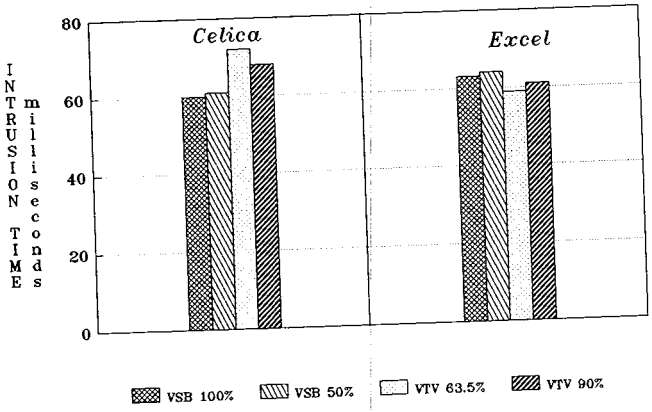

Figure 12. Time of Maximum Displacement of Steering Wheel

unrestrained dummies and the car-to-car tests used restrained dummies.

Figure 13 shows the intrusion velocity. This is the maximum value of the velocity of the steering wheel with respect to the compartment, which occurs prior to the time of maximum rearward displacement. This graph clearly shows that of the two cars, the Hyundai had the highest intrusion velocity and, of the four test conditions, the 63.5% car-to-car had the highest intrusion velocity. The second highest intrusion velocity was seen with the 90% overlap car-to-car tests. The third and fourth rated test condition depends on the car used. Of the remaining two test conditions the Excel performed more poorly with the 50% fixed barrier but the Celica performed more poorly in the full barrier. This intrusion behavior of the Celica was not expected and can be explained by its unusual structure (also see discussion in previous section). In most cars, intrusion of the occupant compartment is caused primarily by rearward motion of the engine into the firewall. In the Celica, a major load path is through the wheels, due to a rigid link from the suspension to the occupant compartment. In addition, there is a crushable load path from the center bumper height to the compartment floor pan. In the barrier test the engine also contributes to intrusion. The combination of these load paths causes earlier and more extensive intrusion in the full barrier test because all are simultaneously engaged by the flat barrier surface.

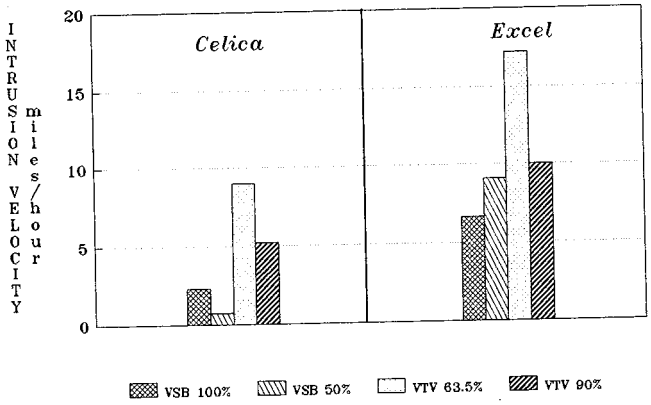

Figure 13. Maximum Rearward Horizontal Velocity of Steering Wheel

Figure 14 shows the maximum vertical steering wheel displacement in each test. From this figure it is apparent that the Hyundai in the fixed barrier test had more vertical displacement. In the Celica the only crash test that produced a significant amount of vertical steering wheel intrusion was the 50% barrier test. It is uncertain whether this is due to loading from the unrestrained occupant via the dummy's knees or due to structurally induced intrusion, such as from the engine, or from crushing of the structure.

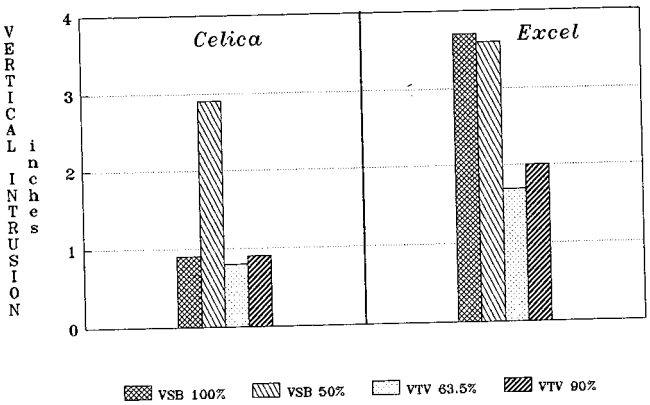

Figure 14. Maximum Upward Dynamic Displacement of Steering Wheel

In summary, the intrusion can be said to be more severe in the car-to-car tests than in the car-to-barrier tests. Intrusion measured in terms of velocity agrees fairly well with the intrusion measured in terms of displacement. From Figures 13 and 14 it is conclusive that intrusion measurements for the Hyundai are greater than for the Celica.

Possible Test Configurations

Several crash test configurations will be discussed for consideration in frontal testing. These test conditions are presented as possibilities to closely simulate a car-to-car overlap test with a car-to-barrier test. In theory the

design of safety systems (structures, air bags, restraints, steering assemblies, etc.) subjected to this crash test condition will improve safety performance in that specific car-to-car crash.

Shaped Fixed Barrier

One test condition which has been used by Mercedes, Auto Motor und Sport, and possibly others is a partial overlap barrier with some degree of shape. The tests analyzed in this paper used a 50% overlap barrier with a squared off flat face. To improve the kinematic comparisons between overlapped barrier and car-to-car testing, one needs to devise a large radius curved surface or an angled barrier face on the barrier face. This test series also suggests that the overlap with a fixed barrier needs to be reduced to achieve the desired match in crash response to the car-to-car test. This variation would probably mean using an overlap of approximately 30 to 50% to achieve the same results as the 63.5% and 90% overlap car-to-car crashes. A large radius edge, a rounded edge and/or a slight angle of the barrier face may further improve results and may improve the direct comparison between a given barrier overlap and a car-to-car overlap.

This type of test is similar in complexity to full barrier impact crash testing. Carefully aligning the vehicle with the barrier to ensure consistent overlap at impact is the only additional requirement. Except for the initial expenditure for the test hardware, the cost of conducting the test would remain unchanged.

Overlap fixed rigid barrier crash testing can not incorporate all of the subtleties of car-to-car crashes. For instance, the Toyota wheel structure contributes significantly to the crash behavior of the car in an offset collision. The wheel within the impacted area loads and penetrates the opposing section of the opposite vehicle. This in turn softens the Toyota crash pulse, especially when the overlap is around 90% and the structure of the opposing vehicle where the Toyota wheel impacts is relatively soft. In this 90% overlap example the intrusion is less than what would be expected in a fixed barrier crash test because the wheel penetrates the opposing vehicle rather than its own compartment (to create intrusion).

Fixed Barrier with Deformable Face

This approach would incorporate some form of deformable element into the face of a fixed barrier. One concept to consider is a deformable honeycomb element with about 5 inches of crushable depth, placed on the barrier in an area representing the engine of the opposing vehicle and approximately 15 inches of crush depth in all other areas representing other structures of a typical vehicle front end. The fixed barrier surface could be stepped, to accommodate the back surface of this geometry, while the front, crushable, surface remains flat. This stepped fixed barrier configuration could serve three purposes. First, it would allow deformation into the opposing structure (up to a point) so that structural hard points would behave similar to hitting a vehicle front end. The second purpose of this configuration would be to allow greater edge deformation, so that the bumper of the subject vehicle can deform at a progressively greater angle—similar to car-to-car behavior. The final purpose of this test configuration could be to promote structural compatibility by matching the crush characteristics of the subject vehicle with the characteristics of the honeycomb for optimum crash performance.

This test type provides a close match to the car-to-car test damage pattern, using a test that is only slightly more involved because of the necessity for careful alignment. It accomplishes this match by allowing for progressively increasing angular crush of the front structure by deformation of the barrier (more on the edge than in the center). Secondly, front-to-front compatibility could be achieved with a standardized crushable element allowing frontal structures to be designed for optimum performance.

Adding the crushable element to the face of a conventional fixed barrier tends to create an unrealistic crash response in terms of energy absorbed at a given speed. This is due to the fact that energy absorbing capability is added to the barrier, while the kinetic energy of the impact remains unchanged from a fixed barrier test. This additional energy absorption needs to be controlled so it is a small percentage of the total, while adding enough crush to be effective for the previously stated advantages. The crash tests may need to be conducted at a higher speed than conventional barrier tests to compensate for this energy discrepancy. There is also increased time and cost burden resulting from the need to replace the crushable element after every test.

Deformable Moving Barrier

This is probably the most complicated test condition. The basic test would utilize a deformable moving barrier impacting the front of a car moving at an equivalent speed in an overlap configuration. If the deformable element of the moving barrier is properly selected, intrusions and crash pulses should very closely simulate a car-to-car test. A non-crushable or stiff element may be required to represent the engine.

This type of test could be made identical to any particular car-to-car match by varying the properties of the honeycomb in the crushable element. By selection of optimized frontal stiffness required for a compatible car fleet, and selection of a matched crushable element for the honeycomb, other cars tested against it would match that stiffness for best performance, thus assuring compatibility. Momentum and energy would be closely matched to a car-to-car collision of equivalent weights. This test, assuming a standardized weight of the deformable moving barrier, would therefore impose a greater severity test on smaller cars than on larger cars. If desired, geo-

metric compatibility could also be addressed by selecting the shape of the deformable moving barrier, assuring load paths are compatible with front, side and rear structures.

However, this type of test imposes an added burden of complication in conducting the test. Both vehicles should be moving, necessitating the test be conducted at mid-track and the tow release point be relatively close to the point of impact, or some means of guidance is provided to ensure proper alignment at impact. Conducting the test with only one vehicle moving is not considered a viable option since it necessitates such a wide angle of film coverage to follow the larger impact area. With both cars moving the cars come to rest near the point of impact. However, with only one car moving, the struck car accelerates rearward to approximately 1/2 of the impact speed. Any test using a deformable barrier has the disadvantage of requiring a new crushable honeycomb face assembly after every test.

Summary and Conclusions

It can be shown from this limited test series that intrusion induced in car-to-car crashes is typically of a higher magnitude than in car-to-full barrier crashes. Intrusion resulting from a narrower overlap impact (63.5%) produced more intrusion than a wider overlap impact (90%). However, there was no consistent correlation between the 50% fixed barrier and the car-to-car overlap tests. The 50% overlap barrier test resulted in approximately the same horizontal intrusion displacement, but slightly lower intrusion velocities than the 90% car-to-car overlap test. Therefore, to simulate the intrusion seen in a car-to-car test via an offset barrier test requires a narrower engagement with the barrier than the actual overlap of interest. To more accurately simulate intrusion extent and velocity may require more sophisticated test tools, such as a deformable moving barrier, a shaped fixed barrier or a deformable fixed barrier.

In attempting to match crash pulses for the Hyundai it is observed that the 50% barrier crash pulse is close to, but more severe than, the 63.5% overlap car-to-car test pulse. In the Celica the 50% barrier crash pulse is very similar to the full barrier and closer to the 90% overlap, than the 63.5% car-to-car pulse. This means that in order to match the crash pulse and intrusion occurring in a car-to-car test with a barrier test one requires a narrower impact overlap with the barrier. This is consistent with the necessity to match intrusion alone by a narrower engagement with the barrier. However, the percentage difference required to match crash pulse and intrusion may vary from car to car. Additionally, this percentage difference may not be the same as required to match intrusion as to match crash pulse.

Due to the relative inconsistency between the two car models in matching the car-to-car test with the car-to-barrier test it is doubtful if one overlap fixed barrier percentage can be used with every model to precisely replicate structural and occupant responses in a given overlap car-to-car impact. Whether or not this objective is feasible is a matter of continuing debate, since it is also recognized that full frontal fixed barrier crashes also cannot always replicate a car-to-car full frontal test. Even though not all possible testing configurations were used, insight was gained for consideration of other potential test configurations.

References

1. Highway Safety Priority Plan, 1991-1993, DOT-HS-807-723, Revised June 1991.
2. Derby, Adele, "Research Priorities in Crashworthiness," Proceedings Twelfth International Technical Conference on Experimental Safety Vehicles, PP 586-588, 1989.
3. Hackney, James R., William T. Hollowell, and Daniel S. Cohen, "Analysis of Frontal Crash Safety Performance of Passenger Cars, Light Trucks and Vans and an Outline of Future Research Requirements," Proceedings Twelfth International Technical Conference on Experimental Safety Vehicles, PP 233-241, 1989.
4. Ragland, C., and G. Klemer, "Intrusion Effects on Steering Assembly Performance in Frontal Crash Testing," Proceedings Twelfth International Technical Conference on Experimental Safety Vehicles, PP 358-387, 1989.

S9-W-32

COVER: "Renault VSS" Safety Vehicle Frontal and Rear Impact Occupant Protection

G. Walfisch, D. Pouget, N. Casadei
Renault

Abstract

The Renault COVER is a synthesis research vehicle built around the Renault 19, a European mid-range, mass production model car (1). Improvements have been made to the basic Renault 19 in order to ensure efficient safety to all occupants, adults and children, particularly in case of asymmetrical impacts, frontal at 65 Km/h and rear at 50 Km/h. Independently of economical standpoint, all improvements chosen are production line feasible and could be progressively be incorporated into future cars. There is a 20 kg weight increase over the Renault 19,

resulting from improved protection in the case of frontal and rear impacts. Structural modifications and the new seat types used are the main causes of this weight increase.

Introduction

After the BRV (2), the Basic Research Vehicle used to study new designs, and the EPURE (3), which was a basis for studying the feasibility and cost/efficacity of a realistic light weight safety vehicule, the COVER prefigures a safety vehicle designed to be production line manufactured and therefore developed with the usual industrial manufacturing constraints: feasibility, weight, performance and cost.

Taking into account the ratio cost/safety leads to adopt different restraint systems for each occupant position. This will guarantee that each position is supplied with an optimized solution and the more convenient one to minimize the injuries observed in real road accidents.

Frontal Impact Protection

Impact Performance Evaluation Criteria for COVER

The effectiveness of the chosen safety devices are evaluated with the following criteria:

For adults. Criteria from FMVSS 208 regulation for the 50th percentile male HYBRID III dummy. In the case of no head impact a criterion is not necessary as actual road situations have shown that no head or neck injury occurs when there is no head impact (4). Moreover, the absence of submarining was considered and verified by high speed film analysis.

For children. Criteria from FMVSS 213 and ECE44 regulations.

Front Structural Improvements

Specific structural reinforcements and design modifications were carried out on different parts of the front structure. These were located in the rear part of the front structure and in the passenger compartment in order to avoid increasing the stiffness of the COVER front end because of inter-vehicule compatibility, especially for side impacts (Figure 1).

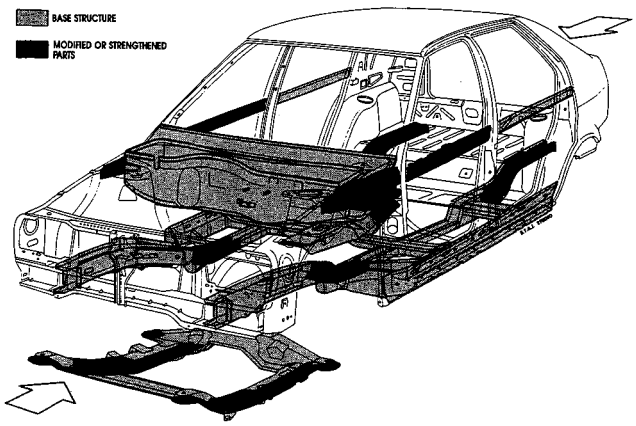

Figure 1. Front and Rear Structural Improvements

Driver Protection

The basic restraint system is the 3-point safety belt with emergency locking retractor.

About this restraint system, it has been shown, from real road accidents, that an improvement of driver protection should be aimed at for each human body part.

Consequently, this safety belt has been improved to increase occupant/vehicule coupling, as follows:

- the upper anchorage has been moved up 60 mm on the b-pillar in order to obtain the optimal shoulder belt position across the chest
- a reel with webbing clamp retractor belt has been chosen to limit the webbing play out due to spooling effect
- a pre-tensioner system at the buckle level has been chosen to make it possible to lower the buckle 80 mm in order to take out slack in the belt and to avoid the risk of submarining. The maximum "normal" retraction force is 350 daN.

The presence of the last two devices together in sled tests without slack between dummy and belt, and (Table 1) resulted in a decrease of:

- 65% in HIC value
- 12% in head excursion
- 15% in head impact velocity
- 15% in thoracic decelerations
- 40% in backward rotation of the pelvis

Table 1. Comparison of Injury Criteria Obtained with a 3-Point Reel Belt and Those Obtained with the COVER Driver Seat Belt

	Head			Chest		Pelvis
	HIC 36ms	Excursion (cm)	Velocity (m/s)	Max. Deceleration (g)	3ms max deceleration (g)	Backwards rotation angle (°)
3-point reel belt	568	590	10	57	50	50
COVER belt webb clamp reel and buckle pre-tensioner	203	520	8.6	47	42	29
% Improvement	65	12	15	17	15	40

Sled tests with a 50th percentile male HYBRID II dummy, in a right front passager environment.

With 50 mm slack (soft padding to simulate clothes) between the safety belt and the 50th percentile male HYBRID II dummy, the standard reel belt results were compared with those of a belt equipped with a pyrotechnical reel and those of the COVER equipped with a pre-tensioner at the buckle level:

- The standard 3-point reel belt resulted in submarining, there was a 50° backward pelvic rotation.
- The belt equipped with a pyrotechnical reel did not result in submarining, but the backwards pelvic rotation was 48°, very near the critical level for submarining.
- The COVER belt with pre-tensioner at the buckle level did not result in submarining, in fact there was a wide margin of safety as to the risk of submarining since the backwards pelvic rotation was 25° only.

Since other head and chest criteria for the different belt types were relatively similar to each other, the above

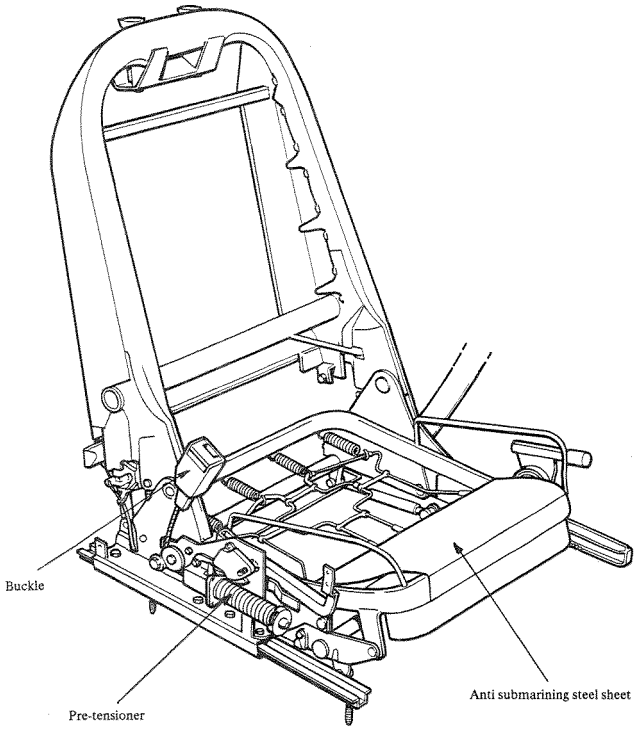

Figure 2. Driver Seat with Pre-Tensioner at the Bucket Level

results were the major reason the belt with pre-tensioner at the buckle level was chosen for the COVER.

Other restraint devices were improved as well:

- *Steering-wheel.* The steering wheel is equipped with a 30-liter airbag with integrated sensor and inflator. In a sled test, HIC results with an airbag were 50% lower than with a steering wheel equipped with a rather effective padding (Table 2). Optimal airbag characteristics (bag and inflator) were determined so as to eliminate the risk of neck injury in the case of static airbag deployment with the head located near the steering wheel (Figure 3, Table 3). Neck injury criteria levels remained below known human limits (7).
- *Seat.* The driver's seat is equipped with two built-in lap belt anchorages and the front anti-submarining seat cross member is reinforced. These two features, used in conjunction with the belt pre-tensioner at the buckle level, ensures that there is no risk of submarining even in the case of a slack in the seat belt.
- *Steering column.* To improve protection to the tibia-knee-femur area a shock absorbing device was placed between, on one side: the lower part of the dashboard and on the other side: the steering adjustment mechanism and the ignition lock of the steering column.

Table 2. The COVER Airbag's Performance Compared to That of Effective Steering Wheel Padding

Restraint type	HEAD	CHEST
	HIC 36ms	3ms resultant acceleration (g)
3-point reel belt and effective wheel padding	1055	54
3-point reel belt and COVER airbag	450	53

Sled test with 50th percentile male HYBRID II dummy

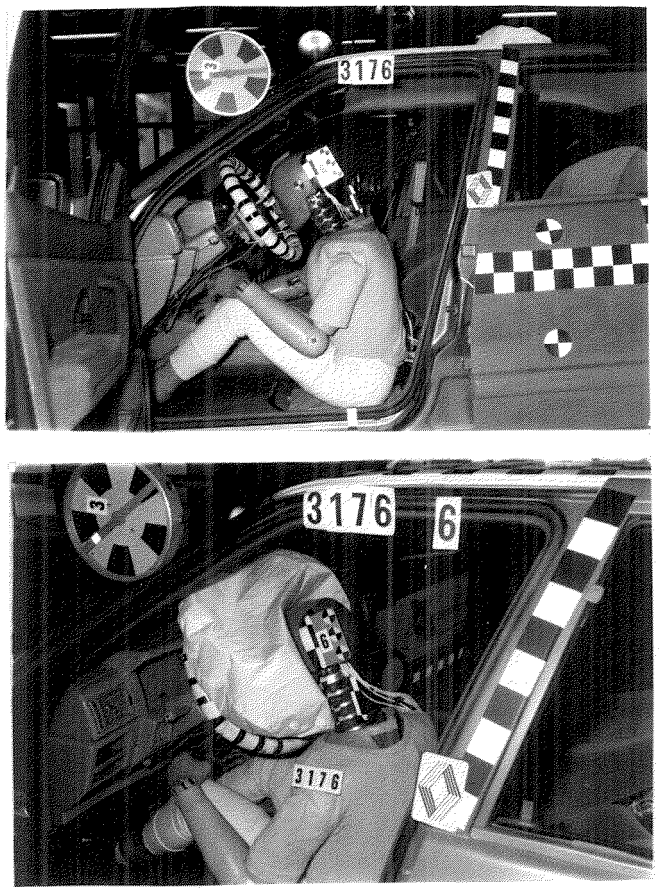

Figure 3. Static Deployment of COVER's Airbag: Out of Position Test

Table 3. Static Airbag Deployment Tests with the Head Located Near the Steering Wheel (Out of Position) with a 50th Percentile Male HYBRID III Dummy

Head to airbag distance (mm)	NECK injury criteria		Head/chest hyperextension angle (°)
	Front to rear shearing force (N)	Hyperextension moment (Nm)	
75	470	22	-
75	670	42	38
125	51	35	16
125	630	50	23
175	430	35	13
175	340	31	15
HUMAN LIMITS	860	57	60

Full-Scale Test Results at 65 km/h Against a 30° Left Angled Barrier (Table 4)

Preliminary adjustments to the aforementioned systems were made based on different sled tests using 5th percentile female, 50th percentile male and 95th percentile male HYBRID III dummies in testing standard injury criteria. The 50th percentile male HYBRID II dummy was used in submarining testing because this dummy seems more convenient for this purpose than the HYBRID III.

Table 4. Injury Criteria Obtained with the COVER at 65 Km/h Against a 30° Left Angled Barrier

Seat occupied	Dummies	HEAD		CHEST				ABDOMEN	FEMURS	
			maximum	acceleration					maximum force	
		HIC 36ms	acceleration (g)	max (g)	3ms (g)	Δ t>60g (ms)	deflection (mm)	submarining	Left (N)	Right (N)
Driver	50th percentile male HIII 25° seat recline position	326	53 AirBag impact	50	48	0	27	No submarining	1970	4620
Front seat passenger	50th percentile male HIII 25° seat recline position	No impact		53	51	0	40	No submarining	1600	2050
	50th percentile male HIII 45° seat recline position	No impact		55	53	0	34	No submarining	1220	1460
Rear seat passenger	50th percentile male HIII	No impact		56	53	0	29	No submarining	-	-
	5th percentile female HIII	No impact		53	50	0	-	No submarining	-	-
FMVSS 208 regulation limits		1000	-	-	60	3	76.2	-	10000	10000

The 30° angled barrier frontal impact test at 65 km/h resulted in injury criteria measurements, for the 50th percentile male HYBRID III dummy driver, much lower than the FMVSS 208 regulation's required limits. Analysis of high speed films confirmed that no submarining occurred. Figures 4 and 5 show the occupants and vehicles before and after impact.

Front Seat Passenger Protection

The abdomen is the more frequently and severely injured body area in the case of frontal impact when a 3-point seat belt is used. Abdominal injuries observed are often due to submarining. The COVER's main objective is therefore to ensure effective protection against this risk, no matter what the seat adjustment position. Protection is particularly important when the seat back is in the "comfort" position, that is to say, at a 45° recline angle instead of the normal 25° recline angle.

To achieve better protection, the following changes have been made (Figure 6):

- the lap belt sides have been moved to a more vertical position
- seat belt buckle position has been moved down lower
- and deformable anti-submarining steel sheet has been placed in the seat bottom forward to the pelvis and parallel to the thighs.

Moreover, to improve seat belt wearing comfort, instead of the normal B-pillar anchorage point, this seat belt anchorage was built into the seat back and the seat cushion is vertically adjustable.

This upper shoulder belt anchorage point was determined in order to optimize thorax restraint and

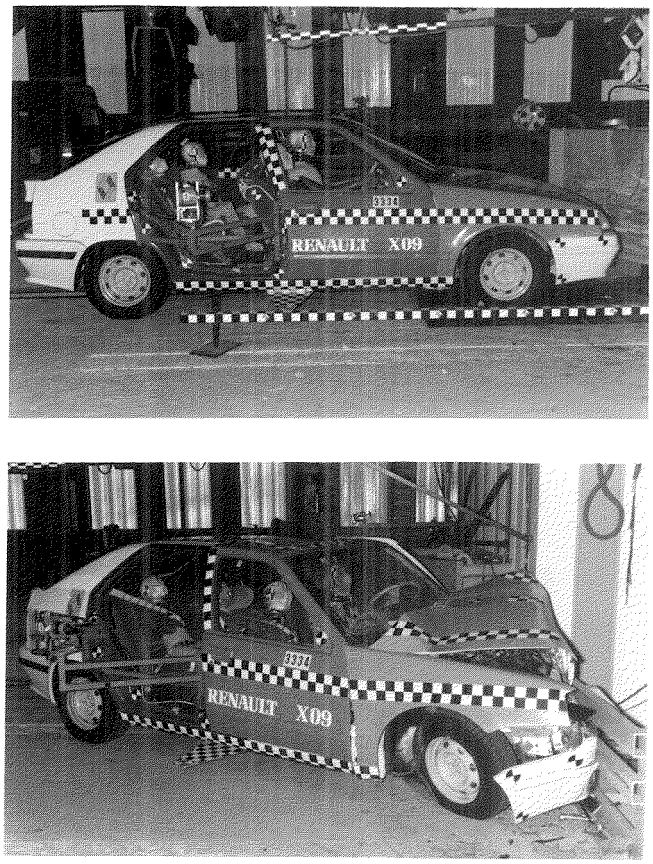

Figure 4. COVER: Before and After Impact

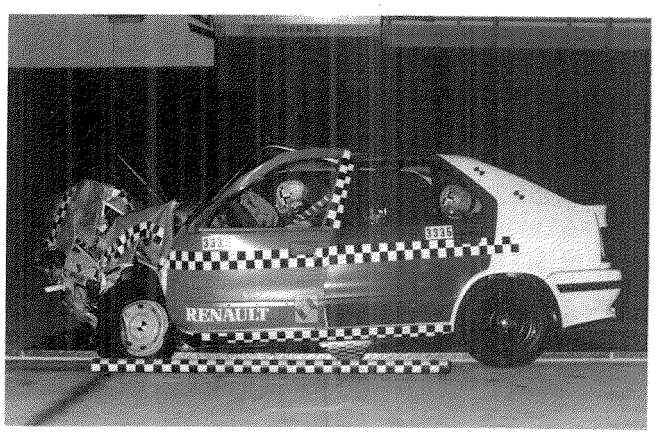

Figure 5. COVER After Impact

particularly to limit the risk of chest sideward movement in asymmetrical collisions thereby avoiding any possible head injury resulting from head impact with the forward interior, an injury risk observes in real accidents (5).

As in the case of the driver, the aforementioned improvements were developed based on sled tests with HYBRID III and HYBRID II dummies.

Table 4 presents the measurements of different injury criteria obtained from tests at 65 Km/h against a 30° left angle barrier. In the standard 25° seat back recline position, as in the 45° "comfort" position, results indicate

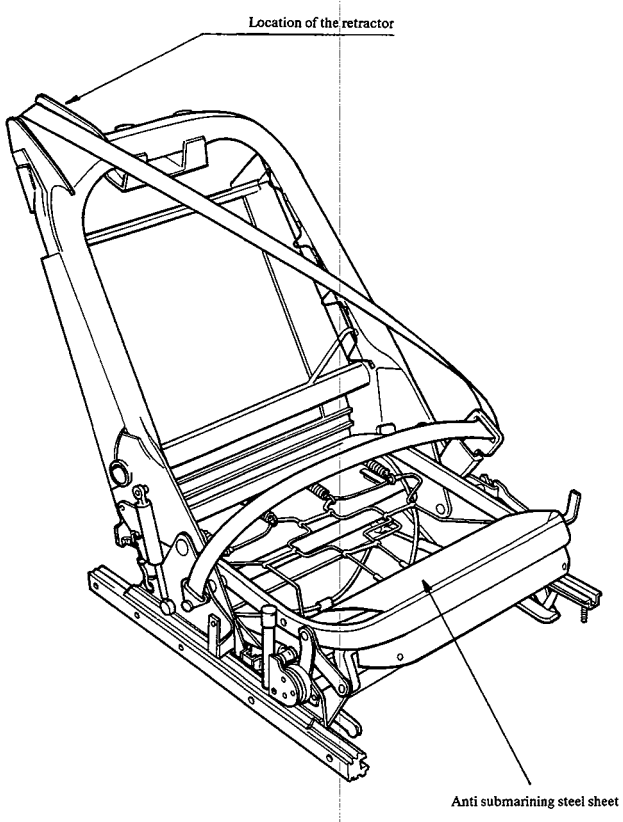

Figure 6. Passenger Seat with the 3-Point Belt Anchorages Built into the Seat

measurement levels lower than the FMVSS 208 regulation's required limits.

Analysis of high speed films confirmed that no submarining, no head impact and no thorax sideward movement occurred.

Rear Passenger Protection

The COVER has 3 rear occupant places which are designed to locate adults, all of which are equipped with three-point reel belts. There is also one rear seat equipped with a built-in supplementary cushion for a child of 3 to 10 years old (integrated booster).

Rear adult passenger protection against submarining is guaranteed by the following improvements:

- *Safety belt improvements* (Figure 7). The lap belt sides, especially the central buckle attachment cables, have been moved to a 70° vertical position and the buckle has been placed level with the seat cushion. This was done so that the strap stays at the pelvic level. This placement has the added advantage of improving safety belt wearing comfort and easier buckling.
- *Seat improvements* (Figure 7). The anti-submarining hump located in the forward seat bottom has been closed by a steel sheet thereby creating a hollow body and increasing its resistance to crushing. Forward seat hinge resistance has been increased in order to better attach the seat to the floor. With the same objective in mind, the back portion of the hole located in the steel sheet in the seat bottom, in which there is an anti-bursting pin, has been reinforced using a 5 mm diameter steel wire.

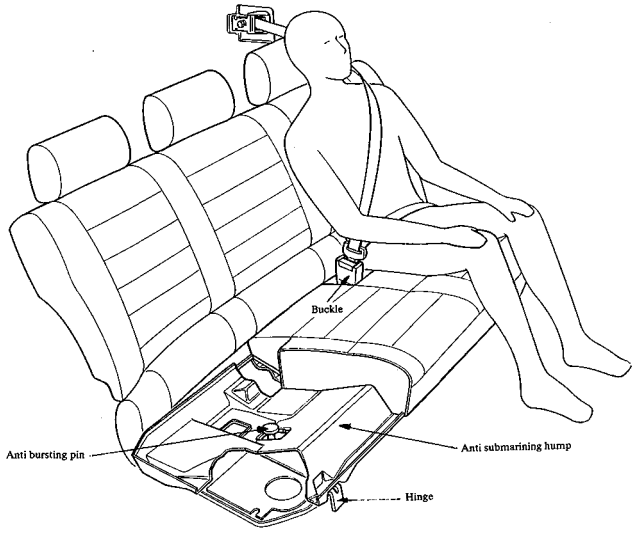

Figure 7. Rear Passenger Seat

Test results at 65 km/h against a 30° left angled barrier. As in the case of front seats, the aforementioned improvements were developed based on sled tests with 5th percentile female and 50th percentile male HYBRID III dummies. In the COVER, at 65 km/h against a 30° left angled barrier, analysis of high speed films confirmed that no head contact or submarining took place. Injury criteria for the chest were lower than required regulatory limits.

Note. The centre rear seat is equipped with a safety belt whose upper attachment is situated on the rear roof crossmember. This attachment is equipped with a system to limit the force applied to the neck by the shoulder strap in case of side impacts.

Child Seat (Figure 8)

For children from 3 to 10 years old, a built-in supplementary cushion has been developed. This cushion is equipped with seat belt strap guides on the sides in order to keep the lap belt in place thereby avoiding any risk of submarining.

In a test at 65 km/h against a 30° left angled barrier, the following injury criteria were obtained:

Table 5. Injury Criteria for Children Obtained with the COVER in a Frontal Impact at 65 km/h Against a 30° Left Angled Barrier

	HEAD		CHEST		
	HIC*	Head excursion max (mm)	max resultant acceleration (g)	3ms resultant acceleration (g)	3ms vertical acceleration (g)
6-years old child Humanetics	691	437	51	47	28
FMVSS 213	1000	-	-	60	-
ECE 44	-	550	-	55	30

* HIC measures throughout the collision

Figure 8. Integrated Booster for Children from 3 to 10 Years Old

Rear Impact Protection

The rear structure of the COVER also received reinforcement to different structural parts, shown in Figure 1. All three rear seats are provided with head rests. These head rests have automatic locking devices whose mechanical characteristics comply with Biomechanical criteria (6). The purpose of these head rests is to minimize movements between the head and the torso during impact.

A 50% offset rear impact was carried out at 50 km/h with a 1,100 kg. rigid mobile barrier, the impact being on the fuel tank filler side. There was no leakage and neck load measurements from the 50th percentile male HYBRID III dummy were much lower than known human limits (7) (Table 6).

Table 6. Front and Rear Passenger Injury Criteria for the COVER in Rear Impact

	Neck injury criteria		
	Front to rear shearing force (N)	Hyperextension moment (m.N)	Hyperextension angle head/chest angle (°)
Front passenger	260	28	24
Rear passenger	800	29	25.5
Human limits	860	57	60

Rollover Impact Protection

The COVER has been tested according to FMVSS 208 test procedure at 50 Km/h. No specific improvements have been done for roll over since the structure behaviour was ensured by the modifications made for side impacts [see paper 91-S5-O-10, reference 8]. The following specifications were controlled:

- no fuel leakage
- no door opening during the crash
- no ejection, even partial of belted dummies
- for each seat range, at least one door can be opened after test.

Conclusion

The COVER illustrates the possibility to offer a satisfying level of safety to all passengers in a mid-range car, even under impact conditions that are very severe in comparison to real-life accidents, using solutions suitable to mass production techniques adapted to the specific problems found at each passenger position. These solutions could be progressively integrated into future Renault cars.

Acknowledgements

We would like to thank the Vehicle Safety Department and the Interior Equipment Engineering Department of the Direction des Etudes Renault as well as Autoliv Klippan Co. for their efficient contribution to the development and adjustments of the COVER's passive safety devices.

References

1. COVER—Syntheses Safety Vehicle, 13th ESV Conference, Paris, November 1991, N. Casadei, Direction des Etudes Renault.
2. Basic Researchs Vehicule, Renault BRV, 5th ESV Conference, London, June 1974, Ph. VENTRE, Direction des Etudes Renault.
3. Status Report of Renault Experimental Safety Vehicule, 7th ESV Conference, Paris, June 1979, Ph. VENTRE, Direction des Etudes Renault.
4. Risque de lésions cervicales en accidents réels et similés, Aguard Conference, Proceeding N°471, Munich, March 1989. C. Tarriere et al., Direction des Etudes Renault.
5. Head risks in frontal impacts: Simulations and Differences Between Tests and Real Life Situations, 12th ESV Conference, May 1979, G. Walfisch et al., Direction des Etudes Renault.
6. Influence of Seat and Headrest Stiffness on the Risk of Cervical Injuries in Rear Impact, 13th ESV Conference, Paris, November 1991, JY. Foret Bruno et al., Direction des Etudes Renault.
7. Human Tolerance to Impact Conditions as Related to Motor Vehicule Design, SAE J885, July 1986.
8. COVER: Renault Safety Vehicule Occupant Safety in Side Impacts, 13th ESV Conference, Paris, November 1991, J. Rio et al., Direction des Etudes Renault.

S9-W-34

Engine Bay Packaging for Crashworthiness Performance

P.V. Skuse, N.D. Grew
Rover Group Limited

Abstract

This paper describes a qualitative technique for assessing the potential crashworthiness performance of vehicles in front impact. The technique is based on experience from accident data and crash tests of known features likely to result in a crashworthy vehicle and is aimed primarily at guiding the concept and early design phases of a new vehicle. The application of this technique is limited to monocoque structures with front wheel drive and transversely mounted engines for passenger car type vehicles. The assessment process has been applied to numerous new vehicle studies and confirmed by crash testing.

Introduction

At the early concept phase of a new vehicle project many of the design parameters start from a clean sheet of paper. Indeed a new vehicle may start life as a number of alternative designs including quite different body and chassis arrangements.

It is important however, that these designs are consistent with the achievement of acceptable standards of crash performance.

To support the early concept phase a methodology for assessing numerous designs quickly has been developed. This technique is based on experience gathered from analysis of accident data and extensive development crash testing over many years.

The methodology set out is for frontal impacts only and its application is limited to monocoque structures for passenger car type vehicles with front wheel drive and transversely mounted engines.

Whilst subjective in its application it seeks to compare new designs with existing vehicle concepts, and features likely to result in crashworthy vehicles.

Methodology

The crash performance of vehicles in front impact is a function of the behavior between the "crumple zone" and the "rigid safety cell."

The packaging of components within the engine bay has a direct result on the collapse behavior of the crumple zone and maintenance of the rigid safety cell for both high speed occupant protection and low speed repairability.

Initially the major configuration and layout of the engine bay should be noted, these are:

- Suspension system
- Extent of subframes
- Engine mounting systems
- Steering column fixing—body and chassis mounts
- Body structure
- Engine variants
- Vehicle mass
- Bumper mounting system
- Clearances—depends on engine variants—but usually engine to brake servo, engine to dash behind engine block/manifolds to bulkhead/dash, engine to radiator etc.

These notes and measured clearances allow the designer to get a 'feel' for the design by comparison of the new layout and clearances with known vehicles of similar size and mass.

Next the detail of a design can be compared with a set of preferred features. Note that at this stage the designer is still considering broad features not detail, e.g. body member section size, gauge of panel etc.

This set of preferred features is not exhaustive nor are the features necessarily mutually compatible i.e. adoption of some features may mean other features cannot be adopted.

Nor is this set of preferred features compulsory, deviation does not indicate a bad design, merely that a more studied analysis be undertaken.

These preferred features have been grouped into seven areas:

- Body Structure
- Engine mounting systems
- Suspension
- Steering column/controls
- Brakes
- Engine design/transmission
- General features

The designer uses his knowledge and expertise to assess his new design against these preferred features.

The Preferred Features

- *Body Structure*
  - Front longitudinals should be of straight; uniform square section
  - Longitudinals should have a structural tie into the suspension towers
  - Longitudinals should be linked to the sills via load-spreading members or outriggers
  - Longitudinals should extend under the floor to the heelboard
  - Longitudinals section size on the dash wall should be comparable to main member size
  - Bumper loads should be channelled through front of longitudinals

- Engine mounts should be kept off the body—if possible
- Avoid reinforcements which could bridge potential collapse zones
- Local reduced section sizes in members should be avoided
- Box member provided as the lower windscreen mounting rail

• *Engine Mounting Systems*
- Engine mounts to the body should be avoided
- For engine mounts fitted to the body, the extent of local stiffening should be minimal
- Engine mounts should provide collapse/deformation and allow engine to move relative to body thus maximizing energy absorption of body
- Engine mounts should mount to chassis subframes
- Short tie-bars should be avoided. Longer tie-bars allow tuning of any collapse loads.
- Heavy gauge and large section fore/aft subframe components should be avoided.

• *Suspension*
- Avoid using front facing brake reaction rods
- Any fore/aft suspension component should have provision for collapse if required

• *Steering Column/Controls*
- Steering column should be of double universal joint type
- Provision of collapse in the upper column to cater for dash intrusion
- Steering column to be mounted off the upper dash/screen rail
- Steering column mount to pedal box to be avoided
- Clearances between pedal box and column components should be maximized

• *Brakes*
- Horizontally mounted brake master cylinders to be as short as possible
- Electronic type ABS systems
- Consider remote servo i.e. package servo on opposite side of dash to engine
- Servo angled from straight forward to allow engine to deflect it.

• *Engine/Transmission*
- Inlet and outlet manifolds to be as short as possible or track routes kept close to engine block
- Avoid packaging ancillaries either side of engine block on the same end, especially in line with brake master cylinder.
- Vulnerable items to be packaged away from the front of the vehicle. This can cause an early load path and they can be easily damaged in Low Speed Impact (repairability).

• *General*
- Tow brackets/recovery eyes/lashing brackets should not provide primary load paths if this results in collapsible structure being bridged
- Bumper system/bumper mounting to maximize energy absorption
- Fuel system components away from front of engine
- Avoid rigid components between engine and dash wall
- Avoid packaging fuel system components between engine and dash wall
- Vulnerable items should not be packaged in front 200mm of bumper/engine bay

Discussion and Conclusions

To achieve a safe product in an efficient manner the basic layout and design has to be well thought out. This paper outlines a methodology and relies on comparing new design with features of known performance. It does allow numerous design alternatives to be compared and evaluated quickly and an approximate measure of potential crash performance established.

This allows a manageable number of alternative designs to be evaluated by computer based analytical methods in pursuit of the final design. [1, 2, 3]

Concurrently this allows design of occupant protection features to proceed with a degree of confidence for design evaluation, costing and feasibility.

Rover has developed this methodology for use in its own design process and is now applying it on future designs.

References

1. Emmerson, W.C. and Fowler, J.E., The application of computer simulations in Vehicle Fifth International Conference on Experimental Safety Vehicles, 1974.
2. Leach, J.H. and Grew, N.D., Application of ADAMS to vehicle crash simulation "Better Bodies" Instn. Mech. Engrs, 1988, S679.
3. Leach, J.H., Practical Tools for Vehicle Impact Simulation. Part 1: vehicle impact simulation in Rover Group. Proc. Instn. Mech. Engrs. Vol. 205, 1991.

S9-W-35

Improving Rear Seat Safety—A Continuing Process

Björn Lundell, Gerd Carlsson, Petter Nilsson, Michael Persson, Camilla Rygaard
Volvo Car Corporation

Abstract

This paper will give an overview of the safety of the rear seat of passenger cars. Accident experience for the rear seat, involving unbelted occupants and occupants wearing three-point belts and two-point lap-belts, will be summarized. Different means of improving the safety of the rear seat for both children and adults, in particular the centre position, will be discussed. The three-point retractor belt is an important safety item, which in some car models has been available for the rear outer seating positions for several years. This has not been the case for the rear centre seating position. Two different types of three-point retractor belts for the centre position in sedan models will be presented. A child cushion integrated in the folding armrest in the centre position will be described. This child restraint has recently been introduced for sedan models and is used together with a standard fitted three-point belt.

Introduction

Safety in passenger cars in industrialized countries has steadily increased for many years. There are several reasons for this. Naturally overall changes such as improvements in the traffic system and in the structure of the cars have affected safety.

The development of the interior protection systems has also had a large influence. These have become more effective as seat belts have improved and in certain cases are equipped with pretensioners, and new protection systems in the form of airbags have been added.

Legislation regarding the installation and usage of restraint systems also influences the total safety. Legal requirements regarding the mandatory installation of seat belts have been introduced in many countries, e.g. requirements regarding the installation of the three-point belts in the rear seat. Requirements regarding the mandatory usage of seat belts also exist in many countries.

Safety in the Rear Seat

During this development, the measures intended to increase safety have, in most cases, applied to the front seat. Safety in the rear seat has lagged a few steps behind but front seat development has helped to call attention to the rear seat as well.

Perhaps the most important means of increasing safety is through the usage of the seat belt. This was shown in a report regarding just this, presented during the 8th ESV Conference in 1980 (1). It was based on traffic accident information obtained from 2000 relatively serious accidents involving Volvo cars with rear seat passengers in Sweden. All the cars were equipped with three-point belts in the outer positions and a lap-belt in the centre position. The injury-reducing effect[1] of the belt for injuries in the AIS 1-6[2] range was 52% for children (1-14 years) and 28% for adults (>14 years).

Krafft et al showed at the 12th ESV Conference in 1989 (2) an injury-reducing effect for children of over 50% and for adults of 22-55%. NHTSA, in its Final Rule for requirements regarding the fitting of three-point belts in the outer positions of the rear seat, estimated that lap shoulder belts are 41% effective in reducing the risk of death (3).

In many countries, requirements already exist stating that passenger cars shall be equipped with three-point belts in the outer positions of the rear seat, e.g. Sweden since 1969, USA since December 1989. On the other hand, unfortunately, many still lack requirements regarding installation of belts in the rear seat. Safety will also be improved if car manufacturers fit belts in the rear seat of a higher standard than those laid out in the legislation of the respective countries. Volvo cars in the 200 400 700 900 800 series, for example, have three-point belts in the outer positions of the rear seat as standard for all markets since the introduction of these models. This means, for example, for the 200 series since 1974. In other words this also applies to those markets where the installation of such belts is not a legal requirement.

The mandatory usage of belts in the rear seat is the law in several countries. In Sweden this has been the law since July 1986.

An analysis of Volvo's traffic accident material up to 1990 has been carried out regarding the proportion of passengers in the rear seat and the frequency of seat belt usage in the rear seat. In total, the material contains information for over 15 000 accidents. All types of accidents are included in the data. A summary of the results for the outer positions in the rear seat is shown in Table 1.

It is clear from Table 1 that the frequency of belt usage has increased markedly during the interval 1986-1990 compared with earlier. We have found that the greatest reason for this has been our law regarding mandatory usage of rear seat belts. The figures for usage during 1986-1990 can be somewhat too high since they

[1] The injury-reducing effect (e) is defined as $e = \frac{\text{injury rate, unrestr. - injury rate, restrained}}{\text{injury rate unrestrained}}$

[2] AIS = Abbreviated Injury Scale.

Table 1. Seat and Belt Usage for Rear Outer Seating Positions (Three-Point Retractor Belt)

Year	1976-80	1981-85	1986-90
No. of accidents	3006	3580	9295
No. of occupants	674	942	1894
No. of belted occupants	74	251	1545
Average usage of left & right seats (%)	11.2	13.2	10.2
Belt usage (%)	11	27	82

are based on the occupant's own information, and can be assumed to be exaggerated after the arrival of the law in 1986.

In order to create a safe environment in the rear seat it is, of course, not only important that belts exist in the car, and are used, but also that they provide effective retention during an accident. Good retention requires an optimised belt and also a good shape of the seat cushion and floor. One example of the latter can be given in Volvo's 700 and 800 series, where the floor under the front edge of the cushion has been raised to help prevent submarining (4).

A comfortable seat belt also contributes to increased usage and in this way an improvement in the total safety. The ESV report from 1980 by Norin et al shows that the frequency of usage for the three-point retractor belt in the rear seat was approximately double that for the fixed three-point belt with manual length adjustment (1).

One important reason for improving the rate of belt usage in the rear seat is that unbelted rear seat occupants increase the injury risk for front seat occupants. This has been confirmed by our own crash testing. Evans gives an estimate of 4% increased fatality risk for front seat occupants caused by unbelted rear seat occupants (5).

The Safety of The Rear Centre Seating Position

The measures introduced to increase safety in the rear seat have, for the most part, applied to the outer positions and not the centre position. One essential reason is that it is difficult to equip this position with a three-point belt, because it is difficult to find an upper attachment point for the three-point belt that gives the necessary strength as well as a good belt geometry. The fact that the measures have not been directed towards the centre position also depends upon the fact that this position is not used very often. According to Volvo's analysis of accident data, the centre position is used in approximately 3-5% of all journeys, as shown in Table 2.

A reduction in the usage of the centre position during the period 1986-1990 can be noted. There is a similar reduction for the outer positions. Apparently the average number of rear seat occupants has decreased. A definite explanation to this does not exist.

Table 2. Seat and Belt Usage for Rear Centre Seating Position (Lap-belt)

Year	1976-80	1981-85	1986-90
No. of accidents	3006	3580	9295
No. of occupants	125	182	241
No. of belted occupants	9	34	168
Centre seat usage (%)	4.2	5.1	2.6
Belt usage (%)	7	19	70

Those people who sit in the centre position in the rear of a five seat car have only had a lap-belt for protection. The three-point belt improves the situation in frontal crashes because the upper part of the body is prevented from folding forwards, thereby avoiding bending of the lumbar spine, intrusion of the belt into the abdomen and head impact. The retractor also makes manual adjustment of the lap-belt unnecessary, thus avoiding the risk of a loosely-fastened belt, which gives poor restraint. Still another advantage with the three-point retractor belt, which has already been mentioned, is that it is convenient to use and is therefore likely to increase the usage rate.

In order to show the potential for safety improvements to the rear centre position, the injury rates for the centre and outer positions are given in Table 3. These figures are based on the same accident data, involving Volvo vehicles, as Tables 1 and 2. The injury-reducing effect derived from Table 3 is shown in Table 4.

As can be seen in Tables 3 and 4, a three-point belt will provide better protection in a crash than a lap-belt. It is, however, important to point out that the lap-belt gives a substantial injury reduction compared with being unbelted.

Table 3. Injury Rate for Rear Seat Occupants

Injury rate	Central rear seat		Outer rear seat	
	Lap-belt	Unrestrained	3-point belt	Unrestrained
AIS 1-6	28.4%	33.8%	26.9%	42.9%
AIS 2-6	5.1%	10.7%	5.4%	13.4%

Table 4. Effectiveness of Rear Seat Belts

Injury rate	Lap-belt in centre seat	3-point belt in outer seats
AIS 1-6	16%	37%
AIS 2-6	53%	60%

As can also be seen in Table 3, the risk of injury to unbelted occupants is greater in the outer positions than in the centre position. On the other hand, the risk of injury to belted passengers is approximately the same in the outer positions as in the centre position. This indi-

cates that a two-point belt is not as effective in reducing injury as a three-point belt, which can also be seen in Table 4. Table 4 shows the injury-reducing effect of the lap-belt and the three-point seat belt.

As can be seen in table 4 there is a clear injury-reducing effect, both for the lap-belt and the three-point belt. However, it is greater for the three-point belt.

An estimate by Evans shows that lap-belts in the outer positions are 18% effective in preventing death (5). A corresponding estimate by Evans for lap-shoulder belts is that they are 43% effective in preventing death (6). NHTSA estimates that the rear seat lap-only belts are 32% effective in reducing the risk of death (3), while the corresponding figures for lap-shoulder belts is 41% (3).

If, on the basis of the figures in Table 4, we assume that a three-point belt has the same injury-reducing effect in the centre position as it has in the outer positions, we can expect a reduction of 25% for AIS 1-6 injuries and 15% for AIS 2-6 injuries if a three-point belt is installed instead of a two-point belt in the centre position (Table 5).

Table 5. Injury-reducing Effect of Changing from Lap-Belt to Three-Point Seat Belt in the Centre Position

Injury rate	Injury-reducing effect
AIS 1-6	25%
AIS 2-6	15%

An increase in safety for the central position of the rear seat corresponds with Volvo's continuing efforts to improve safety in our cars, and to develop our cars with three completely satisfactory positions in the rear seat regarding comfort and safety. An important step in this direction was the introduction of the three-point retractor belt and head restraint for the centre position as an accessory for the 700 series sedan cars in 1986 (7).

A three-point retractor belt in the centre position of the sedan model was introduced as standard equipment in the 900 series in August 1990 (model year 1991) and in the new 800 series in June 1991. As far as we know, this is the first time a three-point belt has been fitted as standard in the centre position of the rear seat of a passenger car. At the same time, an adjustable head restraint was introduced as standard in the same position, which has further contributed to increasing safety. The belt and head restraint are described in more detail in a later chapter.

Integrated Child Safety in The Rear Seat

The introduction of the three-point belt in the centre position of the rear seat has been a basic condition for, and has made it possible to develop, integrated child protection for this position. An integrated child seat was introduced at the same time as the standard fitted three-point belt in the 900 and 850 series sedan cars. This will be described in a later chapter.

We have chosen the centre position for an integrated child protection because this position is especially suitable for children. This position is often more uncomfortable for adults and is most often the position left over for children when all the other positions are taken by adults. In addition, children often like this position because they can get a better frontal view through the front seats. Another reason, which has been mentioned previously, is that with a three-point belt installed, the centre position becomes the safest position in the car.

The idea of integrated child protection has been presented earlier on a number of occasions. During the 12th ESV Conference in Göteborg in 1989, Renault presented an integrated child seat in the outer positions of the rear seat (8). A similar idea has been shown in Renault's concept car, Cover, presented in May 1991. Another report by Karlbrink et al from the ESV Conference in 1989 showed a protection system integrated in the backrest section of the front seat (9). Volvo also showed a prototype of the integrated child seat described in this report at the ESV Conference in 1989.

Three-Point Accessory Belt for the Rear Centre Position

As has been already mentioned, a three-point retractor belt was introduced as an accessory item for the 700 series sedan cars in 1986 (7). The retractor is fitted above the rear shelf with special brackets (Figure 1). The brackets provide the anchorage with the necessary strength and move the upper attachment point to the right height. The installation is covered with a plastic cover. The lower end of the belt is fastened in the same attachment point as the ordinary lap-belt. A head restraint as an accessory also exists for the centre position, and contributes to further increasing the safety of this position.

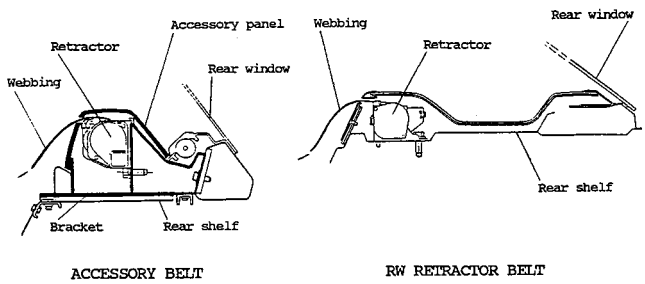

Figure 1. Installation of Retractors on Rear Shelf in 700 Series (Left) and 900 Series (Right) (Difference in Vertical Position of the Rear Shelf Between the 700 and 900 Series is Shown)

Three-Point Standard Belt for the Rear Centre Position

The technology surrounding this belt is described below. The description mainly concerns the 900 series, but the technology is very similar for the 800 series.

Conditions Concerning the Vehicle

During the concept phase of the 900 series sedan model, it turned out that the conditions gave the possibility of attaching the belt to the rear shelf, keeping a good balance between belt geometry, design, visibility and luggage space. The rear shelf provided a possible load-bearing structure for the attachment of a retractor. Therefore a preliminary concept study was initiated. One aim of the study was to place three belt retractors on the rear shelf and thereby one three-point belt in the centre position. Based on the accessory belt introduced earlier and the structural measures necessary to achieve the correct strength and geometry, the following guidelines were drawn up for a cost and weight effective solution:

- a newly developed belt retractor with inverted belt output geometry in order to achieve the correct height geometry
- fastening the belt retractor directly to the plane of the rear shelf
- legal requirements and internal Volvo requirements regarding safety, geometry and strength
- adapting the belt to the integrated child seat for children in the age range 3-10 years

Results of the Concept Study

During the development of the "Reverse Winded Retractor," the belt retractor presented special problems. The first concerns creating sufficient strength in the component parts and attachments of the retractor. Due to the fact that collision forces go directly into the retractor without a seat belt guide, these forces become greater than during a traditional installation with seat belt guide. The loads are guided into the retractor creating a greater bending moment in the attachment plane. This results in other system requirements, e.g. legal requirements, also becoming more difficult to meet. The character of the loading means that the loads into the car body structure, apart from shearing, also have a bending moment component. The development of this retractor was carried out by Autoliv Sweden. (Figure 1).

The geometry which resulted from the concept study produced the desired height position for the belt retractor for all the positions, without the need to introduce any brackets or seat belt guides. The retractor is attached directly onto the plane of the rear shelf. The rear shelf has been raised by approximately 100 mm when compared to the earlier 700 series. The desired position in the other directions (longitudinal and lateral) could also be attained based on the desired belt geometry for different passenger sizes and without conflicting with the standard fitted head restraint.

A good balance between design, visibility, luggage space, etc, was possible for the other requirements. One problem is provided by the Australian requirements for the zone for attachment points. These requirements contain a limitation regarding the position of the upper seat belt guide point rearwards in the vehicle and in our opinion provide an unnecessary limitation for a correct location of the upper attachment point in the rear seat. (Figure 2).

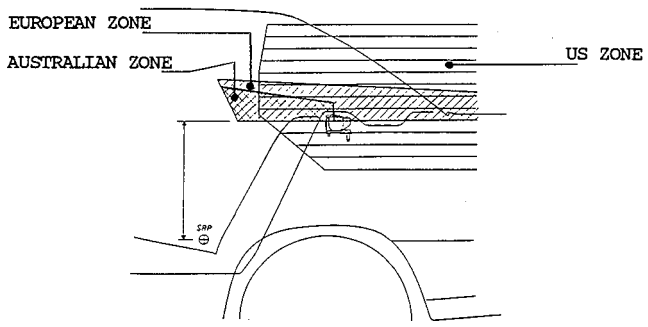

Figure 2. Attachment Point Zones According to Different Regulations

With reference to structural strength, the new concept produced new conditions for absorbing loads. Partly by the rear shelf being used as an attachment point, partly through the increased forces due to the seat belt guide not being used, and partly through the geometry of the RW retractor, apart from shearing forces, producing a bending moment. The local strength was reached on the outer positions by using load distributing brackets. The global strength for these positions was reached by taking up the loads in the body sides and wheel housing.

It became necessary to introduce a spot-welded hat profile for the centre position along the rear seat backrest in order to ensure the global strength. A local reinforcement was integrated in this reinforcement near the retractor attachment.

The results of the preliminary study were, from a cost and weight effectiveness point of view, to be able to offer a three-point belt for all three positions in the rear seat. This in combination with the standard head restraint fitted in all three positions provides fully adequate passenger seating with regard to safety and comfort. The concept also gives rise to the following advantages:

- Low friction losses when taking out and releasing the belt because there is no seat belt guide
- A good belt geometry by placing the seat belt exit from the retractor right behind the passenger's shoulder
- A height-adjustable head restraint on the centre position provides good safety for various sizes of passenger from children to adults and in addition good vision backwards when the centre position is not being used
- The possibility of an integrated child seat in the centre position
- The possibility to fit conventional child seats increases in the centre position, as child restraints requiring three-point belts can be used

The new belts fitted on the rear shelf are in production in the 900 series sedan models as from the 1991 model and were introduced in the new 800 series in June 1991.

Child Cushion for The Rear Centre Position

Conditions

One of the conditions during the development of the 900 series sedan models and the 800 series was that the armrest in the centre position in the rear seat should be able to be replaced with an integrated child cushion. The following conditions were specified (the description applies to the 900 series, but is very similar for the 800 series):

- The cushion should be able to be used for the same ages as the conventional cushions, i.e. children in the age group 3-10 years (groups 2 and 3 according to ECE Regulation 44).
- The centre position should be equipped with a three-point belt and adjustable head restraint as standard.
- The space for the cushion was limited by the outer measurement for the ordinary armrest.
- When the child cushion was folded together it should function as a normal foldable armrest.
- The cushion and armrest should have common attachment points in the car body.
- Legal requirements and internal Volvo requirements regarding safety, geometry and strength should be met.

Technical Solution

The integrated child cushion is constructed in two parts, a seat cushion and a backrest. Both have a steel framework which is cast in expanded polypropylene (EPP). The padding is glued onto the EPP surfaces. The cushion is upholstered in the same material as in the rest of the interior, and the covering is removable for washing (Figure 3).

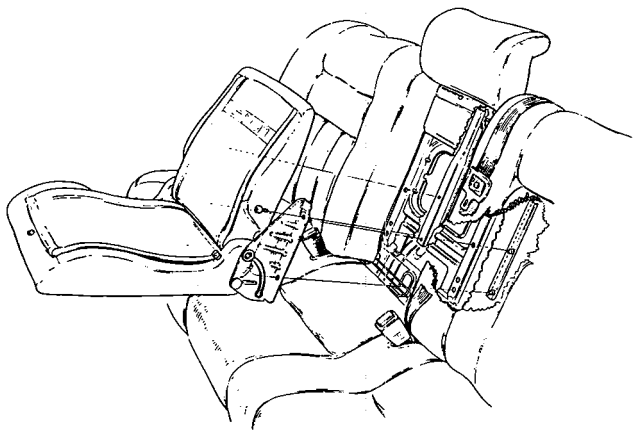

Figure 3. Child Cushion

The backrest and cushion are connected to each other by a hinge system which blocks the backrest both forwards and backwards in relation to the cushion when it is folded up. In addition, the seat cushion is locked to the car body.

All forces which occur in the cushion during a collision are absorbed by the cushion's attachments to the backrest of the rear seat. This is therefore reinforced with two brackets.

The stiffness of the cushion, brackets and backrest of the rear seat is adjusted to retain a controlled movement of the occupant during impact. This results in low injury criteria and helps prevent submarining.

One difference between the 900 and 800 vehicles is worth noting. The 800 rear seat has a narrower armrest and the width is unsatisfactory for a child cushion. Therefore, a special mechanism was developed which widens the cushion when it is unfolded.

Dynamic Testing

The development testing regarding crash safety has primarily been carried out on a sled. Most tests were done according to ECE Regulation 44. This implies specified deceleration pulses with a speed of 50 km h in frontal impact and 30 km h during simulation of a collision from the rear. In order to verify the sled tests, full-scale tests at 30 mph have also been carried out.

The dummies used are the European TNO P3, P6 and P10, i.e. corresponding to the ages 3, 6 and 10 years.

The testing has shown that the integrated cushion affords good protection to children in the age range 3-10 years, during both frontal collisions and collisions from the rear. The results show that the protection is at the same level as, and in some respects better than, a normal accessory cushion.

When comparing the integrated child cushion with the traditional child cushions, their patterns of movement differ from each other during the course of an accident. Since the integrated cushion is fixed at the rear edge, it is prevented from moving longitudinally and therefore a more controlled course of events is obtained during an accident.

During development, there was considerable variation in dummy response in certain test series. When investigating this, it was found that child dummies gave certain doubt regarding their repeatability. Since increasing resources have been invested in order to develop built-in child safety equipment, it is of the utmost importance that the measuring equipment can be trusted. Therefore the same requirements for the checking and calibration of the adult dummies should be used for the child dummies. At present this is not the case with the European dummies.

Test Results

An example of test results from sled testing according to ECE Regulation 44 and from a frontal barrier crash is given below.

The ECE regulation stipulates that the resultant chest acceleration should be below 55 g:s and the vertical chest acceleration below 30 g:s.

It should be noted that the European dummies were not originally intended for measuring head injury criteria (HIC).

All chest accelerations are well below the ECE requirements.

As can be seen from Tables 6 and 8, the measured injury criteria levels are lower in a barrier crash test than in the ECE R44 test.

Table 6. Frontal Crash Tests, ECE R44 Pulse 50 km/h

	HIC	Resultant chest acceleration (g)	Vertical chest acceleration (g)
3 years	435	45	14
6 years	515	47	10
10 years	440	45	21

Table 7. Rear Crash Tests, ECE R44 Pulse 30 km/h

	HIC	Resultant chest acceleration (g)	Vertical chest acceleration (g)
3 years	290	38	20
6 years	200	46	13
10 years	440	37	6

Table 8. Full-scale Frontal Barrier Crash Test at 30 mph

	HIC	Resultant chest acceleration (g)	Vertical chest acceleration (g)
10 years	245	36	12

Certification

For Europe and the other countries which accept the European requirements, the cushion is certified for ECE Regulation 44. The certification occurs in the non-universal category, which means that testing should take place on a car body and not in the standardized test rig.

In the US and Canada, the integrated child cushion is marketed for children weighing more than 50 lbs.

Specific Problems Associated with the Rear Centre Seating Position

There is a potential risk of injury which is unique to the centre position in the rear seat. It is that during side collisions against one side of the car, the belt might possibly produce injuries to the throat spinal region.

This problem has been brought to notice in connection with the introduction of the "reversed belt geometry" in the rear seat (10). A report which was presented at the Stapp conference in 1990, however, showed that the risk of injury is very small (11). Our own testing also shows that loading on the neck is low during side collisions.

When discussing the possible increased risk of injury for a three-point belt located in the centre position, it is important to remember that the alternative to the three-point belt is a lap-belt with a greater risk of injury. The great advantages of the three-point belt, in most types of collision, in our opinion very clearly outweigh the small risk of injury in certain side collisions.

The safety-increasing measures for the rear seat described in this report concern sedan models. There is, as yet, no three-point belt or integrated child cushion for station wagons. The reason for this is that it is more difficult to find a stable and sufficiently high fastening point for the upper attachment point in station wagons, where the rear seat's backrest is often divided and foldable and there is no rear shelf.

Figure 4. Child Cushion Folded Up in the Backrest in the 900 Series

Figure 5. Child Cushion Folded Down as an Armrest in the 900 Series

Conclusions

The introduction of a standard fitted three-point belt in the centre position in sedan cars has meant increased safety for the rear seat. The integrated child seat has further contributed to increasing the safety level in the rear seat.

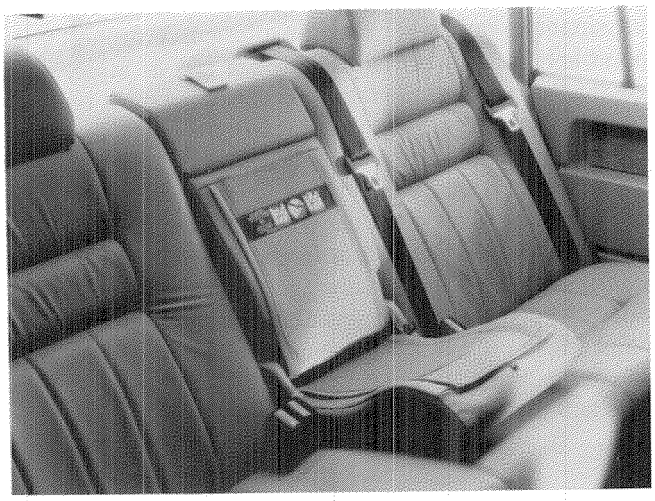

Figure 6. Used as a Child Cushion in the 900 Series

Figure 7. Child Cushion in the 850 Car

During the development of the child cushion it has been observed that the integrated child protection is not consistent with the legislation in certain markets. This constitutes an unfortunate obstacle for safety development.

The testing has also indicated that the repeatability of the child dummies can be a problem. A calibration routine corresponding to that which exists for adult-sized dummies is desirable also for child dummies.

Acknowledgements

The authors wish to thank Hugo Mellander, Magnus Koch, Anders Eugensson and Bill Shapiro, who have reviewed the paper and given valuable comments and suggestions. We also wish to recognize Anne Nyth and her associates for their tireless effort with translation and typing.

References

1. H. Norin, A. Nilsson-Ehle, E. Saretok, C. Tingvall, *Injury Reducing Effect of Seat Belts on Rear Seat Occupants.* 8th ESV Conference, Wolfsburg, October 21-24, 1980.
2. M. Krafft, C. Nygren, C. Tingvall, Rear Seat Protection. *A Study of Children and Adults in The Rear Seat of Cars in Relation to Restraint Use and Car Characteristics.* 12th ESV Conference, Göteborg, May 29-June 1, 1989.
3. 49 CFR Part 571, Docket No. 87-08; Notice 3, June 14, 1989.
4. B. Lundell, H. Mellander, I. Carlsson, *Safety Performance of a Rear Seat Belt System with Optimized Seat Cushion Design.* SAE 810796, 1981.
5. L. Evans, *Rear Seat Restraint System Effectiveness in Preventing Fatalities.* Accident Analysis and Prevention. 20: 129-136, 1988.
6. L. Evans, *The Effectiveness of Safety Belts in Preventing Fatalities.* Accident Analysis and Prevention. 18: 229-241, 1986.
7. L. Karlbrink, H. Mellander, *A Three Point Belt in the Rear Centre Seating Position as Accessories.* SAE 870483, 1987.
8. B. Weber, G. Stcherbatcheff, F. Brun-Cassan, *Protection of Children More Than Three Years Old: Presentation of a Concealable Device Integrated in a Seat.* 12th ESV Conference, Paper No. 89-1A-0-008, Göteborg, May 29-June 1, 1989.
9. L. Karlbrink, M. Krafft, C. Tingvall, *Integrated Child Restraints in Cars for Children Aged 0-10.* 12th ESV Conference, Paper No. 89-1A-0-007, Göteborg, May 29-June 1, 1989.
10. J. Haberl, S. Eichinger, W. Wintershoff, *New Rear Safety Belt Geometry—A Contribution to Increase Belt Usage and Restraint Effectiveness.* SAE No. 870488, 1987.
11. D. Kallieris, G. Schmidt, *Neck Response and Injury Assessment Using Cadavers and the US-SID for Far-Side Lateral Impacts of Rear Seat Occupants with Inboard-Anchored Shoulder Belts.* SAE Paper No. 902313, 34th Stapp Car Crash Conference Proceedings, Orlando, November 4-7, 1990.

S9-W-36

Could a Lap Belt in the Rear Centre Position Save Human Lives?

J.Y. Foret-Bruno, C. Tarriere
Renault
L. Oudenard, C. Got
Institut de Recherches Biomécaniques et Accidentologiques
D. Song
Societé d'Etudes et Recherches des Arts et Métiers
A. Patel
Institut de Recherches Orthopédiques

Abstract

As of January 1992, all back seat passengers in France, in cars equipped with rear seat belts, will be required to buckle up. For side rear seat positions, the use of 3-point belt systems, which have been installed in French vehicles for approximately the last 15 years, will certainly improve passenger protection as they are known to be highly effective. However, almost none of the current vehicles are equipped with a seat belt for the central rear seat position. Vehicle owners, of course, have the possibility of having central 2-point rear seat belts installed after they buy the car, but it has only been recently that car manufacturers have been installing these seat belts on the production line. Given that the effectiveness of these seat belts is often a subject of controversy in the US, will it save lives in France if all occupants of the central rear seat position wear them (using restraining system adaptations appropriate for young children)? The study of past research in this field, accident data, and testing with post mortem subjects and dummies, has shown that the systematic use in the central rear position of a lap belt (even with appropriate restraint adaptations for young children) by all passenger, will result in an increase in the number of occupants killed and seriously injured for accidents on the whole. The number of serious injuries to occupants which can be avoided with such a belt, mainly by preventing occupant ejection, will be lower than the number of additional serious injuries which will be observed in frontal impact accidents. Of course this conclusion, which is based on a given occupant age distribution (accident data from 1980), could change if there were a change in this distribution. For example, if significantly more young occupants (younger than 7) use this central rear position (35% in the studied sample), the protection they would receive with a restraint device adapted to the two-point lap belt could offset the aforementioned risk. It might even decrease the number of seriously injured.

Vehicle Occupancy in Crashes Involving Bodily Injury

In *fatal* crashes, the rear-seat occupancy rate of the vehicles is higher than for crashes involving bodily injury as a whole. From observations made, the presence of three rear passengers is twice as frequent (9% as against 4%).

In 60% of cases, a single rear occupant chooses the right rear position, and in the 30% of cases the left rear. The rear centre position is occupied mostly by children (Table 1).

Table 1. Vehicle Occupancy in Crashes Involving Bodily Injury

	At least one rear occupant	Three rear occupants
LAB file (8,000 vehicles)	25%	4.6%
National Police file (all accidents involving bodily injury)	23%	3.4%
Fatal accidents 1980 (at least one fatality in the vehicle)	31%	9%
Fatal accidents (at least one rear fatality.	14%	4.2%

For all fatal accidents as a whole, a rear centre fatality is observed *in 2% of cases*, and one third of those fatalities are aged less than 10 (in two out of three cases, the fatality is accompanied by two other occupants).

Effectiveness of the Two-Point Lap Belt (Statistical Data)

The available statistics chiefly concern the rear side positions for crashes occurring in the U.S.A. and Canada. The level of effectiveness observed by the various teams can be summarized as follows (references 1 to 7).

- For all crashes taken together, the two-point lap belt reduces the number of fatalities by 15% to 25%, and their severity by 20% to 40%;
- In frontal crashes, the severity of injury and the fatality rate *increase* by O to 30% depending on the source.

All the authors agree that the effectiveness of the rear two-point lap belt is due to the prevention of occupant ejection, especially in the case of rollover.

Therefore in order for the overall effectiveness to be positive, when the effectiveness in frontal crashes is negative, the number of ejections must be greater when no lap belt is worn.

The only available statistics concern ejection for all occupants. For example, the NHTSA states that in 1987

(8), for passenger cars, 24% of all fatalities were observed in *rollovers* (5,976 out of 25,132 fatalities), and for light trucks 52% (3,658 out of 7,008). The percentages of severe injuries and fatalities in rollovers for these two categories represent 16% and 42% respectively. In all these crashes, lap belts were worn by 33% of casualties and 21% of fatalities, these percentages being 50% lower than those observed in the crashes studied by us.

Allowing for this rate of lap belt wearing, it can be estimated that the percentages of severe injuries and fatalities in rollovers observed in the USA are twice as high as those observed in France. According to the authors, the numerous cases of ejection can be attributed to the large side windows (1/3 of the cases) and the doors (1/4 of the cases).

It can therefore be assumed that, given the low ejection rate in France as compared to the U.S.A., the effectiveness of a two-point lap belt in France would be far lower than that indicated by the U.S. statistics, and might even be non-existent. Can we put a figure on this effectiveness? This is what we will try to do with our accident research file after studying U.S. cases.

Effectiveness of a Two-Point Lap Belt (Accident Research Data)

Frontal Impact (NTSB Case Study—Reference 9)

A major report by the NTSB concludes that it is better, in frontal impacts, not to be wearing a seat belt than to be wearing a two-point lap belt in the rear. On the basis of that report, it is possible to define severe injuries and fatalities as a function of impact violence, but also to make comparisons between the various severe injuries observed with and without a lap belt (Table 2).

Table 2. Frequency of Severe Injuries According to Violence of Frontal Impact

	D V	<25 km/h	26 - 40	40 - 56	>56 km/h
NTSB	2-point lap belt	0(0)*	40(20)	76(29)	86(43)
	without lap belt	0(0)	0(0)	13(0)	20(6)
LAB	without lap belt	0(0)	7(1)	18(3)	36(12)

* Severity level (fatality rate)

Frequency of Severe Injuries According to Violence of Frontal Impact

This eloquent table allows us to estimate the effect of wearing a lap belt in the rear centre position. It should be remembered that unrestrained occupants in the rear positions are subjected to the same risk in frontal impact as very young restrained occupants not sustaining intrusion (see Figure 1).

Typology of Severe Injuries Observed for Restrained and Unrestrained Casualties

It is interesting to make a distinction between severe injuries (MAIS 3), very severe injuries (MAIS 4-5) and

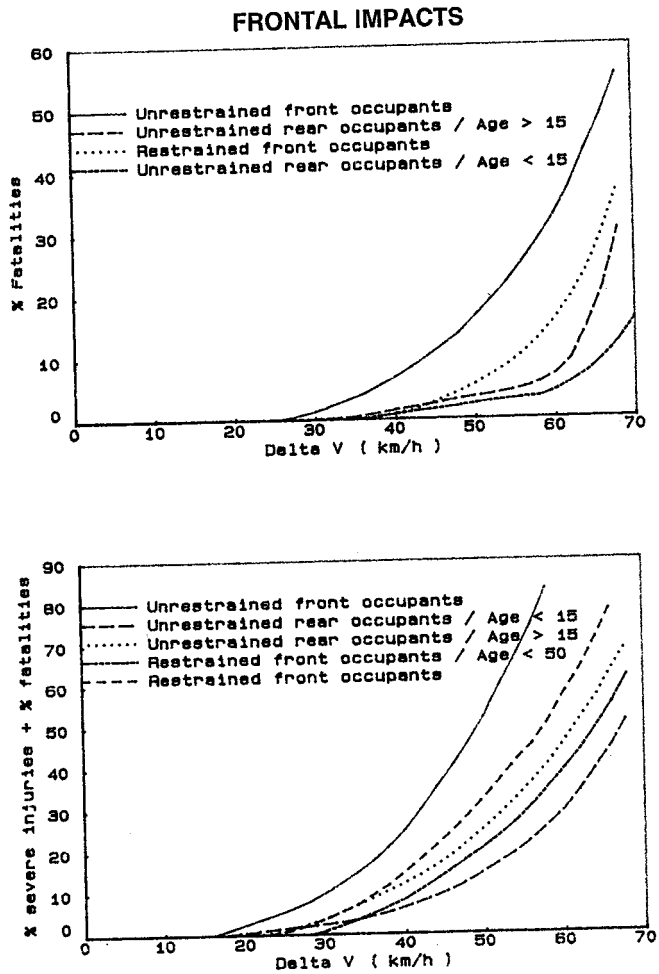

Figure 1. Risks Versus Delta V for Various Configurations

fatalities (MAIS 6). The following table shows that for 100 severe injuries and fatalities, the breakdown among these three categories is very different for two-point restrained casualties and unrestrained casualties (Table 3).

Table 3. Typology of Severe Injuries Observed for Restrained and Unrestrained Casualties

	MAIS 3 severe	MAIS 4- 5 critical	MAIS 6 fatal	TOTAL
2-point lap belt	20	50	30	100
without lap belt	68	8	24	100

With the two-point lap belt, 80% of severe injuries are of MAIS 4-5-6 level, and only 32% for unrestrained casualties.

It is true that the injuries are located in very different body areas, and it is understandable that with the *two-point lap belt, the injury level is often critical* (Table 4).

Table 4. Breakdown of Severe Injuries

	Head	Neck	Thorax	Abdomen	Spinal column	Limbs
2-point lap belt	29	10	--	38	15	8
without lap belt	16	3	4	9	3	64

Estimated Fatality Savings on the Basis of Fatal Accident Police Reports for 1980

We saw that the rear centre occupants are relatively few. Nevertheless, it is interesting to try to calculate the number of human lives that could be saved by wearing the lap belt in the rear centre position.

The figures for 1980 show 1,400 motorist fatalities for all seating positions, including 28 fatalities in the rear centre position, seven of whom were alone in the back seat and 21 accompanied by at least two other occupants.

- Assuming that the sole occupant was wearing a lap belt, *two of the seven* lives could have been saved. The figure is the same for a 2-point or 3-point lap belt (frontal impact with a 5-year old child ejected in rollover).
- For the 21 occupants, one observes that in five cases they were accompanied by three adults in the rear. Assuming a maximum of three rear occupants, the figures classified by type of impact are given in the following table (Table 5).

Table 5. Figures Classified by Type of Impact

	Frontal	Side	Rollover
Single rear fatality	2	1	4
Two rear fatalities	3	4	2
Three rear fatalities	2	3	--

Given the violence of the frontal and side impacts, no savings can be expected in side impact and a maximum savings of two fatalities in frontal impact. In rollovers, ejection is the cause of death (in every case, one or two of the adjacent occupants are ejected). The number of lives saved by wearing a lap belt can be estimated at five in rollovers, giving a total savings of seven out of twenty-one.

On the whole, for all the rear centre positions, the effectiveness would be 32% (9 lives saved out of 28) with a two-point lap belt.

This raw figure is no doubt very positive from the viewpoint of the public authorities, since it corresponds to saving 30 or 40 lives in a year.

The main question now is how many slight or severe injuries would become very severe injuries or fatalities through wearing a lap belt in frontal crashes?

In our file, the number of survivors of fatal frontal crashes can be estimated at 25.

- For six children aged 6, if they had been wearing a suitable restraining system, the severity level would remain unchanged (4 slight injuries, 2 severe injuries).
- For 19 survivors, if they had been wearing a two-point lap belt (10 slight injuries, 9 severe injuries), the severity level would have been very different (7 fatalities, 9 severe injuries, 3 slight injuries).

Hence, in the case of fatal crashes only, the lives saved chiefly by preventing ejection with a two-point lap belt could be offset by an increase in the number of fatalities in frontal crashes. If we consider all frontal impacts, whether fatal or not, the findings are more pessimistic.

We have endeavored to show this on the basis of our file.

Savings in Terms of Severe Injuries and Fatalities for the Cases in Our File

To estimate injury and fatality savings, we analyzed all those cases in which the vehicle had three rear occupants. Taking into account the occupant's age, the impact violence, and ejection, four hypotheses were made considering that the two side occupants were restrained (Table 6).

- One 2-point lap belt in the centre position for all occupants, which must be adapted as a child restraint for very young occupants (scenario 1).
- One 2-point lap belt for very young occupants, with of course the appropriate restraining system (scenario 2).
- No lap belt (scenario 3).
- Lastly, the most pessimistic hypothesis, the two-point lap belt worn without a special restraining system by all occupants (scenario 4).

Table 6. Estimate of Severe Injuries and Fatalities in the Rear Centre Position of Various Scenarios

	Present casualties with 3 rear passengers	Hypothesis 1: The side-position occupants are restrained Hypothesis 2: Centre-position seat belt			
		1 Age > 6 lap belt Age < 6 child restraining sys.	2 no belt child restraining sys.	3 no belt no belt	4 lap belt lap belt
Frontal (101)	10 (3)	23 (8)	7 (1)	10 (3)	36 (13)
Side (38)	6 (1)	4-5 (1)	4-5 (1)	5-6 (1)	4-5 (1)
Rear (13)	4 (1)	1 (1)	1 (1)	1 (1)	1 (1)
Rollover (32)	4 (2)	0	2 (1)	2 (1)	0
Others (9)	3 (2)	2-3 (2)	2-3 (2)	2-3 (2)	2-3 (2)
Total (194)	24 (9)	30-32 (12)	16-18 (6)	20-22 (8)	43-45 (17)

severe injuries and fatalities (fatalities)

Knowing that 35% of casualties and severe injuries are aged less than 7 (45% aged less than 10), the four proposed scenarios give the following results for 194 occupants *including 15 severe injuries and 9 fatalities.*

It is clear that scenarios 2 and 3 give the best results (Table 7). A lap belt should clearly be used only with a child restraining system. When worn by an occupant aged over 6 and 7, the overall risk is greater.

Table 7. Savings in Terms of Severe Injuries and Fatalities for 4 Scenarios

	Severe injuries	Fatalities	Severe injuries and fatalities
Scenario 1	19 (+ 27%)	12 (+ 33%)	31 (+ 29%)
Scenario 2	11 (- 27%)	6 (- 33%)	17 (- 29%)
Scenario 3	13 (- 13%)	8 (- 11%)	21 (- 12%)
Scenario 4	27 (+ 80%)	27 (+ 80%)	44 (+ 83%)

Test with Cadavers

Six cadaver tests were carried out 15 years ago using a two-point lap belt to verify if its installation would not cause severe, non-verifiable injuries in Hybrid II dummies which were used at that time. The conclusion reached from these tests was that a change in the upper

part of the seat back was enough to reduce the risk of serious head injury.

This series of 6 tests at 50 km/h was enough to convince us of the high risk involved in the use of such a restraining device in the case of frontal impact.

Upon being shown films and test results, public officials opted to change their decision and henceforth all vehicles in France have systematically been equipped with 3-point seat belts in the side rear positions. Of course these test results are still pertinent in the case of restraint systems for the centre rear position. Indeed, it can be hypothesized that the probability of the occupant's trajectory following the vehicle's longitudinal axis, thus avoiding head to seat back impact, is statistically not very realistic. Injuries observed in the six tests at 50 km/h are summarized in Table 8. We can see:

- 3 fatal neck injuries and 2 severe injuries,
- 2 severe head injuries accompanied by severe face injuries in one case,
- 4 severe abdominal injuries accompanied by an extremely severe injury to the spinal rachis in one case,
- 3 severe pelvic injuries (fractures to the ilium wings).

Table 8. Results Obtained from Cadaver Tests with a Lap Belt-Only Restraint: Delta V = 50 km/h

Test	CADAVERS AGE	HEIGHT (cm)	WEIGHT	INJURIES	HEAD IMPACT AREA
1	38	166	49	Rupture of abdominal wall, fractures to the ilium wings	On the upper part of front seat back
2	51	169	66	Dislocation of C5-C6, cord transection, 5 rib fractures	On the upper part of front seat back
3	62	154	58	Dislocation of C6-C7, cord transection, fracture of C2, 5 rib fractures, complete fracture of L5, ruptures of colon, jejunum, aorta	On the lower part of front seat back
4	52	162	47	Subluxation of C6-C7 and C2-C3, fractures of C2-C3, 3 rib fractures, ilium wing fracture	On the floor
5	74	172	48	Nose, mandible, maxilla fractures, cord transection, dislocation of C2-C6, contusion of brain stem, 15 rib fractures, ruptures of jejunum and abdominal wall. Ilium wing fracture	On the upper part of front seat back
6	73	153	45	Fractures of spinous process C4-C5, cerebrum contusion, rupture of abdominal wall	On the front seat back

This very high rate of severe injuries, in no way similar to what is found in cadaver tests with 3-point seat belts, indicates an increase in risk. It can even be assumed that, at the same impact speed, the results for non-seat belted passengers would be better (taking into account actual road situations).

Tests with Hybrid III Dummies

Frontal tests at 35, 50 and 56 km/h were carried out with 50th percentile male and 5th percentile female Hybrid III dummies. Table 9 summarizes forces suffered by dummies. The dummies were placed in the center rear position for the tests at 35 and 56 km/h. Their trajectories were at a 20° angle to the longitudinal axis. For both tests at 35 km/h, the 5th percentile and 50th percentile dummies struck the upper seat back. At 56 km/h, after striking the upper seat back, the head violently struck the lower part of the seat, as in the 50 km/h test carried out with the dummy in the left rear seat.

Table 9. Results Obtained from Dummy Tests with a Lap Belt-Only Restraint

TEST N°				1	2	3	4	5
Hybrid III dummy				50th p	50th p	50th p	5th p	5th p
Velocity (km/h)				34	56,8	49,3	34	56,7
Seat Angle about z axis				+20°	+20°	0°	15°	20
HEAD ANGULAR ACCELERATION (ANATOMIC) rad/s²	X	min		-1029	-2049	-2900		
		max		5218	14352	4598		
	Y	min		-10785	-16022	-11319		
		max		4672	3130	4571		
	Z	min		-5517	-7480	-3046		
		max		1831	2354	1623		
HEAD ANGULAR VELOCITY (ANATOMIC) rad/s	X	min		-2	-13	-7		
		max		20	25	19		
	Y	min		-24	-19	-124		
		max		35	48	53		
	Z	min		-8	-9	-16		
		max		15	20	6		
HEAD LINEAR ACCELERATION (G) maximum	X			-126	-299	-142	-119	-248
	Y			-39	-108	-42	-118	-150
	Z			26	-84	-81	25	-80
	resultant			132	318	155	161	299
HIC				529	2794	1878	425	4139
NECK FORCES UPPER (N) maximum	X			-870	-1400	-2190	-394	-940
	Y			-310	-240	-498	/	/
	Z			1350	3250	5897	710	1680
NECK MOMENTS UPPER (Nm) max.	X			30	-31	-48	/	/
	Y			-84	-99	-111	-25	-55
	Z			-31	-35	-2		
NECK FORCES LOWER (N) maximum	X			/	-1650	-2422		
	Y			/	/	-611		
	Z			/	4170	6210		
NECK MOMENTS LOWER (Nm) maximum	X			48	-73	80		
	Y			-47	-271	-280		
	Z			-31	69	40		
FORCE APPLIED ON THE FACE (N)	X			-6110	-13800	-5200		
	Y			-1300	-5000	-1700		
	Z			1600	2100	4200		
	resultant			6450	14900	5200		

The 50th percentile Hybrid III dummies were mounted with a 18 accelerometers to measure head acceleration and angular speed (10). From these measurements it was also possible to know the force applied to the face.

At 50 and 56 km/h, very high HIC values and angular speeds were obtained, as well as neck load and torque measurements that were definitely over the tolerance level (Figures 2, 3 and 4, Test #2).

At 35 km/h, HIC values are below limits for the 5th and 50th percentile dummies (425 and 529 respectively). However, neck load and torque measurements are still very high upon hyperextension (870 N for shearing force, 84 Nm for torque), especially for the 50th percentile dummy (Test #1). As well, angular acceleration in this test reached 15,000 rad/s^2 (difference between minimum and maximum). The load measured to the face reached 6,450 N and is applied at the *eye socket*

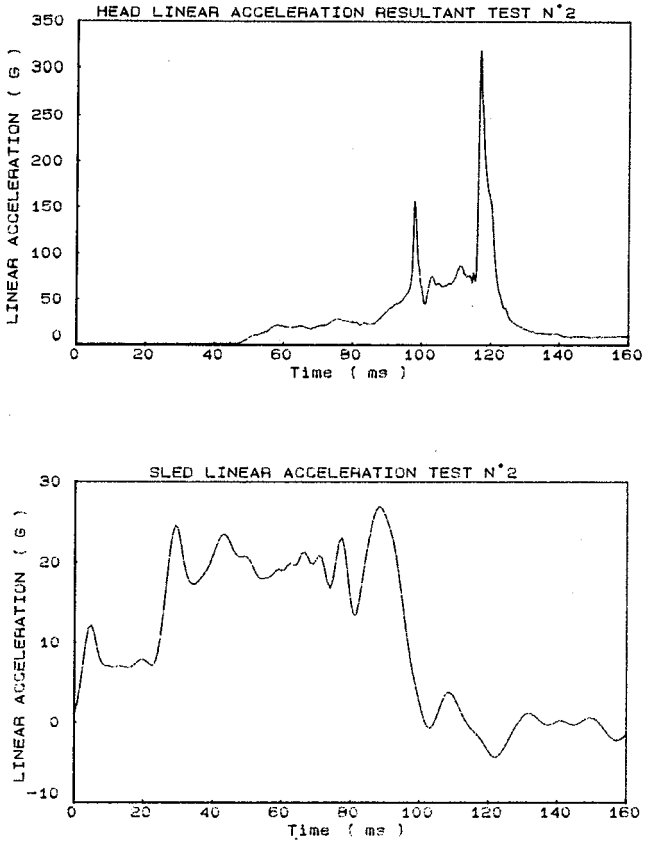

Figure 2. Head Linear Acceleration Resultant and Sled Linear Acceleration for Test N2

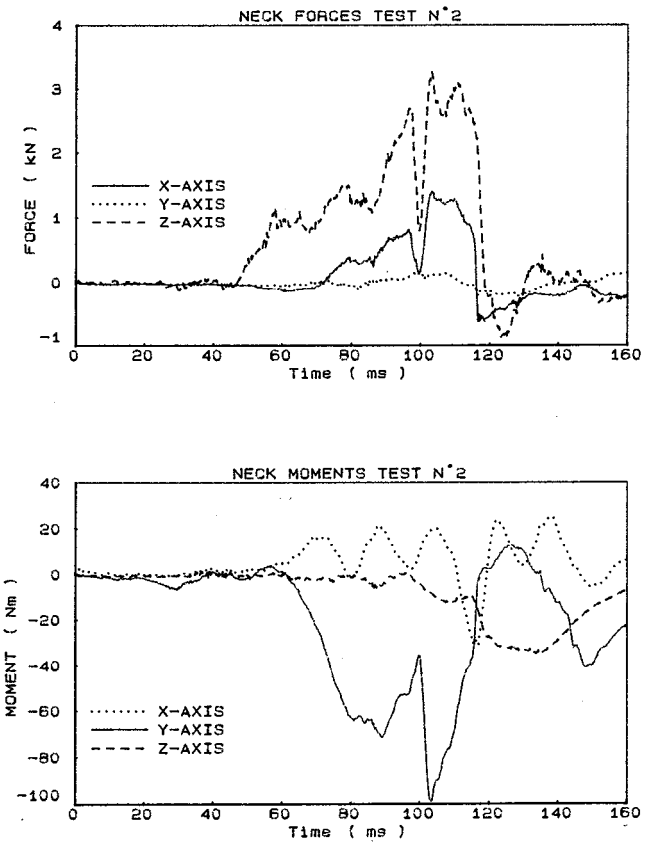

Figure 3. Neck Forces and Neck Moments for Test N2

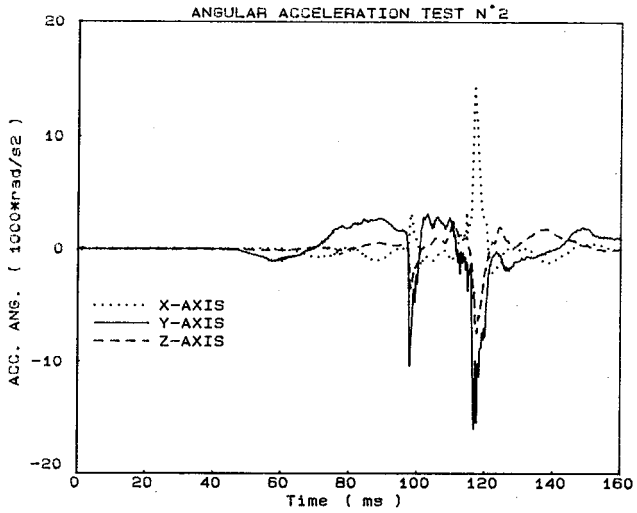

Figure 4. Angular Acceleration for Test N2

level. These tests demonstrate how dangerous loads to the head and neck caused by impact with the upper seat back can already be, for different subject sizes, at 35 km/h. At 50 km/h and up the risk becomes great.

Conclusion

Therefore, it can be concluded that the wearing of a two-point seat belt by all rear seat occupants would increase casualties because of the high risk in the case of frontal impact. This seems to be true even with a restraint system adapted for use by young children, which make up 35% of occupants in this study.

The results would only be positive if the two rear side position occupants wear seat belts and rear centre position occupants younger than 7, and only occupants younger than 7 (no seat belts for older children), wear seat belts with an adapted restraint system.

The larger the number of young children able to use an adequate device in association with the 2-point seat belt, the better the final result. Needless to say, the ideal solution is to install and use the 3-point seat belt for the centre rear position in future vehicles.

References

1. FARS 1987, NHTSA.
2. C. Kahane, "Fatality and Injury Reducing Effectiveness of Lap Belts for Back Seat Occupants," NHTSA, Stapp, 870 486.
3. D. Huelke, "The Rear Seat Automobile Passenger in Frontal Crashes" Proceedings 22nd AAAM Conference (1978).
4. L. Evans, "Rear Seat Restraint System Effectiveness in Preventing Fatalities" Accident Analysis and Prevention, Vol. 20 n°2, pp. 129-136, 1988.
5. D. Dalmotas, "Restraint System Effectiveness as a Function of Seating Position," SAE, Detroit 1987.
6. Campbell, "The Effectiveness of Rear Seat Lap Belts in Crash Injury Reduction," 1986.

7. F. Conley, "An Analysis of Safety Restraint Use and Effects in Passenger Vehicle Accidents in New York States," SAE, Detroit, 1987.
8. Najjar, "Restraint Usage and Effectiveness for Rear Seat Occupants," NCSS, US DOT, 1981.
9. National Transportation Safety Board. Safety study. Performance of Lap Belts in 26 Frontal Crashes. Report number NTSB/SS-86/03, July 1986, US Government, Washington, DC.
10. F. Bendjellal, et al., "Computation of Hybrid III Head Dynamics in Various Impact Situations," SAE, 902320 Paper, Proceedings of the 34th Stapp Car Crash Conference, Orlando, FL, November 1990.

S9-W-38

Parameters Affecting the Performance of Framed Child Seats Anchored by Adult Belts

M.R. Dorn, A.P. Roy
Middlesex Polytechnic
R.W. Lowne
Transport and Road Research Laboratory

Abstract

Framed child seats secured with an adult seat belt have increasingly become the standard child restraint in UK vehicles. However, little work has been undertaken to investigate how the various design parameters affect the dynamic performance. This paper presents the results of a test programme designed to address this question. Parameters such as system centre of gravity, adult belt route, shell inclination and footprint area were varied on a surrogate child restraint, which was subjected to dynamic impact tests in general accordance with ECE R44. The tests were repeated with the child restraint anchored both with adult lap and lap and diagonal belts. The performance was evaluated using the values of 3ms chest acceleration and head forward excursion on the test dummy. A distinction in the effect of each of the parameters was found between the child restraint anchored with a lap belt and that anchored with a 3-point belt. The lowest value of chest acceleration (40g) was observed for the lap belt restrained frame seat with the largest base area while the lowest head excursion was also seen with this arrangement but with the addition of a top tether. Exploring the use of energy absorbing top tethers is suggested.

Introduction

From the early 1960s to mid 1980s the most popular child restraint in the UK for children aged about nine months to about four years was a forward facing shell secured directly to the vehicle structure by four straps, two attached to the shell at the top and two to the bottom (the four point child restraint). The child is held within the shell by an integral five point harness. Recently the four point has been gradually replaced in the UK by the framed reclining version in which the shell is attached to a frame which sits on the vehicle seat and is secured to the vehicle structure using the adult seat belt. This type of child seat has become popular because of the ease of installation and use. While the newer styles of child seat have a marked advantage in simplicity of attachment, the forward excursion of the child in a frontal impact is generally greater than for the earlier four point designs since it is less directly attached to the car and relies on the reaction of the car seat to control forward movement.

Accident investigations of the few cases of restrained child fatality that have occurred suggest that the performance of framed child restraints could be improved (1,2). It would appear that, where the child restraint performance has been considered to have had an influence on the outcome, both excessive forward excursion resulting in head contacts and excessive acceleration resulting in neck injuries have been involved. The performance of such child restraints must be a function of the child restraint itself, the occupant, the car in which it is secured and the means of securing it to the car.

The design of the frame child restraints in the UK has been largely based around the addition of a frame to the existing four point shells. Little work has been published on the identification of the exact parameters that affect their performance. This paper describes a series of tests which attempted to address this question and how far the dynamic performance can be improved. The paper will deal exclusively with the child restraint parameters. Ongoing investigations at Middlesex Polytechnic and TRRL will consider the interaction with the vehicle and to a lesser extent the occupant.

Test Programme

The test programme was designed to study the effects of the route of the adult belt on the frame, the position of the centre of gravity of the child restraint and the size of the base of the frame in contact with the vehicle seat on the forward excursion and on the chest acceleration of the occupant. The study included child restraints held by both adult lap belts and adult lap and shoulder seat belts. For the lap belt configuration, tests were performed also with the addition of a top tether to measure the effect of providing restraint to the top of the frame. Chest acceleration was chosen rather than head acceleration due to the uncertainty of the biofidelity of the neck

and of the chin to chest contact of the TNO P3 dummy used, which will greatly influence the head response.

The initial phase of the programme was a study of a large sample of production UK framed child seats in order to find typical values for the mass and centre of gravity. Some tests (phase 1) were completed using a typical production child restraint but this was found to be unsuitable for multiple testing, due to the excessive distortion of the frame under non-standard conditions. It would also have been difficult to modify the design parameters of the existing child restraint. For these reasons a surrogate child restraint was designed and built.

The dynamic test programme was completed in seven phases. Each phase investigated the effect of a different design parameter. The optimum configuration found in each phase was carried through to the next, thus the child restraint was optimized as each phase was completed.

The Test Series

Phase 1. Variation in adult belt route on typical production child restraint. Seven positions for lap belt. Six for 3-point (lap belt section route was varied).

Phase 2. Variation of shell and hence occupant C of G position using the surrogate child restraint. Nine positions (Figure 1) with lap belt. Only six positions were possible with 3-point.

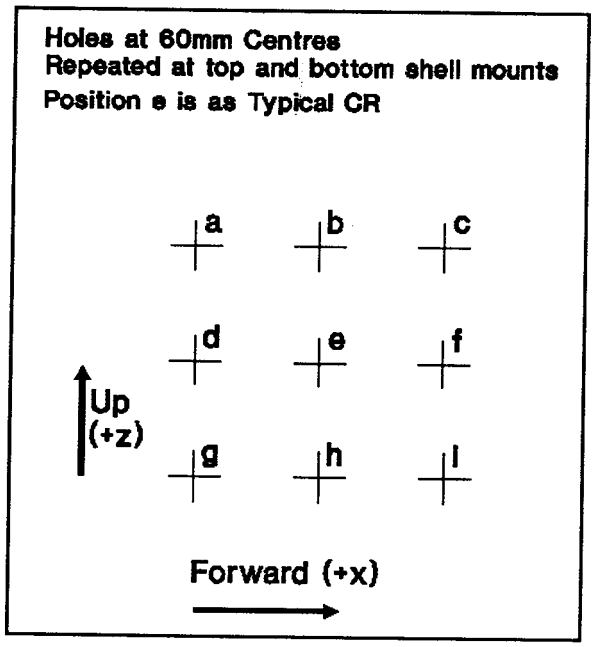

Figure 1. Shell Position

Phase 3. Variation of child restraint foot type and area. Five foot types in total. Standard bar, plate foot at front (one 50x400mm & one 100x400mm) & plate base (one 320x410mm & one 450x460mm).

Phase 4. Variation of child restraint shell inclination. Two positions. Same angle. Reclined about top and reclined about bottom.

Phase 5. Introduction of top tether in lap belt restrained system.

Phase 6. Verification of the effect of adult belt route for the surrogate child restraint. Five positions (Figure 2).

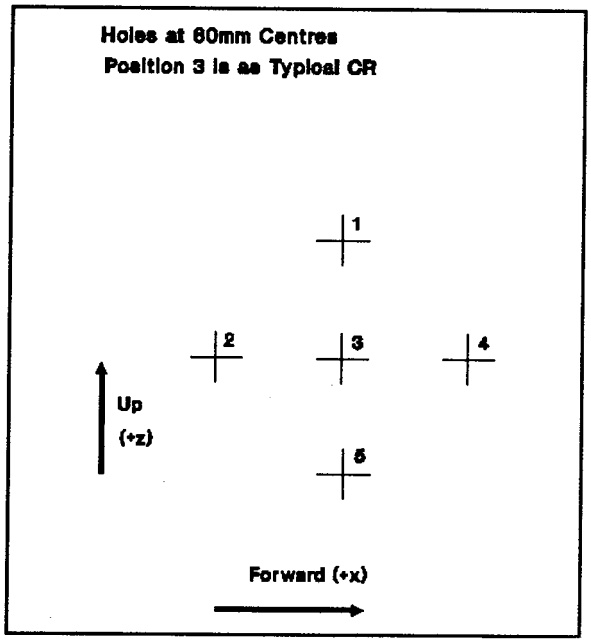

Figure 2. Lap Belt Position

The Surrogate Child Restraint

The surrogate child restraint was designed to have the capability of variation of the parameters mentioned above. The basic dimensions were taken from the typical production child restraint, i.e., foot size/position, shell position, adult belt position etc. A standard production plastic shell and harness were used to simplify the manufacture of the child restraint. The shell and harness were replaced when showing signs of wear. Generally shells were replaced after 3 tests and harnesses after 4. The surrogate child restraint (See Figure 3) was composed of two shaped aluminum alloy 6mm thick side plates, two 25mm diameter aluminum alloy tube cross members (one rear foot and one rear strut) and one 25mm diameter aluminum bar (the front foot).

The side plates were drilled with a series of holes which allowed the shell position and belt route to be moved in the x-z plane (required for phases 1, 2 & 4). In addition to the standard bar, four other foot types could be bolted in place of the bar foot (phase 3).

The mass of the child restraint varied between 7.5 and 8.5 kg, depending on the foot type that was used. This was up to 2.8 kg heavier than the typical production child restraint (5.7 Kg). This unavoidable feature was not thought to effect the performance excessively.

Test Procedure

The dynamic tests were performed at the Road Safety Engineering Laboratory, Middlesex Polytechnic which is

Figure 3. Photograph of Surrogate CR

described elsewhere (3,4). The tests were conducted in general accordance with ECE R44 (5) i.e., velocity 50 Km/h, peak acceleration approximately 25g. As defined in the standard a TNO P3 dummy was used, instrumented with triaxial accelerometers in the head and chest. High speed film and video recording allowed analysis of excursions. The test seat was that specified in R44 and is shown diagrammatically in Figure 4.

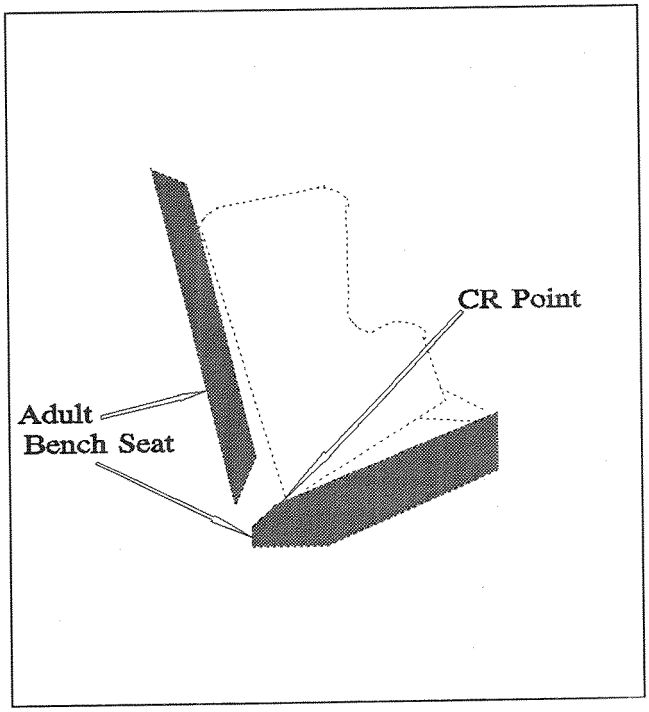

Figure 4. Sketch of Test Seat Showing Cr Point and Surrogate Child Restraint

Surrogate static lap belts were used, which were composed of sections of webbing linked to the child restraint with standard belt anchorages. The 3-point belts were represented by a static belt in which 50mm slack was induced in the diagonal strap, after the belt had been tightened, to simulate the webbing payout observed with inertia reel belts. For the surrogate seat the 3-point belt in the standard position was routed through slots in the side plates. For the variation in belt route (phase 6) it was necessary to use a surrogate belt composed of three separate straps. However it was not considered representative for the majority of testing, as slip between sections was thought to be an important factor that should not be eliminated.

Performance of the child restraint was mainly judged using three parameters:

- Maximum chest 3ms acceleration
- Head maximum excursion, defined as the maximum forward position of the head relative to Cr point (Figure 4)
- Head maximum movement, defined as the maximum forward movement of the head relative to the initial position.

The second parameter gives an absolute measure of the forward movement limit as it would occur in a vehicle. The third parameter, head maximum movement, was defined in order to make comparisons in the second phase where the shell was moved within the frame.

Ideally both forward excursion and chest acceleration should be as low as possible. A short stopping distance, and thus reduced forward movement, would be expected to be accompanied by an increased chest acceleration. It is difficult to establish an optimum compromise as this will depend on the impact speed and acceleration and on the internal dimensions of the vehicle. However, it might be considered that, provided the head forward excursion does not exceed about 550mm from the Cr point (the limit in R44), the performance could be considered to be improved for a reduced chest acceleration.

The estimated accuracy of the measurements is as follows:

- Acceleration ± 5% of reading.
- Excursion and movement ± 8mm.

Results

Phase 1. The Effect of Belt Position on a Typical Production Child Restraint

The dynamic performance was only adversely affected by a change in belt position from the manufacturers' specification. The child restraint frame distortion was increased when the belt load was in the non-specified positions. Chest 3ms accelerations were on the whole increased, as were the maximum head excursions.

Thus the surrogate child restraint for the remaining phases was designed using the standard lap belt positions. However, it was found that a slight lowering of the

3-point lap route slots allowed greater flexibility in the movement of the shell in the next phase.

Phase 2. The Effect of a Change in the System Centre of Gravity Position

The system centre of gravity (C of G) was varied by moving the child restraint shell within the plate frame, thus moving the occupant and the whole C of G. Eight positions other than the typical "e" were utilized with the lap belt restrained tests (see Figure 1). Only six of the nine shell positions were possible with the 3-point restrained child restraint, due to interference with the 3 point belt. The results of the tests are shown in Figures 5 and 6.

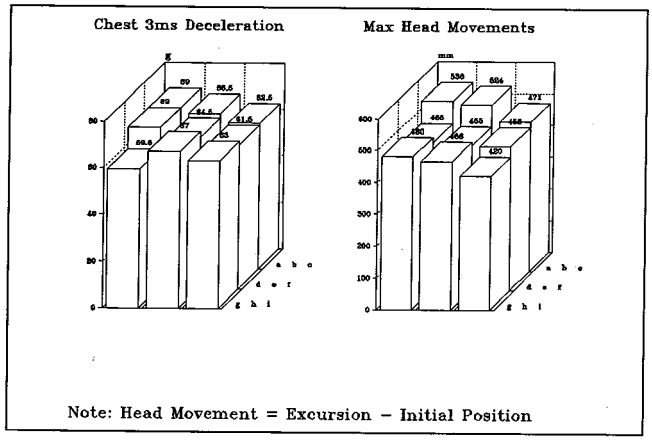

Figure 5. Phase 2, Lap Belt Restrained CR Results

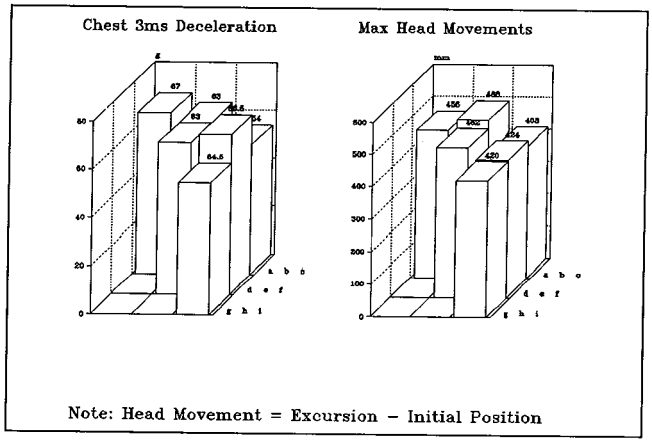

Figure 6. Phase 2, 3-Point Belt Restrained CR Results

The Lap Belt Restrained Child Restraint exhibited a general trend towards lower head *movement* as the shell was moved forward and down (Figure 5). However as expected the maximum head *excursions*, which are measured with respect to the fixed Cr point, increased as the shell, and hence the initial head position, was moved forward. The effect on chest acceleration was less clear, but the lowest acceleration was 59.5g (shell position "g"), and this was achieved without excessive head movement. Thus for the future phases the optimum configuration was chosen to be position "g."

3-Point Belt Restrained Child Restraint showed a similar response to that restrained with a lap belt. As the shell was moved forward the tendency was for absolute movement and chest acceleration to be reduced (Figure 6). The trends are not entirely clear from the limited test results. Although the test data suggest that the results for position "c" were the optimum, computer simulation studies (6) have verified the hypothesis that acceleration is increased, significantly as the shell is moved up while head movement is decreased as the shell is moved forwards. It could be argued that, as for the lap belt tests, head *excursion* would increase for the more forward shell positions giving position "g" as the optimum, but it was not possible to use positions d, g or h for the 3-point belt tests. For this reason position "i" was used for the later phases. It must be noted that the difference in location of the shell between lap belt and 3-point belt tests precludes comparison between these two types of restraint in the following phases.

Phase 3. Effect of a Variation of Foot Size

Since the performance of the child restraint is, to some extent, controlled by the reaction of the seat cushion, the influence of the size of the base of the child restraint in contact with the seat was examined.

Four types of foot were bolted on to the surrogate child restraint. The lap belt restrained tests were completed with the shell in position "g," whereas position "i" was used for the 3-point restrained tests. Thus a direct comparison of the lap belt and 3-point belt results is not possible. The results of the dynamic tests are shown in Figures 7 and 8.

The Lap Belt Restrained Child Restraint results exhibit the largest reduction in 3ms chest acceleration achieved in this series of tests. In general the acceleration decreased and the excursion increased with the larger foot sizes (Figure 7). Thus the largest foot size (450x460mm plate base) yielded the greatest reduction in acceleration (33%). This configuration was chosen as for use in future tests. The acceleration reduction was considered to outweigh the increase in head excursion as all the excursions were within the 550mm limit of ECE Regulation 44.

The reason for the change in child restraint performance is the reduction in overall system stiffness for the larger foot case. The large feet allowed less pre-compression of the seat cushion. The bar foot configured child restraint induced 50mm initial compression of the seat cushion, whereas the largest foot induced negligible pre-compression. Pre-compression reduces the distance the child restraint can travel downwards before hitting the rigid seat pan. Also pre-compression increases the initial horizontal force the cushion can apply and the actual utilized length of lap belt webbing is less. Therefore a reduction of pre-compression reduces system stiffness allowing greater child restraint movements and lower accelerations.

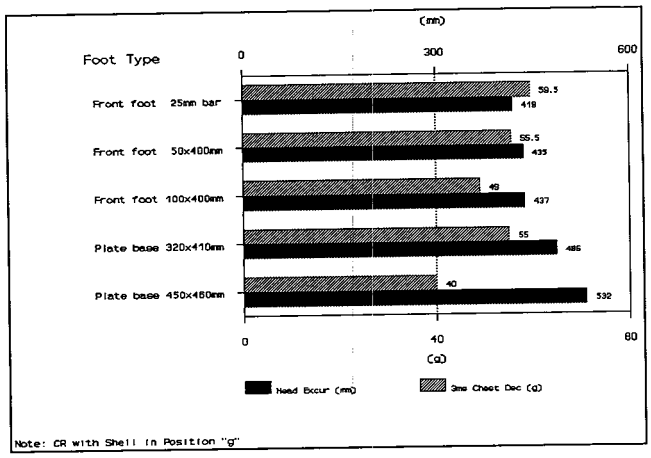

Figure 7. Phase 3 Lap Belt Restrained Results

The 3-Point Restrained Child Restraint tests showed that base area has much less effect on the performance of the child restraint for this configuration (Figure 8). Neither the acceleration of the dummy nor the head excursion were apparently affected in a consistent manner by the change in foot size. The main acceleration forces on a child restraint restrained by a 3-point belt must therefore be those of the belt. The seat squab must play a more minor role than it does with a lap belt.

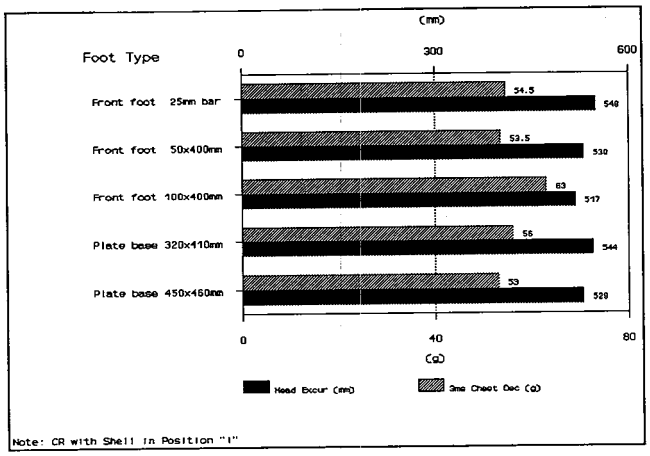

Figure 8. Phase 3, 3-Point Restrained CR Results

It must be noted that the maximum head excursions are in general greater than that of the lap belt restrained child restraint, because of the more forward initial shell position. As no apparent improvement was effected, the bar foot was chosen for the remaining tests on the 3-point restrained child restraint.

Phase 4. The Effect of Child Restraint Shell Inclination

The modern child restraint often includes a reclining mechanism for added comfort of the occupant. The change of inclination of occupant, as well as the induced C of G change, is likely to have some effect on the child restraint performance. To quantify the possible effect of both reclining and the reclining method, tests were completed with the surrogate child restraint shell reclined about both the top and bottom mounting point.

The shell was reclined an extra 21° in addition to the standard 5° which was found in typical production child seats. The shell was rotated about both the top and bottom mounts for the 3-point restrained child restraint using shell position "i." Reclining about the base was not possible for the lap belt restrained case with the shell in position "g." Thus a comparison of the *method* of reclining for the lap belt restrained child restraint was not possible.

The Lap Belt Restrained Child Restraint reclined test was performed with the largest foot and the shell in position "g." The test results (Figure 9) indicate a small increase in chest 3ms acceleration (10%) and a reduction in head excursion in the reclined configuration. Head excursion was reduced mainly due to the more rearward initial position of the head in the reclined position. It was noted that the rebound acceleration of the head (as head hits child restraint shell) was greatly increased in the test.

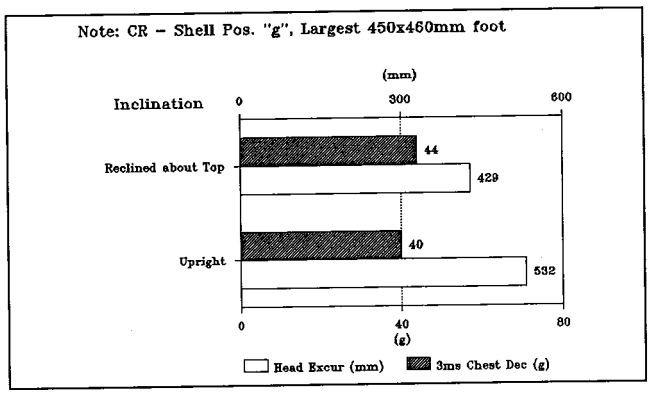

Figure 9. Phase 4, Lap Belt Restrained Results

The 3-Point Restrained Child Restraint results exhibited similar characteristics to the lap belt case (Figure 10). Chest 3ms acceleration was increased slightly whilst head excursion was decreased in the reclined mode. Reclining the shell from lower shell mounting point reduces head excursion by a greater amount than reclining about the top of the shell. However, this also results in the greatest increase in chest acceleration. It

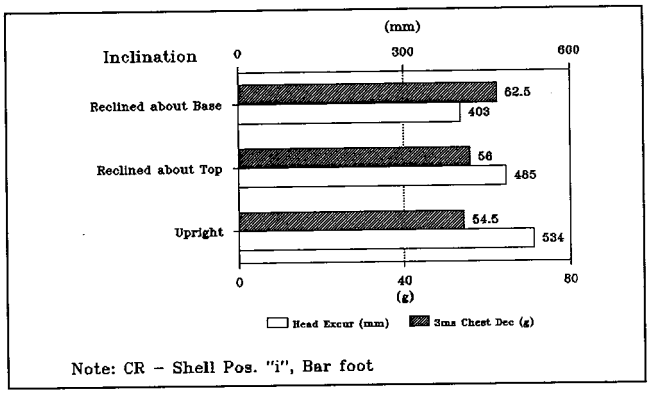

Figure 10. Phase 4, 3-Point Restriained Results

was again observed that rebound of the head seemed to be more violent for the reclined tests.

Phase 5. The Effect of a Top Tether on a Lap Belt Restrained Child Restraint

A top tether was attached to the child restraint and then anchored to the sled at a point simulating a typical car parcel shelf. The child restraint was tested with both the standard bar foot and the previous optimum, the largest foot (450x460mm plate base) . The results of the tests are shown in Table 1.

Table 1. Phase 5, Top Tether Results

Foot Type	Top Tether Used	Chest 3ms Deceleration	Max Head Excursion
Bar	No	59.5	419
Bar	Yes	55.5	396
Evenly Distributed 450x460mm	No	40.0	532
Evenly Distributed 450x460mm	Yes	65.5	319

The results show little effect of the use of a top tether for the child restraint with the narrow bar foot. Only a slight reduction in both acceleration and excursion were observed. The top tether had a large effect on the child restraint configured with the largest foot. Head excursion was greatly reduced (to the lowest level of all the tests), however this was at the expense of a 64% increase in chest 3ms acceleration.

This difference in the effect of top tethers is easily understood. The movement of the child restraint with bar foot is minimal, as the child restraint "bottoms out" on the seat pan (complete cushion crush to the rigid structure below the seat cushion) and is thus restrained by the lap belt and seat reaction. Therefore there is little that the top tether can do. At the other end of the scale is the large foot configured child restraint case, where there is a large child restraint movement. A large force is then applied by the top tether producing a significant effect.

Phase 6. The Effect of Adult Belt Route on the Surrogate Child Restraint

The effect of a variation in belt route was not adequately covered in phase 1 where a typical production child restraint was used. The results were affected by the physical distortion of the child restraint frame. Therefore the effect of this parameter was re-examined using the surrogate child restraint.

The lap belt section of the adult belt route was varied on the surrogate child restraint as shown in Figure 2. As observed in some of the previous phases, there was a difference in the effect of this parameter variation between the lap belt restrained child restraint and the 3-point restrained child restraint. This phase has been repeated and extended using a verified computer model which has aided in the analysis of these results. The child restraint was configured with the standard bar foot and shell position "e."

The Lap Belt Restrained Child Restraint results shown in Figure 11 and an analysis of the film records of the tests suggest that there are two main effects of an alteration in belt route; a variation in the translational movement of the child restraint and an increase in child restraint forward rotation. The increase in translational movement occurs when the initial belt angle to the horizontal is increased which occurs when the belt attachment to the restraint frame is moved back or up. This is because the child restraint, during the impact, attempts to pull the belt to a more horizontal position, which entails a greater forward movement for a larger initial belt angle. The increase in forward rotational movement of the child restraint occurs when the belt force is applied to a more forward or lower position on the child restraint frame. This is due to the increased moment of this force and the child restraint inertial force acting through the centre of gravity.

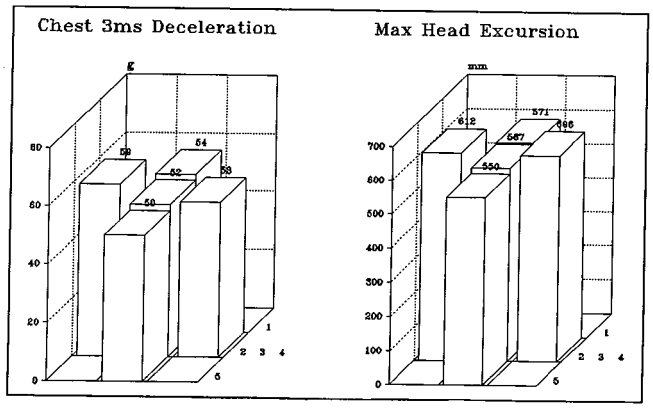

Figure 11. Phase 7, Lap Belt Restrained Results

When the belt attachment point was varied in a vertical plane from point S to point 1, these two effects appear to cancel each other out. When the attachment point was varied in a horizontal plane, from 3 to 2 or 3 to 4, the change in the lap belt angle was greater and the individual effects resulted in an increase in forward excursion away from the standard position, 3.

The 3-Point Restrained Child Restraint results (Figure 12) did not exhibit the same characteristics as discussed for the lap belt above. It is concluded that the restraining force of the diagonal strap nullifies any variation in the lap belt movement. The excursions were not significantly altered as the lap section was moved. The changes in acceleration which occurred are not easily explained.

Discussion

It has been shown that the effect of the variation of a particular parameter is dependant upon the adult restraint

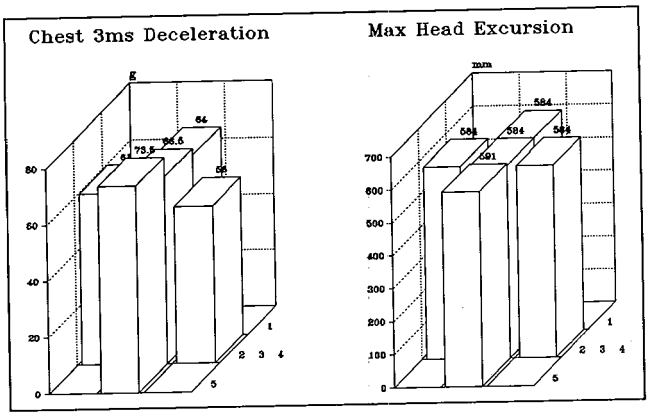

Figure 12. Phase 6, 3-Point Restrained Results

type. In addition, for many of the tests, the shell position in the frame differed between the lap belt and the 3-point belt configurations. Therefore the results for these two attachment configurations are considered separately.

Lap belt. There was not a very large effect on chest acceleration nor on head forward movement between the shell positions used. There was a slight trend to reduce chest acceleration and head *movement* with a lower and more forward location of the shell. However, the differences in the initial location of the head between the shell locations is much greater than any reduction in absolute movement. Consequently, forward excursion for the forward locations considerably exceed those for the rear locations. For instance the head movement with shell position 'g' was 480mm in comparison with 420mm. for position 'i' while the excursions were 419mm and 535mm respectively.

Increasing the foot contact area increases the forward excursion but decreases the chest acceleration, the largest foot producing the lowest chest acceleration of any test. Examination of the film records show that this is due to the higher initial compression of the test seat cushion with a smaller base area which therefore results in earlier 'bottoming out' of the cushion. With a large base area, greater dynamic compression of the cushion is available, resulting in a greater movement of the child restraint, larger head excursion but reduced chest acceleration. This raises the question of the importance of the representativity of the R44 test seat design and initial installation procedures.

The addition of a top tether to the lap belt attached child restraint with the small foot resulted in a small reduction in both the chest acceleration and the head forward excursion. The effects were much greater for the large area foot, reducing the head excursion from 532mm to 319mm, the lowest head excursion observed. However, this was at the expense of a large increase in the chest acceleration. The difference in effects between these two base areas is also attributable to the high pre-compression of the test seat cushion with the small base area resulting in the main reaction force being provided by the test seat structure rather than the cushion for this configuration. As the reaction force for the child restraint with the larger foot comes from compression of the cushion, the addition of the top tether will have a greater effect, as observed. The relevance of this for use in cars will depend on the car seat design and the amount of pre-compression that parents apply in normal use. In view of the potentially large effect on head excursion with a top tether, it would be worth exploring the use of yielding top tethers to reduce the undesirable increase in chest acceleration observed.

The route of the lap belt was seen to affect the performance of the child restraint. Changes from the optimum position increased the forward excursion either through greater translational movement or rotation of the child restraint. Tests on the typical production child restraint showed that the specified belt route gave the optimum performance.

Reclining the shell in the frame about the lower mounting point led to a significant reduction in the head excursion and a small increase in chest acceleration. The test indicated a higher rebound acceleration for the head but it is not known whether this reflects what would happen to a child.

3-Point Belt. Movement of the shell within the frame produced small changes in both head movement and chest acceleration. There was a trend for the chest acceleration to be reduced as the shell was moved forwards and down. There was also an indication of a reduction in head movement as the shell was moved forwards and down which was confirmed by a series of computer simulations. However, as with the lap belt tests, this reduction on head movement was swamped by the differences in initial head position relative to the test seat, resulting in a much greater head excursion as the shell was moved forwards. Again, the optimum position would appear to be as low and as far back in the frame as possible, although the surrogate seat design precluded testing in this location with the 3-point belt.

Changing the area of the base of the child restraint had little effect on the performance when using a 3-point belt suggesting that most of the restraint is controlled by the belt design and layout rather than interaction with the seat cushion.

Very little effect of the location of the lap section was observed on the head excursion when using a 3-point belt. Chest acceleration appeared to increase for lower attachment points of the lap belt and to decrease either side of the standard position. The significance and reasons for this are unclear and should be examined further with the aid of computer simulations.

As with the lap belt configuration, reclining the shell within the frame reduced head forward excursion but increased chest acceleration. Reclining about the lower attachment produced the greatest effect on both parameters. Again, there was an indication of greater head rebound violence with the reclined mode, but the significance of this for injuries in real children is not known.

Where it is possible to compare the performance of the child restraint between being held by a lap belt and held by a 3-point belt, both the head excursions and the chest accelerations are similar or lower with the 3-point belt. The differences are not great but this may be a reflection of the test seat and the installation conditions. The differences when installed realistically in cars should be explored.

Conclusions

- The effects of varying the parameters of a child restraint depend on whether it is anchored with a lap belt or a 3-point belt.
- The lowest chest acceleration was achieved with the surrogate child restraint configured with a large plate foot (as opposed to the standard bar) and anchored with a lap belt although this also resulted in increased head excursion.
- The lowest head excursion was obtained by the addition of a top tether to the child restraint configured with a large foot and anchored by a lap belt. However, this was accompanied by a marked increase in chest acceleration.
- A lower and more rearward position of the shell in the frame was found to produce both lower chest accelerations and head excursions, even though absolute head movement was greater.
- Reclining the shell was found to reduce the head excursion but gave higher chest accelerations. Reclining about the bottom shell mount had the greatest effect.
- In this test series top tethers were found to have a small effect on the standard bar foot configured child restraint, but a large effect in both reducing head excursion and increasing the chest acceleration when the child restraint was configured with the large foot. The applicability of this conclusion to the performance on car seats in normal use is uncertain.
- A variation in the route of the adult belt on the child restraint was found to produce a moderate change in the lap belt restrained child restraint performance, but had a smaller effect on the 3-point restrained child restraint.
- There is a need to explore the potential benefits of energy absorbing top tethers and the extent to which the seat design and installation conditions in the ECE R44 test is representative of normal use of child seats in cars.

Acknowledgments

The Authors would like to thank Chris Witherington and Geoff Savage of RSEL, Middlesex Polytechnic for their part in the testing and Analysis. This work was mainly funded as a research project for the Transport and Road Research Laboratory. Additional support was in the form of a NAB grant. The work described in this paper forms part of the programme of the Transport and Road Research Laboratory and the paper is published by permission of the Director.

References

1. Lowne, R.W., P. Gloyns, and P. Roy, Fatal Injuries to Restrained Children Aged 0-4 years in Great Britain 1972-86, Proc 11th. ESV Conference, Washington, May 1987.
2. Langwieder, K. and Th Hummel, Children in Cars—Their injury Risks and Influence of Child Protection Systems, Proc., 12th. ESV Conference, Sweden, 1989.
3. Hill, K.J., and Roy, A.P., (1982), Simulation of the Effects of Vehicle Impacts on Restrained Child Occupants—Part A: A Description of the KL/MP Dynamic Test Facility, Journal of the Society of Environmental Engineers, 21,1 March 1982. (SEE).
4. Roy, A.P., Hill, K.J., and Mackay, G.M., (1982), Some Limitations of Adult Seat Belts When Used to Restrain Child Dummies in Simulated Frontal Impacts, AGARD Aerospace Medical Specialists Meeting, Koln, Germany, (1982).
5. ECE R44, Economic Commission for Europe, Regulation No.44, Concerning the approval of restraining devices for child occupants of power driven vehicles ("Child Restraints"), 1981.
6. Dorn, M.R., Unpublished MADYMO simulations, Personal communication, 1991.

S9-W-39

Aged, Used, Crashed Seat Belts

Paul Duignan, Michael Griffiths
Roads and Traffic Authority of NSW

Abstract

There is acceptance that some parts of cars wear out and that other parts need replacing after a crash. Vital safety equipment, such as seat belts, should be no exception to this. This paper reports on recent seat belt studies conducted by New South Wales Road Safety Bureau's Crashlab, and attempts to summarize the findings. The studies reported on are: 1) An examination of the static strength of individual components of aged used belts systems from a variety of vehicles; 2) An examination of the dynamic strength of a specific series of aged seat belts; 3) A review of aged crash seat belts from a time series of vehicles with matched pairs of crashed worn, crashed not worn and not crashed seat belts.

Introduction

In Australia it has been mandatory to fit seat belts in vehicles since 1969 and has been compulsory for occupants to wear them since 1971. In 1988 there were over 7 million cars registered with the average age being 8.4 years (1). As the first country to mandate seat belt wearing and to achieve wearing rates of exceeding 90 percent, Australia is ideally placed to do research on the effects of seat belt usage and crash involvement on seat belt performance.

In some vehicles seat belts have fallen apart from the constant use and exposure. It is therefore reasonable to assume that sometime before the complete in-service failure of such belts, there is a point at which they can no longer pass the minimum requirements of the Standard and hence offer adequate protection in a crash.

The Roads and Traffic Authority's, Road Safety Bureau, occasionally receives reports of seat belts breaking in crashes, although there is no routine method of notifying these incidents. Where possible the broken components are obtained and the Bureau logs a formal report. Reports have only been received on fourteen such incidents in the last ten years. These were associated with eleven fatalities. Previous experience has indicated that such failures are generally under-reported because (a) there is no formal system for reporting (b) it is not evident who the responsible body is and (c) the Australian population is less inclined to seek legal redress over such matters because of its personal injury insurance system.

In general the Australian Standard requires seat belts to restrain their occupant in an impact up to around 25g which generally equates to a 50km/h head-on collision (2). In some of the impacts in which seat belts failed, the damage to the vehicle appeared to indicate that the impact would have been of a less severe nature than that specified in the Standard. This supports the idea that the performance of seat belts deteriorates with age and use to such an extent that they do not offer adequate protection to the occupant in a crash.

This report presents the results of a project to determine an objective criteria for the replacement of seat belts worn in a crash (3). The project was sponsored by the National Roads and Motorists Association Insurance Company (NRMA).

The project built on previous studies conducted by Crashlab which investigated the effects of age and use on the crash performance of lap/sash seat belt assemblies.

This study's research strategy required three stages:

- Stage 1. Determine the effects of various crash pulses on belt performance.
- Stage 2. Determine the effects of similar crash pulse with respect to age, seating position and crash involvement on belt performance.
- Stage 3. Determine the effects of multiple impacts on belt performance.

Literature Review

In 1976 Chapman and Cameron (4) conducted testing on old seat belts with the aim of looking for correlation between the visual deterioration of a seat belt and its performance. The sample consisted of 97 lap sash static seat belts which hadn't been involved in crashes and no more than four years old. If the belt had visible signs of damage, then they waived the four year limit. Overall, 66 failed the Australian Standard E35 static assembly test. Of these, 29 had a webbing failure on a piece of hardware, twelve had buckle tongue engagement failure, three had other hardware failure, six failed by excessive slip at adjusters, five had stitching failures and eleven failed the buckle release force test.

A sample of 27 belts was obtained from vehicles which had been involved in crashes. The age of the belts was not controlled. Of the 27 belts, two had failure of the stitching or webbing adjacent to the stitching, six had buckle failures, one failed at the buckle adjuster and four failed the buckle release test force. 13/27 failed.

They tested various models seeking correlation of appearance to performance. They found that "measures and ratings of seat belts were found which were capable of predicting to a limited accuracy, the strength of a seat belt." However of the various models they tried for mechanics of failure, they found "the models do not adequately represent reality." They did not present any results in terms of the comparative ages of the seat belts.

Martin et al. (5) investigated used seat belts in 1979 for the Swiss Commission for Safety Belts (SKASG). Their test program involved testing several types of new belts and 13 used restraint systems both dynamically and statically. Their report recommended that: "A replacement is indicated:

- If any visible damage to the webbing, the buckle or the fittings is present,
- If any visible or non-visible alteration impairs the perfect function of the belt system, and
- If the car exhibits a considerable frontal crush. Side collisions are prone to cause direct damage to the belt system."

In 1985 Pickles and Aldridge (6) conducted "an experiment to substantiate the suggested life expectancy of a belt ... is seven years." They found "a noticeable drop in both assembly strength and webbing strengths from that initially expected. However, this still leaves the majority above the minimum required by the New Zealand Standard NZS 5401:1976." In static tests of the webbing, they found that 80% of seven year old webbing would be expected to pass the requirement of 18 kilo-Newtons. Sixty three percent of the seven year old seat belt assemblies were expected to pass the New Zealand

standard assembly test. Their sample consisted of 13 drivers' static lap-sash belts and four inertia reel drivers' belts. In phase 2 of this study their sample consisted of 16 static lap sash belts which were 12 years old, and 18 static lap-sash belt which were ten years old, to give a total sample of 34 belts. The results were not that clear, but they stated that 83% of assemblies would have passed the requirements of the New Zealand Standard 5401:1982.

In 1987 Griffiths and Skidmore (7) reported on a series of tests on aged used seat belts. Belts were source from vehicles aged from 1970 to 1979. A sample of 10 belts from each year was obtained. Static tests of the individual components of the seat belt were conducted.

The average webbing strength decreased at a fairly constant rate over the 10 year period from approximately 22kN to 15kN. The webbing appeared to be adequate even when 17 years old. All the webbing was polyester.

The average buckle strength varied from 16kN to 10kN at a fairly constant rate according to seat belt age. This could have been due to wear or changes in design.

The average stitching strength was almost constant from 1970 to 1976 and rose sharply from 1976 to 1979. This change from 1976 to 1979 represented a strength change from 9kN to 18kN. This corresponded to a change from nylon to a stronger and more durable polyester thread at about that time.

In the dynamic tests of the total seat belt assemblies, the rate of failure was always the stitching breaking at the top anchorage on the sash part of the seat belt. The breaking loads were all noticeably lower at 6.90, 6.19 and 6.43kN.

In general, the test indicated there was a decline in strength of most components of the seat belt system as they got older. The deterioration appeared to be most noticeable from 8 to 12 years old. Significant changes in seat belt design and materials at around 1976 including the change from manual lap sash belts to automatic locking retractor lap sash seat belts, and a change in stitching thread from nylon to higher grade polyester which is likely to have been responsible for the major change in strength.

The report concluded that the performance of seat belts in crashes from vehicles manufactured in 1976 or earlier, should probably be more closely monitored. If their real world performance substantiates the laboratory assessments, then a retro-fit may be justified.

In 1989 Duignan (8) reported on a more detailed dynamic assessment of seat belts from a consistent stream of seat belts from 1975 to 1980 vehicles. These vehicles were randomly selected from registration records followed by the completion of a questionnaire by the vehicle's owners. As an inducement to responding to the questionnaire, the vehicle owners were promised a new set of seat belts for their vehicles. A sample of 48 belts were selected with 8 belts per year. Belts were divided into garaged and non-garaged, and passengers versus drivers. An even distributed sample across the cells was used. The dynamic test aimed to be sufficiently more severe than the Standard so as to overload each belt system until it broke. Part of the assessment criteria was to measure the load at which the belt system broke.

The test results showed a statistically significant increase in the frequency of breaking rates in older belts when compared in cells of 3 year intervals. Older belts showed significantly lower breaking forces than the younger belts. The average breaking force for 1975 belts was at least 1.5kN less than that recorded for any of the other years tested.

When non-garaged belts were compared to garaged belts, there was statistically significant decrease in the breaking forces in the non-garaged broken belts. This supports the idea that exposure due to sun and weather influence seat belt degradation.

No statistically significant difference in the dynamic breaking forces of the belt assemblies could found between driver and passenger belts.

Research Method

The study was divided into three separate test programs designed to determine:

- Stage 1. Effects of varying crash rates on belt performance,
- Stage 2. Effects of age, use and crash involvement on belt performance and,
- Stage 3. Effects of multiple impacts on belt performance.

Table 1 shows the test matrix used.

Table 1. Test Matrix

	TEST PULSE (G)	NEW BELTS BELT NO. 1 2 3 4 5 6 7 8 9 10	DRIVER'S: AGED CRASHED	DRIVER'S: AGED	PASSENGER'S: AGED CRASHED NOT WORN
STAGE1 EFFECT OF VARIOUS CRASH PULSES	10	X X			
	15	X X			
	20	X X			
	25	X X X X X			
	30	X			
STAGE 2 EFFECT OF AGE, USE AND CRASH INVOLVEMENT	25		X	X	X
STAGE 3 EFFECT OF MULTIPLE IMPACTS	10	X X X X X			

All dynamic testing was conducted using a Hybrid III, 50th percentile male, anthropomorphic test dummy instrumented to measure head, chest and, pelvis accelerations, and chest displacement. Crashlab's Monterey Crash Sled was used as the crash simulator. The sled was instrumented to measure seat belt anchorage loads and sled decelerations. High speed cine-film was used to monitor the seat belt assemblies and the dummy movement during impact.

The Hybrid III dummy was positioned before each dynamic test run with the aid of a laser positioning rig to ensure consistency.

Stage 1

Stage 1 involved dynamically testing 10 new seat belts on the crash sled at five deceleration pulses (2 belts at each pulse, 10 through to 30g's in steps of 5g's).

One seat belt from each deceleration pulse was retested dynamically on the crash sled to the 25g deceleration pulse.

The lap/sash inertia reel seat belts used were new "off the shelf" replacement belts for a popular car. The belts were tested and installed as per instructions and anchorage point geometry specified by the manufacturer for this model car.

All seat belts had post-test visual inspections at both a macro and micro level. Changes in the seat belt assembly were observed and recorded on a check-list.

Stage 2

Stage 2 of the project involved dynamically testing 77 seat belts assemblies from the vehicles which were first registered between 1979 to 1987. 52 belts were driver and passenger assemblies removed from vehicles involved in frontal collisions where the driver was the only occupant. The other 25 belts were driver assemblies removed from non-accident involved cars.

The belts were subdivided as follows:

- 52 belts from 26 vehicles that were involved in frontal collisions. Both the passengers and drivers belts were obtained and tested.
- 25 belts from vehicles which had not been involved in an accident. Only the drivers belts were obtained from this set.

The accident involved vehicles were selected using the following criteria:

- no greater than 30-40 percent frontal offset impact,
- driver is the only occupant at time of accident,
- damage to car is to be economically repairable, that is the vehicle would normally be repaired and put back into use.

For all vehicles selected for this study, it was not possible to establish whether they had been previously involved in an accident or had the seat belts replaced.

The odometer reading was recorded and damage was photographed, to a strict protocol, from several angles for each vehicle. The belts were submitted to a pre-test inspection noting any irregularities to the assembly. Dynamic testing was conducted using the 25g deceleration pulse specified in Stage 1. The test geometry for all belts was the same for all models with only a minor variation between driver and passenger assemblies. The belt assemblies were also submitted to a post-test visual inspection.

Stage 3

Stage 3 of this study involved dynamically testing a new seat belt to the 10g deceleration pulse used in Stage 1 for 5 consecutive tests on the same belt. The belt model and geometry was the same as that used in Stage 1.

The seat belt assembly was subjected to a post-test visual inspection after the fifth test. Comparisons were made with the new belts tested in Stage 1 of the project.

Test Results

Stage 1

Dynamic Tests. Only nine of the ten seat belts scheduled for testing in Part 1 of this stage were tested. One belt could not be tested at 30g as it was found that and above the 20g test pulse, the belts became inoperable and not suitable for retesting in Part 2 of this stage.

Of the nine belts tested two broke (one at 25g's and the only 30g belt tested). The mode of failure in both cases was webbing tearing and breaking in the vicinity of the top anchorage point. The belts tested at 20g and above deceleration levels all became inoperable at the retractor mechanism (i.e., not able to reel in or out).

Two belts were retested at 25g's, one each from the 10g and 15g deceleration levels. Both belts functioned correctly during the second impact, although their retractor mechanisms became inoperable.

The average chest compression and resultant load recorded at the stalk anchorage point (F_{2+4}) was 44 mm and 14.9 kN for the initial 25g tests and 47 mm and 14.2 kN for the repeated tests.

Visual Inspection. The belt assemblies tested were new unused seat belts. A macro pre-test visual inspection was performed on each belt to detect obvious flaws.

Retesting of one 10g belt and one 15g belt showed characteristics similar to those described for the initial 25 g tests. The inspections found that the markings were no more severe as a result of the double impact.

The lower floor mounting anchorage bracket, plastically deforms during impact. The severity of this deformation was recorded.

Stage 2

Dynamic results. Figures 1-4 show the percentage of belt breakages with respect to the vehicle model years. Of the 77 seat belt assemblies tested, 21 broke during the impact. The 1985-87 age group accounted for 15 of the total breakages. The most common breaking mode was webbing tearing at the top anchorage point (18/21). The other breaking modes were retractor mechanism exploding, buckle/tongue disengagement and top anchorage bolt failure.

Analysis was performed on the chest deflection and the force at the stalk anchorage point, namely F_{2+4} (the combined sash and lap webbing load).

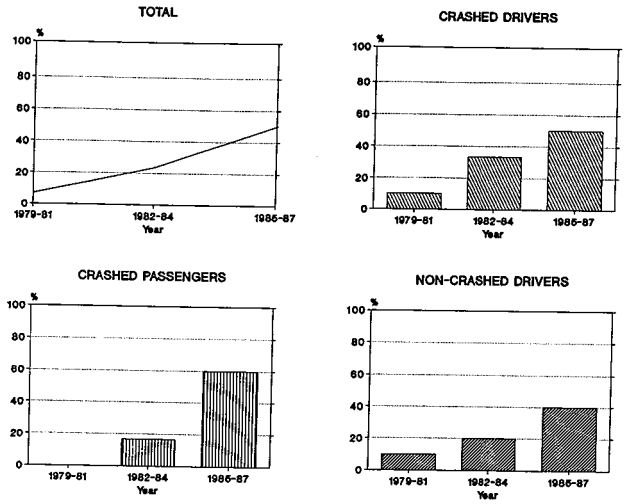

Figures 1-4. Percentage of Belts Broken

This analysis provided the following points:

- a statistically significant difference for the results obtained for both chest deflection and F_{2+4} for moderate severity accident involved driver seat belts and passenger seat belts from the same car. This indicates belt wearing rate has an effect on belt performance.
- no statistically significant difference in the results for both chest deflection and F_{2+4} for moderate severity accident involved driver belts and non-accident involved driver belts. This indicates that moderate severity crash involvement has no effect on the belt effectiveness.
- no statistically significant difference in the results for chest deflection and F_{2+4} between the various age groups of belts. For the period of the study, these results indicate that seat belt age has no effect on restraint effectiveness.
- no statistically significant difference of the results obtained for chest deflection and F_{2+4} between belts which broke and those which didn't break during dynamic testing. This indicates that the belts which broke did not break at a lower load or absorb less energy.

Visual Inspections. Pre and post visual inspections were performed on all seat belt assemblies. The inspection was performed at both a macroscopic and microscopic level.

Pre-test inspections: The pre-test inspections recorded a change in retractor type, upper anchorage guide, tongue attachment and stitching pattern for the years of this study. No changes were recorded for the buckle, stalk and floor anchorage point.

10 of the 26 (48%) drivers belts which were known to be worn during an impact showed some signs of impact similar to those found on the new belts after testing in Stage 1. The signs of impact were very minimal and included:

- tongue plastic rubbing,
- upper anchorage rubbing,
- marks on webbing from upper anchorage.

Of these 10 belts, 4 of them broke by the webbing tearing at the top anchorage point during dynamic testing. A problem which was encountered during visual inspection of aged and used belts was the possible masking of impact indicators by similar signs of age and use.

Post-test inspection: *Retractor*—Two types of retractor were used during the study period. The older style was used in vehicle models manufactured during the period 1979-1985. The newer style was used in 1987 model vehicle.

For the purposes of this study the retractor mechanism was classified as broken if any of the functional requirements could not be performed (for example if the retractor would no longer lock or if the recoil mechanism didn't work). Graphs 5-8 show the percentage of retractors which were non-functional after testing for each study group.

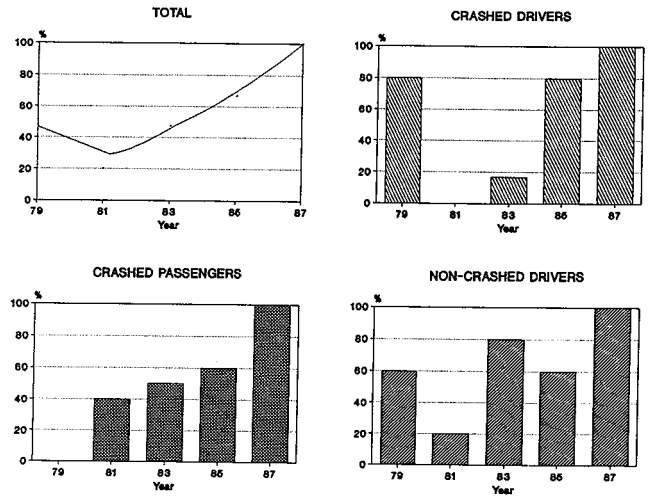

Figures 5-8. Percentage Non-Functional Belts After Testing

Webbing—All webbing breakages occurred in the vicinity of the top anchorage point. The mode of breaking was typically a result of the webbing jamming at the top anchorage and subsequently tearing. Graphs 9-12 show the percentage of webbing breakages with respect to year of manufacture for each study group.

Stage 3

Stage 3 involved testing 1 new seat belt assembly for 5 consecutive tests to determine the effects of multiple impacts on the performance of a seat belt. The belt was tested at a deceleration level of 10g.

Dynamic results. The results did not show any statistically significant difference between the anchorage force and chest displacement for each consecutive test.

Visual inspections. A post-test visual inspection was performed on the belt assembly after the five tests were completed. The inspection of the belt showed the follow-

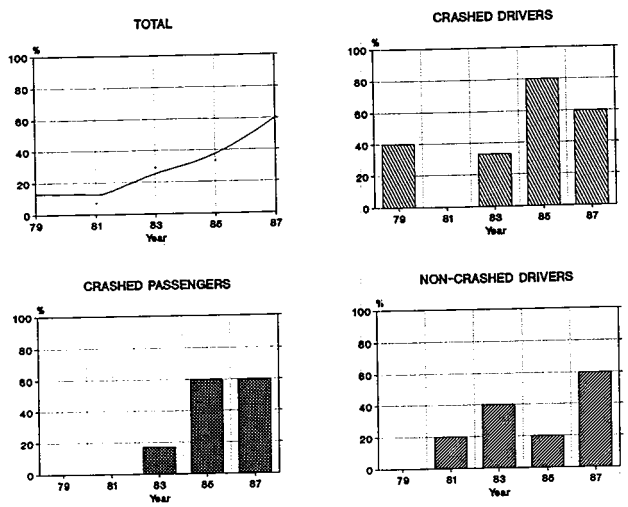

Figures 9-12. Percentage of Webbing Breakages

ing similarities and differences between the seat belt assemblies tested at the 10g level in Stage 1.

Similarities:

- level of damage to retractor
  - flanges bent on spool
  - centre drum on spool cracked
- tongue metal deformation
- level of webbing marking on upper anchorage point
- mark on webbing where tongue attachment rested

Differences:

- clear webbing rub marks on plastic section of tongue *(single impact: only slight rub marks)*
- rub mark over 10 cm in length *(single impact: only over 5 cm length)*

Discussion of Results

Stage 1 (Effects of Various Crash Pulses)

The results show that 50 percent (4/8) of seat belt assemblies dynamically tested at or below that specified by ADR 4/01 were non-functional after testing (i.e., not able to be retested). All belts tested at the 20g level pulse or above became non-functional after testing. A non-functional belt does not necessarily constitute a failure according to the Australian Design Rules.

The dynamic results of the retested belts did not show any significant change in performance to that of the originally tested belts. One belt tested at the initial 25g deceleration pulse broke at the top anchorage point, but both of the retested belts, although not operational afterwards, did not break at any point on the belt assembly. This indicates that low g level crashes do not have adverse effects on the ability of a seat belt to perform to its design requirements in subsequent testing.

The post-test visual inspections on each belt highlighted several distinct marks occurring from crash involvement.

- lower anchorage right angle bracket is usually bent greater than its designed 90°.
- tongue metal shows deformation.
- plastic section of the tongue attachment shows rub markings caused by the webbing.
- plastic section of the upper anchorage shows rub markings caused by the webbing.

The previous observations may be seen by the naked eye and occur on impacts as low as 10g.

Microscopic changes were also observed:

- melted plastic on webbing from top anchorage point and tongue assembly.
- damage to webbing filaments.
- dummy's clothing melted onto webbing.

Microscopic observations in general occurred on higher g impacts.

Stage 2 (Effects of Age, Use, and Crash Involvement)

Stage 2 results did not show any significant difference between seat belts worn during a crash where the vehicle is classified as repairable and those that have not been involved in an accident. A significant difference did exist between the passenger's and the driver's belts. The passenger belts when tested gave a lower chest deflection and lower anchorage point force. This indicates the webbing absorbed more energy in the case of the passenger belt assemblies. An explanation for this is, as a driver's belt has a higher usage rate than a passenger belt, wear effects the stiffness of the belt by either:

- constant bending and rubbing of the webbing over top anchorage point and tongue assembly,
- the accumulation of grease and dirt, and
- degradation by environmental factors.

The pre-test examinations indicated that 10 of the 26 crash involved driver's belts showed minimal signs of crash indicators highlighted in Stage 1 testing. This indicates the sample of frontal accidents investigated were of less severity than the 10g 20 km/h pulse used in Stage 1.

The inspections also suggested that signs of wear through normal usage were indicated by markings on:

- webbing by external means,
- webbing by belt attachments,
- attachments by external means,
- attachments by the webbing.

Irrespective of whether they had been accident involved or not, seat belt assemblies showed the following characteristics because of normal use:

- filaments broken at lower anchorage points,
- rust on the lower anchorage point and stalk mounting point,
- smooth edges due to rubbing on the plastic upper anchorage points,
- edge abrasion.

The signs of wear were more pronounced in older belts.

After dynamic testing the results indicated that there was higher percentage (71%) of non-functional belt

assemblies for the more recently manufactured group (1985-87) whether or not they had been accident involved. This may occur by belt manufacturers designing the belt components to tighter tolerances with smaller factors of safety, but still meeting the minimum performance requirements.

Restraint systems fitted with a plastic upper anchorage point guide were more susceptible to webbing breakage, compared to the older metal type even though this type had significantly older and worn webbing. The loads and anchorage geometry used were similar for both styles of guide. These results suggest that the plastic anchorage fitted to these belts guides are "more aggressive" on the webbing during an impact. It appears that because of the plastic guides shape (although this has not been fully investigated) they tend to snag the webbing and subsequently cut it.

Graphs 5-8 indicate that new style retractors have the greatest probability of being non-operational after a crash than earlier models. This again indicates that engineering modifications have been made which lowers the overall strength of the retractor.

Stage 3 (Effects of Multiple Impacts)

The results in Stage 3 gave no indications that repetitive testing at low g levels (< 10g) has any adverse effects on the dynamic performance of a seat belt assembly or its ability to absorb energy instead of transmitting it to the occupant.

Conclusion

- The test results indicate that prior impacts of minor severity (less than 15g and 30 km/h) have no effect on the ability of a seat belt to perform to its design requirements in a subsequent crash.
- Crash involved belts investigated in Stage 2 (frontal impact accidents which are economically repairable), were of a severity below a comparable sled pulse of 10g and 25 km/h velocity change.
- A seat belt will become non-functional in a moderate to severe accident (sled equivalent to >15g and 30km/h velocity change).
- Later model seat belt assemblies have a greater tendency to become non-functional after crash involvement. Probably because of component design trends.
- There is no measurable effect of multiple 10g impacts on belt performance.
- An additional set of tests on 1989 seat belts found they consistently broke at less severe pulse than the older used seat belts tested.

Recommendations

It is recommended that seat belt assemblies be thoroughly inspected when assessing damage of any vehicle involved in a moderate or more severe crash. The assessment should follow the check-list provided. If the belt does not meet any of the functional requirements specified the belt should be replaced.

Seat Belt Assembly Check List

Tongue/Buckle Assembly

- Engagement
  - the buckle and tongue assemblies should securely latch every time.
- Ejection
  - the tongue should actively eject from the buckle assembly freely when its is released.
- Buckle
  - the buckle assembly should have no visible cracks.
- Tongue
  - the tongue should have no metal deformation, webbing markings or visible cracks on the metal or plastic section of the assembly.

Retractor

- Inertia
  - the inertia locking mechanism on the retractor should be operable throughout its range without any sticking or binding and should lock if the webbing is pulled out suddenly.

Webbing

- the seat belt webbing should be securely attached to its end fittings and the stitching must not be damaged or frayed in any way.
- the webbing should be flat throughout its entire length. Any evidence of warping is a sign that the webbing has been plastically loaded.
- the webbing should not have any plastic burn markings caused by the webbing running over the anchorage point in the vicinity of the top anchorage or tongue sections.

Anchorages

- anchorage points should be free from corrosion and securely fastened to the vehicle structure.
- lower anchorage point should not show any signs of deformation.
- top anchorage should show no signs of webbing burn markings.

References

1. Australian Bureau of Statistics, Motor Vehicle Census, 30 September 1988.
2. Standards Association Australia, Testing Seat Belts AS 2597 (1983), Seat Belt Webbing AS 1753 (1983).
3. Duignan, P., The Performance of Dynamically Tested, Aged, Used Seat Belts. A Crashlab Report. SR91/245 1991. Available from Crashlab. RTA Library, PO Box 110, Rosebery 2018 NSW Australia. Fax 61-2-662 4118.
4. Chapman, C.C. & Cameron, M.A., The Effect of Usage on Seat Belt Strength (1976), published in the

proceedings of Seat Belt Seminar conducted by the Commonwealth Department of Transport.
5. Martin, E., Balmer P. & Remund P. Performance Tests on Used Safety Belts Accident Analysis and Prevention, Vol 12, No. 3 1980.
6. Pickles, R. & Aldridge A.E., Vehicle Seat Belt Degradation, Auckland Industrial Development Division, ISSN 0111-1566. No. G146.
7. Griffiths, M. and Skidmore A., The Performance of Aged Used Seat Belts, 1987 IRCOBI Conference, Birmingham, Inc.
8. Duignan, P., The Performance of Dynamically Tested, Aged, Used Seat Belts, A Crashlab Report. SR89/129 1989. Available from Crashlab. RTA Library, PO Box 110, Rosebery 2018 NSW Australia. Fax 61-2-662 4118.

S9-W-40

Structural Considerations in Air Bag Sensor Activation at Low Threshold Test Speed

Matthew Huang, Cassandra Green, Frederick Samson
Ford Motor Company

Abstract

This paper presents a study of air bag sensor performance in low threshold speed tests where air bag deployment is desired. It presents the effects of the bumper energy absorbing system and the sensor mounting bracket on sensor performance. Vehicle crash deceleration pulses were analyzed for their filtered characteristics and then used as inputs in two mathematical models. One model simulates the dynamic response of a sensor mounting bracket subjected to rotation of the bracket support structure; the other, the dynamics of an air bag ball-in-tube sensor during a crash. The bumper system plays an important role in providing an early deceleration signal needed for air bag sensor activation at low threshold speeds. Sensor bracket support rotation can have an appreciable effect on the deceleration level detected by the sensor. For the type of sensor bracket considered in this study, the vibration of the bracket itself did not significantly change the deceleration level detected by the sensor. Graphs are presented showing the influence of the bumper system and the sensor mounting bracket design on sensor dynamic performance. An animated technique is used to visually present the interaction between the responses of structural components and activation of the air bag sensor. Performance of the air bag sensor under these various test conditions is discussed.

Introduction

The principles of operation, application and simulation of an air bag crash sensing system have been presented by Huang [1] and the development of an advanced air bag crash sensing system has been investigated by Adams, et al. [2]. In this paper, the crash sensor (or discriminating sensor) mounted at the radiator support is used to study the effects of the bumper system and sensor bracket support structure on sensor performance in a low threshold speed impact where air bag deployment is desired.

The low threshold speed is the minimum impact speed at which air bag sensor activation is desired in a crash. A typical low threshold speed in a perpendicular rigid barrier test is 14 mph; in a rigid pole test, 19 mph. These values were chosen based on a review of earlier design criteria and tests in terms of unbelted occupant kinematics and the potential severity of contact with components such as the steering wheel and windshield.

In a low threshold speed test, the vehicle frontal structure deceleration level must equal or exceed the sensor trigger threshold. The critical structural components are the bumper, energy absorber (EA), front rails, and radiator support structure. These structural components not only absorb crash energy but also interact with each other to transmit impact forces to the sensor for prompt sensor activation.

The air bag will be deployed only when at least one crash sensor and one safing sensor (or confirmation sensor) are activated concurrently. The activation of a safing sensor in the passenger compartment requires a lower level of deceleration than is typically required by the crash sensor.

A criterion, known as the 5"-30ms, is used to evaluate sensor effectiveness in this study of air bag deployment at low threshold speed. This criterion states that a sensor must provide 30 milliseconds (ms) of time for air bag deployment before an unbelted occupant has moved 5 inches forward relative to the vehicle compartment. This criterion was derived based on a 30 ms air bag inflation time and an average deployed bag-to-chest dimension of 5 inches.

The air bag sensor system must be activated by deceleration provided by vehicle frontal structural components such as the bumper, EA devices, and radiator supports. A simple, easy to apply, bumper design procedure was presented by Evans, et al. [3] which includes discrete equations for bending strength, torsional strength and dent strength relationships.

Crash test data and two simulation models are utilized in this study. The test data of a mid-sized vehicle in 14

mph perpendicular barrier tests was used as inputs to the models for the sensor mounting bracket and sensor element dynamic simulations.

Methodologies

Crash Pulse Filtering and Haversine

A computer program with the Butterworth second order filter algorithm and a cutoff frequency of 60 Hz[1] were used to filter the wide band (unfiltered) crash test data. The filtered crash data contains harmonic pulses which are useful in evaluating sensor performance through visual inspection.

The crash pulses at the radiators of three mid-size vehicles were filtered at 60 Hz for detailed crash signal analysis. Figure 1 shows the wide band crash pulse at the radiator and its filtered pulse at 60 Hz for a mid-size vehicle in a 14 mph perpendicular barrier impact. The filtered data reveals an approximate haversine pulse between 25 and 43 ms with a duration of 18 ms and amplitude of 41 g. The velocity change in the haversine is then computed as follows.

$$\Delta V = .011 A_p \Delta T$$

where

ΔV = Velocity change associated with the haversine pulse (area under the pulse), mph

A_p = Peak deceleration amplitude, g

ΔT = Duration, ms

Therefore,

$$\Delta V = .011 \times 41 \times 18 = 8.1 \text{ mph}$$

The velocity change of 8.1 mph with a short duration of 18 ms is sufficient to activate the crash sensor mounted at the radiator of Vehicle A. The simulated sensor activation time using the unfiltered crash pulse is 39 ms which occurs near the end of the haversine pulse as shown in Figure 1.

Figure 2 shows the wide band crash pulse at the radiator and its filtered pulse for Vehicle B in a 14 mph barrier impact. The filtered data reveals a double hump haversine pulse between 16 and 54 ms with a valley at 34 ms. Each haversine pulse has a duration of 18 ms and amplitude of 27 g. The velocity change for each haversine is about 5.4 mph which is not sufficient to activate the crash sensor. Together, the two haversine pulses make up a velocity change of 10.8 mph and the simulated sensor activation time using the unfiltered crash pulse is 45 ms which occurs near the end of the double hump pulse.

Role of Bumper

A subsequent study showed that the double hump was caused by the bumper. The design of the bumper was such that the lower part of the housing box (connected to bumper PGM) was weaker than the top, and caused a folding effect during crash. The breakdown of the housing box caused a double hump on the crash pulse which showed a momentary drop in deceleration due to the collapsing of the housing box.

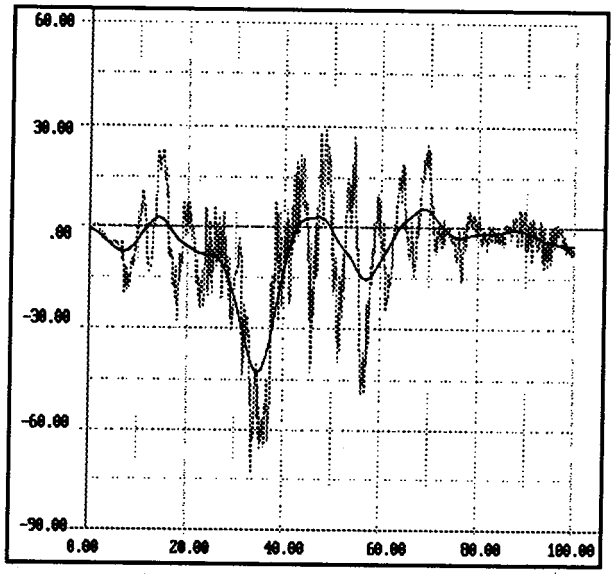

Figure 1. Wide Band Crash Pulse at the Radiator and Its Filtered Pulse at 60 Hz for Vehicle A in a 14 mph Barrier Impact

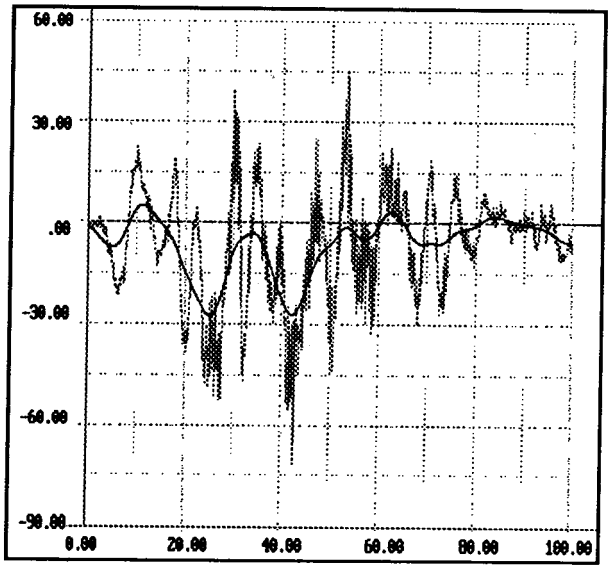

Figure 2. Wide Band Crash Pulse at the Radiator and Its Filtered Pulse at 60 Hz for Vehicle B in a 14 mph Barrier Impact

Figure 3 shows the wide band crash pulse at the radiator and its filtered pulse at 60 Hz for Vehicle C in a 14 mph barrier impact. The filtered data reveals a major haversine pulse between 16 and 43 ms. The duration and amplitude are 27 ms and 28 g respectively with a velocity change of 8.3 mph. The simulated sensor closure

[1]The cutoff frequency in the Butterworth filter algorithm corresponds to the knee frequency, f_N, in the frequency plot shown in SAE J211—Instrumentation for Impact Tests. An f_N of 100 Hz corresponds to Channel Class of 60. There is no Channel Class number that corresponds to the f_N of 60 Hz used in this study.

using the unfiltered crash pulse is 38 ms which occurs near the end of the haversine pulse.

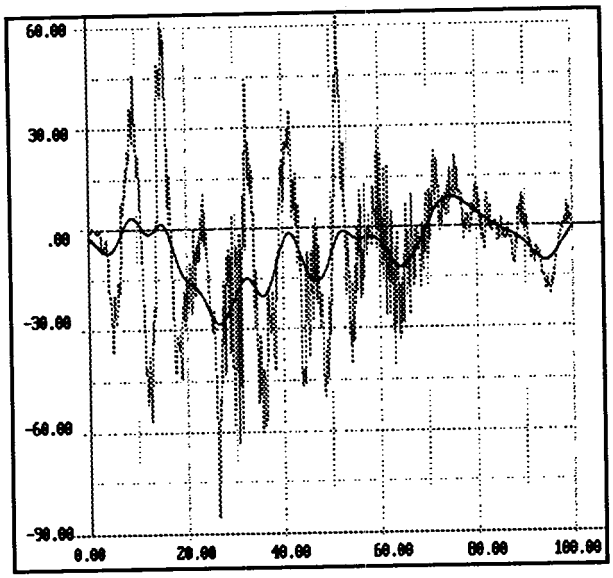

Figure 3. Wide Band Crash Pulse at the Radiator and Its Filtered Pulse at 60 Hz for Vehicle C in a 14 mph Barrier Impact

Since the only major structural difference between Vehicles B and C was the design of the bumper, it was apparent that the bumper design of Vehicle B caused a delay in the sensor activation time. The delay (difference in activation times between Vehicles B and C) was 7 ms (45 minus 38) using the sensor mathematical model and 12 ms (44 minus 32) from the actual crash test data.

Vehicle Kinematics in Crush Zone and Passenger Compartment

Figure 4 compares the filtered pulses at the radiator and rocker panel B-post[2] for Vehicle C. The peak deceleration at the radiator occurs early in the crash and is twice as high as that at rocker panel B-post.

Figure 5 shows the velocity changes at the radiator and rocker panel at the B-post for Vehicle C in a 14 mph barrier impact. The velocity change at the radiator in the window between 25 and 65 ms is higher than that at the rocker B-post (see Figure 4). The deceleration at the radiator starts subsiding after 70 ms and so does the velocity change. The vehicle compartment rebounds from the barrier at around 70 ms where velocity is zero as shown in Figure 6. The corresponding maximum dynamic crush is about 10 inches.

Sensor Dynamics in Crush Zone and Passenger Compartment

The dynamics of the crash and safing sensors were simulated using the crash pulses at the radiator and rocker B-post. Figure 7 shows the ball travel of the crash sensor mounted at the radiator. This crash sensor has a

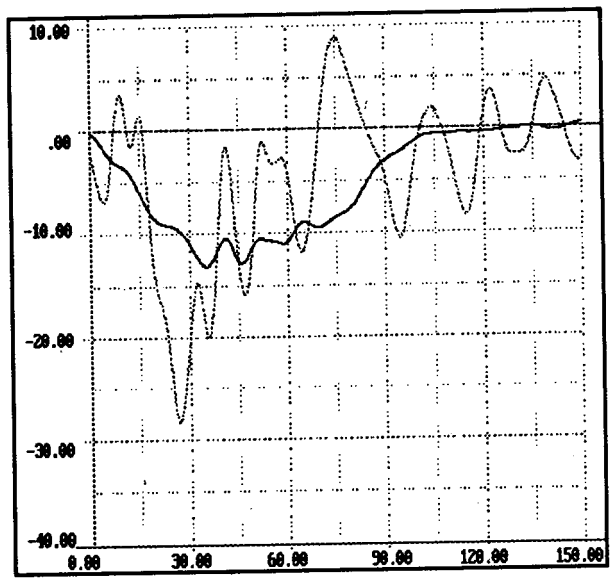

Figure 4. Comparison of the Filtered Pulses at the Radiator and Rocker B-Post of Vehicle C in a 14 mph Barrier Impact

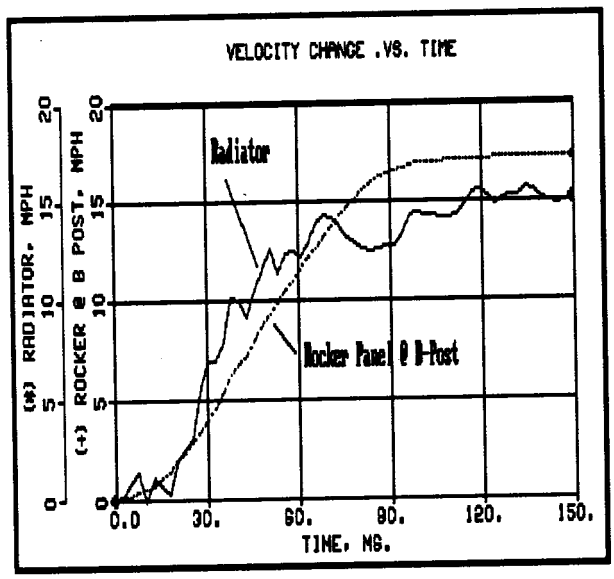

Figure 5. Velocity Changes at the Radiator and Rocker B-Post of Vehicle C in a 14 mph Barrier Impact

simulated activation time at 38 ms with a dwell of 36 ms. Figure 8 shows the ball travel of the safing sensor mounted at the rocker panel B-post. This safing sensor has a simulated activation time at 20 ms with a long dwell.

Using A Simple Sensor Design Criterion

Performing a double integral of the accelerometer data at the rocker B-post location with zero initial velocity yields an unbelted occupant (free-flight mass) displacement relative to an undisturbed point in the rocker panel. The time for an unbelted occupant to move 5 inches forward minus the time needed for the air bag to completely

[2]The accelerometer at the rocker panel B-post, an undisturbed point on the vehicle, records the dynamics of the vehicle passenger compartment in a frontal impact.

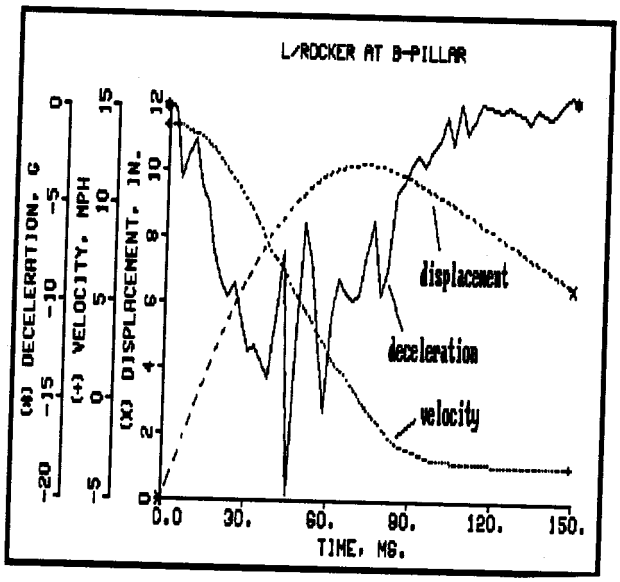

Figure 6. Kinematics of Vehicle C Compartment Based on Accelerometer Data at Rocker B-Post in a 14 mph Barrier Impact

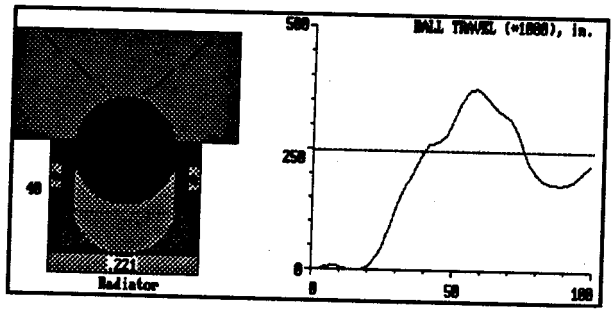

Figure 7. Simulated Ball Travel of the Crash Sensor of Vehicle C in a 14 mph Barrier Impact

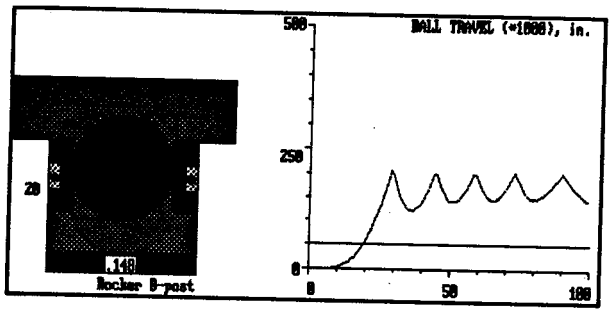

Figure 8. Simulated Ball Travel of the Safing Sensor of Vehicle C in a 14 mph Barrier Impact

deploy (about 30ms) gives the desired sensor activation time.

Figure 9 shows that it takes 61 ms for the unbelted occupant to move five inches in the passenger compartment of Vehicle C in a 14 mph barrier impact. Therefore, the desired sensor activation time, based on the 5"-30 ms criterion, is 31 ms. The actual test sensor activation time of 32 ms is 1 ms later than the activation time determined using the 5"-30ms criterion. In a 14 mph barrier test, 1 ms allows the occupant to move 0.3 inches farther forward than a system meeting the 5"-30ms criterion.

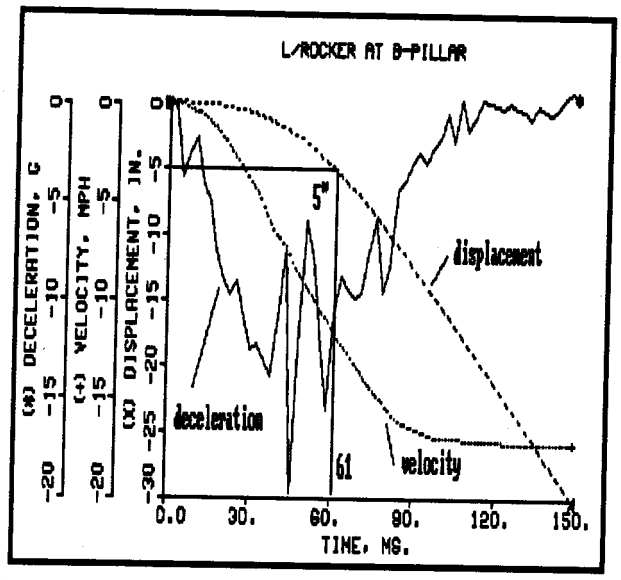

Figure 9. Simulated Unbelted Occupant Displacement in the Passenger Compartment of Vehicle C in a 14 mph Barrier Impact

Figure 10 compares the velocity changes of the A, B and C vehicles at the radiator in a 14 mph barrier impact. The three velocity change traces are quite close to each other except in the window shown. This window covers the region where the sensor activation time should occur, based on the 5"-30ms criterion. The velocity change for Vehicle B is less than that for the other vehicles. The reason for the small velocity change (which tends to slow sensor activation time) at the radiator has been explained previously in the section *Role of Bumper*. The smaller velocity change of Vehicle B is also evident in the response curve at the rocker B-post as shown in Figure 11.

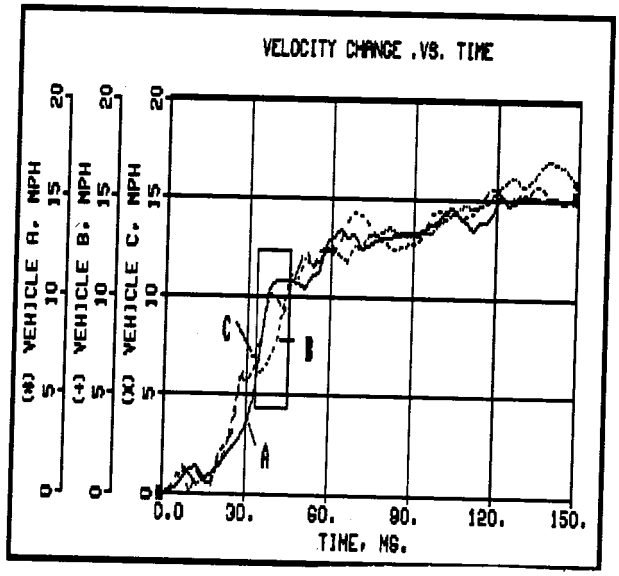

Figure 10. Velocity Change vs Time at Radiators of Vehicles A, B, and C in a 14 mph Barrier Impact

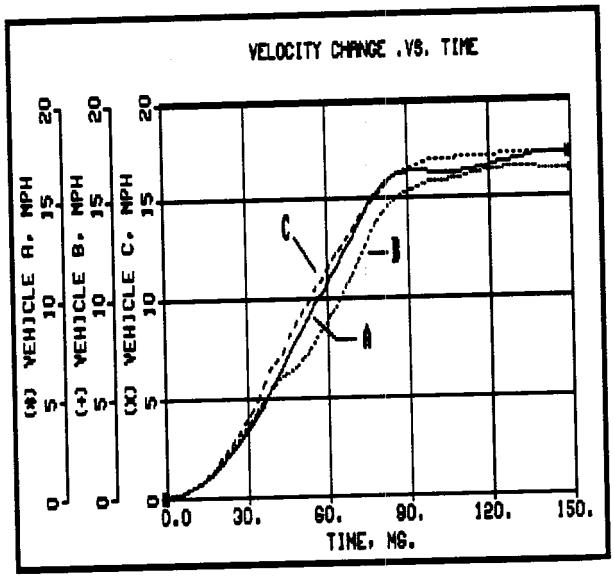

Figure 11. Velocity Change vs Time at Rocker Panel B-Post of Vehicles A, B, and C in a 14 mph Barrier Impact

Table 1 summarizes the results of sensor simulations and tests for the A, B and C vehicles. The effect of a filtered crash pulse on sensor activation time and the computed 5"-30ms (closure time goal) are also listed for comparison. Using sensor simulation, it was found that the filtered crash pulse delayed the sensor activation by an average of 1 ms compared to the wide band data.

Table 1. Summary of Simulation and Test Results

	Vehicle A	Vehicle B	Vehicle C
Weight (lbs)	3924	3531	4000
Closure Time Goal	34	37	31
Simulated Closure Time			
Unfiltered	39	45	38
60 Hz	40	45	40
Actual Closure Time			
Sensor	33	44	32

Sensor Mounting Bracket Model and Impulse Responses

To study the effects of sensor mounting bracket rotation due to structural deformation in a crash, a mathematical model based on the deflection of a beam was formulated. A sensor is mounted at the bottom of a beam supported on the top to simulate a structure such as a radiator support as shown in Figure 12. The assembly is modelled as a beam with a torsional spring loaded at the interface between the bracket and support. The torsional stiffness is based on the dimensions and material property of the bracket.

To verify the dynamic properties of the bracket model, an impulse loading of 3 ms duration and 73 g deceleration level was applied to the undamped system. Figure 12 shows the simulated undamped response of the sensor

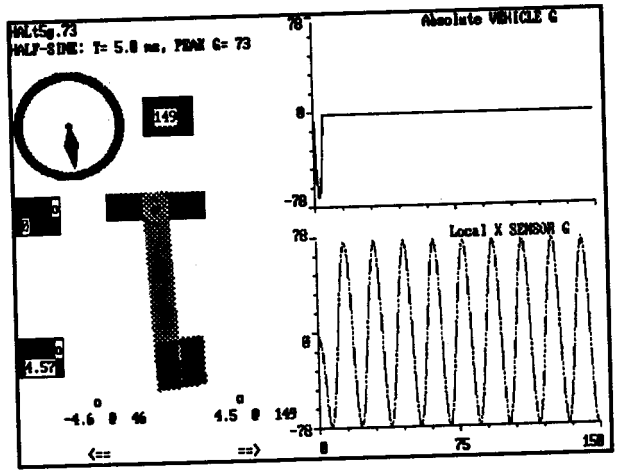

Figure 12. Simulated Response of a Sensor Mounted on Bracket Support with No Damping Subjected to an Impulse to Obtain the Natural Frequency of the Sensor Bracket

on a steel bracket subjected to the impulse shown in the upper right hand corner. The output response shown in the lower right hand corner is an undamped vibration indicating the natural frequency of the bracket assembly is about 60 Hz.

Figure 13 shows the simulated response when a sensor installed on a bracket mounted to provide damping of 100 1/sec[3] is subjected to the same impulse. The output oscillation subsides at about 75 ms after an input excitation of 5 ms duration.

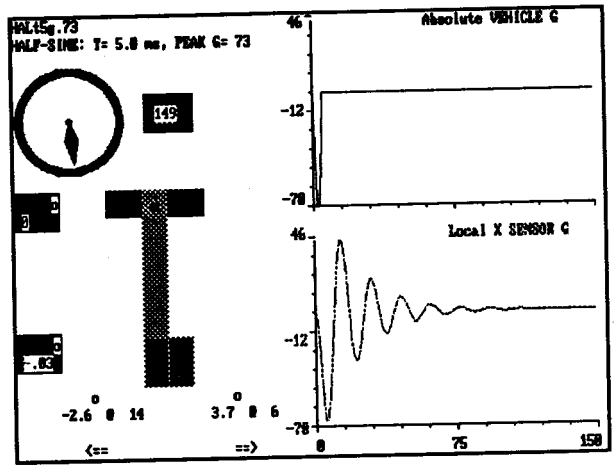

Figure 13. Simulated Response of a Sensor Mounted on Bracket Support with Damping of 100/1 sec Subjected to an Impulse

Effects of Sensor Bracket Stiffness and Support Structure Rotation

Using the same damping value, when the sensor bracket support mounted at the radiator is subjected to an input deceleration, the longitudinal deceleration (g) vs. time (ms) at the radiator of Vehicle C is shown in the upper right hand corner in Figure 14. Assuming no structural rotation during crash, the local longitudinal

[3]In this study, the damping variable, c, is defined as $\Delta\alpha = \omega c$, where $\Delta\alpha$ is change in angular acceleration and ω angular velocity. The unit of c is 1/sec.

deceleration at the sensor location is shown in Figure 14. The local deceleration has lower magnitude than the input deceleration because the input excitation has a frequency higher than the natural frequency of the bracket system and due to the effect of damping. The vibration magnitude of the beam is between 1.8° forward and 1.2° backward.

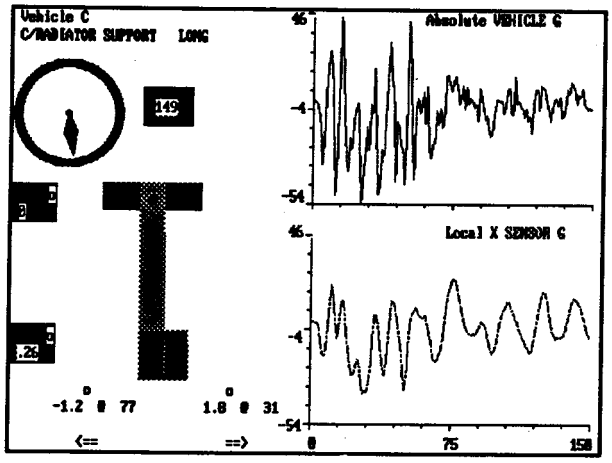

Figure 14. Simulated Response of a Sensor Mounted on a Radiator Support Bracket Having No Structure Rotation in a 14 mph Barrier Test

With the same input excitation at the radiator but with a structure rotation of 60° over the 40 ms after impact, the model predicted a reduced deceleration at the sensor location as shown in Figure 15.[4] Because of the reduction in deceleration, the velocity change or the area under the deceleration curve is not large enough to activate the sensor. If the same structure rotation of 60 degrees occurred over a longer period of time (150 ms) as shown in Figure 16, the deceleration and velocity change are not reduced as much as when rotation occurred during a 40 ms time interval.

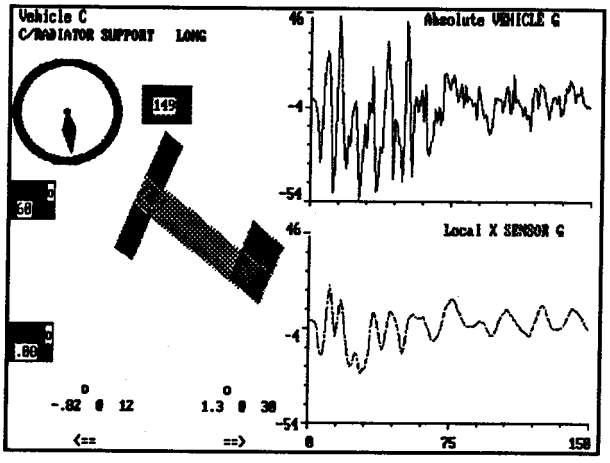

Figure 15. Simulated Response of a Sensor Mounted on a Radiator Support Bracket Having 60 Degree Structure Rotation Over a 40 ms Time Interval in a 14 mph Barrier Test

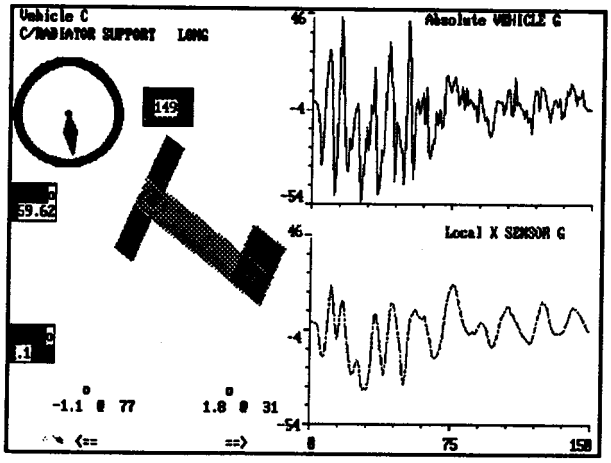

Figure 16. Simulated Response of a Sensor Mounted on a Radiator Support Bracket Having 60 Degree Structure Rotation Over a 150 ms in a 14 mph Barrier Test

Figure 17 shows the simulated response of a sensor mounted on a *softer* bracket made of aluminum with no structural rotation in a 14 mph barrier test. Compared to Figure 12 where the bracket is made of steel, the aluminum bracket has a maximum forward vibration amplitude of 6.1 degrees at 32 ms compared to only 1.8 degrees at 31 ms for the steel bracket. Although the deceleration at the sensor with an aluminum bracket has less high frequency components compared to that with a steel bracket, the peak deceleration magnitude and time at which peak deceleration occurs are about the same for both brackets.

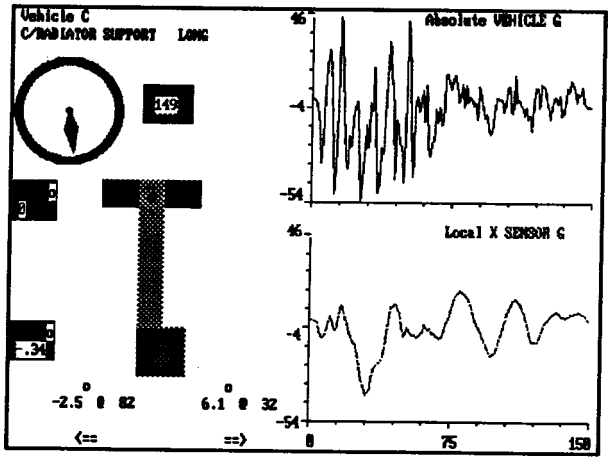

Figure 17. Simulated Response of a Sensor Mounted on a Softer Bracket Having No Structure Rotation in a 14 mph Barrier Test

To minimize the diminution of deceleration level and velocity change at the sensor location, the torsional and flexural rigidity of the bracket system should be designed to reduce the adverse effects of structural rotation and/or vibration.

[4]Due to change in aspect ratio around the video screen, the captured drawing of the bracket assembly was distorted during rotation.

Summary and Conclusions

- Based on mathematical analyses of three vehicles in 14 mph perpendicular barrier tests, Vehicle C has the shortest sensor activation time (38 ms) followed by the Vehicle A (39 ms) and Vehicle B (45 ms). The simulated sensor response of the Vehicle C with revised bumper shows an improvement of 7 ms over the response with the previous bumper system (38 ms vs. 45 ms).
- It was clear that the Vehicle B bumper had a delaying effect on sensor closure compared to Vehicle C. As the only difference between Vehicle C and Vehicle B was the structural design of bumper, it was apparent that the bumper design caused the delay in sensor actuation. Design of the Vehicle B bumper was such that the lower part of the housing box connected to the bumper PGM is weaker than the top, and caused a folding effect during crash. The folding effect in turn caused a double hump on the deceleration pulse with a momentary drop in deceleration due to deformation of the housing box.
- The momentary drop in deceleration is evident when comparing the deceleration crash pulses (filtered at 60 Hz) of the test vehicles at the centerline radiator support and right rocker @ B-Pillar locations. When comparing the velocity vs. displacement and the velocity vs. time at the right rocker @ B-pillar location, the plots displayed a trend caused by the momentary drop in deceleration.
- The effects of a PGM-type energy absorber on sensor closure were examined. The results showed that a "hard" PGM gave a quicker simulated closure time than a "soft" PGM. The "hard" and "soft" PGMs were actually the same energy absorber except that the "hard" PGM had a smaller tube diameter than the "soft" PGM (more energy is required to stroke the shaft of the "hard" PGM than the "soft" PGM for the same travel).
- Based on an analysis of the data and the simulations for the mid-sized vehicles considered, it was concluded that the bumper design yielding the best sensor activation time is the structure that is as rigid as that of Vehicle A, but not much more rigid. The latter condition is necessary to avoid air bag deployment when it is not desired.
- The mathematical model of the sensor mounting bracket predicts the effects of bracket stiffness and rotation of the support structure on the longitudinal deceleration that the sensor will experience. The model can also be used to evaluate dynamic characteristics such as the natural frequency of the bracketry.
- Since the resonant frequency of the sensor mounting bracket is relatively high compared to that of the bracket support structure, bracket vibration does not significantly affect the deceleration amplitude that the sensor experiences. Rotation of the support structure in a frontal crush zone not only decreases the deceleration amplitude but also reduces the velocity change that the sensor experiences during impact.
- The main effect of support structure rotation is that it may delay the sensor activation time (or not activate the sensor at all) in a low threshold speed test. If the rotation occurs over a shorter period of time, the effect is more pronounced than when rotation occurs over a longer period of time.
- As long as the amplitude of bracket vibration is small, the bracket stiffness does not seem to be as important as the support structure rotation with regard to the deceleration level and velocity change read by the sensor.

Acknowledgment

The authors are grateful to Mr. Clay Gabler of the National Highway Traffic Safety Administration for providing the Butterworth second order filtering subroutine, Mr. Michael Lynch of Ford Motor Company, Body Engineering, for providing crash test data for analysis and Mr. Calvin Matle of Ford Motor Company, Automotive Safety Office, for technical consultation.

References

1. M. Huang, "Dynamics and Animation of an Air Bag Ball-in-Tube Sensor System," AMD-Vol. 106, BED-Vol. 13, Crashworthiness and Occupant Protection in Transportation Systems, The Winter Annual Meeting of the American Society of Mechanical Engineers, pp. 81-87, San Francisco, California, December 10-15, 1989.
2. T.G. Adams, M. Huang, R.W. Hultman, J.C. Marsh, S.E. Henson, "The Development of an Advanced Air Bag Crash Sensing System," Paper 905140, XXIII FISITA Congress, The Promise of New Technology in the Automotive Industry, Technical Papers, Vol. II, pp. 159-164, Torino, Italy, May 7-11, 1990.
3. W.J. Evans and C. Haddad, "Select Strength Steel Bumper System," SAE Paper 830397, P-124—High Strength Steel for Automotive Use.

S9-W-42

Application of New Elastic-Plastic-Brittle Material Models to Composite Crash Simulation

E. Haug, O. Fort, G. Milcent, A. Trameçon
Engineering Systems International S.A.
M. Watanabe, I. Nakada
TONEN Corporation
T. Kisielewicz
ESI-APG

Abstract

New materials, such as elastic-plastic-brittle aluminum alloys and predominantly brittle-fracturing fiber reinforced plastic materials (composites) are a potential alternative to the conventional steel materials used in car body structures. While linear elastic stiffness, vibration and stress analyses pose no notable added difficulties, the crashworthiness simulation of structures and components made of composites or aluminum alloys must cope with the basic brittleness and fracturing behaviour of the material and with crash energy absorption modes that may be entirely different from the elastic-plastic crash energy absorbing folding modes, typically encountered in soft steel car body structures. A previous paper outlined a methodology that has been conceived, calibrated, validated and extrapolated for elastic-plastic-brittle and multilayered and multi-material composite sandwich wall and sandwich core models for the numerical crashworthiness prediction of composite components. The new models have been implemented into a crashworthiness simulation program, PAM-CRASH™, and validated on component crash tests. The effects of combining brittle carbon and plastic Kevlar fibers in the sandwich facings of the tested structures have been studied. In the present paper, the models are extrapolated to the numerical crash simulation of a full size composite passenger car cabin.

Introduction

Basic Reference

In Reference [1] the ground has been laid for the present discussion on application of elastic-plastic-brittle material models to crashworthiness simulation of automotive structures, made of composite materials. The present paper discusses the application of the calibrated and validated numerical models to the front and side (pole) impact simulation of a composite prototype passenger car cabin.

Joint Study on Composite Car Crash

Background. In a joint study with the Japanese TONEN Corporation, supported by the Japanese Petroleum Energy Center, the feasibility of industrial crashworthiness calculation and design for composite structures and components is demonstrated on the example of a prototype composite passenger car cabin finite element model of 22000 elements. ESI conceived, calibrated and validated new material models for multilayered thin shell and sandwich core brick finite elements, to be used in the PAM-CRASHTM explicit finite element code. This code was so far predominantly applied to industrial crash simulations and crash design of automobiles made of conventional soft and high strength car body steels. With the new material models, the code can now simulate crash events of structures made of elasto-plastic-brittle fracturing materials, such as composites or aluminum alloys.

Goal. The goal of this study was to demonstrate the feasibility of industrial crash simulation of complex composite sandwich wall structures, the way it has by now become standard practice for car bodies made from soft steel. TONEN Corporation fabricated two prototype composite passenger sports car cabins, one to be used in a fully equipped prototype and the other to be used in strength, vibration and, ultimately, destructive crash tests. The tested cabin was made from carbon-Kevlar-carbon aramid honeycomb sandwich panels. The crash tests were non-standard in the sense that the cabin was crashed as a pure "body in white," i.e., without any of the front and rear attachments of the running prototype. During front and lateral crash tests the expected maximum crash displacement was to be about 10-15 centimeters, i.e., enough to cause realistic large damage, but without complete destruction of the cabin.

Study Outline

Predictive analyses. For that reason the tests were preceded by predictive analyses, where the composite cabin structure was crushed with a quasi-infinite mass, that crushes the structure with almost constant velocity to about the target crash distance, where the computer runs were stopped. From the predicted internal energy absorption curves over calculated crash distance, the real mass to be used during the respective sled tests could be estimated from the required balance of total initial kinetic energy and total absorbed internal energy at maximum crash distance.

Laboratory tests. The tests were then performed by INRETS with the estimated real masses at initial velocities of 50 km/h for the frontal crash (21.4 km/h for the pole impacts). The test results, such as impact force time histories, accelerogrammes, high speed films and damages were recorded for processing and comparison with numerical results.

Final analyses. Finally, the front and side impact simulations were repeated with the real initial velocities and masses attached to the structures during the tests. In

these analyses the predicted and measured maximum crash displacements could be verified.

Applied Methodology

The joint study carried out between TONEN Corporation and ESI comprised three essential study phases.

Calibration Phase 1. During this phase, ESI specified material coupon tests (tensile, compression, bending) that permit access to subcritical material data and data up to specimen failure. The coupon tests were performed by TONEN and the results exploited by ESI for the calibration of the used material models. For this purpose detailed FE models of the coupon tests were prepared and the material model parameters calibrated by comparison between the numerical and laboratory experiments.

Validation Phase 2. Next, the calibrated material models were used to simulate identified benchmark tests of relevant composite sandwich subassemblies. These static and dynamic drop tests on sandwich plates and sandwich box beams, were performed by TONEN and JARI, and the results of the experiments were compared with the numerical results. Coincidence was found quite good and only minor adjustment of the material model parameters of the sandwich core material, calibrated in phase 1, had to be made.

Predictive Phase 3. Finally, the calibrated and validated numerical model was applied to predictive front and side impact analyses of the complete composite sandwich cabin. The indicated 3 phase methodology of calibration, validation and prediction guarantees the best possible results. Detailed proceeding and results for the calibration phase 1 and the validation phase 2 are reported in Reference [1].

Numerical Modelling Aspects

Material Models

Used sandwich material. The basic materials used in TONEN's prototype passenger car cabin are multilayered composite sandwich facings made of high stiffness and high strength unidirectional TONEN FT500 pitch based carbon fiber/epoxy crossply (0°, 90°) layers, a layer of DUPONT aramid fiber based KEVLAR 49 cloth (0°*90°), and of TORAY PAN based T300 carbon/epoxy cloth (45°*-45°), Figure 1. The sandwich core material consists of aramid honeycomb material. The basic sandwich wall structure is provided with additional layers of reinforcements at strategic locations throughout the car cabin.

Material model for sandwich facings. The material models used in the PAM-CRASH simulations were described in detail in Reference [1] and are summarized in Figure 2. The models for each layer of the sandwich facing are bi-phase plane stress material models, by which the rheological behaviour of the constituent monodirectional fiber and orthotropic plane stress matrix

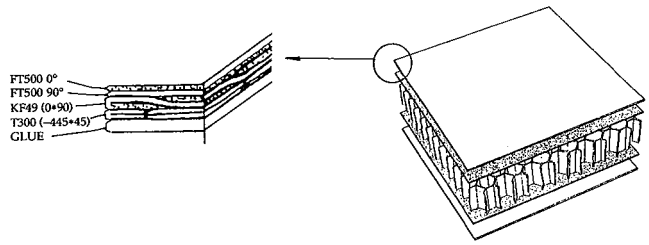

Figure 1. Basic Composite Sandwich Wall Structure

phases can be treated separately. Both material phases obey a brittle fracturing modulus damage description, where the initial modulus, E_o, is damaged by a damage function, $d(\varepsilon)$, such that

$$E(\varepsilon) = E_o\,[1-d(\varepsilon)],$$

where ε is a measure of total deformation. The damage function, d, is assumed to grow from values of zero, at an initial threshold strain, ε_i, to values of one (or almost one for non-vanishing ultimate strength) at an ultimate threshold strain, ε_u, either linearly or non-linearly. The degree of complexity of this function may be assumed, and the coefficients calibrated from basic coupon tests in tension, compression and bending. For symmetric cloth the entire ply behaviour can be represented by the adequately calibrated orthotropic matrix phase of the model, and no fiber phase is needed. Figure 3 shows the tension and compression response in the 0°-direction of each ply in the basic FT500(0°) carbon/K49 (0°*90°) KEVLAR cloth/T300 (+45°*-45°) carbon cloth stackup of the sandwich facings. Similar responses were obtained for other stackups in areas of reinforcements.

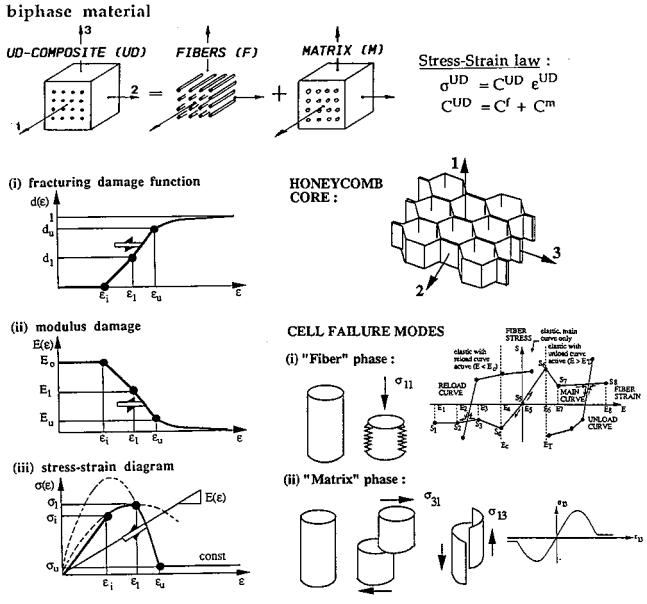

Figure 2. Bi-phase, Fracturing and Sandwich Core Material Models

Material model for sandwich core. The model used for the aramid honeycomb core of the sandwich walls is a specialized 3D bi-phase solid model, where the "fiber" phase is aligned with the axes of the hexagonal honey-

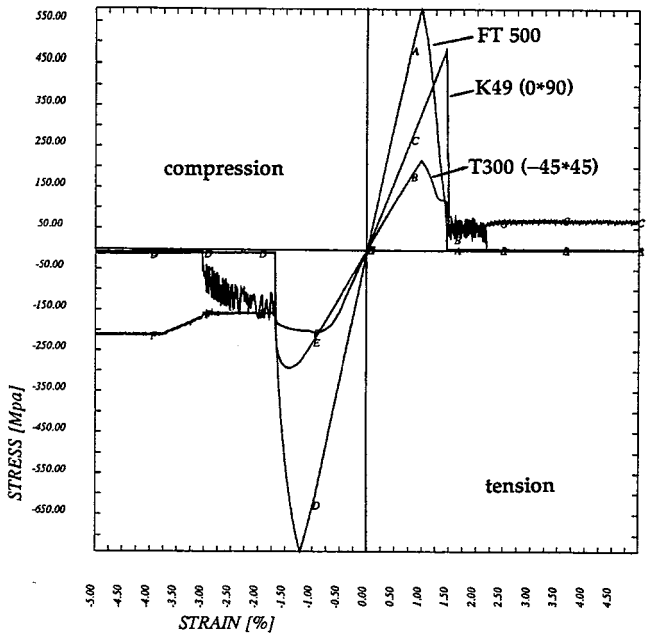

Figure 3. Individual Ply Tensile/Compressive Material Response in Basic Sandwich Facing Stackup

comb cells. In this model, the monodirectional "fiber" properties can be given highly nonlinear tension/compression unloading/reloading properties to represent the complex axial crushing response of the cells, see Figure 2. The transverse shear properties of the core material of a plate made of honeycomb sandwich material is represented by elastic-fracturing terms, with calibrated transverse shear modulus damage, in the "matrix" phase of the adapted 3D bi-phase model. The in-plane stiffness and resistance terms of the honeycomb core material of the sandwich plates are assumed very small and represented by small numbers in the calculations.

Finite Elements

The described composite sandwich material models are built into multilayered Mindlin type under-integrated 4 node and CO compatible triangular shell and plate finite elements for the sandwich facings, and into 8 node under-integrated adapted bi-phase solid brick finite elements for the sandwich core, Figure 4. To make up one "sandwich" element, two multilayered thin shell elements are connected to opposite faces of a brick element, the "fibers" (cell directions) of which are assumed perpendicular to the facings.

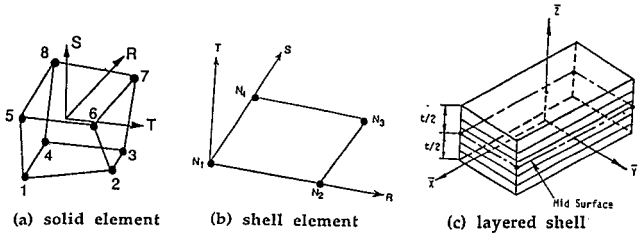

Figure 4. Finite Elements used in PAM-CRASH

Frontal Crash Investigation

Prototype Composite Passenger Car

The layout of the composite two-seater sportscar is shown in Figure 5. The mainframe of the passenger cabin is made 100 % from carbon-Kevlar-carbon aramid honeycomb plate material and has a total mass of about 80 kilograms. The rear engine and gear and the front gear are attached to the cabin rear and front walls at steel insets via tubular metallic subframes. The hood, engine cover and roof are also made of composite material. The car has been built and run on test tracks.

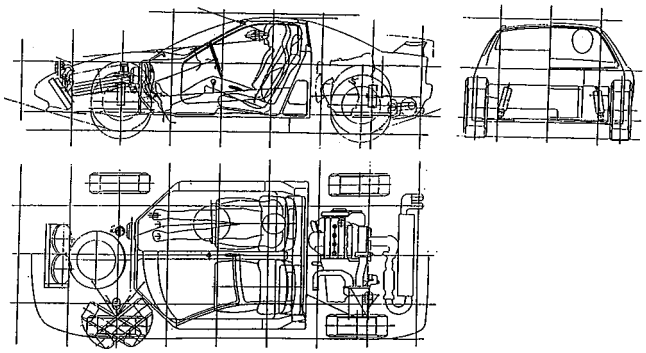

Figure 5. TONEN Composite Prototype Passenger Car

Frontal Crash Test Setup

Figure 6 shows the frontal crash test setup used by INRETS (Lyon-Bron). The cabin is mounted on frictionless rollers on a sled that is stopped short of a rigid barrier. The cabin will then impact on the barrier and the event is recorded via impact force measurement devices, accelerometers and high speed cameras.

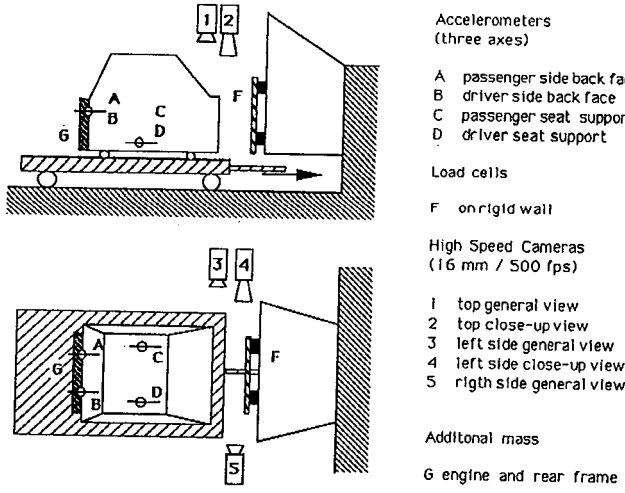

Figure 6. Frontal Crash Test Setup (INRETS Laboratories)

Frontal Crash Simulation

FE-Model. Figure 7 gives an overview on the FE-model of the analyzed half of the prototype composite car cabin ("body in white"). The model comprises about 7000 sandwich elements, i.e., 2 x 7000 = 14000 multilayered composite thin shells and 7000 sandwich core bricks (~22000 finite elements). The boundary conditions

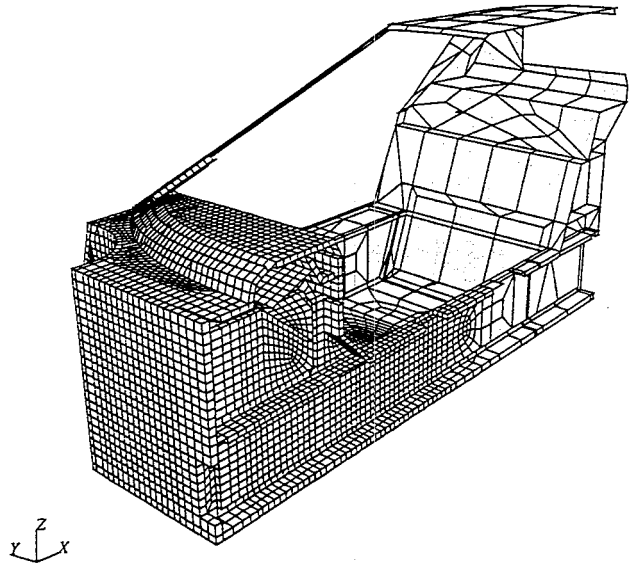

Figure 7. Frontal Crash FE-Model of Composite Car Cabin

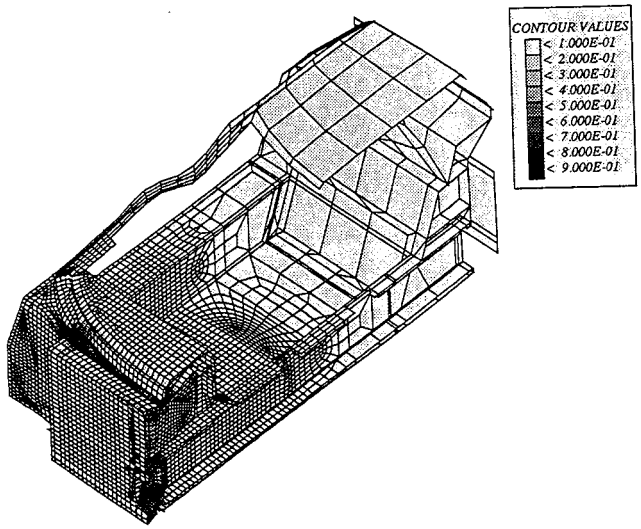

Figure 8. Frontal Crash Simulation: Deformed Shape and Damage Contours at 88 mm Crash Distance (10 ms) (PAM-CRASH/DAISY)

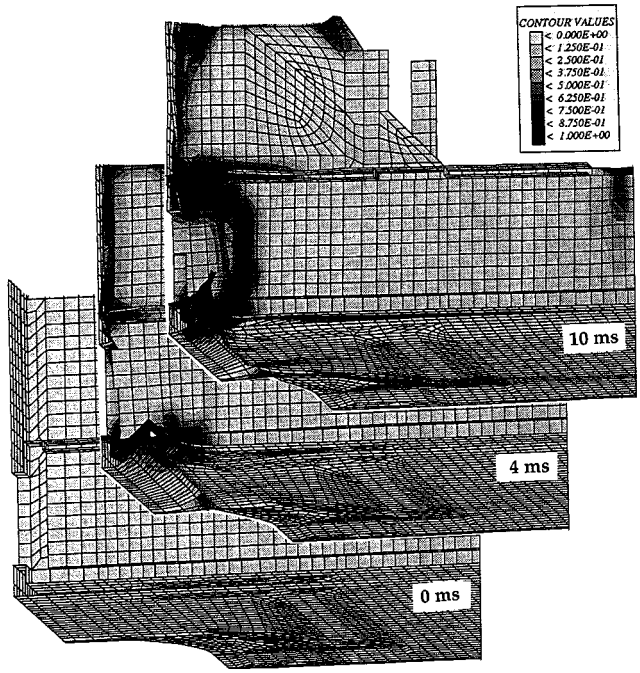

Figure 9. Frontal Crash Simulation: Deformed Shape Zooms and Damage Contours at 0, 4 and 10 ms (0, 39 and 88 mm) (PAM-CRASH/DAISY)

are like in the test with a rigid mass of 180 kilograms attached at the rear wall of the cabin. The cabin model is impacted at 50 km/h against a rigid wall.

Deformed shapes. Figure 8 shows the deformed shape of the crushed cabin model after 10 milliseconds at a total crash distance of 88 millimeters. The crash distance is measured from the relative deformation of the undamaged rear part of the structure with respect to the damaged front end. Figure 9 gives details of the deformed shape near the frontal impact area of the central tunnel at 0, 4 and 10 milliseconds crash duration (0, 40 and 85 millimeters crash distance). The super-imposed average damage contours over the multilayered carbon-Kevlar-carbon sandwich facings indicate the local nature of the damage (in a structure made of soft car body steel the damaged (buckled) areas would spread out much further). Black colour signifies values d = 1.0 of the average damage function, and complete loss of strength. The sandwich core brick elements are not shown in Figure 9 for added clarity.

Figure 10a compares the frontal damage areas of the test (after elastic springback) and of the simulation (before springback). Other than, for example, in soft steel structures, there is significant springback in elastic-fracturing composite structures after removal of the impact loads. This is due to the fact that this type of material tends to recover strain after unloading, nevertheless with severely damaged secant modulus in the stress-strain curve. This is especially true in the presence of more ductile layers of KEVLAR material, that tend to preserve the structural integrity of the damaged wall structure. In elasto-plastic deformation, however, plastic strains are permanent and elastic springback is usually very small.

In the last of the deformed shape plots of Figure 9, a remote area of damage in the vertical wall of the central tunnel can be seen near the central hole for the gear stick. Figure 10b also contains this area, compared to the real damage of the crashed structure.

Further results. The predicted total crash distance of the simulation of the frontal crash test is obtained from the point of zero kinetic energy, Figure 11. The distance is predicted to 13.5 centimeters, which agrees to within a few percent to the total crash distance measured in the frontal crash test. Figure 12 shows the impact force versus crash distance plots of the four force plates attached to the rigid wall in the test and the sum over all forces. The small peaks near 27 mm and 55 mm crash

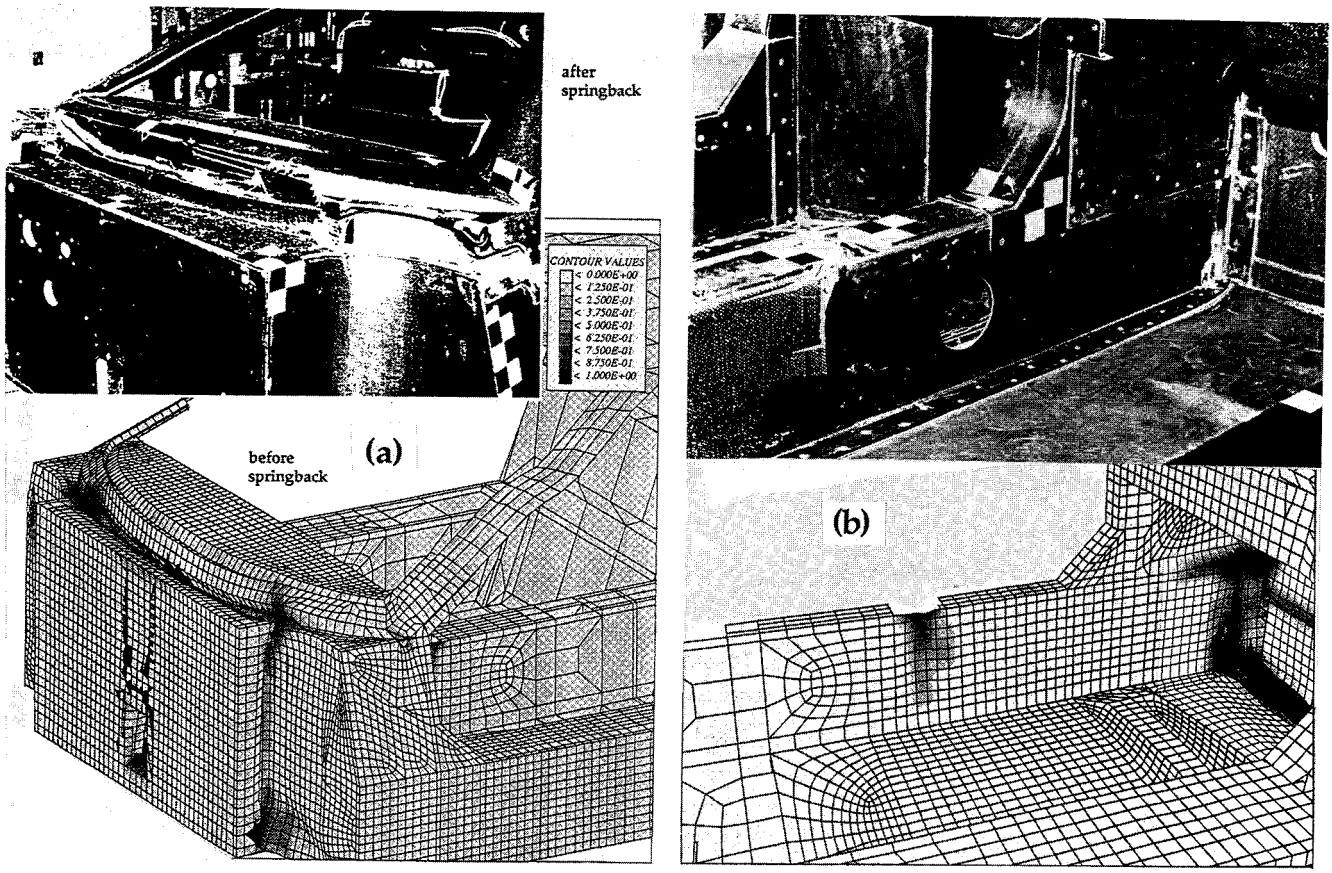

Figure 10. Frontal Crash Simulation: Deformed Shape Test vs. Simulation Comparisons at 10 ms (88 mm) (PAM-CRASH/DAISY)

distance correspond to delayed frontal impacts of the flanges and of the web of the central box beam onto the rigid wall.

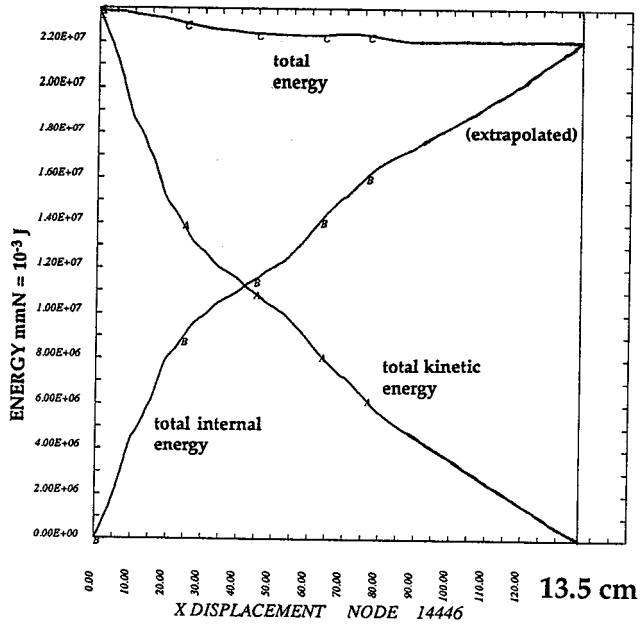

Figure 11. Frontal Crash Simulation: Energy vs. Crash Distance Curves (PAM-CRASH/DAISY)

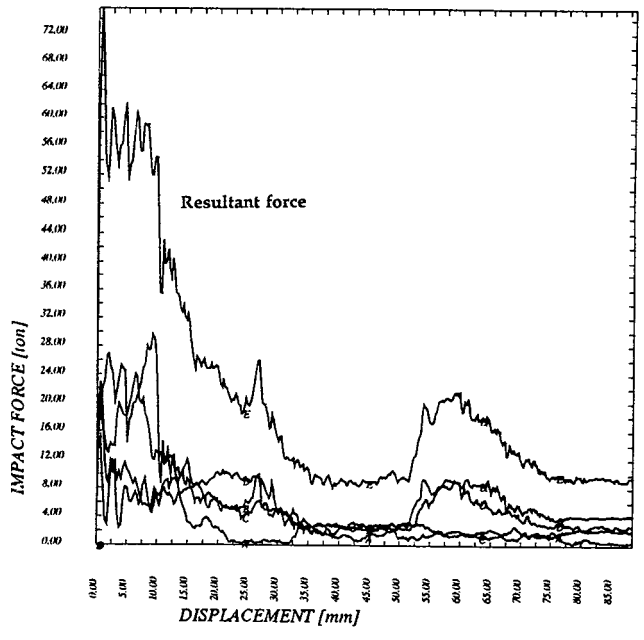

Figure 12. Frontal Crash Simulation: Impact Forces vs. Crash Distance (PAM-CRASH/DAISY)

Pole Side Impact Investigation

Pole Side Impact Test Setup

Following the frontal rigid wall impact test, two lateral pole impacts at about 20 km/h with a total mass

of 288 kilograms were carried out, Figure 13. This was feasible, because the cabin showed no visible damage, neither in the front impact test, nor in the frontal crash simulation, near the areas of the door sill sandwich box beams that were hit by the rigid pole with a diameter of 270 millimeters. In this test, the cabin was positioned laterally against the rigid wall. The "pole" was mounted on a sled that was moving towards the cabin. The sled impact was monitored with an accelerometer mounted on the sled and the impact force of the pole was measured via load cells at the far side of the cabin.

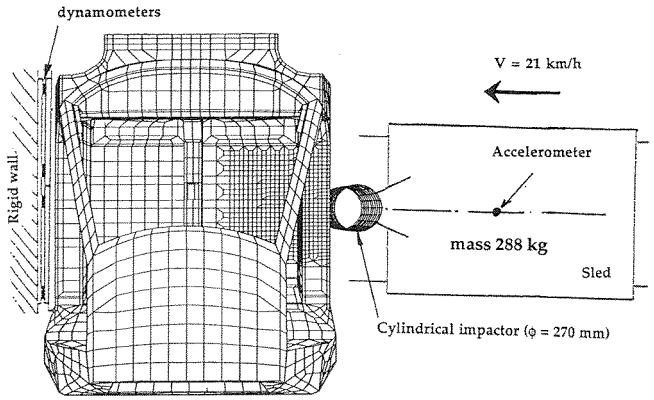

Figure 13. Pole Side Impact Test Setup (INRETS Laboratories)

Pole Side Impact Simulation

FE-Model. Figure 13 also shows the finite element model adapted for the lateral pole impact simulation. For this purpose only the mesh near the impact area around the pole was refined. The mesh contains about 3200 sandwich core brick finite elements and 8800 multi-layered thin shells. The impactor was modelled as a rigid body with mass 288 kilograms and is restricted to move in the impact direction, with an initial velocity of 21.4 m/s (5944.4 mm/s).

Deformed shapes. Figure 14 shows the local nature of the deformation after 18 milliseconds (80 millimeters lateral crash distance) near the sandwich box beam of the door sill, that was hit by the pole. At this time the motion of the sled had decreased to about 20 percent of its initial velocity. For added clarity, the finite elements that had failed were removed from the computer plots. Keeping this in mind, visual comparison of the predicted damage with the photograph from the test is excellent.

Figure 15 contains progressive damage spread in closeup views of the rigid pole impact area at 0, 6, 10 and 14 milliseconds crash duration (0, 35, 52 and 70 millimeters lateral crash distance). For clarity the sandwich core brick elements are not plotted. The contours of the average damage over all plies of the sandwich facings are superimposed on the plots. Black colour signifies a damage function value of d= 1.0, i.e., elements have lost all strength. The pictures clearly show the zip-like tensile ruptures due to membrane stresses to both sides of the pole in the outer facing of the sandwich

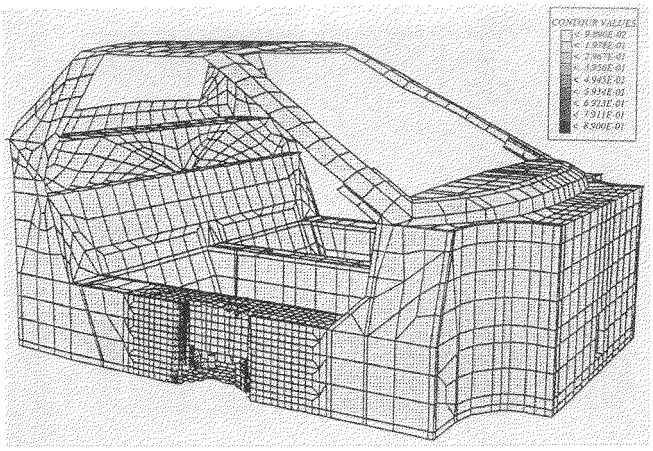

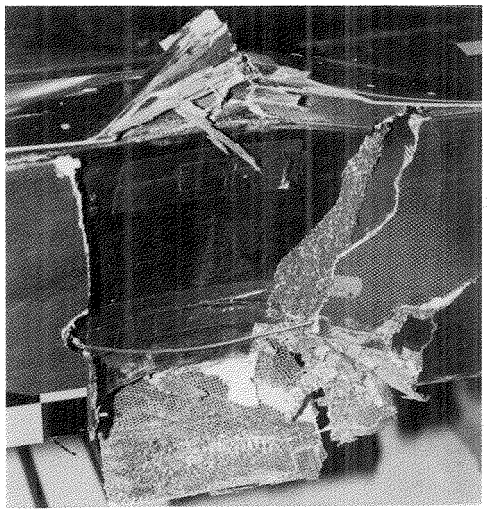

Figure 14. Pole Side Impact Simulation: Deformed Shape and Damage Contours at 14 ms (PAM-CRASH/DAISY)

box beam. The same phenomenon has been found in the test, Figure 14. Similarly, the lower and upper webs of the box beam are seen to undergo severe local bending and compression damage, which has been found in the test. Note that the test picture contains almost totally damaged shreds of the carbon-Kevlar-carbon facings. Such portions were removed from the computer plots. It is mostly the admixture of the KEVLAR plies that preserves this semblance of structural integrity in the tests.

Further results. Figure 16, finally, shows the total impact force near the rigid wall on the far side of the laterally impacted composite car cabin. As a check, this force-time diagram coincides very closely to the direct impact force-time diagram (not shown) that resulted from the accelerations of the impacting mass. This means that the filter effect on the impact signal between the point of impact and the far end rigid wall is quite small.

The figure also contains force-time diagrams from the two lateral impact tests. The simulated curve was found to lay well within the scatter range of the two test curves. This is also confirmed by the absorbed energy plots of Figure 17.

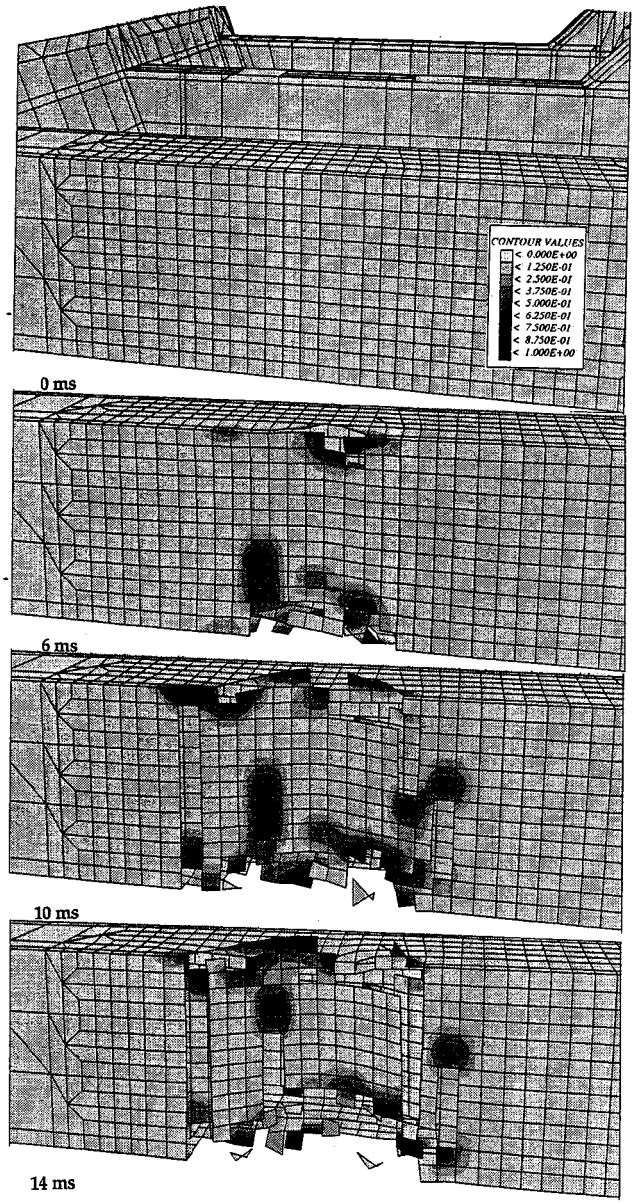

Figure 15. Pole Side Impact Simulation: Deformed Shape Closeup Views with Damage Contours (PAM-CRASH/DAISY)

Conclusions

The methodology outlined in Reference [1] and its successful application to the full scale composite sandwich wall car crash simulations, reported in this paper, permit to conclude that the feasibility of industrial crashworthiness simulation of composite structures has been reached. The crash simulation code, PAM-CRASH, augmented by the options for composite crashworthiness simulation, can therefore be used as a design aid and verification code for the conception of vehicles made from new composite and sandwich wall materials, at no extra CPU cost than needed for crash simulations of conventionally built passenger cars.

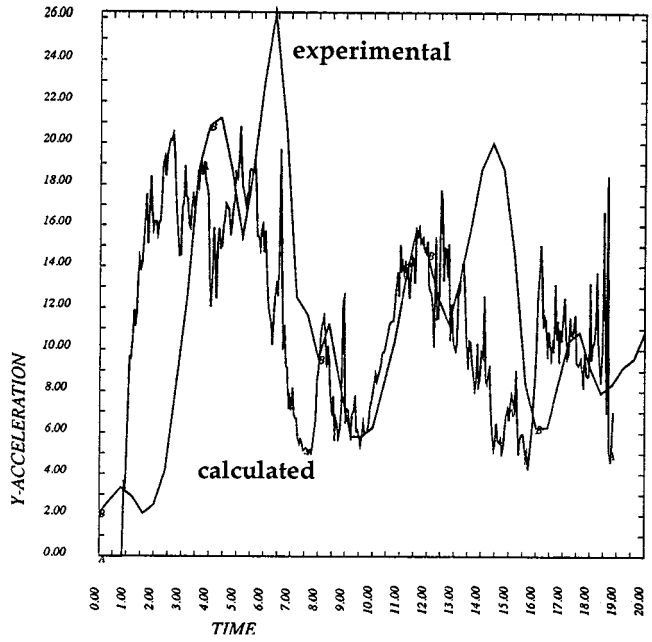

Figure 16. Pole Side Impact Simulation: Impact Force-Time Histories

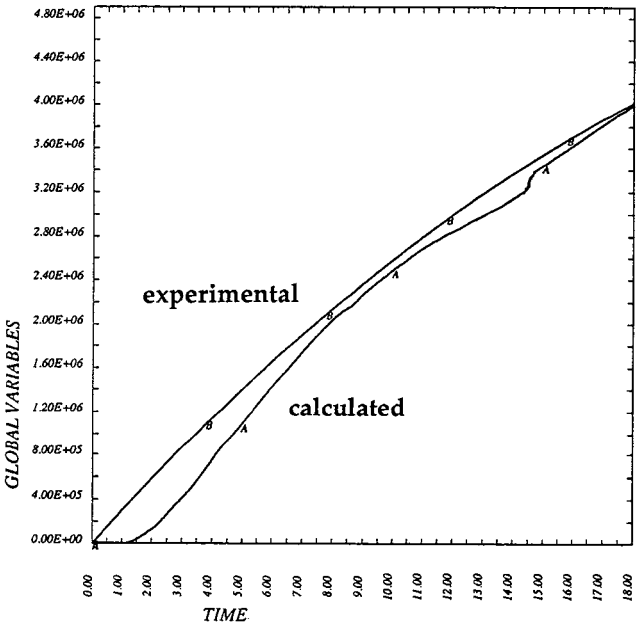

Figure 17. Pole Side Impact Simulation: Absorbed Energy-Time Histories

Acknowledgements

The authors express their gratitude to Dr. D. Cesari and Mssrs. J.A. Bloch and R. Zac of INRETS (Institut National de Recherche sur les Transports et leur Sécurité Bron, France) for having carried out the front and side impact tests at their premisses. The assistance of Mr. L. Penazzi at ESI throughout the project is also gratefully acknowledged.

References

1. Haug, E., Fort, O., Trameçon, A., Watanabe, M. and Nakada, I., "Numerical Crashworthiness Simulation of Automotive Structures and Components made of Continuous Fiber Reinforced Composite and Sandwich Assemblies," SAE Paper 910152, International Congress and Exposition, Detroit, February 25-March 1, 1991.

2. Reference [1] contains a list of 25 references on the subjects of crash simulation, composite component crash experiments, composite car crash experiments and composite damage and strength investigations. The interested reader may consult that list for more information.

S9-W-43

Identification of Automobile Structural Characteristics from Barrier Crash Tests

Clifford C. Chou, Yun S. Lin
Ford Motor Company

Abstract

This interim report documents the progress made in the development of Vehicle Structural Identification Program (VSIP) for determining the non-linear automobile structural characteristics from barrier crash test data. Efforts have been directed toward improving an existing system identification method initiated in 1988 by Hollowell of NHTSA. The improvements made thus far include:

- a provision for predefining certain load paths in a 1-D lumped-mass-spring (LMS) model
- relaxing the requirements of non-negative stiffness parameters in the approximation process.

Good correlations between the extracted results with the actual data either from analytical models or simplified crash test data demonstrate the feasibility of this vehicle structural characterization technique currently under development. Theoretically, the system identification approach has the potential of developing vehicle structural models totally based on accelerometer data from barrier crash tests. The method, when developed and validated, will offer an opportunity in reducing static crusher testings of components traditionally required in LMS model simulations. This opportunity will become evident as the development of the methodology continues. Further applications of this system identification approach to a full scale vehicle system using crash test data need to be explored for identifying feasibilities and issues of the technique.

Introduction

Vehicle crash is a complex dynamic transient event, in that vehicle structures experience large plastic deformations and large strains. The problem of analyzing the crash behavior of vehicle structures has become a challenging analytical subject. The simplest approach to analyze the complex vehicle crash behavior is to use the Lumped-Mass-Spring (LMS) models. Frequently, these models are used through simulation to predict vehicle responses (i.e., the acceleration, velocity and displacement of each mass in the model) based on a given set of structural characteristics. On the other hand, the LMS models can also be used to identify vehicle component structural characteristics represented by the load-deflection of springs connected between masses, provided that all the motions of masses in the model are known. The former approach is referred to as the simulation approach, while the latter one is called the identification approach. The problems solved by an identification approach are also known as inverted dynamics problems.

Simulation Approach

Numerous simulation approaches using various LMS models have been attempted for vehicle structural analysis (Chou, 1986; Kamal, 1970). LMS models, in general, consist of masses and springs. Linear or non-linear springs representing energy absorbing (EA) structural components interconnect the masses. CRUSH (Crash Reproduction Using Static History) II (Motl and Wong, 1975; Herridge and Mitchell, 1972) is a typical LMS simulation program.

In the LMS modeling, inputs of static vehicle structural characteristics into a simulation program are essential for replicating the motion histories of masses. Static crush tests are costly, laborious and time consuming to conduct. In addition, dynamic factors are used in transferring static crush data into dynamic simulation to account for strain rate effects (Prasad and Padgaonkar, 1981). Furthermore, structural collapse modes observed in dynamic crash tests are also difficult to replicate in static crush tests.

In barrier crash tests for vehicle development, accelerometers are normally mounted at various locations for measuring the vehicle response. It is, therefore, desirable to use the available acceleration data for determining the dynamic vehicle structural characteristics directly using an identification approach.

Identification Approach and Its Limitations

A literature review (Hollowell, 1986) reveals that many attempts have been limited to linear structural dynamic systems. This is because, under a normal loading environment, most structures are designed to operate in the linear range. However, non-linearity dominates the behavior of the vehicle structures during a collision. None of the existing linear identification techniques are readily applicable to determine the system parameters of a non-linear vehicle structure in a crash loading condition. An identification program for determining non-linear characteristics is therefore needed.

Non-linear Structural Identification Program

The programs can be classified into two methods: determinate and non-determinate.

Determinate method. This method can only identify the same numbers of spring elements as the number of mass motions provided. Two such methods are:

- FIAT methodology
- SISAME (Structural Impact Simulation and Model Extraction).

FIAT program (Larsen and Shaw, 1980 Revision) was developed, under a sponsorship of FIAT Auto S.p.A., for determination of structural characteristics of a vehicle directly from crash test data. This program is a determinate three-dimensional lumped-parameter vehicle model with non-torsional springs. With the accelerations and/or forces as inputs, the FIAT procedure uses the equations of motion to generate a set of simultaneous algebraic equations. These equations provide solutions for the unknown forces at discrete increments of time. Acceleration-time histories are double integrated to obtain displacements. The force- and displacement-time histories are combined to yield spring force-deflection characteristics.

The SISAME methodology was developed by Mentzer under a NHTSA contract in the early 1980's. Similar to the FIAT approach, SISAME is capable of extracting the non-linear spring characteristics from the acceleration data based on a given model configuration and mass distribution. In addition, it has numerous capabilities for generating vehicle crash models, including pre-defined spring elements and dynamic magnification factors.

Non-determinate method. A non-determinate method for identifying vehicle structural characteristics in crash was developed by Hollowell in mid-1980 (Radwan and Hollowell, 1990; Hollowell et al., 1988; Hollowell, 1986). This computer code, known as the NHTSA's SYSID (SYStem Identification) program, was implemented at Ford in 1989. The identification process is accomplished using adaptive time domain, constrained minimization techniques. The assumptions are:

- the stiffness and damping characteristics of an EA element are separable.
- the characteristics may be approximated piecewise linear.

Hollowell then formulated a set of quasi-linear, time-incremental equations of motion, including error terms. These equations are then solved for non-negative parameters using linear and quadratic programming algorithms.

The non-negative assumption is one of the major limitations of the Hollowell technique. This assumption is valid only for describing a monotonicly increasing force/deformation characteristics of a structural component in certain loading conditions. In a crash loading environment, the requirement of non-negative stiffness parameters is no longer valid.

New Methodology

In the current study, a systematic computer method is developed to handle the negative stiffness parameters. This Vehicle Structural Identification Program (VSIP) is a non-determinate model which is similar to the NHTSA's SYSID. Here, the non-negative requirements for the stiffness parameters are transformed (relaxed) into a standard form of linear programming, from which a solution can be obtained. In addition, a provision is made to allow an analyst to predefine certain spring member's characteristics in the model.

Method of analysis, validation, application and recommendation will be described below.

Method of Analysis

Parameter Estimation Using Optimization

A parametric method is used in this study to determine the values of system parameters in describing a system model. Mathematically, the unknown system parameters are determined in such a way that the errors between the predictions by the equations of motion and the measured acceleration responses are minimized.

The system equations in a compact vector notation for a crash event can be written as

$$\underset{\substack{\text{(Total Spring Force}\\ \text{Exerting on Mass)}}}{F(x,\dot{x})} = \underset{\text{(Inertia Force)}}{m\ddot{x}(t)} \qquad (1)$$

where F is the unknown internal forces exerting on masses by springs connected and is function of the velocity, $\dot{x}$, and the displacement, x; m is the mass of the system; and $\ddot{x}$ is the acceleration. It is assumed that all m, $\ddot{x}$, $\dot{x}$ and x of the system are available from measurements.

For the minimization of errors, the system equations are augmented by introducing an error term, ε:

$$F(x,\dot{x}) + \varepsilon = m\ddot{x}(t),$$

or, equivalently,

$$F_\varepsilon(x,\dot{x}) = m\ddot{x}(t) \qquad (2)$$

where F_ε is the unknown internal forces including the error terms.

Equation (2), when describing the nature of crash event, is a non-linear problem. Use of linearization tech-

nique to Equation (2) reduces the identification problem to a classical linear programming problem (Luenberger, 1984):

$$\textit{Minimize} \quad \sum |\varepsilon| \qquad (3.1)$$

(Sum of Absolute Value of Errors)

$$\textit{Subject to} \quad F_e(x,\dot{x}) = m\ddot{x}(t) \qquad (3.2)$$

$$\textit{and} \quad p \geq 0 \qquad (3.3)$$

Here p is a column parameter vector. It is noted that the vector inequality $p \geq 0$ means that each component of p is non-negative.

Solution Formulation

Identification and simulation are closely related. Vehicle performance simulation needs accurate structural characteristics as inputs in order to predict vehicle dynamic response while identification of a vehicle structure needs an accurate model which is validated by a simulation process in order to generate structurally accurate characteristics of energy absorbing members.

There are two steps involved in an identification process. The first step is to set up a model configuration, allocating masses and collecting respective mass-associated motion data. An analyst needs to use his/her engineering knowledge and experience in arriving at a good sound model during this step. Once the system configuration is ready, the next step is to solve for the structural characteristics of the vehicle under investigation.

The major emphasis of this study is placed on one-dimensional LMS models. A typical model of frontal barrier impact is shown in Figure 1. In this model, five masses representing vehicle radiator, radiator support, engine, sub-frame and occupant compartment are interconnected by eight (8) EA's to represent structural characteristics between these respective adjacent masses. Since the majority of motion occurs along the longitudinal direction in frontal barrier impacts, the assumption for rectilinear motion during collision in an 1-D LMS model is sufficient for the current application.

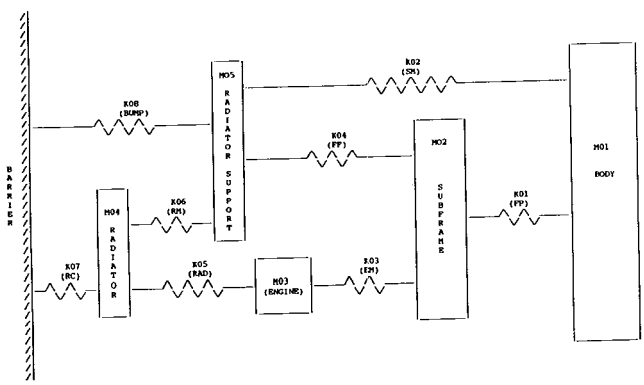

Figure 1. A Typical One-Dimensional Frontal Barrier Crash Lumped-Mass-Spring Model

For a model of M masses interconnected by S non-linear EA elements, the equation of motion for mass i is given by

$$m_i \ddot{x}_i(t) = \sum_{s=1}^{S} (F_s)_i \qquad (4)$$

where

m_i = Mass for mass i

$\ddot{x}_i$ = Acceleration for mass i

$(F_s)_i$ = Internal EA force: $\neq 0$ if EA element s is connected to mass i; $= 0$ if EA element s is not connected to mass i

The internal force is a function of the deformation and deformation rate of an EA element and can be separated by two individual force components: a deformation-dependent non-linear spring force and a deformation rate-dependent damping force. Mathematically,

$$F_s(\delta_s,\dot{\delta}_s) = F_s^{(K)}(\delta_s) + F_s^{(C)}(\dot{\delta}_s) \qquad (5)$$

where

δ_s = Deformation of spring element s

$\dot{\delta}_s$ = Deformation - rate of damping element s

It is noted that both δ_s and $\dot{\delta}_s$ are functions of time, that is, $\delta_s(t)$ and $\dot{\delta}_s(t)$.

Furthermore, by using Hollowell's piecewise linearization, the non-linear force for spring element s at time t_k is the accumulation of previous increments occurred before time t_k, the non-linear force for spring element s at time t, for any time $t \geq t_k$ can be expressed in a series of piecewise linear segments as

$$F_s^{(K)}(t) = K_s(\delta_s(t))[\delta_s(t) - \delta_s(t_k)] + \sum_{\substack{j=0 \\ t \geq tk}}^{k-1} K_s(\delta_s(t_{j+1}))[\delta_s(t_{j+1}) - \delta_s(t_j)], \qquad (6)$$

where

$K_s(\delta_s(t_{j+1}))$ = Stiffness of spring element s at time interval (t_j, t_{j+1})

$\delta_s(t)$ = Deformation of spring element s at time t

On the other hand, the damping force for damping element s is given by

$$F_s^{(C)}(t) = C_s(\dot{\delta}_s(t))\dot{\delta}_s(t) \qquad (7)$$

where

$C_s(\dot{\delta}_s(t))$ = Instantaneous damping coefficient of damping element s at time t

$\dot{\delta}_s(t)$ = Deformation - rate of damping element s at time t

It is noted that the piecewise linearization of EA elements, although permitting conversion of a non-linear problem into a linear programming, has a drawback in the Hollowell's approach. The requirement of non-negative stiffness in solution formulation and the accumulation of linear spring forces at previous time steps keep the extracted spring force increasing monotonicly. This phenomenon precludes identification

of spring characteristics with negative stiffness when structure members collapse under axial/bending loads.

Incorporating Equations (5)-(7) into Equation (4) gives

$$m_i\ddot{x}_i(t) = \sum_{s=1}^{NK}\{K_s(\delta_s(t))\,[\delta_s(t) - \delta_s(t_k)] + \sum_{j=0}^{k-1} K_s(\delta_s(t_{j+1}))\,[\delta_s t_{j+1}) - \delta_s(t_j)]\} + \sum_{s=1}^{NC} C_s(\delta_s(t))\,\delta_s(t) \quad (8)$$

where

NK = Number of non-linear spring elements
NC = Number of damping elements
$N = NK + NC$

Employing an incremental time step approach and discretizing the (equation of motion, Equation (8), in time, a set of M time-incremental system equations can be written for any time increment in terms of the system parameters, i.e., the stiffnesses (K's) and the damping coefficients (C's). Writing these time-incremental equations in matrix forms by including error terms, ε_i's, the mass motion equations can be expressed as

$$\begin{bmatrix} a_{11} & a_{12} & \cdots & a_{1N} \\ a_{21} & a_{22} & \cdots & a_{2N} \\ \vdots & \vdots & \ddots & \vdots \\ a_{M1} & a_{M2} & \cdots & a_{MN} \end{bmatrix} \begin{bmatrix} K_1 \\ \vdots \\ K_{NK} \\ C_1 \\ \vdots \\ C_{NC} \end{bmatrix} + \begin{bmatrix} \varepsilon_1 \\ \vdots \\ \varepsilon_M \end{bmatrix} = \begin{bmatrix} b_1 \\ \vdots \\ b_M \end{bmatrix} \quad (9)$$

where

M = Number of DOF's (degrees of freedom) in the system

The [A] matrix in Equation (9) is referred to as the *motion matrix*. The individual entries of the [A] matrix are attributed by the spring and damping forces and are defined as

$a_{mi} = 0$, if ith spring is not connected to mass m,
$\delta_i(t) - \delta_i(t_k)$, if ith spring is connected to mass m;
$i = 1, \ldots, NK$

and

$a_{mj} = 0$, if jth damper is not connected to mass m,
$\delta_j(t) - \delta_j(t_k)$, if jth damper is connected to mass m;
$j = (NK + 1), \ldots, N$

The [B] vector in Equation (9) is the *inertia force matrix*. Each individual entry of the [B] vector is determined by the instrumented mass weight and its acceleration:

$$b_i = m_i\ddot{x}_i(t)$$

In order to facilitate the solution procedure, the system parameters are further assumed to be constant over a cluster of time increments $[t_k, t_{k+npts}]$, called the *solution span*, namely,

$$K_s(t) = K_s = Constant \qquad C_s(t) = C_s = Constant \qquad t_k \le t \le t_{k+npts} \quad (10)$$

The solution span indeed is defined as *nptsΔt*, and *npts* is an integer parameter chosen in the solution process. Since a set of M time-incremental equations describing the motion of M masses is formed at each time increment, there is a total of T equations (the number of DOF's in the system times the number of time increments) over the solution span. By augmenting the time-incremental motion equations over the solution span and transforming the error terms into the motion matrix, one obtains

$$\left[\begin{array}{c} \overbrace{\begin{bmatrix} a_{11} & a_{12} & \cdots & a_{1N} \\ a_{21} & a_{22} & \cdots & a_{2N} \\ \vdots & \vdots & \ddots & \vdots \\ a_{T1} & a_{T2} & \cdots & a_{TN} \end{bmatrix}}^{N\ terms} \overbrace{\begin{bmatrix} 1 & 0 & \cdots & 0 \\ 0 & 1 & \cdots & 0 \\ \vdots & \vdots & \ddots & \vdots \\ 0 & 0 & \cdots & 1 \end{bmatrix}}^{T\ terms} \end{array}\right] \begin{bmatrix} K_1 \\ \vdots \\ K_{NK} \\ C_1 \\ \vdots \\ C_{NC} \\ \varepsilon_1 \\ \vdots \\ \varepsilon_T \end{bmatrix} = \begin{bmatrix} b_1 \\ \vdots \\ b_T \end{bmatrix} \quad (11)$$

Equation (11) is the equality constraints in a standard form of linear programming problems as stated in Equation (3.2) and is used by minimization techniques stated earlier to solve for the system parameters, K_s and C_s.

Relaxation of Free Variables

It is recalled from Equation (3.3) that the non-negativity constraint on each unknown variable is required in a linear program. However, it is noted that each error term in Equation (11) is a free variable (Luenberger, 1984). A free variable in a linear programming problem is the variable that has no restrictions of non-negativity and is free to take on positive or negative values. Before solving the problem under consideration by linear programming techniques, one has to convert or restrict these free variables to be non-negative. Because ε_i is free to take on either positive or negative values, we then write

$$\varepsilon_i = \varepsilon_i^{(+)} - \varepsilon_i^{(-)} \quad (12)$$

where both components, $\varepsilon_i^{(+)}$ and $\varepsilon_i^{(-)}$, are restricted to be non-negative. If we substitute $\varepsilon_i = \varepsilon_i^{(+)} - \varepsilon_i^{(-)}$ for ε_i in the formulation, the linearity of constraints is preserved and all variables are now non-negative as required. Obviously, by doing so the number of the unknown variables will increase by one as each variable is relaxed.

When a vehicle structural member starts to collapse during a collision, it will generate a force level lower than maximum strength of the structure member. This means that one will see negative slopes in the spring force/deflection curves. Mathematically, all the stiffness parameters (K's) can be treated as free variables. In order to preserve the linearity of constraints and satisfy the non-negative requirements, the stiffness unknowns have to be relaxed or transformed into the standard form of the linear programs. This can be done by employing the same free-variable relaxation method used for the error terms. That is,

$$K_s = K_s^{(+)} - K_s^{(-)} \tag{13}$$

where both new components, $K_s^{(+)}$ and $K_s^{(-)}$, are required to be non-negative. The substitution of the stiffness unknowns with two separate components will augment the motion matrix by additional NK columns for NK nonlinear spring elements. The additional elements of the motion matrix have the same values except the sign.

As in the Hollowell's formulation, limitation bounds of the unknown damping forces are specified and inequality equations are added to the constraints.

Relaxing free variables of error terms and stiffness parameters, expressed by Equations (12) and (13), respectively, in the equality constraint equations, Equation (11) can be re-written as

$$\underbrace{\begin{bmatrix} a_{11} & \cdots & a_{1i} & -a_{1i} & \cdots & a_{1N} \\ a_{21} & \cdots & a_{2i} & -a_{2i} & \cdots & a_{2N} \\ \vdots & \ddots & \vdots & \vdots & \ddots & \vdots \\ a_{T1} & \cdots & a_{Ti} & -a_{Ti} & \cdots & a_{TN} \end{bmatrix}}_{2NK+NC \text{ terms}} \underbrace{\begin{bmatrix} 1 & -1 & \cdots & 0 & 0 \\ 0 & 0 & \cdots & 0 & 0 \\ \vdots & \vdots & \ddots & \vdots & \vdots \\ 0 & 0 & \cdots & 1 & -1 \end{bmatrix}}_{2T \text{ terms}} \begin{bmatrix} K_1^{(+)} \\ \vdots \\ K_i^{(+)} \\ K_i^{(-)} \\ \vdots \\ K_{NK}^{(-)} \\ C_1 \\ \vdots \\ C_{NC} \\ \varepsilon_1^{(+)} \\ \varepsilon_1^{(-)} \\ \vdots \\ \varepsilon_T^{(+)} \\ \varepsilon_T^{(-)} \end{bmatrix} = \begin{bmatrix} b_1 \\ \vdots \\ b_T \end{bmatrix} \tag{14}$$

The objective function in this study is the sum of the absolute values of errors between the predictions by the motion equations and the measured acceleration responses:

$$\sum_{i=1}^{T} |\varepsilon_i| = \sum_{i=1}^{T} \left| b_i - \sum_{j=1}^{2NK+NC} a_{ij} X_j \right| \tag{15}$$

where

$$X_j = K_1^{(+)}, \ldots, K_i^{(+)}, K_i^{(-)}, \ldots, K_{NK}^{(-)}, C_1, \ldots, C_{NC} .$$

This completes the presentation of our formulation of the problem under investigation in the context of linear programming.

Uniqueness Problem

The inability to prescribe the known spring characteristics in the vehicle model to be identified is another shortcoming in the NHTSA Hollowell's system identification formulation. Generally speaking, the more detailed the structural knowledge and test data are, the more accurate the extracted structural information is.

Models which have the same model configurations and mass allocations but differ only in spring characteristics may yield nearly identical motions in a crash simulation. Figures 2, 3 and 4 show two different sets of spring force-deflection curves for the simulation model depicted in Figure 5. The results from the CRUSH II lumped mass simulations are shown in Figures 6 and 7. It is seen that the dynamic responses of masses are nearly identical. This raises an issue regarding the uniqueness problem that needs to be addressed. When extracting automotive structural characteristics from barrier crash tests, one might divert to a mathematically correct but not necessarily realistic vehicle crash model. In order to uniquely identify the system, one may need to provide additional structural information with known characteristics to make the system determinate. Thus, the capability of allowing an analyst to include predefined springs for enhancement of the identification process is implemented.

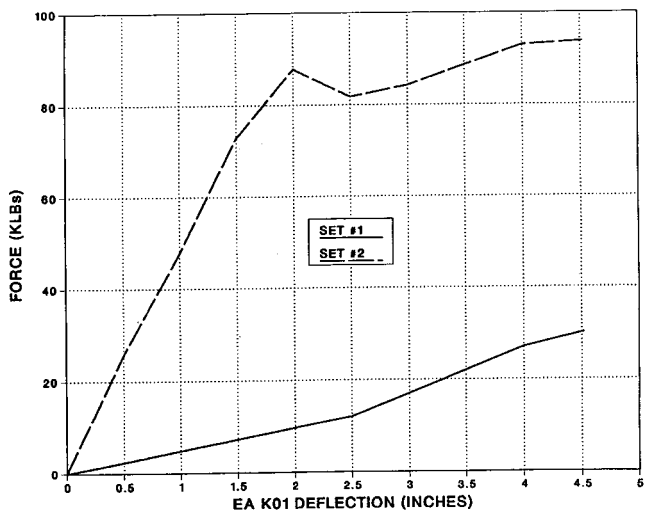

Figure 2. Comparison of Spring K01 Load-Deflection for CRUSH II Input

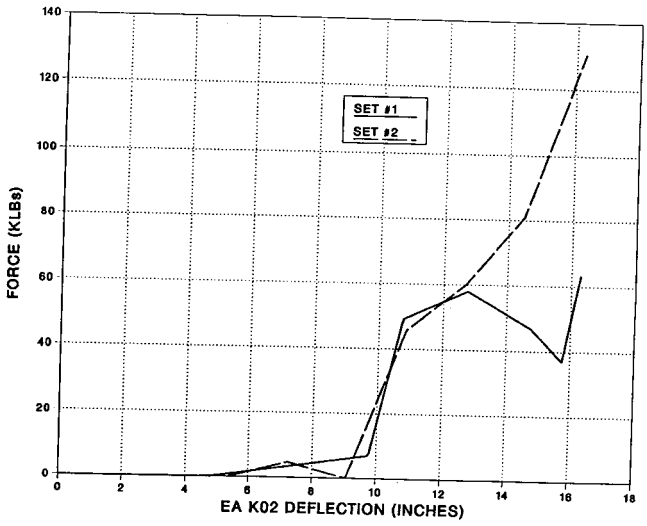

Figure 3. Comparison of Spring K02 Load-Deflection for CRUSH II Input

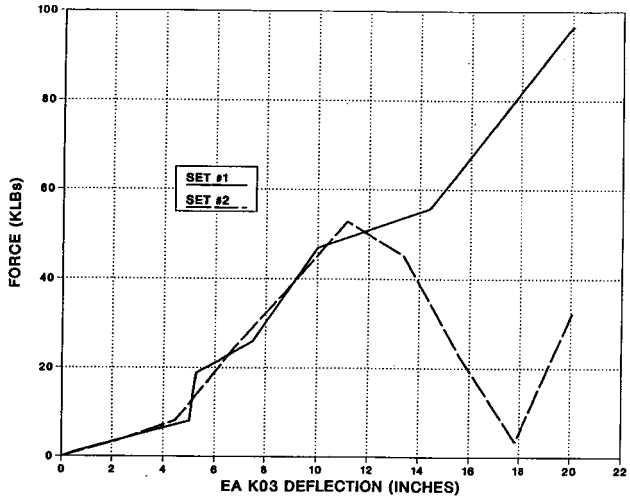

Figure 4. Comparison of Spring K03 Load-Deflection for CRUSH II Input

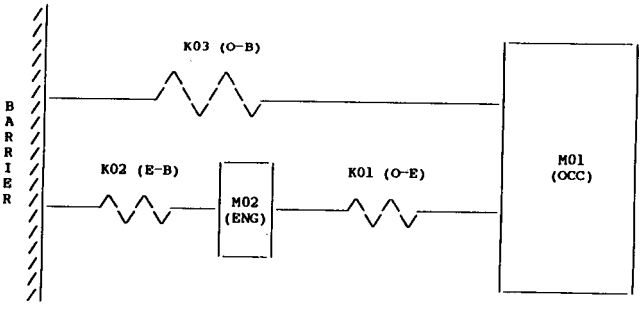

Figure 5. Two DOF System Model with Two Masses and Three Springs

Validation and Application

The non-determinate automobile structure characterization method described in the previous sections has been computerized in a FORTRAN program, VSIP. This Ford structural vehicle model characterization program is different from the Hollowell's system identification

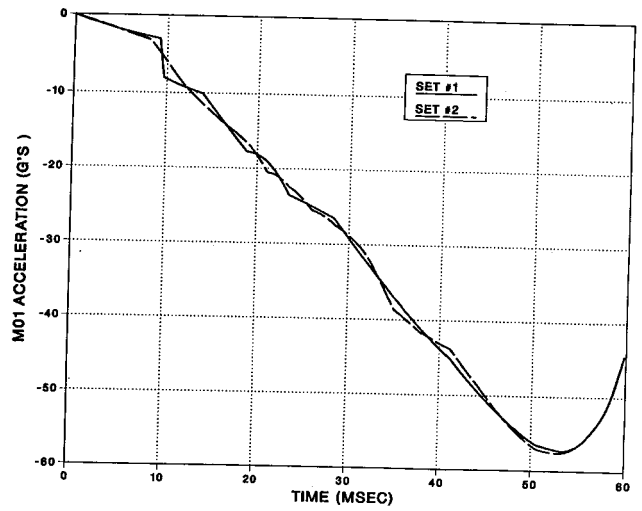

Figure 6. Comparison Between CRUSH II Simulation Results for Mass M01

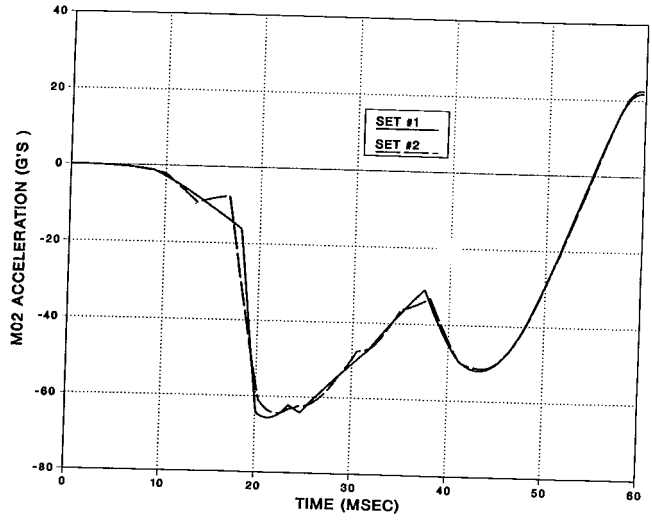

Figure 7. Comparison Between CRUSH II Simulation Results for Mass M02

program by implementing a special algorithm for non-negativity relaxation and provision for prescribing some of spring characteristics in the model. In order to demonstrate and validate the Ford vehicle model characterization system formulation and computer programs, a variety of analytical models and crash test data are used.

Single DOF System with a Non-linear Spring and a Linear Damper. The first model is a single DOF system with a non-linear spring and a linear damper (Figure 8). Use of this model is intended to demonstrate the importance of relaxing the non-negative requirements for stiffness parameters in arriving at the correct solution. The EA's characteristics are extracted with and without relaxations of the requirements of the non-negative stiffness parameters. The extracted characteristics are compared (see Figure 9) with those used in the CRUSH II simulation program to generate motion profiles for the characterization process. An examination of the spring characteristics identified using the Hollowell's system

identification program with non-negative stiffness requirements indicates that the NHTSA's SYSID program has difficulty in predicting the "deep collapse" portion (i.e. a plastic region beyond the maximum load carrying capacity) of the load-deflection characteristics.

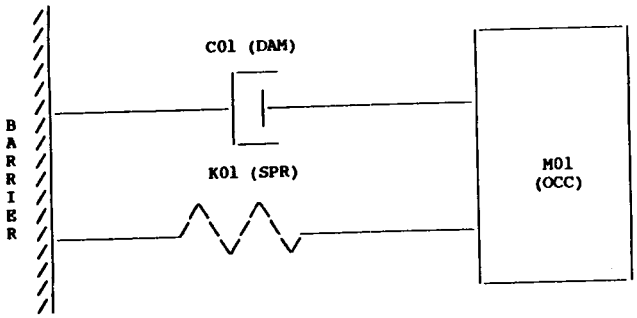

Figure 8. One DOF System with a Non-Linear Spring and a Linear Damper

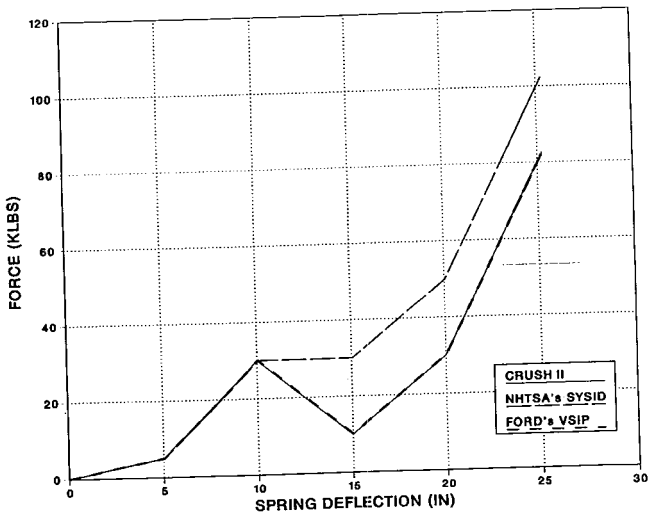

Figure 9. Comparison Between Extracted Results and CRUSH II Input

Additionally, the inability to identify the deep collapse/negative slope of the characteristic curve in the NHTSA's SYSID program leads to cumulative force errors in a non-relaxation process as shown in Figure 9. The Ford vehicle model characterization program, however, extracts the correct EA characteristic for this single DOF model.

The damper results are shown in Figure 10. It is seen that the NHTSA's program identified damper characteristics with a spike, while perfect matches have been found for the relaxed case using the Ford vehicle model characterization program. The spike identified by the NHTSA's program is to balance the accumulated errors in the non-linear spring force.

Single DOF System Using Motion Data from a Crash Test. Again, a uni-mass model is employed using a vehicle occupant compartment acceleration response from a barrier crash test as its motion profile. Three different solution spans, i.e., 3.5 msec, 0.7 msec and 0.07 msec, are used. The identified load/deformation

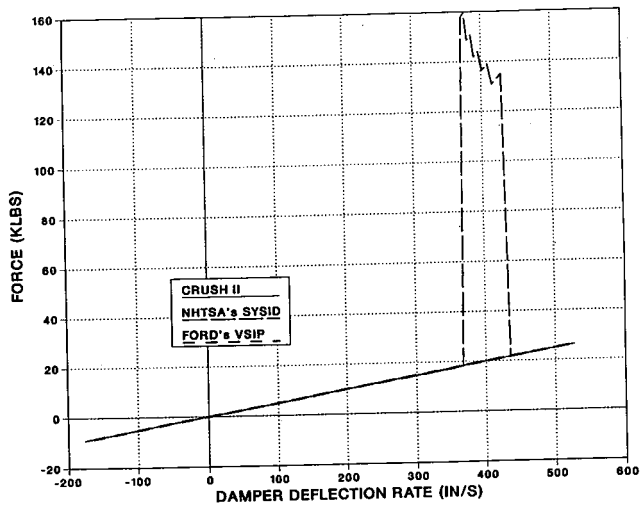

Figure 10. Comparison Between Extracted Results and CRUSH II Input

curves are compared with the characteristics obtained from force based on the product of weight and acceleration and deflection based on integration of acceleration and/or film analysis. Results are shown in Figures 11 to 13, respectively, for 3.5 msec, 0.7 msec and 0.07 msec cases. Referring to Figure 11 for 3.5 msec solution span case, the identified characteristic shows the general trend of matching the shape of load-deflection curve. However, the solution deviates from the correct one at 3.5" of deflection. This is due to a larger solution span (3.5 msec) used in this case. When the solution span is reduced from 3.5 msec to 0.7 msec, the extracted load/deformation characteristic converges to the actual solution, as shown in Figure 12, although a discrepancy still exists. The solution can be further improved by using a finer solution span of 0.07 msec, the identified load/deformation curve matches exactly with the actual characteristics as shown in Figure 13. It is clear from the above discussion that the time increments used in the solution play an important role in the characterization process.

A System Model with Three Masses and Three Springs

This example Is an analytical model with three (3) masses and three (3) non-linear springs in series/parallel connections as shown in Figure 14. Mass M03 is connected to the barrier by the spring element K03. Masses M02 and M01 are connected, in parallel, to Mass M03 by the spring elements, K02 and K01, respectively. It is noted that two types of spring connections have been used in this model: spring elements K01 and K02 are in parallel while the pairs of spring elements (K01, K03) and (K02, K03) are in series.

In order to see whether the VSIP program is capable of extracting the correct characteristics of more EA elements in the model, this analytical model is, first, simulated using the CRUSH II program with known K01, K02 and K03 to generate motion information for all three masses. Referring to Figures 15, 16 and 17, it is

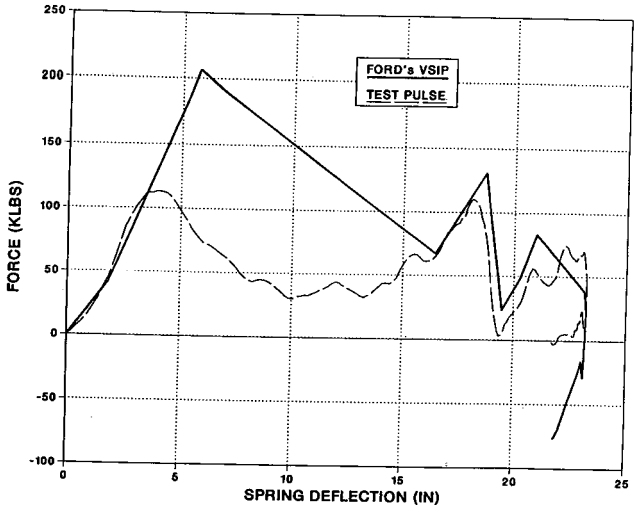

Figure 11. An Uni-Mass Model Using Crash Test Data (Solution Span = 3.5 MS)

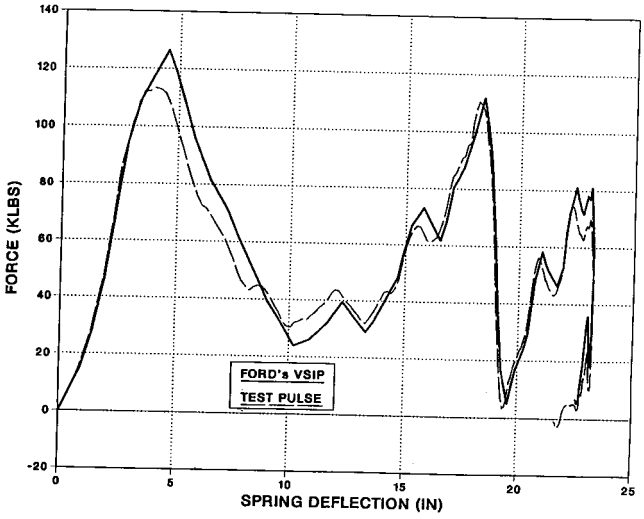

Figure 12. An Uni-Mass Model Using Crash Test Data (Solution Span = 0.7 MS)

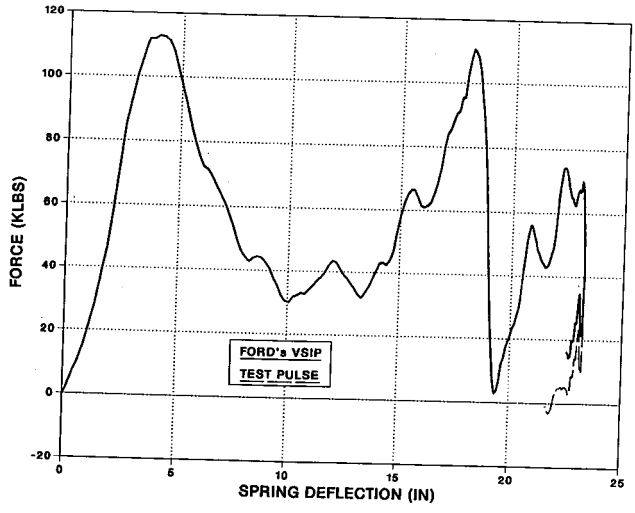

Figure 13. An Uni-Mass Model Using Crash Test Data (Solution Span = 0.07 MS)

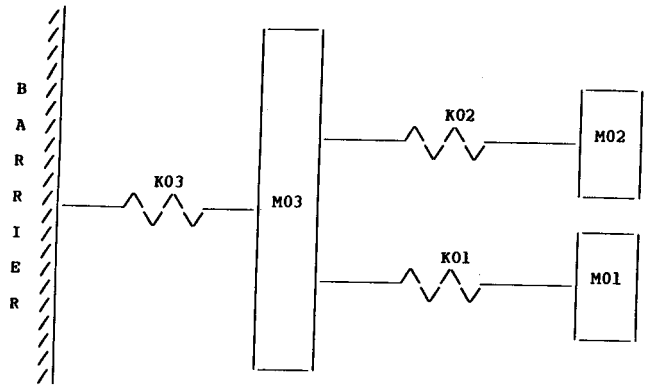

Figure 14. An Analytical LMS Model with 2 Masses and 3 Non-Linear Springs in Series/Parallel Comparison

noted that the spring element K02's force level increases monotonicly in force-deflection curve while spring elements K01 and K03 posses negative stiffness. The acceleration, velocity and displacement time-histories of these masses are then input to the Ford vehicle model characterization program for extracting spring characteristics, K01, K02 and K03. A solution span of 0.07 msec is chosen for this example. The results obtained from the Ford vehicle model characterization program are presented in Figures 15 to 17, showing good correlations between the extracted characteristics and the actual data for all spring elements used in the CRUSH II model.

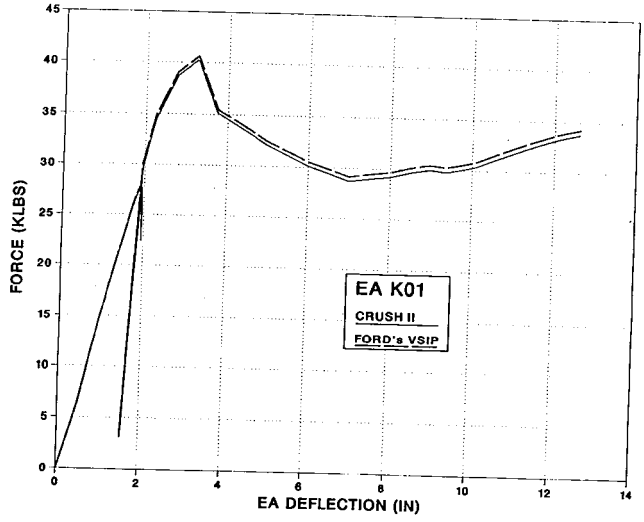

Figure 15. Comparison Between Ford's VSIP Result and CRUSH II Input

Two DOF System Model with Two Masses and Three Springs

The fourth model is a two DOF system consisting of two (2) masses connected by three (3) non-linear spring elements (see Figure 5). Two lumped masses represent the occupant compartment and the engine, and three springs represent radiator, sheet metal and drive line, respectively. It is noted that the previous examples are determinate models in which the number of spring

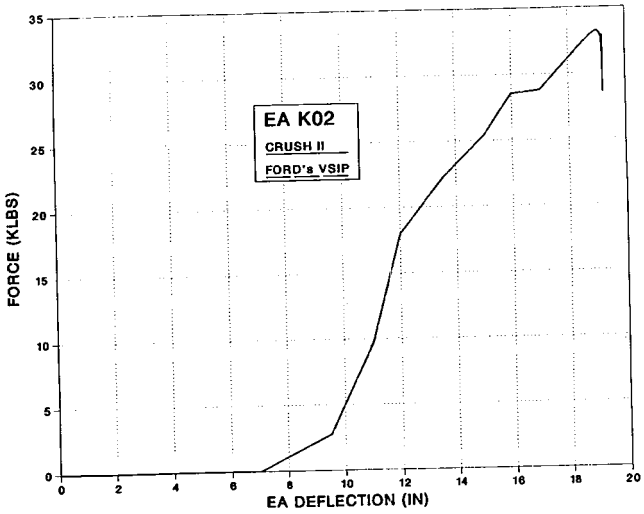

Figure 16. Comparison Between Ford's VSIP Result and CRUSH II Input

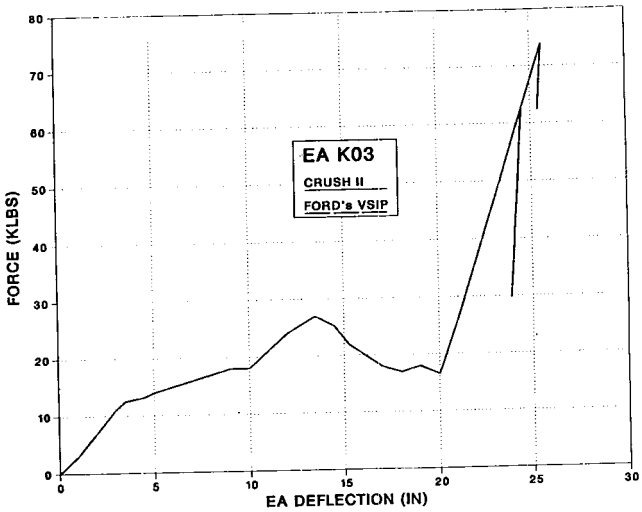

Figure 17. Comparison Between Ford's VSIP Result and CRUSH II Input

elements are equal to number of masses, while this 2-DOF model is a non-determinate dynamic case with the number of springs being greater than that of masses.

The model is used to extract structural component characteristics of a vehicle in a 35 MPH frontal impact simulation. A solution span of 0.07 msec is again used in the characterization process. Since the number of spring elements is greater than that of masses by one (1) in this model, any one of the spring elements K01, K02 and K03 can be prescribed in the solution process. Therefore, three subcases are considered with

- Spring K01 being prescribed;
- Spring K02 being prescribed; and
- Spring K03 being prescribed.

Figures 18 to 23 compare results of these subcases with spring characteristics used in the CRUSH II program for generating the motion profiles. In any subcase,

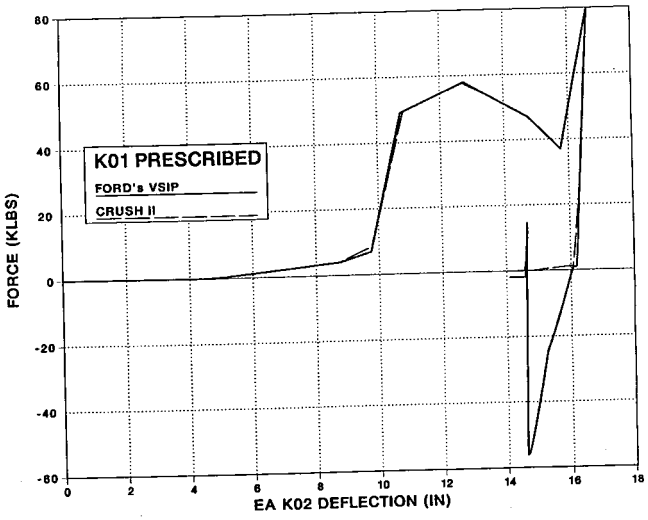

Figure 18. Comparison Between Ford's VSIP Result and CRUSH II Input

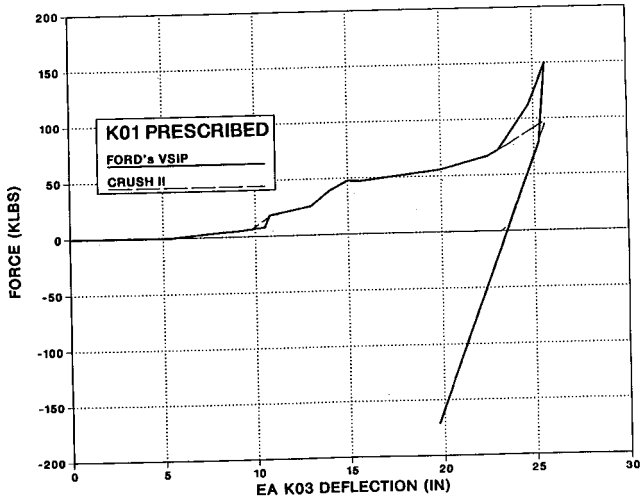

Figure 19. Comparison Between Ford's VSIP Result and CRUSH II Input

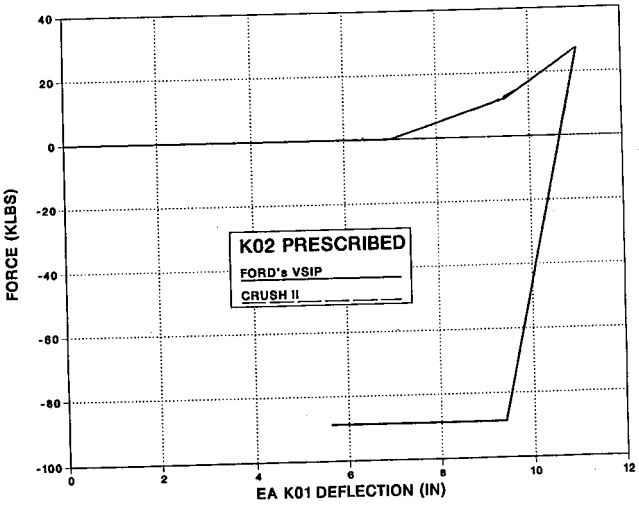

Figure 20. Comparison Between Ford's VSIP Result and CRUSH II Input

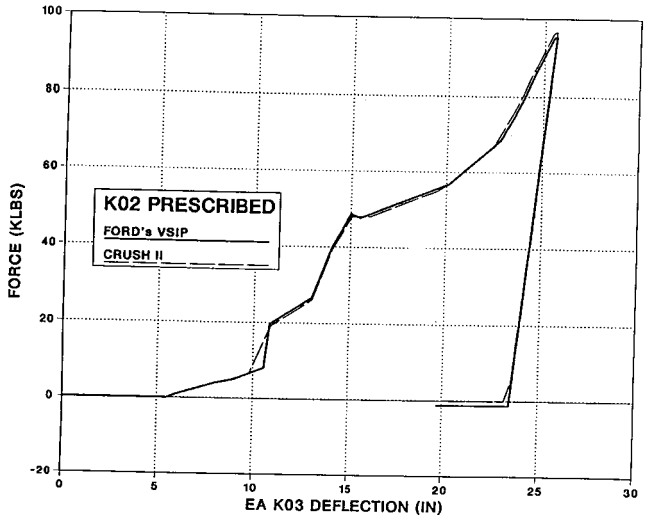

Figure 21. Comparison Between Ford's VSIP Result and CRUSH II Input

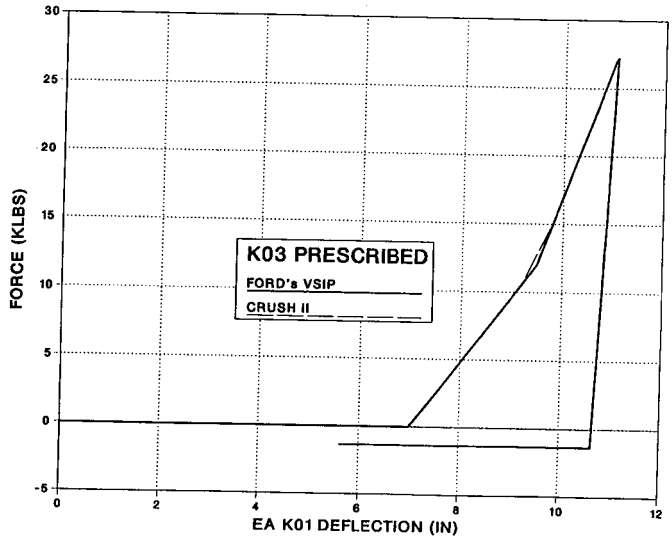

Figure 22. Comparison Between Ford's VSIP Result and CRUSH II Input

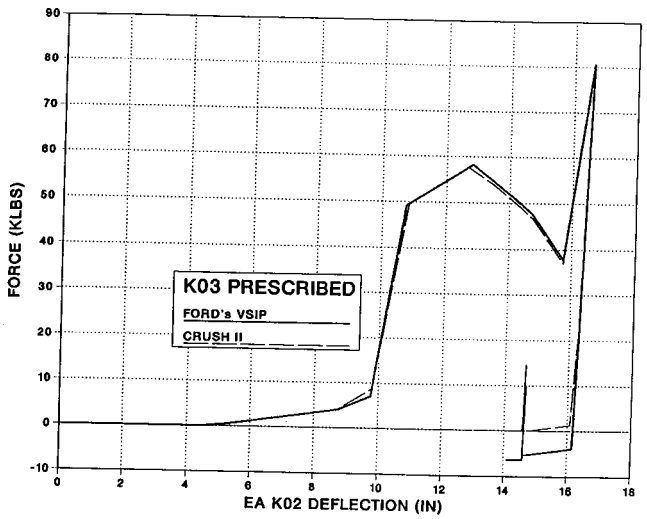

Figure 23. Comparison Between Ford's VSIP Result and CRUSH II Input

a good agreement between the identified and the actual characteristics is found. Thus, the capability of prescribing certain load-paths (springs) to the identification process in optimal determination of more accurate structural characteristics is demonstrated in the model.

With the added capability in the Ford vehicle model characterization program, the question is raised as to how accurately the program can extract the spring characteristics from this model without any spring element's characteristics being prescribed. The model is exercised using the Ford vehicle model characterization program, and the results are then compared with the known characteristics as shown in Figures 24 to 26. Surprisingly, the results are quite satisfactory.

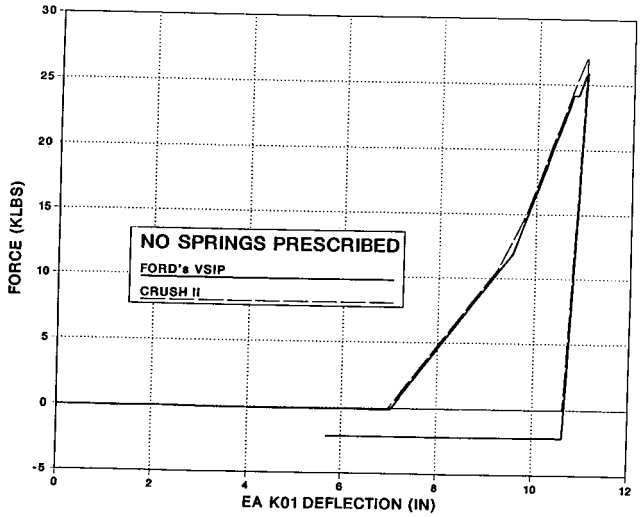

Figure 24. Comparison Between Ford's VSIP Result and CRUSH II Input

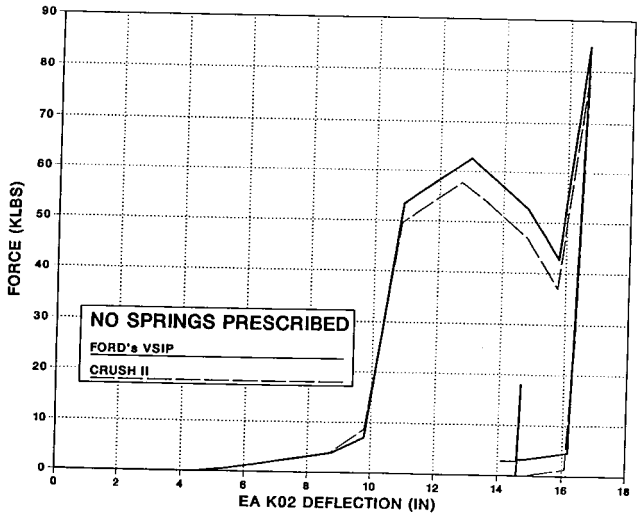

Figure 25. Comparison Between Ford's VSIP Result and CRUSH II Input

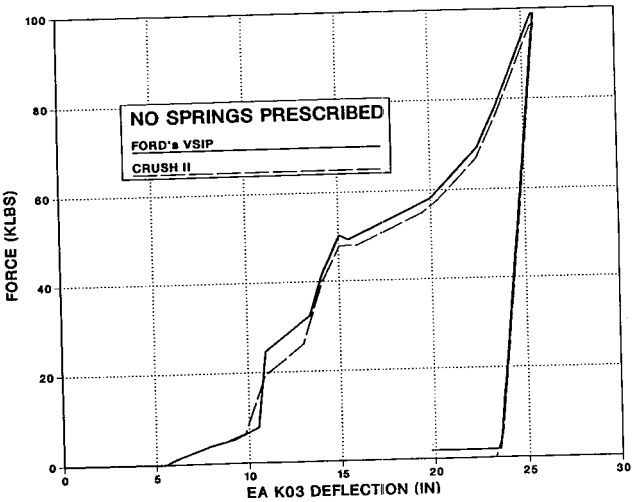

Figure 26. Comparison Between Ford's VSIP Result and CRUSH II Input

Summary and Conclusions

A systematic computer method has been developed to characterize LMS models of automobiles using lumped mass motion data, i.e. acceleration-, velocity- and displacement-time histories. A parameter estimation procedure using non-linear optimization is employed, which approximates the non-linearity of the complex spring characteristics of the EA components with piecewise linear segments. Equal numbers of EA elements (unknowns) and mass acceleration data (inputs) are essential in the characterization process. The provision for predefining certain load paths in the model enables an analyst to uniquely identify a vehicle model. Also, the non-negative requirements for the stiffness parameters are converted (relaxed) into a standard form of linear programming, from which an optimal solution can be obtained for the subject vehicle structural elements.

Theoretically, the system identification approach has the potential of developing vehicle structural models totally based on accelerometer data from barrier crash tests. The method, when developed and validated, will offer an opportunity in reducing static crusher testings of components traditionally required in LMS model simulations. This opportunity will become evident as the development of the methodology continues.

Recommendations

Although satisfactory results have been obtained from this structural characterization technique to analytical systems and simplified models based upon crash test data, further applications to a full scale vehicle system are recommended for identifying feasibilities and issues of the technique.

Acknowledgments

The authors wish to acknowledge Dr. T.W. Hollowell and Ms. R.A. Radwan of NHTSA and Mr. S.G. Mentzer of Automated Sciences Group, Inc., for their valuable technical discussions and suggestions in this study.

References

1. Chou, C.C. (1986), "On the Use of Lumped-Mass-Spring Models for Simulation of Frontal Vehicle Impacts," Engineering and Manufacturing Staff, Ford Motor Company, Technical Report No. EM-86-01, January 7, 1986.
2. Herridge, J.T. and R.K. Mitchel (1972), "Development of a Computer Simulation Program for Collinear Car/Car and Car/Barrier Collisions," DOT-HS 800 645, Prepared by Battelle's Columbus Laboratories for US Department of Transportation under Contract No. FH 7550, 346 pages, also ASME Paper No. 73-ICT-34, 1973.
3. Hollowell, W.T. (1986), Adaptive Time Domain, Constrained System Identification of Nonlinear Structures, Doctoral thesis, University of Virginia at Charlottesville, VA, USA, 174 pages.
4. Hollowell, W.T., W.D. Pilkey and E.M. Sieveka (1988), "System Identification of Dynamic Structures," Finite Elements in Analysis and Design, 4, pp. 65-77.
5. Kamal,M.M.(1970),"Analysis and Simulation of Vehicle to Barrier Impact," 1970 Int'l Automobile Safety Conference Compendium, SAE Report No. 700414, also SAE Transaction, 79, pp. 1498-1503.
6. Larsen, S.E. and L.M. Shaw (1980 Revision), "Technical Justification and User's Manual for FIAT Automotive Structural Crashworthniess Computer Programs," Original Report Aug. 1976, Revised Aug. 1980 (Revision No. 3), Dynamic Science Inc., Program A—Report No. 4890-76-51; Program B—Report No. 4890-76-52.
7. Luenberger, D.G. (1984), Linear and Nonlinear Programming, 2nd Edition, Addison-Wesley Publishing Company, Reading, Massachusetts, USA.
8. Mentzer, S.G. (1984), "Structural Impact Simulation and Model Extraction: The SISAME and MDOP Programs," Automated Sciences Group, Inc., Report No. ASG-TR-A140.05, Prepared for USA DOT/NHTSA under Contract No. DTNH22-83-C-07116.
9. Mentzer, S.G. (1985), "Automated Crash Test Data Assessment and Correction with the VECOR Program," Automated Sciences Group, Inc., Prepared for USA DOT/NHTSA under Contract No. DTNH22-84-R-007368.
10. Motl, D.M. and Wong R.T. (1975), "CRUSH (Crash Reproduction Using Static History)—Reference Guide II," Engineering Technical Services Office, Ford Motor Company, Dearborn, Michigan, CRUSH is Ford's modified version of the system developed by Battelle Laboratories, Columbus, Ohio, under DOT Contract No. FH-11-7550.
11. Prasad, P. and A.J. Padgaonkar (1981), "Static-to-Dynamic Amplification Factors for Use in Lumped-

Mass Vehicle Crash Models," 1981 SAE Int'l Congress and Exposition, Detroit, Michigan, USA, February 23-27, 1981. SAE Report No. 810475.
12. Radwan, R.A. and W.T. Hollowell (1990), "System Identification of Vehicle Structures in Crash Loading Environments," 1990 SAE International Congress & Exposition, Michigan, USA, February 27, 1990. SAE Paper No. 900415, also SAE Series SP-807, Vehicle Crashworthiness and Occupant Protection in Frontal Collisions, February 1990, pp. 41-56.

S9-W-46

An Intelligent Solution to frontal and Side Impact Protection

S. Murtuza
University of Michigan-Dearborn

Abstract

With the availability of anti-skid brakes on automobiles, it becomes feasible to consider automatic braking as a means of absorbing impending crash energy. In this paper we describe an automatic brake actuation system for use on vehicles having an existing braking system. The brake actuation is triggered by an elongate detector fastened to the vehicle which is controllably extendable from the vehicle to contact objects being approached by the vehicle when at predetermined distance therefrom. A compression sensor is included to sense contact between the elongate detector and the object. Provision is made to sense vehicle speed, vehicle-object closing speed, and detector position and to extend and retract the detector and actuate the vehicle braking system in response thereto. Because of practical limitations as to the extent an elongate detector may be extended from the vehicle, the brake actuation system is effective at lower speeds, under 15 miles per hour. It is an excellent solution for the 2.5 mph bumper controversy in the U.S., and facilitates side impact protection.

Introduction

Before 1973 there were no U.S. federal bumper standards for automobiles. In 1973 a federal bumper safety standard was prescribed [1]. The automobile manufacturers were required to provide barrier impact test results on front bumper damage at 5 mph and rear bumper damage at 2.5 mph. The following year the test speed for rear impact was upgraded to 5 mph. Although this was not a property damage standard, it was expected that some reduction in damage would accompany the safety standard. This safety standard remained in effect until 1978.

The Motor Vehicle Information and Cost Savings Act of 1972 required the U.S. Department of Transportation (DOT) to issue a no-damage bumper standard in order to eliminate or reduce substantially physical damage in low-speed collisions. Effective for 1979 model cars, the standard issued under this law first required that all new passenger cars sustain no damage except to bumpers and to their attachment in 5 mph into-barrier tests. These requirements were strengthened for 1980 models, when all but very minor cosmetic bumper damage was restricted.

Despite the success of these standards, DOT rolled back the no-damage bumper standards from 5 mph to 2.5 mph for 1983 and later model cars, saying that the increased crash damage resulting from this action would be offset because the weaker bumpers would be lighter and less expensive than 5 mph bumpers. Yet no evidence of compensatory savings in new car prices has emerged, nor have bumper weight savings been sufficient to balance even a fraction of the cost of the increased crash damage.

The situation by 1990 did not change much. A comparison of the 1983 and 1990 Plymouth Horizon, for example, as shown in Table 1 [2], proves the point.

Table 1. Comparison of 1983 and 1990 Plymouth Horizons Using 1990 Labor Rates and Parts Prices

	Front into Barrier	Rear into Barrier	Front into Angle Barrier	Rear into Pole	Total Damage in All Tests
1983 Horizons with 5 mph Bumpers	$ 0	$ 0	$287	$ 0	$ 287
1983 Horizons with 2.5 mph Bumpers	102	273	296	247	918
1990 Horizons	231	480	341	424	1,476

Similar tests in 1991 found total damages for the same test on the Honda Accord to be $618 and for the Pontiac 6000 to be $3,201 [3]. Honda bumpers are voluntarily designed to withstand 5 mph into-barrier test. A bill to reinstate 5 mph bumpers for cars has been introduced in the U.S. Congress [4], because consumers are spending hundreds of millions of dollars in extra repair costs and higher insurance premiums, as a result of the extra damage incurred in *low speed* accidents. According to another report [5], bumpers, fenders, rear quarter panels and lamps are the car parts most often damaged in urban *low speed* crashes.

The point we want to make here is that there is a specific need to address the issue of safety and protection at *low speeds*, say under 10 mph. Recognizing the need for safety and protection at low speeds, separate from the concerns at all speeds, opens up some innovative solutions which have not been explored before.

Advanced Warning Systems

The ultimate solution to safety and protection concerns lies in managing the absorption of kinetic energy which is otherwise manifested in damaging the car and possibly injuring the occupants. There are basically two approaches to the solution to this problem in practice: (i) design the car body to withstand a collision, and (ii) inform the driver of impending collision so as to facilitate braking the car before a collision takes place. Assuming the car is already designed optimally taking into account safety, protection, cost, weight, etc., we would like to explore the second approach.

A literature search shows that in the past, advanced warning devices have been proposed with three different focuses: (i) collision avoidance during back-up and tailgating, (ii) improved rear/side vision, and (iii) head-on collision avoidance. We are including a selection of references in these categories. References [6]-[9] deal with collision avoidance during back-up and tailgating. There is increased interest in the issue of tailgating, as it is one of the concerns related to the Intelligent Vehicle Highway System (IVHS). References [10] and [11] address improved vision capability behind the driver. The present targets of these inventions are trucks and trailers. A product based on [11] is in the development/ refinement phase [15]. References [12]-[14] deal with head-on collision avoidance and collision avoidance in general. Lichtenberg [14] essentially summarizes the status of activity in this area. Present schemes have limited usefulness; target discrimination is the major problem.

In summary, the current research in advanced warning systems is primarily based on indirect, non-contact means of detecting impending collision objects. While this approach results in elegant and attractive devices, their reliability has been a major cause of concern. Present head-on collision avoidance schemes, even when they are perfected, may not be suitable for detecting objects at smaller distances because of conflicting beam angle requirements. We would like to investigate the use of direct mechanical contact means of detecting impending collision objects as a means of avoiding collision at low speeds. Let us first look into the implications of advanced warning at low speeds.

Implications of Advanced Warning at Low Speeds

Consider a vehicle travelling at a speed of S0 mph. When the brakes are applied to stop the car, the maximum deceleration is giving by Mu.g, where Mu is the coefficient of friction of the road surface and g the gravitational constant (32.2 ft/sec/sec.). A typical value of Mu for a well-travelled portland cement or asphalt road is 0.7 [16]. Now if the brakes are applied for maximum deceleration until the speed reduces to S1 mph, then the distance travelled while the vehicle is decelerating, d (feet), is given by:

$$d = (S0^2 - S1^2) / [2Mu.g\ (3600/5280)^2] \qquad (1)$$

Numerical data based on equation (1) corresponding to S1=2.5 mph and Mu=0.7 is given in Table 2.

Table 2. Distance Travelled to Reach 2.5 mph vs. Initial Speed; Mu = 0.7

S0 (mph)	d (feet)
5	0.89
6	1.42
7	2.04
8	2.76
9	3.57
10	4.47

Take, for example, the third entry in Table 2. If the brakes are applied to a vehicle moving at 7 mph, 2 feet prior to impending collision, then the collision will occur at 2.5 mph. That is, with 2 feet leeway, the vehicle is protected up to 7 mph instead of 2.5 mph as per design. Of course, the computations here are based on some assumptions such as no allowance for driver reaction time, brake system time constant, friction non-linearity, etc. But the fact remains that with advanced warning, effective maximum no-damage speed can be increased. If automatic non-voluntary braking is used, driver reaction time becomes irrelevant. Friction non-linearity at lower speeds would actually aid in stopping. We do need to determine the brake time constant to investigate its impact on our calculations.

Direct Touch Advanced Warning Mechanisms

Any direct touch mechanism which permanently increases the length of a vehicle is neither practical nor acceptable. Here we describe two mechanisms which, in their inactive state, are confined to the nominal envelope of the vehicle. When active, they protrude in front (or back, as the case may be) of the vehicle up to a certain predetermined maximum length. They act as touch feelers to detect the presence of impending collision objects. The active state may be determined by the speed of the vehicle; for example, when the speed is between 2.5 and 10 mph. Since some benefits may be accrued even at higher speeds, the upper speed limit may be selected based on cost and aerodynamic stress consideration.

Figure 1 is a schematic representation of a vehicle with elongate detectors or feelers. Figures 2 and 3 show one embodiment of a detector in inactive and active states, respectively. The feeler probe is moved in and out under controlled action of fluid under pressure. It is returned immediately to inactive state upon contact with an object. Simultaneously, vehicle brakes may be activated automatically to stop or slow down the vehicle. Alternatively, a signal may be sent to the driver for voluntary action. More details on the mechanism are given in a patent application to the U.S. Patent Office [17]. We have received a notice of availability of the patent.

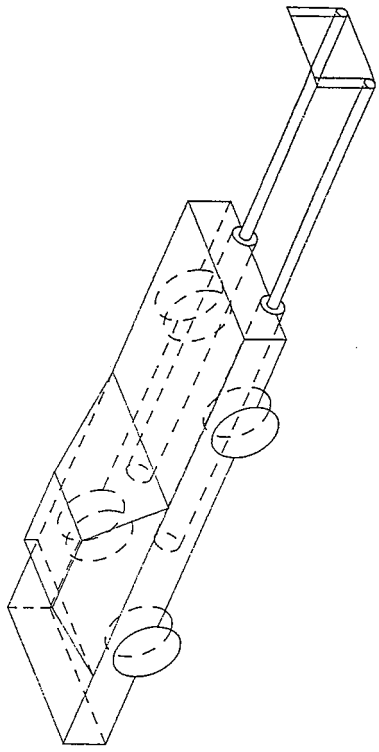

Figure 1. Schematic Representation of Elongate Detectors in Active State

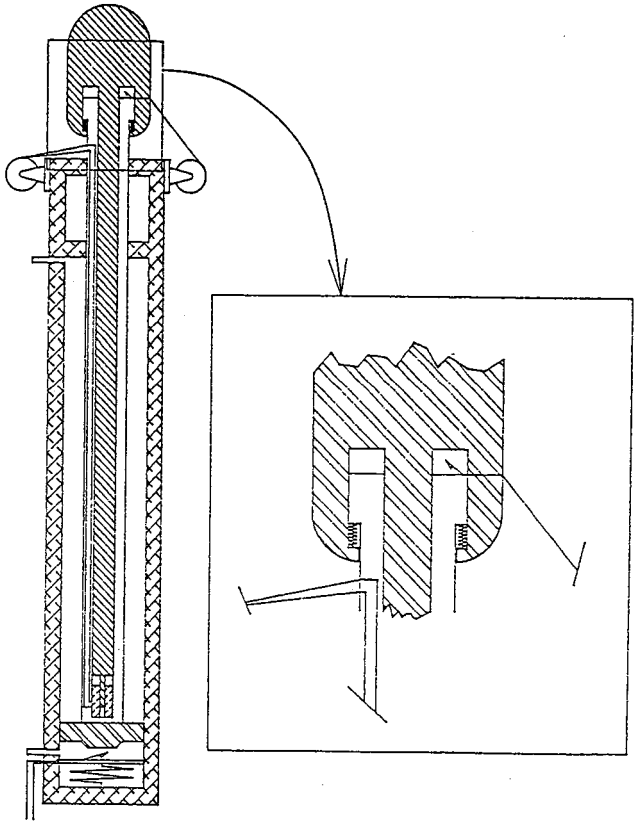

Figure 2. Fluid Actuated Collision Detector in Inactive State

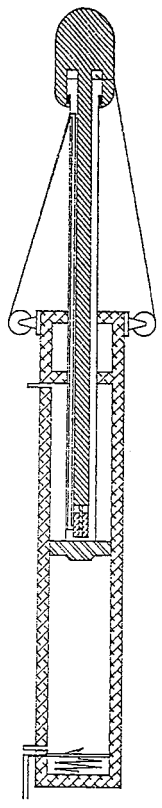

Figure 3. Fluid Actuated Collision Detector in Active State

An alternate embodiment of advanced warning mechanism is shown in Figure 4. Shown in figure 4(a) in its active state is the elongate detector consisting of an inflatable (and inflated) feeler tube having an open end and a closed end. The open end is connected to a controlled source of fluid under pressure for inflating the tube. A touch sensor is attached to the closed end of the tube. When in the inactive state, the feeler tube is deflated and, by design, it coils up neatly within the vehicle envelope as shown in figure 4(b). The coiling of the deflated feeler is aided by a spiral spring mounted along the length of the tube. The spring carries strain gauge sensors to detect sharp curvature changes in the spring caused by frontal or laterally directed impacts. The sensors may be deactivated during inflation and deflation of the tube. As before, upon detection of a collision, either the brakes are applied automatically, or a warning signal is sent to the driver.

Other embodiments based on linear electric actuators and parallel bar mechanisms are possible. Some of them are described in [17].

Autonomous guided vehicles (AGV's) moving on a factory floor have same protection needs as do automobiles at low speeds. The devices described above may also be used for safe operation of AGV's. A device specifically designed for use on AGV's is patented by Krieg [18]. This device is, however, not suitable for use on automobiles.

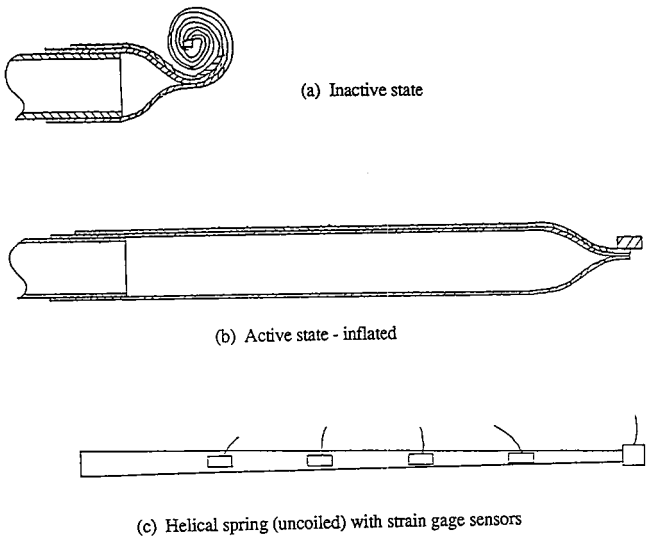

(a) Inactive state

(b) Active state - inflated

(c) Helical spring (uncoiled) with strain gage sensors

Figure 4. Inflatable Collision Detector

Concluding Remarks

There is increasing evidence that automobile accidents at low speeds result in significant property damage. Reduction and even elimination of such losses is possible by proper design of bumpers and use of reliable direct touch advanced warning mechanisms. On the other hand, bumper laws and better bumper designs are not of much help for side impact protection. But advanced warning mechanisms are just as effective in side impacts as they are in frontal collisions. This can be further aided by adopting automatic, non-voluntary braking, once impending collision has been established. With superior reliability of electronic components and increasing acceptance of anti-lock brake systems, there is growing expectation that automatic braking, particularly at low speeds, may be successfully deployed.

The conceptual designs of advanced warning systems suitable in *low speed* situations as presented here warrant prototype design and testing. In the mean time, an organization of a workshop devoted to mitigation of *low speed* automobile accidents for interested researchers in government, industry and academe is highly desirable.

References

1. Insurance Institute for Highway Safety, 1984 *Report on Bumpers,* Watergate 600, Washington, D.C., 1984.
2. Insurance Institute for Highway Safety, *Status Report,* 1005 North Glebe Road, Arlington, Virginia, Vol. 25, No. 3, March 3, 1990.
3. ibid., Vol. 26, No. 2, February 16,1991.
4. ibid., Vol. 26, No. 6, June 15, 1991.
5. ibid., Vol. 26, No. 10, November 30, 1991.
6. Aubert, H., et al, "Equipment of an Automobile or Like Vehicle for the Detection of Obstacles," U.S. Patent No. 3,366,925, January 30, 1968.
7. Huston, V.J., et al, "Photocell Device to Prevent Automobile Rear End Collision," U.S. Patent No. 3,514,610, May 26, 1970.
8. Sztankay, Z.G., "Automobile Collision Avoidance Laser System," U.S. Patent No. 3,891,966, June 24, 1975.
9. Yoshino, Y., and Kodora, M., "Automotive Rear Safety Checking Apparatus," U.S. Patent No. 4,467,313, August 21, 1984.
10. Larka, V.E., "Object Detection Apparatus," U.S. Patent No. 3,681,750, August 1, 1972.
11. Beggs, G. and Speck, R., "Object Detection Apparatus Employing Electro-optics," U.S. Patent No. 4,766,421, August 23, 1988.
12. Troll, W.C., et al, "Results from a Collision Avoidance Radar Braking System Investigation," Society of Automotive Engineers paper no. 770265, 1977.
13. Kowalczyk, T., "Security Eyes For Prevention of Car Accidents," U.S. Patent No. 4,641,136, February 3, 1987.
14. Lichtenberg, C.L., "Application of Radar for Automotive Crash Avoidance," Society of Automotive Engineers paper no. 870496, 1987.
15. Personal correspondence, Auto-Sense Ltd., Englewood, Colorado, November 17, 1989.
16. Baker, S., "Estimating Stopping Distance and Time for Motor Vehicles," Traffic Institute, Northwestern University, 1981.
17. Murtuza, S., "Automatic Brake Actuation," Patent Application to U.S.Commissioner of Patents, S.N. 07/591/963, dated October 2, 1990.
18. Krieg, W., "Driven Vehicle of an Automatic Transport System," U.S. Patent No.4,674,590, June 23, 1987.

S9-O-47

Optimized Passenger Safety in the Compact Class

Prof. Dr.-Ing. U. Seiffert
Volkswagen AG

More than a century has elapsed since the motor vehicle was invented and there is still no convincing alternative as a means of carrying people and freight. Despite many intensive discussions the motor vehicle is now an indispensable element of our daily life in most countries of the world. But, at the same time we must surely recognise the fact, that increasing problems are arising as traffic densities increase.

Cars already account for well over 80% of individual transport needs in the industrial countries of the world and road-going commercial vehicles handle more than

50% of these countries' freight traffic. This automatically leads to a situation in which the road network is unable to absorb the traffic volume which is generated at certain times or seasons. The demands which the automobile is expected to satisfy vary greatly and are sometimes contradictory.

Figure 1 shows conflicting patterns resulting from the desires for low fuel consumption, minimal cost, low exhaust and noise emissions, maximum comfort and convenience, good reliability but also engine performance, generous interior space, and not least, a high level of active and passive safety. During the last few years we have had to add the problems of road traffic and the general acceptance of the automobile to the list.

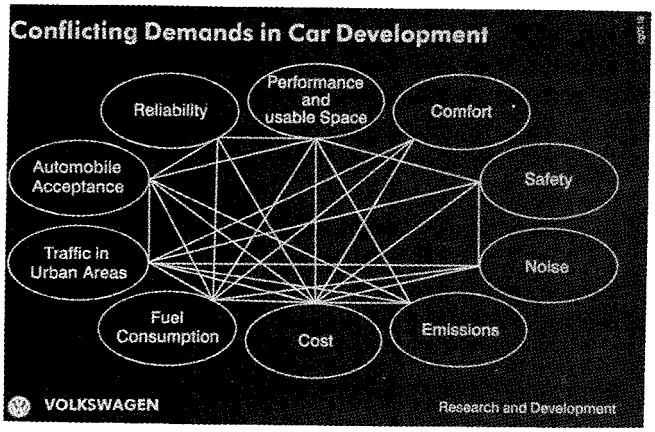

Figure 1. Conflicting Demands in Car Development

The engineers' task is to tackle these various and conflicting demands to arrive at optimum solutions for the customer's specific requirements.

After two unusually successful model generations, the conception and development of the third generation Golf presented an unprecedented challenge to the ability and sense of responsibility of Volkswagen's product strategists and engineers. In order to secure and develop the leading position of the Golf, we not only wanted to make the usual advances progress in all areas but also to dare to achieve a breakthrough.

Volkswagen has comprehensive experience from many years of trailblazing research and development work for active and passive safety. We have been able to further expand this knowledge over the course of the construction of several safety vehicles (ESVWs), with national and international cooperation with scientific and state institutions, particularly with the US safety agency NHTSA. On this basis Volkswagen has made the following strategic decisions:

All future generations of VW vehicles will not only fulfill the European safety regulations but also be oriented towards the US regulations. The 35 mph frontal crash test, which is carried out by the NHTSA—over and above the legal standards—but within the framework of the NCAP programme and published as consumer information, is particularly worthy of mention in this context.

In addition, the new Golf passes the side collision test carried out at a speed of 33.5 mph (54.5 kph) and which by the way does not come into force in the USA until model year 1994. Finally, the new Golf also fulfills our internal specifications for an offset (50%) frontal crash which we carry out at 55 kph in accordance with the test conditions advocated by impartial organisations. In this test, for which there are no legal regulations, we assess the dummies' responses, the survival space and, of course escapeworthiness.

The new Golf is the first vehicle in its class in Europe which has been designed to fulfill 35 mph US frontal crash test *and* a further set of exacting safety standards.

As a further element of Volkswagen's strategy, all other car models from Volkswagen—from the Polo to the Passat—and also Audi vehicles for world-wide markets have reinforcing members in all doors as additional protection against side collisions. Due to its special shape, the VW Transporter fulfills the dynamic test requirements for the 1994 US side crash without reinforcements in the doors.

We are aware that this VW strategy might trigger intensified safety efforts for cars world-wide. A new competitive environment will then come to the fore. In the future, it will be less of a case of national and international laws than competition which will determine the speed of progress which in the field of safety is vital, in the true sense of the word.

Built-in safety is not necessarily one of the obviously visible features of a motor vehicle. The real measure of safety is not found in the visually striking features of a vehicle but in a well thought out, integrated system of design and construction, characterized by a sound underlying concept that coordinates every detail. Crash tests then provide solid evidence as to whether or not the declared aims have been attained.

In the meantime, public interest in the subject of automobile safety has begun to grow, as part of the general shift in priorities from "standard of living" to "quality of life." Crash test results published in speciality magazines attract increasing public attention, even if, for cost reasons, out of many crash modes only *one* is selected which of course, cannot cover all safety aspects of a single car model. All over the world, the modern motorist has quite obviously become more safety conscious. Legal requirements are becoming more stringent, starting in the USA in 1993 with the highest standards that have ever been promulgated for the motor vehicle industry. The European Community will also be developing newer and tougher legislation in the years to come.

With the Golf III Volkswagen has endeavoured to comply with future societal demands and regulatory requirements for improved crash safety, with a dimensionally stable passenger cell, significantly improved side protection and exceptionally efficient crumple zones that progressively absorb the shock of impact according to pre-computed energy lines.

Four basic types of collisions are essentially important and are tested in well over 30 test configurations (Figure 2).

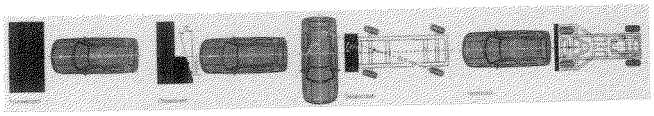

Figure 2. Selected Crash Test Modes

Frontal impact at 30/35 mph (48.3/56.3 km/h)

Going beyond the present US safety standard of 30 mph, the vehicle is also crash-tested at collision speeds of 35 mph into the rigid flat barrier. This represents an increase of 36% of the impact energy. Two test dummies occupy the front seats, and crash performance as well as dummy kinematics are recorded by sophisticated measuring equipment.

Offset impact at 34.2 mph (55 km/h)

This test type is performed in Germany by impartial testing institutes. The vehicle is driven so that half the front end hits a oblique rigid barrier, with an angle of 15°. Two test dummies are seated in the front of the vehicle.

Side impact at 33.5 mph (53.9 km/h)

The left side of the vehicle is impacted at an angle of 27° by a crabbed moving barrier weighing 1365 kg and travelling at 33.5 mph. The driver's seat and left rear passenger seat are occupied by special test dummies (Side Impact Dummy—SID).

Rear impact

An 1800 kg moving barrier strikes the rear of the stationary vehicle at a speed of 30 mph. The front seats of the vehicle are occupied by two test dummies.

Safety obviously is dependent on a variety of factors. Nevertheless, the driver together with his car must be able to deal with all of these imponderables. The vehicle must, therefore, be designed to give the driver maximum support in overcoming critical situations.

Comprehensive experience from previous production and the results of experimental work are a good starting point for safety development. In this process, the computer has become an essential tool for our engineers.

The availability of modern computer technology—including graphics work-stations, CAD/CAM, FEM and the use of super computers—has increasingly made it possible to predict the results of later tests from the earliest stages of development, thereby speeding up the work process.

For example, the crash performance of individual frame components or of the entire front end structure can already be estimated at a very early stage in its development (Figure 3).

These initial calculations take place before any metal sheeting is processed into panels, let alone welded in to place.

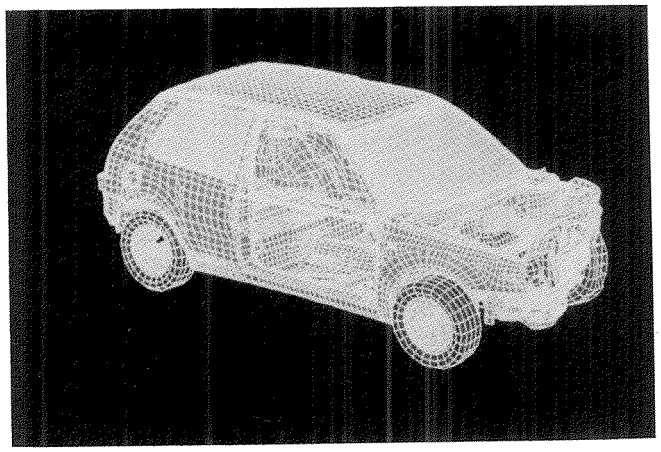

Figure 3. Computed Crash Simulation and Structural Assessment

Safety means additional material ie. increased weight. We know that safety related structures need not be too heavy or uneconomical with respect to fuel consumption. In fact, excessively stiff, unyielding structures outside of the rigid passenger cell impair the controlled and efficient absorption of impact energy.

For example, the front end of the Golf III has two body side members that have been deliberately designed to be able to buckle like an accordion in a predetermined manner. These two side members are joined by a rigid cross-member that helps to spread asymmetrical, one-sided deformation forces to the non-impacted side. The small upper front side rails when collapsed under impact forces, join with their respective A-pillar and door to form a continuous stiffening support that extends to the rear of the vehicle. The schematics in Figures 4 and 5 show the distribution of forces in a head-on collision.

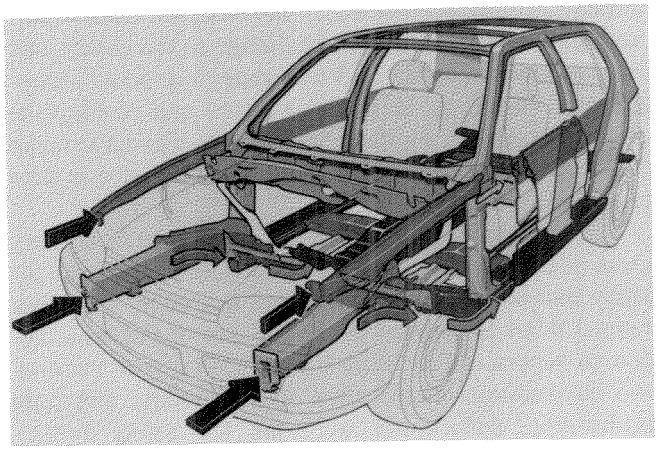

Figure 4. Frame Configuration and Impact Force Distribution

The material and cross-sections of the door sills have been significantly modified to provide increased lateral protection. The door sills, together with the safety cross-member underneath the instrument panel, the cross-beam underneath the front seats and the internal door beams

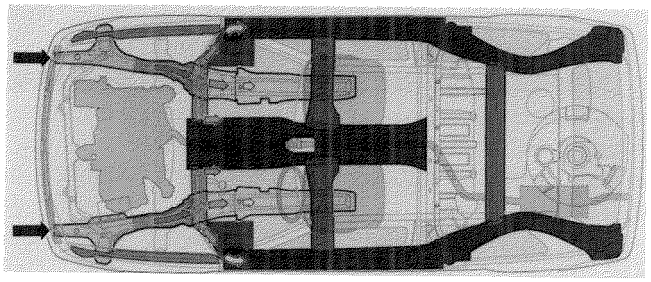

Figure 5. Frame Configuration and Impact Force Distribution

help to maintain the configuration of the passenger compartment, while also improving "escapeworthiness" for the passengers by also helping to ensure that the doors can still be opened even after a more severe collision.

The rear-end also has reinforced side members and thicker floorpan panels for controlled absorption of higher-speed collision energy, while keeping the passenger cell intact.

In the event of "roll-over" accidents, the structure of the A, B and C pillars of the Golf provide extra protection for passengers due to greater resistance to roof deformation.

An entirely new concept was applied in the construction of the lower longitudinal side members of the door sills which include corrugated plates. Their calculated progression of material thicknesses provides progressively increasing resistance to impact energy as well as cost benefits in the event of repair.

The wheel arch connected to the side of the lower front longitudinal side member also plays its part in absorbing crash energy. Stiffeners and ribs in the panelwork and the small upper side rails are also designed for energy absorption (Figure 6).

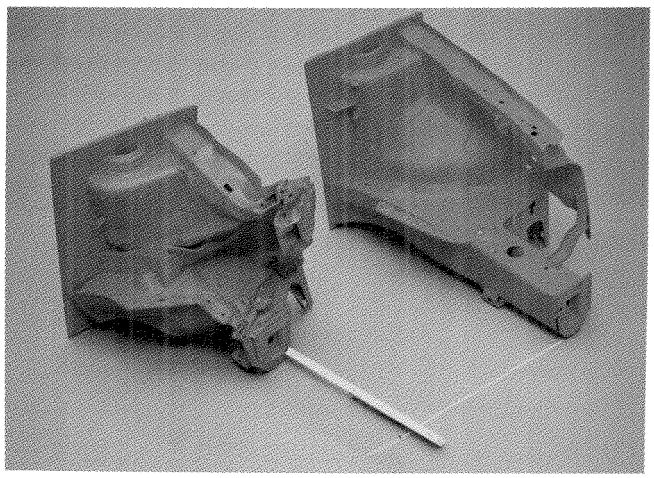

Figure 6. Front Side Members and Wheel Arch Configuration

The main deformation work of the kinetic energy generated is taken by the front lower side members and the upper side rails together with the fenders and wheel arches: all the other frame elements and the floorpan absorb residual energy.

In cases of frontal accidents, the passenger compartment can remain intact, the structure in front of the windscreen crush and deform. The collapsible steering column is designed to telescope into the retracting steering column joint—in order to reduced steering wheel intrusion into the passenger compartment (Figure 7).

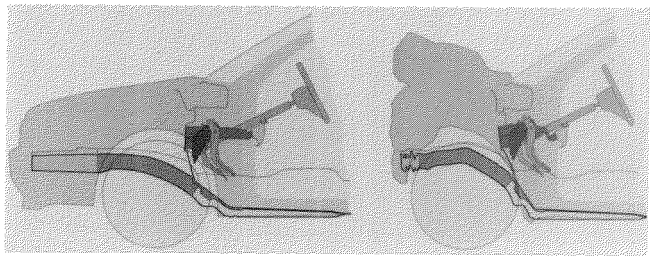

Figure 7. Frontal Crash Configuration

In roughly a quarter of all accidents, impact forces strike the vehicle from the side. Reinforced door sills, the safety cross-member spanning the area underneath the dash panel from one A-pillar to the other, the cross-stiffening in the floorpan underneath the front seats and the door beams built into the doors give the passenger compartment above average strength in the event of a side collision (Figures 8 and 9).

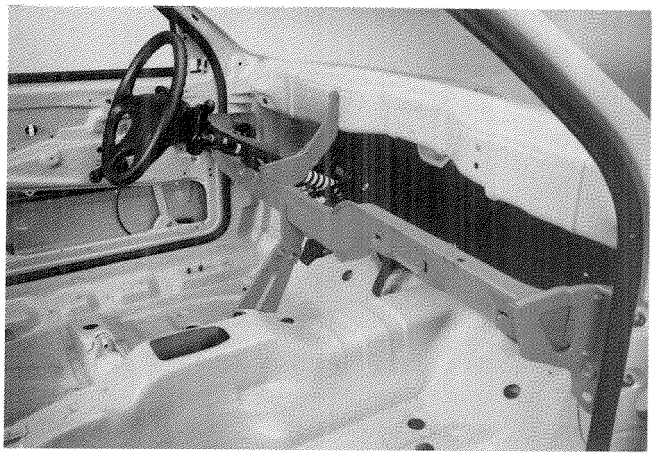

Figure 8. Safety Cross Member

In the 1994 US test procedure side protection integrated into the doors alone increases the car's lateral stiffness by about 30% and reduces penetration by about 50%. The small upper side rails continue underneath the door window (Figure 10), in the form of a profiled stiffening section. Further optimization of the door support on the pillars, door sills and roof frames, has brought about a greater efficiency in the distribution of crash forces. The tougher crash safety requirements also, of course, apply to the driver's cockpit. One of the first precautions taken is the collapsible safety steering column in combination with the folding lower steering column attachment which helps prevent the steering wheel from being projected towards the driver, even in

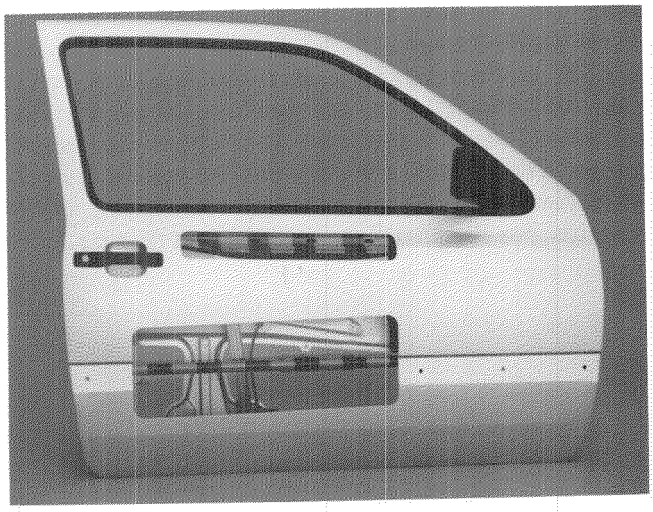

Figure 9. Door Side Rails

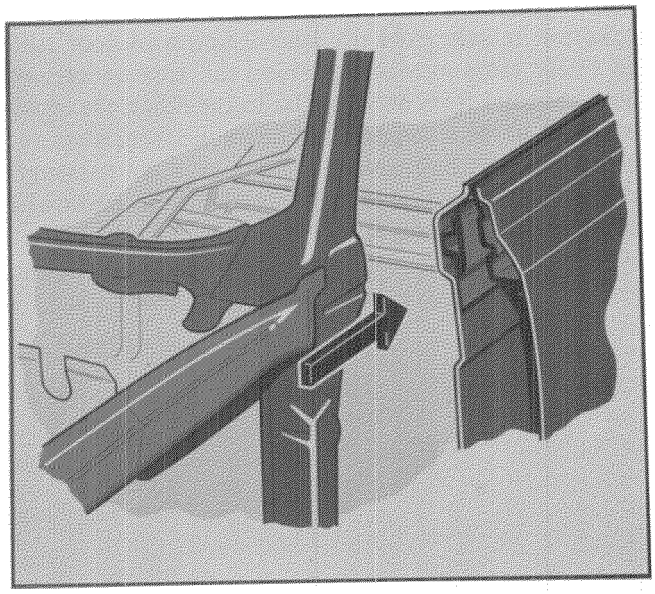

Figure 10. Small Upper Front Side Rails and Door Rails

a 35 mph crash. Secondly, the steering wheel itself incorporates a safety feature in the form of the padded, energy absorbing hub. The rim of the steering wheel can deform in a predetermined manner. In severe accidents the driver's head or chest can contact the steering wheel rim. The steering wheel then acts as a deformation element and reduces impact forces to a more tolerable level. The energy absorbing foam which fills the wheel hub disintegrates and thus further cushions the impact.

The cross-member underneath the dash panel also participates in the good crash performance of the steering wheel. It not only reinforces the rigidity of the passenger cell in the event of a side impact, but it also helps to hold the steering column in position in the event of a frontal impact. In violent collisions, the lower part of the steering wheel can telescope by as much as 170 mm.

The safety of Golf III was complemented by further optimized roadworthiness.

Some other features are worthy of mention:

The torsion beam rear suspension of the Golf III has track correcting mountings, and with the wider track and a larger, self-stabilizing kingpin offset, the front suspension geometry of the Golf provides for improved directional control.

The sophisticated anti-lock brake system (ABS) of the VW Golf combines outstanding active safety with optimum breaking stability.

Unlike many simpler anti-lock systems, the ABS used in the Golf has four electronic sensors, so that it immediately detects even rapidly changing conditions when braking and controls the complete braking process. The potential of the braking system is more fully utilized. All four wheels on the two axles are incorporated in the control process.

Volkswagen has developed an "electric differential lock" (EDS) which provides added safety in handling and steering.

This new EDS traction control is fully automatic. It is constantly on standby and only intervenes when it is actually necessary. As a result, it can do more than just release the car from a sticky situation, for example: icy or muddy conditions.

The Volkswagen seats have been further improved in the new Golf. One important element that remains hidden under the upholstery is the special seat pan with its high strength. The seat pan of course ensures fatigue-free support of the thighs with minimal effect on blood circulation. Moreover, no amount of foam rubber padding of any thickness could act as a substitute for the finer details of its near perfect fit. The front half of the seat has a unique ramp design that rises at a precisely defined angle (Figure 11). This upwards slope helps to prevent the driver from sinking too far into the seat during sharp and heavy braking—and in frontal accidents. This phenomenon which is known as "submarining" can sometimes even result in sliding underneath the lap section of the three-point seat belts. This seat ramp also resits the tendency of the lap position of the seat belt from pressing into the abdomen which can cause internal injuries.

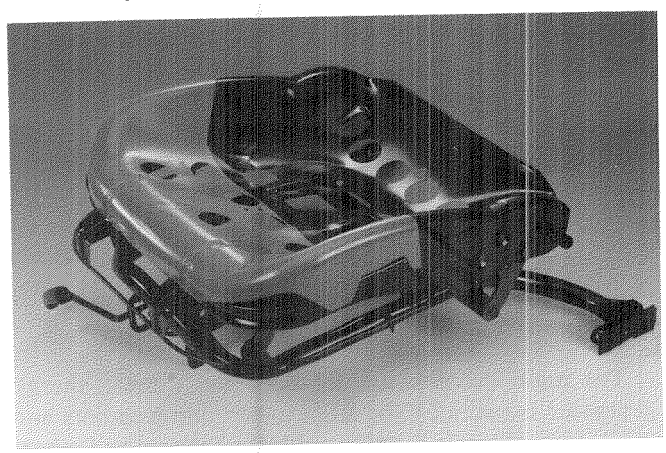

Figure 11. Front Seat Pan Configuration

The fold-down rear seat, which can be separately folded down as needed, has a sheet metal partition and reinforced supports. This can protect the passengers from loose, pointed or bulky articles in the boot which are propelled forward in the event of an accident.

In the new model generation, the occupants of the car are protected by a state-of-the-art seat belt system against many of the consequences of accidents.

Front and rear height (4-door model) adjustments reposition the upper belt anchorage at the appropriate height for occupants of different stature.

To protect child passengers, innovative restraint systems have been introduced in the 3rd generation Golf under the range name of "Bobsy."

In real crash tests and sophisticated simulations the VW's "Bobsy" child safety systems go beyond the test specifications of ECE R 44. These specifications particularly relate to the vehicle specific deceleration behaviour. Being directly integrated into the relevant vehicle range, the "Bobsy" child safety seats provide exemplary protection in both head-on collisions and rear impacts. Improved belt guides and attachment mechanisms help these seats to do their job. The new generation of child safety seats, available for the entire Volkswagen range, has the following outstanding features:

- effective utilization of the protection facility
- individual for each age group
- use of standard seat belt systems
- improved form-fitting seat
- simple operation
- pleasant comfort with pure cotton towelling for active "breathing"
- colours attractive to children

Table 1 shows the range of seats available, as well as the recommended weight and age range for each seat. In Figure 12 all seats are represented.

Table 1

VW Child Safety Systems	Weight of Child	Age of Child	Group in ECE R 44
Bobsy 10	up to 10 kgs	up to 9 months	0
Bobsy 18	9-18 kgs	8 months to 4 years	I
Bobsy 12	up to 25 kgs	up to 7 years	0, 1, II
Bobsy 35	15 - 36 kgs	3 - 12 years	II, III

Bumpers and windscreen/rear window wipers are examples of how the new Golf takes into account the safety of other road users.

The bumpers are now bracketless and, therefore, absorb the energy of impact solely through the flexing capacity of the cover material. Their wide dimensions and rounded corners spread the compressive load over a wide area, thereby minimizing the risk of injury to unprotected road users. These bumpers are part of a

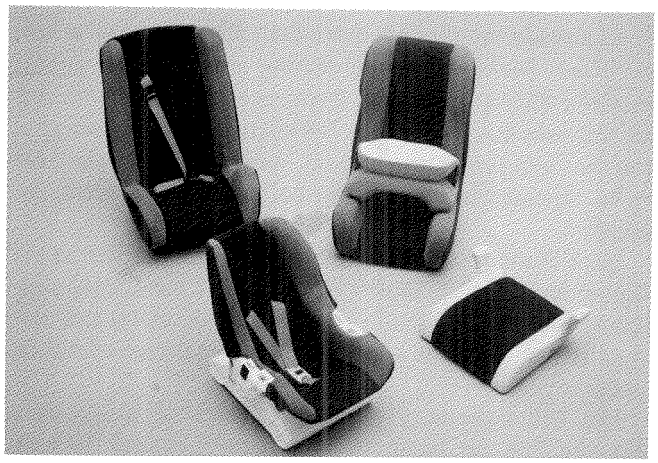

Figure 12. VW Child Safety Systems

safety concept that also includes yielding door mirrors, recessed attachments and fittings, absence of pronounced rain gutters and no sharp body corners or edges. For example, the windscreen wiper shaft bearings that would normally jut out from the surface are concealed by the bonnet, so that they are out of the way of anyone forced over the bonnet, in the event of pedestrian accident.

The fuel tank of the Golf III is made of blow-moulded plastic, with the environmental friendly incorporation of about 40% recycled plastic offcuts from the production process. To ensure that fuel cannot diffuse through the various layers of the fuel tank walls, the inside of the fuel tank has been flourine- treated in a special sealing process.

In 1973 Volkswagen was one of the first automobile companies in the world to use plastic fuel tanks. The fuel tanks have since been constantly optimized.

The Golf III has been equipped with a gravity fuel shut-off valve that is activated in the event the vehicle comes to rest on its roof after an accident.

Returning once again to the subject of accident safety, a glance at the statistics confirms that more than two thirds of all accidents affect the front of the car. The deformation forces act frontally or at an angle, affecting either the entire vehicle width or only parts of it (offset crashes). Roll-over accidents represent the smallest proportion, accounting for 2.8% of all accidents.

It has to be remembered that all these accidents occur between vehicles of widely differing sizes and weights, often travelling at vastly different speeds. Hardly any one head-on or side collision is the same as the next. Roll-overs, for example, can result either from high speeds or centrifugal forces. Customers, accident researchers, experts and car insurers all expect the manufacturer to tell them precisely what degree of damage is done at a particular given speed, how safely the passenger compartment is protected and when repairs can be judged to be economically justified. Consequently, vehicle safety can only be finally assessed on the basis of a whole range of tests covering more than just one limited discipline.

As already mentioned, more than 30 types of tests are, therefore, included in the testing schedule of Volkswagen's Safety Research Department. Since there are several intermediate stages between the first prototypes and the final production model, most of these tests have to be repeated several times before our engineers are satisfied.

Most of the tests on the Golf III were performed at the higher speed of 35 mph (56.3 km/h). These tests confirmed both the computer-aided predevelopment calculations and the results of preliminary tests on individual components.

The biomechanical tolerance limits of US (safety standard 208 for head, chest and thighs) in a 30 mph frontal impact, are clearly met by the new Golf. Even at collision speeds of 35 mph—corresponding to an increase of about 36% in kinetic energy—the expected degree of injury remains below the tolerance limits.

Table 2 shows the test results of four crashes:

- frontal impact at 30 mph
- frontal impact at 35 mph
- side impact at 33.5 mph
- offset crash at 35 mph.

Table 2. Injury Criteria

		Driver				Passenger			
Crash Test	V [mph]	Hic [I]	Chest Acceleration [g]	Thigh Forces [kN] Left	Right	Hic [I]	Chest Acceleration [g]	Thigh Forces [kN] Left	Right
Frontal	30	224	39.3	3.1	7.4	399	51.0	2.9	2.4
Frontal	35	890	58.7	3.2	8.6	453	51.4	3.6	2.2
Side	33.5	301	TTI [I] 75	Pelvis Accel. 82 [g]		392	TTI [I] 81	Pelvis Accel. 115 [g]	
Offset	35	498	59.3	2.5	6.7	239	47.6	2.1	1.0

These numbers underscore the new level which has been reached by the third generation Golf.

Furthermore, the safety level reached is documented by the strength of the passenger compartment, which provides an intact survival space and the greater possibility to protect the occupants' lives even after more severe accidents. Some examples are shown in Figures 13 to 20.

The new Golf has set new safety standards in the compact class, a standard previously only available on luxury cars—if at all. Nevertheless, Volkswagen will continue its endeavour to optimize road safety and crash performance of all its cars.

Figure 13. Frontal Impact Test at 56.3 kph (35 mph)

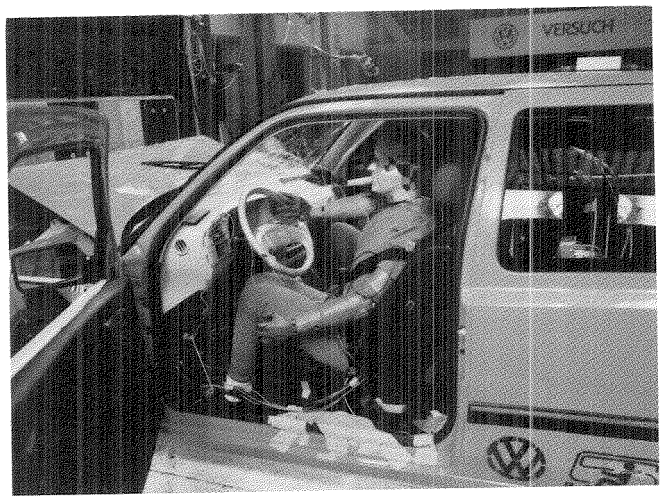

Figure 14. Dummy Position After 56.3 kph (35 mph)

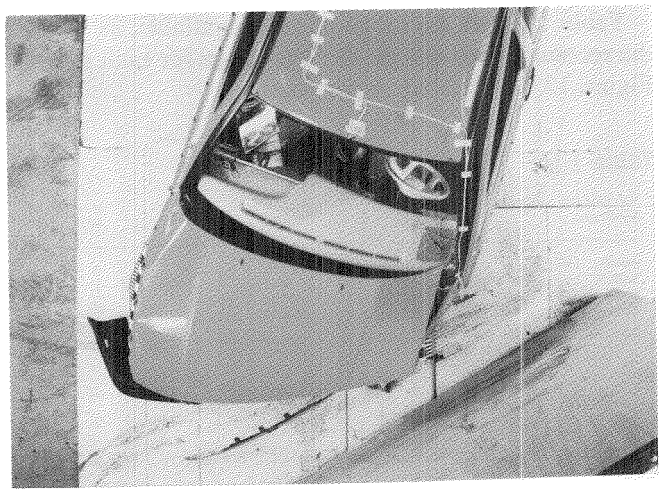

Figure 15. 30° Barrier Impact Test at 48.3 kph (30 mph)

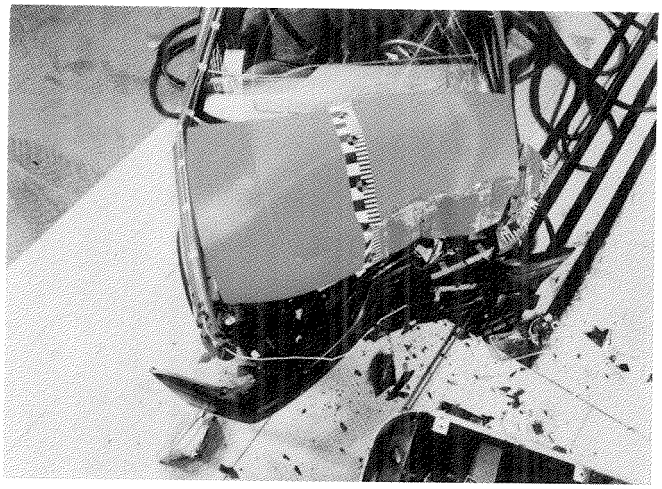

Figure 16. Offset Crash Test at 55 kph (35 mph)

Figure 17. Rollover Test

Figure 18. Rollover Test

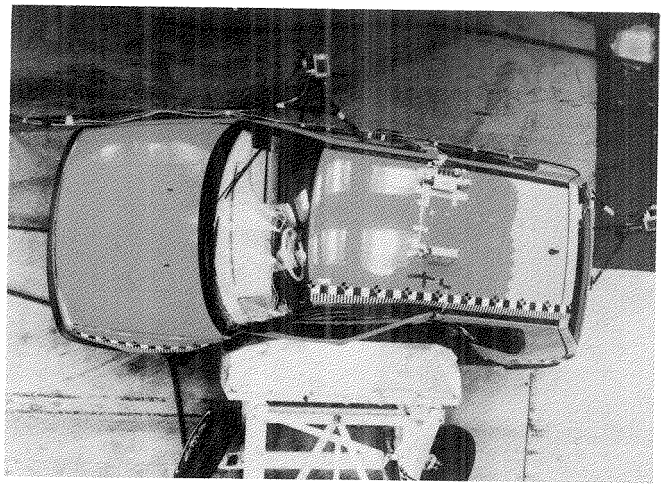

Figure 19. Crabbed Moving Barrier Crash Test at 54 kph (30 mph)

Figure 20. Frontal Crash Test Between Cars of Different Sizes (50 kph) (30 mph)

Figure 21. Rear Crash Test with 1800 kg Moving Barrier (48.3 kph) (30 mph)

Technical Session 10
Heavy Truck Safety

Chairperson: Bernd Friedel, Federal Republic of Germany

S10-O-01

Large Truck Safety in the U.S.

Henry E. Seiff
Motor Vehicle Manufacturers Association
of the U.S., Inc.

Abstract

In contrast to public concern over "killer trucks," large truck fatality and accident rates in the U.S. are falling (fatality rate from $3.64/10^8$ km in 1976 to 2.31 in 1989; accident rate from $2.20/10^6$ km in 1979 to 1.53 in 1989). Large truck occupant fatalities decreased 24% from 1976 to 1989, as safety belt use increased from 6% to 40% (and up to 56% in 1991!). But the fatality rate remains 70% higher than the rate for passenger cars, because the mass of a truck puts occupants in other vehicles at greater risk. Double trailer combinations are not over represented in fatal accidents, but bobtail tractors are. Large trucks are one-fourth as likely to be involved in a fatal accident on limited-access highways as on other highways, and one-third as likely to have a fatal accident in daytime travel as at night.

Introduction

In the late 1970s in the U.S., the subject of large truck accidents became a matter of increasing public concern. Truck manufacturers lacked the data needed to understand the increase in accidents experienced at the time.

In 1979, the Motor Vehicle Manufacturers Association took the initiative in sponsoring a long-term study at the University of Michigan Transportation Research Institute (UMTRI) to provide the detailed accident data needed. The study has the following goals:

- Determine the accident, injury and fatality rates for a broad range of large trucks operating on U.S. highways.
- Determine the causes of accidents involving these trucks.
- Achieve an understanding of the countermeasures likely to prevent or reduce the frequency of such accidents.

The UMTRI study is called the "Acquisition/Analysis of Truck Accident and Exposure Information." I am indebted to Dr. Ken Campbell and his staff at the Center for National Truck Statistics at the University of Michigan Transportation Research Institute for much of the data and many of the insights reported in this paper.

To understand the status of large truck safety in the United States, one must understand a little about the type of trucks and truck operations in use in the U.S.

In contrast to Europe, or at least my observations of Europe, very few truck full-trailer combinations are in use in the U.S. We rely almost exclusively on tractor-trailer combinations for movement of large volumes of freight by highway. In the U.S. in 1987 there were a little over a million tractor-semitrailer combinations in operation, compared with only 60,000 truck full-trailer combinations. There were also 34,000 doubles combinations, and about 500 triples combinations (1) (See Figure 1).

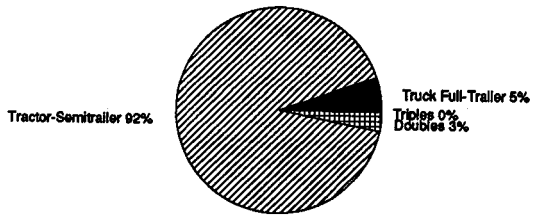

Figure 1. Combination Vehicles in the U.S., 1987

Combination vehicles travel an average of 96,000 km per year (2). Fifty-eight percent of this travel is accumulated on limited-access highways (generally "Interstate Highways") (3).

While railroads move the largest percentage (37.3%) of intercity tonne-kilometers of freight, trucks are second with 25.4%. But in value of freight moved, trucking is the overwhelming leader. Trucks earn 78% of each dollar of total freight revenue; railroads are far behind with 9.1%. In 1989 trucks moved just over a trillion (1.04×10^{12}) tonne-kilometers of freight in intercity operation (4).

In addition to the term "combination vehicles," I will be talking about "heavy" and "large" trucks. The Motor Vehicle Manufacturers Association defines "heavy" trucks as those with a gross vehicle weight rating (GVWR) of over 15,000 kilograms. The term "large trucks" means any truck over 4,545 kg GVWR.

Accident Data Trends

All Motor Vehicle Accident Fatalities

Although U.S. motor vehicle travel has increased some 17 times from 1925 to 1989 (from 195 to nearly 3,371 billion [10^9] km.) highway fatalities have "only" doubled, from 21,877 in 1925 to 45,555 in 1989 (5). There has been a generally constant trend of decreasing accident fatality rate as shown in Figure 2, from 11.9 per hundred million kilometers traveled in 1925, to 1.35 in 1989 (an 88% reduction).

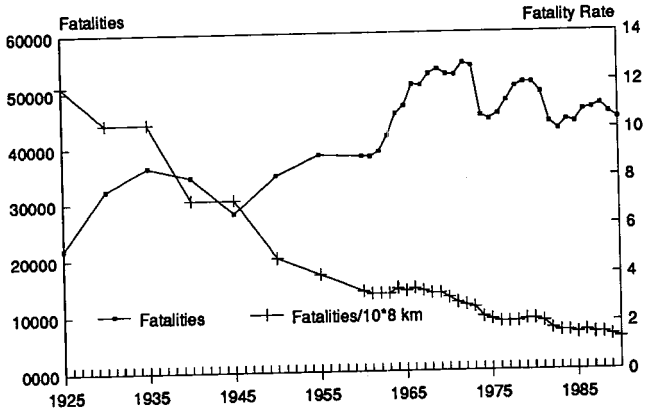

Figure 2. Motor Vehicle Accident Fatalities, 1925-1990 (MVMA, NHTSA)

Large Truck Accident Fatalities

Unfortunately, good data on large truck safety do not go back quite as far as 1925. Beginning in 1976, the National Highway Traffic Safety Administration's Fatal Accident Report System (FARS) provides accurate data on large trucks.

Figure 3 shows a relatively level number of fatalities from 1976-1989. During that period large truck mileage rose substantially, causing a 37% decrease in the fatal accident rate, from 3.64 to 2.31 per hundred million vehicle kilometers. During the same period the fatality rate for passenger cars decreased by 33% from 2.00 to 1.35.

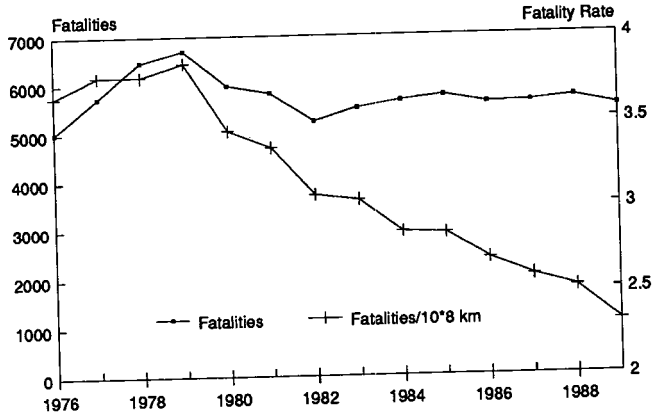

Figure 3. Large Truck Accident Fatalities, 1976-1989 (NHTSA, FHWA)

The good news, of course, is that total fatalities from large truck accidents are essentially level, while the fatality rate is falling even faster than the rate for passenger cars. The bad news is that the rate for large trucks is 70% higher than the passenger car rate. This is primarily a function of vehicle mass. In any accident involving a large truck and a smaller vehicle, such as a passenger car, the sheer size and weight of the truck puts the other vehicle's occupants at greater risk.

Large Truck Occupant Fatalities

Figure 4 shows a clear trend toward a decreasing number of large truck occupant fatalities. While occupant fatalities have fallen 24% (from 1132 to 858) over the 14-year period for which we have good data, large truck travel has increased 73% (from 138 to 238 billion kilometers). The large truck occupant fatality *rate* has therefore fallen even more spectacularly, 57%, from .83 to .36 per hundred million kilometers. As a point of reference, the passenger car occupant fatality rate in the United States was 1.06 in 1989 and has fallen 30% since 1976.

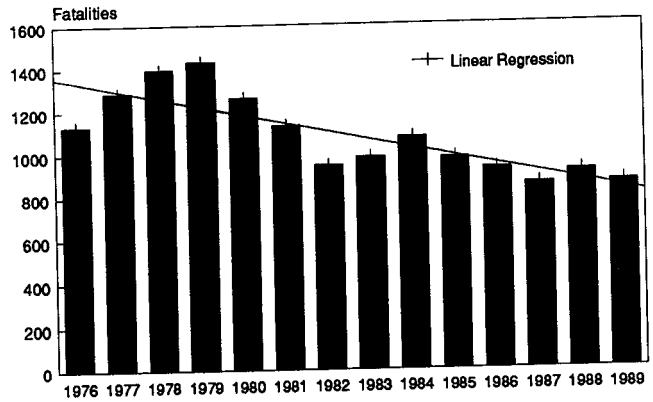

Figure 4. Large Truck Occupant Fatalities, 1976-1989 (NHTSA)

The likely reason for this improvement is the increase in truck driver safety belt use over the period in question. In 1982 the Department of Transportation's National Highway Traffic Safety Administration monitored belt use at four truck weigh stations around the country and found only a 6.3% use rate. Monitoring at the same four stations in the Spring of 1991, NHTSA found the use rate had increased to 56%. These numbers track closely with use rates reported in NHTSA's "Fatal Accident Reporting System." Table 1 shows the trend from 1982 to 1991.

Table 1. Heavy Truck Occupant Safety Belt Usage Rate

Year	Percentage
1982	6.3*
1984	7.9+
1985	16.9+
1986	23.7+
1987	32.7+
1988	37.9+
1989	40.3+
1991	56*

Sources: NHTSA Weigh Station Monitoring (*) and NHTSA FARS (+).

All Large Truck Accidents

To round out the picture a few words should be added about large truck *accidents*. Unfortunately, data on *all* accidents are not nearly as accurate as data on *fatal* accidents. National Highway Traffic Safety Administration figures (Figure 5) from 1979 through 1989 show a

high of 384,000 accidents in 1979 and a low of 280,000 in 1982. In 1989, 365,000 accidents were reported to the police. Of particular interest is the large truck accident rate, which was 1.44 per million vehicle-kilometers compared with an accident rate of 2.14 for passenger vehicles (1988 data) (6).

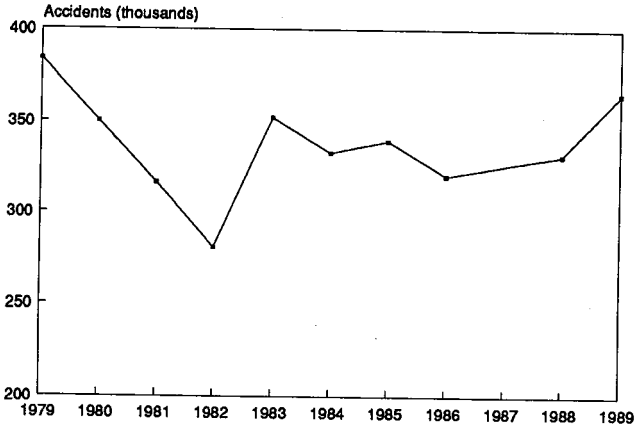

Figure 5. Large Truck Accidents (NHTSA)

So, while large truck experience shows a higher *fatality rate* than passenger vehicles, at the same time trucks have a substantially lower *accident rate*. The truck driver's status as a professional may be credited with at least part of the lower accident rate. A large part of it, however, is the difference in operation between passenger vehicles and large commercial vehicles. Passenger vehicles accumulate only 22% of their travel on the safer, high-speed Interstate Highways while large trucks accumulate 40% of their travel on Interstates.

On the limited-access Interstates, far fewer accidents take place. On the other hand, since vehicles traveling the Interstates are traveling at high speeds, those accidents which do occur tend to be more serious. Add this to the large mass of trucks and it becomes obvious why the fatality rate for accidents involving trucks is higher than that of passenger cars.

Accident Circumstances

Over a five-year period, fatal truck accidents were broken down by vehicle type as shown in Table 2.

Table 2. Types of Trucks Involved in Fatal Accidents

Truck Type	Percentage
Single Unit	23.8
Bobtail	2.5
Tractor-Semitrailer	65.1
Doubles/Triples	3.2
Other/Unknown	5.4

Source: *Trucks Involved in Fatal Accidents, 1980-84*, Carsten and Pettis, UNTRI, p. 84, 8/87.

By comparing fatal accident frequency of various vehicle configurations to miles traveled, the University of Michigan has developed relative risk ("normalized rate") factors. Single-unit trucks are "underinvolved" with a .84 factor, bobtails are substantially "over-involved" with a 2.76 factor, and tractor-semitrailers and doubles experience a "normal" (1.03) involvement rate.

But, since different types of vehicles operate under different circumstances, simple mileage involvement rates do not tell the full story. Day of the week, time of day, and weather conditions under which various types of vehicles operate and driver experience would all be expected to affect accident rate. And, of course, different vehicle configurations might be expected to have different safety records, even if all else were equal.

Analysis of truck accident statistics shows that the kind of road on which a truck travels appears to be the most important single factor in determining accident risk. Figure 6 shows that non limited-access roads are far more dangerous than limited-access roads. Large-truck accidents are comparatively rare during daylight hours on both rural and urban limited access roads. Nighttime travel is more dangerous than daytime travel on the same type of highway.

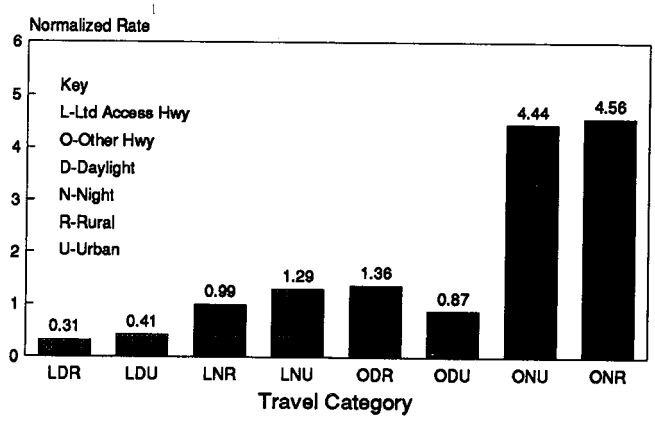

Figure 6. Normalized Fatal Accident Rates by Travel Category (UMTRI)

In 76% of large truck fatal accidents the "first harmful event" was a collision with another motor vehicle. Five percent of the accidents were noncollisions, primarily overturns, and 7% were collisions with fixed objects, such as guardrails or trees (7).

Although multiple-vehicle collisions are the predominant type involving large trucks, the vast majority of truck occupant fatalities (72%) occur in single vehicle accidents (8).

In 1987, rollover was involved in 54% of truck tractor driver fatalities, ejection in 34%, and fire in 14%. Only 23% of the driver fatalities did not involve either rollover, ejection or fire. (Totals add to over 100% since two or more situations may be involved in any one fatality) (9). While the involvement of any of these three events is extremely serious, overall, their likelihood in *all* truck accidents is rare.

Driver Characteristics

Although driving of trucks in interstate commerce is limited to those 21 years of age of over, the same tendency for younger drivers to be involved in a greater percentage of fatal accidents is found in trucks as in cars (Figure 7). Under 21-year old truck drivers are involved in about five times the expected number of accidents. The rate falls to twice the expected number at age 21, and by age 27, younger drivers are safer than the average of all drivers (10).

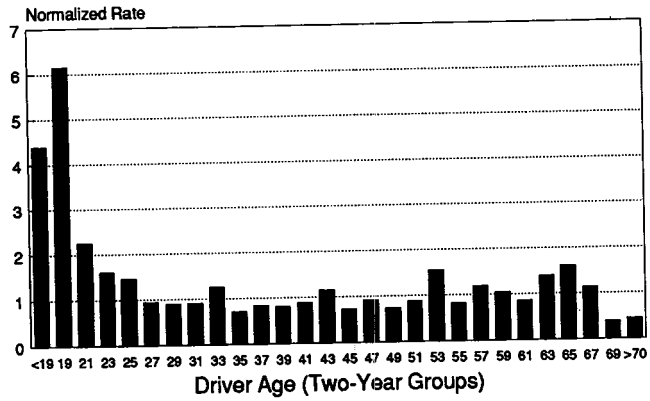

Figure 7. Fatality Rates by Driver Age—All Large Trucks (UMTRI)

As a matter of interest, only 1 percent of the truck drivers involved in fatal accidents are women (11) while 1 percent of the nation's truck drivers are women (12).

The University of Michigan found alcohol use identified in only four percent of truck drivers in fatal accidents (13). But when the National Transportation Safety Board (NTSB) performed in-depth studies of all fatal-to-the-driver heavy truck accidents in eight states for a one year period during 1987-88, they "...found that 33 percent of the *fatally injured* (emphasis added) drivers tested positive for alcohol and other drugs of abuse. The most prevalent drugs found were marijuana and alcohol (13 percent each), followed by cocaine (9 percent), methamphetamine/amphetamines (7 percent)..." (14).

In their study, the NTSB found that fatigue was the probable cause of the fatal accident slightly more often than alcohol and other drugs. "Driver fatigue and loss of alertness behind the wheel is a major cause of highway accidents which has received very little attention to date" (15). Fatigue as a cause of truck accidents is the subject of major studies sponsored by the U.S. Department of Transportation, the American Trucking Associations and the Motor Vehicle Manufacturers Association.

Vehicle Characteristics

Although the tendency is to assume that heavier trucks are more likely than lighter trucks to be involved in fatal accidents, University of Michigan data show that this simple relationship does not hold. Figure 8 plots normalized accident rates (relative risk) of tractor semitrailer combinations by gross weight range, showing an accident rate peak in the 30 tonne range. The rate for heavier vehicles falls substantially. This may simply indicate that the most heavily loaded vehicles stay on the safest (limited-access) highways and that other vehicles tend to operate on less safe roads.

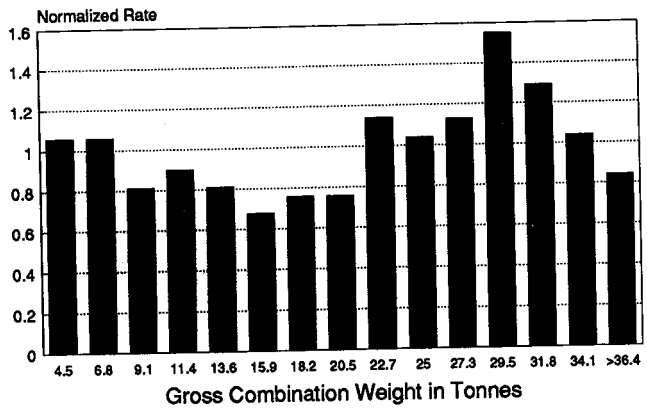

Figure 8. Fatal Accident Rates by Vehicle Weight—Tractor Semi-Trailers (UMTRI)

Most data bases indicate that extremely few accidents involve mechanical defects in the vehicle. According to the Department of Transportation's Office of Motor Carriers "Less than 4 percent of all carriers reporting accidents during 1988 said that their vehicles exhibited mechanical defects or failures at the time of the accident" (16). NHTSA's FARS data as reported by the University of Michigan agree, showing no vehicle related factors in over 93% of fatal truck accidents in 1988 (17). Of those vehicle-related factors which are cited, brakes, followed by tires and wheels, represent by far the major areas of concern.

Contrary to the data noted above, the National Highway Traffic Safety Administration has said that "...vehicle-related topics play a critical, if somewhat unrecognized and underreported role. In many cases, these factors, if they do not directly cause an accident to occur, make it more difficult—or in some cases, impossible—for a driver to recover from an error or avoid an unforeseen conflict" (18). In fact, NHTSA estimates "...that brake system performance could be involved as a contributing factor in as many as one third of all truck accidents" (19). Brake defects are also identified as the cause of a substantial proportion of truck accidents in studies performed by the Insurance Institute for Highway Safety and the National Transportation Safety Board (20).

Highway and Environmental Characteristics

"The typical accident occurred in early winter, on a weekday afternoon. At the time of the accident, weather and road conditions were favorable" (21). Although we have no reliable data on accident *rate* in good versus inclement weather, NHTSA data show that, overall,

about 85% of large truck accidents take place in good weather (22) (see Table 3). For passenger vehicles that figure is 83%. Interestingly, when passenger vehicles have accidents during rain, snow, or fog, they tend to be relatively minor (18% of property damage accidents happen in inclement weather, versus 12% of fatal accidents). In the case of trucks accident severity is about the same (14% of property damage only accidents in inclement weather, and 15% of fatals) in inclement as in good weather.

Table 3. Large Truck Crashes by Atmospheric Conditions

Fatal Crashes	
No Adverse Conditions	84%
Rain, Snow, Fog, etc.	15%
Injury Crashes	
No Adverse Conditions	81%
Rain, Snow, Fog, etc.	19%
Property-Damage-Only Crashes	
No Adverse Conditions	86%
Rain, Snow, Fog, etc.	14%

Sources: NHTSA, *A Summary of Fatal and Nonfatal Crashes Involving Medium and Heavy Trucks in 1988*, Table 18.

Like "vehicle characteristics" discussed above, the highway itself is rarely cited as a cause in a truck accident. Yet, as noted above (see Figure 6) large truck fatal accidents on limited access highways are only about one-fourth as frequent as on non-limited access roads. Likewise, on the same roads, the accident frequency rate during daylight hours is only one-third that during nighttime hours. Again like "vehicle characteristics" one can prognosticate that road conditions "...if they do not directly cause an accident to occur, make it more difficult—or in some cases, impossible—for a driver to recover from an error or avoid an unforeseen conflict" (23).

Seven percent of truck accidents reported to the Federal Highway Administration in 1988 "...occurred on expressway entrance and exit ramps" (24). A study by Ervin, MacAdam and Barnes found that some ramps leave little margin for safe use by large trucks operating at the posted ramp speed. They suggest, given the far lower rollover threshold of combination vehicles, compared to passenger cars, that highway design standards should be reviewed. Without major reconstruction of the ramp, possibilities for safer operation include speed advisories, resurfacing and curb removal (25).

There are many opportunities beyond highway geometric design to improve truck operational safety. A perfect example is those beautiful country roads our host country is famous for—those with lanes of old trees set close beside the road. As lovely as they are, they are recognized as a danger when driver attention wanders and the vehicle goes off the road. Break-away signposts have saved many lives—perhaps our botanists need to work on "break-away trees."

Wayne Muri, former Executive Committee Chairman of the U.S. Transportation Research Board, compliments European road construction, saying that, in addition to longer life, less rutting and the ability to withstand heavier loads, the porous asphalt pavement used in France and other European countries produces a lower noise level, better friction and less hydroplaning than U.S. pavements (26).

In the U.S. we can make big improvements in the economical and safe operation of trucks through better communication between the civil engineers who build the highways and the mechanical engineers who design the trucks. We blame heavy trucks for damaging our highways and at the same time blame poor highways for damaging our trucks and their cargo. It's time we learned to work together (27).

Other Areas of Concern

Enforcement

The Federal Motor Carrier Safety Regulations set safety standards for motor carriers, vehicles and drivers operating in interstate commerce. Before 1984 these regulations were enforced by only a small staff within the Department of Transportation's Federal Highway Administration. In 1984 the Motor Carrier Safety Assistance Program (MCSAP) was implemented, providing funds directly to the states to enforce safety regulations. "Prior to MCSAP funding, 36,000 Federal (commercial vehicle) inspections took place annually. During Fiscal Year (FY) 1990, approximately 3,000 State MCSAP officials conducted over 1.6 million inspections nationwide" (28).

Along with this major Federal program, implemented by the states, went the creation of the Commercial Vehicle Safety Alliance (discussed below), providing for standardized inspection procedures among U.S. and Mexican states and Canadian provinces and assuring carriers that their vehicles, inspected and passed in one jurisdiction, would not be stopped again upon crossing the border.

This year, between May 14-16, "Roadcheck 91" conducted over 46,000 vehicle safety inspections "...at approximately 100 locations throughout North America. For the third consecutive year, the out-of-service rates...declined.... Inspectors removed 12,849 unsafe commercial motor vehicles (28%) and 2,383...drivers (5%) from the highways..." (29).

Deregulation

In the U.S. there was a real concern that economic deregulation in the trucking industry would lead to an increase in truck accidents. It was said that carriers, in an effort to cut costs to stay competitive, would cut their investment in driver and vehicle safety programs. And if

driver wages stayed steady or fell in the more competitive environment, driver quality could fall.

The effect of deregulation on safety is obviously not just a U.S. issue. Although we have economically deregulated on a national basis, many of our states have kept their economic control over intra-state truck operation. Canada, and, I gather, Europe and others are now involved in the deregulation debate.

Although it seems impossible to look at the effect of deregulation on safety in a vacuum, a Canadian trucking industry publication finds that the U.S. data "...certainly don't support a negative link between deregulation and safety. In fact, they present a rather strong case that deregulation has led to improved safety" (30). Their conclusion is based on the fall in the absolute number of large truck fatalities during the decade and the much greater fall in fatality rate shown in Figure 3 above.

Recent Actions to Improve Truck Safety

Highway safety, and especially large truck safety, are active areas of private sector and government concern in the U.S. This is especially true in light of the concern generated by economic deregulation, starting in the late 1970s. Some recent actions which appear to have been successful in cutting the accident and fatality rate include:

Commercial Drivers License (CDL)

By April 1, 1992, all drivers of trucks over 12,000 kg gross vehicle weight rating must have a Commercial Drivers License issued by their state of residence. To obtain this license requires a difficult written test, the ability to conduct a pre-trip inspection and competently drive the type of truck for which the license is issued. Previous to this time some American states allowed an individual who had taken his driving test in a passenger car to drive any type of motor vehicle! The advent of the CDL is expected to substantially improve the skill level of U.S. truck drivers.

Professional Truck Driver Institute of America (PTDIA)

The Professional Truck Driver Institute of America is a non-profit organization sponsored by a broad-based coalition of motor carriers, owner-operators, manufacturers, equipment suppliers, insurers, trade associations and others closely involved with truck safety. The coalition works through the Institute to advance truck driver training, proficiency, safety and professionalism to the highest standards possible. Set up in 1985, the Institute helps assure individuals who aspire to become truck drivers of competent training. PTDIA offers a certification program by which a school or fleet training center voluntarily undergoes a cooperative and comprehensive study and evaluation to demonstrate that its tractor-trailer driver training program meets or exceeds the criteria of the Institute. As of the Summer of 1991, 46 truck driver training schools in the U.S. had been certified by the PTDIA.

Commercial Vehicle Safety Alliance (CVSA)

Begun in 1980, CVSA is an association of U.S., Canadian and Mexican state and provincial officials working together with Federal governments and industry to improve commercial vehicle safety. It provides the basic framework for uniform, compatible and reciprocal truck inspections and safety enforcement activities in member jurisdictions. By coordinating roadside truck inspections, CVSA helps ensure that vehicles on the road are in good mechanical condition and at the same time truckers are not unnecessarily detained for inspection by officials of each state or province through which they drive.

National Governors Association (NGA) Standardized Truck Accident Data Form

To make improvements in truck safety it is necessary to collect and analyze truck accident data. So that data being collected by police in each state in the U.S. is similar, the NGA developed a list of 22 data elements which it has asked each state to collect when investigating a truck accident. Over half the states which responded to a recent NGA survey had already taken action to adopt the recommendations.

Random Drug Testing

On November 14, large motor carrier fleets (50 or more drivers) will begin random driver drug testing. All other fleets must begin testing on January 1, 1992. This applies to drivers of vehicles over 12,000 kg GVWR. In addition drug testing is required as part of the hiring procedure, during the biennial physical evaluation and for "reasonable cause."

Automatic Slack Adjusters (ASAs) and Antilock Brakes (ABS)

As you may remember, the U.S. led the world in requiring antilock brakes on large trucks in the 1970s. ABS braking systems weren't ready for this rigorous application at that time. For that reason and others many provisions of our Federal Motor Vehicle Safety Standard 121 were withdrawn. Since then U.S. carriers, manufacturers and government have become followers, rather than leaders, on ABS. But today most, if not all U.S. truck manufacturers offer ABS as an option and it is generally accepted that the Department of Transportation will begin rulemaking to require it in the near future. A further brake improvement, automatic slack adjusters, is now virtually standard equipment, as are "bobtail proportioning valves" to assure better brake distribution when a tractor is traveling without a trailer.

Three-Point Safety Belts

Although not required by government standards, three-point safety belts are standard equipment on virtually all new large trucks in the U.S. Truck drivers used to complain that safety belts were uncomfortable or got tangled or dirty when they fell to the floor. Manufacturers have changed all that and safety belt use rates have skyrocketed as noted above.

Future Truck Safety Improvements

"Like motor vehicle crashes in general, commercial vehicle crashes are caused by interacting human, environmental, and vehicle factors. Most crashes are attributed to 'driver error'. . . . From a prevention standpoint, attribution of crashes to 'driver error' often obscures the fact that safety enhancements to the environment (e.g., intelligent signing) and/or the vehicle (e.g., collision warning systems, anti-lock brakes) may make 'driver error' less likely to occur" (31). Therefore, in exploring potential truck safety improvements for the near future we shall look at some opportunities in driver, highway environment and vehicle improvements.

Safety Belt Use Rates

As was seen above, large truck occupant fatalities have fallen very substantially over the years, due in major measure to increasing safety belt usage. The occupant fatality rate fell from .83 per hundred million kilometers in 1976, when the safety belt use rate was near zero, to .36 in 1989 when it was around 40%. The use rate is now over 50% and today's trucks are equipped with improved three-point belts. Since rollover and ejection have been seen to be involved in the majority of truck driver fatalities, an increase in belt use to near 100% can be expected to save a great many lives. A 1981 report evaluated specific occupant fatality accidents, finding that, of ejected occupants, "...63 percent were estimated to have had a 60 percent or greater chance of survival had lap and shoulder belts been worn" (32). It is reasonable to expect that increasing public concern, more stringent safety-belt use legislation and stronger carrier enforcement will lead to increased belt use in the future.

Air bags have been suggested for large trucks by some safety advocates. But limited data strongly suggest that accidents which injure truck drivers are usually the result of low deceleration crashes of relatively long duration, for example when a large truck impacts a passenger car or runs off the roadway. And, of course, a large proportion of driver injuries are found in rollover accidents. Driver protection from an air bag in these types of crashes would be minimal, whereas a safety belt would seem to offer optimal protection.

Intelligent Vehicle Highway Systems (IVHS)

"IVHS technologies, though not a panacea, offer a means for directly and dramatically addressing many of the concerns of...commercial vehicle operators regarding the human and economic toll of...traffic accidents" (33).

Automatic Vehicle Identification (AVI), Advanced Vehicle Control Systems (AVCS) and Site Specific Highway Warning Systems are likely to have a positive effect on truck safety within the decade of the '90s. AVI can warn drivers of vehicle safety hazards, assist in vehicle routing and streamline the passage through toll gates, inspection stations and over state borders. AVCS can enhance driver visibility at night or during fog, rain or snow. Active cruise control (decreasing or increasing speed based on a vehicle's distance from the vehicle in front of it) and radar braking (sounding an alarm or even taking over the braking function when an obstacle is sensed) offer potential safety enhancements. Warning systems can ensure that trucks do not move into areas where there are present optical blind spots, such as the right side and the rear. Sensors can detect alcohol or fatigue-impaired drivers. Site-specific warning systems could, for example, broadcast safety advisories of on/off ramp speed, bridge heights, and lane restrictions which would only be picked up on radio frequencies always monitored by large trucks.

Fatigue

"(A) recent study by the National Transportation Safety Board has shown that driver fatigue is more important than drug and alcohol abuse in truck accidents.... Other studies report that falling asleep behind the wheel may account for 15-20 percent of all freeway accidents and up to half of fatal freeway accidents" (34). Since 1939, the Federal Motor Carrier Safety Regulations have regulated a truck driver's hours of service in interstate commerce, in an effort to assure that drivers are properly rested. Knowing that there is far more to assuring alertness than simply limiting drivers to a certain number of hours driving or on-duty, a $3.7 million study is underway, sponsored by the Federal Highway Administration and the American Trucking Associations. "The objectives (of the study) are to measure fatigue indicators and the relationship of fatigue to loss of alertness. Later, alertness-enhancing methods will be tested and we may consider revisions in the regulations governing how long commercial drivers may stay behind the wheel" (35).

The Motor Vehicle Manufacturers Association of the U.S. (MVMA) is sponsoring a study to determine the effect of vibration levels on driver alertness. At various times it has been suggested that high and low cab vibration levels may cause loss of alertness. We hope to determine whether either claim is true, and, more important, whether cab vibration level can be tailored to a driver's need to stay alert when operating on the public highway.

In the foreseeable future, perhaps electronic technology can be melded with new knowledge about alertness and methods to detect it. Non-invasive sensors would then be able to warn the driver of lack of alertness, using such methods as buzzers, audio messages or even taking over control of the truck, bringing it safely to a stop on the side of the road and shutting it down.

Traction Control

Traction control is another development evolving from antilock braking and electronic technology. By sensing when a powered wheel is spinning and automatically decreasing the power supplied and/or applying braking, traction can be improved. Especially in rainy, snowy or

icy conditions, this can substantially improve vehicle controllability and safety. In a very few years traction control will follow ABS in general use on large trucks.

Wide Track Tractors

Since 1983, U.S. law has allowed the operation of 2.6 meter wide vehicles on Interstate Highways. Although most new trailers have been built since that time with a wider track, tractors have stayed with the old 2.44 m overall width to allow them to run over all highways (many states restrict the operation of 2.6 m vehicles to certain highways).

Although the increase in width was designed to expand vehicle carrying capacity and productivity, it also improved vehicle safety. Rollover is a concern with high center of gravity vehicles like trucks. By increasing the trailer width to 2.6 m "...the rollover threshold improve(d) by 4 to 12%, depending upon vehicle configuration and loading scenario" (36). "Tractors which are widened to the 102-inch (2.6 m) dimension provide an additional 8 to 10% improvement in the roll stability of tractor-semitrailers" (37). One would expect that it is only a matter of time before our state officials realize the value of an increase in vehicle stability from permitting wider vehicles on all U.S. highways, especially since most transit buses in our major cities are 2.6 m wide already!

Lower Center of Gravity (CG)

A perennial problem faced by motor carriers, and therefore by trailer and tractor manufacturers, is how to increase productivity by carrying a greater volume of cargo within the size limits imposed by regulation. Since state and Federal regulations limit the cargo container length, height and width, the only reasonable option open is to lower the bottom of the trailer. This has led to some "possum belly" designs, where the trailer floor falls between the axles in the center of the trailer but rises to clear the tractor and trailer wheels. Because it does not provide a smooth trailer floor and therefore limits loading by forklift truck, this design has never become popular.

New tire technology is providing smaller diameter tires with load-carrying capability equal to the old designs. As the new tires come on-line, trailer floors will fall. And even without smaller tires, productivity requirements will force more "possum belly" designs. Along with better productivity comes a lower tractor-trailer center of gravity and with that a greater resistance to rollover. Using a van trailer fully loaded with uniform freight, the CG of the load falls 1 cm for every 2 cm the bottom of the trailer is lowered. Therefore if the floor can be lowered 25 cm, the CG would fall 12.5 cm and the rollover threshold of a typical tractor-semitrailer combination would fall about 12% (38).

Dual Drawbar Dolly

Again looking at vehicle dynamic stability, it can be anticipated that future U.S. regulations will allow increases in vehicle productivity for vehicles with certain specific safety devices. Such a trade off could allow longer or heavier doubles combinations only if some type of "C" or dual drawbar dolly were used between the first and second trailer (as in Canada). Today's typical doubles combination might have a rearward amplification ratio of 2.0 whereas a vehicle with a C-dolly would lower that ratio to 1.35 (39). The rearward amplification ratio is a ratio of lateral acceleration seen at the rear trailer, in comparison to that seen at the tractor. Higher ratios indicate the second trailer is more likely to roll over in an evasive maneuver.

Summary

The large truck fatality and accident rate in the United States has been decreasing dramatically over the last decade and a half. At the same time, public anxiety about truck safety has increased, likely due to the trend toward smaller passenger cars for fuel economy and larger trucks for productivity. The public is aware that most fatalities in large truck accidents are in the other involved vehicles, rather than the truck occupants. They are also aware that heavy trucks and passenger vehicles operate together on increasingly congested highways where a single accident, even without personal injury, can produce extended delay and disruption.

For these reasons it is essential to have facts about truck accidents at hand; facts to allow us to make intelligent decisions to further decrease the number and severity of crashes. Facts, such as those reported in this paper, come from accident data collection and analysis, which the Motor Vehicle Manufacturers Association of the United States is proud to support.

References

1. U. S. Department of Commerce, Bureau of the Census, *1987 Census of Transportation*, Truck Inventory and Use Survey (Washington, D.C.: U.S. Government Printing Office, August 1990), p. US-26.
2. Ibid., Calculated from Tables 6 and 11.
3. Dr. Kenneth L. Campbell, et al., *Analysis of Accident Rates of Heavy-Duty Vehicles*, University of Michigan Transportation Research Institute (Ann Arbor, MI: University of Michigan, April 1988), Table 15.
4. American Trucking Associations, *American Trucking Trends*, 1990-91 Edition (Alexandria, VA: American Trucking Associations), pp 4-6.
5. Motor Vehicle Manufacturers Association, *MVMA Data Digest* (Washington, D.C.: Motor Vehicle Manufacturers Association of the U. S., 1986), p. C-1; Federal Highway Administration, *Highway Statistics 1989* (Washington, D.C.: U.S. Government Printing Office, 11/90), Table VM-1; National Highway Traffic Safety Administration, *Fatal Accident Reporting Systems 1989—A Decade of*

Progress (Washington, D.C.: U.S. Government Printing Office, March 1991), inside front cover.
6. Terry S. T. Shelton, *A Summary of Fatal and Nonfatal Crashes Involving Medium and Heavy Trucks in 1988* (Washington, D.C.: National Highway Traffic Safety Administration, February 1990), Tables 1 & 2.
7. Kathleen P. Sullivan, Daniel Blower, and Leslie Pettis, *Trucks Involved in Fatal Accidents Codebook 1988*, University of Michigan Transportation Research Institute (Ann Arbor, MI: University of Michigan, June 1991), Variable 21.
8. R. M. Clarke and W. A. Leasure, Jr., *Truck Occupant Protection*, (Washington, D.C.: U.S. Department of transportation, National Highway Traffic Safety Administration, December 1986), p. 12.
9. Dawn L. Massie, *Trucks Involved in Fatal Accidents Factbook 1987*, University of Michigan Transportation Research Institute (Ann Arbor, MI: University of Michigan, June 1991), Table 5-22A.
10. Kenneth L. Campbell and Arthur C. Wolfe, *Fatal Accident Involvement Rates by Driver Age for Large Trucks*, University of Michigan Transportation Research Institute (Ann Arbor, MI: University of Michigan, September 1988), p. 2.
11. Massie, *Trucks Involved in Fatal Accidents Factbook 1987*, Table 3-20.
12. U. S. Department of Commerce, Bureau of the Census *Statistical Abstract of the United States 1990* (Washington, D.C.: U.S. Government Printing Office, January 1990), p. 391.
13. Massie, *Trucks Involved in Fatal Accidents Factbook 1987*, Table 3-22.
14. National Transportation Safety Board, *Safety Study—Fatigue, Alcohol, Other Drugs, and Medical Factors in Fatal-to-the-Driver Heavy Truck Crashes*, NTSB/SS-90/01 (Washington, D.C.: National Transportation Safety Board, February 5, 1990), p. v.
15. Drs. Claudio Stampi and Martin Moore-Ede, "Truck Design Technologies to Reduce Driver Fatigue: Relationship between Truck Cab Vibration Levels and Driver Alertness" (proposal to MVMA from of the Institute for Circadian Physiology, Boston, MA, November 27, 1990).
16. J. A. Reyes Associates for the Office of Motor Carriers, U.S. Department of Transportation, *Accidents of Motor Carriers of Property 1988* (Washington, D.C.: Office of Motor Carriers, September 1990).
17. Sullivan, *Trucks Involved in Fatal Accidents Codebook, 1988*, Variable 137.
18. National Highway Traffic Safety Administration, U.S. Department of Transportation, *Heavy Truck Safety Study* (Washington, D.C.: U.S. Department of Transportation, March 1987), p. v.
19. Ibid.
20. Ian S. Jones and Howard S. Stein, *Defective Equipment and Tractor-Trailer Crash Involvement*, Insurance Institute for Highway Safety (Washington, D.C.: IIHS, September 1987), p. 18 and National Transportation Safety Board, *Safety Study—Braking Deficiencies on Heavy Trucks in 32 Selected Accidents* (Washington, D.C.: National Transportation Safety Board, NTSB/SS-88/06, November 30, 1988).
21. U.S. Department of Transportation, *Accidents of Motor Carriers of Property 1988*, p. 29.
22. Shelton, *A Summary of Fatal and Nonfatal Crashes Involving Medium and Heavy Trucks in 1988*, calculated from Table 18.
23. National Highway Traffic Safety Administration, *Highway Truck Safety Study*, p. v.
24. U.S. Department of Transportation, *Accidents of Motor Carriers of Property 1988*, p. 29.
25. R. D. Ervin, C.C. MacAdam and M. A. Barnes, *Truck Control Problems Posed by the Design of Highway Ramps* (Warrandale, PA: SAE Paper 870071, February, 1987).
26. Wayne Muri, "Paving the Way," *The Private Carrier*, August 1991, p. 6.
27. SAE, *Vehicle/Pavement Interaction—where the truck meets the road* (Warrendale, PA: Society of Automotive Engineers, November 1988), preface.
28. U.S. Department of Transportation, *U.S. Department of Transportation Heavy Truck Safety Plan* (Washington, D.C.: U.S. Department of Transportation, May 1991), p. 3.
29. Commercial Vehicle Safety Alliance, "Roadcheck '91'," *"The Newsleader,"* Summer 1991, p. 10.
30. Blair Gough and Ross Gray, "Deregulation can improve safety with right government commitment," *Motor Truck*, July 1991, p. 21.
31. Dr. Michael Walton "CVO Strategic Plan: Safety-Related Aspects," (Draft prepared for IVHS-America, CVO Technical Committee), August 28, 1991.
32. Brian Wolf, Kenneth L. Campbell and James O'Day, *Occupant Survivability in Heavy-Truck Crashes*, University of Michigan Transportation Research Institute (Ann Arbor, MI: University of Michigan, November 1981), p. 10.
33. Walton, "CVO Strategic Plan: Safety-Related Aspects."
34. "Driver Alertness Research Program Launched," *Around the Clock—A Quarterly Report from the Human Alertness Research Center to the Friends of the Institute for Circadian Physiology*, Summer 1991. p. 5.
35. U.S. Department of Transportation Press Release, FHWA 12-91, September 11, 1991.
36. R. D. Ervin, et al., *Influence of Size and Weight Variables on the Stability and Control Properties of Heavy Trucks*, University of Michigan Transportation Research Institute (Ann Arbor, MI: University of Michigan, March 1983), p. 172.
37. Ibid., p. 173.
38. Ibid., Calculated from Figure 38.
39. Ibid., Figure 64.

S10-O-02

Typical Risk Situations in Car to Truck Accidents—The Necessity of Improving the Conspicuity of Trucks

M. Danner, K. Langwieder, H. Bäumler
HUK-Verband

Abstract

Truck accidents are a major factor in the accident statistics. This paper deals with typical risk situations in truck-to-car collisions with respect to accident prevention. From a representative material of nearly 1400 truck-to-car accidents the pre-crash situations are described. It is shown that the signal effect of trucks especially in night-time and in bad weather conditions is insufficient. This results in an increased rate of car crashes into the side and rear end of trucks related with conspicuity problems. Proposals from current research work are made to improve the signal effect of trucks including an efficiency assessment. A passive conture marking seems to be an essential contribution to accident prevention and would enable retro-fitting of existing trucks, which is necessary for short term improvement.

Introduction

In the last few years there has been a sharp increase in the transport performance of all types of traffic. With the introduction of the common European market further growth in transport can be expected, and the opening up of the former Eastern Bloc and the reunification of Germany will boost the growth of traffic even more. In this connection special importance attaches to road haulage, since its share of the total transport of goods is steadily expanding. Whereas 51.5% of all goods were transported by road in 1984, by 1989 it was already 55.7%.

In spite of the rise in the total mileage covered, the number of people killed in truck accidents dropped, also the number of fatalities per Billion kilometres covered fell by 25% from 1984 to 1989, and the number for all vehicles by 36%.

It was therefore not possible for the truck to participate to an adequate extent in the general trend. For this reason it must be the aim of all those involved in road haulage to make the truck even safer.

General Data on Truck Traffic

Each year in the European Community about 52,000 people die in a traffic accident. Truck accidents account for one in four of those killed, and also result in about 300,000 people being seriously injured. The costs incurred by traffic accidents throughout Europe are estimated at DM 140 Billion [1].

In the Federal Republic of Germany in 1989 there were 345,600 accidents resulting in personal injury and in the deaths of 7,995 road users. The proportion of trucks involved in accidents with personal injury was 6.3%, and in accidents with fatalities 11.8% [2]. The car was the principal accident opponent of the truck.

Long-distance trucks, in most cases articulated trucks, cover on average 85,000 km a year [3], night driving accounting for 15,000 km (18%) [4], and its significance will increase as a result of modern logistical systems and new production methods—the catchwords are "night hopping" and "just in time."

The Signal Image of Trucks

Problems with the signal image of trucks arise mainly when visibility is poor i.e. darkness, dusk and bad weather conditions (snow, rain, hail and fog). Another aspect to be considered is the dirt deposited on the lighting, especially on the truck's rear-end.

When visibility is good the signal image of a truck is clearly defined by its contours. It can be obviously recognized as a truck by its size and shape (Figure 1). Once a truck has been recognized as such, the other road users can adjust themselves to a truck's behavior.

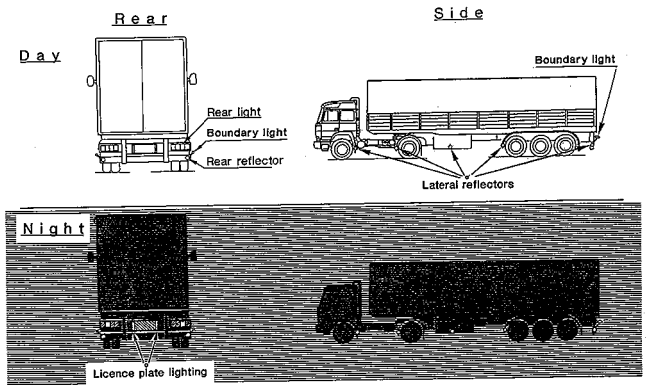

Figure 1. Comparison: Signal Image of a Truck During the Day and at Night

What car drivers tend to associate with a truck was shown by a random sample survey: The respondents replied to the effect that trucks are a danger and that one has to adapt one's driving to the truck's driving behavior.

So after the object has been recognized the signal image evokes behavior which results in a certain action, for example increasing the safety distance to the vehicle ahead.

It is therefore important to create signal images which make it possible to clearly recognize objects—here the truck in various visibility conditions. This is particularly important with regard to the truck's side and rear end. In this connection the front of the truck does not play such an important part, since on-coming drivers receive the

information "wide on-coming vehicle" from the truck's headlights and boundary lights.

Figure 2 gives an overview of the current lighting regulations in Germany (side and rear) for trucks. According to these, two rear lights and two rear reflectors are regarded to be sufficient on the rear end of trucks built before 1987. The legal requirements for new vehicles (first registration in or after 1987) have hardly been tightened up. Commercial vehicles as from this year of construction are required to have two additional boundary lights on either side at the vehicle's rear.

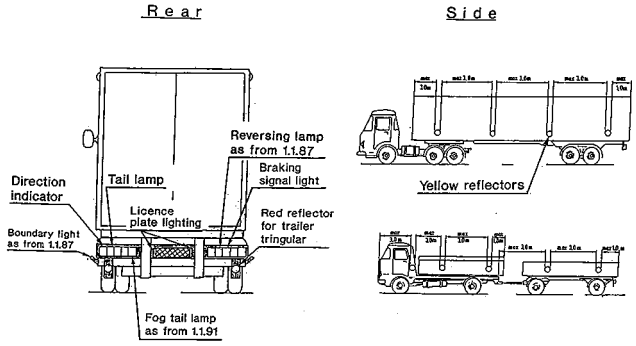

Figure 2. Current Lighting Regulations for Commercial Vehicles in Germany

Since between 72% (tractors) and 77% (rigid trucks) of commercial vehicles were registered before 1987 [5], this measure does not appear to be very effective.

Yellow reflectors have to be mounted at 3 metre intervals on the sides of trucks and articulated trucks. Active lighting equipment is not required at present. According to [6] this kind of identification marking calls for a very high light density to guarantee satisfying conspicuity. It can not be recognized at greater distances.

Factors Influencing the Signal Image

Apart from darkness and dusk, which, of course, result in the use of lights and reflectors, dirtying of the vehicle, bad weather conditions and dazzling by other vehicles make it difficult to recognize trucks.

In the case of the headlights, if the dirtying reaches 50% this can be noticed by the driver [7], while the rear lights and reflectors cannot be checked in this way. The extent of this dirtying is influenced by air turbulence at the rear of the truck caused aerodynamically. They carry large quantities of dirt particles to the vehicle's rear which quickly result in a layer of dirt on the lights. When it is raining this effect is intensified by the formation of a cloud of spray caused by the tyres [8]. In addition, the truck is enveloped in a trail of water, so that a double effect occurs: the truck is, on the one hand, more difficult to recognize and, on the other, the visibility is reduced for cars driving behind it.

One factor that must not be ignored when assessing the signal image is the impairment of the strength of the rear lights on older vehicles. The bulbs get older and their brilliance diminishes. The glass of the lighting equipment, initially colored, becomes lighter and lighter, and the different colors can hardly be distinguished any more, especially of trucks built in the former Eastern bloc. Since between 32% (tractors) and 42% (rigid trucks) of the tractor vehicles are older than 8 years, the importance of the ageing effect on lighting and signalling equipment for traffic safety should not be underestimated.

Traffic observation carried out by HUK engineers on the Munich-Nuremberg A9 motorway revealed that the rear lighting was defective on about 7% of the trucks. The signal image of the vehicles was subjectively assessed by these engineers. In only about 5% of the cases could it be described as good.

To what extent the problems outlined have an effect on accidents involving trucks will be examined more closely below.

The HUK Truck Accident Material

Database

The truck accident material—"Truck Accidents, Bavaria"—comprises over 2,200 truck accidents that caused personal injury. That are all truck accidents with personal injury involving trucks with a gross vehicle weight of over 3.5 tonnes which occurred in Bavaria in 1984 and which were suitable for the defined conditions of the HUK accident research.

The first findings from this study were presented at the 1989 ESV conference, when the structure of the material as dealt with in detail [9]. In the meantime all the cases have been evaluated on an extensive data form with about 260 parameters and are stored in a separate data processing file, where they are available for accident analyses.

Distribution of Truck Accidents

2,615 road users were involved in the 2,216 truck accidents and 216 of these lost their lives. 207 road users were seriously injured (MAIS 3-5). Moderate injuries (MAIS 2) were sustained by 18.1%, slight injuries (MAIS 1) by 51.8%, while 15% remained uninjured.

The mass distribution of the truck/trailer combinations and articulated trucks involved is shown in Figures 3a and 3b. Articulated trucks have a 20% proportion. Trucks and truck/trailer combinations clearly dominate. 37% of the trucks are light trucks (3.5 to 7.5 t gross vehicle weight). Most of them (95%) are operated without trailers. The second largest group are the trucks with a mass of between 12 and 16 t, 58% of which are operated with a trailer.

About two-thirds of all cases were collisions with a car (Figure 4). Two-wheelers follow in second place and, with 15.9%, represent only a quarter of the frequency of car accidents [10]. Truck/truck and single truck accidents, with 9.6% and 6.9% respectively, are not very frequent, but for the truck occupants they are the most serious.

Mass of trailer [t]	Mass of truck [t] 3.6 - 7.5	7.6 - 12	12.1 - 16	16.1 - 22	22.1 - 38	Total
- 3.5	8		6	1		15
3.6 - 7.5	16	12	5	1		34
7.6 - 12	9	23	63	3		98
12.1 - 16		5	63	133	3	204
16.1 - 22		4	214 58%	9	3	230
22.1 - 38		1	18	4	2	25
> 38	1			1	1	3
without trailer	605	99	266	141	10	1,121
Total	639	144	635	293	19	1,730
	36.9 %	8.3 %		16.9 %		

Figure 3a. Mass Distribution of Truck/Truck-Trailer Combinations in the Material

Mass of semi-trailer [t]	Mass of tractor [t] 3.6 - 7.5	7.6 - 12	12.1 - 16	16.1 - 22	22.1 - 38	Total
- 3.5	2		1			3
3.6 - 7.5	1	2	2			5
7.6 - 12	3	7	3	1	2	16
12.1 - 16	1	4	9	14	1	29
16.1 - 22	1	2	89	10	2	104
22.1 - 38	3	6	183 60%	45	3	240
> 38			2	5		7
without trailer	5		16	6		27 6.3 %
Total	16	21	305	81	8	431
			70.7%			

Figure 3b. Mass Distribution of Articulated Trucks in the Material

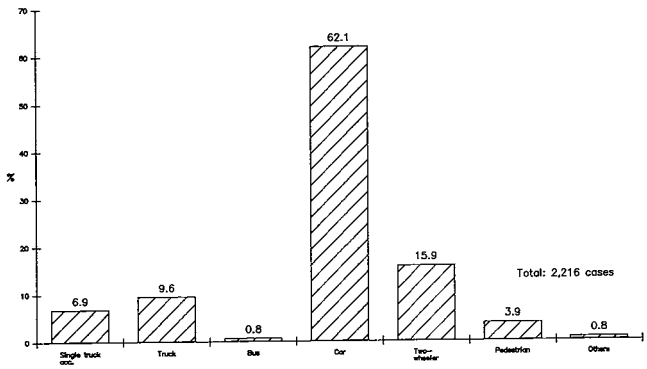

Figure 4. Distribution of the Accident Groups in the Truck Accident Material

The percentage change in the accident groups under the influence of light conditions is shown in Figure 5. As darkness increases the number of unprotected road users decreases. Single vehicle accidents, truck/truck and truck/car accidents rise rapidly. Although the greatest increase is found in the truck/truck accidents, it is the truck/car accidents which clearly represent the largest group. For this reason this group only will be dealt with below.

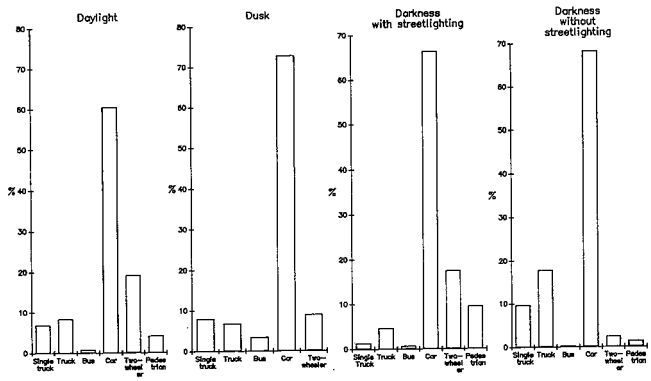

Figure 5. Distribution of the Accident Groups in Various Light Conditions

Crisis Situations in Truck/Car Accidents

In truck/car collisions theoretically three factors that trigger off the accident can be distinguished which are based on the truck's lack of conspicuity:

- The car driver does not recognize the truck or recognizes it too late.
- The car driver does not realize that the vehicle in his traffic lane is in fact a truck.
- The car driver wrongly estimates the speed of the truck and so runs into it.

Figure 6 gives an overview of the distribution of the collision types in truck/car accidents. It can be clearly seen that five collision types differ only slightly with regard to their frequency.

COLLISION TYPE	Total personal injury in car Number	%	of these car occupant fatalities Number	%
FRONT/FRONT	260	15.6	49	38.0
FRONT/SIDE	325	19.4	37	28.7
FRONT/REAR	291	17.4	2	1.5
REAR/FRONT	263	15.8	22	17.1
SIDE/FRONT	343	20.5	10	7.7
OTHERS	189	11.3	9	7.0
TOTAL	1,671	100.0	129	100.0

Figure 6. Distribution of the Truck/Car Collision Types Weighted According to Car Occupant Fatalities

To really be able to differentiate between them the various collision types have to be weighted according to their consequences. 38% of the car occupants killed in truck/car accidents die in frontal collisions. An effective measure for reducing the dangerous nature of the truck's front is the front underride protection [9, 10, 11]. It clearly enables reductions in the seriousness of the accidents to be achieved. In truck-front/car-side collisions (28.7% share of car occupant fatalities) certain improvements are to expected from a front underride protection, too.

The collision types truck-rear/car-front and truck-side/car-front (17.1 and 7.7%) range third and fourth. So almost a quarter of all car occupants killed in truck/car accidents die in collisions in which the truck's lack of conspicuousness can be potentially assumed. Roughly 70% of the truck/car accidents occur in daylight, and the remaining 30% in darkness or at dusk. More than 34% of the car drivers killed loose their lives in darkness or at dusk. There is a slight overrepresentation of dusk or night-time accidents. Much the same can be said for accidents with seriously injured car drivers (MAIS 3-5, 34.6%, Figure 7).

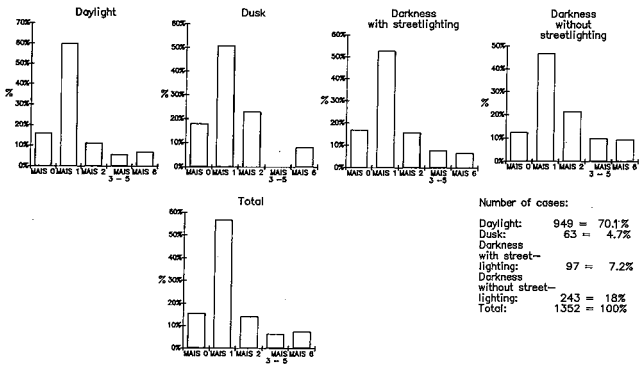

Figure 7. MAIS Distribution of Involved Car Drivers in Different Light Conditions

About 28% of all truck/car collisions occur in bad weather conditions. In a third of these (112 cases) there is the added factor of inadequate light. What influence does the truck's signal image have on the accident in poor visibility?

Figure 8 shows the changes in the accident causes in truck/car collisions for which the car driver is responsible as darkness increases. Accidents caused by driving too close to the truck ahead represent a small proportion of accidents during the day. Only at dusk do they occur in any appreciable numbers, drop slightly in lighted streets and reach their highest level in streets without any lighting.

From this it can be deduced that this kind of accident mainly occurs when the contrast between the truck and its surroundings is too weak. A further indication of trucks' lack of recognizability is the shift of collision types as the light conditions change.

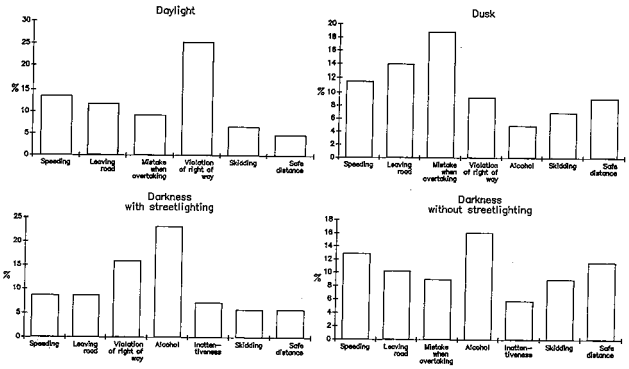

Figure 8. Change in Selected Accidents Causes (≥ 5 %) as Darkness Increases in Truck/Car Collisions Caused by Car Drivers

It should also be borne in mind that truck/car accidents show differing characteristics in the case of different accident sites. A distinction therefore has to be made between different accident sites and different road categories such as motorways.

Truck/car accidents on the motorway make up a share of about 20%. Accidents outside built-up areas on other roads are represented by about 38%. The remainder are accounted for by collisions in built-up areas.

Car/Truck Collisions in Built-Up Areas

Few articulated trucks (13,6%) are involved in accidents in built-up areas. The emphasis here is on tractors of 12 t gvw and above (about 90%). The number of tractors without semitrailers, about 16%, is relatively high. 75% of the trucks involved were driving without a trailer, and 43% were light trucks (3.5-7.5 t gvw). On the whole, lighter commercial vehicles and fewer articulated trucks are involved in accidents in built-up areas. The large number of light commercial vehicles and the lower collision speeds have a positive effect on the death rate of the car drivers involved, which is 2.6%.

Six out of 15 car drivers (40%) died in accidents in the dark, and they are thus clearly overrepresented, since only 22% of truck/car accidents in built-up areas occur at dusk or in the dark (Figure 9). In the case of seriously injured car drivers (MAIS 3-5), too, accidents in the dark are overrepresented (share of 30%).

During the day, collisions in which trucks run into the rear ends of cars predominate (31.7%, Figure 10), while at dusk and in the dark the car runs into the truck (26.6%). Seen absolutely, the number of car/truck rear-end collisions in the dark is also greater than in daylight. Car/truck rear-end collisions in daylight are represented by only 4.4%.

Overtiredness or physical deficiencies on the part of the car driver are not typical in truck/car accidents in built-up areas, on the other hand 24% of the car drivers involved were under the influence of alcohol. These accidents cannot be taken into account in considering the signal image of trucks.

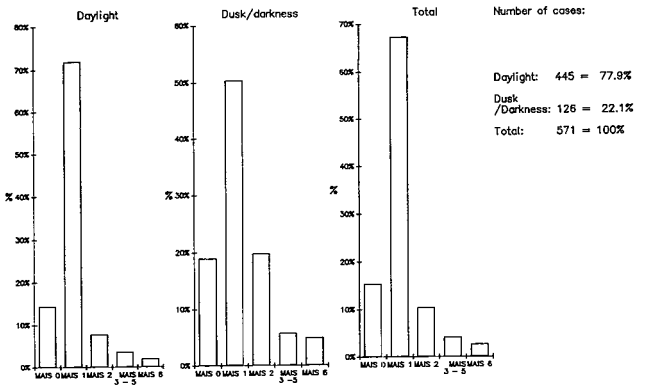

Figure 9. Truck/Car Collisions in Built-Up Areas: MAIS of Car Driver in Daylight and Darkness

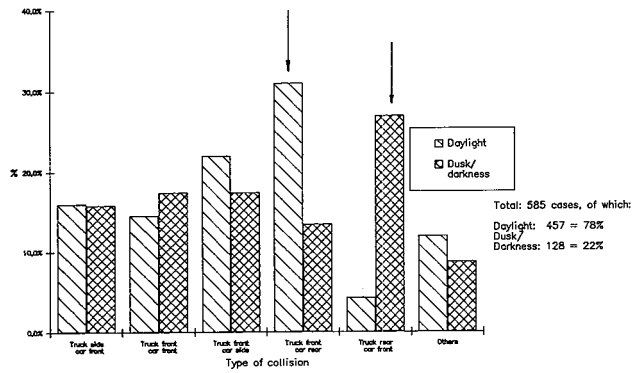

Figure 10. Collision Types in Truck/Car Accidents in Built-Up Areas

Rear-end accidents with car drivers not under the influence of alcohol represent 11.7% of the truck/car accidents in the dark. Their share of night accidents is still 2.6 times higher than in the case of daylight accidents and, also when compared with the average of all car/truck accidents in built-up areas, is slightly over-represented. It cannot be denied that the signal image of the rear ends of commercial vehicles may not be adequate even in illuminated streets in built-up areas.

Truck/Car Accidents Outside Built-Up Areas Excluding Motorways

Related accident risk. In 1985 commercial vehicles drove 27.84 Billion km on roads outside built-up areas (excluding motorways) in the Federal Republic [4]. 8.3% of these were covered at dusk and 16% at night. Three-quarters (75.7%) of the trips were made in daylight, and these account for 70% of the truck/car accidents outside built-up areas. 23.5% and 5.9% of the collisions are distributed over darkness and dusk respectively.

A joint consideration of the distribution of mileage and accidents gives reasons for introducing a weighting of the accident frequency in relation to mileage, so that it is possible to describe the risk distribution in a defined sample of accidents by simply giving a relative number. This "related accident risk (RAR)" represents the quotient of "percentage accident proportion" to "percentage mileage proportion." For the relation of "all accidents (100%)" to the "total mileage (100%)" the RAR = 1.

The "RAR" is therefore only suitable for indicating the risk distribution within a certain group, but it offers a quick overview of a high or low accident risk in certain conditions. For car/truck accidents outside built-up areas in daylight the RAR turns out to be almost 1 (0.93). No great shift in the risk can be observed. Driving at dusk has an RAR of 0.7, a low accident risk. For night driving, however, (RAR = 1.5) the accident risk is very high.

Characteristics of truck/car accidents outside built-up areas. Compared with accident involvement in built-up areas, in accidents outside these areas the proportion of articulated trucks rises from 13.6 to 17.5%, while the mass distribution in the group of articulated trucks remains about the same.

Truck/trailer combinations rise from 25% to 37.4% (Figure 11). Almost 58% of the trucks are heavy trucks with a gross vehicle weight of 12 t or more. Compared with accidents inside built-up areas, there are clearly more heavy trucks to be found outside these areas.

In the 522 truck/car accidents outside built-up areas that were examined 467 car drivers were injured, 64 (12.3%) of them fatally. While there are no unusual features about the fatalities, moderate and serious injuries (MAIS 2 to 5) are relatively more frequent in accidents at night than during the day.

The dominant type of collision in car/truck accidents outside built-up areas is the frontal collision both during the day and at dusk, and they also have a high proportion at night (Figure 12). The proportion of the collision type truck-side/car-front and truck-rear/car-front rises as the darkness increases. If both types of collision are considered together, almost half (48.8%) of all night accidents are collisions of this kind.

Figure 13 shows a rear-end collision with a articulated truck that was difficult to recognize. The car driver crashed with almost unreduced speed into the dry tank semitrailer going ahead of him. It can be clearly seen that almost the whole of the rear section, including the rear lights on the dry tank semitrailer, is covered in dirt, made even worse by driving in rain.

The bulbs of the rear lights were—according to the expert's report—old and therefore sooted up, which reduced their brilliance. How bad the signal image of the articulated truck really was is shown by the reflective traffic signs which can well be seen on the right beside the semitrailer.

Figure 14 shows a typical accident when turning off in which the car driver drove into the side of the truck-trailer combination. All the car occupants sustained considerable injuries. The truck-trailer combination, painted olive-green and dark blue, was standing across the road and it was not possible for the car driver to recognize it; furthermore, it was raining at the time of the accident.

This example shows the importance of a clear signal image of the truck's rear end and side.

Mass distribution of truck/truck-trailer combinations

Mass of trailer [t]	Mass of truck [t] 3.6 - 7.5	7.6 - 12	12.1 - 16	16.1 - 22	22.1 - 38	Total
- 3.5	1					1
3.6 - 7.5	5	2				7
7.6 - 12	1	6	15	1		23
12.1 - 16			19	46	1	66
16.1 - 22		1	54	2		57
22.1 - 38			4			4
> 38						
without trailer	145	17	61	42		265 62.6%
Total	152	26	153	91	1	423
	35.9 %		57.9 %			

Mass distribution of articulated trucks — articulated trucks = 17.5%

Mass of semi-trailer [t]	Mass of tractor [t] 3.6 - 7.5	7.6 - 12	12.1 - 16	16.1 - 22	22.1 - 38	Total
- 3.5	1	1	1			3
3.6 - 7.5	1	2				3
7.6 - 12		2	3	8		13
12.1 - 16	1		10	4		15
16.1 - 22			39	5	1	45
22.1 - 38				2		2
> 38						
without trailer	1		7	1		9
Total	4	5	60	20	1	90

Figure 11. Truck Mass Distribution in Truck/Car Accidents Outside Built-Up Areas (Without Motorways)

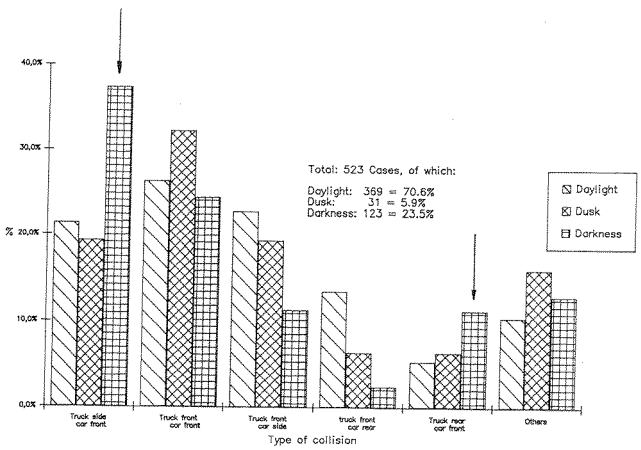

Figure 12. Collision Types in Truck/Car Accidents Outside Built-Up Areas (Without Motorways)

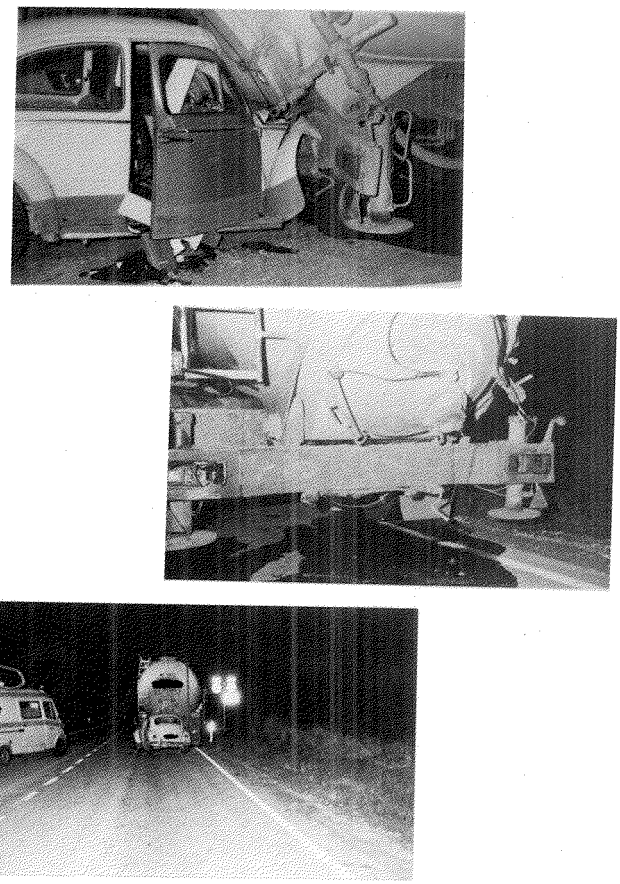

Figure 13. Example of a Truck/Car Rear-End Collision at Night

Motorway Accidents

Mileage and accident risk. Altogether commercial vehicles covered 34.4 Billion km in 1985 [4], over one-third (36.8%) of them on motorways. 68% of the total mileage was covered in daylight, 8.4% at dusk and 23.6% in the night. At night trucks operate far more frequently on motorways than on other kinds of roads.

The accident risk on motorways (about a 20%-share of all truck accidents and of truck/car accidents) is relatively low for trucks, the RAR being 0.5. Within the sample "truck/car motorway accidents" there are, however, marked differences. Daylight accidents (53.4%) and dusk accidents (4.7%) are less frequent than on other roads outside built-up areas. Instead, the proportion of night accidents increases from 23.5% (outside built-up areas) to 42%. This results in a high related accident risk for night driving of RAR = 1.8.

Characteristics of truck/car motorway accidents. On motorways there is one-way, non-intersecting traffic. It could therefore be expected that accidents between trucks and cars are restricted to the collision types rear-end collisions with cars or trucks and the car grazing the truck or vice versa. That this is not the case, but that about one-fifth all of accidents occurring are not typical of motorway collisions (Figure 15) is due to the fact that a high percentage of the cars (about 20%) collide with a truck while they are skidding.

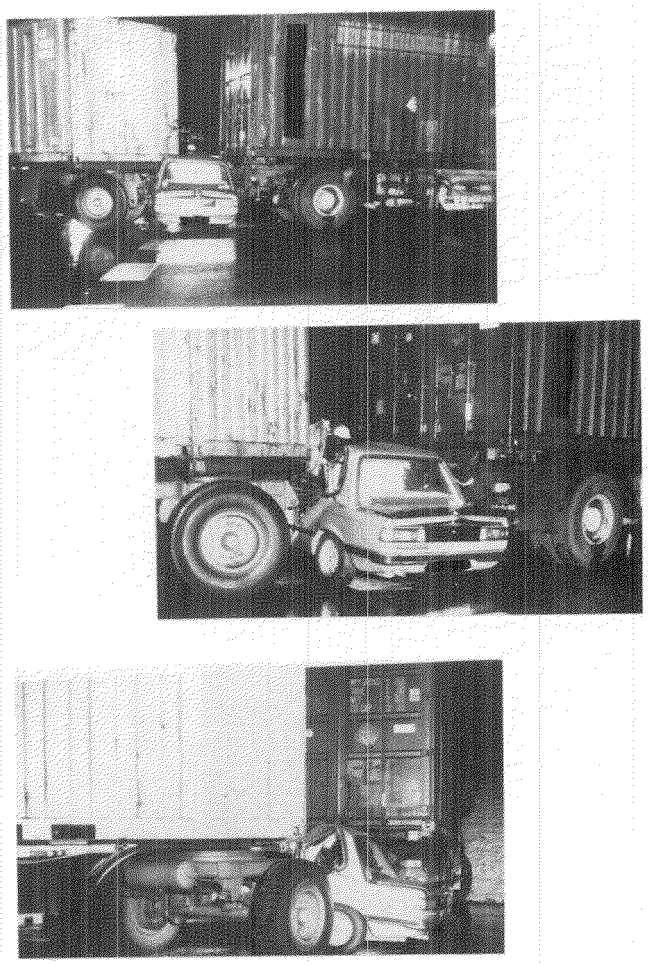

Figure 14. Typical Accident When Turning Off Outside a Built-Up Area

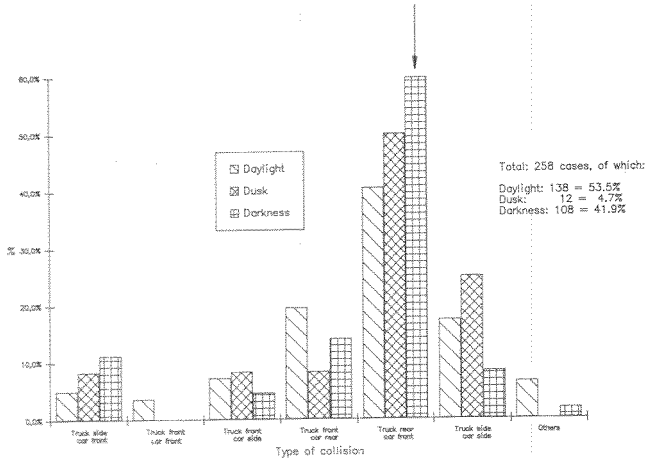

Figure 15. Collision Types in Truck/Car Motorway Accidents

This skidding by the car is triggered, among other things, by the failure of the car driver to adapt his speed to the traffic conditions, by mistakes while overtaking and returning to the inside lane and while changing lanes and by panic braking.

Accidents in which the truck strikes the car's rear-end (16.7%) and glance-off collisions (14%) are of little significance compared with cars running into the rear-ends of trucks (49.2%). Over half (51.2%) of this kind of rear-end accident take place in the night. Their proportion of the total truck/car night accidents on motorways is therefore high. Car drivers under the influence of alcohol are hardly represented at all here.

40% of the commercial vehicles involved in motorway accidents are articulated trucks—a high percentage, but it cannot be said that they are overrepresented, since articulated trucks are typical long-distance vehicles. The overwhelming majority of articulated trucks consist of a tractor with a gross vehicle weight of 12 t or more and a semitrailer with a gross vehicle weight of 16 t or more.

Light trucks are represented far less than on other roads outside built-up areas. 70% of the trucks are heavy trucks with a gross vehicle weight of 12 t or above, two-thirds of them being operated with a trailer weighing between 12 and 38 t.

In the truck/car motorway accidents 18 car drivers were killed, almost half of them (44.5%) in night-time accidents. Serious injuries (MAIS 3-5) to the car drivers are found more frequently in night-time accidents (10 cases = 9%) than in day-time accidents (7 cases = 5%). Night-time accidents are clearly more dangerous for car drivers than day-time accidents, and the number of serious accidents in which the car runs into the back of the truck is considerably higher.

Rear-end collisions at night are characterized by heavier damage to the car than in day-time accidents. This corresponds with a higher collision speed of the car. Some three-quarters of the cars are driving at speeds of over 90 kph when they run into the truck ahead in night-time accidents; one-tenth are well above 125 kph.

In accidents during the day only half of the cars drive into trucks at over 90 kph, and only three percent are going faster than 125 kph. The reason for this is not that there is a higher speed level at night, but that almost half of the car drivers who collide with trucks at night show no braking reaction at all (Figure 16), during the day it is only about one-fifth.

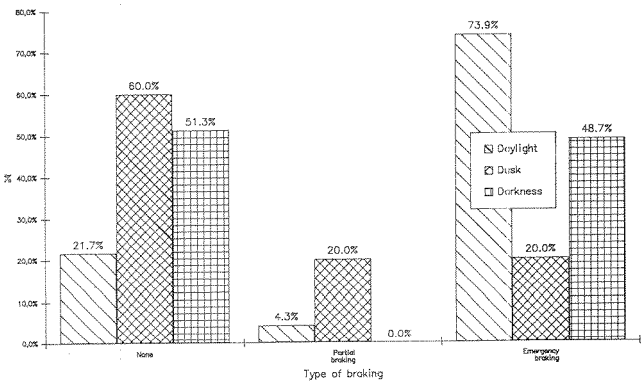

Figure 16. Truck/Car Motorway Accidents: Car Runs into Truck: Braking Reactions of the Car Drivers

Accidents with Slowly Moving Trucks

General remarks. In addition to the generally bad conspicuity of commercial vehicles when the visibility is bad, a further problem is recognizing the often extremely low speeds of commercial vehicles. What exactly is a "slowly moving truck?" German motorways (autobahns) may only be used by vehicles which can reach a speed of at least 60 kph. Analogous to this definition trucks which are driving at a speed of under 60 kph at the time of the collision are referred to as "slowly moving truck."

When perceiving a truck ahead and assessing its speed various physiological problems arise for the cars behind it.

- Big broad roads with no buildings on either side, like motorways, mislead the driver into underestimating his own speed [12].
- Speeds of under 80 kph are overestimated and of over 80 kph are underestimated [13].
- Acceleration is more easily recognized than deceleration.
- The fovea centralis of the eye is the most efficient area for recognizing movement. If the retinal image of the dimensions of the vehicle driving ahead remains within the area of the fovea centralis its change in speed is most easily recognized. If the retinal image exceeds a certain size it appears in the parafoveal region of the retina and the ability of the viewer to correctly assess the speed of the vehicle ahead is greatly diminished [12].
- The more difficult it is to recognize an object, the longer is the so-called latent period, i.e. the interval between recognizing an object and reacting to it [12].

Accident involvement. Over one-third (36.9%) of all rear-end accidents in which the car runs into the truck are collisions with a slowly moving truck. Most of them are driving at between 30 and 45 kph (Figure 17).

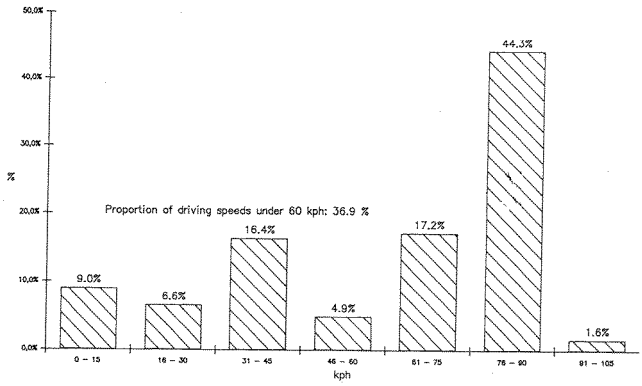

Figure 17. Truck/Car Motorway Accidents: Car Runs into Truck: Driving Speeds of Trucks Involved

Twelve of the 18 car drivers killed in truck/car motorway accidents died in rear-end collisions, and in 4 cases the trucks were driving at less than 60 kph. Straight roads are a typical feature of accidents with slowly moving trucks, and accidents up-hills are frequent (38%, Figure 18).

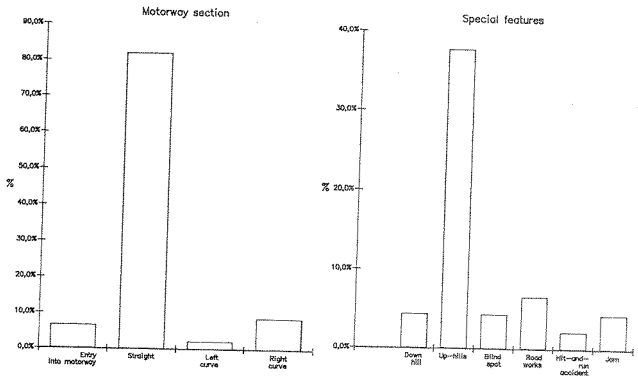

Figure 18. Truck/Car Motorway Accidents: Car Runs into Truck: Motorway Sections and Special Features

A characteristic accident of this kind can be seen in Figure 19. The truck, driving on the extreme right, was going uphills on the motorway at about 40 kph. The articulated truck's lighting was in accordance with the regulations and intact. The car driver coming up behind recognized the slowly moving articulated truck too late and ran into it from a speed of 120 kph almost without braking.

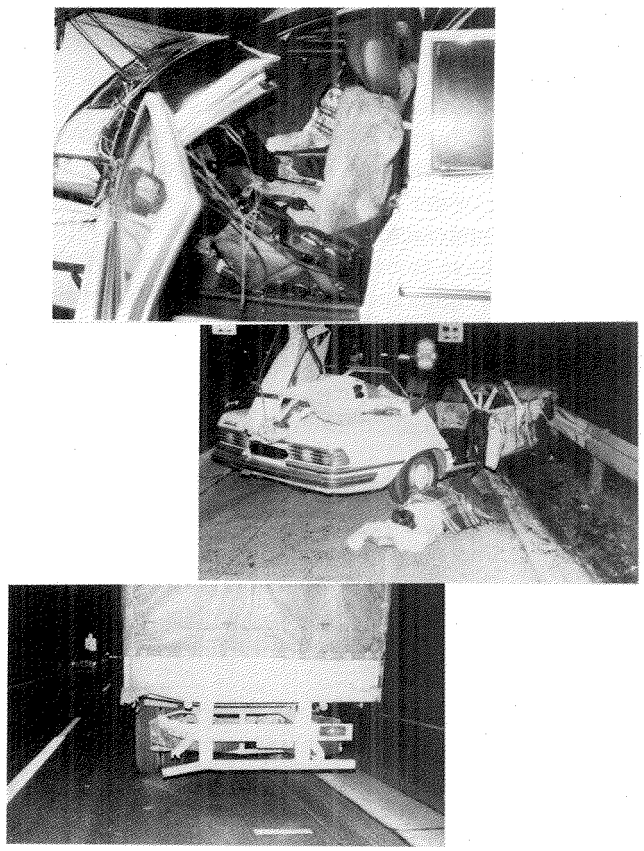

Figure 19. Serious Motorway Accident in which a Car Ran into the Rear-End of a Slowly Moving Truck (v = 40 kph)

The front of the car was badly damaged, and the roof was ripped off as far as to the C pillar. The front seat passenger and the rear occupant were killed; the driver survived because of the only slight overlap, though he was seriously injured. It can be clearly recognized from the retroreflective traffic signs in the background that the signal image of the truck was not satisfactory.

Common Characteristics of the Truck/Car Accidents

It was shown above that truck/car accidents differ considerably in their characteristics depending on the site of the accident. The truck population involved is also different. In accidents in the dark, however, a considerable increase in heavy trucks and articulated trucks can be observed—irrespective of the site of the accident. Both inside and outside built-up areas the number of articulated trucks goes up to 30%, and to 45% in motorway accidents.

At night three-quarters of the trucks involved in truck/car accidents outside built-up areas and on the motorway are heavy trucks of over 12 t.

The number of trucks driving without a trailer drops sharply. Thus night-time accidents are particularly a problem connected with articulated trucks and heavy trucks with a gross vehicle weight of over 12 t with trailers.

Countermeasures

Improving the visibility of trucks is not to be solely achieved by lighting installations. In addition also aerodynamic, electronic and spray-and-splash reducing measures are required. Aerodynamically trucks would have to be optimized with the aim of minimizing the amount of dirt deposited on the truck's rear section. The spray caused by the water thrown up by the wheels can be effectively counteracted by appropriate side guards, which would have to be mounted close to the wheels.

Unusual rear lights and numberplate lighting constitute a considerable danger for the traffic coming up behind. The truck driver should therefore be warned if a light bulb is not working, perhaps by means of an acoustic signal, to prevent him continuing on his way in spite of a defective lamp.

The objective should be to make obvious improvements to the lateral signal image of trucks. This can be done by both active and passive lighting equipment. A passive marking of the contours (Figure 20) would be preferable in that it would achieve a clear identification of the truck. The same applies to the rear-end of the truck.

Physiological processes make it very difficult for the traffic behind to recognize slowly moving trucks. For this reason an additional warning signal, for example a flashing yellow light, ought to be created which automatically warns the traffic coming up from behind when a truck falls below the minimum motorway speed. Another possibility would be the warning system used in Japan.

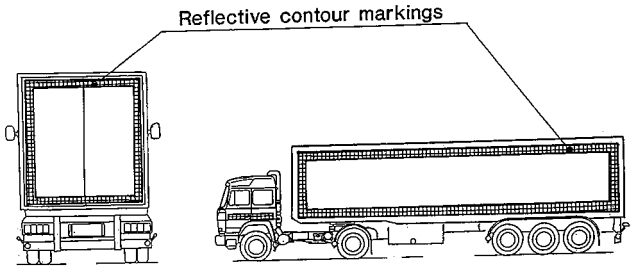

Figure 20. Reflective Contour Markings for the Side and Rear of Commercial Vehicles According to [6]

Commercial vehicles and especially their trailers have a long life. It would therefore be advisable to install this devices in vehicles already on the road.

Summary

The legal requirements for the signal image of trucks today constitutes the minimum standard. On the basis of nearly 1,400 truck/car accidents it was shown that especially in the case of truck-trailer combinations and articulated trucks their sides and rear-ends cannot be seen with adequate clarity.

30% of the truck/car accidents occur when visibility is restricted (darkness or dusk). About 34% of the car drivers killed in truck/car accidents die in accidents at night. In the dark there is a marked increase in the number of accidents car-front/truck-side and car-front/truck-rear.

Accidents caused by failure to keep a safe distance from the vehicle ahead are a problem which chiefly arises when visibility is restricted.

Only one-fifth of accidents in built-up areas are dusk or night-time accidents, whereas this proportion rises to over 40% in the case of motorway accidents.

The related accident risk "RAR" is a good measure of the actual risk distribution within a defined sample of accidents. In night driving by trucks outside built-up areas and on motorways it is 1.5 and 1.8 respectively, quite a high figure. Outside built-up areas collisions with the sides of the truck are clearly dominant in the night time (almost 40%), while on motorways rear-end collisions caused by cars (60%) form the bulk of night-time accidents.

Slowly moving trucks on the motorway are an additional risk. For car drivers approaching from behind it is a problem to recognize the low speeds of these vehicles. Trucks with a speed of under 60 kph are involved in 36% of the truck/car accidents on motorways.

From the point of view of accident research therefore not only an improvement in the lateral and rear signal image of the truck, for example by reflective contour markings, should be the aim, but a possible way should be created of pointing out to the traffic behind an especially slow commercial vehicle.

These measures of better conspicuity must be backed up by a reduction of the spray when it is raining, aerodynamic measures to reduce the dirtying of the truck's

rear and information for the truck driver on the state of his lighting and signalling equipment.

A restriction to new vehicles is not sufficient, since a complete renewal of the registered commercial vehicles takes well over a decade. It therefore appears to be a matter of urgency to apply these measures to commercial vehicles already on the road.

About 6% of all truck/car collisions with personal damage (trucks with a gvw of 3.5 t or more) are accidents in which the truck's inadequate signal image was a mayor cause of the accident. Extrapolated for the Federal Republic (before 3.10.90) a positive influence could be exerted on about 400 to 470 serious truck/car accidents with fatalities and injured persons by improving the signal image.

The measures outlined can therefore achieve a considerable reduction in truck accident figures. This will benefit not only the victims of accidents but also the national economy and, last but not least, the image of road haulage and the transport industry in particular.

References

1. A.P. Goudswaard, E.G. Janssen, P.J.A. de Coo: "Truck Front Underrun Protection," International IRCOBI Conference, Berlin, September 1991
2. Statistisches Bundesamt Wiesbaden: "Reihe 7, Straßenverkehrsunfälle 1989," Verlag Metzler-Poeschel, Stuttgart
3. Der Bundesminister für Verkehr: "Verkehr in Zahlen 1990," Bonn, September 1990
4. D. Heidemann, G. Ionescu: "Untergliederung von Jahresfahrleistungen in der Bundesrepublik Deutschland am Beispiel des Jahres 1985," BAST, Bergisch Gladbach 1988
5. Kraftfahrtbundesamt, Flensburg: "Bestand an Kraftfahrzeugen und Kraftfahrzeuganhängern am 1. Juli 1989," Kirschbaum Verlag, Bad Godesberg
6. H. Finsterer, H. J. Schmidt-Clausen: "Seitenbeleuchtung und rückwärtiges Signalbild von Lkw, Teil 2," Technische Hochschule Darmstadt 1990
7. H.-H. Meseberg: "Beeintrachtigung der Erkennbarkeit von retroreflektierenden Leiteinrichtungen durch fahrzeugspezifische Einflußgroßen," Der Verkehrsunfall, 6/88
8. R. Sagerer: "Messung der Sprühnebelbildung bei schweren Nutzfahrzeugen" ATZ 10/1990
9. M. Danner, K. Langwieder, H. Appel, V. Middelhauve: "Passive Safety Measures for Trucks—Effectiviness and Priorities" 12. ESV-Conference, Goteborg, May 1989
10. K. Langwieder, H. Bäumler: "Effizienz von Unterfahrschutzsystemen für Nutzfahrzeuge," internal paper of the HUK-Verband, February 1991
11. K. Langwieder, H. Bäumler: "Sicherheitsmaßnahmen am Lkw," 7. Internationale Tagung für Straßentransport und Verkehrssicherheit, Budapest, September 1990
12. Amos J. Cohen: "Möglichkeiten und Grenzen visuellerWahrnehmung im Straßenverkehr, Teil I: Wahrnehmung und Schätzung von Geschwindigkeiten," Schriftenreihe Unfall- und Sicherheitsforschung im Straßenverkehr Nr. 57, 1986, Herausgeber BAST, Bergisch Gladbach
13. H. Bubb: "Analyse der Geschwindigkeitswahrnehmung im Kraftfahrzeug," Zeitschrift für Arbeitswissenschaft 31/1977

S10-O-03

Improving HGV Safety—Front Underrun Guards and Anti-Lock Braking Systems

B.J. Robinson, B.S. Riley
Transport and Road Research Laboratory

Abstract

The Transport and Road Research Laboratory has been working to improve the safety of Goods Vehicles for many years. The most recent areas of research have included front underrun guards and anti-lock braking systems. The results of this research are presented and discussed. For a front underrun guard to be fully effective in full frontal and offset frontal impacts, the TRRL research has found that it should be positioned to have a ground clearance no greater than 400 mm. There were approximately 800 fatal accidents involving HGVs in Great Britain in 1988. Two samples of the Police records of these accidents have been analyzed. The results are presented and, in combination with the TRRL track research, used to estimate the potential life-saving benefits of the proposed safety improvements. The analyses have found that front underrun guards fitted to all HGVs in Great Britain would probably save about 80 lives each year. Anti-lock braking systems are likely to save around 70 lives each year.

Introduction

There have been two main areas of research into improving the safety of Heavy Goods Vehicles (HGVs) at the Transport and Road Research Laboratory (TRRL) in recent years. The first part of this paper sets out to describe the work carried out on the impact performance and injury reduction potential of front underrun guards. This is followed by a discussion of research into the

performance and possible accident avoidance benefits of anti-lock braking systems for HGVs.

Front Underrun Guards

Many car occupants are killed when their vehicles impact the front of a lorry. The high front structure of many HGVs allows the much lower bonnet structure of a car to run underneath. This often results in massive intrusion of the lorry into the car's occupant compartment, even at quite low closing speeds. An underrun guard can lower the effective front structure of the lorry, thus preventing cars running underneath, allowing the front structure (crumple zone) of the car to absorb energy and greatly reducing the intrusion and likelihood of fatal or serious injury to the car's occupants.

Work on the construction of energy absorbing underrun guards, their performance in head on frontal car impact tests and potential legislative test procedures has been discussed previously (1,2). Since these reports were published, many more full scale impact tests have been carried out on the TRRL track. The performance of energy absorbing guards in offset frontal collisions has been investigated, as has the effects of using rigid guards and varying the ground clearance of those guards. The results of this research are discussed in this paper.

More recently a sample of about 570 of the 800 Police reports into fatal accidents involving Heavy Goods Vehicles in Great Britain in 1988 has been examined by TRRL. A detailed study of those accidents involving car occupants killed in frontal collisions with HGVs has been undertaken for TRRL by the Accident Research Unit of the Institute for Consumer Ergonomics (ICE). Each accident has been studied in order to assess whether a rigid underrun guard fitted to the front of the HGV involved could have prevented any or all of the fatalities. The results of this work are also presented and discussed in this paper.

Anti-Lock Braking Systems

When an articulated heavy goods vehicle is being braked, instability or longer than necessary stopping distances can result if some or all of the wheels lock. If the steered wheels lock a loss of steering control will be encountered. If the rear wheels of the tractor unit lock there will be a possibility of jack-knifing. Often confused with jack-knifing, but in fact quite different, is trailer swing. This can occur when all the wheels of a semi-trailer lock. Rigid HGVs can also experience loss of control or instability when some or all wheels lock.

An anti-lock braking system can overcome these stability problems by not allowing the wheels to lock under braking. Minimum stopping distances will be obtained if the system can keep the wheels at the point of maximum tyre to road adhesion, but because an anti-lock system removes the braking during part of its cycle it is also possible that anti-lock can cause longer stopping distances than normal braking.

Track tests of two common types of articulated HGV anti-lock system have been carried out. The effects on stopping distances and vehicle stability under heavy braking have been assessed and are discussed in this paper.

The destructive power of an HGV which is out of control due to wheel lock is self evident. A further sample from the accident files described in the previous section has been analyzed at TRRL. For each accident considered, an assessment has been made as to whether the fitting of a typical anti-lock system to the HGV involved could have either prevented the accident from happening or reduced its severity. In making this assessment the results of the track tests at TRRL have been used to justify the assumed performance of an HGV fitted with anti-lock. The accident data analysis results are presented and discussed later in this paper.

Front Underrun Guards—Laboratory Tests

Offset Frontal Impacts with Energy Absorbing Guard

Five tests have been carried out involving various cars impacting the front edge of a Ford D Series truck. The test configuration is shown in Figure 1. To reduce the repairs needed between tests, the cars were impacted into the near-side front of the lorry, thus preventing damage to the lorry's steering system. For all tests the stationary truck was impacted by the car travelling at about 64 km/h (40 mph). The overlap on the truck front was approximately 350 mm.

Figure 1. Test Configuration

Four of the tests involved a truck fitted with the TRRL energy absorbing front underrun guard, the remaining test being with a conventional, unprotected truck. When used the guard was positioned to have a ground clearance of 300 mm. The various impact combinations are shown in Table 1.

The cars were carrying seat belted OPAT dummies in the driver's and front passenger's seats. The dummy in the passenger seat was instrumented with accelerometers, as was the car structure. Each impact was filmed using high speed cameras. These films provide the best guide

Table 1. The Test Vehicles

Test No.	Car	Weight of car (kg)	Underrun guard on truck
1	Renault 5	780	Yes
2	Morris Ital	970	Yes
3	Vauxhall Cavalier	1040	Yes
4	Ford Granada	1185	Yes
5	Renault 5	780	No

to the severity of each impact in terms of intrusion into the car's passenger compartment and the likely occupant injuries resulting. The important results from these tests are presented and discussed in this section.

Results. Figure 2 shows the aftermath of Test No. 1, involving a truck fitted with an underrun guard being impacted by a Renault 5 at a closing speed of approximately 64 km/h. Although the Renault has suffered considerable damage, it is clear that there has not been any contact between the truck structure and the car's A-post. Most of the impact energy was absorbed by the front structure of the Renault. Utilizing this energy absorption capability ensured that the passenger compartment suffered only minor intrusion in this test. It can be assumed that the occupants of such a vehicle, if such a collision had occurred in real-life, would have a high probability of survival if an effective restraint system was used.

Figure 2. Test No. 1—Renault 5, Underrun Guard Fitted to Truck

Figure 3, on the other hand, shows the results of a similar impact between a truck not fitted with an underrun guard and a Renault 5 (Test No. 5). Massive damage has been sustained by the Renault, particularly in the upper bonnet, windscreen and A-post region. It is clear that the main truck structure has impacted this area of the car, causing substantial intrusion into the occupant compartment. The chances of survival for the front seat passenger in this collision would be very low, even if a good restraint system had been used.

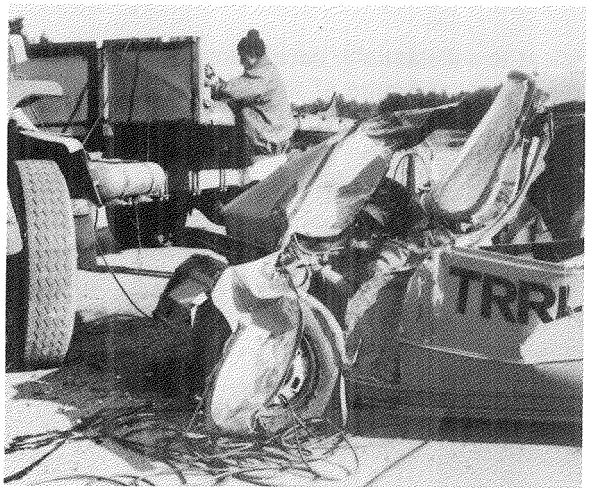

Figure 3. Test No. 5—Renault 5, No Underrun Guard

The remaining tests involved other car types impacting the truck fitted with an underrun guard. Figure 4 shows a typical result. The underrun guard allowed the energy absorbing front structure of the cars to be properly utilized, thus preventing impact of the truck structure into the windscreen and A-post region and minimizing intrusion into the cars' occupant compartments.

Figure 4. Test No. 4—Ford Granada, Underrun Guard Fitted to Truck

Figures 5 and 6 compare results from instrumentation used in Tests 1 (Renault 5, underrun guard on truck) and 5 (Renault 5, no guard). Figure 5 shows the deceleration of the car structure, measured at the base of the near-side B-post. There is a wide variation in the traces from Tests 1 and 5 in the first 60 ms of impact. Test 1, with an underrun guard fitted to the truck, shows that the car was being heavily decelerated from an early stage in the impact. This corresponds to the front of the car crushing, and absorbing energy, as it struck the underrun guard. Test 5, on the other hand, shows that substantial amounts of energy were not absorbed until after 60 ms into the impact. This is because in these early stages the truck only contacted the top of the car's bonnet. This was not

sufficient to substantially decelerate the car. Only when the main front structure of the car hit the truck's front near-side wheel (around 40-60 ms) did the car begin to decelerate heavily. By this time the front structure of the truck was starting to enter the occupant compartment at windscreen level. The trace from Test 5 has a further small peak at around 200 ms. This may correspond to the car turning the truck's front wheel round to full lock, at which point a higher resistive force would be transferred to the car.

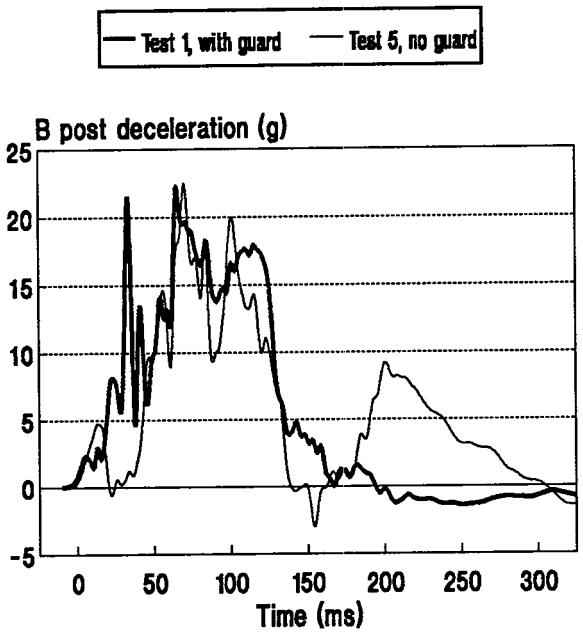

Figure 5. B-Post Deceleration—Tests 1 and 5

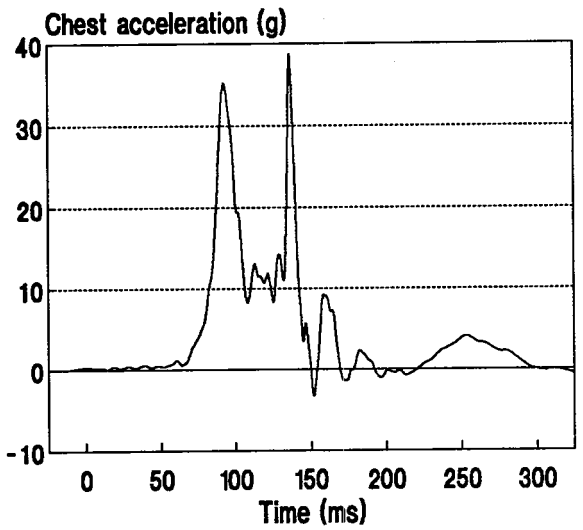

Figure 6. Chest Acceleration—Test 5

Figure 6 shows the chest acceleration, measured in the fore-aft direction, of the front passenger in Test 5, with no underrun guard fitted. The second distinct peak indicates that after the front of the car hit the truck's front wheel the front structure of the truck entered the car's occupant compartment and struck the front seat passenger. Any occupants seated in this position would almost certainly suffer very serious or fatal injuries in a real-life collision of this type.

Previous studies by the Transport and Road Research Laboratory and reported to ESV conferences (1,2) have shown the benefits of energy absorbing underrun guards in head-on frontal impacts between lorries and cars. The series of tests described here shows the potential benefits of properly designed front underrun guards in reducing the injury severities of car occupants involved in offset frontal collisions with lorries.

Head on Impacts to Assess Effects of Ground Clearance

Two tests have been conducted with Ford Fiestas impacting a truck fitted with a strengthened and lowered bumper. The main purpose of these tests was to measure the effects of different underrun guard ground clearances. The ground clearances used were 400 mm and 500 mm. In order to provide the most realistic impact situation, both the car and truck were moving towards each other prior to impact at speeds of about 30 km/h, making a closing speed of 60 km/h. The results and lessons learnt in terms of acceptable ground clearance are given in this section.

Results. The first test involved an impact between a Ford Fiesta and a truck fitted with a rigid underrun guard at a ground clearance of 400 mm. The high speed film showed that the energy absorbing structure of the car was utilized and there was no indication of the truck riding up over the bonnet of the car. The occupants were thus well protected in this situation.

The second test was a repeat of the first but with an underrun guard ground clearance of 500 mm. The high speed film shows that although the guard did just prevent the main truck structure from impacting the car's A-posts, there was still clear evidence of the car underrunning the truck. A slightly higher closing speed or lower car structure would have almost certainly led to substantial intrusion into the car's occupant compartment. Although the occupants were protected in this situation, their margin of safety was very small.

These tests indicate that for underrun guards to be properly effective in all frontal impact configurations between lorries and cars they should be positioned to have a ground clearance well below 500 mm. In one test conducted at 400 mm, and several at 300mm, the guards have been found to be effective. To maximize the number of car occupants that can be protected, including those in very low sports type cars, the ground clearance should be as low as practically possible.

Front Underrun Guards—Overall Summary of Laboratory Tests

Many test impacts between cars and lorries fitted with various underrun guards have been carried out, both in the UK and elsewhere (3). All such studies have concluded that lowering the front structure of trucks in order

to prevent underrun can greatly improve the survival chances of car occupants involved in such crashes.

The tests at the Transport and Road Research Laboratory described in the preceding sections confirm these findings. At the test impact speeds of around 64 km/h the survival chances for front seat, struck-side, car occupants in offset collisions with unprotected trucks are very low. With underrun guards, the survival chances in otherwise identical impacts are much improved, especially for seat belted occupants. The research found that an underrun guard with a ground clearance of 500 mm is not fully effective. At a height of 400 mm the guard was found to be beneficial, though for good protection a ground clearance nearer 300 mm is preferable.

Front Underrun Guards—Accident Data

Proposals for front underrun guards to be introduced into international regulations have been made. To complement these proposals the Transport and Road Research Laboratory and the UK Department of Transport felt it necessary to get an up to date measure of the likely fatality prevention benefits of the widespread fitting of front underrun guards in the UK Heavy Goods Vehicle fleet. Studies conducted in 1981 (4) and 1985 (1) of fatal HGV accidents occurring in 1976 concluded that around 40-80 lives could be saved each year in the UK by underrun guards if all car occupants wore seatbelts. The results of a recent study of fatal HGV accidents in 1988 are described in the following sections.

Overall HGV Accident Situation

In 1988 there were approximately 802 fatal accidents involving at least one HGV in Great Britain. Information on all these accidents is held in the UK's Road Accident Statistics database, STATS 19. Permission was obtained from the Association of Chief Police Officers (ACPO) for the Transport and Road Research Laboratory to obtain the Police reports into the fatal accidents involving Heavy Goods Vehicles in 1988 from all the Police forces in England and Wales, excluding the London Metropolitan area. These Police reports often contain a great deal of useful information, including witness statements, vehicle examiners' reports, Post-Mortem reports and photographs of the vehicles and accident scene.

568 fatal accident reports have been analyzed, representing over two-thirds of the total number of such HGV accidents in 1988. The indications are that 1988 was fairly typical for HGV accidents and hence conclusions drawn from a sample of accidents in that year can be assumed to be applicable in other recent years. In 39 of these 568 accidents either the HGV was not involved in the major impact or the accident did not involve any vehicle over 3500kg Gross Vehicle Weight. A breakdown of the remaining 529 accidents is shown in Table 2.

Table 2. Accident Types within Sample

Road user type killed	No. of accidents	(%)	No.of fatalities
Car occupant	269	(51)	326
Pedestrian	99	(18)	99
Motorcycle rider	55	(10)	59
HGV occupant	51	(10)	52
LGV occupant	30	(6)	38
Pedal cycle rider	22	(4)	22
Other	4	(1)	4
TOTALS	530 *	(100)	600

* 1 accident involved HGV and LGV occupant fatalities

Of the car occupant fatality accidents, 25 were such that the car to HGV collision was not the only major impact involving the car. The remaining 244 accidents involved a car to HGV collision that directly resulted in the death of one or more of the car occupants. The total number of fatalities in this group was 295. Table 3 relates these figures to the overall Great Britain accident situation.

Table 3. Likely HGV/Car Situation in Great Britain

Accident type	No. of accidents in sample	No. of accidents in Great Britain in 1988
All HGV fatal accidents	568	802
HGV directly involved	529	747 (E)
HGV/Car impact directly causing car occupant fatality	244 (295 fatalities)	345 (E) (417 (E) fatalities)

(E) - Estimated

Car to Front of Lorry Accidents

The configurations of the 244 car to HGV impacts were also found. 180 (74 per cent) involved the car impacting the front of an HGV. 219 car occupants were killed as a result of these impacts. In Great Britain overall we can therefore estimate that there were about 250 fatal car to front of lorry impacts, involving some 300 car occupant deaths. It is this figure which front underrun guards for trucks aim to reduce.

Of the 180 car to front of lorry accidents contained within the sample, 80 were chosen for detailed analysis because they included photographs of the vehicles and accident scene and Coroner's Post Mortem reports. Post Mortem reports contain detailed information on all the injuries sustained by the fatality. The resources allocated for the analysis of these files were sufficient to allow a further 15 files, chosen at random from those that contained photographs but no Post Mortem details, to be analyzed. In total, therefore, 95 files have been analyzed in detail. The main purpose of this analysis was to ascertain how many of the fatalities caused by cars impacting

the front of lorries could have been prevented by the fitment of a rigid underrun guard with a ground clearance of between 300 and 400 mm.

The Transport and Road Research Laboratory appointed the Accident Research Unit of the Institute for Consumer Ergonomics, Loughborough University, to conduct the analysis. Reference 5 contains all the detailed results of the study. Some of their most important results are presented here.

Results. There were 111 fatally injured car occupants in this subsample of 95 accidents, with a further 35 sustaining non-fatal injuries. 99 of the fatalities were seated in the front of the car. 66 of these were known to be wearing seat-belts, 12 were known to be unrestrained. The restraint use of the remaining 21 was unknown. Only 1 of the 12 rear seat occupants was known to be restrained, 9 were known to be unrestrained.

For each fatality three assessments of benefits were made. The baseline assumed that all the car occupants were unrestrained and that all HGVs were not fitted with underrun guards. The potential benefit of restraining all the occupants was then assessed. Second, the potential benefit of fitting underrun guards to all the HGVs but having all car occupants unrestrained was assessed. The final assessment assumed that all occupants were restrained and all HGVs had underrun guards.

All assessments were made on a 4-point scale from definite fatality prevention, through high probability of prevention, low probability and on to definitely not prevented by the countermeasure being considered.

The results of these three assessments were then used to find the potential benefit of fitting underrun guards to HGVs for all the car occupants in the sample. For the 23 car occupants whose restraint use was unknown, it was assumed that 85 per cent (18) of the 21 occupants in the front seats were actually restrained. This corresponds to the proportion of front seat occupants whose restraint use was known (78) that were restrained (66). Only 10 per cent of rear seat occupants were known to be restrained so it was assumed that the 2 such occupants in the sample whose restraint use was unknown were both unrestrained.

Table 4 shows the results, broken down according to restraint use, both known and assumed, and probability of fatality prevention.

Table 4. Net Benefits of Underrun Guard Fitment to Car Occupant Fatalities

	Definite prevention	High probability	Low probability	Definitely not prevented	Not known	TOTAL
Restraint use known						
Restrained	7	12	20	25	3	67
Unrestrained						
Front	1	1	1	8	1	12
Rear	1	2	3	3	-	9
Restraint use N/K						
Front assumed restrained	2	3	5	7	1	18
Front assumed unrestrained	-	-	1	2	-	3
Rear	-	-	-	2	-	2
TOTAL	11	18	30	47	5	111

In the cases where restraint use was not known the benefit figures have been calculated from proportions derived from either the study whereby all car occupants were assumed to be restrained and the benefits of underrun guard fitting were assessed or from the assessments made whereby all car occupants were assumed to be unrestrained and underrun guards fitted to the trucks.

In order to estimate the potential fatality reduction of the fitting of front underrun guards to all HGVs in Great Britain, the above sample values need to be multiplied by an appropriate factor.

The sample of 95 accidents represents 53 per cent of the 180 car to front of lorry impacts in the sample. The accident sample of 529 cases represents 71 per cent of the 748 fatal accidents involving at least one HGV over 4 tonnes GVW in Great Britain (England, Wales and Scotland) in 1988. The figure 748 includes an appropriate proportion of those accidents occurring in the London Metropolitan area calculated using STATS 19 data. Thus the weighting factor required is:

$$\frac{1}{0.53 \times 0.71} = 2.7$$

Table 5 shows the estimated benefits of underrun guard fitting in Great Britain. The 'minimum number' is deduced solely from the 'definite prevention' column of Table 4.

Table 5. Summary of Reductions in Car Occupant Fatalities in the Sample and in Great Britain as a Result of Underrun Guard Fitting

Estimate	No. in sample	No. in Great Britain
Minimum Number	11	30
Best Estimate	**32**	**86**
Maximum Number	59	159

In order to obtain a 'best estimate' of the likely numbers of fatalities prevented by underrun guards, each of the two groups of possible benefit were allocated a probability of survival. 75 per cent of those judged to have a high probability of benefit were expected to survive along with 25 per cent of those with a low probability. The best estimate is found by adding the 11 definite cases to 0.75 x 18 high probability cases to 0.25 x 30 low probability cases. This equals 32 fatalities within the sample and 86 when weighted nationally.

The 'maximum number' is derived by assuming that all the fatalities in the definite, high probability and low probability categories would survive.

The "Best Estimate" would suggest that over 80 lives could have been saved by the fitting of underrun guards to all HGVs in Great Britain in 1988. This represents about 30 per cent of the fatalities sustained in car to front of lorry impacts and about 20 per cent of all fatalities in car to lorry impacts.

Front Underrun Guards—Overall Summary of Accident Data

Studies by TRRL of 1976 accident data concluded that up to 80 lives could be saved by front underrun guards each year if all car occupants wore seat-belts. The actual seat-belt wearing rate in the late 70s was probably only about 10-20 per cent. So at that time the widespread introduction of front underrun guards for trucks might actually only have prevented 15 fatalities per year.

Since then seat-belt wearing has been made compulsory for both front and rear car passengers. The wearing rate for front seat occupants is currently near 95 per cent (6). The potential for fatality reduction by underrun guards should therefore be much greater now. The study of 1988 data described above confirms this, concluding that around 80 lives could actually be saved annually.

Gloyns and Rattenbury reported in 1989 (7) on a detailed study of 40 car occupant fatalities killed in front of car to front of lorry impacts during the three year period up to March 1985. They estimated that about 38 per cent of such fatalities could be saved by front underrun guards if all car occupants wore seat-belts. No estimates were made for those car occupants involved in rear or side of car impacts. The study of 1988 data conducted by ICE for TRRL estimated that 45 per cent of the 62 occupants killed in front of car to front of lorry impacts within the sample could be saved by front underrun guards if all wore seat-belts. So there is quite strong agreement between the results of these two studies. Both clearly demonstrate that the widespread fitting of front underrun guards could greatly reduce the annual toll of death and serious injury sustained in car to front of lorry accidents.

Anti-Lock Braking—Laboratory Tests

Tests have been conducted on three HGV anti-lock braking systems, described below. The main purpose was to investigate how well the anti-lock systems could prevent braking instabilities such as jack-knifing and trailer swing. Tests were also conducted to establish if the systems had any adverse effect on stopping distances. Reference 8 gives the main results of this study, but a summary of the most important results is presented in this section.

The Vehicles and Anti-Lock Systems

The test vehicles used were:

- Leyland Roadtrain twin axle tractor unit coupled to a York triaxle semi-trailer.
- DAF FT350 twin axle tractor unit coupled to the same York triaxle semi-trailer.

The Roadtrain was fitted with a Girling Skidchek GX, "Category 2," anti-lock system. With this "select low" system, the pressure to the single air line to each axle is determined by whichever wheel on that axle starts to lock first. The presence of imminent wheel lock is detected by sensors on each wheel, which pass signals to an Electronic Control Unit (ECU). This unit adjusts the braking pressure accordingly.

The DAF was fitted with a more complex Girling Skidchek DGX system. This also has wheel speed sensors passing signals to an ECU, but this ECU can adjust the brake pressures to each wheel independently. This is known as a "Category 1" system. This is the most complex type of HGV anti-lock currently available. Under European law it will soon be required on nearly all new tractor units.

The York triaxle semi-trailer was fitted with a Girling Skidchek MGX system. This is a select low system similar in principle to the GX system fitted to the Roadtrain. Although this system's ECU controls the brake pressures to all three axles, it only receives wheel speed information from two sensors mounted on the middle axle wheels.

Each vehicle combination was tested with the following loading conditions:

- Tractor unit only. Each unit weighed about 7 Tonnes.
- Tractor and unladen trailer. Each unit weighed about 14 Tonnes.
- Tractor and laden trailer. Each unit weighed about 38 Tonnes.

Test Procedures

Braking tests were performed on various surfaces and at various initial speeds. The test surfaces used were a wet gravel (a rounded flint gravel from Bridport which gives a low coefficient of friction), wet Fine Textured Asphalt (FTA) and dry FTA. All the testing was performed in a straight line, with the test speeds increasing from 20 km/h up to 60 km/h in 10 km/h increments. Testing was conducted on all the single, that is uniform, surfaces. In addition, split surface tests were conducted with the vehicle straddling the border between the wet FTA and the low friction wet "Bridport." In this condition the left hand wheels of the vehicle combination are on one surface, while the right hand wheels are on the other at the start of braking.

During the test runs the driver approached the appropriate test surface at the required speed and applied the service brake as hard and as fast as possible. In this way an emergency stop was simulated. To avoid possible injury to the driver and damage to the tractor unit in the event of a jack-knife, a check rope was fitted between tractor and semi-trailer which limited the rotation of the tractor to about 70 degrees.

The tractor units were equipped with a small speed measuring wheel and control box. This box was positioned in the cab and gave a display of vehicle speed. A micro-switch mounted on the brake pedal caused the speed display to freeze as soon as the pedal was depressed. Another display on the control box then showed the braking distance. Thus at the end of each test run a

note of the exact speed upon application of the brakes and the stopping distance could be made. This information was used to calculate the average deceleration for each test run.

Results

Although many combinations of anti-lock on various axles were tested, only the following are considered for the purposes of this paper:

- Full anti-lock on both tractor unit axles and, when used, on the semi-trailer, sensed from the middle axle.
- No anti-lock, that is all anti-lock systems inoperative but with the conventional braking system working normally.

Stopping distances. Some of the results from the single surface braking tests are shown in Figure 7. On the wet "Bridport" surface, both the Category 2 system fitted to the Roadtrain and the Category 1 system fitted to the DAF were able to give higher decelerations, that is shorter stopping distances, than could be obtained from the same vehicles with their anti-lock systems disconnected. Jack-knifing instabilities occurred in some tests on the "Bridport" when the systems were disconnected. There were no instabilities when the systems were operating. On the FTA surfaces there was no consistent difference between the with and without anti-lock conditions.

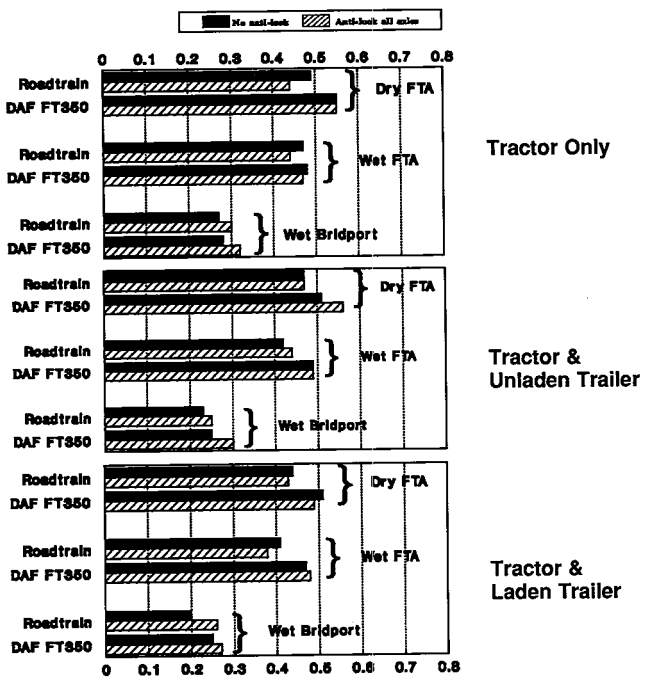

Figure 7. Average Deceleration (g) When Stopping from 60 km/h (50 km/h for Roadtrain on Dry FTA)

Overall it can be concluded that none of the anti-lock systems tested are likely to have a markedly adverse affect on the stopping distances of the vehicle to which they are fitted. On slippery surfaces, such as the wet "Bridport," the systems are in fact likely to give shorter stopping distances.

Braking instability. In the wet "Bridport"/wet FTA split surface tests both types of tractor anti-lock and the trailer anti-lock were very successful at preventing braking instabilities. With the anti-lock systems disconnected, both vehicle combinations were subject to violent jack-knifing and trailer swing at speeds as low as 30 km/h. When the anti-lock systems were connected, however, all the tractor and trailer combinations, under all loading conditions, could be brought to a rapid stable halt when braked heavily on the split surface. All braking instabilities were completely eliminated.

Summary

In estimating the accident avoidance or severity reduction potential of anti-lock, it is necessary to know how HGVs equipped with anti-lock perform in comparison to those without. The tests described here indicate that the greatest potential for accident prevention is in those accidents involving braking instabilities, such as jack-knifing or trailer swing. Stopping distances are not substantially affected by anti-lock, so there is less potential for severity reduction in accidents involving straight line braking on uniform surfaces. Although not investigated here, it is known that by preventing lock-up of the steered wheels, anti-lock systems enable the driver to steer while braking heavily. This also gives rise to accident avoidance and severity reduction potential.

The following sections present the findings of a study by TRRL of 100 fatal HGV accidents to find the possible benefits of widespread use of HGV anti-lock.

Anti-Lock Braking—Accident Data

The Accident Sample and Analysis Procedure

As described earlier, the Transport and Road Research Laboratory has acquired the Police reports into 568 of the 802 fatal accidents involving one or more HGVs in Great Britain in 1988. A breakdown of the sample by accident type is given in Table 2. A sample of 100 accidents was analyzed to find the potential benefits of fitting anti-lock to the HGVs involved. This sample consisted of the correct proportion of each accident type, as set out in Table 2. All the accidents within these groups were chosen at random from an initial sample of 387 fatal HGV accident files containing photographs of the scene and vehicles involved.

Each Police report contained detailed information on the possible causes of the accident, including witness statements, photographs, accident investigation reports, vehicle examiner's reports, and scale plans of the accident scene. This information was analyzed for all 100 accidents in the sample. After reading each file, an assessment was made of whether or not the accident could have been either prevented completely or reduced in severity to non-fatal by the fitting of anti-lock to the HGVs. There is always some degree of uncertainty when

trying to answer questions of this type, so the answers were grouped into orders of probability. There were four categories of probability:

- Accident *definitely* prevented or reduced in severity to non fatal by use of anti-lock brakes on HGV.
- Accident *probably* prevented or reduced in severity to non fatal by use of anti-lock on HGV.
- Accident *possibly* prevented or reduced in severity to non fatal by use of anti-lock on HGV
- Accident not prevented or reduced in severity by use of anti-lock on HGV.

The 100 accidents, in which there were 117 fatalities, involved 104 HGVs, 53 of which were rigid and 51 articulated.

The Results

The results, in the form of number of accidents considered preventable by anti-lock, are given in Table 6. The final column also shows the number of accidents considered possibly or probably able to be reduced in severity to non-fatal. There were no cases that were assessed as definitely able to be reduced in severity.

Table 6. Benefits of HGV Anti-Lock Braking Systems

	NUMBER OF ACCIDENTS					
Road user type killed	In sample	Definitely prevented	Probably prevented	Possibly prevented	Probably reduced in severity to non-fatal	Possibly reduced in severity to non-fatal
Car occupant	51	3	1	1	1	2
Pedestrian	18	1	-	2	-	-
Motorcycle rider	10	-	-	-	-	-
HGV occupant	10	-	1	1	-	-
LGV occupant	6	-	-	-	-	-
Pedal cycle rider	4	-	-	-	-	-
Other	1	-	-	-	-	-
TOTALS	100	4	2	4	1	2

Of the 4 accidents that could definitely have been prevented by anti-lock, 3 involved trailer swing. All these accidents occurred with unladen trailers on wet roads. The remaining case involved a rigid HGV whose driver braked heavily to avoid a pedestrian stepping off the curb. He attempted to steer around the pedestrian, but his front wheels had locked. With an anti-lock system the driver would have been able to steer enough to avoid the pedestrian.

The 9 vehicles involved in the accidents that could probably or possibly have been prevented or reduced in severity by anti-lock consisted of 5 rigids and 4 articulated lorries. In 6 of these accidents, the fitting of anti-lock might have prevented the accident altogether. In the remaining 3 cases anti-lock might have allowed enough steering control to avoid a fatal collision, but not to completely avoid any impact.

The accident assessed as having a high probability of being reduced in severity involved a lorry braking heavily to avoid a stationary car in the road ahead. This rigid vehicle went out of control and after hitting the rear of the first car impacted an oncoming car, killing its driver. Anti-lock would probably have allowed enough steering control to keep the lorry on its correct side of the road, though the first, non-fatal, impact would still have occurred.

The accidents assessed as having a low probability of severity reduction both involved a car pulling out from a side turning into the path of a lorry travelling on the major road. In each case the lorry, under emergency braking, impacted the off-side of the car's occupant compartment, killing the driver. With anti-lock, the lorry driver might have been able to steer sufficiently to avoid direct impact with the driver's door area.

Overall, anti-lock could have prevented as many as 10 (10 per cent) of the accidents analyzed, and reduced in severity a further 3. If a probability of 0.75 is allocated to the "probable" cases and 0.25 to the "possible" cases then a "best estimate" can be found by summing the 4 definitely prevented cases, 0.75 x 2 probably prevented and 0.25 x 4 possibly prevented, namely 7 fatal accidents avoided. A similar sum with the severity reduction cases indicates that a further 1 accident is likely to be so affected.

There were 802 fatal HGV accidents in Great Britain in 1988, involving about 900 fatalities, so multiplying the above figures by 8 will give a rough guide to the benefits of fitting anti-lock to all HGVs in Great Britain. Around 56 (7 per cent) of these accidents might be prevented and a further 8 might be reduced in severity to non-fatal, making a total of 64 accidents affected. Assuming 1988 was a fairly typical year, if anti-lock can prevent fatalities in 64 accidents, then around 70 lives might be saved each year in Great Britain.

Conclusions

Conclusions—Front Underrun Guards

- Impact tests have been carried out to assess the degree of protection offered to car occupants by front underrun guards in offset frontal impacts at a closing speed of approximately 64 km/h.
- An energy absorbing guard, positioned to have a ground clearance of 300mm, prevented severe occupant compartment intrusion in all the tests in which it was used.
- Two tests at closing speeds of roughly 60 km/h have been conducted to assess the effects of varying ground clearance on underrun guard performance. A properly designed underrun guard can protect seatbelted car occupants in full frontal and offset frontal impacts at closing speeds in excess of 60 km/h if it is positioned to have a ground clearance no greater than 400mm.
- 95 police reports of car to front of lorry fatal accidents have been studied by an independent consultancy. It has been estimated that if all the Heavy Goods Vehicles involved had been fitted with a full-width rigid underrun guard with a ground clearance of between 300 and 400mm, then 30 per cent of the 111 fatalities would probably have been prevented.

- If 30 per cent of all car occupant fatalities in frontal collisions with lorries can be prevented, then around 80 lives could be saved by underrun guards each year in Great Britain.

Conclusions—Anti-Lock Braking Systems

- Straight line braking tests have been conducted with various tractor and semi-trailer combinations on various surfaces. Three different anti-lock braking systems have been assessed.
- The systems did not have any seriously adverse effect on stopping distances. On the slippery wet "Bridport" surface the vehicles actually gave shorter stopping distances with their anti-lock systems functioning than with them disabled.
- The systems eliminated jack-knifing and trailer swing instabilities on all surfaces, including a split grip surface combination.
- A stratified sample of 100 police reports of fatal accidents involving Heavy Goods Vehicles has been analyzed to assess the potential benefits of widespread fitment of anti-lock to HGVs. It has been estimated that between 4 and 13 per cent of the fatal accidents in the sample could have been either prevented or greatly reduced in severity had the HGVs involved been fitted with anti-lock. If the 13 per cent figure is used, anti-lock on HGVs might result in 120 lives being saved each year in Great Britain. A more conservative estimate, however, suggests that around 70 lives might actually be saved.

Acknowledgements

The work described in this paper forms part of the programme of the Transport and Road Research Laboratory and the paper is published by permission of the Director. Thanks are due to Pete Thomas and Lawrence Clift at the Institute for Consumer Ergonomics for their efforts in the study of front underrun accidents, and to the TRRL personnel involved in the lorry impact tests and braking tests.

References

1. Riley, B.S., S. Penoyre and H.J. Bates, *Protecting Car Occupants, Pedestrians and Cyclists in Accidents Involving Heavy Goods Vehicles by Using Front Underrun Bumpers and Sideguards*. Proceedings of the Tenth International Technical Conference on Experimental Safety Vehicles, Oxford 1985.
2. Riley, B.S., A. J. Farwell and T.M. Burgess, *Front Underrun Guards for Trucks*. Proceedings of the Eleventh International Technical Conference on Experimental Safety Vehicles, Washington 1987.
3. Gruettert, S., V. Middelhauve, H. Appel, K. Langwieder and M. Danner, *Truck Front-end Protection Systems*. Proceedings of the Twelfth International Technical Conference on Experimental Safety Vehicles, Gothenburg 1989.
4. Riley, B.S., B.P. Chinn and H.J. Bates, *An Analysis of Fatalities in Heavy Goods Vehicle Accidents*. Department of the Environment, Department of Transport, TRRL Report LR1033, Crowthorne, Transport and Road Research Laboratory, 1981.
5. Thomas, P. and L. Clift, *Analysis of Fatal Accidents Involving Heavy Goods Vehicles—Front Underrun Accidents in 1988*. Department of Transport, TRRL Contractor Report CR289, Crowthorne, 1991.
6. Department of Transport, *Road Accidents Great Britain 1989—The Casualty Report*. HMSO, London 1990.
7. Gloyns, P.F. and S.J. Rattenbury, *Cars in Conflict with Larger Vehicles—The Problem of Under-Run*. SAE Paper No. 890746, SAE International Congress & Exposition, Detroit, Michigan, 1989.
8. Riley, B.S., J. Cobb and B.J. Robinson, *Vehicle Primary and HGV Secondary Safety*. Proceedings of SAFETY 91, Transport and Road Research Laboratory, Crowthorne, 1991.

S10-O-04

Passenger Protection in Single and Double-Decker Coaches in Tipping Over

P. Botto, M.C. Caillieret, A. Patel
Institut de Recherches Orthopédiques
C. Got
Institut de Recherches Biomécanique et Accidentologique
C. Tarrière
Renault

Abstract

This paper is based on the accidentology study of 47 real-world coach accidents. From these 47 accidents, a sub-sample of 11 cases of coach "tip overs" have been chosen to be looked at. We will look at the various causes of bodily injury in coach passengers involved in accidents in relation to their position in the coach. Three types of tip overs are studied. They are:

- static tip overs
- dynamic tip overs with side sliding occurring before the coach comes to a full stop
- tip overs involving a fixed obstacle

This study covers tipping over incidents for single as well as double-decker buses. The difference in resulting injury severity between total and partial ejection of coach passengers is also looked at. In conclusion, the various possible countermeasures to ensure better coach passenger safety are discussed.

Introduction

Foreword

Serious coach accidents are fortunately very rare in France and Europe. However, because of their spectacular nature, and the fact that they involve a large number of victims (children or elderly) media coverage of such accidents has a strong impact on the public.

There is no doubt of the high current safety level of coach travel. Statistics show that this means of road transportation has the lowest casualty rate per road kilometer covered (Figure 1).

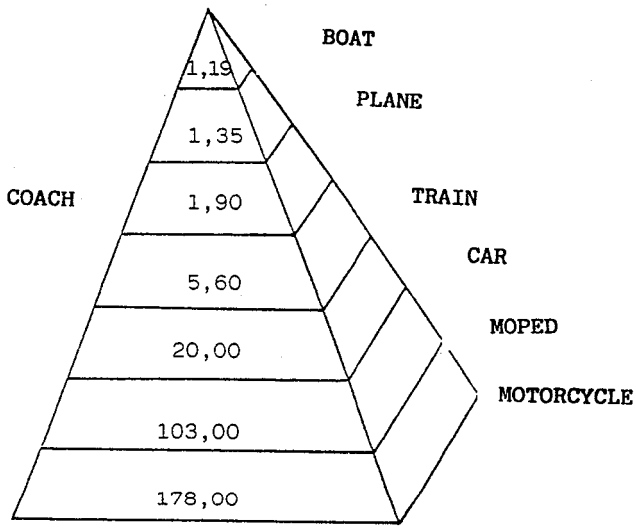

Source : LANGWIEDER (1) 1985

Figure 1. Death Rate per 109 Kilometers per Passenger for the Different Means of Transportation

Looking at road casualty rates, one can note that coach travel involves a very low risk as public transportation casualties (city bus and long distance coach) make up only 0.3% of those killed and injured in road accidents in Europe as well as in the U.S.A. Yet, even though the number of casualties is low, it is still necessary to continue research into ways to reduce even further the current casualty rate and increase coach safety.

Accident Survey Data

This multi-disciplinary study, involving doctors and engineers, covers data collected since 1980. There is currently data from 47 traffic accidents involving coaches, all of these accidents having resulted in bodily injury and having occurred in French territories. Our study looks at accidents involving coaches being driven in France no matter the make of the coach. The worst accidents were chosen and data from them analyzed. To be included in the sample chosen there had to be at least one occupant seriously injured in the accident.

Study of the accidents consisted of the following:

- analysis of accident circumstances, gathering of photographs taken at the scene of the accident and of a diagram showing the layout of the collision. This was done thanks to the French National Gendarmie, (the French state police force).
- technical examination of the coach involved to look at problems in safety.
- measurements of interior and exterior deformation and photos of deformation.
- careful, systematic inspection of all seats. Their characteristics, deformations and any possible impact between occupants and the seats were studied in detail. Above all the seat location of each passenger was determined by cross checking of information collected.
- the medical assessment of injuries. This was obtained from the hospitals having treated the casualties.

Sample Characteristics

The distribution by main impact type of 78 coach accidents involving 2,925 occupants is given in Table 1. The 78 coach accidents looked at include our 47 cases and 31 fatal coach accidents studied in 1984 using information from French National Gendarmerie accident reports.

Table 1. Distribution by Main Impact Type

ACCIDENT CONFIGURATION	NUMBER OF CASES	DISTRIBUTION
FRONTAL IMPACT	35	44 %
TIP OVER	20	26 %
FLIP OVER	6	8 %
ROLL OVER	6	8%
OTHER	11	14 %

Different tip over types are covered in this study. In this impact configuration, the coach tips over onto one of its sides. The sample chosen includes 11 of the 20 cases of tip over which were investigated in detail. Two of the cases were double-decker coach tip overs. Average coach occupancy of those coaches studied was 86% of occupancy capacity.

The breakdown of the injuries sustained by the 512 occupants involved is given in Table 2. Accident victims killed or severely injured make up 18% of the total number of occupants. Those with slight or no injuries make up 39% and 43% respectively. Due to the small numbers of occupants involved, this paper mainly aims to describe the collision conditions.

Table 2. Distribution of Occupant Injury Severity

KILLED	22	4 %
SERIOUSLY INJURED	71	14 %
SLIGHTLY INJURED	198	39 %
UNINJURED	221	43 %
TOTAL	512	100 %

Description of Various Types of Tip Overs

This accident configuration has very different consequences depending on:

- speed upon tip over,
- whether there was an obstacle or no,
- the distance the coach slid on its side.

Tip Over of "Standard" Coaches

Coaches considered as "standard" are those with only one level and 50 to 55 seats.

Quasi-static tip over. In the case of quasi-static tip over, the coach tips onto its side when almost at a full stop. This occurs on a flat surface without any fixed obstacle or major surface unevenness. It is an almost static tip over.

We will look at the following real world case of quasi-static tip over to illustrate: P.L. #95.

This case involved a Renault Vehicules Industriels FR1 GTX coach which was not yet a year old at the time of the accident. After driving up onto a low lane separating wall, the coach tipped onto its side while practically stopped (Figure 2). There were 47 occupants. The following was the medical assessment of the injuries sustained:

- 3 seriously injured (M.AIS 3).
- 27 slightly injured (M.AIS 1-2).
- 17 uninjured (M.AIS 0).

This accident can be considered as having little serious outcome for the occupants.

- Injuries resulted from occupant projection inside of the coach only (Figure 3).
- Occupants were removed from the coach through the front (windshield) (Figure 4).

In the case of quasi-static tip over, the vehicle structure was perfectly intact and the resulting injuries are of very moderate severity.

Dynamic tip over. In this type of accident, the coach tips over onto its side while driving at a relatively high speed and does not come to a stop immediately upon impact with the ground. Vehicle momentum results in various distances of side sliding. These tip overs take place on a flat surface with no fixed obstacle.

The following real world case is an example of dynamic tip over: P.L #68.

This case involved a SCANIA K112 coach carrying 44 people (Figure 6). It was not yet a year old at the time of the accident. After leaving the road at approximately 100 km/h the coach tipped onto its side. It slid on its flank 65 meters before coming to a stop. There was no structural deformation, but three of the five impact side window panels were broken (Figure 5).

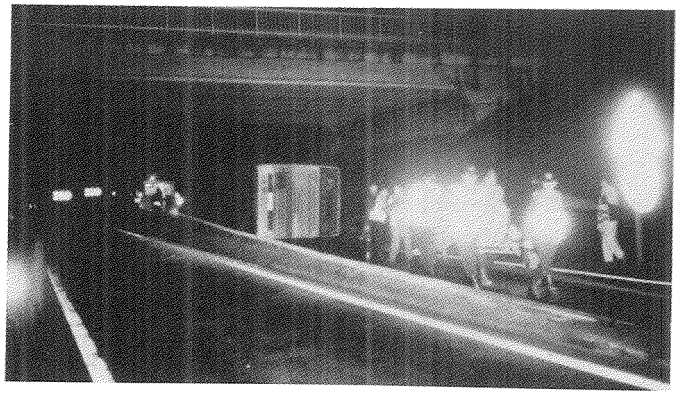

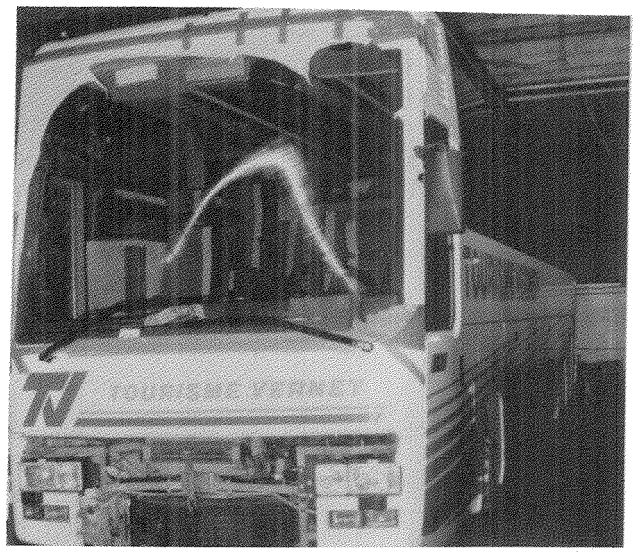

Figures 2, 3, and 4. Photographs of the Coach PL #95

For the 44 occupants, the resulting injury severities were:

- 3 killed (M.AIS 6).
- 6 seriously injured (M.AIS 3).
- 21 slightly injured (M.AIS 1-2).

- 14 uninjured (M.AIS 0).

The overall outcome can be considered relatively serious for those involved.

- Injury causes were as follows:
  - 3 killed through complete ejection from the coach
  - 27 injured through projection
- Occupants were removed from the coach through the front (windshield) without any great difficulty (Figure 7).

During dynamic tip over the sliding distance is a function of the initial coach velocity at the time of tip over. Total or partial ejection are the major causes of serious injury to the occupants.

Tip overs with a fixed obstacle. Coach tip overs onto fixed objects (low wall, tree stumps, road safety barriers, etc...) result in more severe accident conditions for occupants.

The following real world case is an example of this tip over situation: P.L #66.

This accident involved a coach with a VAN HOLL body equipped with a M.A.N. engine which had been in use for a month at the time of the accident. After losing vehicle control on a highway and spinning sideways, the coach tipped over onto the central dividing barriers. Structural damage incurred at the point where the coach struck the barrier was great.

The cars side sustained 60 centimeters intrusion towards the occupants, along with roof panel collapse equal to 30 centimeters at the same point (Figure 8).

For the 46 occupants, the resulting injury severities were:

- 5 killed (M.AIS 6).
- 14 seriously injured (M.AIS 3 or 4).
- 11 slightly injured (M.AIS 1 or 2).
- 16 uninjured (M.AIS 0).

Resulting overall injury severity was very high (Figure 9).

- Injury causes were as follows:
  - through complete ejection from the coach: 5 killed
  - through intrusion: 3 seriously injured, 3 slightly injured
  - through projection: 11 seriously injured, 8 slightly injured

In this accident, as in the preceding one, total ejection was responsible for all fatalities (Figure 10).

Occupants were removed from the coach through the front of the coach (windshield).

In the case of coach tip overs onto fixed objects, total ejection from the coach is also the major cause of the most serious injuries. However, this ejection is facilitated by the deformations induced by the obstacle. Therefore the intrusion of the vehicle wall is an additional cause of serious injury. This intrusion is the result of structural deformations caused by striking a fixed object. These causes of injury result in increased outcome severity for those involved.

Figures 5, 6, and 7. Photographs of the Coach PL #68

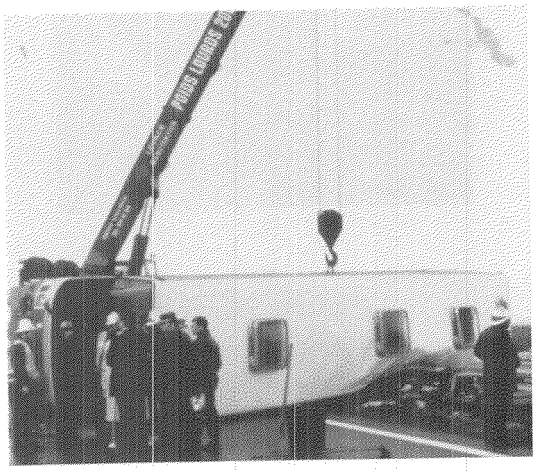

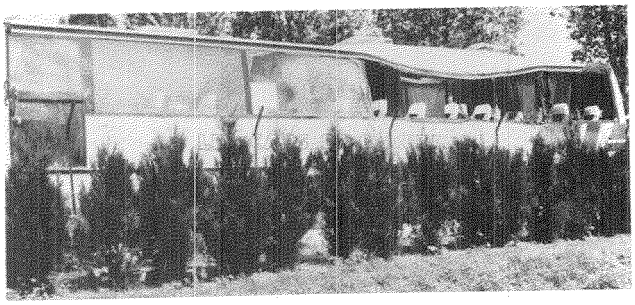

Figures 8, 9, and 10. Photographs of the Coach PL #66

Double-Decker Coach Tip Over

This type of coach with two levels has, on the average, 75 to 79 seats.

Quasi-static tip over. As with "standard" coaches, in the quasi-static tip over accident configuration a coach tips onto its side when almost at a full stop on a flat surface without any fixed obstacle. It is an almost static tip over.

We will look at the following real world case of quasi-static tip over to illustrate: P.L. #94.

This case involved a DAF SBR 3000 coach. After driving off the road, the coach tipped onto its side at a very low speed and came to a stop at the point of impact. No structural deformation occurred (Figure 11).

The following was the medical assessment of the injuries sustained by the 69 occupants:

- 2 seriously injured (M.AIS 3).
- 35 slightly injured (M.AIS 1 or 2).
- 32 uninjured (M.AIS 0).

Victim distribution, all injuries mixed, between the upper (55 seats) and lower deck (19 seats) is as follows:

- Lower deck: 2 slightly injured
- Upper deck: 2 seriously injured and 33 slightly injured.

Despite the fact that there were more seats in the upper deck, the proportion of injuries to occupants of the upper deck was 6 times higher than to those in the lower deck (Figure 12).

Injury causes were as follows:

- through complete ejection from the coach: 1 seriously injured, 1 slightly injured
- through projection: 1 seriously injured, 34 slightly injured

Evacuating passengers from the lower deck was particularly long and tricky. The windshield, the usual exit used in evacuating (Figure 13) was obstructed by the raised driver's bunk and a television set. It was therefore necessary to remove lower deck passengers by passing through the upper level. This was a difficult operation and was made all the more arduous by the presence of dislodged seats throughout the coach interior.

In the case of quasi-static tip over with a double-decker coach, vehicle structure was perfectly intact. Only occupant projection in the upper deck was responsible for injuries.

One can conclude that victim evacuation in double-decker coaches is abnormally long and difficult.

Dynamic tip over of a double-decker coach. In this accident configuration, the coach tips over onto its side while advancing at a relatively high speed and does not come to a stop immediately upon impact with the ground as kinematic energy is dissipated through side sliding. Such tip overs take place on a flat surface with no fixed obstacle being struck.

We will look at the following real world case of dynamic tip over to illustrate: P.L #92.

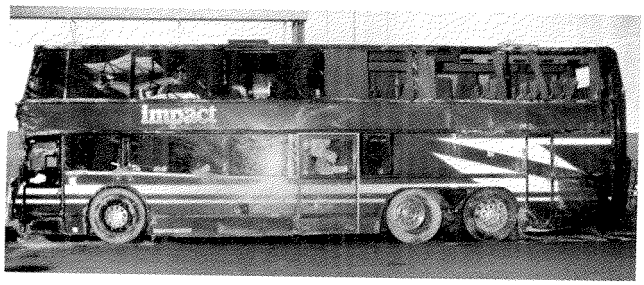

Figures 11, 12, and 13. Photographs of the Coach PL #94

This case involved a VAN HOOL TD 824 coach (Figure 14). After a tire blow-out while driving on a highway, the coach left the road, continued along the shoulder and tipped onto its side. It slid on its flank 56 meters before coming to a stop. There was considerable structurae deformation to the upper part of the downward side. The deformation consisted of a roof fold and inward crushing of the window pillars on the impact side. Roof intrusion was 32 centimeters.

The resulting injury severities for the 76 coach occupants was extremely severe (Figure 15):

- 11 killed (M.AIS 6).
- 16 seriously injured (M.AIS 3,4,5).
- 40 slightly injured (M.AIS 1 and 2).
- 9 uninjured (M.AIS 0).

The distribution of occupants in the coach by injury severity is given in Table 3.

Table 3. Distribution of Occupants by Injury and Their Coach Level Position

	UPPER DECK	LOWER DECK	TOTAL
KILLED	8	3	11
SERIOUSLY INJURED	15	1	16
SLIGHTLY INJURED	25	15	40
UNINJURED	5	4	9
TOTAL	53	23	76

As in the preceding accident, the majority of victims were found in the upper deck. It should be noted that the three passengers killed in the lower deck were elderly people (Figure 16).

A new cause of injury, partial ejection, appears in this accident type. Due to roof deformation and lateral crushing of the window pillars, occupants sitting next to the window on the impact side find themselves partially outside the vehicle. This takes place while the occupants are still in their seats. This situation, called "partial ejection," is particularly dangerous as these passengers are in contact with the ground, due to window breakage, while the coach slides along its flank.

Two other causes of injury found in this accident situation are total ejection and projection (Table 4).

Table 4. Distribution of Casualties by Cause of Injury

	PARTIAL EJECTION	TOTAL EJECTION	PROJECTION	TOTAL
KILLED	8	- -	3	11
SERIOUSLY INJURED	5	5	6	16
SLIGHTLY INJURED	- -	4	36	40

Occupants were removed from the upper and lower coach decks through the windshield. During this accident, structural deformation and long sliding distance resulted in the cases of partial ejection. These factors explain the severity of occupant injuries.

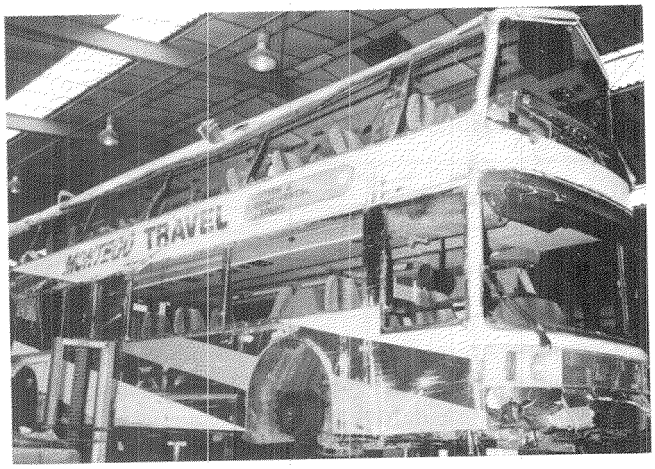

Figures 14, 15, and 16. Photographs of the Coach PL #92

Summary of the Important Results

Four causes of injury have been revealed through these 5 real world accidents studied. The are projection, partial ejection, total ejection and intrusion. Of course, for some occupants there can be more than one cause of injury. In order to simplify the study, the cause of injury considered to have played the largest part was chosen (Table 5).

Table 5. Distribution of the 291 Casualties by Cause of Injury

	VICTIMS	FREQUENCY
PROJECTION	239	82 %
TOTAL EJECTION	23	8 %
PARTIAL EJECTION	15	5 %
INTRUSION	14	5 %
TOTAL	291	100 %

The majority of injured occupants receive their injuries by being projected (82%). It is important however to look at degree of injury severity in such cases. This information is given in Table 6 which shows the breakdown of the 291 victims in the 11 coaches by the severity of their injuries and injury cause.

Table 6. Distribution of Casualties by Injury Severity and Cause of Injury

	PROJECTION	TOTAL EJECTION	PARTIAL EJECTION	INTRUSION	TOTAL
KILLED	14 %	50 %	36 %	- -	100 %
SERIOUSLY INJURED	68 %	8 %	10 %	14 %	100 %
SLIGHTLY INJURED	95 %	3 %	- -	2 %	100 %

It would seem that:

- total or partial ejection is responsible for:
  - 86% of deaths
  - 18% of serious injuries.
- projection, which concerns 82% of the victims, is responsible for:
  - 95% of slight injuries
  - 68% of serious injuries.

Possible Countermeasures

From the results presented above, it is evident that it is primordial to avoid total or partial occupant ejection. An effective countermeasure would seem to be to install restraint systems which would protect against total ejection of coach occupants. Accident study data shows that, in the most severe frontal impacts, mean decelerations are at an acceptable level for coach occupants. The use of simple 2-point restraining system would therefore seem sufficient to help avoid total ejection.

Potential Effectiveness of a Restraining System

An analysis of the 93 killed and seriously injured found in this study was carried out to determine the potential effectiveness of this countermeasure. Figure 17 shows the results for the 22 fatalities.

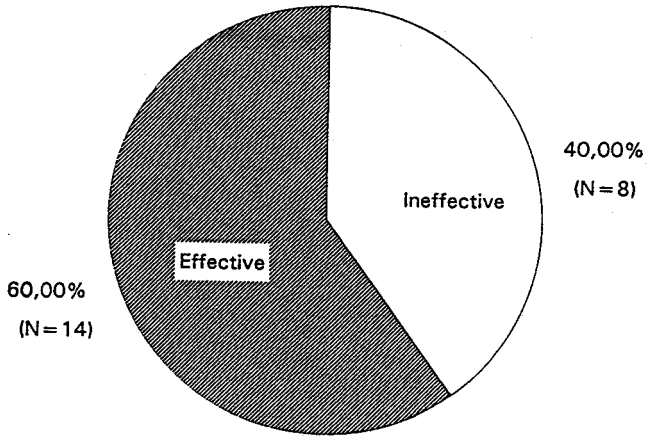

Figure 17. Probable Effectiveness of a Restraining System for Fatalities

The use of this type of restraint system would probably have resulted in avoiding 14 of the 22 deaths (Figure 17).

Figure 18 shows the effectiveness for the 71 seriously injured occupants.

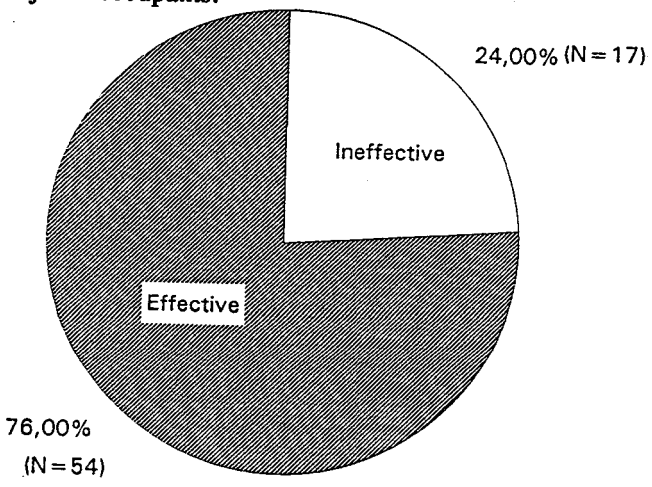

Figure 18. Probable Effectiveness of a Restraining System for Severe Injuries

The use of this restraint system would have resulted in avoiding 54 of the 71 serious injuries (Figure 18).

One would expect a much higher level of effectiveness in the case of slight injuries. Nonetheless, in the case of serious injuries resulting from intrusion or partial ejection the wearing of a seat belt is not effective.

Effectiveness of Side Window Panels Remaining in Place

Another possible countermeasure, which would be complementary to the first, is the use of side window panels that remain in place after impact no matter what the structural deformation. This should avoid partial ejection of occupants.

These window panels must be removable only after the coach comes to a stop, so that occupant evacuation can be carried out easily and rapidly.

In this impact configuration, the benefit from these two aforementioned countermeasures together should be:

- saving of the life of 100% of fatalities
- as well as avoiding 86% of serious injuries.

Countermeasures to Improve Victim Evacuation from the Coach

It is also essential to keep the exit routes free after the coach has come to a stop. It would seem to be of the utmost importance that the two most practical openings, the windshield and the rear window in this accident configuration, be maintained as exit routes. Therefore it seems important to have a transparent rear window if one wishes to facilitate evacuation by way of this exit. Roof trap hatches, ejectable after impact, are also useful and effective exit routes.

Conclusions

The study of these 11 coach tip over accident seems to indicate that:

- In coach tip overs, 20% of occupants are either killed or seriously injured while 80% are either slightly injured or uninjured.
- Of the main causes of injury found in this type of accident, total or partial ejection are responsible for the majority of serious casualties. As well the majority of occupants are projected inside the coach. This is true for almost all occupants receiving slight injuries as well as for a large number of those with serious injuries.
- Correct wearing of restraining system would be a beneficial countermeasure to combat projection and avoid total ejection.
- Side window panels capable of adapting to structural deformations while still remaining in place would result in avoiding all ejection and more particularly, partial ejection.
- To guarantee rapid and easy evacuation of victims after the accident, it is necessary to maintain the use of transparent rear windows.

These proposed countermeasures, like all present or future regulations, should be applied to both single deck and double-decker coaches. Of course they are necessary as well in both the upper and lower decks of double-decker coaches.

Through such studies of real world accident data, Renault Vehicules Industriels is developing its voluntary safety policy for its range of public transportation vehicles. For example, crash tests carried out to complement accidentology studies, have revealed the necessity of a safety belt in coaches.

There is no doubt that there are numerous applications of this sort of study to vehicles and that findings from such studies will progressively be incorporated into vehicles.

References

1. K. Langwieder, M. Danner and T. Kummel, "Collision types and characteristics of bus accidents. Their consequences for the passengers and the accident opponent." Proceedings of the 10th ESV Conference, Oxford, England, July 1-4, 1985.
2. Rickey L. Stansifer and Robert A. Romberg, "An analysis of accidents involving buses and an assessment of the need for safety belt requirements in such vehicles."
3. Klaus Rompe and Haus J. Krüger, "Improvements for bus safety," Proceedings of the 10th ESV Conference, Oxford, England, July 1-4, 1985.
4. Merrit M. Davis, "A study of some school bus crashes," Proceedings of 21st A.A.A.M. Conference, Vancouver, British Columbia, September 15-17, 1977.
5. André St. Laurent and Dan Rolfe, "School bus seat backs and their relation to facial injuries," Proceedings of the Canadian Multidisciplinary Road Safety Conference, Montréal, Québec, May 26-28, 1985.
6. P. Botto, C. Thomas, C. Tarrière, "Accidents Mortels d'Autocars", June 1984.
7. C. Thomas, F. Hartemann, C. Tarrière, P. Botto, C. Got and A. Patel, "Severe coach accident survey," Proceedings of the 10th ESV Conference, Oxford, England, July 1-4, 1985.
8. P. Botto, C. Thomas, C. Tarrière, C. Got and A. Patel, "Lésions imputables aux sièges dans les accidents d,autocars," Conference internationale sur la Sécurité Routière en Europe, Göteborg, Suède, 12-14 octobre 1988.
9. American Association for Automotive Medicine, 1980 Revision "The Abbreviated Injury Scale."
10. P. Botto, C. Thomas, C. Tarrière, C. Got and A. Patel, "Injuries caused by coach crashes in France," Elmmia Ergonomics 1989, Jonkoping, Sweden.

S10-O-05

Influence of Different Loading Configurations on the Driving Behaviour of Heavy Commercial Vehicles

Andreas Schindler
TÜV Rheinland e.V., Institute of Traffic Safety

Introduction

Commercial vehicles such as coaches or trucks represent an important economic factor in the Federal Republic of Germany. A great part of the transport service is produced by commercial vehicles, for example in 1989 approximately 14% of passenger transportation was serviced by coaches and about 55% of ton-kilometers were brought by trucks. Related to the covered distances this means that commercial vehicles and coaches with a proportion of 5% in the total number of registered motor vehicles meet about 10% of the whole annual kilometers of driving distance.

At the same time commercial vehicles and coaches are involved in about 7% of the motor vehicle accidents with casualties. With regard to an improvement in traffic safety the adaption of vehicles to the needs and capabilities of the drivers and the requirements of road traffic is of great importance. Hence to an increasing extent the handling characteristics of heavy commercial vehicles which play an important part in accident avoidance become a main field of development.

Sophisticated investigations of 182 commercial vehicle accidents conducted by the Medical University of Hannover in cooperation with the Technical University of Berlin allow some statements about the part of handling characteristics in accident events (Figure 1).

According to this the following order with regard to the relevance in accident events can be specified (multiple specifications are possible):

- braking performance: 86%
  (locked wheel braking: 45%)
- steering performance: 39%
- directional control: 21%

behaviour in case of accidents in %	type of vehicle: truck n = 82	truck train n = 50	semitrailer train n = 29	bus n = 21	total n = 182
braking performance					
braking	82,9	88,0	89,7	90,5	86,3
of that braking with locked wheels	43,9	42,0	41,4	57,1	44,5
steering performance					
steering input	30,5	42,0	58,6	38,1	39,0
directional control					
unstable	13,4	34,0	31,0	9,5	21,4
of that travel of trailer	-	12,0	13,8	-	
jackknifing	-	10,0	6,9	-	

ref.: UFO MHH / TUB / BAST 1985

Figure 1. Handling Performance of Commercial Vehicles Related to Accidents

Present State of Objective Test Procedures

The evaluation of handling characteristics of motor vehicles was mainly carried out by means of subjective assessments by experienced drivers or research engineers so far. But in recent years objective test procedures with

comparable measuring and evaluation criteria have reached significance [1].

In the years past quite a number of relevant test procedures including appropriate criteria of description and evaluation respectively have been developed to objectively describe and assess handling and braking characteristics of passenger cars and passenger car-trailer combinations. After comprehensive testing and discussion some of these test procedures were laid down as test standards in the national DIN working committee AA-I9 and the international ISO technical committee TC22/SC9. At present, however, commercial vehicles are not included in standardized test manoeuvers but these procedures are basically applicable to heavy vehicles and combinations as well provided that either the starting conditions or the criteria of evaluation and description are adapted to the special features of this particular class of vehicles.

At present state of knowledge the following six test procedures have proved their feasibility and expressiveness for the objective evaluation of handling and braking characteristics of heavy commercial vehicles in practical testing (Figure 2):

- Steady state cornering to determine the understeer/oversteer behaviour as a function of lateral acceleration or driving speed.
- Step steering input to determine the promptness of vehicle response.
- Frequency response measurement to determine the extent and promptness of vehicle response as a function of steering angle input.
- Braking during steady state turning to determine yaw stability and steerability.
- Straight line braking on a split adhesion surface (μ-split) to determine deceleration capability and driving stability.
- Lane change to determine the steering effort and the effect of a lane change as an excitation function for yaw angle oscillations.

Within this paper some measurement results obtained by application of the test procedures mentioned above will be presented which point out the influence of different loading conditions on the driving behaviour of two trucks with a vehicle gross weight of about 14 tons. The investigation referred to was conducted on behalf of public authorities in particular the German Federal Minister of Defense.

Measuring Instrumentation

In contrast to the subjective assessment of handling characteristics which generally is performed by experienced drivers with the help of rating charts the application of objective test procedures necessitates measuring devices to record the driver's input and the resulting vehicle response.

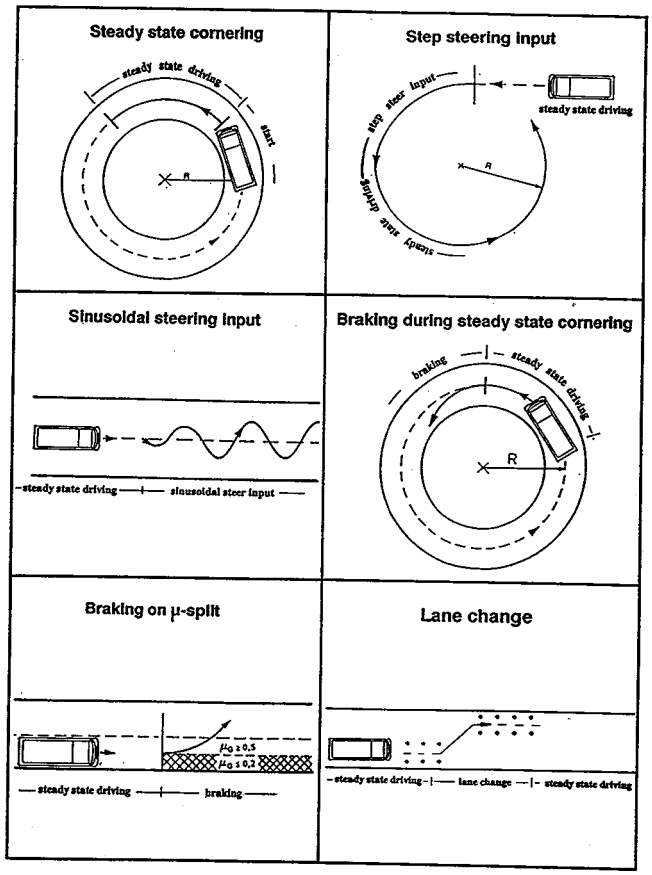

Figure 2. Objective Test Procedures for the Evaluation Handling Characteristics of Commercial Vehicles

Figure 3 shows a selection of the required measuring variables illustrated by the example of a truck-trailer combination. There is evidence that the standard variables referring to the towing vehicles such as steering angle, driving speed, lateral and longitudinal acceleration and yaw velocity are needed and so are corresponding variables referring to the further elements of the combination and the relative yaw angles at the different joints and couplings. Depending on the setting of the task and the specific vehicle type it may be necessary to measure and record additional variables e.g. separated for the driver's cabin and the platform.

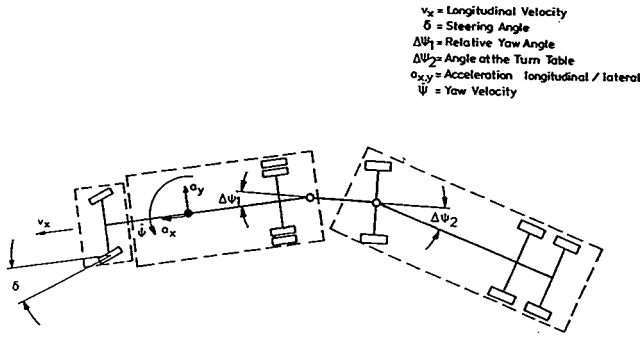

Figure 3. Commercial Vehicles Measuring Variables

In order to assess the dynamic capabilities of commercial vehicles up to limit performance depending on the specific vehicle type a rollover protection or a safety device to prevent jackknifing may be necessary to reduce the danger of accidents during the driving tests. The influence of these devices on the handling characteristics has to be determined in pre-tests.

Test Results

Steady-State Circular Test

The steady-state circular test procedure is the method most frequently used to provide data on the steering tendency i.e. on the driving course as a function of steering angle and lateral acceleration. Furthermore this manoeuvre especially for commercial vehicles with a high centre of gravity gives a suitable approach to assess roll behaviour and dynamic roll resistance. The conditions for implementation as relating to passenger cars are specified in ISO Standard 4138.

The steering wheel angle measured with both 14-t-trucks in the steady-state circular test on a constant radius of 40 m is illustrated in Figure 4 as function of lateral acceleration. The diagram's upper part refers to the loading condition test weight (TN) whereas the lower part describes the characteristic curves for the gross vehicle weight (GVW).

The test weight of the vehicles characterizes the curb weight plus the weight of the measuring equipment and the driver. The loading condition gross vehicle weight was simulated by concrete ballast which was fastened in a frame on the vehicle's platform.

Both unloaded trucks show an understeering behaviour. This finds expression in a with increasing driving speed and lateral acceleration respectively also increasing steering wheel angle required to keep the course. The understeer characteristic of truck B is comparatively distinctive whereas truck A up to a lateral acceleration of 3 m/s² shows an almost neutral behaviour that only in the range of higher lateral accelerations changes into a moderate understeering performance. For truck A a remarkably high steering wheel angle can be perceived when cornering with very low driving speeds (Ackermann driving condition) which indicates a comparatively high-ratio steering.

In contrast to truck B which retains its understeering performance even in the loaded condition the load alternation to gross vehicle weight with truck A is combined with a significant change in steering tendency. With increasing lateral acceleration the steering wheel angle necessary to follow the marked out course continuously reduces equivalent to an oversteering behaviour of the vehicle. At the same time the obtainable maximal lateral acceleration decreases from 5.2 m/s² to about 2.9 m/s². This overall steering tendency of truck A in gross vehicle weight is mainly caused by roll steer effects of the rear axle and clearly differs from the known and

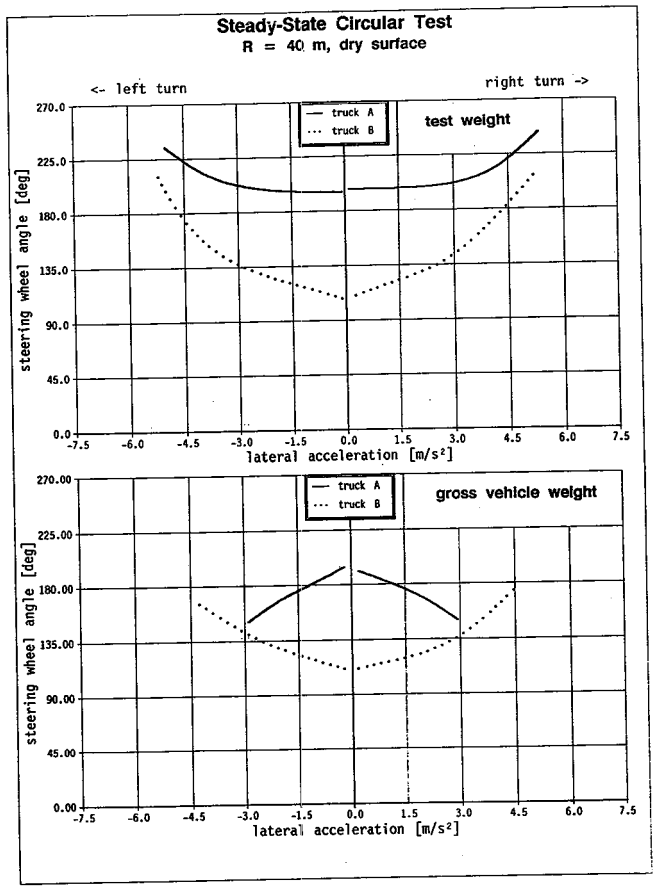

Figure 4. Steady-State Circular Test; Steering Wheel Angle as Function of Lateral Acceleration for Two 14-t-Trucks in Different Loading Conditions

normal layout of cars and trucks. In dangerous situations the driver therefore could have difficulties in controlling it.

Step Steering Input

The step steering input test describes the vehicle response to a sudden steering input and simulates a driving situation that can occur in everyday traffic, e.g. an avoidance manoeuvre which requires a rapid steering input by the driver to make way for an obstacle. The manoeuvre as applied to heavy commercial vehicles is comparable to that applied to passenger cars with the exception that the driving velocities only range from 50 km/h to 80 km/h and the lateral accelerations obtained during the steady-state cornering condition of the test are reduced to 2.5 m/s².

The handling performance evaluated within this test procedure contain two essential qualities: on the one hand the magnitude of the vehicle response (gain) and the promptness of the response on the other hand. In addition to the yaw stability which becomes evident by the maximum values of yaw velocity and sideslip angle for the assessment of directional control of heavy commercial vehicles in particular the rollover resistance is of great importance. With regard to this a suitable criterion

of evaluation is represented by the maximum values of roll angles measured during the peak response of the vehicle.

Figure 5 illustrates these maximum roll angle values measured with two military 8-t-trucks as function of the steady-state lateral acceleration obtained after the steering input [2]. Both trucks were driven in unloaded condition and with a special telecommunication cabin. With increasing lateral acceleration the roll angles also increase. The higher values and the greater relative increase of peak roll angles of the loaded vehicles are not only influenced by the changed centre of gravity height but also by the effective moments of inertia according to load contribution. Compared with the unloaded condition the limit of rollover stability characterized by the maximum lateral acceleration obtained decreases with cabin from 5.2 m/s² to 4.6 m/s². At this level of lateral acceleration the peak roll angles reached with cabin exceed the values of the unloaded vehicles by 4° to 5°.

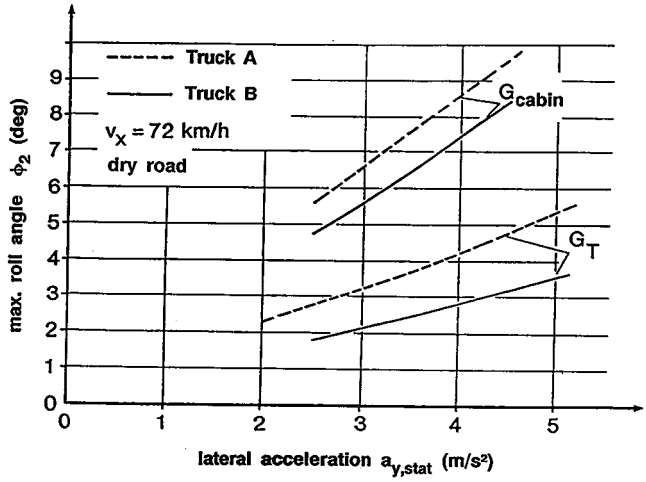

Figure 5. Maximum Roll Angles in Transient Response as Function of Steady State Lateral Acceleration for Step Steering Input Under Test Weight and Cabin Loading Condition

The time histories of characteristic values recorded in a step steering input test with both 14-t trucks previously mentioned in unloaded condition are pictured in Figure 6. The steering wheel angle of 62° (truck A) and 55° (truck B) respectively is chosen in such a way that with a driving speed of 72 km/h a steady-state lateral acceleration of about 2.5 m/s² is obtained. In test weight condition both vehicles respond without a great time delay to the rapid steering input which becomes evident by the quick and abrupt increase of yaw velocity and lateral acceleration. Already about 1.2 s after the steering input has been applied the characteristic values of vehicle motion show an almost steady-state driving condition. As a consequence of the high system damping an overshoot of the measured variables which is typical for test results with passenger cars cannot be observed.

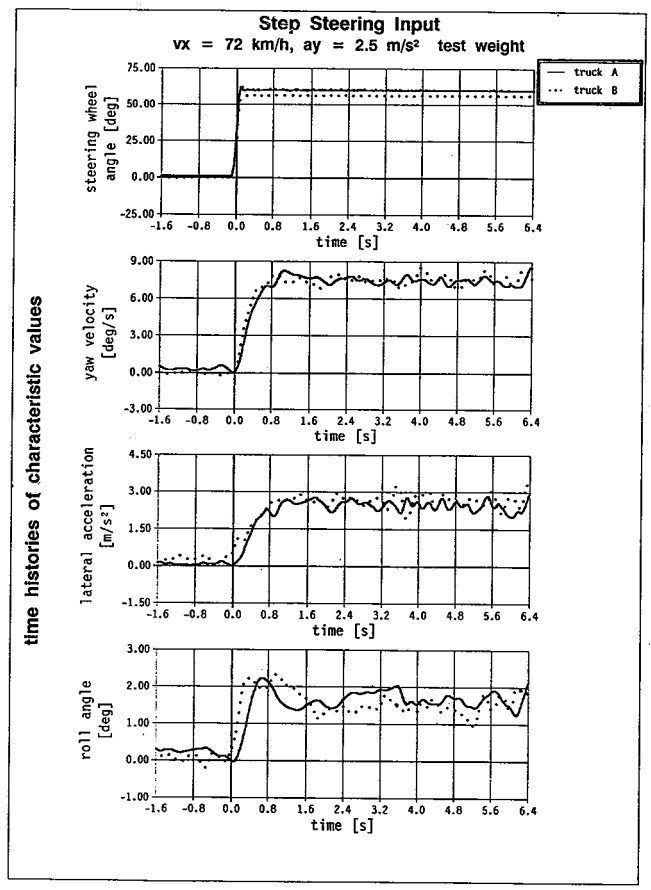

Figure 6. Step Steering Input: Time Histories of Characteristic Values for Two 14-t Trucks in Test Weight Condition

The corresponding time histories for truck A and B loaded up to gross vehicle weight are illustrated in Figure 7. Similar to the results of the steady-state circular test shown before the transient response behaviour of truck A is effected in a decisive manner by the changed loading condition whereas the response of truck B in gross vehicle weight to the rapid steering input only differs insignificantly from that in test weight condition. With truck A the steering wheel angle necessary to reach a lateral acceleration of 2.5 m/s² decreases to only 22° and the response times of yaw velocity and lateral acceleration extend to more than 4 s. With regard to accident relevant driving situations the transient response behaviour of the vehicle in loaded condition has to be evaluated unfavorably because this dynamic oversteer on the one hand can hardly be foreseen by the driver and the small steering wheel angles required in connection with the extended response time on the other hand will probably provoke a driver's reaction which is too intense.

Continuous Sinusoidal Steering Input

The continuous sinusoidal steering input is used to determine the frequency response characteristics as the ratio of a periodic steering wheel input to vehicle reaction according to amplitude and phase at different

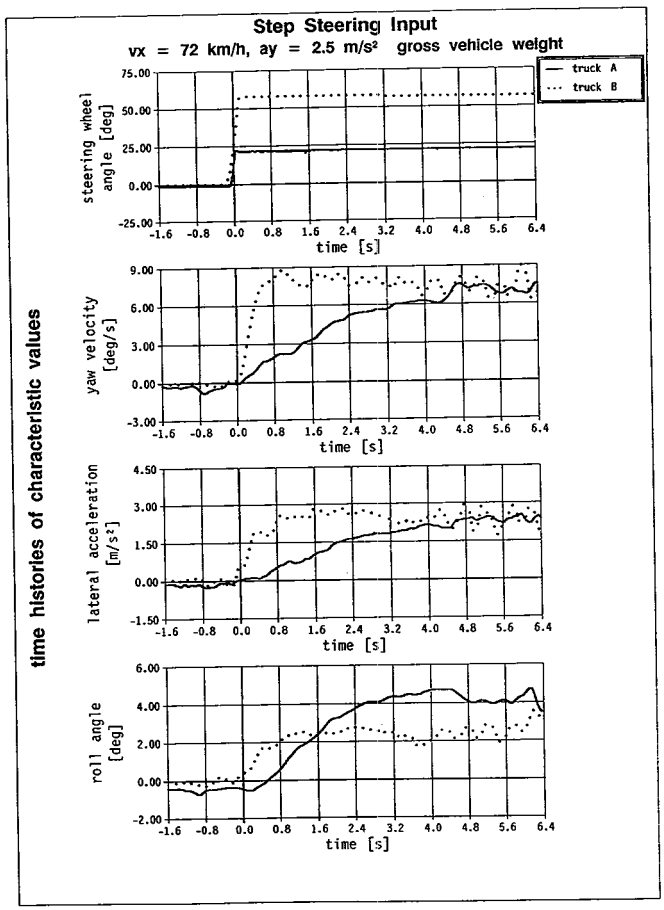

Figure 7. Step Steering Input: Time Histories of Characteristic Values for Two 14-t Trucks in Gross Vehicle Weight

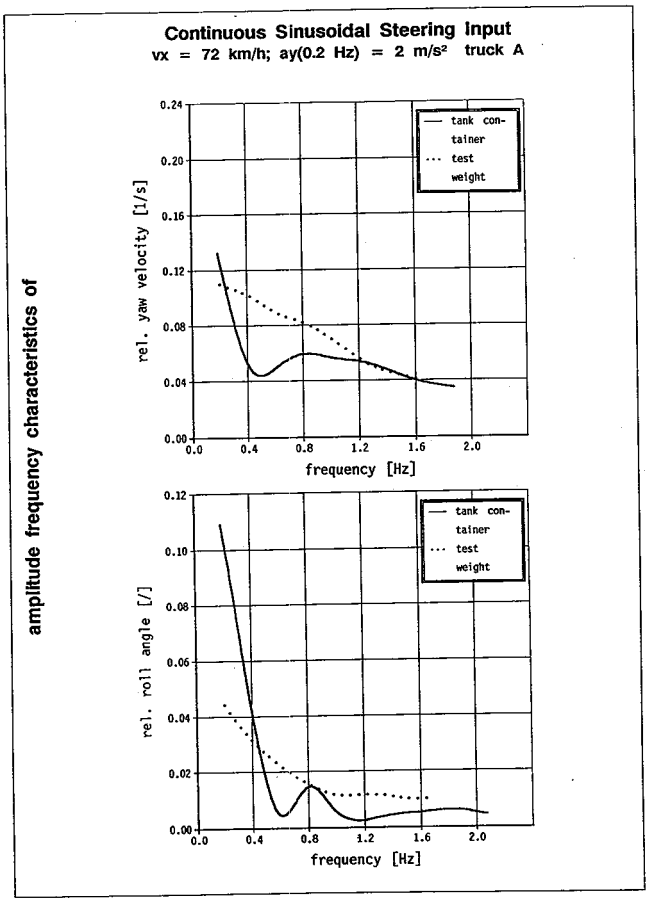

Figure 8. Continuous Sinosoidal Steering Input: Amplitude Frequency Characteristics of Yaw Velocity and Roll Angle for a 14-t Truck in Different Loading Conditions

steering frequencies. The procedure assumes that the transfer characteristics of the vehicle can be described in a linear way with good approximation. The frequency response of a linear dynamic system is a function which describes the amplitude ratio of output and input signals and the phase lag between both signals in periodic steady-state condition depending on frequency. In comparison to other test procedures specified in ISO 7401 the continuous sinusoidal steering input provides for heavy commercial vehicles the most reliable results in frequency domain.

To evaluate the influence of a liquid loading on the transient response behaviour truck A was equipped with two tank containers which were attached upon the loading space. The tank containers with a total capacity of 4.600 l were filled up to about 60% with water. The amplitude frequency characteristics of yaw velocity and roll angle measured in this loading condition are illustrated in Figure 8 in comparison to the test weight condition. The actual tests started with a steering frequency of 0.2 Hz which gradually was increased up to 1.8 Hz. The amplitude of the steering wheel input was previously defined so that with a driving velocity of 72 km/h and a steering frequency of 0.2 Hz a periodic steady-state lateral acceleration of 2 m/s² was obtained.

In test weight condition the amplitude frequency characteristic of yaw velocity starting from 0.2 Hz continuously decreases with increasing steering frequency because the vehicle responds in a reduced way to the steering wheel input. Because of the high system damping a resonance range in the amplitude frequency characteristic as typical for passenger cars cannot be observed under these test conditions.

Compared with the test weight condition the truck equipped with tank containers shows a higher gain at a steering frequency of 0.2 Hz which can be attributed to the lower steering wheel angle required to obtain the planned level of periodic steady-state lateral acceleration. Then the amplitude ratio of yaw velocity decreases comparatively sharp. At steering frequencies above 0.6 Hz the effect of liquid surge becomes evident leading to a relative rise of the amplitude ratio within the frequency range up to 1.0 Hz. This resonance effect can also be detected in the amplitude frequency characteristic of vehicle roll angle. However the peak amplitude ratio at this point only amounts 15% of the initial value obtained at 0.2 Hz so that a reduction in yaw stability and roll stability respectively caused by the surge of liquid loading cannot be stated.

Braking During Steady-State Turning

The braking characteristics of vehicles represent an essential quality of handling performance and are directly associated with safety in road traffic. In this context the test procedure braking in a turn originally designed for passenger cars is used to provide information about the vehicle behaviour on a braking action effected simultaneously by lateral forces. For heavy commercial vehicles the test manoeuvre laid down in ISO standard 7975 has to be adapted especially with regard to the initial steady-state driving conditions. The reasons are primarily the lower physically obtainable lateral acceleration during cornering and the comparatively long time delay until the deceleration and the corresponding vehicle reaction is built up [3].

Figure 9 shows the time histories of characteristic values for a brake test at a high deceleration level with the unloaded truck A. The initial driving velocity is 53 km/h equivalent to a lateral acceleration of about 2 m/s^2 on a radius of 100 m. The brakes at the front axle of the truck are operated hydraulically whereas the braking forces at the rear axle are generated by a pneumatic system and are adjusted to the specific loading condition by an automatic load-depending brake force proportioning (ALB). Approximately 0.4 s after brake application the hydraulic pressure at the front axle reaches its final value of about 160 bar. At the same time a rapid increase of yaw velocity and lateral velocity can be observed due to an early lock-up of the rear wheels. In spite of the ALB the rear axle of truck A is overbraked in test weight condition and as consequence of this the vehicle spins and looses driving stability.

To describe the vehicle response during braking in the whole deceleration range in detail from the time histories of the variables recorded in brake tests with varying brake pressure values at a time of 1.5 s after brake application are determined and presented as a function of the vehicle deceleration. These characteristic values are usually divided by the corresponding values of the steady-state driving period to equalized minor variations in the test conditions. In addition reference curves are used for evaluation purposes which characterize the behaviour of a vehicle travelling exactly along the initial radius after braking.

Figure 10 illustrates the characteristic curves of yaw velocity and sideslip angle for truck A in the loading conditions test weight and gross vehicle weight. With increasing deceleration the characteristic functions of yaw velocity in both loading conditions show increasingly higher values than the reference curve. Hence it follows that as a consequence of the braking process the vehicle goes off the lane towards the inside of the bend. Up to a deceleration of 3.5 m/s^2 the tendency of turning inwards with the loaded truck is comparatively stronger than in test weight condition. With further increasing deceleration the yaw reaction of the fully loaded vehicle diminishes again because the front wheels reach the

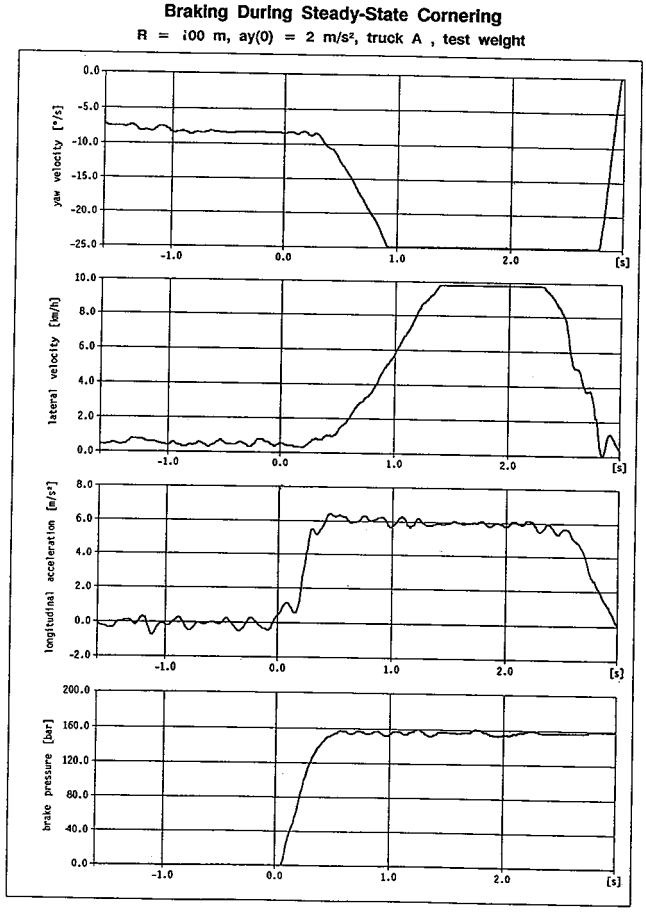

Figure 9. Braking During Steady-State Cornering: Time Histories of Characteristic Values for a 14-t Truck in Test Weight Condition at Full Braking

wheel lock limit. In contrast to this the locked rear axle of the truck in test weight condition results in a rapid increase of yaw velocity in combination with great sideslip angles indicating a vehicle behaviour that cannot be controlled even by an experienced driver.

The test results demonstrate that even a brake balance that complies to national and international regulations of type approval can lead to a loss of driving stability especially when braking in a turn. Here antilock brake systems can show a good potential with regard to an improvement of traffic safety although such a system cannot be an equivalent to a good layout of the brake system.

Conclusions

Heavy commercial vehicles and busses represent an important economic factor in the Federal Republic of Germany. Against the background of a continuously growing transport service brought by these vehicles on a limited traffic network research on the handling characteristics of commercial vehicles in order to improve traffic safety becomes increasing significance.

For the assessment of passenger car and passenger car-trailer combination handling characteristics a number

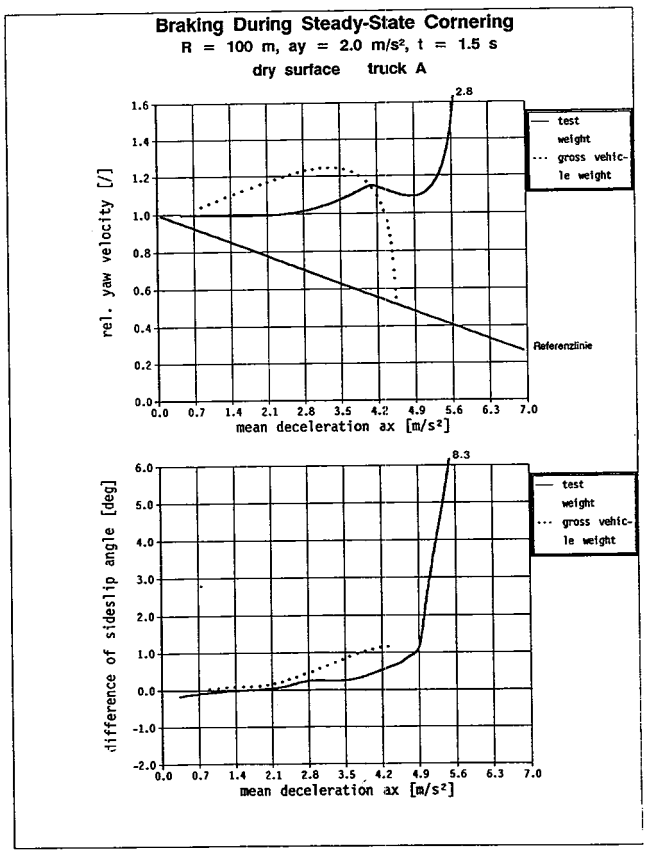

Figure 10. Braking During Steady-State Cornering: Ratio Between Yaw Velocity and Difference of Sideslip Angle 1.5 s after Brake Application as Function of Mean Deceleration for a 14-t Truck in Different Loading Conditions

of objective test procedures are available which are basically applicable to heavy commercial vehicles as well. In doing so it has to be considered that there is a need for adapting either the initial driving conditions or the criteria of evaluation accordingly.

With regard to the variety of commercial vehicle configurations it will be necessary in some cases to confine to comparative tests in order to evaluate basic conceptions and the effects of special parameters respectively. As illustrated by the example of different loading conditions then these test procedures form expressive facilities to assess the handling and braking characteristics of commercial vehicles. Consequently it seems necessary and useful to continue with the work in applying these test procedures to adapt vehicle technology to the human capabilities for a further improvement in traffic safety.

References

1. Rompe, K.; Heißing, B: Objektive Testverfahren für die Fahreigenschaften von Kraftfahrzeugen Verlag TÜV Rheinland, Koln 1984
2. Ehlich, J.; Rompe, K.; Schüßler, J.: Objektive Meß- und Bewertungsverfahren für die Fahreigenschaften von Nutzfahrzeugen der Bundeswehr
3. Heißing, B.; Ehlich, J.: Fahrverhalten von schweren Nutzfahrzeugen beim Bremsen in der Kurve DKF-Heft Nr. 281, VDI-Verlag 1983

S10-O-06

Reliability, Maintainability, and Durability of Heavy Truck ABS Systems

Robert M. Clarke
National Highway Traffic Safety Administration

Abstract

Efforts in the 1970's to require that U.S. heavy vehicles be equipped with antilock braking systems (ABS) were unsuccessful, in part, because of truck user concerns about the in-service operational reliability and serviceability of the systems. As a necessary pre-step to reconsidering a requirement for ABS, the National Highway Traffic Safety Administration began, in 1988, a large in-service field evaluation of current-generation ABS systems in order to determine if they would function reliably in U.S. trucking operations. Reliability and serviceability has been tracked on 200 ABS-equipped truck tractors, operated by seventeen fleets in six U.S. cities for a two year period beginning in late 1988/early 1989. Beginning in late 1990, 50 ABS-equipped trailers were added to the program. These will also operate for a two-year period. Maintenance records and specially designed on-board monitor/recorder systems have been used to monitor system operation. Data from the recorders indicates the ABSs function more frequently than might have been expected and that the frequency of operation increases, as would be expected, during the winter months. Driver acceptance of the systems has been favorable. Maintenance information collected to date indicate that if quality control of the ABS and its installation in the vehicle is kept high, and if good maintenance is available, from a reliability and maintenance perspective, ABS can be successfully installed and maintained on U.S. heavy vehicles.

Introduction

Development work on ABS for heavy trucks began in the 1950's with commercial products becoming available in the late 1960's (Leasure and Williams, 1989). Aware

of these developments, and wishing to achieve improvements in then-current truck brake system performance, NHTSA, in 1970, proposed a stringent set of truck braking requirements. Federal Motor Vehicle Safety Standard (FMVSS) 121 was subsequently published in 1971, with an original effective date of 1973. It effectively required ABS by requiring trucks to stop within 216 feet on dry pavement from 60 mph, without more than momentary wheel lock-up. The effective date of the rule was subsequently changed twice, while the stopping distance requirement was increased to 293 feet. By March 1, 1975, the final effective date, there were seven commercially available systems.

On March 1, 1975, a petition for judicial review was filed with the Ninth U.S. Circuit Court of Appeals asking that the stopping distance requirements of the rule be set aside, in part, because it was felt that the systems then available were not reliable. There had been reports of brake system failures that were attributed to the ABS.

In 1978, the Appeals Court rendered its decision, agreeing with the petitioners. It set aside the "no-wheels locked" stopping distance test requirements of the Standard based, in part, on a determination that the Agency had not independently established that reliable systems were available. This ruling effectively precluded the Agency from again proposing the use of heavy truck ABS without first establishing such a record.

Development work, as well as production, of U.S. truck ABS effectively halted as a result of the ruling. A-C Sparkplug was the last U.S. manufacturer to offer a system. Prior to the Court's ruling, A-C produced about 180,000 units per year. By 1980, this figure was 3500 and in 1984 it was 500 (Leasure and Williams, 1989).

In Europe, Grau-Girling, WABCO, Bosch, and Bendix-France continued to work on ABS. Second-generation digital systems were offered on European model trucks beginning in 1981. European government interest in the systems increased as a result.

In 1986, in an effort to harmonize standards that were proliferating among its member countries, the European Economic Community (Common Market) adopted EEC Directive 71/320/EEC which established categories or descriptions of various types of ABSs and defined performance requirements for each. It permitted member countries to type-approve ABS-equipped heavy trucks, but did not require ABS. In 1988, as anticipated, the EEC stiffened its heavy vehicle braking requirements (88/194/EEC), stipulating that for the purposes of international type approval:

- Type approval had to be granted to ABS-equipped trucks, trailers and buses certified after October 1, 1988;
- All new model heavy trucks and buses and trailers receiving type-approval for the first time after October 1, 1989, had to be equipped with ABS; and
- After October 1, 1991, all new heavy trucks, buses, and trailers have to be equipped with ABS, regardless of when they were first type-approved.

U.S. interest in the European systems was increasing at this time. The Freightliner Corporation began, in June 1987, to offer the WABCO 6-channel ABS as an option on its U.S. vehicles. It still remained to be proven, however, whether the European systems could be successfully adapted over the long term to typical U.S. trucking environments. One major difference between U.S. and European vehicles is their electrical systems. U.S. vehicles employ 12 volt systems, whereas European vehicles use 24 volts. A record had yet to be established as to whether modified versions of the European systems, plus several newly-developed U.S. systems, would function reliably under U.S. operating conditions.

European/Australian Experience with Heavy Truck ABS

Before developing a program to determine the reliability of heavy truck ABS in U.S. operating environments, NHTSA sponsored a review of the European and Australian experience with the systems in order to establish a base against which comparisons could later be made. The study was conducted in 1987. It consisted of interviews and fact gathering to:

- Establish the then-current, as well as future projected, market penetration of ABS within the population of European and Australian heavy trucks;
- Determine, based on a limited number of interviews, European motor carriers' opinions relative to the systems; and
- Establish the extent and nature of ABS failure histories/patterns and warranty claims experienced by European ABS suppliers.

Based on information supplied by European ABS manufacturers, it was estimated that in 1987 there were approximately 1.5 million heavy trucks (including those designed to tow full trailers), and tractors and an additional 1 million semi and full trailers, in service in Western Europe. In Australia, 92,000 trucks and tractors and 80,000 trailers were estimated to be in service. This compares with estimates of 900,000 truck tractors, 740,000 heavy single-unit trucks and 2.5 million trailers in use in the U.S. in 1982.

As can be seen from the data in Figure 1, the largest penetration of ABS among these vehicles in 1987 was in the U.K. and West Germany. In the U.K., approximately 25 percent of the in-service truck tractors (20,000) and 24 percent of the semitrailers (38,000) were equipped with ABS. In West Germany, where truck/full trailer combinations are prevalent, 25 percent of the truck tractors (15,000), 7 percent of the semitrailers (4,000) and 7 percent of the single-unit trucks (20,000) were ABS-equipped. In all of Western Europe, in 1987, less

than 10 percent of the various vehicle combinations were equipped with ABS.

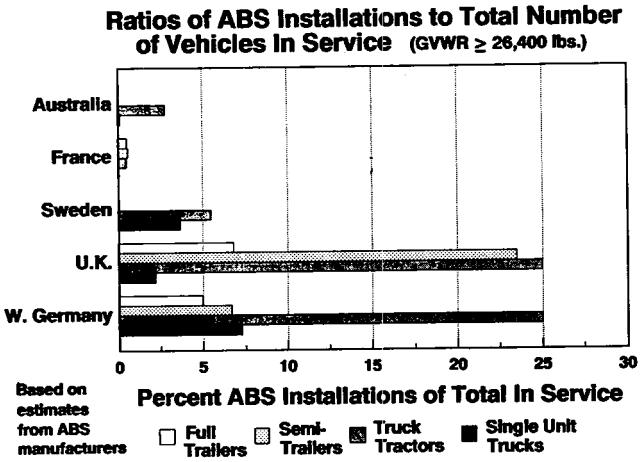

Figure 1. Ratio of ABS Installations to Total Number of Vehicles In Service (GVWR ≥ 26,400) (Fancher 1988)

It was projected then, that by the end of 1988, 37 percent of the truck tractors in West Germany and 30 percent of the truck tractors and semitrailers in the U.K. would be equipped with ABS. The validity of those forecasts has not been verified.

European and Australian fleet experience with ABS was based on discussions with 3 fleets in England, 6 in Germany, 2 in France, 2 in Sweden, 3 in Norway, and 5 in Australia. In general it was found that:

- Maintenance was done only when a malfunction warning light came on.
- Failure warning indications did not disrupt operations; the vehicles were able to continue on their routes if a failure warning was indicated.
- No special maintenance was performed on the ABS beyond routine periodic inspections.
- Radio frequency interference (RFI) problems were not evident.
- With proper maintenance, ABS life was expected to equal that of the vehicle.
- Carriers reported that drivers liked driving ABS-equipped vehicles.

ABS maintenance histories and experiences were developed primarily from ABS truck manufacturer supplied information. In 1985, Lucas Girling reported on a survey of their service visits for the period of January 1983 to May 1985. There was a rapid increase in the population of ABS-equipped vehicles during that time period. Service calls ranged from 5 to 30 per month on from 6,000 vehicle at the beginning of the period to approximately 18,000 vehicles in May 1984. The ABS components needing servicing are shown in Figure 2 The "Other" category includes a wide range of miscellaneous items such as welding near wires or components causing failures, unintentional disabling of the system during maintenance, etc., as well as many cases in which service visits were made, but no problems were found.

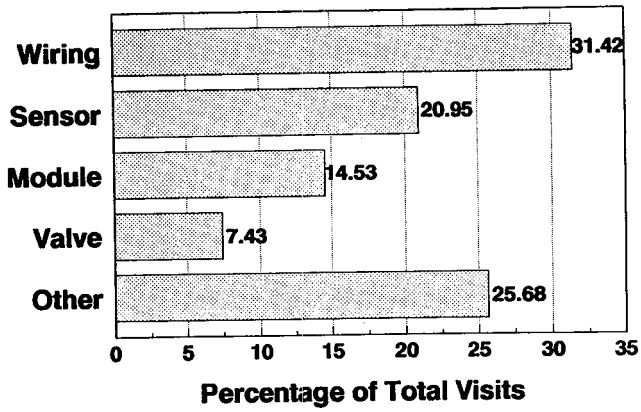

Figure 2. Service Visit Analysis by Component (Lucas-Girling, 1988)

Approximately 1.7 percent of the vehicles in use had a problem difficult enough to merit a service call in a year.

Crane Fruehauf reported that of the 14,860 warranty claims it experienced on its trailers for the 1982-87 time period, 5.7 percent were ABS related.

One German ABS manufacturer supplied information relating to the number of defective components it had received back from the field in the mid-1980's. Out of approximately 250,000 sensors it had produced, 21 (.008 percent) were found to have defects. Similarly, for approximately 250,000 solenoid valves, 55 (.02 percent) were found to have defects created during production. Out of approximately 60,000 electronic control units, 55 (.09 percent) were found to have production defects. Daimler-Benz reported it sold approximately 40,000 ABS-equipped vehicles 1982-87. Approximately 2 percent of the ABS-equipped vehicles sold in 1987 experienced some type of problem. The causes of those failures were divided among components as follows: sensors, 25 percent; cable and connectors, 50 percent; ECUs, 21 percent; and solenoid valves, 4 percent. They expected the failure rate to drop to about 1 percent of the vehicles produced in 1988 and beyond.

Australian reliability data were scarce. Between 1983-87 Daimler Benz produced 1186 ABS-equipped tractors in Australia. Those vehicles experienced 22 ECU failures (2 percent), 2 sensor failures (0.2 percent), and 4 (0.3 percent) solenoid valve failures. Two (2) of the ECU failures were caused by mechanics welding around wires/cables. In all, 2.4 percent of the Australian population of ABS-equipped vehicles experienced a failure.

Synthesizing all these reports, the study author concluded that if ABS was placed in U.S. fleet service, between 1 and 5 malfunctions could be expected to occur per 100 vehicles per year.

The NHTSA ABS Fleet Evaluation Program

Planning for a U.S. field test of the new generation of ABSs began in 1986. The first trucks became operational in the fall of 1988. The program's objective is to ascertain the reliability, maintainability, and durability of currently available (1988) heavy truck ABSs.

Participants

NHTSA's fleet evaluation of ABS-equipped heavy trucks is a cooperative effort with industry, without whose help the program would otherwise not have been possible. ABS suppliers, the major U.S. truck manufacturers, and truck user groups (such as the National Tank Truck Conference of the American Trucking Associations and the National Private Truck Council) were instrumental in providing technical advice, manpower, and hardware to make the program possible.

The initial focus of attention was on truck tractors. These vehicles were chosen because:

- Combination-unit trucks are much more frequently involved in serious (fatal/injury producing) crashes than are single-unit trucks;
- There were fewer tractor manufacturers in the U.S. (7 major) compared to trailer manufacturers (over 400) and, in general, their engineering capability to adapt the systems to their vehicles, within the time frame desired, was more extensive; and
- Tractor ABSs were further along in terms of development and commercial availability than were trailer systems.

Fleet participants were sought using the following criteria:

- Planned acquisition of new tractors in the 4th quarter of 1988 or the 1st or 2nd quarters of 1989;
- Location in northern, cold weather climate cities in order to expose the ABSs to as rigorous an environmental (and, therefore, operational) test as possible;
- Centralized fleet operations, where vehicles were dispatched from and returned to the same location frequently (preferably once or more a week) and all vehicle maintenance was done on the vehicles at that location (thereby facilitating access to records on all maintenance work done on a particular vehicle);
- Availability of a credible maintenance record keeping system, preferably automated, that would give a complete accounting of all maintenance performed on the vehicles; and
- Interest in the program, and a willingness and commitment to provide access to records and participate in the data collection process.

The industry program participants are shown below. WABCO and Rockwell have since formed a joint venture (Rockwell/WABCO Vehicle Control Systems Co.) to market a combined line of products. Table 1 further describes the nature and type of trucking operations involved in the test.

- Truck Manufacturers:
  - Ford
  - Freightliner
  - Kenworth
  - Mack
  - Navistar
  - Peterbilt
  - Volvo-GM
- ABS Suppliers:
  - Bendix
  - Bosch
  - Midland
  - Rockwell
  - WABCO
- Manufacturers of Axles with In-Axle Sensors:
  - Dana
  - Eaton

Table 1. Participants In the ABS In-Service Fleet Evaluation

FLEET NAME	LOCATION	TYPE OPERATION	TRAILER TYPE	TYPE ROUTES	DATE TEST VEHICLES WENT INTO OPERATION	TRACTOR MANUFACTURER	ABS SUPPLIER (# Each)
Associated Grocers	Seattle	Private Carrier, Grocery Distribution	Dry & Refrigerated Vans	Local & Regional	10/88	Freightliner	WABCO (9) Rockwell (5)
KMD Inc.	Seattle	Contract/Common Carrier, Truck Load	Dry Van	Over-the-Road	12/88	Kenworth	Rockwell (8)
DiPietro Trucking Co. Inc.	Seattle	Contract/Common Carrier, Truck Load	Dry Van	Over-the-Road	5/89	Peterbilt	WABCO (8)
Safeway Food Stores	Seattle	Private Carrier, Grocery Distribution	Dry & Refrigerated Vans	Local & Regional	2/89	Navistar	Bosch (9) Bendix (10)
Mobil Oil Co.	Chicago	Private Carrier, Gasoline Distribution	Tankers	Local	11/88	Freightliner	Rockwell (4) WABCO (4)
Transport Services Inc.	Chicago	Contract/Common Carrier, Chemicals & Petroleum Products	Tankers	Over-the-Road	7/89	Mack	Midland (9)
Certified Grocers Inc.	Chicago	Private Carrier, Grocery Distribution	Dry & Refrigerated Vans	Local	3/89	Ford	Bendix (13)
Continental Baking Co.	Chicago	Private Carrier, Food Products	Dry Vans	Local & Regional	2/89	Freightliner	Rockwell (4) WABCO (4)
A.M. Castle Co.	Chicago	Private Carrier, Specialty Metals Wholesaler/Distributor	Flatbeds (1 doubles unit)	Regional	2/89	Kenworth	Bendix (9)
Manfred Motor Transit Co.	Detroit	Contract/Common Carrier Food Products, Chemicals, Petroleum Products	Tankers	Local & Regional	5/89	Freightliner	WABCO (8)
Chrysler Transport Co.	Detroit	Private Carrier, Motor Vehicle Parts	Dry Vans	Regional	6/89	Volvo-GM	Rockwell (8) WABCO (8) Midland (5) Bosch (5) Bendix (8)
Frito Lay	Detroit	Private Carrier, Food Products	Dry Vans	Regional	3/88	Ford	Rockwell (7)
Markem Co. Inc.	Joplin	Contract/Common Carrier, Truck Load	Dry Vans	Over-the-Road	5/89	Freightliner	Midland (12)
Matlack Inc.	Columbus, OH	Contract/Common Carrier, Chemicals & Petroleum Products	Tankers	Over-the-Road	8/89	Mack	Midland (11)
Perlman-Rocque Inc.	Minneapolis	Private Carrier, Food Products Distribution	Dry & Refrigerated Vans	Regional	4/89	Volvo-GM	Bosch (6)
Super Valu Food Stores	Minneapolis	Private Carrier, Grocery Distribution	Dry & Refrigerated Vans	Local & Regional	6/88	Peterbilt	Bosch (12) Rockwell (6)
Wayne Transport Inc.	Minneapolis	Contract/Common Carrier Chemicals & Petroleum Products	Tankers	Over-the-road	6/89	Peterbilt	Bosch (5)

Types of Systems Under Test

Because there are no regulations governing the design or performance of heavy truck ABS brake systems, designers have taken a number of different approaches to configuring their systems for U.S. applications. Those differences are evident in:

- System configuration, i.e., the number and location of wheel-speed sensors and the controlling function of the brake air pressure modulating valves used in the system; and
- The type of wheel-speed sensor used (i.e., wheel-end versus in-axle).

System configurations. A major distinction among the systems is whether they sense and control wheel-slip at both the drive and steer-axles of the vehicle or at the drive-axle(s) alone. Figure 3 is a schematic of a full individual wheel control, 6-channel ABS for a 3-axle truck or truck tractor. For the NHTSA test, WABCO was the only supplier of this system configuration designated as a 6S/6M (6 sensors; 6 modulator valves).

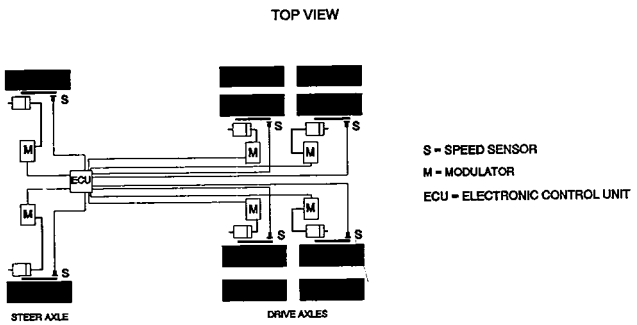

Figure 3. Schematic of a 6S/6M ABS

With this system, the speed at each individual wheel position is sensed. Brake application air pressure is individually modulated should wheel-slip occur at that wheel. Systems that control steer-axles typically employ a modified individual wheel regulation (MIR) scheme for the front axle wherein both steer-axle brakes are modulated simultaneously on a select-low at the onset of braking, but gradually shift to individual wheel regulation (IR) as the vehicle decelerates.

A 4S/4M system, that treats both drive and steer-axles, is a variation of the full 6S/6M system that employs fewer wheel-speed sensors and modulators. Like the 6S/6M system, it employs MIR on the steer-axle. Wheel-speeds are also sensed on one of the two drive-axles (typically the lead axle on a four spring suspension and the trailing axle on an air bag suspension). When wheel-slip is noted, braking air pressure is modulated to the wheels on both drive-axles on that side of the vehicle, yielding a side-to-side control strategy. WABCO, Bosch, and Midland all supplied versions of this configuration for the test. It is shown schematically in Figure 4.

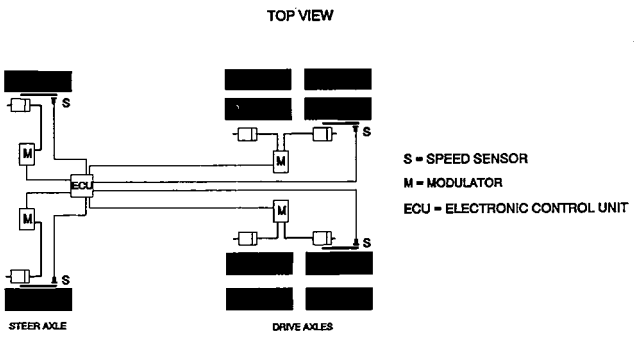

Figure 4. Schematic of a 4S/4M ABS

Also included in the NHTSA test program are several variations of systems that control only the drive-axle(s) of the tractor. One, a 4S/2M system, is shown schematically in Figure 5. This system is essentially two independently acting, select-low axle control systems, one mounted on the lead axle of the tandem drive-axle set, the other on the trailing axle of the set. Bendix supplied this system for the test.

Another version of a drive-axle-only system in the NHTSA test is a 2S/2M configuration. Wheel-speeds are

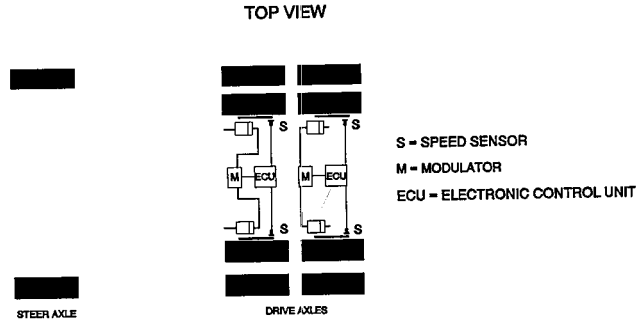

Figure 5. Schematic of a 4S/2M ABS

sensed on one of the two drive-axles and, as before, when wheel-slip is noted, braking air pressure is modulated to the wheels on both drive-axles on that side of the vehicle, yielding a side-to-side control strategy. Bosch supplied a version of this configuration for the test. It is shown schematically in Figure 6.

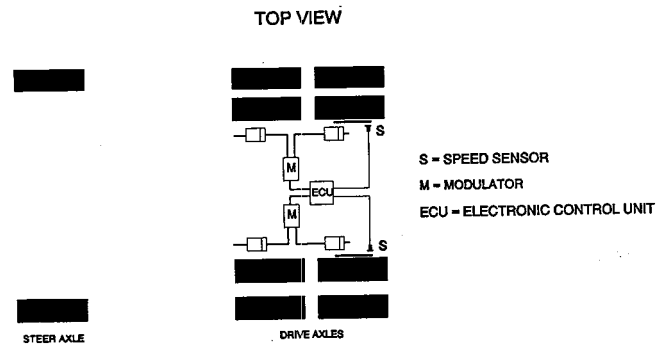

Figure 6. Schematic of a 2S/2M ABS

Bendix also supplied a single-axle version of their system shown schematically in Figure 7, a 2S/1M configuration. With this configuration, wheel-speeds are sensed on the lead axle of the tandem drive-axle set. When wheel-slip is noted, on either side, brake pressure to all four wheel positions in the tandem-axle set are modulated as a group.

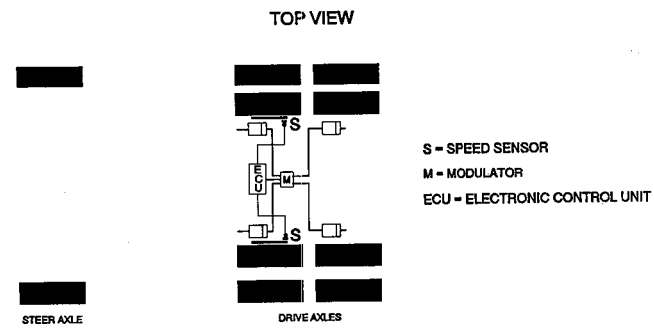

Figure 7. Schematic of a 2S/1M ABS

The least complex system in the NHTSA test, a 1S/1M is shown schematically in Figure 8. It employs one speed sensor, mounted on the differential of the trailing axle of the tandem drive-axle set, which monitors gear speed in the differential from which wheel- speed activity is

computed. When wheel-slip is noted, all the wheels in the tandem-axle set are modulated simultaneously, yielding a tandem-control strategy. Rockwell supplied this configuration system for the test.

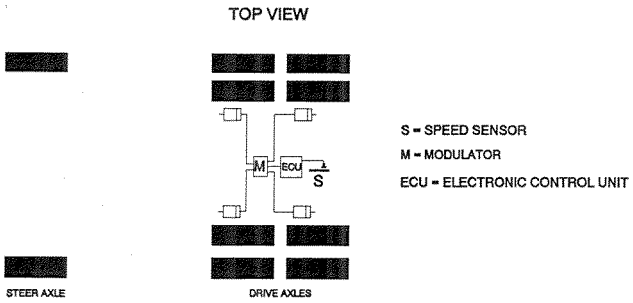

Figure 8. Schematic of a 1S/1M ABS

Wheel-speed sensor types. There are two approaches to sensing wheel-speeds represented in the test: wheel-end and in-axle. The wheel-end approach utilizes a single point, variable reluctance, fixed sensor and rotating exciter ring that is mounted within the foundation brake drum and shoe assembly at the wheel hub end. Figure 9, the Midland unit, is an example of this type sensor. Bosch and WABCO supplied sensors for the test that are similar in concept but utilize a forged rather than a stamped exciter ring that is press-fit onto the wheel hub rather than being bolted to it. The Bosch/WABCO sensor arrangement is shown in Figure 10.

A variation on the wheel-end sensing approach utilizes a fixed sensor mounted external to the brake drum assembly that is excited by notches in the rear of the brake drum itself. Bendix employed this sensing approach on some of its test systems. It is shown in Figure 11.

Eaton and Dana supplied drive-axles for this test that were equipped with in-axle speed sensors mounted in the area of the differential. The objective of in-axle sensing is to remove the sensor from the potentially "hostile" wheel-end operating environment, thereby improving its reliability. The Eaton in-axle sensor, shown in Figure 12, was mated with the Bendix system, as was the Dana in-axle sensor system. The Dana sensor arrangement is shown in Figure 13.

Finally, the Rockwell ABS employs an in-axle sensor mounted in the differential of the trailing axle of the Rockwell tandem drive-axle set. It is shown in Figure 14.

The matrix of ABS configurations and wheel sensing approaches for the test vehicles is shown in Table 2.

Maintenance Data Collection

Records obtained from each of the participating fleets are the basis for the maintenance service histories on each of the ABS-equipped trucks in the NHTSA test program. The fleets were asked to keep detailed records of each and every incident involving any maintenance work done on the test trucks on subsystems/components

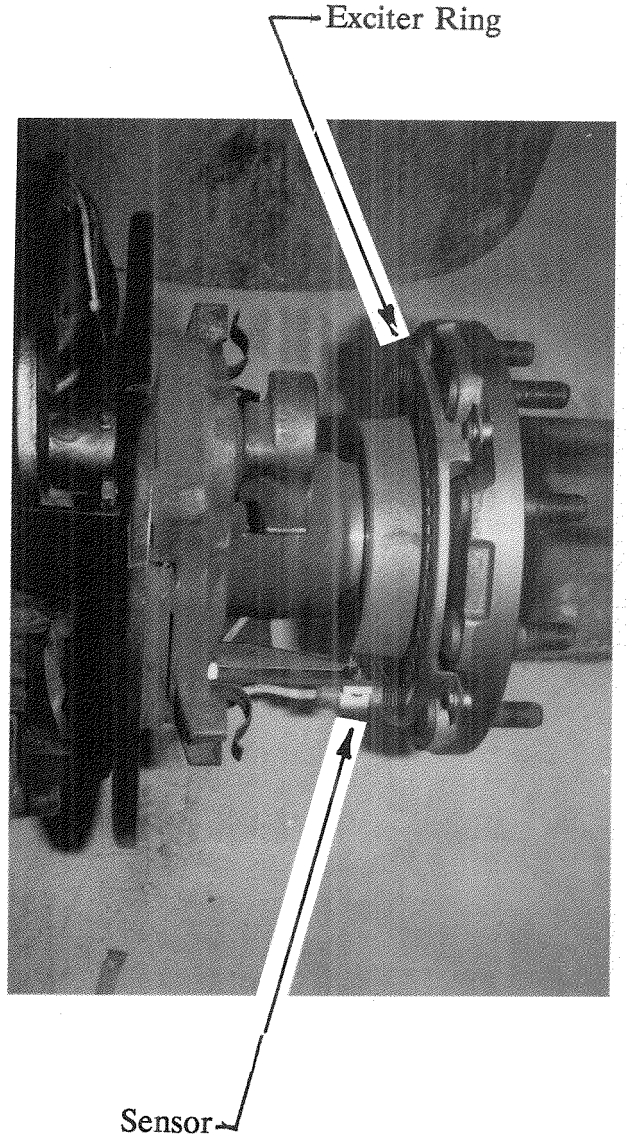

Figure 9. Midland Wheel Sensor Configuration

of interest in this test program. In addition, drivers' reports of failure warning light indications or other comments were solicited.

Periodically (at least once a week), on-site contractor personnel visited each fleet to gather new maintenance records and talk to drivers and mechanics about their experiences or to clarify recorded information. The recorded information, supplemented and verified by conversations with mechanics and drivers, was encoded into an automated data file.

The American Trucking Associations' Vehicle Maintenance Recordkeeping System (VMRS) is a detailed data collection system that enables fleets to track maintenance activities and costs by major subsystems/components. The VMRS was screened for those activities/costs which might be affected by the change of the truck's brake system to include an ABS.

Accordingly, maintenance data on the following items/systems were collected for each test vehicle in the

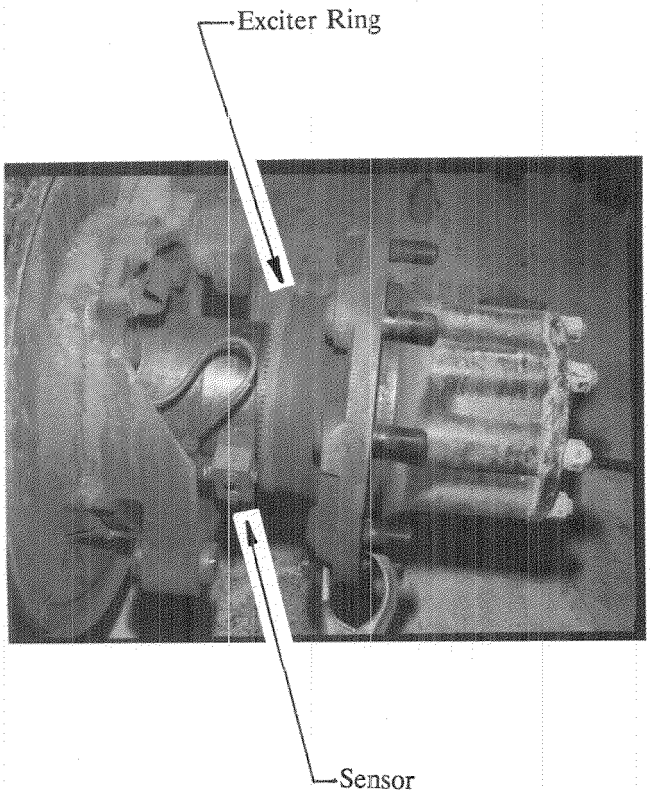

Figure 10. Bosch/Wabco Wheel Sensor Configuration

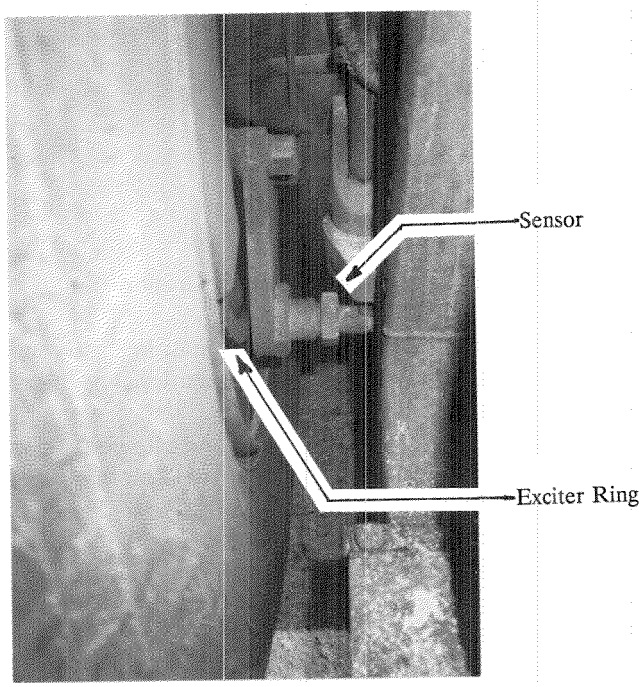

Figure 11. Bendix Wheel Sensor Configuration

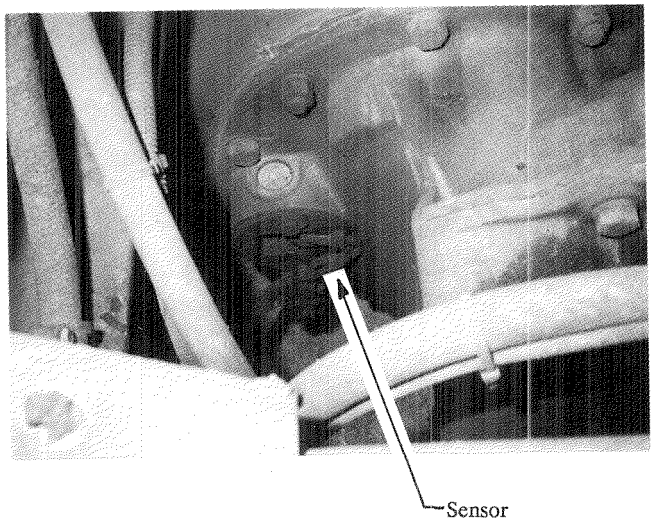

Figure 12. Eaton In-Axle Sensor

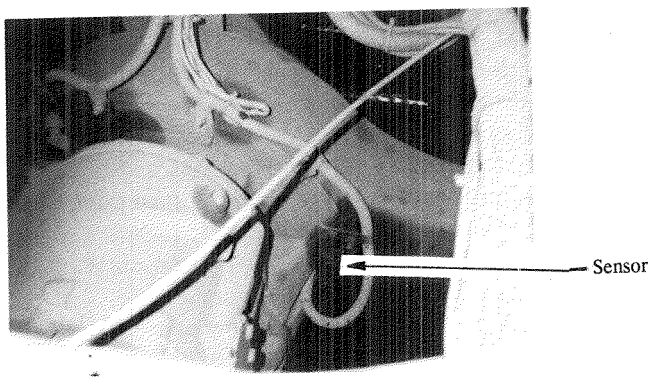

Figure 13. Dana In-Axle Sensor

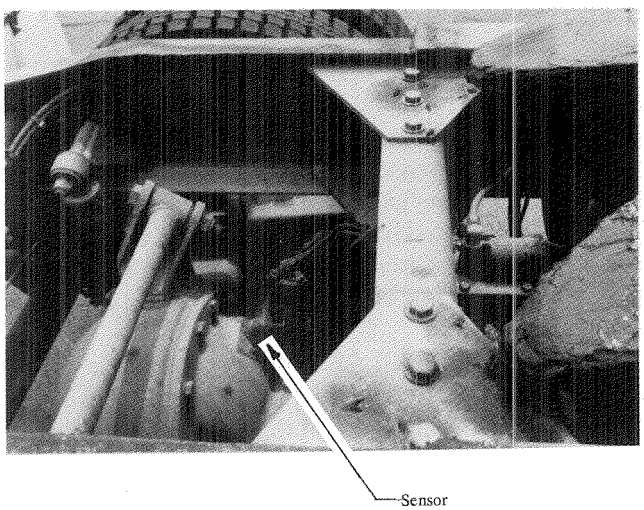

Figure 14. Rockwell In-Axle Sensor (Inside Differential)

study. In addition, the maintenance histories on the same components, on an equivalent sample of non-ABS-equipped trucks in the same fleets were also collected or reconstructed in order to provide a comparison set of data on the non-ABS-related components listed below.

- *ABS*—including wiring, connectors, sensors, modulator valves, electronic control units, and associated miscellaneous parts;
- *Brakes*—including the foundation brake assembly (drums, shoes, linings, S-cams) and slack adjusters;

Table 2. ABS Configurations and Fleet Evaluation Program

ABS Configuration	ABS Supplier	Fleet (No. in Test)	Wheel-Speed Sensors
Drive-Axle-Only Systems			
1S/1M	Rockwell	Associated Grocers (5) Chrysler Transport Co. (8) Continental Baking Co. (4) KMD Inc. (6) Frito Lay (7) Mobil Oil Co. (4) Super Valu Food Stores (6)	Rockwell/In-Axle
2S/1M	Bendix	Safeway Food Stores (10)	Dana/In-Axle
2S/2M	Bosch	Perlman Rocque (6)	Bosch/Wheel-End
4S/2M	Bendix	A.M. Castle Co. (9) Certified Grocers, Inc. (13) Chrysler Transport Co. (4) Chrysler Transport Co. (4)	Eaton/In-Axle Eaton/In-Axle Eaton/In-Axle Bendix/Notch-Drums
Drive and Steer Axle Systems			
4S/4M	Bosch	Chrysler Transport Co. (8) Safeway Food Stores (9) Super Valu Food Stores (12) Wayne Transport, Inc. (5)	Bosch/Wheel-End
4S/4M	Midland	Chrysler Transport Co. (8) Matlack Inc. (11) Monkem Co., Inc. Transport Services, Inc. (9)	Midland/Wheel-End
4S/4M	WABCO	Chrysler Transport Co. (8)	Wabco/Wheel-End
6S/6M	WABCO	Associated Grocers (9) Continental Baking Co. (4) Dipietro Trucking Co. (9) Manfredi Motor Transit Co. (6) Transport Services, Inc. (6) Mobil Oil Co. (4)	Wabco/Wheel-End

- *Air System*—including all air brake pneumatic valves, air brake chambers, hoses, air compressor, air reservoirs, and associated miscellaneous parts;
- *Tires/wheels*—as well as bearings and wheel seals; and
- *Electrical System*—including wiring, gauges, lights, fuses, battery, alternator, switches, and other miscellaneous electrical components.

The collected data were subdivided into two major categories: "start-up" and "in-service" maintenance/repairs. Start-up problems were those present when the vehicle was delivered to the motor carrier and typically were attributable to installation oversights/problems. This distinction was felt necessary to differentiate between problems that were the result of operational use (i.e., "running" or "in-service" problems) and, therefore, were an indication of the ABSs reliability, and those which could not be attributed to ABS design/performance characteristics.

The maintenance needed to make the system functional was further subdivided into four categories describing the extent or nature of the work done. The following descriptions were applied:

- *Inspect*—this category includes all incidents in which the failure warning light on the dash activated, but no problem was found and the system was merely reset. In some instances this problem would not manifest itself again on that vehicle. In others, the failure warning was intermittent and occurred multiple times on the same vehicle. In most instances, the cause of the failure warning indication could not be determined. In others, after repeated instances, the cause became apparent and was corrected. That corrective action was noted separately.
- *Adjust*—this category includes all incidents involving an adjustment to correct a failure warning light indication. In almost all instances, this involved adjusting the air gap between the wheel-speed sensor and the tone-wheel to correct an apparent failure of a wheel-speed sensor. In other instances, connector pins were straightened or the connectors were simply snapped together tighter.
- *Repair*—this category includes all incidents in which physical repairs had to be made to an ABS component in order to make the system functional again after a failure warning light indication. Examples include reconnecting totally disconnected or partially connected connector fittings or cleaning the fitting of contaminants. It also includes a number of cable rerouting and securements with wire harness tie-wraps.
- *Replace*—this category includes all incidents involving failure and replacement of an ABS component part. This is the only category in which replacement parts costs were incurred.

Start-up incidents. As previously noted, at the time the NHTSA test program began, only the Freightliner Corp. offered ABS as an available option, specifically the WABCO system. As such, Freightliner was the only truck manufacturer with experience doing the detailed engineering and product development test work necessary to ensure that the systems were properly packaged and installed on their vehicles. Even Freightliner had no experience installing the other ABSs which were installed on some of its trucks as part of this test program. As a result, many of the ABS installations for this test were being done for the first time by the truck manufacturers and suppliers involved.

Additionally, the various ABSs under test were in various stages of product development and, therefore, design "maturity." The three European systems (WABCO, Bosch, and Midland) have been in production and use since the early 1980's, but two of them had only recently been modified to operate using a 12 volt, rather than 24 volt, power supply. The Rockwell and Bendix designs were newer and not available as production items at the time the test program began. The Rockwell system is still not commercially available. Test units of these systems were pre-production prototypes or early versions of evolving designs.

The truck manufacturers and ABS suppliers worked together closely to install the systems on the test vehicles. In some cases they were done on the truck manufacturer's assembly line, while in others it was done "off line" in special vehicle preparation areas. In two instances, it was done by a manufacturer/supplier

team at the manufacturer's local dealer before the trucks were delivered to the carrier.

Due to the quasi-experimental nature of some of the installations and state of product development of some of the ABSs, it is not surprising that some of the test vehicles were delivered to the participating motor carriers with pre-existing problems that, for one reason or another, caused the ABS to not function properly. In order to differentiate these type problems from those that could be attributed to the ability of the ABSs to function properly in normal in-service use, they were separated and categorized as one-time "start-up incidents."

Several groups of vehicles experienced similar start-up problems, whereas in other cases, isolated problems arose with only one vehicle. For example:

- One of the ABS supplier's systems experienced an unusually high number of failure warning indications from the beginning of their test vehicles' operation. Fifty-nine (59) inspections/ECU resets occurred on 17 vehicles before the cause of the problem was determined. After extensive diagnostic work by the supplier, it was determined that the computer algorithm used to test wheel-speed sensor electrical signal integrity was overly conservative and, as a result, false sensor-failure warnings were being triggered. This necessitated changing the ECUs on the entire group of 19 tractors in service at that point, which were equipped with this ABS, to a model with a different algorithm. This "new" ECU was also installed on the remaining 21 test units that had not yet been built and placed in service. This change eliminated this source of failure warnings.
- The electrical power source to the ECU on a group of four trucks was incorrectly wired, at installation, through the starter solenoid. These four trucks had to be rewired to make the ABS function properly.
- In a similar incident, another group of 23 tractors had to be rewired to provide a separate electrical power source for the dash-mounted failure warning lamp in order for it to function properly.
- Intermittent failure warnings were noted on 3 trucks from the beginning of their operation. Upon inspection, some of the trucks were found with a connector in the wiring harness that was incompletely assembled. All 17 vehicles using connectors of that type were inspected by disassembling and reassembling the connector, in some cases pushing the connector pins into position better, in most others doing nothing other than the disassembly/reassembly. Incorrect failure warnings on the 3 trucks ceased after this.
- On another truck, a sensor cable needed to be rerouted and resecured because of an interference/pinching problem with the wire and the steering gear.
- A group of 12 tractors experienced physical interference problems between ABS modulator valves installed on the tractor's frame rail and the tractor's driveshaft. The modulator valves were inadvertently installed at a location such that the pipe thread fitting on the air output port of the valve came in contact with the driveshaft if it moved upward with drive-axle suspension travel. All 12 valves were relocated. The fittings on five of these modulator valves had to be replaced due to damage they sustained before the relocation could be accomplished. On two of the trucks, contaminants were discovered in the pipe thread fitting. The valves were cleaned before the fittings were reinstalled.
- In another fleet, the modulator valve on one truck was found to contain a liquid residue that remained from a quality control check done on the valve at its point of assembly. It could not be repaired and was replaced.
- The modulator valve on another truck was delivered with a slight air leak that was attributed to a "stack-up" of tolerances on internal components in the pneumatic portion of the valve. It was replaced.
- On delivery check-out of one truck, the locking ring on the wire connector to a modulator valve was found to be loose. On another truck the power cable to the ABS ECU was found to be incompletely connected. In both cases, the problem was corrected before the vehicle was placed in service.
- One truck experienced problems with wheel-speed sensor attachment hardware, which was adjusted and tightened, making the system functional.
- Finally, two wheel-speed sensors on two trucks were not adjusted properly when the ABS was installed. When the sensor's air gap was adjusted, the ABS functioned properly.

In all, 59 trucks out of the 200 (29 percent) experienced start-up problems of one type or another. This relatively high percentage is indicative of the "newness" of the systems in North American applications. Problems of this type are not uncommon when new models of vehicles or new systems are first produced and delivered. A major complaint of trucking fleets is that their newly-purchased vehicles rarely can be operated immediately. In general, they always experience some down time to make the minor adjustments needed to make the vehicle operational.

Table 3 lists the number of trucks requiring start-up maintenance as a function of which ABS component required servicing. In some cases, individual trucks needed maintenance on more than one component and, therefore, the numbers are not additive. Problems were relatively evenly distributed among the components in the ABS needing work.

In the case of components that had to be replaced in order to make the system functional, wiring and ECU replacements were most prevalent. Each of these, however, was attributable to one generic "problem" (e.g., the replacement of ECUs because of the conservative failure

Table 3. ABS Start-Up Maintenance by System Component Needing Work

ABS Component	Number of Trucks Needing "Start-up" Inspections, Adjustments or Repairs on this Component	Number of Trucks Requiring Replacements of this Component
Wiring Cables	13	17**
Wiring Connectors	16	0
Sensors and Related Parts	19	0
Modulator Valves	12	2
ECU's	17	19**
Other*	9	0
Total	52	42

*Other includes: Checking and resetting the system-no other failure apparent, relocating a number of solenoids; rewiring due to installation oversights; and one wire resecurement.
**One problem represented all these replacements
Note: Individual column numbers are not additive since specific trucks may have needed maintenance on more than one component. Source: NHTSA, 1991

warning logic) that necessitated work on a number of trucks.

In-service maintenance work. For the purposes of this analysis, April 30, 1990, was chosen as "cut-off" date for including in-service maintenance work done on the test vehicles. For many of the test vehicles, this represents less than one year of operational use. For a small number, it represents 18 months of operational service. All the trucks have been in operation during at least one Winter. As of April 30, 1990, 19,792,131 miles of travel had been accumulated by the 200 test vehicles (98,960 miles avg/vehicle).

As was the case with start-up problems, a number of generic or similar in-service incidents have occurred on multiple numbers of trucks. These have included the following:

- A total of 63 trucks have experienced intermittent failure indications during their operation. In 36 of the cases (57 percent), the vehicle experienced one of these types of failure warnings and the source/cause of the problem could not be found. In these cases the ABS either was manually reset or the warning light did not reactivate when the truck's ignition was turned off and subsequently turned on again at some later time. All five ABSs in the test have had this experience with at least one of their forty test trucks.
  - The problem with seven of the remaining 27 vehicles was ultimately traced to an inadequate wheel-speed sensor retaining clip that allowed the speed sensor to get out of adjustment. It was replaced on all 7 vehicles. This could justifiably be considered a start-up problem that was not uncovered until later in the vehicles' service life.
  - One other vehicle ultimately had its ECU replaced, only to have it fail a second time and have to be replaced again.
  - The remaining 19 vehicles have experienced more than one failure warning, interspersed over time (two vehicles experiencing 17 and 15 separate indications respectively), without the source of the problem being uncovered yet.
- Four (4) trucks, besides the one described above, have had failed ECUs replaced.
- In a group of 4 trucks with notched-drum wheel-speed sensors, 3 trucks have needed defective wheel-speed sensors replaced; one truck requiring two replacements. Two wheel-end speed sensors on two other trucks also were replaced.
- Thirteen (13) different trucks have had the air gap on a wheel-speed sensor adjusted in order to rectify a failure warning, three trucks having this done twice each.
- Miscellaneous wiring or connector problems, most of them single incidents, have had to be repaired on 24 different trucks at one time or another during the course of their operation.
- One truck experienced a failure of its combination modulator/relay valve that effectively restricted supply air from being transmitted to all the wheels on the tandem drive-axle set when the driver was attempting to make a stop. Braking effectiveness was substantially reduced as the vehicle was essentially reduced to having brakes only on its steer and trailer axles under this condition. Upon a subsequent tear-down of the valve, the coating on a sliding piston in the modulator section of the valve was found to have corroded. On this brake application, the piston "froze" in such a position as to prevent air from exiting from the output ports of the relay valve. The supplier recognized this to be a manufacturing defect. All 40 of the test units were inspected for this defect and this portion of the valve was replaced on all 39 of the remaining test units as a precaution. The supplier of this ABS does not plan to use this valve design in subsequent models of its product.

In all, 114 trucks out of the 200 (57 percent) have experienced incidents involving the ABS at one time or another during their in-service operation. However, 40 of these incidents were essentially one problem—the modulator valve slide piston manufacturing defect—and 36 of these incidents were involved one failure light warning indication for undetermined causes. The work done on most of the trucks was of a minor adjustment nature (recrimping wires, snapping loose connectors together, etc.), or involved inspections for intermittent problems with undetermined causes.

Excluding the trucks that experienced the modulator valve slide piston manufacturing defect (which is, in effect, one problem) 15 trucks have had a total of 20 deficient/defective ABS component parts replaced; 7 wheel-speed sensor retaining clips, 6 ECUs and 7 wheel-speed sensors. The retaining clip problem could, from one perspective, be considered a start-up incident, leaving the ECU and wheel-speed sensor failures as the relevant ones to consider.

Five of the seven wheel-speed sensors in question were the exposed, notched-drum type from the early FMVSS 121 era. This design is not likely to be used beyond this test. Thus, the 6 ECU failures, and the two other wheel-end speed sensor failures are the only significant ABS component failures that have occurred during this test, to date.

It is interesting to compare these results to those that were predicted three years ago based on the study of European experience with ABS (Fancher, 1988). The study predicted 2-10 malfunctions for the entire 2-year NHTSA study, based on experiences of European truck operations. If the slide piston valve and the notched drum speed sensor failures are each considered to be one problem, then 10 failures have been noted to date and the study is essentially 60% completed. Thus, the number of failures that have occurred are within the range predicted by the European study and, if anything, may be overstated since the present study captured virtually all maintenance work done, whereas the European/Australian study relied exclusively on warranty data.

Frequency of ABS Actuation

In addition to maintenance data, electronically measured information is being continuously recorded on each test truck, as well as 16 non-ABS-equipped control trucks. These systems would enable continuous monitoring of whether the ABSs are operating. This capability amounts to having a "check" on whether drivers report ABS failure warning indications. In some cases, they were not. Having this capability has enabled problems to be quickly identified, diagnosed, and corrected. Data from these systems also allow development of statistical summaries describing how often and under what operating conditions, the systems activate.

These systems have also enabled detailed analyses of system functioning/operation in critical situations. Analysis of recorder data has verified that none of the crashes in which test vehicles have been involved were attributable to improper ABS functioning. The recorder was especially useful in determining that, during a very serious crash that occurred during the test program, the truck's ABS functioned properly. In that case, the ABS's operation probably enabled the truck driver to avoid having a fatal crash.

The recorder that was designed for this test (shown in Figure 15) monitors and records the following parameters:

- Brake application pressure at the treadle (foot) valve;
- Air brake pressures at the brake chambers of wheels controlled by ABS modulator valves;
- Electrical current flowing to modulator valves, thus indicating modulator valve actuation;
- Wheel rotational speeds at wheels controlled by ABS modulator valves; and
- Vehicle deceleration.

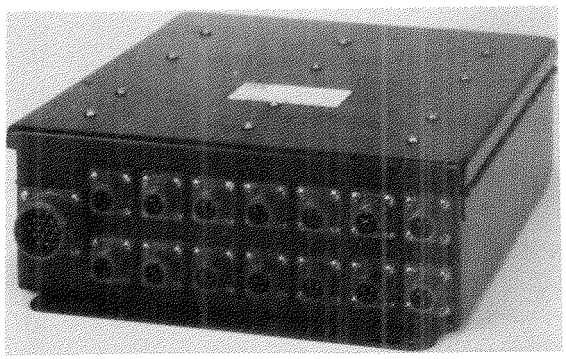

Figure 15. ABS-Data Recorder

When the brake system is functioning in its normal mode, the recorder counts the number of times the brakes are applied and measures the amount of air pressure applied at the treadle valve. Vehicle deceleration is also measured. This capability enables histograms to be developed describing the frequency and range of brake applications at various application pressures and deceleration levels.

The data in Figures 16 and 17 show averages for all the stops made by all the test trucks for the time period February-April 1990 (plots from different time periods are similar to these). The vast majority of these brake actuations are at very low application pressures and deceleration levels, indicating that most drivers attempt to anticipate the need to stop and, therefore, gradually slow and stop their vehicles without having to make "hard" stops. As could be expected, under these conditions, the vehicle's ABS rarely needs to activate.

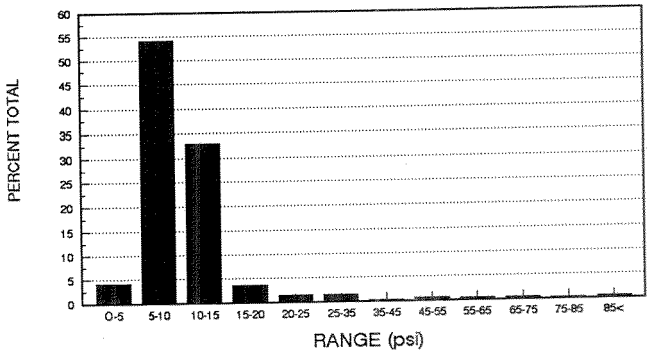

Figure 16. Treadle Valve Pressure History (February 1990-April 1990)

In situations where either an ABS modulator valve actuates, a wheel begins to lock up, or a pressure differential is noted across a modulator valve, the recorder detects these occurrences and records all measured parameters at 100 millisecond intervals for 1 second before the event starts, at 20 millisecond intervals during the time the ABS is functioning, and again at 100 millisecond intervals for 1 second after the ABS event ends. It does this by continuously recording the measured

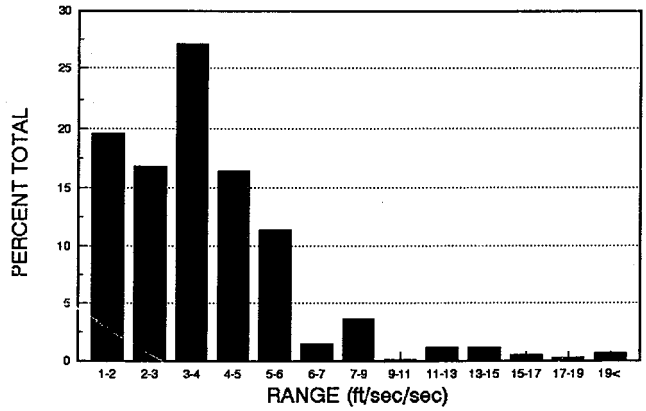

Figure 17. Deceleration Rate History (February 1990-April 1990)

parameters in a buffer memory which is only transferred to permanent memory if an ABS actuation takes place, otherwise it is written over. This type of recorder is analogous to the flight data recorder installed on commercial aircraft.

An example of an ABS event "captured" by the recorder is shown in Figure 18.

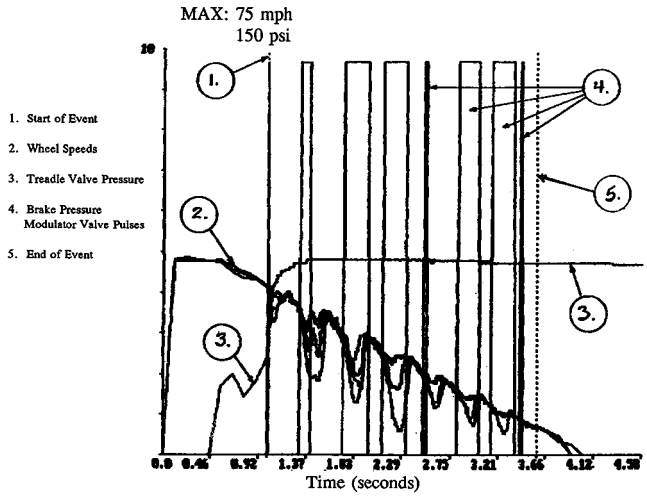

Figure 18. Recorder ABS Event

After recorder data are collected from each of the trucks, they are checked for accuracy and then pooled with data from other test trucks to enable the generation of statistical summary reports. One such report is shown in Figure 19.

This summary reflects only those ABS events which potentially have safety relevance, that is, a sufficient amount of wheel-slip (20 percent) to begin the onset of loss-of-control. It does not include counts of every ABS activation as there are an appreciable number of non "significant" ABS events that typically involve single activations of the modulator at one wheel of the system, at wheel-speed levels that may have been 85-95 percent of that of the other wheels on the vehicle. This could occur, for example, if a wheel hit a bump in the road or momentarily slipped on dirt or gravel when the vehicle

Summary For: All ABS Equipped Tractors
February, March, April 1990 - 1555 Files

73,776.5	hours of tractor operation
2,781,822	miles travelled
1,780,845	brake applications
3,250	Significant ABS events (*)
333	Major ABS events (**)
8,353	miles per major ABS event
5,347	brake applications/Major ABS event
1.6	miles per brake application

Significant Event (*) Distribution by Vehicle Speed and Solenoid Activity

Vehicle Speed (mph)	1 Cycle	2, 3, or 4 Cycles	5 or more Cycles
<25	1280	1091	238
25 - 45	273	203	83
>45	46	24	12

* A Significant ABS event is defined as one during which at least one wheel speed decreases to 80% or less of vehicle speed during braking and then increases speed coincident with solenoid operation at that wheel.

** A Major ABS event is a subset of the "Significant" ABS event population. It is defined as a single event which contains 5 or more instances in which a wheel slows to 80% or less of vehicle speed and then increases speed coincident with solenoid operation at that wheel.

Figure 19. Data Summary Report

was being braked. The consequences of such an event would not be "significant" and, therefore they were not included in the summary. The fact that they do occur, however, is an indication of the sensitivity of the systems.

The further differentiation of "major" ABS events from among the "significant" events is an attempt to estimate more conservatively the number of times the ABS activates in situations that could have led to loss of vehicle control. Thus, "major" ABS events were defined as being those in which the ABS's modulator valve(s) cycled 5 or more times, indicating that the system had to repeatedly activate to prevent the vehicle's wheel(s) from locking. It is easier to postulate that these ABS events might have involved loss-of-control had not the ABS been present. This would especially be true in cases involving initial vehicle speeds greater than 45 mph.

The data in Figure 19 indicate that, for the time period from February 1990 to April 1990, there was an average of one "significant" ABS event every 856 miles of vehicle travel and a "major" event every 8,353 miles of travel. Many of the trucks involved in this test accumu-

late 100,000 miles per year of operation. For a vehicle in this type of operation, the ABS is activating approximately once every 3 days, while a "major" ABS event occurs approximately once a month.

As could be expected, the average number of "significant" and "major" ABS events occurring per mile of travel varies depending on the time of year, regional location in which the truck is operated and, type of operation in which the truck is used. Figure 20 shows the seasonal variation in the number of "major" ABS events occurring per 10,000 miles of travel. The mean number of major ABS events per 10,000 miles was 65 percent higher during months in which slippery roads were more likely (December-February) compared to months in which slippery roads are less likely (October, November, March-May).

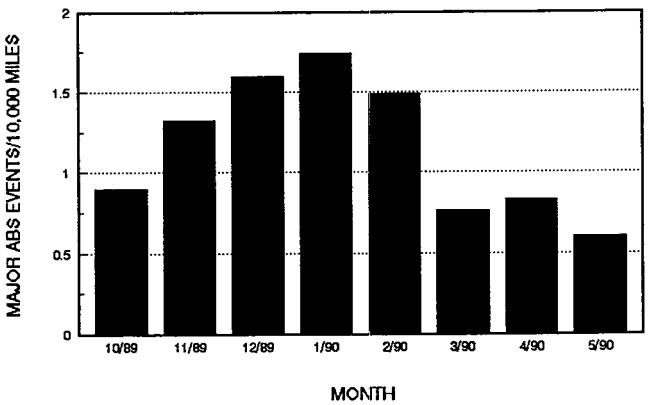

Figure 20. ABS Activity of Test Fleet by Month

Figure 21 shows the same metric, for October 1989-May 1990 time period, as a function of the individual fleets involved in the test, grouped by the region of the country in which the trucks operated, with a further notation as to the type of operation in which the fleet is engaged. Data from two of the fleets were unavailable for this time because changes in vehicle-dispatching practices precluded frequent enough recorder data off-loadings to prevent overwriting data and losing it. Changes have been made to correct this problem. One of the fleets had no major ABS events during this time period. As can be seen, there are wide variations as a result of these operational differences.

Finally, and possibly most importantly, differences among individual vehicles, the route(s) over which they are operated and the way the individual drivers handle their vehicles have a large influence on the number of times the ABS is likely to activate. Figure 22 shows the average number of "major" ABS events that were noted between October 1989 and May 1990 for 34 individual trucks in the program that were selected because of the comparatively high number of ABS activations they experienced compared to other vehicles in the test. The frequencies of ABS activations for these vehicles are compared to the overall average for the entire 200 truck

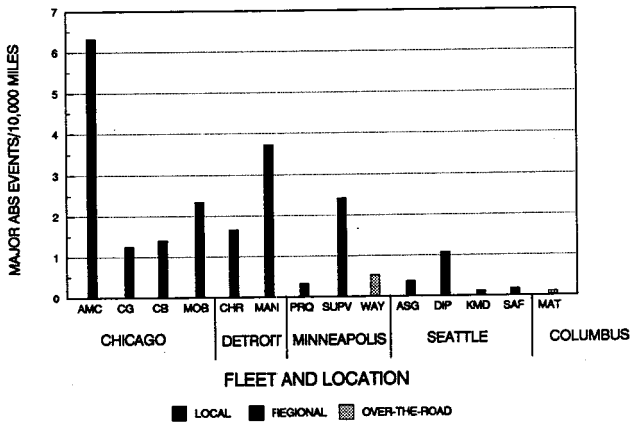

Figure 21. ABS Activity of Fleets by Location and Type

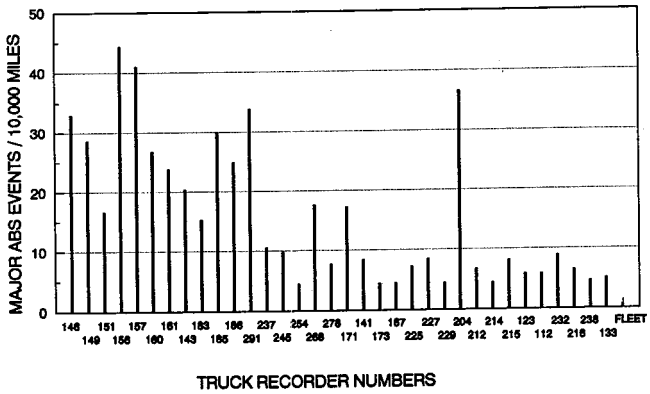

Figure 22. ABS Activity of Individual Trucks

fleet. There are extremely large differences between many of the individual trucks and the overall fleet average. These individual driver/vehicle/route differences may be much more significant as a determinant of the frequency of ABS activation than are factors associated with ABS design differences.

Driver Comments/Reactions

During the course of the field evaluation, drivers of ABS-equipped test trucks have been informally interviewed to elicit their opinions and experiences with the vehicles. The interviewers use an open-ended format to promote frank comments that are not biased by having to respond to a fixed set of questions. Results/findings are later transcribed and tabulated.

The results from a sample of 280 recent interviews are as follows:

- 259 (92.5 percent) of the interviewed drivers expressed moderate to high acceptance of ABS. Typical comments were: "Like system very much ...," "System works well in the snow and ice ...," "Works well on icy and wet pavement...," "I didn't realize how good it (ABS) is until I got a truck without it...," and "I prefer ABS over standard brakes...."
- 17 (6.1 percent) of the drivers expressed neutral feelings toward ABS. Many of these were new

drivers and, therefore, likely had not driven the vehicle long enough to form an opinion.

- Only 4 (1.4 percent) of the drivers indicated a low or very low acceptance of ABS with comments such as, "...system worked on ice but is too touchy...," and "I think the truck would stop better if the brakes locked...."
- 132 (47.1 percent) of the drivers made positive statements about the operation of the ABS on slippery road surfaces.
- 108 (38.6 percent) of the drivers felt that ABS should be on trailers as well. Several drivers (8 percent) mentioned specific instances where the ABS kept the tractor straight and under control while braking, while the trailer slid sideways.
- Drivers reported 20 instances in which they felt the ABS allowed them to avoid a crash which they could not have avoided if they had been driving a tractor without ABS.

Electrical Circuit Performance of In-Service Truck Trailers

One of the principal issues that must be resolved before ABS can be successfully equipped on trailers is providing adequate electrical power to the systems. Current trailer ABS's need approximately 8-10 volts in order to operate properly. Designers are working to develop future systems that will function at levels as low as 6 volts, but these are not now available.

If the trailer ABS senses that it is not receiving a predetermined minimum amount of voltage, it automatically shuts itself down, leaving the trailer with the performance capabilities of its basic braking system. While this is no worse than the present situation, there is concern that adequate electrical power be available in order to ensure that the benefits of trailer ABS are realized.

The options for powering trailer ABS are to use the stop-lamp circuit, as is currently done, or to use a separate circuit. There are two ways of providing a separate circuit: through the present, or a modified version of the "7-pin" tractor/trailer electrical connector, or; through another separate electrical connector. There are unresolved issues associated with all of these options. Nevertheless, the results of a recent study (Copenhaver, et al, 1990) make it clear that a change in the way trailer ABS is powered will likely be necessary to ensure that adequate power is available.

The study, conducted at four locations throughout the country (Dumfries, VA, New Market, MD, Woodburn, OR, and Brownville, TN), measured 561 in-service trucks and truck trailers to determine trailer stop-lamp circuit voltage and current at tractor engine speeds of 700 and 1100 RPM, with all lights and accessories "on."

The type and number of vehicles/trailers included in the sample were:

- Single-unit dump trucks—15
- Single semitrailer, van—178
- Single semitrailer, tank—62
- Single semitrailer, flatbed—32
- Double-trailers—12
- Triple-trailers—62

In each case, readings were taken at the rear of the rearmost vehicle in the combination. Observed voltage readings, at the higher 1100 RPM level, on just the trailer portion of the sample were as follows:

The findings noted in Table 4 do not reflect the extra load that would be imposed on the trailers' electrical circuitry if ABS was also present. In that case, the readings would be even lower. These findings suggest that while it may be possible to power some configurations of ABS on single semitrailers using the existing stop-lamp circuit, it is problematic for double trailers, and virtually impossible for triples.

Table 4. Observed Trailer Stop-Lamp Circuit Voltage Readings (Copenhaver et al., 1990)

VEHICLE TYPE	VOLTAGES		
	MINIMUM	MAXIMUM	MEAN
VANS	8.65	13.78	11.70
TANKS	8.61	13.77	11.58
FLATBEDS	6.80	13.35	11.42
DOUBLES	6.08	12.58	9.87
TRIPLES	5.56	11.29	8.55

Summary/Discussion of ABS Field Evaluation Results to Date

The present NHTSA study of U.S. vehicles has endeavored to portray as complete a picture as possible of *all the work* that has been done on the ABS-equipped test vehicles. Thus, these data include many more maintenance-related activities (namely, inspections, adjustments, and repairs) than would normally be reported. These activities, while not insignificant, would normally go unnoticed in most maintenance reporting systems. Indeed, extraordinary efforts have had to be expended to get the participating fleets to take note of and record the fact that these activities were performed. In normal circumstances, they would simply be done as part of routine new vehicle preparation work or as part of normal periodic inspection activities. Most of this maintenance work would not even be recorded/noted.

Most of the maintenance work has been minor in nature, with the exception of the "frozen" valve problem encountered with one supplier's system, and the "conservative failure warning logic" problem encountered with another supplier's ECU. Both these problems were attributable to the early developmental nature of those systems. These type problems should, and likely will, be resolved and eliminated as more experience is gained by

ABS suppliers and truck manufacturers and their dealers installing this type of electropneumatic system. This test program was instrumental in helping identify those product development problems and making certain they do not show up in future production versions of those ABSs.

The remaining problems that have occurred are of a quality control nature that are ultimately traceable to the way the systems were installed. In general, the widespread system design-related failures that were reported to have occurred during the early FMVSS 121 era have not been noted during this test program.

Despite the fact that the source/cause of most of these problems was minor and easily fixed, and was not related, for the most part, to ABS component part design deficiencies, a number of other issues uncovered by this study, need to be addressed if ABS is ultimately to be successful in U.S. operations.

- The U.S. truck-building business is unique in that component parts suppliers and truck users play large roles in determining the ultimate design and product content of the vehicle. In many instances, customer-driven market "pull" forces dictate that truck manufacturers install component parts and systems, without the benefit of very extensive engineering testing or evaluation of that component/system as part of their overall vehicle design. As a result, the type of quality control problems that have been encountered to date with ABS are not atypical for many other types of components/systems as well. Based on this past and reoccurring experience, many of the problems encountered in this test program would likely persist even if ABS was in more widespread use. The incidence of these problems would be significantly reduced if truck manufacturers could concentrate their engineering and quality control resources on only one or two designs, but this is unlikely in the U.S. truck market. As a result, the "price" users may have to pay for infinite flexibility in "spec'ing" their trucks, may have to be a certain amount of tolerance for "teething problems" while yet another ABS configuration/design is adapted to a given manufacturer's product. Given the slow voluntary introduction rate of ABS into the U.S. heavy truck market (by 1990, 3 years after it was made commercially available in the U.S., approximately 3000 commercial vehicles had been equipped with ABS), these problems would likely persist even if market demand for ABS increased.
- Because there has been so little market demand for ABS, most truck manufacturers have expended only minimal amounts of engineering and product development resources to integrate ABS into their designs. Indeed, most of the truck manufacturers involved in the Agency's test program had not adapted any of the current ABS designs to their product line before they were requested to do so for this test. Until demand increases, this situation is not likely to change, especially in a market that is in a downturn. Also, truck manufacturers face substantial engineering and financial challenges to integrate cleaner burning engines into their product lines before the 1994 deadline specified in current emissions standards. The type of quality control improvements that seem to be needed will be slow in coming until more resources are available for engineering and quality control work. Simply stated, more market demand for ABS is needed to enable this work to be done.
- Truck drivers are not reticent about reporting failures. They are, however, often powerless to get those problems fixed. If their complaints are not addressed, two things are likely to happen. They become cynical and less inclined to report failures in the future, and they are likely to remove ABS failure warning lamp bulbs, or the ABS fuse itself, to prevent being annoyed by the constantly lit lamp.
- Despite training that was given to the mechanics in all the fleets in this test program by the ABS manufacturers on how to troubleshoot and repair their systems, many are either reluctant to attempt to repair/maintain an electronic piece of equipment such as ABS or, given that they attempt to fix the systems, are unable to do so correctly. A large-scale information dissemination/training effort by ABS suppliers and truck manufacturers will be necessary to deal with this problem. In addition, a strong local service support network, backed by such things as service "Hotlines," will be essential so that fleet maintenance personnel with questions can quickly and easily get answers/help. These measures will be necessary to give them the confidence to attempt to diagnose and fix problems.
- In one sense, most ABS failures are benign events; they do not prevent the safe continued operation of the truck—the "safety insurance policy" simply lapses. The pursuit of productivity often is not conducive to performing anything other than essential maintenance on vehicles if carriers are to achieve the vehicle utilization rates they seek. Under these conditions, there is a strong incentive to let ABS failures "slide" until they can be more conveniently fixed. Examples of this have occurred in the NHTSA's fleet evaluation program. Two of the participating fleets experienced operational changes that necessitated their vehicles being away from their home base of operation much longer than originally envisioned when the test began. As a result, long time periods elapsed between when failures occurred and when they were addressed. Sometimes it was difficult to address them at all. These types of failures can easily be ignored with no

immediate or direct adverse consequences. Carriers simply must be willing, or be convinced, to maintain these systems.

- Intermittent failures, whose cause is difficult/impossible to determine, can become major annoyances to drivers and fleet maintenance personnel, especially if they occur repeatedly. No problems were found with many of these warnings but, nevertheless, they required maintenance time to address. ABS suppliers should endeavor to minimize the likelihood of these occurrences. They undermine drivers' confidence in the systems and frustrate mechanics, making them less inclined to attend to "real" problems.
- It would greatly facilitate maintaining ABSs if ABS suppliers developed very simple, fool-proof methods for diagnosing ABS problems. Additionally, it would be very beneficial if the SAE, in conjunction with the American Trucking Associations' Truck Maintenance Council, began work now to develop recommended practices that would standardize the way failure diagnostic messages are formatted and presented. Thought needs to be given to standardizing the color and location of failure warning lights on power units and trailers, (if trailer failure warning indications are not transmitted to the power unit cab), and whether the light is "off" when the ABS is fully operational and "on" when it has failed, or vice versa. In this regard, it has been noted that some suppliers of trailer systems intend to have the trailer failure warning lamp "on" when the system is functional. Tractor ABS failure warning lamps are typically just the opposite, "off" when the system is functional. Driver and mechanic confusion are likely in this situation.
- Even if a standard failure warning format is developed, it will not help mechanics diagnose and locate many of the wiring/connector problems that have been encountered to date in the NHTSA test program, especially the intermittent ones. ABS suppliers and truck manufacturers should work to ensure that the number of these problems is substantially reduced and that simple diagnostic techniques are developed to identify them when they do occur.

There can be no doubt that the problems that have occurred are real and would render the ABS's inoperative if not addressed. This highlights the need to provide service assistance to motor carriers to enable them to quickly and easily diagnose minor problems and quickly fix them. If this does not occur, carriers will likely form strongly adverse opinions about these systems, as they did in the case of early "121" systems. On the other hand, if quality control is kept high, and if good service support is available, the preliminary results of this field study indicate that, from a reliability and maintenance perspective, ABS can be successfully installed and maintained on U.S. heavy trucks.

References

1. Copenhaver, M., Gurrier, J., and Ching, H., "Photometric and Electrical Performance Characteristics of Rear Lighting Systems on In Service Truck Trailers," USDOT/NHTSA Report No. DOT HS 807 545, February, 1990.
2. Fancher, P.S., "European/Australian Experience with Antilock Braking Systems in Fleet Service," USDOT/NHTSA Report No. DOT HS 807269, March, 1988.
3. Leasure, Jr., W.A., and Williams, S.F., "Antilock Systems for Air-Braked Vehicles," Society of Automotive Engineers (SAE) Technical Paper No. 890113, February, 1989.

S10-O-07

New Concept of Brake for Heavy Duty Vehicle

Tohru Kuwahara
Isuzu Motors Ltd.
Kenji Araki
Sumitomo Metal Industries Ltd.

Abstract

As performance and speed of heavy duty vehicles become higher there are much market needs of higher performance of brake system for higher safety. Recently load on wheel brake mainly for high speed vehicles is increasing by lowered engine brake force and exhaust brake force caused by adoption of small swept volume diesel engine with turbo and inter cooler coupled with fast ratio final gear for fuel economy of heavy duty vehicles. Besides that, load on wheel brake is also increased by reduced rolling resistance of tire and aerodynamic drag force. In the past wheel brake size was increased (mainly width of brake drum was increased) to remedy the situation, but now because of space problem further increase of width is impossible. As a result various kinds of study were conducted such as material change of lining, improvement of cooling performance of brake drum, adoption of retarder and etc, from among them retarder was the best choice. But there were many problems of electro-magnetic or hydrodynamic retarders also such as heavy weight, space for installation and etc, and retarder is not so popular in Japan. Under these circumstances, authors succeeded for the first time in the world to develop epoch-making eddy-current retarder

featuring light weight, compact and easy installation by using very powerful Nd-Fe-B base permanent magnet. This paper describes about this new retarder and improvement of safety at the time of brake application while running at high speed based on test results of express way on mountainous district. This new retarder can be incorporated to conventional brake system as an integral part, and for improvement of brake safety retarder is to be used mainly at high speed while conventional wheel brake system is to be used at low speed running or in an emergency. This paper is to deal with new concept of braking system of heavy duty vehicles in this way.

Introduction

With the expansion of express way network the volume of cargo transport in long distance at high speed has been increasing recently in Japan, and in order to meet this requirements characteristics of heavy duty trucks are tended to be higher power and speed. Brake system is also requested to be of higher performance and safety.

Besides that engine brake and exhaust brake force has been sacrificed recently by adoption of smaller swept volume diesel engine with turbo & inter-cooler coupled with fast ratio final gear, and wheel brake has been subjected to larger load because of reduced rolling resistance of tire and aerodynamic drag force for fuel economy.

Under these circumstances, the authors were interested in retarder which is to decelerate or restrict automobile speed as an auxiliary system of wheel brake, and succeeded to develop new compact and light weight retarder not requiring electricity consumption by adoption of very powerful Nd-Fe-B base permanent magnet and the retarder was placed in the market in January 1991.

This paper describes about required performance, principle of operation and construction of this newly developed retarder. Moreover, improvement of safety of brake application at high speed and future requirements of brake system of heavy duty vehicle are to be discussed by referring to the test results obtained while driving on express way in mountainous districts.

Braking Work on Express Way

Kinetic energy absorbed by brake application of heavy duty truck running on express way was measured and Figure 1 shows these results obtained while this test truck was running on Chugoku Express Way in mountainous districts. Test truck was ISUZU CXG23X with GVW approximately 20,000kg powered by small swept-volume diesel engine of approximately 9.8ℓ with turbo-charger and inter cooler.

As shown here wheel brake absorbed energy occupies share of over 60% of total energy absorption while shares of engine brake and exhaust brake are much smaller. In this case average vehicle desolation is 0.5 ~

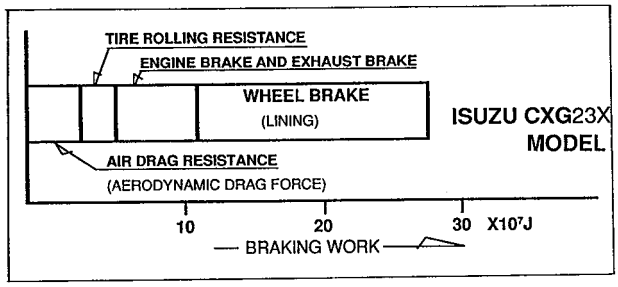

Figure 1. Braking Work on Express Way

0.7m/sec^2 which is not so much deceleration, but wheel brake absorbed energy is very high because braking time and distance are rather long caused by high vehicle speed.

In the past this problem of increased wheel brake absorbed energy was addressed by size-up of wheel brake (larger lining area by larger width of lining) and Figure 2 shows trend of lining area/axle for heavy duty vehicle in Japan for the past 10 years.

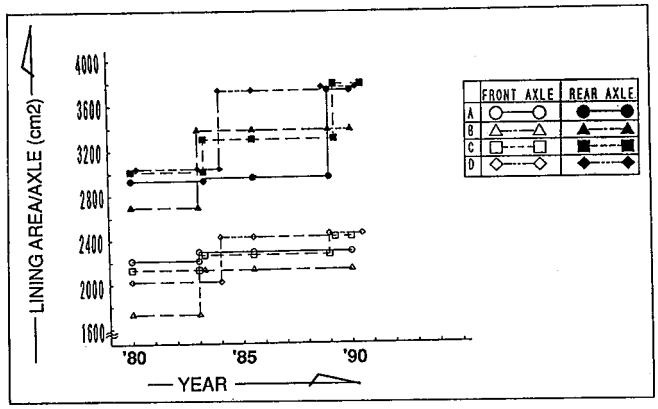

Figure 2. Trend Lining Area/Axle for Heavy Duty Vehicle in Japan

But, this approach is almost not practical at present because of limited space.

Consequently, various engineering studies were conducted such as to adopt better lining with higher fade resistance or to provide air cooling fin on drum for higher cooling efficiency. From among various possible solutions the adoption of retarder as an auxiliary brake was the best choice, and in this case not high braking force is required but this retarder must withstand continuous application for a long time.

Conventional electro-magnetic or hydrodynamic retarder has high performance but heavy weight are problems, and moreover large scale chassis modification is required. So, in Japan retarder has not been popular.

Purpose of Development of New Retarder

For popularization of retarder in Japan the new retarder was developed with the purposes listed below.

- Improvement of brake performance at high speed running of heavy duty truck of GVW 20,000Kg

powered by small swept volume diesel engine with turbo-charger and inter-cooler.

- Sufficient performance to be secured together with existing exhaust brake.
- Small size and light weight.
- Chassis modification for retarder mounting shall be kept minimum.
- Construction and system shall be simple for securing reliability.

Estimation of Required Performance

Market survey centering on vehicle powered by turbo-charged engine was conducted to estimate required performance matching with Japanese market, and required performance of retarder was obtained by simulation as shown by Figure 3 based on data of market survey and test data of wheel brake basic characteristics.

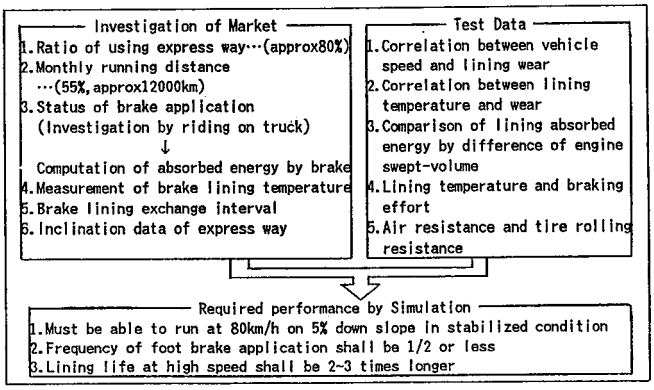

Figure 3. Required Performance

Principle of Operation and Construction

In order to achieve the purpose of development, our engineering effort was directed to simplify construction and system for large scale weight reduction by using very powerful permanent magnet of Nd-Fe-B base.

Principle of Operation

Principle of permanent magnet type eddy-current retarder is same as conventional coil type electro-magnetic retarder. As shown by Figure 4 when permanent magnet comes near to rotating metal plate eddy-current is generated on metal plate by magnetic field of permanent magnet and braking force in opposite direction of metal plate rotation is created by Fleming's rule.

The above rotor was changed to be of drum structure and 12 pieces of permanent magnet were arranged on outer surface of yoke so that neighboring pole would face opposite pole each other. This permanent magnet never rotates.

As shown by Figure 5 when brake is applied these permanent magnets are set in matching position inside of drum by the force of air cylinder and magnetic circuit is formed by permanent magnet and drum through pole piece.

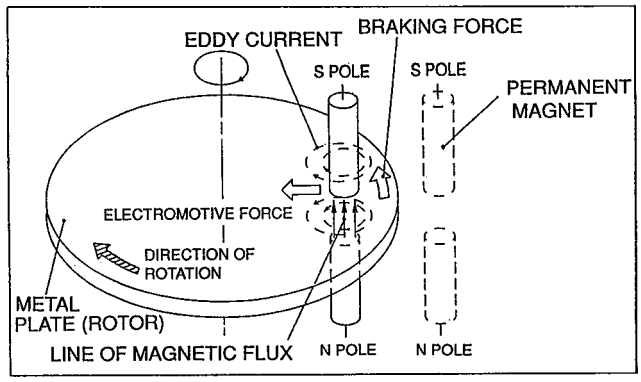

Figure 4. Principle of Retarder

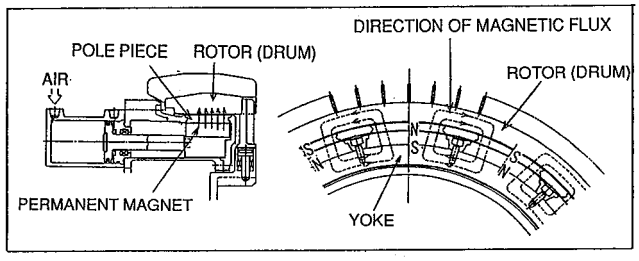

Figure 5. Magnetic Circuit During Braking

If drum rotates under these conditions eddy-current is generated around inner surface of drum and braking force works in reverse direction of drum rotation.

When retarder switch is not on, the permanent magnets are separated from inside surface of drum and magnetic circuit is formed by permanent magnet and case as shown by Figure 6. By this reason magnetic circuit by drum and permanent magnet is shut-out, and magnetic force is re-routed to inside of case where there is no leakage of magnetic force.

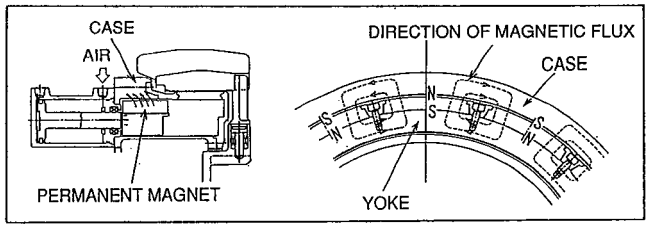

Figure 6. Magnetic Circuit During Non-Braking

Basic Equation

Lorentz force of permanent magnet type eddy-current retarder was obtained from Maxwell equation (1).

Lorentz force (braking force) created on drum by approximation is as follows.

$$T = F_1(M) \cdot F_2(k,a,b,\omega) \cdot F_3(s,\mu r,k b)$$

This is multiplication of terms of M (permanent magnet force), geometric shape of equipment and magnetic permeability of material and S (speed parameter).

$F_1 \sim F_3$ are as follows.

$$F_1 = (4\mu_0 M^2)/\pi^2$$

$$F_2 = \sin^2(k\omega/2)\,(\sinh(ka)/\cosh(kb))^2\,(1-\tanh(kc)/kc)$$

$$F_3 = \frac{S}{\alpha}\,\frac{\mu r^2}{\sqrt{1+\mu r^2 s^2+2\alpha\mu r\tanh(kb)+\mu r^2\tanh^2(kb)}}$$

where

$a, b, c, \omega, k = \tau$; Parameter of shapes shown by Figure 7.

$\mu r, \sigma$; Relative magnetic permeability and electrical conductivity.

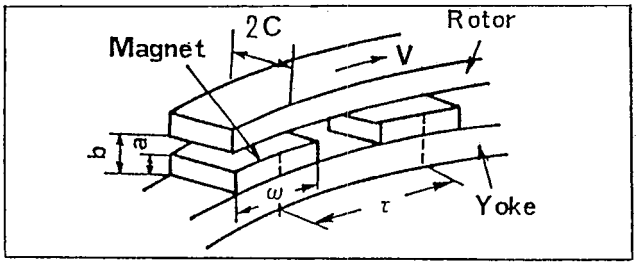

Figure 7. Model and Notations

Results of these theoretical calculation indicate that torque efficiency can be improved if optimum selection of electrical conductivity and relative magnetic permeability (factor of parameter S) of drum material is made.

This time, comparatively low carbon steel alloy with high relative magnetic permeability was selected as drum (rotor) material after paying due engineering attention to braking force and thermal strength at high speed.

Construction

As this retarder was designed to be very compact with light weight almost no reinforcement of chassis is required for mounting at rear side of transmission.

Further more retarder is fastened to drive line together with parking brake system and design change of both parking brake and propeller shaft was also not required. In another words,light weight (40kg) and almost no requirement of chassis modification are the special design features of this retarder.

Figure 8 shows location of retarder, Figure 9 shows detailed construction and Figure 10 shows retarder cut model.

Here, given are the detailed descriptions of stator and rotor.

Stator. Together with yoke 12 pieces of permanent magnet are sealed inside of magnetic sealed case and inside surface of drum 12 pieces of pole piece are arranged corresponding to each pole of permanent magnet. When permanent magnet comes inside of pole piece then this pole piece functions as magnetic pole. Parts other than pole piece are made of aluminum which is nonmagnetic material. Store area of permanent magnet after separation from drum is covered by magnetic sealing material. Permanent magnet is protected against

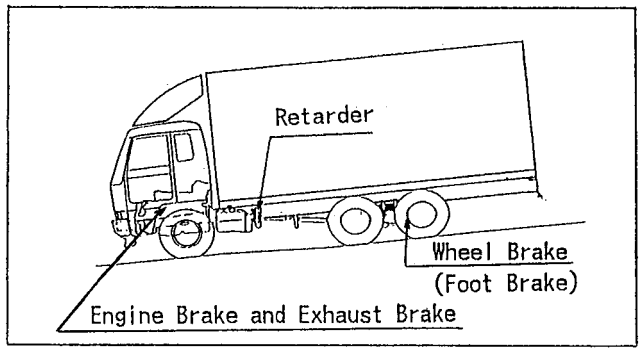

Figure 8. Location of Retarder

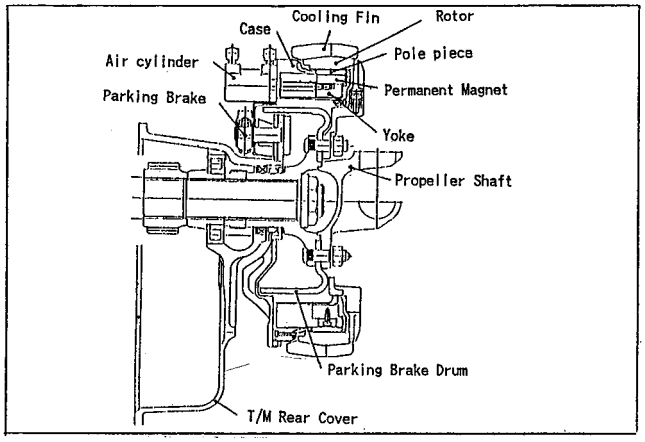

Figure 9. Construction (Rear Side of Transmission)

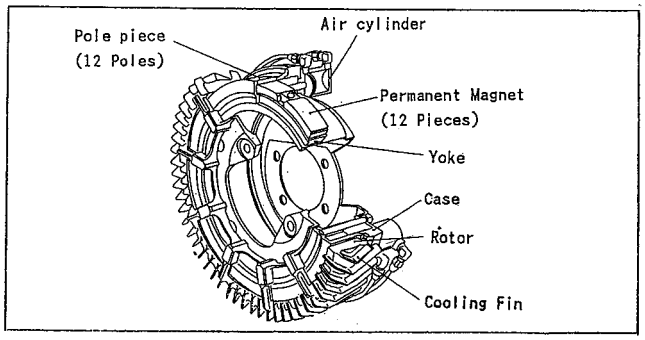

Figure 10. Cut Model

heat, water and dust coming in from out-side by this sealed case.

Table 1 shows specification of permanent magnet.

Table 1. Specification of Magnet

RESIDUAL MAGNETIC FLUX DENSITY Br (T)	COERCIVE FORCE iHC (KA/m)	MAXIMUM ENERGY PRODUCTS [HB] MAX (KJ/m)	TEMPERATURE COEFFICENT OF Bf $\frac{\triangle Br}{\triangle T}\times 100/Br$ (%/°C)	TEMPERATURE COEFFICENT OF iHc $\frac{\triangle iHc}{\triangle T}\times 100/iHc$ (%/°C)	THERMAL RESISTANCE (°C)
1.16	OVER 1353	255	-0.12	-0.58	140

Rotor. When brake is applied magnetic flux density becomes higher and also eddy current is concentrated inside surface of drum. Continuous brake application at

high speed generates eddy current of several thousands ampere and temperature of inner surface of drum reaches over 600°C, this heat is radiated by V type fin on outer surface of drum. Air cooling fin is quite necessary for obtaining stabilized braking force at high speed in continuous application.

Control System

Same control system as conventional exhaust brake was adopted for simplification and can be controlled by manually operating combination switch provided on steering column. This switch can be operated in 2 stages—1st position for exhaust brake and 2nd position for exhaust brake and retarder together. Retarder on-off is controlled by 2 sets of magnetic valve which sends air to either left or right chamber of air cylinder alternately to move permanent magnet (see Figure 11.).

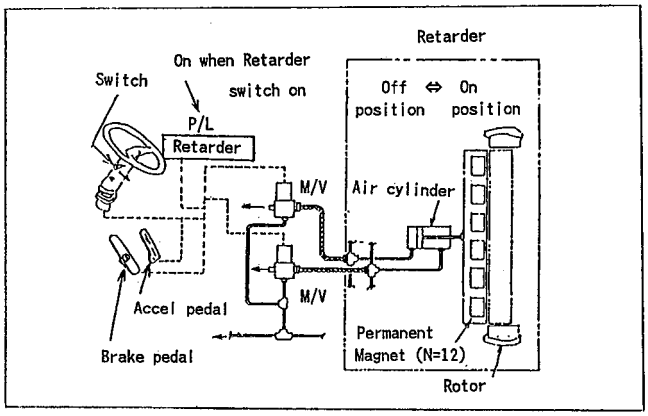

Figure 11. Control System

Moreover retarder starts operation when service brake pedal is pressed and retarder is released by pressing accelerator pedal.

Evaluation of Performance

In order to confirm if required performance is satisfied or not performance test was conducted by using heavy duty truck(ISUZU CXM23V Model, GVW 19,785kg) powered by small swept volume(9.8ℓ) diesel engine with turbo and inter-cooler coupled, because wheel brake of this model is subjected to heavy load. As shown by Figure 12. together with exhaust brake deceleration 0.49m/sec^2 at vehicle speed 80km/h was secured and this vehicle could run on 5% down slope at high speed without acceleration in a stabilized condition.

In Japan, brake application frequency is very high on Chugoku Express Way where there are many slopes, and test was conducted between Miyoshi I.C. and Yamaguchi I.C. because brake application frequency becomes highest in this area.

Figure 13 shows one part of vertical section of slope.

Figure 14 shows that when "only exhaust brake" is compared with "exhaust brake + retarder" the lining absorbed energy of "exhaust brake + retarder" is less

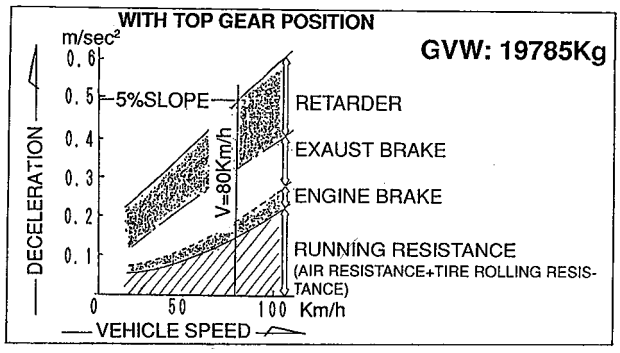

Figure 12. Deceleration by Retarder

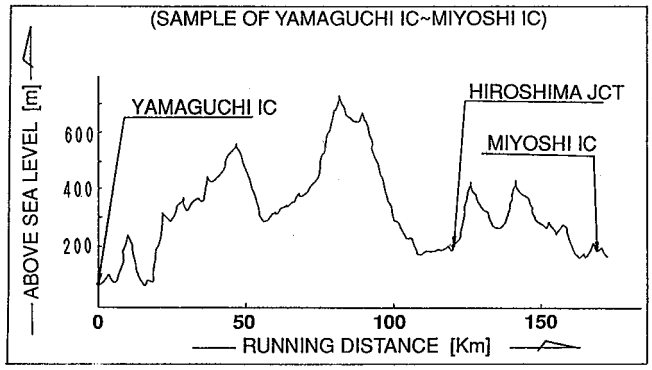

Figure 13. Vertical Section of Chugoku Express Way

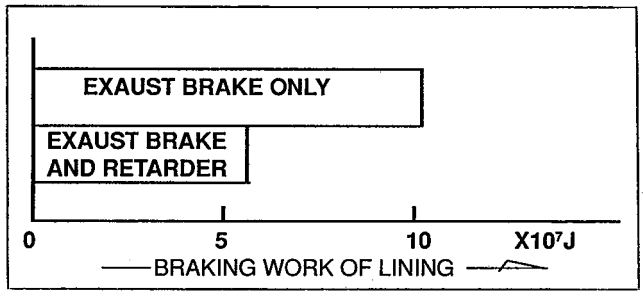

Figure 14. Braking Work of Lining

than 1/2 of "only exhaust brake." Because of lower frequency of wheel brake application.

Figure 15 shows that lining temperature goes up over 200°C when "only exhaust brake" is applied, but when "exhaust brake + retarder" applied lining temperature is lower than 150°C where braking effort of lining is stabilized (see Figure 16) (2) under these conditions service life of lining was successfully elongated to 3 times which is almost same value obtained by initial simulation calculation.

Evaluation by Monitoring Test

Before introduction of new retarder in the market many monitoring test were conducted to survey evaluation in the Japanese market. Some of the user's comments were that:

- Can run winding down slope at high speed easily,

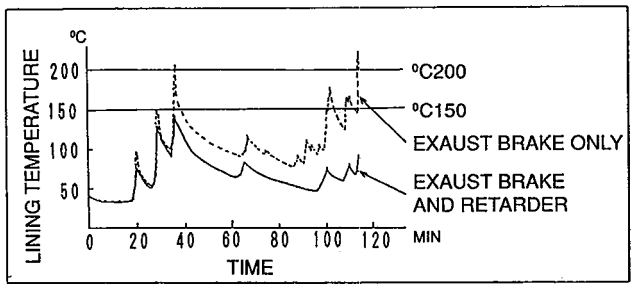

Figure 15. Lining Temperature

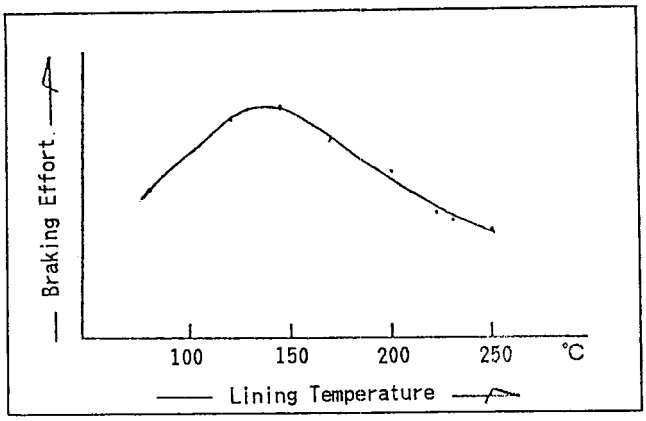

Figure 16. Lining Temperature and Braking Effort

- Brake application frequency reduced to less than half which in turn helped reduce driver's fatigue.

This new retarder was highly evaluated by users as expected and design engineers were deeply impressed by high market needs.

Conclusion

Max inclination angle of slope of express way in Japan is approximately 5% in average, and it was possible to negotiate down-hill of 5% at 80km/h (speed limit on express way in Japan) without acceleration in stabilized condition by application of retarder and conventional exhaust brake. As a result retarder was found out to be very effective for improvement of brake performance at high speed. Based on these required performance the authors succeeded to develop new compact retarder featuring light weight, easy to be mounted on chassis and not consuming electricity by using powerful permanent magnet (Nd-Fe-B bese). By incorporating this new type retarder to conventional brake system centering on high speed truck transportation, new concept was formulated where retarder acting as main brake in high speed area while conventional wheel brake as main brake in slow speed area or emergencY case. Our engineers are firmly convinced that this kind of braking system must be adopted by heavy duty trucks which are tended to be higher speed and larger engine out-put in future.

As there are much demands from market the brake system of heavy duty vehicles expected to be revolutionized.

References

1. Haruo Sakamoto and others, "Lorentz force analysis for eddy current brake system," 68th JSME spring annual meeting, Vol. No. 910-17 pp. 525-527 (1991.3.30).
2. Automobile engineering hand book (1990) by JSAE, "basic and theory, 4th chapter, basic and theory of braking performance", p. 126.

S10-O-08

Experimental Accident Simulation for Improved Safety of Tank Vehicles for Dangerous Goods

K. Rompe
TÜV Rheinland e.V., Institute of Traffic Safety

Abstract

An investigation termed THESEUS which is scheduled to last for several years has been initiated by the German Federal Minister for Research and Technology. This investigation is intended to generate measures designed to improve tank trucks transporting hazardous substances. For this purpose, the safety of the overall system consisting of vehicle, tank components and safety devices, participants in the accident and the type of accident will be considered. Relevant accident statistics and analyses of accidents by teams involved in the project will create the parameters for the experimental and theoretical investigations. Crashes will be simulated with original tank vehicles in the form of vehicle-to-vehicle collisions and overturning tests which have proved to be important since hazardous goods are frequently released. The experimental simulation of the overall vehicle will be supplemented by the systematic testing of tank components in order to examine the behaviour of the walls when exposed to puncturing and flat loads. These investigations should result in sound, simplified test methods for the approval of tanks. The experiments will be accompanied by numerical calculations. The first step will be to validate the mathematical model with experimental results and then to calculate conditions not covered by experiments. The second step should provide a better understanding of the mechanisms of deformation and the criteria of rupture. In addition to this, the driving behaviour of tank vehicles will be investigated by means of objective driving maneuvers

such as steady-state turning, step steering input and sinusoidal steering input. The most important parameter to be varied will be the loading condition of the tank vehicle. The most significant results are expected to be the non-steady-state overturning limits of the vehicles under investigation. These limits will be compared to those obtained under steady-state conditions during tests on a turntable. These experiments will also be supplemented by numerical calculations. The numerical model will be validated by experimental results obtained with a modern truck-trailer combination with a low center of gravity. The model will then be used to study the influence of parameters. The objective of the investigation which commenced in summer 1990 is described and the results which have been obtained so far are presented.

Introduction

About 23,500 tank trucks are currently licensed for the transportation of hazardous goods in the Federal Republic of Germany. Their transport capacity is increasing steadily and is slightly more than 12% of the total quantity of goods transported on the road. Although the number of road accidents involving hazardous goods is comparatively low, amounting to about 800 per year, the risk potential of these accidents is relatively high.

With the agreement of the Federal Ministry of Transport, the Federal Ministry for Research and Technology has therefore appropriated funds for a comprehensive joint research venture by the Technischer Überwachungs-Verein Rheinland (TÜV), DEKRA, the Federal Institute for Materials Testing and Research (BAM), the Federal Institute for Road Research (BASt) and subcontractors from industry.

THESEUS, the name of this project, is derived from the German "Tankfahrzeuge mit höchst erreichbarer Sicherheit durch experimentelle Unfallsimulation," which can be roughly translated as Tank Trucks with Maximum Achievable Safety through Experimental Accident Simulation.

The main objective of the project is to consider the overall system consisting of vehicle, tank components and safety devices, participants in the accident and the type of accident from the point of view of safety. Vehicle-to-vehicle collisions and overturning tests will be carried out for this purpose. Investigations of tank components should provide information on failure behaviour and lead to simpler test methods. The limits of the dynamics of vehicle movement and overturning immunity will also be examined experimentally. Both the investigations with permanent deformation of the tank walls and the driving tests will be supplemented with numerical simulations to permit variation of the parameters after validation of the models.

Statistical accident data will be collected to allow parameters to be selected for the experimental investigations.

These main objectives of the THESEUS project are taken into account in the project structure as shown in Figure 1. The activities which have been carried out in the main job packages (AP) up to now are described in the following.

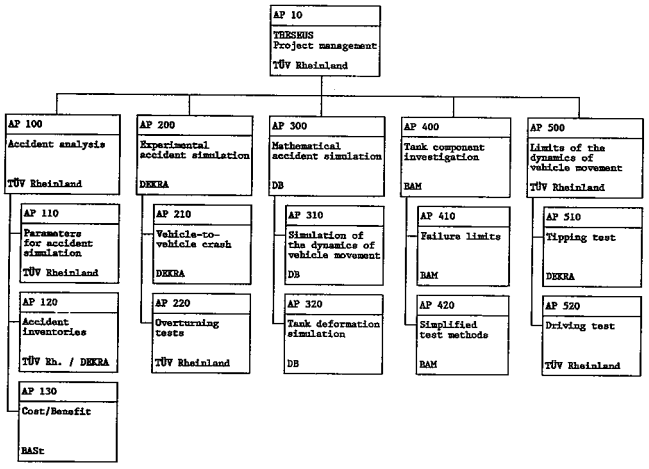

Figure 1. Project Structure

Accident Analysis

Accident analyses are based on already available data on the one hand and on data collections carried out specially for this project on the other. The results of these data collections are recorded in a four-part questionnaire.

These questionnaires were subjected to a preliminary evaluation in order to check the accident simulation parameters specified at the start of the project. The experimental boundary conditions obtained during this evaluation were compared to the figures defined at the start of the project and used for definition of the accident simulation parameters.

The number of tank trucks and cylindrical tanks involved in accidents is almost the same as that obtained in the course of an investigation performed by BASt from 1982 to 1984. In contrast, the number of articulated vehicles involved in accidents has almost doubled (approximately 58%) while that of box tanks has more than doubled (approximately 68%).

The accidents assessed in the course of this evaluation show that the list of accidents to be simulated, which was specified at the beginning of the project on the basis of a literature study, is still valid. These are rear-end collisions, accidents at intersections and self-initiated overturning accidents.

It is interesting to consider the behaviour of cylindrical tanks as compared to box types which is apparent from Table 1.

The results obtained from an evaluation of the accidents up to now (59 cases) are in contrast to the general opinion that the risk of a release of hazardous substances from a cylindrical tank is much lower than from a box tank.

Table 1. Tank Shapes Related to the Type of Vehicle and the Release of Hazardous Goods

	Box Tank HG Release with/without		Cyl. Tank HG Release with/without		Ell. Tank HG Release with/without	
Articulated vehicle	8	11	6	8	0	1
Tank truck	6	6	2	2	0	0
Tank truck with trailer	6	3	0	0	0	0
Total	20	20	8	10	0	1
Total	40		18		1	

The evaluation shows that there was a release of hazardous substances from 50% of the 40 box tanks involved in accidents, while such a release was detected in 44% of the 18 cylindrical tanks involved in accidents.

The objective of accident analyses is to keep the parameters as close to the real accident sequence as possible when planning the experimental program and to describe accidents with tank trucks containing hazardous goods in greater detail than is presently the case.

Experimental Accident Simulation

A preliminary program encompassing about 30 tests was drawn up from an analysis of the usage and accident frequencies of various vehicle types. The impacting vehicle is always a truck. The tank shape, tank material, center of gravity, vehicle type, number of axles, suspension and tyres of the tank truck were taken into account.

The points at which accelerations and internal tank pressures are measured on or in the tank truck are coordinated with the other job packages. The global tank acceleration (its central axis) is always measured on the outside in three orthogonal directions parallel to the main axes of the tank at the center of the front and back tank bottom. Other acceleration measuring points are located in a ring on the inside of the wall of the tank chamber which is filled to the allowable level with water and suffers a direct impact during the crash. Sensors for measuring the internal tank pressure are also positioned here, Figure 2. Additional pressure measuring points are installed on a partition of the directly loaded chamber.

A method is currently being tested for deformation measurements. It can record a surface form by means of moire effects. Acceleration measurements are also carried out at the impacting truck. In the side collision tests performed so far, a 16 t truck (forward control vehicle) crashed head-on into the side of the tank truck, whereby the longitudinal axes of the vehicles were at an angle of 60°. Figure 3 shows the deformations of a tank which suffered an impact at 40 km/h.

Since accidents with material release are particularly dangerous and since the vehicle overturns in 60 to 70% of these accidents, this point is considered in great depth.

According to the concept developed for overturning tests, the wheels on the left side of the vehicle roll along the road while those on the right side roll over a ramp.

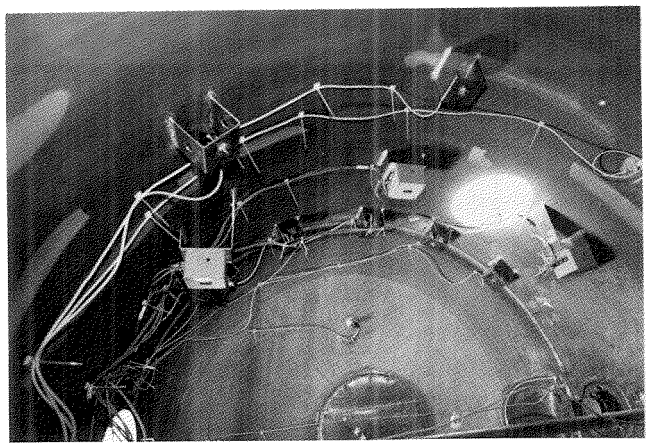

Figure 2. Part View of Pressure Sensors and Acceleration Sensors Installed in Measuring Boxes Inside a Tank Chamber Which is Filled with Water to the Allowable Level During the Crash Test

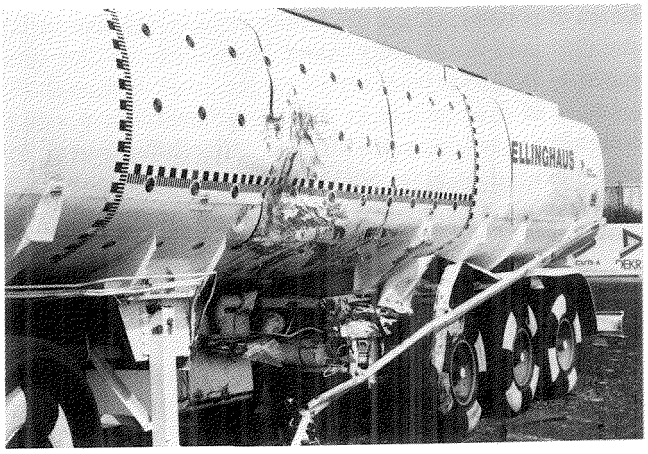

Figure 3. Deformation of the Side Wall of the Tank Due to the Head-On Impact of a Truck Travelling at 40 km/h

A rail is used for lateral control. The overturning kinematics still have to be investigated in order to calculate the point of impact as accurately as possible.

Mathematical Accident Simulation

The investigations involving permanent deformations of the tank walls and the driving tests will be supplemented by mathematical simulations.

A three-dimensional, non-linear simulation model to calculate tank truck dynamics will be prepared for simulation of the dynamics of vehicle movement. For this purpose, the existing truck model must be extended to include the semitrailer, fifth wheel coupling and air suspension.

Simple model approaches for a fifth wheel coupling with locally concentrated degrees of freedom of the articulated joints, as frequently described in literature, are not suitable for more accurate investigations of the dynamics of vehicle movement. In this case, an accurate consideration of the positions of the individual spin axes is necessary to correctly depict the dynamic effects and

moments between the towing vehicle and the semitrailer. A model to depict a standard fifth wheel coupling is currently being prepared.

In the course of a literature study it became apparent that models for the simulation of pneumatically sprung axles have not been documented to date in the time range. A new model approach was therefore derived. This reproduces both transient (adiabatic) and steady-state (isothermal) behaviour of the pneumatic springs. In the intermediate ranges, one obtains the hysteresis loops known from measurements, which are primarily caused by heat transfers (air in the vicinity of the cushion type pneumatic spring).

In the sector tank deformation dynamics, additional information is expected to be obtained on the influence exerted by energy input, mass distribution, the speed of the event and geometric boundary conditions on the failure limits. The calculations will be performed with the crash program DYNA3D. A tank drop test was simulated in order to prepare the necessary tools.

The steel tank (fine-grain structural steel TTStE) used for this test had a diameter of 2000 mm and was dropped from a height of 1.33 m onto a sharp mandrel with a diameter of 150 mm. The tank was filled with water and weighed 19.5 t. The impact speed was 5.1 m/s.

Figure 4 shows the completely punctured structure after 100 ms. The maximum mandrel force amounted to 1830 kn and the maximum deceleration was around 90 g.

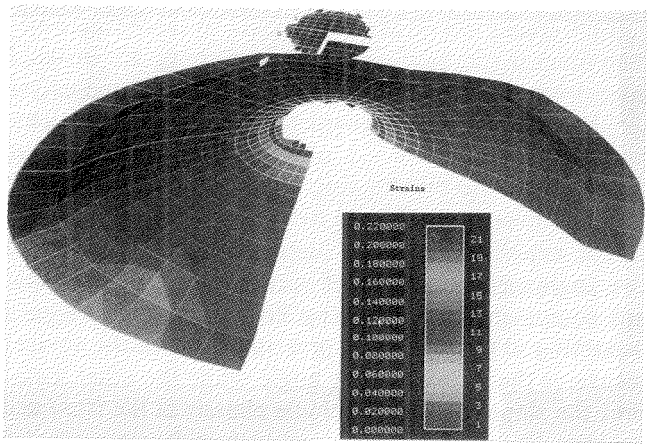

Figure 4. Puncturing of the Tank Bottom After 100 ms

After adapting the calculation to the smaller mass of the test tank of 5.3 t, the force-time curves (Figure 5) and the deformation were in good agreement. The force profile measured in the test is presented in flattened form in the figure. The measuring strip chart contains fluctuations similar to those in the calculated profile. The contact force fluctuates; after impact, the tank briefly lifts off the mandrel again several times. The force level in the test and in the calculation is approximately the same for the first two impacts. The force peaks decrease more quickly in the test, presumably on account of the damping effect of the water in the tank; only the damping effect of the tank plays a role in the calculation. In order to simulate the test conditions more accurately, another calculation will be performed with a different program system. In this case, the interaction of the structural deformations and the motion of the liquid in the tank will be described.

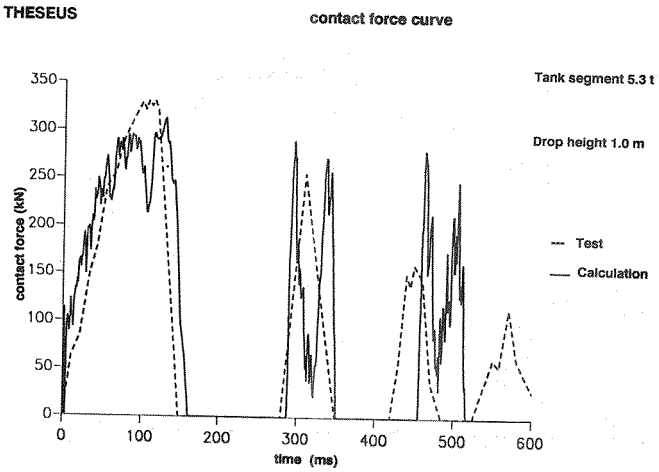

Figure 5. Contact Force Curve

An investigation of the intrinsic forms of the tank segment gives a possible explanation for the fact that the calculation results are not rotationally symmetrical. The intrinsic forms exhibit mirror-symmetrical or quadruple symmetry at different frequencies. These deformations may have been caused by vibrations initiated during contact. In the experiment, the tanks have a similarly severe, cross-shaped deformation pattern.

Tank Components

Local impacts of pointed structures on tanks constitute a major type of loading in real accidents. In this context, a literature study was also performed at the beginning of the project with the following objectives:

- To analyze known, real accidents involving vehicles transporting hazardous goods in order to define suitable test objects and calculation models for experimental and mathematical studies on the basis of the typical damage patterns.
- To determine fundamental characteristic values for real accidents.
- To systematically document publications dealing with the failure behaviour of thin plates and shells. As an example, Figure 6 summarizes known investigations of the puncturing behaviour of plates of various metallic materials which are frequently used for tank construction.

Steady-state and dynamic puncturing tests were then carried out on tank components to obtain an overall picture of failure behaviour. These included:

- Static puncturing tests (mandrel diameter 80 mm) on spherical bottoms of varying thickness manufactured from structural steel St 37-2 with the aid of a 25 MN test machine (see Figure 7a). The force/deformation

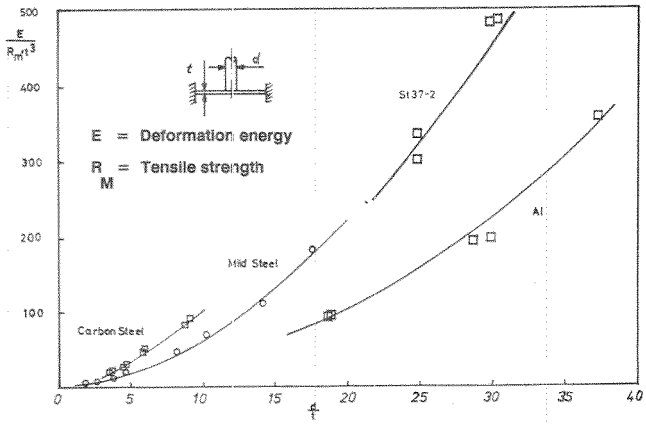

Figure 6. Results of Puncturing Tests

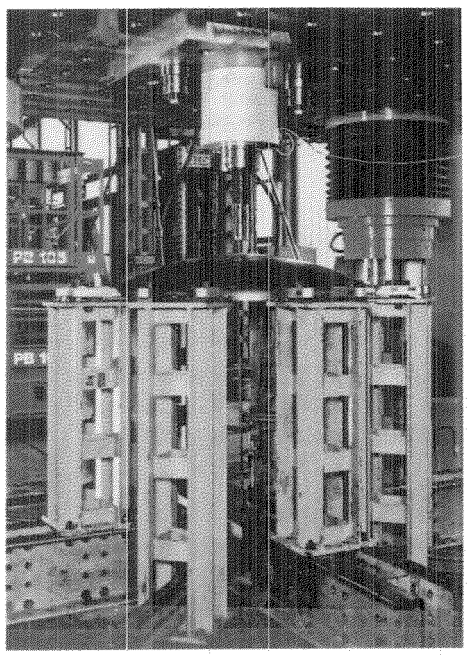

Figure 7a. Test Setup and result of a Static Puncturing Test—25MN Test Machine for Puncturing Test

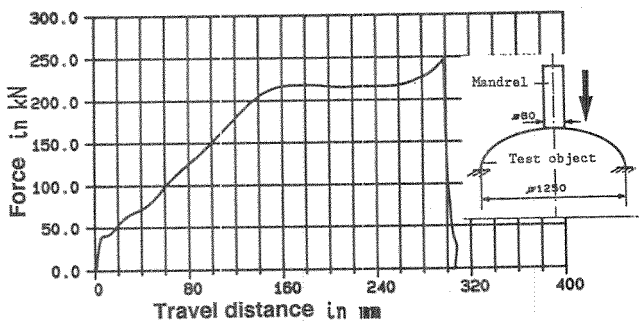

Figure 7b. Test Setup and result of a Static Puncturing Test—Force/Deformation of a 5 mm Spherical Bottom

behaviour recorded during the measurements (see Figure 7b) was used to determine the energy absorbing capacity at the failure limit.

- Instrumented drop tests with bottoms having the same geometry and material properties and with welded-on cylindrical section (diameter 1250 mm, height 990 mm). The test object was filled with about 1000 l water to simulate the real content. It therefore had a total mass of 1300 kg. A potential energy corresponding to the deformation energy which can be taken from the static puncturing test (Figure 7b) is obtained with this mass at a drop height of 4.1 m.

The main result obtained in the course of these tests is that the spherical bottom is totally penetrated even in the case of a deformation path of about 180 mm (static drop: 300 mm, see Figure 7b), whereby the failure force of approximately 280 kN is comparable to that of the static puncturing test. The numerical integration of the force/deformation profile recorded during the impact duration points to a failure energy which is much lower than that encountered during static loading. This result is in contrast to the results obtained from static and dynamic puncturing tests of flat plates which, in the dynamic case, always show a larger energy absorbing capacity at the low impact speeds under discussion here. It would therefore be sensible to perform a drop test with a critical drop height based on the failure behaviour of flat plates.

Limits of the Dynamics of Vehicle Movement

Tank trucks are involved in accidents more frequently than other trucks as a result of overturning, for instance after driving into a bend too quickly. In order to analyse the basic overturning characteristics of tank trucks, investigations are carried out to determine the static overturning limit on a tipping bridge and to establish the dynamic overturning limits by means of driving tests.

The experiments on the tipping bridge make use of two angle measuring devices which are part of the standard equipment of the tipping bridge and are designed according to the pendulum principle. One of the devices measures the tipping bridge angle while the other measures the slope of the test vehicle chassis at the front and the rear. Chassis inclination and tank inclination are also recorded with inclination measuring systems consisting of a sensor and a display unit.

Two vehicle conditions are considered in the tipping tests: In condition A, one single wheel loses contact with the tipping bridge surface. In condition B, all wheels of a vehicle unit lose contact with the tipping bridge surface. The respective conditions are reached in a quasi-static manner by increasing the slope of the tipping bridge very slowly. Figure 8 illustrates tipping to the right. The vehicle-related inclination measuring points and the associated measuring systems are documented photographically together with a list of other relevant vehicle data, e.g. data required to review tipping angle calculation formulae at a later date.

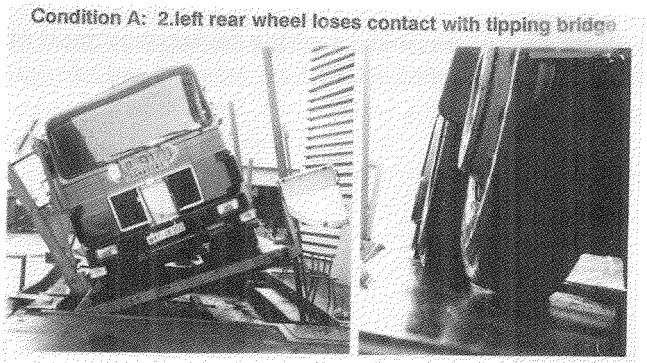

	Measured values	Mean value
Tipping bridge inclination:	20,5°/21,4°/21,0°	21,0°
Chassis inclination at rear:	25,8°/26,9°/26,6°	26,4°
Chassis inclination at front:	24,6°/25,1°/25,0°	24,9°
Tank inclination at front:	26,2°/26,8°/26,5°	26,5°
Tank inclination at rear:	25,9°/26,5°/26,4°	26,3°

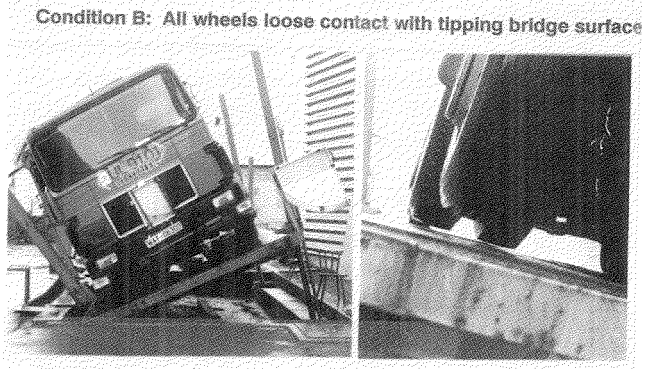

	Measured values	Mean value
Tipping bridge inclination:	23,5°/23,6°/23,5°	23,5°
Chassis inclination at rear:	30,5°/30,8°/30,5°	30,6°
Chassis inclination at front:	28,0°/27,7°/27,7°	27,8°
Tank inclination at front:	29,8°/30,2°/29,7°	29,9°
Tank inclination at rear:	29,4°/29,6°/29,4°	29,5°

Figure 8. Tilting to the Right

Driving tests are carried out with objective maneuvers to determine the dynamic overturning limit for realistic driving maneuvers prior to accidents and to compare these to the values obtained on the tipping bridge.

The first series of driving tests was carried out with a four-wheel towing vehicle and a six-wheel semitrailer with insulated stainless steel tank. Figure 9 shows the inside of the cab with the installed equipment to measure the variables

- Steering wheel angle
- Steering wheel moment
- Longitudinal acceleration of driver's cab
- Lateral acceleration of driver's cab
- Yaw velocity of driver's cab
- Roll angle of driver's cab
- Pitch angle of driver's cab
- Differential roll angle between driver's cab and chassis
- Lateral acceleration of chassis (chassis rigid)
- Buckling angle
- Relative pitch angle between chassis and semitrailer
- Longitudinal velocity
- Lateral velocity

at the towing machine, and the variables

- Lateral acceleration
- Longitudinal acceleration
- Yaw velocity
- Roll angle
- Pitch angle

at the semitrailer. The test program included 5 loading conditions and three driving maneuvers.

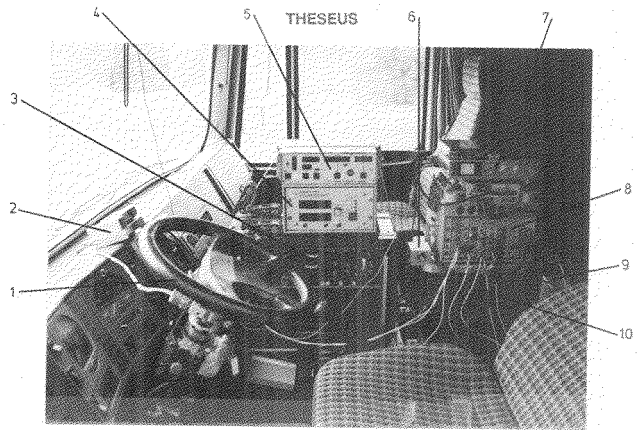

Figure 9. Measuring Equipment in the Driver's Cab

First evaluations of the circular driving maneuver show neutral steering to slight understeering for all loading conditions (Figure 10, top). The achievable lateral accelerations are larger for an unloaded semitrailer than for a loaded one. The buckling angle (Figure

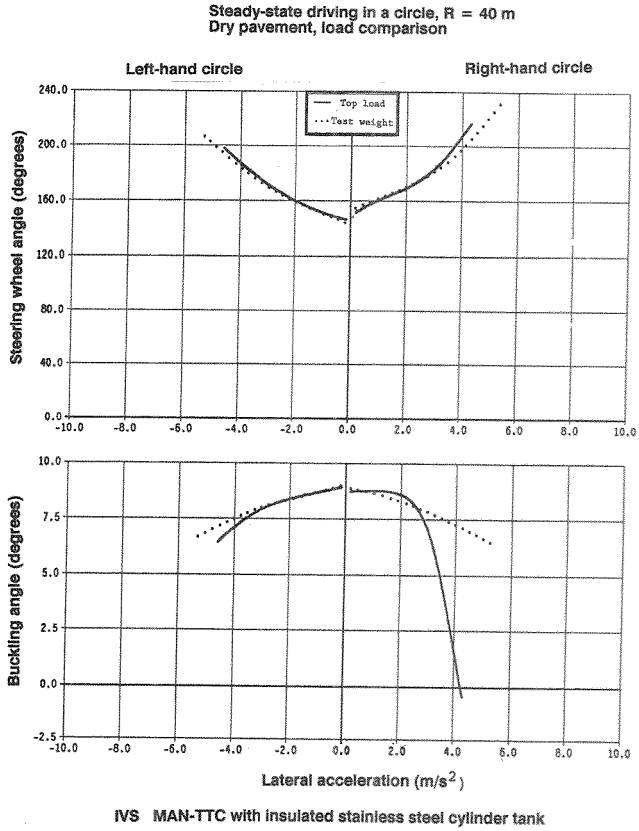

Figure 10. Buckling and Steering Wheel Angle as a Function of Lateral Acceleration

10, bottom) between the towing vehicle and the semitrailer is clearly positive when steering to the left, while negative values are obtained at larger lateral accelerations while steering to the right. This is due to the fact that the last axle of the semitrailer helps to steer the vehicle when driving in a left-hand circle but not when driving in a right-hand one.

In the case of sinusoidal steering angles, movement of the semitrailer around its vertical axis can only be observed at low steering frequencies. Vehicle reactions are very slight at high steering frequencies. However, the driver's cab does move considerably.

S10-O-09

UNITAS 2000—Environment and Nature Protection Related Integrated Tanker Safety

Hans-Eggert Tonnesen
Anton Ellinghaus GmbH & Co. KG

Abstract

TOPAS (tank truck with optimum and active safety equipment) was a research project of the BMFT in the mid-1980s. In view of the increase in the safety of tank trucks that became evident from this research project and of the results obtained from tanker crash tests carried out in conjunction with the DEKRA, Ellinghaus saw the need to apply the knowledge gained to cylindrical pressure tanks as well. The result of this was the enhanced-safety tank truck UNITAS 2000. The biggest difficulty in realizing this project was to lower the centre of gravity, in order to achieve not only a high level or stability against overturning, as in the case of TOPAS, but also the excellent road performance of this vehicle type, whereby it had to be born in mind that cylindrical tanks are all tested with an internal pressure of 4 bars. To attain this goal while retaining strength against the 4-bar internal pressure, the forward part of the tank deviated from the ideal cylindrical form and a so-called aerofoil profile was used in this area instead. The special feature of such a profile is that in the upper shell pressure-stresses occur and in the lower shell tensile-stresses, while the disastrous bending-stresses are almost completely obviated. The necessary static calculations for type approval were carried out using a finite element program that was hired in America. The usual hoop has been replaced on the UNITAS 2000 by an arrangement that provides the same level of safety with a normal wall thickness of 5,12 mm. The dome fittings were lowered into the outer contour of the tank, thus achieving a vehicle height saving of 400 mm. As a result, the dome fittings are protected in the case of the vehicle overturning in an accident, and a protection cover for the dome fittings is no longer necessary. The trapezoidal profile also had the advantage of making it possible to reduce the normal vehicle length, leading to better manoueuverability. The vehicle has been tested for operational safety by the Vehicle Owner's Trade Association and is permitted to display the GS sign.

Introduction

In the mid-Eighties a research project of the Ministry of Research and Technology was carried out under the name TOPAS which is the abbreviation for: "Road Tanker with Optimised Passive and Active Safety Features."

Out of the results of the TOPAS Project, the lowering of the centre of gravity must be classed as the most outstanding safety improvement (Figure 1).

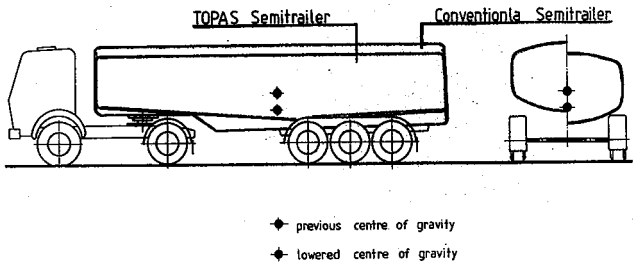

Figure 1. Cofferdam Bulkhead Tank

The reason why the lowering of the centre of gravity of road tankers, i.e. vehicles with moving load, is so important and offers an enormous safety improvement is something which I should like to explain by means of the following diagram (Figure 2).

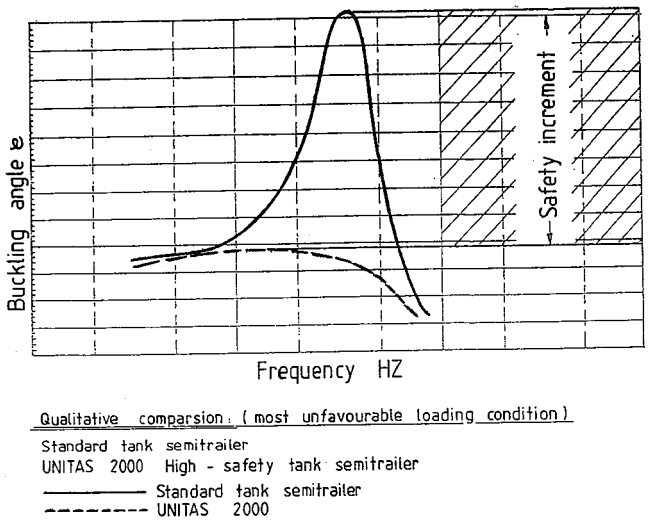

Figure 2. Trails of Dynamics of Vehicle Movements

The results from a trial of the dynamics of vehicle movements are illustrated in the diagram. In this trial with the most unfavourable loading condition, i.e. the front compartments partially loaded and the rear compartments fully loaded, the buckling angle between the tractor and semitrailer axle was measured as a function of the steering frequency. The buckling angle is plotted on the ordinate of the diagram, and the frequency in Hz on the abcissa. In this trial, the steering wheel of the tractor was periodically moved out to the right and left with the aid of a steering machine while driving straight ahead at about 45 km/h. The first trial was run with a standard tank semitrailer and high centre of gravity. During this trial, a very strong increase in amplitude of the buckling angle occurred within the range of the so-called natural frequency; this can be clearly seen in the steep ascent of the curve for the standard tank semitrailer.

In the case of unskilled drivers and vehicles which are not properly prepared, this strong increase in amplitude will, inevitably, result in overturning of the entire tank semitrailer. We were able to prevent this by means of laterally arranged supporting wheels under our test conditions.

In normal traffic situations, a tank semitrailer may get caught up in this resonant range if, at a relatively high speed, the driver has to avoid sudden unexpected obstacles or suddenly drops off to sleep.

The disastrous aspect of this situation lies in the fact that the tanker driver appears to have no chance of getting his vehicle under control within the range of this natural frequency.

This is where the enormous safety improvement of the lowering of the centre of gravity lies since, as you can see, the course of the curve for the TOPAS within the range of the natural frequency is extremely flat and does not show any increase in amplitude. With this safety road tanker it is possible to drive around obstacles without any problem and without the slightest tendency towards self-reinforcing. The self-reinforcing—increase of the buckling and swaying angle—which occurred up to now is eliminated completely.

We realised the necessity to transfer the experience gained from the TOPAS Project, from our road tanker crash trials and our trials of the dynamics of vehicle movements also to cylindrical pressure tanks. The result was the high-safety road tanker UNITAS 2000—a cylindrical tank with a lowest possible centre of gravity.

In this implementation the designer has to allow for certain limitations and boundary conditions. First of all, he has to adhere to the maximum permissible dimensions of the StVZO (Regulations Authorising the Use of Vehicles for Road Traffic). Another criterion is the tractor required for semitrailers. Since a modification of the tractor would be much more expensive, the designer has to adapt the tank semitrailer to the conditions of the tractor (Figure 3).

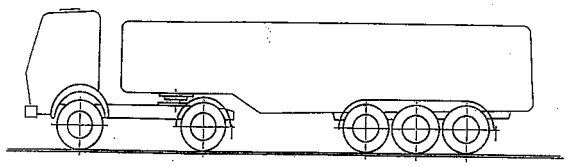

Figure 3. Tank with Lowered Centre of Gravity

As you can see on this illustration, the area of the tractor must be recessed from the tank in order to permit the useful volume of the tank behind the tractor to be lowered to a great extent.

This requires a substantial design and manufacturing-engineering expense. The expenditure largely depends on the test or service pressure of the tank.

This illustration shows the design of an aluminum cofferdam bulkhead tank with lowered centre of gravity. Due to the low test pressure of approx. 0,25 bar, the design and calculation expenditure is small in this case. The designer can use level walls and small wall thickness since the compressive load is insignificant.

In the case of a cylindrical pressure tank, however, the expenditure is several times higher because of the high test pressure of 4 bar (Figure 4).

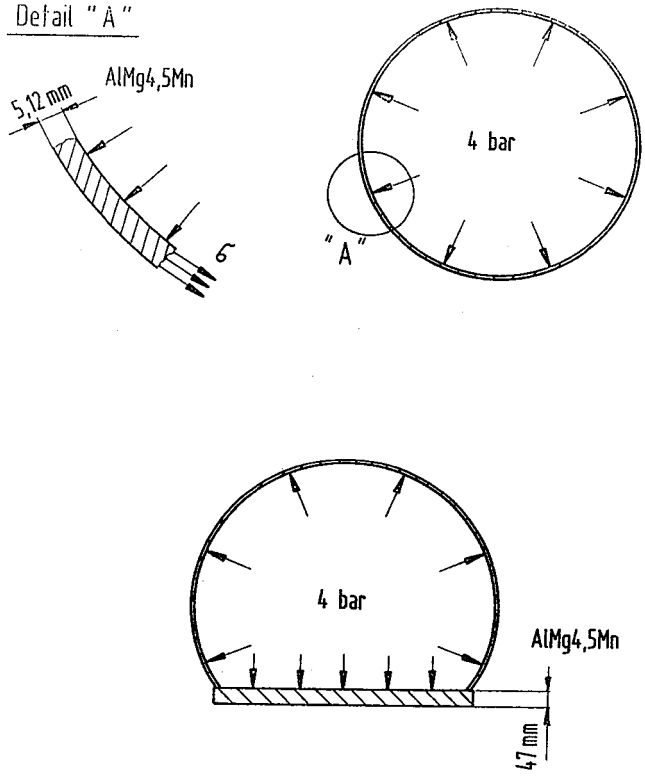

Figure 4. Pressure Tank—4-Bar

We know from physics that the most favourable geometrical form for an internal compressive load is the ball and/or the circle. As a consequence, pressure tanks usually have circular cross-sections.

Since the forces are distributed uniformly here, so-called membrane stresses acting as tensile stress prevail

in the tankwall. Tensile stresses are the most favourable condition of loading for inherent stability and strength of a component.

Since, as you have seen, we need the space for the tractor in the front area of the tank, we have to deviate from the idea circular form here. After we had simply cut off the lower tank shell, we now had to reconstruct a component which was level towards the outside in order to close the tank at this point. This component had to be capable of absorbing both the compressive forces and the bearing relations of the fifth wheel coupling. As you see, however, a wall thickness of 47 mm would be required here because of the high bending load of the plate compared to 5,12 mm in the case of the cylindrical wall. The absurdity of the a design is obvious. The main point now was to design a stress-resistant section which would be capable of absorbing the high compressive forces despite a small wall thickness.

Out of several approaches a so-called airfoil section (or wing profile) was, finally, selected (Figure 5).

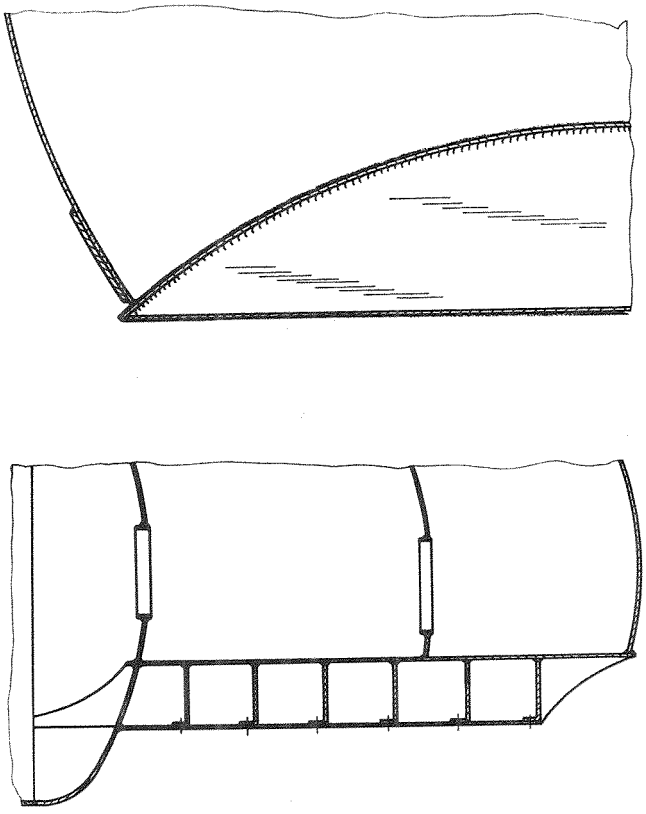

Figure 5. Wings Profile

This section is characterized by the fact that compressive stresses prevail in the top shell, and tensile stresses in the lower shell. Unfavourable bending stresses are avoided as far as possible. This is why we were able to choose the required wall thicknesses relatively small at approx. 8 mm and, thus, favourable as to weight (Figure 6).

A far more difficult hurdle had to be cleared, however: the necessary model approval of the tank with

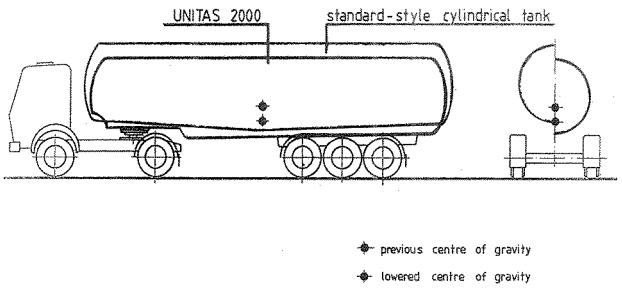

Figure 6. Cylindrical Tank

the appropriate computation. Because of the intricate shape of the airfoil section, the computation could only be completed with a Finite Element Program. Since it was not possible to obtain a suitable computer program in Germany, we had to borrow one in the United States against a high license fee. The program was then radio relayed to Germany via satellite and inputted into the mainframe of the Hannover Technical Control Association.

This illustration (Figure 7) shows one of approx. 50 result plots in which the different colours illustrate differently high stress conditions. The highest loads are shown in red.

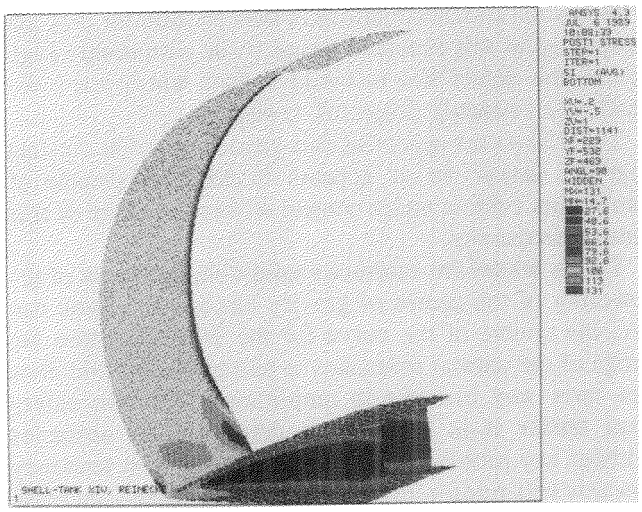

Figure 7. Comparison Stress SI (Shear Hypothesis) on the Inside

After the Finite Element Computation and a stress-strain check measurement had resulted in an adequate component strength, we were granted the model approval by the competent authority and this tank construction went into quantity production as UNITAS 2000.

Figure 8 shows the new development as it is used now. The tank is built in different wall thickness from aluminum or high-grade steel according to customer specifications.

In addition to road safety, industrial safety was, likewise, improved considerably and covered by a model test of the Main Professional Association. The UNITAS 2000 is the first road tanker permitted to carry the German GS symbol (symbol for tested safety).

Figure 8. Examples

A further, substantial safety improvement was achieved with regard to the dome arrangement of this tank semi-trailer. The dome cover and all dome fittings such as ventilation, overfilling protection etc. as well as the associated pipings are located within the tank contour and are optimally protected from damage and leakage.

As further features of this high-safety road tanker, we only name by key words those items which are not common:

- rigidly arranged three-axle steering unit, fully manoeuvrable (short-term steerable within a range of up to 25 km/h)
- high level stop lights and flashing trafficators
- reflecting strips at the rear deck and on the sides
- double bottoms at the front and rear (crash zone)
- salvage eyes on the tank and at the rear deck (for raising the fully tank semitrailer)
- complete all-round panelling as additional lateral tanker starting protection, passive cyclist and pedestrian protect

Specifications:

approx. 39.000-41.500 l capacity
6 to 8 compartments
full air suspension
lifting and lowering device
all-aluminum construction
all attachments of light-metal (axle attachment, air chamber, retainers, pipes, walkway etc.)
light-metal rims
Unladen weight: 5.700-6.450 kg

S10-O-11

Micro-Level Analysis of Large Truck Accidents in a Freeway Environment —

F.F. Saccomanno
University of Waterloo
S.W. Read
M.M. Dillon and Associates

Abstract

A statistical procedure is presented for determining the probabilities of accident involvement for certain truck configurations given specific manoeuvres and a mix of road and traffic conditions. The approach consists of a micro-level simulation applied to a controlled freeway environment, to obtain the pattern of manoeuvres over time and space for each truck in the traffic stream. The methodology is applied to three freeway test sections, with given road and traffic characteristics. Manoeuvres that are most problematic from the perspective of accident involvement are noted for different truck configurations and loading conditions. The results of this analysis are useful in establishing accident reduction strategies for freeways that are sensitive the specific requirements of different truck configurations and loading conditions.

Introduction

The process wherein large truck accidents take place is affected by individual vehicle operating characteristics. It is generally recognized that all drivers do not behave in a like manner, nor are they exposed to the same level of accident risks. For example, for the same road and traffic conditions, drivers with a more erratic driving pattern are more likely to be involved in accidents than drivers with a more stable driving pattern. Erratic driving caused by frequent lane changes, overtaking, and speed fluctuations increases the likelihood of an accident for the same road and traffic mix.

The nature of the relationship between the individual vehicle operating environment and the overall road and traffic mix is not well understood. Recent studies of large truck accidents by Carsten (1987), Jovanis and

Chang (1989) and Lyles and Stamatiadis (1989) have not addressed the effect of vehicle operating characteristics on accident involvement. The focus of this work has been to explain variations in truck accident rates in terms of different mixes of road and traffic characteristics. By adopting an aggregate approach, these studies assume that all trucks travelling along a section of roadway in a given traffic stream behave in a like manner, and are exposed to the same accident risk. Situational factors that reflect differences in accident risks for individual trucks are essentially ignored.

To fully understand the incidence of large truck accidents in a given road/traffic environment, a complete appreciation is required of the types of manoeuvres experienced by certain truck types and the proportions of these manoeuvres that actually result in accidents. In this paper, a micro-level analysis of large truck accidents is presented, that makes use of simulation techniques as applied to a controlled freeway environment. The approach incorporates information extracted from accident data on the proportions of unsafe manoeuvres for various truck configurations and loading conditions. Using a Baeysian formulation, inferences are drawn on the pattern of unsafe manoeuvres for selected truck types, and the conditions under which these manoeuvres are most problematic for truck accident occurrence.

Methodology

For truck type t, the conditional probability of an accident (A_t) given a manoeuvre (M_i) and road/traffic environment (E_j) can be stated as:

$$P\ (A_t | M_i \cap E_j)$$

In this section of the paper, a general mathematical expression is established for this relationship.

Consider a set of aggregate environmental factors, E_j, representing a mix of road geometric characteristics, traffic composition and weather conditions affecting truck accident rates. These "environmental factors" are established *by definition* to be mutually-exclusive, i.e., membership in each set E. cannot be shared with any other set of environmental factors, E_k. For example, if trucks are observed to undergo lane changes and accelerating operations together, then a new manoeuvre comprising the combination of these two operations is defined, such that overlaps with this combined operational set would not be permitted.

For each truck type t, the union of all environmental factors, i.e., $\cup E_j$, must be fully contained in the union of the subsets for all accidents (A_t) and non-accidents (NA_t), such that:

$$(E_1 \cup E_2 \cup \ldots E_j) \supset \{ A_t \cup NA_t \} \qquad (1)$$

The conditional probability of an accident for each manoeuvre can be obtained by applying Bayesian techniques of experimentation. The proportion of manoeuvres in the union of sets A_t and NA_t is unknown, but the proportion of manoeuvres in the set of accidents alone (A_t) can be obtained directly from police accident reports. Information concerning the proportion of manoeuvres (set M_i) in the set of accidents (A_t) for truck type t is used to provide information on the "posterior probability" of an accident for a given manoeuvre, road/traffic mix, and truck type, such that:

$$P(A_t | M_i \cap E_j) = \frac{P(M_i | A_t \cap E_j)\ P(A_t | E_j)}{P(M_i | E_j)} \qquad (2)$$

where

A_t = accident for truck type t.
M_i = manoeuvre type i.
E_j = road/traffic environment j.

Since all road/traffic environments have been defined to be mutually-exclusive, the posterior probability in Eq. 2 can be summed over all possible environments along a given road section, to yield the cumulative accident probability for each manoeuvre and truck type, $P[A_t | M_i]$.

The proportion of critical manoeuvres in the truck accident data base serves as a basis for estimating the term $P(M_i | A_t \cap E_j)$ in Eq. 2, where this term is part of the larger expression:

$$\begin{aligned} P(M_i | E_j) &= P(M_i | E_j \cap A_t)\, P(A_t | E_j) \\ &\quad + P(M_i | E_j \cap NA_t)\, P(NA_t | E_j) \\ &= P(M_i | E_j \cap A_t)\, P(A_t | E_j) \\ &\quad + P(M_i | E_j \cap NA_t)\{1 - P(A_t | E_j)\} \end{aligned} \qquad (3)$$

The term, $P(M_i | E_j \cap A_t)$ in Eq. 3 can be estimated directly from the accident data, controlling for the prior occurrence of an accident (A_t) in a given environment (E_j). The term $P(M_i | E_j \cap NA_t)$ for a non-accident situation, however, is difficult to obtain directly without continuously monitoring each vehicle in the traffic stream over time and space.

In this analysis, the distribution of vehicle manoeuvres is obtained by simulating traffic on selected freeway sections, while controlling for various exogenous conditions that affect the pattern of these manoeuvres, for example, operating speed, volumes and percentage trucks.

Simulation of Freeway Truck Manoeuvres Using "FREEVU"

The underlying premise of this analysis is that for a given mix of road and traffic conditions, large truck accidents are affected by unique vehicle operating characteristics at the time of the accident. In the absence of certain manoeuvres many accidents would take place or would occur with reduced frequency. Critical weight and dimensional factors place severe restrictions on the maneuverability of certain large trucks, creating instability and unsafe conditions. A good appreciation of the relationship between these manoeuvres and accident involvement could reduce a large proportion of accidents

involving large trucks under certain road and traffic conditions.

An analysis of 1983 Ontario truck accidents by Buyco (1987) indicated that large truck accidents are influenced by certain critical manoeuvres. These manoeuvres were identified based on an over-representation of trucks in the accident data base in relation to the general vehicle populations for the same road/traffic environment (Table 1). From this analysis, certain manoeuvres were found to be especially problematic for certain types of trucks and loading conditions, for example, going ahead, overtaking, changing lanes, pulling in and merging.

Table 1. Involvement Ratios for Different Manoeuvres for Ontario Highway Accidents

CATEGORY	TRUCK ACCIDENT	ALL VEHICLE ACCIDENT**	EXP. # OF TRUCK ACC.	IR
MANOEUVRE				
GOING AHEAD	3062	184935	2484	1.233 †
SLOW/STOP	263	21041	283	0.931 †
OVERTAKING	184	5676	76	2.414 †
TURNING LEFT	189	34878	468	0.403
TURNING RIGHT	83	10907	146	0.567
U-TURN	14	1138	15	0.916
CHANGING LANES	232	10572	142	1.634 †
MERGING	29	1018	14	2.121 †
REVERSING	58	8427	113	0.512
STOP/PARKED	213	42680	573	0.372
PULL AWAY CURB	11	2298	31	0.356
PULL INTO CURB	15	562	8	1.987
UNKNOWN/OTHER	24	7309		
TOTAL *	4353	324132	4353	
* NOT INCLUDING UNKNOWN CATEGORY				
** FROM MOTOR VEHICLE ACCIDENT FACTS FOR ONTARIO 1983				

† Manoeuvres retained for further analysis.

While the above manoeuvres indicate an over-representation in the truck accident data base, it doesn't necessarily follow that they also cause more accidents per truck-kilometer travelled. Over-representation may be due solely to higher levels of exposure. For example, one would expect that given higher vehicle stability, fewer truck accidents are likely to take place while the vehicle is going ahead at a uniform speed. The higher truck involvement ratios in Table 1 for this manoeuvre may be due to a higher proportion of time in travel spent going ahead at a constant speed. When exposure is taken into account, the going ahead manoeuvre could be very safe under most road/traffic conditions and truck configurations.

In this study, the pattern of manoeuvres for large trucks in a freeway environment is obtained through a micro-level simulation program called FREE W. FREE W is based on FOMIS, an earlier freeway simulator developed by A.G. Bullen at the University of Pittsburg. The purpose of these packages is to model traffic flow along a specified freeway section controlling for various traffic inputs, such as, volume, average traffic stream speeds, truck composition, and geometric characteristics. The basic features of FREEVU have been documented by Hellinga and Shortreed (1990).

FREEVU is used in this exercise to obtain a distribution of simulated truck manoeuvres along a given freeway section, controlling for various traffic factors such as, volume, percentage trucks, and speed. The ability of FREEVU to adequately represent the pattern of manoeuvres in a traffic stream was reviewed by comparing the simulated pattern with observations from 1985 Federal Highway Administration (FHWA) freeway studies in the United States (Smith, 1985). Read (1991) and Hellinga (1990) have shown that the simulated pattern of manoeuvres from FREEVU closely mirrors the pattern reported in the FHWA data, for an assumed mix of geometrical features and traffic composition. Three test sections were used for these comparative tests (Table 2).

Table 2. FHWA Freeway Sections Used for Validating FREEVU

Site No.	Location	Section Type
2	I-95 S.B. at Backlick Road (Rte 617) in Fairfax County, VA	On-Ramp
3	I-395 S.B. (Shirely Highway) at Duke Street (Rte 236) in Alexandria, VA	Off-Ramp
4	I-405 N.B. at Mulholland Drive Los Angeles, CA	Tangent
5	I-405 S.B. at Santa Monica Blvd. Los Angeles, CA	On-Ramp

Site No.	Observed			Simulated			Error (%)
	Left	Right	Total	Left	Right	Total	
2	0.217	0.135	0.352	0.285	0.091	0.376	6.8[a]
3	0.082	0.140	0.222	0.195	0.254	0.449	102.3[b]
4	0.186	0.234	0.420	0.307	0.173	0.480	14.3[c]
5	0.386	0.098	0.484	0.416	0.094	0.510	5.4

[a] simulated volumes approximately 10% low
[b] simulated volumes approximately 17% low
[c] simulated volumes approximately 13% low with breakdown occurring

FREEVU Input Specifications

It should be noted that FREEVU is based on an accident-avoidance algorithm. As such, the program cannot be used to simulate accident occurrence directly. Since the proportion of accidents involving selected manoeuvres is negligible in relation to the total distribution of similar manoeuvres in the traffic stream, the distribution of manoeuvres for a non-accident environment can be used to approximate the distribution of manoeuvres for both accident and non-accident situations. Hence for truck type t the term, $P(M_i \mid E_j)$ in Eq. 3 can be approximated by $P(M_i \mid E_j \cap NA_t)$.

FREEVU can model a large number of vehicle types. Each type is distinguished by its length, desired speed, power/mass ratio, frontal area, and weight (Table 3). In this analysis, five truck configurations are considered: single unit truck, truck and trailer, tractor without trailer, tractor-trailer and tractor-twin-trailer units. For each

truck type, excluding tractors, both fully loaded and unloaded conditions are considered.

Table 3. Truck Configuration Characteristics

Vehicle Type	Load Status	HP	GVW (tonne)	Frontal Area (m^2)	Length (m)
Truck	Loaded	250	25.0	7.0	10.0
	Unloaded	250	10.4	7.0	10.0
Truck+Trailer	Loaded	350	42.2	7.0	16.0
	Unloaded	350	14.5	7.0	16.0
Tractor	Unloaded	350	7.5	8.0	9.0
Tractor+Trailer	Loaded	400	50.0	8.25	22.5
	Unloaded	400	18.0	8.25	22.5
Tractor+2 Trailers	Loaded	400	63.5	8.25	23.0
	Unloaded	400	21.6	8.25	23.0

Manoeuvres which were found to be over-represented in the 1983 Ontario road accident data base for large trucks were modified for input into the simulation package. Four distinctive truck manoeuvres have been simulated using FREEVU: 1) Overtaking, 2) Changing Lanes and Merging, 3) Slowing and/or Stopping and 4) Going Ahead. Lane change manoeuvres were classified initially into mandatory or desired, and later combined for the purpose of analysis. Mandatory lane changes occur when a vehicle must merge with the current physical section due to geometric constrictions. Desired lane changes are dictated by the vehicles' desired speed of operation, and its desire to be in a designated lane at a particular point along the freeway section. Passing manoeuvres (overtaking), going ahead, and yielding manoeuvres (slowing and stopping) are not dictated by the physical characteristics of the section but by the desired speeds and attainable accelerations of the individual vehicles.

A considerable amount of uncertainty bounds the simulated estimate of the vehicle manoeuvre rate, when this estimate is applied to a block of trucks in a given traffic stream. This is due to the fact that no simulation package can fully incorporate all factors affecting individual vehicle operations. Uncertainty in the pattern of manoeuvres can be considered by treating the mean manoeuvre rate for a block of trucks as a Poisson process, such that for each estimate of the manoeuvre rate there is a corresponding probability measure. However, since the simulated mean manoeuvre rate in this analysis is small, the probability of getting more than one manoeuvre in the assumed simulation period is negligible. As a result, the probability of getting at least one manoeuvre can approximated by the mean manoeuvre rate for the assumed block of trucks, and the incorporation of the Poisson process was not warranted.

Application to Selected Freeway Corridor

In this section of the paper, the methodology is applied to three representative freeway sections along the Queen Elizabeth Way from Fort Erie to Toronto in Southern Ontario (Figure 1). The corridor begins with low volume, non-commuter traffic near Fort Erie and ends with high volume commuter traffic in the vicinity of Toronto. High volume non-commuter traffic applies to the middle section from St. Catherines to Hamilton. These sections were chosen because of their proximity to truck inspection stations used in the 1983 Ontario Commercial Vehicle Survey (CVS). The nature of the information available at these stations is discussed by Perrera and Corupe (1984). The geometric and traffic characteristics associated with each of the three freeway Environments (A, B and C) are given Figure 2.

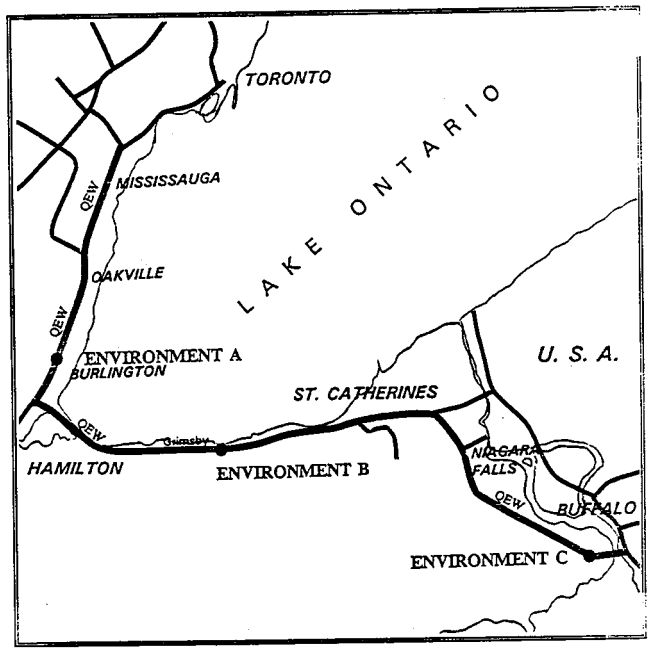

Figure 1. Queen Elizabeth Way Freeway Corridor in Southern Ontario

Estimating Freeway Accident and Manoeuvre Probabilities

Many studies have estimated large truck accident rates based on various road and traffic classifications. The thrust of these studies has been to establish truck accident rates accounting for the presence of statistically determined environmental features explaining variations in these rates. Saccomanno and Buyco (1989) used a GLIM loglinear approach to obtain rates in Ontario for large trucks, while controlling for truck type and loading status, freeway location, and various other road and traffic conditions. Using these GLIM loglinear expressions, average accident rates by truck type were

Environment A - Freeway: High Volume Commuter

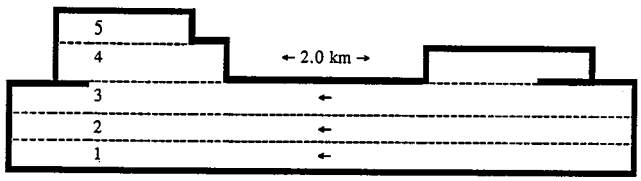

AADT..... 88000
DIR. SPLIT..... 74%
DHF..... 9.8%
PHV..... 6382 VPH
%CV..... 10%

Environment B - Freeway: High Volume Non-Commuter

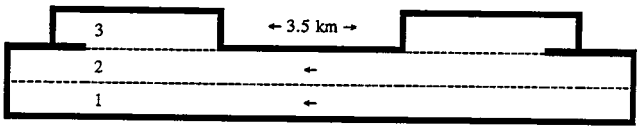

AADT..... 51200
DIR. SPLIT..... 62%
DHF..... 10.2%
PHV..... 3238 VPH
%CV..... 20%

Environment C - Freeway: Low Volume Non-Commuter

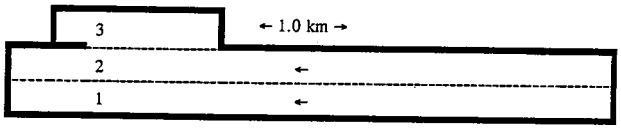

AADT..... 12300
DIR. SPLIT..... 64%
DHF..... 10.2%
PHV..... 804 VPH
%CV..... 10%

Figure 2. Freeway Test Section Characteristics (Environments A, B, and C)

obtained for any combination of road and traffic factors (i.e., Environments A, B and C). These estimates correspond to the term $P(A_t \mid E_j)$ in Eq. 2. and have been summarized in Table 4.

Table 5 gives the distribution of manoeuvres by truck type extracted from the Ontario truck accident data base for the period 1982-86. The probability of a manoeuvre given an accident and a road/traffic environment can be obtained directly from this Table by dividing manoeuvre frequencies by the number of accidents in each environment for each type of truck. These estimates correspond to the term $P(M_i \mid A_t \cap E_j)$ in Eq. 2.

The results summarized in Table 5 indicate that Environment A (high volume, commuter) traffic is most represented in the accident data. Approximately 80% of all truck accidents occurred during the "going ahead" manoeuvre. Tractor-trailer combinations were involved in 78% of all large truck accidents during the 1982-86 period; the majority of these accidents took place while the vehicle was fully loaded.

FREEVU was applied to each representative freeway/traffic section and the probability of manoeuvres was estimated for different truck types and loading conditions. For 10% trucks and high volume traffic (Environment A), the percentage of time during which trucks experience specific manoeuvres is summarized in Table 6 for each truck type being considered. For over 95% of the time during the simulation, all trucks were observed to be moving a straight direction at a uniform speed. Tractors were observed to experience a significant proportion of overtaking and slow/stopping manoeuvres relative to other configurations, although going straight ahead continues to dominate operations for this type of truck (94.89%). Irrespective of loading, the longer and less maneuverable configurations represented the highest going ahead time share of all trucks on the freeway sections. Unloaded tractor-trailer combinations experienced a significant level of slow/stopping operations.

Table 4. Truck Accident Rates for Three Freeway Environments

TRUCK TYPE	LOADING	ACCIDENT RATE (per 10^6 km)		
		ENV A	ENV B	ENV C
TRUCK	LOADED	1.283	1.125	0.600
	UNLOADED	0.249	1.802	
TRUCK+TRAILER	LOADED	0.1780	0.177	0.095
	UNLOADED	0.2490	0.170	
TRACTOR	UNLOADED	1.774	1.499	0.488
TRAC+TRAILER	LOADED	0.889	0.609	0.390
	UNLOADED	1.601	0.766	
TRAC+2TRAILERS	LOADED	0.980	0.567	0.431
	UNLOADED	0.179	0.074	

ENV A: Commuter Traffic Pattern; High Volumes

ENV B: Non-Commuter Traffic Pattern; High Volumes

ENV C: Non-Commuter Traffic Pattern; Low Volumes

Table 5. Pattern of Manoeuvres in the 1982-86 Ontario Truck Accident Data Base

		ENVIRONMENT A				ENVIRONMENT B				ENVIRONMENT C			
VEHICLE TYPE	STATUS	M1	M2	M3	M4	M1	M2	M3	M4	M1	M2	M3	M4
TRUCK	LOADED	0.0021	0.0432	0.2119	0.7428	0	0.0551	0.2047	0.7401	0	0	0	0
	UNLOADED	0.0056	0.0367	0.1808	0.7768	-	-	-	-	-	-	-	-
TRUCK+TRAILER	LOADED	0	0	0.2857	0.7143	-	-	-	-	-	-	-	-
	UNLOADED	0	0.0250	0.1500	0.8250	0.0833	0	0	0.9166	-	-	-	-
TRACTOR	UNLOADED	0.0083	0.0413	0.1818	0.7686	0.0555	0.0277	0.0555	0.8611	-	-	-	-
TRAC+TRAILER	LOADED	0.0096	0.0311	0.1222	0.837	0.0446	0.0292	0.1000	0.8262	0.0955	0	0.0756	0.8288
	UNLOADED	0.0054	0.0453	0.1133	0.836	0.0022	0.0465	0.1867	0.7314	-	-	-	-
TRAC+2TRAILERS	LOADED	0.0479	0.0616	0.0274	0.863	0.0606	0.0606	0.0606	0.8181	0.0952	0	0.0471	0.8571
	UNLOADED	0.1020	0.0612	0	0.8367	-	-	-	-	-	-	-	-

Manoeuvres: M_1 Overtaking
M_2 Changing Lanes/Merging
M_3 Slow/Stopping
M_4 Going Ahead

Environment: A Commuter; High Volume
B Non-Commuter; High Volume
C Non-Commuter; Low Volume

Source: 1982-1986 Police Report Accident Data (MTO) Tabulation

Probabilities of Truck Accidents Given Manoeuvres

The application of FREEVU to the three representative freeway sections of the QEW yields probability distributions of manoeuvres for a block of trucks of designated

Table 6. Conditional Truck Accident Probabilities for Different Manoeuvres, Configurations, and Loading Conditions (Freeway Environment A with 10 Percent Trucks)

TRUCK	MAN	P[M/NA]	P[M/NA]	P[A]	P[A/M]
Loaded Truck					
1	1	0.00539	0.00200	1.28e-04	4.7572e-05
	2	0.00430	0.04320	1.28e-04	1.2862e-03
	3	0.01175	0.21190	1.28e-04	2.3094e-03
	4	0.97855	0.74270	1.28e-04	9.7374e-05
Unloaded Truck					
2	1	0.00936	0.00560	2.49e-05	1.4905e-05
	2	0.00460	0.03670	2.49e-05	1.9884e-04
	3	0.02171	0.18070	2.49e-05	2.0721e-04
	4	0.96431	0.77680	2.49e-05	2.0058e-05
Loaded Truck + Trailer					
3	1	0.00095	0.00000	1.78e-05	0.0000
	2	0.00923	0.00000	1.78e-05	0.0000
	3	0.00485	0.28570	1.78e-05	1.0481e-03
	4	0.98497	0.71420	1.78e-05	1.2907e-05
Unloaded Truck + Trailer					
4	1	0.00818	0.00000	2.49e-05	0.0000
	2	0.00522	0.02500	2.49e-05	1.1929e-04
	3	0.02363	0.15000	2.49e-05	1.5805e-04
	4	0.96297	0.82500	2.49e-05	2.1332e-05
Tractor					
5	1	0.01370	0.00820	1.77e-04	1.0621e-04
	2	0.00352	0.00820	1.77e-04	2.0755e-03
	3	0.03392	0.18180	1.77e-04	9.4987e-04
	4	0.94886	0.76850	1.77e-04	1.4367e-04
Loaded Tractor + Trailer					
6	1	0.00060	0.00960	8.89e-05	1.4276e-03
	2	0.00535	0.03110	8.89e-05	5.1673e-04
	3	0.00617	0.12220	8.89e-05	1.7568e-03
	4	0.98788	0.83700	8.89e-05	7.5320e-05
Unloaded Tractor + Trailer					
7	1	0.00509	0.00530	1.60e-04	1.6672e-04
	2	0.00393	0.04530	1.60e-04	1.8431e-03
	3	0.01762	0.11320	1.60e-04	1.0274e-03
	4	0.97336	0.83600	1.603-04	1.3750e-04
Loaded Tractor + 2 Trailers					
8	1	0.00051	0.04790	9.80e-05	9.2103e-03
	2	0.00431	0.06160	9.80e-05	1.4004e-03
	3	0.00264	0.02730	9.80e-05	1.0144e-03
	4	0.99255	0.86300	9.80e-05	8.5205e-05
Unloaded Tractor + 2 Trailers					
9	1	0.00221	0.10200	1.79e-05	8.2585e-04
	2	0.00427	0.06120	1.79e-05	2.5625e-04
	3	0.00747	0.00000	1.79e-05	0.0000
	4	0.98604	0.83670	1.79e-05	1.5189e-05

configurations and loadings, and a mix of road and traffic conditions. The lion's share of manoeuvres do not result in accidents. The central point of interest in this analysis is to determine the proportion of manoeuvres of a given type that result in accidents, and to assess how these probabilities are affected by truck type, loading and road/traffic conditions.

It isn't clear from the above analysis whether specific manoeuvres are equally represented in accident and non-accident data. If this is not the case, specific manoeuvres would have a disproportionate effect on accidents involving each truck type for each freeway test section. Conditional probabilities of accidents for specific manoeuvres and differing truck types were estimated using Eq. 2. These results are summarized in the right most column of Table 6 for road/traffic environment A (high volume, commuter with 10% trucks).

In general, the posterior probabilities in Table 6 suggest that for most manouevres and truck types a considerable amount of travel would be required before a vehicle has a reasonable chance of being involved in an accident as a direct result of a specific manoeuvre. All probabilities lie in the 10^{-3} to the 10^{-5} range per truck-kilometer of exposure. Assuming one million truck-kilometers of exposure per year for a large urban jurisdiction, many of these manoeuvres would not give rise to more than 100 freeway accidents per year overall.

The range of posterior probabilities (accident given manoeuvre and environment) by truck type and loading are illustrated in Figure 3 for 10 trucks and high volume traffic (Environment A) and in Figure 4 for 20% trucks and low volume traffic (Environment B). These Figures indicate significant variation in conditional accident probabilities for different truck types, loading conditions, and road/traffic environment. Variations in conditional probabilities among trucks of different configurations appears to be significant for all manoeuvres. Independently of truck type, the highest conditional probabilities of an accident were obtained for the lane change and slow/stop manoeuvre. The highest conditional accident probabilities were observed for tractor units for most manoeuvres, followed by loaded single unit trucks. Single and double trailer combinations were most likely to be involved in accidents during the overtaking manoeuvre, regardless of load status. The effect of load status on conditional accident probabilities is affected by truck type and manoeuvre. Some trucks are more likely to experience accidents when loaded, while other are more likely to experience accidents when empty.

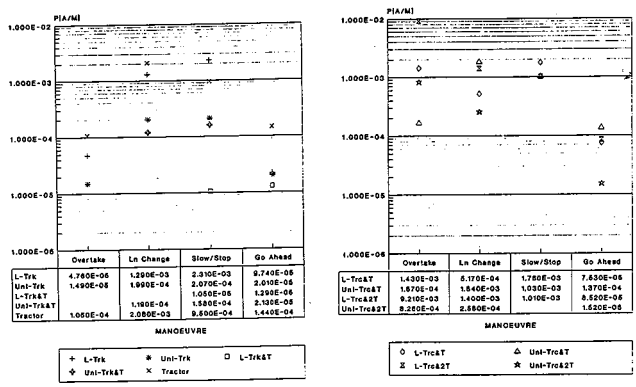

Figure 3. Posterior Accident Probabilities Given Manoeuvres and Truck Configurations for Freeway Environment A

A comparison between Figure 3 and 4 suggests that the conditional probabilities of accidents are affected by the total volume and percentage trucks in the traffic stream. These factors were found to have a disproportionate effect on accidents depending on truck configuration and loading. Less congested conditions, represented by lower volumes on the freeway test section, reduced the conditional probabilities of accidents significantly for all manoeuvres, especially for lane change and slow/stopping. The effect was found to be greater for the smaller truck than for longer combination units. The most problematic manoeuvres for high volume freeway traffic were identified as:

Truck Type	Load Status	Manoeuvre
Truck	Loaded	Slow\stopping and lane change
	Unloaded	Slow\stopping and lane change
Truck & trailer	Loaded	****
	Unloaded	Slow\stopping and lane change
Tractor	Unloaded	Lane change and slow\ stopping
Tractor-Trailer	Loaded	Slow\stopping and overtaking
	Unloaded	Lane change and slow\ stopping
Tractor-Twin Trailer	Loaded	Overtaking and lane change
	Unloaded	Slow\stopping and overtaking

Although the differences between them are negligible, these manoeuvres have been listed in descending order of probabilities or importance.

It should be noted that while going ahead was over-represented in the simulated traffic data for all truck types, the conditional probabilities of accidents for the going ahead manoeuvre is considerably lower than for other manoeuvres. Loaded and unloaded tractor trailers, tractor, and loaded trucks were observed to reflect the highest accident potential for the going ahead manoeuvre.

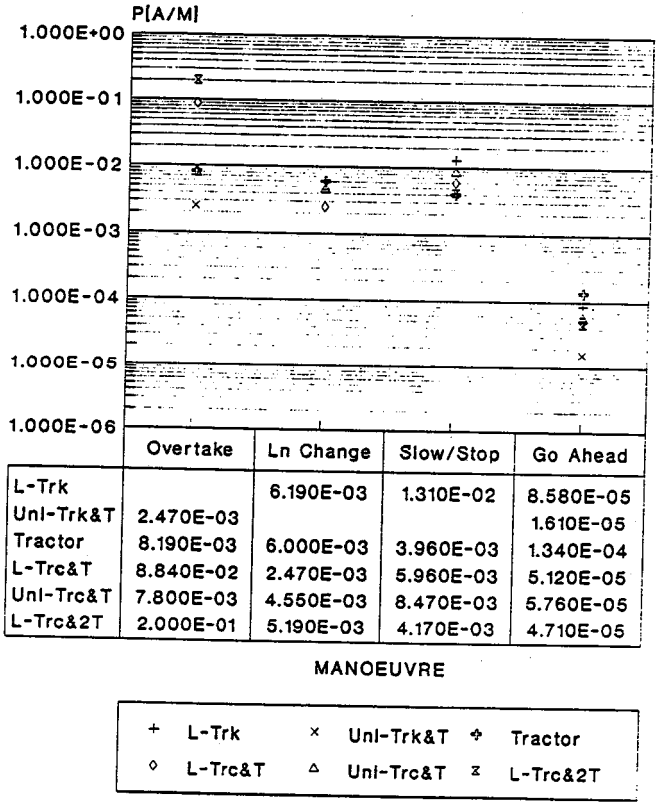

	Overtake	Ln Change	Slow/Stop	Go Ahead
L-Trk		6.190E-03	1.310E-02	8.580E-05
Unl-Trk&T	2.470E-03			1.610E-05
Tractor	8.190E-03	6.000E-03	3.960E-03	1.340E-04
L-Trc&T	8.840E-02	2.470E-03	5.960E-03	5.120E-05
Unl-Trc&T	7.800E-03	4.550E-03	8.470E-03	5.760E-05
L-Trc&2T	2.000E-01	5.190E-03	4.170E-03	4.710E-05

Figure 4. Posterior Accident Probabilities Given Manoeuvres and Truck Configurations for Freeway Environment B

Conclusions

A probabilistic relationship has been established between truck configuration and vehicle operating characteristics controlling for a mix of road and traffic conditions. The approach has permitted a more complete understanding of the nature of large truck accidents than would otherwise be available from an aggregate analysis of accident frequencies and rates, where all trucks in a traffic stream are considered together with regard to accident risk.

The results of this analysis have shown that conditional probabilities of truck accidents are affected by road/traffic environment, truck type, load status and the nature of the manoeuvre being undertaken at the time of the accident. Despite higher exposure levels, the conditional probability of a truck accident for the going ahead manoeuvre was typically less than other manoeuvres for all truck types and loadings. Going ahead appeared to have special problems for longer tractor-trailer combinations on a high volume freeway environment.

Truck type and loading were found to be significant factors in the accident profile for most manoeuvres, especially for Environment A. Smaller truck configurations were most likely to experience accidents during lane changes and slow/stopping manoeuvres.

The results of this analysis are useful in identifying the most unsafe vehicle operating features, and the conditions under which these features are most problematic. Effective accident reduction strategies can be established for each freeway section, taking into account the specific demands placed on safety by certain configurations and loading conditions. The information provided by this approach may be useful in highway truck inspection programs, traffic management and routing, and highway and vehicle design standards.

References

1. Buyco, C. "Analysis of factors affecting truck accident rates," Unpublished M.A.Sc. Thesis, Department of Civil Engineering, University of Waterloo, 1987.
2. Buyco, C. and Saccomanno, F.F., "Analysis of truck accident rates using loglinear models," *Canadian Journal of Civil Engineering*, Vol. 5, 1988.
3. Carsten, O., "Safety implications on truck configurations," Paper presented at the 66th Annual Meeting of the Transportation Research Board, Washington, D.C., 1987.
4. Hellinga, B., and Shortreed, J.H., "FREE W—A potential computer freeway traffic analysis tool," Report prepared for the Research and Development Branch, Ministry of Transportation of Ontario, 1990.
5. Jovanis, P.P. (et.al.), "A comparison of accident rates for two truck configurations," Paper presented at the 69th Annual Meeting of the Transportation Research Board, Washington, D.C., 1989.

6. Perera, M.H. and Corupe, E.G. "Ontario Commercial Vehicle Survey—1983," Policy Planning Branch, Ontario Ministry of Transportation, 1984.
7. Read, S. "Analysis of large truck freeway accidents utilizing Bayesian analysis," Unpublished M.A.Sc. thesis, Department of Civil Engineering, University of Waterloo, 1991.
8. Smith, S.A., "Freeway data collection for studying vehicle interactions," Technical report. FHWA/RD-85/108, US Department of Transportation, 1985.

☆ US GOVERNMENT PRINTING OFFICE : 1993 O - 354-702 (vol.2)

Motorists at Risk: Defective Seat Belts and Seat Backs

Edward M. Ricci

Many unwary motorists are driving cars and trucks equipped with seats no stronger than ordinary lawn chairs and seat belts that can kill or maim. The laws of physics, which dictate how these devices work, go back as far as Sir Isaac Newton, but automakers continue to disregard the realities of motor vehicle crashes and do little to protect the motoring public.

When Newton first theorized that for every action there is an equal and opposite reaction, he also formulated the basis for today's occupant containment theory in motor vehicles. In frontal collisions, seat belts protect motorists from striking steering wheels, dashboards, and windshields. Seat backs provide protection in the opposite direction, preventing motorists from catapulting rearward and breaking their necks and backs.

Motor vehicle safety is not optional. It is an entitlement of every motorist. Disregard for consumer safety will lead the public to insist that the National Highway Traffic Safety Administration (NHTSA) revise its standards to assure crash protection and will lead victims to continue to seek redress in the courts.

How should a properly designed seat belt perform? What protection should its wearer expect?

The answer is found in the dynamics of the car crash. In the car's impact with a fixed object or another vehicle—the "first collision"—the occupant continues to move after the car has decelerated. The movement will only be slowed or arrested when the occupant's body meets an opposing structure in the "second collision."

If that structure is a rigid metal roof rail, jagged windshield glass, or the hard pavement surface outside the car, the results can be devastating. If the structure is protective—if it spreads the crash forces across the occupant's body, diverts them from areas especially vulnerable to life-threatening injuries, and yields sufficiently to the body's impact—injuries can be prevented or substantially minimized.

Seat back failures in low-impact accidents have resulted in severe or fatal injuries.

The role of a properly designed seat belt system is to provide just that kind of protection in the second collision because, when worn, it is the first structure met by the occupant's moving body. As stated by the principal research scientist at General Motors (GM): "A snug-fitting lap/shoulder belt ties the occupant directly to the passenger compartment and allows that occupant to 'ride down' the crash," eliminating "the more severe occupant-to-interior 'second collisions,' provided the belts are themselves fairly tight." And, "Belts are also designed to distribute restraining loads over strong skeletal structures, including the shoulder, rib cage, and pelvis, to optimize protection during deceleration."[1]

These principles are violated in many belt designs. A belt that is not properly designed, a former Ford engineer warned as early as 1970, "may itself contribute to injury in specific circumstances."[2]

Despite these and other warnings, motorists are still being urged to buckle up for safety with seat belts that are defective and dangerous. The following are the most common hazards.

▸ Rear lap belts. In July 1986, the public was jolted by a National Transportation Safety Board (NTSB) study that revealed rear lap belts were a deadly menace in common crashes, especially to children.[3] For years, however, auto manufacturers had been informed in medical and engineering literature that lap-only belts not only would permit needless injuries in some crashes, but also would cause injuries. Manufacturers also knew that properly designed lap-shoulder belts would eliminate these hazards.

The NTSB warned: "Lap belts may induce injury, ranging in severity from minor to fatal, to the head; spine; abdomen; intra-abdominal viscera, connecting tissue, and blood vessels; and intrathoracic viscera, connecting tissue, and

Edward M. Ricci is a partner in Edward Ricci & Associates in West Palm Beach, Florida.

blood vessels. Such injuries may occur singly or in combination."[4] As the agency noted, the belts promote head injury by allowing the upper torso to swing forward, and abdominal and spinal cord injury by overloading the lower torso with crash forces.

Rear-belt use has increased since 1986, and so have injuries. Even NHTSA, which has failed to recall lap-only belts or effectively promote the retrofitting of rear lap-shoulder belts, has admitted to Congress that as many as 6,000 deaths and injuries per year could be prevented by the replacement of lap-only rear belts with lap-shoulder belts.[5]

One reason for the injuries is that the lap belts often slip off the pelvis in crashes, violating Federal Motor Vehicle Safety Standard (FMVSS) 209. If the belt rides up, the crash load is distributed over the soft tissue and viscera of the abdomen. This further increases the likelihood of severe abdominal and spinal cord trauma, especially to children, who have delicate muscular and skeletal structures and are frequently seated in back seats.

► "Windowshades." In the early 1970s, the lap-shoulder belts in most U.S. cars were so poorly designed that they squeezed the wearer's body uncomfortably. They were routed across the necks and faces of shorter wearers, which created or increased injury risks in crashes and discouraged use.

Rather than redesigning the belts, the companies instead equipped them with a tension-relieving device known as a "windowshade." This device allows for several inches of slack to be introduced into the belt system.

Unfortunately, a loose belt is a grave hazard in a crash. According to NHTSA tests, even two inches of slack can substantially raise head-injury force levels, and a few inches can largely eliminate a belt's effectiveness.[6] Further, a slack belt can promote or allow ejection or submarining (the occupant sliding out of the belt).

In June 1979, a NHTSA contractor, completing an exhaustive analysis of belt design problems, warned that windowshades "should not be employed" because they "often allow excessive and dangerous slack in the shoulder belt."[7] NHTSA also indicated that removal of these devices would save not only lives but money, since the resulting cost of belts to car buyers would be less.[8] Two seat belt manufacturers and Japanese, German, and French automakers have also warned about the hazards of seat belt slack and slack-inducing devices.[9] Manufacturers, though, ignored the warnings.

In 1988, the NTSB referred to data indicating that "increasing slack in a windowshade-equipped lap/shoulder belt increases the chance of serious or fatal head injuries."[10] It urged curtailment of the devices.

Although manufacturers appear to have begun phasing out windowshades, they refuse to recall them in cars already on the highways, leaving at risk hundreds of millions of motorists who travel on U.S. roads.

Motorists are being urged to buckle up for safety with seat belts that are defective and dangerous.

► Door-mounted belts. These buckle with no help from the user. If a door opens during a crash, an occupant whose belt is anchored to the door may be ejected, a leading cause of catastrophic injury in rollover and other crashes.

In late 1990, a Brunswick, Maine, police officer died after the door of his GM patrol car opened in a side impact and the door-anchored automatic belt system automatically disengaged.[11] The city has since retrofitted its police cars with manual belts. Yet automakers continue to equip many new cars with door-mounted belts and do nothing to retrofit ones already on the road or to warn owners about ejection risks.

► Shoulder-only belts. This design has been known to be hazardous since at least 1970.[12] Because there is no lap belt to restrain the torso, occupants can suffer severe internal and neck injuries. Although manufacturers have altered the design and some governments prohibit their production, these belts were in cars sold as late as 1990 and are still permitted under the NHTSA vehicle safety standards.

► Front release buttons. Seat belts with release buttons on the front face of the buckle are prone to release in some types of crashes, especially side impacts and rollovers. The release can occur when the rear face of the buckle is hit by a solid part of the user's body (such as the pelvic or hip bone) or by a child safety seat that the belt is supposed to secure. NHTSA has refused to issue a recall despite mounting complaints by motorists. The government of Australia criticized this belt buckle design as early as 1973.[13]

► Fixed anchorages on three-point lap-shoulder belts. Several car models popular in the United States are equipped with fixed-anchorage three-point lap-shoulder belts. The upper anchorage locations provide a dangerous fit for many users because the belt may be too high or too low. If it is too high, a user may suffer neck injury; a belt that is too low may not properly restrain the user. Despite the simplicity and low cost of adjustable anchorages, they are found on very few models.

► "Convenience" apparatus. An example is a device in some Ford cars. To keep its rear lap-only belts from slipping behind the seat of many Escort models, Ford attached the belt buckle to the seat by an elastic strap retainer. Tragically, the retainer applies forces that pull the belt off the wearer's pelvis. In a crash, it becomes a lethal threat to abdominal organs and the spinal cord. Ford provided no rear-seat lap-shoulder belts in its U.S. cars until the 1990 model year, unlike European Escorts, which had these devices at least a decade earlier.

► Excessive slack. In normal use the seat belt must be reasonably snug across the chest and pelvis to minimize forward motion of the wearer. However, many belts are designed with too much slack. A long-available but rarely used remedy is the pre-tensioner, which tightens the belt around the wearer when a crash is sensed. Although the technology is simple, it is currently available in only a few high-priced automobiles.

Role of Seat Backs

Although much public attention has been focused on seat belt restraint systems, most car companies and NHTSA have remained silent about occupant restraint protection in rear-impact crashes.

In front-end crashes the vehicle's forward movement is abruptly stopped, and seat belts and air bags keep the occupants from hurling forward. The goal is to maintain the occupant in an upright position and to prevent the body from striking hard surfaces and other occupants or from being ejected.

When a car is struck from the rear, the forces work in the opposite direction. The car is then abruptly propelled forward, and occupants are thrown backward. The safety objective of a seat back

is to remain upright while cushioning and containing the occupant's body.

If the seat back collapses, the occupant can be ejected or lose control of the vehicle and be exposed to otherwise avoidable multiple crashes. The occupant can also be hurled into the vehicle's rigid interior structures or other occupants. The collapsed seat back can make it difficult for crash victims to get out of the car, an especially hazardous defect when a fuel system has ruptured and a vehicle is on fire.

In real-world, low-speed, rear-impact crashes, flimsy seat backs have failed to provide adequate protection. Fully investigated "fender bender" cases dramatically demonstrate that seat back failures in low-impact accidents have resulted in severe or fatal injuries. Poorly designed adjustable head restraints add to the hazard because they can be adjusted flush with the top of the seat back, allowing the occupant's head to pivot over the headrest. This can cause severe spinal injury, even quadriplegia.

The importance of seat rigidity in rear-impact crashes has been known for many years. Studies show the industry was well aware of the need for properly designed seat backs as early as the 1960s.

After conducting an extensive test program of rear-impact collisions, a researcher concluded in 1968 that

> rigid seat backs assure more effective support of the occupant during rear-end collisions, providing the seat back support is high enough to also resist rearward movement of the head. Conversely, a seat that yields appreciably rearward . . . places the motorist in a semi-reclined posture that may serve to attenuate some of the injury-producing forces but at the same time adversely displaces the motorist to high elevations relative to the seat back, thereby reducing the measure of support that may be derived.[14]

The same year, another researcher noted that

> a seat back as part of the restraint system should be designed with the following objectives:
>
> 1. It should be strong enough not to fail under heavy torso loads resulting from a rear-end impact of some design speed (30 mph?).
>
> 2. If the seat back does fail, it should do so in a manner involving a considerable expenditure of energy—crumpling or tearing of metal, or hydraulic damping—as this will limit the energy still to be dissipated by the occupant being protected.[15]

Noncatastrophic injuries to the head and neck have also been documented in engineering and scientific literature. These injuries are exacerbated by poor seat back construction, including poorly designed headrests.

Inadequate Standards

It has been reported by researchers that seats and seat backs are failing to provide adequate restraint against injuries in rear impacts and that alternative safer designs are possible.[16] For years, however, NHTSA has lacked the courage to stand up to pressure from the auto industry and has failed to enact meaningful motor vehicle safety standards for seat back and headrest performance in rear-impact collisions.

The government has been privy to rear-impact crash tests for two decades. In virtually every instance, the films accompanying the test reports document the failure of the seat backs; the dummies fly from the front seats into the rear seats or are ejected from the vehicles. Nevertheless, NHTSA has chosen to turn a blind eye to this safety problem.

In 1967, the agency promulgated FMVSS 207, which calls for a static loading test for seats and seat backs. The test simply requires that an empty seat be attached to a pulley and a static load 20 times the empty seat weight be applied with minimal rearward bending. For example, an empty seat that weighs 10 pounds is required to withstand a static load of only 200 pounds before collapsing. FMVSS 202, adopted in 1968, similarly sets static loading limits for headrests.

As cars have become lighter to meet fuel economy requirements, so have car seats. The result has been a corresponding reduction in the minimal level of protection provided by a grossly inadequate standard.

No Crash Test for Seats

While seat belts and shoulder harnesses are required to meet dynamic crash test conditions in which the test vehicle collides with a concrete wall at 30 miles per hour, no similar requirement exists for the seat back in rear-impact collisions. Tests dramatically illustrate how a seat back can collapse in a real-world, rear-impact crash and still meet the performance requirements of FMVSS 207.

Products Liability Section: Safe Products, Safe People

The ATLA Products Liability Section is working toward a product-safe society. "Our section is clearly committed to educating members on the cutting edge of product safety issues," notes chair Edward Ricci of West Palm Beach, Florida. "We will network with other safety and pro-consumer organizations around the country to unmask anti-safety lobbying efforts and other negative tactics of industry."

One key benefit of section membership is a subscription to the *Products Liability Law Reporter*. Any member in good standing who subscribes to the reporter by calling the ATLA Membership Department at (800) 424-2727 will automatically become a member of the section. A subscription costs $110 per year.

Another advantage of membership is access to the The Exchange's Brief Bank of depositions, briefs, complaints, jury instructions, and memoranda on products-related issues.

In addition, an electronic bulletin board has been established for section members who have an IBM-compatible computer, a modem, and a communications software package. For information about the bulletin board or other Exchange offerings, please contact Peter Larsen at (800) 344-3023.

The section also works with the National College of Advocacy to plan educational programs focusing on the needs of section members. For example, at the 1993 Annual Convention, discussions of discovery, expert testimony, and foreign products were on the agenda. Specific topics included medical devices, sudden acceleration of cars, and complex machine liability.

For more information, contact section secretary Gary Robb in Kansas City, Missouri, tel. (816) 474-8080, fax (816) 474-8081. □

In 1974, NHTSA proposed to strengthen these standards by combining head restraint and seat performance requirements into a single rule. The rule would have imposed dynamic crash test requirements on the overall rear-impact restraint system incorporating these components.[17] These requirements would have been similar to those in FMVSS 301, which sets test criteria to determine fuel system integrity in rear-impact crashes.

Faced with industry opposition, NHTSA halted all action on the proposal in April 1979. The agency replaced it with a regulatory plan that would "significantly increase the level of occupant protection" in rollovers and frontal, side, and rear impacts.[18] In a November 1980 letter to car manufacturers, NHTSA's administrator said tests revealed a number of failures involving seat backs and seat tracks and urged the companies to "review their designs to insure that seats do not fail catastrophically in crashes."[19]

The 1979 regulatory plan was abandoned by the incoming Reagan administration, and NHTSA failed to follow up and determine the manufacturers' responsiveness to the November 1980 letter.

In 1989, NHTSA received two petitions requesting rules that would require adequate rear-impact crashworthiness and dynamic testing of seats and seat backs.[20] Although NHTSA officially granted the petitions, it has done little to protect motorists.

The agency invited submissions on a wide range of topics related to seat performance, frontal restraint systems, and side impacts and other types of crashes. Most responses were from manufacturers, the vast majority of whom opposed strengthened standards for seats and seat backs and dynamic crash testing of components. NHTSA has yet to act on these submissions.

Degradation of Safety

Current standards actually encourage a degradation of safety. As vehicles get lighter, manufacturers can comply with regulations but provide less protection.

Motorists must be given seat belts and seat backs that provide reasonable protection in real-world crashes. The necessary technology has long been available, but it cannot protect motorists unless manufacturers are willing to use it. Until that day arrives, the only recourse available to victims will continue to be the tort system. □

Notes

1 David C. Viano, *Cause and Control of Automotive Trauma*, 64 BULL. N.Y. ACAD. MED. 376 (1988).
2 Richard G. Snyder, *The Seat Belt as a Cause of Injury*, 53 MARQ. L. REV. 211, 213 (1970).
3 NATIONAL TRANSP. SAFETY BD., PUB. NO. NTSB/SS-86/03, SAFETY STUDY: PERFORMANCE OF LAP BELTS IN 26 FRONTAL CRASHES 29 (1986).
4 *Id.* at 33.
5 NATIONAL HIGHWAY TRAFFIC SAFETY ADMIN., U.S. DEP'T OF TRANSP., REAR SEAT LAP/SHOULDER BELT RETROFIT KIT REPORT TO CONGRESS, REPORT TO THE COMM. ON APPROPRIATIONS, U.S. HOUSE OF REPRESENTATIVES & U.S. SENATE 11 (1991).
6 NATIONAL HIGHWAY TRAFFIC SAFETY ADMIN., U.S. DEP'T OF TRANSP., 30 MPH SLED TESTS OF WINDOW-SHADE TYPE SEATBELTS (1982).
7 THEODORE TAYLOR, JR., & NORMAN F. LUDTKE, CORPORATE-TECH PLANNING, INC., IMPACT OF FMVSS 208, COMFORT AND CONVENIENCE ON VEHICLE MANUFACTURING 1-2 (prepared for Nat'l Highway Traffic Safety Admin., 1979).
8 *Id.* at 1-15.
9 INSTITUTE FOR INJURY REDUCTION, SEAT BELT WINDOWSHADES: A BACKGROUND REPORT 4 (1988).
10 NATIONAL TRANSP. SAFETY BD., PUB. NO. NTSB/SS-88/02, 1 SAFETY STUDY: PERFORMANCE OF LAP/SHOULDER BELTS IN 167 MOTOR VEHICLE CRASHES 82 (1988).
11 CALSPAN CORP., ACCIDENT RESEARCH SECTION, CALSPAN ON-SITE AUTOMATIC SEAT BELT INVESTIGATION, CASE NO. 90-17 (prepared for Nat'l Highway Traffic Safety Admin., 1990).
12 Snyder, *supra* note 2, at 218-19.
13 DAVID HERBERT ET AL., DEPARTMENT OF MOTOR TRANSP., DYNAMIC TESTING FOR SEAT BELTS 76 (1973) (N.S.W., Austl.).
14 DERWYN M. SEVERY ET AL., BACKREST AND HEAD RESTRAINT DESIGN FOR REAR-END COLLISION PROTECTION 107 (Society of Automotive Engineers Technical Paper No. 680079, 1968).
15 JOHN L. MARTINEZ, HEADREST AND SEAT BACK DESIGN PROPOSALS (Society of Automotive Engineers Technical Paper No. 680775, 1968).
16 *See, e.g.*, KENNETH J. SACZALSKI, FIELD ACCIDENT EVALUATIONS AND EXPERIMENTAL STUDY OF SEAT BACK PERFORMANCE RELATIVE TO REAR-IMPACT OCCUPANT PROTECTION (Society of Automotive Engineers Technical Paper No. 930346, 1993).
17 39 Fed. Reg. 10,268 (1974).
18 NATIONAL HIGHWAY TRAFFIC SAFETY ADMIN., U.S. DEP'T OF TRANSP., FIVE YEAR PLAN FOR MOTOR VEHICLE SAFETY AND FUEL ECONOMY RULEMAKING CALENDAR YEARS 1980-1984 39 (1979).
19 Letter from Joan Claybrook, Administrator, Nat'l Highway Traffic Safety Admin., to auto manufacturers (Nov. 28, 1980) (on file with author).
20 PRM-207-001, submitted by Dr. Kenneth Saczalski (Apr. 18, 1989); PRM-207-002, submitted by Alan Cantor (Dec. 28, 1989).

DOT HS 807 991
JULY 1993